Foundations of Engineering Mechanics

Sergey M. Aleynikov

Spatial Contact Problems in Geotechnics

Boundary-Element Method

Springer

Foundations of Engineering Mechanics

Series Editors: V.I. Babitsky, J. Wittenburg

For further volumes:
http://www.springer.com/series/3582

Sergey M. Aleynikov†

Spatial Contact Problems in Geotechnics

Boundary-Element Method

With 295 Figures

Springer

Series Editors:

V.I. Babitsky
University Loughborough
Department of Mechanical Engineering
Loughborough LE11 3TU, Leicestershire
United Kingdom

J. Wittenburg
Universität Karlsruhe
Fakultät Maschinenbau
Institut für Technische Mechanik
Kaiserstrasse 12
76128 Karlsruhe
Germany

Author:

Sergey M. Aleynikov†
Voronezh State Architecture and Civil
Engineering University
20-Letya Oktyabrya Street, 84
394006, Voronezh
Russia
e-mail: alasmbkb@box.vsi.ru

Originally published in Russian as "Boundary Element Method in Contact Problems for Elastic Spatial-and-Nonhomogeneous Bases", in 2000 by Publishing House of Civil Engineering Universities Association, Moscow, Russia, ISBN 5-93093-053-8, 601 p.

ISSN 1612-1384 e-ISSN 1860-6237
ISBN 978-3-540-25138-5 e-ISBN 978-3-540-44776-4
DOI 10.1007/b11479
Springer Heidelberg Dordrecht London New York

Library of Congress Control Number: 2009934850

Cover design: deblik, Berlin

Printed on acid-free paper

Springer is part of Springer Science+Business Media (www.springer.com)

Obituary

The author of this monograph – Dr. Sergey M. Aleynikov, a well-known specialist in the field of numerical simulation of soil-foundation contact interaction, passed away on August 4, 2009.

Sergey M. Aleynikov graduated from the Department of Applied Mathematics and Mechanics of the Voronezh State University, then he took a Postgraduate Course at the Heat and Gas Transfer Institute of the USA Academy of Science in the city of Minsk, the capital of Belorussia. After defending the PhD thesis in 1983, he started working at the High Mathematics Chair at the Voronezh State University of Architecture and Civil Engineering, and finally, he was the Head of this Chair for five last years.

At the university he began, in close collaboration with Dr. S.V. Ikonin, actively developing the Boundary Integral Approach (BEM approach) for solving non-classical problem analyses of foundation engineering interaction. In co-authorship with Dr. A. A. Sedaev, he generalized the method of duel grids for numerical solution of elastic Hertzian contact problems and suggested the method of generation of random (or irregular) dual grids. On the base of N.K. Snitko's ideas, Dr. Aleynikov proposed the integrated approach to the definition of dominant function for basement soil with a depth variable modulus of elasticity.

He became a recognized specialist in the area of modern method analyses of foundation engineering interaction. More than once he went abroad with lectures and for conducting mutual research in Denmark, Spain, Poland, Canada, Germany, Belgium, the Netherlands and Croatia.

In 2007 S. M. Aleynikov made the translation of the book 'Boundary Elements. Theory and Applications' "written by G.T. Katzikadelis".

His professional competence was highly appreciated and widely recognized. He was a full member of Russian Transport Academy, a member of the panel of Russian Society for Soil Mechanics and Geotechnical Engineering, a member of the International Society for Soil Mechanics and Geotechnical Engineering (ISSMGE), and the European Technical Committee ERTC7 "Numerical Methods in Geotechnical Engineering". Dr. S.M. Aleynikov a big was a member of the Expert Council of the Highest Certification Commission of Education and Science Ministry of the Russian Federation.

This survey monograph by S. M. Aleynikov was published in Russia in 2001 and won a high appraisal of the Russian academic community in the field. There is no doubt its English translation will be useful for Western readers as well.

The image of this indefatigable and original person will be held in our remembrance forever.

Voronezh, Russia

Professor Igor S. Surovtsev
(VSUAC)

Foreword

The theory of elasticity occupies a prominent position in the development of geomechanics and in particular the study of interaction between structural elements and geomaterials. The general area of contact between geomaterials and structural elements is referred to as soil–structure interaction and solutions based on the theory of elasticity have been successfully applied for the study of structural foundations, layered soil systems, earth-retaining structures and tunnels. The subject matter related to soil–structure interaction also forms an important component in work related to the mathematical theory of contact problems starting with the pre-eminent work of Boussinesq and Hertz. The mathematical theory of elastostatic contact problems in particular attracted the attention of the earlier Russian school of eminent elasticians, including Galin, Ufliand, Muskhelishvili, Shtaerman, Koronev, Popov, and others, with special emphasis on the application of elastic contact problems to structural foundations made by Gorbunov-Posadov and colleagues. These contributions were less well known in the English literature in the middle of the last century and a systematic exposition of the contributions of the Russian researchers to soil–structure interaction was documented in the treatise by Selvadurai and to contact mechanics documented in the comprehensive volume by Gladwell. Since the publication of these expository volumes in the 1980s, a number of authoritative volumes have appeared in the area of elastostatic contact problems, where both classical and non-classical contact mechanics problems were discussed; a critical examination of the influences of frictional and unilateral contact problems have found applications in the treatment of traditional interface mechanics problems as well as new developments in materials science and advanced materials modelling.

The present volume is a welcome addition to the literature on elastostatic contact problems with special reference to geomechanics. The volume commences with a systematic exposition of the fundamental solutions of Kelvin, Boussinesq, Cerruti and Mindlin, which is the underpinning of many interesting applications of elastostatics to contact problems in geomechanics. An aspect of spatial non-homogeneity, which is relevant to accreted materials that attain increases in the stiffness with depth due to gravitational effects, is also included in the presentation. The volume proceeds to the presentation of the traditional contact problems in elastostatics that include axisymmetric and torsional indentation problems. A chapter in the volume is devoted to the numerical implementation of the contact problem by appeal to

boundary elements. This is a useful development that complements the analytical aspects and contains sufficient depth to enable the reader to appreciate the contributions that numerical schemes can make to the formulation and solution of contact problems in geomechanics. The treatment of the class of contact problems is not restricted to linear responses; non-linear effects arising from non-linear deformability of the geomaterial is also presented, with the approaches encompassing both finite difference and boundary element methods. The conventional analytical approaches to the formulation and solution of contact problems in geomechanics are by necessity restricted to simplified geometries. The author has ventured to include approaches that can be used for the study of complex foundation shapes associated with pile foundations and other interactions between piles and foundation bases. Finally, the volume culminates with the study of the mechanics of contact between a structure and a poroelastic material saturated with an incompressible fluid. The integral equations governing this class of poroelastic contact problem are summarized and numerical techniques for their solution are presented.

The volume is a very useful contribution to the literature in geomechanics of contact problems as applied to practical problems involving the interaction of geomaterials and supporting soils. It contains a balance of analytical and computational approaches and this makes it a volume that will be of benefit to the researcher and practitioner alike.

William Scott Professor and James McGill Professor A.P.S. Selvadurai FRSC
McGill University, Montreal, QC, Canada

Preface

The studies of contact interaction in the mechanics of deformable solids have been carried out since late 19th century, starting from the works of Winkler (1867), Hertz (1881), and Boussinesq (1885). These studies have been further developed by specialists in the mechanics of deformable solids as well as in structural mechanics, bases and foundations. Thousands of papers on this topic have been published, most of their authors using simplifying assumptions of theoretical modeling on a flat or axially symmetrical stressed state of a base under a punch (a foundation model). It is seen from the detailed analysis of references found in literature that mathematical modeling of essentially spatial contact interaction is in its early stage.

The existing methods for the calculation of complex-shaped foundations are, as a rule, based on a bed coefficient hypothesis. This results in the introduction of empirical coefficients into the calculation methods, thus restricting the range of their application. In the recent years more attention is paid to finite-element approach to mathematical modeling of spatial contact interaction of foundations with bases. However, in such studies the dimensionality of the algebraic analogue of the contact problem sharply increases and the problem must be restricted to a number of partial problems – for example, by imposing restrictions to shape and size of both the foundations themselves and the soil massifs around the foundations, by considering loads in assumption of existence of symmetry axes or planes in the calculation scheme etc. Such studies are rather rare and lack proper consideration of loads of general spatial type (horizontal, vertical forces and moments) and the possibility of their combined action. And extremely rare are studies where the complex shape of various foundations, applied in industrial and civil engineering, is fully taken into account and theoretically based calculations are made.

Creation of new progressive foundation structures and solution of current problems of geotechnical engineering result in more complicated problems to be solved and in the increasing accuracy of the calculation results. The mathematical description of the problems has become so complicated that traditional methods are no longer suitable for their solution. The lack of reliable mathematical methods to a certain extent retards elaboration and implementation of new foundation structures in engineering. Hence, the development of boundary element method (BEM), a relatively new trend in structural mechanics, based on boundary integral equations, seems to be quite promising from the point of view of both theory and application as

an efficient tool for solving 3-D problems. The BEM advantages over other methods of numeric modeling consist in lowering the problem dimensionality (not the whole calculation domain is subject to discretization, but only the boundary surface), in the possibility of a detailed analysis of separate stressed areas, in the simplified data preparation stage etc. This determines the broad application of BEM for solving various problems of structural mechanics, especially the unlimited domains. Simultaneously, by the present time numerical implementation of BEM to the spatial problems of structural mechanics in the field of interaction of foundations and bases has not been sufficiently elaborated yet and appropriate boundary element algorithms and software are still unavailable. Therefore, there is an urgent need to develop efficient numeric approaches using the BEM to solve spatial contact problems of interaction of complex-shaped volumetric punches with deformed bases.

The present book is devoted to one of the BEM application areas – numerical modeling of contact interaction of rigid foundation structures with soil. The main attention is paid to the specific features of stress-strained states of elastic bases at spatial conditions. Contrary to the finite element method, special literature for the BEM application in mechanics of spatial contact interactions between bases and foundations is at present unavailable. In recent publications, devoted to the calculation of bases and foundations, BEM is merely mentioned. On the other hand, well-known books, describing theory and application of BEM, do not appropriately cover the issues of creating calculation models and numerical algorithms for analyzing spatial contact interaction of foundation structures with soil bases.

The whole material is set in six chapters. The first chapter presents some introductive data while reviewing spatial contact models in geotechnics. Classical fundamental solutions for the spatial theory of elasticity obtained by Boussinesq, Cerruti, Mindlin are quoted as well as their generalizations, suitable for calculating constructions on elastic nonclassical bases. The properties of the influence functions are analyzed, required for characterizing elastic bases with nonhomogeneous deformation properties (connected half-spaces, elastic layers of constant and variable thickness).

In the same chapter a numerical-and-analytical procedure is developed for construction of fundamental solutions of spatial elasticity theory for multilayer bases without restrictions on the layer thickness and elastic parameters. Using the two-dimensional Fourier transform, the formulae have been derived, enabling three-dimensional contact problems for complex-shaped structures deepened into spatially nonhomogeneous (layered) soils to be solved in the framework of the BEM numerical algorithm. The final part of the first chapter contains the results on the formulation of influence functions for elastic bases with variable deformation properties. The Boussinesq problem is solved for an elastic half-space when the deformation modulus increases with depth according to a most general law. Proper relations, enabling adequate description of the experimental data, are considered. An efficient numerical-and-analytical procedure is developed for construction of the influence functions, taking into account the soil deformation modulus variation with depth. All the theoretical results for the influence functions were obtained within a unique approach enabling all the main types of nonhomogeneities of natural soil bases to be taken into account.

The second chapter is devoted to the mathematical formulation of mixed problems of the elasticity theory for a half-space and to the numerical-and-analytical methods of their solution. The results obtained in this chapter on developing the mathematical means are the reference data for BEM-based numerical modeling of the spatial contact interaction. The boundary integral equations of the spatial contact problem are written for the case when the calculation scheme is accepted in the form of variously deepened punches undergoing the action of the spatial system of forces. It is shown how to reduce the initial integral equation system of the contact problem with respect to the contact stress function and the punch displacement parameters to the appropriate finite-dimensional algebraic analogue. Much attention is paid to calculating the matrix coefficients of the resolving system of algebraic equations. A numerical-and-analytical procedure is given for integrating Mindlin's fundamental solutions over flat triangular and quadrangular boundary elements, arbitrary oriented in the half-space. For convenience, to apply the developed approach in practical calculations, the boundary integral equations of the spatial contact problems for a number of essential special cases are presented. The contact problems at axial loading and torsion of absolutely rigid rotation bodies deepened into the half-space, are considered. Boundary-element formulations of the contact problems for complex-shaped punches with flat and smooth bases (shallow foundations), situated on spatially nonhomogeneous bases of the semi-infinite elastic massif type are presented.

The third chapter deals with practical implementation of the developed numerical algorithms and substantiation of the reliability of the numerical solutions. It presents the general characteristics and structure of the *Rostwerk* software package for investigating three-dimensional stress-strained states of elastic bases corresponding to the interaction of foundation structures with soil under force factors of general kind. Procedures for creating input databases are described in detail. Algorithms and modules for automatic formation of boundary element grids in plane and in space are presented. An original algorithm for triangulation of flat single- and multiply connected domains, bounded by straight line segments or circle arcs, is described. An algorithm of generation (according to the given triangulation) of dual polygonal boundary element grids of Dirichlet cell type is considered. The created object library of boundary element modules, partitioned into boundary elements, enabling spatial discretization of complex-shaped surfaces of foundation structures, is described. Specific features of solving the systems of linear algebraic equations with asymmetric and close-packed matrices, arising in boundary element analysis, are considered. For solving such systems by direct (Gauss type) methods a special scaling procedure is applied, improving the conditioning of matrices for the finite-dimensional algebraic analogue of a contact problem. The data about the reliability of the numerical solutions are presented. The BEM accuracy and efficiency are demonstrated by the examples of the solved test problems for flat punches of circular, annular and polygonal shapes. Boundary-element solutions for spatial contact problems concerning a rigid spherical inclusion and a cylindrical deepened punch in an elastic half-space are obtained. The final part of the chapter gives the results for numerical-and-analytical solution of the spatial contact problem on impressing a deepened conical punch into an elastic half-space. The method of determination

of the deformation modulus from tests for deepened conical indenters with different angles by static loading is substantiated theoretically.

In the fourth chapter the results of the boundary-element solutions of spatial contact problems for complex-shaped punches, located on the surfaces of elastic nonclassical bases, are analyzed. The problems under consideration correspond to the modeling of contact interaction of shallow foundations with elastic nonhomogeneous bases. Contact pressure fields under punches of various shape under an eccentric load (a contact problem on a strongly inclined punch) are obtained. The influence of non-uniform (over the area) compressibility as well as depth-dependent nonhomogeneity of the base deformational properties on the formation and development of detachment zones, settlements and slopes of punches with the increase of the absolute values of overturning moments is shown. An algorithm to calculate the boundaries of the section core for rigid complex-shaped foundation plates from the stress values is described. Some optimization problems are solved for load and shape parameter control in order to provide uniform settlement of rigid foundation. As an example for the application of the developed boundary element method, a contact problem is solved and the elastic base stress-strained state is determined for a rigid strip foundation of variable width. In the same chapter a spatial contact model of the base is built taking into account nonlinear elastic soil properties. A procedure for the model parameter characterization based on the direct punch test data is considered. Finally, the chapter contains the studies of contact problems of bending of orthotropic plates situated on elastic nonclassical bases, performed by BEM combined with finite difference method.

In the fifth chapter BEM is applied to calculate contact interaction of foundation structures with soil, taking into account the deepening factor. The need for spatially-based calculation of bases of deepened foundations is explained. The principles for foundation structure calculations from the base deformations are briefly reviewed as well as the existing problem formulations and solution methods for spatial problems of contact interaction of deepened foundation structures with soil bases. Solutions of spatial contact problems for deepened monolithic-type foundation structures most widely used in the recent years are also considered, namely for (1) pyramidal piles; (2) foundations made of short vertical or inclined bored piles with caps; (3) bored pile foundations with support extensions; (4) slot foundations with the longitudinal cross-section of various shape. Heterogeneous stress-strained states of the base are taken into account as well as the formation of cavities between the soil and the foundation structures. The effect of the foundation shape on its displacement and slope at various spatial loading is estimated quantitatively. Numerous examples show the results of the boundary-element modeling to be in good agreement with the experimental measurements performed for spatial foundation structures, in most cases BEM results being closer to the experiment than those obtained by other known calculation methods.

Finally, the sixth chapter presents solutions of spatial problems of applied geomechanics related to variation of pore pressure in the soil. The influence of the pore pressure decline on the soil settlement and cracking as well as the induced seismicity and other environmental hazards due to pumping out gas and oil deposits or

intense removal of underground water at industrial or civil engineering is discussed. The methods for numerical modelling of soil mass deformations due to the reduction of the pore pressure are described. The approach is based on the application of integral representations for displacements in a half-space saturated with liquid (or gas) according to the theory of linear pore-elasticity (filtration consolidation). Spatial deformation of the earth surface due to operating horizontal gas-and-oil wells or water drains is studied with the account of the run-off mode. Finally, the results for boundary-element solutions of the spatial contract interaction of structures with the soil at reduced pore pressure are presented.

The studies, presented in the book, are of applied character and have been initially oriented at geotechnical objects in industrial and civil engineering. The boundary element methods developed are suitable for wide applications to calculate the spatial deformation of soil bases. They provide high reliability and efficiency of design solutions for foundation structures. Moreover, the boundary element approach presented here can be helpful for solving other spatially-based problems of mechanics and mathematical physics.

The book summarizes the studies performed in the recent years in Voronezh State University of Architecture and Civil Engineering. The author is grateful to Prof. Viktor N. Nikolaevskiy for his all-round support as well as to Dr. Sergey V. Ikonin and Dr. Alexandr A. Sedaev for fruitful communications and helpful discussions which have enabled the book to be made more substantial.

The preparation of the book for publication was essentially supported by the Dean of Geotechnical Faculty in Varaždin, University of Zagreb (Croatia), Prof. Mladen Kranjčec and the Vice Dean of the faculty Dr. Božo Soldo. The translation from Russian would not have been possible without the key professional contribution of Dr. Yuriy Azhniuk from Institute of Electron Physics, Ukr. Nat Acad Sci (Uzhhorod, Ukraine). The author is truly indebted to all of them.

The author hopes that the work presented in the book can be a helpful study for numerical experiments in geotechnical engineering and will be grateful to the readers for their comments.

Voronezh, Russia Sergey M. Aleynikov

Contents

1 Spatial Contact Models of Elastic Bases 1
1.1 Fundamental Solutions of Static Problems of Spatial Theory of Elasticity 1
1.1.1 Concentrated Forces in an Elastic Body 1
1.1.2 Green's Displacement Tensor 2
1.1.3 Kelvin's Tensor of Influence 3
1.2 Elastic Homogeneous Isotropic Half-Space 5
1.2.1 Mindlin's Solution 5
1.2.2 Boussinesq and Cerruti Solutions 6
1.3 Coupled Half-Spaces 8
1.4 Elastic Layered Bases 12
1.4.1 Constant-Width Elastic Layer 12
1.4.2 Variable-Thickness Elastic Layer 17
1.4.3 Multilayer Elastic Half-Space 25
1.5 Elastic Bases with the Deformation Modulus, Variable with Depth 55
1.5.1 Variation of Deformation Modulus with Depth 55
1.5.2 Normal Concentrated Force Acting on the Half-Space Surface 58
1.5.3 Settlement of a Nonhomogeneous Half-Space Surface . . . 63
References 83

2 Static Analysis of Contact Problems for an Elastic Half-Space 91
2.1 Boundary Integral Equations of the Contact Problem for an Absolutely Rigid Punch, Deepened into an Elastic Half-Space, Under a Spatial Load System 91
2.2 Finite-Measure Analogue of the Contact Problem Using Direct Boundary-Element Method 96
2.3 Numerical-and-Analytical Method of Integration of Fundamental Mindlin's Solutions 101
2.4 Punch in the Shape of a Rotation Body, Deepened into an Elastic Half-Space 108
2.4.1 Axisymmetric Contact Problem 110
2.4.2 Torsion of an Axisymmetric Punch in an Elastic Half-Space 115

2.5 Contact Problems for Rigid Punches Located on the Elastic Base Surface . . . 119
2.5.1 Indentation of a Punch with a Flat Smooth Base into an Elastic Half-Space . . . 121
2.5.2 Torsion of an Elastic Half-Space by a Rigid Punch . . . 126
References . . . 131

3 Computer Implementation of Boundary-Element Algorithms . . . 135
3.1 Software for Solving Spatial Problems of Contact of Foundations with Soil Bases . . . 136
3.2 Specific Features of Numerical Solutions of Linear Algebraic Equation Systems with Non-symmetrical Matrices, Arising in Boundary-Element Analysis . . . 146
3.3 Effective Discretization of 2-D Domains of Complex Shape at Numerical Solving of Spatial Contact Problems of Theory of Elasticity . . . 150
3.3.1 Algorithm of Triangulation in the Boundary-Element Method . . . 151
3.3.2 Dual Grids and Their Application in Boundary-Element Method . . . 162
3.4 Automated Construction of Spatial Grids of Boundary Elements on the Surfaces of Contact of Deepened Foundation Structures with Soil . . . 174
3.5 Test Examples of Numerical Modeling of Spatial Problems of Contact Interaction . . . 192
3.5.1 Contact Problems for Flat Punches with a Smooth Base . . . 192
3.5.2 Contact Problems with the Account of the Deepening Factor for Axisymmetric Punches, Interacting with an Elastic Half-Space . . . 218
References . . . 243

4 Contact Interaction of Shallow Foundations with Nonhomogeneous Bases . . . 251
4.1 Spatial Contact Problems for Rigid Flat-Bottom Punches . . . 253
4.2 Contact Problems for Rigid Rectangular Punches, Resting on Elastic Nonhomogeneous Bases . . . 278
4.2.1 Contact Interaction at Central Loading . . . 282
4.2.2 Contact Interaction at Off-Centre Loading with the Account of Unilateral Constraints . . . 295
4.3 Control of the Parameters of Loading and Shape to Provide a Uniform Settlement of Rigid Foundation Plates . . . 300
4.3.1 Formulation of the Problem and Its Numerical Implementation . . . 301
4.3.2 External Load Control . . . 303
4.3.3 Shape Parameter Control . . . 307

4.4 Spatial Stress-Strained State of the Base of a Rigid Strip Variable-Width Foundation . . . 311
4.4.1 Contact Problem for a Variable-Width Strip Foundation . . 312
4.4.2 Stress-Strained State of a Strip Foundation Base . . . 315
4.4.3 Contact Pressure Distribution in the Area of the Strip Foundation Width Variation . . . 317
4.5 Calculation of the Section Kernel Boundary for Rigid Foundation Plates . . . 323
4.6 Numerical Algorithms of Solving Boundary Integral Equations in Spatial Contact Problems for a Nonlinearly Deformable Base . . . 334
4.6.1 Spatial Contact Model for a Nonlinearly Deformable Base . . . 335
4.6.2 System of Nonlinear Contact Equations of the Contact Problem for Absolutely Rigid Punches of a Complex Shape with a Flat Base . . . 337
4.6.3 Iterative Processes of Solving a Finite-Measure Analogue of the Spatial Contact Problem for a Nonlinearly Deformable Base . . . 339
4.6.4 Contact Problem for a Round Punch on a Nonlinearly Deformable Base . . . 341
4.6.5 Estimation of Nonlinear Deformation Effects from Punch Test Results . . . 348
4.7 Contact Problem for Orthotropic Foundation Plates with the Account of the Specific Features of Spatially Nonhomogeneous Base Deformation . . . 351
4.7.1 Static Calculations of Foundation Plates on Elastic Bases . 352
4.7.2 System of Integro-Differential Equations of Bending of a Plate, Resting on an Elastic Base . . . 358
4.7.3 Calculation of Rectangular Orthotropic Plates Based on Combining Finite-Difference and Boundary-Element Methods . . . 361
4.7.4 Examples of Numerical Modelling of the Contact Interaction of Plates with Elastic Bases . . . 364
References . . . 372

5 Calculation of Bases for Rigid Complex-Shaped Deepened Foundations According to the Second Limiting State in a Three-Dimensional Formulation . . . 385
5.1 General Information on the Calculation of Bases for Foundation Structures from the Deformations . . . 390
5.2 Spatial Problems for Calculation of Foundation Bases with the Account of the Depth Factor . . . 396
5.3 Calculation of Bases for Pyramidal Piles Under Vertical, Horizontal, and Momental Loads . . . 415

5.3.1 Existing Approaches to the Calculation of Piles with a Variable Cross-Section . . . 416
5.3.2 Calculation for the Vertical Load . . . 420
5.3.3 Calculation for the Action of a Horizontal Load . . . 420
5.3.4 Calculation for the Action of an Inclined Load . . . 422
5.3.5 Calculation for the Combined Action of an Inclined Force and a Moment . . . 423
5.4 Interaction of Bases and Rigid Bored Foundations with Vertical and Inclined Piles . . . 424
5.4.1 Structure, Design, and Specific Features of Calculation of Rigid Pile Foundations with Short Piles and a Pile Raft . . . 425
5.4.2 Vertical Cylindrical Piles Under an Inclined Load . . . 428
5.4.3 Foundations with Inclined Piles and a Rectangular Pile Raft . . . 435
5.5 Spatial Contact Problem for a Bored Pile Foundation with a Widening . . . 438
5.5.1 Production and Structures of Bored Pile Foundations with a Support Widening . . . 439
5.5.2 Engineering Methods for Calculation of Bored Pile Foundation Bases from the Base Deformation . . . 441
5.5.3 Calculation of Deformations of the Base of a Bored Pile Foundation with a Spheroconical Widening Under a Central Loading (Axisymmetric Contact Problem) 443
5.5.4 Calculation of Displacements and Slopes of a Bored Pile Foundation Under an Inclined Load . . . 448
5.6 Calculation of Contact Interaction of Bases with Slotted Foundations of Industrial and Civil Buildings . . . 454
5.6.1 Slotted Foundations of Various Structural Shapes . . . 454
5.6.2 Calculation of Slotted Foundations Based on the Base Deformation . . . 457
5.6.3 Contact Stress on the Lateral Surface of a Slotted Foundation . . . 476
5.6.4 Slotted Foundations with Lateral Widenings . . . 491
References . . . 493

6 Spatial Contact Problems for Porous Elastic Bases . . . 505
6.1 Soil Mass Deformation Due to the Pore Pressure Decline . . . 509
6.1.1 Integral Representation of Displacements in a Porous Elastic Medium . . . 509
6.1.2 Dilatation Relations . . . 512
6.2 Distribution of Pressure in a Layer in Case of Functioning Horizontal Wells . . . 514
6.2.1 Distributed Sources of Predetermined Intensity . . . 514
6.2.2 Account of the Finite Radius of the Well . . . 516

6.3 Contact Problems for Foundation Structures at a Reduced Pore Pressure in the Soil . . . 517
6.3.1 Integral Equations of a Spatial Contact Problem . . . 517
6.3.2 Finite-Dimensional Algebraic Analogue of the Integral Equation System . . . 519
6.3.3 Numerical Algorithm of Solution of the Contact Problem . . . 520
6.3.4 Contact Problem for Shallow Foundations . . . 522
6.4 Examples of Numerical Calculations . . . 524
6.4.1 Spatial Deformation of the Land Surface . . . 526
6.4.2 Surface Deformations of the Layer . . . 532
6.4.3 Settlements and Slopes of Rigid Foundation Plates . . . 533
References . . . 534

Conclusions . . . 537

Appendix A Fundamental Solutions of Spatial Theory of Elasticity for a Homogeneous Isotropic Half-Space . . . 543

Appendix B Numerical Schemes for Surface Integral Calculations . . . 555

Appendix C Round Punch on an Elastic Layer of Variable Thickness at Central and Off-Centre Load . . . 569

Appendix D Foundation Under a Tower-Type Structure on a Wedge Base . . . 581

Appendix E Finite-Difference Equations of Cylindrical Bend of Orthotropic Slabs Located on an Elastic Foundation . . . 591

Appendix F Calculation of the Base for a Pyramidal Pile Under Vertical Load According to the "Instructions Manual for Design of Foundations Made of Pyramidal Piles" . . . 603

Appendix G Isolines of Contact Stress on a Lateral Surface of a Slotted Foundation . . . 613

Appendix H Numeric Schemes of Volume Integration . . . 629

Index . . . 637

Chapter 1
Spatial Contact Models of Elastic Bases

Abstract The first chapter presents some introductive data while reviewing spatial contact models in geotechnics. Classical fundamental solutions for the spatial theory of elasticity obtained by Boussinesq, Cerruti, Mindlin are quoted as well as their generalizations, suitable for calculating constructions on elastic nonclassical bases. The properties of the influence functions are analyzed, required for characterizing elastic bases with nonhomogeneous deformation properties (connected half-spaces, elastic layers of constant and variable thickness). A numerical-and-analytical procedure is developed for construction of fundamental solutions of spatial elasticity theory for multilayer bases without restrictions on the layer thickness and elastic parameters. Using the two-dimensional Fourier transformation, the formulae have been derived, enabling three-dimensional contact problems for complex-shaped structures deepened into spatially nonhomogeneous (layered) soils to be solved in the framework of the boundary-element method numerical algorithm. The final part of the first chapter contains the results on the formulation of influence functions for elastic bases with variable deformation properties. The Boussinesq problem is solved for an elastic half-space when the deformation modulus increases with depth according to a most general law. Proper relations, enabling adequate description of the experimental data, are considered. An efficient numerical-and-analytical procedure is developed for construction of the influence functions, taking into account the soil deformation modulus variation with depth. All the theoretical results for the influence functions were obtained within a unique approach enabling all the main types of nonhomogeneities of natural soil bases to be taken into account.

1.1 Fundamental Solutions of Static Problems of Spatial Theory of Elasticity

1.1.1 Concentrated Forces in an Elastic Body

One of the most important problems of mathematical theory of elasticity is construction of a solution of the problem of determination of displacements and stresses in an elastic body, loaded by a unit concentrated force. In case such solutions exist in

S.M. Aleynikov, *Spatial Contact Problems in Geotechnics*, Foundations of Engineering Mechanics, DOI 10.1007/b11479_1, © Springer-Verlag Berlin Heidelberg 2011

linear theory of elasticity, the solutions for the same body at arbitrary loading can be obtained rather easily (in quadratures).

A unit concentrated force, acting in a point $K(\xi,\eta,\zeta)$ (the "source point") of an elastic body V in the direction of OX_k axis, is treated [92] as a singular distribution of mass forces in the form

$$A_i = \delta(N-K)\delta_{ik} \tag{1.1}$$

where δ_{ik} is the Kronecker symbol, $\delta(N-K) = \delta(x_1-\xi)\delta(x_2-\eta)\delta(x_3-\zeta)$, $\delta(t)$ is the Dirac delta function [151].

It follows from Eq. (1.1) that

$$\int_V A_i dV = \int_V \delta(N-K)\delta_{ik} dV(N) = \delta_{ik}, \tag{1.2}$$

i.e. the components of the concentrated force of Eq. (1.1) in the direction of the OX_i axis are nonzero, and in all points $N(x_1,x_2,x_3) \neq K(\xi,\eta,\zeta)$ the distribution of Eq. (1.1) is zero. In the point $K(\xi,\eta,\zeta)$ itself the mass force value is infinite, and according to Eq. (1.2), the integral over the volume of the elastic body V is unit.

In the point of application of the concentrated force infinite displacements arise what is inconvenient for using the corresponding solutions in theory of elasticity. However, in all applications of the idealized solution under consideration integration of products of the infinite solutions and elementary volumes of areas is performed, finally resulting in finite values of displacements and stresses in the elastic body.

Note that the idealized condition of the concentrated force action corresponds to the problem of a load, distributed over a small area, degenerating into a point, under a condition of the value of the main traction vector remaining unchanged. As noted in [95], introduction of concentrated forces is justified by essential advantages for solving boundary problems in the integral formulation.

1.1.2 Green's Displacement Tensor

Let a unit concentrated force, acting in an elastic body V, result in displacements $U_i^{(j)}(N,K)$ where $i = 1, 2, 3$ is an index, indicating the displacement vector component number, $j = 1, 2, 3$ is an index, indicating the concentrated force direction, $N(x_1, x_2, x_3)$ is the observation point, $K(\xi,\eta,\zeta)$ is the concentrated force application point (Fig. 1.1). The mathematical problem of determination of the displacements $U_i^{(j)}(N,K)$ is reduced to the integration of a system of three non-uniform second-order partial differential equations of elliptical type (fundamental Lamé equations)

$$\mu\,\Delta U_i^{(k)} + (\lambda+\mu)U_{j,\,ji}^{(k)} + \delta_{ik}\delta(N-K) = 0(i,j,k = 1,2,3) \tag{1.3}$$

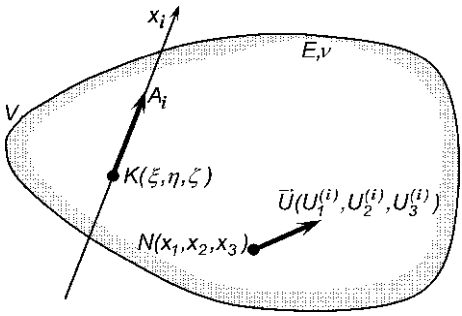

Fig. 1.1 Components of the displacement vector due to the action of a unit concentrated force A_i, applied in the point $K(\xi,\eta,\zeta)$ in an elastic body V

with given boundary conditions. In Eq. (1.3) λ and μ are the Lamé elastic constants, Δ is a three-dimensional Laplace operator in a Cartesian coordinate system $OX_1X_2X_3$, comma means differentiation; as usual, summation over the repeated indices is assumed. It is shown in [92] that the displacement matrix

$$\begin{pmatrix} U_1^{(1)} & U_1^{(2)} & U_1^{(3)} \\ U_2^{(1)} & U_2^{(2)} & U_2^{(3)} \\ U_3^{(1)} & U_3^{(2)} & U_3^{(3)} \end{pmatrix}$$

forms a symmetrical second-rank tensor, i.e. $U_i^{(j)}(K,K') = U_j^{(i)}(K',K)$ (the Maxwell theorem for work reciprocity for concentrated forces). Consequently, for the displacement functions $U_i{}^{(j)}$, called the fundamental solutions of static theory of elasticity (Green's displacement functions), tensor notations are convenient. $U_i^{(j)} = U_j^{(i)} = U_{ij} = U_{ji}$.

1.1.3 Kelvin's Tensor of Influence

As noted above, by using the Green's displacement functions, the solutions of boundary problems of theory of elasticity are obtained in quadratures. Therefore, a key point of solving the problems of theory of elasticity is of the Green's function determination. However, in the three-dimensional case the problem of the Green's function determination for bounded domains meets strong difficulties [92, 151]. Now this function has been obtained for a class of elastic bodies, rather limited in shape. The most easily obtained [92] is the expression for the displacement tensor in an unlimited domain (fundamental Kelvin's solution for an elastic space):

$$U_{ij}(N,K) = A\left[\frac{B}{R}\delta_{ij} - R_{,ij}\right]$$

where $R \equiv R(N,K) = [(x_1-\xi)^2+(x_2-\eta)^2+(x_3-\zeta)^2]^{1/2}$ is the distance between the point $K(\xi,\eta,\zeta)$, to which the load is applied, and a point $N(x_1, x_2, x_3)$ of the space (the observation point),

$$A = \frac{\lambda+\mu}{8\pi\mu(\lambda+2\mu)}, B = \frac{2(\lambda+2\mu)}{\lambda+2\mu}.$$

In an extended form Eq. (1.4) is given by

$$U_{ij}(K,N) = \frac{1}{16\pi G(1-\nu)} \cdot \left[\frac{3-4\nu}{R}\delta_{ij} - z_j \frac{\partial}{\partial x_i}\left(\frac{1}{R}\right)\right] =$$

$$= \frac{1}{8\pi G}\left[\delta_{ij}\Delta R - \frac{1}{2(1-\nu)} \cdot \frac{\partial^2 R}{\partial x_i \partial x_j}\right] = \frac{1}{16\pi G(1-\nu)} \cdot \left[\frac{3-4\nu}{R}\delta_{ij} + \frac{z_i z_j}{R^3}\right],$$

$$z_i = x_i - \zeta_i, \zeta_1 = \xi, \zeta_2 = \eta, \zeta_3 = \zeta; i,j = 1,2,3.$$

As one can see, the components of the fundamental Kelvin's solution have a singularity of the order of $1/R$ in the concentrated force application point K. According to Sect. 1.1.1, the fundamental Kelvin's solution (1.4) corresponds to the displacements arising in the point $N(x_1, x_2, x_3)$ of an infinite body due to a unit concentrated force, applied to the point $K(\xi,\eta,\zeta)$ in the direction of the OX_j axis. This solution can be treated as the Green's function of the influence function for an infinite elastic medium. Using the Hooke law, one can easily obtain stresses, corresponding to the Kelvin displacements

$$\sigma_{jki}(N,K) = \frac{-1}{8\pi(1-\nu)R^2}\left[(1-2\nu)(R_{,k}\delta_{ij} + R_{,j}\,\delta_{jk} - R_{,i}\delta_{jk}) + 3R_{,i}R_{,j}R_{,k}\right].$$

The fundamental Kelvin's solution for the displacements Eq. (1.5) and stresses Eq. (1.6) enables one to obtain the solution of any spatial problem of theory of elasticity for a homogeneous isotropic linearly deformable medium. The fundamental Kelvin's solution is most successfully applied for solving spatial problems of theory of elasticity using the boundary integral equation method for finite-size bodies embedded in an infinite space with the same elastic properties [29].

The solution of contact (mixed) problems for elastic spatially nonhomogeneous half-spaces, being the most popular geomechanical models of soil bases, on the surface of which uniform boundary conditions for the stresses are given, is most effectively accomplished by using special fundamental solutions. In the subsequent sections of this chapter such fundamental solutions of spatial theory of elasticity are considered when unit concentrated forces act inside or on the surface of elastic layers and half-spaces, whose mechanical characteristics take into account the natural conditions of soil masses. The main advantages in using such fundamental solutions (influence functions, calculated or contact models of bases) consist in the boundary conditions on the free surface and on the surfaces of separation of different elastic layers being automatically fulfilled as well as variation of the deformation properties with depth, anisotropy, etc. being taken into account.

1.2 Elastic Homogeneous Isotropic Half-Space

1.2.1 Mindlin's Solution

Consider a unit concentrated force, acting inside a homogeneous half-space $x_3 \geq 0$, whose boundary plane $x_3 = 0$ is load-free. This problem was first solved by Mindlin [77–79] who used the method of superposition of special partial solutions for the infinite space. Later the Mindlin displacement tensor was obtained using different approaches: integral Fourier transformation method [92], reflection method [72], Green's function method for the harmonic Dirichlet problem [136]. The Mindlin's solution is obtained in an explicit form [29] by summation of 18 deformation kernels, following from the Kelvin's solution (six for each of the three force components).

The most compact of the known forms of expressions for the Mindlin displacement $U_i^{(j)}$ and stress $\sigma_{mq}{}^{(i)}$ tensors is as follows:

$$
\begin{aligned}
&U_{ij}(K,N) = [16\pi G(1-\nu)]^{-1}\{(3-4\nu)\delta_{ij}R_1^{-1} + z_i^{(1)}z_j^{(1)}R_1^{-3} + (8\nu^2 - 12\nu + 5)\times \\
&\delta_{ij}R_2^{-1} + (3-4\nu)[z_i^{(2)}z_j^{(2)} - 2\xi_3(z_i^{(2)}\delta_{j3} + z_j^{(2)}\delta_{i3})(1-\delta_{i3}\delta_{j3})]R_2^{-3} + \\
&+2\xi_3(z_3^{(2)} - \xi_3)(1-2\delta_{i3})(R_2^2\delta_{ij} - 3z_i^{(2)}z_j^{(2)})R_2^{-5} - \\
&-4(1-\nu)(1-2\nu)[z_3^{(2)}\delta_{ij}(1-\delta_{i3}) - z_i^{(2)}\delta_{j3} + z_j^{(2)}\delta_{i3} + \\
&+z_i^{(2)}z_j^{(2)}(1-\delta_{i3})(1-\delta_{j3})(R_2 + z_3^{(2)})^{-1}]R_2^{-1}(R_2 + z_3^{(2)})^{-1}\},
\end{aligned}
\tag{1.7}
$$

$$
\begin{aligned}
&\sigma_{mq}^{(i)}(K,N) = [8\pi(1-\nu)]^{-1}\{(1-2\nu)(z_i^{(1)}\delta_{mq} - z_q^{(1)}\delta_{im} - z_m^{(1)}\delta_{iq})R_1^{-3} \\
&-3z_i^{(1)}z_m^{(1)}z_q^{(1)}R_1^{-5} - (1-2\nu)(z_i^{(2)}\delta_{mq} - z_q^{(2)}\delta_{im} - z_m^{(2)}\delta_{iq})R_2^{-3} \\
&-2(1-2\nu)\xi_3[3\delta_{mq}\delta_{i3} + (\delta_{m3}\delta_{qi} + \delta_{q3}\delta_{mi})(1-2\delta_{m3}\delta_{q3}\delta_{i3})]R_2^{-3} \\
&-3(3-4\nu)z_m^{(2)}z_q^{(2)}(z_i^{(2)} - 2\xi_3\delta_{i3})R_2^{-5} + 6\xi_3(1-2\delta_{i3})[\xi_3 z_i^{(2)}\delta_{mq} \\
&-(z_3^{(2)} - \xi_3)(z_q^{(2)}\delta_{im} + z_m^{(2)}\delta_{iq}) + (1-2\nu)(z_i^{(2)}z_q^{(2)}\delta_{3m} + z_i^{(2)}z_m^{(2)}\delta_{3q} \\
&-z_3^{(2)}z_i^{(2)}\delta_{mq})]R_2^{-5} + 30(z_3^{(2)} - \xi_3)\xi_3 z_i^{(2)}z_m^{(2)}z_q^{(2)}(1-2\delta_{i3})R_2^{-7} \\
&+4(1-\nu)(1-2\nu)\left\{(\delta_{mq} - \delta_{m3}\delta_{q3})\left[z_i^{(2)}R_2^{-2} - \delta_{i3}(R_2 + z_3^{(2)})^{-1}\right]\right. \\
&-(1-\delta_{q3})(1-\delta_{m3})\left[(1-\delta_{i3})(z_i^{(2)}\delta_{mq} + z_q^{(2)}\delta_{im} + z_m^{(2)}\delta_{iq})\right. \\
&-\delta_{i3}z_m^{(2)}z_q^{(2)}(2R_2 + z_3^{(2)})R_2^{-2} - (1-\delta_{i3})z_i^{(2)}z_m^{(2)}z_q^{(2)}(3R_2 + z_3^{(2)})R_2^{-2} \\
&\left.\left.\times(R_2 + z_3^{(2)})^{-1}\right](R_2 + z_3^{(2)^{-2}}\right\}R_2^{-1}\Big\}
\end{aligned}
\tag{1.8}
$$

where G is the shear modulus and ν is the Poisson ratio of the soil,

$$z_1^{(1)} = \zeta_1 - \xi_1 = z_1^{(2)}; z_2^{(1)} = \zeta_2 - \xi_2 = z_2^{(2)}; z_3^{(1)} = \zeta_3 - \xi_3;$$

$$z_3^{(2)} = \zeta_3 + \xi_3; R_1 = (z_1^{(1)^2} + z_2^{(1)^2} + z_3^{(1)^2})^{0.5};$$

$$R_2 = (z_1^{(2)^2} + z_2^{(2)^2} + z_3^{(2)^2})^{0.5}.$$

In Eqs. (1.7) and (1.8) R_1 is the distance between the observation point N and the loading point K (point of application of the concentrated force), R_2 is the distance between the point N and a point $\tilde{K}(\xi, \eta, \zeta)$, being a mirror reflection image of the point K with respect to a free surface $x_3 = 0$ of the half-space (Fig. 1.2).

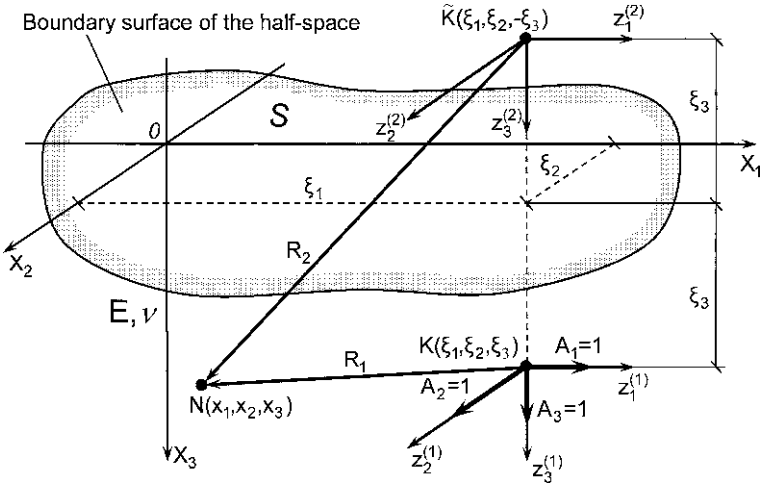

Fig. 1.2 Geometrical scheme of the Mindlin problem of action of concentrated forces in an elastic half-space

For a given direction of the unit concentrated force the first terms for each component of the Mindlin displacement and stress tensors are the corresponding Kelvin's solutions. In Eqs. (1.7) and (1.8) all terms of the tensor components, except the first ones, contain the coordinates of the imaginary loading point $\tilde{K}$, what, as shown by Mindlin, enables the condition of vanishing of stresses at the boundary surface $x_3 = 0$ to be fulfilled. As one can see, at large distances $R = R_1 \approx R_2$ from the loading point the displacement $U_i^{(j)}$ and stress $\sigma_{mq}{}^{(i)}$ functions decrease as $1/R$ and $1/R^2$, respectively. Consequently, Eqs. (1.7) and (1.8) determine the stress-strained state near the point of application of the concentrated force with respect to the points of the elastic body, located at a large distance from the point K ($R \to \infty$) where the half-space can be nominally considered as if they were fixed [54].

1.2.2 Boussinesq and Cerruti Solutions

Consider a particular case of the Mindlin's solution when unit concentrated forces act in the point $K(\xi,\eta,\zeta)$, located on the elastic half-space surface (Fig. 1.3). With a limiting transition in Eqs. (1.7) and (1.8) at $\zeta \to 0$, assuming $R_1 = R_2 = R =$

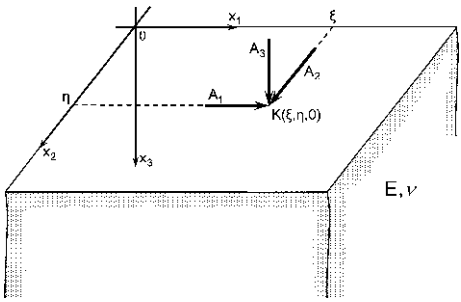

Fig. 1.3 Calculation scheme to the problems of Boussinesq and Cerruti

$\sqrt{(x_1-\xi)^2+(x_2-\eta)^2+x_3^2}$, one obtains an expression for the fundamental tensors of displacements and stresses in the following form:

$$U_{ij}(K,N)=(4\pi G)^{-1}\{(2\nu-1)\delta_{ij}R^{-1}+z_iz_jR^{-3}-(1-2\nu)[B_{ij}z_iz_jR^{-1}(R+z_3)^{-2}$$
$$+(A_{ij}z_3-z_i\delta_{3j}+z_j\delta_{ij})R^{-1}(R+z_3)^{-1}]\}, \tag{1.9}$$

$$\sigma_{ml}^{(i)}(K,N)=\frac{3}{2\pi}\left\{\frac{z_iz_mz_l}{R^5}+\frac{1-2\nu}{3}\left[A_{ml}\frac{z_i(R+z_3)-R^2\delta_{i3}}{R^3(R+z_3)}+D_{iml}\frac{z_mz_l(2R+z_3)}{R^3(R+z_3)^2}\right.\right.$$
$$\left.\left.+C_{iml}\frac{z_iz_mz_l(3R+z_3)-(z_i\delta_{ml}+z_l\delta_{im}+z_m\delta_{il})R^2(R+z_3)}{R^3(R+z_3)^3}\right]\right\} \tag{1.10}$$

where $R=\sqrt{z_1^2+z_2^2+z_3^2}$; $z_1=x_1-\xi_1$; $z_2=x_2-\xi_2$; $z_3=x_3$; $A_{im}=\delta_{im}-\delta_{i3}\delta_{3m}$; $B_{im}=(1-\delta_{i3})(1-\delta_{3m})$;$D_{iml}=B_{ml}\delta_{i3}$; $C_{iml}=B_{im}(1-\delta_{3l})$; $i,j,l,k,m=\overline{1,3}$.

As follows from the quoted expressions, the obtained equations combine the known fundamental Boussinesq solutions [40, 50, 54, 92] (for a concentrated force, acting normally to the half-space surface $A_1=A_2=0$, $A_3=1$) and Cerruti solutions (for tangential forces, acting on the half-space surface, $A_1=1(0)$; $A_2=0(1)$; $A_3=0$).

Equations (1.9) and (1.10) for the fields of deformations and stresses caused by concentrated normal and tangential forces, in principle, enable one to solve the problems of a stress-strained state of an elastic half-space, on the surface of which given, in general case, inclined, loads act. The resulting displacements and stresses from the action of loads, distributed over an arbitrary finite domain on the half-space surface, are obtained by integration, using the superposition principle [54, 92]. In a closed form, determination of the stress-strained state in a half-space under surface loads has been performed only for the domains of the most simple geometrical shape: circular and ring-shaped [40, 54, 146], rectangular [68], elliptical [71, 110, 141].

The difficulties of application of analytical methods for the loads being distributed over domains of complex geometry can be overcome using various numerical methods of integration of the Boussinesq and Cerruti fundamental solutions. We

have proposed [8, 9] an effective version of the numerical method of calculation of displacements and stresses in the case of surface loads of arbitrary form, distributed over the areas of a given geometry. The possibilities of this approach were tested for the example of analysis of the stress-strained state of the elastic half-space in case its square domain being loaded by a uniformly distributed load or a load, being varied linearly or parabolically. In particular, the range of relative depths, for which the angular point method [140] is applicable independently of the loading type, is determined. Using the developed approach, for practical geotechnical purposes the surface deformations of various elastic bases were determined for circular, elliptical and ring-shaped (concentric and eccentric) loading domains [9, 12].

The expressions for the Mindlin, Boussinesq, and Cerruti fundamental solutions in the extended form are given in Appendix A. From the literature the most important are fundamental solutions of spatial theory of elasticity for a homogeneous half-space with a fixed boundary [128, 135], for a nonhomogeneous half-space with the Poisson ratio variable in depth [24], for anisotropic half-spaces [36, 60, 64, 117, 123, 145].

1.3 Coupled Half-Spaces

Consider a full system of expressions for the components of the Green's displacement tensor, obtained from the solution of the problem of the action of concentrated forces within contacting half-spaces with different deformational characteristics. This system is convenient for application in the boundary-element analysis. No displacement of layers along the boundary is assumed for both vertical and horizontal directions, i.e. the case of two coupled half-spaces with different elastic constants E_1, ν_1 and E_2, ν_2 is considered. The forces ate applied in the point $K(\xi, \eta, \zeta)$ (Fig. 1.4). The origin of coordinates is set on the elastic half-space separation surface; the OZ axis is directed towards the first half-space normally to the common

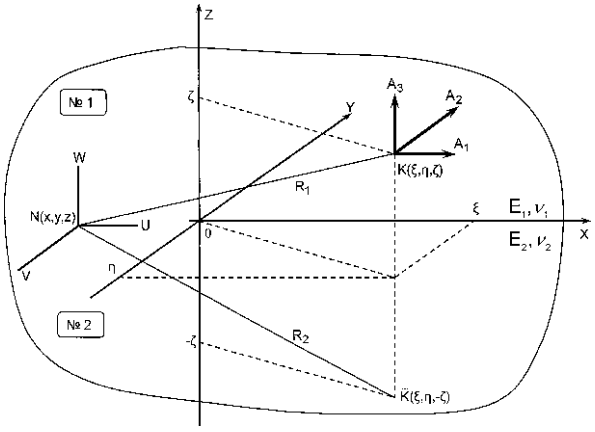

Fig. 1.4 Unit concentrated forces in coupled half-spaces

half-space boundary, which is the *OXY* plane. The problem under consideration was solved by Plevako [100], using the representation of the displacement vector components in terms of Galerkin vector and three arbitrary biharmonical functions which are unambiguously determined due to the boundary conditions of the half-space coupling being satisfied. Equality of all three displacements as well as of normal and two tangential stresses are taken as such conditions. In view of the Plevako fundamental solution being sufficiently universal, here we quote the expressions for the displacement tensor components for each of the half-spaces:

Half-space No. 1

$$U^{(1)}(K,N)=\frac{1}{16\pi G_1(1-\nu_1)}\left[\frac{x_1^2}{R_2^3}-\frac{3-4\nu_1}{R_2}+\frac{4(1-\nu_1)-2\gamma}{R_1}+\right.$$
$$+2\beta\zeta z\left(\frac{1}{R_1^3}-\frac{3x_1^2}{R_1^5}\right)-\frac{\alpha+2(1-\nu_1)(3-4\nu_1)\beta+(1-2\nu_1)\beta-2\gamma+3-4\nu_1}{R_1+z_1}\times$$
$$\left.\times\left(1-\frac{x_1^2}{R_1(R_1+z_1)}\right)+(3-4\nu_1)\beta\left(\frac{1}{R_1}-\frac{x_1^2}{R_1^3}\right)\right], \tag{1.11}$$

$$V^{(1)}(K,N)=\frac{x_1y_1}{16\pi G_1(1-\nu_1)}\left[\frac{1}{R_2^3}-\frac{(3-4\nu_1)\beta}{R_1^3}-\frac{6\beta\zeta z}{R_1^5}+\right.$$
$$\left.+\frac{\alpha+2(1-\nu_1)(3-4\nu_1)\beta+(1-2\nu_1)\beta-2\gamma+3-4\nu_1}{R_1(R_1+z_1)^2}\right], \tag{1.12}$$

$$W^{(1)}(K,N)=\frac{x_1}{16\pi G_1(1-\nu_1)}\left[\frac{-z_2}{R_2^3}+\frac{(3-4\nu_1)\beta z_2}{R_1^3}+\frac{6\beta\zeta zz_1}{R_1^5}-\right.$$
$$\left.-\frac{\alpha-\beta-4(1-\nu_1)(1-2\nu_1)\beta-1}{R_1(R_1+z_1)}\right], \tag{1.13}$$

$$U^{(2)}(K,N)=\frac{1}{16\pi G_1(1-\nu_1)}\left[\frac{y_1^2}{R_2^3}-\frac{3-4\nu_1}{R_2}+\frac{4(1-\nu_1)-2\gamma}{R_1}+\right.$$
$$+2\beta\zeta z\left(\frac{1}{R_2^3}-\frac{3y_1^2}{R_2^5}\right)-\frac{\alpha+2(1-\nu_1)(3-4\nu_1)\beta+(1-2\nu_1)\beta-2\gamma+3-4\nu_1}{R_1+z_1}\times$$
$$\left.\times\left(1-\frac{y_1^2}{R_1(R_1+z_1)}\right)+(3-4\nu_1)\beta\left(\frac{1}{R_1}-\frac{y_1^2}{R_1^3}\right)\right], \tag{1.14}$$

$$V^{(2)}(K,N)=\frac{-x_1y_1}{16\pi G_1(1-\nu_1)}\left[\frac{1}{R_2^3}-\frac{(3-4\nu_1)\beta}{R_1^3}-\frac{6\beta\zeta z}{R_1^5}+\right.$$
$$\left.+\frac{\alpha+2(1-\nu_1)(3-4\nu_1)\beta+(1-2\nu_1)\beta-2\gamma+3-4\nu_1}{R_1(R_1+z_1)^2}\right], \tag{1.15}$$

$$W^{(2)}(K,N)=\frac{-y_1}{16\pi G_1(1-\nu_1)}\left[\frac{-z_2}{R_2^3}+\frac{(3-4\nu_1)\beta z_2}{R_2^3}+\frac{6\beta\zeta z z_1}{R_1^5}-\right.$$
$$\left.-\frac{\alpha-\beta-4(1-\nu_1)(1-2\nu_1)\beta-1}{R_1(R_1+z_1)}\right], \tag{1.16}$$

$$U^{(3)}(K,N)=\frac{-x_1}{16\pi G_1(1-\nu_1)}\left[\frac{-z_2}{R_2^3}+\frac{(3-4\nu_1)\beta z_2}{R_1^3}-\frac{6\beta z\zeta z_1}{R_1^5}-\right.$$
$$\left.-\frac{\beta+4(1-\nu_1)(1-2\nu_1)\beta-\alpha+1}{R_1(R_1+z_1)}\right], \tag{1.17}$$

$$V^{(3)}(K,N)=\frac{-y_1}{16\pi G_1(1-\nu_1)}\left[\frac{-z_2}{R_2^3}+\frac{(3-4\nu_1)\beta z_2}{R_1^3}-\frac{6\beta z\zeta z_1}{R_1^5}-\right.$$
$$\left.-\frac{\beta+4\nu_1(1-\nu_1)(1-2\nu_1)\beta-\alpha+1}{R_1(R_1+z_1)}\right], \tag{1.18}$$

$$W^{(3)}(K,N)=\frac{-1}{16\pi G_1(1-\nu_1)}\left[\frac{3-4\nu_1}{R_2}+\frac{z_2^2}{R_2^3}-\frac{4(1-\nu_1)(1-2\nu_1)\beta+\alpha-1}{R_1}\right.$$
$$\left.-\frac{\beta[(3-4\nu_1)z_1^2+2\zeta z]}{R_1^3}+\frac{6\beta z\zeta z_1^2}{R_1^5}\right]. \tag{1.19}$$

Half-space No. 2

$$U^{(1)}(K,N)=\frac{1}{16\pi G_2(1-\nu_1)}\left[\frac{2\gamma}{R_2}+\frac{2z(\alpha-\beta-1)}{R_2(R_2-z_2)}\left(1-x_1^2\frac{2R_2-z_2}{R_2^2(R_2-z_2)}\right)\right.$$
$$+\frac{(3-4\nu_2)\alpha+[1-2(\nu_1-\nu_2)](\beta+1)-2\gamma}{R_2-z_2}\left(1-\frac{x_1^2}{R_2(R_2-z_2)}\right)$$
$$\left.-(\beta+1)\left(\frac{1}{R_2}-\frac{x_1^2}{R_2^3}\right)\right], \tag{1.20}$$

$$V^{(1)}(K,N)=\frac{x_1y_1}{16\pi G_2(1-\nu_1)}\left[-2(\alpha-\beta-1)\frac{z(2R_2-z_2)}{R_2^3(R_2-z_2)}\right.$$
$$\left.-\frac{(3-4\nu_2)\alpha+[1-2(\nu_1-\nu_2)](\beta+1)-2\gamma}{R_2(R_2-z_2)^2}+\frac{(\beta+1)}{R_2^3}\right], \tag{1.21}$$

$$W^{(1)}(K,N) = \frac{x_1}{16\pi G_2(1-\nu_1)}\left[\frac{(3-4\nu_2)\alpha - [3-2(\nu_1+\nu_2)](\beta+1)}{R_2(R_2-z_2)}\right.$$
$$\left. - \frac{(\beta+1)\zeta + z(2\alpha-\beta-1)}{R_2^3}\right], \tag{1.22}$$

$$U^{(2)}(K,N) = \frac{1}{16\pi G_2(1-\nu_1)}\left[\frac{2\gamma}{R_2} + \frac{2z(\alpha-\beta-1)}{R_2(R_2-z_2)}\left(1 - x_1^2\frac{2R_2-z_2}{R_2^2(R_2-z_2)}\right)\right.$$
$$+\frac{(3-4\nu_2)\alpha + [1-2(\nu_1-\nu_2)](\beta+1) - 2\gamma}{R_2-z_2}\left(1 - \frac{x_1^2}{R_2(R_2-z_2)}\right)$$
$$\left. - (\beta+1)\left(\frac{1}{R_2} - \frac{x_1^2}{R_2^3}\right)\right], \tag{1.23}$$

$$V^{(2)}(K,N) = \frac{x_1 y_1}{16\pi G_2(1-\nu_1)}\left[-2(\alpha-\beta-1)\frac{z(2R_2-z_2)}{R_2^3(R_2-z_2)^2}\right.$$
$$\left. - \frac{(3-4\nu_2)\alpha + [1-2(\nu_1-\nu_2)](\beta+1) - 2\gamma}{R_1(R_1+z_2)^2} + \frac{(\beta+1)}{R_2^3}\right], \tag{1.24}$$

$$W^{(2)}(K,N) = \frac{x_1}{16\pi G_2(1-\nu_1)}\left[\frac{(3-4\nu_2)\alpha - [3-2(\nu_1+\nu_2)](\beta+1)}{R_2(R_2-z_2)}\right.$$
$$\left. - \frac{(\beta+1)\zeta + z(2\alpha-\beta-1)}{R_2^3}\right], \tag{1.25}$$

$$U^{(3)}(K,N) = \frac{-x_1}{16\pi G_2(1-\nu_1)}\left[\frac{[3-2(\nu_1+\nu_2)](\beta+1) - (3-4\nu_2)\alpha}{R_2(R_2-z_2)}\right.$$
$$\left. - \frac{2\alpha z - z_1(\beta+1)}{R_2^3}\right], \tag{1.26}$$

$$V^{(3)}(K,N) = \frac{-y_1}{16\pi G_2(1-\nu_1)}\left[\frac{[3-2(\nu_1+\nu_2)](\beta+1) - (3-4\nu_2)\alpha}{R_2(R_2-z_2)}\right.$$
$$\left. - \frac{2\alpha z - z_1(\beta+1)}{R_2^3}\right], \tag{1.27}$$

$$W^{(3)}(K,N) = \frac{-1}{16\pi G_2(1-\nu_1)}\left[\frac{2(\nu_2-\nu_1)](\beta+1) + (3-4\nu_2)\alpha}{R_2}\right.$$
$$\left. + \frac{[2\alpha z - z_1(\beta+1)]z_2}{R_2^3}\right], \tag{1.28}$$

where $x_1 = x - \xi$; $y_1 = y - \eta$; $z_1 = z - \zeta$; $z_2 = z + \zeta$; $R_1 = \sqrt{x_1^2 + y_1^2 + z_1^2}$; $R_2 = \sqrt{x_1^2 + y_1^2 + z_2^2}$;

ξ, η, ζ are the coordinates of the point K of application of the unit concentrated forces, $N(x, y, z)$ – is a field point (observation point),

$$k = \frac{G_2}{G_1} = \frac{E_2(1+\nu_1)}{E_1(1+\nu_2)}; \alpha = \frac{8\,k(1-\nu_1)[k(1-\nu_1)+(1-\nu_2)]}{(k+3-4\nu_2)[k(3-4\nu_1)+1]};$$
$$\beta = \frac{k-1}{k(3-4\nu_1)+1}; \gamma = 4(1-\nu_1)\frac{k}{k+1}.$$

The necessary execution of limiting transitions is checked directly.

The Kelvin's solution for an infinite homogeneous elastic body follows from Eqs. (1.11)–(1.28) if the deformation parameters of the two half-spaces coincide ($E_1 = E_2$, $\nu_1 = \nu_2$). One also arrives at the same result at $\zeta \to \infty$, since the terms, containing R_1, disappear, and deals with a fundamental solution for an infinite elastic medium with the deformation parameters E_1, ν_1.

If one implies $\zeta = 0$ and $E_2 = 0$, then the Plevako solution is transformed into a combined Boussinesq-Cerruti solution for the half-space No. 1.

At $E_2 = 0$ one arrives at the Mindlin's solution for a concentrated force, acting inside an elastic half-space No. 1.

At $\zeta = 0$ the concentrated force acts on the boundary of the coupled half-spaces. The Plevako solution coincides with the Vasilyev solution [149].

If the lower half-space is absolutely rigid ($E_2 = \infty$), one obtains a solution of the Shandru problem [128, 135] of a concentrated force, acting in a homogeneous half-space with a restrained boundary.

It is seen that the Plevako solution (1.11)–(1.28) generalized all main fundamental solutions for an elastic half-space. Meanwhile, this solution is also of an independent interest. The application of the Mindlin's solution is known to be justified for spatial problems of theory of elasticity in case of relatively small depth of structures in the soil base. The Kelvin's solution is advisable to be applied at large distances from the base surface. The Plevako equations are useful for geotechnical calculations in the case when a deep foundation structure is located near the boundary of two layers of a thick base, the mechanical characteristics of these layers being different.

1.4 Elastic Layered Bases

1.4.1 Constant-Width Elastic Layer

An infinite elastic medium, restricted by parallel plane, is called a spatial elastic layer [92]. Denote the layer thickness as H and introduce a Cartesian coordinate system with an origin on the upper boundary of the layer $x_3 = 0$ (Fig. 1.5). If an infinite elastic layer is resting on an incompressible half-space, such calculation scheme corresponds to a popular model of a finite-thickness elastic base, substantiated by many authors and included into the engineering regulations for the determination of the stress-strained state in soil bases [144]. This base model is applicable in the

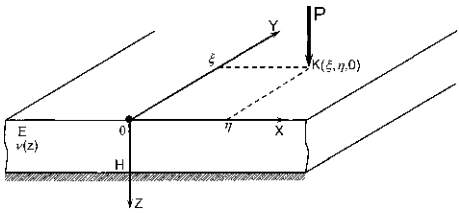

Fig. 1.5 Concentrated force, acting on the free surface of an elastic layer with an absolutely rigid base as an underlayer

cases of rocks or low-compressible soils lying at a certain depth. If there is no rigid underlying half-space, then a nominal compressible layer is introduced into consideration, its thickness being set from long-term observations of settlements of large-scale foundations [143]. It is noted in a number of papers that a constant-thickness elastic layer as a calculation model for a soil base smoothes some disadvantages, inherent to the elastic half-space. When the elastic layer model is used, the settlements are smaller and their decay with the distance from the load application point is faster than for the elastic half-space. In such model the calculated forces in the structures, resting on elastic bases, are reduced. It should be noted that typically the calculations of the soil bases themselves and foundation structures, interacting with them, are reduced to the determination of normal displacements of the base surface points as well as an a priori unknown distribution of contact pressures over the areas of the structure contact with the base. In general, such problems result in integral or integro-differential equations. A very important characteristic, introduced into these equations, is the fundamental solution for the problem of action of a normal concentrated force on the layer boundary. In particular, for the deformation-and-strength calculation of shallow foundation structures (typically rigid or flexible plates and beams) it is sufficient to know only the dependence of the base surface vertical displacements on the normal load or, in other words, to know the calculation model (in our case – the contact model) of the base. The equations for the normal displacements of the layer surface points $x_3 = 0$ due to a unit normal force applied in an arbitrary point of this surface are given below in the explicit form. Suitable for practical application contact models of nonhomogeneous bases whose properties vary with depth, are considered.

Elastic layer, nonhomogeneous with depth. Consider an isotropic layer $S = \{ |x_1, x_2| < \infty, 0 \le x \le H \}$ with a one-dimensional nonhomogeneity of elastic properties with depth. Let the shear modulus G of the layer material be constant and the Poisson ratio $\nu(x_3)$ be an arbitrary differentiable function of coordinate along the layer thickness. In this case the modulus of elasticity of the layer material $E(x_3) = 2G[1+\nu(x_3)]$ will be a positive function of the coordinate x_3.

The problem of action of a unit concentrated force, normal to a layer with no tangential stress ($\sigma_{\alpha 3}(x_1, x_2, 0) = 0$), is solved by Borodachev [25] in the assumption of absence of friction forces at the contact of a layer with an absolutely rigid base ($U_3(x_1, x_2, H) = 0$, $\sigma_{\alpha 3}(x_1, x_2, 0) = 0$, $\alpha = 1, 2$). The influence function for the base model under consideration with sufficiently general nonuniformity of elastic properties can be presented in the form

$$W^{(3)}(K,N) = W(x,y,\xi,\eta) = W(x-\xi\,, y-\eta) = W(r) = \frac{1}{4\pi G}\int\limits_0^\infty Q(k)J_0(rk)dk \tag{1.29}$$

where $r = \sqrt{(x_1-\xi)^2+(y-\eta)^2}$; $J_O(t)$ is the Bessel function of the first kind of the zeroth order;

$$Q(k) = \frac{4\sinh^2(Hk)}{k(2L+E_2^2+E_1^2L_2)};$$

$$E_1(k) = \exp(-Hk);\ E_2(k) = \exp(Hk);\ L = \int\limits_0^H \gamma(s)ds;$$

$$L_1(k) = \int\limits_0^H \gamma(s)\exp(-2ks)ds;\ L_2 = \int\limits_0^H \gamma(s)\exp(2ks)ds;$$

$$\gamma(s) = [1-\nu(s)]^{-1}.$$

The construction of the influence function (1.29) for such character of nonuniformity of elastic properties with the layer thickness was enabled by introduction of stress functions, satisfying second-order partial differential equations with constant coefficients and subsequent application of theory of two-dimensional integral Fourier transformation [141]. As an example, Borodachev has analyzed in detail the law of variation of elastic properties of the layer material, when

$$\gamma(x_3) = \alpha_1 + \alpha_2\cos(n\pi\frac{x_3}{H}), \tag{1.30}$$

$n = 1, 2, 3,\ldots$, α_1 and α_2 are the model parameters. Figure 1.6 shows the examples of Poisson ratio dependences in accordance with Eq. (1.30). In case of variation of deformation properties of the elastic layer with depth according to Eq. (1.30), the influence function is given by

$$W(r) = W_0(r)[1-\psi(R)] \tag{1.31}$$

where

$$\psi(R) = T_1(R) - \alpha T_2(R);\ T_1 = \int\limits_0^\infty X\left(\frac{k}{R}\right)J_0(k)\,dk;\ T_2 = \int\limits_0^\infty Y\left(\frac{k}{R}\right)J_0(k)\,dk;$$

$$X(k) = 1 + [1-\cosh(k)]\,[k+\sinh(k)]^{-1};$$

$$Y(k) = \frac{[\cosh(k)-1]\,\{k+[1-\theta(k)]\sinh(k)\}}{[k+\sinh(k)]\,\{k+[1+a\theta(k)]\sinh(k)\}};$$

$$\theta(k) = k^2\left(k^2+n^2\pi^2\right)^{-1};\ a = a_2/a_1;\ R = r/2H;$$

$W_0(r) = \dfrac{1-\nu(0)}{2\pi G}\cdot\dfrac{1}{r}$ is the influence function (the Boussinesq problem solution) for a homogeneous elastic half-space with a shear modulus G and Poisson ratio

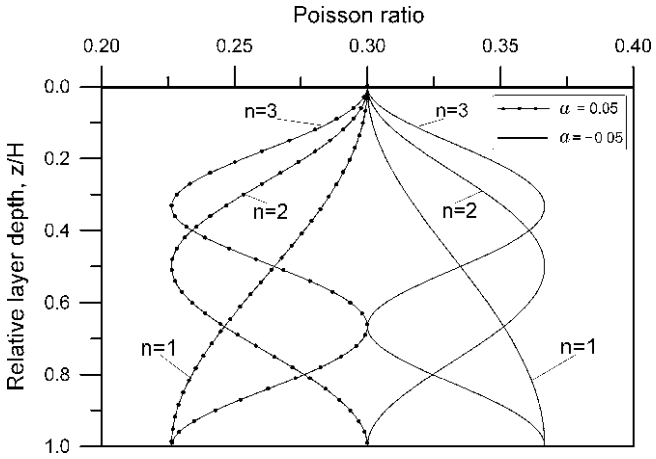

Fig. 1.6 Variation of the Poisson ratio across the finite-thickness nonhomogeneous elastic layer; $\nu(0) = 0.3$

$\nu = \nu(0)$. In a particular case, when in Eq. (1.31) $H \to \infty$ (in this case the elastic nonhomogeneous layer $0 \le x \le H$ is transformed into a half-space $x_3 \ge 0$), the influence function for an elastic half-space with a variable Poisson ratio [24, 43] is obtained:

$$W^{\infty}(r) = \frac{1}{4\pi G} \int_0^{\infty} \frac{J_0(rk)dk}{\Lambda(k)k}, \; \Lambda(k) = \int_0^{\infty} \gamma(s) \exp(-2ks)ds.$$

Elastic homogeneous layer. In the case of a homogeneous layer material, when $\nu(x_3) = \nu = \text{const}$, the function $Q(k)$ from the integral representation of Eq. (1.29) is given by

$$Q^o(k) = \frac{4(1-\nu)\sinh^2(Hk)}{2Hk + \sinh(2Hk)}, \tag{1.32}$$

and a well-known [37] formula for the vertical displacements of the elastic layer surface is valid:

$$W^H(r) = \frac{2(1-\nu^2)}{\pi E} \int_0^{\infty} \frac{\sinh^2(Hk)}{2Hk + \sinh(2Hk)} J_0(rk)dk. \tag{1.33}$$

One should note that Eq. (1.33), similarly to Eq. (1.31), corresponds to the condition of zero tangential stress on the lower surface of the layer, i.e. when there are no obstacles for horizontal displacements. According to the Egorov solution [37], the function $Q(k)$ for a layer, rigidly restrained ($U = V = W = 0$) on the lower surface $x_3 = H$, is given by

$$Q^1(k) = \frac{[(3-4\nu)\sinh 2\alpha - 2\alpha](1-\nu)}{(3-4\nu)\cosh^2\alpha + \alpha^2 + (1-2\nu)^2}, \alpha = kH, \tag{1.34}$$

and the corresponding fundamental solution is written in the form

$$W^E(r) = \frac{(1-\nu^2)}{2\pi E}\int\limits_0^\infty \frac{(3-4\nu)\sinh 2\alpha - 2\alpha}{(3-4\nu)\cosh^2\alpha + \alpha^2 + (1-2\nu)^2} J_0(rk)dk. \tag{1.35}$$

A check for the asymptotic behaviour of the integrals in Eqs. (1.33) and (1.35) at $H \to \infty$, using a known equality

$$\int\limits_0^\infty J_0(r\alpha)d\alpha = \frac{1}{r},$$

results, as one should expect, to the classical Boussinesq solution $W_0(r) = (1-\nu^2)/\pi Er$. In other words, with the layer thickness increase the type of boundary conditions on its lower boundary will not affect the settlement values of the free boundary.

It is noted in [37] that the improper integrals in Eqs. (1.33) and (1.35) are not expressed in a finite form in terms of elementary functions. On the other hand, direct numerical integration (e.g., using the Simpson rule) is noted to be ineffective in this case. Following [18], Egorov suggested the following approximation, applicable for practical purposes:

$$\frac{2\sinh^2\alpha}{2\alpha + \sinh 2\alpha} = \sum_{i=0}^{4} B_i e^{-A_i\alpha} \tag{1.36}$$

where $A_0 = 0$, $A_1 = 0.8$, $A_2 = 1.4$, $A_3 = 0$, $A_4 = 0.6$, $B_0 = 1$, $B_1 = 0.426$, $B_2 = -6.051$, $B_3 = 7.395$, $B_4 = -2.770$.

As a result, the improper integral (1.33) can be expressed in terms of elementary functions by means of the equation [49]

$$\int\limits_0^\infty e^{-\alpha a} J_0(b\alpha)d\alpha = (a^2 + b^2)^{-1/2}.$$

Thus, the fundamental solution for an elastic layer with a slippage on the lower boundary is presented in the following explicit algebraic form:

$$W_1(r) = \frac{1-\nu^2}{\pi E}\sum_{i=0}^{4} B_i \int\limits_0^\infty e^{-A_i kH} J_0(rk)dk = \frac{1-\nu^2}{\pi E}\sum_{i=0}^{4} \frac{B_i}{\sqrt{A_i^2 \cdot H^2 + r^2}}. \tag{1.37}$$

One should note that, contrary to Eq. (1.33), the solution (1.35) requires approximation of the integrand function for each given value of the Poisson ratio ν. Therefore, for the value of $\nu = 0.3$, the most widely used in soil mechanics, Egorov [37] proposed a rather successful approximation of the fundamental solution (1.35), corresponding to the condition of rigid constraint of the elastic layer on the lower boundary $x_3 = H$

$$W_2(r) = W_1 - \frac{1-\nu^2}{\pi HE} \cdot 0.2086 \cdot e^{-\frac{25}{22}\left(\frac{r}{H}\right)^2} \tag{1.38}$$

It is quite evident that in case of necessity similar approximations of the displacement function $W_2(r)$ can be constructed for any other value of the ν coefficient.

In the studies where the elastic base model is used in the form of a finite-thickness layer with constrained lower boundary (e.g. [34, 110]), the calculations are performed, based on the Burmister solution [31]. It can be easily shown that this solution exactly coincides with the corresponding Egorov solution (1.35). However, it should be noted that the Burmister solution was obtained 2 years earlier and has an advantage, additionally giving the distribution of vertical compressive stress in the layer.

Finally note that the influence functions from the action of concentrated forces within the finite-thickness layer are obtained below (Sect. 1.4.3) as a particular case of solution of the spatial problem for a to-layer base.

1.4.2 Variable-Thickness Elastic Layer

A spatial elastic wedge is used as the model of a base with a linearly varied depth (variable-thickness elastic layer). The necessity of taking into account the compressed layer thickness variation in the soil base calculation scheme often arises in practice when the underlying dense layer (e.g. rock) is inclined. Related issues are also problems of calculation of foundation structures, located near slopes (the base model is also an elastic spatial wedge). The wedge angle for such bases is obtuse (or at least right) and both faces outside the contact domain are stress-free. Both variants of the calculation scheme of the base as a variable-thickness layer have been studied rather incompletely. The solutions for most of the contact problems for an elastic wedge have been obtained, as a rule, in a flat formulation [7, 30, 41, 73, 116, 122, 130, 131, 133, 153].

In cylindrical coordinates r, ϕ, z where the z axis is directed along the wedge rib, consider normal P and directed along the r axis tangential Q concentrated forces, acting on the $\phi = \alpha$ face of the spatial elastic wedge in the points $r = x$, $z = \pm y$ (Fig. 1.7a). The boundary conditions on this wedge face can be written in the following form:

$$\sigma_\varphi = P\delta(r-x)\delta(|z|-y),\ \tau_{r\varphi} = -Q\delta(r-x)\delta(|z|-y),\ \tau_{\varphi z} = 0 \tag{1.39′}$$

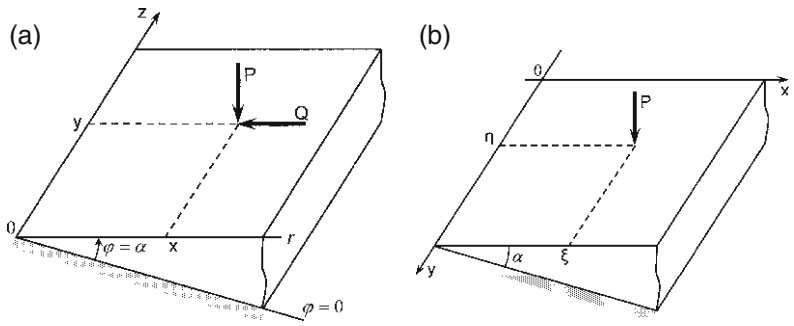

Fig. 1.7 Coordinate systems for a variable-thickness elastic layer: (**a**) polar, (**b**) Cartesian

On the face $v = 0$ one of the following conditions is supposed to be fulfilled:

$$\begin{aligned} &\text{(a) } \sigma_\varphi = \tau_{r\varphi} = \tau_{\varphi z} = 0 \text{ (zero stress)},\\ &\text{(b) } v = \tau_{r\varphi} = \tau_{\varphi z} = 0 \text{ (sliding fixation)},\\ &\text{(c) } u = v = w = 0 \text{ (rigid fixation)}. \end{aligned} \tag{1.39″}$$

In [69] exact Green's formulae are derived (in the form of Neumann series over the powers of (1–2 ν) where ν is the Poisson ratio) for displacements and stresses in a variable-thickness elastic layer. A method for solving the first boundary problem for the spatial wedge is used, consisting in its reduction to the Gilbert boundary problem, generalized according to Vekua [94, 148]. Using the known formulae [148], the stresses and displacements were expressed in terms of three harmonic functions, determined in the form of Fourier and Kontorovich-Lebedev integrals in the complex plane. A transition is made from the boundary conditions (1.39) to the Gilbert boundary problem, generalized according to Vekua [94], in which the functional equations with shift are reduced to the second-order Fredholm integral equations with respect to auxiliary functions $\Phi_n(\mu)$, $n = 1, 2, 3, 4$, being contained later in the expressions for the stresses and displacements in the wedge ($0 < \mu < \infty$; transformation parameter $\beta x > 0$)

$$\begin{aligned} &\phi(\mu) - (1-2\nu)\int_0^\infty L_n(\mu,y)\,\phi_n(y)\,dy = \left[P + \frac{Qf_{n(\mu,\alpha)}}{2(1-\nu)(1-2\nu)}\right]\times\\ &\times\cosh\frac{\pi\mu}{2}K_{i\mu}(\beta\ x) - \frac{Q}{2(1-\nu)}\cosh\frac{\pi\mu}{2}\int_0^\infty h_n(t,\alpha)\,K_{it}(\beta\ x)\times\\ &\times\frac{\sinh(\pi\ t)\,dt}{\cosh(\pi\ t) - \cosh(\pi\ \mu)} \end{aligned} \tag{1.40}$$

where $K_{it} = \int_0^\infty \exp[-x\cosh(t)]\cos(\tau t)dt$ is the modified second-order Bessel function (Macdonald function);

$$L_n(\mu,y) = 2\cosh\frac{\pi\ \mu}{2}\sinh\frac{\pi\ y}{2}W_n(y,\alpha)\int_0^\infty \times$$

$$\times\frac{\sin\pi\, t\, g_n(t,\alpha)\, dt}{(\cosh\pi\, t+\cosh\pi\,\mu)(\cosh\pi\, t+\cosh\pi\, y)}$$

$$\text{(a) } W_{1,2}(\mu,\alpha) = \pm\frac{\cosh\alpha\mu\mp\cos\alpha}{\cosh\ \alpha\mu\pm\mu\sin\alpha}g_{1,2}(\mu,a) =$$

$$=\left\{\begin{matrix}\coth\alpha\mu/2\\ \tanh\alpha\mu/2\end{matrix}\right\}\frac{\sin^2\alpha}{\cosh\alpha\mu\mp\cos 2\alpha},$$

$$f_{1,2}(\mu,\alpha) = \frac{\mu}{W_{1,2}(\mu,\alpha)}\pm\frac{2(1-\nu)(1-2\nu)\sin\alpha}{\cosh\ \alpha\mu\mp\cos\alpha}$$

$$h_{1,2}(\mu,\alpha) = \frac{(1-2\nu)\sinh\ \alpha\mu\mp\mu\sin\alpha}{\cosh\alpha\mu\mp\cos\alpha}$$

(b) $W_3(\mu,\alpha) = W_1(\mu,2\alpha), g_3(\mu,\alpha) = g_1(\mu,2\alpha), f_3(\mu,\alpha) = f_1(\mu,2\alpha)$,
$h_3(\mu,\alpha) = h_1(\mu,2\alpha)$;

$$\text{(c) } W_4(\mu,\alpha) = \frac{2k\ \sinh 2\alpha\mu - 2\mu\sin 2\alpha}{2k\ \cosh 2\alpha\mu + 2\mu^2 - 2\mu^2\cos 2\alpha + k^2 + 1},\quad k = 3-4\nu,$$

$$g_4(\mu,\alpha) = -g_2(\mu,2\alpha) + \left\{\sin^2 a\left(g_5(\mu)\left[2g_6(\mu) - \mu g_1(\mu)\right] + \right.\right.$$

$$+g_8(\mu)\left[2g_1(\mu) - \mu g_6(\mu)\right]/\cosh\alpha\mu - 2(1-\nu)\sin\alpha\ g_5(\mu)\times$$

$$\left.\left.\times(\sin 3\alpha - \sin 2\alpha\ \cosh 2\alpha\mu) - g_8(\mu)\cos 2\alpha\ \sinh 2\alpha\mu)\right\}/g_9(\mu)\right.$$

$$g_5(\mu) = k\sinh 2\alpha\mu\ \cos 2\alpha - \mu\ \sin 2\alpha,$$

$$g_6(\mu) = \cosh 2\alpha\mu\ \cos 2\alpha - \cosh 3\alpha\mu - \cosh\alpha\mu\ \cos 4\alpha,$$

$$g_7(\mu) = \sinh 2\alpha\mu\ \sin 2\alpha + \sinh\alpha\mu\ \sin 4\alpha, g_8(\mu) = (k\ \cosh 2\alpha\mu - 1)\sin 2\alpha,$$

$$g_9(\mu) = \left[g_5^2(\mu) + g_8^2(\mu)\right]\left(\sinh^2 2\alpha\mu + \cos^2 2\alpha\right)$$

$$f_4(\mu,\alpha) = \frac{\mu}{W_4(\mu,\alpha)} + \frac{4(1-\nu)(1-2\nu)\mu\sin^2\alpha}{k\ \sin 2\alpha\mu - \mu\ \sin 2\alpha}$$

$$h_4(\mu,\alpha) = \frac{k(1-2\nu)(\cosh 2\alpha\mu - 1) - 2\mu^2\sin^2\alpha}{k\sinh 2\alpha\mu - \mu\sin 2\alpha} \tag{1.41}$$

It should be noted that the kernel of the integral equation (1.40) depends on the boundary conditions at $\phi = 0$, and the right-hand part depends as well on the type of the load on the other face of the wedge.

In [94, 148] Eq. (1.40) was obtained for the problem (b) and a normal load, symmetrical with respect to z, applied to the face $\phi = \alpha$; it is proven that if this load is such that the right-hand side of Eq. (1.40) belongs to the space $L_2(0,\infty)$, then the method of successive approximations is applicable for solving such an equation.

At $Q = 0$, $P \neq 0$ the right-hand part of Eq. (1.40) does not belong to $L_2(0,\infty)$, but lies within the space of continuous and restricted on the semiaxis functions $C_M(0,\infty)$. In [69] it is shown that in the case of the problem (b), the corresponding integral operator in the left-hand part of Eq. (1.40) for all $\alpha \in [0, 2\pi]$ is the operator of compression in the space $C_M(0,\infty)$ at least at $\nu > 0.053$. For the problem (c) the calculations have shown that at $\alpha = \pi k/12$, $k = 1, 2, \ldots, 24$, $\nu = 0.25, 0.30; 0.35$ the solution of the integral equation (1.40) can be also constructed by the method of successive approximations. Besides, a detailed analysis, based on numerical integration, has shown that for the problem (a), e.g. for the case of $\alpha = \pi/2$ the solution of Eq. (1.40) at $n=2$ can be presented as a Neumann series, if the condition $\nu > 0.116$ is fulfilled; and in the case $\alpha = 3\pi/4$ already for any $\nu \in [0, 1/2]$. At $\alpha \to 0$ the method of successive approximations is applicable at $\nu > 0.092$. For a fixed angle $\alpha \in [0, 2\pi]$ in the problems (a) and (c) the corresponding Neumann series, as a rule, converge practically at any practically significant value of the Poisson ratio.

Using the solution of the integral equation (1.40) in the form of the Neumann series and denoting the right-hand part of Eq. (1.40) as $G_n(\mu, \beta x)$, one can present the expression for the normal displacements on the wedge face $\phi = \alpha\,(z \geq 0)$ as follows:

$$v = \frac{4}{\pi^3} \cdot \frac{1-\nu}{G} \int_0^\infty \int_0^\infty \sinh \frac{\pi\mu}{2} W(\mu,\alpha,\beta x) K_{i\mu}(\beta r) \cos \beta y \cos \beta z d\beta d\mu; \qquad (1.42)$$

$$(a)\ W(\mu,\alpha,\beta x) = W_1(\mu,\alpha) B_1^\mu \{G_1(y,\beta x)\} - W_2(\mu,\alpha) B_2^\mu \{G_2(y,\beta x)\};$$

$$(b)\ (n = 3), (c)(n = 4)\ W(\mu,\alpha,\beta x) = 2W_n(\mu,\alpha) B_n^\mu \{G_n(y,\beta x)\};$$

$$B_n^\mu = \sum_{m=0}^{\infty} (1-2\nu)^m (A_n^\mu)^m,$$

$$A_n^\mu \{G_n(y,\beta x)\} = \int_0^\infty L_n(\mu,y) G_n(y,\beta x) dy.$$

The explicit form of the kernel of the integral equation obtained on the base of Eq. (1.42), enabled different analytical methods to be applied for its solution [41]. It is the uniform convergence of functional series over the powers of $(1–2\nu)$ in $C_M(0,\infty)$ that is important to be used in Eq. (1.42). In [70] a spatial contact problem of a punch in the shape of an elliptical paraboloid being indented into a face of an elastic wedge (without the account of friction). For solving the corresponding

integral equation the asymptotic method of "high λ" is applied [153], enabling at $\alpha = \pi/2$ the contact domain and the punch settlement to be determined (however, with a limited accuracy). Note that here the dimensionless parameter λ characterizes the relative distance of the contact domain from the wedge rib.

For the case (a) at $\alpha = \pi$ one can obtain the following expressions from Eq. (1.42) after integration [69]:

$$v = \frac{P(1-\nu)}{2\pi G}\left(\frac{1}{R_+} + \frac{1}{R_-}\right) + \frac{Q(1-2\nu)(r-x)}{4\pi G}\left(\frac{1}{R_+^2} + \frac{1}{R_-^2}\right),$$

$$R_\pm = \sqrt{(r-x)^2 + (z \pm y)^2},$$

what, with the account of parity of the problem with respect to z, coincides with the known solutions of Boussinesq and Cerruti problems for a half-space.

If the right-hand side of Eq. (1.42) for the displacements is multiplied by $\cos\epsilon z$, integrated over z from 0 to ∞, and then a limiting transition at $\epsilon \to 0$ is performed, then, according to [69], one arrives at the corresponding equations of the flat problem for a wedge, given in [7] for a normal load.

Note that the possibility of obtaining a solution of a problem of action of a concentrated force in a spatial wedge at $\nu \neq 1/2$ in the form of an expansion into series over the powers of (1–2 ν) was first formulated by Uflyand [147]. The problems for concentrated forces in a wedge are known to be solved exactly at $\nu = 1/2$ (the deformation is not accompanied by the volume variation), when fragmentation of boundary conditions occurs to determine three harmonic functions in the Papkovic-Neuber representation [5, 51, 147, 156]. In [147], while the first boundary-value problem is being solved using the integral transformation method, it is partitioned into a symmetrical one and a skew-symmetrical one with respect to the angular coordinate, and the quadratures, being contained in the explicit solution, are then obtained using residues. In [156] the Kantorovich-Lebedev method of integral transformations is extended to the case of an elastic incompressible wedge with a right dihedral angle (an elastic quarter-space). Using a limiting transition, the problem of a concentrated force on the elastic wedge rib is solved, and then the solution is extended to the case of any dihedral angle value. In a recent paper [51] a dual integral transformation is applied – the Fourier transformation along the wedge rib and the Kantorovich-Lebedev transformation along the radial coordinate in the section plane perpendicular to the wedge rib. Problems for a wedge, loaded by a concentrated internal force or a force, concentrated in a point at the wedge rib, are solved in images. For a particular case, when the force acts within the wedge cross-section and is directed normally to the radius-vector of its application point, the image reversals are reduced to one-dimensional integrals. Note that at $\nu = 1/2$ Eqs. (1.42) give the Green's functions for an incompressible wedge from [5, 6]. At $\nu \neq 1/2$ approximate solutions of the first boundary-value problem for a spatial wedge were constructed only for a quarter-space either asymptotically, or numerically [27, 28, 52, 55, 61].

Equation (1.42), though with difficulties, can be used for solving spatial contact problems of theory of elasticity for a wedge (including the account of friction),

arising at deformation-and-strength calculations of foundation structures, resting on non-uniformly compressible bases. However, in spite of all advantages of the fundamental solution of Eqs. (1.42) for a spatial wedge, described in [6, 69], its practical application cannot be admitted without reservation as convenient and efficient. The main difficulty here consists in the necessity of a preliminary solution of integral equations using expansions into functional series whose convergence at certain parameters of the problem can be rather slow. In particular, the authors of [69] have drawn attention to a considerable slowdown of convergence of the Neumann series (1.42) for $\alpha = \pi/2$. The developed method is rather cumbersome and complicated, it requires high mathematical culture of the calculators, and there is no guarantee of the solution convergence at some combinations of the parameters α and ν. Besides, one should add that the fundamental solution of Eq. (1.42) has been obtained only for a normal load, symmetrical with respect to z. As follows from the analysis of the spatial contact problem [70], using of the fundamental solution, proposed in [69], can be finally accomplished only on the base of asymptotic methods (e.g., the "high λ method"), which are efficient at sufficient distance of the contact domain from the wedge rib, i.e. the solutions being obtained are mostly of theoretical importance. We can hardly believe that the expression of Eq. (1.42) can be directly applied for practical solution of spatial problems with contact domains of complicated geometry. A more simple and convenient from the practical point of view is the use of an approximate solution of the mixed spatial problem of a vertical concentrated force acting on a horizontal face of an elastic wedge proposed by Fedorovskiy and Onopa [39] (Fig. 1.7b). While constructing the solution, the authors have invoked the "fictitious force" method (or the source method) in combination with the collocation method [105]. Displacements in the spatial wedge are determined in the form of superposition of two solutions for a half-space with a stress-free boundary: the Boussinesq solution and a solution, corresponding to the location of fictitious forces in an imaginary point, symmetrical to the point of application of the real concentrated force with respect to the restrained face of the elastic layer. The second solution is built on the base of the choice of intensities of the fictitious forces (the sources) to provide automatic fulfillment of boundary conditions on the wedge faces.

According to [39], the influence function, corresponding to the action of a unit concentrated load normally to the elastic wedge free surface, is given by

$$W^{(3)}(K,N) = \omega(x,y,\xi,\eta) = \frac{1-\nu}{2\pi G}\left(\frac{1}{R} - \frac{1}{R_1}\sum_{k=1}^{4}\frac{a_k}{\sqrt{(R/R_1)^2 + (kb)^2}}\right), \quad (1.43)$$

$$R = \sqrt{(x-\xi)^2 + (y-\eta)^2}, R_1 = \sqrt{(x+\xi)^2 + (y-\eta)^2}$$

where b, a_k, $k = \overline{1,4}$ are coefficients, depending on α, ν, ξ, η are the coordinates of the point of application of the concentrated force, x, y are the coordinates of the field (the observation point), α is the angle of inclination of a rigid underlying soil, ν is the Poisson ratio, $G = E/2(1+\nu)$ is the shear modulus.

The coefficients b, a_k, $k = \overline{1,4}$ in Eq. (1.43) for various values of the wedge angle α and the Poisson ratio ν are proposed to be found by the least-square method [39]. The values of the coefficients b, a_k, $k=\overline{1,4}$, used in our calculations, are listed in Table 1.1. References [39, 115] give more detailed tables of these coefficients for the values $5° \le \alpha \le 89°$ and $0 \le \nu \le 0.5$. The tables do not contain the angle $\alpha = 90°$, since in this case the equation system is degenerate. As in the case of the constant-thickness layer, Eq. (1.43) contains only four additive terms to the Boussinesq solution. Using of simple algebraic functions in Eq. (1.43) results in a considerable simplification of the calculation methods and shortage of the calculation scope for the studies of the contact interaction processes.

As an example, Fig. 1.8 shows isolines of dimensionless settlements W/W_O ($W_O = P(1–\nu)d/2\pi G$ is the characteristic displacement measure) of the free surface of the elastic wedge ($a = 30°$) and a half-space with the same deformation characteristics ($\nu = 0.25$) under a vertical concentrated force P in the point K with coordinates $\xi = d$, $\eta = 0$. Due to the presence of a rigid underlying soil base, the settlements of the surface of the variable-thickness layer will always be smaller than for the corresponding values for the half-space. As seen from the comparison of the calculation data (Fig. 1.8a, b), besides the quantitative differences, the fundamental solution of Eq. (1.43) differs from the classical Boussinesq solution ($a_k = 0, k = \overline{1,4}$) in a number of qualitative features. First, the domain of definition of the influence function (1.43) is not the plane, but the half-plane $x \ge 0$. Second, the fundamental solution of Eq. (1.43), having the following structure:

$$W^{(3)}(K,N) = \omega(x-\xi,x+\xi,y-\eta) = \omega(x,\xi,y-\eta)$$

is not a difference solution with respect to the variables x, ξ (i.e. in the direction of the layered base depth increase), and, consequently, is nonlinear and anisotropic.

In a small vicinity of the point $K(\xi, \eta, \zeta)$ of the concentrated force application, the influence functions for the half-space and the variable-thickness layer behave qualitatively similar, this being revealed in an unlimited growth of settlements according to hyperbolic law. However, with the increase of the distance form the point $K(\xi, \eta)$ the difference of the two solutions becomes more essential. As is clearly seen from the settlement isolines, plotted in Fig. 1.8b, the solution of Eq. (1.43), due to its approximate character, has a noticeable defect, resulting in the formation of an area of negative (opposite to the force direction) displacements, arising between the elastic wedge rib and the concentrated force application point. Note that the authors of [39] did not discuss this defect (probably, they have not found it). The discussed character of deformation of the horizontal surface of the variable-thickness elastic wedge is quantitatively rather small and diminishes to zero rather soon with the increase of the distance between the concentrated force application point and the wedge rib. It is quite clear that in case of high accuracy of solution of contact problems in the direct vicinity of the wedge rib being required, the situation can be improved only by increase of the number of additional terms in the approximate representation of Eq. (1.43).

Table 1.1 Values of a_k and b coefficients at various ν and α

α	ν	a_1	a_2	a_3	a_4	B
5°	0	−0.1859	−4.179	−4.415	−1.410	0.0194
	0.25	−0.2084	−0.3373	3.587	−2.765	0.0194
	0.35	−0.2371	−2.584	9.778	−6.037	0.0194
0.50	−0.2084	−10.09	26.03	−14.75	0.0194	
15°	0	−0.1013	−1.751	5.778	−3.129	0.0405
	0.25	−0.0877	−1.77	6.412	−3.755	0.0405
	0.35	−0.0889	−1.966	7.389	−4.553	0.0405
0.50	−0.1008	−2.589	10.34	−6.928	0.0405	
20°	0	0.0211	−0.7522	4.894	−3.208	0.0697
	0.25	−0.0326	−0.1323	4.086	−2.984	0.0697
	0.35	−0.0645	0.2019	3.911	−3.127	0.0697
0.50	0.1405	0.9806	3.894	−3.849	0.0697	
25°	0	−0.020	−0.1491	4.187	−3.096	0.0979
	0.25	−0.0799	0.6939	2.76	−2.458	0.0979
	0.35	−0.1181	1.212	2.120	−2.312	0.0979
0.50	−0.2112	2.505	0.8496	−2.279	0.0979	
30°	0	−0.1261	3.619	−2.193	0.6272	0.175
	0.25	−0.0916	1.019	2.277	−2.313	0.125
	0.35	0.1324	1.636	1.368	−1.992	0.125
0.50	0.2345	3.220	−0.6396	−1.504	0.125	
40°	0	−0.0918	2.183	0.7424	−2.08	0.2249
	0.25	−0.0684	0.7601	3.108	−2.977	0.1749
	0.35	−0.1063	1.394	2.106	−2.594	0.1749
0.50	−0.2040	3.050	−0.1037	−2.015	0.1749	
45°	0	−0.1033	3.971	−3.079	−0.0604	0.2974
	0.25	−0.1224	2.935	−1.224	−0.7867	0.2474
	0.35	−0.0803	0.9443	3.195	−3.308	0.1974
0.50	−0.1687	2.445	1.412	−3.053	0.1974	
60°	0	0.0555	−1.580	8.086	−5.799	0.2531
	0.25	−0.0596	1.341	4.130	−5.023	0.3531
	0.35	−0.010	2.585	0.9658	−2.980	0.3531
0.50	−0.1309	2.378	2.644	−4.627	0.3031	
75°	0	0.0596	−1.527	6.112	−3.550	0.2880
	0.25	0.0416	−1.179	5.223	−3.012	0.2880
	0.35	0.0369	−1.166	5.702	−3.607	0.2880
0.5	0.0335	−1.432	8.570	−6.614	0.2880	
80°	0	0.0509	−1.253	4.590	−2.123	0.2946
	0.25	0.0338	−0.9102	3.591	−1.457	0.2946
	0.35	0.0299	−0.909	4.009	−1.966	0.2946
0.50	−0.0325	−1.287	6.968	−4.941	0.2946	
89°	0	0.0215	−0.4724	1.099	0.9120	0.2999
	0.25	0.0206	−0.4447	1.020	0.8807	0.2999
	0.35	0.0237	−0.5434	1.548	0.3678	0.2999
0.5	0.0375	−0.9932	3.905	−1.785	0.2999	

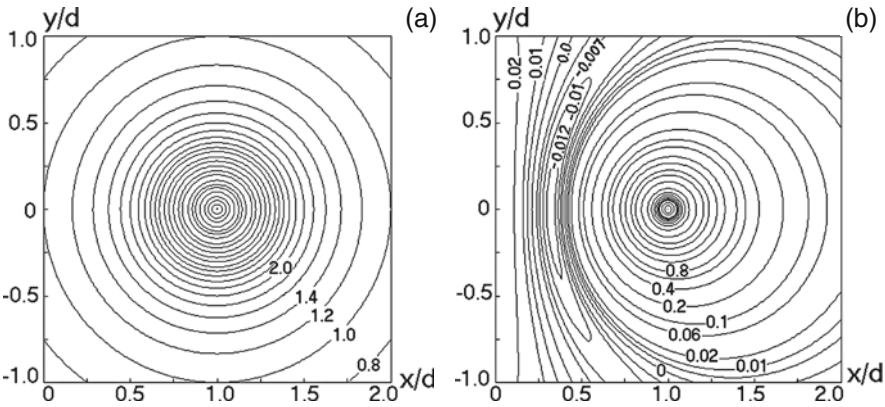

Fig. 1.8 Isolines of dimensionless settlements of the surface of (**a**) an elastic half-space, (**b**) of variable-thickness elastic layer ($\alpha = 30°$) under a normal concentrated force, $\nu = 0.25$

The experience of numerous calculations of spatial problems of contact interaction has shown that, in spite of its approximate character, the influence function (1.43) enables the non-uniform compressibility of the base to be taken into account with sufficient accuracy, what is important for rational design of foundations at complicated engineering-and-geological conditions.

1.4.3 Multilayer Elastic Half-Space

Models of elastic layered media with plane-parallel layers rather adequately reflect mechanical properties of many objects, widely spread in practice. In the field of geotechnics these are first of all road and airfield surfaces, soil bases with natural layering. The effect of the base lamination should be estimated while designing such important objects as high-rise buildings, funnels, barrages, dams, mines.

The main advantage of the models of multilayer media is the possibility of a stepwise variation of the soil base mechanical properties at the transition from one layer to another to be described. A number of studies are devoted to the issues of theory and calculation of multilayer bases. Among the most significant studies in this field of mechanics of nonhomogeneous media one should mention Refs. [20, 58, 59, 82, 89, 90, 91, 106, 137, 152, 110]. The overwhelming majority of studies regarding the problems of static of elastic multilayer bases deal with the issues of the medium deformation by surface loads only. The most convenient methods of solution of these problems of theory of elasticity for multilayer bases are such methods when the conditions of joint deformation of layers finally result in the problem of finding auxiliary functions, determining the stress-strained state of the upper layer. The parameters of the stress-strained state for other layers are found from special recurrent relations. It is quite important that the order of the resolving system of linear algebraic equations does not depend on the number of layers in the base.

In spite of a considerable success in developing methods for solving the problems of theory of elasticity for multilayer bases under a surface load, the number of publications devoted to the case of loading inside the layers or at interlayer boundaries, is quite limited [32, 33, 38, 129, 132, 134]. The investigation of the stress-strained state of multilayer media due to internal forces is the basis for working out a general approach to solving the boundary problems of theory of elasticity for bases of complex structure, containing cavities, inclusions, various defects and gaps between the layers. In geotechnics, the field of application of such studies is rather broad: essentially deepened foundation structures, wells, mine working, etc. The classical method of superposition of singularities, once having been applied by Mindlin for a homogeneous isotropic half-space, is inapplicable for more complicated systems, which are layered media. As a rule, in such cases integral transformations are required.

Pioneer studies by Shekhter and Prikhodchenko [129, 132] present a general method for the exact solution of the problem of the distribution of stresses and displacements in an elastic layer under a vertical force and a horizontal force acting inside it, at the conditions of a flat problem of theory of elasticity, and under a vertical force in the case of an axisymmetric spatial problem. Later the same authors have also solved the spatial problem for a layer under a horizontal force acting inside it [134]. The essence of the method used consists in the following: on the stress-strained state due to the action of a concentrated force within the space (the Kelvin's solution) a continuous trained solution is superimposed, which is chosen in such a way that the boundary conditions at the upper and lower faces of the layer be satisfied. However, the proposed method has not been applied for multilayer bases (with the account of satisfaction of the conjugation conditions at the boundaries of each layer). Besides, no numerical results have been obtained even for a one-layer system, since the representation of the displacement vector components in terms of the Galerkin vector contains unlimited functions. This is an essential inconvenience for the numerical application of the methods, since inadmissibly large numbers appear at high and low values of the Hankel transformation parameters. Later, an axisymmetric problem of action of a concentrated vertical force inside an elastic half-space, consisting of a finite number of plane-parallel layers, was considered by Yegorov, Barvashov, and Fedorovskiy [38]. These authors seek for the solution in each layer, using the biharmonic Love function, presented using the Hankel transformation. The stress function is partitioned into two terms: the stress function, corresponding to the Kelvin's solution for the action of a concentrated force in the space, and a stress function, determined from the layer contact conditions and satisfying the zero stress conditions for the free surface. An approximate solution of the resolving system of linear algebraic equations is found in the form of a matrix power series, each term of which induces a correction due to the decrease of the approximation discrepancies by "reflection" from the layer boundaries. By means of a transition from the Hankel transformations to the Fourier transformation, the approach proposed in [38] can be extended to the spatial non-axisymmetric problem. As one should expect, the calculations have shown the satisfactory accuracy of approximation to be obtained only for the points close to the point of application of the concentrated load. However, besides the same difficulties as for the application of the Shekhter

method, a necessity of representation of the approximate solution using the partial sums of the matrix series, is added. To our knowledge, no solutions of practical problems regarding calculation of deepened foundation structures using the method proposed by Yegorov, Barvashov, and Fedorovskiy, are available. Therefore, there are no data available, enabling the fundamental solutions for layer bases of [38] to be considered suitable for broad practical application.

A considerable success in solving the spatial problem of the action of concentrated forces directed vertically and horizontally within a layered half-space, was achieved in [32]. The solution for a two-layer system (an elastic layer, resting on an elastic half-space) was obtained in a closed form as Hankel integrals from exponential decay functions. A general solution of the Navier's equations of elastic equilibrium for non-axisymmetric problems was used in the form of Muki [83] by means of expansion into Fourier series over the angular coordinate and the Hankel transformation over the radial coordinate. A special numerical method was developed for the evaluation of improper integrals, including an exponential approximation of high accuracy for the reciprocal values of common denominators of the integrands using the least-square method in the integral formulation. The fundamental solutions for the two-layer system, presented in [32], were thoroughly tested in the limiting cases, using the Mindlin's solution. The proposed closed form of the approximate solution enables the results to be obtained with high accuracy and can be extended to another, more complicated multilayer bases. Meanwhile, the efficiency of practical application of the approach is rather limited, since it requires labour-consuming approximation of the reciprocal values of the integrand function denominators at each specific combination of the elastic parameters of the layers. Note, that the fundamental solution for the two-layer system, presented in [32], was later repeated by Davies and Bannerjee [33] for the forces inside the base, acting on the contact surface of separation of the layer and the half-space. These authors presented the fundamental solution in an improved (for the purpose of numerical integration) form due to the analytical evaluation of slowly decreasing terms in the integrand expressions.

Below the closed solutions of spatial problems of theory of elasticity for multilayer media, obtained on the basis of the two-dimensional Fourier transformation, are presented. The elaborated formulae can be conveniently used as fundamental singular solutions for layered media in the framework of the numerical algorithm of the boundary-element method. For the sake of better visual understanding of the results, a three-layer system is considered, the two-layer one being considered as a particular case. The first case is most often met in the geotechnical practice, when the foundation base contains an internal layer of strongly or weakly compressible soil. Another typical case in subterranean geomechanics is a three-layer elastically deformable system "elastic layer + elastic oil(gas)-containing layer + finite-thickness elastic layer (or elastic half-space)". If two adjacent layers of the base have the same elastic parameters, then the three-layer system becomes a two-layer one and one of the interlayer boundaries becomes fictitious. One arrives at the problem of concentrated forces acting within the upper or the lower layer. In the two-layer system the assignment of the fictitious boundary enables the problem of concentrated forces, acting within a finite-thickness layer, to be solved. In case of

necessity, the formulations proposed for the two- and three-layer systems, can be without any principal difficulties generalized, in a more cumbersome form, for any finite number of layers. The most convenient for visualization results are obtained for the number of layers, not exceeding five, what corresponds to the geotechnical conditions in practice.

Three-layer base. The calculation scheme for a three-layer deformable system is presented in Fig. 1.9. Let us consider each layer to be solid, and in case of deformation the adjacent layers to be deformed together. The component layers have their own independent thicknesses h_k, elastic parameters E_k, ν and are related to a local orthogonal Cartesian coordinate system X_k, Y_k, Z_k $(k = 1, 2, 3)$ with the origin on the upper boundary of the layer. Let us find the displacements, stresses and dilatation functions due to unit concentrated forces on the upper boundaries of each layer. This will enable the deformation of the daylight surface as well of the surfaces, bounding each layer, to be calculated based on the integral representations. It is convenient to characterize the stressed state at each of the nine concentrated forces (three per each layer) by a separate component of the matrix

$$\begin{Vmatrix} T_1^x & T_1^y & Q_1 \\ T_2^x & T_2^y & Q_2 \\ T_3^x & T_3^y & Q_3 \end{Vmatrix} \tag{1.44}$$

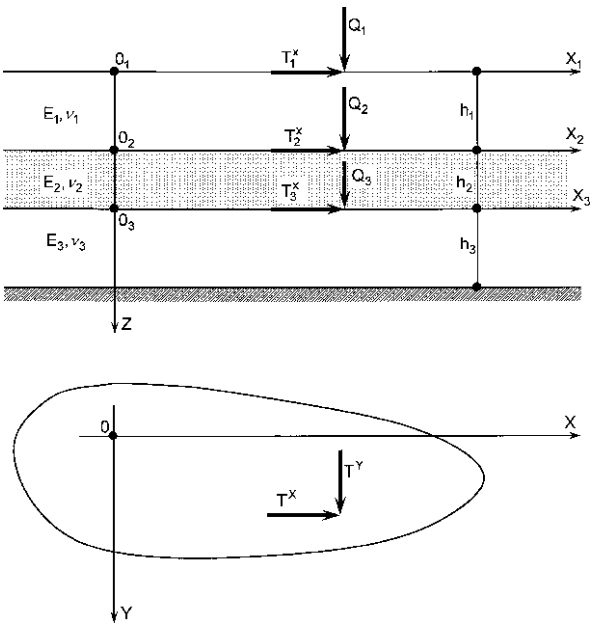

Fig. 1.9 Concentrated forces on the separation surfaces in a three-layer base

where $T_k{}^x$ and $T_k{}^y$ are tangential and Q_k are normal concentrated forces on the upper boundary of the k-th layer.

Take the advantage of the Lamé equations of spatial theory of elasticity [71], performed for each layer

$$\begin{cases} \dfrac{2G(1-\nu)}{1-2\nu}\dfrac{\partial \varepsilon_v}{\partial x} + G\Delta U = 0, \\ \dfrac{2G(1-\nu)}{1-2\nu}\dfrac{\partial \varepsilon_v}{\partial y} + G\Delta V = 0, \\ \dfrac{2G(1-\nu)}{1-2\nu}\dfrac{\partial \varepsilon_v}{\partial z} + G\Delta W = 0 \end{cases} \tag{1.45}$$

where G and ν are the elasticity parameters,

$$\varepsilon_v = \frac{\partial U}{\partial x} + \frac{\partial V}{\partial y} + \frac{\partial W}{\partial z};\ \Delta = \frac{\partial^2}{\partial x^2} + \frac{\partial^2}{\partial y^2} + \frac{\partial^2}{\partial z^2}.$$

Now apply the two-dimensional Fourier transformation

$$\bar{f}(\xi,\eta) = F\left[f\right] = \int_{-\infty}^{\infty}\int f(x,y)e^{i(\xi x+\eta y)}dxdy \text{ (direct)}, \tag{1.46}$$

$$f(x,y) = \frac{1}{4\pi^2}\int_{-\infty}^{\infty}\int \bar{f}(\xi,\eta)e^{-i(\xi x+\eta y)}d\xi\, d\eta \text{ (inverse)} \tag{1.47}$$

to Eqs. (1.45). Taking into account that

$$F\left[\frac{\partial^{m+n} f}{\partial x^m \partial y^n}\right] = (-i\xi)^m(-i\eta)^n \bar{f},$$

one obtains instead of Eqs. (1.45) the following system of ordinary differential equations:

$$\begin{cases} \dfrac{2G\,(1-\nu)}{1-2\nu}\left(-\xi^2\bar{U} - \xi\eta\bar{V} - i\xi\dfrac{\partial \bar{W}}{dz}\right) - G\ p^2\bar{U} + G\dfrac{d^2\bar{U}}{dz^2} = 0, \\ \dfrac{2G\,(1-\nu)}{1-2\nu}\left(-\xi\eta\bar{U} - \eta^2\bar{V} + i\eta\dfrac{\partial \bar{W}}{dz}\right) - G\ p^2\bar{V} + G\dfrac{d^2\bar{V}}{dz^2} = 0, \\ \dfrac{2G\,(1-\nu)}{1-2\nu}\dfrac{d}{dz}\left(-i\xi\bar{U} - i\eta\bar{V} + \dfrac{\partial \bar{W}}{dz}\right) - G\ p^2\bar{W} + G\dfrac{d^2\bar{W}}{dz^2} = 0 \end{cases} \tag{1.48}$$

where $p^2 = \xi^2 + \eta^2$.

If now in the image space a transition is performed to new functions S and T, related to $\bar{U}$ and $\bar{V}$ as follows:

$$S = i\xi\bar{U} + i\eta\bar{V}, T = i\eta\bar{U} - i\xi\bar{V}, \tag{1.49}$$

then a new system of differential equations with respect to the functions S, T, and $\bar{W}$ is obtained:

$$\begin{cases} \dfrac{2G(1-\nu)}{1-2\nu}p^2\left(\dfrac{d\bar{W}}{dz} - S\right) + G\left(\dfrac{d^2S}{dz^2} - p^2S\right) = 0, \\ \dfrac{2G(1-\nu)}{1-2\nu}\left(\dfrac{d^2\bar{W}}{dz^2} - \dfrac{dS}{dz}\right) + G\left(\dfrac{d^2\bar{W}}{dz^2} - p^2\bar{W}\right) = 0, \\ \dfrac{d^2T}{dz^2} - p^2T = 0. \end{cases} \tag{1.50}$$

Note that as a result of the transition to the system (1.50), the third equation becomes independent of the first and the second one. The common solution of the system (1.50) is easily obtained in a standard way and is given by

$$\begin{aligned} p\bar{W} &= \frac{L}{4(1-\nu)^2}\left(\alpha\left[(3-4\nu)\ \sinh pz - pz\ \cosh pz\right] + 2(1-\nu)\right. \\ &\beta\left[2(1-\nu)\cosh pz - pz\ \sinh pz\right] \\ &\left.+2(1-\nu)\gamma\left[(1-2\nu)\ \sinh pz - pz\ \cosh pz\right] - \delta\ pz\ \sinh pz\right), \\ S &= -\frac{L}{4(1-\nu)^2}\left(\alpha\ pz\ \sinh pz + 2(1-\nu)\beta\left[(1-2\nu)\sinh pz + pz\ \cosh pz\right]\right. \\ &\left.+2(1-\nu)\gamma\left[2(1-\nu)\cosh pz + pz\ \sinh pz\right] + \delta\left[(3-4\nu)\sin pz + pz\cosh pz\right]\right), \\ T &= L\left[\bar{\gamma}\cosh pz + \frac{1}{1-\nu}\tilde{\delta}\sinh pz\right] \end{aligned} \tag{1.51}$$

where $L = 2(1-\nu^2)/E$ and the integration functions α, β, γ, δ, $\bar{\gamma}$, $\bar{\delta}$ of the parameters ξ and η of the integral Fourier transformation are determined from the boundary conditions, given on the surfaces, bounding each layer.

Since the boundary conditions are formulated in terms of characteristics of the stress-strained state, the transforms of the displacements and stress tensor components should be expressed in terms of S, T, and $\bar{W}$ functions.

Application of the direct Fourier transformation to the Hooke's law

$$\sigma_{ij} = G\left(\frac{\partial U_i}{\partial x_j} + \frac{\partial U_j}{\partial x_i}\right) + \frac{2G\nu}{1-2\nu}\varepsilon_v\delta_{ij}$$

enables the transforms of stresses and dilatation function to be obtained in the following form:

$$
\begin{aligned}
\bar{\sigma}_x &= 2G(-i\xi\bar{U}) + \frac{2G\nu}{1-2\nu}\bar{\varepsilon}_v,\\
\bar{\sigma}_y &= 2G(-i\eta\bar{V}) + \frac{2G\nu}{1-2\nu}\bar{\varepsilon}_v,\\
\bar{\sigma}_z &= 2G\frac{d\bar{W}}{dz} + \frac{2G\nu}{1-2\nu}\bar{\varepsilon}_v,\\
\bar{\tau}_{yz} &= G\left(-i\eta\bar{W} + \frac{d\bar{V}}{dz}\right),\\
\bar{\tau}_{xz} &= G\left(-i\xi\bar{W} + \frac{d\bar{U}}{dz}\right),\\
\bar{\tau}_{xy} &= G\left(-i\eta\bar{U} - i\xi\bar{V}\right),\\
\bar{\varepsilon}_v &= -i\xi\bar{U} - i\eta\bar{V} + \frac{d\bar{W}}{dz}.
\end{aligned}
\tag{1.52}
$$

Using Eq. (1.49) in combination with Eq. (1.52), for each layer one will have in the Fourier transforms the sought expressions of the stress-strained state components, using the S, T, and $\bar{W}$ functions.

$$
\begin{aligned}
&\bar{U} = -\frac{1}{p^2}(i\xi S + i\eta T),\ \bar{V} = -\frac{1}{p^2}(i\eta S - i\xi T),\\
&\bar{\sigma}_x = -2G\left[\frac{\xi^2}{p^2}S + \frac{\xi\eta}{p^2}T - \frac{\nu}{1-2\nu}\left(\frac{d\bar{W}}{dz} - S\right)\right],\\
&\bar{\sigma}_y = -2G\left[\frac{\eta^2}{p^2}S - \frac{\xi\eta}{p^2}T - \frac{\nu}{1-2\nu}\left(\frac{d\bar{W}}{dz} - S\right)\right],\\
&\bar{\sigma}_z = 2G\left(\frac{1-\nu}{1-2\nu}\frac{d\bar{W}}{dz} - \frac{\nu}{1-2\nu}S\right),\\
&\bar{\tau}_{yz} = -G\left(i\eta\bar{W} + \frac{i\eta}{p^2}\frac{dS}{dz} - \frac{i\xi}{p^2}\frac{dT}{dz}\right),\\
&\bar{\tau}_{xz} = -G\left(\xi\bar{W} + \frac{\xi}{p^2}\frac{dS}{dz} + \frac{\eta}{p^2}\frac{dT}{dz}\right),\\
&\bar{\tau}_{xy} = G\left(\frac{\xi^2-\eta^2}{p^2}T - \frac{2\xi\eta}{p^2}S\right),\\
&\bar{\varepsilon}_v = \frac{d\bar{W}}{dz} - S.
\end{aligned}
\tag{1.53}
$$

Thus, the boundary problem under consideration is reduced to the determination of functional coefficients α, β, γ, δ, $\bar{\gamma}$, $\bar{\delta}$, for each elastic layer. Using these coefficients, based on the conditions of continuity of displacements and stresses on the layer surface, the auxiliary functions S and T become unambiguous as well as

the transforms of the displacements and stresses and the dilatation function. After rather cumbersome intermediate transformation, the further required (additionally to Eq. (1.51)) relations in a detailed notation are given by

$$\bar{\sigma}_z = \alpha\left[\cosh pz - \frac{1}{2(1-\nu)}pz\ \sinh pz\right] + \beta\,(\sinh pz - pz\ \cosh pz) - \\ -\gamma\, pz\ \sinh pz - \frac{1}{2(1-\nu)}\delta\left[(1-2\nu)\sinh pz + pz\ \cosh pz\right], \tag{1.54}$$

$$\tau = -\frac{1}{p}\left(i\bar{\xi}\,\bar{\tau}_{xz} + i\eta\bar{\tau}_{yz}\right) = \frac{\alpha}{2(1-\nu)}\left[pz\ \cosh pz - (1-2\nu)\sinh pz\right] + \\ +\beta pz\ \sinh pz + \gamma\,(\sinh pz + pz\ \cosh pz) + \delta\left[\cosh pz + \frac{pz\ \sinh pz}{2(1-\nu)}\right], \tag{1.55}$$

$$\tilde{\tau} = -\frac{1}{p}\left(i\eta\bar{\tau}_{xz} - i\bar{\xi}\,\bar{\tau}_{yz}\right) = \tilde{\gamma}\,(1-\nu)\sinh pz + \tilde{\delta}\cosh pz, \tag{1.56}$$

$$\bar{\varepsilon}_\nu = \frac{(1+\nu)(1-2\nu)}{E(1-\nu)}\left\{\left[\alpha + 2\gamma\,(1-\nu)\right]\cosh pz + [\delta + 2\beta\,(1-\nu)]\sin pz + \\ +\frac{\delta}{1-2\nu}pz\ \cosh pz\right\}. \tag{1.57}$$

Now consider the formulation of the boundary conditions, corresponding to the common deformations in the three-layer system (Fig. 1.9) with the account of the action of concentrated forces of the form of Eq. (1.44). Let a uniform normal pressure $q = \text{const}$ act on the upper boundary ($z = 0$) of one of the layers, being distributed over a circle $x^2 + y^2 \le a^2$:

$$\sigma_z = \begin{cases} q,\ x^2 + y^2 \le a^2 \\ 0,\ x^2 + y^2 > a^2 \end{cases}$$

where $q = Q/\pi a^2$, Q is the main traction vector.

If now the known transition equation [19]

$$\int_{-\infty}^{\infty}\int f(r)\ e^{\pm i(\xi x+\eta y)}dxdy = 2\pi\int_0^\infty r\cdot f(r)J_0(r\rho)\,dr$$

is used, as well as the property of the Bessel function [63]

$$\int_0^1 x\,J_0(ax)dx = \frac{1}{a}J_1(a),$$

one obtains

$$\bar{\sigma}_z = \frac{2Q}{a^2} \int_0^a r\, J_0(rp) dr = 2Q \frac{J_1(ap)}{ap}$$

Here $J_m(x)$ i the Bessel function of the first kind of the order m, $r = \sqrt{x^2 + y^2}$.

Making, as usual, the load action radius a tend to zero and keeping constant the main traction vector Q, with the account of the limiting relation

$$\lim_{\rho \to 0} \frac{J_1(\rho)}{\rho} = \frac{1}{2},$$

finally for a normal concentrated force one obtains

$$\bar{\sigma}_z = Q.$$

Similarly, for the action of tangential concentrated forces T^x and T^y, directed along the x and y axes and applied to the coordinate origin, accordingly, one arrives at

$$\bar{\tau}_{xz} = T^x,\ \bar{\tau}_{yz} = T^y. \tag{1.58}$$

Thus, the boundary conditions, expressing the absence of stress on the free surface of the first layer, the continuity of the U, V, and W displacements, the balance of normal σ_z and tangential τ_{xz}, τ_{yz} stresses on the common boundary of two adjacent layers as well as the equality of the displacements on the lower boundary of the last layer to zero

$$U(x,y,h_3) = V(x,y,h_3) = W(x,y,h_3) = 0,$$

for the Fourier transforms will take the form:

1st layer (at $z = 0$):

$$\bar{\sigma}_z = Q_1,\ \bar{\tau}_{xz} = T_1^x,\ \bar{\tau}_{yz} = T_1^y; \tag{1.59}$$

2nd layer:

$$\begin{cases} \bar{U}_2 \mid_{z=0} = \bar{U}_1 \mid_{z=h_1} \\ \bar{V}_2 \mid_{z=0} = \bar{V}_1 \mid_{z=h_1} \end{cases} \text{or} \quad \begin{matrix} \mathrm{S}_2 \mid_{z=0} = S_1 \mid_{z=h_1} \\ T_2 \mid_{z=0} = T_1 \mid_{z=h_1} \end{matrix},$$

$$\bar{W}_2 \mid_{z=0} = \bar{W}_1 \mid_{z=h_1},$$

$$\bar{\sigma}_z^{(2)} \Big|_{z=0} + Q_2 = \bar{\sigma}_z^{(1)} \mid_{z=h_1},$$

$$\bar{\tau}_{xz}^{(2)}\,|_{z=0} + T_2^x = \bar{\tau}_{xz}^{(1)}\,\big|_{z=h_1}\,,$$

$$\bar{\tau}_{yz}^{(2)}\,|_{z=0} + T_2^y = \bar{\tau}_{yz}^{(1)}\,\big|_{z=h_1}\,; \tag{1.60}$$

3rd layer:

$$\begin{cases} \bar{U}_3\,|_{z=0} = \bar{U}_3\,\big|_{z=h_2} \\ \bar{V}_3\,|_{z=0} = \bar{V}_2\,\big|_{z=h_2} \end{cases} \text{or} \quad \begin{matrix} \mathrm{S}_3\,|_{z=0} = S_2\,\big|_{z=h_2} \\ T_3\,|_{z=0} = T_2\,\big|_{z=h_2}\,, \end{matrix}$$

$$\bar{W}_3\,|_{z=0} = \bar{W}_2\,\big|_{z=h_2}\,,$$

$$\bar{\sigma}_z^{(3)}\,\Big|_{z=0} + Q_3 = \bar{\sigma}_z^{(2)}\,\big|_{z=h_2}\,,$$

$$\bar{\tau}_{xz}^{(3)}\,|_{z=0} + T_3^x = \bar{\tau}_{xz}^{(2)}\,\big|_{z=h_2}\,,$$

$$\bar{\tau}_{yz}^{(3)}\,|_{z=0} + T_3^y = \bar{\tau}_{yz}^{(2)}\,\big|_{z=h_2}\,,$$

$$\begin{cases} \bar{U}_3\,\big|_{z=h_3} = 0 \\ \bar{V}_3\,\big|_{z=h_3} = 0 \end{cases} \text{or} \quad \begin{matrix} \mathrm{S}_3\,\big|_{z=h_3} = 0 \\ T_3\,\big|_{z=h_3} = 0, \end{matrix}$$

$$\bar{W}_3\,\big|_{z=h_3} = 0. \tag{1.61}$$

On the upper boundary of each layer ($z = 0$), as follows from Eqs. (1.51), (1.53), ((1.54), (1.55), (1.56), (1.57), the following conditions are fulfilled:

$$\alpha = \bar{\sigma}_z\,|_{z=0}\,,$$

$$\beta = \frac{E}{2(1-\nu^2)} p\bar{W}\,|_{z=0}\,,$$

$$\gamma = -\frac{E}{2(1-\nu^2)}(i\xi\bar{U} + i\eta\bar{V})\,|_{z=0} = -\frac{E}{2(1-\nu^2)} S\,|_{z=0}\,,$$

$$\delta = \tau|_{z=0} = -\frac{1}{p}(i\xi\,\bar{\tau}_{xz} + i\eta\bar{\tau}_{yz})\,|_{z=0}\,, \tag{1.62}$$

$$\tilde{\gamma} = \frac{E}{2(1-\nu^2)}(i\eta\bar{U} - i\xi\,\bar{V})\,|_{z=0} = \frac{E}{2(1-\nu^2)} T\,|_{z=0}\,,$$

$$\tilde{\delta} = \tilde{\tau}|_{z=0} = \frac{1}{p}(i\eta\bar{\tau}_{xz} - i\xi\,\bar{\tau}_{yz})\,|_{z=0}\,.$$

Therefore, by using Eqs. (1.51), (1.52), (1.54), (1.55), (1.56), (1.57) as well as relations

$$\bar{\tau}_{yz} = \frac{1}{p}(i\xi\bar{\tau} + i\eta\tau),\ \bar{\tau}_{xz} = \frac{1}{p}(i\xi\tau - i\eta\bar{\tau}),$$

the boundary conditions (1.59)−(1.61) in a detailed notation will be given by

$$\alpha_1 = Q_1, \tag{1.63}$$

$$\delta_1 = -\frac{i}{p}(T_1^x\xi + T_1^y\eta), \tag{1.64}$$

$$\tilde{\delta}_1 = \frac{i}{p}(T_1^x\eta - T_1^y\xi), \tag{1.65}$$

$$\begin{aligned}\gamma_2 = \frac{L_1}{4L_2(1-\nu_1)^2}&\left\{\alpha_1 p_1 \sinh p_1 + 2(1-\nu_1)\beta_1\left[(1-2\nu_1)\sinh p_1 + p_1\cosh p_1\right]\right.\\ &+2(1-\nu_1)\gamma_1\left[2(1-\nu_1)\cosh p_1 + p_1\sinh p_1\right]\\ &\left.+\delta_1\left[(3-4\nu_1)\sinh p_1 + p_1\cosh p_1\right]\right\},\end{aligned} \tag{1.66}$$

$$\tilde{\gamma}_2 = \frac{L_1}{L_2}(\tilde{\gamma}_1\cosh p_1 + \frac{1}{1-\nu_1}\tilde{\delta}_1\sinh p_1), \tag{1.67}$$

$$\begin{aligned}\beta_2 = \frac{L_1}{4L_2(1-\nu_1)^2}&\{\alpha_1[(3-4\nu_1)\sinh p_1 - p_1\cosh p_1] +\\ &+2(1-\nu_1)\beta_1\left[2(1-\nu_1)\cosh p_1 - p_1\sinh p_1\right] +\\ &+2(1-\nu_1)\gamma_1\left[(1-2\nu_1)\sinh p_1 - p_1\cosh p_1\right] - \delta_1 p_1\sinh p_1\},\end{aligned} \tag{1.68}$$

$$\begin{aligned}\alpha_2 + Q_2 = \alpha_1[\cosh p_1 - \frac{1}{2(1-\nu_1)}p_1\sinh p_1] + \beta_1(\sinh p_1 - p_1\cosh p_1)\\ -\gamma_1 p_1\sinh p_1 - \frac{\delta_1}{2(1-\nu_1)}[(1-2\nu_1)\sinh p_1 + p_1\cosh p_1],\end{aligned} \tag{1.69}$$

$$\begin{aligned}\delta_2 = \frac{i}{p}(\xi T_2^x + \eta T_2^y) + \frac{1}{2(1-\nu_1)}&\{\alpha_1[-(1-2\nu_1)\sinh p_1 + p_1\cosh p_1] +\\ &+2(1-\nu_1)\beta_1 p_1\sinh p_1 + 2(1-\nu_1)\gamma_1[\sinh p_1 + p_1\cosh p_1] +\\ &+\delta_1[p_1\sinh p_1 + 2(1-\nu_1)\cosh p_1]\},\end{aligned} \tag{1.70}$$

$$\tilde{\delta}_2 = -\frac{i}{p}(\eta T_2^x - \xi T_2^y) + (1-\nu_1)\tilde{\gamma}_1\sinh p_1 + \tilde{\delta}_1\cosh p_1, \tag{1.71}$$

$$\gamma_3 = \frac{L_2}{4L_3(1-\nu_2)^2}\left\{\alpha_2 p_2 \sinh p_2 + 2(1-\nu_2)\beta_2\left[(1-2\nu_2)\sinh p_2 + p_2\cosh p_2\right]\right.$$
$$+2(1-\nu_2)\,\gamma_2\left[2(1-\nu_2)\cosh p_2 + p_2\sinh p_2\right]$$
$$\left.+\delta_2\left[(3-4\nu_2)\sinh p_2 + p_2\cosh p_2\right]\right\}, \tag{1.72}$$

$$\tilde{\gamma}_3 = \frac{L_2}{L_3}(\tilde{\gamma}_2\cosh p_2 + \frac{1}{1-\nu_2}\tilde{\delta}_2\sinh p_2), \tag{1.73}$$

$$\beta_3 = \frac{L_2}{4L_3(1-\nu_2)^2}\{\alpha_2[(3-4\nu_2)\sinh p_2 - p_2\cosh p_2]$$
$$+2(1-\nu_2)\beta_2\left[2(1-\nu_2)\cosh p_2 - p_2\sinh p_2\right] \tag{1.74}$$
$$+2(1-\nu_2)\,\gamma_2\left[(1-2\nu_2)\sinh p_2 - p_2\cosh p_2\right] - \delta_2 p_2\sinh p_2\},$$

$$\alpha_3 + Q_3 = \alpha_2[\cosh p_2 - \frac{1}{2(1-\nu_2)}p_2\sinh p_2] + \beta_2(\sinh p_2 - p_2\cosh p_2)$$
$$-\gamma_2 p_2\sinh p_2 - \frac{\delta_2}{2(1-\nu_2)}[(1-2\nu_2)\sinh p_2 + p_2\cosh p_2], \tag{1.75}$$

$$\delta_3 = \frac{i}{p}(\xi T_3^x + \eta T_3^y) + \frac{1}{2(1-\nu_2)}\{\alpha_2[-(1-2\nu_2)\sinh p_2 + p_2\cosh p_2] +$$
$$+2(1-\nu_2)\beta_2 p_2\sinh p_2 + 2(1-\nu_2)\gamma_2[\sinh p_2 + p_2\cosh p_2] + \tag{1.76}$$
$$+\delta_2[p_2\sinh p_2 + 2(1-\nu_2)\cosh p_2]\},$$

$$\tilde{\delta}_3 = -\frac{i}{p}(\eta T_3^x - \xi T_3^y) + (1-\nu_2)\tilde{\gamma}_2\sinh p_2 + \tilde{\delta}_2\cosh p_2, \tag{1.77}$$

$$\alpha_3 p_3\sinh p_3 + 2(1-\nu_3)\beta_3[(1-2\nu_3)\sinh p_3 + p_3\cosh p_3] + 2(1-\nu_3)$$
$$\gamma_3[2(1-\nu_3)\cosh p_3 + p_3\sinh p_3] + \delta_3[(3-4\nu_3)\sinh p_3 + p_3\cosh p_3] = 0, \tag{1.78}$$

$$\tilde{\gamma}_3\cosh p_3 + \frac{1}{1-\nu_3}\tilde{\delta}_3\sinh p_3 = 0, \tag{1.79}$$

$$\alpha_3[(3-4\nu_3)\sinh p_3 - p_3\cosh p_3] + 2(1-\nu_3)\beta_3[2(1-\nu_3)\cosh p_3 - p_3\sinh p_3] +$$
$$+2(1-\nu_3)\gamma_3[(1-2\nu_3)\sinh p_3 - p_3\cosh p_3] - \delta_3 p_3\sinh p_3 = 0 \tag{1.80}$$

where $p_k = h_k p$ $(k = 1, 2, 3)$.

Thus, for each of the nine concentrated forces under consideration in Eq. (1.44), a system of 15 linear algebraic equations (1.63)–(1.80) to determine 15 functions α_k, δ_k, $\tilde{\delta}_k$, γ_m, β_m, $\tilde{\gamma}_k$ $(k = 2,3;\ m = 1, 2, 3)$ of the parameters ξ, η (α_1, δ_1, $\tilde{\delta}_1$ being always given on the upper boundary of the 1st layer) is obtained, its solution determining the transforms of the stress-strained state and the dilatation function for each layer.

Note some features of the system of Eqs. (1.63)−(1.80) whose account is important for the numerical implementation of the method proposed. The unknowns $\tilde{\gamma}_m$, $\tilde{\delta}_k$ ($m = 1, 2, 3$; $k = 2, 3$) are included only in Eqs. (1.67), (1.71), (1.73), (1.77), (1.79) and can be found independently of α_k, β_m, γ_m, δ_k ($k = 2,3$; $m = 1, 2, 3$). When a normal concentrated force acting on the upper surface of any layer is considered, then the system of Eqs. (1.67), (1.71), (1.73), (1.77), (1.79) is uniform and, consequently, has a trivial solution. In this case the functions $T_k = 0$, and all equations for the transforms of the displacements and stresses are considerably simplified. Simultaneously, when each tangential concentrated force is considered, the system is nonuniform. However, its solution by the substitution method can be easily obtained in an analytical form, what is taken into account while developing the computation algorithm. The solution of the system of the rest ten equations to determine α_k, β_m, γ_m, δ_k ($k = 2,3$, $m = 1, 2, 3$) is also presented in an analytical form and used in the calculations by sequential substitutions without application of standard routines of matrix algebra, requiring much computation time.

When a concentrated force, acting solely on the free surface of a multilayer system, is considered, a rather effective way to speed up the computation process is the method of compliance functions [111, 112], depending only on the integral transformation parameters, thicknesses and moduli of elasticity of the base layers, and do not depend on the loads being applied. The compliance functions are found prior to the boundary problem solution, rather simple recurrent relations existing for their determination. When the compliance functions are used, there is no need to deal with any auxiliary systems of high-order linear algebraic equations, what is essentially important for large number of layers. Note that the compliance functions were first considered for solving contact problems for a one-layer base (an elastic layer on a non-deformable half-space) [3, 15, 18, 66, 154], and then for two-layer bases as well [109, 150]. Later Petrishin, Privarnikov, Shevlyakov, and Naumov described the properties of the compliance functions for essentially multilayer bases both in the case of smooth and bonded layers [87, 96, 97].

If the account of concentrated forces acting on interlayer boundaries within the base is required, the compliance functions are inapplicable. Therefore, all the calculations performed here were carried out using a common method, applicable in case the base being loaded both on the free surface and on the internal surfaces of contacting layers.

After the functions α_k, β_{m}, γ_m, δ_k, $\tilde{\gamma}_m$, $\tilde{\delta}_k$ ($k = 2,3$, $m = 1, 2, 3$) having been found, it is possible to determine the stress-strained state and the dilatation functions for each layer of the soil base in the Fourier transforms based on the following expressions:

$$\bar{U} = -\frac{1}{p^2}(i\xi S + i\eta T), \bar{V} = -\frac{1}{p^2}(i\eta S - i\xi T), \bar{W} = \bar{W}(p),$$

$$\bar{\sigma}_x = -2G\left(\frac{\xi^2}{p^2}S + \frac{\xi\eta}{p^2}T - \frac{\nu}{1-2\nu}\bar{\varepsilon}_v\right), \tag{1.81}$$

$$\bar{\sigma}_y = -2G\left(\frac{\eta^2}{p^2}S - \frac{\xi\eta}{p^2}T - \frac{\nu}{1-2\nu}\bar{\varepsilon}_v\right),$$

$$\bar{\sigma}_z = 2G\left(\frac{1-\nu}{1-2\nu}\frac{d\bar{W}}{dz} - \frac{\nu}{1-2\nu}S\right),$$

$$\bar{\tau}_{yz} = \frac{i}{p}(\tau\eta + \tilde{\tau}\xi), \bar{\tau}_{xz} = -\frac{i}{p}(\tilde{\tau}\eta - \tau\xi),$$

$$\bar{\tau}_{xy} = G\left(\frac{\xi^2-\eta^2}{p^2}T - \frac{2\xi\eta}{p^2}S\right), \bar{\varepsilon}_v = \frac{d\bar{W}}{dz} - S.$$

The functions S, T and $\bar{W}$, τ, $\tilde{\tau}$, being contained in Eqs. (1.81), have been determined above in Eqs. (1.51), (1.55), and (1.56).

Application of the inverse Fourier transformation (1.47) to the transforms (1.81) in combination with the Eq. [19]

$$\int\limits_{-\infty}^{\infty}\int f(p)e^{\pm i(\xi x+\eta y)}d\xi\,d\eta = 2\pi\int\limits_0^{\infty} pf(p)J_0(pr)dp$$

$$\int\limits_{-\infty}^{\infty}\int i\xi f(p)e^{\pm i(\xi x+\eta y)}d\xi\,d\eta = \mp\frac{2\pi x}{r}\int\limits_0^{\infty} p^2 f(p)J_1(pr)dp$$

$$\int\limits_{-\infty}^{\infty}\int (i\xi)^2 f(p)e^{\pm i(\xi x+\eta y)}d\xi\,d\eta = -2\pi\left[\frac{x^2}{r^2}\int\limits_0^{\infty} p^3 f(p)J_0(pr)dp + \right.$$

$$\left. + \frac{y^2-x^2}{r^2}\int\limits_0^{\infty} p^3 f(p)\frac{J_1(pr)}{pr}dp\right],$$

$$\int\limits_{-\infty}^{\infty}\int (i\eta)^2 f(p)e^{\pm i(\xi x+\eta y)}d\xi\,d\eta = -2\pi\left[\frac{y^2}{r^2}\int\limits_0^{\infty} p^3 f(p)J_0(pr)dp + \right.$$

$$\left. + \frac{x^2-y^2}{r^2}\int\limits_0^{\infty} p^3 f(p)\frac{J_1(pr)}{pr}dp\right]$$

$$\int\limits_{-\infty}^{\infty}\int (i\xi)(i\eta) f(p)e^{\pm i(\xi x+\eta y)}d\xi\,d\eta = -\frac{2\pi xy}{r^2}\left[\int\limits_0^{\infty} p^3 f(p)J_0(pr)dp - \right.$$

$$\left. - 2\int\limits_0^{\infty} p^3 f(p)\frac{J_1(pr)}{pr}dp\right],$$

$$\int\limits_{-\infty}^{\infty}\int (i\xi)^3 f(p)e^{\pm i(\xi x+\eta y)}d\xi\,d\eta = \pm 2\pi\left[\frac{x^3}{r^3}\int\limits_0^{\infty} p^4 f(p)J_1(pr)dp - \right.$$

$$\left. - \frac{x(3y^2-x^2)}{r^3}\int\limits_0^{\infty} p^4 f(p)\frac{prJ_0(pr)-2J_1(pr)}{(pr)^2}dp\right],$$

$$\int\limits_{-\infty}^{\infty}(i\xi)^2(i\eta)f(p)e^{\pm i(\xi x+\eta y)}d\xi d\eta = \pm 2\pi\left[\frac{yx^2}{r^3}\int\limits_0^{\infty}p^4f(p)J_1(pr)dp-\right.$$

$$\left.-\frac{y(y^2-3x^2)}{r^3}\int\limits_0^{\infty}p^4f(p)\frac{prJ_0(pr)-2J_1(pr)}{(pr)^2}dp\right],$$

$$\int\limits_{-\infty}^{\infty}(i\eta)^2(i\xi)f(p)e^{\pm i(\xi\, x+\eta\, y)}d\xi d\eta = \pm 2\pi\left[\frac{xy^2}{r^3}\int\limits_0^{\infty}p^4f(p)J_1(pr)dp-\right.$$

$$\left.-\frac{x(x^2-3y^2)}{r^3}\int\limits_0^{\infty}p^4f(p)\frac{prJ_0(pr)-2J_1(pr)}{(pr)^2}dp\right],\ r=\sqrt{x^2+y^2}$$

enables the true values of the stress-strained state characteristics and dilatation functions to be calculated for each layer. Here we present in an extended form the formulae, corresponding to Eq. (1.81), obtained using the Hankel integrals.

The displacement and stress fields, when a normal concentrated force Q_i is acting on the upper boundary of the i-th layer ($i = 1, 2, 3$), are determined from the following expressions:

$$U^{(i)}(x,y,z) = -\frac{Q_i}{2\pi}\frac{x}{r}\int\limits_0^{\infty}S^{(i)}(p)J_1(pr)dp, \tag{1.82}$$

$$V^{(i)}(x,y,z) = -\frac{Q_i}{2\pi}\frac{y}{r}\int\limits_0^{\infty}S^{(i)}(p)J_1(pr)dp, \tag{1.83}$$

$$W^{(i)}(x,y,z) = \frac{Q_i}{2\pi}\int\limits_0^{\infty}p\bar{W}^{(i)}(p)J_0(pr)dp, \tag{1.84}$$

$$\sigma_z^{(i)}(x,y,z) = \frac{Q_i}{2\pi}\int\limits_0^{\infty}p\bar{\sigma}_z^{(i)}(p)J_0(pr)dp, \tag{1.85}$$

$$\sigma_x^{(i)}(x,y,z) = \frac{Q_iG_i}{\pi}\left[\frac{x^2}{r^2}\int\limits_0^{\infty}pS^{(i)}(p)J_0(pr)dp+ + \frac{y^2-x^2}{r^2}\int\limits_0^{\infty}pS^{(i)}(p)\frac{J_1(pr)}{pr}dp\right]+$$

$$+\frac{Q_iG_i}{\pi}\cdot\frac{\nu_i}{1-2\nu_i}\int\limits_0^{\infty}p\bar{\varepsilon}_v^{(i)}(p)J_0(pr)dp, \tag{1.86}$$

$$\sigma_y^{(i)}(x,y,z) = \frac{Q_iE_i}{2\pi(1+\nu_i)}\left[\frac{y^2}{r^2}\int\limits_0^{\infty}pS^{(i)}(p)J_0(pr)dp+\frac{x^2-y^2}{r^2}\int\limits_0^{\infty}pS^{(i)}(p)\frac{J_1(pr)}{pr}dp\right]+$$

$$+\frac{Q_iG_i\nu_i}{\pi(1-2\nu_i)}\int\limits_0^{\infty}p\bar{\varepsilon}_v^{(i)}(p)J_0(pr)dp, \tag{1.87}$$

$$\tau_{yz}^{(i)}(x,y,z) = \frac{Q_i}{2\pi} \cdot \frac{y}{r} \int_0^\infty p\tau^{(i)}(p) J_1(pr)dp, \tag{1.88}$$

$$\tau_{xz}^{(i)}(x,y,z) = \frac{Q_i}{2\pi} \cdot \frac{x}{r} \int_0^\infty p\tau^{(i)}(p) J_1(pr)dp, \tag{1.89}$$

$$\tau_{xy}^{(i)}(x,y,z) = \frac{Q_i G_i}{\pi} \cdot \frac{xy}{r^2} \left[\int_0^\infty pS^{(i)}(p) J_0(pr)dp - 2 \int_0^\infty pS^{(i)}(p) \frac{J_1(pr)}{pr} dp \right], \tag{1.90}$$

$$\varepsilon_v^{(i)}(x,y,z) = \frac{Q_i}{2\pi} \int_0^\infty p\bar{\varepsilon}_v^{(i)}(p) J_0(pr)dp. \tag{1.91}$$

If a tangential concentrated force T^x is acting in the positive direction of the x_i axis on the upper boundary of the i-th layer, the following equations are obtained to determine the stress-strained state in an elastic base:

$$\begin{aligned} U^{(i)}(x,y,z) = \frac{T_i^x}{2\pi} \left[\frac{x^2}{r^2} \int_0^\infty S^{(i)}(p) J_0(pr)dp + \frac{y^2 - x^2}{r^2} \int_0^\infty S^{(i)}(p) \frac{J_1(pr)}{pr} dp + \right. \\ \left. + \frac{y^2}{r^2} \int_0^\infty T^{(i)}(p) J_0(pr)dp + \frac{x^2 - y^2}{r^2} \int_0^\infty T^{(i)}(p) \frac{J_1(pr)}{pr} dp \right], \end{aligned} \tag{1.92}$$

$$\begin{aligned} V^{(i)}(x,y,z) = \frac{T_i^x}{2\pi} \left\{ \frac{xy}{r^2} \left[\int_0^\infty S^{(i)}(p) J_0(pr)dp - 2 \int_0^\infty S^{(i)}(p) \frac{J_1(pr)}{pr} dp - \right. \right. \\ \left. \left. - \int_0^\infty T^{(i)}(p) J_0(pr)dp + 2 \int_0^\infty T^{(i)}(p) \frac{J_1(pr)}{pr} dp \right] \right\}, \end{aligned} \tag{1.93}$$

$$W^{(i)}(x,y,z) = \frac{T_i^x}{2\pi} \cdot \frac{x}{r} \int_0^\infty p\bar{W}(p) J_1(pr)dp, \tag{1.94}$$

$$\begin{aligned} \sigma_x^{(i)} = \frac{G_i T_i^x}{\pi} \left[\frac{x^3}{r^3} \int_0^\infty pS^{(i)}(p) J_1(pr)dp - \frac{x(3y^2 - x^2)}{r^3} \int_0^\infty pS^{(i)}(p) \frac{prJ_0(pr) - 2J_1(pr)}{(pr)^2} dp + \right. \\ + \frac{xy^2}{r^3} \int_0^\infty pT^{(i)}(p) J_1(pr)dp - \frac{x(x^2 - 3y^2)}{r^3} \int_0^\infty pT^{(i)}(p) \frac{prJ_0(pr) - 2J_1(pr)}{(pr)^2} dp + \\ \left. + \frac{\nu_i}{1 - 2\nu_i} \cdot \frac{x}{r} \int_0^\infty p\bar{\varepsilon}_v^{(i)}(p) J_1(pr)dp \right], \end{aligned} \tag{1.95}$$

$$\sigma_y^{(i)}(x,y,z) = \frac{G_i T_i^x}{\pi}\left[\frac{xy^2}{r^3}\int_0^\infty pS^{(i)}(p)J_1(pr)dp - \right.$$
$$-\frac{x(x^2-3y^2)}{r^3}\int_0^\infty pS^{(i)}(p)\frac{prJ_0(pr)-2J_1(pr)}{(pr)^2}dp - \frac{xy^2}{r^3}\int_0^\infty pT^{(i)}(p)J_1(pr)dp +$$
$$+\frac{x(x^2-3y^2)}{r^3}\int_0^\infty pT^{(i)}(p)\frac{prJ_0(pr)-2J_1(pr)}{(pr)^2}dp +$$
$$\left. + \frac{\nu_i}{1-2\nu_i}\cdot\frac{x}{r}\int_0^\infty p\bar{\varepsilon}_v^{(i)}(p)J_1(pr)dp\right], \tag{1.96}$$

$$\sigma_z^{(i)}(x,y,z) = \frac{T_i^x}{2\pi}\cdot\frac{x}{r}\int_0^\infty p\bar{\sigma}_z^{(i)}(p)J_1(pr)dp, \tag{1.97}$$

$$\tau_{yz}^{(i)}(x,y,z) = \frac{T_i^x}{2\pi}\left\{\frac{xy}{r^2}\left[2\int_0^\infty p\tau^{(i)}(p)\frac{J_1(pr)}{pr}dp - \int_0^\infty p\tau^{(i)}(p)J_0(pr)dp - \right.\right.$$
$$\left.\left. - \int_0^\infty p\tilde{\tau}(p)J_0(pr)dp + 2\int_0^\infty p\tilde{\tau}(p)\frac{J_1(pr)}{pr}dp\right]\right\}, \tag{1.98}$$

$$\tau_{xz}^{(i)}(x,y,z) = -\frac{T_i^x}{2\pi}\left[\frac{x^2}{r^2}\int_0^\infty p\tau^{(i)}(p)J_0(pr)dp + \frac{y^2-x^2}{r^2}\int_0^\infty p\tau^{(i)}(p)\frac{J_1(pr)}{pr}dp - \right.$$
$$\left. -\frac{y^2}{r^2}\int_0^\infty \tilde{\tau}^{(i)}(p)J_0(pr)dp - \frac{x^2-y^2}{r^2}\int_0^\infty p\tilde{\tau}^{(i)}(p)\frac{J_1(pr)}{pr}dp\right], \tag{1.99}$$

$$\tau_{xy}^{(i)}(x,y,z) = \frac{G_i T_i^x}{2\pi}\left[2\frac{y(y^2-3x^2)}{r^3}\int_0^\infty pS^{(i)}(p)\frac{prJ_0(pr)-2J_1(pr)}{(pr)^2}dp - \right.$$
$$-2\frac{yx^2}{r^3}\int_0^\infty pS^{(i)}(p)J_1(pr)dp - \frac{y^3}{r^3}\int_0^\infty pT^{(i)}(p)J_1(pr)dp + \tag{1.100}$$
$$\left. +\frac{x(3y^2-x^2)}{r^3}\int_0^\infty pT^{(i)}(p)\frac{prJ_0(pr)-2J_1(pr)}{(pr)^2}dp\right],$$

$$\varepsilon_v^{(i)}(x,y,z) = \frac{T_i^x}{2\pi}\cdot\frac{x}{r}\int_0^\infty p\bar{\varepsilon}_v^{(i)}(p)J_1(pr)dp. \tag{1.101}$$

In the case of the tangential concentrated force T_i^y, acting in the positive direction of the y_i axis on the upper boundary of the i-th layer, one should replace x with y and, vice versa, y with x, in the corresponding equations for the case of the T_i^x force.

Two-layer base. The calculation scheme for a two-layer deformable system is presented in Fig. 1.10. The dimensionality of the functional system of equations, corresponding to the boundary conditions of the displacement and stress continuity, is reduced due to the presence of only one internal contact layer and, consequently, obtaining their solutions becomes less labour-consuming. Here we present the form of the reduced system in case concentrated forces acting only on the interlayer surface, having implied $Q_1 = 0$, ${T_1}^x = {T_1}^y = 0$, what at once results in

$$\alpha_1 = \delta_1 = \tilde{\delta}_1 = 0, \tag{1.102}$$

$$\begin{aligned}\gamma_2 = \frac{L_1}{2L_2(1-\nu_1)} &\left\{\beta_1\left[(1-2\nu_1)\sinh p_1 + p_1\cosh p_1\right]\right. \\ &\left.+\gamma_1\left[2(1-\nu_1)\cosh p_1 + p_1\sinh p_1\right]\right\},\end{aligned} \tag{1.103}$$

$$\begin{aligned}\beta_2 = \frac{L_1}{2L_2(1-\nu_1)} &\left\{\beta_1\left[2(1-\nu_1)\cosh p_1 - p_1\sinh p_1\right]\right. \\ &\left.+\gamma_1\left[(1-2\nu_1)\sinh p_1 - p_1\cosh p_1\right]\right\},\end{aligned} \tag{1.104}$$

$$\alpha_2 + Q_2 = \beta_1(\sinh p_1 - p_1\cosh p_1) - \gamma_1 p_1\sinh p_1, \tag{1.105}$$

$$\delta_2 = \frac{i}{p}(\xi T_2^x + \eta T_2^y) + \left[\beta_1 p_1\sinh p_1 + \gamma_1(\sinh p_1 + p_1\cosh p_1)\right], \tag{1.106}$$

$$\begin{aligned}&\alpha_2 p_2\sinh p_2 + 2(1-\nu_2)\beta_2\left[(1-2\nu_2)\sinh p_2 + p_2\cosh p_2\right] \\ &+2(1-\nu_2)\gamma_2\left[2(1-\nu_2)\cosh p_2 + p_2\sinh p_2\right] \\ &+\delta_2\left[(3-4\nu_2)\sinh p_2 + p_2\cosh p_2\right] = 0,\end{aligned} \tag{1.107}$$

$$\begin{aligned}&\alpha_2\left[(3-4\nu_2)\sinh p_2 - p_2\cosh p_2\right] + 2(1-\nu_2)\beta_2\left[2(1-\nu_2)\cosh p_2 - p_2\sinh p_2\right] \\ &+2(1-\nu_2)\gamma_2\left[(1-2\nu_2)\sinh p_2 - p_2\cosh p_2\right] - \delta_2 p_2\sinh p_2 = 0\end{aligned}, \tag{1.108}$$

$$\tilde{\gamma}_2\cosh p_2 + \frac{1}{1-\nu_2}\tilde{\delta}_2\sinh p_2 = 0, \tag{1.109}$$

$$\tilde{\gamma}_2 = \frac{L_1}{L_2}\tilde{\gamma}_1\cosh p_1, \tag{1.110}$$

$$\tilde{\delta}_2 = -\frac{i}{p}(\eta T_2^x - \xi T_2^y) + (1-\nu_1)\tilde{\gamma}_1\sinh p_1 \tag{1.111}$$

where

$$p_k = h_k p\ (k = 1,2)\,.$$

The functional system of Eqs. (1.103−1.111) should be solved by the method of sequential elimination using the same scheme, as in the case of the three-layer base, considering separately the vertical Q_2 and the horizontal forces ${T_2}^x$, ${T_2}^y$.

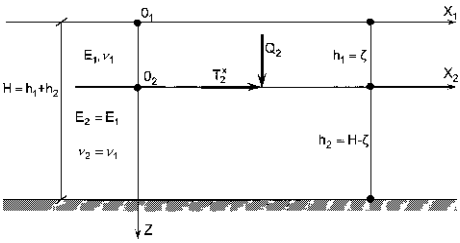

Fig. 1.10 Concentrated forces in a finite-thickness elastic layer

In a particular case, when the deformation parameters of both layers are equal ($\nu_1 = \nu_2 = \nu$, $E_1 = E_2 = E$), one arrives at the simplest case for the two-layer base under concentrated forces acting on a fictitious surface $z = \zeta$ separating the homogeneous layers (Fig. 1.10). Such calculation scheme corresponds to the problem of action of concentrated forces within a homogeneous finite-thickness layer and is of separate interest. Since while solving problems of concentrated forces, acting inside a multilayer half-space, according to the approach applied, a fictitious separation surface should be introduced at the level of the force application point, this problem has important methodological aspects and deserves a more detailed consideration.

Concentrated forces, acting in a finite-thickness elastic layer. At equal deformation parameters of the layers and $L_1 = L_2 = L = 2(1-\nu^2)/E$, the system of Eqs. (1.103–1.111) is written in the form

$$\gamma_2 = \frac{1}{2(1-\nu)}\left\{\beta_1\left[(1-2\nu)\sinh p_1 + p_1\cosh p_1\right]\right. \\ \left.+\gamma_1\left[2(1-\nu)\cosh p_1 + p_1\sinh p_1\right]\right\}, \tag{1.112}$$

$$\beta_2 = \frac{1}{2(1-\nu)}\left\{\beta_1\left[2(1-\nu)\cosh p_1 - p_1\sinh p_1\right]\right. \\ \left.+\gamma_1\left[(1-2\nu)\sinh p_1 - p_1\cosh p_1\right]\right\}, \tag{1.113}$$

$$\alpha_2 + Q_2 = \beta_1(\sinh p_1 - p_1\cosh p_1) - \gamma_1 p_1\sinh p_1, \tag{1.114}$$

$$\delta_2 = \frac{i}{p}(\xi T_2^x + \eta T_2^y) + \left[\beta_1 p_1\sinh p_1 + \gamma_1(\sinh p_1 + p_1\cosh p_1)\right], \tag{1.115}$$

$$\alpha_2 p_2\sinh p_2 + 2(1-\nu)\beta_2\left[(1-2\nu)\sinh p_2 + p_2\cosh p_2\right] \\ +2(1-\nu)\gamma_2\left[2(1-\nu)\cosh p_2 + p_2\sinh p_2\right], \\ +\delta_2\left[(3-4\nu)\sinh p_2 + p_2\cosh p_2\right] = 0 \tag{1.116}$$

$$\alpha_2\left[(3-4\nu)\sinh p_2 - p_2\cosh p_2\right] + 2(1-\nu)\beta_2\left[2(1-\nu)\cosh p_2 - p_2\sinh p_2\right] + \\ +2(1-\nu)\gamma_2\left[(1-2\nu)\sinh p_2 - p_2\cosh p_2\right] - \delta_2 p_2\sinh p_2 = 0, \tag{1.117}$$

$$\tilde{\gamma}_2\cosh p_2 + \frac{1}{1-\nu_2}\tilde{\delta}_2\sinh p_2 = 0, \tag{1.118}$$

$$\tilde{\gamma}_2 = \tilde{\gamma}_1 \cosh p_1, \tag{1.119}$$

$$\tilde{\delta}_2 = -\frac{i}{p}(\eta T_2^x - \xi T_2^y) + (1-\nu)\tilde{\gamma}_1 \sinh p_1 \tag{1.120}$$

where $p_k = h_k p$ $(k = 1, 2)$.

Further on we consider the most important from the practical point of view case when only the vertical force Q_2 is acting. By assuming $T^x = T^y = 0$ in the system of Eqs. (1.112–1.120) and by denoting

$$e_1 = \exp(-2p_1),\ e_2 = \exp(-2p_2),\ c_k = (1+e_k)/2,\ s_k = (1-e_k)/2,$$

$$\varepsilon = \exp(-p_1),\ n_1 = 2(1-\nu),\ n_2 = 1-2\nu,\ n_3 = 3-4\nu,$$

one arrives at a relatively simple linear algebraic system with respect to the values $\beta_1, \gamma_1, \beta_2, \gamma_2, \alpha_2, \delta_2$:

$$\beta_1(n_2 s_1 + p_1 c_1) + \gamma_1(n_1 c_1 + p_1 s_1) - n_1 \varepsilon \gamma_2 = 0, \tag{1.121}$$

$$\beta_1(n_1 c_1 - p_1 s_1) + \gamma_1(n_2 s_1 - p_1 c_1) - n_1 \varepsilon \beta_2 = 0, \tag{1.122}$$

$$\beta_1(s_1 - p_1 c_1) - \gamma_1 p_1 s_1 - \varepsilon \alpha_2 = \varepsilon Q_2, \tag{1.123}$$

$$\beta_1 p_1 s_1 + \gamma_1(s_1 + p_1 c_1) - \varepsilon \delta_2 = 0, \tag{1.124}$$

$$\alpha_2 p_2 s_2 + n_1\beta_2(n_2 s_2 + p_2 c_2) + n_1\gamma_2(n_1 c_2 + p_2 s_2) + \delta_2(n_3 s_2 + p_2 c_2) = 0, \tag{1.125}$$

$$\alpha_2(n_3 s_2 - p_2 c_2) + n_1\beta_2(n_1 c_2 - p_2 s_2) + n_1\gamma_2(n_2 s_2 - p_2 c_2) - \delta_2 p_2 s_2 = 0. \tag{1.126}$$

The solution of the system of Eqs. (1.121–1.126) is presented in the explicit form:

$$\beta_1 = \frac{1}{2\mu_1} e^{-\alpha\bar{\zeta}} \frac{N_{\beta_1}}{D}, \tag{1.127}$$

$$\gamma_1 = \frac{1}{2\mu_1} e^{-\alpha\bar{\zeta}} \frac{N_{\gamma_1}}{D}, \tag{1.128}$$

$$\beta_2 = \frac{1}{8\mu_1^2} \cdot \frac{N_{\beta_2}}{D}, \tag{1.129}$$

$$\gamma_2 = \frac{1}{4\mu_1^2} \cdot \frac{N_{\gamma_2}}{D}, \tag{1.130}$$

$$\delta_2 = -\frac{1}{4\mu_1} \cdot \frac{N_{\delta_2}}{D}, \tag{1.131}$$

$$\alpha_2 = -\frac{1}{2\mu_1} \cdot \frac{N_{\alpha_2}}{D} \tag{1.132}$$

where the following notations are used:

$$
\begin{aligned}
&D(\alpha) = 2\left(\mu_5 + 2\alpha^2\right)e^{-2\alpha} + \mu_3\left(1 + e^{-4\alpha}\right),\\
&N_{\beta_1}\left(\alpha,\bar{\zeta}\right) = \mu_3\left(2\mu_1 + \alpha\bar{\zeta}\right) + \left[2\mu_1\mu_3 + \alpha\left(1-2\alpha\right)\bar{\zeta} + 2\alpha\left(\alpha - 2\mu_1\right)\right]e^{-2\alpha} +\\
&+\left[-2\mu_1\mu_3 + \alpha\left(1+2\alpha\right)\bar{\zeta} - 2\alpha\left(\alpha + 2\mu_1\right)\right]e^{-2\alpha\left(1-\bar{\zeta}\right)} +\\
&+\mu_3\left(-2\mu_1 + \alpha\bar{\zeta}\right)e^{-2\alpha\left(2-\bar{\zeta}\right)},\\
&N_{\gamma_1}\left(\alpha,\bar{\zeta}\right) = -\mu_3\left(\mu_2 + \alpha\bar{\zeta}\right) + \left[\mu_2\mu_3 - \alpha\left(1+2\alpha\right)\bar{\zeta} + 2\alpha\left(\alpha - \mu_2\right)\right]e^{-2\alpha} +\\
&+\left[\mu_2\mu_3 + \alpha\left(1-2\alpha\right)\bar{\zeta} + 2\alpha\left(\alpha + \mu_2\right)\right]e^{-2\alpha\left(1-\bar{\zeta}\right)} +\\
&+\mu_3\left(-\mu_2 + \alpha\bar{\zeta}\right)e^{-2\alpha\left(2-\bar{\zeta}\right)},\\
&N_{\beta_2}\left(\alpha,\bar{\zeta}\right) = 4\alpha\left[2\alpha^2\bar{\zeta}^2 + 2\left(2\nu\mu_4 - \alpha^2 - 2\right)\bar{\zeta} - \mu_5\right]e^{-2\alpha} +\\
&+\mu_3^2\left(1 - e^{-4\alpha}\right) +\\
&+\mu_3\left[2\alpha^2\bar{\zeta}^2 + 2\mu_3\alpha\bar{\zeta} + \mu_5\right]e^{-2\alpha\bar{\zeta}} +\\
&+\left[-2\alpha^2\bar{\zeta}^2 + 2\alpha\left(2\alpha + \mu_3\right)\bar{\zeta} - 2\alpha\mu_3 - 2\alpha^2 - \mu_3^2\right]e^{-2\alpha\left(1-\bar{\zeta}\right)} +\\
&+\mu_3\left[-2\alpha^2\bar{\zeta}^2 + 2\mu_3\alpha\bar{\zeta} - \mu_5\right]e^{-2\alpha\left(2-\bar{\zeta}\right)} +\\
&+\left[2\alpha^2\bar{\zeta}^2 - 2\alpha\left(2\alpha - \mu_3\right)\bar{\zeta} - 2\alpha\mu_3 + 2\alpha^2 + \mu_3^2\right]e^{-2\alpha\left(1+\bar{\zeta}\right)},\\
&N_{\gamma_2}\left(\alpha,\bar{\zeta}\right) = 2\mu_3\left[-2\alpha^2\bar{\zeta} + 2\mu_1\mu_2 + \alpha^2\right]e^{-2\alpha} +\\
&+\mu_3\left[\alpha^2\bar{\zeta}^2 - 2\mu_1\mu_2\right]e^{-2\alpha\bar{\zeta}} +\\
&+\alpha^2\left(1-\bar{\zeta}\right)^2 e^{-2\alpha\left(1-\bar{\zeta}\right)} +\\
&+\mu_3\left[\alpha^2\bar{\zeta}^2 - 2\mu_1\mu_2\right]e^{-2\alpha\left(2-\bar{\zeta}\right)} +\\
&+\alpha^2\left(1-\bar{\zeta}\right)^2 e^{-2\alpha\left(1+\bar{\zeta}\right)},\\
&N_{\delta_2}\left(\alpha,\bar{\zeta}\right) = 4\alpha\left[2\alpha^2\bar{\zeta}^2 + 2\left(2\nu\mu_4 - \alpha^2 - 2\right)\bar{\zeta} + \mu_2\right]e^{-2\alpha} +\\
&+\mu_2\mu_3\left(1 - e^{-4\alpha}\right) +\\
&+\mu_3\left[2\alpha^2\bar{\zeta}^2 + 2\mu_2\alpha\bar{\zeta} - \mu_2\right]e^{-2\alpha\bar{\zeta}} +\\
&+\left[-2\alpha^2\bar{\zeta}^2 + 2\alpha\left(2\alpha + \mu_2\right)\bar{\zeta} - 2\alpha\left(\alpha + \mu_2\right) - \mu_2\mu_3\right]e^{-2\alpha\left(1-\bar{\zeta}\right)} +\\
&+\mu_3\left[-2\alpha^2\bar{\zeta}^2 + 2\mu_2\alpha\bar{\zeta} + \mu_2\right]e^{-2\alpha\left(2-\bar{\zeta}\right)} +\\
&+\left[2\alpha^2\bar{\zeta}^2 - 2\alpha\left(2\alpha - \mu_2\right)\bar{\zeta} + 2\alpha\left(\alpha - \mu_2\right) + \mu_2\mu_3\right]e^{-2\alpha\left(1+\bar{\zeta}\right)},\\
&N_{\alpha_2}\left(\alpha,\bar{\zeta}\right) = 2\left[\alpha^2\left(\mu_3 - 2\mu_2\bar{\zeta}\right) + \mu_1\mu_6\right]e^{-2\alpha} + \mu_1\mu_3\left(1 + e^{-4\alpha}\right) +\\
&+\mu_3\left[\alpha^2\bar{\zeta}^2 + 2\mu_1\alpha\bar{\zeta} + \mu_1\right]e^{-2\alpha\bar{\zeta}} +
\end{aligned}
$$

$$+\left[\alpha^2\bar{\zeta}^2 - 2\alpha\left(\alpha+\mu_1\right)\bar{\zeta} + \alpha\left(\alpha+2\mu_1\right) + \mu_1\mu_3\right]e^{-2\alpha\left(1-\bar{\zeta}\right)} +$$
$$+\mu_3\left[\alpha^2\bar{\zeta}^2 - 2\mu_1\alpha\bar{\zeta} + \mu_1\right]e^{-2\alpha\left(2-\bar{\zeta}\right)} +$$
$$+\left[\alpha^2\bar{\zeta}^2 - 2\alpha\left(\alpha-\mu_1\right)\bar{\zeta} + \alpha\left(\alpha-2\mu_1\right) + \mu_1\mu_3\right]e^{-2\alpha\left(1+\bar{\zeta}\right)},$$

$$\mu_1 = 1-\nu,\ \mu_2 = 1-2\nu,\ \mu_3 = 3-4\nu,\ \mu_4 = 3-2\nu,$$

$$\mu_5 = 8\nu^2 - 12\nu + 5,$$

$\mu_6 = 16\nu^2 - 20\nu + 7$ are dimensionless parameters, $\alpha = \rho H$, $\bar{\zeta} = \zeta/H$, $\rho = r/H$ are dimensionless variables.

The dependence of the functional coefficients β_1, γ_1, β_2, γ_2, α_2, δ_2 on the dimensionless parameter α of the Hankel transformation for the fixed values of $\nu = 0.3$, $\bar{\zeta} = 0.25$ is illustrated by Fig. 1.11a. As follows from the plotted data, all the dependences, with the exception of α_2, have a non-monotonous character of the initial part with distinct extrema. However, with the increase of the transformation parameter all the dependences rather soon (at $\alpha \approx 25$) achieve their limiting values.

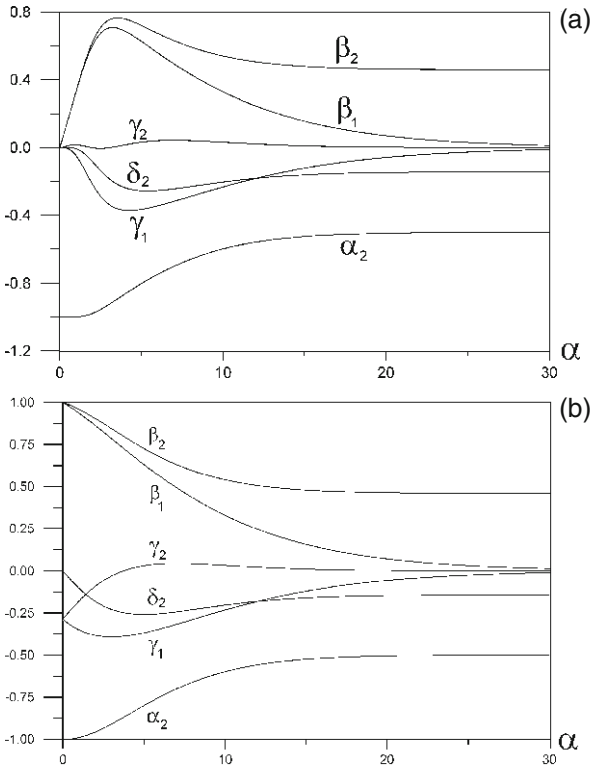

Fig. 1.11 Dependence of functional coefficients on the transformation parameter α (**a**) for a constant-thickness elastic layer and (**b**) for a half-space; $\nu = 0.3$, $\zeta/H = 0.2$

When the elastic layer is of infinite thickness, one arrives at the classical base model in the form of a homogeneous half-space with the fundamental singular Mindlin's solution. The limiting transition at $H \to$ in Eqs. (1.84)–(1.89) results in

$$\beta_1(\alpha,\bar{\zeta}) = \frac{1}{2\mu_1} e^{-\alpha\bar{\zeta}}(2\mu_1 + \alpha\bar{\zeta}),$$

$$\gamma_1(\alpha,\bar{\zeta}) = -\frac{1}{2\mu_1} e^{-\alpha\bar{\zeta}}(\mu_2 + \alpha\bar{\zeta}),$$

$$\beta_2(\alpha,\bar{\zeta}) = \frac{1}{8\mu_1^2}\left[\mu_3 + (2\alpha^2\bar{\zeta}^2 + 2\mu_3\alpha\bar{\zeta} + \mu_5)e^{-2\alpha\bar{\zeta}}\right],$$

$$\gamma_2(\alpha,\bar{\zeta}) = \frac{1}{4\mu_1^2}(\alpha^2\bar{\zeta}^2 - 2\mu_1\mu_2)e^{-2\alpha\bar{\zeta}},$$

$$\delta_2(\alpha,\bar{\zeta}) = -\frac{1}{4\mu_1}\left[\mu_2 + (2\alpha^2\bar{\zeta}^2 + 2\mu_2\alpha\bar{\zeta} - \mu_2)e^{-2\alpha\bar{\zeta}}\right],$$

$$\alpha_2(\alpha,\bar{\zeta}) = -\frac{1}{2\mu_1}\left[\mu_1 + (\alpha^2\bar{\zeta}^2 + 2\mu_1\alpha\bar{\zeta} + \mu_1)e^{-2\alpha\bar{\zeta}}\right].$$

The dependences of the functional coefficients β_1, γ_1, β_2, γ_2, α_2, δ_2 on the transformation parameter α, corresponding to the Mindlin's solution, for the same ν and $\bar{\zeta}$ values as for the case of Fig. 1.11a, are plotted in Fig. 1.11b. It is seen that in this case β_1, β_2, and α_2 are already strictly monotonous. The extrema in the plots of δ_2, γ_1, and γ_2 are rather weak and, as shown by the calculations, soon disappear with the increase of the $\bar{\zeta}$ parameter, i.e. with the increase of the distance between the force application point from the half-space surface.

The obtained expressions for the functional coefficients β_1, γ_1, β_2, γ_2, α_2, δ_2 together with Eqs. (1.82)–(1.91) enable the stress-strained state to be calculated at any point of the elastic layer. We investigate the settlements of the free layer surface in case a vertical concentrated force acting inside it at different depth of its application. Since the free surface ($z = 0$) belongs to the first fictitious layer, its vertical displacements are fully characterized by the functional coefficient β_1 The dependences of the latter coefficient for a finite-thickness layer and a half-space at different depths of the concentrated force application point are illustrated by Fig. 1.12. As should be expected, for both cases the areas, encompassed with the calculated curves, decrease with $\bar{\zeta}$, tending to zero in the limit. At $\alpha \to \infty$ the character of the β_1 function decrease is monotonous in all cases, determined by the most slowly decreasing exponent $e^{-\alpha\bar{\zeta}}$. The initial part of the β_1 curves for the finite-thickness layer and the half-space is qualitatively different. In the first case the β_1 dependences, starting from the zero point, increase, possess a characteristic maximum, decreasing with $\bar{\zeta}$ increase. In the case of the elastic half-space the curves under consideration exhibit strictly monotonous exponential decay from the unit value. In fact, the $\beta_1(\alpha, \bar{\zeta}, \nu)$ function determines the character of free surface settlements,

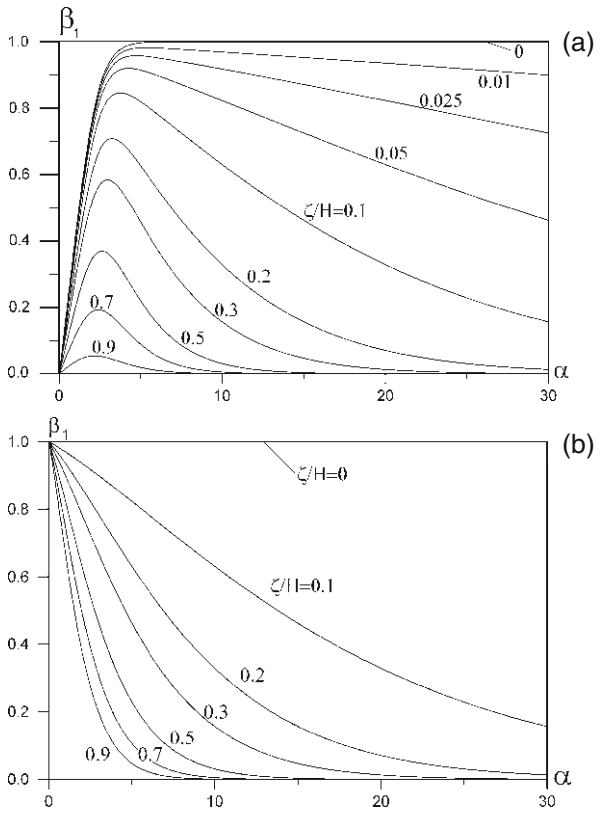

Fig. 1.12 Dependence of functional coefficient β_1 on the transformation parameter α: (**a**) for a constant-thickness elastic layer and (**b**) for a half-space at various values of ζ/H; $\nu = 0.3$

whose values, according to Eq. (1.84), can be presented in the form

$$W(p,\bar{\zeta},z=0) = Q_2 \frac{(1-\nu^2)}{\pi EH} \int_0^\infty \beta_1(\alpha,\bar{\zeta},\nu) J_0(\alpha\rho) d\alpha. \tag{1.133}$$

The results of the numerical calculations according to Eq. (1.133) are illustrated by the plots (Figs. 1.13, 1.14, and 1.15) of dimensionless settlements $\bar{W} = W/W_*$ where $W_* = Q_2/\pi EH$ is the chosen displacement measure. The largest settlement values are observed when the force is acting on the base free surface ($\zeta = 0$). The functional coefficient $\beta_1(\alpha,0,\nu)$ for this case is given by

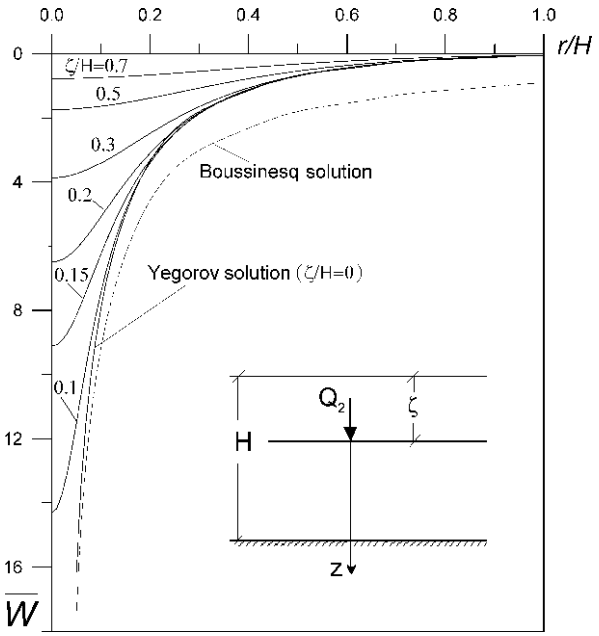

Fig. 1.13 Elastic base free surface settlements due to a vertical concentrated force

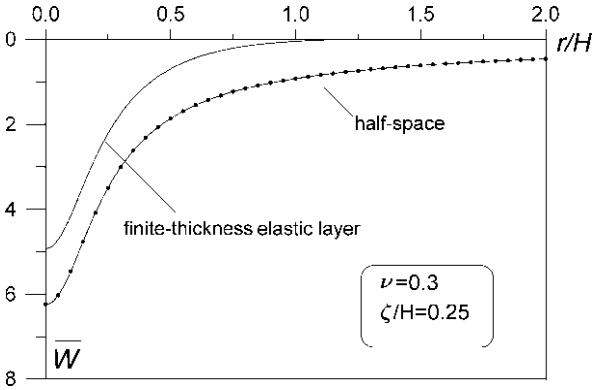

Fig. 1.14 Elastic base free surface settlements due to a vertical concentrated force acting inside elastic bases

$$\beta_1 = \frac{\mu_3(1-e^{-4\alpha}) - 4\alpha e^{-2\alpha}}{2(\mu_5 + 2\alpha^2)e^{-2\alpha} + \mu_3(1+e^{-4\alpha})} = \frac{1}{2}\frac{\mu_3 \sinh(2\alpha) - 2\alpha}{\mu_3 \cosh^2\alpha + \alpha^2 + \mu_2^2}, (H < \infty),$$

$$\beta_1 = 1, (H \to \infty).$$

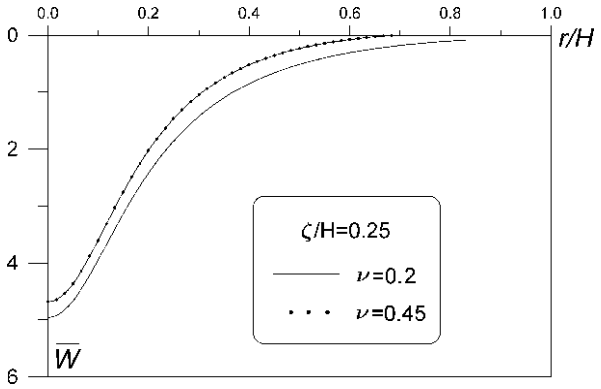

Fig. 1.15 Elastic base free surface settlements due to a vertical concentrated force acting inside a finite-thickness elastic layer at different Poisson ratio values

At such values of β_1 Eq. (1.133) produces the Yegorov (1.35) and Boussinesq $W_0(r) = (1-\nu^2)/\pi Er$ solutions, respectively. At $\rho \to 0$, i.e. near the vertical force application point, the settlement values for both contact models behave in a similar way, unlimitedly increasing according to a hyperbolic law (Fig. 1.13). Due to the infinite half-space depth, the Boussinesq solution always gives the largest settlement values with the lowest decay rate at $\rho \to \infty$.

Action of the concentrated force inside the layer ($\bar{\zeta} \neq 0$) results in finite surface displacements (Figs. 1.13, 1.14, and 1.15). The smaller is the depth of the force application point, the larger will be the settlement cone (Fig. 1.13). As one should expect, the deeper is the elastic layer, the larger are the free surface settlements for a fixed $\bar{\zeta}$. Such comparison of the settlements is performed in Fig. 1.14 for the layer and the half-space in the layer depth scale. The calculation data for the settlements of a finite-thickness elastic layer surface at $\bar{\zeta} = 0.25$ and $\nu = 0.2$ and 0.45 are shown in Fig. 1.15. These data enable the effect of compressibility on the base free surface deformation to be estimated. In particular, with the increase of the Poisson ratio the settlements decrease, simultaneously their decay rate with $\rho \to \infty$ increases.

The determination of other characteristics of the stress-strained state in the layer does not experience any difficulties either. For example, the calculation formula to determine the horizontal (radial) displacements of the layer surface can be given by

$$U_r(r,\bar{\zeta},z=0) = Q_2 \frac{(1-\nu^2)}{\pi EH} \int_0^\infty \gamma_1(\alpha,\bar{\zeta},\nu) J_1(\alpha\rho) d\alpha. \tag{1.134}$$

The results of the calculations, performed in accordance with Eq. (1.134), are shown in Fig. 1.16. The horizontal displacement curves for $\bar{\zeta} \neq 0$ start from the

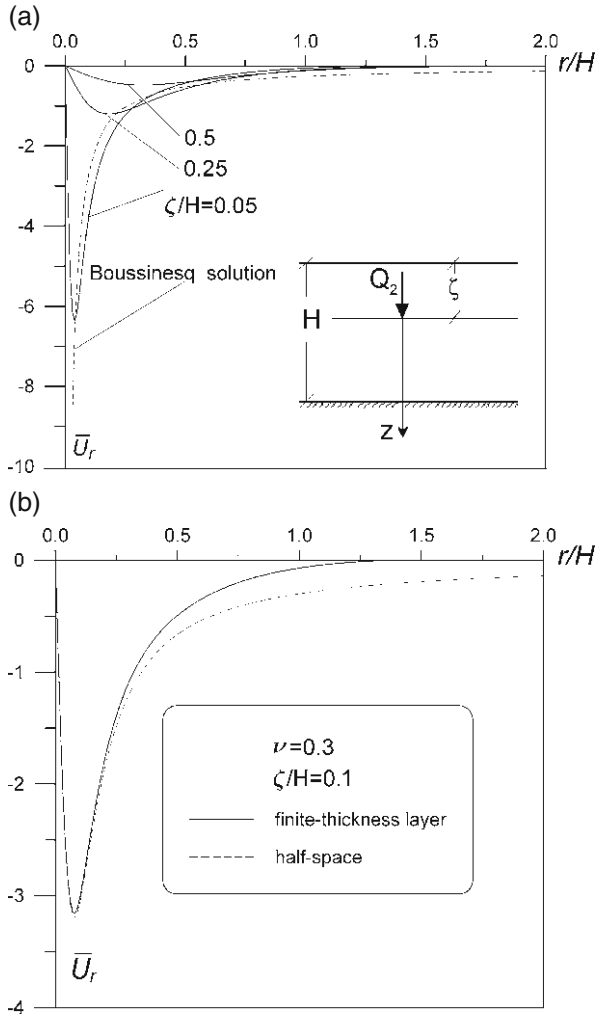

Fig. 1.16 Horizontal displacements of elastic base free surfaces at different depths of a vertical concentrated force application

zero value, exhibit a characteristic maximum of the absolute values, and then monotonously decay at $\rho \to \infty$. As shown by the calculations, horizontal displacements near the concentrated force action line (below the point of the characteristic maximum of the absolute value) are practically independent of the layer thickness and are determined solely by the depth of the concentrated force application point. Simultaneously, with the increase of the distance from the concentrated force line of action, the difference in the models of the elastic bases (layers of different thickness) is revealed quite significantly.

In order to obtain equations, determining the stresses and displacements in a multilayer base loaded by a tangential concentrated force T, one should at first find the functional coefficients from the system of Eqs. (1.112)–(1.120) at unit right-hand parts, and then multiply the obtain results by $i\xi T/p$ or by $-i\eta T/p$ in accordance with the separation of Eqs. (1.112)–(1.120) into independent subsystems, and add the obtained so5s in order to determine finally the transforms of the sought values. This procedure does not meet any principal difficulties, but results in quite cumbersome formulations and, therefore, is not presented here. A more careful attention is required to calculate the Hankel integrals from the oscillating functions contained in the final equations for the stresses and displacements, obtained by application of the inverse Fourier transformations to the transforms found.

Quite popular is a direct method of calculation of improper integrals with weights in the form of the Bessel functions [124]. In order to obtain results of the required accuracy, for each value of the oscillation parameter the integration interval is partitioned by the Bessel function zeroes into the segments of constant sign of the integrand; on each of the segments the Gauss-Legendre quadrature formula with fifteen nodes is applied. The calculation error is checked by the absolute values of the integration results on each segment. It is quite clear that achievement of the required calculation accuracy at high values of the oscillation parameter by the direct method under consideration is related to large computation time.

The difficulties arising at the calculation of improper integrals from oscillating functions (too large computation time or too low calculation accuracy), can be overcome by improvement of the known quadrature formulae. A rather efficient method of calculation of the Hankel integrals for solving axisymmetric problems, torsion problems, and some three-dimensional boundary problems of theory of elasticity was proposed by Godes and Privarnikov [45]. Similarly to the Filon method for the calculation of sine- and cosine-Fourier transformations, these authors have developed special quadrature formulae with a given absolute error, independent of the oscillation parameter. The experience of numerical calculations ha shown the application of the quadrature formulae proposed in [45] to result in the accuracy not worse than the Gauss method with six nodes, when the integration interval was partitioned for each value of the oscillation parameter into such number of intervals that each of them should contain not more than one extremum point of the integrand function. The time of calculation of integrals using the Gauss method linearly increased with the oscillation parameter, while for the special quadrature formulae it was independent of this parameter. Note that an inconvenience of application of the Godes and Privarnikov quadrature formulae consists in the necessity of a correct preliminary choice of a finite integration interval, large enough for the remainder to be negligible. A method of the Hankel integral calculation based on the same idea was later proposed by Minoru et al. [80]. However, this method implies the use of the Lommel function and the hypergeometrical function what encumbers its computer implementation.

For mass calculations of improper Hankel integrals, arising in the framework of the boundary-element method, we used an effective numerical-and-analytical method, including presentation of the integrals in terms of two components

$$\int_0^{\infty} \frac{N(\alpha)}{D(\alpha)} J_m(\alpha\rho)d\alpha = \int_0^{A} \frac{N(\alpha)}{D(\alpha)} \left(1 - \frac{D(\alpha)}{D_*}\right) J_m(\alpha\rho)d\alpha + \frac{1}{D_*} \int_0^{\infty} N(\alpha) J_m(\alpha\rho)d\alpha \tag{1.135}$$

where D_* is the limiting value of the integrand denominator at $\alpha \to \infty$, A is the finite upper limit when at $\alpha > A$ one can with high accuracy imply that $D(\alpha) \approx D_*$, $m = 0,1$. The first term in Eq. (1.135) is rather effectively estimated on the basis of the adaptive numerical Romberg integration scheme similarly to the way it was done in our earlier paper [11]. The second term is expressed in a closed form, using the formula [49]

$$\int_0^{\infty} \alpha^n e^{-q\alpha} J_m(\alpha\rho)d\alpha = (-1)^n \rho^{-m} \frac{\partial^n}{\partial q^n} \left[\frac{(\sqrt{q^2+\rho^2} - q)^m}{\sqrt{q^2+\rho^2}} \right], q > 0.$$

The upper limit value A is determined for each multilayer system in accordance with the law of the asymptotic behaviour of the integrand denominator. For example, for a concentrated force in an elastic layer the estimation of the approximation of $D(\alpha)$ to D_* has enabled one to assume $A = 10$ with a relative error of $\epsilon = 10^{-6}$ for all Poisson ratio values (Table 1.2).

The proposed approach to the calculation of the two-layer system deformation can be easily generalized for the case of existence of elastic constraints between the

Table 1.2 $D(\alpha)/D_*$ ratio at different values of the transformation parameter α

α	Poisson ratio ν					
	0	0.1	0.2	0.3	0.4	0.5
0.5	2.484227	2.374806	2.279106	2.206273	2.175909	2.238974
1.0	1.649880	1.630448	1.623633	1.637851	1.691125	1.830327
1.5	1.317797	1.323414	1.338315	1.368690	1.427803	1.550136
2.0	1.159071	1.167712	1.182160	1.206285	1.248381	1.330017
2.5	1.078655	1.084944	1.094499	1.109500	1.134612	1.181970
3.0	1.038014	1.041725	1.047148	1.055420	1.068986	1.094199
3.5	1.017935	1.019908	1.022732	1.026972	1.033845	1.046507
4.0	1.008275	1.009259	1.010650	1.012718	1.016045	1.022141
4.5	1.003743	1.004213	1.004871	1.005844	1.007401	1.010243
5.0	1.001665	1.001882	1.002184	1.002629	1.003339	1.004631
5.5	1.000729	1.000827	1.000963	1.001162	1.001479	1.002054
6.0	1.000315	1.000359	1.000418	1.000506	1.000645	1.000897
6.5	1.000135	1.000154	1.000180	1.000218	1.000278	1.000386
7.0	1.000057	1.000065	1.000076	1.000093	1.000118	1.000165
7.5	1.000024	1.000027	1.000032	1.000039	1.000050	1.000069
8.0	1.000010	1.000011	1.000013	1.000016	1.000021	1.000029
8.5	1.000004	1.000005	1.000006	1.000007	1.000009	1.000012
9.0	1.000002	1.000002	1.000002	1.000003	1.000004	1.000005
9.5	1.000001	1.000001	1.000001	1.000001	1.000001	1.000002
10.0	1.000000	1.000000	1.000000	1.000000	1.000001	1.000001

layers in the following way [44]. The k-th and the $(k+1)$-th layers are assumed to be connected by elastic constraints with a coefficient μ_k, i.e. the stresses σ_z, τ_{yz}, τ_{xz} and vertical displacements W on their common boundary coincide, and

$$u_j^{(k+1)}(x,y,0) - u_j^{(k)}(x,y,h_k) = \frac{1-\nu_k}{G_k}\mu_k \tau_{jz}^{(k)}(x,y,h_k)$$

where ν_k is the Poisson ratio of the k-th layer, $j = x,y$. At $\mu_k = 0$ the case of the half-space cohesion is obtained, at $\mu_k \to \infty$ the layers can slide without friction along their common boundary. Thus, the boundary conditions of conjugation of the contacting layers in the matrix form are given by

$$\begin{pmatrix} \sigma_z^{(k+1)} \\ \tau_{xz}^{(k+1)} \\ \tau_{yz}^{(k+1)} \\ u_x^{(k+1)} \\ u_y^{(k+1)} \\ u_z^{(k+1)} \end{pmatrix} \begin{pmatrix} 1 & 0 & 0 & 0 & 0 & 0 \\ 0 & 1 & 0 & 0 & 0 & 0 \\ 0 & 0 & 1 & 0 & 0 & 0 \\ 0 & \psi_k & 0 & 1 & 0 & 0 \\ 0 & 0 & \psi_k & 0 & 1 & 0 \\ 0 & 0 & 0 & 0 & 0 & 1 \end{pmatrix} \begin{pmatrix} \sigma_z^{(k)} \\ \tau_{xz}^{(k)} \\ \tau_{yz}^{(k)} \\ u_x^{(k)} \\ u_y^{(k)} \\ u_z^{(k)} \end{pmatrix} \tag{1.136}$$

where $\Psi_k = (1-\nu_k)\mu_k/G_k$. The limiting cases of such conditions of the simultaneous layer deformation are full cohesion and smooth contact.

Application of the contact conditions of a general type (1.136) enables one to model the phenomena of interaction at the layer boundaries, encountered in practice. For example for a soil with an underlayer of a rigid base of a rock type, it is quite natural to assume the condition of full cohesion ($\mu_k = 0$) at moderate loads. A smooth contact (zero tangential stress, $\mu_k = \infty$) is characteristic, e.g., for the boundary between the thawed frozen soil when there is a water-saturated interlayer, eliminating friction between the layers. It is quite clear that this case is characterized by minimal mathematical difficulties. Intermediate cases ($0<\mu_k<\infty$) can be accomplished when artificial bases are constructed using modern geosynthetic materials, accepting considerable tensile forces even at small elongation: geogrids, geotextiles (fabrics and grids), applied for the separation and binding of layers, drainage in ground and hydrotechnical engineering, reinforcement of asphalt concrete road pavement, etc.

Thus, using the two-dimensional Fourier transformation, a numerical-and-analytical method of construction of fundamental solutions of spatial problems of theory of elasticity for multilayer bases without any restrictions on the layer thicknesses and elastic parameters has been developed. The method includes the effective procedure of calculation of improper Hankel integrals with exponentially decaying kernels. The obtained results enable three-dimensional contact problems for complex-shaped structures, deepened into spatially nonhomogeneous (layered) soils to be solved within the numerical algorithm of the boundary-element method.

Based on the solutions, developed for the layered linearly deformable half-space, numerical modelling of spatial contact interaction of soil bases with drop caissons of bridge piers was performed [10]. Attempts to solve such problems had been made earlier in a number of studies where the interaction of the foundation with a multilayer base was modelled by Winkler constraints. Such solutions do not take into account the distributive ability of the soil base and interaction of the layers with each other: the rigidity of the constraints on the contact surface is determined by a rough indirect method. The noted shortcomings were overcome when the model of elastic layered media, more adequate to the nature, was applied. To estimate the possibilities and advantages of the proposed method of calculation of drop caissons based on the base deformations, the examples of deepened foundation structures, penetrating through the layers of sand loam, dense fine sand, and low-plasticity clay, were considered. The proposed fundamental solutions are shown to give more reliable predictions of interaction of the drop caissons with the layered bases in comparison with the methods, using the Winkler model of the soil.

1.5 Elastic Bases with the Deformation Modulus, Variable with Depth

In the literature in mechanics of deformable solids a number of dependences are quoted for the account of spatial nonuniformity of mechanical properties of various type [4, 13, 23, 24, 26, 46, 58, 59, 67, 74, 75, 88, 93, 98, 101–104, 107, 108, 118, 120, 137–139]. An important geotechnical problem consists in the determination of the stress-strained state in an elastic nonhomogeneous half-space whose modulus of deformation (or shear modulus, at a constant Poisson ratio) is varied with depth [2, 16, 21, 22, 35, 56, 42, 57, 62, 65, 76, 81, 84–86, 113, 114, 119, 121, 125–127, 142, 155, 157]. This problem is most successfully solved on the basis of development of contact models of the soil base of natural bedding. A review of publications on the problem of application of theory of elasticity of nonhomogeneous media for solving contact problems for a half-space, when the elastic parameters are functions of the spatial parameters, was recently performed by Selvadurai [126]. As follows from a number of studies, the contact model of the elastic base in the form of a nonhomogeneous half-space with a deformation modulus, regularly increasing with depth, describes the deformational properties of real bases more exactly than widely applied base models in the form of a homogeneous elastic half-space of a finite-thickness layer and, hence, it corresponds better to the mechanism of contact interaction of soil bases and foundation structures.

1.5.1 Variation of Deformation Modulus with Depth

As a result of processing of the experimental data, obtained at static tests, performed on the base surface, an average value of the deformation modulus E of the punch

base active area is determined, its value being usually smaller than for the deeper layers of the soil. Simultaneously, the available experimental data on the soil mass deformability give the evidence for a regular increase of the deformation modulus with depth and show a noticeable increase of the soil deformability at open surfaces in underground workings. Thus, the average constant value of E, obtained from the measurements of displacements of test site surface, based on the solutions of theory of elasticity for a homogeneous half-space, is rather approximate and does not enable the real properties of soil bases to be characterized with the required reliability. Besides, its value will evidently be lower than the real one since the major part of the punch base corresponds to the loss of strength area.

In the simplest case, the dependence of the deformation modulus on depth is determined, using flexible punches, from the measurement of the test site surface in the direction of the load application in 15–20 points. In this case the solution of the problem of theory of elasticity regarding a homogeneous elastic half-space or a homogeneous limited-thickness layer under a uniform load [121].

A rather pronounced increase of the deformation modulus with deepening into the mass soil arises due to the pressure of the upper layers of the soil onto the lower ones, the stressed state due to the surface load as well as natural bedding of the mass soil itself and is experimentally confirmed in a number of studies. The form of the $E(z)$ dependence is determined for specific engineering-and-geological conditions and is specific for soils of various type. Empirical parameters, characterizing the base nonhomogeneity, can be obtained at standard soil tests in a well at various depth or from field experiments using punches of various bearing area [35].

In the literature, the main attention was paid to the $E(z)$ dependences, enabling the exact solutions of contact problems to be obtained for punches of canonical shape. The account of the experimental data for the deformational characteristics at the natural bedding of the soil mass by the $E(z)$ dependence itself was not sufficiently correct. The most known is [4, 16, 21, 22, 62, 81, 84, 108, 113, 119, 120] the model of a nonhomogeneous half-space with the deformation modulus, increasing according to the power law

$$E(z) = E_0 \cdot z^n; \tag{1.137}$$

$$E_0, n - \text{const.}$$

Evidently, in this case the results of calculation, using the corresponding influence functions, are hardly suitable for practice since the deformation modulus tends to zero at the daylight surface. References [14, 35, 56, 57, 67, 76, 85, 102, 142] employed more realistic dependences (Fig. 1.17), taking into account the nonzero deformation modulus value $E(0) = E_0 \neq 0$ on the half-space surface

$$E(z) = E_0 + E_n \cdot z^n, \tag{1.138}$$

$$E(z) = E_0(1 + k \cdot z)^b, \tag{1.139}$$

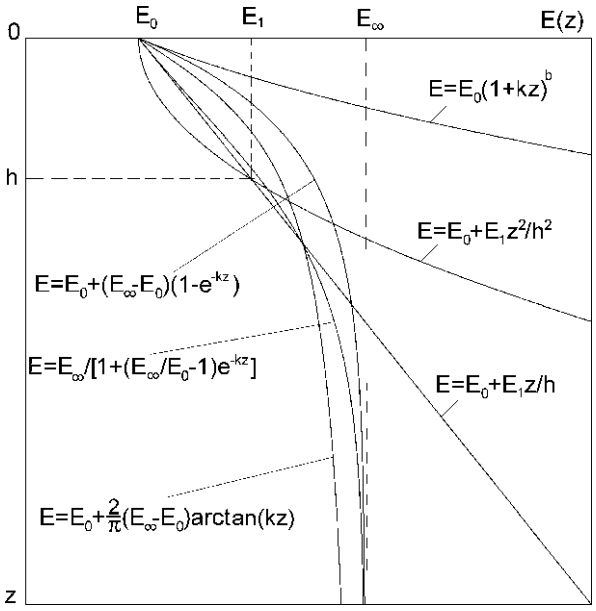

Fig. 1.17 Various laws of deformation modulus increase with depth

$$E(z) = E_0 \cdot e^{kz} \tag{1.140}$$

where E_n, n, b, and k are empirical parameters, characterizing the variation of the soil properties with depth.

Though for Eqs. (1.138), (1.139), and (1.140) the exception $E(0) = 0$ does not hold (like it was for Eq. (1.137)), still these dependences (1.138), (1.139), and (1.140) are not free from disadvantages. The use of the influence functions, found for Eqs. (1.138) and (1.139), is limited due to the "rigid" relationship of the n and b parameters with the Poisson ratio value for the soil. The dependences (1.138), (1.139), and (1.140) have one more common shortcoming revealed in an unlimited growth of the deformation modulus with the base depth increase. This fact contradicts with the field observation data [125], which indicate a characteristic stabilization of the deformation modulus with the increase of the compressed base thickness (depth), when, with the increase of natural stress and the decrease of the soil jointing, soil and rock properties are converging to those of a homogeneous linearly deformable medium. Therefore, increasingly important for practical purposes becomes the development of influence functions (solution of the Boussinesq problem), in case dependences of a more general form being used [86, 114, 125, 126, 155, 157]

$$E = E(z,E_0,E_\infty,n,k,a,b,...), \tag{1.141}$$

taking into account the realistic variation of the deformation modulus with depth due to the intrinsic weight of the soil, history of the layer formation, distribution of water, etc.

Below we consider contact models of a nonhomogeneous elastic half-space whose deformation modulus increases with depth according to the dependences of a rather general form. It is admissible to assume the Poisson ratio for soils to be constant since its value varies insignificantly and makes no essential effect on the stress-strained state characteristics. Taking into account the known relationship between the elastic constants $G = E/2(1+\nu)$, at such consideration the shear modulus $G = G(z)$ will also be variable with depth.

1.5.2 Normal Concentrated Force Acting on the Half-Space Surface

Let a concentrated force P act orthogonally to the plane $z = 0$ of a nonhomogeneous half-space along the z axis, directed inside the half-space (Fig. 1.18). Let the origin of a cylindrical (r,ϕ,z) and a spherical (R,Θ,Ψ) coordinate systems be put in the point O of the force application. Due to the axial symmetry of the problem, similarly to the case of a homogeneous half-space, let the following distribution of radial displacements be assumed:

$$u_R = \frac{D \cdot \cos\theta}{R} \tag{1.142}$$

where θ is the angle, counted from the z axis, $0 \le \theta \le \pi/2$. For the radial deformations ϵ_R and stresses σ_R

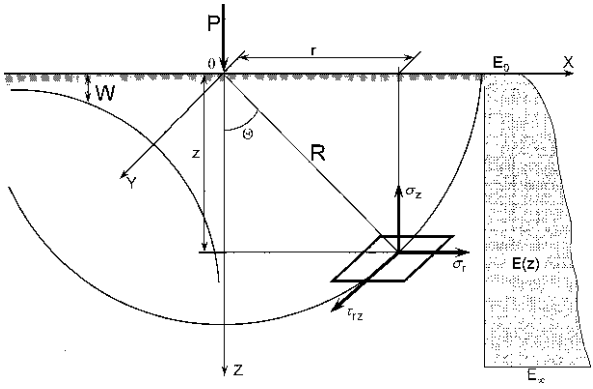

Fig. 1.18 Calculation scheme to the problem of a concentrated force acting on a nonhomogeneous elastic half-space

$$\varepsilon_R = -\frac{D \cdot \cos\theta}{R^2}, \sigma_R = E(z) \cdot \varepsilon_R = -E(z)\frac{D \cdot \cos\theta}{R^2}. \tag{1.143}$$

Using the formulae for a transition to the cylindrical coordinates, one obtains

$$\sigma_z = \sigma_R \cos^2\theta. \tag{1.144}$$

Since (See Fig. 1.18)

$$\cos\theta = \frac{z}{R}, R = \sqrt{z^2 + r^2},$$

then

$$\sigma_R = -E(z) \cdot \frac{D \cdot z}{R^3}, \tag{1.145}$$

$$\sigma_z = -E(z) \cdot \frac{D \cdot z^3}{R^5}. \tag{1.146}$$

The factor D, contained in Eqs. (1.143), (1.145), and (1.146), can be determined from the equilibrium equation of a hemisphere, cut out in the vicinity of the point O of application of the force P, by collecting the pressures from the surface of this hemisphere

$$P + \int\limits_S \int \sigma_R \cdot \cos\theta dS = 0,$$

or, in an extended notation,

$$P + \int\limits_0^{2\pi} d\varphi \int\limits_0^{\pi/2} \sigma_R \cdot \cos\theta \cdot R^2 \cdot \sin\theta \cdot d\theta = 0.$$

Taking into account Eq. (1.145), for the constant D one can obtain

$$D = \frac{P}{2\pi \int\limits_0^1 E(Rt)t^2 dt}. \tag{1.147}$$

At $E = E_0 = \text{const}$, Eq. (1.147) takes the form of the known Boussinesq solution [17]:

$$D = \frac{3P}{2\pi E_0}.$$

Using Eqs. (1.146) and (1.147) with the account of transformation of stress into the cylindrical coordinate system, the vertical stress σ_z is given by

$$\sigma_z = -\frac{P \cdot E(z)}{2\pi \int\limits_0^1 E(Rt)t^2 dt} \cdot \frac{z^3}{R^5}. \tag{1.148}$$

Hence, as should be expected, at $E(z) = E_0 = \text{const}$ the known Bousinesq formula for compressive stress in a homogeneous half-space is obtained:

$$\sigma_z = -\frac{3P}{2\pi} \cdot \frac{z^3}{R^5}. \tag{1.149}$$

In order to determine the spatial stress-strained state of the nonhomogeneous elastic base, at first the vertical deformation should be found, using the Hooke's law:

$$\varepsilon_z = \frac{1}{E(z)} \left[\sigma_z - \nu(\sigma_x + \sigma_y)\right], \tag{1.150}$$

or, in case of an axisymmetric stress-strained state,

$$\varepsilon_z = \frac{1}{E(z)} \left[\sigma_z - \nu(\sigma_r + \sigma_\varphi)\right]. \tag{1.151}$$

Since the distributions of the σ_r and σ_ϕ stresses in the nonhomogeneous half-space are unknown, we take advantage of the semi-inverse method, assuming the hypotheses for the distribution of σ_r and σ_ϕ (or σ_x and σ_y). Following [142], we make the simplest assumption of proportionality of the normal stresses:

$$\sigma_r - \sigma_z, \quad \sigma_\varphi - \sigma_z. \tag{1.152}$$

Then

$$\varepsilon_z = \frac{\gamma}{E(z)}\sigma_z = -\frac{P \cdot \gamma}{2\pi \int\limits_0^1 E(Rt)t^2 dt} \cdot \frac{z^3}{R^5} = -\frac{P \cdot \gamma}{2\pi \cdot e(R)} \cdot \frac{z^3}{R^5} \tag{1.153}$$

where γ is an indefinite coefficient and a notation is introduced:

$$e(R) = \int\limits_0^1 E(Rt)t^2 dt. \tag{1.154}$$

The function $e(R)$ characterizes the degree of the elastic base nonhomogeneity due to the deformation modulus variation with depth.

Now, using the expression for the vertical deformation

$$\varepsilon_z = \frac{dw}{dz},$$

one can easily find settlements (vertical displacements) depending on the depth z:

$$w(r,z) = \frac{P \cdot \gamma}{2\pi} \int_z^\infty \frac{\varsigma^3 d\varsigma}{e(R) \cdot R^5}. \tag{1.155}$$

The proportionality coefficient γ can be easily determined from the comparison (at any depth) of w values, obtained from Eq. (1.155) and for the case of the homogeneous half-space ($E(z) = E_0 = \text{const}$). Since on the surface $z = 0$ of the homogeneous half-space

$$w_0 = \frac{(1-\nu^2) \cdot P}{\pi \cdot E_0} \cdot \frac{1}{r}, r = \sqrt{x^2 + y^2}, \tag{1.156}$$

and the integral value

$$\int_0^\infty \frac{z^3 dz}{R^5} = \frac{2}{3} \cdot \frac{1}{r}, \tag{1.157}$$

and taking into account that

$$e(R) = \int_0^1 E_0 t^2 dt = \frac{E_0}{3}, \tag{1.158}$$

one obtains for the indefinite factor $\gamma = 1-\nu^2$. Thus, Eq. (1.155) is obtained on the basis of the hypothesis

$$\sigma_r = \sigma_\varphi = 0.5\nu \cdot \sigma_z \tag{1.159}$$

which is in agreement with the assumption of Eq. (1.152) used earlier [142]. As seen from Eq. (1.159), according to the assumed hypothesis, vertical stresses in the nonhomogeneous half-space are distributed in the horizontal plane in accordance with the Poisson's law in equal ratios both in radial and tangential directions. Let us find other components of the stress-strained state.

In a cylindrical coordinate system tangential stress τ_{rz} is given by [17]

$$\tau_{rz} = \frac{1}{2}\sigma_R \sin 2\theta.$$

Since in our case

$$\cos\theta = \frac{z}{R},\ \sin\theta = \frac{r}{R},\ \frac{1}{2}\sin 2\theta = \frac{rz}{R^2},\ R = \sqrt{z^2 + r^2},$$

then

$$\tau_{rz} = -\frac{P}{2\pi} \cdot \frac{E(z)}{e(R)} \cdot \frac{z^2 \cdot r}{R^5}. \tag{1.160}$$

For the normal stresses σ_r and σ_ϕ (or σ_x and σ_y), according to Eqs. (1.148) and (1.159), one obtains

$$\sigma_r = \sigma_\varphi = \frac{\nu}{2}\sigma_z = -\frac{P}{4\pi} \cdot \frac{E(z)}{e(R)} \cdot \frac{z^3}{R^5}. \tag{1.161}$$

The radial displacement u_r is found, using the dependence

$$\varepsilon_\varphi = \frac{u_r}{r}$$

where

$$\varepsilon_\varphi = \frac{1}{E(z)}\left[\sigma_\varphi - \nu(\sigma_r + \sigma_z)\right].$$

In our case, with the account of Eq. (1.161),

$$u_r = \frac{\nu(1+\nu)P}{4\pi \cdot e(R)} \cdot \frac{rz^3}{R^5}. \tag{1.162}$$

At $R \to \infty$, as should be expected, $u_r \to 0$.

Finally, we calculate the stressed state dilatation in the half-space due to the force P:

$$\varepsilon_V^{(3)} = \frac{1-\nu}{E(z)}\left[\sigma_z + \sigma_\varphi + \sigma_r\right] = -\frac{(1-2\nu)(1+\nu)P}{2\pi \cdot e(R)} \cdot \frac{z^3}{R^5}. \tag{1.163}$$

Now, if necessary, one can easily obtain the six components of stress and three components of displacement in the Cartesian coordinate system. If the cylindrical coordinate system is converted to a Cartesian coordinate system, the stress components σ_r, σ_ϕ, τ_{rz} will be converted to the components σ_x, σ_y, τ_{xy}, τ_{yz}, τ_{zx} as follows:

$$\begin{cases} \sigma_x = \sigma_r \cdot \cos^2 \varphi + \sigma_\varphi \cdot \sin^2 \varphi, \\ \sigma_y = \sigma_r \cdot \sin^2 \varphi + \sigma_\varphi \cdot \cos^2 \varphi, \\ \tau_{xy} = (\sigma_r - \sigma_\varphi) \cdot \sin^2 \varphi / 2, \\ \tau_{zx} = \tau_{rz} \cdot \cos \varphi, \\ \tau_{yz} = \tau_{rz} \cdot \sin \varphi. \end{cases} \tag{1.164}$$

The displacements u, v in the x and y directions, respectively, are expressed in terms of the radial displacement u_r:

$$u = u_r \cdot \cos \varphi, \, v = u_r \cdot \sin \varphi. \tag{1.165}$$

The vertical stresses σ_x and displacements w are not converted and are found, using Eqs. (1.148) and (1.155) at $\gamma = 1 - \nu^2$. For Eqs. (1.164) and (1.165) one should use the known transformation formulae

$$x = r \cdot \cos \varphi, \, y = r \cdot \sin \varphi;$$

$$\cos 2\varphi = 1 - 2 \cdot \frac{y^2}{r^2} = \frac{x^2 - y^2}{r^2}, \; \sin 2\varphi = \frac{2xy}{r^2}.$$

As one can see, the consideration of the proposed nonhomogeneous base model results in formulae whose structure is similar to those of classical theory of elasticity. Simultaneously, one should expect that the predictions of the nonhomogeneous base model, using Eqs. (1.155), (1.160)–(1.166), will be closer to the characteristics of real soil bases. In particular, the experimental data show that the distributive properties (the ability of distribution of a vertical load in the horizontal direction) of a homogeneous elastic base are exaggerated [47, 48]. As shown in the subsequent section, the application of the nonhomogeneous base calculation models considered here, results in a reduction of the base distributive ability and, consequently, a decrease of the calculation forces for design of shallow foundation structures of beam or plate type on elastic bases.

1.5.3 Settlement of a Nonhomogeneous Half-Space Surface

For solution of practical geotechnical problems the most interesting is calculation of vertical displacements (settlements) of the soil base surface. For the model of a nonhomogeneous elastic half-space under consideration, when the modulus of elasticity is a given function of depth $E = E(z)$, according to Eqs. (1.154) and (1.155) one obtains

$$w\,|_{z=0} = w(r) = \frac{(1-\nu^2)\cdot P}{2\pi}\int\limits_0^\infty \frac{z^3 dz}{e(R)\cdot R^5}. \tag{1.166}$$

Here $e(R) = \int\limits_0^1 E(Rt)t^2 dt$ is the function of the nonhomogeneity degree.

First consider the cases of linear and square nonlinearities (Fig. 1.17), proposed to be taken into account by Snitko [142]. He gave some estimations of the nonhomogeneous half-space surface settlements when the deformation modulus increases with depth according to a linear or a parabolic law. Even rather rough estimations for such cases of nonhomogeneity show much lower distributive ability of the soil than for the homogeneous half-space model, what is important to be taken into account at the design and calculation of foundation structures. However, no formulae were given in [142] for the influence functions which enable the mixed (contact) problems of theory of elasticity to be reduced to boundary integral equations and numerical methods to be applied for solving spatial problems of soil mechanics, first of all, for the calculation of contact stresses and settlements for foundation structures of given geometry. Note also that the knowledge of the influence functions in the explicit form is important since it enables not only more effective numerical algorithms to be constructed, but also the applicability of an influence function to be evaluated qualitatively in view of the account of the nonhomogeneity characteristics.

Linear law of the deformation modulus increase. Let the soil deformation modulus vary with depth according to a linear law

$$E(z) = E_0 + \alpha\cdot z = E_0 + \frac{E_1 - E_0}{h}\cdot z = E_0\left(1 + B\frac{z}{h}\right) \tag{1.167}$$

where E_0 is the deformation modulus value at the soil daylight surface, E_∞ is its value at the depth $z = h$, $B = (E_1–E_0)/E_0$

In the case under consideration.

$$e(R) = \int\limits_0^1 e(Rt)t^2 dt = \int\limits_0^1 (E_0 + \alpha Rt)\cdot t^2 dt = \frac{E_0}{3} + \frac{\alpha R}{4}, \tag{1.168}$$

and the integral (1.166) after rather cumbersome transformations can be calculated in the finite form, and the following expression for the settlement of the daylight surface is obtained:

$$w|_{z=0} = w(r) = \frac{2(1-\nu^2)P}{\pi}\int\limits_0^\infty \frac{z^3 dz}{\left(\frac{4}{3}E_0 + \alpha R\right)\cdot R^5} = \frac{(1-\nu^2)\cdot P}{\pi\cdot E_0}\cdot\frac{1}{r} + \\ + \frac{(1-\nu^2)\cdot P}{\pi\cdot E_0 h}\cdot\frac{B}{A^2}\left[\frac{1}{2} - \frac{B\cdot r}{A\cdot h} + \left(1 - \frac{B^2\cdot r^2}{A^2\cdot h^2}\right)\ln\frac{B\cdot r}{B\cdot r + A\cdot h}\right] \tag{1.169}$$

where for the sake of simplicity a notation $A = 4/3$ is introduced.

If dimensionless settlements

$$V = \frac{w}{w^*}, w^* = \frac{(1-\nu^2)\cdot P}{\pi \cdot E_0 \cdot h} \tag{1.170}$$

and distance

$$\tilde{r} = \frac{r}{h} = \sqrt{\left(\frac{x}{h}\right)^2 + \left(\frac{y}{h}\right)^2} \tag{1.171}$$

are introduced, then Eq. (1.169) can be written in a more convenient form

$$V = \frac{1}{\tilde{r}} + \frac{B}{A^2}\left[\frac{1}{2} - \frac{B\cdot\tilde{r}}{A} + \left(1 - \frac{B^2\cdot\tilde{r}^2}{A^2}\right)\ln\frac{B\cdot\tilde{r}}{B\cdot\tilde{r}+A}\right]. \tag{1.172}$$

It is easily seen that the first terms in Eqs. (1.169) and (1.172) are the Boussinesq solutions for a homogeneous elastic half-space, to which the obtained solution is reduced at $B \to 0$.

Parabolic law of the deformation modulus increase. Dependence of the deformation modulus on depth is given by

$$E(z) = E_0 + \beta \cdot z^2 = E_0\left(1 + B\frac{z^2}{h^2}\right) \tag{1.173}$$

where the notation $B = (E_1 – E_0)/E_0$ is still used for the deformation modulus relative variation with depth. Then consecutively calculate

$$e(R) = \int_0^1 E(Rt)t^2 dt = \int_0^1 (E_0 + \beta R^2 t^2)\cdot t^2 dt = \frac{E_0}{3} + \frac{\beta R^2}{5}, \tag{1.174}$$

$$w|_{z=0} = w(r) = \frac{3(1-\nu^2)P}{2\pi}\int_0^\infty \frac{z^3 dz}{\left(E_0 + \frac{3}{5}\beta R^2\right)\cdot R^5}. \tag{1.175}$$

The latter improper integral after rather cumbersome transformations is reduced to a set of elementary functions, and Eq. (1.175) for the settlement of a nonhomogeneous elastic half-space in the dimensionless form is given by

$$V = \frac{1}{\tilde{r}} + \frac{3C}{2}\left[C\cdot\tilde{r} - (1 + C^2\cdot\tilde{r}^2)\cdot \operatorname{arccot}(C\cdot\tilde{r})\right], C = \sqrt{0.6B}. \tag{1.176}$$

Comparative calculations of the settlements of a nonhomogeneous half-space surface for the cases of linear and square increase of the deformation modulus with

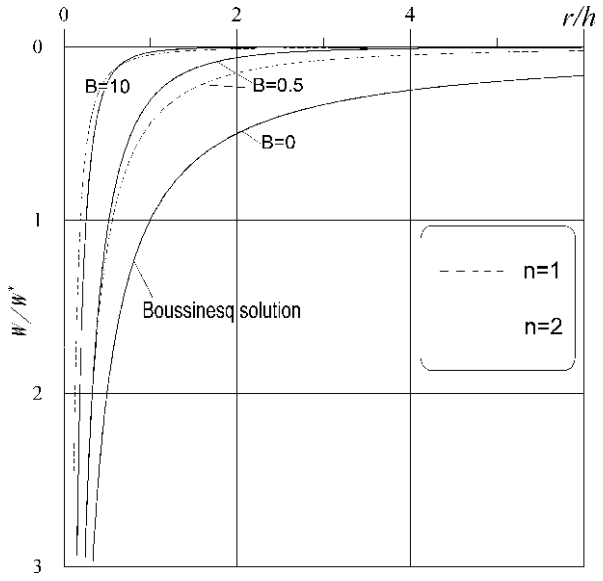

Fig. 1.19 Settlements of the surface of elastic bases with linear ($n = 1$) and parabolic ($n = 2$) nonuniformities due to a vertical concentrated force

depth are presented in Fig. 1.19. The same figure shows the settlements plotted versus the distance from the point of application of the concentrated force P for a homogeneous half-space (the Boussinesq solution). As one can see, with the increase of the B parameter, characterizing the degree of the soil base nonhomogeneity with depth, higher concentration of stresses occurs and the distributive ability of the soil is revealed to a lower extent. Simultaneously, with the increase of the B parameter, characterizing the rate of the deformation modulus increase with depth, the difference in the soil surface settlements for the linear and square variation law becomes less significant. At B>20 the surface deflections resemble the Dirac δ-function and the nonhomogeneous base contact models (1.172) and (1.176) approach the Winkler type model.

Note that the direct application of Eq. (1.176) is rather complicated for calculations. This is related to the specific features of computer arithmetic in case of multiplication of factors of essentially different orders of magnitude. The experience of numerical calculations has shown that with the increase of the B parameter, direct calculations using Eq. (1.176) at $C\tilde{r} > 5$, due to the loss of accuracy, result in negative deflections. A detailed analysis has shown that even double precision in using standard computer mathematical procedures cannot overcome the errors arising at the calculation of a term, containing an inverse trigonometric function. The problem could be solved only by application of a special subroutine for the calculation of $y = \arctan x$ function for x>1, using a power series [49]

$$\arctan x = \frac{\pi}{2} - \frac{1}{x} + \frac{1}{3x^3} - \frac{1}{5x^5} + \ldots = \frac{\pi}{2} - \sum_{k=0}^{\infty} \frac{(-1)^k}{(2k+1)\,x^{2k+1}}, x > 1. \quad (1.177)$$

Application of not more than 50 terms of the series (1.177) provided the correct calculation of settlements, using Eq. (1.176) for all $C\tilde{r}$>1 with the guaranteed accuracy.

Note the character of the asymptotic behaviour of the solutions found at $r \to 0$ and $r \to \infty$.

Using the known expansions of elementary functions, contained in Eqs. (1.172) and (1.176) into power series, one obtains

$$w \approx \frac{1-\nu^2}{\pi E_0} \cdot \frac{1}{r} + O(r^{-1}),\ r \to 0 \quad (1.178)$$

where O is the Landau order symbol. Consequently, at variable modulus of elasticity, the settlements due to a normal concentrated force have the same singularity in the point $r = 0$, as in the case of a homogeneous half-space with the modulus of elasticity E_0. In other words, near the concentrated force application point the surface settlements do not undergo any influence of variation of the base mechanical properties with depth.

Let us estimate the character of the displacement decay with the increasing distance from the concentrated force application point. We take the advantage of asymptotic expressions, following from Eqs. (1.172) and (1.176) at $r \to \infty$:

$$V \approx \frac{1}{2\tilde{r}} (n = 1), \tilde{r} >> \frac{4}{3} \cdot \frac{1}{B}; \quad (1.179)$$

$$V \approx \frac{1}{3B} \cdot \frac{1}{\tilde{r}^3} (n = 2), \tilde{r}^2 >> \frac{5}{3} \cdot \frac{1}{B}. \quad (1.180)$$

As seen from Eqs. (1.179) and (1.180), with the increase of the degree of nonuniformity of mechanical properties (i.e. with the increase of the n parameter) an increase of the rate of the settlement decrease with the distance from the concentrated force application point is observed. For the linear law of the deformation modulus increase ($n = 1$) the surface settlements far from the concentrated force application point are exactly twice smaller than for the homogeneous half-space. Simultaneously, it follows from Eq. (1.180) that at the square law of the deformation modulus increase ($n = 2$) this decrease rate also increases with the nonhomogeneity parameter B.

General power laws of increase of the deformation modulus. In Refs. [35, 56] a base model is considered with the deformation modulus, varied according to the law

$$E(z) = E_0 + E_n \cdot z^n,\ n \geq 0 \quad (1.181)$$

where E_0 is the deformation modulus under the foundation bottom. The book [35] also suggests possible methods for determination of the empirical parameters in Eq. (1.181) using punch test data or well measurements.

It is difficult to find the soil base displacements in a closed analytical form according to Eq. (1.166) in the case of the law of Eq. (1.181). Barvashov [14] obtained an expression for the influence function of integral type, corresponding to Eq. (1.181) in a simplifying assumption of the soil base being presented by a parallel combination of a homogeneous half-space with the deformation modulus E_0 and a half-space, for which the deformation modulus varies with depth according to the law $E_n \cdot z^n$. In order to obtain a more simple and explicit formula for the calculation of the nonhomogeneous base settlements, it is convenient to apply the following engineering approach [35].

For the nonhomogeneous soil base model, when $E(z) = E_n \cdot z^n$, in [4] the vertical displacements of points in the half-space, loaded normally by a concentrated force, applied to the surface, were obtained in the form

$$w_n = \frac{(1+\nu)\cdot P}{E_n \cdot R^{n+1}} \sum_{m=0}^{\infty} A_m \left[\frac{(1-\nu)(m+n+1)m}{(m+n)(n+1)} + \frac{z^2}{R^2} \right] \cdot \left(\frac{z}{R} \right)^{m-1} \tag{1.182}$$

where

$$R = \sqrt{x^2+y^2+z^2}, A_m = \frac{c_0 a_m \Gamma\left(\frac{m+n+2}{2} \right)}{2\sqrt{\pi}\,\Gamma\left(\frac{m+n+3}{2} \right)}, \quad m = 0,1,2,\ldots,$$

$$a_0 = \cos\frac{\pi q}{2}, \quad a_1 = q \cdot \sin\frac{\pi q}{2}, \quad a_m = \frac{p^2 - q^2}{m(m-1)} a_{m-2}, \quad m \geq 2;$$

$p = m-1$, if m is odd, $p = m-2$, if m is even;

$$q = \sqrt{(1+n)(1-n\nu/(1-\nu))}, \quad 0 < n < 1;$$

$$C_0 = \frac{2^{n+3}}{4\pi\,\Gamma(n+2)} \Gamma\left(\frac{n+3+q}{2} \right) \cdot \Gamma\left(\frac{n+3-q}{2} \right),$$

$\Gamma(x)$ is a gamma function.

The series of Eq. (1.182) converges everywhere, except $R = 0$. At $n = 0$, i.e. in the case of a half-space with a constant deformation modulus, the known Boussinesq solution is obtained:

$$w_0 = \frac{P(1+\nu)}{2\pi E_0} \cdot \left[\frac{z^2}{R^3} + \frac{2(1-\nu)}{R} \right].$$

Then the solution (1.182) is used to find the base settlements at $E(z)=E_0+E_n \cdot z^n$ in the following way [35]. The nonhomogeneous half-space is nominally partitioned into a homogeneous half-space with the deformation modulus E and a nonhomogeneous half-space with the deformation modulus $E_n \cdot z^n$. If the fraction of the entire force, accepted by the homogeneous half-space is denoted as λ, then the fraction of the entire force, accepted by the half-space with the deformation modulus, increasing as $E_n \cdot z^n$, will be $(1-\lambda)$. At such consideration, the displacements of any point of the nominally homogeneous half-space will be given by

$$w = \lambda \cdot w_0. \tag{1.183}$$

The displacement of the same point due to the force under consideration, corresponding to the nominal half-space with the variable deformation modulus, should then be assumed

$$w = (1 - \lambda) w_n. \tag{1.184}$$

Since the components, nominally comprising the half-space, should be presented as functioning together, one should equalize the right-hand parts of Eqs. (1.183) and (1.184), i.e. assume

$$\lambda w_0 = (1 - \lambda) w_n.$$

After simple transformations the unknown factor is found:

$$\lambda = 1/\left[\frac{(E_n/E_0)(z^2 R^{n-2} + 2R^n(1-\nu))}{2\pi \sum\limits_{m=0}^{\infty} A_m \left[\frac{(1-\nu)(m+n+1)m}{(m+n)(n+1)} + \frac{z^2}{R^2} \right] \cdot \left(\frac{z}{R} \right)^{m-1}} + 1 \right], \tag{1.185}$$

and then from Eq. (1.183) the sought displacement for the half-space with the deformation modulus, varied according to the power law (1.181), is determined:

$$w = \frac{P(1+\nu)\left[\frac{z^2}{R^3} + \frac{2(1-\nu)}{R} \right]}{\frac{E_n \left(z^2 R^{n-2} + 2R^n (1-\nu) \right)}{\sum\limits_{m=0}^{\infty} A_m \left[\frac{(1-\nu)(m+n+1)m}{(m+n)(n+1)} + \frac{z^2}{R^2} \right] \cdot \left(\frac{z}{R} \right)^{m-1}} + 2\pi E_0}. \tag{1.186}$$

For the vertical displacements of points on the half-space surface ($z = 0$) Eq. (1.186) is considerably simplified and at $n > 0$ is given by

$$w = \frac{P(1-\nu^2)}{\pi E_0 r} \cdot \frac{1}{\left[\frac{2(1-\nu)}{\beta} \cdot \frac{E_n}{E_0} \cdot r^n + 1\right]} \tag{1.187}$$

Where

$$\beta = \frac{C_0\sqrt{\pi}(1-\nu)\Gamma\left(\frac{n+1}{2}\right)}{(n+1)\Gamma\left(\frac{n+2}{2}\right)} \cdot q \cdot \sin\frac{\pi q}{2}, r = \sqrt{x^2+y^2}.$$

According to Klein and Durayev [56], the settlements of a half-space with a deformation modulus, increasing with depth according to the law of Eq. (1.181), can be found, using the following formula

$$w = \frac{P(1-\nu^2)}{\pi r E_0} \cdot \frac{1}{\left[\frac{2(1-\nu^2)(1+n)}{(3+n)(1-\nu-n\nu)} \cdot \frac{E_n}{E_0} \cdot r^n + 1\right]}. \tag{1.188}$$

This formula is obtained, based on an assumption of a relationship between the Poisson ratio ν and the power index n being fulfilled:

$$(2+n) \cdot \nu = 1. \tag{1.189}$$

In case this condition being not obeyed, Eq. (1.188) becomes theoretically unreasonable. Comparison of the displacements, calculated according to Eqs. (1.187) and (1.188), performed in [35] as well as our calculations show that the settlement values are sufficiently close, but not identical at $(2+n)\cdot\nu = 1$. Difference between the settlements, calculated according to these formulae depending on ν at $(2+n)\cdot\nu \neq 1$, can be quite essential, e.g.
at $\nu = 0.27$; $n = 0.4$–16%,
at $\nu = 0.42$; $n = 1.3$–29%.

Therefore, Eq. (1.187) is more suitable for practical application, since it is not related to the requirement of the condition of Eq. (1.189) to be fulfilled. The comparative calculations performed for the nonuniformity model of Eq. (1.181) according to Eqs. (1.172), (1.176), (1.187), and (1.188) at $n = 1, 2$ have shown that the most decisive effect on the settlements is made by the deformation modulus variation rate with depth: at fixed values of B, n, and ν the difference in the calculated settlement values did not exceed 1.5%. Therefore, when the deformation modulus variation law (1.181) is used, for significant simplification of the calculations the application of Eq. (1.188) is justified, since it will fully meet the accuracy requirements for practical application.

Plevako [102] has emphasized physical irreality of a medium with the deformation modulus varying according to the power law (1.137) and studied the stress-strained state of a half-space with the elasticity modulus as a function of z-coordinate given by

$$E(z) = E_0(1 + k \cdot z)^b, \tag{1.190}$$

and a constant Poisson ratio. The conditions, at which the common solution of the flat, axisymmetric, and spatial problems of theory of elasticity can be expressed in terms of harmonic functions, were found. The corresponding values of the Poisson ratio ν which determine the particular cases of nonuniformity, enabling the common solution of equations of theory of elasticity to be obtained, are listed in Table 1.3 for all possible $b \leq 10$ (according to [102]).

Table 1.3 Values of ν for different magnitudes of b

b	2	3	4	5	6	7	8	8	9	10	10
ν	1/4	0	1/6	1/6	1/8	1/15	0	1/10	1/16	1/56	1/10

Note that for a soil medium, as follows from the table, the most appropriate is the value $\nu = 1/4$ which is "rigidly" connected to the value of $b = 2$.

The results, obtained in [102], were, in particular, applied to solve the problem of the stress-strained state of the half-space with the nonuniformity function of Eq. (1.190) under a concentrated force applied normally to the boundary surface. In the final form the formula for the vertical displacements ($b = 2$, $\nu = 1/4$) is given by

$$w(r,z) = \frac{kP}{4\pi G_0(1+\varsigma)} \int_0^\infty e^{-\lambda\varsigma\lambda} \cdot \frac{2\lambda^2\varsigma + \lambda(\varsigma+3) + 2}{2\lambda^2 + 6\lambda + 3} J_0(\lambda\rho)d\lambda \tag{1.191}$$

where

$$\rho = kr, \quad \varsigma = kz, \quad r = \sqrt{(x-\xi)^2 + (y-\eta)^2},$$

$J_0(t)$ is the Bessel function of the first kind of the zeroth order.

At $z = 0$ Eq. (1.191) produces the desired expression to determine the displacements of the points of the homogeneous half-space surface

$$w|_{z=0} = w(r,0) = \frac{kP}{4\pi G_0} \int_0^\infty \lambda \cdot \frac{3\lambda + 2}{2\lambda^2 + 6\lambda + 3} J_0(\lambda p)d\lambda, \tag{1.192}$$

$$w(r,0) = \frac{3P}{8\pi G_0 r} - \frac{kP}{4\pi G_0} \int_0^\infty \frac{9/2 + 7\lambda}{2\lambda^2 + 6\lambda + 3} J_0(\lambda\rho)d\lambda. \tag{1.192'}$$

The first term of Eq. (1.192′) corresponds to the homogeneous half-space with the same Poisson ratio ν and shear modulus $G_0 = E_0/2(1+\nu)$.

In order to calculate the nonhomogeneous half-space surface settlements, in [102] Eq. (1.192), using the known formulae [49, 53]

$$\int_0^\infty J_0(\lambda\rho)d\lambda = \frac{1}{\rho}, \quad \rho > 0, \tag{1.193}$$

$$\int_0^\infty \frac{J_0(\lambda\rho)}{\lambda+\gamma}d\lambda = \frac{\pi}{2}T_0(\gamma\rho),\ T_0(\gamma\rho) = H_0(\gamma\rho) - N_0(\gamma\rho), \quad |\arg\gamma| < \pi, \tag{1.194}$$

is given by

$$w|_{z=0} = \frac{3P}{8\pi G_0 r}\left\{1 - \frac{\pi}{3}\rho\left[\left(\frac{7}{4}+\sqrt{3}\right)T_0(\gamma_1\rho) + \left(\frac{7}{4}-\sqrt{3}\right)T_0(\gamma_2\rho)\right]\right\} \tag{1.195}$$

where $\gamma_1 = \frac{1}{2}(3+\sqrt{3})$, $\gamma_2 = \frac{1}{2}(3-\sqrt{3})$, and the Struve $H_0(\gamma\rho)$ and Neumann $N_0(\gamma\rho)$ functions are calculated with the required degree of accuracy by summation of the corresponding series.

Note that the approach to the solution of problems of theory of elasticity of nonhomogeneous media using harmonic functions has a limited practical value since the solution of the corresponding equations encounters strong difficulties even when the nonuniformity functions are specified; besides, it is possible only for certain values of the elasticity parameters. Furthermore, the approach to the determination of the surface deformation, used in [102], is not only restricted by the choice of the nonuniformity function, but also related to an inconvenience of carrying out engineering calculations due to the necessity of special functions to be calculated.

According to the method proposed here, at any dependence of the deformation modulus $E = E(z)$, the calculation of the nonhomogeneous half-space surface settlements can be reduced, according to Eqs. (1.157) and (1.166), to the calculation of vertical displacements as follows:

$$w(r) = \frac{(1-\nu^2)\cdot P}{\pi\cdot E_0}\cdot\left[\frac{1}{r} - \int_0^\infty \Phi(b,kR)\cdot\frac{z^3}{R^5}dz\right] \tag{1.196}$$

where

$$\Phi(b,kR) = \frac{1}{2}\cdot\frac{3e(\hat{R})/E_0 - 1}{e(\hat{R})/E_0}; \quad \hat{R} = kR. \tag{1.197}$$

The function of the degree of nonuniformity $e(\hat{R})$ for the deformation modulus increase law (1.190) after transformations, using integration by parts, is given by

$$e(\hat{R}) = E_0 \int_0^1 (1 + kRt)^b \cdot t^2 dt =$$

$$= \frac{E_0}{\hat{R}^3(b+1)} \left[\hat{R}^2(1+\hat{R})^{b+1} - \frac{2\hat{R}(1+\hat{R})^{b+1}}{b+2} + \frac{2(1+\hat{R})^{b+3}}{(b+2)(b+3)} - \frac{2}{(b+2)(b+3)} \right]. \tag{1.198}$$

Note that the limiting values of the function $\Phi = \Phi_1$ (corresponding to the law (1.190)) are obtained, using Eq. (1.198):

$$\lim_{kR \to 0} \Phi_1(b,kR) = 0, \lim_{kR \to \infty} \Phi_1(b,kR) = \frac{3}{2}. \tag{1.199}$$

Both limits in Eq. (1.199) have fixed values, independent of the nonuniformity parameter b. The dependences of the Φ_1 function on the reduced distance kR at various values of b are illustrated by Fig. 1.20. As seen from the figure, at $b > 1$ the Φ_1 function tends rather fast to its limiting value. On the contrary, at $b \leq 1$ the character of Φ_1 variation is sufficiently smooth.

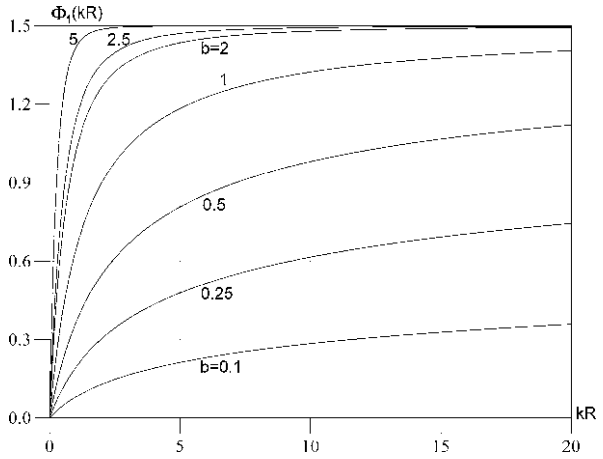

Fig. 1.20 Weight function for the power law of the deformation modulus variation with depth, Eq. (1.180)

Figure 1.21 shows the vertical displacements of the nonhomogeneous base surface at $b = 2$, $\nu = 1/4$ and various values of the parameter $c = kh$ (the value of $c = 0$ corresponds to the homogeneous half-space, h is the chosen linear measure). As follows from the data presented, the surface settlements, obtained using the equations of theory of elasticity (1.195) slightly differ from the values obtained using the approximate calculation model of Eq. (1.196): not more than by 1.5% at $c = 1$, and by 3.2% at $c = 5$, what is almost unresolved graphically. Consequently, it is reasonable to consider the proposed numerical-and-analytical approach to the calculation of nonhomogeneous base settlements to be applicable for wide practical application

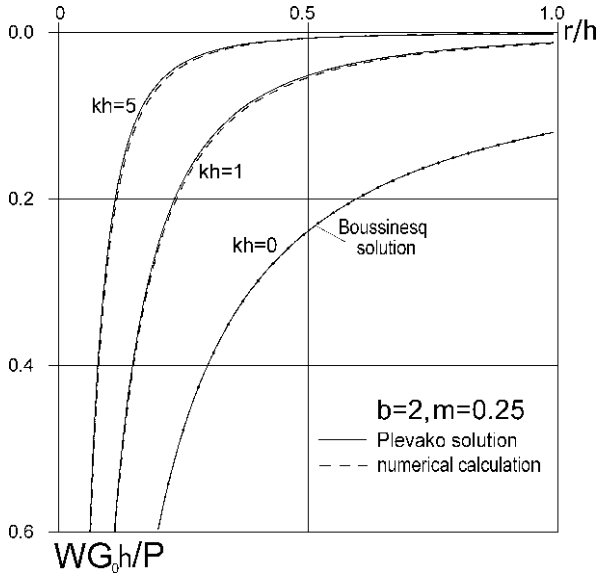

Fig. 1.21 Settlements of the surface of elastic bases with the power-law nonuniformity, Eq. (1.180), due to a vertical concentrated force

of Eq. (1.190) at various values of ν and b. Being simple in realization and simultaneously possessing sufficient accuracy of calculation, the approach is also helpful from the practical point of view, in particular, due to the possibility of strict account of experimental data regarding the growth of the soil deformation modulus with depth.

Though the considered laws of the deformation modulus variation (1.138) and (1.139) of power type, contrary to the purely theoretical one of Eq. (1.137), result in finite values of E on the soil base surface, still they produce an unlimited growth of $E(z)$ with depth. This circumstance contradicts the realistic concept of the deformation modulus stabilization with the increase of z. The data of the experimental studies show that in most cases the elastic nonuniformity is localized near the soil base surface, being the result of the processes of weathering, thawing, chemical effects, and a number of other geoecological phenomena.

Consider the deformation of nonhomogeneous base surfaces for the dependences $E(z)$, obtained by approximation of the experimental data and corresponding to the real growth of the deformation modulus with depth from the minimal value E_0 at the base daylight surface to a certain limiting finite value E_∞ at a considerable depth (Fig. 1.17). Variation of the deformation properties between these two limiting values of the deformation modulus can occur with different rate and is determined in accordance with an a priori substantiated empirical dependence.

For empirical dependences of the deformation modulus growth with depth, as a rule, no exact solutions of the problem of action of a concentrated force can be obtained. Therefore, it becomes necessary to develop efficient, sufficiently universal

numerical algorithms of representation of influence functions, which do not require large computer resources. Below, with an example of several dependences, adequate to the experimental data, which correctly correspond to the soil densification with depth, the possibilities of the elaborated numerical-and-analytical method of representation of influence functions are illustrated.

Exponential laws of the deformation modulus increase

$$E(z) = E_0 \cdot \left[1 + \alpha(1 - e^{kz})\right]. \tag{1.200}$$

Here $\alpha = (E_\infty - E_0)/E_0$, k is an empirical parameter, determining the deformation modulus increase rate, $0 \le k \le \infty$. Note that in this case the deformation modulus increases at large depths by factor of not higher than $(1+\alpha)$ in comparison with its daylight surface value.

While constructing the influence function for an elastic half-space with deformational nonuniformity of Eq. (1.200), first one calculates $e(R)$, using Eq. (1.154), obtaining

$$e(R)/E_0 = \frac{\alpha + 1}{3} + \alpha\left[\frac{e^{-kR}}{kR}\left(1 + \frac{2}{kR}\right) + \frac{2}{k^3R^3}(e^{-kR} - 1)\right]. \tag{1.201}$$

Substitution of the obtained expression into Eq. (1.166) results in the following expression for the nonhomogeneous base surface settlement

$$w|_{z=0} = w(r) = \\ = \frac{(1-\nu^2)P}{2\pi E_0}\int_0^\infty \frac{z^3 dz}{\left\{\frac{\alpha+1}{3} + \alpha\left[\frac{e^{-kR}}{kR}\left(1 + \frac{2}{kR}\right) + \frac{2}{k^3R^3}(e^{-kR} - 1)\right]\right\} \cdot R^5}. \tag{1.202}$$

Direct application of the obtained expression is hardly efficient due to a considerable loss of accuracy in the integrand calculations and the necessity of application of special adaptive integration schemes, requiring considerable computer resources in order to achieve the required accuracy at the variation of the r parameter in a semi-infinite interval $0 < r < \infty$. The experience of numerical calculations has enabled an optimal (from the point of view of labour consumption) method, enabling the sought integral value to be obtained with a high degree of accuracy. The efficiency of this method is achieved due to the selection of the main part of the integrand expression and calculation of the remaining improper integral using the quadrature formulae of the highest accuracy degree.

Taking into account Eq. (1.157), one can present Eq. (1.202) in the following form:

$$w(r) = \frac{(1-\nu^2)\cdot P}{\pi \cdot E_0}\left(\frac{1}{r} - \int_0^\infty \Phi_2(\alpha,kR)\cdot\frac{z^3}{R^5}dz\right) \tag{1.203}$$

where the weight function $\Phi_2(\alpha, kR)$ is given by

$$\Phi_2(\alpha,kR) = \frac{3}{2}\cdot\frac{\frac{\alpha}{3}k^3R^3 + \alpha\left[e^{-kR}(k^2R^2+2kR)+2(e^{-kR}-1)\right]}{\frac{1+\alpha}{3}k^3R^3 + \alpha\left[e^{-kR}(k^2R^2+2kR)+2(e^{-kR}-1)\right]}. \tag{1.204}$$

As one can see, at such formulation of the displacement function, the first term in Eq. (1.203) is the classical Boussinesq solution for the homogeneous elastic half-space, and the second (integral) term determines the effect of the soil deformation properties nonuniformity with depth.

The integral

$$\int_0^\infty \Phi_2(\alpha,kR)\cdot\frac{z^3}{R^5}dz \tag{1.205}$$

is calculated numerically, the knowledge of the characteristic features of behaviour of the weight function $\Phi_2(\alpha,kR)$ being used. It directly follows from Eq. (1.204) that

$$\lim_{kR\to 0}\Phi_2(\alpha,kR) = 0,\ \lim_{kR\to\infty}\Phi_2(\alpha,kR) = \frac{3}{2}\cdot\frac{\alpha}{1+\alpha}.$$

The function $\Phi_2(\alpha,kR)$ is plotted in Fig. 1.22 versus a dimensionless variable kR for various values of the α parameter. With the increase of $\hat{\boldsymbol{R}} = \boldsymbol{kR}$ from 0 to ∞ the function $\Phi_2(\alpha,kR)$, being limited, monotonously increases from 0, asymptotically approaching its limiting value in the infinity. Thus, the convergence of the integral (1.205) increases at small R and is of the same rate as that for the integral (1.157) at moderate and high R.

In order to estimate the improper integral of Eq. (1.205) with a guaranteed accuracy and minimal computation time, we convert it to a definite integral on the standard interval [−1,1], using a transformation

$$q = \frac{z-a}{z+a},$$

i.e. we assume in Eq. (1.205)

$$z = a\frac{1+q}{1-q}.$$

Then

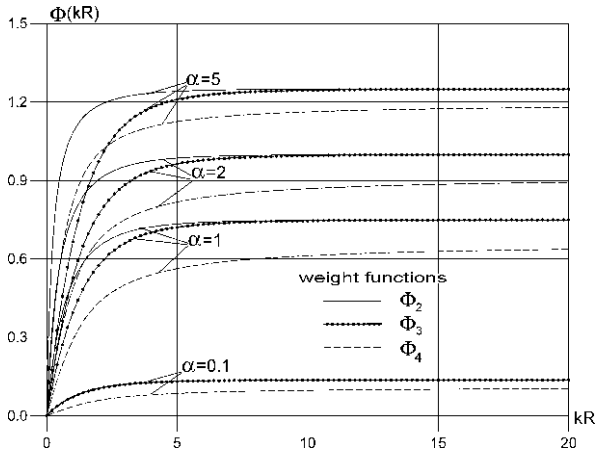

Fig. 1.22 Weight functions for various laws of elastic modulus variation with depth

$$\int_0^\infty \Phi(\alpha,kR)\frac{z^3}{R^5}dz = \int_0^\infty G(z)dz = 2a\int_{-1}^{1}\frac{G\left(a\frac{1+q}{1-q}\right)}{(1-q^2)}dq = \int_{-1}^{1}\hat{G}(q)dq. \quad (1.206)$$

The obtained integral is calculated, using the known Gauss-Legendre quadrature formula of the highest degree of accuracy [1]

$$\int_{-1}^{1}\hat{G}(q)dq \approx \sum_{i=1}^{m}\hat{G}(q_i)\cdot c_i$$

where q_i and c_i are the quadrature nodes and weights. The working formula to calculate the integral (1.206) under consideration finally takes the form

$$\int_0^\infty G(z)dz \approx \sum_{i=1}^{m}G(z_i)\cdot p_i \quad (1.207)$$

where

$$p_i = \frac{2ac_i}{(1-q_i)^2};\ z_i = a\frac{1+q_i}{1-q_i};\quad i = 1,\ldots,m.$$

Equation (1.207) is exact, when $G(z)$ is a linear combination of poles $1/(z+\alpha)^i$, $i = 2,3,\ldots,2m+1$. In other cases, when $G(z)$ is not an exact combination of poles, or when $G(z)$ contains poles of the power higher than $2m+1$, as noted in [99], Eq. (1.207) gives the best regards by the optimal choice of the (free) transformation parameter a value. The calculations regarding the numerical evaluation of the inte-

gral (1.157), possessing an exact value, have shown that application of Eq. (1.157) gives the results, practically coinciding with the exact ones, at $m = 10$ and $a = s \cdot r$ where $s = 1{,}3$. Using of higher (m>10) number of terms of the quadrature formula Eq. (1.207) does not result in a noticeable increase of the calculation accuracy.

Calculations of the half-space surface settlements, performed using Eq. (1.207) with various values of the nonuniformity parameters, are shown in Fig. 1.23. As one can see, the main effect on the decrease of the distributive ability of the base is made by the deformation modulus difference value $\alpha = (E_\infty\text{-}E_0)/E_0$. With the increase of the k parameter, the rate of variation of the deformation properties, the settlement curves are transformed, getting steeper what also indicates the decrease of the base distributive ability.

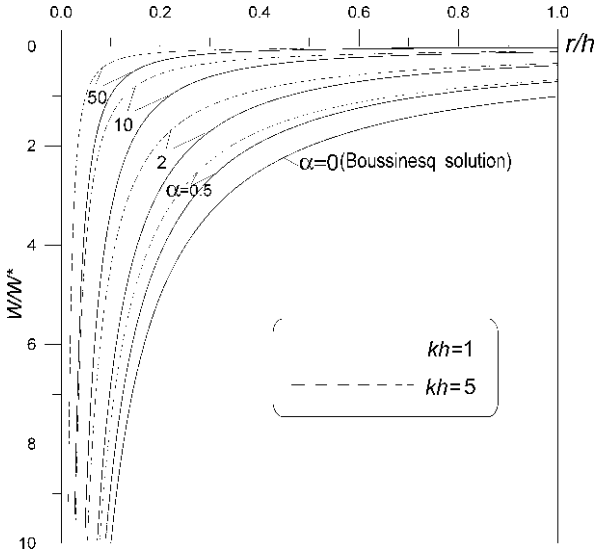

Fig. 1.23 Settlements of the surface of elastic bases with the exponential nonuniformity of Eq. (1.200) type due to a vertical concentrated force

2^0. Sapegin, Nikitina, and Shvedova [121] have experimentally justified the formula

$$E(z) = \frac{1}{Q_1 + Q_2 e^{-kz}} \tag{1.208}$$

where Q_1 and Q_2 are parameters, characterizing a given soil base. For further consideration, the dependence of Eq. (1.208) can be conveniently presented in one of the following forms:

$$E(z) = \frac{1}{\dfrac{1}{E_\infty} + \left(\dfrac{1}{E_0} - \dfrac{1}{E_\infty}\right) e^{-kz}}, \tag{1.209}$$

$$E(z) = E_0 \frac{1+\alpha}{1+\alpha e^{-kR}} \tag{1.210}$$

where, similarly to the above case, $\alpha = (E_\infty - E_0)/E_0$.

Development of the experimental data, obtained at specific engineering-and-geological conditions, using Eq. (1.208), results in [121]

$$E(z) = \frac{10^4}{0.445 + 1.555 \cdot e^{-4.3z}} \text{MPa}, \tag{1.211}$$

or, in the notations, used above,

$$k = 4.3\text{m}^{-1}, \quad E_0 = 0.5 \cdot 10^4 \text{MPa}, \quad E_\infty = 2.247 \cdot 10^4 \text{MPa}, \quad \alpha = 3.494.$$

According to Eq. (1.154),

$$e(kR) = \int_0^1 E(Rt) t^2 dt = E_0(1+\alpha) \int_0^1 \frac{t^2 dt}{1+\alpha e^{-kRt}}. \tag{1.212}$$

The latter integral can be evaluated only numerically. The dependences $e(kR)/E_0$ for different α are plotted in Fig. 1.24. Note that the numerical values of the integral converge very fast for all values of the $kR \geq 0$ and α parameters. The use of a maximum of 10 nodes in the Gauss-Legendre quadrature formula has proven to be sufficient in order to provide the calculation accuracy $\varepsilon = 10^{-5}$.

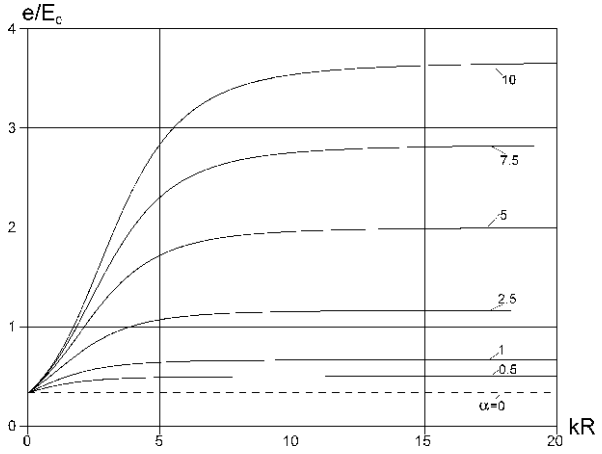

Fig. 1.24 Dimensionless nonuniformity function for the exponential law of deformation modulus variation, Eq. (1.210)

For a known $e(R)$ function, the nonhomogeneous base settlements are determined using Eq. (1.166), which, similarly to the above case, is presented in a form, conve-

nient for numerical calculations:

$$w(r) = \frac{(1-\nu^2)\cdot P}{\pi \cdot E_0}\left(\frac{1}{r} - \int_0^\infty \Phi_3(\alpha,kR)\cdot\frac{z^3}{R^5}dz\right), \tag{1.213}$$

$$\Phi_3(\alpha,kR) = \frac{1}{2}\cdot\frac{3e(\hat{R})/E_0 - 1}{e(\hat{R})/E_0};\quad \hat{R} = kR. \tag{1.214}$$

Here, similarly to the above case, the limiting values are the following:

$$\lim_{kR\to 0}\Phi_3(\alpha,kR) = 0,\ \lim_{kR\to\infty}\Phi_3(\alpha,kR) = \frac{3}{2}\cdot\frac{\alpha}{1+\alpha}.$$

Comparison of the weight functions for the exponential laws of the deformation modulus variation shows (Fig. 1.22) that the difference in the values of Φ_2 and Φ_3 occurs at $kR \leq 10$, increasing, as one should expect, with the nonuniformity parameter α. Using the weight function Φ_3 in Eq. (1.213), nonhomogeneous half-space surface settlements were calculated (Fig. 1.25). The distributive ability of the base decreases both with the deformation modulus difference $\alpha = (E_\infty - E_0)/E_0$, and with the increase of the deformation properties variation rate k. However, the settlement values are much less sensitive to the nonuniformity parameters than in the above case of the nonuniformity of exponential type (Fig. 1.23).

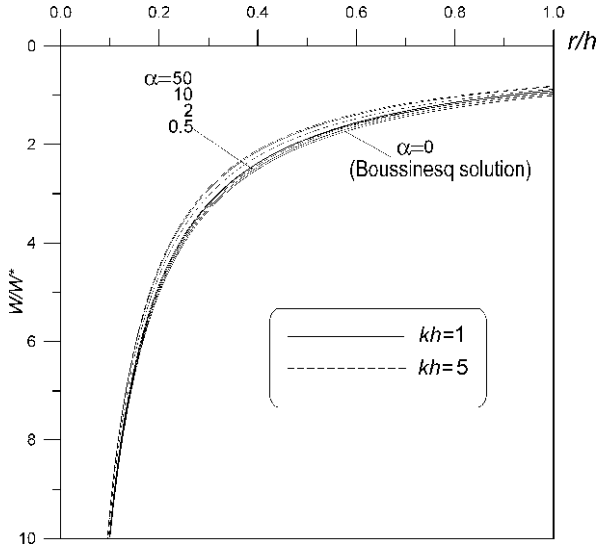

Fig. 1.25 Settlements of the surface of an elastic half-space with the exponential nonuniformity of Eq. (1.210) type due to a vertical concentrated force

Inverse trigonometric law of the deformation modulus increase. Consider the formulae for calculating the nonhomogeneous base surface settlements when the

deformation modulus experimental data are processed according to the following dependence:

$$E(z) = E_0 \cdot \left[1 + \alpha \frac{2}{\pi} \arctan(kz)\right] = E_0 \cdot (1 + \hat{\alpha} \cdot \arctan \hat{z}) \tag{1.215}$$

where $\hat{\alpha} = \alpha \frac{2}{\pi}$; $\hat{z} = kz$; $\alpha = (E_\infty - E_0)/E_0$ and, still, $\alpha = (E_\infty - E_0)/E_0$; k is an empirical parameter, determining the deformation modulus increase rate with depth, $0 \le k < \infty$.

The required calculations sequentially result in:

$$e(R) = \frac{E_0}{3}\left[1 + \alpha \cdot \left(\arctan(kR) - \frac{1}{2kR} + \frac{1}{2k^3R^3}\ln(1 + k^2R^2)\right)\right], \tag{1.216}$$

$$w|_{z=0} = w(r) = \frac{3(1-\nu^2)P}{2\pi E_0} \int_0^\infty \frac{z^3 dz}{\left[1 + \alpha \left(\arctan(kR) - \frac{1}{2kR} + \frac{1}{2k^3R^3}\ln(1 + k^2R^2)\right)\right] \cdot R^5}. \tag{1.217}$$

Similarly to the above case, we present the latter expression in the form, convenient for numerical calculations:

$$w(r) = \frac{(1-\nu^2) \cdot P}{\pi \cdot E_0}\left(\frac{1}{r} - \Phi \int_0^\infty {}_4(\alpha, kR) \cdot \frac{z^3}{R^5} dz\right) \tag{1.218}$$

where

$$\Phi_4(\alpha, kR) = \frac{3\alpha}{2} \cdot \frac{2k^3R^3\arctan(kR) - k^2R^2 + \ln(1 + k^2R^2)}{2k^3R^3 + \alpha\left[2k^3R^3\arctan(kR) - k^2R^2 + \ln(1 + k^2R^2)\right]}.$$

Accordingly, the limiting transitions lead to

$$\lim_{kR \to 0} \Phi_4(\alpha, kR) = 0, \lim_{kR \to \infty} \Phi_4(\alpha, kR) = \frac{3}{2} \cdot \frac{\pi}{1 + \alpha\pi}.$$

The $\Phi_4(\alpha, kR)$ dependences are plotted in Fig. 1.22, and the plots of vertical displacements of the surface of a soil base with spatial nonhomogeneity of Eq. (1.215)-type are shown in a dimensionless form in Fig. 1.26. As seen from the calculation results, the displacements according to Eq. (1.218) are in a qualitative agreement with the predictions of the above considered contact model (1.203), and the quantitative differences are related to the character of the deformation modulus variation with the base depth.

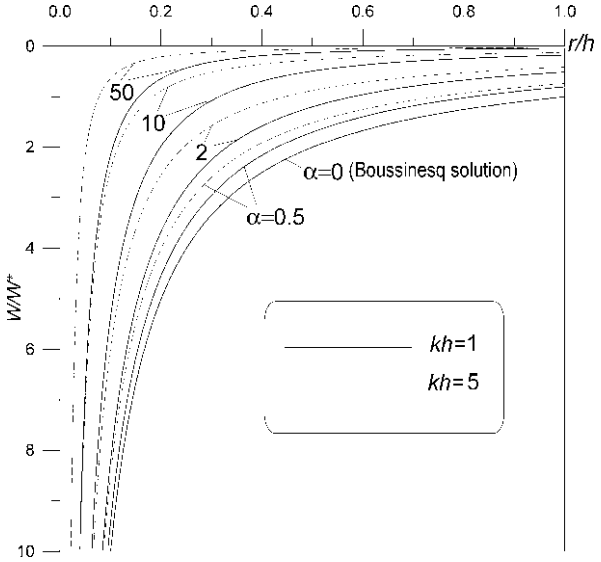

Fig. 1.26 Settlements of the surface of an elastic half-space with the inverse trigonometric nonuniformity of Eq. (1.215) type due to a vertical concentrated force

Thus, a numerical-and-analytical method for calculation of settlements of a nonhomogeneous half-space settlements is developed for different laws of the deformation modulus increase from the value $E_0 \neq 0$ at the daylight surface to the final limit E_∞ at considerable depths. Improper integrals in the calculation formulae are determined on the basis of an efficient procedure of numerical integration, optimal from the point of view of computation time due to the application of quadratures of the highest degree of accuracy. In the particular cases of linear and parabolic laws of the deformation modulus increase with depth, analytical expressions for the influence functions are obtained. The analysis of a large series of the calculations performed has shown the soil base surface settlements to be essentially affected by the nonuniformity of their elastic properties. The proposed influence functions are applicable for the description of the soil functioning in the course of condensation, setting much lower distributive ability of the nonhomogeneous base than for the homogeneous half-space model. The empirical parameters of the contact models under consideration, characterizing the base nonhomogeneity, can be determined from processing the data of standard soil tests in a well at different depths, or from punch tests, using punches of different bearing area.

At the end of this chapter we should note that the developed method of construction of influence function for bases with the deformation modulus, increasing with depth, results (in the framework of the boundary-element method) to effective numerical algorithms of solution of spatial contact problems of soil mechanics for shallow foundations. As shown below (Sect. 4.2), one can take into account the effect of the soil nonhomogeneity degree on the contact interaction of bases and foundations, especially with big dimensions.

References

1. Abramowitz M, Stegun I A (1972) Handbook of mathematical functions with formulas, graphs, and mathematical tables, 10th edn. Dover, New York
2. Aizikovich S M, Aleksandrov V M (1984) Axially symmetrical problem of impression of a round punch into an elastic half-space, nonhomogeneous in depth. Mekh Tverd Tela (issue 2): 73–82 (in Russian)
3. Aleksandrov A Ya (1963) On the solution of certain contact problems of the theory of elasticity. J Appl Math Mech 27: 1490–1494
4. Aleksandrov A Ya, Solovyov Yu I (1978) Spatial problems of theory of elas-ticity (application of methods of theory of complex-variable functions). Nauka, Moscow (in Russian)
5. Aleksandrov V M, Pozharskii D A (1989) Action of a strip-shaped stamp on an elastic incompressible three-dimensional wedge. Intern Appl Mech 25: 749–756
6. Alexandrov V M, Pozharskii D A (2001) Three-dimensional contact problems. Kluwer, Amsterdam
7. Alexandrov V M, Romalis B L (1986) Contact problems in machine building. Mashinostroyenie, Moscow (in Russian)
8. Aleynikov S M, Ikonin S V (1988) Numerical integration of singular solutions of theory of elasticity applied to the calculation of soil bases. In: Applied problems of me-chanics of solid media. Voronezh State University, Voronezh, pp. 132–136 (in Russian)
9. Aleynikov S M, Ikonin S V (1990) Three-dimensional deformation of the surface of a tapered elastic layer. Soil Mech Found Eng 27: 218–222
10. Aleynikov S M, Ikonin S V (1996) Numerical modeling of contact interac-tion of bases with dredging wells of bridge piers. In: Geotechnical engineering for transporta-tion infrastructure. Proc 12th Europe Conf Soil Mech Found Eng (Amsterdam, 7–10 June 1999), vol. 3. Theory and practice, planning and design, construction and maintenance. Balkema, Rotterdam, pp. 1719–1724
11. Aleynikov S M, Nikolaevskiy V N, Ramazanov T K (1994) Migration the stresses for two-level tectonic models. In: Dynamic processes in geophysical medium. Nauka, Moscow, pp. 11–21 (in Russian)
12. Aleynikov S M, Sedaev A A (1990) Calculation of ring-shaped foundations at complicated geotechnical conditions. In: Calculation and design of bases and foundations at complex geotechnical conditions. VPI, Voronezh, pp. 19–26 (in Russian)
13. Awojobi A O (1976) On the hyperbolic variation of elastic modulus in a non-homogeneous medium. Intern J Solids Struct 12: 81–92
14. Barvashov V A (1976) Composite models of an earth foundation bed. Soil Mech Found Eng 13: 61–65
15. Belenkiy M Ya (1952) Mixed problem of theory of elasticity for an infinitely long strip. Prikl Mat Mekh 16: 283–292 (in Russian)
16. Belik G I, Rvachev V L (1962) On the main integral equation of contact problem of theory of elasticity for a half-space whose elasticity modulus is a power function of depth. Dokl AN UkrSSR (issue 8): 1041–1044 (in Russian)
17. Bezukhov N I (1968) Fundamentals of theory of elasticity, plasticity and creep. Vysshaya Shkola, Moscow (in Russian)
18. Birman S Ye (1953) On the settlement of a rigid punch on an elastic layer resting on an incompressible base. Dokl AN SSSR 93(issue 5): 791–794 (in Russian)
19. Bochner S (1959) Lectures on Fourier integrals. Princeton University Press, Princeton, NJ
20. Bolotin V V, Novichkov Yu N (1980) Mechanics of multilayer structures. Mashinostroyenie, Moscow (in Russian)
21. Booker J R, Balaam N P, Davis E H (1985) The behaviour of an elastic non-homogeneous half-space. Part 1. Line and point loads. Intern J Num Anal Method Geomech 9: 353–367
22. Booker J R, Balaam N P, Davis E H (1985) The behaviour of an elastic non-homogeneous half-space. Part 2. Circular and strip footings Intern J Num Anal Method Ge-omech 9: 369–381

23. Borodachev A N (1984) Pressure of an elliptical punch on a nonhomogene-ous elastic half-space. Dokl AN UkrSSR Ser A (issue 7): 30–33 (in Russian)
24. Borodachev A N (1985) Kernel matrix for an elastic half-space with a vari-able Poisson ratio. Dokl AN UkrSSR Ser A (issue 12): 21–23 (in Russian)
25. Borodachev A N (1988) Elastic equilibrium in a layer inhomogeneous with depth. Intern Appl Mech 24: 753–758
26. Borodachev A N, Dudinskii V I (1986) Contact problem for an elastic half-space with a variable Poisson ratio. Mech Solids 21(issue 1): 86–91
27. Bosakov S V (1988) Action of a concentrated force on an elastic quarter-space. Teor i Prikl Mekh. Vysheyshaya Shkola, Minsk 15: 100–108 (in Russian)
28. Bosakov S V, Fomicheva N M (1986) Displacements of a spatial wedge boundary due to a normally concentrated force at arbitrary Poisson ratio. Vopr Stroit i Arkhit. Vysheyshaya Shkola, Minsk 15: 53–56 (in Russian)
29. Brebbia C, Telles J, Wrobel L (1984) Boundary element techniques. Springer-Verlag, Berlin
30. Bronshtein M I (1970) On the calculation of a base underlaid by an inclined incompressible layer and loaded by a concentrated force or a punch. In: Bases, foundations and underground structures. Tr NIIOSP 60: 40–82 (in Russian)
31. Burmister D M (1956) Stress and displacement characteristics of a two-layer rigid base soil system: influence diagrams and practical applications. Proc Highway Res 35: 773–814
32. Chan K S, Karasudhi P, Lee S L (1974) Force at a point in the interior of a layered elastic half-space. Intern J Solids Struct 10: 1179–1199
33. Davies T G, Banerjee P K (1978) The displacement field due to a point load at the inter-face of a two layer elastic half-space. Geotechnique 28: 43–56
34. Dempsey J P, Li H (1989) A rigid rectangular footing on an elastic layer. Geotechnique 9: 147–152
35. Durayev A Ye (1991) Calculation of structures on a soil base with a defor-mation modulud increasing with depth. Mordovian University, Saransk (in Russian)
36. Dymek F, Dymek J (1988) Funkcje Greena gla polprzestrzeni sprezystej transwersalnie izotropowej. Gornictwo 12: 211–229
37. Egorov K E (1958) On the deformation of a finite-thickness base. In: Bases and foundations. Soil Mech Tr NIIOSP 34: 5–33 (in Russian)
38. Egorov K E, Barvashov V A, Fedorovskii V G (1973) On the application of theory of elasticity to the calculation of bases under structures. In: Proc 8th Intern Conf Soil Mech Found Eng, Stroyizdat, Moscow, pp. 72–83 (in Russian)
39. Fedorovskii V G, Onopa I A (1985) Surface settlements of a wedge-shape bed under a concentrated load. Soil Mech Found Eng 22: 79–84
40. Florin V A (1959) Fundamentals of soil mechanics. Stroyizdat, Mos-cow/Leningrad (in Russian)
41. Galin L A (ed) (1976) Development of theory of contact problems in the USSR, Nauka, Moscow (in Russian)
42. Gibson R E (1967) Some results concerning displacements and stresses on a non-homogeneous elastic half-space. Geotechnique 17: 58–67
43. Gibson R E, Sills G C (1969) On the loaded elastic half-space with a depth varying Poisson's ratio. ZAMP 20: 691–695
44. Godes Yu Ya (1987) Functions of compliance of a multilayer base with elas-tic constraints between the layers. In: Nonlinear problems of hydroaeromechanics and theory of elasticity. Dnipropetrovsk State University, Dnipropetrovsk, pp. 92–97 (in Russian)
45. Godes Yu Ya, Privarnikov A K (1983) Quadrature formulae for Hankel inte-grals. Dnipropetrovsk State University, Dnipropetrovsk, VINITI No. 327-84Dep (in Russian)
46. Golecki J J, Knops R J (1969) Introduction to a linear elasto-statics with variable Poisson's ratio. Acad Gorn-Hutn w Krakowie 30: 81–92
47. Gorbunov-Posadov M I, Malikova T A, Solomin V I (1984) Calculation of structures on an elastic base. Stroyizdat, Moscow (in Russian)

48. Gorlov A M, Serebryaniy R V (1968) Automated calculation of rectangular plates on an elastic base. Stroyizdat, Moscow (in Russian)
49. Gradshtein I S, Ryzhyk I M (1980) Tables of integrals, series and products. Academic Press, New York
50. Hahn H G (1985) Elastizitatstheorie. Teubner, Stuttgart
51. Hanson M T, Xu Y, Keer L M (1994) Stress analysis for a tree-dimensional incompressible wedge under body force or surface loading. Q J Mech Appl Math 47: 141–158
52. Hetenyi M A (1970) A general solution for the elastic quarter space. Trans ASME Ser E J Appl Mech 37: 70–76
53. Janke E, Emde F, Lösch F (1966) Tafeln Höherer Funk-tionen. Teubner, Stuttgart
54. Johnson K L (1985) Contact mechanics. Cambridge University Press, Cam-bridge
55. Keer L M, Lee J C, Mura T (1984) Hetenyi's elastic quarter space problem revisited. Intern J Solids Struct 20: 513–524
56. Klein G K, Durayev A Ye (1971) Account of increase off the soil deforma-tion modulus with depth at the calculation of beams on a solid base. Gidroteh Stroit (issue 7): 19–21 (in Russian)
57. Kogan B M, Zinchenko V D (1960) Stressed state of a nonhomogeneous layer, resting on an elastic half-space. Izv Vuzov Stroit Arkhit (issue 3): 8–18 (in Russian)
58. Kolchin G B, Faverman E A (1972) Theory of elasticity of nonhomogeneous bodies. Bibliographical index. Stiinţa, Chişinău (in Russian)
59. Kolchin G B, Faverman E A (1977) Theory of elasticity of nonhomogeneous bodies. Bibliographical index (1970–1973). Stiinţa, Chişinău (in Russian)
60. Koning H (1957) Stress distribution in a homogeneous, anisotropic, elastic semi-infinite solid. In: Proc 4th Intern Conf Soil Mech Found Eng, Butterworths, London, pp. 335–338
61. Kopasenko V Yu, Kebedev V K (1977) Mixed problem of theory of elastic-ity for a quarter-space. Izv SKNC VSH. Nat Sci (issue 3) 30–31 (in Russian)
62. Korenev B G (1957) Punch, resting on an elastic half-space whose deforma-tion modulus is a power function of depth. Dokl AN SSSR 112: 823–826 (in Russian)
63. Korenev B G (1971) Introduction into Bessel function theory. Nauka, Mos-cow (in Russian)
64. Kupradze V D, Gegeliya T G, Basheleyshvili M O, Burchuladze T V (1979) Three-dimensional problems of the mathematical theory of elasticity and thermoelasticity. North-Holland, Amsterdam
65. Kushner S G (1990) Calculation of settlements of bases under buildings and structures. Budivelnyk, Kyiv (in Russian)
66. Lebedev N N, Ufliand Ia S (1958) Axisymmetric contact problem for an elastic layer. J Appl Math Mech 22: 442–450
67. Lomakin V A (1976) Theory of elasticity of nonhomogeneous bodies. Mos-cow State University, Moscow (in Russian)
68. Love A E H (1959) A treatise on the mathematical theory of elasticity, 4th edn. Cambridge University Press, Cambridge
69. Lubyagin I A, Pozharskii D A, Chebakov M I (1991) Generalization of Boussinesq and Cerruti problems for the case of an elastic spatial wedge. Dokl AN SSSR 321(issue 1): 58–62 (in Russian)
70. Lubyagin I A, Pozharskii D A, Chebakov M I (1992) Embedding of a punch in the form of an elliptic paraboloid into an elastic spatial wedge. J Appl Math Mech 56: 244–252
71. Lur'e A I (1964) Three-dimensional problems in the theory of elas-ticity. Interscience, New York
72. Lur'e A I (1970) Theory of elasticity. Nauka, Moscow (in Russian)
73. Lur'e A I, Brachkovskii B S (1941) Solution of a flat problem of theory of elasticity for a wedge. Works Leningrad Polytechnic Institute 3: 158–165 (in Russian)
74. Makovenko S Ya (1988) The influence tensor for an elastic medium with Poisson's ratio varying in one direction. J Appl Math Mech 52: 263–266

75. Martynenko M D, Dashkevich A A (1985) Some problems of bending of round plates and slabs on a nonhomogeneous half-space. In: Boundary problems and automa-tion of their solution. KhAI, Kharkiv, pp. 168–170 (in Russian)
76. Martynenko M D, Dashkevich A A (1989) Bending of slans on a nonho-mogeneous base of exponential type with the account of their thickness deformability. Probl Mashinostr 32: 57–60 (in Russian)
77. Mindlin R D (1936) Force at a point in the interior of a semi-infinite solid. Physics 7: 195–202
78. Mindlin R D (1953) Force in the interior of a semi infinite solid. In: Proc First Midwestern Conf Solid Mech Univ Illinois, Urbana, pp. 111–118
79. Mindlin R D, Cheng D H (1950) Nuclei of strain in the semi-infinite solid. J Appl Phys 21: 926–931
80. Minoru H, Koji K, Jun K (1984) A numerical method of Hankel transform for axisymmetric problems of elasticity. Bull JSME 27: 1333–1338
81. Mossakovskii V I (1958) Pressure of a circular die on an elastic half-space, whose modulus of elasticity is an exponential function of depth. J Appl Math Mech 22: 168–171
82. Mozharovskii V V, Starzhinskii V Ye (1988) Applied mechanics of layered bodies of composites: Flat contact problems. Nauka i tekhnika, Minsk (in Russian)
83. Muki R (1960) Asymmetric problems of the theory of elasticity for a semi-infinite solid and a thick plate. In: Sneddon I N and Hill R (eds) Progress in solid mechanics. North-Holland, Amsterdam, vol. 1, pp. 399–439
84. Muravskii G (1997) Green functions for a compressible linearly non-homogeneous half-space. Archive Appl Mech 67: 521–534
85. Muravskii G (1997) Time-harmonic problem for a non-homogeneous half-space with exponentially varying shear modulus. Intern J Solids Struct 34: 3119–3139
86. Muravskii G (1997) Time-harmonic problem for a non-homogeneous half-space with shear modulus limited at infinite depth. Eur J Mech A/Solids 16: 277–294
87. Naumov Yu A, Shevlyakov Yu A (1967) On the bending of round plates on a multilayer base. Inzh Zh Mekh Tverd Tela (issue 1): 154–167 (in Russian)
88. Naumov Yu A, Shevlyakov Yu A, Chistyak V I (1970) On solving the fun-damental problems of the theory of elasticity for a layer with an arbitrary nonhomogeneity along its thickness. Intern Appl Mech 6: 406–711
89. Nikishin V S, Shapiro G S (1970) Spatial problems of theory of elasticity for multilayer media. VC AN SSSR, Moscow (in Russian)
90. Nikishin V S, Shapiro G S (1973) Problems of theory of elasticity for multi-layer media. Naula, Moscow (in Russian)
91. Novotný B, Hanuška A (1983) Teória vrstev-natého polpriestoru [Theory of layered half-space]. Veda, Bratislava (in Slo-vak)
92. Nowacki W (1970) Teoria sprezystosci. PWN, Warszawa
93. Olszak W (ed) (1958) Non-homogeneity in elasticity and plasticity. In: Proc IUTAM Symp (Warsaw, September 2–9 1958). Pergamon Press, Lon-don
94. Orlyuk Ye I (1979) Functional equations of the spatial problem of theory of elasticity for a wedge and their solution. Dokl AN USSR Ser A (issue 3): 194–198 (in Russian)
95. Parton V Z, Perlin P I (1981) Methods of mathematical theory of elasticity. Nauka, Moscow (in Russian)
96. Petrishin V I (1965) On the torsion of a multilayer base. Prikl Mekh 1(issue 6): 127–129 (in Russian)
97. Petrishin V I, Privarnikov A K (1965) Main boundary problems of theory of elasticity for multilayer bases. Prikl Mekh 1(issue 4): 58–66 (in Russian)
98. Piskunov V G, Prisyazhnyuk V K (1985) Calculation of nonhomogeneous plates on a non-homogeneous half-space. Stroit Mekh Raschet Sooruzh (issue 1): 25–28 (in Russian)
99. Pissanetzky S (1983) An infinite element and a formula for numerical quad-rature over an infinite interval. Intern J Num Method Eng 19: 913–927

100. Plevako V P (1969) A point force inside a pair of cohering half-spaces. Soil Mech Found Eng 6: 165–169
101. Plevako V P (1971) On the theory of elasticity of inhomogeneous media. J Appl Math Mech 35: 806–813
102. Plevako V P (1972) On the possibility of using harmonic functions for solv-ing problems of the theory of elasticity of nonhomogeneous media. J Appl Math Mech 36: 834–842
103. Plevako V P (1972) The state of stress of a nonhomogeneous layer resting on an elastic half-space. Intern Appl Mech 8: 397–403
104. Plevako V P (1973) The deformation of a nonhomogeneous half-space un-der the action of a surface load. Intern Appl Mech 9: 593–598
105. Pobedrya B Ye (1981) Numerical methods in theory of elasticity and plas-ticity. Moscow State University, Moscow (in Russian)
106. Pobedrya B Ye (1984) Mechanics of composite materials. Moscow State University, Moscow (in Russian)
107. Popov G Ya (1982) Concentration of elastic stress near punches, cuts, fine inclusions and supports. Nauka, Moscow (in Russian)
108. Popov G Ya (1982) Contact problems for a linearly deformable base. Vyshcha Shkola, Kyiv/Odesa (in Russian)
109. Potelezhko V P, Filippov A P (1967) The contact problem for a slab lying on an elastic base. Intern Appl Mech 3(issue 1): 49–51
110. Poulos H G, Davis E H (1974) Elastic solutions for soil and rock mechan-ics. Wiley, New York
111. Privarnikov A K (1973) Spatial deformation of a multilayer base. In: Stabil-ity and strength of structural elements. Dnipropetrovsk State University, Dnipropetrovsk, pp. 27–45 (in Russian)
112. Privarnikov A K, Godes Yu A (1986) On the solution of the first boundary problem for an elastic multilayer base. In: Stability and strength of structural elements. Dni-propetrovsk State University, Dnipropetrovsk, pp. 6–28 (in Russian)
113. Rakov A K, Rvachev V L (1961) Contact problem of theory of elasticity for a half-space with an elasticity module being a power function of depth. Dokl AN UkrSSR (is-sue 3): 286–290 (in Russian)
114. Rao C R A (1970) On the integration of the axisymmetric stress equations of motion for nonhomogeneous elastic media. Arch Mech Stosow 22: 63–73
115. Recomendations on the calculation of settlements and slopes for rectangular foundations on a wedge-shaped base (1985) Gersevanov NIIOSP, Moscow (in Russian)
116. Reut V V, Tikhonenko L Ia (1980) Bending of wedge-like plates with elas-tically-fastened or reinforced edges. J Appl Math Mech 44: 104–110
117. Romanchik V S, Knyazeva L P (1983) Stress-strained state of a cubic ani-sotropic space. Teoret i Prikl Mekh. Vysheyshaya Shkola, Minsk 10: 41–47 (in Russian)
118. Rostovtsev N A (1964) On the theory of elasticity of a nonhomoqeneous medium. J Appl Math Mech 28: 745–757
119. Rostovtsev N A, Khranevskaia I E (1971) The solution of the boussinesq problem for a half-space whose modulus of elasticity is a power function of the depth. J Appl Math Mech 35: 1000–1009 (in Russian)
120. Rvachev V L, Protsenko V S (1977) Contact problems of theory of elastic-ity for nonclassical domains. Naukova Dumka, Kyiv (in Russian)
121. Sapegin D D, Nikitin A A, Shvedova T K (1976) Study of deformational properties of rock bases with the account of their deformability in depth. Izv VNIIG Ve-deneyeva 111: 67–73 (in Russian)
122. Sarkisyan V S, Avetikyan V K (1987) On the solution of a contact problem for an elastic wedge reinforced by a finite and a semifinite stringers on its boundary. In: Me-chanics. Yerevan State University, Yerevan (issue 6), pp. 65–70 (in Russian)
123. Schclar N A (1994) Anisotropic using boundary elements. Computational Mechanics Publications, Southampton

124. Selvadurai A P S (1979) Elastic analysis of soil-foundations interaction. El-sevier, Amsterdam
125. Selvadurai A P S (1995) On the indentation of a non-homogeneous elastic geomaterial: Analytical and computational estimates. In: Pande & Pitrusczak (eds) Numerical Models in Geomechanics-NUMOG V: Proc. 5th Intern Symp (Davos, Switzer-land). Balkema, Rotterdam, pp. 381–389
126. Selvadurai A P S (1996) The settlement of a rigid circular foundation rest-ing on a half-space exhibiting a near surface elastic non-homogeneity. Intern J Num Anal Method Geomech 20: 251–364
127. Selvadurai A P S, Lan Q (1998) Axisymmetric mixed boundary value prob-lems for an elastic halfspace with a periodic non-homogeneity. Intern J Solids Struct 35: 1813–1826
128. Shandru N (1964) On internal point loads in an elastic half-space with fixed edges. Bull Math Soc Sci Math Phys RPR 5: 205–224
129. Shekhter O Ya (1965) A horizontal force in a three-dimensional layer on a rigid base. Soil Mech Found Eng 2: 11–14
130. Shekhter O Ya (1965) A point force applied inside an elastic wedge. Soil Mech Found Eng 2: 334–337
131. Shekhter O Ya (1970) On the solutions of problems for an infinite elastic wedge with loads inside. In: Bases, foundations and underground structures. Tr NIIOSP 59: 22–30 (in Russian)
132. Shekhter O Ya, Prikhodchenko O E (1964) Stress and displacement distri-butions in an elastic layer acted on by internal point forces. Soil Mech Found Eng 1: 275–279
133. Shekhter O Ya, Bronshtein M I (1970) Some practical applications of prob-lems for an infinite elastic wedge. In: Bases, foundations and underground structures. Tr NIIOSP 60: 12–40 (in Russian)
134. Shekhter O Ya, Prikhodchenko O E (1966) Distribution of stresses and dis-placements in an elastic wedge with a free surface, resting on a rigid base, with concentrated forces acting inside. In: Bases and foundations. Tr NIIOSP 56: 12–35 (in Russian)
135. Sheremet V D (1982) Green's displacement tensor for an elastic half-space with a fixed boundary plane. In: Numerical analysis in the problems of mechanics. Stiinta, Chisinau 70: 139–143 (in Russian)
136. Sheremet V D (1983) A new solution and generalization of the Mindlin's problem for an elastic half-space with a fixed boundary plane. In: Mathematical studies: Numerical analysis in the problems of mechanics. Stiinta, Chisinau 75: 134–140 (in Russian)
137. Shevlyakov Yu A (1977) Matrix algorithms in theory of elasticity of non-homogeneous media. Vyshcha Shkola, Kyiv/Odesa (in Russian)
138. Shevlyakov Yu A, Naumov Yu A, Chistyak V I (1968) On calculating in-homogeneous foundations. Intern Appl Mech 4(issue 9): 42–45
139. Shirinkulov T Sh (1972) Calculation of engineering structures on a nonho-mogeneous elastic base. FAN, Tashkent (in Russian)
140. Shvets V B, Ginzburg L L, Goldshtein V M et al. (1987) Handbook on me-chanics and dynamics of soils. Budivelnyk, Kyiv (in Russian)
141. Sneddon I (1995) Fourier transforms. Dover, New York
142. Snitko N K (1980) On the action of a concentrated force on a nonhomoge-neous elastic half-space. Stroit Mekh Raschet Sooruzh (issue 2): 76–78 (in Russian)
143. Solomin V I, Shmatkov S B (1986) Methods of calculation and optimal de-sign of ferroconcrete foundation structures. Stroyizdat, Moscow (in Russian)
144. Sorochan E A, Trofimenkov Yu G (ed.) (1985) Bases, foundations and un-derground structures: Designer's handbook. Stroyizdat, Moscow (in Russian)
145. Sveklo V A (1964) Boussinesq type problems for the anisotropic half-space. J Appl Math Mech 28: 1099–1105
146. Timoshenko S, Wojnowski-Krieger S (1959) Theory of plates and shells. McGraw Hill, New York

147. Ufliand Ia S (1972) Some spatial problems of theory of elasticity for a wedge. In: Mechanics of a solid medium and related problems of analysis. Nauka, Moscow, pp. 549–554 (in Russian)
148. Ulitko A F (1979) Method of vector eigenfunctions in spatial problems of theory of elasticity. Naukova Dumka, Kyiv (in Russian)
149. Vasilyev Yu N (1965) Problem of action of a concentrated force applied to the boundary of coupled half-spaces. Stroit Mekh Raschet Sooruzh (issue 4): 15–16 (in Russian)
150. Vilkov I M (1963) Flat contact problem for a two-layer base under a sym-metrical load acting on a rigid punch. Izv AN SSSR Mekh Mashinostr (issue 4): 172–174 (in Russian)
151. Vladinirov V S (1967) Equations of mathematical physics. Nauka, Moscow (in Russian)
152. Vlasov V Z, Leontiev N N (1960) Beams, plates and shells on an elastic base. Phys Math Liter Publ, Moscow (in Russian)
153. Vorovich I I, Aleksandrov V M, Babeshko V A (1972) Nonclassical mixed problems of theory of elasticity. Nauka, Moscow (in Russian)
154. Vorovich I I, Ustinov Yu A (1959) Pressure of a die on an elastic layer of finite thickness. J Appl Math Mech 23: 637–650
155. Vrettos C (1991) Time-harmonic Boussinesq problem for a continuously non-homogeneous soil. Earthquake Eng Struct Dynam 20: 961–977
156. Yefimov A B, Yefimov D G (1966) Concentrated effects on an elastic in-compressible wedge. Izv AN SSSR Mekh Tverd Tela (issue 6): 89–92 (in Russian)
157. Yevdokimov P D, Sapegin D D (1964) Strength, resistance to shear, and de-formability of bases of buildings on rock. Energiya, Moscow (in Russian)

Chapter 2
Static Analysis of Contact Problems for an Elastic Half-Space

Abstract The second chapter is devoted to the mathematical formulation of mixed problems of the elasticity theory for a half-space and to the numerical-and-analytical methods of their solution. The results obtained in this chapter on developing the mathematical means are the reference data for BEM-based numerical modeling of the spatial contact interaction. The integrated boundary equations of the spatial contact problem are written for the case when the calculation scheme is accepted in the form of variously deepened punches undergoing the action of the spatial system of forces. It is shown how to reduce the initial integral equation system of the contact problem with respect to the contact stress function and the punch displacement parameters to the appropriate finite-dimensional algebraic analogue. Much attention is paid to calculating the matrix coefficients of the resolving system of algebraic equations. A numerical-and-analytical procedure is given for integrating Mindlin's fundamental solutions over flat triangular and quadrangular boundary elements, arbitrary oriented in the half-space. For convenience, to apply the developed approach in practical calculations, the boundary integral equations of the spatial contact problems for a number of essential special cases are presented. The contact problems at axial loading and torsion of absolutely rigid rotation bodies deepened into the half-space, are considered. Boundary-element formulations of the contact problems for complex-shaped punches with flat and smooth bases (shallow foundations), situated on spatially nonhomogeneous bases of the semi-infinite elastic massif type are presented.

2.1 Boundary Integral Equations of the Contact Problem for an Absolutely Rigid Punch, Deepened into an Elastic Half-Space, Under a Spatial Load System

Consider an elastic homogeneous half-space $z \geq 0$, containing a cavity $S$with a boundary Γ from the side of the surface $z = 0$. The mechanical properties of the half-space are determined by the elastic modulus E and Poisson's ratio ν. We assume the surface $z = 0$, being the boundary of the half-space, to be free from any

S.M. Aleynikov, *Spatial Contact Problems in Geotechnics*, Foundations of Engineering Mechanics, DOI 10.1007/b11479_2, © Springer-Verlag Berlin Heidelberg 2011

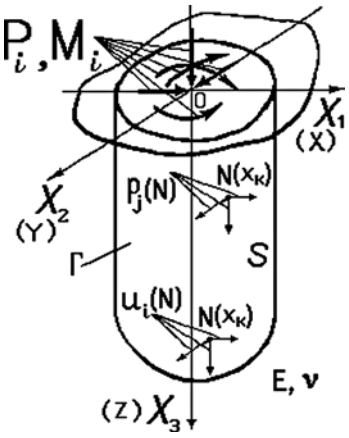

Fig. 2.1 Calculation scheme for the contact problem of a volumetric punch, deepened into an elastic half-space

load. In the cavity S an absolutely rigid volumetric punch is deepened, subject to a static load, reduced to a resultant force $P = \{P_1, P_2, P_3\}$ and a resultant moment $M = \{M_1, M_2, M_3\}$ where P_i, M_i $(i = 1, 2, 3)$ are the projections of the corresponding vectors onto the axes of the Cartesian coordinate system $OX_1X_2X_3$ *(OXYZ)* (Fig. 2.1). The contact problem of spatial theory of elasticity for the deepened punch consists in the determination of contact stress on the surface of interaction of the elastic medium with the punch as well as the determination of the parameters of its displacement as a rigid solid. We assume the punch to be welded with the elastic half-space, i.e. on the contact surface of the punch and the base the displacements coincide (the second-order boundary conditions according to Galin [14] are fulfilled). In order to derive the main equations of the contact problem we follow a rather demonstrative method, first considered by Kovneristov [20] and later applied by Shishov [29] while solving the problems in an axisymmetric arrangement. The method suggests the involvement of Betti's theorem of reciprocity [24] that requires the concept of basic and auxiliary states of an elastic body to be introduced.

As a basic state we consider an elastic half-space with a cavity S, in each point of whose surface the displacements $u_i(N)$ are given and the stresses $P_j(N)$ are acting, being a distributed reaction from the side of the punch (Fig. 2.1). The stress-strained state of the base in the initial contact problem will be equivalent to the basic state introduced into the consideration.

In order to build auxiliary states consider a solid elastic half-space, loaded in a point $K(\xi,\eta,\zeta)$ by unit concentrated forces

$$A_j = \delta(x - \xi, y - \eta, z - \zeta), \quad i = 1,2,3 \tag{2.1}$$

directed along the coordinate axes, respectively. The load point $K(\xi,\eta,\zeta)$ is chosen outside the domain bounded by the surface Γ. Virtually remove the elastic body S' from the half-space, the surface Γ of the body S' being identical to that of the rigid punch. In order to keep the half-space, weakened by the cavity, in equilibrium,

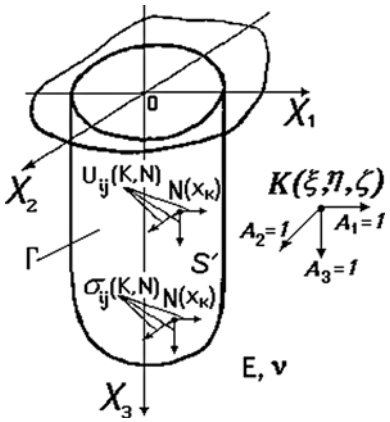

Fig. 2.2 Elastic half-space, weakened by a cavity, corresponding to the deepened punch shape

forces $\sigma_{ij}(N, K)$ and displacements $U_{ij}(N, K)$, being the fundamental Mindlin's solutions, should be distributed over the surface Γ (Fig. 2.2).

We take the advantage of the Betti's theorem of reciprocity [24], linking the solution of two different problems for the same domain of an elastic body: the work of the system of forces of the basic state on the displacements of the auxiliary state is equal to the work, performed by the system of forces of the auxiliary state on the displacements of the basic state. The equations of reciprocity of the works for the basic and the auxiliary states considered in this contact problem, are given by

$$\begin{aligned}&\iint_{\Gamma}\left[p_1(N)U_{1i}(K,N)+p_2(N)U_{2i}(K,N)+p_3(N)U_{3i}(K,N)\right]d\Gamma=\\&=\iint_{\Gamma}\left[\sigma_{1i}(K,N)u_1(N)+\sigma_{2i}(K,N)u_2(N)+\sigma_{3i}(K,N)u_3(N)\right]d\Gamma+u_i(K),\\&i=1,2,3.\end{aligned}\tag{2.2}$$

Equation (2.2) gives the integral representation of displacements at any point (outside the punch) of the elastic half-space and is known as Somigliana identity for the displacements [10, 24]. This equation could be immediately used formally as an initial one. Note that Eq. (2.2) lacks the integrity over the half-space surface, since the absence of stress at the free surface of the elastic half-space in the basic state had been initially assumed, and the fundamental Mindlin equation was obtained under the same condition. The Somigliana equation explains the main advantage of the boundary integral equation method (and the boundary-element method as a method of its numerical implementation), consisting in the fact the displacement vector components (and, consequently, the stresses) are determined solely by the boundary data at the punch surface. In other words, if the displacement values u_i and forces p_j at the Γ boundary are known, then using the Somigliana identity (2.2) one can always find the displacements and, consequently, deformations and stresses at any internal point $K(\xi, \eta, \zeta)$ of the elastic half-space.

The deformations of the half-space can be determined using Eq. (2.2) in a conventional way after differentiating and using the Cauchy relations

$$\varepsilon_{11} = \frac{\partial u_1}{\partial \xi}(K), \quad \varepsilon_{22} = \frac{\partial u_2}{\partial \eta}(K), \quad \varepsilon_{33} = \frac{\partial u_3}{\partial \zeta}(K),$$

$$\varepsilon_{12} = \varepsilon_{21} = \frac{1}{2}\left(\frac{\partial u_1}{\partial \eta}(K) + \frac{\partial u_2}{\partial \xi}(K)\right), \quad \varepsilon_{23} = \varepsilon_{32} = \frac{1}{2}\left(\frac{\partial u_2}{\partial \zeta}(K) + \frac{\partial u_3}{\partial \eta}(K)\right),$$

$$\varepsilon_{13} = \varepsilon_{31} = \frac{1}{2}\left(\frac{\partial u_1}{\partial \zeta}(K) + \frac{\partial u_3}{\partial \xi}(K)\right),$$

which afterwards enables the stress tensor components in the elastic half-space for the basic state to be determined using Hooke equations

$$\sigma_k(K) = 2G\left[\frac{\nu}{1-2\nu}\theta(K) + \varepsilon_k(K)\right], \quad k = 1,2,3,$$

$$\tau_{12} = 2G\varepsilon_{12}(K), \quad \tau_{23} = 2G\varepsilon_{23}(K), \quad \tau_{13} = 2G\varepsilon_{13}(K)$$

where $G = E/2(1+\nu)$ is the shear modulus, $\theta(K) = \varepsilon_{11}+\varepsilon_{22}+\varepsilon_{33}$ is dilatation. The obtained equations are cumbersome and, therefore, not given here in the extended form.

In order to obtain the equations of the contact problem, we direct the point $K(\xi,\eta,\zeta)$ of application of the unit concentrated forces toward the deepened punch surface, i.e. perform a limiting transition from the internal point to the boundary one. The limiting transition results in a system of three boundary integral equations

$$\frac{1}{2}u_i(K) = \iint\limits_{\Gamma}\left[\sum_{j=1}^{3}(p_j(N)U_{ji}(K,N) - u_j(N)\sigma_{ji}(K,N))\right]d\Gamma, \tag{2.3}$$

$$i,j = 1,2,3; \quad K(\xi,\eta,\zeta) \in \Gamma, \quad N(x_1,x_2,x_3) \in \Gamma.$$

The factor 1/2 on the left-hand side of Eq. (2.3) arises due to the fact the unit forces in the point $K(\xi,\eta,\zeta)$ in the auxiliary state are divided by the surface Γ in two parts: one acts at the half-space with the cavity, the other acts at the punch-shaped elastic body being removed. The singularity of the equations consists in an unlimited increase of the integrands at $N \to K$. It will be shown below (Sect. 2.3) that all the integrals, containing functions $U_{ij}(N, K)$ with a weak singularity (of the $1/R$ type), can be calculated for flat integration surfaces numerically-and-analytically with any degree of accuracy. Integrals, containing functions $\sigma_{ij}(N, K)$ with a strong singularity (of the $1/R^2$ type), require special calculation in the sense of the Cauchy principal value. Below it will be shown that for the contact problems considered here the integrals, containing cores with strong singularities, can be excluded out of

consideration after the account of displacements of the punch as a rigid solid as well as the application of equilibrium equations for the auxiliary state.

The displacement of the punch as a rigid solid enables the following relation to be written for the points on the contact surface [21]:

$$u_i(K) = \Delta_i - \varepsilon_{ijk}\zeta_j\psi_k \tag{2.4}$$

where Δ_i are translational displacements of the punch, ψ_k are small rotations of the punch with respect to the coordinate axes, $i,j,k = 1,2,3$, $K(\xi,\eta,\zeta) \in \Gamma$, $\zeta_1 = \xi$, $\zeta_2 = \eta$, $\zeta_3 = \zeta$.

The boundary integral equations (2.3) of the contact problem for the deepened punch with the account of Eq. (2.4) take the following form (summation over the repeated indices is assumed):

$$\frac{1}{2}\left(\Delta_i - \varepsilon_{ijk}\zeta_j\psi_k\right) = \iint\limits_{\Gamma} p_j U_{ji} d\Gamma - \Delta_j \iint\limits_{\Gamma} \sigma_{ji} d\Gamma + \psi_k \iint\limits_{\Gamma} \varepsilon_{jlk}\zeta_l \sigma_{ji} d\Gamma, \tag{2.5}$$

i, j,k,l =1, 2, 3.

The three obtained equations (2.5) can be essentially simplified by using the equilibrium equations for the elastic body S' in the shape of the deepened punch for the auxiliary states from the action of the unit concentrated forces on the surface Γ:

$$\iint\limits_{\Gamma} \sigma_{ji} d\Gamma = \frac{1}{2}\delta_{ji}, \iint\limits_{\Gamma} \varepsilon_{jlk}\zeta_l \sigma_{ji} d\Gamma = \frac{1}{2}\varepsilon_{ijk}\zeta_j, \quad i,j,k,l = 1,2,3. \tag{2.6}$$

With the account of Eq. (2.6) the boundary integral equations of the spatial contact problem for the rigid punch deepened into an elastic half-space, are given by

$$\iint\limits_{\Gamma} \left[\sum_{j=1}^{3} \left(p_j(N) U_{ji}(K,N)\right)\right] d\Gamma = \Delta_i - \varepsilon_{ijk}\zeta_j\psi_k, \quad i,j,k,l = 1,2,3. \tag{2.7}$$

Equation (2.7) assert that the displacement of any point on the punch contact surface is numerically equal to the work of contact forces $p_j(N)$ in the basic state on the displacements $U_{ji}(K, N)$ of the auxiliary state.

Rigid displacements Δ_i and rotations ψ_k of the punch (i, k = 1, 2, 3) are also unknown, and to determine them one should invoke six equations of the punch equilibrium (in the basic state):

$$P_i = \iint\limits_{\Gamma} p_i(N) d\Gamma, \quad M_i = \iint\limits_{\Gamma} \varepsilon_{ijk} x_j p_k(N) d\Gamma, \quad (i,j,k = \overline{1,3}). \tag{2.8}$$

Thus the solution of the spatial contact problem for an absolutely rigid punch of arbitrary shape, deepened into an elastic half-space, under an external static load

of a general type is determined by a system of nine integral equations (2.7), (2.8) which for convenience hereinafter can be presented in the following extended form:

$$\begin{cases} \iint\limits_{\Gamma} \left[p_1(N)U_{11}(K,N) + p_2(N)U_{12}(K,N) + p_3(N)U_{13}(K,N)\right] d\Gamma = \Delta_1 + \eta\psi_3 - \zeta\psi_2, \\ \iint\limits_{\Gamma} \left[p_1(N)U_{21}(K,N) + p_2(N)U_{22}(K,N) + p_3(N)U_{23}(K,N)\right] d\Gamma = \Delta_2 + \zeta\psi_1 - \xi\psi_3, \\ \iint\limits_{\Gamma} \left[p_1(N)U_{31}(K,N) + p_2(N)U_{32}(K,N) + p_3(N)U_{33}(K,N)\right] d\Gamma = \Delta_3 + \xi\psi_2 - \eta\psi_1, \end{cases} \tag{2.9}$$

$$\begin{cases} \iint\limits_{\Gamma} p_1(N)d\Gamma = P_1, \quad \iint\limits_{\Gamma} p_2(N)d\Gamma = P_2, \quad \iint\limits_{\Gamma} p_3(N)d\Gamma = P_3 \\ \iint\limits_{\Gamma} \left[p_3(N)x_2 - p_2(N)x_3\right] d\Gamma = M_1, \\ \iint\limits_{\Gamma} \left[p_1(N)x_3 - p_3(N)x_1\right] d\Gamma = M_2, \\ \iint\limits_{\Gamma} \left[p_2(N)x_1 - p_1(N)x_2\right] d\Gamma = M_3. \end{cases} \tag{2.10}$$

Having solved the system of Eqs. (2.9), (2.10), one can determine three functions of contact stresses p_i and six parameters Δ_i, $\psi_i\psi_i$ $(i = 1, 2, 3)$ of the punch displacement as a rigid solid, i.e. the stress-strained state at the contact surface Γ is determined.

2.2 Finite-Measure Analogue of the Contact Problem Using Direct Boundary-Element Method

Analytical solutions of the system of integral equations (2.7), (2.8) formulated in Sect. 2.1 for deepened punches of any particular geometrical shape have not been obtained yet even for the simplest loading schemes. The main difficulty here, as has been noted by many authors, concerns the integration of the fundamental Mindlin's solution.

For the numerical solution of the spatial contact problem, formulated in the most general way, we use the boundary-element method in its direct formulation [7, 10, 34] when the unknown function values on the boundary have the physical sense of contact pressures and play the role of source densities determining the stress-

strained state inside the stressed domain. The method application to an essentially spatial contact problem under consideration is reduced to the following stages:

(1) discretization of the boundary surface Γ by means of a finite element ensemble;
(2) determination for the boundary elements of a finite set of nodes with respect to which the collocation method is applied, enabling the node values of the unknowns to be related based on a finite-measure analogue of the initial integral equations;
(3) formation of the resolving system of algebraic equations whose coefficients are calculated by analytical and/or numerical integration over each boundary element;
(4) direct or iterative solution of the resolving system of algebraic equations;
(5) finding of the stress-strained state in the given internal points of the stressed medium with invoking the schemes of numerical integration of various orders.

Hereinafter we restrict ourselves to the discretization of the contact surface Γ with a set of boundary elements of polygonal (as a rule, triangular, and/or quadrangular) shape (Fig. 2.3). The overwhelming majority of volumetric deepened punches in the problems of civil engineering (first of all, for geotechnical purposes, see Sects. 3.3 and 3.4) are restricted by fragments of planes or second-order (conical, cylindrical, or spherical) surfaces. A moderate number of flat boundary elements enables the punch boundary of practically any geometrical shape to be approximated with a required accuracy. Therefore, application of non-flat boundary elements in the contact problems of geotechnics is hardly appropriate. Here we note once again that, since in this approach one uses the fundamental Mindlin's solution for the problem of the concentrated force inside the elastic half-space (automatically satisfying the boundary conditions on the stress-free base surface), only the contact surface of the punch and the base can be discretized.

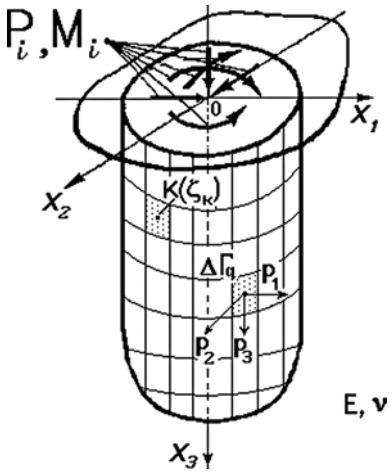

Fig. 2.3 Discretization of the contact surface of the punch and the elastic base using the boundary elements

After the boundary-element discretization of the boundary Γ the integral equation system of the contact problem is given by

$$\begin{cases} \Delta_i = \sum\limits_{q=1}^{m} \iint\limits_{\Delta\Gamma_q} p_j(N) U_{ji}(K_f, N) d\Gamma + \zeta_k \psi_j \varepsilon_{ijk}; \\ P_i = \sum\limits_{q=1}^{m} \iint\limits_{\Delta\Gamma_q} p_i(N) d\Gamma; \quad M_i = \sum\limits_{q=1}^{m} \iint\limits_{\Delta\Gamma_q} \varepsilon_{ijk} p_j(N) x_k d\Gamma; \\ i,j,k = \overline{1,3},\ f,q = 1,2,...m \end{cases} \tag{2.11}$$

where m is the number of the boundary elements on the punch contact surface, $\Delta\Gamma_q$ is the surface of the q-th boundary element, K_f are the collocation points (the finite-element gravity centres), ζ_k are the coordinates of the point K_f ($\zeta_1 = \xi,\ \zeta_2 = \eta,\ \zeta_3 = \zeta$).

The system of Eqs. (2.11) is the consequence of the system of Eqs. (2.7), (2.8) where the calculation of 2-D integrals over the surface Γ is substituted by the sum of integrals over the flat surfaces of the introduced boundary elements $\Delta\Gamma_q$, $q = 1, 2...m$.

Within each boundary element one should assume that the contact forces p_i vary according to a pre-given law. As a rule, polynomial (constant, linear, quadratic, or higher-order) approximation is applied [7, 10, 17, 34, 36]. Application of the boundary-element method to the solution of spatial static problems for finite-size bodies (local strength problems) shows that quite satisfactory results are achieved already at application of piecewise constant or piecewise linear approximation of the unknown densities, in particular, of the stress function. Note that in [16], based on the analysis of the literature, a hypothetic idea is suggested to choose the order of approximation for each boundary element by a unit higher than the order of approximation of the functions to be found. Though this statement has not been proved strictly (it is only confirmed by calculations for the flat and the axisymmetric cases), a conclusion is made that it is appropriate to combine flat boundary elements and constancy of the sought function, second-order elements and linear variation of the sought functions etc. Violation of this correspondence is not justified since it does not result in a guaranteed increase of the accuracy of the approximate solution. Thus, at further application of flat boundary elements the approximation of piecewise constant variation of the sought function of contact stress will be to a certain extent justified. Then, taking into account that stress p_i in theory of elasticity is presented by a derivative of displacement u_i, the application of constant stress on a boundary element corresponds to a linear variation of displacement in the plane of each finite element. This is in agreement with the linear distribution of displacements of the boundary surface of an absolutely rigid punch and is an additional argument for the piecewise constant approximation of the contact stress function in the proposed version of the numerical boundary-element method with application of flat boundary elements.

For m collocation nodes, in which the condition of fulfillment of boundary integral equations is set, we choose points, uniformly distributed over the discretized punch surface. It is quite natural to obtain the first $3m$ equations of the algebraic system of the boundary-element method by locating the unit forces of the auxiliary state in the gravity centres of the boundary elements. Then, in accordance with the approximation applied, the system of integral boundary equations of the spatial contact problem for the absolutely rigid punch deepened into a half-space together with the integral equilibrium equations can be given in the following discrete form:

$$\begin{cases} \Delta_i = \sum\limits_{q=1}^{m} p_j(N_q) \iint\limits_{\Delta\Gamma_q} U_{ji}(K_f, N_q) d\Gamma + \zeta_k \psi_j \varepsilon_{ijk}; \\ P_i = \sum\limits_{q=1}^{m} p_j(N_q) \Delta s_q; \quad M_i = \sum\limits_{q=1}^{m} p_j(N_q) \varepsilon_{ijk} x_k \Delta s_q; \\ i,j,k = \overline{1,3},\ q,f = 1,2,...m \end{cases} \tag{2.12}$$

where $p_j(N_q) = p_j^{(q)}$ are the averaged values of contact stresses in the j-th direction within the q-th boundary element, $N_q \in \Delta\Gamma_q$, $\Delta\Gamma_q$ is the surface of the q-th boundary element, $\Delta S_q = mes(\Delta\Gamma_q)$ is the surface of the q-th boundary element.

In an extended notation the equation system (2.12) is given by

$$\sum_{q=1}^{m} \left[p_1(N_q) \iint\limits_{\Delta\Gamma_q} U_{1j}(K_f, N_q) d\Gamma + p_2(N_q) \iint\limits_{\Delta\Gamma_q} U_{2j}(K_f, N_q) d\Gamma + \right.$$

$$\left. + p_3(N_q) \iint\limits_{\Delta\Gamma_q} U_{3j}(K_f, N_q) d\Gamma \right] = \begin{cases} \Delta_1 + \zeta_f \psi_2 - \eta_f \psi_3, & j = 1, \\ \Delta_2 + \xi_f \psi_3 - \zeta_f \psi_1, & j = 2, \\ \Delta_3 + \eta_f \psi_1 - \xi_f \psi_2, & j = 3, f = 1,...,m, \end{cases} \tag{2.13}$$

$$\sum_{q=1}^{m} p_1(N_q) \Delta s_q = P_1, \sum_{q=1}^{m} p_2(N_q) \Delta s_q = P_2, \sum_{q=1}^{m} p_3(N_q) \Delta s_q = P_3, \quad \text{(2.14a, b, c)}$$

$$\sum_{q=1}^{m} \left[p_3(N_q) y_q - p_2(N_q) z_q \right] \Delta s_q = M_1, \tag{2.14d}$$

$$\sum_{q=1}^{m} \left[p_1(N_q) z_q - p_3(N_q) x_q \right] \Delta s_q = M_2, \tag{2.14e}$$

$$\sum_{q=1}^{m} \left[p_2(N_q) x_q - p_1(N_q) y_q \right] \Delta s_q = M_3 \tag{2.14f}$$

and enables the resolving system of linear algebraic equations of the boundary-element method to be set in a matrix form

$$\mathbf{A}\cdot Z = B \tag{2.15}$$

where $\mathrm{A} = \begin{pmatrix} \mathrm{D}_{3m\times 3m} & \mathrm{C}_{3m\times 6} \\ \mathrm{T}_{6\times 3m} & 0 \end{pmatrix}$ is a square block matrix of the order of $(3m+6)$, $\mathrm{D}_{3m\times 3m} = \left(\delta_{ij}^{(fq)}\right)$ is the influence matrix, $\delta_{ij}^{(fq)} = \begin{pmatrix} \delta_{11}^{(fq)} & \delta_{12}^{(fq)} & \delta_{13}^{(fq)} \\ \delta_{21}^{(fq)} & \delta_{22}^{(fq)} & \delta_{23}^{(fq)} \\ \delta_{31}^{(fq)} & \delta_{32}^{(fq)} & \delta_{33}^{(fq)} \end{pmatrix}, f, q = \overline{1,m}$;

$$C_{3m\times 6} = -\begin{pmatrix} 1 & 0 & 0 & 0 & z_1 & -y_1 \\ 0 & 1 & 0 & -z_1 & 0 & x_1 \\ 0 & 0 & 1 & y_1 & -x_1 & 0 \\ \ldots & \ldots & \ldots & \ldots & \ldots & \ldots \\ 1 & 0 & 0 & 0 & z_m & -y_m \\ 0 & 1 & 0 & -z_m & 0 & x_m \\ 0 & 0 & 1 & y_m & -x_m & 0 \end{pmatrix},$$

$$T_{6\times 3m} = \begin{pmatrix} \Delta s_1 & 0 & 0 & \vert & \Delta s_2 & 0 & 0 & \vert \ldots \\ 0 & \Delta s_1 & 0 & \vert & 0 & \Delta s_2 & 0 & \vert \ldots \\ 0 & 0 & \Delta s_1 & \vert & 0 & 0 & \Delta s_2 & \vert \ldots \\ 0 & -z_1\Delta s_1 & y_1\Delta s_1 & \vert & 0 & -z_2\Delta s_2 & y_2\Delta s_2 & \vert \ldots \\ z_1\Delta s_1 & 0 & -x_1\Delta s_1 & \vert & z_2\Delta s_2 & 0 & -x_2\Delta s_2 & \vert \ldots \\ -y_1\Delta s_1 & x_1\Delta s_1 & 0 & \vert & -y_2\Delta s_2 & x_2\Delta s_2 & 0 & \vert \ldots \end{pmatrix}$$

$$\begin{pmatrix} \ldots & \vert & \Delta s_m & 0 & 0 \\ \ldots & \vert & 0 & \Delta s_m & 0 \\ \ldots & \vert & 0 & 0 & \Delta s_m \\ \ldots & \vert & 0 & -z_m\Delta s_m & y_m\Delta s_m \\ \ldots & \vert & z_m\Delta s_m & 0 & -x_m\Delta s_m \\ \ldots & \vert & -y_m\Delta s_m & x_m\Delta s_m & 0 \end{pmatrix},$$

Z and **B** are column vectors of the size $(3m + 6)$:

$$\mathrm{Z} = (p_1(N_1), p_2(N_1), p_3(N_1)..p_1(N_m), p_2(N_m), p_3(N_m); \Delta_1, \Delta_2, \Delta_3, \psi_1, \psi_2, \psi_3)^{\mathrm{T}},$$

$$\mathrm{B} = (0,0,0,...;P_1, P_2, P_3, M_1, M_2, M_3)^{\mathrm{T}}.$$

The dimensionality of the system of Eq. (2.15) equals $(3m+6)_{\times}(3m+6)$ where m is the total number of the boundary elements used for the approximation of the contact surface of the punch and the elastic base. The vector of the unknowns Z includes $3m$ components of contact stresses $p_i(N_k) = p_i^{(k)}$ as well as six parameters Δ_i, ψ_i of the punch displacement as a rigid solid ($i = 1, 2, 3$; $k = 1, 2,...m$). In a general case, the block $\mathbf{D}_{3m\times 3m}$ of the matrix **A** is non-symmetrical and completely filled. This block is characterized by the diagonal predominance of coefficients.

Application of a conventional Gauss elimination method to solve the linear algebraic equation system (2.15), as shown by a vast experience of calculations performed, results in the numerical solution accuracy and stability, sufficient for the practical purposes. The details of efficient implementation of algorithms of solutions of linear algebraic equation systems of the boundary-element method, appropriate for the specific features of Eq. (2.15), are given below in Sect. 3 (Sect. 3.4).

The coefficients of the main block $\mathbf{D}_{3m\times 3m}$ of the matrix $\mathbf{A}$ are surface integrals of the fundamental Mindlin's solution

$$\delta_{ij}^{(fq)} = \iint\limits_{\Delta\Gamma_q} U_{ij}(K_f, N)d\Gamma(N) \tag{2.16}$$

The analytical calculation of these integrals over flat triangular or quadrangular domains, arbitrarily oriented in an elastic half-space, seems impossible. In practice we have carried out the efficient integration by means of an original numerical-and-analytical approach. It can be assumed that formation of the matrix coefficients of Eq. (2.15) is the key point of the whole boundary-element method since it requires both regular and improper integrals to be calculated with high precision and simultaneously in an optimal way from the point of view of the computation time. These issues need to be considered in more detail what is performed in the following subsection.

2.3 Numerical-and-Analytical Method of Integration of Fundamental Mindlin's Solutions

Formation of the matrix of coefficients of the resolving system (2.15) of linear algebraic equations of the boundary-element method is reduced to the calculations of surface integrals of the fundamental Mindlin's solution for the displacements

$$\delta_{ij} = \iint\limits_{\Delta\Gamma_q} U_{ij}(K_f, N)d\Gamma(N) \tag{2.17}$$

The domains of integration of Eq. (2.17) are the simplest flat polygons (triangles and quadrangles), arbitrarily oriented in the half-space.

The difficulties in the calculation of the integrals of Eq. (2.17) consist in the fact that when the double integrals are reduced to iterated integrals, the primitives cannot be found; besides, near the collocation points (when they belong to the integration domain $\Delta\Gamma$) the integrands become unlimited. In the last case direct application of standard procedures of numerical integration does not lead to the desired results since for 2-D improper integrals it is very difficult to reveal the specific features in the vicinity of the point $K(\xi,\eta,\zeta)$ of application of unit concentrated force by a finite number of summands of the cubature formulae. The experience of numerical calculations has shown that this requires a quite considerable increase of the number of integration points and, simultaneously, their concentration near the integrand

singularities (adaptive numerical integration [34]) in order to obtain the result of the desired accuracy. As a result, sufficient accuracy of the approximate values of improper surface integrals requires too much computer time.

Consider the calculation of surface integrals of $U(K,N)$ Mindlin displacements based on the complementary possibilities provided by analytical and numerical integration methods with direct account of the integrand structure.

In Mindlin equations (1.7) for the displacements the singular terms are fundamental Kelvin's solutions for the whole space, other terms have no singularities (since they correspond to an imaginary point $\tilde{K}(\xi,\eta,-\zeta)$ of unit concentrated force application). Hence, similarly to [9, 10], it is natural to present Mindlin formulae in the form

$$U_{ij} = (U_{ij})^K + (U_{ij})^C \tag{2.18}$$

where superscripts K and C correspond to the singular Kelvin's solution and the auxiliary (regular) solution, respectively. As shown by the experience of numerous calculations, analytical determination of improper integrals of the Kelvin functions (containing only R_1 powers, at $K \in \Delta\Gamma$) and numerical integration of complete Mindlin's solutions at $K \notin \Delta\Gamma$ has appeared an efficient (both in accuracy and in speed) combined method of calculation of improper surface integrals in the spatial problems of elasticity theory for a half-space.

Numerical integration was performed using the cubature formulae of various order with the highest accuracy degree. In each separate case the choice of the number of nodes of the cubature formulae was performed on the base of empiric criteria obtained from an extended series of numerical experiments, including the dependences on the discretization degree and the contact surface shape. A common feature of the obtained regularities was an increase of the order of quadratures with the decrease of the distance from the point K to the integration domain. The detailed data on the numerical integration procedures are presented in Appendix B.

In order to determine the improper surface integrals with a weak (integrable) singularity in the centre of gravity of the boundary element one can apply analytical transformations. As mentioned above, the singularities in the integrand expressions are determined by the summands of the fundamental Kelvin's solutions for an unbounded elastic space [7]:

$$(U_{ij})^K(K,N) = \frac{1}{16\pi G(1-\nu)} \cdot \left[\frac{3-4\nu}{R}\delta_{ij} + \frac{z_i z_j}{R^3}\right] \tag{2.19}$$

where $z_i = \zeta_i - \xi_i$, $R = \sqrt{z_1^2 + z_2^2 + z_3^2}$, $N(\zeta_1,\zeta_2,\zeta_3)$ is a point in the integration domain, $K(\xi_1, \xi_2, \xi_3)$ is the point of application of a unit force (source), ξ_i are global Cartesian coordinates. Note that the Kelvin's solution is a special case of the Mindlin's solution and can be obtained from it at $R_1 = R$, $R_2 \to R$.

From the tensor notation of Eq. (2.19) it follows that the problem is reduced to the exact calculation of the following integrals with a singularity in the centre of gravity of a flat boundary element

$$I_1 = \iint\limits_{\Delta\Gamma} \frac{d\Gamma}{R_1}, I_2 = \iint\limits_{\Delta\Gamma} \frac{z_1 z_3}{R_1^3} d\Gamma, I_3 = \iint\limits_{\Delta\Gamma} \frac{z_2 z_3}{R_1^3} d\Gamma, I_4 = \iint\limits_{\Delta\Gamma} \frac{z_1^2}{R_1^3} d\Gamma, \quad (2.20)$$

$$I_5 = \iint\limits_{\Delta\Gamma} \frac{z_2^2}{R_1^3} d\Gamma, I_6 = \iint\limits_{\Delta\Gamma} \frac{z_3^2}{R_1^3} d\Gamma, I_7 = \iint\limits_{\Delta\Gamma} \frac{z_1 z_2}{R_1^3} d\Gamma.$$

If boundary elements on the surface of the half-space $x_3 = 0$ are used, an additional pair of surface integrals should be included into consideration:

$$I_8 = \iint\limits_{\Delta\Gamma} \frac{z_1}{R_1^2} d\Gamma, I_9 = \iint\limits_{\Delta\Gamma} \frac{z_2}{R_1^2} d\Gamma. \quad (2.21)$$

We connect the point of application of the unit concentrated force $K(\xi,\eta,\zeta) \in \Delta\Gamma$ with the vertices of the boundary element $\Delta\Gamma_j$ (Fig. 2.4) within which this point is located. As a result, the flat integration domain will be divided into $\bar{m}$ additional triangular subelements $\Delta\Gamma_{jk}$ where $k = 1, 2, .., \bar{m}$. Here $\bar{m} = 3$ for a triangular boundary element, $\bar{m} = 4$ for a quadrangular one. It is clear that such an additional mesh, being internal for each boundary element, does not lead to any changes in the general approximating grid on the contact surface. Then, each of the improper integrals considered in Eqs. (2.20) and (2.21) should be substituted by a sum

$$\iint\limits_{\Delta\Gamma_j} \frac{z_1^\alpha z_2^\beta z_3^\gamma}{R_1^\delta} d\Gamma = \sum_{k=1}^{\bar{m}} \iint\limits_{\Delta\Gamma_{jk}} \frac{z_1^\alpha z_2^\beta z_3^\gamma}{R_1^\delta} d\Gamma. \quad (2.22)$$

Here α, β, γ, δ are integer powers, determined in accordance with Eqs. (2.18) and (2.19).

Separate terms in the sum of Eq. (2.22) will be reduced to a set of elementary functions by performing calculations according to a uniform procedure. The apices

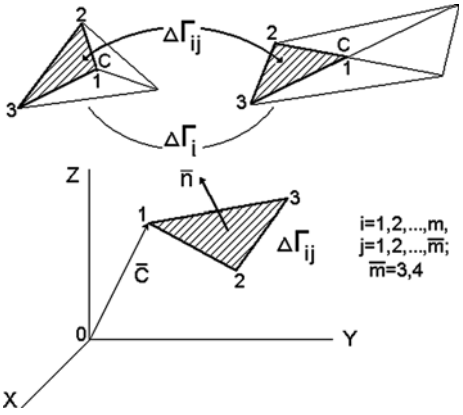

Fig. 2.4 Representation of triangular and quadrangular elements using triangular subelements with a common vertex

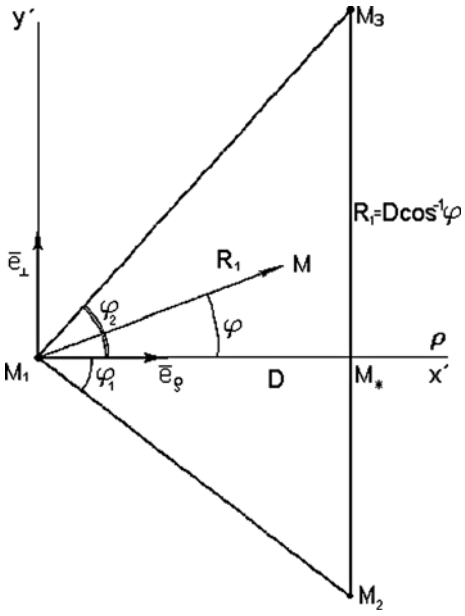

Fig. 2.5 Geometrical representations for integration over a flat triangular domain with a singularity of the integrand in one of the vertices

of a currently considered fragment $\Delta\Gamma_{jk}$ anti-clockwise are put into correspondence with the points $M_1(X_1, Y_1, Z_1)$, $M_2(X_2, Y_2, Z_2)$, $M_3(X_3, Y_3, Z_3)$ in such a way that the first of them be simultaneously the point of application of the unit concentrated force (the boundary-element centre of gravity). In the plane of the triangle $M_1M_2M_3$ we introduce a polar coordinate system with a pole in the point M_1, the polar axis being normal to the M_2M_3 side (Fig. 2.5). We will show that the singularities of the integrands for the integrals under consideration in the point M_1, due to the introduction of the above polar coordinate systems, annihilate.

Denote $\left|\overline{M_1M_*}\right| = |\bar{r}_*| = D$, $\overline{M_1M_3} = \bar{r}_{13}$, $\overline{M_1M_2} = \bar{r}_{12}$. Then

$$\bar{R}_1 = R_1\left(\cos\varphi \cdot \bar{e}_\rho + \sin\varphi \cdot \bar{e}_\perp\right)$$

where $\bar{e}_\rho = \frac{\bar{r}_*}{|\bar{r}_*|} = \{A_1, A_2, A_3\}$; $\bar{e}_\perp = \frac{\bar{r}_{23}}{|\bar{r}_{23}|} = \{B_1, B_2, B_3\}$.

After the transition to the polar coordinates (R_1, φ) I_1 can be readily calculated:

$$I_1 = \iint\limits_{\Delta\Gamma_{jk}} \frac{d\Gamma}{R_1} = \int\limits_{\varphi_1}^{\varphi_2} d\varphi \int\limits_0^{D/\cos\varphi} dR_1 = D\int\limits_{\varphi_1}^{\varphi_2} \frac{d\varphi}{\cos\varphi} =$$

$$= \frac{D}{2} \cdot \ln\left(\frac{1+\sin\varphi_2}{1-\sin\varphi_2} \cdot \frac{1-\sin\varphi_1}{1+\sin\varphi_1}\right) = D\ln\left(\frac{1+\tan\frac{\varphi_2}{2}}{1-\tan\frac{\varphi_2}{2}} \cdot \frac{1-\tan\frac{\varphi_1}{2}}{1+\tan\frac{\varphi_1}{2}}\right). \tag{2.23}$$

The components of the vector $\bar{R}_1$ are written as

$$\begin{aligned} z_1 &= R_1 \left(A_1 \cdot \cos\varphi + B_1 \cdot \sin\varphi\right), \\ z_2 &= R_1 \left(A_2 \cdot \cos\varphi + B_2 \cdot \sin\varphi\right), \\ z_3 &= R_1 \left(A_3 \cdot \cos\varphi + B_3 \cdot \sin\varphi\right) \end{aligned} \tag{2.24}$$

or, since $x' = R_1 \cos\varphi$, $y' = R_1 \sin\varphi$ are the components of the $\bar{R}_1$ vector in the plane of the triangle $M_1M_2M_3$ (in the Cartesian coordinate system $OX'Y'$, formed by e_ρ,$e_\perp$ vectors), then

$$\begin{aligned} z_1 &= A_1 \cdot x' + B_1 \cdot y', \\ z_2 &= A_2 \cdot x' + B_2 \cdot y', \\ z_3 &= A_3 \cdot x' + B_3 \cdot y'. \end{aligned} \tag{2.25}$$

Using Eqs. (2.24), (2.25), the sought integrals can be given by

$$I_q = Q_q \cdot J_1 + S_q \cdot J_2 + T_q \cdot J_3, \quad q = 2,3,...,7;$$
$$I_8 = A_1 \cdot J_4 + B_1 \cdot J_5, \quad I_9 = A_2 \cdot J_4 + B_2 \cdot J_5$$

where

$$\begin{aligned} &Q_2 = A_1 \cdot A_3, \quad S_2 = B_1 \cdot B_3, \quad T_2 = A_3 \cdot B_1 + A_1 \cdot B_3; \\ &Q_3 = A_2 \cdot A_3, \quad S_3 = B_2 \cdot B_3, \quad T_3 = A_3 \cdot B_2 + A_2 \cdot B_3; \\ &Q_4 = A_1^2, \quad S_4 = B_1^2, \quad T_4 = 2A_1 \cdot B_1; \\ &Q_5 = A_2^2, \quad S_5 = B_2^2, \quad T_5 = 2A_2 \cdot B_2; \\ &Q_6 = A_3^2, \quad S_6 = B_3^2, \quad T_6 = 2A_3 \cdot B_3; \\ &Q_7 = A_1 \cdot A_2, \quad S_7 = B_1 \cdot B_2, \quad T_7 = A_2 \cdot B_1 + A_1 \cdot B_2; \\ &J_1 = \iint\limits_{\Delta\Gamma_j k} \frac{\left(x'\right)^2}{R_1^3} d\Gamma, \quad J_2 = \iint\limits_{\Delta\Gamma_j k} \frac{\left(y'\right)^2}{R_1^3} d\Gamma, \quad J_3 = \iint\limits_{\Delta\Gamma_j k} \frac{x'y'}{R_1^3} d\Gamma, \\ &J_4 = \iint\limits_{\Delta\Gamma_j k} \frac{x'}{R_1^2} d\Gamma, \quad J_5 = \iint\limits_{\Delta\Gamma_j k} \frac{y'}{R_1^2} d\Gamma. \end{aligned}$$

Now the integrals J_1, J_2,..., J_5 after the transition to the polar coordinates are obtained in quadratures

$$\begin{aligned} &J_1 = D\left(\sin\varphi_2 - \sin\varphi_1\right), \quad J_2 = I_1 - J_1, \quad J_3 = -D\left(\cos\varphi_2 - \cos\varphi_1\right), \\ &J_4 = D\left[A_1\left(\varphi_2 - \varphi_1\right) + B_1 \ln\left|\frac{\cos\varphi_1}{\cos\varphi_2}\right|\right], \quad J_5 = D\left[A_2\left(\varphi_2 - \varphi_1\right) + B_2 \ln\left|\frac{\cos\varphi_1}{\cos\varphi_2}\right|\right]. \end{aligned} \tag{2.26}$$

Considering the coordinates X_i, Y_i, Z_i, (i= 1, 2, 3) of the apices of the triangular subelement $\Delta\Gamma_{jk}$ to be known, for the sake of completeness we give the formulae to determine the A_i, B_i (i= 1, 2, 3), and D values:

$$A_1 = \frac{X_* - X_1}{D}, \quad A_2 = \frac{Y_* - Y_1}{D}, \quad A_3 = \frac{Z_* - Z_1}{D},$$
$$B_1 = \frac{X_3 - X_2}{\hat{R}}, \quad B_2 = \frac{Y_3 - Y_2}{\hat{R}}, \quad B_3 = \frac{Z_3 - Z_2}{\hat{R}},$$
$$\hat{R} = \sqrt{(X_3 - X_2)^2 + (Y_3 - Y_2)^2 + (Z_3 - Z_2)^2},$$
$$D = \sqrt{(X_* - X_1)^2 + (Y_* - Y_1)^2 + (Z_* - Z_1)^2},$$
$$X_* = X_2 + (X_2 - X_3) \cdot t, \quad Y_* = Y_2 + (Y_2 - Y_3) \cdot t, \quad Z_* = Z_2 + (Z_2 - Z_3) \cdot t,$$
$$t = ((X_2 - X_1)(X_3 - X_2) + (Y_2 - Y_1)(Y_3 - Y_2) + (Z_2 - Z_1)(Z_3 - Z_2)) / \hat{R}^2.$$

The presented expressions Eqs. (2.23), (2.26) for the improper integrals over a flat triangular domain with a singularity in one of its apices enable the accuracy of calculation of the diagonal coefficients of the canonical equation matrix to be essentially increased at a simultaneous decrease of the computation time (in comparison with only numerical integration being used).

In the analytical integration we mostly followed the approach suggested by Cruse [12] who was among the first to obtain analytical expressions for diagonal coefficients of the influence matrix for a flat triangular boundary element. In addition to [12], we have also obtained analytical expressions for special (limiting) integrals, arising at the application of boundary elements on the half-space surface. As one should expect, the final equations (2.23), (2.26) with the accuracy to identity transformations, are in agreement with the results of [12]. Besides, note that the expressions obtained here have the advantages of giving directly the formulae with the known coordinates of the boundary-element nodes what is convenient for practical applications.

In a series of numerical comparison experiments it has been found that the presented analytical-and-numerical integration method appeared comparable in efficiency with the known methods (in view of speed at the given calculation accuracy). In our case the natural increase of the computation time for the integration of the Mindlin's solution is caused by the fact the latter being more complicated than the Kelvin's solution (the presence of additional eighteen deformation cores) and is to a great extent justified by the condition of vanishing of stress at the half-space surface being automatically satisfied.

In view of the comparison performed we would give a brief account of other existing approaches to the formation of influence matrices in the direct boundary-element method for spatial problems of theory of elasticity [5, 6, 35–38]. In all of the known studies the results are obtained in closed form only in the case when the external normal does not change its direction, i.e. for flat boundary elements being used.

A rather descriptive numerical-and-analytical method of calculation of the matrix of an algebraic analogue of the system of boundary integral equations was suggested by Yakimchuk and Kvitka [38]. In the boundary-element plane a local polar coordinate system was introduced. The surface integrals were reduced to iterated integrals for which the integration over the polar radius was performed analytically using a

software for computation of indefinite integrals (*Analytic* language). Numerical integration over the angular variable, using the quadrature formulae, is recommended. The procedure of formation of the influence matrix, suggested in [38] which its authors call semianalytical, does not seem to have visible advantages and has not been further developed or spread for the solution of spatial problems of theory of elasticity in the studies performed by other groups. Since we have performed efficient numerical integration of the fundamental Mindlin's solutions over the optimal quadrature formulae without a transition to consideration of iterated integrals, the semianalytical method, proposed in [38], in case being applied to a half-space, will only create additional difficulties and will obviously be inefficient.

Expressions of a rather cumbersome structure at the analytical calculation of integrals from the Kelvin's solution with density functions in the form of algebraic polynomials are given in [36]. The formulae have a sufficiently general form and are applicable both in the cases the collocation point (pole) belonging to the integration domain ($K \in \Delta\Gamma$) and being located outside it ($K \notin \Delta\Gamma$). Parallel translation and rotation of the Cartesian coordinate system axes are used for the transition to the plane of the boundary element $\Delta\Gamma$. Later, in [37], Roytfarb et al. have also obtained in a closed analytical form the expressions for the coefficients of the Kelvin influence matrix in a special case (with respect to [37]) of piecewise constant approximation of the sought densities and using a local polar coordinate system linked to a side of a polygon, arbitrarily oriented in space. In spite of the obvious efficiency of the methods developed in [36, 37], they possess certain inconveniences in the practical application of the obtained results for solution of problems for an elastic half-space. Namely, the formulae for the primitives contain a great number of transcendental functions, the reliable calculation of which is known to require double-precision computations and, hence, additional computation time. In the case under consideration, when part of the terms $(U_{ij})^c$ in the Mindlin's solution is always subject to numerical integration, the use of analytical transformation to obtain all the coefficients of the Kelvin influence matrix (the total number of integrals is $3m \times 3m$ where m is the number of the boundary elements on the contact surface) is absolutely unjustified. As has been shown by intentional numerical experiments, this increases the computation time by factor of 1.5/2 without a noticeable increase of the calculation accuracy.

In [5, 6, 35], the earlier approach of [36] is developed, using the method of analytical integration of the Mindlin's solutions over triangular flat elements. The practical applicability of the proposed method was restricted by the presence of primitives only for the cases when the flat integration domain was parallel to the axes of the global coordinate system, in which the expressions for the integrands were written. Such approach leaves beyond consideration a great class of problems, important for applications, when at the approximation of contact surfaces boundary elements with different angles of inclination with respect to the coordinate axes arise (Sect. 3.4). Unfortunately, until now we failed to obtain primitives in double integrals from the additional terms of the Mindlin's solution for flat, arbitrarily oriented boundary elements even using such modern powerful software for analytical transformations as *Matcad, Maple, Mathematica, Derive* etc.

2.4 Punch in the Shape of a Rotation Body, Deepened into an Elastic Half-Space

If the contact surface of a punch is a rotation surface and its loading and the boundary conditions possess axial symmetry, the spatial problem of theory of elasticity is essentially simplified. In this case it is quite natural to use more precise and efficient procedures of numerical solution, taking into account the symmetry of the problem. This will save the computation resources and revise the calculation formulae, finally resulting in a more rational design solutions.

In a cylindrical coordinate system (r, φ, z), for which the Oz axis is combined with the punch axis, all the parameters of the stress-strained state are independent of the angular coordinate ϕ and, due to such azimuthal symmetry, the contact problem becomes two-dimensional. The simplest axisymmetric punches are a sphere, a cylinder, a cone (including a frustum of a cone). More complicated axisymmetric structures are presented in Sect. 3.4.

Contact problems with an axial symmetry for punches, deepened into an elastic half-space, can be divided in two groups. The first one corresponds to the forced

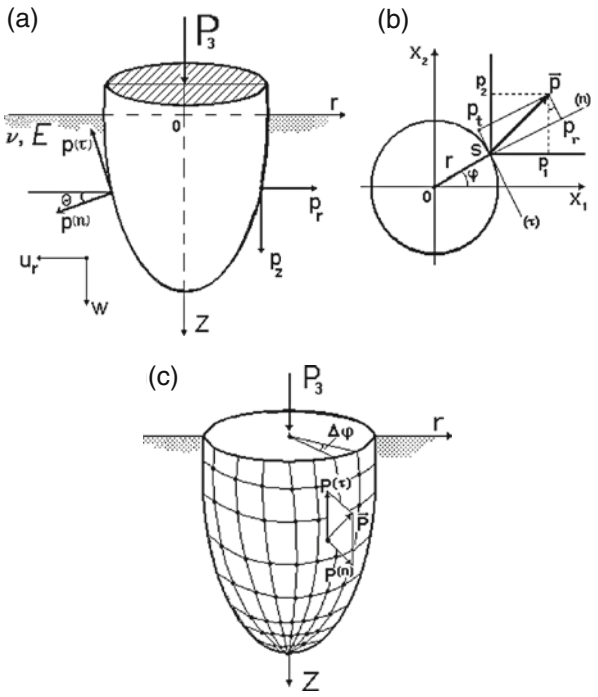

Fig. 2.6 Axially symmetrical contact problem for a rigid punch, deepened into an elastic half-space: (**a**) calculation scheme; (**b**) contact stress in the horizontal plane; (**c**) cyclic (over the angular coordinate) discretization of the contact surface and representation of the contact stress vector on the boundary elements

loading of the punch along the symmetry axis and is characterized by action of tangential and normal stresses on the contact surface as well as radial and axial displacements in the stressed base (Fig. 2.6a). The second group corresponds to the punch torsion under a torque, collinear to the symmetry axis, and is characterized by the action of a pair of tangential contact stresses and solely tangential displacements in the elastic half-space, i.e. the stress distribution, inversely symmetrical with respect to the axis (Fig. 2.7a).

For axisymmetric problems, being one of the most important classes of spatial problems of theory of elasticity, there are efficient methods of solution; a great number of forms of general solution are known [31]. The problem is eventually two-dimensional, for its solution well developed means of theory of analytic and *p*-analytic functions can be used [3, 26]. According to [31], the studies of axisymmetric stress-strained state of bodies of finite size is one of the most extensively developed fields of theory of elasticity, the better results have been achieved only for the flat problem. Nevertheless, still no analytical solutions of contact problems with axial symmetry for punches of even the simplest shape, deepened into an elastic half-space, are available.

Below we present the integral equations for contact problems with axial symmetry and construct efficient boundary-element algorithms of their solution, suitable

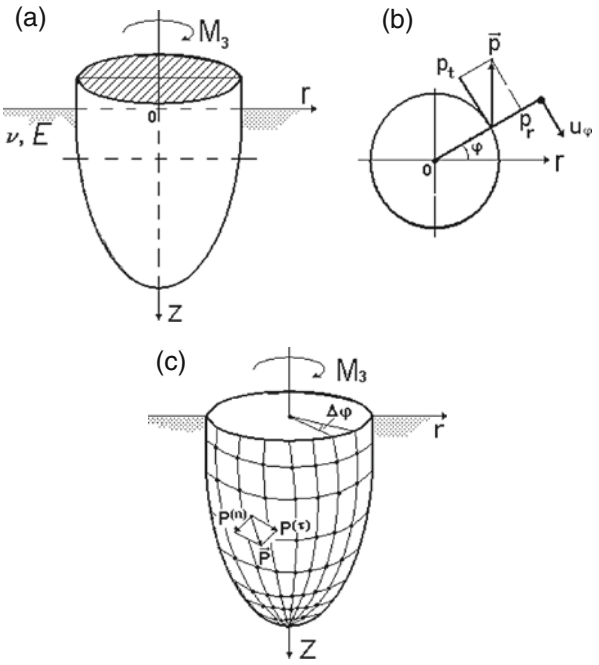

Fig. 2.7 Torsion of an elastic half-space by a rigid deepened punch in the shape of a rotation body: (**a**) calculation scheme; (**b**) stress-strained state of the horizontal plane; (**c**) cyclic (over the angular coordinate) discretization of the contact surface and representation of the contact stress vector on the boundary elements

for punches in the shape of rotation bodies without any restrictions on the meridional cross-section shape.

2.4.1 Axisymmetric Contact Problem

At central loading by an axial force $P_3 = P_z$ a deepened absolutely rigid punch in the shape of a rotation body will be displaced only vertically. The stressed state of an elastic half-space is characterized by radial p_r and vertical p_z components of the contact stress vector (there is no tangential stress due to the axial symmetry) which depend only on the vertical coordinate (Fig. 2.6a, b).

The system of equations of the spatial contact problem for a deepened axisymmetric punch, written using the theorem of reciprocity of works for the basic and the auxiliary states (see Sect. 2.1), is given by

$$\begin{cases} \iint\limits_{\Gamma} \left[p_r(N) U_r^{(1)}(K,N) + p_z(N) W^{(1)}(K,N) \right] d\Gamma - \Delta_3 \iint\limits_{\Gamma} p_z^{(1)}(K,N) d\Gamma = 0, \\ \iint\limits_{\Gamma} \left[p_r(N) U_r^{(3)}(K,N) + p_z(N) W^{(3)}(K,N) \right] d\Gamma - \Delta_3 \iint\limits_{\Gamma} p_z^{(3)}(K,N) d\Gamma = \frac{1}{2} \Delta_3 \end{cases} \tag{2.27}$$

where Δ_3 is vertical displacement of the punch, $p_r(N)$, $p_z(N)$ are the projections of the contact stress vector in the point N on the cylindrical coordinate system axes, $U_r^{(k)}(K,N)$, $W^{(k)}(K,N)$ are displacements of points of the elastic half-space, determined from the following formulae

$$\begin{cases} U_r^{(k)}(K,N) = U_{1k}(K,N) \cdot \cos\varphi + U_{2k}(K,N) \cdot \sin\varphi, \\ W^{(k)}(K,N) = U_{3k}(K,N), \quad k = 1,3 \end{cases} \tag{2.28}$$

$U_{ij}(K,N)$, $i,j = \overline{1,3}$ is the fundamental Mindlin's solution, written in the global Cartesian coordinate system, Γ is the punch contact surface, points $N \in \Gamma$ and $K \in \Gamma$.

The obtained integral equations (2.27) are essentially simplified if one takes into account the equilibrium equations of an elastic body in the shape of the deepened punch in the auxiliary state under the action of unit concentrated forces (see Sect. 2.1):

$$\iint\limits_{\Gamma} p_z^{(1)}(K,N) d\Gamma = 0, \quad \iint\limits_{\Gamma} p_z^{(3)}(K,N) d\Gamma = \frac{1}{2}. \tag{2.29}$$

After substitution of Eq. (2.29) into Eq. (2.27), one obtains integral equations of the axisymmetric contact problem for a rigid punch, deepened into an elastic half-space in the shape of a rotation body, under an axial load:

$$\begin{cases} \iint\limits_{\Gamma} \left[p_r(N) U_r^{(1)}(K,N) + p_z(N) W^{(1)}(K,N) \right] d\Gamma = 0, \\ \iint\limits_{\Gamma} \left[p_r(N) U_r^{(3)}(K,N) + p_z(N) W^{(3)}(K,N) \right] d\Gamma = \Delta_3, \end{cases} \tag{2.30}$$

Boundary integral equations for the axisymmetric problem of Eq. (2.30) can be as well obtained in a formal way using the general equations of the spatial contact problem (2.9) in a special case when the punch does not undergo any rotations ($\psi_1 = \psi_2 = \psi_3 = 0$) and displacements across the symmetry axis ($\Delta_1 = \Delta_2 = 0$). Then the integral equation system (2.9) is given by

$$\begin{cases} \iint\limits_{\Gamma} \left[p_1(N) U_{11}(K,N) + p_2(N) U_{12}(K,N) + p_3(N) U_{13}(K,N) \right] d\Gamma = 0, \\ \iint\limits_{\Gamma} \left[p_1(N) U_{21}(K,N) + p_2(N) U_{22}(K,N) + p_3(N) U_{23}(K,N) \right] d\Gamma = 0, \\ \iint\limits_{\Gamma} \left[p_1(N) U_{31}(K,N) + p_2(N) U_{32}(K,N) + p_3(N) U_{33}(K,N) \right] d\Gamma = \Delta_3. \end{cases} \tag{2.31}$$

In the plane, orthogonal to the punch symmetry axis, for each contact point S we introduce a local coordinate system whose axes are directed tangentially (t) and normally (n) to the cross-section contour (Fig. 2.6b). Then, using the formulae for transformation of the displacement and stress vector components at the axis rotation

$$\begin{cases} p_1 = p_r \cdot \cos\varphi - p_t \cdot \sin\varphi, \\ p_2 = p_r \cdot \sin\varphi - p_t \cdot \cos\varphi, \end{cases} \quad \begin{cases} U_1 = U_r \cdot \cos\varphi - U_t \cdot \sin\varphi, \\ U_2 = U_r \cdot \sin\varphi - U_t \cdot \cos\varphi, \end{cases} \tag{2.32}$$

the system (2.31) can be presented in projections on the cylindrical coordinate system axes

$$\begin{cases} \iint\limits_{\Gamma} \left[p_r(N) U_r^{(1)}(K,N) + p_t(N) U_t^{(1)}(K,N) + p_3(N) U_3^{(1)}(K,N) \right] d\Gamma = 0, \\ \iint\limits_{\Gamma} \left[p_r(N) U_r^{(2)}(K,N) + p_t(N) U_t^{(2)}(K,N) + p_3(N) U_3^{(2)}(K,N) \right] d\Gamma = 0, \\ \iint\limits_{\Gamma} \left[p_r(N) U_r^{(3)}(K,N) + p_t(N) U_t^{(3)}(K,N) + p_3(N) U_3^{(3)}(K,N) \right] d\Gamma = \Delta_3. \end{cases} \tag{2.33}$$

Due to the symmetry at the axial loading the tangential components of the contact stress vector will be zero ($p_t = 0$) what considerably simplifies the system (2.33). Taking into account the fact that the first and the second equations of Eq. (2.33) are linearly dependent (i.e. one of them is a consequence of the other), the integral equation system of the axisymmetric contact problem takes the above form of Eq. (2.30).

Equation (2.30) should be complemented with an integral equation of equilibrium

$$\iint_{\Gamma} p_z(N)\, d\Gamma = P_3 \tag{2.34}$$

where P_3 is the resultant of the external forces, applied to the punch in the direction of the z axis.

Note that other five integral equations of equilibrium in the system (2.10) are fulfilled identically since at the axial loading $P_1 = P_2 = M_1 = M_2 = M_3 = 0$, p_r and p_z are independent of the angular coordinate φ, and after the transition form double integrals to iterated integrals each of the terms will contain zero factors

$$\int_0^{2\pi} \cos\varphi d\varphi = 0, \int_0^{2\pi} \sin\varphi d\varphi = 0.$$

Thus, the axisymmetric problem of theory of elasticity, consisting in the determination of the contact forces p_r, p_z and vertical displacements Δ_3, is reduced to the solution of the integral equation system (2.30) under the integral condition of Eq. (2.34) being fulfilled. Having found the solution, one can easily calculate the normal $p^{(n)}$ and tangential $p^{(\tau)}$ contact stresses based on the known relations

$$\begin{cases} p^{(n)} = p_r \cdot \cos\theta + p_z \cdot \sin\theta, \\ p^{(\tau)} = -p_r \cdot \sin\theta + p_z \cdot \cos\theta \end{cases} \tag{2.35}$$

where θ is the angle between the external normal to the contact surface and the horizontal plane (Fig. 2.6a).

For an approximate solution of the axisymmetric contact problem under consideration we use the direct boundary-element method combined with the piecewise constant approximation of the contact stress function what will enable the integral equations (2.30) and (2.34) to be reduced to a system of linear algebraic equations.

The most convenient way is to divide the contact surface of the punch in the shape of a rotation body into flat boundary elements whose nodes are formed by intersection of the "geographical" system of coordinate lines. For this purpose we build Q planes, containing the symmetry axis, turned by equal angles $\Delta\varphi = 2\pi/Q$. As a result, on the punch surface Q meridional zones will be formed. Then we build $M' = M+1$ horizontal planes, not necessarily equidistant. Consequently, the surface of the deepened part of the punch will be divided into $M \times Q$ boundary elements, among which there will be Q triangular and $(M-1) \times Q$ quadrangular elements

(Fig. 2.6c). We can say that we use cyclic discretization of the rotation surface over the angular coordinate since at a rotation around the symmetry axis by an angle, multiple of $\Delta\varphi = 2\pi/Q$, there will be a coincidence of all the boundary-element nodes with their initial positions. Note that the variation of the distance between the horizontal planes enables one, taking into account the curvature of the punch generatrix, to perform discretization uniformly with the required vertical condensation.

After the discretization of the surface of contact between the deepened part of the punch and the elastic half-space, the formed system of linear algebraic equations of the boundary-element method is given by

$$\begin{cases} \sum\limits_{n=1}^{N} [p_r(N_n) \iint\limits_{\Delta\Gamma_n} d\Gamma + p_z(N_n) \iint\limits_{\Delta\Gamma_n} W^{(1)}(K_i, N) d\Gamma] = 0, \\ \sum\limits_{n=1}^{N} [p_r(N_n) \iint\limits_{\Delta\Gamma_n} U_r^{(3)}(K_i, N) d\Gamma + p_z(N_n) \iint\limits_{\Delta\Gamma_n} W^{(3)}(K_i, N) d\Gamma] = \Delta_3, \\ \sum\limits_{n=1}^{N} p_z(N_n) \Delta s_n = P_3, \quad i = 1,2,...,N. \end{cases} \tag{2.36}$$

Here the following notations are used: $N = M \times Q$ is the total number of the bound elements on the punch contact surface; $p_r(N_n)$, $p_z(N_n)$ are the averaged values of the radial and vertical contact stress, respectively, within the n-th boundary element; K_i are the collocation points (the gravity centres of the boundary elements); ΔS_n is the area of the n-th boundary element.

We further reduce the system (2.36), assuming the above discretization of the contact surface between the punch and the base to be regular, cyclic over the angular coordinate. The latter condition enables one to increase essentially the dimensionality of the algebraic analogue in comparison with the system of Eqs. (2.10) and (2.9) for the general spatial contact problem. If the punch generatrix was divided by the horizontal planes into M sections, and over the angular coordinate into Q meridional zones (being determined by equal dihedral angles $\Delta\varphi = 2\pi/Q$), then the system (2.36) with the account of the cyclicity requirement is given by

$$\begin{cases} \sum\limits_{m=1}^{M} \left[p_r(N_m) \sum\limits_{q=1}^{Q} \iint\limits_{\Delta\Gamma_{M(q-1)+m}} U_r^{(1)}(K_i, N) d\Gamma + p_z(N_m) \sum\limits_{q=1}^{Q} \iint\limits_{\Delta\Gamma_{M(q-1)+m}} W^{(1)}(K_i, N) d\Gamma \right] = 0, \\ \sum\limits_{m=1}^{M} \left[p_r(N_m) \sum\limits_{q=1}^{Q} \iint\limits_{\Delta\Gamma_{M(q-1)+m}} U_r^{(3)}(K_i, N) d\Gamma + p_z(N_m) \sum\limits_{q=1}^{Q} \iint\limits_{\Delta\Gamma_{M(q-1)+m}} W^{(3)}(K_i, N) d\Gamma \right] = \Delta_3 \\ \sum\limits_{m=1}^{M} p_z(N_m) \Delta s_m = P_3/Q, \quad i = 1,2,...,M. \end{cases} , \tag{2.37}$$

Here $M = N/Q$ is the number of boundary elements in a single meridional zone of the punch contact surface.

For the sake of convenient realization of numerical algorithms the algebraic analogue Eq. (2.37) of the integral equation system of the axisymmetric contact problem is presented in the matrix form:

$$\mathbf{A}\cdot Z = B \tag{2.38}$$

where $\mathrm{A} = \begin{pmatrix} \mathrm{D}_{2M\times 2M} & \mathrm{C}_{2M\times 1} \\ \mathrm{T}_{1\times 2M} & 0 \end{pmatrix}$ is a square block matrix of the order $(2M + 1)$,

$$\mathrm{D}_{2M\times 2M} = \begin{pmatrix} a_{11}^{(1)} & b_{11}^{(1)} & a_{21}^{(1)} & b_{21}^{(1)} & \ldots & a_{M1}^{(1)} & b_{M1}^{(1)} \\ a_{11}^{(3)} & b_{11}^{(3)} & a_{21}^{(3)} & b_{21}^{(3)} & \ldots & a_{M1}^{(3)} & b_{M1}^{(3)} \\ \ldots & \ldots & \ldots & \ldots & \ldots & \ldots & \ldots \\ a_{1M}^{(1)} & b_{1M}^{(1)} & a_{2M}^{(1)} & b_{2M}^{(1)} & \ldots & a_{MM}^{(1)} & b_{MM}^{(1)} \\ a_{1M}^{(3)} & b_{1M}^{(3)} & a_{2M}^{(3)} & b_{2M}^{(3)} & \ldots & a_{MM}^{(3)} & b_{MM}^{(3)} \end{pmatrix} \text{ is the influence matrix,}$$

$$\mathrm{C}_{2M\times 1} = -\begin{pmatrix} 0 \\ 1 \\ 0 \\ 1 \\ \vdots \\ 0 \\ 1 \end{pmatrix}, \quad \mathrm{T}_{1\times 2M} = (0,\Delta s_1;0,\Delta s_2;\ldots;0,\Delta s_M)\,;$$

Z and **B** are column vectors of the size $(2M + 1)$:

$$\mathbf{Z} = (p_r(N_1), p_z(N_1);\quad p_r(N_2), p_z(N_2);\ldots p_r(N_M), p_z(N_M);\Delta_3)^T\,,$$

$$\mathbf{B} = (0,0;0,0;\ldots;P_3)^T\,;$$

ΔS_i $(i = 1, 2,\ldots M)$ are the areas of flat triangles or quadrangles, dividing the meridional zone into the boundary elements whose numbering is determined in accordance with the vertical coordinate variation;

$$a_{im}^{(k)} = \sum_{q=1}^{Q} \iint\limits_{\Delta\Gamma_{M(q-1)+m}} U_r^{(k)}(K_i, N)d\Gamma =$$

$$= \sum_{q=1}^{Q} \cos\varphi_q \iint\limits_{\Delta\Gamma_{M(q-1)+m}} U_{1\,k}(K_i, N)d\Gamma + \sum_{q=1}^{Q} \sin\varphi_q \iint\limits_{\Delta\Gamma_{M(q-1)+m}} U_{2\,k}(K_i, N)d\Gamma;$$

$$b_{im}^{(k)} = \sum_{q=1}^{Q} \iint\limits_{\Delta\Gamma_{M(q-1)+m}} W^{(k)}(K_i, N)d\Gamma = \sum_{q=1}^{Q} \iint\limits_{\Delta\Gamma_{M(q-1)+m}} U_{3\,k}(K_i, N)d\Gamma$$

are the coefficients of the influence matrix $\mathbf{D}_{2M\times 2M}$, determined by the numerical-and-analytical integration method, described above in Sect. 2.3, $\varphi_q = (2q-1)\pi/Q$, $k = 1, 3; 4$, $m = 1, 2, \ldots, M$.

It is seen that the dimensionality of the algebraic analogue of the boundary contact problem equals $(2M+1)$ with respect to the values of Δ_3 and $p_r(N_m)$, $p_z(N_m)$ $(m = 1, 2, \ldots M)$ where M is the boundary element number along the punch generatrix.

2.4.2 Torsion of an Axisymmetric Punch in an Elastic Half-Space

Consider a punch in the shape of a rotation body, deepened into an elastic half-space, under the action of a sole torque $M_3 \neq 0$ ($P_1 = P_2 = P_3 = M_1 = M_2 = 0$). Then the punch displacement will be determined only by the angle $\psi_3 \neq 0$ ($\psi_1 = \psi_2 = \Delta_1 = \Delta_2 = \Delta_3 = 0$), characterizing the punch rotation around the Oz axis (Fig. 2.7a). The equation system (2.9) in the special case under consideration is given by

$$\begin{cases} \iint\limits_{\Gamma} \left[p_1(N)U_{11}(K,N) + p_2(N)U_{12}(K,N) + p_3(N)U_{13}(K,N)\right] d\Gamma = \eta \cdot \psi_3, \\ \iint\limits_{\Gamma} \left[p_1(N)U_{21}(K,N) + p_2(N)U_{22}(K,N) + p_3(N)U_{23}(K,N)\right] d\Gamma = -\xi \cdot \psi_3, \\ \iint\limits_{\Gamma} \left[p_1(N)U_{31}(K,N) + p_2(N)U_{32}(K,N) + p_3(N)U_{33}(K,N)\right] d\Gamma = 0. \end{cases} \tag{2.39}$$

Similarly to the case of the axisymmetric problem (see Sect. 2.4.1), using the formulae (2.32) for the transformation of the vector components at the axis rotation, the system (2.39) is presented in projections onto the cylindrical coordinate system axes

$$\begin{cases} \iint\limits_{\Gamma} \left[p_r(N)U_r^{(1)}(K,N) + p_t(N)U_t^{(1)}(K,N) + p_z(N)U_z^{(1)}(K,N)\right] d\Gamma = \eta \cdot \psi_3, \\ \iint\limits_{\Gamma} \left[p_r(N)U_r^{(2)}(K,N) + p_t(N)U_t^{(2)}(K,N) + p_z(N)U_z^{(2)}(K,N)\right] d\Gamma = -\xi \cdot \psi_3, \\ \iint\limits_{\Gamma} \left[p_r(N)U_r^{(3)}(K,N) + p_t(N)U_t^{(3)}(K,N) + p_z(N)U_z^{(3)}(K,N)\right] d\Gamma = 0. \end{cases} \tag{2.40}$$

Since, according to the problem formulation, the punch does not undergo axial forces, there will arise no vertical stress on the contact surface, i.e. $p_z = 0$. Besides,

the system (2.40) will be additionally simplified due to the fact that its first and second equations are linearly dependent (one is the consequence of the other). As a result, the system of boundary integral equations for the contact problem of an elastic half-space torsion due to the axial rotation of a deepened punch will be given by

$$\begin{cases} \iint\limits_{\Gamma} \left[p_r(N) U_r^{(1)}(K,N) + p_t(N) U_t^{(1)}(K,N) \right] d\Gamma = \eta \cdot \psi_3, \\ \iint\limits_{\Gamma} \left[p_r(N) U_r^{(3)}(K,N) + p_t(N) U_t^{(3)}(K,N) \right] d\Gamma = 0, \end{cases} \tag{2.41}$$

where

$$\begin{cases} U_r^{(k)}(K,N) = U_{1k}(K,N) \cdot \cos\varphi + U_{2k}(K,N) \cdot \sin\varphi, \\ U_t^{(k)}(K,N) = -U_{1k}(K,N) \cdot \sin\varphi + U_{2k}(K,N) \cdot \cos\varphi, k = 1,3. \end{cases} \tag{2.42}$$

The equation system (2.41) becomes closed if it is complemented by the integral equilibrium equation

$$\iint\limits_{\Gamma} \left[x_1 p_2(N) - x_2 p_1(N) \right] d\Gamma = M_3. \tag{2.43}$$

Evidently, the other five equilibrium equations of the system (2.10) will be identically fulfilled due to the symmetry of the problem and independence of the contact stress on the angular coordinate, similarly to the case of the axial loading (Sect. 2.4.1).

The equilibrium equation (2.43), similarly to the boundary integral equations (2.41), can be written in terms of the radial and tangential projections of the stress vector. Taking into account that $x_1 = r\cos\varphi$, $x_2 = r\sin\varphi$, and p_1 and p_2 are expressed in terms of p_r and p_t using Eq. (2.32), the equilibrium equation (2.43) is given by

$$\iint\limits_{\Gamma} p_t \cdot r d\Gamma = M_3 \tag{2.44}$$

where $r = \sqrt{x_1^2 + x_2^2} = r(z)$ is the radial coordinate of the contact surface points.

Thus, the inverse symmetrical problem of theory of elasticity, consisting in the determination of the contact forces p_r and p_t and rotation angles ψ_3, is reduced to the solution of the integral equation system (2.41), the integral condition of Eq. (2.44) being fulfilled. Note that the found solution will simultaneously determine the normal $p^{(n)} = p_r$ and tangential $p^{(\tau)} = p_t$ contact stresses (Fig. 2.7c).

The approximate solution of the inverse symmetrical contact problem will be obtained similarly to the above considered (Sect. 2.4.1) axisymmetric problem, using the direct boundary-element method in combination with the piecewise

constant approximation of the contact stress function. Assuming the discretization with the cyclic symmetry to be performed (Fig. 2.7c) and omitting cumbersome intermediate calculations, the integral equations (2.41) and (2.44) can be readily reduced to the following system of linear algebraic equations of the direct boundary-element method:

$$\begin{cases} \sum\limits_{m=1}^{M}\left[p_r(N_m)\sum\limits_{q=1}^{Q}\iint\limits_{\Delta\Gamma_{M(q-1)+m}} U_r^{(1)}(K_i,N)d\Gamma + p_t(N_m)\sum\limits_{q=1}^{Q}\iint\limits_{\Delta\Gamma_{M(q-1)+m}} U_t^{(1)}(K_i,N)d\Gamma\right] = \eta_i\cdot\psi_3, \\ \sum\limits_{m=1}^{M}\left[p_r(N_m)\sum\limits_{q=1}^{Q}\iint\limits_{\Delta\Gamma_{M(q-1)+m}} U_r^{(3)}(K_i,N)d\Gamma + p_t(N_m)\sum\limits_{q=1}^{Q}\iint\limits_{\Delta\Gamma_{M(q-1)+m}} U_t^{(3)}(K_i,N)d\Gamma\right] = 0, \\ \sum\limits_{m=1}^{M} p_t(N_m)r_m\Delta s_m = M_3/Q, \quad i = 1,2,...,M. \end{cases} \tag{2.45}$$

Here $p_r(N_m)$ and $p_t(N_m)$ are the averaged values of the radial and tangential contact stress, respectively, within the m-th boundary element, the rest of notations being the same as those in Sect. 2.4.1.

In the matrix form the algebraic analogue (2.45) of the integral equation system is given by

$$\mathbf{A}\cdot Z = B \tag{2.46}$$

where $\mathrm{A} = \begin{pmatrix} \mathrm{F}_{2M\times 2M} & \mathrm{G}_{2M\times 1} \\ \mathrm{H}_{1\times 2M} & 0 \end{pmatrix}$ is a square block matrix of the order $(2M+1)$,

$$\mathrm{F}_{2M\times 2M} = \begin{pmatrix} g_{11}^{(1)} & h_{11}^{(1)} & g_{21}^{(1)} & h_{21}^{(1)} & \ldots & g_{M1}^{(1)} & h_{M1}^{(1)} \\ g_{11}^{(3)} & h_{11}^{(3)} & g_{21}^{(3)} & h_{21}^{(3)} & \ldots & g_{M1}^{(3)} & h_{M1}^{(3)} \\ \ldots & \ldots & \ldots & \ldots & \ldots & \ldots & \ldots \\ g_{1M}^{(1)} & h_{1M}^{(1)} & g_{2M}^{(1)} & h_{2M}^{(1)} & \ldots & g_{MM}^{(1)} & h_{MM}^{(1)} \\ g_{1M}^{(3)} & h_{1M}^{(3)} & g_{2M}^{(3)} & h_{2M}^{(3)} & \ldots & g_{MM}^{(3)} & h_{MM}^{(3)} \end{pmatrix} \text{ is the influence matrix,}$$

$$\mathrm{G}_{2M\times 1} = -\begin{pmatrix} \eta_1 \\ 0 \\ \eta_2 \\ 0 \\ \vdots \\ \eta_M \\ 0 \end{pmatrix}, \mathrm{H}_{1\times 2M} = (0,r_1\Delta s_1;0,r_2\Delta s_2;...;0,r_M\Delta s_M);$$

Z and **B** are column vectors of the size $(2M + 1)$:

$$\mathrm{Z} = (p_r(N_1),\, p_t(N_1);\, p_r(N_2), p_t(N_2); \ldots p_r(N_M), p_t(N_M); \psi_3)^T,$$

$$\mathrm{B} = (0,0;0,0;\ldots;M_3)^T;$$

$$g_{im}^{(k)} = \sum_{q=1}^{Q} \iint\limits_{\Delta\Gamma_{M(q-1)+m}} U_r^{(k)}(K_i, N)\, d\Gamma =$$

$$= \sum_{q=1}^{Q} \cos\varphi_q \iint\limits_{\Delta\Gamma_{M(q-1)+m}} U_{1\,k}(K_i, N)\, d\Gamma + \sum_{q=1}^{Q} \sin\varphi_q \iint\limits_{\Delta\Gamma_{M(q-1)+m}} U_{2\,k}(K_i, N)\, d\Gamma;$$

$$h_{im}^{(k)} = \sum_{q=1}^{Q} \iint\limits_{\Delta\Gamma_{M(q-1)+m}} U_t^{(k)}(K_i, N)\, d\Gamma =$$

$$= -\sum_{q=1}^{Q} \sin\varphi_q \iint\limits_{\Delta\Gamma_{M(q-1)+m}} U_{1\,k}(K_i, N)\, d\Gamma + \sum_{q=1}^{Q} \cos\varphi_q \iint\limits_{\Delta\Gamma_{M(q-1)+m}} U_{2\,k}(K_i, N)\, d\Gamma$$

are the coefficients of the influence matrix $\mathbf{F}_{2M\times 2M}$, $\varphi_q = (2q-1)\pi/Q$, $k = 1, 3$; $i, m = 1, 2, \ldots, M$.

Evidently, the dimensionality and the structure of the matrix representation of the algebraic analogue of the boundary contact problem in terms of ψ_3 and $p_r(N_m)$, $p_z(N_m)$ $(m = 1, 2, \ldots M)$ values are the same as in the above axisymmetric case.

Thus, we have considered the integral equations of the contact problems for deepened punches with axial symmetry and have constructed an efficient method of their solution ob the base of direct boundary-element formulation. The results of the formulations presented in Sects. 2.4.1 and 2.4.2 enable numerical solutions of the class of contact problems of theory of elasticity, important for practical application, to be effectively constructed. Attention should be paid to the following main advantages of the elaborated algorithms, increasing the efficiency of application of the boundary-element method in engineering.

As noted above, spatial contact problems of theory of elasticity with axial symmetry are two-dimensional, since, due to the independence of the geometrical shape of the punch and the boundary conditions on the angular coordinate, the characteristics of the stress-strained state of the base will be determined only by virtue of the radial r and vertical z coordinates. The application of the boundary-element method with a special cyclic discretization of the contact surface additionally reduces the geometrical dimensionality of the problem: the contact stresses are to be determined only for the points of the broken line, approximating the punch generatrix. Consequently the application of the boundary-element method, enabling the possibility of further reduction of dimensionality, reduces the axisymmetric contact problem to a one-dimensional one.

The time, required for the solution of the contact problems with axial symmetry, will be essentially shortened in comparison with the problems in general spatial formulation, due to the two reasons. First, the dimensionality of the resolving systems of algebraic equations is reduced, and for these systems, in case Gauss elimination method being used, the solution time is proportional to N^3 (N is the number of the equations). Besides, due to the angular (cyclic) symmetry the time for the computation of the influence matrix coefficients will be reduced by factor of $3Q/2$. In practice, in our calculations of contact problems with axial symmetry, based on the proposed reduced formulation, with the number of the boundary elements of about 400, the total computation time was reduced in average by factor of 20 in comparison with that required in case of application of the spatial scheme of the most general way. It should be also mentioned that by increasing the number of the boundary elements along the angular coordinate one can increase the accuracy of the numerical solution of contact problems with axial symmetry without increasing the dimensionality of the system of resolving algebraic equations, increasing only the computation time for the formation of the influence matrix, i.e. without extending the computer RAM resources.

Finally we note that in a great many of studies, devoted to the solution of axisymmetric problems of theory of elasticity for the finite-size bodies, using the Kelvin's solution, the implementation of the boundary-element method implies a procedure of analytical integration over the angular coordinate (See, e.g., the references in [7, 10, 17]). This results in complete elliptical integrals of the first and second order, which, in turn, for the sake of convenience of further numerical calculations, are presented in the form of an expansion over polynomials [1]. A number of authors note that in the axisymmetric case the integral cores have a rather complicated form and the related calculations are cumbersome. In [29], devoted to the axisymmetric contact problem for a rigid deepened punch, integration of the Mindlin's solution over the angular coordinate is performed numerically. Evidently, such an algorithm can be efficient only for the punches of cylindrical shape when the radial coordinate of the contact surface points remains constant. The approach developed here seems more convenient since it enables the solutions for both axisymmetric problems and problems of general spatial formulation to be obtained, based on the same computation algorithm of formation of influence matrices, without loss in accuracy.

2.5 Contact Problems for Rigid Punches Located on the Elastic Base Surface

Considering a spatial contact problem for a rigid punch and an elastic base, we analyze a limiting case when the punch is not deepened, i.e. is located on the elastic base surface (Fig. 2.8). We also assume the punch bottom to be flat; then the contact domain F will be a part of the half-space surface. Hence, in the boundary integral equations of the general spatial contact problem (2.9), (2.10) one should imply $z = \zeta = 0$, and the fundamental Mindlin's solution to be transformed into a

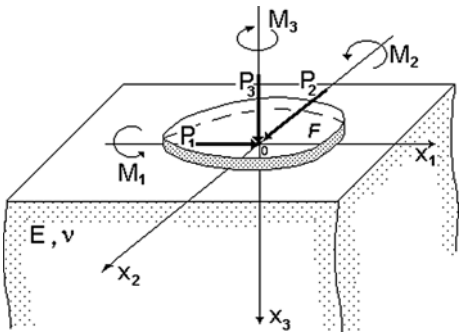

Fig. 2.8 Calculation scheme for the spatial contact problem for a non-deepened rigid punch with a flat bottom, located at the surface of the elastic base

combined Boussinesq-Cerruti solution. The account of the above statements enables the boundary integral equations of the spatial problem of theory of elasticity for a flat rigid punch, contacting an elastic half-space on its surface, to be written in the following form:

$$\begin{cases} \iint\limits_F \left[p_1(N)U^{(1)}(K,N) + p_2(N)V^{(1)}(K,N) + p_3(N)W^{(1)}(K,N)\right] ds = \Delta_1 + \eta \cdot \psi_3, \\ \iint\limits_F \left[p_1(N)U^{(2)}(K,N) + p_2(N)V^{(2)}(K,N) + p_3(N)W^{(2)}(K,N)\right] ds = \Delta_2 - \xi \cdot \psi_3, \\ \iint\limits_F \left[p_1(N)U^{(3)}(K,N) + p_2(N)V^{(3)}(K,N) + p_3(N)W^{(3)}(K,N)\right] ds = \Delta_3 - \eta \cdot \psi_1 + \xi \cdot \psi_2. \end{cases} \tag{2.47}$$

To make the system (2.47) closed we take into account six static equilibrium equations whose form is more simple than in Eqs. (2.10):

$$\begin{cases} \iint\limits_F p_1(N)ds = P_1, \iint\limits_F p_2(N)ds = P_2, \iint\limits_F p_3(N)ds = P_3 \\ \iint\limits_F p_3(N)x_2 ds = M_1, \iint\limits_F p_3(N)x_1 ds = -M_2, \iint\limits_F \left[p_2(N)x_1 - p_1(N)x_2\right] ds = M_3. \end{cases} \tag{2.48}$$

In Eqs. (2.47), (2.48) the following notations are assumed: $p_1(N) = p_x(x, y)$, $p_2(N) = p_y(x, y)$, $p_3(N) = p_z(x, y)$ are the sought contact stress functions, acting in a flat domain F; $U^{(k)}$, $V^{(k)}$, and $W^{(k)}$ $(k = 1, 2, 3)$ are the components of the combined Boussinesq-Cerruti solution for the displacements of the half-space surface due to unit concentrated forces, acting in the direction of the coordinate axes $x_k (k = 1, 2, 3)$.

In comparison with the initial system of Eqs. (2.9), (2.10) for the general spatial contact problem for a deepened punch, the integral equation system (2.47) and (2.48) is simpler. First, the contact pressure functions have to be determined in a flat domain and, hence, both the discretization of the contact domain and the interpolation of the discrete numerical results at the analysis of the contact problem solution will be easier than for a curved surface. Second, the integration procedure at the formation of the influence matrix of the resolving system of algebraic equations of the boundary-element method will require less time than in the case of the full Mindlin's solution. Nevertheless, the total computation time for the solution of the spatial contact problem for a non-deepened punch will be of the same order as for the solution of the contact problem in the most general spatial formulation.

Then we consider two important special cases of spatial loading of non-deepened punches, for which the integral equation system (2.47), (2.48) is essentially simplified, following separately the force balance at contact deformation in the vertical and horizontal planes, respectively. The first case corresponds to the punch indentation by a vertical force and pull-out torques, acting with respect to the coordinate axes in the punch base plane; in the contact domain only vertical (normal) stress exists. In the second case, the punch, linked to the half-space, undergoes a torque; only horizontal (tangential) stresses act on the contact surface.

2.5.1 *Indentation of a Punch with a Flat Smooth Base into an Elastic Half-Space*

Let the punch base be smooth, i.e. in the contact domain F tangential stress is zero. In this case the external load system will not include horizontal forces P_1, P_2 and torque M_3 leading to the tangential stress in the contact domain. The punch will be indented into the base by a vertical force P_3 and torques M_1, M_2, rotating the punch around the axes Ox_1 and Ox_2. Besides, since no friction between the punch bottom and the base surface is assumed, then only one of the three displacement vector components will be varied, namely the vertical one. Thus, in the system (2.47), (2.48) one should imply $\Delta_1 = \Delta_2 = 0$, $\psi_3 = 0$, $P_1 = P_2 = M_3 = 0$, $p_1 = p_2 = 0$. Then the interaction of the punch with the base will be characterized by the function of vertical stress (contact pressure) $p_3 = p(x, y)$ and vertical displacement of the points of the flat punch bottom $W = \Delta_3 - \eta \cdot \psi_1 + \xi \cdot \psi_2$. The above assumptions will reduce the integral equation system of the spatial contact problem for a smooth punch with a flat base to a single equation

$$\iint_F p_3(N) W^{(3)}(K, N) = \Delta_3 - \eta \cdot \psi_1 + \xi \cdot \psi_2. \tag{2.49}$$

In the equilibrium equation system (2.48) three conditions, corresponding to the horizontal force balance, are fulfilled identically, and the other three are given by

$$\begin{cases} \iint\limits_F p_3(N)ds = P_3, \\ \iint\limits_F p_3(N)x_2 ds = M_1, -\iint\limits_F p_3(N)x_1 ds = M_2. \end{cases} \tag{2.50}$$

The system (2.49), (2.50) can be written in the form, corresponding to the notations, established in the literature

$$\iint\limits_p (\xi,\eta)\omega(x,y,\xi,\eta)d\xi d\eta = W_c + \psi_x \cdot (x - x_c) + \psi_y \cdot (y - y_c), \tag{2.51}$$

$$\begin{gathered} \iint\limits_F p(x,y)dxdy = P, \iint\limits_F p(x,y)ydxdy = P \cdot y_c - M_x, \\ \iint\limits_F p(x,y)xdxdy = P \cdot x_c + M_y \end{gathered} \tag{2.52}$$

where

F is the domain of the punch contact with the elastic base;
$p(x, y) = p_3(x, y, 0)$ is the sought contact pressure function,
$W(x,y) = W_c + \psi_x \cdot (x - x_c) + \psi_y \cdot (y - y_c)$ is the displacement of the point $N(x,y)$ of the contact surface of the punch and the elastic base,
W_c is the vertical displacement of the punch centre (x_c, y_c) (point of application of the external forces and torques),
ψ_x and ψ_y are the punch slopes with respect to the coordinate axes,
$\omega(x, y, \xi, \eta) = W^{(3)}(K, N) = (1 - \nu^2)/\pi E\sqrt{(x - \xi)^2 + (y - \eta)^2}$ is the influence function (Boussinesq solution),
P, M_x, M_y are the external vertical force and tilting moments.

Equation (2.51) expresses the fact that the punch displacement $W(N)$ is numerically equal to the sum of works from the contact forces $p\ (x,\ y)$ in the basic state on the vertical displacements of the base surface

$$\omega\ (x, y, \xi, \eta) = \frac{(1 - \nu^2)}{\pi E} \cdot \frac{1}{R}, \quad R = \sqrt{(x - \xi)^2 + (y - \eta)^2}$$

of the auxiliary state, resulting from the action of a unit vertical concentrated force.

Thus, the spatial contact problem on the indentation of a rigid punch with a smooth flat bottom into an elastic half-space is reduced to the finding from a 2-D integral equation (2.51) of the parameters W_c, ψ_x and ψ_y, determining the punch position, and the contact pressure function $p(\xi,\eta)$ over its bottom, satisfying the equilibrium conditions (2.52).

While characterizing the integral equation (2.51), note that, in spite of its simple form, the general studies of the corresponding mixed problem of theory of elasticity are far from being finished [4, 15, 30]. A closed solution of the integral equation (2.51), except for its axisymmetric case, has been found only for elliptical and ring-shaped contact domains. Construction of approximate solutions of the integral equation (2.51) for contact domains of a rather general shape is a serious computational problem. Our overview of the main solution methods for the spatial contact problem for flat complex-shaped punches, interacting with elastic, spatially nonhomogeneous bases, is presented in Sect. 4.1.

We obtain a finite-measure algebraic analogue of the integral equation system (2.51), (2.52) of the contact problem under consideration using the boundary element method. For this purpose first we approximate the contact surface by boundary elements of, in general, polygonal shape. This can be done using practically any of the known considerable amount of mesh generators for arbitrary flat domains, used in finite-difference, finite- and boundary-element methods and having their own specific features. The proposed and applied here algorithms of automatic mesh of flat surfaces of a rather general shape are considered in Sect. 3.3. They are rather economical (require small computation time in comparison with the numerical solution of the problem, for which the mesh is built) and are capable of controlling the mesh geometry using easily treated "free" parameters (condensation degree, maximal and minimal boundary element size etc.).

In the simplest version of the boundary-element method the points of application of the unit concentrated forces are located in the gravity centres of the boundary elements and a piecewise contact approximation of the contact pressures $p(\xi, \eta) = \text{const}$ within each boundary element is assumed. Then, instead of Eqs. (2.51) and (2.52), a linear algebraic equation system with $(m+3)$ unknowns is obtained:

$$\begin{cases} p_1\delta_{i1} + p_2\delta_{i2} + \ldots + p_m\delta_{im} - W_c - \psi_x \cdot (x_c - x_i) - \psi_y \cdot (y_c - y_i) = 0,\ i = \overline{1,m}, \\ p_1\Delta s_1 + p_2\Delta s_2 + \ldots + p_m\Delta s_m = P, \\ p_1\Delta s_1 x_1 + p_2\Delta s_2 x_2 + \ldots + p_m\Delta s_m x_m = P \cdot x_c + M_y, \\ p_1\Delta s_1 y_1 + p_2\Delta s_2 y_2 + \ldots + p_m\Delta s_m y_m = P \cdot y_c - M_x, \end{cases} \tag{2.53}$$

Here $p_i(\xi_i,\ \eta_i)$ are the sought contact stresses for the boundary elements ($i = 1, \ldots, m$),

$$\delta_{ij} = \iint\limits_{F_j} \omega\,(x, y, \xi, \eta)\, d\xi\, d\eta \tag{2.54}$$

is the vertical displacement of the base surface in the point $(x_i,\ y_i)$ coinciding with the gravity centre of the i-th element, due to a unit load, uniformly distributed over the domain F_j of the j-th element, ΔS_i ($i = 1, 2, \ldots m$) are the areas of the flat boundary elements whose combination approximates the contact domain F.

For numerical solution of the system (2.53) one can take the advantage of its matrix form

$$\mathbf{A} \cdot Z = B \tag{2.55}$$

where

$\mathbf{A} = \begin{pmatrix} \mathbf{D}_{m\times m} & \mathbf{C}_{m\times 3} \\ \mathbf{T}_{3\times m} & 0 \end{pmatrix}$ – is a block matrix of the size $(m+3)\times(m+3)$,

$\mathbf{D} = \|\delta_{ij}\|$ is the influence matrix, $i, j = 1,...m$; $\mathbf{C}$ and $\mathbf{T}$ are rectangular matrices

$$\mathbf{C} = -\begin{pmatrix} 1 & x_1 - x_c & y_1 - y_c \\ 1 & x_2 - x_c & y_2 - y_c \\ \ldots & \ldots & \ldots \\ 1 & x_m - x_c & y_m - y_c \end{pmatrix}, \mathbf{T} = \begin{pmatrix} \Delta s_1 & \Delta s_2 & \ldots & \Delta s_m \\ \Delta s_1 \cdot x_1 & \Delta s_2 \cdot x_2 & \ldots & \Delta s_m \cdot x_m \\ \Delta s_1 \cdot y_1 & \Delta s_2 \cdot y_2 & \ldots & \Delta s_m \cdot y_m \end{pmatrix};$$

$\mathbf{Z}$ and $\mathbf{B}$ are column matrices of the size $(m+3)$:

$$Z = \left(p_1, p_2 \ldots p_m; W_c, \psi_x, \psi_y\right)^T, \mathrm{B} = \left(0,0,\ldots 0; P; P \cdot x_c - M_y; P \cdot y_c + M_x\right)^T.$$

The discretization of the contact domain (the punch bottom) will result in the location of all the boundary elements in the same plane (the half-space surface $z = 0$). Therefore, in order to increase the computation algorithm efficiency and accuracy we use in Eq. (2.54) the same procedure of analytical calculation of both singular $(i = j)$ and regular $(i \neq j)$ surface integrals over an arbitrary boundary element with a polygonal contour. This is achieved on the base of algebraic assembling (according to the choice of sign while moving along a closed circuit) of singular integrals over triangles with a singularity in the concentrated force application point. For example, for a triangular boundary element with the apices *A, B,* and *C* and an arbitrary point $K(\xi, \eta)$, located outside (Fig. 2.9a) and inside (Fig. 2.9b) the integration domain the same sum

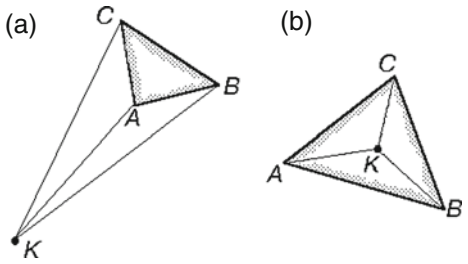

Fig. 2.9 Geometrical scheme of the integration domain in case the point *K* of application of a unit concentrated force being located (**a**) outside and (**b**) inside the boundary element

$$\int\limits_{ABC} = \int\limits_{KAB} + \int\limits_{KBC} + \int\limits_{KCA} .$$

is used, corresponding to the positive (anti-clockwise) direction of moving along the circuit.

The exact calculation of integrals of the form

$$\int\int \omega(x, y, \xi, \eta) d\xi d\eta,$$

over a triangular domain $\Delta F = M_1M_2M_3$, when the integrand has a singularity in the first apex, is reduced to the above obtained integral I_1 (Sect. 2.3). According to Eq. (2.23), in a general case, when the triangle is arbitrarily oriented in the elastic half-space, the latter integral can be found by a combination of logarithmic and trigonometric functions. In our case, when the punch is located on the half-space surface ($Z_1 = Z_2 = Z_3 = 0$), Eq. (2.23) remains unchanged, and the expressions for its parameters are considerably simplified, having the form

$$D = \sqrt{(X_* - X_1)^2 + (Y_* - Y_1)^2}, \quad \hat{R} = \sqrt{(X_3 - X_2)^2 + (Y_3 - Y_2)^2},$$
$$X_* = X_2 - (X_3 - X_2) \cdot p, \quad Y_* = Y_2 - (Y_3 - Y_2) \cdot p,$$
$$p = ((X_2 - X_1)(X_3 - X_2) + (Y_2 - Y_1)(Y_3 - Y_2)) / \hat{R}^2.$$

The simplest form of the system (2.53) is achieved for a circular punch at central ($x_c = 0, y_c = 0$) loading (axisymmetric contact problem). Due to the axial symmetry ($M_x = M_y = 0$), ($\psi_x = \psi_y = 0$), hence instead of Eq. (2.53) one obtains

$$\begin{cases} p_1\delta_{i1} + p_2\delta_{i2} + ... + p_m\delta_{im} - W_c = 0, \, i = \overline{1, m}, \\ p_1\Delta s_1 + p_2\Delta s_2 + ... + p_m\Delta s_m = P. \end{cases} \tag{2.56}$$

The reduction of the system (2.56) is performed similarly to the case of the axisymmetric problem of a deepened punch indentation (Sect. 2.4.1), assuming cyclic discretization of the circular (or the ring-shaped) contact domain. A typical example of such discretization by means of a regular ($\Delta\varphi = \text{const}$) grid of boundary elements whose nodes are obtained by intersection of rays and concentric circles in a polar coordinate system, is shown in Fig. 2.10. Afterwards the system (2.56) is transformed in the following way. In each line of this system there are several terms which, due to the cyclic symmetry, contain the same contact force values, corresponding to the same boundary element number along the radius (or the number of the ring-shaped layer). Combine all such terms in the line, corresponding to each ring-shaped layer. If L is the number of the boundary elements along the punch radius, then the algebraic analogue of the integral equation system on the contact problem for central indentation of a circular (or ring-shaped) punch with a flat smooth bottom takes its most simple form

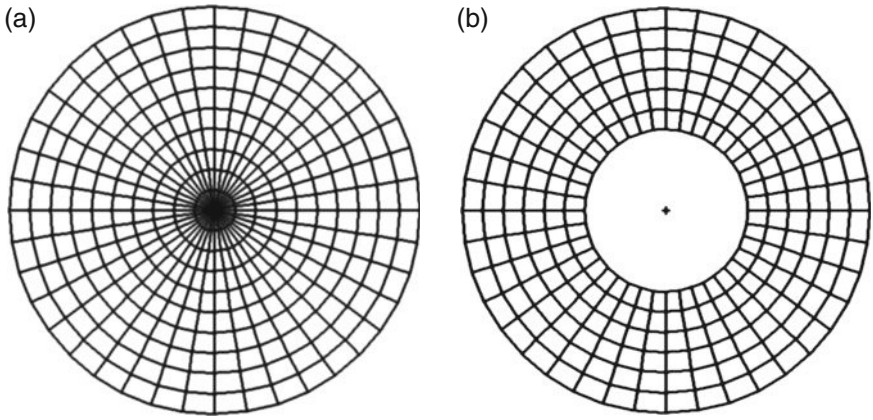

Fig. 2.10 Cyclically symmetrical discretization of circular (**a**) and ring-shaped (**b**) contact domains

$$\sum_{j=1}^{L} A_{ij} \cdot p_j - W_c = 0,\ i = \overline{1,L},\ \sum_{j=1}^{L} p_j \cdot \Delta s_j = \frac{P \cdot L}{m} \tag{2.57}$$

Here the values A_{ij} are found using the influence coefficients δ_{ij} ($i = 1,\ldots, L$; $j = 1,\ldots, m$) from the formula

$$A_{ij} = \sum_{k=1}^{m/L} \delta_{i,j+L(k-1)}.$$

It is evident that the system (2.57) can be also easily obtained from the system (2.37) as a degenerate case of a deepened punch with a smooth bottom $W^{(3)}(K,N) = \omega(x,y,\xi,\eta), \rho_\tau = 0$.

2.5.2 Torsion of an Elastic Half-Space by a Rigid Punch

Let the system of the external load on the punch include only a torque M_3, resulting in the formation of tangential stresses in the contact domain. Neither other torques M_1, M_2, nor both vertical P_3 and horizontal P_1, P_2 external forces are assumed. In this case the punch will rotate with the elastic base, and its position is characterized only by the rotation angle ψ_3 around the Oz axis. In the system (2.47) let $\Delta_1 = \Delta_2 = \Delta_3 = 0$, ($P_1 = P_2 = M_1 = M_2 = 0$). Due to the absence of vertical loads and tilting moments it can be reasonably assumed that the torsion does not affect the pressure distribution below the punch bottom, hence $p_3 = 0$ [19]. Contrary to the above case of the punch indentation (Sect. 2.5.1), now the contact interaction of the punch with the base will be characterized by two functions of contact tangential stress $p_1 = p_x(x, y)$ and $p_2 = p_y(x, y)$. The integral equations (2.47) of the spatial

contact problem of torsion for the case of a flat-bottom punch are reduced to the following system:

$$\begin{cases} \iint\limits_F \left[p_1(N)U^{(1)}(K,N) + p_2(N)V^{(1)}(K,N)\right] ds = \eta \cdot \psi_3, \\ \iint\limits_F \left[p_1(N)U^{(2)}(K,N) + p_2(N)V^{(2)}(K,N)\right] ds = -\xi \cdot \psi_3. \end{cases} \tag{2.58}$$

As follows from Eq. (2.48), the system (2.58) is made closed by a single (the others are fulfilled identically) equilibrium equation, given by

$$\iint\limits_\Gamma \left[p_2(N)x_1 - p_1(N)x_2\right] ds = M_3. \tag{2.59}$$

In Eqs. (2.58) and (2.59) $p_1(N) = p_x(x, y)$ and $p_2(N) = p_y(x, y)$ are the sought functions of tangential stresses acting in the contact domain F;$U^{(k)}$ and $V^{(k)}$ $(k = 1, 2)$ are the components of the Cerruti solution for the half-space surface displacements under unit concentrated horizontal forces in the direction of the Ox and Oy axes, respectively.

Having introduced commonly used notations, we present the system (2.58), (2.59) in a more convenient form for the subsequent analysis:

$$\begin{cases} \iint\limits_F \left[p_1(\xi,\eta)\Omega_1(x,y,\xi,\eta) + p_2(\xi,\eta)\Omega_2(x,y,\xi,\eta)\right] d\xi\, d\eta = y \cdot \psi, \\ \iint\limits_F \left[p_1(\xi,\eta)\Omega_2(x,y,\xi,\eta) + p_2(\xi,\eta)\Omega_3(x,y,\xi,\eta)\right] d\xi\, d\eta = -x \cdot \psi, \end{cases} \tag{2.60}$$

$$\iint\limits_\Gamma \left[p_2(x,y)x - p_1(x,y)y\right] dxdy = M \tag{2.61}$$

where $p_1(x, y)$ and $p_2(x, y)$ are the sought contact tangential stress functions, $\Omega_i(x, y, \xi, \eta)$, $(i = 1, 2, 3)$ are the Cerruti displacement functions:

$$\Omega_1(x,y,\xi,\eta) = U^{(1)}(K,N) = \frac{1+\nu}{\pi E}\left[\nu\frac{x_1^2}{R^3} + (1-\nu)\frac{1}{R}\right],$$

$$\Omega_2(x,y,\xi,\eta) = U^{(2)}(K,N) = V^{(1)}(K,N) = \frac{\nu(1+\nu)}{\pi E}\frac{x_1 y_1}{R^3},$$

$$\Omega_3(x,y,\xi,\eta) = V^{(2)}(K,N) = \frac{1+\nu}{\pi E}\left[\nu\frac{y_1^2}{R^3} + (1-\nu)\frac{1}{R}\right];$$

$x_1 = x - \xi$, $y_1 = y - \eta$, $R = \sqrt{x_1^2 + x_2^2}$; M is the external torque rotating the punch in the horizontal plane by an angle ψ.

Thus, the spatial contact problem on surface torsion of an elastic base by a rigid flat-bottomed punch at full coupling is reduced to the following: from the two-dimensional integral equation system (2.60) one should find the angle ψ and two functions $p_1(x, y)$ and $p_2(x, y)$, satisfying the integral equilibrium condition (2.61).

The exact solutions of the mixed problem of theory of elasticity (2.60) and (2.61) are known only for circular and elliptical punches [19]. Approximate solutions of contact problems on torsion of elastic bases of various types have been obtained by a number of authors [2, 8, 11, 13, 23, 25, 27, 28, 33], but in most cases for circular and ring-shaped punches. For a rectangular domain, the punch rotation angle due to a given torque was determined by Mozhevitinov [22]; however, the contact problem was not solved, but a linear distribution of tangential stresses, depending on the contact point distance from the rotation axis, was suggested. As will be shown below, the numerical solution of the integral equation system (2.60), (2.61) for punches with complex-shaped bottom can be efficiently performed using the boundary-element method in its direct formulation.

If the discretization of the contact domain F is performed by any of the available methods, then a finite-measure algebraic analogue of the system (2.60), (2.61) can be readily obtained in the approximation of piecewise constant functions of contact tangential stresses on the boundary elements similarly to how it has been made in Sect. 2.4.2. We write the resolving solutions of the torsion contact problem under consideration in a discrete form:

$$\begin{cases} \sum\limits_{q=1}^{M} \left[p_1(Q_q) \iint\limits_{\Delta F_n} \Omega_1(P_i, Q) dF + p_2(Q_q) \iint\limits_{\Delta F_n} \Omega_2(P_i, Q) dF \right] = y_i \cdot \psi, \\ \sum\limits_{q=1}^{M} \left[p_1(Q_q) \iint\limits_{\Delta F_n} \Omega_2(P_i, Q) dF + p_2(Q_q) \iint\limits_{\Delta F_n} \Omega_3(P_i, Q) dF \right] = -x_i \cdot \psi, \\ \sum\limits_{q=1}^{M} \left[p_2(P_q) x_q - p_1(P_q) y_q \right] \Delta s_q = M, \quad q = 1,2,...,m. \end{cases} \tag{2.62}$$

Here the following notations are used: $p_1(Q_q)$, $p_2(Q_q)$ are the averaged values of the corresponding radial and vertical contact stress within the q-th boundary element, P_i are the collocation points (the boundary element gravity centres), ΔS_q is the q-th boundary element area, m is the total number of the boundary elements.

In the matrix notation the algebraic analogue Eq. (2.62) of the integral equation system is given by

$$\mathbf{A} \cdot \mathbf{Z} = \mathbf{B} \tag{2.63}$$

where $\mathbf{A} = \begin{pmatrix} \mathbf{F}_{2m\times 2m} & \mathbf{G}_{2m\times 1} \\ \mathbf{H}_{1\times 2m} & 0 \end{pmatrix}$ is a square block matrix of the order $(2m + 1)$,

$$\mathbf{F}_{2m\times 2m} = \left(\begin{array}{cc:cc:c:cc} f_{11} & g_{11} & f_{21} & g_{21} & \cdot\ \cdot & f_{m1} & g_{m1} \\ g_{11} & h_{11} & g_{21} & h_{21} & \cdot\ \cdot & g_{m1} & h_{m1} \\ \hdashline \cdot & \cdot & \cdot & \cdot & \cdot\ \cdot & \cdot & \cdot \\ \cdot & \cdot & \cdot & \cdot & \cdot\ \cdot & \cdot & \cdot \\ \hdashline f_{1m} & g_{1m} & f_{2m} & g_{2m} & \cdot\ \cdot & f_{mm} & g_{mm} \\ g_{1m} & h_{1m} & g_{2m} & h_{2m} & \cdot\ \cdot & g_{mm} & h_{mm} \end{array}\right)$$ is the influence matrix

$$\mathbf{G}_{2m\times 1} = -(y_1, -x_1, y_2, -x_2, ..., y_m, -x_m)^T,$$

$$\psi = \pi q_0/(4G),\ \tau(r) = q_0 r(a^2 - r^2)^{-1/2},\ (q_0 = 3M/4\pi a^3).$$

Z and **B** are column vectors of the size (2*M*+1):

$$\mathbf{Z} = (p_1(P_1), p_2(P_1); p_1(P_2), p_2(P_2); ... p_1(P_m), p_2(P_m); \psi)^T,$$

$$\mathbf{B} = (0,0;0,0;...;M)^T;$$

$$f_{iq} = \iint\limits_{\Delta F_q} \Omega_1(P_i, Q)dF = \iint\limits_{\Delta F_q} \Omega_1(x_i, y_i, \xi, \eta)d\xi d\eta,$$

$$g_{iq} = \iint\limits_{\Delta F_q} \Omega_2(P_i, Q)dF = \iint\limits_{\Delta F_q} \Omega_2(x_i, y_i, \xi, \eta)d\xi d\eta,$$

$$h_{iq} = \iint\limits_{\Delta F_q} \Omega_3(P_i, Q)dF = f\Omega_3(x_i, y_i, \xi, \eta)d\xi d\eta$$

are the coefficients of the influence matrix $\mathbf{F}_{2m\times 2m}$, $i, q = 1, 2, \ldots, m$.

It is evident that the structure of the given matrix representation of the algebraic analogue of the boundary contact problem with respect to the values of ψ_3 and $p_1(P_q)$, $p_2(P_q)$ $(q = 1, 2, \ldots m)$ is similar to the case of the half-space torsion by a deepened punch in the shape of a rotation body considered above in Sect. 2.4.2 with the only difference that the blocks in the influence matrix $\mathbf{F}_{2m\times 2m}$ for a flat-bottomed punch are symmetrical. The coefficients f_{iq}, g_{iq}, h_{iq} of the influence matrix for the Cerruti solution used here are determined analytically using the primitives for the integrals I_1, I_4, I_5, I_7, obtained in Sect. 2.3 in a closed form. Here, similarly to the case of the punch indentation (Sect. 2.5.1), for the calculation of both singular and regular integrals the same method is used, based on the algebraic assembling of integrals over triangles, resting on the sides of flat polygon-type boundary elements. The formulae of the primitives (2.26) for I_1, I_4, I_5, I_7 remain unchanged, and their

parameters are determined from simplified 2-D formulae due to the zero values of the node z-coordinates for all the boundary elements.

We finish the consideration of a half-space torsion by a rigid flat-bottomed punch by a boundary-element formulation of the problem for the circular (or ring-shaped) contact domain.

First we perform cyclic discretization into boundary elements (Fig. 2.10). Then we take into account the axial symmetry of the problem, for which only tangential stresses are possible. Similarly to the above case, we locate the points of application of unit concentrated forces in the boundary-element gravity centres and assume tangential forces $p_t = \tau$, acting in the direction, normal to the radius, to be constant within each boundary element. The algebraic analogue of the integral equation system of the contact problem of a rigid rotation under the torque of a circular (or ring-shaped) punch, bound to the half-space, will be obtained from the system (2.45) as a limiting case of the deepened punch in the shape of a rotation body ($U_t^{(1)}(P,Q) = \tilde{\Omega}(x,y,\xi,\eta)\, p_r = p_z = 0$) in the form

$$\begin{cases} \sum\limits_{j=1}^{L} B_{ij} \cdot \tau_j - y_i \cdot \psi = 0, i = \overline{1,L} \\ \sum\limits_{j=1}^{L} \tau_j \cdot r_j \cdot \Delta s_j = \frac{M \cdot L}{m} \end{cases} \tag{2.64}$$

where

$$B_{ij} = \sum_{k=1}^{m/L} \lambda_{i,j+L(k-1)};\ \lambda_{qn} = \iint\limits_{\Delta F_n} \tilde{\Omega}(P_q, Q) dF = \iint\limits_{\Delta F_n} \tilde{\Omega}(x_q, y_q, \xi, \eta) d\xi d\eta;$$

$$\tilde{\Omega}(x,y,\xi,\eta) = -\Omega_1(x,y,\xi,\eta) \cdot \cos\varphi + \Omega_2(x,y,\xi,\eta) \cdot \sin\varphi;$$

$n = 1,\ldots,m$; m is the total number of boundary elements in the contact domain, $q = 1,\ldots,L$; L is the number of boundary elements along the radial direction.

Note that the problem of torsion of an elastic half-space by a round punch of the radius a has an exact solution [19], enabling the rigid rotation ψ of the punch and the distribution of tangential forces $\tau(r)$ below the punch to be obtained:

$$\psi = \pi q_0/(4G),\ \tau(r) = q_0 r (a^2 - r^2)^{-1/2} (q_0 = 3M/4\pi a^3).$$

An approximate analytical solution of the problem of an elastic half-space torsion due to a ring-shaped punch rotation was obtained in [8].

In the algebraic analogues (2.53), (2.62), and (2.64) the influence matrix coefficients are presented for the classic contact model of an elastic homogeneous half-space. However, all the formulations of spatial contact problems for flat-bottomed punches considered remain valid also for non-classic bases, for which the influence functions exist or can be obtained. The algorithm of solution of such contact problems remains the same, except for the calculation of the influence matrix coefficients. The literature analysis shows that the great majority of the influence functions for non-classic elastic bases can be given by

$$\Lambda_i(x,y,\xi,\eta) = \Lambda_0(x,y,\xi,\eta) + \Lambda_*(x,y,\xi,\eta)$$

where $\Lambda_0(x, y, \xi, \eta)$ is the influence function for a homogeneous elastic half-space (a combined Boussinesq-Cerruti solution), and $\Lambda_*(x, y, \xi, \eta)$ is an additional (non-classic) component, taking into account nonhomogeneity, anisotropy, lamination and other mechanical characteristics of the bases. The additional components of the influence functions $\Lambda_*(x, y, \xi, \eta)$ are regular and do not introduce any principal difficulties in numerical integration. Here, similarly to the case of the Mindlin's solution integration, a numerical-and-analytical procedure, described in Sect. 2.3 and consisting in analytical integration of the components of the influence functions Λ_0 for the elastic half-space and numerical integration of the non-classic component Λ_*, appears to be efficient.

Concerning the above boundary-element formulations of contact problems for a round (or ring-shaped) punch (2.57) and (2.64), it should be noted that in spite of the existing corresponding exact solutions, these algebraic analogues are of great importance for the general development of the proposed version of the numerical boundary-element method. First, they serve as a convenient tool for numerical algorithm testing. Second, these formulations remain unchanged (except for the technical procedure of the influence matrix determination) for various spatial contact models being used and, hence, are a universal tool for the studies of spatial contact interaction of the simplest type (a centrally loaded round punch). The latter case is important for the identification of the parameters of the existing and constantly elaborated influence functions. The formulations of Eqs. (2.57) are (2.64) are undoubtedly helpful as well due to the fact they are valid for practically any important contact problem with axial symmetry, namely for a flat ring-shaped punch. The numerical solution of this problem using the proposed boundary-element algorithms requires, in comparison with the round punch problem, only an obvious slight modification at the contact domain discretization under the condition of the cyclic symmetry being preserved (Fig. 2.10b). Not so many solutions have been obtained for the ring-shaped punch problem (much less than for the round punch, see Sect. 4.1); however, the practical interest to it is rather high [18, 32].

In spite of the simplicity and convenience of the given boundary-element formulation of the contact problems with axial symmetry (2.57) and (2.64), one should take into account that they remain valid only for the base models, for which the influence functions are symmetrically-differential, i.e. when $\Lambda(x,y,\xi,\eta) = \Lambda(x-\xi,y-\eta)$. Otherwise, for the numerical solution of contact problems for round and ring-shaped punches the general boundary-element algorithms of Eqs. (2.53) and (2.62) should be used.

References

1. Abramowitz M, Stegun I A (1972) Handbook of mathematical functions with formulas, graphs, and mathematical tables, 10th edn. Dover, New York
2. Aizikovich S M (1978) Torsion of a nonhomogeneous half-space by a round punch. In: Calculation of shells and plates. Rostov University, Rostov, pp. 156–169 (in Russian)

3. Aleksandrov A Ya, Solovyov Yu I (1978) Spatial problems of theory of elasticity (application of methods of theory of complex-variable functions). Nauka, Moscow (in Russian)
4. Alexandrov V M, Kovalenko E V (1986) Problems with mixed boundary conditions in continuum mechanics. Nauka, Moscow (in Russian)
5. Aleynikov S M, Ikonin S V (1989) Effect of depth factor on the foundation displacements. Bases and Foundations. Budivelnyk, Kyiv 22:6–8 (in Russian)
6. Aleynikov S M, Ikonin S V, Rashutina G N (1993) Numerical solutions of nonlinear spatial contact problems of soil mechanics for pile structures. In: Nonlinear soil mechanics. Proc 6th Russ Conf St Petersburg, vol. 1, pp. 155–160 (in Russian)
7. Banerjee P K, Butterfield R (1981) Boundary element methods in engineering science. McGraw-Hill, New York
8. Borodachev N M, Borodacheva F N (1966) Torsion of an elastic half-space due to a ring-shape punch rotation. Inzh Zh Mekh Tverd Tela (issue 1): 94–99 (in Russian)
9. Brebbia C, Telles J, Wrobel L (1984) Boundary element techniques. Springer-Verlag, Berlin
10. Brebbia C A, Walker S (1980) Boundary element techniques in engineering. Newnes-Butterworths, London
11. Chistyak V I, Ryabokon T N (1988) On the solution of the problem of torsion of a nonhomogeneous elastic layer by a punch. In: Stability and strength of structural elements. Dnipropetrovsk State University, Dnipropetrovsk, pp. 56–64 (in Russian)
12. Cruse T A (1969) Numerical solution in three dimensional elastostatics. Intern J Solids Struct 5: 1259–1274
13. Dudinskiy V I (1984) Torsion of an elastic nonhomogeneous half-space by a circular die. Intern Appl Mech 20: 913–917
14. Galin L A (1980) Contact problems of theory of elasticity and viscoelasticity. Nauka, Moscow (in Russian)
15. Galin L A (ed) (1976) Development of theory of contact problems in the USSR. Nauka, Moscow (in Russian)
16. Goldshtein R V (1978) Supplement. On the issue of application of boundary integral equation method for solving problems of mechanics of solid media. In: Mechanics. New in foreign science. Boundary integral equation method. Computational aspects and applications in mechanics. Mir, Moscow, pp. 182–209 (in Russian)
17. Hartmann F (1989) Introduction to boundary elements: Theory and applications. Springer, Berlin/Heidelberg/New York
18. Instructions on design of plate foundations for tower-type skeleton buildings and structures (1984) Gersevanov NIIOSP, Stroyizdat, Moscow (in Russian)
19. Johnson K L (1985) Contact mechanics. Cambridge University Press, Cambridge
20. Kovneristov G B (1962) Integral equations of the contact problem of theory of elasticity for deepened punches. Works of Kyiv Engineering Institute 20: 200–213 (in Russian)
21. Loytsyanskii L G, Lurye A I (1982) Course of theoretical mechanics. Vol. 1: Statics and kinematics. Nauka, Moscow (in Russian)
22. Mozhevitinov A L (1989) Rotation of a rigid foundation due to a spin torque. In: Bases of power structures. Izv VNIIG Vedeneyeva 215: 76–80 (in Russian)
23. Naumov Yu A, Chistyak V I (1973) Torsion of a nonhomogeneous rigid layer by a punch. In: Dnipropetrovsk State University, Dnipropetrovsk, pp. 12–21 (in Russian)
24. Nowacki W (1970) Teoria sprezystosci. PWN, Warszawa
25. Petrishin V I (1988) Torsion of a multilayer base by a ring-shaped punch. In: Stability and strength of structural elements. Dnipropetrovsk State University, Dnipropetrovsk, pp. 96–99 (in Russian)
26. Polozhiy G I (1963) On the boundary problems of axisymmetrical theory of elasticity. Method of p-analytical functions of complex variable. Ukr Math Zh 15: 25–45 (in Russian)
27. Protsenko V S (1968) Twisting of a generalized elastic half-space. Intern Appl Mech 4 (issue 6): 56–58

28. Rostovtsev N A (1955) To a problem of torsion of an elastic half-space. Prikl Mat Mekh 19 (issue 1): 55–60 (in Russian)
29. Shishov O V (1971) Contact problem for axisymmetrical deepened punches. In: Resistance of materials and theory of structures. Budivelnyk, Kyiv 13: 60–66 (in Russian)
30. Shtayerman I Ya (1949) Contact problem of theory of elasticity. Gostekhizdat, Moscow (in Russian)
31. Solyanik-Krassa K V (1987) Axisymmetrical problem of theory of elasticity. Stroyizdat, Moscow (in Russian)
32. Sorochan E A, Trofimenkov Yu G (ed.) (1985) Bases, foundations and underground structures: Designer's handbook. Stroyizdat, Moscow (in Russian)
33. Ufliand Ia S (1965) Survey of articles on the application of integral transforms in the theory of elasticity. North Carolina State University
34. Ugodchikov A G, Khutoryanskiy N M (1986) Boundary-element method in mechanics of deformable solids. Kazan State University, Kazan (in Russian)
35. Veryuzhskii Yu V, Ikonin S V, Savitskii V V (1982) Application of potential method in calculation of rigid foundations. In: Bases and foundations. Budivelnyk Kyiv 15: 21–25 (in Russian)
36. Veryuzhskiy Yu V (1978) Numerical methods of potential in some problems of applied mechanics. Vyshcha Shkola, Kyiv (in Russian)
37. Vinnik A I, Vorona Yu V, Roytfarb I Z, et al. (1981) Calculation of triaxial stressed state of structural elements using the potential method. In: Resistance of materials and theory of structures. Budivelnyk, Kyiv 38: 77–82 (in Russian)
38. Yakimchuk D K, Kvitka A L (1979) Application of the boundary integral equation method for solving spatial problems of static theory of elasticity. Preprint Inst. Problems of Strength, Kyiv (in Russian)

Chapter 3
Computer Implementation of Boundary-Element `Algorithms`

Abstract This chapter deals with practical implementation of the developed numerical algorithms and substantiation of the reliability of the numerical solutions. It presents the general characteristics and structure of the *Rostwerk* software package for investigating three-dimensional stress-strained states of elastic bases corresponding to the interaction of foundation structures with soil under force factors of general kind. Procedures for creating input databases are described in detail. Algorithms and modules for automatic formation of boundary element grids in plane and in space are presented. An original algorithm for triangulation of flat single – and multiply connected domains, bounded by straight line segments or circle arcs, is described. An algorithm of generation (according to the given triangulation) of dual polygonal boundary element grids of Dirichlet cell type is considered. The created object library of boundary element modules, partitioned into boundary elements, enabling spatial discretization of complex-shaped surfaces of foundation structures, is described. Specific features of solving the systems of linear algebraic equations with asymmetric and close-packed matrices, arising in boundary element analysis, are considered. For solving such systems by direct (Gauss type) methods a special scaling procedure is applied, improving the conditioning of matrices for the finite-dimensional algebraic analogue of a contact problem. The data about the reliability of the numerical solutions are presented. The boundary-element method accuracy and efficiency are demonstrated by the examples of the solved test problems for flat punches of circular, annular and polygonal shapes. Boundary-element solutions for spatial contact problems concerning a rigid spherical inclusion and a cylindrical deepened punch in an elastic half-space are obtained. The final part of the chapter gives the results for numerical-and-analytical solution of the spatial contact problem on impressing a deepened conical punch into an elastic half-space. The method of determination of the deformation modulus from tests for deepened conical indenters with different angles by static loading is substantiated theoretically.

S.M. Aleynikov, *Spatial Contact Problems in Geotechnics*, Foundations of Engineering Mechanics, DOI 10.1007/b11479_3,

3.1 Software for Solving Spatial Problems of Contact of Foundations with Soil Bases

Determination of parameters of contact interaction of foundation structures with soil still remains a complicated problem. This is related mostly to the two reasons: (i) appearance of new foundation structure types accepting force and torque loads of the most general spatial type; (ii) increased demands to the calculation method accuracy.

In the first case, the existing calculation methods are often unable to take into account a variety of features of operation of the new-type foundation structures. In the second case, as a rule, one intends to obtain an economical solution at minimal safety factor values.

The methods of foundation structure calculations from deformation, having been used until the recent time, use simplified models what is explained, on one hand, by the structural complexity of a number of foundation structures and, on the other hand, by the foundation operation being considered without a detailed account of the spatial effect from the above-foundation structures. However, the appearance and development of such a powerful tool for the studies of interaction processes in the "foundation + soil base" system as the boundary-element method, enables a qualitatively new level of calculations of foundation structures of complicated shapes under the spatial type of external factors affecting the foundation from the load carrying structures to be achieved. The calculation model becomes able to take into account a variety of features of real operation of the foundation structures: a complicated shape of the bottom, the presence of extensions on the lateral surface and its non-prismatic shape, nonuniformity of the mechanical properties of the base, action of off-centre loads, impossibility of tensile functioning of soil, etc. Combination of numerical and analytical approaches in the boundary-element method enables rather efficient calculation algorithms to be obtained and the possibilities of modern computer facilities to be fully used. The boundary-element method enables the calculation of foundations of various structure shapes from the base deformation to be performed from the general methodological position. The calculator has no need to make pre-calculation assumptions on the contact stress distribution character, on the presence and localization of areas of the foundation uplifting from the soil, neither to invoke any additional speculations taking into account the specific features of the stress-strained state on the contact surface of the considered foundation structure type and the soil. All the features of the contact stress distribution for a foundation structure are revealed in the course of solving the problem using the boundary-element method. Note that in order to obtain high accuracy of calculations, the time required for the computation, input data preparation, requirements for the computer memory size for the boundary-element method are by two or more orders of magnitude lower than in case finite-element or finite-difference methods being used.

Basic characteristics of the Rostwerk *software.* In order to implement the boundary-element algorithms for solution of spatial contact problems, discussed in Sect. 2, we have worked out and developed a *Rostwerk* code, written using

FORTRAN-77 algorithmic language and oriented for personal computers of various modifications.

We have chosen FORTRAN language since it is available in a great number of operating systems and, being rather simple, still enables efficient program debugging and creating object modules. It is also important that different versions of the FORTRAN language are rather standardized and the transfer of programs from one environment into another will not make great difficulties. Besides, many graphic programs, being used in the input/output programs, are graphic extensions of FORTRAN.

The *Rostwerk* software is intended for the studies of contact interaction of foundation structures with linearly stressed bases under spatial static loading of a general type. The software package enables both deep and shallow rigid foundations of various structural types to be analyzed regarding the second limit state (from the base deformations). The software takes into account the possibility of partial contact of the foundation with soil as well as a variety of non-classical properties of soil bases (lamination, non-uniform compressibility, dependence of mechanical properties on depth etc). The software enables one to calculate deformations of foundation bases of practically any known shape whose contact surface can be (automatically or manually) discretized into flat boundary elements. The external load acting on the foundation should be reduced within the foundation section plane to six components of main vectors of forces and moments along the OX, OY, and OZ axes of the global Cartesian coordinate system. The results of the calculation enable one to determine stress on the contact surface of the foundation and the soil, foundation displacements and slopes as well as areas of the foundation uplifting from the soil.

Processor time required for one version of calculation is not more than 10 min for any PC type in case the contact surface being discretized into 400 boundary elements with the account of tangential stress. In the case of calculation for shallow foundation structures, when one can reduce the problem to the determination of contact pressures, the calculation time is shortened more than three times. The calculation time is reduced even more (by an order of magnitude) in case the foundation has the shape of a rotation body under axial loading (axisymmetric contact problems).

Elaboration of software for boundary-element method was aimed at the following five main objectives:

(1) the software package should be universal in the sense of its applicability to rigid foundation structures of various type (both shallow and deep);
(2) the calculations should enclose interaction of the foundation structure with soil bases characterized by spatial nonhomogeneity;
(3) preparation of the input data should be simple and unified;
(4) computation time required for the input data preparation and requirements for the computer parameters should be minimized;
(5) data interchange between the software package and other software applications should be available.

The first requirement is achieved by the fact that the configuration of the known relatively complex foundation structures can be without principal difficulties described using typical polygonal, conical, spherical, and cylindrical shapes. By locating the foundation structure fragments of the above shapes in the required geometry, one can obtain different types of deep and shallow foundations, used in engineering practice. The software performs the choice (assignment) of the foundation structure shape with simultaneous mesh of its surface into boundary elements semi-automatically, what is described in detail in Sects. 3.3 and 3.4. Extensive practical application of the software has shown the high accuracy of the boundary-element description of the foundation structure geometry (the errors in the determination of contact surface area and volume of bodies even for the moderate number of boundary elements lie within $0.01 \div 01\%$).

The second requirement for the software is satisfied by module assignment of influence functions for elastic bases, being singular fundamental solutions of three-dimensional theory of elasticity. The usage of an influence function is related to the initial data input and can be performed in an explicit way without principal difficulties for all known up to now contact models of elastic non-classical bases. The formulations for some influence functions, most often occurring in practical calculations, have a uniform character and have been considered above in Chap. 1.

In order to satisfy the third demand the input data preparation is organized as follows. It is assumed that the input data are standardized independently of the foundation structure type, shape, type of loading and mechanical (contact) model of the soil base. Similarly the force data (external forces and moments) and geometrical data (boundary-element node coordinates and the direction along the contour) are given. Note that, due to the dicretization of only the contact surface between the foundation and the soil, the input data size is almost by two orders of magnitude smaller than for the finite-element or finite-difference methods which are known to require detailed discretization of the foundation active area in the soil base.

The fourth requirement is satisfied due to the creation of optimal algorithms with analytical solutions being provided to maximally possible depth. This first of all concerns the operation of integration of fundamental solutions for a homogeneous half-space (Kelvin's kernels) at building up the influence coefficient matrices. Numerical integration of singular solutions is known to require long computation times and is avoided in the elaborated algorithm (Sect. 2.3) due to the fact that the software contains the analytical expressions for the results of integration of singular functions over a flat area of boundary elements, arbitrarily oriented in space. Besides, the economy of time and manual work for input data preparation is achieved, on one hand, due to the relatively small size of the input data itself, and on the other hand, due to the elaboration of software modules oriented at automatic discretization of the contact surface of the foundation structure of a given type. A considerable decrease of manual labour for input data preparation as well as the computation time can be achieved for axisymmetric foundation structures as well as for those possessing symmetry planes in the case the foundation being loaded axially or under the action of a flat system of forces.

Finally, the fifth requirement is in the simplest way satisfied by a set of intermediate files being organized in the course of the program performance. These files will become an input data flow for various specialized or general application software.

Structure and main stages of operation of the Rostwerk *software.* The software package has a module structure with partial or complete overlay of common areas to save the computer RAM at each stage of the problem solution. The package consists of the main routine and more than forty subroutines which do not require any additional mathematical software.

The block structural scheme of the software is shown in Fig. 3.1

The `WERK` module controls the sequence of performance of all steps of the boundary-element algorithm.

The `DAN` module is responsible for the input data processing, performs discretization of the contact surface into triangular and quadrangular flat boundary elements, global enumeration of the boundary elements and local enumeration of their nodes in counterclockwise direction (observed from the side of the external normal to the contact surface of the foundation structure), as well as formation of nonyero components of the load vector. The discretization unit is protected from user errors. In case of incorrect input data the program does not continue running and shows an error or a list of possible errors. Besides, in the course of the `DAN` module being run, the coordinates of gravity centres of boundary elements, their areas, direction cosines of external normal vectors are stored on a hard disk. As a result, a file of input geometrical information is formed, whose graphical processing enables the user to "view" the discretized surface of the foundation structure on the screen from any point in space.

After processing the input data, the `SBOR` module is started, forming the influence coefficient matrix for the resolving system of linear algebraic equations with respect to unknown contact stresses. The `SBOR` module itself has a multilevel structure, including subdivision of the boundary elements into triangular subelements with a common vertex in the gravity centres, as well as units responsible for analytical and numerical integration. In the last case the process is performed adaptively with the reduction of the number of the integration nodes at the increase of the distance from the observation point to the centre of the integration domain.

The constructed influence coefficient matrix, complemented by matrix blocks with the data on the static moments of the boundary elements with respect to the coordinate axes, is written to the hard disk for on-run storage. This enables the computation time to be saved at multivariant calculations.

In the course of operation of the `GAUSS` program module the constructed system of linear algebraic equations is solved by Gauss elimination method with selection of the main element in a row. Simultaneously the conditionality number is calculated, characterizing the closeness of the system matrix to degeneration, the numerical solution stability, accumulation of rounding-based errors due to arithmetic operations performed by the computer.

The components of contact stress vectors `PX(I), PY(I), PZ(I), I = 1,N`, obtained by solving the linear algebraic equation system, are transferred to the `STRESS` program module where for each boundary element tangential `PT(I)`

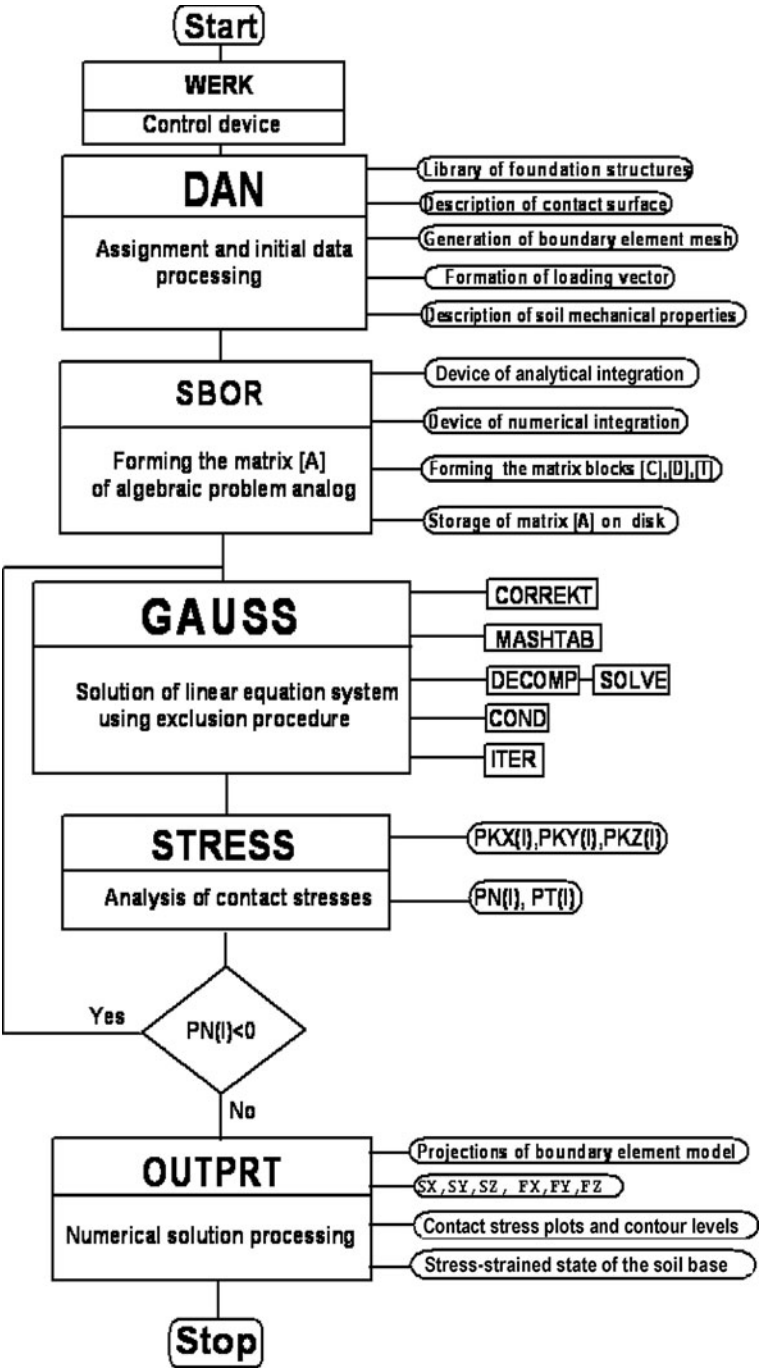

Fig. 3.1 Structural scheme of *Rostwerk* software

and normal PN(I) contact stresses are computed. The numbers of the boundary elements, for which PN(K)<0, are stored for subsequent elimination while considering the contact interaction process. For this purpose the influence matrix elements A(I,J), corresponding to the boundary elements with the number K, are made zero (except the diagonal ones). As a result, for the boundary elements of such type at subsequent calculations the contact stress values will always be zero. The above process is performed by iteration until none of the boundary elements is characterized by tensile stress (PN(I)<0).

From the solution, obtained from the iteration process, the OUTPRT software module prints out (or to a file) the components SU, SV, SW of the displacement vector for the foundation structure centre, its slopes FX, FY, FZ with respect to the coordinate axes, the components of contact stress vectors PX(I), PY(I), PZ(I), PT(I), PN(I), acting on the boundary elements as well as auxiliary geometrical information, required for the description of the results of the numerical solution of the problem. From the programming point of view, the OUTPRT module is standard and does not contain new elements. After its operation being finished, the processing of the computation results can be performed in the user-defined form using various graphical software providing visualization of 2-D and 3-D images.

Input data preparation. All the input data are divided into the data on the type and topology of the foundation structure surface, load-and-geometrical data, containing the data on the structure dimensions and external forces, as well as the data on the soil deformation properties.

First of all the characteristic of the foundation structure type is specified:

IK = 1 – shallow foundation,
IK = 2 – deep foundation.

Then, for each foundation type the contact surface shape should be specified.

For *shallow foundations* in the *Rostwerk* software the following system of characteristics is accepted:

JF = 1 – circle,
JF = 2 – ellipse,
JF = 3 – square,
JF = 4 – rectangle,
JF = 5 – trapezoid,
JF = 6 – quadrangle of general type,
JF = 7 – rectangle with angular cut-outs (cross),
JF = 8 – rectangle with lateral cut-outs (I-beam),
JF = 9 – T-beam,
JF = 10 – L-shaped contact domain,
JF = 11 – closed rectangular-shaped strip bottom,
JF = 12 – symmetrical ring,
JF = 13 – eccentric ring,
JF = 14 – ring with cut-off internal circle,

JF = 15 – rectangle with a circular cut-out,
JF = 16 – circle with a rectangular cut-out.

For *deep foundations* in the *Rostwerk* software the following system of characteristics is accepted:

JZ = 1 – rectangular prismatic,
JZ = 2 – pyramidal,
JZ = 3 – pyramidal with a prismatic head,
JZ = 4 – wedge,
JZ = 5 – stepwise,
JZ = 6 – rectangular prismatic with a set-off in the bottom,
JZ = 7 – prismatic with oblique bottom,
JZ = 8 – slotted with longitudinal cross-section of rectangular shape,
JZ = 9 – slotted rectangular with curved bottom shape,
JZ = 10 – slotted with curved longitudinal cross-section shape,
JZ = 11 – slotted with support widenings,
JZ = 12 – wedge-slotted with a broadened toe,
JZ = 13 – vertical cylindrical,
JZ = 14 – vertical cylindrical with a pile raft of rectangular (JZ = 141) or circular (JZ = 142) shape,
JZ = 15 – inclined cylindrical,
JZ = 16 – inclined cylindrical with a pile raft of rectangular (JZ = 161) or circular (JZ = 162) shape,
JZ = 17 – cylindrical with a spheroconical bearing,
JZ = 18 – cylindrical with an anchor plate,
JZ = 19 – common conical (JZ = 191) and biconical (JZ = 192),
JZ = 20 – deepened sphere.

Then, in accordance with the characteristics JF and JZ, the geometrical characteristics of a specific foundation structure are interactively specified using the following parameters:

DL – length,
DS – width,
DH – thickness,
DZ – depth,
DR – radius,
DA1, DB1, DC1,..., DR1, ... – other characteristic dimensions of the foundation structure (size of set-offs, cut-outs, cross-sections, tilt angles etc.).

The programs for automatic mesh of the contact surface PJF1–PJF15, PJZ1–PJZ20 perform the mesh into boundary elements in accordance with the user-specified degree of discretization density, as a result arrays of spatial coordinates of the boundary-element vertices AX(I,J), AY (I,J), AZ(I,J) being formed,

where I is the global number of the boundary element, J = L(I), L(I) is the attribute vector whose components are assigned values 3 or 4 for triangular or quadrangular boundary elements, respectively.

The library of routines for automatic boundary-element grid formation on the contact surface of the foundation and soil can be supplemented by user in the course of using the *Rostwerk* software. In case the program of automatic mesh being absent, user can form the corresponding arrays manually and transfer them to the main routine via shared space

```
COMMON/ELPS/AX(510,4),AY(510,4),AZ(510.4),L(510).
```

For the accuracy of the obtained results it is very important to provide rational mesh of the foundation structure contact surface into boundary elements. These issues are considered in detail in Sects. 3.3 and 3.4. Here we only note the following basic recommendations concerning discretization:

(a) it is preferable that boundary elements should have regular geometrical shape: triangular boundary elements should be close to equilateral triangles, quadrangular boundary elements – close to squares; the presence of triangular boundary elements with obtuse angles or prolate quadrangular boundary elements results in a decrease of the accuracy of calculation of contact stress values as well of foundation displacements and slopes,
(b) the grid of boundary elements should be condensed near ribs, angular points, and edges where a sharp local increase of contact stress occurs (so-called edge effects in theory of elasticity); if the stress distribution is a priori unknown, in the contact domain a uniform mesh should be performed with maximal density,
(c) discretization of separate fragments, units, or faces of the contact surface should be performed in agreement with the discretization of adjacent areas; if this requirement is fulfilled, the numerical solutions (the calculated contact stress values) will be obtained with higher smoothness degree.

The input data preparation is finished by specifying the values for the soil deformation modulus E and Poisson ratio PU, nonhomogeneity parameters, lamination etc as well as external load vector

```
{PX,PY,PZ,PMX,PMY,PMZ} .
```

These parameters can be specified both in the input data file and interactively by typing on keyboard.

The input data can be printed out, output to a file or the screen on the user's request.

Description of the numerical modeling results. After the problem solving being finished, the calculation results are output to a file RESULT.

This file sequentially contains the data on the dimensionality of the discrete problem:

KR – number of the boundary elements,
3*KR + 6 – total number of unknowns at the calculation of a deepened foundation structure,
KR + 3 – total number of unknowns at the calculation of a shallow foundation structure

as well as

COND – condition number of the matrix of the resolving linear equation system,
S(I), XA(I), YA(I), ZA(I), CNR(I,3) – areas, gravity centre coordinates and direction cosines (components of external normal unit vectors) for the I-th boundary element.

Then the file contains contact stress arrays in the global coordinate system OXYZ, normal and tangential stresses, acting in the I-th boundary element plane (I = 1, 2,..., N)

PKX(I),PKY(I),PKZ(I),PN(I),PI(I)

and vectors of linear {SU, SV, SW } and angular {FX, FY, FZ} displacement of the foundation as a rigid solid.

In case domains of the foundation uplifting being present, the contact stress and displacement arrays can be, on the user's request, output to the RESULT file at each iteration step what enables the development of the foundation uplifting areas to be traced. Besides, as a result of solving the problem, the value S of the total possible area of the foundation contact with soil is output as well as the sum of areas of the boundary elements SK, at which compressive normal stresses act. This enables one to estimate the fraction of the foundation structure surface which interacts with the soil mass.

Stages and specific features of practical calculation. Calculation using the *Rostwerk* software should be performed in the following sequence:

(1) make the calculation scheme, reducing all forces from the above-foundation structure to the centre at the foundation edge to the system of forces and moments $\overline{P}$ = {PX, PY, PZ},-M = {PMX, PMY, PMZ},
(2) analyze the calculation scheme from the point of view of existence of symmetry axes and planes and take these data into account in order to reduce the dimensionality and shorten the time of formation of the influence coefficient matrix,
(3) indicate the topological scheme of the foundation structure surface among the preset schemes (JF = 1, 2,..., 15, JZ = 1, 2,..., 20) or work out a program for automatic mesh of the contact area into boundary elements,
(4) input the input data for geometrical and physical characteristics of the "foundation + soil base" system by their formation within the input data file or interactive typing,
(5) using the visualization program, check the correct enumeration of vertices (counterclockwise) for each boundary element in accordance with the external normal direction (towards the soil),

(6) run the program according to the requirements of the computer operating system.

The following conditions should be obeyed at calculations using the *Rostwerk* software:

- the total number of boundary elements N, into which the foundation structure contact surface is discretized, at general spatial formulation of the problem should not exceed 510 (with the account of tangential stress) and 1530 (without the account of the latter),
- global enumeration of the boundary elements in the software is not strictly determined, but nodes within each boundary element should be enumerated counterclockwise at the observation from the side of the external normal (directed towards the soil),
- influence functions being used (singular fundamental solutions) are set in the form of subroutine functions, whose formal parameters are coordinates of points of observation and application of unit concentrated forces. Mechanical parameters of the elastically stressed base should be transferred to the subroutines using the shared space,
- to provide visual interpretation of the numerical solution of the problem all the data, processed and created by the routines of the *Rostwerk* software, are stored in direct-access files in accordance with the requirements of the graphic software applications used. Therefore, the format of the data storage should be modified in accordance with the rules of the specific graphic data processing software. There is a variety of such software tools which are constantly updated.

The above restrictions are determined by the RAM value and can be revised while using modern hardware. The restriction for the number of the boundary elements was determined by the RAM size and CPU speed of computers, for which the first working version of the software was implemented. While more powerful computers are used, no above noted restrictions are required.

Experience of implementation and work with Rostwerk *software.* The analysis of the results of both test and practical calculations for the second limit state, being considered in detail in the subsequent sections of the book, has shown that the boundary-element *Rostwerk* software has a number of clear advantages over the known software of similar purpose (worked out on the base of finite-element and finite-difference methods).

The software combines the depth of theoretical studies with the simplicity of use and enables one to carry out with the required accuracy calculations of contact interaction of foundations with soil bases which earlier had been considered hardly possible or totally impossible.

The *Rostwerk* code can be easily adapted for any computer with various speed and RAM size, since the routines it contains are written using FORTRAN, a classic language for technical applications.

The organization of the *Rostwerk* software operation with the formation of intermediate files of input data and calculation results enables the elaborated boundary-element software to be linked with other calculation applications as well as computer-aided design tools. In turn, the software can also serve as a base for working out specialized software for computer-aided design of foundations for both typical structures and specialized important objects.

High efficiency of the *Rostwerk* software is also determined by the possibility of calculations to be performed directly in practice since it requires rather small computation time and does not impose any special requirements to the computer hardware. This results in a decrease of manpower effort and reduction of the design work execution period, ability to optimize the calculation schemes, shape and loading parameters of the known and new foundation structures.

3.2 Specific Features of Numerical Solutions of Linear Algebraic Equation Systems with Non-symmetrical Matrices, Arising in Boundary-Element Analysis

Spatial contact problems for rigid punches, interacting with a linearly distorted base, are reduced, as shown in Chap. 2, to the solution of linear algebraic equation systems. The dimensionality of such systems, due to the discretization of only the contact boundary, lower than in the case of finite-element being used; however, the system matrices are completely filled, nonsymmetrical and not always well conditioned [32].

Note that in the finite-element method the matrix of a linear equation system is symmetrical, positively determined and band at corresponding enumeration of node unknowns. For such systems effective methods for numerical solution have been elaborated, requiring relatively small computation time, with high accuracy and numerical stability (square root, block diagonalization, tridiagonalization and other methods [60]).

In [154] the first schemes for numerical solution of boundary integral equations were proposed in the form of boundary-superelement method, resulting in equation systems with symmetrical band matrices. The advantages of the above approach are easy programming of the numerical algorithm and possibility to connecting to finite-element method routines. Simultaneously the boundary-superelement approach has an essential shortcoming: when the equation system for each superelement is built, a matrix, whose dimensionality is proportional to the number of the superelement nodes, needs to be inverted. This essentially reduces the method efficiency and prevents its wide practical application. Tsybenko and Lavrikov [137] proposed a version of direct formulation of boundary integral equation method, directly following from the method of weighted residuals [33] and resulting in a symmetrical and completely filled matrix of resolving equation system.

In the case under our consideration a matrix equation

$$\mathbf{A} \cdot \mathbf{Z} = \mathbf{B} \tag{3.1}$$

corresponding to a resolving system of linear algebraic equations for the spatial contact problem for a rigid punch, will have a nonsymmetrical matrix **A**, containing four blocks. It can be presented in the following form:

$$\mathbf{A} = \begin{pmatrix} \mathbf{D} & \mathbf{C} \\ \mathbf{T} & 0 \end{pmatrix} \tag{3.2}$$

In Eq. (3.2) $\mathbf{D}_{3m\times 3m}$ is a nonsymmetrical square matrix of influence coefficients, m is the total number of boundary elements on the contact surface. Due to the properties of integral operator kernels for problems of theory of elasticity (they are positively determined functions [81, 144]) the matrix **D** is positively determined and possesses a dominant main diagonal. Rectangular sparse matrices $\mathbf{C}_{6\times 3m}$ and $\mathbf{T}_{3m\times 6}$ are determined by the presence of six linear equations being an algebraic analog of integral equilibrium equations. The elements of these matrices are the coordinates of gravity centres, areas and static moments of boundary elements in the global coordinate system (for details see Sect. Section 2.2). First $3m$ components of the solution vector X are unknown contact stress values p_X, p_Y, p_Z, and the rest six components are the parameters of the punch displacement as a rigid solid U, V, W, ψ_X, ψ_Y, ψ_Z.

It should be noted that the elements of the matrix **D** have quite small values in comparison with the nonzero elements of the blocks **C** and **T**. The difference is on the average by factor of E where E is the soil deformation modulus with typical values of 10–20 MPa and reaching the values of the order of 40 MPa and higher for some soil masses of rock type. Hence, the matrix **A** of the resolving system of linear equations (3.1) is nondegenerate, almost completely filled, nonsymmetrical, and with a considerable nonuniformity of coefficients. The nonuniformity will increase with the punch size, i.e. with the increase of the contact surface area of the foundation and soil. According to [45], the matrix **A** belongs to the matrices of storable type since at least $(3m)^2$ of its elements should be stored in the computer's RAM.

From the above stated, as well as with the account of recommendations for application of direct methods of linear equation systems [93] we conclude that for the numerical solution of the equation system (3.1) one should apply a known, widely spread, based on the *LU*-expansion Gauss method of successive elimination of unknowns with a choice of the main (with the largest absolute value) element in a row, column or in the whole matrix. Gauss elimination, expressed in matrix notation, can be treated as triangular factorization of the matrix **A** (*LU*-expansion)

$$\mathbf{A} = \mathbf{LU}$$

and the solution of the system (3.1) is reduced to the solution of two systems

$$\mathbf{LY} = \mathbf{B},\ \mathbf{UZ} = \mathbf{Y}$$

with the lower **L** and the upper **U** triangular matrices.

The most suitable for our calculations are two routines – DECOMP and SOLVE [45]. The DECOMP routine performs the part of the Gauss elimination, depending solely on the matrix. Besides, it stores factors and information on the main elements. The SOLVE routine uses these results to obtain a solution for an arbitrary right-hand part. It is important that DECOMP also evaluates the matrix condition number, being a reliable and useful measure of its closeness to non-degeneracy, stability of the numerical solution, rounding errors, sensitivity to specifying the input data in the right-hand sides of system of Eq. (3.1). Note that the estimated condition number is obtained at a rather easy rate after the triangular expansion of the matrix **A**. having been found by the Gauss method.

In spite of the Gauss method belonging to direct methods of solution (i.e. it should give an exact solution after a finite number of actions), no exact solution is achieved by computer calculation due to computation errors. According to [116], accumulation of rounding errors at solving linear algebraic equation system by Gauss method using floating-point computations results in the sought solution being determined with a relative error

$$\frac{\|\overline{Z} - Z\|}{\|Z\|} = o\left[\text{cond}(\mathbf{A}) \cdot n \cdot 2^{-t}\right] \tag{3.3}$$

where $\text{cond}(\mathbf{A}) = ||\mathbf{A}|| \cdot ||\mathbf{A}^{-1}||$ is the condition number of the matrix **A**, n is the order of the matrix **A**, t is the number of digits in the mantissa of a floating-point number in binary representation. For a typical personal computer 2^{-t} is approximately equal to 10^{-6}–10^{-8}.

In the case under consideration direct application of the Gauss elimination method (routines DECOMP, SOLVE etc.) results in a rather high overall computation error, evidenced by the increase of condition numbers cond(**A**), reaching the order of 10^6 and higher. Besides, note that if the matrix **A** of the system (3.1) is not degenerate, then by increasing the computer word length one can always reduce the rounding error and obtain a numerical solution close to the exact solution of the problem. However, calculation with double or triple number of digits accordingly increases the computation time and computer RAM size which, even at current level of computer equipment, is not available for the most of the practical problems.

On the other hand, it follows from Eq. (3.3) that in order to reduce the numerical solution error one should try to increase the input data accuracy or to reformulate the algebraic analog (3.1) of the integral equation system for the spatial contact problem with respect to other parameters.

Since the right-hand sides of the system (3.1) are given exactly, and the coefficients of the matrix **A** are determined by numerical-and-analytical method with controlled accuracy, then in order to obtain a well conditioned system some artificial-looking steps should be taken.

First, in order to reduce the condition number of the matrix **A** we effectively use scaling of a linear equation system or, in other words, multiplication of the matrix equation (3.1) at the left-hand side and at the right-hand side by diagonal matrices $\mathbf{Q}_1$ and $\mathbf{Q}_2$. In a general case, scaling of the system (3.1) can be given by

$$\mathbf{Q_1 A Q_2 Y = Q_1 Y, Z = Q_2 Y}. \tag{3.4}$$

Studies of a number of authors show [28, 43] that a successful scaling improves the computation process, increasing the stability of the numerical solution to the effect of rounding errors. For many practical problems unilateral scaling, i.e. transition from the matrix **A** to the matrix **AQ** or **QA** appears to be sufficient.

We have performed numerical experiments on unilateral scaling of the system (3.1) for a number of models and practical problems of contact deformation of foundations with soil bases. The last six columns of the matrix **A** (containing coefficients at unknown punch displacements) were divided by the same constant number μ. As a result of an extensive series of calculations, we have found an optimal value $\mu \approx 10^2$ resulting to the decrease of the condition number on the average by 3–4 orders of magnitude. Note that, in accordance with the rules of linear algebra in the solution, obtained after scaling, the last six components determine the sought displacement values with the accuracy of a constant factor, i.e. in the form

$$\mu U, \mu V, \mu W, \mu\psi_x, \mu\psi_y, \mu\psi_z.$$

Therefore, in order to obtain a physical solution one should in a {3*m*+ 6}-dimensional solution vector divide only last six components by the scaling factor μ, in this scaling method first 3*m* components corresponding to invariable contact stress values, i.e. those which do not need to be corrected. Note also a possible method of multiparametric (μ_i, $i = 1, 2, \ldots 6$) scaling of the matrix of system (3.1) over each of the components of displacement vectors of the punch as a rigid solid. However, such approach requires extensive methodological studies which we have not performed. This approach can be, undoubtedly, quite useful for the numerical solution improvement in case specific types of foundation structures and spatial loading types being considered.

The estimated value cond(**A**) of 10^2, obtained in our practical calculations, is the evidence for the good condition of the system (3.1) transformed by scaling, i.e. for the closeness of the approximate numerical solution to the exact one. This can be confirmed by iterative refinement of numerical solutions, intentionally performed for many problems. The value of correction to the obtained solution always was small, and in most cases even zero. From this one can conclude that numerical solutions, obtained using scaling, coincide with the exact solution of the system (3.1) within the machine word length.

Second, the experience of the numerical calculations performed has shown that along with the scaling of the matrix **A** of the system (3.1) a reduction of the condition number (hence, an increase of accuracy of the numerical solution being obtained) is possible due to rearrangement of first 3*m* its variables (unknown contact stress

values). In the initial formulation of the system (3.1) the vector of unknowns **Z** was determined as

$$\mathbf{Z} = (P_{\mathrm{x}}^{(1)}, P_{\mathrm{y}}^{(1)}, P_{\mathrm{z}}^{(1)}, P_{\mathrm{x}}^{(2)}, P_{\mathrm{y}}^{(2)}, P_{\mathrm{z}}^{(2)}, \ldots, P_{\mathrm{x}}^{(\mathrm{m})}, P_{\mathrm{y}}^{(\mathrm{m})}, P_{\mathrm{z}}^{(\mathrm{m})}, \Delta_{\mathrm{x}}, \Delta_{\mathrm{y}}, \Delta_{\mathrm{z}}, \psi_{\mathrm{x}}, \psi_{\mathrm{y}}, \psi_{\mathrm{z}}) .$$

At such order of unknown contact stress values there is alteration of columns of different types: projections of contact stress vectors on different coordinate axes can be essentially different in the order of magnitude. If the vector of unknowns is transformed to the form

$$Z = \left(P_{\mathrm{x}}^{(1)}, P_{\mathrm{x}}^{(2)}, P_{\mathrm{x}}^{(3)}, \ldots, P_{\mathrm{x}}^{(\mathrm{m})}, P_{\mathrm{y}}^{(1)}, P_{\mathrm{y}}^{(2)}, \ldots, P_{\mathrm{y}}^{(\mathrm{m})}, P_{\mathrm{z}}^{(1)}, P_{z}^{(2)}, \ldots, P_{\mathrm{z}}^{(\mathrm{m})}, \Delta_{\mathrm{x}}, \Delta_{\mathrm{y}}, \Delta_{\mathrm{z}}, \psi_{\mathrm{x}}, \psi_{\mathrm{y}}, \psi_{\mathrm{z}}\right),$$

then the columns of the matrix **A** appear arranged in groups with close values of components and thereby improve the structure of the matrix **A**.

The corresponding numerical experiments have revealed a quite noticeable decrease of the condition numbers of the matrix **A** after the above rearrangement of unknowns. Besides, a general acceleration of the program performance for solving linear equation systems for matrices with improved structure was noticed (rearrangement and selection of the main element consume much computation time). Afterwards all calculations of processes of contact interaction of foundation structures with soil were carried out with mandatory scaling of the matrix A of the resolving system of linear equations, and in the cases of deepening – also with the rearrangement of the system (3.1) over uniform variables.

Finally note that for a more accurate check of the effect of rounding errors being introduced at each arithmetic operations, *Rostwerk* software package contains a routine, using the algorithm of Godunov et al. [51], which takes into account the effect of the rounding errors at the specific computer used for the calculations and outputs the result of solving linear algebraic equation systems by Gauss method with a guaranteed accuracy. Besides, this program can in the course of computation find out that a given system possesses a condition level insufficient to guarantee any accuracy at a computer of the given capacity. In practice, due to high computation time, we used the routine for solving systems with guaranteed accuracy only for test calculations before a series of computations for foundations of a given type or while using different contact models of elastic bases for the sake of additional substantiation of reliability of the numerical solutions being obtained.

3.3 Effective Discretization of 2-D Domains of Complex Shape at Numerical Solving of Spatial Contact Problems of Theory of Elasticity

It is well known that numerical implementation of the boundary integral equation method for solving contact (mixed) problems of spatial theory of elasticity assumes a stage of mesh of the contact surface into boundary elements, resulting in the

discretization of the initial problem. The arising linear algebraic equation systems have asymmetrical, completely filled matrices whose orders correspond to the number of the mesh elements. With the increase of the number of boundary elements a trend to worse condition of such matrices is observed, and this affects the accuracy of the results being obtained. This feature of the boundary-element method as well as restricted capacities of the computing facilities urge the elaboration of such an algorithm of contact surface mesh which could possibly satisfy the following, in general, contradicting requirements. On one hand, it should be aimed at obtaining minimal number of the mesh elements, on the other hand it should be universal enough and generate a high-quality mesh, adaptive to the problem requirements. These circumstances result in the necessity to apply mostly piecewise constant approximation of the contact pressure field in the boundary-element method as well as to reduce the number of the mesh elements. Hence, the problems arise, concerning compensation of the above disadvantages and smoothing of numerical solution results, obtained for not dense grids.

Section. 3.3.1 describes a universal algorithm of triangulation of a 2-D domain, aimed at minimizing the number of the mesh elements with the mesh quality being preserved. The examples of the algorithm application for triangulation of flat domains of non-canonical shape are also given.

In Sect. 3.3.2 a concept of a dual grid pair is introduced, akin to the concept of duality in planar graph theory. Application of dual grids in the boundary-element method is considered. A preprocessor algorithm is described for building up a dual grid of the type of mesh into Voronoy polygons according to the given triangulation of the domain. The preprocessor application enables the dimensionality of the resolving linear equation system to be reduced (on the average by factor of 1.8) with respect to the initial one, and, accordingly, its conditionality to be improved. A postprocessor is elaborated, enabling a new, more smooth and exact solution to be obtained based on the simultaneous use of two approximate boundary-element solutions, found in the nodes of a dual grid pair.

3.3.1 Algorithm of Triangulation in the Boundary-Element Method

The main idea, pursued at discretization in numerical modeling of contact interaction, is to give such a mesh of the calculation domain into boundary elements that will provide obtaining the most exact solution of boundary integral equations. For this purpose an algorithm and a software application were elaborated [16], in particular, intended to perform discretization of flat simply and multiply connected domains, bounded by straight segments or circular arcs. The following types of mesh are provided: (i) close to uniform, (ii) with condensation near the boundary or in separate areas of the domain.

The proposed algorithm, contrary to the procedures quoted in [68, 83, 101, 114, 115], is neither frontal, nor iterative. In the first approximation it can be assigned to the class of blockwise discretization methods [114]. However, in the case under

consideration blocks are formed by subdomains of a rather general nature; blocks can be either selected from the domain by user (in a dialog), or automatically formed by the software (in the independent mode). The main stages of the proposed algorithm of triangular discretization are the following:

(a) mesh of the domain near the boundary in order to provide the grid condensation,
(b) sequential detachment of large blocks from the rest of the domain,
(c) stratification of the blocks into strips,
(d) mesh of the strips into elements.

Main conventions on the terminology. Part of a plane bounded by a closed connected polygonal line without transversal self-crossing of its segments, will be called a *domain*, and the polygonal line itself – its boundary (Fig. 3.2). The parts of the polygonal line will be called *segments*, their ends – *vertices*.

Vertices will be considered enumerated counterclockwise along the boundary path.

Let us define section (*I, J*) as a straight-line segment totally inside the domain, connecting the vertices with numbers I and J of its boundary. A segment is also a section.

Let H be a number. We will consider a number S *comparable* with H if $H/d \leq S \leq dH$ where $d > 1$ is a constant (in our consideration d, as a rule, equals 2 or 3).

Let us call a mesh of the polygonal line segments into the minimal number of equal parts, not exceeding H, an*additional mesh* of the polygonal line with a step H.

Let us call a domain a *strip* in case if in its any point P the minimal diameter does not exceed the value, comparable with H (Fig. 3.3).

Algorithm of strip discretization according to a given step. Let Q be a strip. Apply an additional mesh to its boundary with a step H, and let the obtained mesh points be enumerated from 1 to N. In the course of discretization we will operate with a movable section (*I, J*) and a subdomain of the strip at one side of the section. This section and this subdomain will be called current and possess an ordinal number. At the initial moment of time $I = 1$, $J = 1$, and the whole strip is the current domain with the ordinal number 1. Let $I1 = I + 1$ and $J1 = J - 1$. In the course of the mesh I, $I1$, J, $J1$ will vary, but always $I < I1 < J1 < J$.

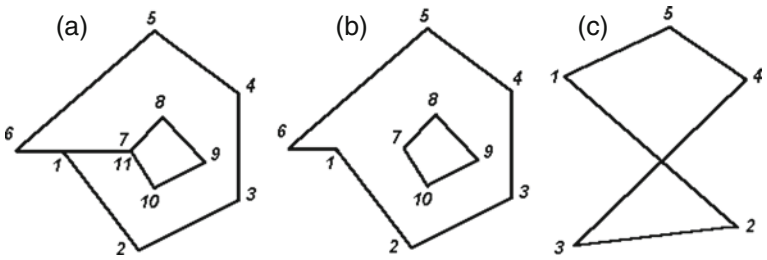

Fig. 3.2 To the definition of a domain: (**a**) a simply connected domain with non-transversal crossing of ribs (6, 7) and (11, 1); (**b**) a doubly connected domain, bounded by two boundaries; (**c**) an example of a polygonal line, which does not bound any domain

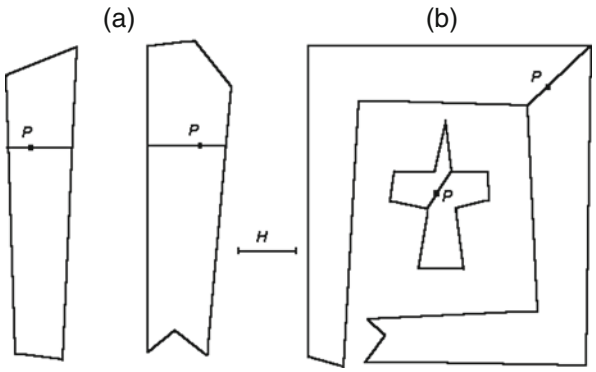

Fig. 3.3 To the definition of a strip: (**a**) "typical" strips; (**b**) example of complex-shaped strips

Then, among the chords, outgoing from *I*, and the chords, outgoing from `J`, find the minimal one, entirely belonging to the current domain. This will be a new section. As per construction, it length does not exceed a value, comparable with H. Two cases are possible.

A. The new section cuts off a triangle from the current domain. Then its sides do not exceed a value, comparable with *H*, and it is considered a next element of discretization. Then evident corrections are made for `I, J, I1, J1`, and the process is repeated (Fig. 3.4a).

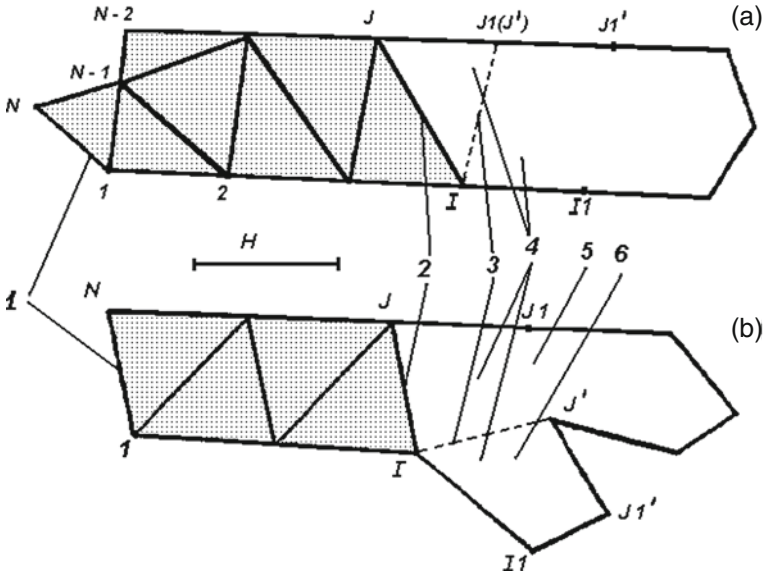

Fig. 3.4 Mesh of a strip: (**a**) the case of splitting off a triangular element; (**b**) the case of the process branching; 1 – initial section, 2 – current section, 3 – new current section, 4 – current domain, 5 – old current domain, 6 – new current domain

B. The new chord divides the current domain into two subdomains of a general nature which, evidently, are also strips (Fig. 3.4b). In this case the subdomain, containing (I, J), is given the old ordinal number, and for some time is out of consideration. The other subdomain is given a number, greater by 1, and becomes the current subdomain along with the new section. Accordingly, I, J, I1, J1 are changed (Fig. 3.4b), and then the discretization procedure is applied to a new current domain.

As a result of such a process, first the range of the highest order will be meshed, then we return to the next-highest order range and repeat the procedure once again. Finally, such recursive algorithm will result in a complete mesh of the whole strip.

Note 1. If the values of the segments of the strip boundary and their sections are limited from below (e.g., to $H/2$), this increases the uniformity and quality of the mesh.

Note 2. A procedure is provided, preventing appearance of triangles with great obtuse angle. Here we do not pay special attention to it.

Note 3. Evidently, the algorithm provides a procedure to check whether a new section is entirely within the strip.

Condensation of mesh near the domain boundary. Cutting off singularities. Let Q be an arbitrary domain. The mesh can be condensed along separate parts of the boundary or along the whole boundary. In each of the cases the corresponding part of the boundary is called the part of condensation. Its mesh is supposed to be already performed. A number of vertices of the part of condensation, called reference vertices, is displaced into the interior of the domain (Fig. 3.5). The displaced vertices,

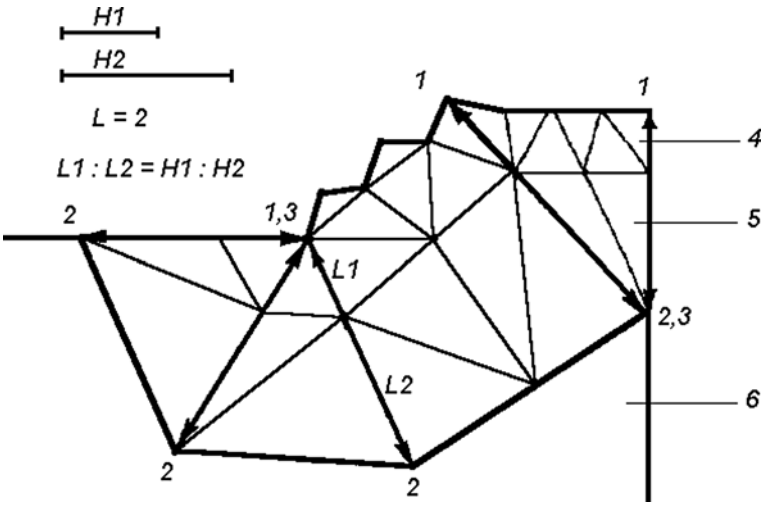

Fig. 3.5 Mesh condensation near the boundary and cutting off singularities: 1 – reference vertices of the part of condensation, 2 – vertices of the new boundary, obtained by shifting of the reference vertices, 3 – multiple vertices, 4 – the first condensation strip, 5 – the second condensation strip, 6 – domain Q, remaining after the singularities being cut off

being connected by straight lines, form a part of the boundary (or the whole boundary) of the part $\overline{Q}$ of the domain Q having remained after the condensation. This result can be treated as cutting off from Q the parts with the boundary nodes, containing small singularities and segments whose size is much less than the step value H of the mesh of the remaining part $\overline{Q}$ of the domain Q.

Note that between the new (displaced) and the old (to be displaced) vertices a one-to-one correspondence is set (with the account of the repetition multiplicity). It is indicated by arrows in Fig. 3.5. Between the old and the new parts of the boundary a subdomain of the domain Q is formed, called the *condensation subdomain*.

Then the number of condensation layers L and steps H_1, H_L, $H_1 < H_L$ are specified. Let the sequence $H_1 < H_2 < ... < H_K < ... < H_L$ (e.g., geometrical) "connect" H_1 and H_L. Partition the segments, connecting the corresponding vertices of the old and the new parts of the boundary, in such a way that their lengths be proportional to $H_1, H_2, \ldots, H_L$ (Fig. 3.5). By straight connecting the corresponding partitioning points of different segments one stratifies the condensation domain into L strips whose transverse size varies in accordance with the sequence $H_1, H_2, \ldots, H_L$.

At the next stage at first an additional mesh of the first strip boundary and a mesh of the first strip with a step H_1 is performed, then an additional mesh of the second strip boundary and a mesh of the second strip with a step H_2 etc. until the L-th strip with a step H_L. Thus, the required condensation near the boundary is obtained. The remaining part $\overline{Q}$ of the domain is afterwards independently meshed accordingly with a step $\overline{H}$, comparable with H_L.

The position of the displaced vertices can be specified in different ways. The algorithm provides the following options:

(a) let a vertex I be angular for two adjacent segments f_1 and f_2. Displace f_1 and f_2 parallel to themselves to the interior of the domain by distances d_1 and d_2, respectively (usually $d_1 = d_2 = d$ and is comparable with H). The new vertex position will be placed in the point of intersection of the displaced segments,
(b) the initial position of the displaced vertices is determined similarly to the case of (a), but afterwards the user makes corrections of position of some vertices (e.g. combines them in multiple vertices),
(c) the user himself specifies the position of new vertices. For this purpose the software provides a graphic cursor.

Note 4. Figure 3.5 shows the procedure to be applicable for an economical (in the sense of the number of elements) cutting off small singularities and irregularities at the boundary that simplifies the mesh inside the domain.

Note 5. Based on the above procedure, a final mesh of a doubly connected domain can be obtained. The idea is clear from Fig. 3.6.

Note 6. The displacement of vertices to the interior can be used for an essential simplification of the boundary of the remaining domain. This simplifies the mesh and increases its quality.

In the proposed method the mesh of the remaining domain (close to a uniform one) is, in general, performed in the following way: the domain is cut (if necessary)

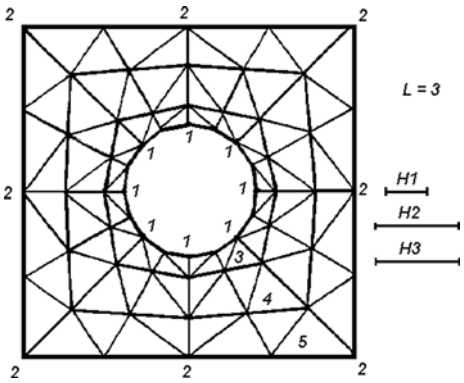

Fig. 3.6 Example of a mesh of a doubly connected domain using a condensation procedure: 1 – reference vertices, 2 – shifted vertices, 3, 4, 5 – condensation strips

into "regular" in their coordinate systems blocks. The blocks are stratified into strips and the strips are partitioned into elements. Now consider stratification into strips and decomposing into blocks.

Stratification of a regular domain into strips. A domain Q is called *regular* if in a Cartesian rectangular coordinate system XOY any straight line, parallel to the OY axis, intersects Q over a connected set. For such a domain, naturally, *upper* and *lower* boundaries are specified (Fig. 3.7). Besides, it makes sense to distinguish *left* and *right* segments, connecting the initial and end-point of the upper and lower boundaries, respectively (Fig. 3.7).

Let us introduce order among the points of the plane: A is less than B if the abscissa of A is less than the abscissa of B.

Let a step H be given, and let the segments of the upper and lower boundaries be additionally meshed with a step H, and concerning the left and right segments we assume (without a restriction of generality) that their projection on OX do not exceed $H/2$. One should cut Q into strips, the width of whose projections on OX is not less than $H/2$ and not more than $2.5–3H$ (the projection of the whole Q on OX is assumed more than $H/2$). We also demand that the projections of all the sections on OX should not exceed $H/2$.

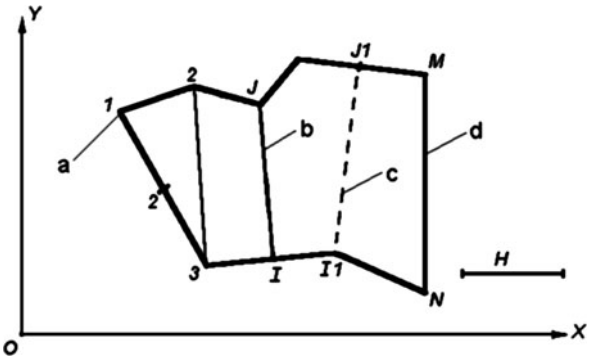

Fig. 3.7 Stratification of a regular domain into strips: a – left segment (1, 1), b – right segment (N, M), c – current section (I, J), d – new section (I1, J1)

Let us build sections from left to right. The first section is the left segment (*I, J*) (in Fig. 3.7 $I = 1$, $J = 1$, a possible case of degeneration of a segment into a point is shown). Consider a general situation. Let the last built section (*I, J*) connect the *I*-th vertex of the lower and the *J*-th vertex of the upper boundary, and let at first the distance along OX between the midpoint of the section (*I, J*) and the midpoint of the right segment (*N, M*) is larger than 3*H*. Find on the lower and upper boundaries the closest to *I* and *J*, respectively, vertices *II* and *JJ* in such a way that that were at a distance from the centre (*I, J*) along the OX axis direction not closer than 0.75*H*. Choose the largest of them (in the sense of a certain order) and find (in the sense of the same order) the one closest to it on the opposite boundary. Denote these vertices *I*1 and *J*1. Then the projection of (*I*1, *J*1) on OX does not exceed *H*/2 (since the boundaries are additionally meshed) and, as can be readily seen, the strip located between (*I, J*) and (*I*1, *J*1) (denote it as {*I, J, I*1, *J*1}) has projections on OX not smaller than 0.75*H* and not larger than 2.5*H*. If the chord (*I*1, *J*1) does not entirely belong to the domain Q, it can be easily corrected by substitution of I1 or J1 by the vertex appearing to be inside the {*I, J, I*1, *J*1} strip. Thus, a new strip with required properties is cut off from the domain Q. Then the process is repeated with substitution of (*I, J*) by (*I*1, *J*1).

If the distance between the centres (*I, J*) and (*N, M*) is shorter than 2.5*H*, than tale the whole strip {*I, J, N, M*}. If this distance is longer than 2.5*H* and shorter than 3*H*, than the strip {*I, J, N, M*} is divided in two.

A disadvantage of this method of mesh is the possibility of appearance of long narrow strips that generates, after them having been meshed, a great number of narrow elements (Fig. 3.8). The reason for this is the fact that on the boundaries of the domain Q segments with very large angular coefficients in the XOY coordinate system are possible. Such segments will be called *critical*. If there are no such segments, a great number of narrow elements will not arise.

A coordinate system X′O′Y′ will be called *inverse* to the XOY system if O′X′||OY, O′Y′||OX. Note that if a segment, critical in XOY, is considered in the inverse system X′O′Y′, it is no longer critical. This suggests an idea to decompose Q into blocks, part of which is to be partitioned in strips in the XOY system, and

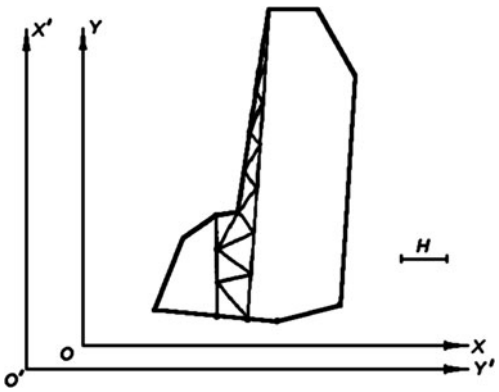

Fig. 3.8 Example of a strip containing a critical segment and narrow elements

the other part – in the inverse X′O′Y′ system. Such operation can be performed manually, and the software provides such option along with the choice of the corresponding coordinate system. We have worked out a procedure to automate this process. Its idea is in brief described below.

Division of a normal domain into blocks to be stratified into strips in mutually inverse coordinate systems. A domain Q is called *normal* if it is regular both in XOY and X′O′Y′ coordinate systems.

Let $K > 1$ be a number (usually $K = 1.7, 2, 3$). Boundary segments will be called *critical* if their angular coefficients k in XOY are larger than K (the absolute value).

Let M be a set of points on OX which is the projection of all the critical segments of the boundary, and let [a, b] be a connected component of this set. A part of the domain Q, located above [a, b], will be called critical (Fig. 3.9). If long narrow set-offs arise on the left side or on the right side (or on both sides) of this domain, then emborder the domain at this side by a strip of a width comparable with $H/2$ at the expense of the area with precritical slopes of the boundary segments. As a result, the critical domain is confined between two sections in a domain without narrow set-offs.

The same procedure can be performed with other components of the set M. Embordering can result in merging of some critical domains into one. Finally the whole domain Q will be cut into parts, some of which containing critical segments, the others – not containing them (Fig. 3.9).

The parts, which do not contain critical segments, are, according to the above described algorithm, cut into strips and meshed into elements. The others are in turn considered in the inverse coordinate system X′O′Y′, and the same procedure, as in the case of the initial domain, is applied to them. Inside them critical and noncritical domains are again formed. The noncritical domains are immediately meshed in

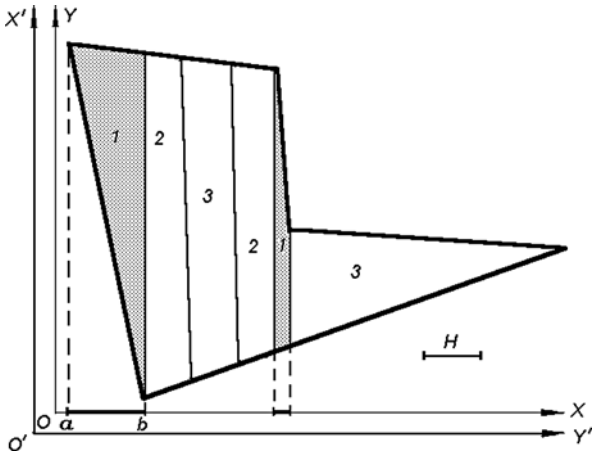

Fig. 3.9 Decomposing of a normal domain into blocks: 1 – critical domains, 2 – embordering of critical domains, 3 – non-critical domains (these blocks are meshed in XOY system)

$X'O'Y'$, and the critical ones are subject to the above procedure, but in XOY system, etc. Hence, Q will be gradually partitioned into smaller and smaller blocks. If a block is entirely critical both in $X'O'Y'$ and XOY systems, then either the coordinate system should be turned, or K increased, or the block should be meshed as it is. If a block achieves size comparable with H, it is immediately meshed into elements as a strip. Thus, the process is finished in any case, and though slim elements can arise, their number is sharply decreased and their location is dispersed.

Practical application examples. While analyzing the results of the algorithm operation, note that in a number of simple, but typical cases the described algorithm enables the user's activity in the discretization process to be reduced to a minimum. It is sufficient to input the coordinates of the boundary vertices in the counterclockwise order in a basic coordinate system (further address to the vertices will be reduced to specifying of their numbers), specify condensation areas, number of layers L, steps of condensation H_1, H_L and the boundary segment displacement value d. Then the step H of uniform mesh of the remained domain is specified and automatic operation mode is chosen if the domain, having remained after the condensation, is normal. As a result, the program will perform discretization independently and output the geometry of the boundary elements in the basic coordinate system.

Simultaneously, the directed (not iterative) structure of the program enables the mesh results to be foreseen and the mesh to be actively planned:

- user can in a dialogue mode specify the initial domain sections, the order of mesh of the arising partitions, steps and coordinate systems of the mesh as well as continuously check the discretization process visually,
- by means of sections as well as the choice of position of the boundary vertices being displaced at the condensation, the domain, remaining for the uniform mesh, can be simplified and made close to regular,
- the routine can be assisted to bypass difficulties arising due to the critical boundary segments,
- finally, lack of iteration reduces the program runtime duration.

The program code is written in the FORTRAN-77 language.

Figure 3.10 shows the examples of mesh (close to uniform) of domains of circular and typical polygonal shapes.

For the mesh of the circular domain (Fig. 3.10a) the input data were the circle radius R, number of vertices of uniform mesh of the boundary (36), the domain mesh step $H = R/5$. The domain was meshed independently in the initial coordinate system.

An example of a uniform mesh of an I-beam is presented in Fig. 3.10b. The input data were 12 I-beam vertices, boundary additional mesh step; domain mesh step. By three sections the domain was divided into four equal parts, each of them being meshed independently in its own coordinate system. In a similar way a uniform mesh of a cross-shaped domain (Fig. 3.10c) and a domain with angular cutoffs (Fig. 3.10d) is carried out. The mesh of the cross-shaped domain is performed

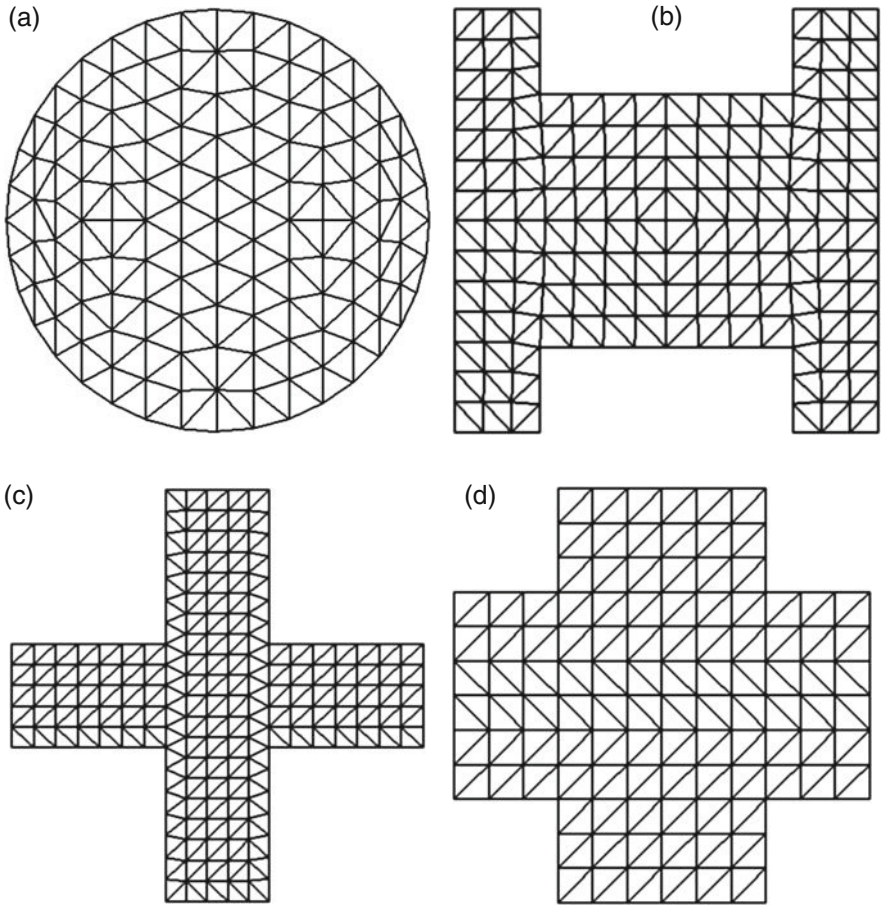

Fig. 3.10 Examples of uniform discretization: (**a**) circular domain; (**b**) I-shaped domain; (**c**) cross-shaped domain; (**d**) square with angular cutoffs

independently in the initial coordinate system, while the domain with angular cut-offs is divided by a horizontal section into two parts, each of them being meshed independently in its own coordinate system.

An example of mesh of a circular domain with a near-boundary condensation is shown in Fig. 3.11. The number of the condensation layers is four, the number of the reference vertices – 12, the displaced vertex has a multiplicity of 12.

Figure 3.12 illustrates the automatic mesh of a circular domain (Fig. 3.12a) and circular domains with cut-offs (Fig. 3.12b–d) with the optimization of the number of boundary elements.

The mesh, shown in Fig. 3.12a is performed similarly to the example of Fig. 3.10a. The number of boundary elements is 110.

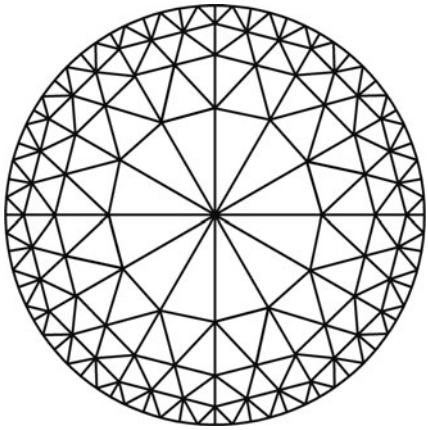

Fig. 3.11 Discretization of a circular domain with condensation at the boundary

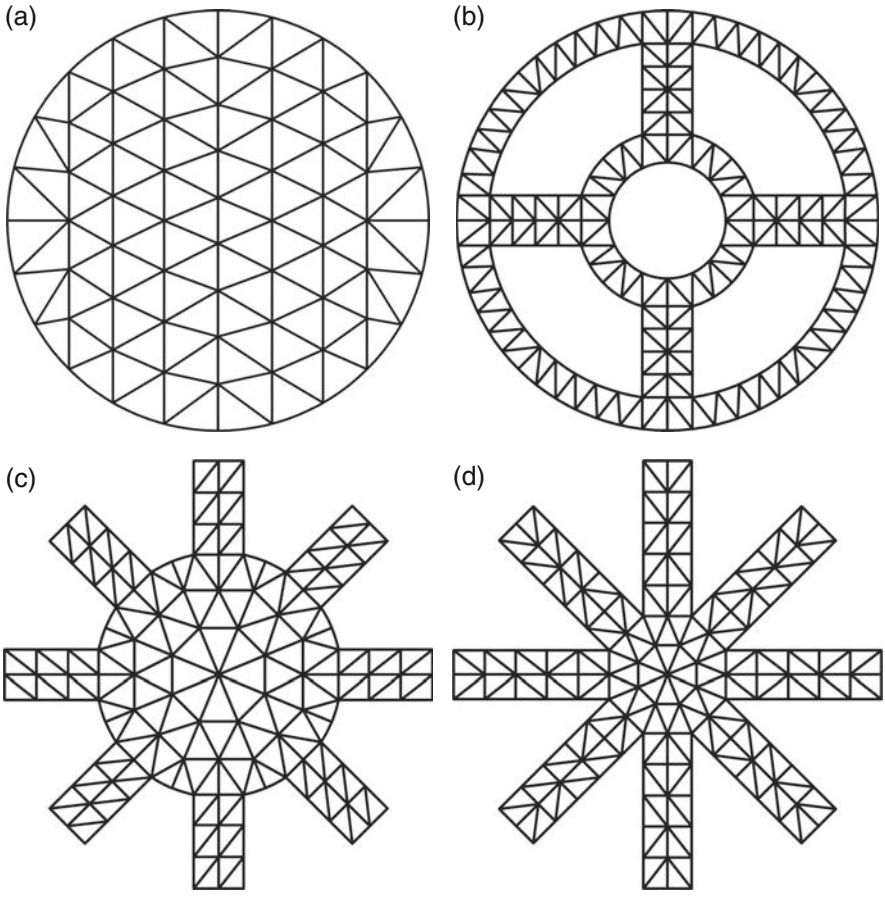

Fig. 3.12 Examples of condensation for a circular domain with cutoffs

At discretization domain, shown in Fig. 3.12b initially a quarter of the domain within the sector ($\pi/4$, $\pi/4$) is considered. It is divided by two vertical sections into a rectangular subdomain and two circular strips. The boundaries of these parts are additionally meshed according to the specified step; afterwards, each of them is independently triangulated. The total mesh of the domain is obtained by triple rotation. The total number of boundary elements is 208.

Figure 3.12c gives an example of a domain obtained from a circular one by means of eight cut-offs. For discretization initially an eighth part of the domain is considered. By a section it is divided into a rectangle and a circular sector. The rectangle is meshed at once, and the sector is meshed with condensation near the circular arc. Three condensation layers are seen in the figure. The final mesh of the entire domain is obtained by means of seven rotations. The total number of boundary elements is 176. The discretization of the domain shown in Fig. 3.12d is performed in a similar way. The number of boundary elements is 192.

The program, in which the above triangulation algorithm is implemented, possesses a user interface (in fact, an internal graphic software tool) enabling not only the input data (domain boundaries, mesh steps, condensation areas etc.) to be specified by observing them on the screen, but also all the mesh stages to be actively controlled, choosing the mode which is the most effective for the problem solution. As a result, the user obtains the triangular element coordinates as well as the necessary geometrical data, required in the boundary-element method. The computation time for formation of a hundred of mesh elements for a low-speed computer is on the average 3–5 s.

The elaborated algorithm of triangulation was applied to solve a number of geotechnical problems on the calculation of parameters of contact interaction of flexible and rigid punches as well as foundation plates of complex geometrical shape resting on elastic nonclassical bases. Results on geometrical optimization of the objects under study at different conditions of spatial loading were obtained (See Chapter 4). The elaborated software can be without essential changes applied to obtain numerical solutions of spatial boundary problems of mechanics and mathematical physics with mixed boundary conditions (fracture mechanics, calculations of structural element strength, heat and mass transfer, electrostatics etc.) based on boundary integral equations.

3.3.2 Dual Grids and Their Application in Boundary-Element Method

Here we state the practical approach developed for the solution of the above problems of reduction of the number of boundary elements and obtaining a smoothed numerical solution on grids with a moderate number of elements [2, 17]. The main idea consists in proceeding from a solution on one grid to a pair of approximate solutions obtained on two grids in duality. Construction of grids in duality is a preprocessor problem. Joint processing of two solutions, obtained for the dual grids, is a postprocessor problem. Development and joint inclusion of a preprocessor and a

postprocessor into the software package is of great practical interest since it enables solutions of spatial contact problems for complex-shaped punches to be built effectively and with high accuracy without preliminary prediction of the contact pressure field structure, as well as numerical solutions to be interpolated.

Dual grids on a plane. Main definitions. Let R be a flat polygonal domain and $\mathbf{A} = \{A_{ij}\}$ is a mesh of R into polygons A_i, $i = 1, 2, \ldots, M$. The polygons A_i will be called mesh elements or cells, the polygon vertices – nodes the polygon sides – ribs, and the mesh $\mathbf{A}$ itself – a grid. If a node belongs to the domain boundary, it is called a boundary node, otherwise – an internal node.

The concept of duality, used hereinafter, characterizes mutual location of the elements and nodes of a pair of grids related to the meshes of one or two domains. This concept naturally arises at numerical modeling in finite-element and boundary-element methods for the problems of mathematical physics. Due to the specific features of the problems, it is convenient to use several *definitions* of duality given below which are close essentially, but differ in details.

If R does not coincide with the whole plane, then by adding to $\{A_j\}$ a polygon A_0, coinciding with the closure of the complement of the domain R to the whole plane, we come to a mesh $\overline{\mathbf{A}} = \{A_j\}_{j=0}^{M}$ of the whole plane. The collection of nodes and ribs of the grid $\overline{\mathbf{A}}$ (or, what is the same, $\mathbf{A}$) forms a flat graph $\tilde{A}_A$ without isolated and pendant vertices [59], for which in graph theory a concept of a dual graph Γ'_A is known. The latter is built in the following way. In each polygon A_0, $A_1, \ldots$ an internal point b_0, $b_1, \ldots$ is chosen (among them one can be infinitely remote). The collection of these points forms a set of nodes of the dual graph Γ'_A. A rib in Γ'_A is an arc l', connecting those, and only those b_k and b_j, for which the cells of the initial mesh A_k and A_j which contain them, have a common rib l. Such ribs l and l' will be called corresponding.

The graph $\tilde{A}_A$ is known to be dual to the graph Γ'_A up to isomorphism. Consequently, $\tilde{A}_A$ and Γ'_A will be mutually dual. The graph Γ'_A also generates a mesh of the plane, denoted as $\overline{\mathbf{A}'}$. It follows directly from the definition that if N, L, M and N', L', M' are the numbers of nodes, ribs and cells for the meshes $\overline{\mathbf{A}}$ and $\overline{\mathbf{A}'}$, respectively, then $N = M'$, $M = N'$, $L = L'$.

It follows from the definition of dual graphs that location of their nodes is determined by far not uniquely. Therefore, while defining plane meshes dual to each other, with the account of their further application in numerical analysis, we have to impose additional requirements.

Definition 1. Two grids $\mathbf{A}$ and $\mathbf{B}$ on a plane are called dual if:

(1) the corresponding graphs $\tilde{A}_A$ and $\tilde{A}_B$ are dual,
(2) each node of one grid is contained in a cell of the other grid,
(3) each cell of one grid contains a single node of the other grid,
(4) all ribs are straight lines and each rib of one grid intercepts only the corresponding rib of the other grid in a point, internal for these ribs (Fig. 3.13a).

It is clear that Definition 1 (with an evident modification of item 4) is also extended for grids, given on a 2-D sphere or on a smooth surface of a 3-D body, homeomorphic to a sphere.

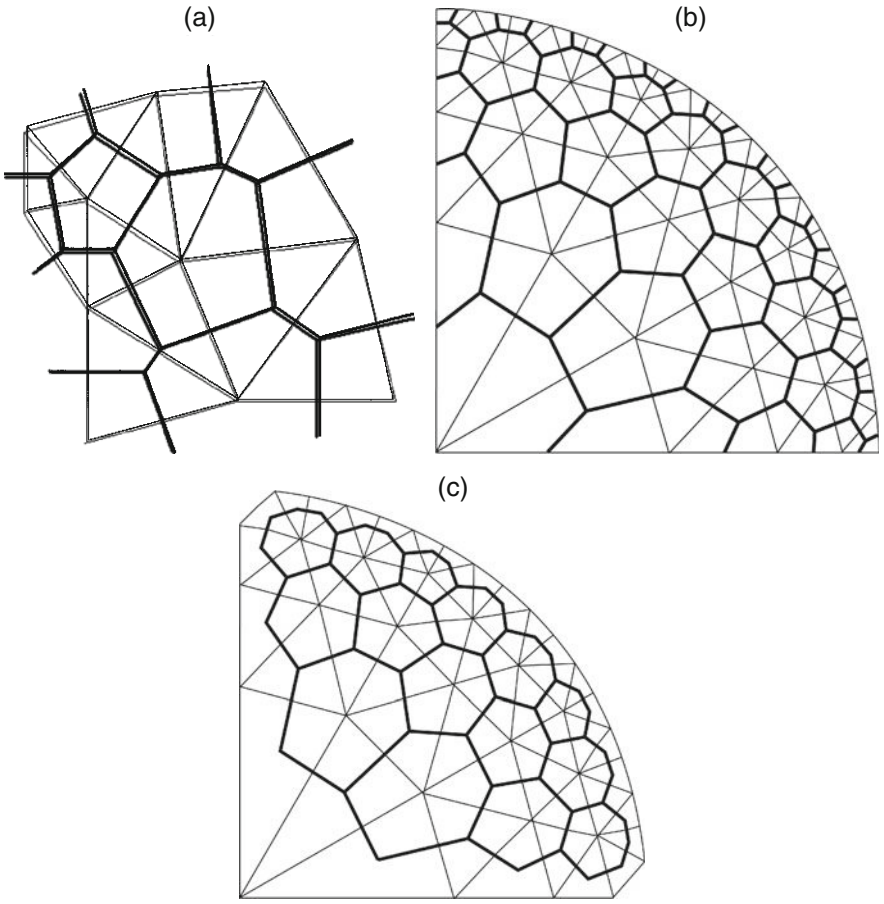

Fig. 3.13 Dual grids generated by triangulations: (**a**) delaunay triangulation and Voronoy polygons; (**b**) grids, satisfying definition 1; (**c**) grids, satisfying definition 2

Now let R be a subdomain of a plane and **A** be a grid on R, $\overline{\mathbf{A}}$ is the corresponding mesh of the whole plane, and let $\overline{\mathbf{B}}$ be a mesh, dual for A in the sense of Definition 1.

Definition 2. A mesh **B** of the domain R, consisting of polygons $B_j = R \cap \bar{B}_j$ where $\overline{B}_j$ are the elements of the mesh $\overline{\mathbf{B}}$ (Fig. 3.13b), is called dual to the mesh **A**.

Note that for grids, dual in the sense of Definition 2, the properties (2), (3), and (4), are, in general, not fulfilled in the pure sense and require a certain modification of statements.

For such meshes each internal node of one grid is contained in a cell of the other grid, and different internal nodes are contained in different cells.

Each cell of one grid contains one internal and (or) one boundary node of the other grid.

Corresponding ribs of the dual grids intercept.

The meshes **A** and **B** are disparate and not mutually dual.

Consider one more definition of duality for grids on domains, not coinciding with the whole plane.

Definition 3.Two grids **A** and **B**, specified on two different domains R and Q, are called dual if each element of one grid contains inside it a single node of the dual grid, and the grids themselves can be extended to two dual (in the sense of Definition 1) grids on the whole plane (Figs. 3.13c and 3.13 a,b).

For such grid the following property is also valid: each internal node of one grid is contained in a single element of the other grid.

We should emphasize that though for a grid **A,** specified on R, dual (in the sense of Definition 3) grids are defined not uniquely, nevertheless they can differ from each other only in the vicinity of the domain R boundary and should be in fact identical inside R. Among them one should pay particular attention to those, for which the domains Q and R are inside each other (the case of maximal and minimal dual grids).

Thus, the main feature of all the above defined dual grids is a matched location of their nodes, cells and ribs, for which each internal node of one grid is in the environment of nodes of the other grid. This with necessity determines high correlation of approximate solutions, found independently in the nodes of grids, dual between each other.

Examples of dual grids

1. Let a domain R be the whole plane and points P_i, $i = 1, 2,\ldots,N$ be located on it in a rather regular way. Using a construction from the book [106], consider a grid **B** on R to be a set of Voronoy polygons (Dirichlet cells) with centres in the points P_i. Consider **A** to be a grid, in which a rib connects those pairs of points P_i and P_j, for which the Voronoy polygons have a common rib. Such grids **A** and **B** are dual in the sense of flat graph theory [59, 106]. The grid **A** is a mesh of the domain R', coinciding with a convex shell of the set of points P_i, $i = 1, 2,\ldots, N$, into triangles. Such triangulation is called Delaunay triangulation [66]. In the general case **A** and **B** are not dual in the sense of Definition 1 since the properties (2), (3), and (4) can be not fulfilled. One can easily check that the grids **A** and **B** are dual in the sense of Definition 1 then, and only then when all elements of the Delaunay triangulation **A** are acute-angled (Fig. 3.13a).
2. Let **A** be a triangulation of the domain R. Let the gravity centres of triangles of **A** be the nodes of a mesh **B**; join by segments those of them which belong to the triangles A_i and A_j possessing a common side. The grid **B** is a mesh of a subdomain of the domain R. It can be easily shown that if for all the triangles A_i of the grid **A** with sides $a_i > b_i > c_i$ the condition

$$a_j < b_j + 3c_j \tag{3.5}$$

   is valid, then the grids **A** and **B** are in duality in the sense of Definition 3 (Fig. 3.13c).
3. Figure 3.13b shows two grids **A** and **B** on the same domain, satisfying Definition 2.

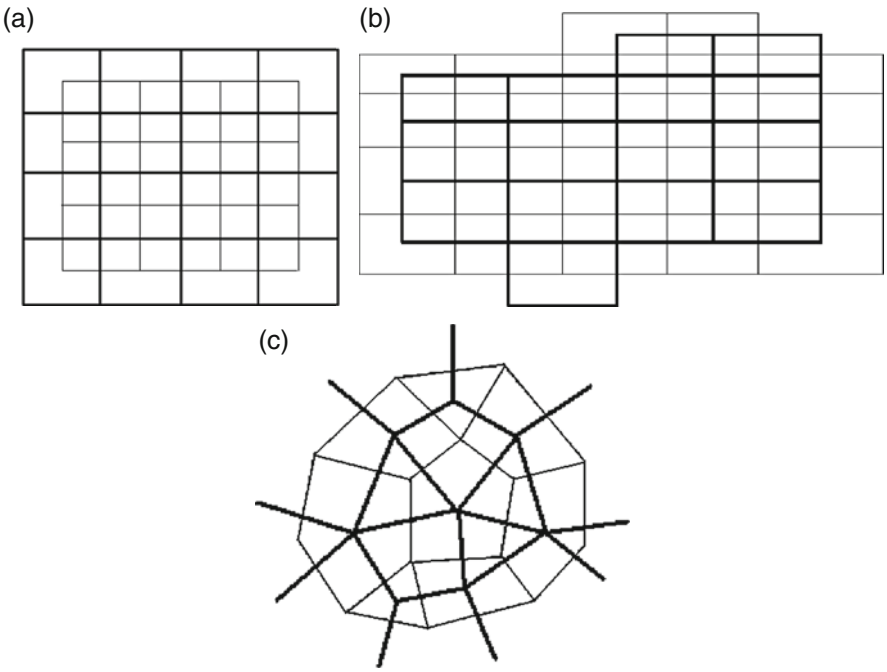

Fig. 3.14 Dual rectangular grids (**a**, **b**) and dual grids, consisting of arbitrary polygons (**c**)

4. Let **A** be a grid of rectangular elements. There exist many grids B, consisting of rectangular elements, dual to **A** in the sense of Definition 3 (Fig. 3.14a, b). In particular, among them there is a dual grid whose nodes are the gravity centres of elements of **A**.
5. Figure 3.14c shows a pair of grids, dual in the sense of Definition 1, whose elements are arbitrary polygons.

It is worth to make some remarks concerning the number of elements of the grids **A** and **B** from the first three examples. Let N be the total number of nodes of a triangulation **A**, $N_{\tilde{\Gamma}}$ being the number of nodes, belonging to the boundary, M being the number of elements from **A**, and L being the number of ribs connecting the nodes. For any triangulation the following formulae are valid:

$$M = 2(N-1) - N_{\Gamma}, \quad L = 3(N-1) - N_{\Gamma} \, . \tag{3.6}$$

If a grid on the whole surface (boundary) of a three-dimensional finite body is dealt with, then the corresponding formulae are given by

$$M = 2(N-2), \quad L = 3(N-2) \, . \tag{3.7}$$

Hence, if $N_{\tilde{\Gamma}}$ is small in comparison with N, then the number of elements N of the dual grid **B** is approximately twice smaller than the initial number of elements of the triangulation **A**.

The latter remark enables the following approach to the problem of improvement of conditionality of the system matrix in the boundary-element method to be proposed. In the case of a condensed triangular grid on a 2-D domain or on the boundary of a 3-D body, which generates a matrix of high dimensionality and bad conditionality, resulting due to errors to an inaccurate solution, it is recommended to pass to a dual grid **B** with N ($N \approx M/2$) elements (of Dirichlet cell type) that will reduce the dimensionality of the discrete problem and improve its conditionality. One should keep in mind that the mesh density, accuracy of the boundary approximation, and, hence, the accuracy of the solution itself in the boundary-element method theoretically can be reduced.

Preprocessor algorithm. Here we describe the preprocessor algorithm which on the base of a given grid **A** creates a grid **B**, dual to **A**. The description is given for the most important case when **A** is a triangulation of the domain R (examples 2 and 3).

Let a triangulation **A** of the domain R with N nodes and M elements be given. In this case at least we know two-dimensional arrays `KNOTS(2,N)` and `ELEM(3,M)`. The first one contains coordinates X_i, Y_i of all the nodes P_i, $i = 1, 2, \ldots, N$ of the triangulation, and the second one for each $k = 1, 2, \ldots, M$ contains the numbers i_1, i_2, i_3 of those nodes which form the vertices of the element with the number k. Let the order of i_1, i_2, i_3 correspond to counterclockwise direction.

By a simple procedure these simplest data concerning the mesh **A** is complemented with one-dimensional arrays `NNBE(N)` and `NBE(NK)` which explain the triangulation structure. Namely, `NNBE(i)` is the number of the triangulation elements, for which the node P_i is a vertex. Such elements will be called possessions of the node P_i. The array `NBK(NK)` contains possession numbers for all the nodes, recorded consecutively (first for P_1, then for P_2, etc.). Thus,

$$\mathtt{NK} = \sum_i \mathtt{NNBE(i)} = 3M \ .$$

Note that the record of numbers of adjacent to P_i elements, contained in the array `NBE`, does not yet in any way correspond to their order at counterclockwise encircling P_i. This problem is solved by a separate procedure, accompanied by formation of further important one-dimensional arrays `NNBK(N)` and `NBK(NK)` which for each node P_i contain the number of neighbouring nodes (i.e. nodes connected by a rib to P_i) and the numbers of these nodes (similarly to the `NBE` array), respectively. Note that in `NBK` array the enumeration of the nodes, neighbouring to P_i, already corresponds to the counterclockwise direction around P_i. Moreover, if P_{i_1}, P_{i_2},..., P_{i_q}, the neighbours of P_i and P_j, belong to the domain boundary, then P_{i_1} and P_{i_q} also belong to the boundary.

Based on the data obtained, below we describe building up elements V_i of a new mesh of a subdomain of the domain R, each of which contains one node P_i, that will finish construction of the dual grid **B**. Building up V_i differs for the nodes P_i, belonging to the interior of the domain R and to its boundary.

Let at first P_i be an internal node and P_{i_1}, P_{i_2},..., P_{i_q} be the neighbours of P_i. Denote C_1,...,C_q to be the gravity centres of triangles $P_iP_{i_s}P_{i_{s+1}}$, $s = 1,2,\ldots,q$, where $P_{i_{q+1}} = P_i$. Then the polygon line $\tilde{\mathrm{A}}_i = C_1, \ldots, C_{\mathrm{q}}$ which does not contain self-

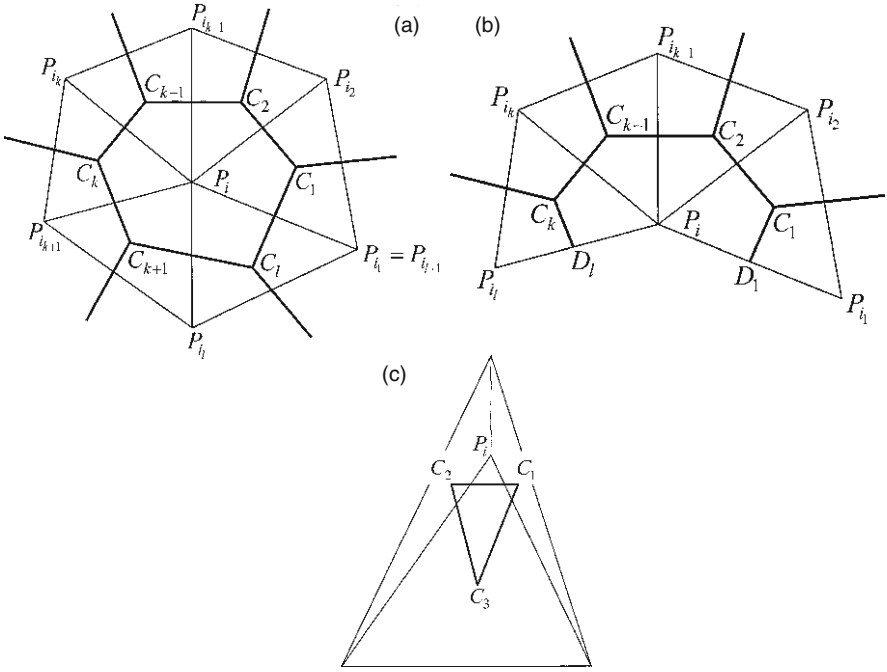

Fig. 3.15 Schemes of building up dual grids based on a given triangulation: (**a**) internal node; (**b**) boundary node; (**c**) the case when the grid building method does not work

crossings, bounds a domain V_i (Fig. 3.15a) and, if the triangulation is of sufficient quality (See, e.g., the condition of Eq. (3.5)), then V_i contains the node P_i. A case of bad triangulation, i.e. when the algorithm under consideration does not work, is shown in Fig. 3.15c. It is evident from the construction that the vertices of the domains V_i, are, in turn, contained in the mesh elements **A**. Thus, according to Definition 3, the mesh **B**, consisting of V_i, where P_i are internal nodes of the domain R, form a mesh, dual to **A**, which covers all the nodes of the **A** grid, except the boundary ones (Fig. 3.13b).

If the triangulation of **A** is an approximation of a complete boundary of a 3-D body, then all the nodes of **A** are internal and, consequently, **B** is also a mesh, approximating the boundary of the same 3-D body. By applying the boundary-element method to **A** and **B** we can obtain two approximate solutions of a 3-D problem, the resolving system matrix for the mesh **B** being almost twice smaller in size than the matrix for the mesh **A**.

Let now P_i belong to the boundary of the domain R. Consider a polygon line $\tilde{A}_i = P_i D_1 C_1 \ldots C_{q-1} D_q$ where C_s, $s = 1,2,...,q-1$ are the same as above and D_1, D_q are the midpoints of the ribs $P_i P_{i_1}$ and U_i, respectively. Then F_i is closed, does not contain self-crossings and encloses the domain V_i, including P_i (Fig. 3.15b). A collection of all V_i, built for P_i both inside the domain R and on its boundary, forms a new mesh **B** of the same domain R. **B** will not be dual to **A** in the sense

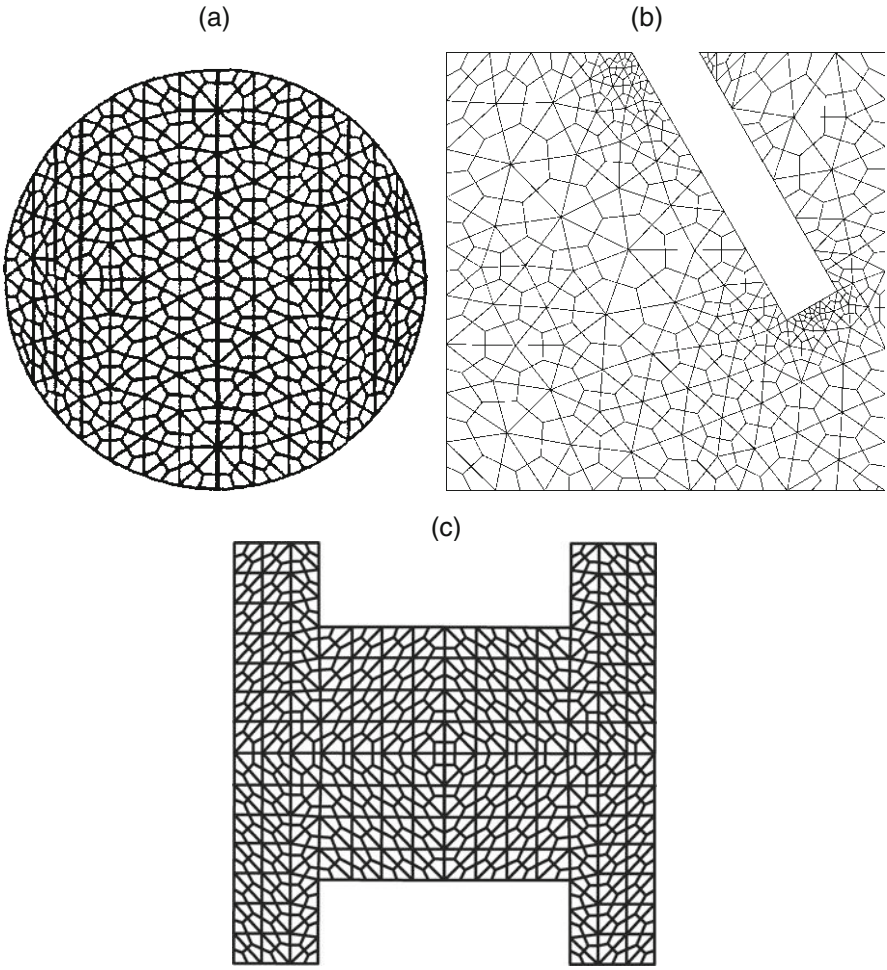

Fig. 3.16 Examples of the preprocessor algorithm application

of Definition 3, since e.g. nodes of **B** of D_1 and C_1 type simultaneously belong to the same element of the mesh **A**, but will be dual to **A** in the sense of Definition 2 (Fig. 3.13b). The examples of application of the described method are shown below (Fig. 3.16) where the initial triangulation is created by a routine of triangular grid generation (See Sect. Section 3.3.1, [16]).

It should be also noted that the proposed preprocessor algorithm includes the following important functions: (1) by means of it the dual grids, having been built before, are redefined in such a way that each internal node of one grid be either the centre of gravity of the dual grid cell to which it belongs (Fig. 3.17a–c), or the arithmetic mean of its vertices (Fig. 3.17b–d), (2) for each pair of dual grids a general triangulation of the whole domain is built, whose nodes are all the nodes

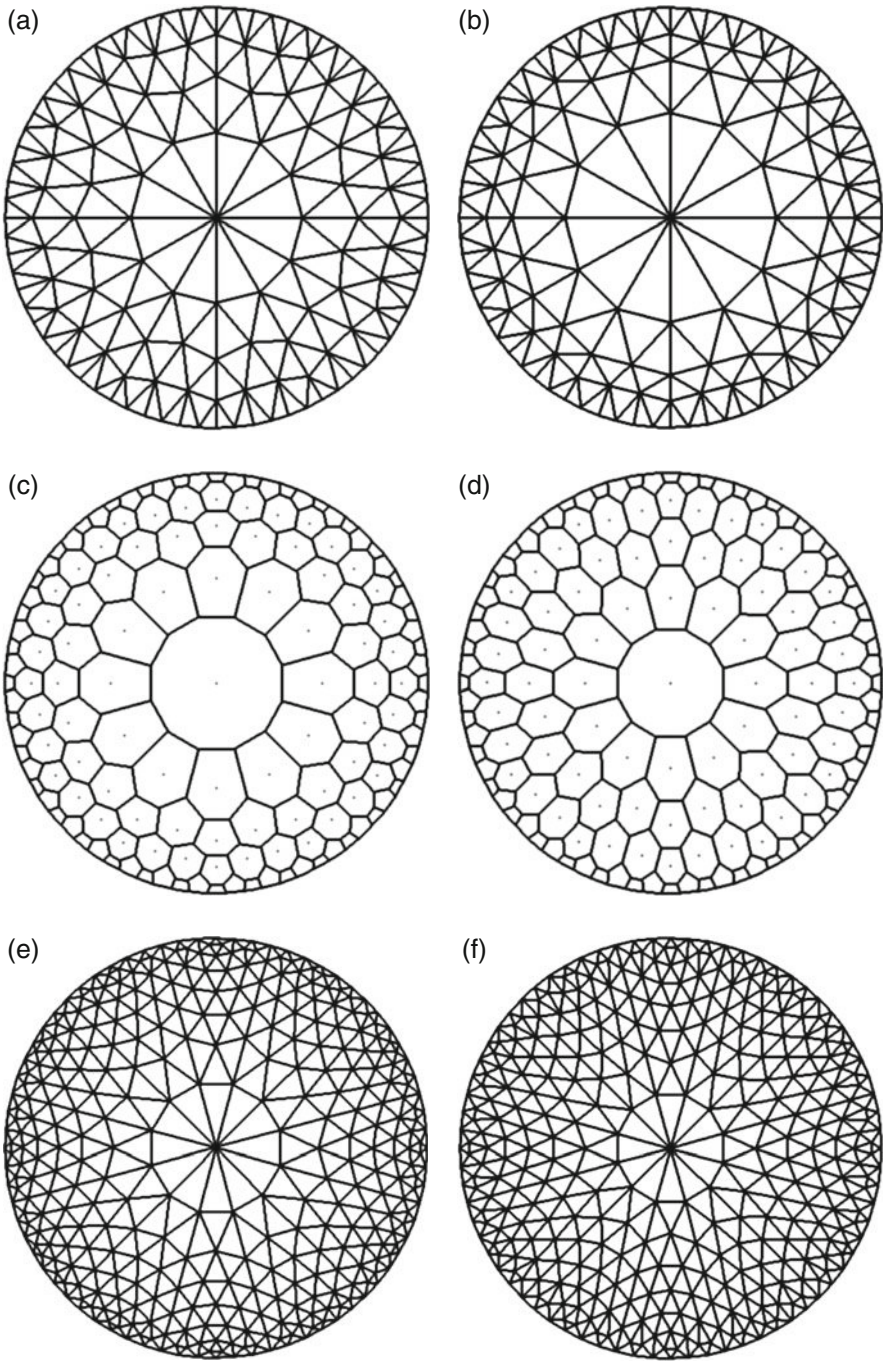

Fig. 3.17 Pairs of dual grids on a circle: internal nodes of the grids are (**a**, **c**): the gravity centres of the cells to which they belong and (**b**, **d**): mean arithmetic points of the vertices of the cells to which they belong; (**e**, **f**): triangulation of a circular domain over the nodes of a dual grid pair

of both grids (Fig. 3.17e, f). The latter triangulation (being of independent value) is important for the postprocessor application and at construction of isolines of the numerical solution, obtained for the pair of the dual grids.

A large series of numerical experiments on dual grids has enabled us to evaluate the efficiency of the proposed approach as well as to compare (for a number of problems) the results of calculations of contact interaction parameters obtained by boundary-element method and by other known methods. In typical cases substitution of a triangular grid by a dual grid of generalized Dirichlet-Voronoy cells results in the reduction of dimensionality of the resolving finite-measure equation system by factor of at least 1.5. In this case, even if the accuracy of the new solution id decreased, this decrease is slight (by 5–10%), though often the accuracy is increased due to a successful choice of the initial grid. Practical examples of solving the spatial problems of theory of elasticity for non-canonical (simply and multiply connected) contact domains using dual boundary-element grids, are given in Sect. 3.5.1.

Postprocessor algorithm for dual grids. Let one, as a result of a numerical experiment, in the nodes P_i, $i = 1, 2,\ldots, M$ and Q_j, $j = 1, 2,\ldots, N$ of the grids **A** and **B**, which are in duality, have obtained approximate values F_i, $i = 1, 2,\ldots, M$ and G_j, $j = 1, 2,\ldots, N$ of a function $z = f(x, y)$ of two variables. The sets $\{F_i\}$, $\{G_j\}$ are assumed to be obtained independently and to contain errors (deviations from the exact values of the function $z = f(x, y)$ both of random character and related to the errors of the numerical method itself). Since the nodes of one grid are located inside (and even in the geometrical centre of) the other grid cells, evidently there should be an internal relationship between the values of $\{F_i\}$, $\{G_j\}$. The presence of two approximations enables one to suppose that on their base, with the account of the interdependent location of the nodes P_i and Q_j of the dual grids, a new approximation for $z = f(x, y)$ can be obtained, being of a better quality than each of $\{F_i\}$, $\{G_j\}$ separately. Namely, using the approximate value sets $\{F_i\}$, $\{G_j\}$, one should:

(1) specify new approximate values $\{U_i\}$, $\{V_j\}$, $i = 1, 2,\ldots, M$; $j = 1, 2,\ldots, N$ simultaneously on the whole system of points P_i, Q_j;
(2) while specifying U_i, V_j, take into account their natural relation to $\{F_i\}$, $\{G_j\}$ and with each other;
(3) try to specify the new values in such a way that sharp oscillations of the neighbouring approximate values be possibly smoothed and the effect of random experimental errors be reduced.

Concerning the function $f(x, y)$ itself we assume that within one element of mesh **A** or **B** the sought function $f(x, y)$ is rather well approximated by its first-order Taylor polynomial. The latter fact means that either the grad$f(x, y)$ variation rate is small, or the grids **A** and **B** are sufficiently dense.

Construct a new approximate solution using the least-square method. For the sake of simplicity consider the problem for the grids of the example 3. Let **A**be a square grid, containing $\mathtt{kk} = \mathtt{k}.\mathtt{k}$ nodes, and **B** be a square grid, containing $\mathtt{kk1} = (\mathtt{k}-1)\cdot(\mathtt{k}-1)$ nodes. Each node Q_j of the second grid is enclosed by some nodes

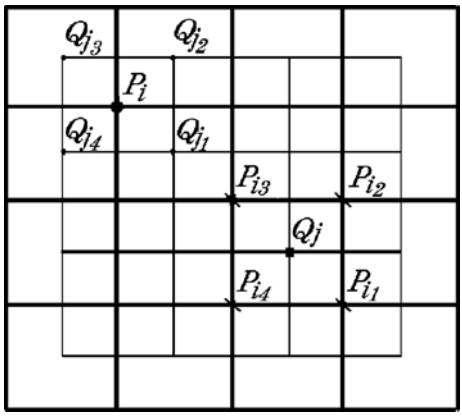

Fig. 3.18 Neighbouring nodes for rectangular dual grids

P_{i_1}, P_{i_2}, P_{i_3}, P_{i_4} of the first grid and is their centre of gravity, and each internal node P_i of the first grid is enclosed by some nodes Q_{j_1}, Q_{j_2}, Q_{j_3}, Q_{j_4} of the second grid and also is their centre of gravity (Fig. 3.18).

The simplest way is to imply $U_i = F_i$ and $V_j = G_j$. Then the requirement (1) will be satisfied, but the requirements (2) and (3) will be not. Nevertheless, it is evident that U_i and V_j should not essentially be far from F_i and G_j. This means that the value

$$\varphi_1(\overline{U}, \overline{V}) = \sum_{i=1}^{k\,k} (U_i - F_i)^2 + \sum_{j=1}^{k\,k\,1} (V_j - G_j)^2$$

should not be large. Here $\overline{U} = \{U_i\}$,$\overline{V} = \{V_j\}$.

Then, due to the assumption of *f(x, y)* within one mesh element being close to a linear function, one concludes its value in the point Q_j not to be strongly different from the arithmetic mean of its values in the neighbouring points P_{i_1}, P_{i_2}, P_{i_3}, P_{i_4}, and the value in the point P_i not to be strongly different from the arithmetic mean of its values in the points Q_{j_1}, Q_{j_2}, Q_{j_3}, Q_{j_4}. This leads to a conclusion that at the correct choice of $\overline{U} = \{U_i\}$,$\overline{V} = \{V_j\}$ the following two values should not be large:

$$\varphi_2(\overline{U}, \overline{V}) = \sum_j \left(\frac{U_{i_1} + U_{i_2} + U_{i_3} + U_{i_4}}{4} - G_j \right)^2 + \sum_i \left(\frac{V_{j_1} + V_{j_2} + V_{j_3} + V_{j_4}}{4} - F_j \right)^2,$$

$$\varphi_3(\overline{U}, \overline{V}) = \sum_j \left(\frac{V_{j_1} + V_{j_2} + V_{j_3} + V_{j_4}}{4} - U_i \right)^2 + \sum_j \left(\frac{U_{i_1} + U_{i_2} + U_{i_3} + U_{i_4}}{4} - V_j \right)^2.$$

Here i runs the numbers of the internal nodes of the grid **A**, a j runs the numbers of all the nodes of the grid **B**.

From these considerations, the following criterion of choice of U_i and V_j can be stated. U_i and V_j should be sought in such a way that the minimum value of

$$\varphi(\overline{U}, \overline{V}) = \gamma_1\varphi_1(\overline{U}, \overline{V}) + \gamma_2\varphi_2(\overline{U}, \overline{V}) + \gamma_3\varphi_3(\overline{U}, \overline{V}) \tag{3.8}$$

be obtained, γ_1, γ_2, and γ_3 being weight coefficients.

It is evident that if γ_2 and γ_3 are very small in comparison with γ_1, then U_i, V_j coincide with F_i, G_j, respectively. If γ_2 is large while γ_1 and γ_3 are small, then U_i will be expressed in terms of G_j, and V_j – in terms of F_i. Finally, if $\gamma_1$and γ_2 are small in comparison with γ_3, then the solution will be any U_i, V_j, expressed in terms of arithmetic mean values in the neighbouring nodes of the dual grid, but having no relation to the initial F_i, G_j. The correct choice of the weight ratio γ_1, γ_2, γ_3 can give the values of U_i and V_j, satisfying to a certain extent all the requirements of the problem under consideration. By variation of weights an accent can be made on this or that (possibly, known a priori or a posteriori) property of the sought solution.

The minimum point of the sum of squares of Eq. (3.8) always exists. It can be found from a system of `kk + kk1` equations with `kk + kk1` unknowns$\{U_i\}$, $\{V_j\}$, obtained by making partial derivatives equal zero:

$$\frac{\partial\varphi}{\partial U_i} = 0 \quad \text{and} \quad \frac{\partial\varphi}{\partial V_j} = 0.$$

By solving this system, one obtains new approximate values U_i, V_j for the function $f(x, y)$ in the nodes P_i, Q_j of both grids simultaneously. It is worth noticing that while the system matrix being composed, the analogues for the `NNBK` and `NBK` arrays, but for rectangular grids, are essentially used. Note that in such formulation the system matrix is obtained symmetrical and sparse.

For carrying out numerical experiments on checking the above method a program was composed using the FORTRAN 77 language. The results, illustrating the operation of the described algorithm for a spatial contact problem of off-centre loading of a square punch, located on a nonhomogeneous elastic half-space, are given in Sect. 3.5.1.

Additionally, we pay some attention to the properties of a similar postprocessor which we have developed on the base of an arbitrary triangulation of a general-type domain. In this case the dual grid are Dirichlet–Voronoy type polygons, formed by the preprocessor. The solution is sought in the nodes of the general triangulation of the domain (see the preprocessor algorithm) in such a way that it has minimum deviation from the two solutions, specified on dual grids in a metric l_2 with weights. Similarly to the postprocessor algorithm on a square, described here, the choice of weights affects the properties of the sought solution. One of the functions, provided by the postprocessor, is a possibility of extrapolation of any of the dual solutions to the whole general triangulation, and then to the whole domain.

Thus, application of grids in duality in the boundary-element method enables:

– an essentially new numerical solution of the problem, still genetically related to the one, built on the initial grid, to be obtained without large extra efforts;
– approximate solutions to be easily interpolated to the whole domain since they are located in the nodes of the two known grids;
– an efficient postprocessor algorithm to be built due to the interdependent location of nodes of the two grids when each node of one grid is enclosed by the known nodes of the other one;
– new smoothed solutions to be obtained by means of the postprocessor, which, inheriting the most important features of the two initial ones, have much less numerical error.

3.4 Automated Construction of Spatial Grids of Boundary Elements on the Surfaces of Contact of Deepened Foundation Structures with Soil

Application of boundary-element method for numerical modeling of processes of contact interaction of deepened foundation structures with soil media required a boundary-element grid to be built on a contact surface, the quality of the grid being to a great extent responsible for the numerical solution to be obtained. Since a correct calculation should take into account the contact interaction of the foundation and the soil not only on the bottom, but also on the lateral surfaces, the contact domains to be discretized are in general for foundation structures of a non-canonical, piecewise smooth shape. Therefore, the description of geometry of such contact surfaces by an explicit functionality of $z = f(x, y)$ type can be used, as a rule, only for separate areas.

At present, for some spatial problems of computational mechanics considerable progress has been achieved in plotting calculation grids on complex-shaped bodies.

In spatial problems of gas dynamics, liquid mechanics, heat and mass transfer formation of high-quality grids on a given boundary surface provides further constructions of 3-D finite-element or finite-difference grids [48, 49, 52, 64, 65, 86, 87, 133, 145]. Surfaces whose geometry can be easily described (or whose structural topology is known) by an initial rough discretization, are considered. Using the theory of Gaussian surfaces for obtaining spatial surface grids with specified properties, a multistep numerical procedure is built, including:

– parametrization of the surface area within the specified boundaries;
– numerical solution of the boundary problem of elliptical type to determine the field of parameters in the nodes of a natural or a rough grid on a specified surface;
– determination of new grid nodes on the surface in accordance with the parametric coordinates found;
– finding Gaussian surface equations provided that the calculation grid nodes belong to a simplest curved surface.

Note that one of the main requirements of most of the algorithms to the properties of the approximating spatial grids of the given type, is the grid line orthogonality.

The necessity of discretization of a complex-shaped surface arises in the problems of calculation of thin-walled structures, in particular, complex-shaped shells whose median surface is not described by a simple analytical expression [58, 78, 148]. After the choice of the reduction surface (in general, of a non-canonical shape), the main attention is paid to efficient procedures of parametrization of these surfaces. Shells of various geometry are effectively calculated using the finite-element method. Therefore, application of flat finite elements as well as those based on the relations of three-dimensional theory of elasticity, simplifies the surface parametrization. Surface approximation in theory of shells assumes for a discrete set of points on the median surface a coordinate system to be introduced and coefficients of the first and the second quadratic forms to be found, i.e. values of the vector function

$$r = X(u, v)i + Y(u, v)j + Z(u, v)k$$

for the introduced coordinate system to be found as well as the derivatives of r over u and v up to the third order inclusive. As noted in [148], in order to obtain high-accuracy numerical results on the static and vibrations of shell structures one should apply either a dense grid of mesh into flat finite elements, or apply approximations of higher accuracy.

All the experience on the discretization of complex-shaped surfaces, known from the studies in the above fields of computational mechanics, can be without principal modifications applied for boundary-element modeling of contact deformation processes. However, in the spatial contact problems for rigid punches under our consideration, when flat boundary elements with piecewise constant approximation of contact pressures are used, direct application of methods of approximation of higher-order surfaces, developed in liquid mechanics and theory of shells will be hardly justified. These methods, can be, above any doubt, more efficient for solving spatial contact problems for flexible foundation structures, i.e. for the problems with the account of local strength.

In accordance with the above stated, for the approximation of contact surfaces of rigid foundation structures constant boundary elements (for which the unknown contact stress has the same value over the whole element [33]) of triangular and quadrangular shape will be used. The vertices of the elements will be located on the contact surface itself. Note that at such approach for flat contact domains the boundary elements will always entirely belong to the foundation structure surface.

For the parts, characterized by a curvature, we assume that the required accuracy of the surface approximation can be achieved with the increase of the discretization degree.

It should be noted that our analysis of the geometrical shape of most of the real foundation structures has shown that they can be divided in two large categories: block type configurations with flat faces and rotation bodies. Therefore, the description of the discretization methods will be performed in detail for the foundation structures of these two types. The examples of methods of surface discretization will

be shown for foundation structures of various shapes, their parts being described by known equations in a Cartesian coordinate system.

Hereinafter it will be demanded that at any method of the contact surface mesh into boundary elements there should be no crossings or overlaps, and points on a non-flat surface should be the nodes of the adjacent boundary elements. In general, the mesh is supposed to be mixed, i.e. with simultaneous presence of triangular and quadrangular boundary elements. Global enumeration of elements is used with a possibility of preferential selection of a certain group of elements for the sake of convenience of subsequent processing of the numerical results. This is caused by the piecewise constant approximation of the unknowns and the completely filled structure of the matrix of the resolving linear equation system. Local enumeration of nodes for each element is also taken counterclockwise, the observation being performed from the direction of the external normal to the contact surface (i.e. from the side of soil).

High efficiency of the automatic generation of boundary-element vertices is favoured by the concept of boundary macroelements being used, which has been for a long time applied for computer implementation of the finite-element method [120, 123]. This concept is used mostly for automatic generation of coordinates and numbers of node points for flat problems [120]. Some details of the software implementation of the macroelement concept in the finite-element method for spatial problems are described in [123]. Spatial surface macroelements of various types will be also used here in the proposed algorithm of construction of boundary-element grids. Then some specific features of application of macroelements in the boundary-element method will be discussed, since there is not much literature available concerning this approach.

For all surface types fragmental discretization is performed that corresponds to a preliminary mesh of the foundation structure surface into boundary macroelements. At the next stage boundary macroelements are meshed into separate boundary elements with automatic generation of coordinates and nodes. Surface fragments with the simplest topology are taken as boundary macroelements. As a rule, these are flat quadrangles, parts of cylindrical, conical and spherical surfaces. In specific cases boundary macroelements, for which surface equations can be given in a determined way, are used.

The mesh of boundary macroelements into separate boundary elements is performed regularly and not necessarily uniformly. The degree of nonuniformity in a separate boundary macroelement over different directions is given parametrically and, if possible, takes into account the presupposed character of contact stress variation.

An important aspect of the fragmental discretization is adjustment of number of boundary elements at the lines of conjugation of complex boundary macroelements. It is required to improve the numerical solution and for the convenience of processing and treatment of the obtained results.

Now consider the procedures, used for automatic construction of the boundary-element grid for the main types of boundary macroelements.

Flat boundary macroelements. The geometry of each flat boundary macroelement is determined by its vertices. Let the global coordinates of the node points of a triangular (quadrangular) boundary macroelement be known:

$$\left(X_i, Y_j, Z_i\right), \quad i = 1,2, \ldots, l; \quad l = 3\,(4)\,.$$

The mesh of boundary macroelements into separate elements is performed on the base of isoparametrical element technique [22].

The description of geometry in the plane of a quadrangular boundary macroelement is obtained by using interpolation formulae

$$\begin{aligned} X &= X_1\varphi_1 + X_2\varphi_2 + X_3\varphi_3 + X_4\varphi_4, \\ Y &= Y_1\varphi_1 + Y_2\varphi_2 + Y_3\varphi_3 + Y_4\varphi_4, \\ Z &= Z_1\varphi_1 + Z_2\varphi_2 + Z_3\varphi_3 + Z_4\varphi_4 \end{aligned} \tag{3.9}$$

where φ_i, $i = \overline{1,4}$ are simplest linear shape functions given by

$$\phi_1 = \frac{1}{4}\cdot(1-\xi_1)\cdot(1-\xi_2)\,, \quad \phi_2 = \frac{1}{4}\cdot(1+\xi_1)\cdot(1-\xi_2)\,,$$

$$\phi_3 = \frac{1}{4}\cdot(1-\xi_1)\cdot(1-\xi_2)\,, \quad \phi_4 = \frac{1}{4}\cdot(1+\xi_1)\cdot(1-\xi_2)\,.$$

Dimensionless variables ξ_1 and ξ_2 are identified with local coordinates in the plane of a standard square $|\xi_1| \le 1, |\xi_2| \le 1$. If now a uniform (Fig. 3.19a) or condensing towards the boundary (Fig.3.19b) grid of elements is applied to a standard square, then a linear isoparametric transformation (3.9) will transform them into global boundary elements without violation of interelement continuity and with required regular enumeration of nodes and vertices.

Based on the above interpolation algorithm a subroutine `TRPSPS` was developed for discretization of an arbitrary quadrangular boundary macroelement with the following call:

```
CALL TRPSPS(M,N,X,Y,Z,ALPHA,K1,K2),
```

where `M, N` is the number of the boundary element grid lines along two adjacent directions, `X, Y, Z` are 4-component arrays of global coordinates of the boundary macroelement vertices, `ALPHA` is a parameter of the boundary-element grid condensation at the boundary element edges (`ALPHA` = Ø at uniform discretization), `K1` is the number of boundary elements having been created before calling the subroutine `TRPSPS`; `K2` is the total number of boundary elements after calling the subroutine `TRPSPS`, `K2 = K1 + M * N`.

Discretization of the contact surface of a foundation structure of the block type with flat quadrangular faces into boundary elements is reduced in the case under

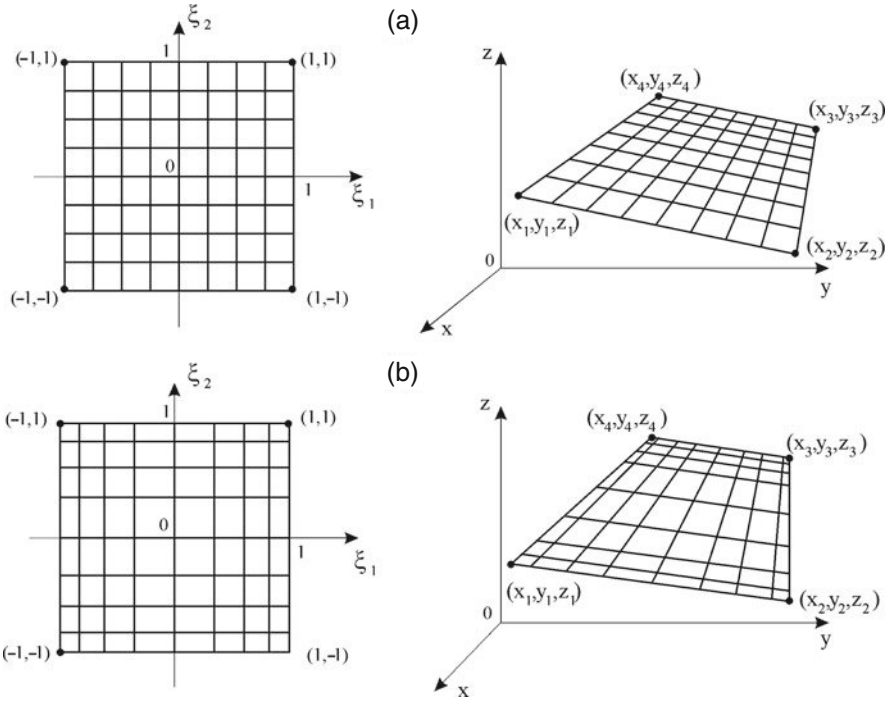

Fig. 3.19 Local coordinates for a quadrangular boundary macroelement: (**a**) uniform grid; (**b**) non-uniform grid

consideration to specifying the global coordinates of vertices and a subsequent call to the subroutine TRPSPS. For example, discretization of the contact surface of a pyramidal foundation (with five flat faces) with a uniform boundary element grid is obtained as a result of the following set of FORTRAN statements:

```
K1 = Ø
CALL TRPSPS(N1,N2,X1,Y1,Z1,Æ,K1,K2)
CALL TRPSPS(M,N1,X2,Y2,Z2,Ø,K2,K3)
CALL TRPSPS(M,N2,X3,Y3,Z3,Ø,K3,K4)
CALL TRPSPS(M,N1,X4,Y4,Z4,Ø,K4,K5)
CALL TRPSPS(M,N2,X5,Y5,Z5,Ø,K5,KK).
```

As a result, the common area of global coordinates of vertices and characteristics of the boundary elements will be filled:

```
COMMON /ELPS/ AX(KK,4),AY(KK,4),AZ(KK,4),L(KK).
```

The practical experience of discretization of contact surfaces of various foundation structures of block type with flat faces has shown that the most often repeated

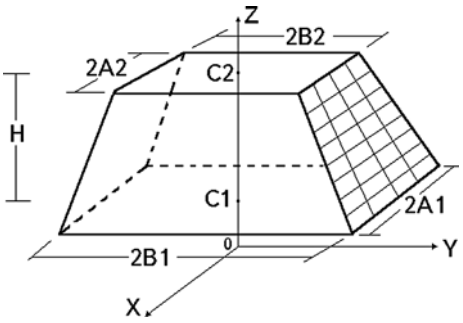

Fig. 3.20 Scheme of discretization of a tetrahedral boundary macroelement

module (substructure) is a four-faced belt with the height H, symmetrical with respect to the planes OXZ and OYZ and possessing rectangular shape with the dimensions 2*A1 ×2*B1, 2*A2 ×2*B2 at the depths Z = C1 and Z = C2, (H = C2 −C1) (Fig. 3.20). For the convenience of discretization of this substructure a special subroutine NABS was developed, called by the following statement:

```
CALL NABS(M,N1,N2,A1,A2,B1,B2,C1,C2,K1,K2).
```

The formal parameters of the NABS subroutine are described as follows:

M is the number of divisions of the boundary-element grid vertically (in depth);
N1, N2 are the numbers of divisions of the boundary-element grid horizontally for two faces of the belt, respectively;
A1, B1 and A2, B2 are half-sizes of the belt rectangles in the Z = C1 and Z = C2 planes, respectively;
K1, K2 are the parameters of the amount of the boundary elements with the same sense as in TRPSPS subroutine.

The result of NABS subroutine is, similarly to the case of TRPSPS subroutine, the filled common area COMMON/ELPS/ for the vertice coordinates and characteristics of the boundary elements. The total number of boundary elements, formed by NABS subroutine, is KK = 2 M*(N1 + N2).

For the discretization of triangular flat faces (triangular boundary macroelements), the necessity of which happens not so often, the most convenient is application of a mesh of a standard triangle (a 2-D simplex) $\{0 \le \xi_1 \le 1, 0 \le \xi_2 \le 1 - \xi_1\}$ with subsequent interpolation (Fig. 3.21). For a given integer $m \ge 1$ in the standard triangle a system of points is introduced [139]:

$$\xi_1 = i/m, \xi_2 = j/m, 0 \le i, j \le m, 0 \le i + j \le m\,. \tag{3.10}$$

System (3.10) includes the triangle vertices as well as the points obtained by mesh of each side of the triangle into m equal parts as the points of intercept of the

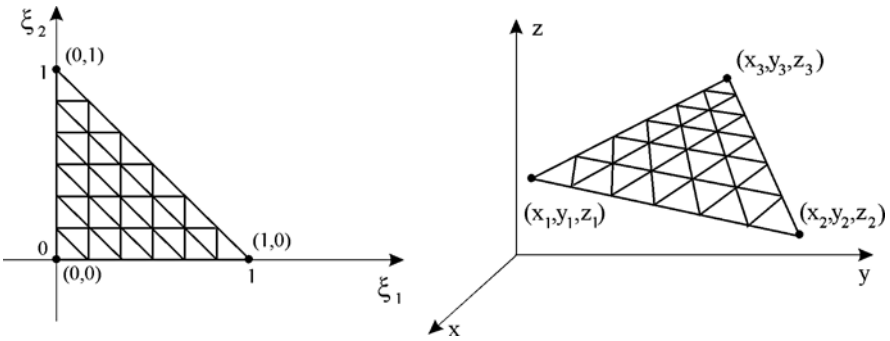

Fig. 3.21 Local coordinates for a triangular boundary macroelement

straight lines parallel to the triangle sides and passing through the mesh points. A uniform mesh of an arbitrary flat triangular face with the vertices

$$P_1\,(X_1,Y_1,Z_1)\,,P_2\,(X_2,Y_2,Z_2)\,,P_3\,(X_3,Y_3,Z_3)$$

into m^2 triangular boundary elements is easily obtained after the application of the following parametric interpolation [33]:

$$\begin{aligned} X &= X_1\xi_1 + X_2\xi_2 + X_3\xi_3, \\ Y &= Y_1\xi_1 + Y_2\xi_2 + Y_3\xi_3, \\ Z &= Z_1\xi_1 + Z_2\xi_2 + Z_3\xi_3, \\ \xi_1 &+ \xi_2 + \xi_3 = 1\,. \end{aligned} \tag{3.11}$$

This results in an algorithm for discretization of triangular boundary macroelements, which enables the required triangular boundary-element grid condensation degree to be achieved rather easily. Besides, triangles, similar to the initial macroelement, are formed. If necessary, the obtained boundary-element grid can be easily condensed near the selected vertex of the boundary macroelement using, e.g. quasi-uniform grids [69] instead of Eq. (3.10).

Figure 3.22 shows the surface of rectangular prismatic foundation blocks discretized by means of uniform grids of quadrangular boundary elements. Rigid plates or monolithic blocks with dimensions as shown in Fig. 3.22a, are used, e.g. to design foundations for forging hammers as well as molding foundry machines, crushers, mills, presses etc. [62, 118, 152]. Rectangular prismatic monolithic concrete foundations with relative deepening $h/d \sim 2 \div 4$ (Fig. 3.22b) are widely applied for contact-line (console, anchor, fixing etc.) masts [71, 80], bridge piers of caisson type [140] etc. The experience of foundation engineering of the recent years shows the efficiency of application of trench (or slotted) foundations (Fig. 3.22c), built by diaphragm wall method under columns and walls of buildings and structures [34, 98, 99, 132], as well as for high-voltage power line masts [82].

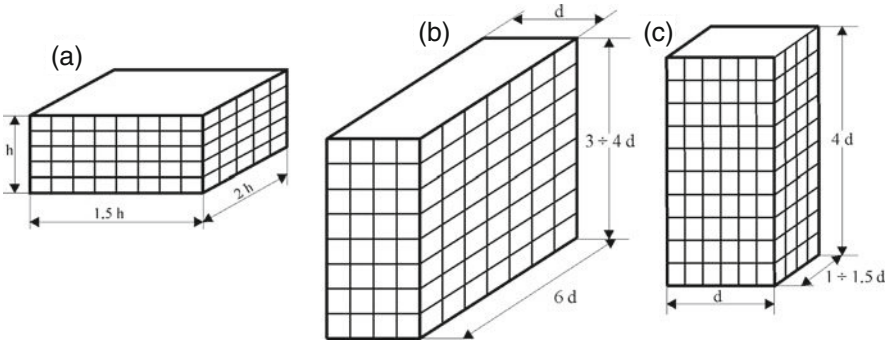

Fig. 3.22 Rectangular prismatic foundations of various dimensions

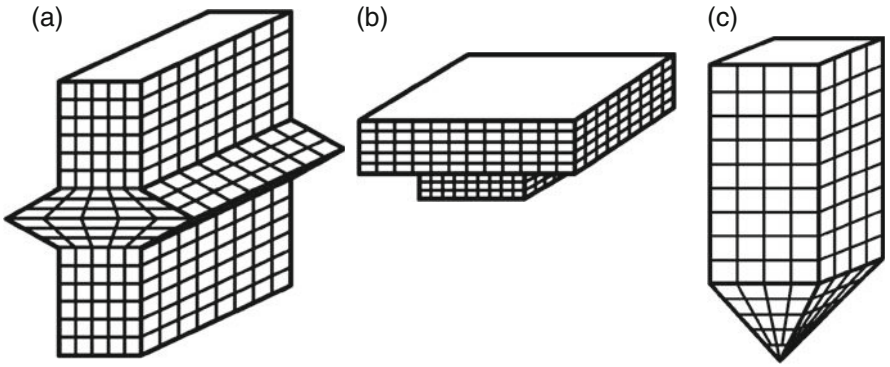

Fig. 3.23 Rectangular prismatic foundations with structural modifications: (**a**) slotted foundation with lateral widenings; (**b**) with a set-off in the bottom; (**c**) with a pyramidal tip

Rectangular prismatic foundations with simplest structural modifications are shown in Fig. 3.23. Slotted foundation structures with lateral extensions in the form of longitudinal ribs of various cross-section configuration [8] (Fig. 3.23a). Calculations and the experimental data [18, 19, 130] show that foundations with a set-off in the bottom (Fig. 3.23b) (with intermediate preparation, variable cross-section) work more efficiently than those with a flat bottom. Rectangular prismatic foundations with a pyramidal tip (displacement piles) are widely applied in industrial and civil engineering (Fig. 3.23b).

In industrial engineering the most spread foundation structures are massive pedestal footings [130]. Figure 3.24a, b show pedestal footing constructions for one and two treads, respectively. The cross-section shape of such foundations is square or rectangular for central and off-centre loading, respectively.

In pile foundation construction common prismatic piles are with high efficiency replaced with foundations of short pyramid-shaped piles in view of their load capacity for the same volume [26, 63, 119]. Figure 3.25 shows discretized contact surfaces

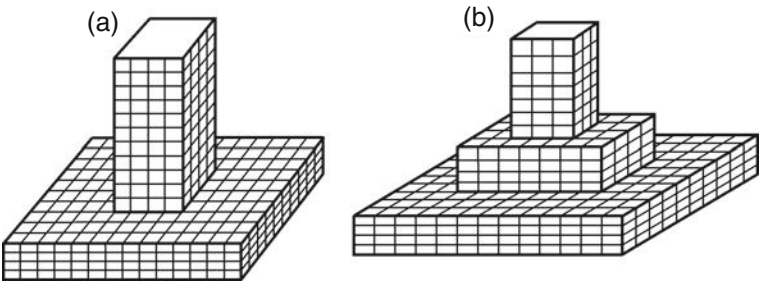

Fig. 3.24 Benched pier foundations: (**a**) with one bench; (**b**) with two benches

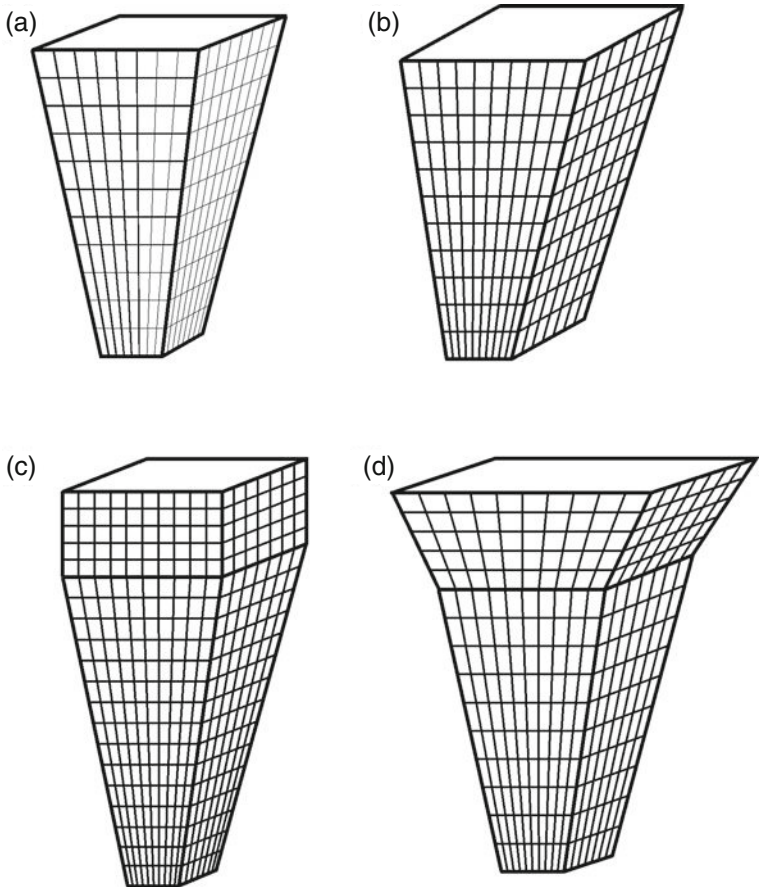

Fig. 3.25 Pyramidal foundations: (**a**) with square cross-section; (**b**) with rectangular cross-section; (**c**) with a prismatic head; (**d**) a bipyramidal pile

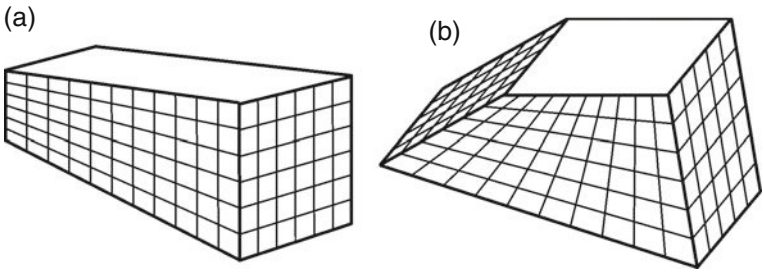

Fig. 3.26 Block foundations with an inclined bottom: (**a**) vertical lateral sides; (**b**) inclined lateral sides

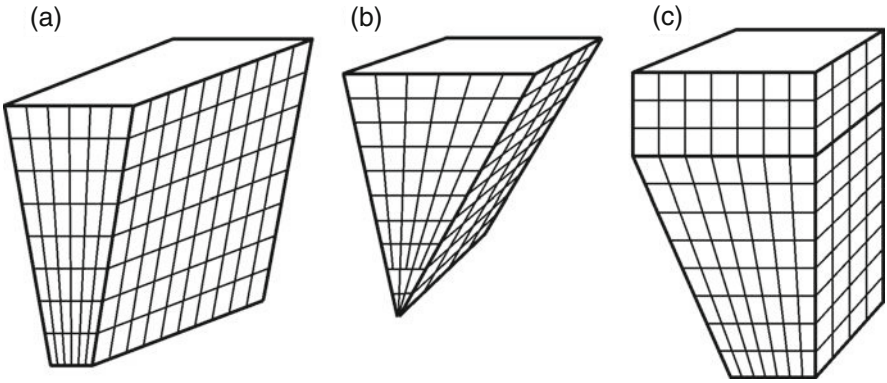

Fig. 3.27 Wedge-type foundations: (**a**) wedge-slotted; (**b**) asymmetrical wedge pile; (**c**) wedge pile foundation with a console block

with soil for pyramidal foundations of most of the known shapes, operating well at horizontal and momental loads [4, 5, 55, 72, 84].

For structures with strutted elements, e.g. three-hinged frames, application of foundations with oblique bottom is advisable [130]. The size of such foundation and the angle of the bottom inclination with respect to horizontal is chosen in such a way that the eccentricity of load resultant on the foundation founding level be close to zero [109]. Massive foundations with oblique bottom and vertical or slanted lateral faces, with plotted boundary-element grids are shown in Fig. 3.26a, b respectively.

To reduce horizontal displacements and to increase the load-carrying capacity under horizontal forces various wedge foundations are used [71, 73, 98, 117]. The examples of wedge foundations are presented by a wedge-slotted foundation and an asymmetric wedge pile shown in Fig. 3.27a, b respectively, along with the boundary-element grids, as well as wedge pile foundation with a corbel block (Fig. 3.27c).

Figure 3.28 presents variations of post foundations of complex shape, widely used in practice, for which the contact surface with soil is formed by planes [98, 130, 134]. They can be easily discretized. The extended lateral surface of such foundation structures is the main factor responsible for the increase of their characteristics.

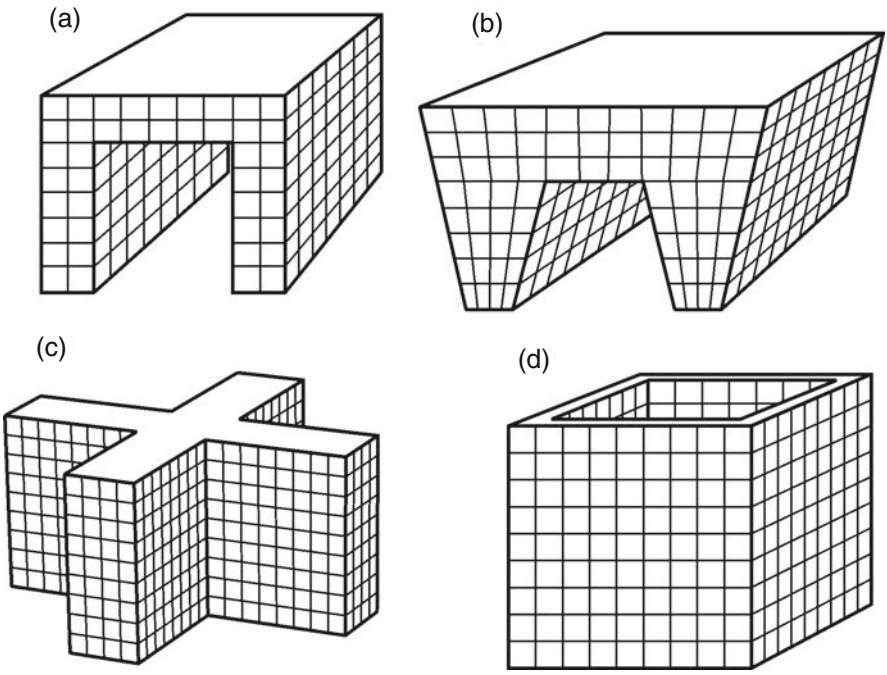

Fig. 3.28 Complex-shaped foundations with flat sides: (**a**) double-slotted; (**b**) double-wedge; (**c**) slotted cross-like; (**d**) box-like

Boundary macroelements on the surfaces of rotation bodies. An axisymmetric surface is obtained as a result of rotation of a curve around the axis of symmetry. Assume OZ to be the symmetry axis. Then, due to the axial symmetry, the equation of the curve in the cylindrical coordinate system is given by

$$r = F(z), F''(z) \neq 0, r = \sqrt{x^2 + y^2}, C_1 \leq z \leq C_2 \tag{3.12}$$

In order to plot the boundary-element grid on the rotation surface (Fig. 3.29) the segment $[C_1, C_2]$ is divided into m parts, not necessarily equal, by points $z_k = C_1 + (C_2 - C_1) \cdot q(\alpha, t_k)$, $k = 1, 2, \ldots, m+1$ where $t_k = (k-1)/m$, $\cdot\ q(\alpha, t)$ is a function, mapping the [0, 1] segment into itself and chosen, depending on the form of $F(z)$ for condensation of the points of division near the $[C_1, C_2]$ segment ends, α is the condensation parameter.

The interval $[0, 2\pi]$ of the angular coordinate φ variation is meshed into n equal parts by $\varphi_j = \Delta \cdot j$, $j = 0, 1, \ldots, n-1$ planes with a step $\Delta\varphi = 2\pi/n$. Considering each two consecutive meridional sections φ_j, φ_{j+1} $(j = \overline{0, n-1})$, form flat boundary elements by calculating the coordinates of their vertices as follows:

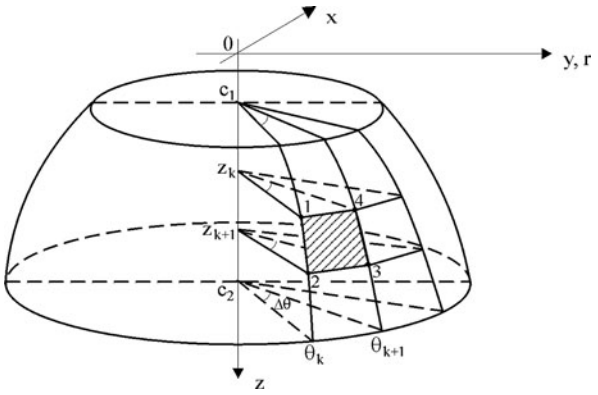

Fig. 3.29 Discretization of a rotation surface into boundary elements

$$X_1^{(j)}(k) = F(z_k) \cdot \cos\left(\phi_j\right); Y_1^{(j)}(k) = F(z_k) \cdot \sin\left(\phi_j\right); Z_1^{(j)}(k) = Z_k;$$

$$X_2^{(j)}(k) = F(z_{k+1}) \cdot \cos\left(\phi_j\right); Y_2^{(j)}(k) = F(z_{k+1}) \cdot \sin\left(\phi_j\right); Z_2^{(j)}(k) = z_{k+1};$$

$$X_3^{(j)}(k) = F(z_{k+1}) \cdot \cos\left(\phi_{j+1}\right); Y_3^{(j)}(k) = F(z_{k+1}) \cdot \sin\left(\phi_{j+1}\right); Z_3^{(j)}(k) = Z_{k+1};$$

$$X_4^{(j)}(k) = F(z_k) \cdot \cos\left(\phi_{j+1}\right); Y_4^{j}(k) = F(z_k) \cdot \sin\left(\phi_{j+1}\right); Z_4^{(j)}(k) = Z_k;$$

$$k = 1,2,\ldots,m+1; j = 0,1,2,\ldots,n-1.$$

Note that in the case when $F(z) = 0$ (i.e. in the foundation structure endpoint) the second and third vertices of the boundary elements merge and quadrangular boundary elements are degenerated into triangular. The total number of the flat boundary elements on the rotation body fragment under consideration is $K = m \cdot n$, increasing with the mesh number both in depth (m), and in the angular coordinate (n).

According to the accepted terminology, the rotation surface fragment, approximated by using flat quadrangular and triangular boundary elements will present a boundary macroelement on a rotation body. Subroutines for automatical discretization of boundary macroelements have been developed for the most often used rotation surface fragments:

cylindrical: $F(z) = R = \text{const}$;

conical: $F(z) = R_1 + \dfrac{R_2 - R_1}{C_2 - C_1}(z - C_1)$;

spherical: $F(z) = \pm\sqrt{R^2 - (z - z_0)}$

where R is the cylinder or sphere radius, R_1, R_2 are the radii of the upper and lower bases of a truncated cone, respectively, z_0 is the Z-coordinate of the centre of the sphere.

Another rather efficient method of discretization of boundary macroelements should be mentioned. It is more convenient than the above one for the cases when the rotation body surface is given by an equation of the type

$$z = f(r), \quad r = \sqrt{x^2 + y^2} \tag{3.13}$$

We take the advantage of the fact that any rotation surface fragment located between the $z = C_1$ and $z = C_2$ planes, is always projected onto XOY plane as a circle or a ring. Then, possessing the discretization of these planar canonical domains and by applying Eq. (3.13), one can easily approximate boundary macroelements on a rotation body by planar boundary elements of triangular and quadrangular type, the requirements of interelement continuity being directly fulfilled. Subroutines, elaborated for the boundary macroelement mesh on a

plane: $z = C = \text{const}$,
conical surface: $z = z_0 \pm a\sqrt{x^2 + y^2}$,
spherical surface: $z = z_0 \pm \sqrt{R^2 - r^2}$

employ regular uniform and non-uniform grids on a circle and a ring, enabling the spatial discretization of the required quality to be obtained.

Full discretization of the foundation structure in the form of a rotation body is obtained by combining boundary macroelements of simplest shapes considered above. When the total number of the boundary elements is sufficiently large and their size is sufficiently small, then, as follows from the knowledge of physics, it is natural to expect the contact interaction of such foundation structure with soil (after the surface approximation by an ensemble of flat boundary elements) under external load not to be much different from the real foundation behaviour, and the approximate solution of the contact problem to converge to the exact one at the increase of the number of flat boundary elements and at their size decrease. Practical calculations, described in the subsequent sections, show a rather good convergence.

Figures 3.30–3.32 show typical examples of mesh of the contact surface of axisymmetric foundation structures with soil, using flat boundary elements.

Boundary-element discretization is performed most easily when the foundations have only cylindrical components (Fig. 3.30). In such cases boundary macroelements of only three types are used: a circle, a concentric ring, and the lateral surface of a cylinder. Rigid cylindrical foundations (Fig. 3.30a) (short single bored piles, short-length shell-piles, caissons and shell caissons) are now rather widely applied in industrial, agricultural and transport engineering [25, 50, 74, 79, 100, 153]. They appear economically justified for construction of industrial and civil buildings with rather small number of storeys (workshops, garages, warehouses, shops etc.), livestock factories, greenhouses, pipe bridges, city transportation contact-line masts,

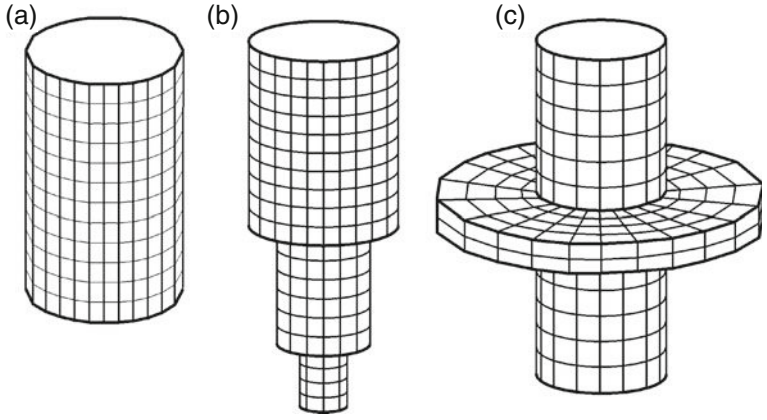

Fig. 3.30 Foundations of cylindrical components: (**a**) simple; (**b**) telescopic; (**c**) with a collar

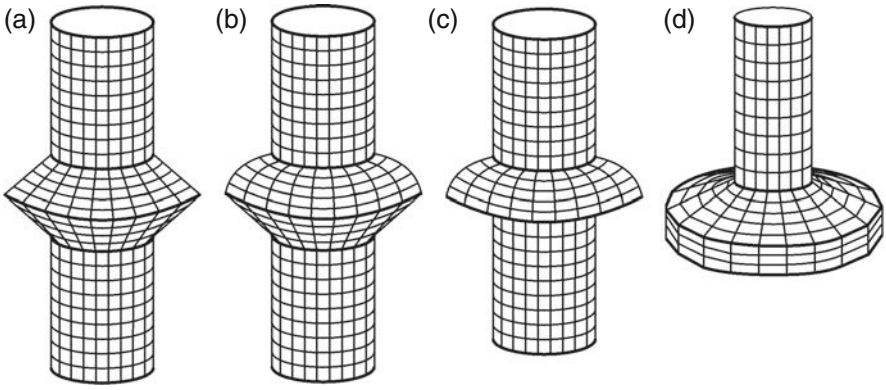

Fig. 3.31 Foundation with shaft widenings of various type: (**a**) bored pile foundation with a conical widening; (**b**) bored pile foundation with a spheroconical widening; (**c**) bored pile foundation with a hemispherical widening; (**d**) mushroom-shaped foundation

power transmission towers, bridges. Telescope-shaped cylindrical foundations (Fig. 3.30b) find application for construction of oil and gas drilling platform legs on the sea shelf [146]. Sometimes near the cylindrical pile heads a stabilizing collar is made (Fig. 3.30c) what enables the load-carrying capacity of the foundation structure to be essentially increased [79].

A considerable effect on the increase of the load-carrying capacity of short cylindrical foundations can be achieved due to widening of a part of their shank (bottom, head or the intermediate part) [143, 153]. The surfaces of cylindrical foundations with different widenings, discretized by means of flat boundary elements, are shown in Fig. 3.31. In accordance with soil drilling technology, the shape of the widening surface is determined by the junction of conical, cylindrical, and spherical fragments. As seen from Figs. 3.31a–d application of circular, ring-shaped, cylindrical,

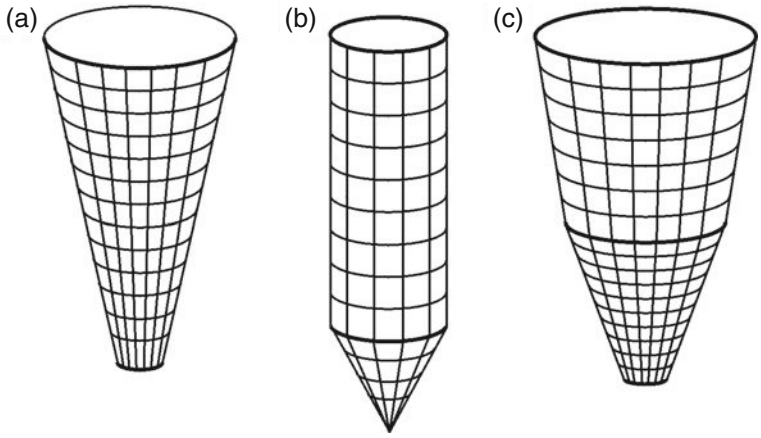

Fig. 3.32 Conical foundations: (**a**) in the shape of a truncated cone; (**b**) cylindrical pile with a conical tip; (**c**) biconical

conical, and spherical boundary macroelements in a required sequence automatically provides consistent discretization of the foundation structures with various types of widenings.

A relatively new, progressive type of foundations are now short conical piles (Fig. 3.32), especially hollow ones, whose application enables the concrete consumption to be reduced by 25–30% [25, 27]. The shape of the lateral surface results in an explicitly pronounced increase of the load-carrying capacity due to the formation of a compression area around the pile. A good-quality approximation for conical surfaces is achieved using 2–3 boundary macroelements at relatively small total number of flat boundary elements (Fig. 3.32a–c).

Figures 3.33–3.35 present the versions of discretization of contact surfaces for various complex-shaped foundation structures. Each of the configurations considered is characterized by simultaneous presence of both flat elements and fragments of second-order surfaces, mostly cylindrical. When the surface fragments are combined in a whole unit with the required conjunction of the boundary-element vertices at adjacent partitions, an individual approach to each foundation structure is required, preferably taking into account the specific features of the contact stress distribution.

A version of almost uniform discretization of the contact surface of the soil and a caisson with rounded (cylindrical) abutting ends is presented in Fig. 3.33 [140]. Two flat rectangles and two symmetrical halves of straight circular cylinder surface are taken as boundary macroelements on the lateral surface (Fig. 3.33a). The bottom is discretized by using three boundary macroelements – a rectangle in the middle and two semicircles, each of them possessing only two triangular boundary elements, all other boundary elements being quadrangular (Fig. 3.33b).

Typical examples of discretized surfaces of contact with soil for slotted foundations with non-flat bottom shape [98] are shown in Fig. 3.34. The slotted foundation

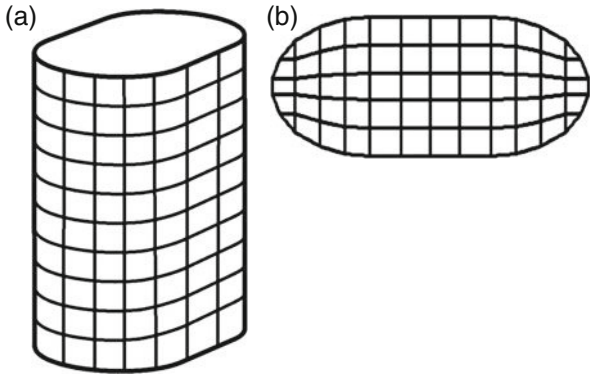

Fig. 3.33 Caisson with rounded walls: (**a**) lateral surface; (**b**) bottom

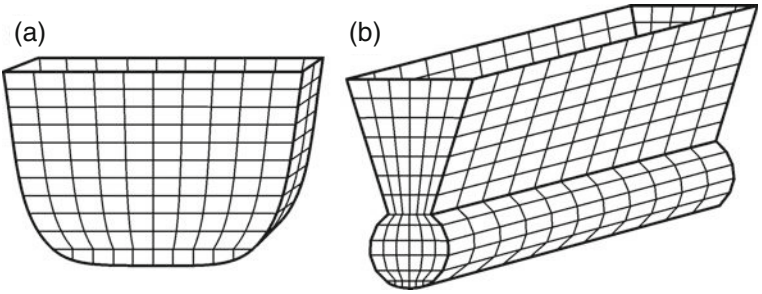

Fig. 3.34 Slotted foundations with non-flat bottom: (**a**) curved bottom shape in the longitudinal cross-section; (**b**) wedge-slotted with an enlarged footing

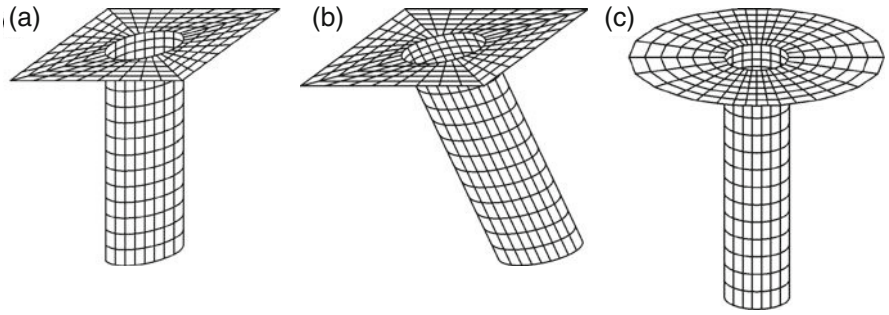

Fig. 3.35 Pile raft foundations: (**a**) vertical cylindrical pile with a rectangular raft; (**b**) inclined cylindrical pile with a rectangular raft; (**c**) vertical cylindrical pile with a circular raft

surface with a curved bottom shape first was presented as a combination of three boundary macroelements (Fig. 3.34a): a rectangular prismatic one in the upper part, two symmetrical segments on the lateral surface as well as a ruled surface on the bottom. Not that the shape of the bottom has no major importance for the program

module developed to perform the discretization and can be determined by a subroutine function. A rather complex structure of a wedge-slotted foundation with a pedestal [53] was subject to surface discretization using the following standard boundary macroelements: a four-faced belt-shape part of a pyramid, an open lateral surface of a circular cylinder with a horizontal axis, and two truncated circles at the abutting ends (Fig. 3.34b). The program provides consistence of the discretization while combining of the above boundary macroelements as well as a possibility to specify different widening shapes and boundary-element grid condensation degree for the given type of the foundation structures and enables a good-quality surface approximation to be obtained using a moderate ($\approx 300 \div 350$) number of flat boundary elements.

Discretization of foundations with pile rafts needs special attention. A low pile raft is a concrete block of rectangular or circular cross-section, mounted on the pile's head to transfer the load from the structure. Such structures combine typical features of both shallow foundations and pile foundations.

Figure 3.35 shows boundary-element grids on the surfaces of pile raft foundations with single vertical (Fig. 3.35a–c) and inclined (Fig. 3.35b) piles. Such foundations are effectively used for structures with relatively small number of storeys as well as for reconstruction of buildings and structures [77]. Since, in general, a pile and a pile raft can be located eccentrically, special boundary macroelements of circular and rectangular shape with internal cutoffs of various shape had to be developed. The discretization on the internal contour was consistent with the boundary-element nodes in the horizontal sections of the pile substructure.

A rather typical one among the foundations with pile rafts under consideration is the discretization of the contact surface for a foundation with an inclined cylindrical pile and a rectangular pile cap (Fig. 3.35b). A scheme, explaining the sequence of formation of the boundary-element grid on the surfaces of contact of the pile raft and the pile with soil, is shown in Fig. 3.36. Three consistent boundary macroelements were used: the lateral surface of a straight circular cylinder, restricted by an orthogonal planar section and a planar section, inclined at an angle φ (φ being the angle of the cylinder axis inclination to the horizontal plane), a circle on the cylinder's abutting end, and a rectangle with an ellipse-shaped cutoff. For the convenience of computation of the boundary-element vertex coordinates on the inclined cylinder surface an auxiliary coordinate system $O'X'Y'Z'$ is introduced with the origin in the centre of the cylinder's abutting end and the coordinate axis $O'Z'$ coinciding with the cylinder axis. This corresponds to a counterclockwise rotation of the global OXYZ system by angle $\alpha = \pi/2 - \varphi$ around the OX axis and a transfer of the coordinate system origin to the $(0, L\cdot\cos\varphi, L\cdot\sin\varphi)$ point. The formulae for the coordinate transformation to the global system are as follows

$$\begin{cases} x = x', \\ y = z' \cos\varphi + y' \sin\varphi + L \cdot \cos\varphi, \\ z = z' \sin\varphi - y' \cos\varphi + L \cdot \sin\varphi \end{cases} \tag{3.14}$$

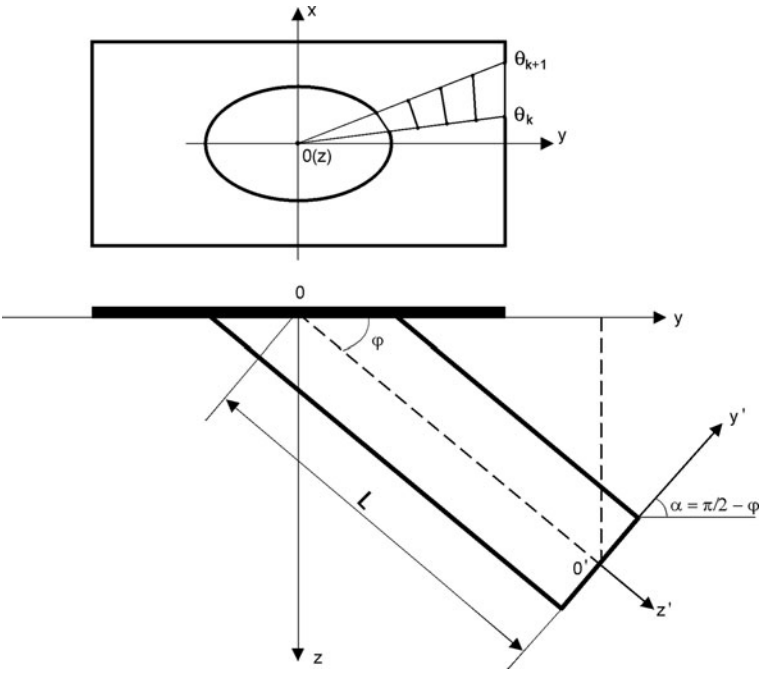

Fig. 3.36 Scheme of discretization of the contact surface of soil and an inclined pile with a low rectangular raft

and the formulae for the coordinate transformation from the global system are given by

$$\begin{cases} x' = x, \\ y' = y \cdot \sin\varphi - z \cdot \cos\varphi, \\ z' = y \cdot \cos\varphi + z \cdot \sin\varphi + L \end{cases} \tag{3.15}$$

where L is the length of the segment on the cylinder axis between the restricting upper and lower sections. The equation of the elliptical cut-off in the pile raft

$$\mathrm{x}^2 + \mathrm{y}^2 \sin^2\varphi = R^2$$

is obtained as the line of interception of the straight circular cylinder

$$(x')^2 + (y')^2 = R^2$$

with the plane

$$z = 0 \quad (z' = y' \cot\varphi - L)\,.$$

Further mesh of the contact surface into the boundary elements is performed by sectioning by planes, passing through the cylinder axis. It is convenient at first to obtain the coordinates of flat boundary-element vertices from the formulae of Eq. (3.15)-type in the cylinder-linked O′X′Y′Z′ system, and then to transform them to the global OXYZ system according to Eq. (3.14). The considered example shows how one can semiautomatically obtain discretization of various non-axisymmetric surfaces by preliminary introduction of local coordinate systems for separate surface fragments (boundary macroelements).

Thus, the developed algorithms of boundary-element discretization of contact surfaces of deepened foundations with soil are characterized by a simple logical structure and short computation time (due to the use of the explicit formulae to determine the coordinates of the boundary-element vertices). Besides, the possibility of automatic mesh of grids enables a sequence of naturally nested discretizations to be created. As a result, at the application of condensing grids, numerical solutions are effectively extrapolated with the estimation of accuracy. The proposed simplified construction of grid approximations enables the grids to be automatically reconstructed multiply, adapting them by local condensations to the sought solution.

3.5 Test Examples of Numerical Modeling of Spatial Problems of Contact Interaction

3.5.1 Contact Problems for Flat Punches with a Smooth Base

Numerical solution of spatial contact problems on regular grids. Consider as the main example a spatial contact problem for a rigid punch with a circular cross-section, interacting with an elastic homogeneous half-space. No friction in the contact domain is considered. Suppose the punch to be loaded at the centre by a vertical force P. It is known [67] that in such a case the problem has an exact solution

$$W = \frac{P\left(1-\nu^2\right)}{2Ea}, p\,(r) = \frac{P}{2\pi a\sqrt{a^2-r^2}} = \frac{p_*}{2\pi\sqrt{1-(r/a)^2}},$$

where α is the punch radius, r is the distance from the punch centre to the observation point, E is the deformation modulus, ν is the Poisson ratio, $p_* = P/\alpha^2$. This problem is one of the few spatial contact problems having an analytical solution what enables one to estimate the accuracy of its numerical solutions, obtained on different grids.

Compare the numerical solutions of this problem using the boundary-element method for four types of the circular domain discretization:

(1) mesh into triangles and quadrangles by coordinate curves in polar coordinate system with a constant radial step (a uniform mesh, Fig. 3.37a);

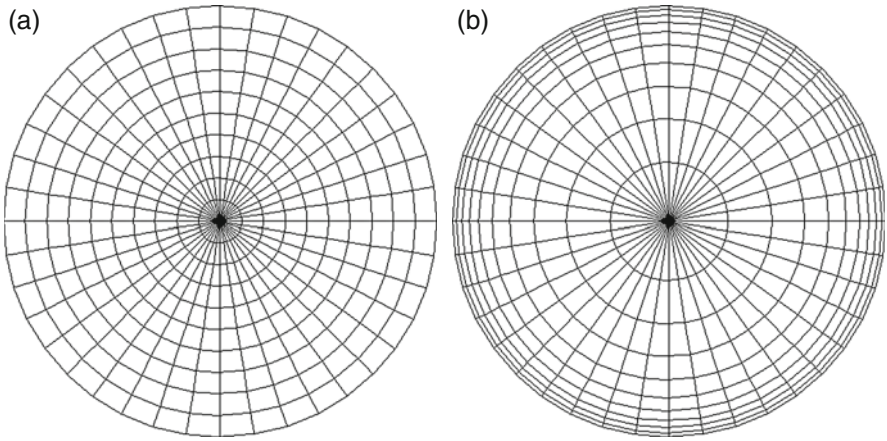

Fig. 3.37 Regular grids of boundary elements, applied for solving the contact problem of a centrally loaded circular punch: (**a**) uniform; (**b**) with condensation at the boundary

(2) mesh into triangles and quadrangles using the polar coordinate system with a variable radial step (a non-uniform mesh with condensation towards the boundary, Fig. 3.37b);
(3) cyclic mesh into triangular elements with condensation at the boundary (Fig. 3.17a);
(4) dual mesh into Dirichlet-Voronoy type cells (Fig. 3.17c), obtained by the method described in Sect. 3.3.2.

At the numerical solution of the problem in the second case the circular contact domain was discretized into triangular and quadrangular elements by means of radii and concentric circles condensing towards the boundary. The condensation was applied to take into account a sharp increase of contact stress near the punch edge. The radii of the concentric circles were calculated using the following quasiuniform dependence:

$$r_j = a\frac{\exp\left(\beta \cdot t_j\right) - 1}{\exp\left(\beta\right) - 1}, t_j = \frac{j}{L}, j = 1, 2, \ldots, L.$$

The condensation degree was controlled by the choice of the parameter β.

The first and the second grids consist of 400 elements and contain 10 concentric layers. The third grid contains 216 elements and consists of four concentric layers. Finally, the last grid contains 145 elements, located in five concentric layers, the first (central) layer containing only one element. Note that the number of Dirichlet–Voronoy elements of the last grid is by one and half times smaller than the number of elements of the triangular grid (3) and by factor of 2.76 smaller than the number of elements of the first two grids.

Table 3.1 Characteristics of the boundary-element solution of the contact problem for a round punch on regular grids

Discretization type	N	S/α^2	W/α	σ	Mean square deviation
Uniform in polar coordinates ($\beta = 0$)	400	3.12869	0.47802	274.0	4.3265×10^{-3}
Non-uniform in polar coordinates ($\beta = -3$)	400	3.12869	0.47114	147.0	3.3212×10^{-2}
Triangulation with a displacement on the boundary	216	3.13761	0.47760	100.6	1.3489×10^{-2}
Dual Dirichlet–Voronoy grid	145	3.13761	0.46868	274.2	1.0686×10^{-3}
Exact solution	–	3.14153	0.46875	–	0

The results of the numerical solution of the contact problem for the four discretization schemes as well as the exact solution data for $\nu = 0.25$, $P = E\alpha^2$ are listed in Table 3.1and shown in Fig. 3.38.

As follows from the presented data, the calculation using the uniform grid of 400 elements produces results which are quite acceptable from the engineering point of view. At the same number of elements the accuracy of the solution can be, though slightly, increased by the grid condensation near the punch boundary (what is seen in Table 3.1 for the calculations while choosing the condensation parameter

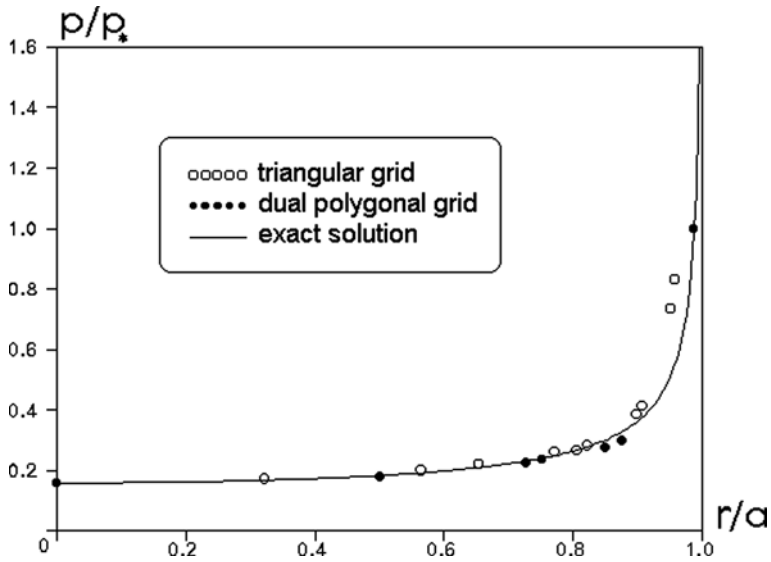

Fig. 3.38 Exact and approximate solutions of the contact problem for a centrally loaded circular punch using regular dual grids

$\beta = -3$). In this case the total (mean square) error increases by an order of magnitude and the condition number of the matrix of the resolving system of linear algebraic equation is reduced almost twice. This means that at $\beta = -3$ the boundary-element grid rather correctly takes into account the unlimited growth of the solution (contact pressures) near the punch boundary. The increase of the mean square error here is most likely due to the extension of the numerical results for the contact pressure function on the condensed grid to the area where the solution varies with increasing rate. Evidently, for each non-uniform discretization of the type under consideration an optimal value of the condensation parameter β exists, whose determination requires additional computation time consumption. For example, the calculations at $\beta = -5$ give the following characteristics of the numerical solution:

$$W/a = 0.47032,\ \sigma = 384.8,\ \text{mean square error} = 2.94958 \times 10^{-1}$$

It is seen that at a slight correction of the relative settlement, which is an integral characteristic of the numerical solution, the boundary-element function of contact pressures is determined with higher error near the punch edge. Simultaneously the condition number strongly increases, which can be related to the degeneracy of the boundary elements into rectangles of a rather small thickness. In order to obtain uniformly suitable numerical solution over the whole circular domain one should simultaneously with the grid condensation near the punch edge increase the discretization degree over the angular coordinate.

The triangular discretization according to the scheme (3) in comparison with the above cases contains almost twice less boundary elements, but leads to the numerical results of practically the same degree of accuracy. The accompanying decrease of the condition number σ by factor of 3 and 1.5, respectively, is related to a successful choice of the size of the triangular elements, close in shape to equilateral, as well as to the decrease of their area with moving away from the centre of the circle.

Proceeding from the triangular grid to the dual mesh of Dirichlet–Voronoy type polygons enables not only the discretization degree to be reduced almost by factor of 1.5, but also the numerical results with the improved accuracy both for displacements and contact pressures to be obtained (Table 3.1, Fig. 3.38).

The most essential effect of application of the dual grid of Dirichlet–Voronoy polygons is a considerable decrease of the mean square error with respect to all the cases of discretization considered, as well as the possibility of a practically exact solution to be obtained in a sufficient vicinity to the punch boundary. Besides, the numerical solution, obtained using the dual grid, gives the values for the boundary-element vertices what is convenient for interpolation.

Then we give an example of application of a postprocessor to the results calculated on the base of the boundary-element method. Consider the contact problem for a square punch $2\alpha \times 2\alpha$, loaded by an eccentric vertical force $P = E_0\alpha^2$, $\varepsilon_x = 0.1\alpha$, $\varepsilon_y = 0.1\alpha$. The punch rests on an elastic nonhomogeneous half-space with deformation module increasing with depth $E = E_0\ (1 + Bz/h)$ (See Sect. Section 1.5.3). The computations have been performed for two dual grids containing 8×8 and 7×7 nodes, provided that $h/\alpha = 1.0$, $B = 1.0$, and the Poisson ratio $\nu = 0.25$. Level

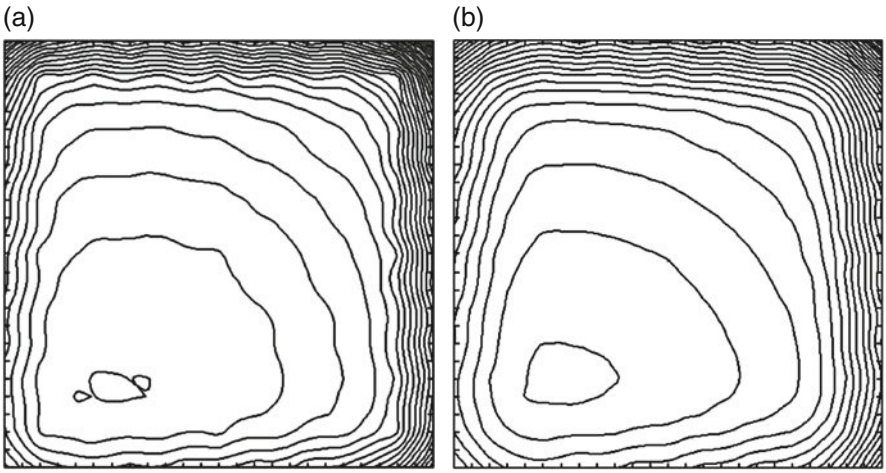

Fig. 3.39 Lines of equal dimensionless contact pressure for an off-centre loaded square punch (**a**) before and (**b**) after the postprocessor application

lines for the contact pressures $\bar{p}(x,y) = p(x,y)/p_{\text{av}}$ ($p_{\text{av}} = P/4\alpha^2$), built using all the 113 values in the nodes of both dual grids, are shown in dimensionless coordinates $\bar{x} = x/\alpha, \bar{y} = y/\alpha$ in Fig. 3.39a.

The boundary-element solutions were also processed by the postprocessing method proposed in Sect. 3.3.1. Since the postprocessing algorithm (or simply postprocessor) depends on the ratio $\gamma_1 : \gamma_2 : \gamma_3$, then, without any loss of generality, suppose $\gamma_2 = 16$ and denote γ_1 and γ_3 as ω_1 and ω_2, respectively. Here ω_1 is the weight of the "old" values and ω_2 is the weight of the "new" values in the grid nodes. To obtain the best result one should choose ω_1 and ω_2 according to the specific features of the problem being solved. For the present example by a series of test calculation the following parameters were chosen: $\omega_1 = 256$, $\omega_2 = 16$. This has led for the whole set of 113 nodes to a new approximate solution whose level lines are shown in Fig. 3.39b. Comparison of the level lines in Fig. 3.39a, b has shown the prostprocessor to result in a noticeable data smoothing. Unfortunately, for the contact problem under consideration the exact solution is unknown what does not enable us to compare the accuracy of the approximate solution before and after the postprocessing. A considerable excess of $\gamma_1 = \omega_1 = 256$ over $\gamma_2 = \omega_2 = 16$ and $\gamma_3 = \omega_3 = 16$ was caused by the requirement of the new smoothed solution not to be very much different from the two initial ones.

In practice, in case the boundary-element method being applied, the contact domain often has complex shape. For the punches of noncanonical shape under spatial loading of a general type it is, as a rule, impossible to predict in detail the solution character. For the correct simulation of the contact pressure field a nonuniform grid is required with condensations in the expected areas of rapid variation of the solution. Simultaneously, the triangulation of complex-shaped flat domains by various methods results, as a rule, in irregular grids with a large number of bound-

ary elements. By the example of the numerical solution of the contact problem for a round punch using regular (uniform and non-uniform) grids it was shown that the application of dual polygonal grids of Dirichlet–Voronoy type results in an essential decrease of dimensionality of the algebraic analogue of the problem and, due to the adaptation to the solution, does not decrease its accuracy. Therefore, for the punches of various cross-section shape at spatial loading of a general type (with possible uplifting of the bottom from the base) the following procedure of obtaining a numerical solution is proposed:

(1) a possibly uniform triangulation of the contact domain is performed using a relatively large number of triangles, close to equilateral (at the a priori known character of contact pressure variation the triangular grid is condensed in the areas of rapid variation of the solution);
(2) switching to a dual polygonal grid of Dirichlet–Voronoy cell type is performed, and on this grid the numerical solution of the contact problem with the pressure values in the nodes of the initial triangular grid;
(3) the found discrete solution is interpolated for the whole contact domain and visualized using isobar lines.

Below we present the results of numerical experiments for irregular grids, having enabled us to check the efficiency of the proposed approach, to evaluate the accuracy of the boundary-element algorithm by comparing the solutions found to the known analytical solutions or those obtained on the base of other known methods, as well as to show the possibilities of the proposed method for finding the contact interaction parameters in practical problems.

A round punch at central and off-centre loading (irregular grids of boundary elements). Figures 3.40–3.43 and Table 3.2 present the numerical solutions of the contact problem for a round punch in case it being pressed into a homogeneous elastic half-space ($\nu = 0.25$) by a central force P. The obtained boundary-element solutions on a sequence of condensed, essentially irregular grids were compared with the known exact solution of this problem [67]. Consider a dimensionality reduction coefficient $K_{TV} = N_T/N_V$ where N_T is the number of equations of the resolving system of the problem on a triangular grid, N_V is the number of equations of the corresponding system on a dual polygonal grid. As one can see, the increase of the contact domain discretization degree results in stable numerical solutions which at linear extrapolation over the value $(N_V)^{-1}$ in the limit at $(N_V)^{-1} \to 0$ (or $(N_V)^{-1} \to \infty$) lead to a result, practically not differing from the exact one (Table 3.2). The application of dual grids in the examples under consideration has enabled the dimensionality of the discrete analogue of the contact problem to be reduced by the factor of $K_{TV} = 1.5$, 1.8, and 1.84, respectively. With the increase of the triangulation density the K_{TV} value is seen to have, though a slight, but a stable trend to increase what is extremely important while solving real problems, requiring always as minute discretization as possible.

It is seen from Figs. 3.40c and 3.41c, and 3.42d where the isolines of dimensionless contact pressures $\bar{p}(x,y) = p(x,y)/p_{aV}$ ($p_{aV} = p/S$ is the average pressure in

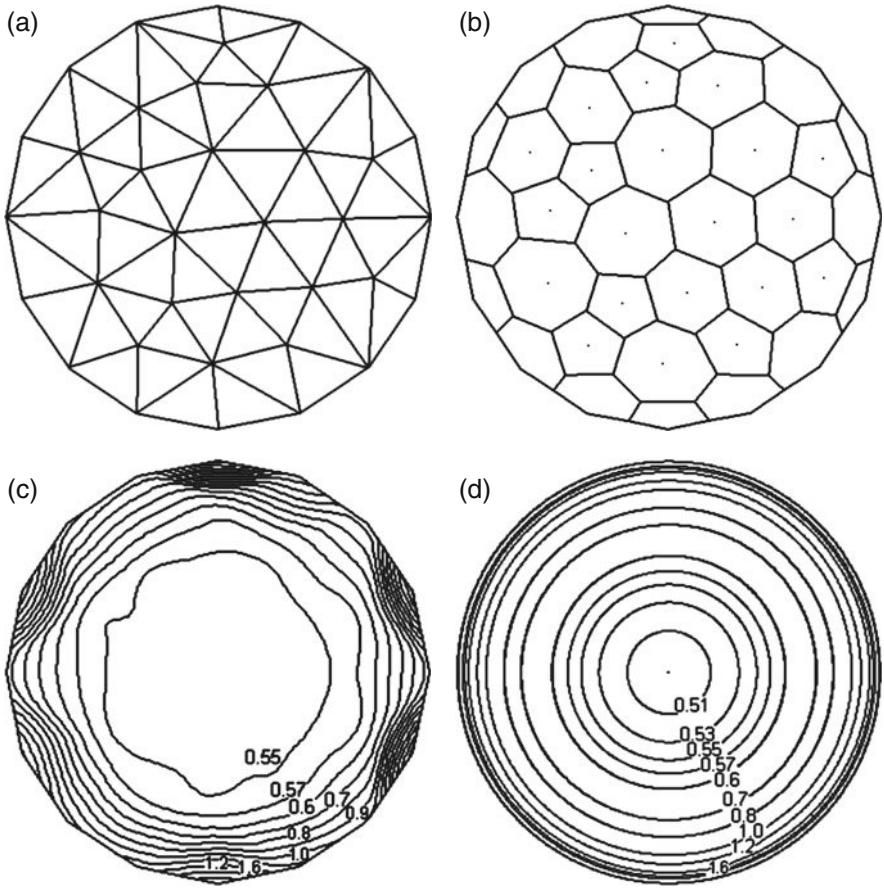

Fig. 3.40 To the solution of the contact problem for a circular punch on an elastic half-space (C37): (**a**, **b**) discretization of the contact surface using dual triangular ($N_T = 56$) and polygonal ($N_V = 37$) grids; (**c**) isolines of dimensionless contact pressure; (**d**) exact solution

the contact domain with the area S) are shown, that with the increase of the number of the triangular grid nodes (or the number of Dirichlet–Voronoy type polygonal boundary elements) the isobars are still less sensitive to the character of irregularity of the boundary-element grid and take the shape of concentric circles. As follows from Fig. 3.40c, d the calculated pressures for a rough grid (ℂ37), though slightly differ from the exact values in the central part of the punch ($r/a \leq 0.6$), still do not enable one to obtain isolines, independent of the boundary element shape. Application of essentially dense grids (ℂ307and ℂ513) results in a contact pressure distribution, practically coinciding with the exact one almost in the whole punch area ($r/a \leq 0.9$) with the except of a narrow zone near its edges ($0.9 \leq r/a \leq 1$). Comparison of the solutions for two dense grids ℂ307 and ℂ513 shows that the solution correction near the punch edge due to a mere increase of the number of the bound-

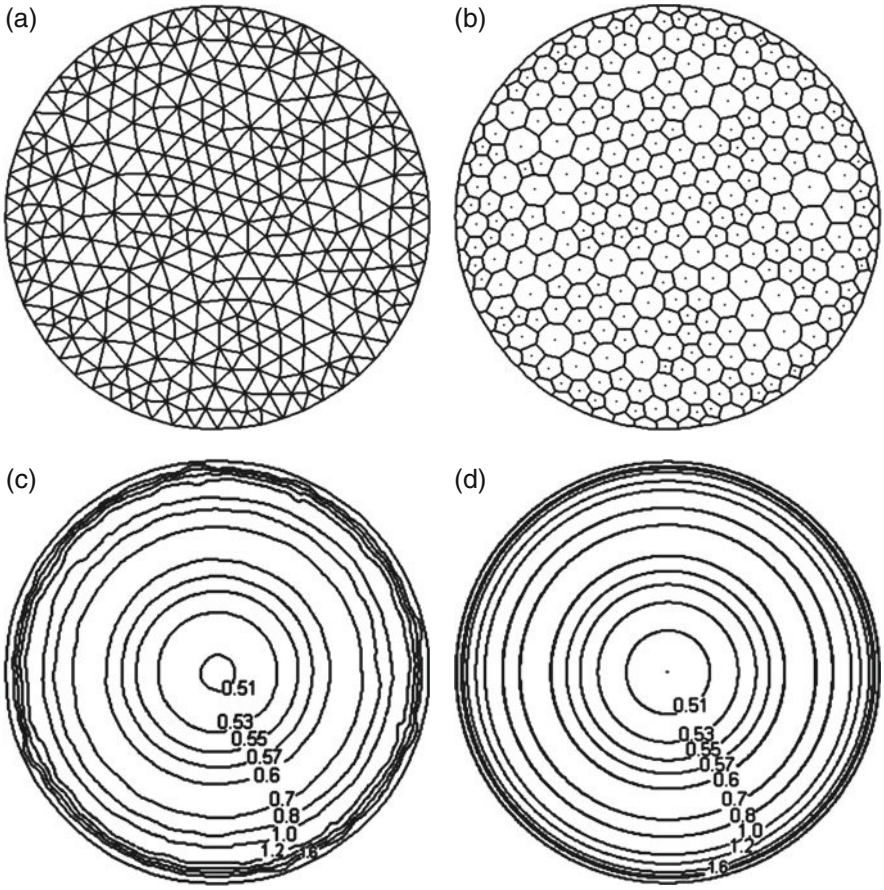

Fig. 3.41 To the solution of the contact problem for a circular punch on an elastic half-space (C307): (**a**, **b**) discretization of the contact surface using dual triangular ($N_T = 552$) and polygonal ($N_V = 307$) grids; (**c**) isolines of dimensionless contact pressure; (**d**) exact solution

ary elements of the irregular (rather uniform, without condensations) grid is rather small. The solution just moves towards the boundary due to the general decrease of the boundary element size (Fig. 3.43). A considerable effect in the increase of the solution accuracy near the boundary condition separation line can be evidently also achieved, similarly to the case of application of non-uniform regular grids (see Sect. Section 3.3), when the contact pressure variation near the punch edge is correctly taken into account.

Application of a detailed discretization of the circular contact domain by a $\mathbb{C}513$ grid has enabled the contact pressure distribution at the asymmetric loading of the punch to be studied (Fig. 3.44). It follows from the results of the calculations performed that the application of a vertical force even with a slight eccentricity results in a rather noticeable violation of the contact pressure field symmetry, characterized

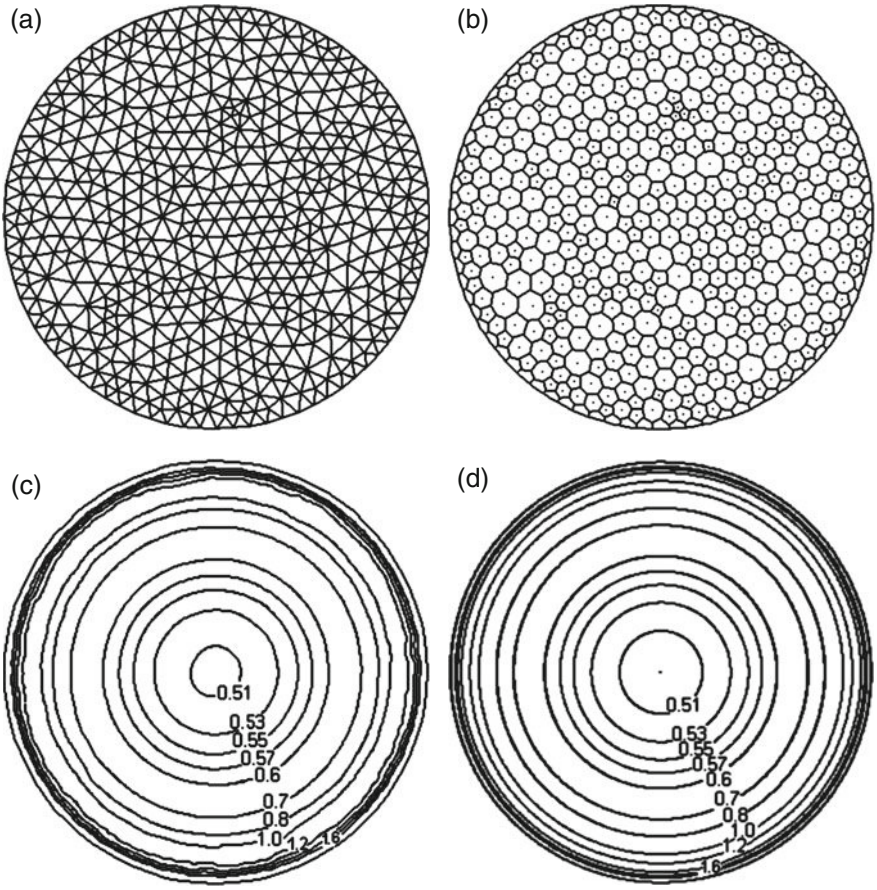

Fig. 3.42 To the solution of the contact problem for a circular punch on an elastic half-space (C513): (**a**, **b**) discretization of the contact surface using dual triangular (N_T= 904) and polygonal (N_V= 513) grids; (**c**): isolines of dimensionless contact pressure; (**d**) exact solution

by an under pressure zone located opposite to the direction of the eccentric displacement of the applied vertical force. The obtained numerical solution of the problem of the asymmetric full contact of a round punch with an elastic homogeneous half-space (Fig. 3.44a) has practically coincided (cannot be distinguished on the plot) with the known exact solution [1, 37, 90, 94]

$$p(x,y) = \frac{1}{2\pi a^2\sqrt{a^2 - r^2}}(P \cdot a + 3 \cdot \frac{x}{a} \cdot M),$$

$$W(x,y) = \delta + \varepsilon_x \cdot \left(\frac{x}{a}\right)$$

where the axial force P and the overturning moment M with respect to the OY axis are related to the punch centre displacement δ under impression and the maximal

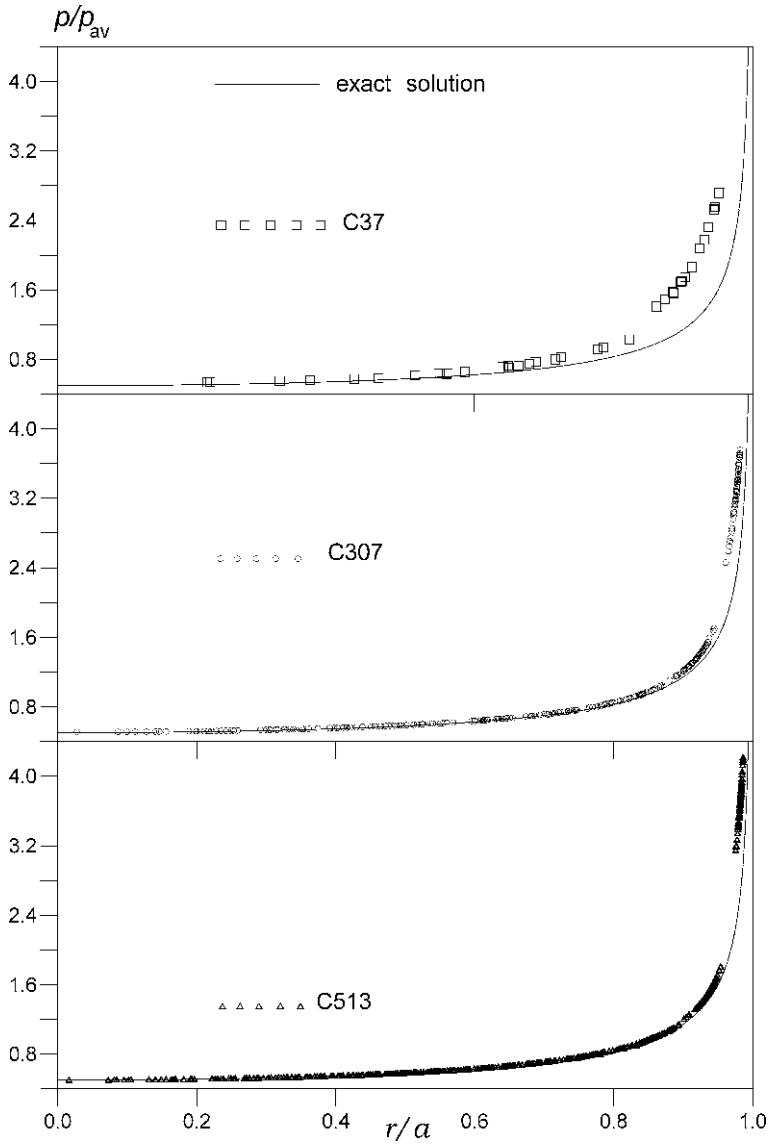

Fig. 3.43 Contact pressures for a circular punch on an elastic half-space, obtained using dual grids of different condensation degree

displacement ε_x at the rotation, respectively, according to the formulae

$$P = \frac{2a^2E}{1-\nu^2}\left(\frac{\delta}{a}\right), M = \frac{4}{3}\cdot\frac{Ea^3}{1-\nu^2}\cdot\left(\frac{\varepsilon_x}{a}\right).$$

The solution of a similar problem, when an elastic half-space with the deformation module increasing with depth $E = E_0(1 + Bz/h)$ is considered as a base, is

Table 3.2 Characteristics of the boundary-element solution of the contact problem for a round punch on irregular grids

Discretization type	Contact domain area S/α^2	Contact pressures p_{min}/p_{max}	Slopes $\frac{\psi_x \cdot 10^4}{\psi_y \cdot 10^4}$	Relative settlement W/α	Condition number σ	Mean square deviation
$N_V = 37$ $N_T = 56$, $K_{TV} = 1.514$	3.12869	$\frac{0.5381}{2.7163}$	$\frac{-5.695}{-4.944}$	0.49003	93.61	$2.2191\times10^{-}$
$N_V = 307$ $N_T = 552$, $K_{TV} = 1.798$	3.12869	$\frac{0.5084}{3.7560}$	$\frac{-0.653}{-1.098}$	0.47334	70.76	$1.8368\times10^{-}$
$N_V = 513$ $N_T = 944$, $K_{TV} = 1.840$	3.13761	$\frac{0.5065}{4.2218}$	$\frac{-0.0321}{-0.6978}$	0.47216	115.3	$1.7783\times10^{-}$
Extrapolation	3.14242	$\frac{0.5036}{4.9165}$	$\frac{-0.0004}{-0.3551}$	0.47041	–	$1.6911\times10^{-}$
Exact solution	3.14159	$\frac{0.5}{\infty}$	$\frac{0}{0}$	0.46875	–	0

shown in Fig. 3.44b (see Sect. Section 1.5). The considered example shows that the proposed boundary-element method of numerical integration enables to take into account simultaneously, within a unique approach, complex spatial loading of rigid punches and nonclassical properties of elastic bases.

Negative (tensile) contact stress is not taken up by an elastically compressed medium, and at the area of their formation within the contact area an uplifting zone (gap) is formed. Therefore, the developed algorithm takes into account unilateral constraints. The specific feature of the calculation in this case consists in the fact that in the course of the punch loading process the calculation scheme can vary (a part of the punch surface will not participate in the contact interaction). Thus modified formulation of the problem qualitatively changes the contact interaction pattern since the calculation scheme becomes a function of load. Since the uplifting zone is not known a priori, the solution is sought by iteration, by means of correction and switching unilateral constraints. For the elements in the contact area it is necessary that the condition $p_i \geq 0$, $W_i^{(n)} = 0$ be fulfilled, and the elements on which tensile stress arises (p_i<0), are included into the uplifting zone only in case the condition $W_i^{(n)} \geq 0$ being valid, where $W_i^{(n)} = W_i^+ - W_i^-$ is the gap opening value, equal to the difference of the base and the punch displacements. The process of more exact specification of the contact domain is performed by iteration, the equilibrium conditions being fulfilled, until in the subsequent approximation all the included forces p_i are positive and the calculation results coincide with initial prerequisites. In the problems, having been solved using this algorithm, the number of approximations seldom exceeded 7 cycles. Note that our calculations and studies of contact interaction with the account of unilateral constraints were based on

the general properties of the systems containing unilateral constraints. For this case convergence of iterative processes of finding the functioning system is shown e.g. in the book by Reznikov [110], and its uniqueness – in the studies of Rabinovich [107, 108]. It is noted in the latter of the above references that by a limiting transition the theorem of uniqueness is extended to the systems with infinitely large number of unilateral constraints, including structures, resting on an elastic continuum with unilateral consraints.

Figure 3.44c, d demonstrate the abilities of the developed method for solving the contact problem of an essentially inclined round punch with areas of uplifting from the elastic homogeneous half-space on its bottom. We used an irregular boundary-element grid $\mathbb{C}513$ with a sufficient degree of condensation for calculations and for interpolation of the contact pressures at off-centre punch loading. It is seen from the calculation data that the increase of eccentricity of the external vertical force appli-

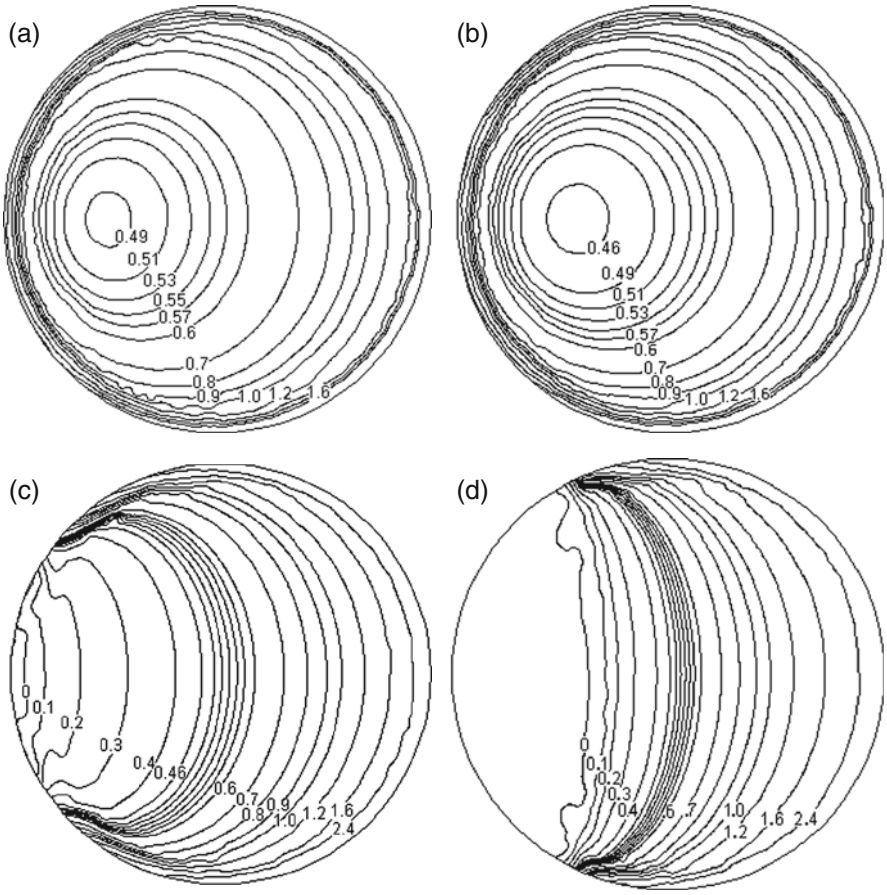

Fig. 3.44 Contact pressure isolines at off-centre loading of a round punch (C513): (**a**, **b**) $e_x/\grave{a}$= 0.15; (**c**) $e_x/\grave{a}$= 0.35; (**d**) e_x/a= 0.5; (**a**, **c**, **d**) homogeneous elastic half-space; (**b**) elastic half-space with the deformation modulus, linearly increasing with depth ($B = 1.0$, $\mu = h/a = 1.0$)

cation point results in an appearance and subsequent broadening of uplifting areas and an increase of the number of iteration process cycles for their determination. Evidently, the numerical solution of the problem of an essentially inclined punch will be the more accurate, the higher is the degree and the better is the quality of discretization of the contact domain into boundary elements.

Note that the solution of the contact problem at the asymmetric loading of a round punch when the contact domain is a part of a circle, has been considered earlier in [21, 111, 112, 125]. Rvachev with collaborators [21, 111, 112] have carried out a study to determine the contact domain of a round punch with a half-space depending on the eccentricity of the force application using the structural method. They have found the problem solution in the form of a linear combination of the complete system of Chebyshev polynomials, and for the calculations they had to make the type of the function, determining the line L_0 of the punch uplifting from the base, completely specified. This line was assumed to be a two-parameter parabola. The results we have obtained without any assumptions on the contact domain shape, show (Fig. 3.44c, d) that the L_0 line is not a parabola, its configuration being to a great extent more complicated with approaching the angular points of the L_0 line interception with the punch contour. In the vicinity of these points a complicated character of the stressed state is observed, when the pressure varies from zero to infinity depending on the direction of approach to these points.

A rigid round punch with partial uplifting of its bottom from an elastic homogeneous half-space due to asymmetrical impression was also considered in [125]. To determine the contact domain, to calculate contact stress and parameters of the punch displacement as a rigid solid, a numerical method is applied, much similar to the boundary-element method. The circular contact domain is meshed into 316 squares, entirely inside the circle, which are identified with circular boundary elements with the same centres and equivalent areas. For each such circular element a constant pressure is assumed. Displacements of the homogeneous linearly stressed half-space surface in the centres of the circular boundary elements due to a uniform pressure over the circular domain are found from explicit formulae using a combination of full elliptic integrals of the first and second order. Besides, the proposed algorithm [125] takes essential advantage of the symmetrical shape of the punch. The actual contact domain is determined by iteration using a simple switching of unilateral constraints. The zero-pressure line L_0, bounding the contact domain, is obtained by square interpolation of discrete values from two points in the directions, parallel to the diameter, passing through the circle centre and the point of application of the off-centre vertical force. For different eccentricities of the external force after such extrapolation the uplifting lines L_0 are completely determined in the course of the numerical solution of the problem and, contrary to the structural method [112], without any additional assumptions. Essentially, one should confess that the method of solving the problem of an essentially inclined round punch, proposed in [125], has set the foundation of direct numerical solving of spatial contact problems for rigid flat punches in partial contact with elastic bases. Nevertheless, an essential limitation for this approach is the application of the exact solution of the problem (expressed via Bessel functions) of a load, uniformly distributed over elements

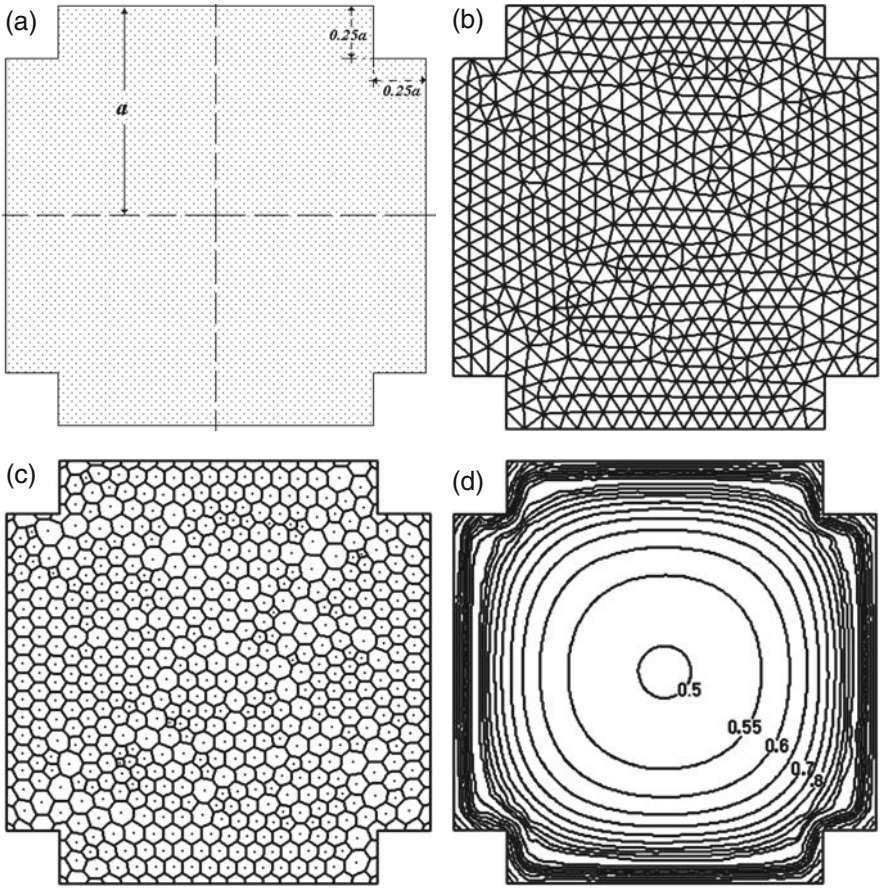

Fig. 3.45 Square punch with angular cutoffs at central loading: (**a**) contact domain; (**b**) irregular triangular grid ($N_T = 1118$); (**c**) dual polygonal grid ($N_V = 608$); (**d**) dimensionless contact pressure isolines

of circular shape, acting on an elastic homogeneous half-space. Such approach is related to the contact domain discretization performed using a square grid, whose cells are to be put into correspondence to circles of equivalent area. However, the most convenient and widely used method of discretization of flat complex-shaped domains is non-uniform triangulation with a required condensation in the supposed areas of the solution variation with considerable gradients. Therefore, it is rather evident that the boundary-element approach using adaptive irregular grids, proposed here, is well applicable for the class of spatial contact problems under consideration. As noted before, such an approach is also indifferent with respect to the contact model of the elastic base under consideration. If for the base contact model, the influence function can be integrated analytically over the circular domain, then the application of the boundary-element method becomes even more efficient. Indeed, since the calculation grids of Dirichlet–Voronoy type consist mostly of the boundary

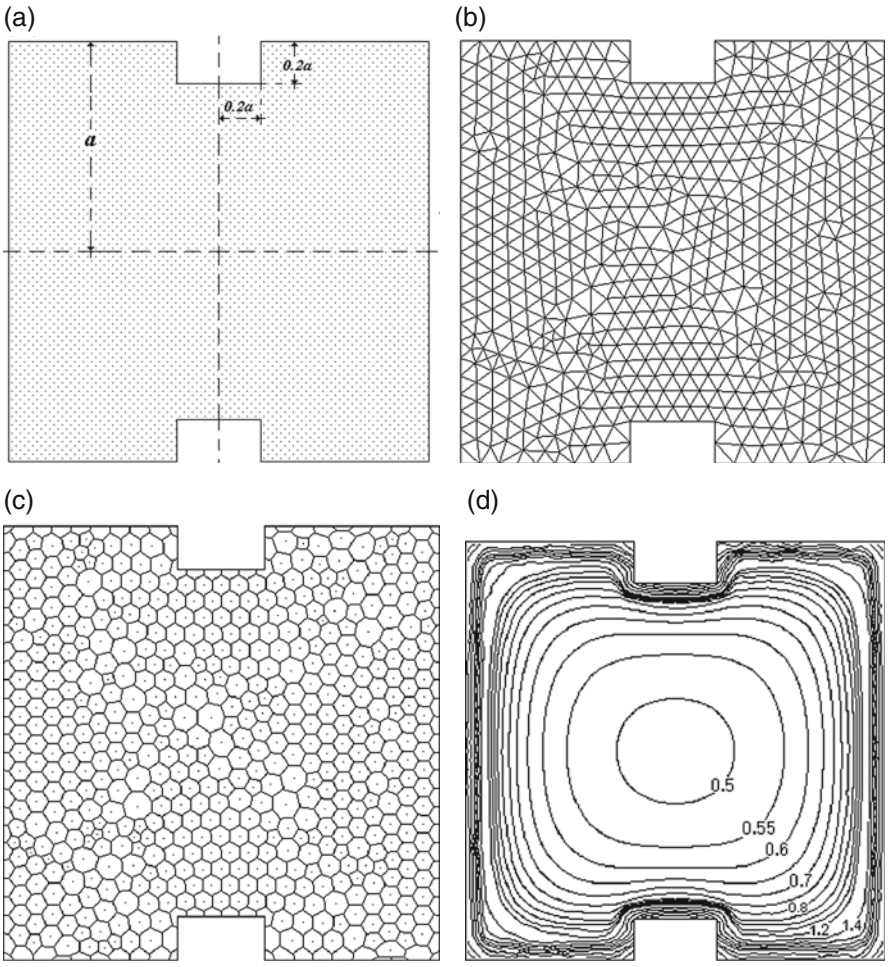

Fig. 3.46 Square punch with side cutoffs at central loading: (**a**) contact domain; (**b**) irregular triangular grid ($N_T = 1156$); (**c**) dual polygonal grid ($N_V = 630$); (**d**) dimensionless contact pressure isolines

elements, rather close in shape to regular polygons with the number of angles from 6 to 8 (Figs. 3.40b–3.43b, 3.45c–3.56c), the replacement of the latter by circles of equivalent area will result in a more accurate approximation of the contact domain after the corresponding aggregation of the elementary circles with less error than in the case of replacement of traditional square elements [46, 125].

Thus, the performed comparison of the solutions of the problem of an essentially inclined circular punch has shown that among the known approaches the developed boundary-element method, including the application of dual, in the general case irregular grids, possesses high university and universality, being revealed in (a) con-

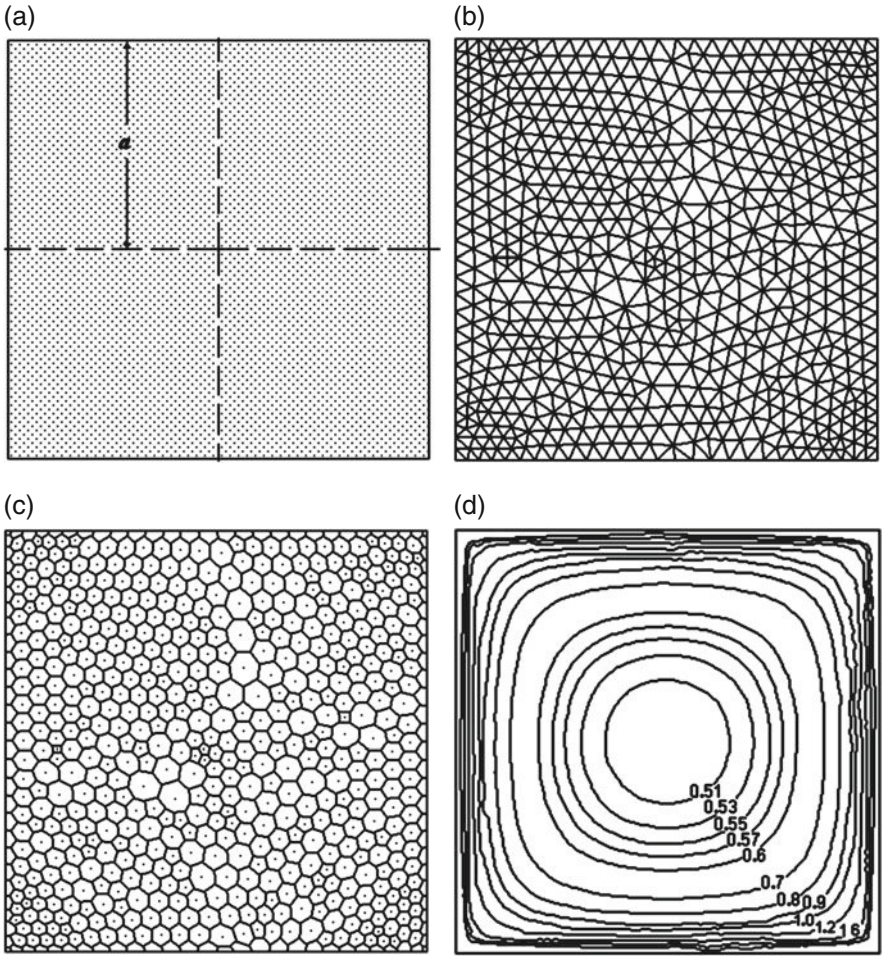

Fig. 3.47 Square punch at central loading: (**a**) contact domain; (**b**) irregular triangular grid ($N_T = 1202$); (**c**) dual polygonal grid ($N_V = 656$); (**d**) dimensionless contact pressure isolines

sideration of contact domains of practically any complexity and their discretization by any of the known methods, (b) interpolation of the numerical solution in automatic mode with simultaneous determination of the a priori unknown shape of the contact domain, (c) application of a broad spectrum of spatial contact models specifying the mechanical properties of elastic bases by means of the known influence functions.

Below we consider the examples of solving spatial contact problems for the punches of complex (noncanonical) shape, being first of all directly related to the design of shallow foundation structures, having no exact solutions even in the case of the classical model of a homogeneous elastic half-space being used as a base.

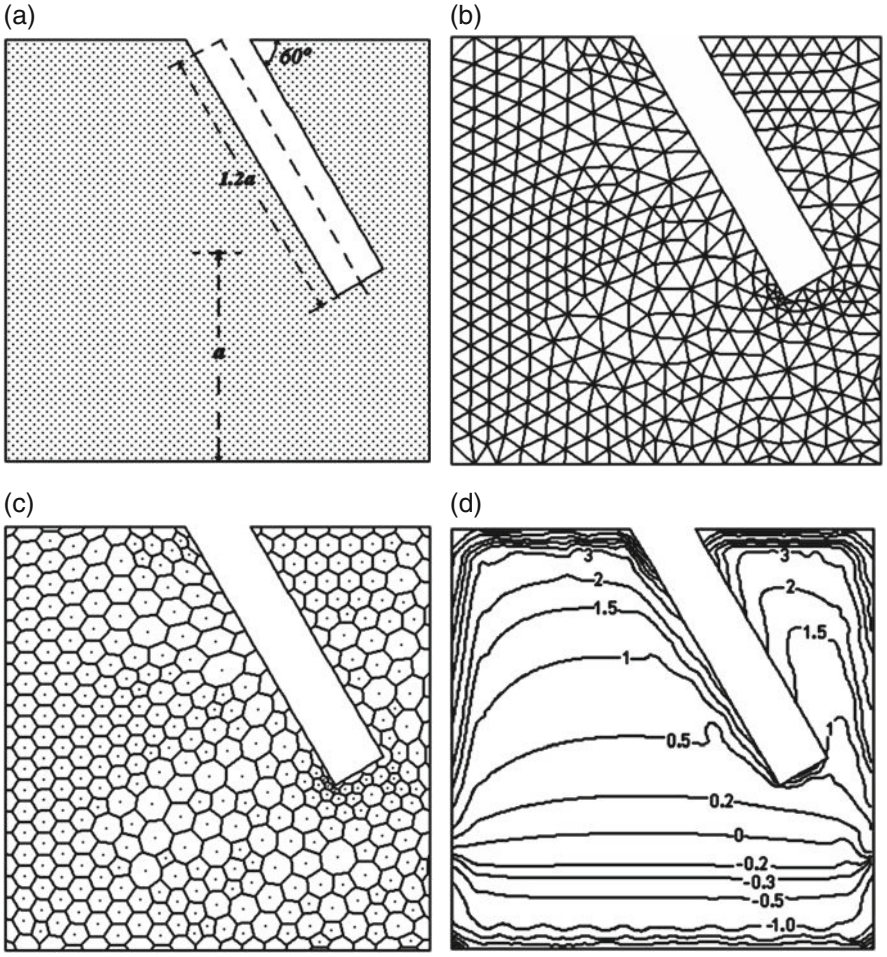

Fig. 3.48 Square punch with an inclined asymmetric cutoff at central loading: (**a**) contact domain; (**b**) irregular triangular grid ($N_{\mathrm{T}} = 724$); (**c**) dual polygonal grid ($N_{\mathrm{V}} = 415$); (**d**) dimensionless contact pressure isolines

Punches of polygonal cross-section. Figures 3.45 and 3.46 show the dual boundary-element grids and the results of solving spatial contact problems for square punches with symmetrical cut-outs, the depth of the latter being 1/8 of the square side, loaded by a central force. For the punch with angular cut-outs N_T= 1118, N_V= 608, K_{TV}= 1.839, for the one with lateral cut-outs N_T= 1156, N_V= 630, K_{TV}= 1.835. It is seen from the equal contact pressure lines plotted in Figs. 3.45d and 3.46d that in both cases the stressed states under the punches have characteristic features, being revealed only near the punch boundaries. For the central part of the punches, due to the small values of the cut-out depth parameter $\alpha = D/a$, the contact pressure isolines have the shape of regular ovals, practically the same as the

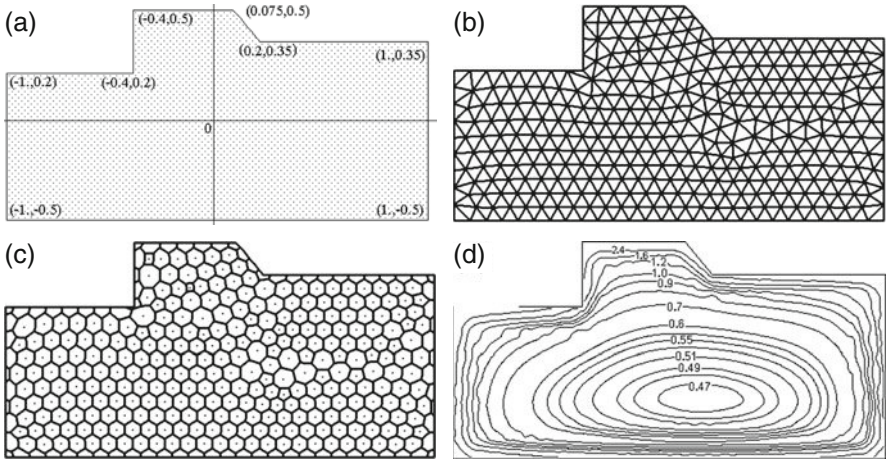

Fig. 3.49 Polygonal punch (foundation under a locomobile): (**a**) contact domain; (**b**) irregular triangular grid ($N_T = 659$); (**c**) dual polygonal grid ($N_V = 370$); (**d**) dimensionless contact pressure isolines

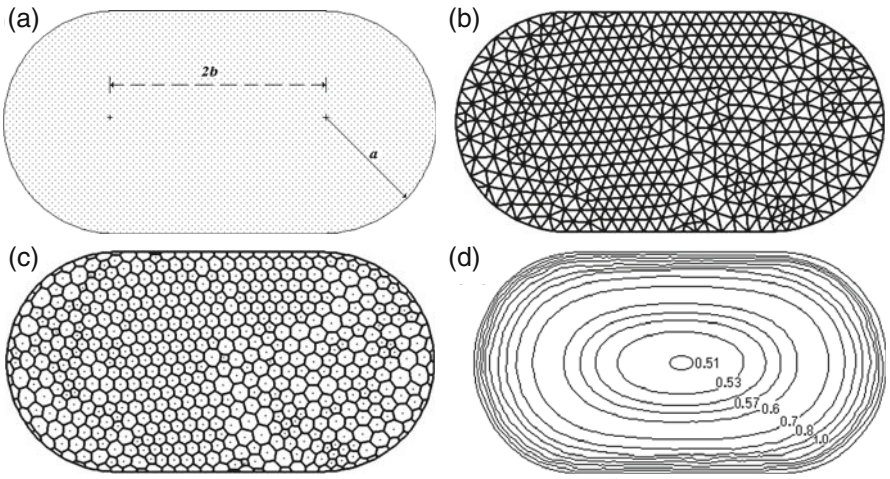

Fig. 3.50 Strip punch with semicircular face ends: (**a**) contact domain; (**b**) irregular triangular grid ($N_T = 1046$); (**c**) dual polygonal grid ($N_V = 567$); (**d**) dimensionless contact pressure isolines

corresponding isobars for the square punch without cut-outs (Fig. 3.47). Note that the punches, considered in Figs. 3.45 and 3.46, are the models of variable-width foundations. Application of such foundations is economically sound since the soil in the cut-out area participates in the foundation functioning and at equal external load they can be used instead of rectangular (constant-width) foundations with the same dimensions [130].

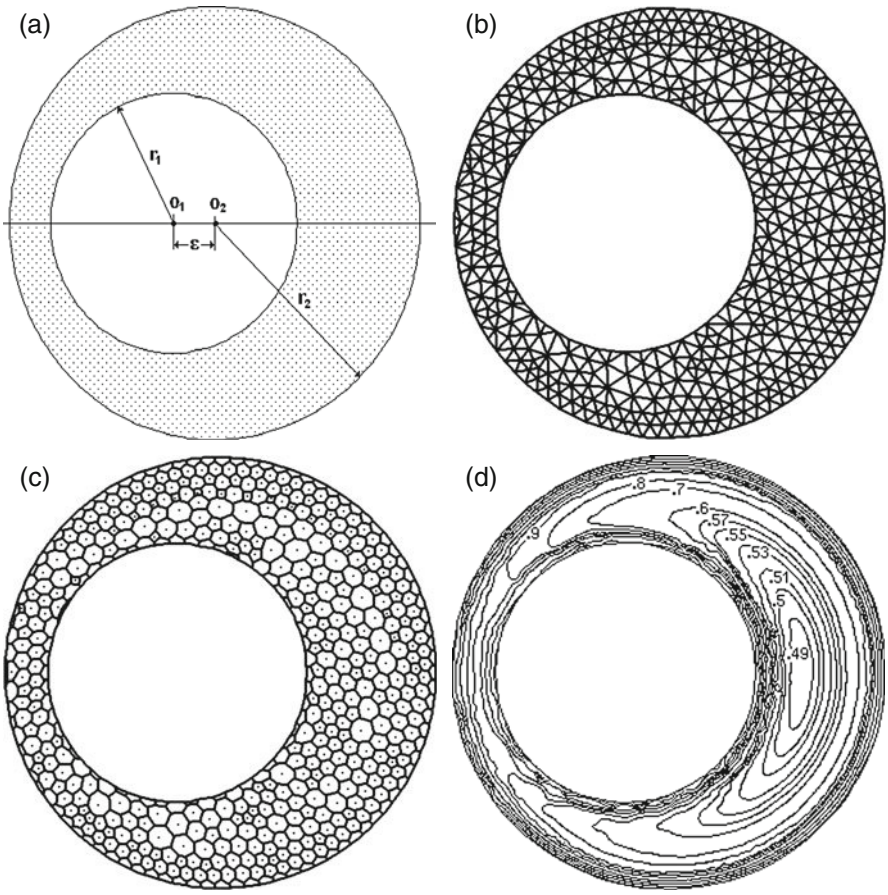

Fig. 3.51 Eccentric ring-shaped punch: (**a**) contact domain; (**b**) irregular triangular grid (N_T = 929); (**c**) dual polygonal grid (N_V= 539); (**d**) dimensionless contact pressure isolines

Along with the punches with symmetrical cut-outs we have also considered (Fig. 3.48a) a square punch with a "deep", asymmetrical (inclined at 60° to the side) cut-out (a rigid foundation plate with a cut-out for the equipment). The triangulation of the domain contained N_T= 724 elements (Fig. 3.48b). Proceeding to a dual polygonal grid, we have reduced the number of the boundary elements to N_V= 415 what corresponds to the value K_{TV}= 1.745 (Fig. 3.48c). The equal contact pressure lines, built from the results of the numerical solution of the problem, indicate that due to a strong asymmetry at the punch loading in the centre of the external square contour, a complex stressed state with the presence of negative (tensile) stress is formed. This means that for the final solution of the contact problem one should consider in detail the iteration process of determination of the contact domain where the contact pressures will be negative. In practice, variation of

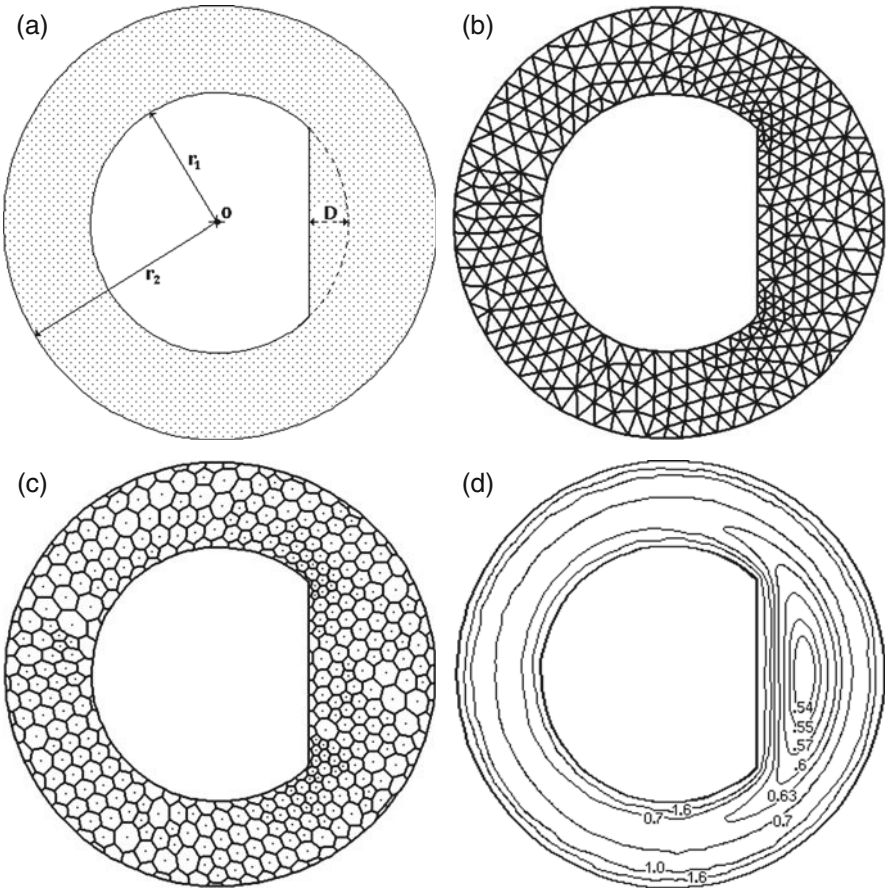

Fig. 3.52 Ring-shaped punch with a cutoff in the inner circle: (**a**) contact domain; (**b**) irregular triangular grid ($N_T = 710$); (**c**) dual polygonal grid ($N_V = 419$); (**d**) dimensionless contact pressure isolines

the shape and load parameters in order to accept a design solution, excluding the foundation functioning with the bottom uplifting from the base, is usually applied [102, 113].

A foundation for a locomobile is considered as a typical example of the solution of a spatial contact problem for a punch of a rather complex polygonal cross-section shape [135]. The geometrical dimensions of the punch loaded by a vertical force with the application point in the coordinate origin are shown in Fig. 3.49a. A triangular (N_T= 659) and a polygonal (N_V= 370) grids in duality (Figs. 3.49b, c) were used for the numerical solution of the contact problem. The parameter of reduction of dimensionality of the discrete problem in this example K_{TV}= 1.781. Interpolation of the numerical solution, found in the triangular grid nodes, enabled a detailed pattern of the stressed state under the punch to be obtained using the lines of equal

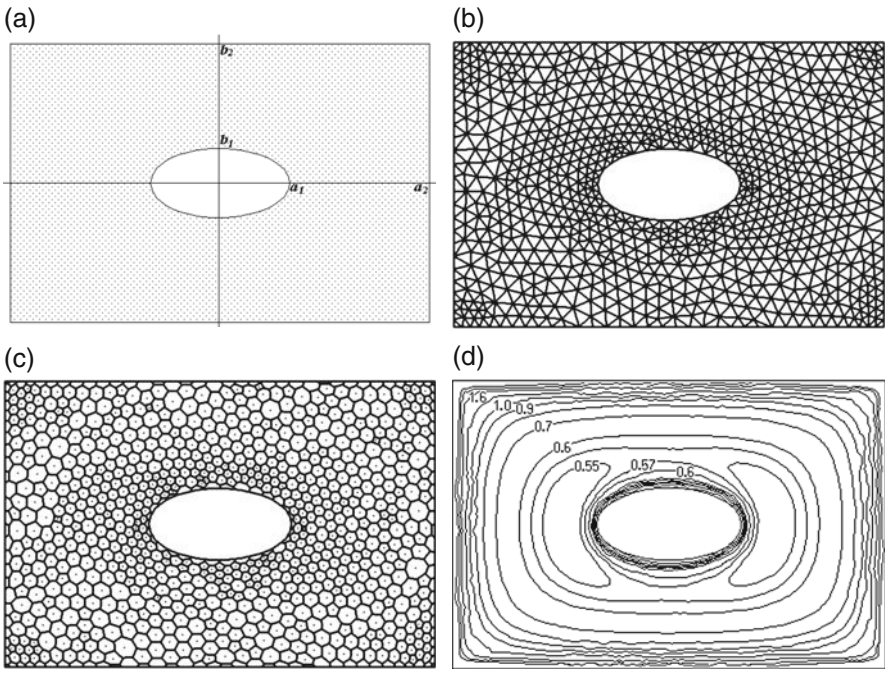

Fig. 3.53 Rectangular punch with an elliptical cutoff: (**a**) contact domain; (**b**) irregular triangular grid ($N_T = 1688$); (**c**) dual polygonal grid ($N_V = 919$); (**d**) dimensionless contact pressure isolines

values of dimensionless contact pressures $\bar{p}\,(x,y)$ (Fig. 3.49d). Note that the spatial contact problems for polygonal punches on a homogeneous half-space, shown in Figs. 3.45, 3.46 and 3.49, have been studied earlier using electrical analogy method [30, 31]. The comparison of the experimental isobars and our theoretical solutions has shown a good not only qualitative, but also quantitative agreement of the results.

A strip-shaped punch with half-round abutting ends. The shape and dimensions of the punch are presented in Fig. 3.50. The punch under consideration corresponds e.g. to a bottom in caissons with rounded walls constructed as deep foundations for bridge piers [140]. The dual grids, discretizing the contact domain, are shown in Figs. 3.50b, c and contain $N_T = 1046$ and $N_V = 567$ elements, respectively ($K_{TV} = 1.845$). Figure 3.50d shows the plots of isolines of dimensionless reactive pressures, corresponding to central impression of the punch ($a = 3.0$, $b = 2.85$) into an elastic homogeneous half-space. Here we also note that the results of calculation, performed at the parameter values $a = 0.2$, $b = 0.4$ with a high degree of accuracy (the error does not exceed 1.3%) agree with the solution obtained earlier by structural R-function method [112].

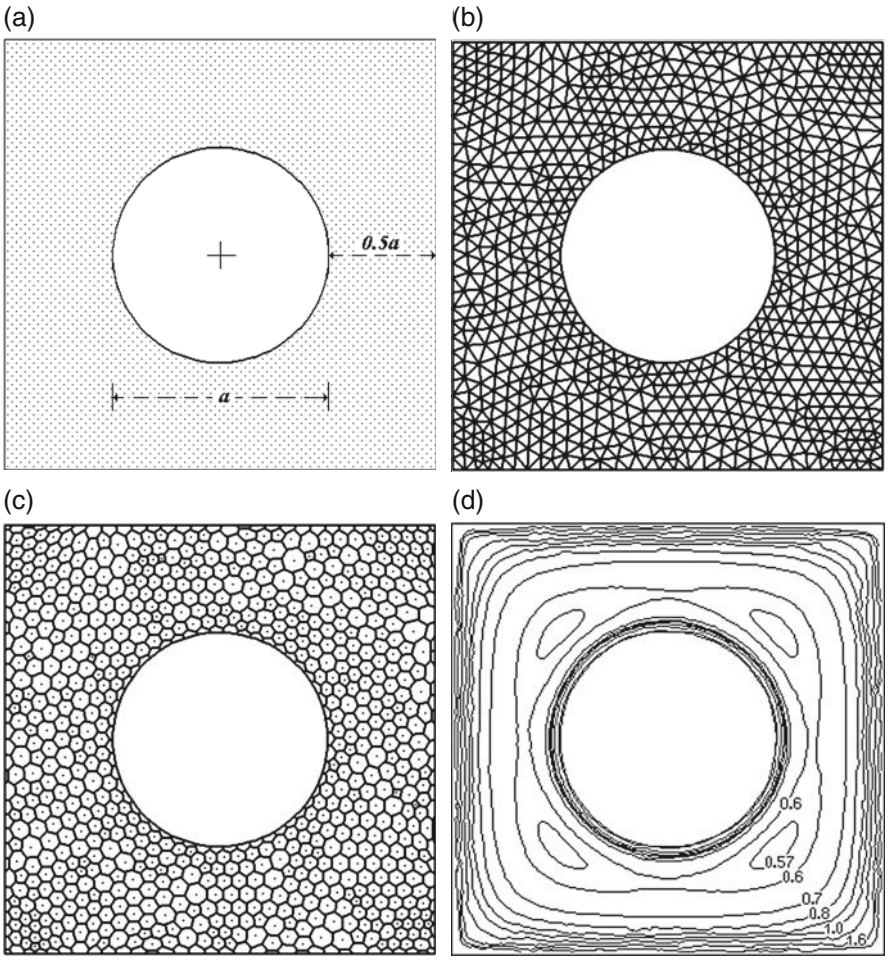

Fig. 3.54 A square punch with a circular cutoff: (**a**) contact domain, (**b**) triangular irregular grid (N_T= 1521), (**c**) dual polygonal grid (N_V=848), (**d**) dimensionless contact pressure isolines

Punches with multiply connected contact domain. Figures 3.51 and 3.52 illustrate the solution of the spatial contact problem for centrally loaded asymmetrical ring-shaped punches. Such punches are the models for foundations under tower-type structures to be erected on non-uniformly compressed bases or on uniformly compressed ones subject to momental loads in a given direction [7, 11, 13–15]. For both punches r_1/r_2= 0.6 is assumed.

For the eccentric ring-shaped punch the value of eccentricity ε_0, by which the internal circle is displaced with respect to the centre, is taken as $0.2r_2$ (Fig. 3.51a). The initial triangular grid contains N_T= 929 elements (Fig. 3.51b). The dual polygonal grid is composed of N_V= 539 elements (Fig. 3.51c), K_{TV}=

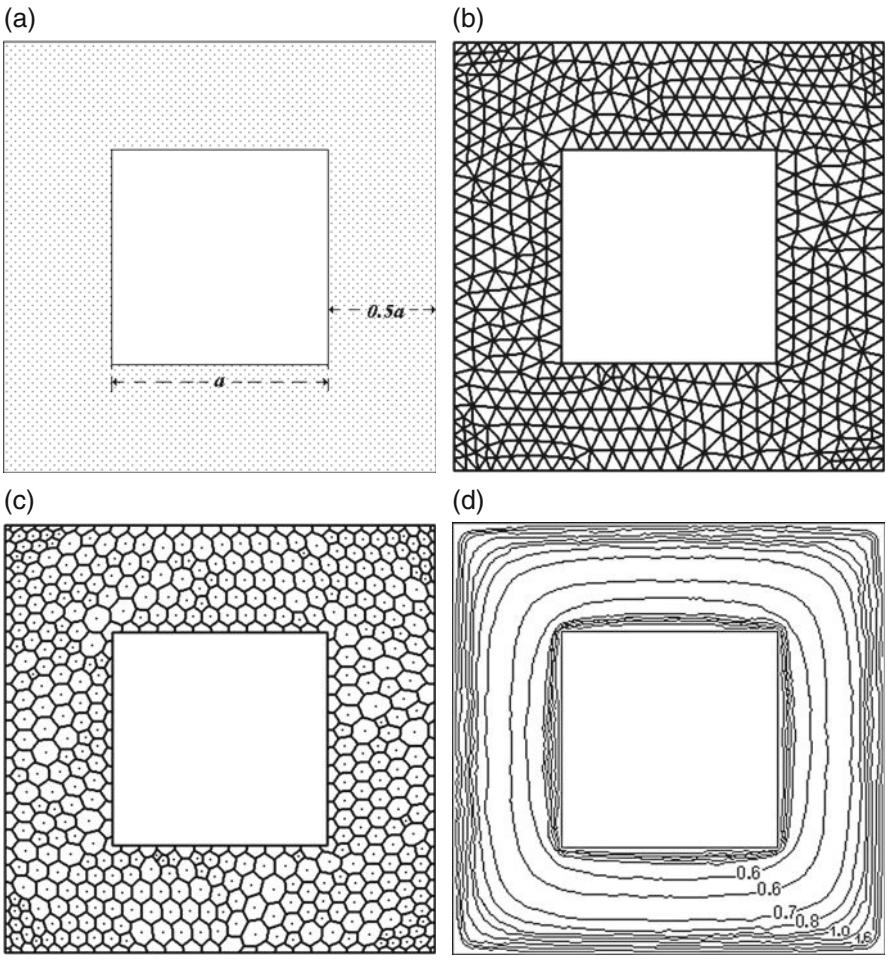

Fig. 3.55 Square punch with a square cutoff: (**a**) contact domain; (**b**) irregular triangular grid ($N_T = 1448$); (**c**) dual polygonal grid ($N_V = 814$); (**d**) dimensionless contact pressure isolines

1.724. The ring-shaped punch, shown in Fig. 3.52a, has the value of the parameter D, characterizing the internal circle cut-off, equal to $0.19r_2$. The triangular grid contains $N_T = 710$ elements and has condensed areas in the vicinity of the angular points on the internal contour of the punch (Fig. 3.52b). By proceeding to the dual polygonal grid we managed to reduce the discrete problem dimensionality with respect to $N_V = 419$ unknown contact pressures by factor of $K_{TV} = 1.695$ (Fig. 3.52c).

Plotted from the calculation results equal contact pressure lines, reproducing the features of the stressed state under the asymmetric ring-shaped punches at ver-

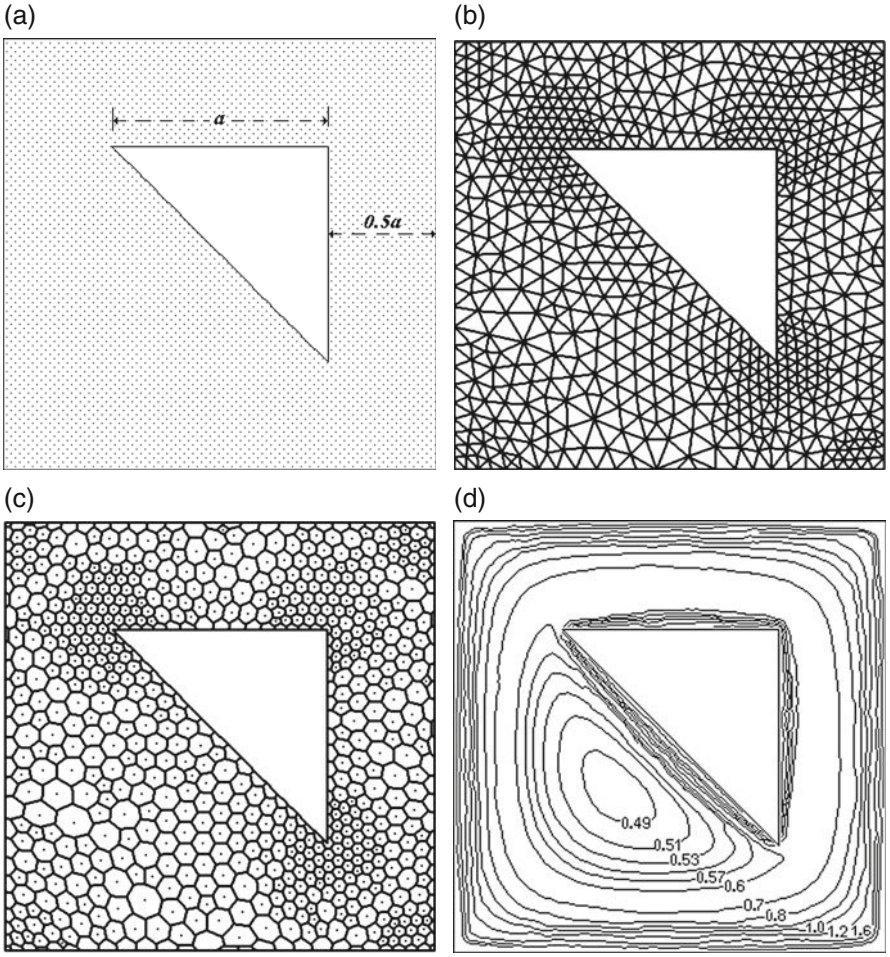

Fig. 3.56 Square punch with a triangular cutoff: (**a**) contact domain; (**b**) irregular triangular grid ($N_T = 1332$); (**c**) dual polygonal grid ($N_V = 745$); (**d**) dimensionless contact pressure isolines

tical loading in the centre of the external circle, are shown in Figs. 3.51d and 3.52d. It should be noted that while for the symmetrical ring-shaped punch different forms of analytical and approximate solutions are well known [20, 29, 38–40, 47, 56, 57, 96, 112, 141], no spatial contact problem solution for the asymmetrical ring-shaped punches considered here has been proposed before by any of the methods.

Consider the solution of a practically important spatial problem for the multiply connected contact domain when the punch has a rectangular shape with an elliptical cut-out (Fig. 3.53a). Due to such shape of the bottom, the foundation can be made with smaller support point. The presence of the unsupported elliptical area in the

central part of the foundation results in the fact that the compressive stress from the central load grows faster than the tensile stress due to moments [88]. Besides, the choice of the elliptical shape for the internal contour leads to the minimal decrease of the moment of inertia of the foundation bottom what enables it to bear higher bending moments than at any other cut-out shape. Note that the contact domain under consideration in this example (and its particular case of a square with a circular cut-out, Fig. 3.54) also arises at the interaction of rectangular pile rafts (for inclined or vertical cylindrical piles) with the soil surface [12]. Figures 3.53b, c show a triangular (N_T= 1688) and a polygonal (N_V= 919) grids (K_{TV}= 1.857) in duality which were used for the numerical solution of the contact problem for a centrally loaded rectangular punch (a_2= 1.5, b_2= 1.0) with an elliptical cut-out (a_1= 0.5, b_1= 0.25). The obtained solution along the long axis of the punch appeared graphically indistinguishable from the solution, obtained by structural method (*R*-function method) in [112]. The full pattern of the stressed state under the punch is shown in Fig. 3.53d where the equal contact pressure lines are built based on interpolation (using the initial triangular grid) of the boundary-element solution found on a dual polygonal grid.

Solutions for contact problems at multiply connected contact domain of polygonal shape with rectangular and triangular internal cut-outs in a square punch are considered in Figs. 3.55 and 3.56, respectively, as examples to demonstrate the proposed boundary-element algorithm, including the dual grid application. The contact pressure isolines built using the results of the numerical solution on irregular dual grids (Figs. 3.55d and 3.56d) as well as the solutions of the above considered contact problems for the punches with cut-outs, show wide abilities of the proposed approach in the case of different doubly connected contact domains bounded by piecewise smooth curves.

Quantitative characteristics of the developed method based on the results of its application in 28 contact problems for complex-shaped punches with different degree of non-uniform discretization of the contact domain are given in Fig. 3.57. Figure 3.57a shows the dimensionality reduction coefficient $K_{TV}= N_T/N_V$ and Figure 3.57b illustrates computation time for dual grid calculations. It is seen that in problems important for practical applications (with the number of the boundary elements above 250) the proposed method enables one to reduce essentially the dimensionality of the algebraic analogue of the contact problem (on the average by factor of 1.8) as well as to decrease the computation time (which is varied as a square of the system dimensionality) in comparison with the case only triangular grids being applied.

Thus, the performed comparison of the numerical results with both analytical solutions and those obtained by other approximate methods enables the boundary-element method to be successfully applied for solving engineering problems of calculation of rigid foundation structures from the base deformation. The boundary-element method is made much more efficient due to the application of not one grid, but two interlinked (dual) grids for the solution finding domain, which are used both at the preliminary stage of discretization and directly in the course of compu-

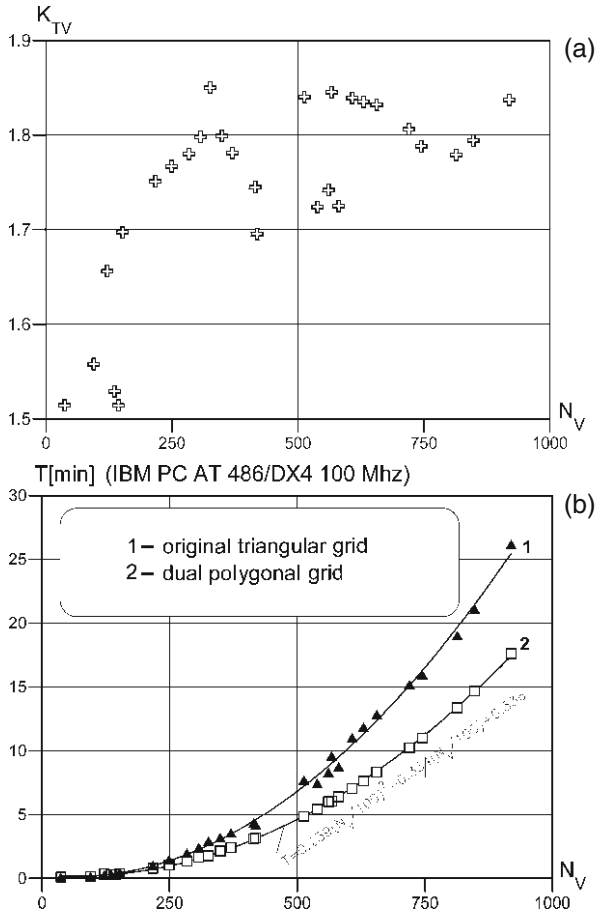

Fig. 3.57 Efficiency characteristics in case irregular dual boundary-element grids being used: (**a**) dimensionality reduction coefficient; (**b**) computation time

tations as well as for subsequent processing of approximate solutions. In particular, it is shown that the problems of numerical modeling of contact interaction of rigid punches with nonclassical elastic bases can be without particular difficulties solved at any shape of bottom. The proposed boundary-element method is applicable with equal convenience to simply and multiply connected contact domains. The accuracy of the numerical results, by far sufficient for practical purposes, is obtained at relatively small dimensionalities of the algebraic analogue of boundary integral equations and piecewise constant approximation of the contact pressure field.

3.5.2 Contact Problems with the Account of the Deepening Factor for Axisymmetric Punches, Interacting with an Elastic Half-Space

Spatial contact problems for rigid inclusions and deepened punches in an elastic medium have been the subject of numerous studies causes by the necessity of investigation of stress concentration issues in a spatial formulation and their significance for the development of mechanics of composite materials [6, 105] as well as for geotechnical problems regarding the studies of contact interaction of the foundation structures with soil [24]. By now the problems of such type have been studied most extensively for the case the elastic medium being infinite space. Approaches have been developed for studying axisymmetric stress-strained state of the elastic medium near the cavities or rigid inclusions, as a rule, of spherical or ellipsoidal shape, when at the infinity the stress components are arbitrary linear functions of the Cartesian coordinates [103, 104]. In the case of semi-infinite domains (of elastic half-space or elastic layer type), solution of this class of problems becomes much more complicated due to the necessity to satisfy the boundary conditions of the absence of stress on a free surface or the conditions of continuity of stress and displacements on the surfaces of the layer contact. Approaches with the application of finite-difference and finite-element methods appear hardly efficient in this case.

Below we consider the examples of application of numerical-and-analytical boundary-element method for solving spatial contact problems for an absolutely rigid inclusion and deepened punches in an elastic isotropic linearly stressed half-space (with stress-free boundary surface) at their force loading along the symmetry axis. As an auxiliary state consider an elastic half-space with a cavity whose boundary is totally identical to the contact surface of the rigid inclusion or the deepened punch. The fundamental singular Mindlin's solution for an elastic half-space is used. The structure nonlinearity due to the introduction of unilateral constraints on the contact between the rigid inclusion and the elastic half-space, not being under tension and resulting in the violation of the full contact conditions, is taken into account. Six equilibrium conditions are included into the integral equation system of the spatial contact problem, which are required to determine the parameters of the displacement of the inclusion of an arbitrary shape as a rigid solid (See Sect. Section 2.1).

For numerical solution of these problems direct boundary-element method is applied (in the assumption of a piecewise constant approximation of the contact stress function), resulting in linear algebraic equation systems with constraints in the form of inequalities $p^{(n)} \geq 0$. Discretization of the rigid inclusion contact surface is performed automatically, using flat boundary elements of triangular and quadrangular shape according to the method employing boundary module-elements (Sect. 3.4). A possibility of non-uniform condensation of the boundary element grid in the areas of contact stress concentration. While calculating the matrix coefficients

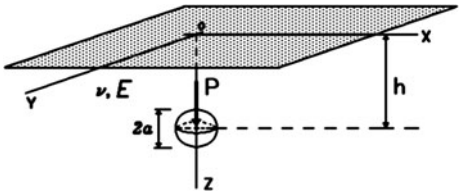

Fig. 3.58 Calculation scheme for the contact problem of a rigid sphere in an elastic half-space

for the resolving system of the linear algebraic equations, the integrals of the singular part of the Mindlin's solution are determined analytically, and those of the regular part are obtained numerically, using quadratures whose order depends on the size and remoteness of the boundary element under consideration from the collocation point (See Sect. Section 2.3, See Appendix B). Having solved the finite-measure analogue of the integral equation system, one can determine the displacements and rotation angles of the rigid inclusion with respect to the chosen spatial coordinate system as well as contact stress vector components for each boundary element, averaged over its area. The stress-strained state in any point of the elastic half-space, containing the rigid inclusion or the deepened punch, can be then easily calculated by direct integration of the found solution of the contact problem.

Test calculations have been performed for few exact solutions of contact problems for an elastic half-space, known from the literature, as well as for the solutions, obtained numerically in the axisymmetric formulation using other approximate approaches, available for the case of the half-space. The effect of the elastic properties of the medium as well as of relative deepening on the characteristic of contact stress distribution and load-displacement plots for the inclusions and the punches, is shown.

A rigid spherical inclusion in an elastic half-space. In an elastic homogeneous half-space $z > 0$ consider a nonhomogeneity in the form of an absolutely rigid inclusion of spherical type. A vertical force P is acting on a rigid sphere of radius a, deepened inside by distance h; the half-space is considered free of stress at the boundary surface (Fig. 3.58). In such formulation there is no exact solution of this spatial contact problem. For its numerical solution using the boundary-element method, the spherical contact surface is subject to discretization into flat triangular and quadrangular boundary elements by means of vertical and horizontal sections in a way shown in Fig. 3.59. Some results of the performed extensive systematic calculations, enabling the numerical solution convergence to be estimated, are listed in Tables 3.3 and 3.4. It should be noted that in all cases the solutions of the problem in the full (Sect. 2.2) and axiially symmetrical (Sect. 2.4.1) formulations have been always coinciding within the machine accuracy. Since in the first case the condensation degree of the discretization is limited by the computer resources, for numerous calculations using dense boundary element grids the axisymmetric version was applied.

Fig. 3.59 Discretization of a spherical surface using flat boundary elements

Table 3.3 Normal σ and tangential τ contact stress in meridional section of a spherical inclusion at relative deepening $h/a = 1, 100, 1000$

m	z/a	Without the account of unilateral constraints		With the account of unilateral constraints	
		σ	τ	σ	τ
1	2	3	4	5	6
$h/a = 1$					
1	0.01831	−0.00860	−0.01293	0.0	0.0
2	0.06152	0.17345	0.22415	0.17031	0.22180
3	0.13095	0.46263	0.50427	0.46271	0.50425
4	0.21212	0.53004	0.59668	0.52998	0.59676
5	0.29733	0.42830	0.63391	0.42830	0.63398
6	0.38246	0.28918	0.69239	0.28920	0.69245
7	0.46555	0.17608	0.77105	0.17612	0.77110
8	0.54600	0.10246	0.85703	0.10250	0.85708
9	0.62433	0.06466	0.94225	0.06470	0.94229
10	0.70236	0.05619	1.02382	0.05624	1.02384
11	0.78493	0.08194	1.11162	0.08200	1.11164
12	0.91268	0.14357	1.17952	0.14363	1.17952
13	1.08732	0.29764	1.26111	0.29770	1.26120
14	1.21507	0.43373	1.32531	0.43375	1.32519
15	1.29764	0.53920	1.29886	0.53926	1.29889
16	1.37567	0.64018	1.27954	0.64027	1.27965
17	1.45400	0.74622	1.24718	0.74624	1.24713
18	1.53445	0.85917	1.19827	0.85923	1.19828
19	1.61754	0.97979	1.12833	0.97985	1.12834
20	1.70267	1.10679	1.03076	1.10681	1.03073
21	1.78788	1.23694	0.89749	1.23704	0.89753
22	1.86905	1.36458	0.71814	1.36460	0.71813
23	1.93848	1.48182	0.48317	1.48189	0.48318
24	1.98169	1.53174	0.19160	1.53178	0.19160

Table 3.3 (continued)

m	z/a	Without the account of unilateral constraints		With the account of unilateral constraints	
		σ	τ	σ	τ
1	2	3	4	5	6
$h/a = 100$					
1	99.0183	−0.97820	0.12789	0.0	0.0
2	99.0615	−0.94687	0.32283	0.0	0.0
3	99.1309	−0.87206	0.48338	0.0	0.0
4	99.2121	−0.78950	0.60984	0.0	0.0
5	99.2973	−0.70392	0.70811	0.0	0.0
6	99.3825	−0.61843	0.78433	0.0	0.0
7	99.4656	−0.53536	0.84426	0.0	0.0
8	99.5460	−0.45503	0.89124	0.0	0.0
9	99.6243	−0.37681	0.92860	0.0	0.0
10	99.7024	−0.29907	0.95918	0.0	0.0
11	99.7849	−0.21416	0.99599	0.0	0.0
12	99.9127	−0.08870	0.98830	0.0	0.0
13	100.0873	0.08874	0.98831	1.19945	3.39521
14	100.2151	0.21423	0.99611	0.80355	1.73530
15	100.2976	0.29914	0.95922	0.94858	1.66283
16	100.3757	0.37694	0.92886	1.00226	1.50023
17	100.4540	0.45517	0.89144	1.06916	1.37119
18	100.5344	0.53550	0.84433	1.14257	1.24983
19	100.6175	0.61867	0.78465	1.22256	1.12638
20	100.7027	0.70417	0.70830	1.30763	0.99164
21	100.7879	0.78983	0.61007	1.39522	0.83720
22	100.8690	0.87243	0.48356	1.48159	0.65311
23	100.9385	0.94728	0.32298	1.56360	0.43159
24	100.9817	0.97867	0.12792	1.59142	0.16676
$h/a = 1000$					
1	999.018	−0.97847	0.12795	0.0	0.0
2	999.063	−0.94702	0.32299	0.0	0.0
3	999.131	−0.87212	0.48316	0.0	0.0
4	999.212	−0.78981	0.61009	0.0	0.0
5	999.297	−0.70408	0.70824	0.0	0.0
6	999.382	−0.61837	0.78478	0.0	0.0
7	999.466	−0.53544	0.84399	0.0	0.0
8	999.546	−0.45508	0.89122	0.0	0.0
9	999.624	−0.37693	0.92861	0.0	0.0
10	999.702	−0.29923	0.95932	0.0	0.0
11	999.785	−0.21420	0.99616	0.0	0.0
12	999.913	−0.08869	0.98836	0.0	0.0
13	1000.087	0.08869	0.98831	1.19940	3.39520
14	1000.215	0.21421	0.99604	0.80363	1.73524
15	1000.298	0.29921	0.95935	0.94884	1.66314
16	1000.376	0.37698	0.92875	1.00247	1.50019
17	1000.454	0.45506	0.89122	1.06917	1.37103
18	1000.534	0.53550	0.84433	1.14274	1.24996
19	1000.617	0.61819	0.78414	1.22209	1.12588
20	1000.703	0.70422	0.70867	1.30777	0.99215

Table 3.3 (continued)

m	z/a	Without the account of unilateral constraints		With the account of unilateral constraints	
		σ	τ	σ	τ
1	2	3	4	5	6
21	1000.788	0.78961	0.60950	1.39514	0.83655
22	1000.869	0.87252	0.48384	1.48178	0.65347
23	1000.938	0.94672	0.32268	1.56316	0.43132
24	1000.982	0.97862	0.12801	1.59143	0.16688

Contact stress values on the surface of the spherical inclusion in a meridional cross-section, obtained from the results of calculation for a sufficiently dense boundary-element grid (N = 24×72 = 1728), are listed in Table 3.3. Both the tangential $\tau = p_\tau/\sigma_0$ and normal $\sigma = p_n/\sigma_0$ stress values are made dimensionless using a nominal pressure $\sigma_0 = P/4\pi\alpha^2$ being the average pressure on the surface of the sphere. At the discretization of the contact surface sectioning by horizontal planes was performed with condensation towards the centre of the sphere what ha enabled non-prolate boundary elements (close to squares and equilateral triangles) to be used. As seen from the data presented, at different values of the sphere deepening on its rear side (in the pole, closer to the half-space surface) negative both tangential and normal stress values arise. The calculations show that with the increase of the deepening parameter the absolute values of the negative contact stress increase and the contact area, where they are revealed, expands. As could be expected, the account of unilateral constraints at any deepening parameter $h/a \geq 2$ results after an iterative process in a complete uplifting of the upper half of the sphere from the elastic medium. In turn, the contact domain decrease leads to the increase of stress as well as additional displacements acquired by the rigid sphere. Variation of displacements of the rigid spherical inclusion versus depth at different values of the Poisson ratio ν of the elastic half-space can be traced from Fig. 3.60. The calcu-

Table 3.4 Comparative characteristics of calculation of displacements of a rigid sphere at different relative deepening values in an elastic half-space on condensed boundary-element grids ($\nu = 0.3$, $P = E \cdot a^2$)

Number of boundary elements $N = m \times n$	$S/4\pi a^2$	W/a		
		$h/a = 1$	$h/a = 100$	$h/a = 1000$
$144 = 6 \times 24$	0.92279	0.29198	0.163789	0.162152
$240 = 10 \times 24$	0.95780	0.28478	0.161602	0.159967
$384 = 16 \times 24$	0.97416	0.28136	0.160836	0.159200
$480 = 20 \times 24$	0.97886	0.28034	0.160649	0.159014
$720 = 20 \times 48$	0.98305	0.27944	0.160035	0.158401
$1440 = 20 \times 72$	0.98384	0.27928	0.159918	0.158284
$1728 = 24 \times 72$	0.99399	0.27684	0.159815	0.158180
Linear extrapolation	0.99804	0.27624	0.159331	0.157697
According to Eq. (3.16)	1.00000		0.157639	

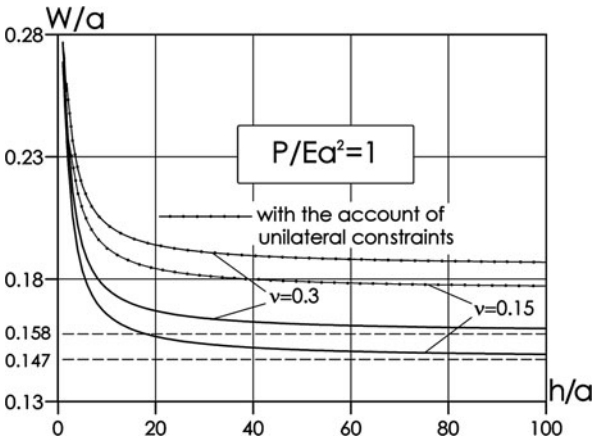

Fig. 3.60 Relative displacements of the rigid sphere depending on its depth in the elastic half-space

lation results here were obtained in the axisymmetric formulation using the most dense among the boundary-element grids we have used, providing high calculation accuracy at different depths (See Table 3.4). The calculated curves show that with the increase of the relative deepening *h/a* the vertical displacements *W/a* of the rigid sphere monotonously decrease, unlimitedly approaching the values determined based on the known solution of the Roben elastostatic problem for a rigid sphere, sealed into an unlimited elastic space [92]

$$W = \frac{(5 - 6\nu)(1 + \nu)}{12\pi E(1 - \nu)a} P \tag{3.16}$$

The displacements of the rigid sphere, calculated from Eq. (3.16), are also shown in Fig. 3.60 by dotted lines. At high values of the relative deepening *h/a* the calculated values of *W/a* practically coincide with the exact ones, what shows that the displacement values, obtained according to the proposed boundary-element approach, can be considered reliable. In particular, it is seen from the plots that the displacements of the rigid sphere monotonously grow with the increase of the Poisson ratio ν of the elastic half-space.

Similarly to the considered contact problem for a rigid sphere, the cases of inclusions of different shapes can be also studied. The most frequent in the literature [41, 42, 91, 97, 124, 151] are the studies of axisymmetric problems for rigid inclusions in the shape of rotation bodies: rotational ellipsoids (spheroids), finite cylinders, smoothly conjugated with half-spheres at abutting ends, circular cones, smoothly conjugated with spherical segments, and some more. In the boundary-element approach being developed, the inclusion can have any shape and undergo a spatial load of a general type. The accuracy of the contact problem solution will

mostly depend on the degree and quality of the contact surface discretization and finally will be determined by the computer resources.

In geotechnics, rigid flat inclusions of various shape in an elastic half-space are considered as a mathematical idealization of anchor foundation plates [121]. A solution of the axial loading problem for an ellipsoid, for whose semiaxes the following condition is valid

$$a_1 = a_2 = \alpha, a_3 \to 0,$$

is often used in order to estimate the displacement versus load dependences of such anchors. Under such consideration, the inclusion becomes an infinitely thin circular disc (penny-shaped). Due to the above mentioned advantages of the boundary-element approach it becomes possible to obtain rigidity characteristics of the "deepened anchor + elastic geomaterial" system independently of the simplifying assumptions concerning the anchor shape, thickness, direction of the pulling load, etc.

Note that the problem of a rigid sphere deepened into an elastic half-space is especially important for geotechnical calculations. This problem models the functioning of a spherical enlarged footing of bored piles. Experimentally the absence of limit equilibrium areas under the sphere and uplifting from the soil is observed only in the upper part of the enlarged footing [23]. Besides, there is a good coincidence of normal contact stress diagrams. This confirms the validity of application of theory of elasticity to calculate the footings of bored piles with enlarged bases. It should be also noted that in a prelimit state the soil under the tip of a pile without enlarged footing also moves together with the pile. In the course of impression and at pile driving a condensed core is formed which should be treated together with the pile as a whole unit body. The core, independently of the tip shape, acquires a shape close to hemispherical [85]. Note that for both flat and conical pile footing the core shape has no significant differences. Therefore, while performing pile calculations for the impression load, one can specify boundary conditions not for the tip surface, but for the hemispherical core surface. Consequently, while developing engineering calculation methods, solution of contact problem for a rigid sphere in an elastic half-space enables a more substantiated, with the account of the deepening factor, evaluation of pile displacements and soil resistance at their tip.

Cylindrical punch, deepened in an elastic half-space. Figure 3.61a shows a calculation scheme for the axisymmetric contact problem for an absolutely rigid cylinder, deepened into an elastic half-space and undergoing a vertical impressing load P. Consider the punch and the half-space to be soldered at the contact surface. Due to the axial symmetry of the problem, in the elastic half-space only radial p_r and vertical p_Z stresses arise, and the punch will be displace only in the direction of the force P.

In such formulation the axisymmetric contact problem for a deepened cylinder was first solved numerically by Shishov in 1971 [126]. He averaged the contact stresses over m cylindrical belts of a finite height on the punch lateral surface and ring-shaped belts of a finite width on its bottom. The integral equation system of theory of elasticity and the punch equilibrium equations are, due to such averaging,

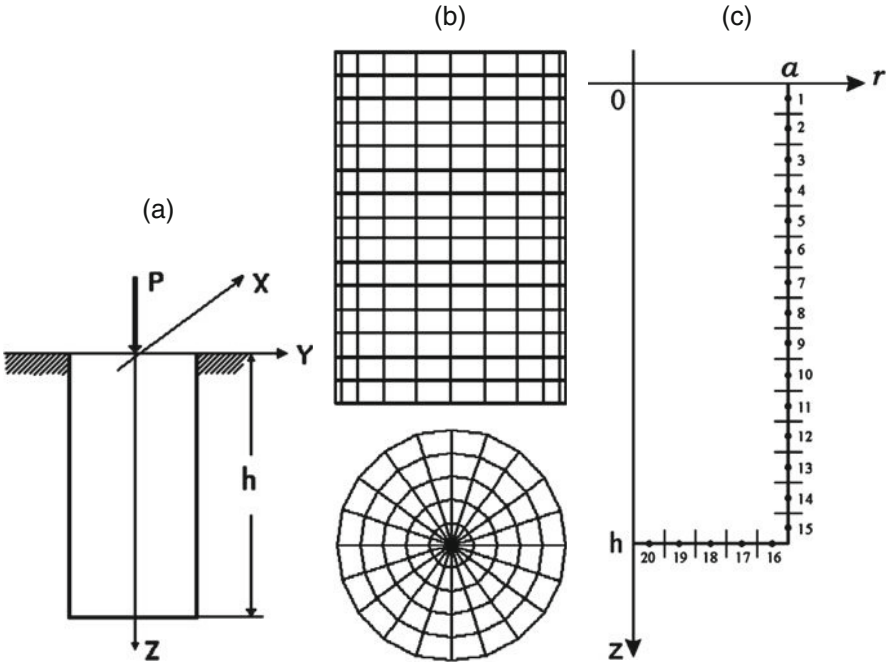

Fig. 3.61 Axisymmetrical contact problem for a cylindrical punch, deepened in an elastic half-space: (**a**) calculation scheme; (**b**) discretization of the contact surface by flat boundary elements; (**c**) location of collocation points on the generatrix

reduced to an algebraic equation system of the (2*m*+ 1)-th order with respect to 2*m* unknown contact stress values and vertical displacement Δ_Z. The coefficients at the unknowns are found by numerical integration of the fundamental solution over the circular coordinate. The results of the problem solution with respect to normal σ and tangential τ stresses in fractions of the mean contact stress $\sigma_{av} = P/2\pi Rh$ (*R* being the cylinder radius, *h* – its height) are given in the end of Table 3.5. The calculations were performed for the relative punch deepening $h/R = 3$ and for the contact surface discretization into 20 belts (5 on the bottom and 15 on the lateral surface, Fig. 3.61c). A characteristic feature of the solution is the presence of negative (tensile) normal stress at the punch lateral surface in the area close to the bottom.

Our calculations, performed using the boundary-element method, are presented in Table 3.5 at different density of the contact surface mesh into flat boundary elements. For all cases the cylindrical punch surface approximation was agreed with the discretization into cylindrical and ring-shaped belts of the numerical study of Shishov (15 + 5 = 20 boundary elements) in each meridional section $\theta_k = 2\pi k/n$, $k = 1, 2, \ldots n$ (Fig.3.61b). The problem was solved both based on a full spatial formulation and on the axisymmetric approach. For the cases of n= 12 (240 boundary elements) and n= 20 (400 boundary elements) the calculation results have coincided within the machine accuracy.

Table 3.5 Normal σ and tangential τ contact stress in the axial section of a cylindrical punch on a succession of condensing boundary-element grids ($h/R = 3$, $\nu = 0.3$)

		$n = 12$			$n = 20$		
m	z/a	r/a	σ	τ	r/a	σ	τ
1	0.1	0.966	1.97843	0.72064	0.988	1.99296	0.71949
2	0.3	0.966	0.87163	0.58824	0.988	0.87118	0.59347
3	0.5	0.966	0.61466	0.62024	0.988	0.61681	0.61874
4	0.7	0.966	0.45167	0.64667	0.988	0.45410	0.64528
5	0.9	0.966	0.34663	0.67429	0.988	0.34899	0.67323
6	1.1	0.966	0.27256	0.70191	0.988	0.27469	0.70115
7	1.3	0.966	0.21733	0.72988	0.988	0.21915	0.72939
8	1.5	0.966	0.17409	0.75911	0.988	0.17555	0.75890
9	1.7	0.966	0.13854	0.79091	0.988	0.13960	0.79104
10	1.9	0.966	0.10758	0.82723	0.988	0.10818	0.82783
11	2.1	0.966	0.07842	0.87125	0.988	0.07848	0.87251
12	2.3	0.966	0.04770	0.92846	0.988	0.04717	0.93077
13	2.5	0.966	0.00850	1.01241	0.988	0.00739	1.01725
14	2.7	0.966	−0.03929	1.11874	0.988	−0.04046	1.13133
15	2.9	0.966	−0.38419	1.98107	0.988	−0.40651	2.00987
16	3.0	0.874	2.60622	0.48425	0.893	2.56068	0.47496
17	3.0	0.681	1.53689	0.08493	0.696	1.49349	0.07438
18	3.0	0.489	1.35948	0.05645	0.500	1.32977	0.05175
19	3.0	0.301	1.25883	0.02817	0.307	1.23436	0.02596
20	3.0	0.129	1.21725	0.01037	0.132	1.19175	0.00957

		$n = 24$			$n = 40$		
m	z/a	r/a	σ	τ	r/a	σ	τ
1	0.1	0.994	1.99712	0.72097	0.997	1.99927	0.72252
2	0.3	0.994	0.87088	0.59342	0.997	0.87071	0.59255
3	0.5	0.994	0.61744	0.61783	0.997	0.61780	0.61734
4	0.7	0.994	0.45481	0.64478	0.997	0.45519	0.64449
5	0.9	0.994	0.34969	0.67288	0.997	0.35006	0.67270
6	1.1	0.994	0.27532	0.70092	0.997	0.27566	0.70077
7	1.3	0.994	0.21969	0.72925	0.997	0.21998	0.72917
8	1.5	0.994	0.17599	0.75886	0.997	0.17622	0.75881
9	1.7	0.994	0.13991	0.79109	0.997	0.14008	0.79114
10	1.9	0.994	0.10835	0.82802	0.997	0.10844	0.82813
11	2.1	0.994	0.07849	0.87288	0.997	0.07849	0.87309
12	2.3	0.994	0.04700	0.93146	0.997	0.04691	0.93183
13	2.5	0.994	0.00696	1.01844	0.997	0.00668	1.01913
14	2.7	0.994	−0.03990	1.13430	0.997	−0.03937	1.13541
15	2.9	0.994	−0.41540	2.02530	0.997	−0.42099	2.03601
16	3.0	0.898	2.54350	0.47215	0.901	2.53226	0.47007
17	3.0	0.700	1.47932	0.07000	0.703	1.47161	0.06755
18	3.0	0.504	1.32144	0.05058	0.505	1.31710	0.04998
19	3.0	0.309	1.22781	0.02533	0.310	1.22472	0.02501
20	3.0	0.133	1.18297	0.00933	0.133	1.17720	0.00918

		$n = 60$			$n = 72$		
m	z/a	r/a	σ	τ	r/a	σ	τ
1	0.1	0.988	2.00045	0.72366	0.999	2.00083	0.72395
2	0.3	0.988	0.87062	0.59176	0.999	0.87059	0.59152
3	0.5	0.988	0.61800	0.61709	0.999	0.61806	0.61704
4	0.7	0.988	0.45540	0.64433	0.999	0.45547	0.64428
5	0.9	0.988	0.35027	0.67258	0.999	0.35034	0.67256
6	1.1	0.988	0.27585	0.70071	0.999	0.27591	0.70068
7	1.3	0.988	0.22015	0.72913	0.999	0.22021	0.72910
8	1.5	0.988	0.17636	0.75880	0.999	0.17641	0.75878
9	1.7	0.988	0.14019	0.79114	0.999	0.14023	0.79113
10	1.9	0.988	0.10851	0.82817	0.999	0.10855	0.82816
11	2.1	0.988	0.07852	0.87320	0.999	0.07855	0.87318
12	2.3	0.988	0.04688	0.93200	0.999	0.04691	0.93203
13	2.5	0.988	0.00655	1.01946	0.999	0.00656	1.01947
14	2.7	0.988	−0.03898	1.13589	0.999	−0.03881	1.13591
15	2.9	0.988	−0.42433	2.04240	0.999	−0.42514	2.04359
16	3.0	0.903	2.52557	0.46857	0.903	2.52438	0.46812
17	3.0	0.704	1.46757	0.06629	0.704	1.46666	0.06604
18	3.0	0.406	1.31548	0.04966	0.506	1.31553	0.04960
19	3.0	0.311	1.22326	0.02487	0.311	1.22297	0.02484
20	3.0	0.133	1.17372	0.00908	0.133	1.17286	0.00906

		Calculation by Shishov [126]		
m	z/a	r/a	σ	τ
1	0.1	1.0	1.952	0.715
2	0.3	1.0	0.877	0.600
3	0.5	1.0	0.614	0.620
4	0.7	1.0	0.451	0.646
5	0.9	1.0	0.346	0.674
6	1.1	1.0	0.272	0.702
7	1.3	1.0	0.216	0.730
8	1.5	1.0	0.173	0.760
9	1.7	1.0	0.137	0.792
10	1.9	1.0	0.106	0.829
11	2.1	1.0	0.076	0.875
12	2.3	1.0	0.045	0.934
13	2.5	1.0	0.005	1.024
14	2.7	1.0	−0.044	1.149
15	2.9	1.0	−0.424	2.013
16	3.0	0.9	2.488	0.443
17	3.0	0.7	1.490	0.078
18	3.0	0.5	1.322	0.006
19	3.0	0.3	1.223	0.000
20	3.0	0.1	1.221	0.000

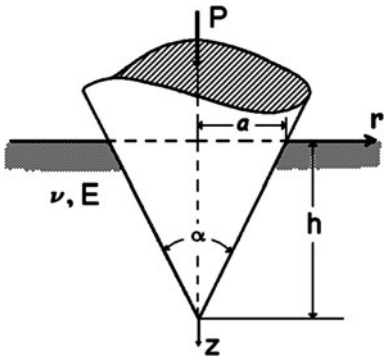

Fig. 3.62 Calculation scheme to the problem of impression of a deepened cone into an elastic half-space

The calculations for $n = 28, 40, 60$, and 72, due to the limitations of the computer RAM size, were performed only in the axisymmetric approach and have shown a stable increase of the approximate solution accuracy with the increase of the number of the boundary elements (the correction regards the 4–5-th digit after the decimal point, Table 3.5). The calculations performed by boundary-element method at $n = 20$ gave the result which appeared to be the closest to the numerical calculations of Shishov. Additional calculations for this case of discretization when the cylindrical punch radius was increased in such a way that the boundary-element polyhedron surface corresponded to the contact surface for the initial cylinder and the collocation points on the bottom were chosen not in the gravity centres of the boundary elements, but in the geometrical centres of the circular sectors, has led to a practically full coincidence of the numerical boundary-element values with the calculation data of Shishov (the difference was observed only for the 5th, only sometimes for the 4th digit after the decimal point). Consequently, the results of the contact problem solution for a deepened cylindrical punch using the proposed boundary-element method, are reliable and the calculation accuracy can be increased due to the increase of the number of boundary elements. To obtain the results with an accuracy, sufficient for practical purposes, the contact surface discretization degree can be limited to 400–500 boundary elements.

Note that the successful approbation of the contact problem for a deepened cylindrical punch subsequently enabled the boundary-element approach to be applied with better substantiation for the calculation of base deformations for rigid foundation structures of vertical and inclined cylindrical bored piles as well as bored piles with footings under spatial loading of general type (see Sects. Section 5.4 and Section 5.5).

Impression of a cone into an elastic half-space. Consider a spatial contact problem for a deepened conical punch being impressed by an axial force P into an elastic homogeneous half-space with the deformation modulus E and the Poisson ratio ν. Consider the punch to be soldered with the half-space which has a conical cavity of the depth h and radius a (the angle at the cone vertex $\alpha = 2\text{arccot}(h/a)$). The calculation scheme of the problem and the notations used are shown in Fig. 3.62.

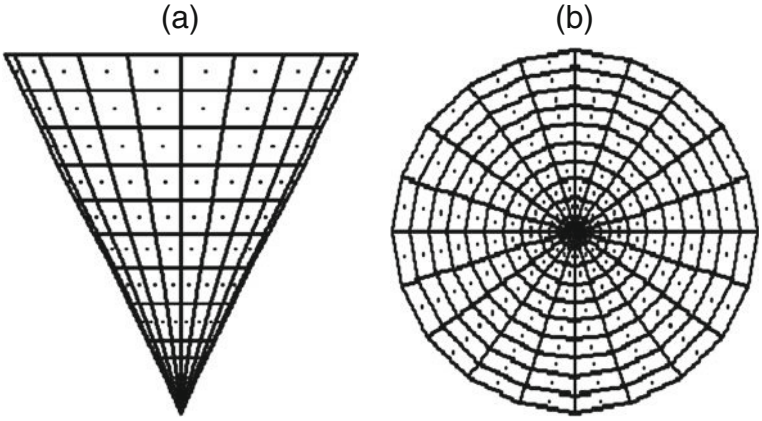

Fig. 3.63 Discretization of the contact surface of a deepened conical punch by flat triangular and quadrangular boundary elements: (**a**) lateral view; (**b**) view from below

Since no analytical solution of the problem under consideration is available, we study it numerically using the boundary-element method. The contact surface of the cone and the half-space is meshed into flat boundary elements whose nodes are formed at the intercepts of horizontal (equidistant) and vertical (passing through the cone axis and forming equal angles between the neighbouring ones) planes (Fig. 3.63). Such discretization of the cone lateral surface enables the contact problem to be solved in both axisymmetric and general spatial formulation for the same boundary-element grid. Note that, similarly to the above contact problems for the rigid sphere and cylinder, comparison of the results in both formulations at the number of boundary elements not higher than 500 gives the results, coinciding within the machine accuracy. This is the evidence for the applied boundary-element algorithm to be correct and reliable. On the other hand, since central loading of the conical punch is of the main practical interest, this enables us hereinafter to solve the contact problems in the axisymmetric formulation what increases practically unlimitedly the number of boundary elements to obtain numerical solutions with a required accuracy.

The results of the numerical solution of the contact problem for a conical punch with a depth $h = 2a(\alpha/2 = 26.57°)$, being impressed by a force $P = Ea^2$ into an elastic half-space with the Poisson ratio $\nu = 0.3$, are presented in Tables 3.6 and 3.7and in Fig. 3.64. The cone generatrix was meshed into ten parts of equal length (m= 10), in the centres of which the values of normal σ and tangential τ contact stress were determined, normalized by the average contact stress $\sigma_{av} = P/S$ where S is the cone lateral surface area. The calculation data give the evidence for a rather fast convergence of the numerical solution with the increase of the number of the boundary elements n in the circular direction, i.e. with the increase of the degree of the contact surface approximation by an ensemble of flat boundary elements. Table 3.6 contains also contact stress extrapolation, obtained from the calculation

Table 3.6 Normal σ and tangential τ contact stress in the axial section of a deepened conical punch ($h/a = 2.0$, $\nu = 0.3$, $P = E \cdot a^2$)

			$n = 40$		$n = 60$	
m	z/a	r/a	σ	τ	σ	τ
1	0.0983	0.94795	1.89056	0.54453	1.89209	0.54555
2	0.2980	0.84836	0.71133	0.56688	0.71052	0.56578
3	0.4978	0.74880	0.60811	0.59814	0.60822	0.59758
4	0.6974	0.64927	0.54249	0.63204	0.54267	0.63131
5	0.8969	0.54982	0.52223	0.67833	0.52255	0.67730
6	1.0963	0.45046	0.53094	0.74526	0.53163	0.74389
7	1.2952	0.35129	0.56938	0.84678	0.57088	0.84517
8	1.4933	0.25255	0.65315	1.01607	0.65623	1.01557
9	1.6889	0.15508	0.83164	1.37025	0.83421	1.37094
10	1.8667	0.06646	1.23047	2.56431	1.22676	2.55185

			$n = 100$		$n = 160$	
m	z/a	r/a	σ	τ	σ	τ
1	0.0983	0.94795	1.89379	0.54561	1.89744	0.54428
2	0.2980	0.84836	0.79814	0.56466	0.70856	0.56345
3	0.4978	0.74880	0.60861	0.59665	0.60938	0.59558
4	0.6974	0.64927	0.54331	0.63017	0.54435	0.62917
5	0.8969	0.54982	0.52370	0.67604	0.52524	0.67517
6	1.0963	0.45046	0.53353	0.74259	0.53566	0.74212
7	1.2952	0.35129	0.57395	0.84438	0.57677	0.84465
8	1.4933	0.25255	0.66101	1.01712	0.66453	1.01923
9	1.6889	0.15508	0.83772	1.37386	0.83942	1.37689
10	1.8667	0.06646	1.22158	2.53778	1.21563	2.52637

data in the assumption of a linear dependence of the numerical solutions on n^{-1}. It is seen that at n= 400 the relative error δ of determination of dimensionless contact stress seldom exceeded 0.5% and relative punch displacement W/a has three correct digits after the decimal point (Table 3.7), what is by far sufficient for practical calculations. In order to visualize the contact interaction character, normal and tangential stress diagrams, built along the cone generatrix from the numerical solution extrapolation data, are shown in Fig. 3.64.

Note that the solution of the above contact problem for the cone with the same vertex angle had been performed earlier by Aleksandrov and Solov'ev [3] using a contour integral method. Unfortunately, the quoted reference does not contain the Poisson ratio value ν, for which the numerical results were obtained. Therefore, we have performed additional calculations for various most widely used ν values. The calculated displacement data are presented in Table3.8. The numerical results, obtained by different methods, are seen to be close. It should be noted that application of the contour integral method in [3] implied neglection of horizontal displacements in the points of the punch contact with the base what, in turn, resulted in a

			$n = 400$		Extrapolation		δ (%)	
m	*z/a*	*r/a*	σ	τ	σ	τ	σ	τ
1	0.0983	0.94795	1.91321	0.53968	1.92372	0.53661	0.55	0.57
2	0.2980	0.84836	0.70244	0.56152	0.69836	0.56023	0.58	0.23
3	0.4978	0.74880	0.61113	0.59408	0.61230	0.59308	0.19	0.17
4	0.6974	0.64927	0.54612	0.62806	0.54730	0.62732	0.22	0.12
5	0.8969	0.54982	0.52753	0.67447	0.52906	0.67400	0.29	0.07
6	1.0963	0.45046	0.53825	0.74195	0.53998	0.74184	0.32	0.02
7	1.2952	0.35129	0.57951	0.84524	0.58134	0.84563	0.31	0.05
8	1.4933	0.25255	0.66711	1.02167	0.66883	1.02330	0.26	0.16
9	1.6889	0.15508	0.83813	1.37988	0.83727	1.38187	0.10	0.14
10	1.8667	0.06646	1.20232	2.50906	1.19345	2.49752	0.74	0.46

hardly probable law of contact stress distribution over the lateral surface of the cone (the normal and tangential stress diagrams appeared to be practically identical). A removal of this limitation would undoubtedly enable even better compatibility of the results of the solution of the contact problem under consideration for the deepened cone using two different approaches.

Consider in more detail the results of the boundary-element solution of the contact problem for obtuse-angle conical punches, deepened into an elastic half-space whose Poisson ratio is taken as 0.3. The punch contact surface approximation in this case was performed using 4000 boundary elements (50 along the cone gener-

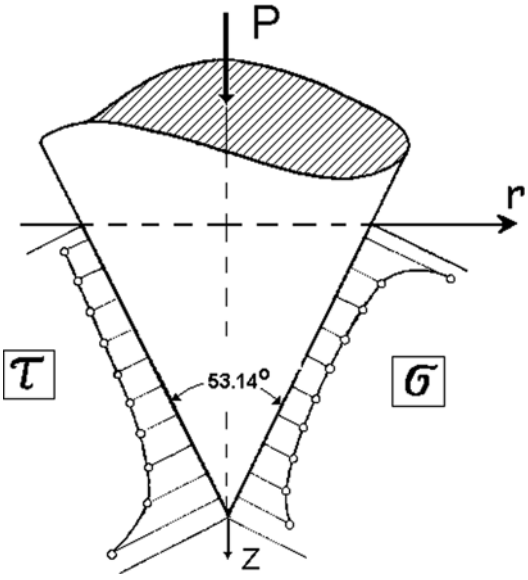

m	z/a	r/a	σ	τ
1	0.098	0.9479	1.9237	0.5366
2	0.298	0.8484	0.6984	0.5602
3	0.498	0.7488	0.6123	0.5931
4	0.697	0.6493	0.5473	0.6273
5	0.897	0.5498	0.5291	0.6740
6	1.096	0.4505	0.5399	0.7418
7	1.295	0.3513	0.5813	0.8456
8	1.493	0.2526	0.6688	1.0233
9	1.689	0.1551	0.8373	1.3819
10	1.867	0.0665	1.1935	2.4975

Fig. 3.64 Profiles of dimensionless tangential **τ** and normal **σ** contact stress for a deepened conical punch ($h/a = 2.0$; $\nu = 0, 3$; $P = Ea^2$)

Table 3.7 Comparative characteristics of settlements of a deepened cone, calculated for a sequence of condensed boundary-element grids ($\nu = 0.3$, $P = E \cdot a^2$,$h/a = 2.0$)

Number of boundary elements $N = m \times n$	$S/\pi a\sqrt{a^2 + h^2}$	W/a
$400 = 10 \times 40$	0.99836	0.34571
$600 = 10 \times 60$	0.99927	0.34538
$1000 = 10 \times 100$	0.99974	0.34516
$1600 = 10 \times 160$	0.99990	0.34498
$4000 = 10 \times 400$	0.99998	0.34446
Linear extrapolation	1.00002	0.34411

Table 3.8 Comparison of the calculated values of relative displacements$W/a$of a deepened conical punch depending on the Poisson ratio ν of the elastic half-space ($h/a = 2.0$, $P = E \cdot a^2$)

ν	Contour integral method	Boundary-element method	Relative error (%)
0.3	0.31955	0.34525	7.4
0.35	0.33184	0.34493	3.8
0.4	0.34413	0.34302	0.32

atrix and 80 along the circular coordinate), what for the case of the axisymmetric formulation of the problem corresponds to a system of 101 linear algebraic equations with respect to the averaged 50 vertical p_z and 50 radial τ_{rz} stress values along the generatrix as well as the punch vertical displacement W in the direction of the external force. The cone radius a and the external impressing force value $P = Ea^2$ were fixed at the calculations. The h/a ratio, i.e. the relative deepening of the punch was used as a variable parameter. The calculations were performed for the values h/a= 0.5. 0.3, 0.2, 0.1, 0.03, and 0.01, what corresponds to a gradual increase of the angle at the cone vertex. In the limit (at small h/a) it tends to the solution of the problem of a flat circular punch, linked to a half-space, which has been solved analytically at least several times [70, 138, 142]. In the most convenient visual form (on the base of the numerical data) the solution of the problem in question is presented in [129] and is treated here as the case of a degenerate conical punch (h/a= 0). The above limiting transition is illustrated by Fig. 3.65where an example with vertical contact stress diagrams along the cone generatrix is shown. Complementing Fig. 3.65, one should note that the contact stress diagrams, built for h/a= 0.01, have practically coincided with the corresponding diagrams for the circular punch with flat bottom (dotted curve in Fig. 3.65).

The calculated settlement values for the series of the above considered obtuse-angle conical punches are shown in Fig. 3.66. In the same figure the value W_0/a= 0.044234 for the flat-base punch settlement is indicated, determined at $\nu = 0.3$ and $P = Ea^2$ using the formula [129]

$$W = \frac{(1 - 2\nu)(1 + \nu)}{2Ea \cdot \ln(2 - 4\nu)} P.$$

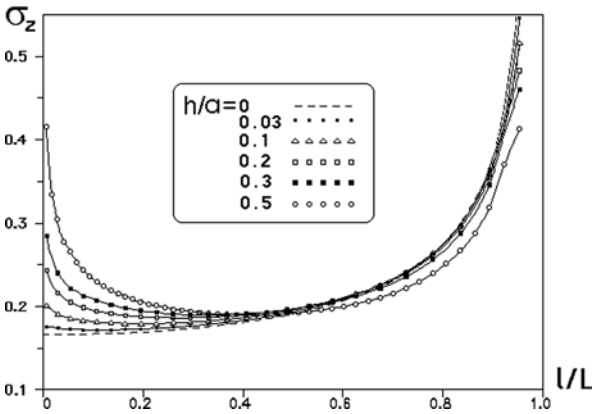

Fig. 3.65 Profiles of dimensionless vertical contact stress $\sigma_z = p_z Ea^2/P$ along the cone generatrix at different depths ; $\nu = 0.3$

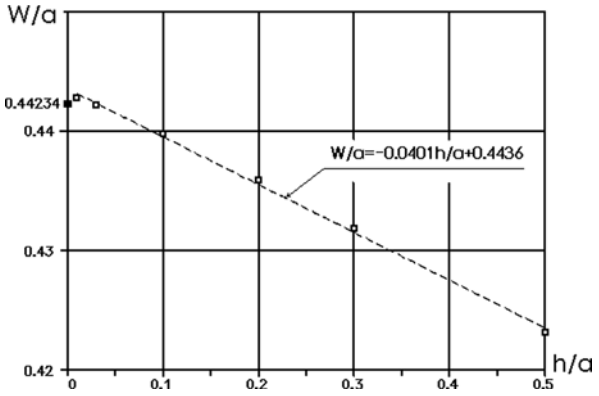

Fig. 3.66 Dimensionless settlements of obtuse-angled cones at different relative depths; $\nu = 0.3$; $P = Ea^2$

The relative settlement value for the conical punch with the deepening parameter $h/a = 0.03$, calculated by the boundary-element method, is 0.44222 what is rather close to the exact result for the flat-base punch. At $0 \leq h/a \leq 0.01$ the numerical values of relative displacements of the cone within the machine accuracy were practically indistinguishable between each other and from the W_0/a value. As one can see, the calculated data of the settlements of conical punches with increasing vertex angle show the applicability of the proposed boundary-element algorithm and the reliability of the results obtained using this approach. Besides, from the performed numerical study an important feature of contact interaction of obtuse-angle conical punches with an elastic half-space should be noted, namely the practically linear law of their settlement decrease with the relative depth increase (Fig. 3.66).

The performed formulation and boundary-element solution of the spatial contact problem for the deepened conical punch is highly important in geotechnics for the development of punch (field-based and laboratory-based) methods of determination of mechanical properties of soils. In practical studies of soils for engineering purposes, in the recent years intense improvement of methods of determination of physical and mechanical properties of soils by various punches and tips, namely flat circular, conical (penetrating and immersing), spherical, torvane, cylindrical, pile, etc. [35, 44, 75, 76, 89, 95, 127, 128, 136, 149, 150]. Application of various tips increases the reliability of the obtained soil characteristics at their natural conditions. Since a considerable interval of the soil functioning belongs to the compression phase with a linear (or close to linear) relation between the load and the settlement, one should note that while calculating foundation bases, solutions of linear theory of elasticity can be used for the absolute majority of the soils. In turn, the experimentally obtained plots of the indenter (tip) settlement versus the load (or pressure) being transferred to it, form a basis for the determination of deformational properties of the soil and for checking its strength properties.

The most important deformational characteristic of the soil is its deformation modulus E. The correct evaluation of this parameter is quite important for the accuracy of determination of settlements of buildings and structures. Variation of another deformational parameter, the Poisson ratio ν, is known to affect much less the stress-strained state of soils. Usually it is sufficient to take the Poisson ratio from handbook data, depending on the soil type [131]. Besides, while assigning the Poisson ratio it is rather convenient to apply the known Wet formula [147].

At present the most elaborated both from theoretical and practical point of view is soil examination method by a test static load using test circular punches (first of all, in order to determine the deformation modulus) [35, 127, 131]. However, in spite of the simplicity of the equipment, the flat punch test methods possess a number of essential disadvantages [44]. The main of them is low representability of the obtained results for characterization of the soil properties from the deposit profile. The test results for the base surface, which usually have a random character, are extended to the whole depth of the soil mass. Then, the contact stress under the flat punch is characterized by a considerable nonuniformity due to a sharp increase of gradients with approaching the punch edges. This results in residual plastic deformations along the punch perimeter, determined by the soil strength properties and not characterizing its compactability (elastic compressibility). Discrepancies between theoretical solutions and experimental data are often revealed, especially in case punches of small size being used [44, 128]. Besides, soil tests using flat circular punches are rather labour-consuming and expensive, therefore wide application of this method for examination of construction sites for residential building development or, moreover, for engineering-and-geological survey, is still limited.

Based on a review of physical and mechanical characteristics, which, according to the construction codes and regulations, should be used for foundation and base calculation, and which are determined by different tips, Yeltsov has convincingly shown the advantage of conical methods of soil tests [149]. These tests are suitable both for the Earth and other planets [36], both for field-based and laboratory studies.

They are characterized by simplicity and portability, low price and high performance speed, are easily automated and enable continuous mechanical characteristics across the soil section to be obtained at minimal labour and power expense. Application of conical tips in the measuring device is especially important for road construction, which is characterized by long road extension and requires determination of soil properties in a very great number of points [35].

In spite of the mentioned advantages, wide application of tips, first of all conical, is retarded by insufficient development of experimental and theoretical fundamentals of determination of mechanical properties of soils by static load. A number of authors note that the existing theoretical solutions in many cases considerably differ from the experimental data and are even contradictory [75, 136]. Then boundary-element results of a systematic and rather strict solution of the problem on cone impression into an elastically compressible medium are analyzed in detail. The investigation performed has enabled data of fundamental character to be obtained, which are required for working out a substantiated method of soil testing using deepened conical punches.

Figure 3.67 presents the values of a dimensionless function

$$\frac{\pi WEa}{P} = q(\alpha,\nu) \tag{3.17}$$

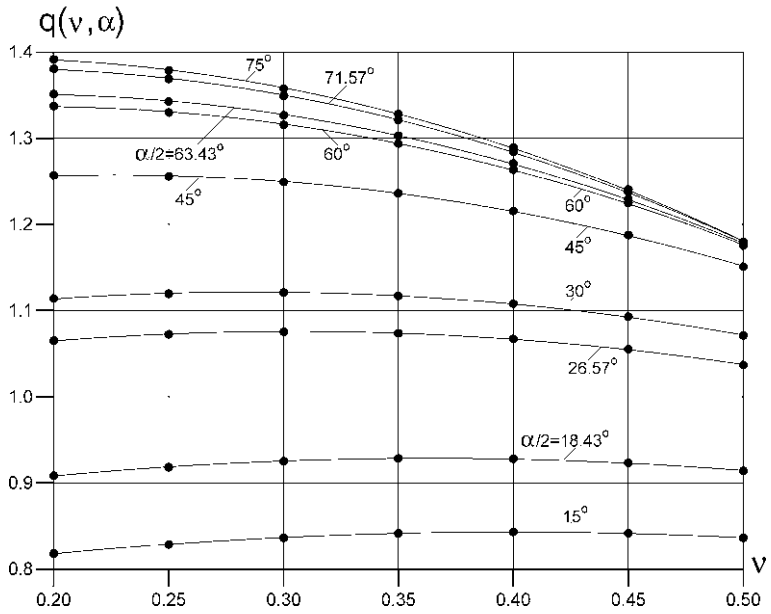

Fig. 3.67 Calculated values of a dimensionless function $q(\alpha,\nu)$ which determines the settlement of cones, deepened into an elastic half-space

obtained from the results of settlement calculations for cones, deepened into an elastic half-space, with various vertex angles ($\alpha/2 = 15°, 18.43°, 30°, 45°, 60°, 63.43°, 71.57°, 75°$) and at the Poisson ratio ν values from 0.2 to 0.5 with a step 0.05 what in a rather detail covers the real possible interval of variation of volume compressibility of solid media ($\nu = 0.27$ for macrofragmental soils, $\nu = 0.3$ for sands and clayey sands, $\nu = 0.35$ for clayeys, $\nu = 0.42$ for clays [127]). A detailed analysis of the calculation data has shown that at fixed cone opening angle α the values of q can be rather successfully approximated by a parabolic dependence

$$q(\alpha,\nu) = K(\alpha) \cdot \left[1 + A(\alpha) \cdot \nu - B(\alpha) \cdot \nu^2\right]$$

its parameters as well as the high approximation accuracy being indicated in Table 3.9. For the intermediate values of a with approximation, sufficient for practical purposes, the coefficients K, A, and B can be obtained from the data of Table 3.9 by linear interpolation. For the sake of convenient application of Eq. (3.18) Figure 3.68 contains auxiliary plots of $K(\alpha)$, $A(\alpha)$, $B(\alpha)$, obtained from square approximation. The corresponding formulae are given by

$$\begin{aligned} K &= K_0 + K_1\left(\frac{h}{a}\right) + K_2\left(\frac{h}{a}\right)^2, \\ A &= A_0 + A_1\left(\frac{h}{a}\right) + A_2\left(\frac{h}{a}\right)^2, \\ B &= B_0 + B_1\left(\frac{h}{a}\right) + B_2\left(\frac{h}{a}\right)^2 \end{aligned} \tag{3.19}$$

where $h/a = \cot(\alpha/2)$ is the relative deepening of the cone, K_i, A_i, B_i (i= 0, 1, 2) are regression parameters, listed in Table 3.10. Note that for obtuse-angle conical punches ($h/a \leq 1$) the $K(h/a)$, $A(h/a)$, and $B(h/a)$ plots have appeared practically linear (Fig. 3.68). This enables one to use for the cones with the vertex angles $\alpha \geq 90°$ less complicated, but not less exact linear approximations instead of the dependences given by Eq. (3.19):

Table 3.9 Parameters of the approximation dependence Eq. (3.18) for deepened cones with different vertex angles

h/a	$\alpha/2$, deg	K	A	B	Mean square deviation
0.26795	75	1.342	0.46319	1.40716	5.38×10^{-6}
0.33333	71.57	1.32848	0.46983	1.38527	5.01×10^{-6}
0.5	63.43	1.29322	0.48806	1.33147	4.24×10^{-6}
0.57735	60	1.27657	0.49679	1.30787	3.94×10^{-6}
1.0	45	1.18423	0.54349	1.19669	2.78×10^{-6}
1.73205	30	1.03221	0.60650	1.06071	1.67×10^{-6}
2.0	26.57	0.98241	0.62364	1.02334	1.42×10^{-6}
3.0	18.43	0.82771	0.66912	0.91932	8.33×10^{-7}
3.73205	15	0.74099	0.69074	0.86571	5.99×10^{-7}

Table 3.10 The parameters of square, Eq. (3.19), and linear, Eq. (3.20), approximations for the coefficients *K, A, B*in Eq. (3.18)

i	K_i	A_i	B_i	$\tilde{K}_i$	$\tilde{A}_i$	$\tilde{B}_i$
0	1.41259	0.42289	1.47791	1.40053	0.43332	1.47888
1	−0.25241	0.12901	−0.3072	−0.21584	0.11003	−0.28596
2	0.019314	−0.01589	0.03893			
Mean square deviation (s 10^5)	7.28	2.71	55.6	0.1508	0.02713	9.57

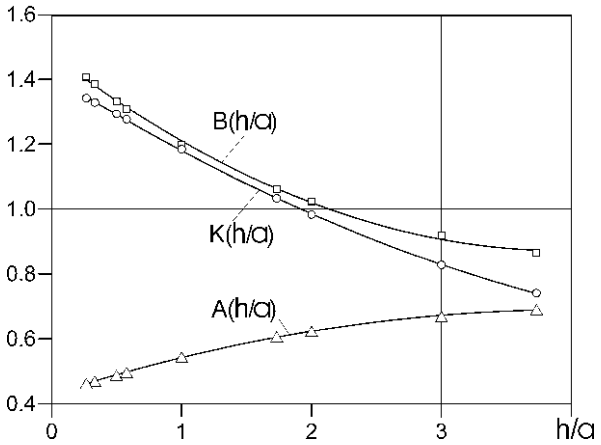

Fig. 3.68 Coefficients of Eq. (3.18) depending on the cone relative depth, α =2arccot(h/a)

$$\begin{aligned} K &= \bar{K}_0 + \bar{K}_1 \left(\frac{h}{a}\right), \\ A &= \bar{A}_0 + \bar{A}_1 \left(\frac{h}{a}\right), \\ B &= \bar{B}_0 + \bar{B}_1 \left(\frac{h}{a}\right) \end{aligned} \tag{3.20}$$

whose coefficients are also listed in Table 3.10.

Consider an example of calculation the cone settlement using the obtained dependences. Let the settlement value for a deepened conical punch with the vertex angle $\alpha = 100°$ and radius $a = 5$ cm at the half-space surface, be required to estimate. The punch is deepened into a fine grained sand by a vertical force P= 15 kN. The deformation parameters of the elastic base are taken as follows: E= 28 MPa, ν = 0.333.

First consider the relative punch depth $h/a = \cot(\alpha/2) = \cot(50°) = 0.8391$. Using Eqs. (3.19) with the account of Table 3.10, one can find the coefficients

$$K = 1.2143, A = 0.52591, B = 1.24754$$

and then the value q(100°, 0.333) = 1.25896. The sought value of the cone settlement will be $W_1 = qP/\pi Ea = 0.42937$ cm. Since the angle at the cone vertex is obtuse, the calculation can be also performed using a more simple equation (3.20), what results in a value $W_2 = 0.43154$ cm, what is slightly different from the one obtained earlier. A direct calculation using the developed program employing the boundary-element method, leads to a result $W_3 = 0.43935$ cm which, as could be expected, is close to the settlements obtained earlier, and the differences between the three values are within the measurement accuracy.

The developed numerical-and-analytical approach to determine the relationship between W and P for a deepened cone, similarly to the flat punch [54, 127], can be used to determine the soil deformation modulus according to the formula

$$E = \frac{q(\alpha,\nu) \cdot \Delta P}{\pi a \cdot \Delta W} \tag{3.21}$$

where ΔP and ΔW are the variations of load and settlement, respectively, at static tests within the soil linear displacement phase. This dependence for the determination of the deformation modulus is the consequence of Eq. (3.17), the values of P and W being replaced with their increments, since the settlement at the initial loading stages will always be related to deviations due to a loose contact of the punch and the soil in the cavity, breaking down surface irregularities, etc.

The procedure of testing and processing of the results for static loading of a cone using Eq. (3.21) is similar to that for flat-bottom punches and consists in application of a central force to the conical punch with subsequent stepwise loading with a step ΔP whose value should depend on the soil grain composition, dampness and density, consistency, and porosity coefficient. Contrary to the flat punch tests, when the settlement should be determined in several points of the punch, for impression of a cone it is sufficient to determine the axial displacement. Note that, similarly to the case of the flat punch, for a conical punch the critical pressure (corresponding to the proportionality limit) can be determined from a sharp kink of the experimental curve $W = W(P)$. Thus, application of static loading of a conical punch can be regarded as improvement of the existing methods of determination of deformational parameters and checking the strength properties of soils.

An important feature of static examination based on the theoretical solution of Eq. (3.21) consists in the fact that impression of a cone, having been deepened into the soil before, is performed. When disturbed soils are examined, the samples are formed using liners, forming conical cavities after their removal [76]. In the natural soil samples the cavity is made using a special device of helical drill type. Near walls and pits, as well as in order to determine anisotropic properties of the soil, the cone can be impressed both in horizontal and in vertical direction.

Equation (3.21) enables the impression of a conical punch, deepened from the elastic base surface. Application of this formula for the cases of impression of the cone on the bottom of a pit, a trench, or a well will introduce an error into the deformation modulus value, depending on the conical punch location depth. The evidence for this is the above considered solution of the contact problem for a

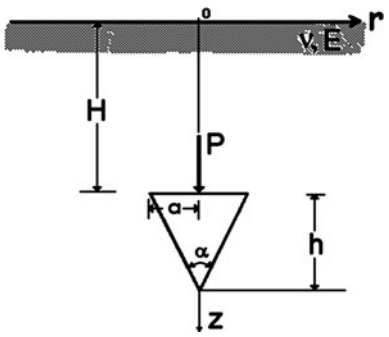

Fig. 3.69 Calculation scheme of the contact problem for a conical punch inside an elastic half-space

deepened spherical inclusion as well as the solution of the problem for a flat circular punch, deepened into an elastic half-space [95]. Evidently, the settlement of the cone inside the half-space will be smaller than the settlement of the cone on the surface, since part of the transferred load will be accepted by the soil mass, located above the punch level. This was confirmed by the calculations which we performed for a conical punch with the vertex angle 60° at the relative depth H/a from 1 to 1000. The calculation scheme of the contact problem for the conical punch inside an elastic half-space is shown in Fig. 3.69. As follows from the calculation data (Table 3.11), the similarity function $q_0 = q(H/a)/q(0)$, taking into account the cone depth, is characterized at first by a rather sharp decrease (below $H/a \approx 50$), followed by a rather slow stabilization towards the limiting value at $H/a \to \infty$. Note that the volume compressibility has practically no effect on these tendencies. The dependence $q_0(\nu)$, obtained by approximation of the calculation data at high relative depth of the cone ($H/a = 1000$), is shown in Fig. 3.70. The formula

$$W = \frac{b_0 + b_1\nu + b_2\nu^2}{\pi E a} P\,, \tag{3.22}$$

found by numerical-and-analytical method, where $b_0 = 0.43808$, $b_1 = 0.51284$, $b_2 = -0.67609$, mean square error 2.6877×10^{-5}, can be treated as a kind of analogue of the Roben equation for the cone with the vertex angle $\alpha = 60°$. In case of necessity similar dependences can be without major difficulties also obtained for cones with different vertex angles and appear helpful for theoretical substantiation of issues concerning static probing by cone-shaped tips [44, 136].

The data of Table 3.11 and Eq. (3.22) are, in principle, quite sufficient to determine the deformation modulus with the account of depth correction for the standard cone with the vertex angle $\alpha = 60°$. Note that such angle is recommended for conical tips by European standard on probing. Meanwhile, the analytical expression of the dependence of q_0 on H/a can be helpful for the calculations. However, approximation of slowly decreasing functions of $q_0(H/a)$ type on a half-infinite interval is known to be a rather difficult problem to solve. For example, we have managed to

Table 3.11 Similarity function $q_0(\nu)$ values at different Poisson ratios and depths for a standard cone ($\alpha = 60°$)

z/H	$\nu = 0.2$	$\nu = 0.25$	$\nu = 0.3$	$\nu = 0.35$	$\nu = 0.4$	$\nu = 0.45$	$\nu = 0.5$
0	1.00000	1.00000	1.00000	1.00000	1.00000	1.00000	1.00000
1	0.81687	0.82181	0.82688	0.83197	0.83686	0.84116	0.84396
2	0.71404	0.72023	0.72629	0.73195	0.73666	0.73938	0.73729
3	0.66061	0.66715	0.67335	0.67885	0.68291	0.68412	0.67859
4	0.62916	0.63585	0.64209	0.64744	0.65109	0.65142	0.64400
5	0.60869	0.61547	0.62172	0.62699	0.63039	0.63018	0.62166
6	0.59437	0.60121	0.60748	0.61268	0.61592	0.61536	0.60614
7	0.58381	0.59069	0.59698	0.60214	0.60526	0.60448	0.59478
8	0.57571	0.58263	0.58893	0.59407	0.59711	0.59615	0.58612
9	0.56930	0.57626	0.58256	0.58769	0.59066	0.58958	0.57929
10	0.56411	0.57109	0.57741	0.58252	0.58545	0.58427	0.57379
15	0.54819	0.55526	0.56161	0.56669	0.56949	0.56804	0.55703
20	0.54005	0.54715	0.55352	0.55859	0.56134	0.55976	0.54852
30	0.53177	0.53892	0.54532	0.55038	0.55309	0.55139	0.53993
40	0.52758	0.53476	0.54117	0.54624	0.54892	0.54718	0.53561
50	0.52506	0.53225	0.53867	0.54374	0.54641	0.54463	0.53301
100	0.51997	0.52719	0.53364	0.53871	0.54135	0.53952	0.52779
200	0.51742	0.52466	0.53111	0.53617	0.53881	0.53696	0.52518
1000	0.51536	0.52262	0.52908	0.53415	0.53678	0.53489	0.52308

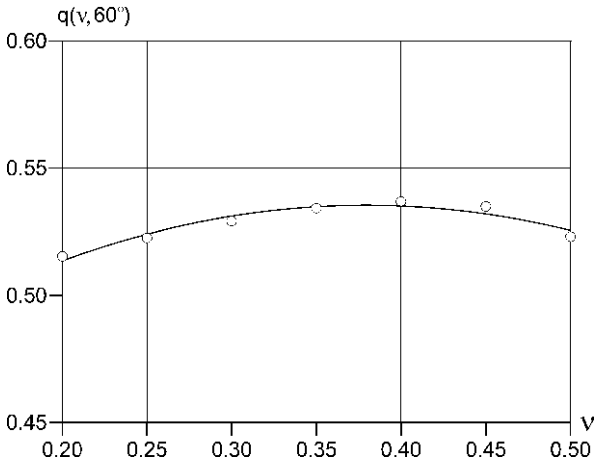

Fig. 3.70 Quadratic approximation of the function of similarity $q_0(\nu)$ for a standard cone ($\alpha = 60°$) at H/a=1000

approximate the dependence $q_0 = q_0(H/a)$ at $\nu = 0.35$, $1 \leq H/a \leq 200$ rather accurately (Fig. 3.71) only in logarithmic coordinates $X = \ln(1-H/a)$, $Y = \ln(1-q_0)$ using a 9-th order polynomial approximation

$$Y = a_0 + a_1 X + a_2 X^2 + a_3 X^3 + a_4 X^4 + a_5 X^5 + a_6 X^6 + a_7 X^7 + a_8 X^8 + a_9 X^9 \quad (3.23)$$

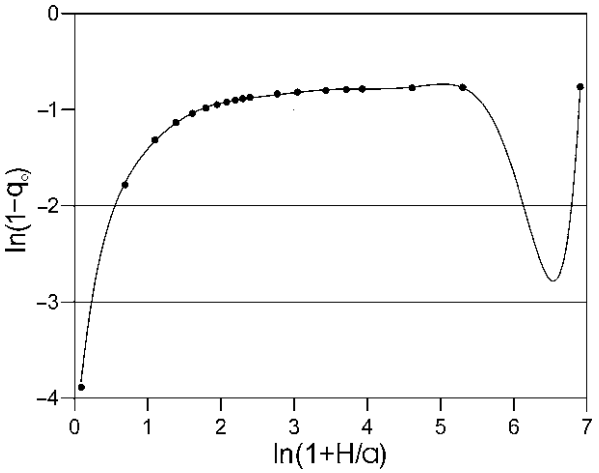

Fig. 3.71 Approximation of the function of similarity $q_0(H/a)$ for a standard cone ($\alpha = 60°$) in logarithmic coordinates; ν=0.35

where $a_0 = -4.6179$, $a_1 = 9.50151$, $a_2 = -13.9894$, $a_3 = 13.3122$, $a_2 = -8.08656$, $a_5 = 3.12577$, $a_6 = -0.761261$, $a_7 = 0.11267$, $a_8 = -0.00922487$, $a_9 = 0.000319464$, mean square error is 0.017685.

Though the approximation of Eq. (3.23) provides a good accuracy of approximation (Fig. 3.71), its practical application is not always effective due to computational difficulties. For the same reason hardly applicable is Shapery method [122], often used for approximation of slowly decreasing functions, where the approximation is performed by a set of a great number of exponents. Our calculation experience has shown a rather good effectivity (at fixed ν values) of interpolation of the considered dependences $q_0 = q_0(H/a)$ using cubic splines on the base of a numerical algorithm, proposed in [45] and implemented in a Fortran routine `SPLINE`. This approach can be especially convenient for numerical calculations with direct application of the data of Table 3.11. Finally, we show an example of our successful, in our opinion, approximation of the dependence $q_0 = q_0(H/a)$ (Table 3.11, $\nu = 0.35$), obtained based on a combination of two exponential splines [61]:

$$q(t) = q(0)\left[\left(1 - ct^{\alpha}e^{-\chi t}\right)h(t) - b\left(1 - e^{-\beta(t-\xi)}\right)h(t-\xi)\right],$$

where $h(t)$ is the Heaviside function, $t = H/a$, $b = 1-q(1000) = 0.46585$, $c = 0.1901$, $\alpha = 0.87511$, $\beta = 0.8689$, $\chi = 0.15545$, $\xi = 5.82654$. From Table 3.12 one can see a rather small discrepancy between the calculation data and the values of analytical expression of Eq. (3.24) (mean square error is 2.1489×10^{-3}).

Finalizing the analysis of solution of the contact problem for a deepened cone, note that application of the proposed boundary-element procedure of solving soatial contact problems for an elastic half-space has enabled an alternative (along with the application of flat punches) method of determination of the most important

Table 3.12 Approximation of the similarity function $q_0(\nu = 0.35, \alpha = 60°)$ by two exponential splines at various depths of a standard cone

z/H	BEM calculations	Spline approximation	δ (%)
0	1.00000	1.00000	0.0
1	0.83197	0.83727	0.64
2	0.73195	0.74449	1.71
3	0.67885	0.68812	1.37
4	0.64744	0.65659	1.41
5	0.62699	0.64264	2.49
6	0.61268	0.63456	3.57
7	0.60214	0.60549	0.56
8	0.59407	0.58532	1.47
9	0.58769	0.57174	2.71
10	0.58252	0.56302	3.35
15	0.56669	0.55524	2.02
20	0.55859	0.56208	0.63
30	0.55038	0.56238	2.18
40	0.54624	0.55238	1.12
50	0.54374	0.54387	0.02
100	0.53871	0.53434	0.81
200	0.53617	0.53415	0.38
1000	0.53415	0.53415	0.0

deformational characteristic of soil, the deformation modulus E, from the results of impression of deepened cones with different vertex angles [9, 10]. The obtained theoretical dependences are not much more complicated that the equations used in the procedure of standard examination by a test static load of experimental punches with a flat bottom [54, 95, 127, 136]; however, they have higher generality. In particular, a possibility of theoretically substantiated experimental studies for identification of deformational properties of materials based on the results of impression of different-angled (both acute-, and obtuse-angled) cones is being open. In our opinion, it will enable a fast and rather reliable determination of the deformation modulus of soils with different consistency, porosity and genetic type. Finally, the corrected values of the soil deformation modulus will result in higher reliability of determination of the calculated values of foundation settlements at construction of building and structures at various engineering-and-geological conditions.

The analysis of numerous examples, presented in this subsection, is a rather convincing evidence for the broad opportunities being opened by applying the boundary-element method to solve spatial contact problems. The test and model calculations, which we have performed using the *Rostwerk* software, have been compared with other results for the problems having analytical solutions or obtained by alternative approximate methods. Besides, high efficiency and reliability of the proposed boundary-element algorithms has been shown. These algorithms are characterized by module structure, low computation time and computer RAM requirements. In comparison with other popular numerical methods (e.g., finite-difference or finite-element methods which require discretization not only of the boundaries,

but also inside the calculation domains) the input data size has been considerably reduced and their preparation procedure has been simplified. Vast methodological calculations enable us to conclude on a good convergence of the numerical results and a sufficiently high for practical purposes accuracy of the boundary-element method even at piecewise constant approximation of the contact pressure field on the contact surfaces of rigid punches (at different depth). The possibilities of the boundary-element approach to be applied for spatial contact deformation studies are definitely shown, in particular, to perform structural analysis of rigid foundations from base deformations, to determine soil base deformation parameters, to calculate rigid anchor bearing plates of various plate depth.

References

1. Abramov V M (1939) Study of a case of asymmetric pressure of a punch of round cross-section on an elastic half-space. Dokl Akad Nauk SSSR 23(issue 8):759–763 (in Russian)
2. Aleinikov S M, Sedaev A A (1999) Dual grids and their application in the boundary-element method. Comput Math Math Phys 39:228–241
3. Aleksandrov A Ia, Solov'ev Iu I (1964) The solution of the three-dimensional axisymmetric problem in the theory of elasticity by means of line integrals. J Appl Math Mech 28:1106–1112
4. Alekseyev V M, Lipson G A, Mitrenko Yu A (1980) Study of the bearing capacity of pyramidal piles on a vertical load. In: Soil mechanics, bases and foundations. Voronezh State University, Voronezh, pp. 72–81 (in Russian)
5. Alekseyev V M, Lipson G A, Mitrenko Yu A (1984) Studies of bearing capacity of pyramidal piles under an inclined force. In: Studies of rational structures of foundations. Voronezh State University, Voronezh, pp. 17–24 (in Russian)
6. Alexandrov V M, Smetanin B I, Sobol B V (1993) Thin stress concentrators in elastic solids. Nauka, Moscow (in Russian)
7. Aleynikov S M (1996) Ring-shaped foundation with an internal cut-off circle. In: Calculation and design of bases and foundations at complex geotechnical conditions. VGASA, Voronezh, pp. 9–16 (in Russian)
8. Aleynikov S M (1997) Calculation of slotted foundations in spatial stress-strain state of soil base. In: Proc 14 Intern Conf Soil Mechanics and Found Eng (6–12 Sept. 1997, Hamburg), Balkema, Rotterdam, vol 1, pp. 629–632
9. Aleynikov S M (1998) Method for the determination of modulus of deformation. Patent 2145655, MPK6 E02D 1/00; G01N 3/42. No. 98117270/28 (Russia)
10. Aleynikov S M (1999) Deformation of deformation modulus from soil test data by indentation of a conical punch. In: Geotechnics-99. Proc Int. Conf. PGASA, Penza, pp. 9–12 (in Russian)
11. Aleynikov S M, Ikonin S V (1994) Design and calculation of ring-shaped foundation on variable-thickness bases. Energ Stroit (issue 11):66–70 (in Russian)
12. Aleynikov S M, Ikonin S V (1995) Calculation of inclined foundations for high-voltage power line metal supports from the base deformations. Energ Stroit (issue 3):63–66 (in Russian)
13. Aleynikov S M, Ikonin S V (1995) Foundation for tower building on tapered base. Patent 2043462 RU, MKI6 E 02 D 27/42. No. 92010566/33 (Russia)
14. Aleynikov S M, Ikonin S V (1996) Control of foundation shape and loading parameters to preserve uniform settlement. Commun Numer Methods Eng 12:745–754.

15. Aleynikov S M, Ikonin S V (1996) Prevention of nonuniform settlement of foundations. Build Res J 44 (issue 2):69–89
16. Aleynikov S M, Sedaev A A (1995) Algorithm of grid generation in the boundary-element method for flat domains. Mat Modelirovanie 7(issue 7):81–93 (in Russian)
17. Aleynikov S M, Sedaev A A (1998) Implementation of dual grid technique in BEM analysis of spatial contact problems. In: Numerical methods in continuum mechanics: Proc. 7th Intern. Conf. (High Tatras, Slovak Republic, 6–9 October 1998), pp. 113–118
18. Anan'ev I V, Andronov Ya L, Shlafman Sh M (1988) Three-dimensional problem of interaction between a rigid die and an inhomogeneous foundation. Mech Solids 23 (issue 3):76–79
19. Andronov Ya L (1985) Numerical solution of the spatial problem of the interaction of a rigid punch with a protrusion in the footing, with a nonhomogeneous base. Rostov Institute of Engineering, Rostov-na-Donu, VINITI No. 2631-85Dep (in Russian)
20. Antipov Yu A (1987) Exact solution of a problem of impression of a ring-shaped punch into a half-space. Doklady AN UkrSSR Ser A (issue 7):29–33 (in Russian)
21. Arkhipova E S, Protsenko V S, Rvachev V L (1974) Indentation in an elastic half-space of a plane, circular, inclined stamp. Int Appl Mech 10:567–573
22. Banerjee P K, Butterfield R (1981) Boundary element methods in engineering science. McGraw-Hill, New York
23. Baranov V S, Romanov D A, Romanov K D, Sidorchuk V F (1973) Investigation of the pressure distribution in the soil around piles with spherical enlarged bases. Soil Mech Found Eng 10:96–99
24. Barbakadze V Sh, Murakami S (1989) Calculation and design of engineering structures in deformable media. Stroyizdat, Moscow (in Russian)
25. Bartolomei A A (1994). Modern state and problems of pile foundation engineering. In: Proc. 4th Int. Conf. on Pile Foundation Engineering Problems. Pt 1. Improvement of methods of calculation and technology of pile foundations. PGTU, Perm, pp. 38–43 (in Russian)
26. Bartolomei A A, Pilyagin A V (1988) Stress-strain state of the beds of pyramidal pile foundations. Soil Mech Found Eng 25:136–140
27. Bartolomey A A, Ponomaryov A B, Yushkov B S (1994) Foundations of hollow conical piles. In: Bases and foundations in geological conditions of the Urals. PPI, Perm, pp. 13–17 (in Russian)
28. Bayer F L (1963) Optimally scaled matrices. Numer Math 5:73–87
29. Borodachev N M, Borodacheva F N (1966) Impression of a ring-shaped punch into an elastic half-space. Inzh Zh Mekh Tverd Tela (issue 4):158–161 (in Russian)
30. Borodachev N M, Tarikov G P (1972) Determination of the reaction pressure under a foundation by the electrical modeling method. Soil Mech Found Eng 9:428–429
31. Borodachev N M, Tarikov G P (1974) Solution of three-dimensional contact problems in elasticity theory by the method of electrical simulation. Mech Solids 9 (issue 3):84–87
32. Brebbia C A, Walker S (1980) Boundary element techniques in engineering. Newnes-Butterworths, London
33. Brebbia C, Telles J, Wrobel L (1984) Boundary element techniques. Springer-Verlag, Berlin
34. Bykov V I (1995) Foundations for individual residential buildings. Soil Mech Found Eng 32:66–68
35. Cherkasov I I (1976) Mechanical properties of soils in road engineering. Transport, Moscow (in Russian)
36. Cherkasov I I, Shvarev V V (1970) Basics of Moon soil studies. Nauka, Moscow (in Russian)
37. Egorov K E (1948) Deformation of the base of a round rigid foundation under an eccentric load. In: Bases and foundations. Issues of soil mechanics. Tr NIIOSP 11: 119–138 (in Russian)
38. Egorov K E (1958) On the issue of the base calculation under a foundation with a ring-shaped footing. In: Bases and foundations. Soil Mech Tr NIIOSP 34:34–57 (in Russian)
39. Egorov K E (1963) Indentation of a punch with a flat ring-shaped bottom into a half-space. Izv AN SSSR Mekh i Mashinostr (issue 5):187–196 (in Russian)

40. Egorov K E (1965) Calculation of bed for foundation with ring footing. In: Proc. 6th Intern. Conf. Soil Mech. Found. Eng., vol. 2, pp. 41–45
41. Eshelby J D (1957) The determination of the elastic field of an ellipsoidal inclusion and related problems. Proc R Soc Lond A 241:376–396
42. Eshelby J D (1959) The elastic field outside an ellipsoidal inclusion. Proc R Soc Lond A 252:561–569.
43. Faddeev D K, Faddeeva V N (1968) Problems of scaling for linear systems. In: Modern numerical methods: Proc Intern School on Numerical Methods (Kyiv). VC AN SSSR, Moscow, issue 1, pp. 76–84 (in Russian)
44. Ferronskii V I (1969) Penetration and carotage methods of engineering and geological studies. Nedra, Moscow (in Russian)
45. Forsythe G E, Malcolm M A, Moler C B (1977) Computer methods for mathematical computations. Prentice-Hall, Englewood Cliffs
46. Galanov B A (1981) Approximate solution of some problems of elastic contact between two bodies. Mech Solids 16(issue 5):61–67
47. Galin L A (ed.) (1976) Development of theory of contact problems in the USSR, Nauka, Moscow (in Russian)
48. Giannakoglou K C, Chaviaropoulos P, Papailiou K D (1994) A numerical structured grids of desired properties, on complex 3-D surfaces. Proc. 2nd ECCOMAS Conf. Stuttgart (Sept. 5–8, 1994), pp. 701–710
49. Giannakoglou K C, Chaviaropoulos P, Papailiou K D (1996) Boundary-fitted parameterization of unstructured grids on arbitrary surfaces. Adv Eng Software 27:41–49
50. Glotov N M, Luga A A, Silin K S et al. (1975) Pile foundation. Transport, Moscow (in Russian)
51. Godunov S K, Antonov A G, Kirilyuk O P et al. (1988) Guaranteed accuracy of solving linear equation systems in Euclid spaces. Nauka, Novosibirsk (in Russian)
52. Godunov S K, Zabrodin A V, Ivanov M Ya et al. (1976) Numerical solution of multidimensional problems of gas dynamics. Nauka, Moscow (in Russian)
53. Goncharov B V, Yenikeyev A Kh, Kogan V L (1991) Slotted foundations in tamped pits. In: Pile foundations. Stroyizdat, Moscow, pp. 87–90 (in Russian)
54. GOST 20276-85 (1985) Soils. Methods of field determination of deformability characteristics. Standard Publishers, Moscow (in Russian)
55. Gotman A L (1987) Analysis of tapered piles under combined action of vertical, horizontal, and flexural loads. Soil Mech Found Eng 24:7–12
56. Gubenko V S, Mossakovskii V I (1960) Pressure of an axially symmetric circular die on an elastic half-space. J Appl Math Mech 24:477–486
57. Gubenko V S, Nakashidze G M, Pyatovolenko V G (1986) Exact solution of the problem of a ring-shaped punch. Dokl AN UkrSSR Ser A (issue 3):40–44 (in Russian)
58. Gulyayev V I, Bazhenov V A, Gotsulyak Ye A et al. (1990) Calculation of complex-shaped shell. Budivelnyk, Kyiv (in Russian)
59. Harary F (1969) Graph theory. Addison-Wesley, Reading
60. Ikramov Kh D (1988) Numerical methods for symmetrical linear systems. Nauka, Moscow (in Russian)
61. Ilyin V P, Maltsev L Ye, Sokolov V G (1991) Calculation of engineering structures of viscoelastic materials. Stroyizdat, Leningrad (in Russian)
62. Instructions on design of foundations for machines subject to dynamic loads (1982) Gersevanov NIIOSP, Stroyizdat, Moscow (in Russian)
63. Instructions on design of pyramidal pile foundations (1983) Glavn Upr Project Organiz, Moscow (in Russian)
64. Ivanenko S A (1993) Adaptive grids and grids on surfaces. Zh Vychisl Matem Matem Fiz 33:1333–1355 (in Russian)
65. Ivanenko S A, Prokopov G P (1997) Methods of adaptive harmonic grid generation. Comput Math Math Phys 37:627–645 (in Russian)

66. Joe B (1986) Delaunay triangular meshes in convex polygons. SIAM J Sci Stat Comput 7: 514–539
67. Johnson K L (1985) Contact mechanics. Cambridge University Press, Cambridge
68. Kalinnikov A Ye, Yefremov S M, Vakhrushev F V (1985) Algorithm for automatic mesh of a two-dimensional domain for solving contact problems by boundary-element method. Probl Prochnosti (issue 2):106–108 (in Russian)
69. Kalitkin N N (1978) Numerical methods. Nauka, Moscow (in Russian)
70. Kapshivyi A N, Maslyuk G F (1967) The solution of the mixed axisymmetric problem from the theory of elasticity for a half-space by the method of p-analytical functions. Int Appl Mech 3 (issue 7):13–16
71. Kazarnovskii I I (1997) Experience of design of monolithic foundations for contact-line supports. Transp Stroit (issue 7):21–23 (in Russian)
72. Khazin V I (1984) Foundation structures for rural buildings on short pyramidal piles. Budivelnyk, Kyiv (in Russian)
73. Khilobok V G, Yudin A V (1984) On some specific features of functioning of asymmetric wedge-shaped piles. In: Study of rational design of foundations. Voronezh State University, Voronezh, pp. 78–81 (in Russian)
74. Klein G K, Cherkasov I I (1985) Foundations of urban transport structures. Stroyizdat, Moscow (in Russian)
75. Klemyatsionok P L (1987) Indirect methods of determination of parameters of soil properties. Stroyizdat, Leningrad (in Russian)
76. Klemyatsionok P L (1994) Obtaining and studies of theoretical balance dependences of the penetration method of determination of soil deformation modulus. In: Reliability of bases for transport structures. SPBGUPS, St. Petersburg, pp. 41–48 (in Russian)
77. Konovalov P A (1988) Soil bases and foundations of buildings under reconstruction. Stroyizdat, Moscow (in Russian)
78. Kornishin M S, Paymushin V N, Snigiryov V F (1989) Computational geometry in the problems of shell mechanics. Nauka, Moscow (in Russian)
79. Kosorukov I I (ed.) (1974) Pile works. Vysshaya Shkola, Moscow (in Russian)
80. Kryukov K P, Kurnosov A I, Novgorodtsev B P (1975) Construction and design of metal and ferroconcrete power line supports. Energiya, Leningrad (in Russian)
81. Kupradze V D, Gegeliya T G, Basheleyshvili M O, Burchuladze T V (1979) Three-dimensional problems of the mathematical theory of elasticity and thermoelasticity. North-Holland, Amsterdam
82. Kuzma I, Nikitenko M I (1984) Experimental studies of slotted foundations for the supports of high-voltage lines. Soil Mech Found Eng 25:176–180
83. Kuznetsov A Yu (1990) Algorithm of construction of two-dimensional triangulation. preprint VC SO AN SSSR No. 909, Novosibirsk (in Russian)
84. Lapshin F K (1986) Baes and foundations in diploma project design. Saratov State University, Saratov (in Russian)
85. Levachev S N, Fedorovskiy V G, Kurillo S V, Kolesnikov Yu M (2002) Piles in hydrotechnical engineering. Balkema, Rotterdam
86. Liseykin V D (1991) Technology of construction of three-dimensional grids for aeromechanical problems. In: Vopr Atom Nauki Tekhn Ser Mat Modelirovaniye Fiz Protsessov 31:1670–1683 (in Russian)
87. Liseykin V D (1996) Review of methods for construction of structural adaptive grids. Zh Vychisl Mat Mat Fiz 36: 3–41 (in Russian)
88. Luchinskiy I A, Maliy E Yu, Povolotskaya I R, Ostrovskiy B S (1992) Foundation. USSR Authors' Certificate 1758169, MKI5 E 02 D 27/04, 27/44. No. 4737430/33 (in Russian)
89. Lupan Yu T, Klemyatsionok P L (1988) Tests of soils by penetration and combined probing. UMK VO UkrSSR, Kyiv (in Russian)
90. Lur'e A I (1964) Three-dimensional problems in the theory of elasticity. Interscience, New York

91. Lur'e A I (1967) Elastostatic Roben problem for a triaxial ellipsoid. Inzh Zh Mekh Tverd Tela (issue 1):80–83 (in Russian)
92. Lur'e A I (1970) Theory of elasticity. Nauka, Moscow (in Russian)
93. Molchanov I N (1987) Machine methods for solution of applied problems: algebra and approximation of functions. Naukova dumka, Kyiv (in Russian)
94. Muki R (1960) Asymmetric problems of the theory of elasticity for a semi-infinite solid and a thick plate. In: Sneddon I N and Hill R (eds.). Progress in solid mechanics. North-Holland, Amsterdam, vol. 1, pp. 399–439
95. Ogranovich A B (1993) On the issue of determination of soil deformation modulus from punch test data. Izv Vuzov Stroit (issue 10):129–131 (in Russian)REF>
96. Olesiak Z (1965) Annular punch on elastic semi-space. Arch Mech Stosow 17: 633–648
97. Ovsyannikov A S, Starikov V A (1989) Method of superposition of singular solutions in axially symmetrical problems of theory of elasticity. Naukova dumka, Kyiv (in Russian)
98. Pavlov V V (1992) Slotted foundation of buildings. Stroyizdat, Krasnoyarsk (in Russian)
99. Pavlov V V, Katsov K P, Smorodinov M I (1992) Slit foundations of industrial and civic buildings in the middle Urals. Soil Mech Found Eng 29:140–143
100. Perley Ye M (1969) Tubular ferroconcrete piles for industrial and civil engineering. Stroyizdat, Leningrad (in Russian)
101. Piskunov V G, Prisyazhnyuk V K (1985) Calculation of nonhomogeneous plates on a nonhomogeneous half-space. Stroit Mekh Raschet Sooruzh (issue 1):25–28 (in Russian)
102. Plevkov V S, Polishchuk A I (1990) Size determination of off-centre loaded foundations of various geometrical shape. TPI, Tomsk (in Russian)
103. Podilchuk Yu N (1979) Three-dimensional problems of theory of elasticity. Naukova Dumka, Kyiv (in Russian)
104. Podilchuk Yu N (1984) Boundary problems of statics of elastic bodies. Naukova Dumka, Kyiv (in Russian)
105. Popov G Ya (1982) Concentration of elastic stress near punches, cuts, fine inclusions and supports. Nauka, Moscow (in Russian)
106. Preparata F P, Shamos M I (1985) Computational geometry: an introduction. Springer-Verlag, New York
107. Rabinovich I M (1961) On the problem of calculation of statically undetfinable systems with unilateral constraints (proof of the uniqueness of the solution). In: Gvozdev A A (ed.) Studies in theory of structures, Gosstroyizdat, Moscow, issue 10, pp. 163–169 (in Russian)
108. Rabinovich I M (1975) Problems of theory of static calculation of structures with unilateral constraints. Stroyizdat, Moscow (in Russian)
109. Recommendations on the calculation of bases under foundations with an inclined bottom (1983) Gersevanov NIIOSP, Moscow (in Russian)
110. Reznikov R A (1971) Solving problems of engineering mechanics using a computer. Stroitelstvo, Moscow (in Russian)
111. Rvachev V L, Protsenko V S (1970) On the structure of solution of a contact problem with an inclined punch. Dokl AN UkRSSR Ser A 11:1023–1026 (in Russian)
112. Rvachev V L, Protsenko V S (1977) Contact problems of theory of elasticity for nonclassical domains. Naukova Dumka, Kyiv (in Russian)
113. Rybin V S (1990) Design of foundations of buildings under reconstruction. Stroyizdat, Moscow (in Russian)
114. Sabonnadière J-C, Coulomb J-L (1986) La méthode des éléments finis. Du modèle... a la CAO. Hermes, Paris – Londres – Lausanne
115. Sakalo V I, Shkurin A A (1985) Universal program for triangulation of a two-dimensional domains of an arbitrary shape with grid condensations. Probl Prochn (issue 1):106–108 (in Russian)
116. Samarskiy A A, Gulin A V (1989) Numerical methods. Nauka, Moscow (in Russian)

117. Savchenko F M, Oding B S (1988) Economically efficient foundations under strutted structures of agricultural buildings. In: Pile foundation studies. Voronezh State University, Voronezh, pp. 162–167 (in Russian)
118. Savinov O A (1979) Modern design of foundations under machines and their calculation. Stroyizdat, Leningrad (in Russian)
119. Sazhin V S, Shishkin V A, Zhanalinov B N (1991) Design and technology of erection of foundations on heaving soils. Gylym, Almaty (in Russian)
120. Segerlind L J (1976) Applied finite element analysis. J. Wiley & Sons, New York
121. Selvadurai A P S (1994) On the problem of a detached anchor plate embedded in a crack. Int J Solids Struct 31:1279–1290
122. Seo T, Mura T (1979) The elastic fields in half space due to ellipsoidal inclusions with uniform dilatational eigen-strains. Trans ASME J Appl Mech 46:568–572
123. Shabrov N N (1983) Finite-element method in calculation of details of heat engines. Mashinostroyenie, Leningrad (in Russian)
124. Shapery R A (1962) Approximate methods of transform inversion for viscoelastic stress analysis. In: Proc. 4th US Nat. Congr. Appl. Mech. ASME, New York, vol. 2, pp. 1075–1085
125. Shibuya T, Koizumi T, Takakuda K, Takagi T (1982) Partial contact problem of an elastic half-space pressed aslant by a circular rigid punch. Bull JSME 25:1366–1372
126. Shishov O V (1971) Contact problem for axisymmetrical deepened punches. In: Resistance of materials and theory of structures. Budivelnyk, Kyiv 13:60–66 (in Russian)
127. Shvets V B, Lushnikov V V, Shvets N S (1981) Determination of engineering properties of soils: handbook. Budivelnyk, Kyiv (in Russian)
128. Sidorov N N, Sipidin V P (1972) Modern methods of determination of characteristics of mechanical properties of soils. Stroyizdat, Leningrad (in Russian)
129. Solovyov L Yu, Solovyov Yu I (1995) Distribution of stress at the action of a circular punch on an elastic half-space. Izv Vuzov Stroit (issue 9):22–26 (in Russian)
130. Sorochan E A (1986) Foundations of industrial buildings. Stroyizdat, Moscow (in Russian)
131. Sorochan E A, Trofimenkov Yu G (ed.) (1985) Bases, foundations and underground structures: designer's handbook. Stroyizdat, Moscow (in Russian)
132. Sorochan E A, Piven V G, Rybnikov A M (1991) Monolithic foundations with an effective lateral surface. Soil Mech Found Eng 28:99–102
133. Spekreijse S P, Boerstoel J W, Kuyvenhoven J L, Van der Marel M J (1992) Surface grid generation for multi-block structured grids. Comput Fluid Dynam 2:937–944.
134. Studies of interaction of wedge-slotted foundations (double wedge) with a nonhomogeneous loess base (1989) Research report. Rostov Institute of Engineering, Rostov-na-Donu (in Russian)
135. Telezhnikov V Ye (1956) Foundations under the equipment of small and medium power plants. RSFSR Ministry of Public Service Publishers, Moscow (in Russian)
136. Trofimenkov Yu G, Vorobkov L N (1981) Field methods for the studies of constructive properties of soils. Stroyizdat, Moscow (in Russian)
137. Tsybenko A S, Lavrikov S A (1984) Direct symmetrical formulation of the method of boundary integral equations. Probl Prochn (issue 11):48–50(in Russian)
138. Ufliand Ya S (1977) The dual equation method in the problems of mathematical physics. Nauka, Leningrad, 219pp. (in Russian)
139. Ugodchikov A G, Khutoryanskiy N M (1986) Boundary-element method in mechanics of deformable solids. Kazan State University, Kazan (in Russian)
140. Ukhov S B, Semenov V V, Znamenskii V V et al. (1994) Soil mechanics, bases and foundations. Association of Engineering Institutions, Moscow (in Russian)
141. Valov G M (1968) Infinite elastic layer and half-space under the action of a ring-shaped die. J Appl Math Mech 32:917–930
142. Valov G M (1989) Method of solving the main mixed problem of theory of elasticity for a half-space with circular line of separation of boundary conditions. In: Applied problems of

strength and elasticity. Methods of solution. Gorkiy Technical University, Gorkiy, pp. 77–82 (in Russian)
143. Vershinin V P, Kovalev I P, Chelnokov Ye L (1978) Bored pile foundations with support widenings. Stroyizdat, Leningrad (in Russian)
144. Vladimirov V S (1976) Generalized functions in mathematical physics. Nauka, Moscow (in Russian)
145. Warsi Z U A (1986) Numerical grid generation in arbitrary surfaces through a second-order differential-geometric model. J Comput Phys 64:82–96
146. Werno M (1994) Statecznosc platformy Petrobaltic. In: Geotechnika w inzynierii wodnej i ladowej. Gdansk, pp. 35–44
147. Wet J (1966) Application of energy hypothesis in soil mechanics. In: Soil mechanics and foundation engineering. Proc 5th Intern Conf. Stroyizdat, Moscow, pp. 105–114 (in Russian)
148. Yakupov N M, Serazutdinov M N (1993) Calculation of elastic thin-walled structures of complex geometry. KNC, Kazan (in Russian)
149. Yeltsov Yu A (1991) Studies of soil with indentors. Izhevsk mechanical Institute, Izhevsk (in Russian)
150. Yeltsov Yu A (1993) Mechanics of effect of indentors on soil. Udmurt University, Izhevsk (in Russian)
151. Yu H Y, Sanday S C (1990) Axisymmetric inclusion in a half space. Trans ASME J Appl Mech 57:74–77
152. Zabylin M I, Linovskii S V, Nuzhdin L V (1991) Design of pile foundations under machines. NISI, Novosibirsk (in Russian)
153. Zhukov N V, Dondysh A M, Pogosyan Z G et al. (1972) Short piles in rural engineering. ONTI CNIIEPSelstroy, Moscow (in Russian)
154. Zienkiewicz O C, Kelly D W, Bettess P (1977) The coupling of the finite element method and boundary solution procedures. Int J Num Method Eng 11:355–375

Chapter 4
Contact Interaction of Shallow Foundations with Nonhomogeneous Bases

Abstract In the fourth chapter the results of the boundary-element solutions of spatial contact problems for complex-shaped punches, located on the surfaces of elastic nonclassical bases, are analyzed. The problems under consideration correspond to the modeling of contact interaction of shallow foundations with elastic nonhomogeneous bases. Contact pressure fields under punches of various shape under an eccentric load (a contact problem on a strongly inclined punch) are obtained. The influence of non-uniform (over the area) compressibility as well as depth-dependent nonhomogeneity of the base deformational properties on the formation and development of detachment zones, settlements and slopes of punches with the increase of the absolute values of overturning moments is shown. An algorithm to calculate the boundaries of the section core for rigid complex-shaped foundation plates from the stress values is described. Some optimization problems are solved for load and shape parameter control in order to provide uniform settlement of rigid foundation. As an example for the application of the developed boundary element method, a contact problem is solved and the elastic base stress-strained state is determined for a rigid strip foundation of variable width. In the same chapter a spatial contact model of the base is built taking into account nonlinear elastic soil properties. A procedure for the model parameter characterization based on the direct punch test data is considered. Finally, the chapter contains the studies of contact problems of bending of orthotropic plates situated on elastic nonclassical bases, performed by BEM combined with finite difference method.

Foundations with small ratio of the depth to the width (the smaller side) of the bottom are called shallow foundations. A characteristic feature of shallow foundations is load transfer to the soil mostly through their bottom [258, 269]. Therefore, at the calculation of shallow foundations, their depth is neglected and the calculation scheme for a foundation, located on the base surface, is used. Besides, in order to simplify the calculations for the most of shallow foundations, the latter are considered not as a rigid body (punch) on a natural base whose properties are determined by the chosen mechanical model of the soil. If the knowledge of the average settlement of the structure is sufficient and the calculation of the foundation strength is not required, then the distribution of reactive pressures under its bottom has no

S.M. Aleynikov, *Spatial Contact Problems in Geotechnics*, Foundations of Engineering Mechanics, DOI 10.1007/b11479_4,

special importance and load transfer to the soil can be considered as a distributed load, i.e. using the calculation scheme for a flexible punch. If an economical design solution for foundation structures of steel and reinforce concrete is required, the issue of reactive pressure distribution becomes very important since the determination of bending moments and shearing forces in the foundation structures depends on its solution. Various models of soil bases being used as well as a representation of the foundation as a rigid punch enable the slopes of the structures to be determined and, the forces in the foundation structures to be assigned more reasonably, though with a certain allowance, after the contact problem of the soil mechanics having been solved. Note that the foundation of a structure can be treated as a rigid body in case the main condition being fulfilled: the foundation deformations should not make a noticeable effect on the base deformations.

Shallow foundations on a natural base are the most widely spread in our country and constitute about 75% of the gross volume of the foundation engineering. For their construction annually about 40 million m^3 of concrete; 11.9 million tons cement, 1.69 million tons metal are spent. The costs of their construction in 1992 was estimated as about 4.4 billion roubles [197, 257]. Hence, the rational solution for a foundation essentially determines the cost of its construction and, therefore, the reduction of materials consumption for shallow foundations is an important economic problem.

Design of shallow foundations (free-standing, plate foundations, etc.) is a rather complicated and labour-consuming problem, especially under several combinations of loads. The main stages in this case are the choice of the foundation depth, determination of its bottom dimensions, determination of pressures over the bottom, calculation of the foundation settlements and their nonuniformities, calculation of the foundation strength etc. The calculation of off-centre loaded shallow foundations (taking into account their rigidity and using modified base models) is rather complicated, especially in the case of a complicated foundation shape. At present such calculations are performed in a rather approximate way, the solutions being often ambiguous what not always provides the choice of economical solutions. A particular uncertainty is induced by an assumption of a linear distribution of contact forces over the foundation bottom [124, 162, 197, 226, 249]. Many important features of engineering-and-geological conditions (in particular, non-uniform compressibility of the base) that are rather essential for large-size foundations, are not taken (or practically not taken) into account. In this chapter we apply the algorithm of calculation of settlements, slopes and contact pressures over the bottom of centrally and off-centre loaded separate shallow foundations of various geometrical shape, considered in Sect. 2.5. The developed method is shown to enable not only the contact stress distribution features, displacements and slopes for foundations, loaded by a spatial force system of a general type to be studied in detail (Sects. 4.2, 4.4 and 4.6, Appendix B), but also important practical problems related to the determination of section kernels of complex-shaped foundations to be solved (Sect. 4.5). The section kernel boundaries are a convenient geometrical characteristic of the foundation stability under various technical and geological conditions. The proposed boundary-element approach combined with intentionally developed procedures of

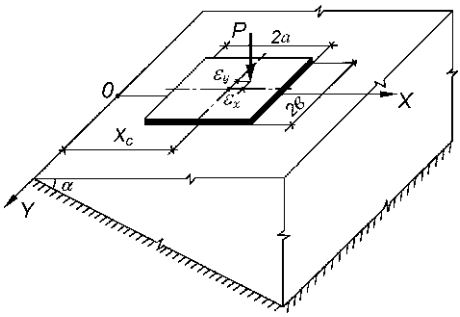

Fig. 4.1 Calculation scheme for a rectangular punch on a variable-thickness elastic layer

shape and load parameter control provides design solutions on uniform settlement of shallow foundations at the conditions of the spatial stress-strained state of the base (Sect. 4.3). Using the developed semi-empirical models of contact deformation, the elaborated boundary-element algorithm enables the deformations of natural and artificial bases of structures and buildings to be predicted with the account of nonlinear properties of soils (Sect. 4.6). Combination of boundary-element and finite-difference methods has enabled contact problems of bending of orthotropic foundation plates of finite rigidity, resting on soil bases, to be effectively solved in the framework of elastic non-classical models (Sect. 4.7). At various type of loading and boundary conditions at the plate contours the effect of the plate material orthotropy degree on the stress-strained state of the plates (on the deflections, shearing forces, bending moments and torques) is determined. Elastic layers of constant or variable thickness (Fig. 4.1) as well as an elastic half-space with deformation modulus, increasing with depth, are used as models for the soil bases. The latter case corresponds to the interaction of foundation structures with real soil bases, nonhomogeneous both over the area and in depth [86]. Due to a convenient module structure of the software developed for the elaborated numerical algorithm, the use of influence functions for any of the known models of linearly deformable base of non-classical type does not result in any substantial difficulties and can lead only to the total computation time increase.

Before considering special issues, the chapter begins with a review of main studies devoted to the solution of spatial contact problems for rigid flat-bottom punches and directly related to the foundation construction problems (Sect. 4.1).

4.1 Spatial Contact Problems for Rigid Flat-Bottom Punches

The problem of contact pressure distribution over the foundation bottom of various shape is of high practical importance, especially when their dimensions are being assigned and the foundation plate reinforcement is determined.

At present, two-dimensional (planar and axisymmetric) problems are solved rather successfully, contrary to the three-dimensional solutions which are very rare

[8, 92, 98, 99, 117, 128, 159, 160, 203, 205, 225, 278]. Meanwhile, it is well known [194] that for a number of geotechnical problems the approximations of flat deformation and axially deformed stress-strained state will not correspond to the real interaction pattern in the "foundation – soil base" system, or they will lead to unreasonably high allowances. First of all, among such problems there are calculations of foundation bases of rectangular or more complex (e.g. polygonal) shape of solid plate type under buildings and structures, roads as well as foundations under machines and equipment etc. [121, 123, 125, 197, 226, 257]. Therefore, the development of the corresponding spatial solutions is of considerable interest to substantiate economical technical solutions.

Experimental studies. An all-round experimental study of the mechanism of interaction of foundation models and soil bases is a rather complicated problem requiring the improvement of the experimental technique, its automation, processing of the measured data [178]. As a result, at the present stage of development of soil mechanics and foundation engineering experimental studies strongly lag behind theoretical investigations. Simultaneously, along with the difficulties in using new experimental techniques, carrying out expensive and labour-consuming experiments, the development of the experimental studies is hindered by a practically total absence of strict theoretical solutions of essentially spatial problems of mechanics of continuous media. The presence of such solutions enables the measurement accuracy to be estimated and the experiment to be planned more substantially, the measurement gauges to be located, the correspondence of the boundary conditions for the experiment and theory to be determined, etc.

The available experimental data on the spatial distribution of contact pressures, obtained from field and laboratory studies, often results to disputable and even contradictory conclusions [72, 83, 96, 144–147, 177, 178, 264]. In most cases the experimental studies enable the data to be obtained only for the specific conditions which can be extended to other cases only with great precaution. It is mostly explained by the use of different measurement techniques. In order to compare the data of different experiments, the size and shape of the foundation models should be determined from the similarity conditions and the experimental data processing should be performed in the same way. At the present stage of development of the experimental techniques one should consider the most reliable the data obtained at symmetrical loading under a rigid circular or rectangular punch, for which rather detailed studies have been performed concerning the contact stress profile transformation with load increase, the distribution of stresses and their invariants in the soil mass, the base deformation along the punch axis in horizontal and vertical directions, compressible soil mass depth, corresponding to the depth of the sand base density variation range.

Besides the field and laboratory experimental studies, a certain progress in the description of the processes of spatial contact interaction of foundations with soil bases can be achieved by the method of mathematical analogies. The contact problems possess a certain similarity with the problems of electrostatics. From this point of view one should mention the studies of Borodachev and Tarikov [45, 46] where the results of the experimental solution of spatial contact problems of theory of

elasticity for complex-shaped punches are given using electrical modelling. In such approach the problem of determination of the reactive pressure under the punches in accordance with the similarity of partial differential equations is reduced to a problem of determination of charge density on an electrically conductive plate with a shape of the punch base. After an additional mathematical processing of the experimental data by least-square method, the distribution of the reactive pressure under the punches at their translational motion due to the vertical force, applied at the punch gravity centre, is found. In all cases under consideration the contact area was supposed to coincide with the flat area of the punch base. The effect of cutout in the bases of punches of polygonal shape is studied. The electric modelling method has an advantage over other (direct) experimental methods due to its high stability; meanwhile the measurement accuracy is sufficient for the practical engineering purposes. Nevertheless, the electric modelling of contact interaction can be realized yet only in the framework o the elastic half-space model as well as at the conditions of direct contact of the punch with the base. Although practical problems of determination of reactive pressure under punches (foundations) of rather complex shapes can be solved, the experiments carried out by this method are still expensive and labour-consuming.

In spite of the great scope of the experimental studies having been performed, a number of issues still remain unsolved, regarding experimental procedures for the studies of essentially spatial processes of deformation of soil masses under foundations. In particular, this concerns experimental studies devoted to the contact pressure distribution over the punch foundation bottom under an off-centre load. The scope of these studies having been performed so far, is still insufficient [145, 178, 197]. This is one of the reasons for the fact that in practical design (according to the valid regulations [124, 162, 197, 226, 258]) under an off-centre load the shape of the contact pressure profiles is simplified and for separate foundations is assumed to be linear. Depending on the load application eccentricity, rectangular, triangular, or trapezoidal type profiles are used. Note that in a number of situations the reactive pressure distribution scheme can be used only as a tentative one, mostly for the rectangular-shape foundations.

Exact analytical solutions. The analysis of numerous literature sources has shown that the contact pressure distribution over a rigid foundation bottom depends on the bottom shape, load application eccentricity value, nonuniformity degree and many other factors. In practical design preference is given only to such calculation models of soil bases, the use of which enable the theoretical law of contact pressure distribution to be obtained. The main calculation models of soil bases, for which the greatest number of theoretical solutions have been obtained and which to a sufficient extent provide an adequate description of spatial functioning of shallow foundations, are an elastic half-space and a finite-thickness layer.

The known exact analytical solutions of spatial contact problems for a linearly deformed half-space have been built mostly for circular, elliptical and ring-shaped punches. Note that the necessity of the contact problem solution for the circular and ring-shaped punches is caused by the wide application of circular and ring-shaped

foundations under tower-type structures (funnels, cooling towers, water towers, TV towers, etc.) in engineering.

The most effective solution has been obtained for the problem of a circular punch, being impressed without friction into an elastic half-space. Boussinesq was the first to solve the problem of a rigid circular punch impression by a central force [55]. He obtained a formula to determine the pressure under the punch:

$$p(r) = \frac{P}{2\pi a\sqrt{a^2 - r^2}}, \quad r = \sqrt{x^2 + y^2} < a$$

where a is the punch radius, r is the distance from the punch centre to the observation point, P is a force, acting on the punch. This formula was the first to show the general law of the contact pressure being unlimited near a fixed smooth boundary of a contact domain. Boussinesq has not determined the stress-strained state in the internal points of the elastic base. Such study for an axisymmetric case was performed by Dinnik [71]. In particular, he has shown a fact, very important for the strength calculations, that the maximal tangential stress is reached under the punch at a distance from the half-space surface, approximately equal to half radius of the contact area. Much later Egorov and Shelest [81] have given the full pattern of the stress-strained state in an elastic half-space under a centrally loaded round foundation in the form of isolines of vertical and horizontal displacements as well as tangential and normal stresses. Comparison with the corresponding results for a flexible foundation has shown an essential effect of the foundation rigidity and the Poisson ratio of the soil upon the stress-strained state of the base, mostly near the half-space surface. The obtained formulae for the displacement and stress components were concluded to be very useful for the design of bases under tower-type structures (cooling towers, funnels, reservoirs, etc.).

Leonov [153] and Mossakovskii [170, 171] have solved the problem of pressure of a circular punch on an elastic half-space in the most general formulation already in 1953, the expressions for the contact pressure having been obtained in a closed form – as integral-differential operators from given functions.

This problem has been further considered mainly with the aim to obtain the results in a more convenient form, more suitable for computations, as well as to evaluate the efficiency of methods being used to solve contact problems. Detailed reviews of studies regarding the spatial contact problem for round punches and for different equations of the punch bottom were published in a book [99] and a topical review [174]. The analysis of the studies of the problem of a round punch being impressed without friction into an elastic half-space, has shown that at present this problem is fully studied. For a punch with a polynomial base the problem solution is expressed in elementary functions. Such solution is a convenient object to estimate the efficiency of approximate methods, aimed at the investigation of more complicated contact problems with non-canonical contact domains and for non-classical bases. Most of the contact problem solutions quoted in [99, 174] are applicable for flat-bottom punches, which to the greatest extent correspond to shallow foundation structures design.

In the overwhelming majority of the investigated contact problems the lack of friction forces between the punch and the half-space is assumed. In a rather recent paper [256], based on the spatial problems of theory of elasticity solved using analytical functions of a complex variable [8], the solution of the contact problem for a rigid punch, fully coherent with an elastic half-space, is analyzed. The studies of the stressed state inside the half-space and under the bottom of the punch subject to a pressing force and a displacive force as well as an overturning moment, have been carried out. The effect of contact stress oscillation in the vicinity of the punch edge (similar to the Abramov effect [1] in the planar problem), typical for the contact problems of linear theory of elasticity with the account of the friction forces has been studied. Due to the complicated character of the formulae in the obtained solution, they were treated using numerical integration.

Lur'e [159, 160] has performed analytical studies of asymmetrical pressure of rigid planar punches of circular and elliptical cross-section, completely adjacent to the elastic half-space.

Relatively recently exact solutions of the contact problem of a centrally loaded ring-shaped punch (or action of a hollow circular cylinder on a half-space) were obtained [25, 113]. For this problem the exact solution in [113] is expressed in terms of a sequence of powers of infinite-measure matrix, while in [25] the solution is found as a dual series, for its coefficients explicit formulae having been obtained. The results of both works [25, 113] have mostly a pure theoretical significance, since their application requires rather complicated computations.

The book by Rvachev and Protsenko [225] describes exact solutions of spatial contact problems of an infinite stripe punch and a system of infinite stripe punches, located on an elastic half-space, obtained as improper integrals of series over Mathieu functions. It is shown that the problem of a punch, whose cross-section is restricted by two osculant circles, can be reduced by Kelvin transformation to the problem of a stripe-shaped punch. The same book also quotes the exact solution for a spatial problem of a simultaneous contact of a system of stripe-shaped punches with a combined elastic Shtayerman base [245], being a combination of the elastic half-space model with the Winkler model. In spite of the obtained formulae for the contact pressure function being rather complicated, the application of the combined base model enables the character of the contact pressure distribution to be preserved similarly to the case of the elastic half-space; however, in this case their values at the punch edges are not restricted.

Thus, the known exact solutions of the contact problems are obtained for particular, relatively simple domains and classical base models under full contact. The methods being used for this purpose settle upon a classical mathematical apparatus – theory of potential, Fourier method, integral transformations, integral equations, solution of infinite systems of algebraic equation and some others. Solution of almost each type of the problems requires a high qualification of the researcher, enabling considerable mathematical difficulties to be overcome. As a result, for practical purposes engineers use only few analytical solutions, the most simple from the computational point of view [92, 117, 205, 258].

Approximate analytical solutions. Due to the difficulties of solving spatial contact (mixed) problems of theory of elasticity, the possibilities of construction of their exact analytical solutions without introducing simplifying assumptions regarding the geometrical (circular and elliptical line of separation of boundary conditions) and mechanical (isotropic and homogeneous medium) parameters are rather limited. Therefore, most of the studies of spatial contact problems now are related to the construction of various approximate solutions.

A mixed boundary (contact) problem of theory of elasticity can be, using integral transformations, reduced to paired or triple functional (integral or ordinary) equations [99]. As a result, finally such equations are transformed into a second-order Fredholm integral equation that can be effectively solved by one of the approximate methods.

The method of paired integral equations for spatial contact problems of theory of elasticity was first applied by Abramov [2], where a solution of the problem on impression of a round punch with a flat base into an elastic half-space under an eccentrically applied vertical force was obtained. The contact pressures were determined provided the whole punch bottom being in contact with the elastic medium. Later the same problem for a finite-thickness layer was considered by Egorov [74]. The solution obtained there is still being used in Russian handbooks and regulations [125, 258]. The handbook [258] quotes a table to determine slopes of round foundation plates depending on the eccentricity of the vertical component of the resultant load and the relative depth of the base mass being compressed. Graphs for the determination of settlements and slopes of a round absolutely rigid foundation on a linearly deformed half-space and a finite-thickness layer under off-centre vertical load are presented in [125]. An approximate formula for the calculation of horizontal displacements in an elastic layer under a centrally loaded round-shaped foundation is given in [82]. For different ratios of the compressed layer thickness to the foundation radius tables are composed and isolines of horizontal displacements of soil are built which should be taken into account in case of design of tower-type structures which produce high load on the foundation.

The method of paired integral equations was rapidly developing in the 1950–1970s. As noted by Popov [92], at present this method is the most flexible and universal among the analytical methods for solving mixed problems of mathematical physics. Reviews of contact problem studies, performed using the method of paired integral equations, are given in books by Ufliand [266, 267] and a book edited by Galin [99]. Mostly the problems of determination of contact stresses under a round punch, coherent with an elastic layer, including an anisotropic one, have been solved.

Among the recent studies of applications of the theory of paired integral equations, one should mention two papers by Borodachev [36, 37] regarding the generalized Hankel operator. An axisymmetric mixed boundary problem of the pressure of a circular punch on a nonhomogeneous elastic half-space (in the absence of friction and coherence forces), investigated in [36], is generalized for the case of off-centre impression in [37]. A non-classical model of the elastic base is considered, for which the elastic modulus and the Poisson ratio vary with the base depth

in a sufficiently arbitrary way. The problems under consideration are shown to be reduced to a succession of one-dimensional second-order Fredholm integral equations, in case the punch equilibrium equations being fulfilled. A periodical law of variation of elastic properties of the half-space material with depth was found, for which the obtained integral equations admit exact solutions to be constructed. The regularities of the influence of the base nonhomogeneity on the characteristics of its interaction with the rigid foundation are shown. As follows from the author's estimations, the account of the elastic base nonhomogeneity can result in the settlement variation for a round foundation of up to 33% in comparison with the homogeneous base model. The contact problem for a centrally loaded elliptical punch on an elastic base with a variable Poisson ratio is considered using the Hankel transformation in [35, 39].

One should mention rather scarce [53, 63, 151, 175, 204, 212, 231, 248, 286] exact and approximate analytical solutions of spatial contact problems for circular and elliptical punches, having been obtained rather long ago and included into handbooks [205].

Distribution of vertical stresses at various depths under an asymmetrically loaded round punch, coherent with an elastic half-space, was obtained by Muki [175]. Earlier Bycroft [63] had obtained formulae for horizontal displacements for a round punch at the same coherence conditions at horizontal loading. A solution for slopes of a round punch, coherent with a half-space, under momental load, was first obtained by Borowicka [55], while Sneddon obtained the distribution of contact pressures and vertical stresses in the half-space for the problem in question [248]. Reisner and Sagoci obtained a solution for the rotation angle of a round punch, coherent with a half-space, under a torque load [212]. Approximate solutions for slopes and contact pressures for a round punch under a momental load on a finite-thickness layer were obtained by Egorov and Nitchiporovich [286]. Poulos determined the contact pressures, vertical compressive stresses and displacements along the vertical axis of a centrally loaded round punch with a smooth base, located on an elastic layer of finite thickness [204]. A centrally loaded elliptical punch on an elastic half-space was studied in [231] where a distribution of contact pressures and vertical compressive stresses under the centres of ellipse of different eccentricity was obtained. An exact solution for horizontal displacements of the half-space surface under an elliptical punch was obtained by Lee [151].

An efficient method of solution of a spatial contact problem for punches with a cross-section close to circular, on an elastic half-space, is given in the book [172]. Mossakovskii and co-authors have reduced the contact problem to a problem of potential theory for a half-plane and is solved approximately. Pressures under punches with a flat bottom in the shape of a rectangle, a parallelogram, a triangle, a hexagon are determined as well as for the case of the punch bottom being an area restricted by elliptical arcs, when the impression is performed without an inclination (the contact area is a priori known: it coincides with the punch bottom). The unknown functions of the problem are found using an expansion over a small parameter characterizing the contact area shape deviation from a circle. Reliability of the obtained solutions was estimated using a similarity between pressure isolines

and Prandtl function level lines at a rod torsion with a cross-section corresponding to that of the punch [255].

Galin in his book [97] was the first to formulate the contact problem of a ring-shaped punch, having set an analogy with a problem of electric charge distribution on a ring-shaped conductor. He had not performed specific calculations concerning the problem because the specific functions, contained in the solution, were not tabulated.

Egorov has made a considerable progress in investigating the problem of a ring-shaped punch [75, 77], using an approximate approach based on fulfillment of only the stress boundary conditions. He obtained approximate formulae for settlements and contact pressures under a centrally loaded ring-shaped punch at different ratios of the inner and outer ring radii as complete second-order elliptical integrals. The numerical results have enabled one to reveal that the ring-shaped punch settlement remains almost unchanged with the variation of the inner-to-outer radii ratio within $0 < R_2/R_1 < 0.6$ in case the overall load on the punch remaining constant. It was shown that at $m = R_1/R_2 > 0.9$ the contact pressure distribution is similar to the case of a rigid strip foundation. Besides, in [77] the dimensionless values of the ring-shaped punch vertical displacements were tabulated depending on the parameter m.

In a number of subsequent publications the axisymmetric contact problem of a ring-shaped punch was solved by various techniques based on the method of triple integral equations [43, 76, 186, 272], power expansion of a singular integral equation kernel [112], application of the work reciprocality theorem [176], using asymptotic representations separately for large and small values of the parameter characterizing the relative thickness of the ring-shaped contact area [9], using toroidal coordinates [28], by expansion of the contact pressure function in a dual series with subsequent determination of the coefficients from recurrent relations [214], using a representation of the contact pressure function on the base of the expansion into trigonometrical series [240], by collocational fulfillment of boundary equations in case contact pressures being presented as a sum of boundary values of two analytical functions of a complex variable [173]. Note that the results of the first Egorov's study [75] appeared to be in a good agreement with subsequent more accurate data [112, 176, 240]. Besides, since now the exact solutions for an axisymmetric contact problem of a ring-shaped punch on an elastic half-space are known, the quoted papers [9, 28, 43, 75–77, 112, 173, 176, 185, 214, 240, 272] are mostly of methodological character. The approaches, developed in these studies, have enabled the contact problems of the pressure of a ring-shaped punch on an elastic layer of a finite thickness to be solved approximately (Valov [272], Gubenko [111]), the solution of non-axisymmetric problems of an elliptical punch with a circular opening of a small radius to be obtained (Aleksandrov [9]) as well as the one for a ring-shaped punch with a flat oblique base (Hara, Shibuya et al. [116], Popov [200], Borodacheva [47, 48]), the action of a ring-shaped punch on a nonhomogeneous half-space to be studied (Popov [200], Protsenko [208]) as well as its action on multilayer bases (Lamzyuk, Privarnikov [149], Nikishin and Shapiro [180]). One should also mention important from the practical point of view studies of Borodacheva [49–52] where the field of displacements and stresses in an elastic half-space due to

a ring-shaped punch was investigated as well as a work by Borodachev [42] where the character of distribution of pressures under a ring-shaped punch is studied in detail.

An approximate analytical solution of a rather general form for a flat ring-shaped punch on elastic homogeneous and nonhomogeneous (with a power dependence of the deformation modulus $E = E_0\ z^n$ on depth) bases under an eccentrically applied vertical force is given in [225]. Ordinary assumptions are made regarding the absence of friction in the contact area and the absence of the bottom uplifting from the base. The problem is reduced to a system of triple integral equations which is solved by expansion of the sought functions into power series whose coefficients are found in the third approximation using a small parameter method. The value $\varepsilon = a/b$ where a and b are the inner and outer radii of the ring, respectively, is taken as the small parameter. Unfortunately, the found approximate analytical solution has a limited applicability in construction of foundations since it is valid only for very broad punches and non-realistic bases (with zero deformation modulus on the surface).

The asymptotical method and its modifications for solving contact problems were developed in numerous studies by Vorovich, Aleksandrov, and Babeshko. A generalizing book by these authors [281] contains mixed (contact) problems of two-dimensional and three-dimensional theory of elasticity on the interaction of strip, circular, and elliptical punches with non-classical bases of layer and wedge type. Mostly so-called asymptotic methods of 'large and small λ' are used. In particular, in the problem of interaction of a round punch with an elastic layer the λ parameter is the ratio of the layer thickness to the characteristic size of a contact area, equal to the punch diameter. The proposed method is based on an idea of a transition from the known solution of the classical problem of the punch action on an elastic half-space to the approximate solution of impression of the same punch into an elastic body with finite dimensions in one direction. The main advantage of such an approach is obtaining the contact pressure function in a closed and rather simple analytical form, convenient for engineering applications. However, the generality and efficiency of the method are low – the asymptotic approach has been developed only in the case of building approximate solutions of spatial problems for punches of circular and elliptical cross-section impressed into an elastic layer.

The problem of pressure of a punch with a wedge-shape cross-section on an elastic half-space in the presence of a load outside the punch was first solved by Galin [97]. Later Rvachev solved this problem without an additional load and simultaneously revealed a singularity of contact pressures in the vicinity of the wedge vertex [222]. He found an approximate solution using a semi-inverse method together with Galerkin method. This solution is especially important for the determination of singularity indices in the angular points of polygonal domains in case the contact problems being solved by numerical methods. It should be also noted that later the problem of an infinite wedge was studied by the asymptotic method by Aleksandrov and Babeshko [10].

The problem of an off-centre loaded punch of an arbitrary cross-section resting on an elastic homogeneous linearly deformed half-space was considered in

[84]. An approximate semi-inverse analytical method of determination of the punch inclinations with respect to the coordinate axes is proposed. The method does not require preliminary calculation of contact pressures. The general formula for the angular displacements of the punch is rather complex, being an infinite series of integrals of the hypergeometrical Gaussian function. In the case of an elliptical punch this method leads to an exact result. By truncation of the solution to five harmonics, the developed approach is applied to punches with the cross-section in the shape of a rectangle, a rhombus, a circular sector, or a segment. The obtained results, having been compared with the known numerical solutions [225], show the applicability of the developed approximate formulae in practical design.

Rvachev in his earlier studies on theory of contact problems paid main attention to the influence of geometrical factors on the character of the contact stress distribution. The search for approaches to the solution of contact problems for punches of polygonal cross-section has led him in 1963 to the development of a new mathematical approach – the *R*-function method [223], combining logic algebra methods with classical methods of mathematical physics and computational mathematics. In the book [225] the structural method developed by Rvachev (the *R*-function method) is applied to find approximate solutions of the contact problems for punches of a rather arbitrary cross-section shape (the contact area can be bounded by a piecewise smooth curve). The contact problems for punches on a half-space with contact areas in the shape of polygons, an elliptical ring, a rectangle with an elliptical cutout, a part of a circle, etc. have been solved. A characteristic of this approach is the construction of series using coordinate successions for non-traditional (non-classical) contact domains in the framework of elementary functions, exactly satisfying the boundary conditions of the contact problem being solved by a variation method of Bubnov-Galerkin type.

When the contact area is known (in axisymmetric problems as well as at central loading of punches of canonical shape), an approximate method consisting in setting the contact pressure function as an infinite series over known (coordinate) functions but with unknown coefficients, is rather widely spread. The boundary conditions are satisfied approximately when a finite number of terms in the series are preserved. As noted in [99], similar approaches as well as the *R*-function method are, in general, badly conditioned and can result in big errors if the coordinate functions (polynomials) are chosen for the given geometry of the contact area boundary in a wrong way. The examples of solution of contact problems using expansions into power series as well as into series over orthogonal polynomials (Gegenbauer, Chebyshev, Jacobi, Laguerre, Hermit, etc. [3, 259]) are described in detail in known books [105, 201–203, 235, 241, 242].

In a rather simple and most widely spread in practice case of a rectangular foundation, the solutions of the contact problem at central and off-centre loading (under full contact) were obtained by various methods only approximately, with different degree of accuracy in [31, 41, 57, 105, 154].

Whitman and Richart [285] have obtained approximate solutions for vertical displacements of a rectangular punch with a smooth base at central vertical load.

Barkan in his book [30] gives an approximate solution for horizontal displacements of a rectangular punch undergoing a horizontal load in the direction of one of the central axes. His results are presented in a tabulated form depending on the ratio of the punch sides and Poisson ratio values for the soil base. Way has obtained an approximate solution for the slopes i_m of rectangular foundations, loaded by a moment in one of the directions and presented tabulated values of i_m at different ratios of the punch sides [284]. The results of the studies [30, 284, 285] were later quoted in a handbook [205].

The contact problem solution for a narrow punch of a rectangular cross-section (a narrow girder) on an elastic half-space in an approximate formulation was considered by Borodachev and Galin [40, 44]. It was implied that the pressure value by unit length of the girder is subject to be determined and contact pressures in each cross-section agree with the solution of the corresponding flat problem. At such assumptions the problem is reduced to a one-dimensional integral first-order Fredholm equation with a kernel containing a complete first-order elliptical integral. After polynomial approximation of the regular part of the kernel the problem is finally reduced to the solution of an infinite system of linear algebraic equations. This system was approximately substituted by a finite system of the 11th order and solved for different values of a small parameter $\varepsilon = \delta/a = 0.02 \div 0.2$ where $2a$ and 2δ are the length and the width of the rectangular contact domain of the punch (the girder). The distribution of pressures per unit length of the punch was obtained as well as its settlement under a central vertical force. An important result of the investigation performed was the consideration of an issue regarding the range of applicability of the Winkler hypothesis in the engineering theory of beam bending on an elastic base.

Burmistrov [62] suggested an asymptotic method of solution of the contact problem for the punches of prolate shape, not necessarily with a straight axis. In order to simplify the problem, a small parameter is used, related to the narrowness of the contact domain. The initial problem with a two-dimensional integral equation is shown to split into two one-dimensional integral equations, being solved sequentially. A number of asymptotically exact and one polynomially exact solution have been obtained (for an elliptical domain). In the author's opinion, the developed method is very important for the problem of contact of a roller with a bearing ring. However, in our opinion, the asymptotic method of Burmistrov can also be successfully used for the calculations of structures of prolate shape (beam type structures or strip foundations of finite length) on elastic bases.

Numerical solutions. The performed analysis of exact and approximate solutions has shown that a strict mathematical study of the processes of spatial contact interaction can be performed for a known contact domain only for the punches of the simplest geometry and, as a rule, at central loading. Mathematical difficulties while finding the exact and approximate solutions of the spatial contact problem still remain insurmountable in case the punch geometry being more complex as well as with the account of various sorts of nonhomogeneity, laminarity, anisotropy, etc. for the elastic base [59, 73, 179, 239]. Therefore, of high practical importance are contact interaction studies, carried out using computer modelling.

In case spatial contact problems being solved, including those with an a priori known contact domain, the most efficient are numerical methods based on discretization with subsequent piecewise constant, linear, or quadratic approximation of the contact stress function. Among the numerical method of this trend, used for the design of foundation bases, the most widely spread are finite-difference method (FDM), finite-element method (FEM), and boundary-element method (BEM). It should be noted that the finite-difference and finite-element methods assume the discretization of the base area, which is active for the foundation (punch) being calculated. In the case of spatial problems both methods, though formally allow the physical and geometrical nonlinearity of the base material as well as bulk forces to be formally taken into account, still result in the solution of algebraic equation system of a very high order. On the other hand, in the boundary-element method the account of the above factors makes the problem solution much more labour-consuming; thus such main advantages of the method as discretization of only the domain boundary and small amount of input and output data, can vanish.

Finite-difference method. Using the finite-difference method, Vinokurov in the end of the 1960s elaborated an iterative method of calculation of bases and foundations in planar and spatial formulations [279]. The numerical algorithms and solution method constructed have enabled the elastic-plastic-viscous soils to be considered with and without the account of structural strength for a number of cases when solutions in the closed form are missing. As a field of application of the elaborated method stress-strained states of soil bases are considered, including the case of being subject to the action of a rigid punch. Main finite-difference equations to determine settlements and slopes of a rigid square punch located on a transversely isotropic base and loaded by a vertical force and moments in two orthogonal planes. Both the settlements and slopes can be found only after the calculation of the stress-strained state of the base. The book [279] contains only theoretical issues of calculation of bases and foundations. The practical application of the elaborated finite-difference approach to the solution of the essentially spatial contact problem for a rectangular punch on a linearly deformed base was given much later (in almost two decades) in the studies by Shevchuk [133, 238] which now, in fact, determine the level having been achieved for the solution of spatial contact problems using the finite-difference method.

Shevchuk has worked out a finite-difference algorithm to solve the spatial contact problem for punches of rectangular cross-section located on an anisotropic and simultaneously nonhomogeneous with depth layer [238]. The formulation of the problem includes complete determination of the stress-strained state of the layer under the flat punch undergoing all six components of load. The finite-difference approximation has been performed for differential equations of equilibrium, Cauchy equations, and physical equations of an anisotropic nonhomogeneous body. On a bounded (prismatic) domain of the layer under the punch a regular spatial grid is built. The condition of full coherence of the punch and the elastic layer is accepted. Equations, obtained from the condition of normal and tangential stress being equal to zero, are used to calculate the displacements of the finite-difference nodes of the free surface. Due to the great number of the finite-difference equations and to the

coefficient matrix being very sparse, an iterative Seidel method is used to obtain a solution. The studies of the iterative scheme have resulted in a condition of the numerical solution stability relating the Poisson ratio of the layer and the ratio of moduli of elasticity in the horizontal and vertical directions. Comparison of the results obtained for the grids of various step has shown the approximation errors to be localized, as it should be expected, near the punch edges at a distance from them of half of the punch bottom width. The effect of remoteness of the lateral boundaries of the base approximation area is traced only for the overall settlement of the punch. The effect of the lateral sides is shown to be insignificant in case they being remote from the punch centre by more than the triple width of its bottom. Comparison of the finite-difference calculations with the results of experiments and field studies of real structures has shown rather high discrepancies (up to 12%), especially near the contact surface.

The necessity of solving contact problems for various types of structures interacting with soil bases, requires influence functions to be used. Shevchuk managed to build a discrete analogue of the latter, using the finite-difference approach in the following way. From the calculation for an elastic anisotropic layer loaded by a unit vertical force, uniformly distributed within one cell of the finite-difference grid, influence coefficients are determined, numerically equal to vertical displacements of the layer surface nodes. From the influence coefficients an influence matrix is built in a standard way which was used for the combined calculation of the frame system and the base.

Only a rather small number of publications available touch the problem of account of physical nonlinearity of the base material when the problems are solved using the finite-difference method [161, 207, 243, 244].

Malyshev and Proskuryakov in [207] present the results of numerical solution of the problem of the stress-strained state of a half-space subject to a flexible load uniformly determined over a square area. The half-space is characterized by nonlinear deformational properties, described by nonlinear relations of deformational theory of plasticity. The bulk deformation modulus is taken constant and the generalized secant shear modulus is determined by the Botkin dependence [54]. The dependences between the stresses and deformations are taken in the form of Hencky equations. The problem is solved by the finite-difference method in displacements. An integral-interpolational method is used to construct the difference scheme. The obtained difference equation system is solved iteratively using the Seidel method. In view of the symmetry of the calculation scheme only a quarter of the base and the load area is considered. The account of the nonlinearity of the soil physical properties was carried out incrementally: the nonlinear problem of the action of a load of a given intensity on a half-space is reduced to a succession of problems of the action of an incremental load with constant deformation moduli. As noted in [207], convergence of the incremental iteration method was not always easily achieved, what made the computations much longer (the number of iterations in each approximation was not less than 10). Therefore, the need of the discretization degree to be increased in the areas of high displacement gradients for the case of the three-dimensional soil mass requires a sharp increase of the computation time.

Probably, this did not enable the authors of [207] to solve the contact problem of a rigid rectangular punch by finite-difference method even for the case of a symmetrical calculation scheme.

The contact problem for a rigid punch on a physically nonlinear base is more efficiently solved by the finite-difference method in the case of axial symmetry what practically corresponds to the planar formulation. The contact problem of the deformation of a nonlinearly elastic base under a round rigid punch, studied by Solomin et al. using the finite-difference method [161, 243, 244], is discussed below when the numerical solutions of the contact problem for round punches is specially considered.

In opinion of a number of authors, among the main disadvantages of the finite-difference method, revealed at the contact problems being solved, one should mention considerable difficulties of finite-difference formulations for different boundary conditions as well as violation in a number of cases of symmetry of the resolving algebraic equations what finally does not enable this method to be recognized as a sufficiently universal one.

Finite-element method. Recently the finite-element method has become more widely applied for numerical solving geotechnical problems than the finite-difference method. The finite-element method is especially efficient to evaluate the stress-strained state of bodies of a finite size and a complex shape both in planar and spatial problems of mechanics of solid deformed bodies. In the framework of a unique approach this method is used to solve many complicated geotechnical problems of joint deformation of a foundation and soil with the account of geometrical and physical nonlinearities, factors of nonhomogeneity, anisotropy, consolidation, etc. Different approaches to the investigation of the stress-strained state of soil bases using the finite-element method can be found in the studies of prominent geotechnicians [24, 70, 85, 107, 114, 142, 194, 196, 216, 218, 236, 268, 287–289, 292–294], devoting the main attention to the solution of planar and axisymmetric problems.

In comparison with the planar and axisymmetric problems, the number of degrees of freedom in the finite-element method for three-dimensional (essentially spatial) problems increases by several orders of magnitude. This results in such insurmountable yet difficulties in practical application of the finite-element method to solve geotechnical spatial problems as the required computer RAM size and speed increase as well as the increase of input and output data size. Therefore, even at contemporary level of computer systems application of the finite-element method in spatial geotechnical problems still remains rather limited. The situation is even more complicated for the solution of problems (nonlinear, with a priori unknown contact domains, etc.), requiring various iterative processes to be organized when the elastic calculation procedure is to be repeated many times.

Pilyagin and Kazantsev in their papers [193, 195] and book [194] were the first to give the solution of a spatial elastoplastic problem of evaluation of the stress-strained state of bases. They also describe a software package with numerical algorithms of the problem produced using the finite-element method. The FEM is considered there for the case of symmetrical foundation structures at central loading. This has enabled the solution of the discrete problem to be essentially simplified by

storing only the symmetrical part of the rigidity matrix in the computer RAM and using effective methods of solving systems of linear equations with symmetrical matrices.

Based on the results of the solution of a spatially symmetrical elastoplastic problem, the analysis of the influence of rectangular foundation size on the development of settlements at different physical and mechanical parameters of the soil was carried out. The influence of the foundation bottom shape on the soil base deformation was studied only by variation of the ratio $\eta = l/b$ of its length to its width. In particular, at $\eta \geq 6$ the rectangular foundation settlement is shown to be practically equal to that of a strip foundation of the same width. For an absolutely rigid square punch being impressed into a homogeneous soil base by a central force, the calculated results are compared with the experimental studies by Rabotnikov and Kovanev [209]. The experimental data and the FEM theoretical solution for the settlement versus load dependences appeared to be in a good agreement. As one could expect, the difference between the calculated and experimental curves increases with the load increase. The different soil strength conditions being used have made the settlement values for the linearly elastic solution more exact, but still differing from the actual values by up to 7% at the Mohr-Coulomb strength condition, and up to 14% at the Mises-Schleicher-Botkin strength condition.

The method of solving a mixed spatial problem of theories of elasticity and plasticity, quoted in [193–195], as well as the analysis of influence of various factors on the variation of the stress-strained state of the soil base have shown a conceptual possibility of the finite-element method to be applied in practical design of foundations for buildings and structures. However, the variety of factors affecting the stress-strained state of the bases, the long computation time for spatial elastic and elastoplastic problems strongly encumber the application of the three-dimensional FEM in practical engineering. This has made Pilyagin and Kazantsev [194] to suggest a way to apply the solutions of mixed problems of soil mechanics for elucidating the factors affecting the settlement, for choice of versions most widely used in real design of bases and foundations as well as for obtaining corresponding approximate dependences or making alignment charts. It should be noted that due to the above difficulties in solving essentially three-dimensional problems, the obtained finite-element solutions in [194] are made ready for practical application in the form of alignment charts and multifactor power models only for the strip type foundations, i.e. for the conditions of flat deformation of the soil bases when the two-dimensional formulation of the contact problems essentially simplifies the contact interaction analysis.

The known general approaches to the solution of static planar and axisymmetric contact problems by the finite-element method are discussed in detail in [198]. The influence of various contact conditions, rheological properties of the material (creep and plasticity) and contact domain variation in the course of loading on the character of functioning of the contacting structure elements, mostly of machine-building type, has been studied. The analysis of the contact interaction of elastic and elastoplastic bases with rigid punches, performed in [198], has a direct similarity with the problems of calculation of bases and foundations. A test solution of the classical

problem in an axisymmetric formulation of impression of a rigid circular punch into an elastic half-space and a constant-thickness layer has clearly shown some shortcomings of using the finite-element method for solving contact problems for infinite domains. For numerical modelling the semi-infinite elastic half-space was approximated by a finite-size domain ($0 \le r/a \le 30.0 \le z/a \le 150$), at the boundaries of which the resting conditions were formulated. In order to obtain a satisfactory numerical solution, the meridional cross-section of the deformed base domain was meshed into finite elements with condensation towards the contact domain boundary. The total number of the grid nodes was 1230, among them only 15 (i.e. slightly above 1%) being on the contact area. Comparison of the numerical values for pressures under the punch with the data of analytical solutions, an exact one for the half-space [128] and an asymptotic one for the layer [281] appeared interesting. The general conclusion of the comparison of the above problems was made that in the areas adjacent to the punch edge, a considerable error of the numerical solution is observed. For these areas the stress-strained state of the base is of complicated character and cannot be approximated in a satisfactory way by bilinear coordinate functions of the finite element. It is noted that obtaining more exact numerical results in the presence of areas with rapidly growing solutions makes the contact problems of the class under consideration (for rigid punches on infinite bases) rather labour-consuming in case the finite-element method being used.

While performing calculations for the stress-strained states of bases under punches the most convenient is to apply linear theory of elasticity, but the load value should be restricted in accordance with the average pressure over the bottom (calculated soil resistance) [258, 269]. This restriction is abandoned in case nonlinear (elastoplastic) models of soil bases being used. Axisymmetric problems regarding stresses and displacements of a nonlinearly deformed half-space, on whose surface a circular or a ring-shaped centrally loaded punch being located, are considered in [12, 64, 101, 161, 198, 243, 244, 258, 269]. In all cases no slippage of the soil under the bottom was assumed to occur, i.e. there were no horizontal displacement over the contact of the soil and the punch.

The problem of a circular rigid punch on a soil base is the simplest problem of spatial type and the most widely spread in soil mechanics and foundation engineering [12]. On one hand, a wide experimental material has been obtained for the problem of a circular punch. On the other hand, a nonlinear solution of this problem can be used for the adjustment of equations of the soil state and practical calculations of strip and columnar foundations. Therefore, it is this contact problem, from which many authors begin the application of a new calculation method; besides, the solutions of this problem are complex enough and enable one to judge upon the efficiency of the calculation method applied.

A method of calculation of soil bases for rigid circular foundations at axisymmetric conditions using the finite-element method in combination with the initial stress method is proposed in [12]. A model of soil as a strengthening elastoplastic medium of modified "Cam-Clay" model is considered [232]. The node coordinates of the calculated finite-element grid were given analytically as the intercepts of confocal ellipses and hyperbolae [292]. This discretization has enabled a rather large

base area (by 3.8R in radius and by 3.6R in depth where R is the punch radius) to be embraced using a small amount of elements (24 finite elements bound by 20 nodes). Based on the calculations, settlement versus load plots are built, which enabled the effect of initial porosity on the deformational properties of the soil to be revealed. A typical more intense increase of stress under the punch edge (in comparison with the centre) with load increase was found.

Glushkov has obtained solutions for mixed elastoplastic problems in an axisymmetric formulation for ring-shaped and circular foundations [101]. Using the finite-element method, the effect of strength characteristics (φ and c) and deformational characteristics (E and ν) of soil as well as the foundation size on the variation of the stress-strained states of bases to be studied. The stressed state of the soil medium was determined only under an external load. The soil in the prelimit state was considered as a solid linearly deformable medium, being transformed under further loading to a limit (plastic) state in accordance with the Mohr-Coulomb criterion of fluidity (strength). The calculations were performed using a stepwise procedure of load application. Regarding the contact of the foundation bottom with the base full adhesion is assumed. With the account of the natural stressed state the calculations were carried out to determine the effect of strength characteristics (φ and c) and deformational characteristics (E and ν) of the soil on the stress-strained state in the foundation active zone. The analysis of the results has shown that the settlement versus load dependences are generally nonlinear (bilinear). With the exception of a small initial part these dependences are almost linear, and their slope and the load bearing capacity of the base are essentially dependent of the soil strength parameters φ and c as well as of the ratio of the inner and outer radii of the ring. Detailed isoline patterns of horizontal and vertical displacements of the soil, main and tangential stresses in the foundation base were also obtained. An important result of the investigation carried out in [101] consists in finding the laws of formation and development of a plastic deformation zone in the base active area under an axisymmetric loading of ring-shaped and circular foundations. These zones arise in an area, directly adjacent to the bottom, and develop laterally and downward with the increase of the load on the foundation. The character of formation and development of the plastic zones mostly depends on the strength characteristics of the soil: the smaller are φ and c values, the earlier are the plastic zones in the base formed and the more intense is their growth rate. Similarly to the case of strip foundations [194], a rather high computation time for the axisymmetric problems with a variety of factors affecting the stress-strained state of the ring-shaped and circular foundation bases did not enable Glushkov to apply the elaborated method in the engineering practice. Similarly to [194], for wide application of the solutions of axisymmetric problems of soil mechanics, the author proposes to determine the parameters (strength-related, deformational, geometrical), affecting the settlement, search through the variants, the most widely involved at real conditions, and obtain the corresponding approximate dependences and homographs. In particular, a multifactor power dependence, assumed in [101] for the settlement of a round foundation under a central force, has shown a good agreement with the experimental data and can be applied in practical design. However, for practically important cases of off-centre loading no effect of

the strength and deformational properties of soil on the settlements and slopes of ring-shaped and circular foundations have been found using the FEM in the quoted papers [12, 101, 198].

The authors of [64] propose to use local variation method for solving the axisymmetric problem of impression of an absolutely rigid flat-bottomed punch into an elastoplastic base. The unlimited base area in polar coordinates $r \geq 0$, $z \geq 0$ is substituted by a finite-size domain $0 \leq r \leq R$, $0 \leq z \leq H$ where R and H are sufficiently large. At the boundary of the domain under investigation $r = R$, $z = H$ the conditions for displacements are given from the known solution of the problem of action of a concentrated force on an elastic half-space (from the Boussinesq problem). The main equations of the elastoplastic problem under consideration, besides the equilibrium equation, included the Mises plasticity condition and the Prandtl-Reiss equation of state. The variational principle of theory of plastic flow is applied, according to which the real increments of vertical and radial displacements are the realizations of the minimum of the increment energy functional. The proposed algorithm for solving the variational problem has the following stages: (i) meshing of the stressed base domain ($0 \leq r \leq R$, $0 \leq z \leq H$) into triangular cells by a non-uniform grid, (ii) combining the neighbouring triangular cells into one cell and calculation of integrand functions in the energy functional using the finite-element expressions, (iii) solving the obtained variation-difference problem using the local variation method.

The calculation data enabled the development of plastic zones, arising at the punch edges, to be traced. Comparison of the exact solution with a numerical solution in a purely elastic formulation has shown the difference not to exceed 2.5% for the calculation domain discretization by a 7×7 grid and 1% for the 11×11 grid. Due to the presence of several nested iterative processes as well as the formulae used being rather cumbersome, the scope of calculations required to solve the problem, is very large. In spite of the possibility of complex rheology to be taken into account (both in the framework of the plastic flow theory and for the deformational theories of plasticity) and a rather high calculation accuracy, the algorithm of solving the contact problem of a punch on an elastoplastic base, proposed in [64], is elaborated only for solving two-dimensional and axisymmetric problems.

In order to solve the contact problem of a round punch, in [161, 243, 244] the relation between the stress and deformation components was taken in the form of the generalized Hooke's law where the shear modulus and the modulus of dilatation are scalar functions of the stress tensor invariants. The form of the functional dependence was determined experimentally. The contact problem is reduced to a system of nonlinear differential equations with respect to the vertical and radial components of the displacement vector. The solution is obtained using the successive approximation method (Ilyushin elastic solutions) in combination with the finite-difference method. While the problem being solved, the half-space was substituted by a cylinder with a radius $16R$ and height $8R$ where R is the punch radius. The calculations have revealed the effect of the variation character and value of the secant shear modulus on the stress-strained state of the base at the same value of the modulus of dilatation. The issue of expediency of account of the soil structural strength is studied at the example of a sand base. Two solutions are compared. The first one was

obtained using the Botkin model whose parameters were taken from the test data for the sand of disturbed structure. The second solution takes into account the structural strength at shear. A quantitative discrepancy in the data consisted mostly in the fact that the account of the structural strength enabled the calculated settlement to be essentially reduced (based on the calculation data – almost by three times). Besides, the account of the structural strength enabled a number of new qualitative effects to be revealed, corresponding to the experimental data: formation and development of a compressed zone; formation of an elastic kernel; concentration of vertical deformations on the foundation axis directly under the elastic kernel; more intense damping of displacements with depth and corresponding to the experimental data more complicated (in comparison with the Botkin model-based solution) character of transformation of the reactive pressure profile.

Some important features of the numerical solution of problems of interaction of punches with soil bases were noted by Likhovtsev and Estrin [155]. They have performed comparative calculations of interaction of a punch with a base (of a finite-thickness layer type) both for a cinematic (traditional) and a force loading schemes in the planar problem formulation.

In the case of the cinematic loading scheme the punch is considered absolutely rigid. At each loading step an increment of the punch settlement is given, a contact pressure profile is determined and from the latter the loading step value is determined. This process is performed iteratively until the given load is reached or the base loses its carrying capacity. At this loading scheme there is no necessity to discretize the foundation itself (this reduced the computation time and makes the computer RAM less loaded), the matrix of the resolving system of linear algebraic equations is obtained well conditioned and, consequently, when the global rigidity matrix is formed there are no truncation errors (due to the arithmetic operation between numbers of the same order of magnitude). Nevertheless, such approach does not take into account deformational characteristics of the punch; besides, the problems with off-centre and horizontal application of load cannot be considered. Note that numerical data for the case of the spatial contact problem when the finite-element method at the cinematic loading scheme was used for a rectangular punch on an elastic two-layer base, were obtained in [95].

At the force loading scheme, the punch (with a finite rigidity) and the base are considered as a compound body with different mechanical characteristics. Similarly to the base, the punch is subject to discretization into finite elements. The problems of interaction of the foundation with the base at off-centre load application can be solved, the effect of the deformational characteristics of the punch on the contact pressures and the stress-strained state of the base can be estimated, stress and bending moments in the foundation can be determined with the account of its deformational characteristics. Consequently, the application of the force scheme enables a broader class of problems to be solved in comparison with the cinematic loading scheme. However, the calculations have shown [155] that numerical application of the force loading scheme (especially, using a computer), should be performed with double-precision data format. This requirement follows from the appearance of truncation errors at the formation of the global matrix of rigidity for the different-type

materials whose deformational characteristics differ by several orders of magnitude. According to the data of [155], the single-precision calculations, performed according to the force scheme (at central loading), have shown a symmetry violation for the displacements and stresses in the nodes located symmetrically with respect to the punch axis, i.e. the results become erroneous. Thus, when the force loading scheme for solving the spatial problems of interaction of rigid punches with soil bases by finite-element method is used, the requirement of the calculations to be performed with double precision (to avoid numerical errors) will require a rather essential extra increase of the computer RAM size and the computation time.

Boundary-element method. As seen form the analysis of the available literature, for solving planar and axisymmetric contact problems as well as spatial contact problems in case the contact domain size being comparable with the characteristic size of the contacting bodies, a boundary-element method is efficiently used [22]. For solving essentially spatial problems in soil mechanics and foundation engineering when one of the deformed bodies (base) is infinite (half-space, unlimited layer, wedge, etc.), the boundary-element method is being used more and more. In this method continuous contact forces are substituted by discrete values in accordance with the mesh of the contact domain only into boundary (contact) elements.

While searching for the discrete contact forces, maximally satisfying the boundary conditions, as a rule, two approaches are used [128]: a direct approach when the boundary equations are satisfied exactly in the given collocation points (These are usually taken in the boundary-element centres), and a variational approach when the discrete force values are chosen from the conditions of the energy function minimum. Aleksandrov was one of the first to propose a method of solving three-dimensional problems of theory of elasticity by numerical implementation of the integral equation method [6]. He constructed solutions for circular and ring-shaped punches with a flat bottom based on the elaborated method of determination of stresses and displacements due to a load, uniformly distributed over a ring [7]. The proposed method was tested by a problem of pressure of a circular flat-bottomed punch on a half-space. The possibilities of this variant of the boundary-element method appeared to be essentially dependent of the accuracy of the contact pressure calculation from the algebraic analogue of the boundary integral equations of the problem. Simultaneously, determination of tangential stress field in the half-space by this method gives the results that are in a good agreement with the experimental data [174].

Most of the essentially spatial problems were solved using different variations of the BEM for the foundation models with rectangular cross-section [34, 68, 140, 165, 166, 182, 186, 187, 192, 213, 270, 276]. Only several studies consider circular, ring-shaped, and elliptical punch foundations [6, 88, 140, 276].

Relatively recently Bokiy and Petrishin elaborated an algorithm for numerical solution of the pressure of a smooth punch of square cross-section on an elastic half-space [34]. A case of central loading is considered, resulting in the symmetry of the unknown pressures on elementary squares, discretizing the square contact domain. The coefficients of the resolving system of integral equations, being the dual integrals of the Boussinesq solutions for a vertical concentrated force, are

calculated in the finite form via elementary functions. The approximate solutions of this problem at various degrees of discretization, obtained in [34], correct the errors in the solution of the same problem, quoted in a manual [213] and using the tabulated values of the influence matrix coefficients (according to Zhemochkin), correct only for certain directions.

Novotný and Hanuška also studied the contact problem for a rigid rectangular punch resting on an elastic homogeneous half-space [182]. As in similar works by most of other authors, while determining the contact pressures, horizontal stress was not accounted. A unilateral constraint on the contact of the punch and the base, preventing from tensile contact stress, was taken into account. This requires the integration domain (contact domain) to be defined while solving the main integral equation of the problem and the equations of equilibria. Numerical solution of the problem is performed using the boundary-element grid of right-angle triangles, on each of which the contact stress is taken according to a linear law. The algorithm of the problem solution includes an iterative process of removal of negative contact stresses. The calculations have shown the non-uniform discretization with condensation of triangular elements near the punch angles to produce essentially better results than a uniform one. Detailed studies of the ratio of the angle uplifting and the centre settlement for a square punch at eccentric application of the resultant vertical force have been performed.

Veryuzhskii et al. [276] proposed a general approach to the solution of spatial contact problems regarding the interaction of soil and rigid foundations, using potential methods. The main concepts of the potential method, stated in [277], are based on the consideration of unit point forces acting in a soil medium, and enable the method in question to be considered as a numerical-and-analytical form of the boundary-element method. Based on the application of Betti's theorem to the basic state under consideration and an auxiliary state constructed, an algebraic analogue of the Somigliana integral equation is derived. In general, Mindlin's solutions are used as the integral equation kernels [169]. The main attention in the work is paid to the increase of efficiency of the contact problem solution method due to analytical determination of antiderivatives for the integrals contained in the algebraic analogues of the Somigliana formulae. In order to estimate the abilities of the numerical-and-analytical potential method, test problems for rigid round and square punches resting on the surface of an elastic half-space and loaded by a central vertical force, were solved in [276]. The punch settlement values and the contact stress profiles over the punch bottom were obtained for a different density of the contact surface mesh. For a square punch the settlement value obtained by the numerical-and-analytical potential method on a 6×6 boundary-element grid appeared practically the same as the one found from the Schleicher formula [260]. A rather good coincidence with the Boussinesq solution is also noted for the contact stress distribution in the soil under a rigid round punch: the discrepancies obtained are within the accuracy of graphic interpolation. The circular contact domain was approximated by a regular hexadecagon, meshed using 68 contact (boundary) triangular and quadrangular elements. In spite of the approach proposed being rather general, the contact problems for punches of complex-shaped cross-sections, resting on non-classical bases and

loaded by off-centre forces (what results in the bottom uplifting from the base), have not been solved.

Numerical implementation of the integral equation method in contact problems for an orthotropic half-space was performed by Martynenko, Knyazeva, and Romanchik [140, 165, 166]. An approach to the numerical solution of integral equations developed in [167], was used to solve the problem of pressure of a coherent (without slippage) [165] and a smooth [166] punches of rectangular cross-section on a half-space. The rigid punch displacement parameters are determined by invoking six equilibrium equations. Three contact stress functions are proposed to be sought in the form of a product of a specific part of the solution and a linear combination of Sobolev δ-shaped averaging functions [103] whose coefficients are found by collocation method. In order to describe the contact domain boundaries R-function representations are used. A number of problems for complex-shaped punches with the cross-section of triangular, rectangular, elliptical shape and their combinations have been also solved [140].

A number of experiments performed have shown that many important features of the engineering and geological conditions, affecting the contact interaction of the foundation with the soil base can be successfully taken into account in the framework of the boundary-element method: the compressible soil mass variability [186, 187], non-uniform salinity [192] and laminarity [68, 88, 270] of the soil bases.

Onopa and Fedorovskii have solved the spatial problem of the settlements and slopes of a rectangular punch on a wedge-shaped base, i.e. on a compressed layer whose thickness varies linearly [186, 187]. A kernel of the wedge-shaped base contact model, found earlier [89], is used, relating the pressure to the vertical displacements on the base surface. A punch can be subject to an off-centre vertical load, reduced to a central force and two moments, acting in orthogonal directions. As a result of the discretization by the punch bottom into rectangular boundary elements, the unknown averaged contact pressures on each of them as well as the punch settlement and slopes with respect to the coordinate axes are found from the solution of a linear algebraic equation system being an analogue of the equality of the punch and the base vertical displacements as well as three integral equations of equilibrium. The authors of [186, 187] have succeeded to avoid the difficulties of the numerical integration of singular functions at the calculations of the influence matrix coefficients due to the analytical calculations of the terms in the contact model corresponding to the Boussinesq equation for a unit vertical concentrated force. Dependences of the punch settlements and slopes on the wedge angle at various Poisson ratio values ν, relative depth of the compressed mass under the punch centre H/b, its side length ratio a/b were obtained for three main combinations of the external loads: at separate action of the vertical force P and each of the moments M_x and M_y. Subsequently, based on the results of [14], recommendations were made for the calculations of the settlements and slopes of rectangular foundations on a wedge-shaped base [211]. The studies of contact pressure fields while solving the above problems were not detailed enough [186]. Practically significant cases of complex-shaped foundations were not considered as well as off-centre loaded with the bottom uplifting from the base. The latter case is especially important to be taken

into account while designing foundation structures at complicated geotechnical conditions (on bases with compressible soil mass depth, variable over their area).

Petrukhin [192] proposed a method to calculate non-uniform settlements of free-standing rigid smooth-bottomed foundations on a nonhomogeneous base of salinated soils, including the case of the presence of oblique layers. Using the boundary-element method, for a rectangular foundation contact pressures and settlements are determined as well as slopes in two planes due to the action of a complex external load including a vertical force and an overturning moment of arbitrary direction. In the proposed approach the total settlement of a base composed of the salinated soils, is found as the sum of the base settlement prior to the beginning of the suffusion process (using the scheme of a linearly deformed half-space and the total deformation modulus of the soil in a natural state), and the base settlement due to the suffusion, determined by integration over the depth of relative suffusion deformation, depending on the desalination degree and the value of the vertical stress in the soil. The resolving system of equations of the discrete contact problem was solved iteratively: at each approximation step the suffusion-related part of the base deformation at each boundary element is determined according to the experimental curves between the relative suffusion-related compression of the soil and the vertical pressure applied. The performed boundary-element calculations for a single shallow square foundation on a nonhomogeneous base (with three layers of soil of various of salinity level) at the discretization of its bottom even by a rather rough grid (five elements along each side of the square) produced results which agree well with the experimental data. This has enabled the author of [192] to propose, after a required refinement, the boundary-element method of solving the contact problem for a shallow rigid foundation on a salinated soil for other types of structurally unstable soils as well.

Dempsey and Li applied the boundary-element method to solve the contact problem for a rigid centrally loaded rectangular punch on an elastic layer resting on a non-compressible underlayer base [68]. They used the Burmister solution [60] as the influence function. A similar problem had been solved earlier by Urisman [270] without studying the distribution of vertical compressive stress in the base at the off-centre loading of a rectangular punch located on a finite-thickness elastic layer with the Egorov influence function [75]. Urisman considered the contact surface of the rectangular punch as a single boundary element, the unknown pressure function on which was presented in the form of a two-dimensional polynomial of the 12th order, similarly to [105]. The unknown polynomial coefficients were proposed to be determined by the least-square method. With this purpose, the coordinates of points, belonging to the punch domain, re substituted into the main integral equation of the problem; the number of these points is taken greater than the number of the parameters to be determined, thus enabling a redetermined system of linear algebraic equations to be built. Thus formed redetermined system is solved by the least-square method, after which the punch displacement parameters and a polynomial function of reactive pressures are found. Subsequently, using the software elaborated by Urisman, extensive calculations of settlements and slopes were performed for rectangular rigid foundations on a linearly deformed half-space and a

finite-thickness layer due to a vertical off-centre load of a general type (with eccentricities along the longitudinal and transverse axes). The corresponding graphs were included into an appendix to a manual for design of plate foundations for frame constructions and tower-type structures [125].

Using the boundary-element method, Fedorovskiy and Dokhnyanskiy have solved an axisymmetric contact problem for rigid ring-shaped and circular smooth punches (foundations) on the base formed by an elastic layer resting on a more rigid half-space [88]. The domain of the contact of the punch and the base was meshed into ring-shaped boundary elements of equal area, the pressure on each of them being assumed constant. In order to calculate the coefficients of the influence matrix of the resolving system of linear algebraic equations, a representation of displacements and stresses in a multilayer elastic medium by integral Hankel transformation is used in the form, proposed earlier by Fedorovskii et al. [78]. According to the algorithm elaborated, automated calculations were performed using a high-speed *Koltso* software. Based on the great scope of multivariant calculations performed using this software, simple formulae (of the Schleicher formula type) were constructed for the settlements of ring-shaped and circular foundation punches depending on the punch radii ratio and the deformational properties of the base. The boundary-element approach to the calculation of the settlements of ring-shaped foundations and the stress-strained state of their bases, proposed by Fedorovskii and Dokhnyansky in [88], at the presence of the influence functions for the layered bases is more general and accurate than the approximate method of evaluation of settlements of ring-shaped foundations on a combined base [80]. A comparison of the calculation data with the measurements of the average settlements of the ring-shaped foundations performed in [80, 88], confirmed the application of the solutions of the contact problem of a rigid ring-shaped punch to be correct for the design of foundations under high funnels. According to [80, 88], the ring-shaped foundations can be effectively used instead of expensive pile foundations and solid round foundation plates at complicated geotechnical conditions.

Thus, the review performed enables one to conclude that the abilities of most of the numerical methods available for solving essentially three-dimensional contact problems of foundation engineering, problems still remain rather limited.

Finite-difference and finite-element methods enable a considerable success to be achieved in planar and axisymmetric problems of foundation base calculation. However, they appear rather ineffective for solving essentially spatial problems even for elastic linearly stressed bases. Size assignment of the foundation active area, required in case these methods being used, is an independent and labour-consuming problem, and in order to solve it one should take into account the mechanical properties of the base and the load type as well as the problem solution method. The requirements of a detailed discretization of the base stressed area result in too high computer RAM size and computation time required. The quantity and size of the finite elements should be chosen in such a way that the effect of the planes, restricting the foundation active zone, be reduced to minimum.

The broad application of the finite-element methods for planar and axisymmetric contact problems is caused by the possibility of taking into account the material nonhomogeneity and anisotropy, complex rheological properties, slippage conditions, etc. at rather high calculation speed. Therefore, the amount of publications devoted to the FEM applications in soil mechanics and foundation engineering is extraordinarily high: almost every third paper in geotechnical journals is somehow related to the FEM [85]. The account of nonlinear regularities, inherent to soils, is undoubtedly essential, but results in a considerable complication of the contact problem. The requirements to the computer speed and RAM size increase by several orders of magnitude in the case of spatial problems of nonlinear soil mechanics. This is the reason for the essentially spatial problems having not been considered using the finite-element method.

Comparison of the solutions, obtained for rigid punches in an axisymmetric formulation by boundary-element and finite-element methods, have shown [198] that using the boundary-element method provides higher accuracy and working efficiency in the areas of high stress gradients (below the punches where the solution for the theory of elasticity tends to infinity) even in case piecewise constant approximation of the contact pressure field being used. Besides, the data preparation procedures (discretization into the boundary elements) are reduced by several orders of magnitude in comparison with the expenses for discretization in the finite-element method what finally results in a considerable decrease of the computer resources for solving the problems of the class under consideration.

Thus, among the numerical methods one of the most promising and efficient for solving mixed problems of theory of elasticity is the boundary-element method which successfully competes in a number of aspects with the finite-element method. The BEM is characterized by an essential reduction of the data preparation procedure and a decrease of the dimensionality of the resolving system of equations. At present, the BEM has an explicit advantage over the FEM for the problems of theory of elasticity, especially for infinite domains. The boundary-element method to a considerable degree uses the superposition principle and can be applied to the problems where the initial differential equations are linear or assume a stepwise linear approximation with respect to the increments. This has enabled the authors of the known book regarding the BEM applications [29] to conclude that, in principle, only a very few problems exist which can be solved by the finite-element method and which could not be solved with at least the same efficiency solved using the BEM. The BEM has not been yet studied in such a detail as the FEM, and not all its possibilities are revealed, both concerning the increase of the calculation accuracy and the reduction of the computation labour consumption. The known few solutions of the spatial contact problems for rigid punches, obtained by the boundary-element method, enable a high efficiency of this method to be predicted in case the elastic base models with different influence functions being used.

The analysis of the reference data also shows that the difficulties in creation of universal algorithms of mathematical modelling of processes of interaction of foundations with soil masses are related to the necessity of the simultaneous account of the geometrical and physical nonlinearities of the soil base, contact friction, and

slippage effects on the contact surface of the foundation and the soil, search for the a priori unknown contact domains of complex shape, etc. The FEM computation schemes, due to the superimposement of various iterative procedures, appear so cumbersome that they result in a deterioration of the general convergence of the numerical solution processes and extraordinarily high consumption of computer resources. Therefore, elaboration of new efficient methods of solving the contact problems of interaction of foundations with soil, with the account of the complex shape of their section, essentially spatial loading conditions, close to the real physical and mechanical properties of soils and deformational characteristics of foundation structures, is still an up-to-date task. In our opinion, combined application of the boundary-element and finite-element methods should enable more effective solutions of important and practically significant problems of interaction of foundations with soil in spatial formulation.

Optimal application of advantages of the boundary-element and finite-element methods appeared rather fruitful for solving the modified problems of contact interaction of foundations with soil bases. In this view one should mention a series of publications of Rozin et al. [217–221], devoted to working out a combined numerical method of solving the problems for infinite domains of complex structure. The proposed combined method is based on iterative combination of the boundary-element and finite-element methods. The iterative process of solving the spatial problem of interaction of the foundation with the soil is proposed to be built in the following way [217–221]. At each step the finite-element method is applied in a finite domain of complex structure (being the foundation together with the area of plastic deformation of the base) using the Somigliana formula on a boundary surface of the rest of the infinite homogeneous area of the base. All the calculations in the specified finite domain can be performed using traditional grid methods (FDM, FEM). The iterations continue until the displacements on a certain finite convolute (auxiliary) surface will differ within the given computation error. Solutions of a number of test (non-contact) problems for infinite domains, performed by Rozin et al., have shown higher accuracy and considerable computational benefits in case the combined method being used, in comparison with the application of the FEM with truncation of the infinite base domain.

Evidently, the effective application of the combined method for contact interaction calculations in the “foundation + soil base” system will require the use of the boundary-element solutions of contact problems for infinite elastic bases in an essentially spatial formulation.

4.2 Contact Problems for Rigid Rectangular Punches, Resting on Elastic Nonhomogeneous Bases

Consider spatial contact problems for rigid rectangular punches, resting on elastic, in general case spatially nonhomogeneous bases. Elastic solutions. corresponding to such formulation, are important for the design of extensively used foundations

with a rectangular bottom shape: under elevators, under columns of buildings and structures, for equipment, etc.

Let us consider an absolutely rigid punch of a rectangular shape with a flat bottom to undergo a spatial static load, reduced to a vertical resultant force P and moments M_x, M_y (Fig. 4.1). We also assume that vertical displacements of the punch and the base surface are equal, and there is no tangential stress in the contact plane. The latter assumption is based on the results of solving similar problems for a half-plane and a half-space with the account of tangential stress in the contact domain which have shown that the effect of tangential reactions under the punch can be neglected while determining the main characteristics of the contact interaction (First of all, normal forces) [1, 91, 127, 128, 135]. Note that the account of friction forces in the contact domain is required in a number of machine-building problems, e.g. the evaluation of wear strength of contacting elements in various mechanisms and machines, estimation of the probability of fatigue crack nucleation, etc. when the friction coefficient depends on the acting stress and relative velocity of the bodies in contact [26, 108].

As noted above, there are no exact solutions for the punches of rectangular cross-section. Therefore, for a rectangular punch, as well as for the punches of more complex shape, one should apply numerical methods for solving the contact problem.

For numerical solution of the contact problems by the boundary-element method the contact domain was preliminarily discretized into rectangular boundary elements. Figure 4.2 shows a scheme of a uniform mesh of a rectangular domain into 96 quadrangular boundary elements. At the calculations of the contact interaction of punches with the variable-thickness elastic layer the number of elements in the direction of the OX axis was always equal or exceeding the number of elements along the OY axes. This is required for the correct account of the contact interaction characteristics in the direction of the maximal variation of the elastic layer thickness. The optimal number of the elements at the calculations was taken as $12 \times 8 = 96$ what enables one to obtain relatively exact values of integral characteristics of the contact interaction (the settlements and slopes of the punches as a rigid body).

Since the contact stresses near the edge (under a full contact with the base) are of singular character, in order to increase the accuracy of the solution of the contact problem for a half-space, on the edge boundary elements the known asymptotic was taken into account [27, 31, 183, 225]:

$$\begin{aligned} &\text{in the vicinity of the right angle } \; p(r,\varphi) = C_1(\varphi) \cdot r^{-\gamma_1},\ \gamma_1 \approx 0.7; \\ &\text{at straight sides } \; p(r,\varphi) = C_2(\varphi) \cdot r^{-\gamma_2},\ \gamma_2 \approx 0.5 \end{aligned}$$

where $r = 0$ is a point on the punch contour.

No similar estimations have been performed for punches on elastic non-classical bases. Therefore, at numerical calculations for bases of different type, in order to "soften" the contact pressure field near the punch edge. The rectangular boundary-element grid was condensed towards the edges of the rectangular punch contact area. The nodes of the boundary-element grid were chosen at the intercepts of straight

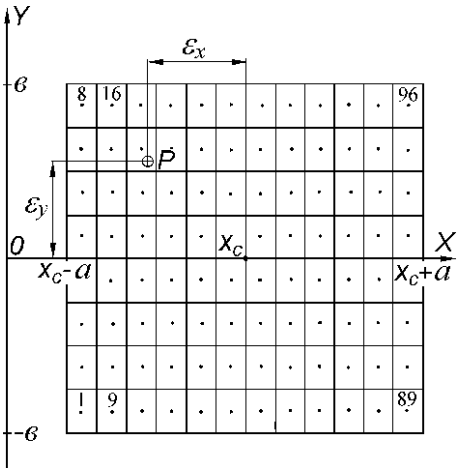

Fig. 4.2 Uniform discretization of a rectangular domain into boundary elements

lines, located at the distances from the punch symmetry axes, given by a quasiuniform dependence

$$\rho_m = \rho_0 \frac{e^{\gamma t_m} - 1}{e^{\gamma} - 1}, \quad t_m = \frac{m-1}{L}, \quad m = 1,2,...,L$$

where ρ_0 is a half of the rectangular punch side length, $2L$ is the number of nodes in one of the directions. The condensation degree was controlled by the choice of an empirical parameter γ. The series of test calculations for test problems have enabled the value $\gamma = -2$ to be chosen, at which the numerical results of the reactive pressure distribution at the full contact of the rectangular punches with the base are obtained with acceptable accuracy. To calculate the integral characteristics of the contact interaction (settlements and slopes), a boundary-element grid of the optimal density 10×10 was effectively used (Fig. 4.3a). A quasiuniform grid of rectangular boundary elements, enabling reliable contact pressure fields to be obtained at complex loadings on elastic bases of different type, is shown in Fig. 4.3b.

At the contact domain discretization for rectangular punches, located in the *XOY* plane of arbitrary orientation, as well as for punches of quadrangular cross-section of general type (not necessarily rectangular), the following transformation was used [56]:

$$U = \varphi_1 U_1 + \varphi_2 U_2 + \varphi_3 U_3 + \varphi_4 U_4$$

with the interpolating functions

$$\varphi_1 = \frac{1}{4}(1-\xi_1)(1-\xi_2), \quad \varphi_2 = \frac{1}{4}(1+\xi_1)(1-\xi_2),$$
$$\varphi_3 = \frac{1}{4}(1+\xi_1)(1-\xi_2), \quad \varphi_4 = \frac{1}{4}(1-\xi_1)(1+\xi_2)$$

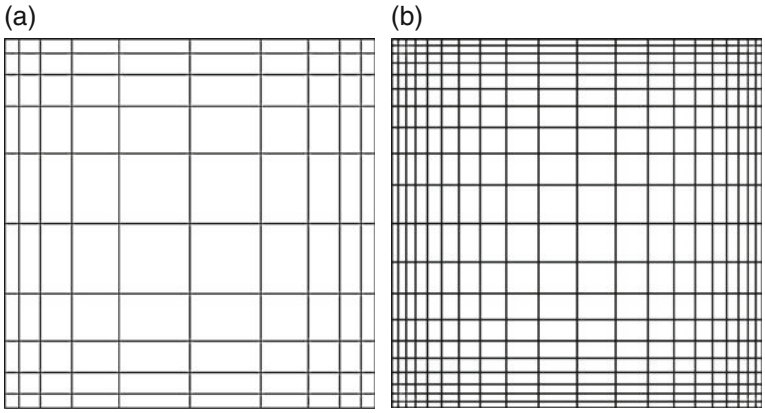

Fig. 4.3 Quasiuniform discretization of a square domain into (**a**) 10 × 10 and (**b**) 20 × 20 boundary elements ($\gamma = -2$)

where U_i $(i = \overline{1,4})$ are the X or Y coordinates of the four angular points of the contact domain, ξ_1 and ξ_2 are the coordinates of points of a standard square $|\xi_1| \leq 1$, $|\xi_2| \leq 1$.

The subsequent subsections of this section contain the results of numerical studies of the contact interaction of rectangular punches resting on elastic bases with non-uniform compressibility.

For an elastic layer of variable thickness, the calculation results for punches, whose centre is located at a distance x_c from the elastic wedge rib $x = 0$, $-\infty<y<\infty$, $z = 0$, and loaded by a vertical central or off-centre force P, are analyzed. For the calculations the following values of the punch loading parameters and the elastic base characteristics were used:

$$M_x = M_y = 0,\ P = (10 \cdot a)^2 E\ k\text{N},\ \text{E} = 10\,\text{MPa}.$$

In all cases, except those directly specified otherwise, the calculations were performed with the Poisson ratio $\nu = 0.25$. The constant vertical load was applied at the point with the coordinates $x = x_c + \varepsilon_x$, $y = y_c + \varepsilon_y$ where $(\varepsilon_x, \varepsilon_y)$ is the eccentricity of the force P with respect to the punch centre $C(x_c\ ,\ y_c)$, $2a$ is the characteristic size of the punch.

In a similar formulation the contact problem solution for punches of circular cross-section, resting on an elastic layer of variable thickness, is described in Appendix B. Settlements and slopes of a rectangular punch on a wedge-shaped base without the analysis of contact pressure fields and without the account of unilateral constraints in the contact domain were studied in [187].

4.2.1 Contact Interaction at Central Loading

Elastically compressible bases of constant and variable thickness. The results of calculation of parameters of interaction of rectangular punches with an elastic half-space and layers of variable and constant thickness are given in Figs. 4.4–4.12 and 4.14 and in Tables 4.1–4.3.

Figure 4.4 shows the calculated dependences of contact pressures for a centrally loaded square punch at different values of the tilt angle α of the underlayer and fixed values $\nu = 0.25$ and $x_c = 2a$. For the sake of comparison the same figure contains the contact pressure curve, corresponding to the calculations for an elastic half-space. The contact pressure values p_i, calculated at the solution of the boundary problem in the centres of gravity of the elements located along the *OY* axes, were afterwards interpolated using cubic splines [93]. It is seen from the comparison of the calculated dependences, presented in Fig. 4.4, that the pressure field under the square punch on a variable-thickness layer is essentially asymmetrical. With the increase of the tilt angle α of the rigid underlayer the difference between the solution for the half-space and the calculation results for the elastically compressible wedge becomes smaller, this being the consequence of the increase of the thickness of the compressible layer under the punch. A more detailed pattern of the non-uniform distribution of the contact pressure under the square punch is seen in Figs. 4.5 and 4.6 where the equal contact pressure lines are presented, plotted using the interpolation of functions of two variables. For the square punch on an elastic half-space the obtained solution is in a qualitative agreement with the one given in [154]. For this solution the isoline pattern for the contact pressure is symmetrical with respect to the symmetry axes of the square and its centre (Fig. 4.5), in the greater part of the contact domain the equal pressure lines being practically indistinguishable from circles. With the increase of the distance form the centre the equal pressure lines are taking the shape of squares with rounded angles.

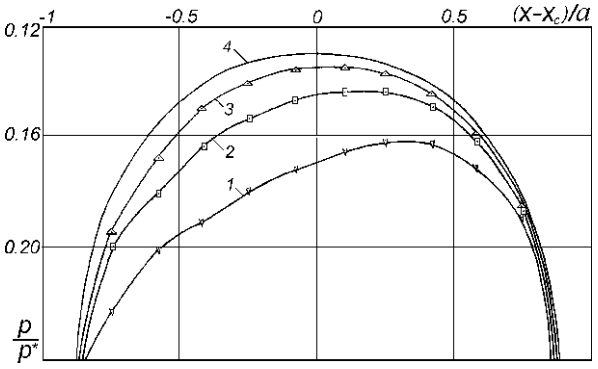

Fig. 4.4 Contact pressures in the $y = 0$ section for a centrally loaded square punch, resting on a variable-thickness elastic layer ($x_c = 2a$) at $\alpha = 30°, 45°, 60°$ (1–3); (4) elastic half-space

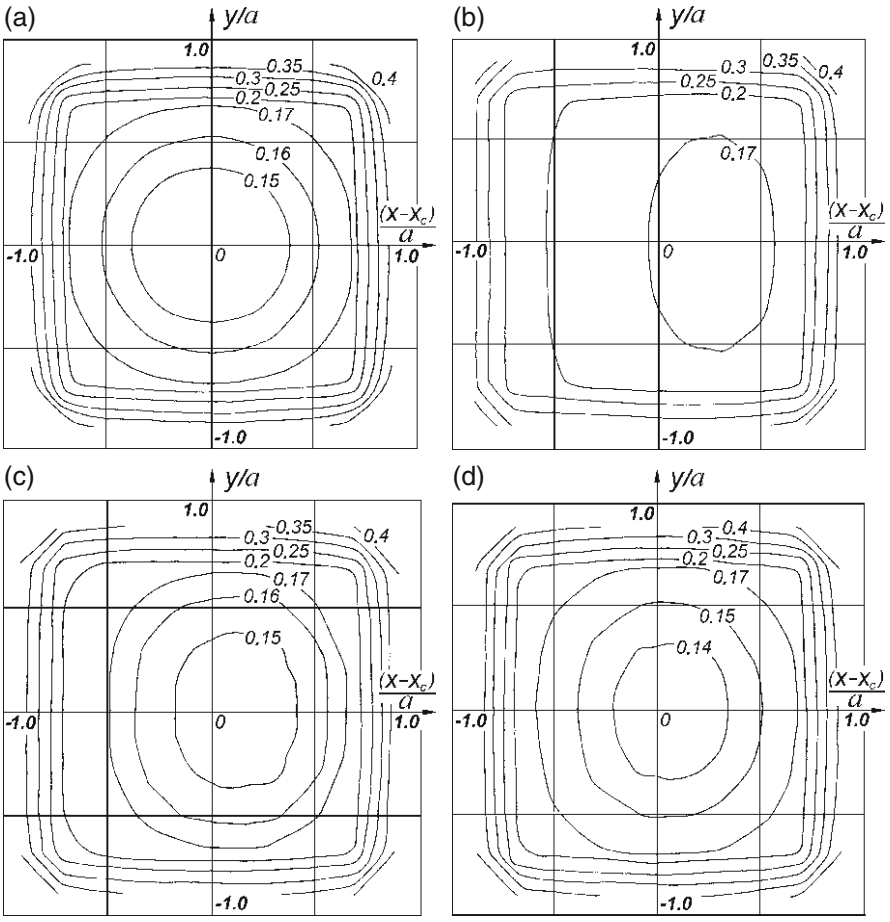

Fig. 4.5 Equal contact pressure linesp/p^* for a centrally loaded square punch, resting on an elastic half-space (**a**) and on a variable-thickness elastic layer ($x_c = 2a$), $\alpha = 30°$ (**b**), 45° (**c**), 60° (**d**)

For a square punch on an elastically compressible layer of variable thickness, contact pressure isolines are always asymmetrical with the contours displaced from the centre of the square towards the increase of the layer thickness. An evident condensation of the isolines occurs in the same direction. The asymmetry in the pattern of the equal pressure lines is noticeably manifested in the central part of the punch with the decrease of the α values. However, with the increase of α, as well as with approaching the punch contour, the effect of the elastic layer thickness variation is smaller. As follows from the calculations (Figs. 4.5 and 4.6), in the considered cases of the contact interaction of a square punch with a non-uniformly compressible base, a rather considerable contact domain exists, in which the pressure is practically constant. With the decrease of α these domains are distorted, acquiring a prolate shape along the OY axis, and shift towards the increasing thickness of the

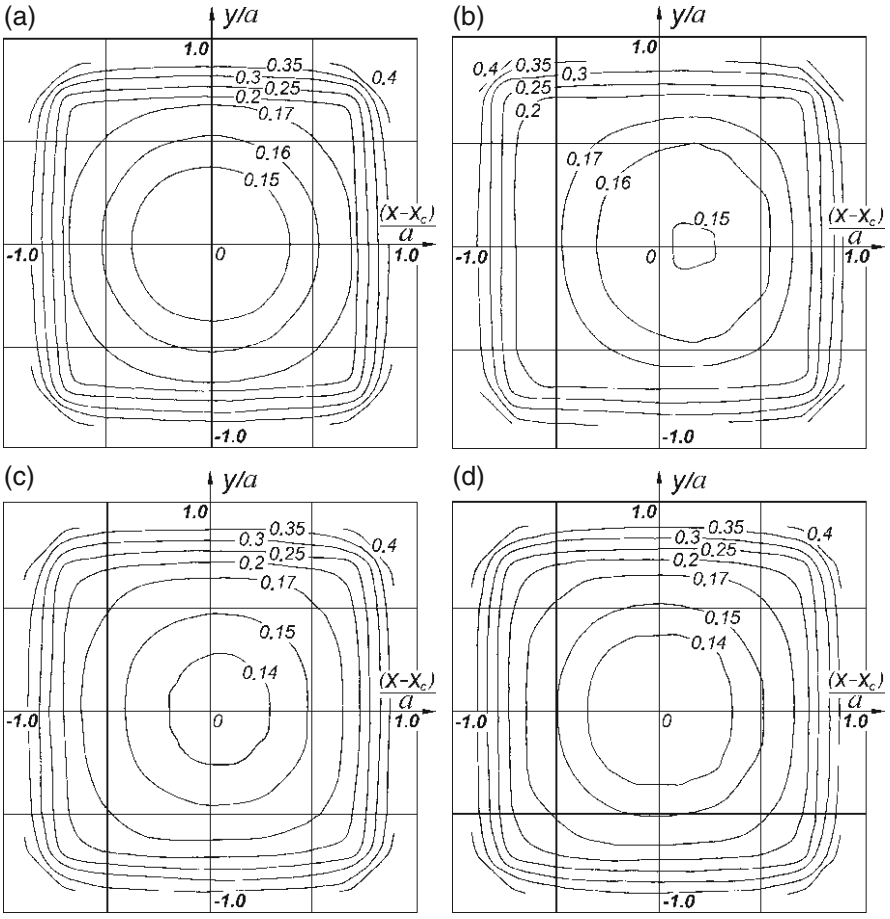

Fig. 4.6 Equal contact pressure linesp/p^* for a centrally loaded square punch, resting on an elastic half-space (**a**) and on a variable-thickness elastic layer ($x_c = 3a$), $\alpha = 30°$ (**b**), 45° (**c**), 60° (**d**)

elastically compressible wedge (normally to its rib). As follows from the calculations performed, for the contact domains, more remote from the elastic wedge rib, at a fixed angle α value the described characteristics of the contact interaction are also revealed, but to a much smaller extent: the domains of constant contact pressure are of more rounded shape and the displacement from the punch centre is essentially smaller. Already for $\alpha = 60°$ and $x_c/a = 3$ the contact pressure field both qualitatively and quantitatively practically does not differ from the corresponding field for an elastic half-space. Contact pressure field variations with the increase of the punch distance from the elastic wedge rib at a fixed value of $\alpha = 45°$ are illustrated by Fig. 4.7. As seen from the figure, with the increase of the x_c/a values the asymmetry of the contact pressure profile rather quickly vanishes, and already at x_c/a

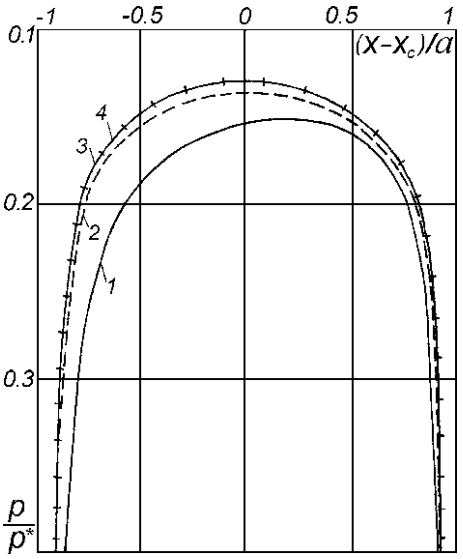

Fig. 4.7 Equal contact pressure linesp/p^* for a centrally loaded square punch in the$y = 0$ section, resting on a variable-thickness elastic layer ($\alpha = 45°$) at $x_c = a$(1), $3a$(2),$30a$ (3); (4) elastic half-space

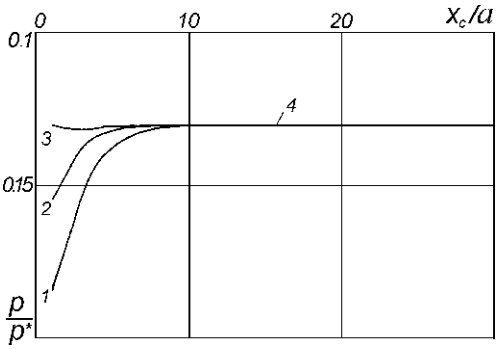

Fig. 4.8 Dependence of pressures in the centre of a square punch on the distance from the elastic wedge rib ($\varepsilon_x = \varepsilon_y = 0$) at $\alpha = 30°$ (1), 45° (2), 60° (3); (4) elastic half-space

$= 30$ the contact pressures for a square punch on the half-space and on the elastic layers (with various values of α) practically coincide.

Figures 4.8–4.11 illustrate the variation of the integral characteristics of the contact interaction of a square punch at different values of x_c/a and α: the pressure p_c and the centre settlement W_c, as well as the punch slopes ψ_x. As follows from the calculations, presented in Fig. 4.8, the contact pressures p_c in the square punch centre for $x_c/a \leq 10$ are essentially dependent of the values of α, growing with the increase of the latter. However, for $x_c/a \geq 10$ no dependence of the pressure values p_c on α is observed, and the corresponding solutions for the half-space can be used to estimate p_c without any essential error.

The punch centre settlements increase with the increase of its distance from the elastic compressible wedge rib, as well as with the increase of the tilt angle α of

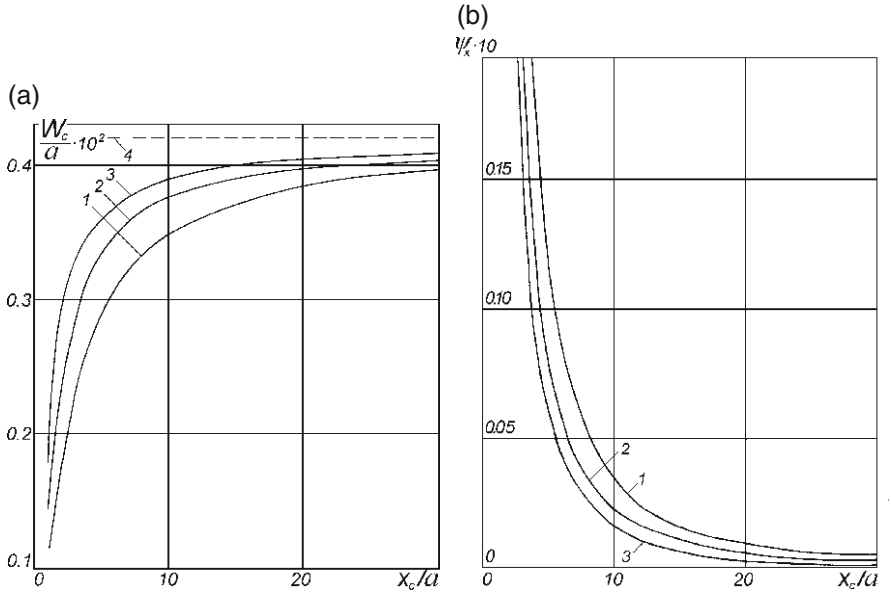

Fig. 4.9 Settlements of the centre (**a**) and slopes (**b**) of a centrally loaded square punch versus the distance from the elastic wedge rib at $\alpha = 30°$ (1), 45° (2), 60° (3); (4) half-space

the lower surface of the distorted base (Fig. 4.9a). With the increase of x_c/a the settlement values unlimitedly approach the punch settlement values on the half-space what is related to the increase of the compressible layer thickness under the punch and the corresponding small range of the compressed soil mass thickness variation.

The influence of the relative distance x_c/a and angle α on the slopes at central loading of the square punch is shown in Fig. 4.9b. As follows from the calculations, with the increase of x_c/a values the punch slope ψ_x in the interval $a \leq x_c \leq 30a$ rapidly decreases to zero, the higher values of a corresponding to smaller slopes and their more rapid decrease. Note that the results of calculations for the centrally loaded square punch, shown in Figs. 4.8 and 4.9, are in full qualitative agreement with those we have obtained from the calculations of pressures p_c, settlements W_c and slopes ψ_x of a centrally loaded round punch (See Appendix B).

Figure 4.10a–c illustrate the quantitative effect of the punch geometrical shape on the pressures p_c, settlements W_c and slopes ψ_x of the round and square punches, loaded by equal vertical forces and having the same contact area. Centrally loaded punches of circular (with a radius $r = a\sqrt{\pi/2}$) and square (with the lateral size $2a$) shape of equal area were compared. It follows from the obtained calculation data (Fig. 4.10a) that the round punch centre settlements are always smaller than those of the square shape, independently of the elastic base type. The larger is the angle α at the elastically compressible wedge rib, the greater is the difference in the settlements. It is seen from the plots of Fig. 4.10b that the circular punch slopes are

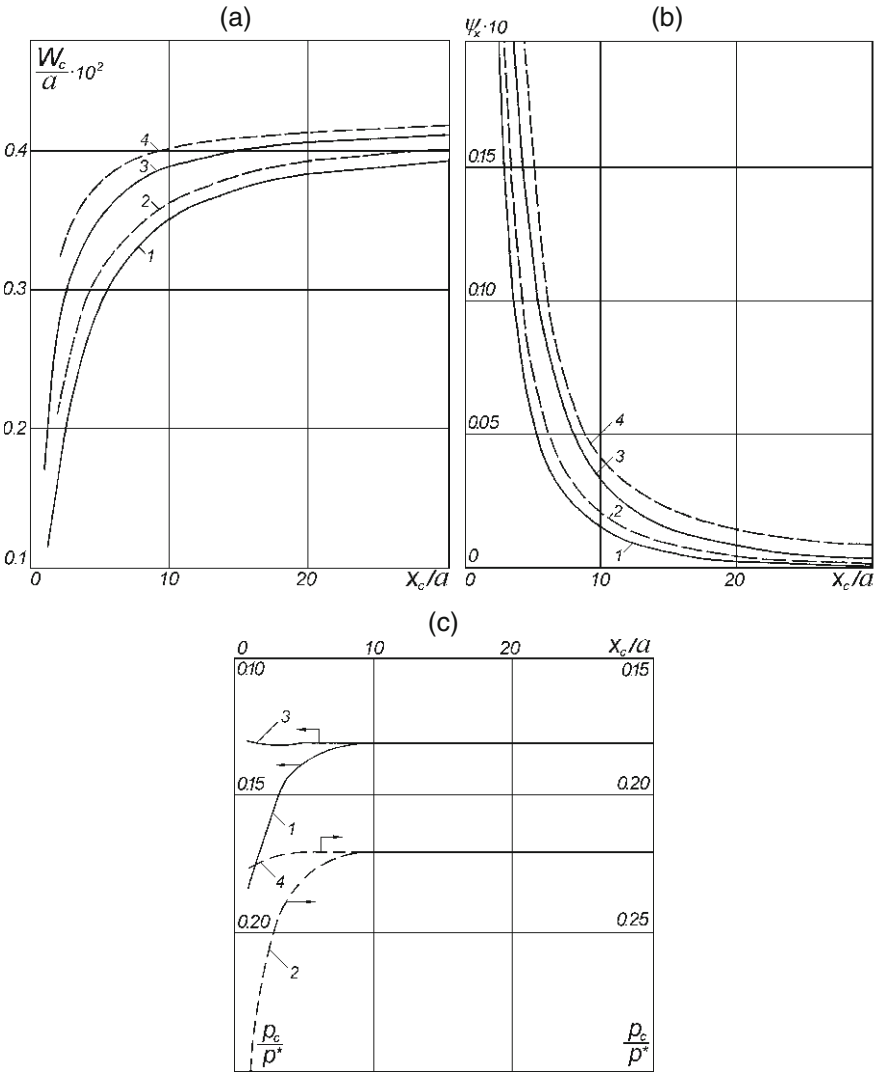

Fig. 4.10 Settlements of the centre (**a**), slopes (**b**) and pressures in the centre (**c**) of rigid punches ($\varepsilon_x = \varepsilon_y = 0$) of equal area, resting on a variable-thickness elastic layer for $\alpha = 30°$(1,2), 60° (3,4); *solid line* – square punch, *dashed line* – circular punch

larger, though slightly, than those for the square one of the same area. The absolute increment of the round punch slopes is the most considerable in the area, adjacent to the elastic wedge rib. The influence of the punch bottom shape is the most essential for the contact pressure distribution. The pressures p_c in the centres of the square and the round punches of equal area are plotted in Fig. 4.10c versus the relative distance of their centres to the elastic wedge rib for the values of $\alpha = 30°$ and 60°.

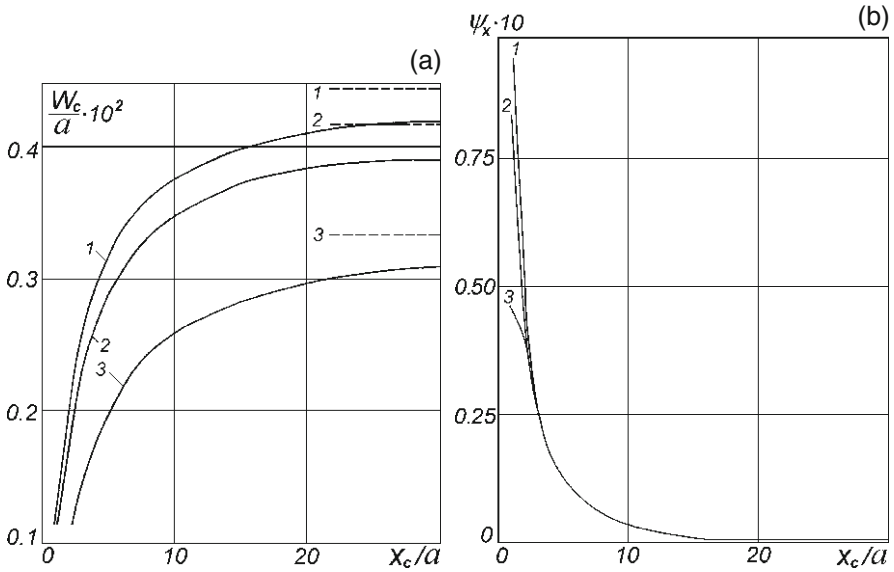

Fig. 4.11 Settlements of the centre (**a**) and slopes (**b**) of a centrally loaded square punch at $\nu = 0$ (1), 0.25 (2), 0.5 (3). *Solid line* – a variable-thickness elastic layer ($\alpha = 30°$), *dashed line* – elastic half-space

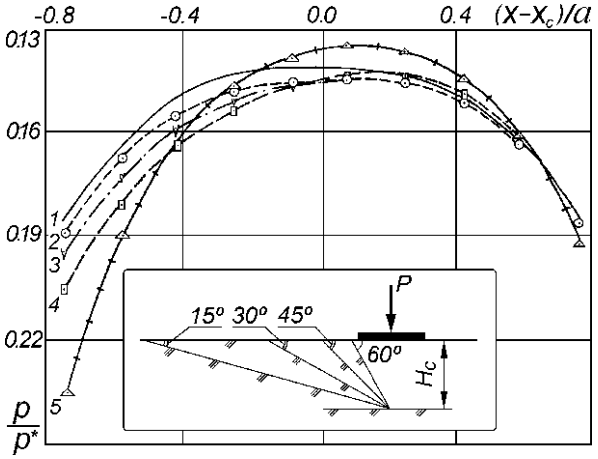

Fig. 4.12 Distribution of contact pressures in the $y = 0$ section of a centrally loaded square punch for constant-thickness $H_c = 2a$ (1) and variable-thickness layers at $\alpha = 15°$ (2), 30° (3), 45° (4), 60° (5)

Table 4.1 Characteristics of the contact interaction of a centrally loaded square punch on elastic bases of different type ($\nu = 0.25$)

Elastic base type	Settlement of the punch centre $(W_c/a) \times 10^2$	Slope $\psi_x \times 10$	Pressure in the punch centre p_c/p_*, $p_* = P/a^2$
Half-space	0.4209	0	0.1305
Constant-thickness layer $H_c = 2a$	0.2672	0	0.1414
Elastic wedge:			
$\alpha = 15°$	0.2495	0.1004	0.1477
$\alpha = 30°$	0.2461	0.2170	0.1464
$\alpha = 45°$	0.2339	0.4003	0.1457
$\alpha = 60°$	0.1989	0.8579	0.1371

Table 4.2 Settlements and slopes of a square punch with a side $2a$ on a variable-thickness elastic layer ($\nu = 0.25$; $\alpha = 45°$, $x_C = 2a$) at different orientation angles β in the contact plane

β	0°	22.5°	45°
$(W_c/a) \times 10^2$	0.2339	0.2338	0.2337
$\psi_x \times 10$	0.4003	0.4101	0.4197
$\psi_y \times 10^3$	0	0.8958	0

Table 4.3 Characteristics of the contact interaction of rectangular punches with different side ratio a/b, resting on a variable-thickness elastic layer ($x_c = 3a$, $\nu = 0.25$, $\alpha = 45°$)

a/b	$\psi_x \times 10$	p_c/p_*	$(W_c/a) \times 10^2$
1.0	0.2097	0.1367	0.2840
0.25	0.1586	0.1409	0.2575
4.0	0.2452	0.1477	0.2454

As seen from the calculated plots, due to the concentration of the pressure field near the angular points, the contact pressures in the central part of the square punch are essentially lower than in the central part of the circular punch. At $\alpha \geq 30°$ for both the circular and the square punches, variation of the contact pressures p_c in the centre occurs only in the area, adjacent to the rib of the elastically compressible wedge, with the size $x \div 10a$. For $x_c \geq 10a$ the contact pressures p_c in the centre of both the circular and the square punches are the same as the corresponding values for the elastic half-space (Fig. 4.10c). Thus, the performed comparative analysis of the contact interaction of the circular and square punches of equal area with the elastic layer of variable thickness shows the necessity of a more detailed discretization of the contact domain towards the decrease of the base depth to be performed at the design of rigid and flexible structures on elastic bases with variable compressible thickness.

The calculated dependences, plotted in Fig. 4.11 show the effect of the Poisson ratio on the punch centre displacements and slopes with the increase of the distance from the elastic compressible wedge rib. As seen from the plots, the increase of ν most essentially affects the settlement of the square punch centre. With the increase of the punch distance from the rib ($x = 0$) the corresponding settlement values asymptotically tend to the values, corresponding to the punch settlements on the half-space (Fig. 4.11a). Numerous calculations have shown that the increase of α leads to the size of the domain where the settlement values for the square punch centre on a variable-thickness elastic layer will be practically indistinguishable for the Poisson ratio values ν in the whole range of its possible variation. The numerical calculations have also shown the increase of ν to cause the growth of p_c values. Note that the contact pressure values in the centre of the square punch become practically equal for the different values of the Poisson ratio ν at essentially lower values of the relative distance x_c/a in comparison with those, for which the levelling of the relative settlements W_c/a occurs. The dependence of the punch rotation angles versus the Poisson ratio values is illustrated by the calculated plots, given in Fig. 4.11b for the angle $\alpha = 30°$. Similarly to the circular punch (Appendix B), at $x_c \geq 5a$ the square punch slopes are practically independent of the Poisson ratio value.

The obtained numerical values for the parameters of the contact interaction for the square punch on the elastic layer with a linearly varied thickness were compared with the calculation data based on the known Egorov solution [75] for a concentrated normal load on the surface of an elastic layer of a constant thickness H. The depth of the layer under the square punch centre was fixed ($H_c/a = 2$), the tilt angles of the lower surface of the elastic compressible layer of variable thickness were varied. The analysis of the data presented in Fig. 4.12 and Table 4.1 gives the evidence for the necessity of the account of the elastic base thickness variation, especially for the estimation of such parameters of contact interaction of rigid punches as settlements and slopes.

The above considered calculation data for the square punch correspond to such its location when one of the sides is parallel to the elastic compressible wedge rib. In order to investigate the effect of the punch rotation angle in the XOY plane on the characteristics of its contact interaction, additional calculations were performed, their results being presented in Table 4.2. An angle $\beta \leq \pi/4$ between the symmetry axis of the square and the OX axis is used as a parameter, determining the punch location on the free surface of the elastic wedge (Fig. 4.13). As it should be expected,

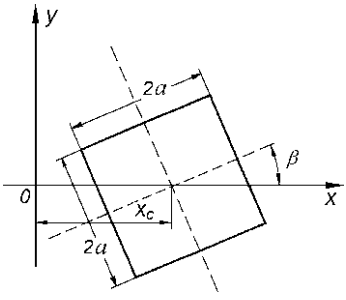

Fig. 4.13 Scheme of a square punch orientation on the surface of an elastic wedge-type base

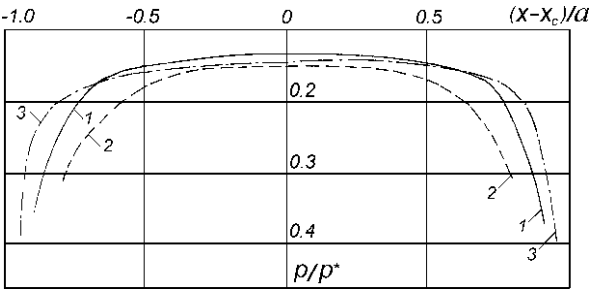

Fig. 4.14 Contact pressures in the $y = 0$ section of rectangular punches with the side ratio a/b: 1.0 (1), 0.25 (2), 4.0 (3), resting on a variable-thickness elastic layer ($x_c = 3a$, $\alpha = 45°$)

the slope ψ_x is always nonzero, and at $\beta \neq 0°, 45°$ one also has $\psi_y \neq 0$. Note that the ψ_x slope values are more than by an order of magnitude higher than the ψ_y slopes. The relative settlement values W_c/a remain practically unchanged. As follows from the numerical calculations, for a centrally loaded square punch its rotation at a fixed value $x_c = 2a$ results in the corresponding variation of ψ_x not more than by 5%. Therefore, for square punches of arbitrary orientation on a variable-thickness elastic layer, the values of W_c and ψ_x, obtained at $\beta = 0$, can be used with a sufficient accuracy. At different β one should correctly estimate the corresponding slope ψ_y variations.

Consider some results of calculations for punches of rectangular cross-section shape with different side ratio. The calculation results for centrally loaded rectangular punches of equal area with the side ratio $a/b = 0.25, 1, 4$ at $\alpha = 45°$, $x_c/a = 3$ are presented in Fig. 4.14 and Table 4.3. For the discretization of the contact domain grids of 100 square boundary elements arranged as 4×25, 10×10, 25×4, respectively, were applied. Such system of the contact domain discretization has enabled the contact interaction to be reproduced at the numerical calculations with minimal errors. The relative settlement W_c/a of a rectangular punch is always smaller than for the square punch of the same area (Table 4.3). On the other hand, relative pressures p_c/p_* in the rectangular punch centre will be higher than for the square punch. The calculations have shown the relative pressure p_c/p_* in the centre of the rectangular punch with longer dimension along the rib ($a/b = 0.25$) of the elastic compressible wedge, to be by 4.6% lower than for the rectangular punch with longer dimension ($a/b = 4$) along the OX axis. The influence of the a/b ratio is the most essential for the angular displacements ψ_x of rectangular punches. For a rectangular punch with the side ratio $a/b = 0.25$ the slope ψ_x decreases by 24.3% with respect to the slope of the square punch. Simultaneously, for a rectangular punch with longer dimension in the direction of the elastic layer depth increase ($a/b = 4$), its slope ψ_x increases by 17% in comparison with that of the square punch. The calculations for rectangular punches have also shown that, contrary to the square punch, the slope values ψ_x and ψ_y are comparable and strongly depend on the a/b ratio at different values of the angle β.

Elastic half-space with an increasing deformation modulus. Consider a spatial contact problem for a rigid rectangular punch resting on an elastic nonhomogeneous base with an increasing deformation modulus, loaded by a central force *P*. Fundamental solutions $\omega^{(n)}(x–\xi,\ y–\eta)$ for a nonhomogeneous base with linear (n=1) and parabolic (n=2) dependences of the deformation modulus on the depth (Sect. 1.5.3) are used as influence functions. The Poisson ratio, as a rule, varies only slightly, its value does not produce any essential effect on the stress-strained state characteristics and hereinafter is assumed constant. Since there is a known relationship between the elastic constants $G = E/2(1+\nu)$, at such consideration the shear modulus $G = G(z)$ will be variable with depth.

The main regularities of the contact interaction can be traced from the calculation results, obtained for a square punch ($a/b = 1$). In Table 4.4 the calculation data for the settlements W_0/a and contact pressures in the centre p_0/p_{av} ($p_{av} = P/S$ being the average pressure over the bottom, $S = 4ab$) illustrate convergence of the numerical solutions with the increase of the discretization degree for a punch located on an elastic half-space ($B = 0$) and elastic non-classical bases with different nonhomogeneity degree ($B = 5$, $n = 1, 2$). The upper values in the table cells correspond to dimensionless pressures, the lower ones – to dimensionless settlements. The calculations were carried out for the values $n = 0.25$, $P = E_0 \times a^2$, and $\mu = h/a = 0.5$. The same table contains the corresponding extrapolated values obtained using the Richardson method in the assumption of the second order of accuracy of the numerical method being used. As follows from Table 4.4, with the increase of the discretization degree a stable increase of the accuracy of the obtained results is observed. On a 20 × 20 grid the relative error of the numerical solutions does not exceed 1.5% for the settlements and 2% for the contact pressures what is quite sufficient for practical calculations.

Contact pressure $p = p(x, y)/p_{av}$ isolines for the punch on an elastic homogeneous half-space ($B = 0$) and on elastic punches with different degrees of nonhomogeneity of the deformational properties ($B = 1, 5$, $n = 1, 2$) are plotted in dimensionless coordinates $\bar{x} = x/a$, $\bar{y} = y/a$ in Fig. 4.15. In all cases the contact pressure distribution patterns are qualitatively similar: in the punch bottom centre a constant-pressure

Table 4.4 Studies of convergence of numerical solutions of the contact problem of a square punch on nonhomogeneous elastic bases

Base parameters	$N_x = N_y$					Extrapolation values
	8	12	16	20	24	
$B = 0$	0.5296 0.4236	0.5144 0.4181	0.5069 0.4153	0.5025 0.4137	0.4996 0.4125	0.4931 0.4099
$B = 5.$ $n = 1$	0.6026 0.2599	0.5844 0.2557	0.5758 0.2536	0.5707 0.2524	0.5674 0.2516	0.5598 0.2498
$B = 5.$ $n = 2$	0.8118 0.114	0.7957 0.1093	0.7873 0.1082	0.7820 0.1075	0.7785 0.1071	0.7704 0.1060

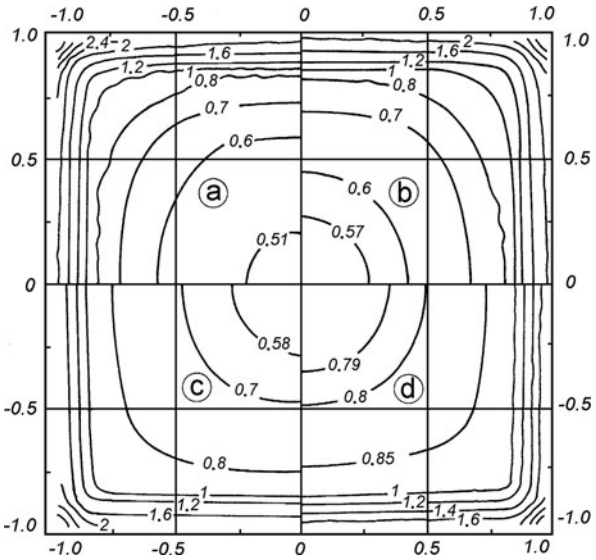

Fig. 4.15 Contact pressure p/p^* isolines for a square punch on the bases of different nonhomogeneity degree atμ=1: **(a)**$B = 0$; **(b)**$n = 1$, $B = 1$; **(c)** $n = 2$, $B = 1$; **(d)** $n = 2$, $B = 5$

area with a nearly circular shape exists, with the increase of the distance from the centre the isobars from the circles are transformed into symmetrical ovals, and in the vicinity of the foundation edges they take the shape of similar squares with rounded corners. For both contact models of the elastic nonhomogeneous base an unlimited growth of the contact pressures occurs at the foundation boundary contour. Simultaneously, as seen from the calculation data presented, the contact pressure field is rather sensitive with respect to the distributive properties of the base, determined by the nonhomogeneity parameters. The circular central constant-pressure area has the minimal size in the homogeneous half-space case (Fig. 4.15a). For nonhomogeneous bases the area in question broadens with the increase of both the n parameter (Fig. 4.15b, c), and the B parameter (Fig. 4.15c, d). Simultaneously the values of the contact pressures themselves increase for these areas as well (Figs. 4.15b–d and Fig. 4.16a). Thus, with the increase of the nonhomogeneity parameters, due to the variation of the distributive properties, for different contact models of nonhomogeneous bases redistribution (levelling) of the reactive pressures in the contact domain occurs with the pressure decrease near the boundaries and increase in the central area.

The relative settlements W_0/a of the punch are plotted across the values of the deformation modulus B variation range on nonhomogeneous bases of different type ($n = 1, 2$) at $\mu = 0.5$, 1, and 2 in Fig. 4.16b. It is seen from the figure that an increase of the nonhomogeneity parameter B within one order of magnitude can result in the punch settlement decrease more than by factor of 5 what is related to the relaxation of the base distributive properties with the increase of their nonhomogeneity

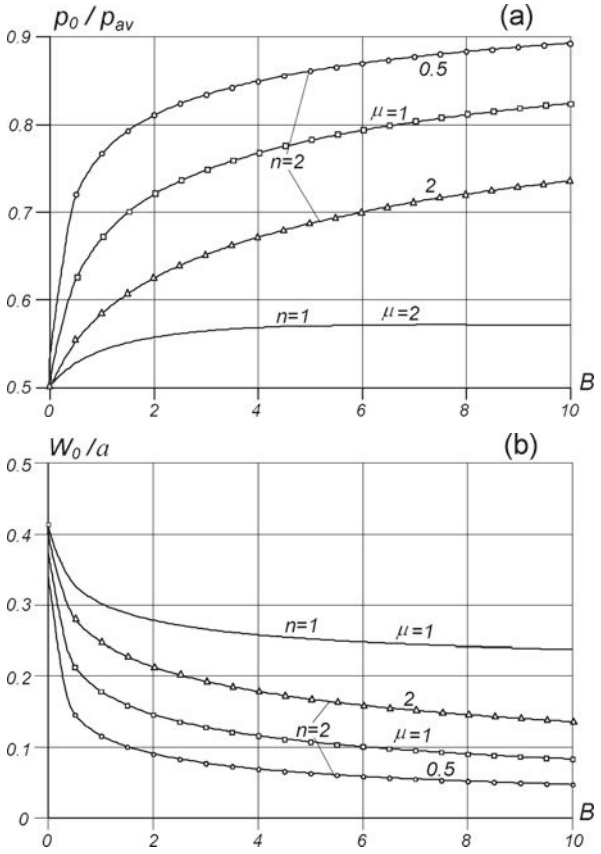

Fig. 4.16 Contact pressures (**a**) and settlements (**b**) in the centre of a square punch on nonhomogeneous bases with increasing deformation modulus

degree. A rather considerable (≈70%) settlement decrease occurs already in the case when at the depth of half the punch side width ($\mu = 1$) the deformation modulus increases not more than twice ($B \leq 1$). Besides, numerous calculations have shown that at a fixed μ the above noted character of the settlement decrease is essentially affected by the type of the base nonhomogeneity: at the linear increase of the deformation modulus with depth ($n = 1$) the settlements are always larger than at the parabolic variation ($n = 2$). Depending on the deformation modulus variation law employed, the difference in the settlement determination can reach up to 45%.

It should be noted that the account of nonhomogeneity, inherent to real soil bases, is rather important for the evaluation of internal forces in complex-shaped foundations since it enables the above considered trend to the contact pressure field levelling to be estimated at the design stage. The more uniform pressure over the foundation bottom than in the case of the homogeneous base will be helpful for the decrease of the slopes and levelling of the settlements.

4.2.2 *Contact Interaction at Off-Centre Loading with the Account of Unilateral Constraints*

Multivariant numerical studies have shown that at certain conditions related to the action of external moments or an eccentric load on a punch of a regular geometrical shape as well as at contact interaction of complex-shaped punches with elastic bases of half-space type, constant- or variable-thickness type, negative pressure zones can arise [13, 16, 17, 76, 225]. Since the soil medium does not work for tension, then, for a correct description of the real pattern of interaction of foundations with the base a unilateral character of constraints in the contact domain should be introduced into consideration.

Consider the results of calculations for off-centre loaded rectangular punches. Equal pressure lines $\bar{p} = p/p_*$ (hereinafter $p_* = P/a^2$) in the contact domain of a square punch under an eccentric load on an elastic wedge for $\alpha = 45°$, x_c=3a are plotted in Fig. 4.17. As seen from the calculations performed, the off-centre punch loading results in the formation of areas with rather low contact pressure (Fig. 4.17a) or even negative pressure (Fig. 4.17b) in the contact domain. In accordance with the unilateral constraint principle, in the presence of negative (tensile) stress the calculation was performed iteratively, excluding the boundary elements, for which p_i<0. A large series of the calculations performed has shown the iterative process to be, as a rule, convergent even at considerable eccentricities of the vertical load applied and the maximum iteration number not to exceed eight. By interpolation of the contact pressure function the contact zone configurations in the presence of the punch uplifting are plotted in Fig. 4.18 and the contact domain variation for the square punch loaded by an eccentric force for ε_x= 0, ε_y= 0.7, x_c= 2a, ν = 0.25, $\alpha = 45°$ in the course of the iterative process is shown. After the iteration process being

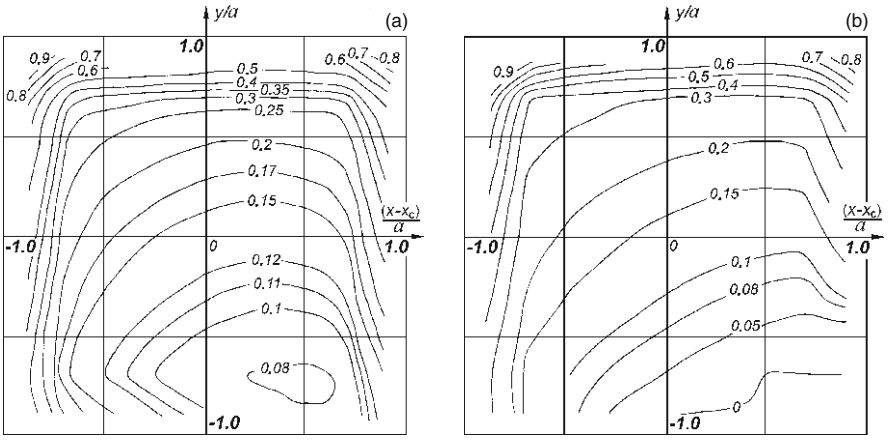

Fig. 4.17 Equal contact pressure lines p/p^* at off-centre loading of a square punch, resting on a variable-thickness elastic layer ($\alpha = 45°$, x_c= 3a): **(a)** (ε_x= – 0.1a, ε_y= 0.3a), **(b)** (ε_x= –0.2a; ε_y= 0.4a)

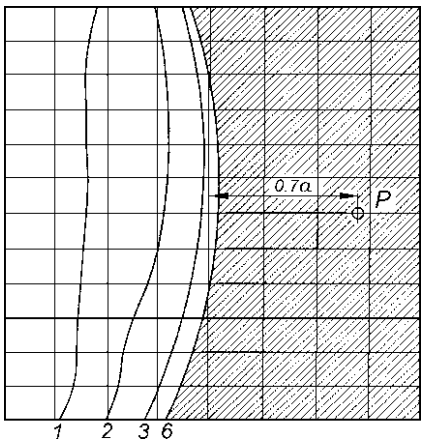

Fig. 4.18 Contact domain variation at off-centre loading ($\varepsilon_x = 0$; $\varepsilon_y = 0.7a$) of a square punch, resting on a variable-thickness elastic layer ($\alpha = 45°$, $x_c = 2a$) in the course of iterations, $N = 1,2,3,6$

finished, when all the values $p_i \geq 0$, the zone of the punch uplifting from the elastic base surface and, accordingly, the contact zone are determined. With the increase of the distance of the load application point from the rectangular punch centre the uplifting zone covers broader area (Fig. 4.19). The analysis of the great amount of numerical calculations performed shows that at $\varepsilon_x, \varepsilon_y \geq 0.8a$ a square punch undergoes a sharp increase of slopes what finally results in its overturn. In the case when $\varepsilon_y = 0$, the contact area of a rectangular punch with its side being parallel to the elastic wedge rib, is symmetrical with respect to the *OX* axis at any values $\varepsilon_x \neq 0$. At $\varepsilon_x \neq 0$, $\varepsilon_y \neq 0$ simultaneously as well as in the case when $\varepsilon_x = 0$, due to the variable thickness of the elastically compressed layer the area of contact of the rectangular with the base will be asymmetrical at any values $\varepsilon_y \neq 0$ (Fig. 4.19). The analysis of the contact area shape has shown the asymmetry degree to increase with eccentricity ε_y.

Figures 4.20 and 4.21 show the results of calculations of the settlements of the centre of a square punch and its slopes for various cases of off-centre loading with and without the account of unilateral constraints in the contact area. The distance of the punch centre from the elastic wedge rib $x_c = 2a$ and the Poisson ratio of the stressed base $\nu = 0.25$ were considered constant. As follows from the calculation performed (Fig. 4.20), the dependences of the rectangular punch centre settlements on ε_x (at $\varepsilon_y = 0$) and on ε_y (at $\varepsilon_x = 0$) are strictly linear what fully corresponds to the superposition principle in linear theory of elasticity. Similarly to the case of a round punch (Appendix B), at $\varepsilon_y = 0$, $\varepsilon_x \neq 0$ (Fig. 4.20a), the angular coefficients for the corresponding straight-line dependences of the variable-thickness layer are obviously nonzero and weakly depend on the angle α. It should be noted that at $\varepsilon_x = 0$ for an elastically compressed variable-thickness layer as well as for a half-space (Fig. 4.20a, b) the settlement of the punch centre does not depend on ε_y.

The results of the calculations performed show that an approach without the account of unilateral constraints does not enable one to describe the rigid punch

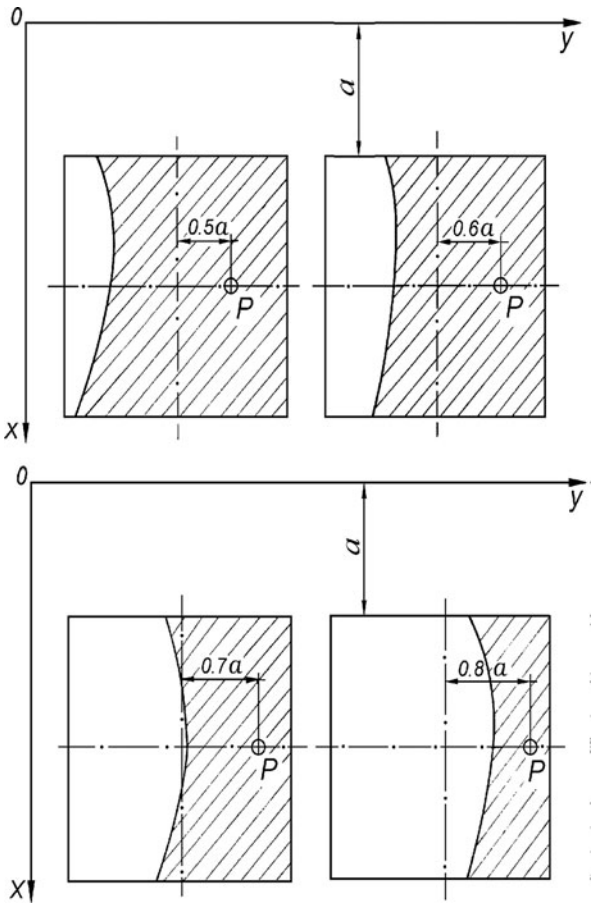

Fig. 4.19 Contact domains at off-centre loading (ε_x=0, ε_y/a= 0.5, 0.6, 0.7, 0.8) of a square punch, resting on a variable-thickness elastic layer ($\alpha = 45°$, $x_c = 2a$)

uplifting from an elastic base and the unlimited increase of its slope with the external force application point approaching the punch boundary. These shortcomings of the contact problem solution in the classical (linear) formulation are corrected by the account of the unilateral character of constraints in the contact area. From the calculations performed it follows (Fig. 4.20) that when the zones of the punch uplifting form the elastic base surface arise and the contact area decreases, a nonlinear dependence of the slopes ψ_x, ψ_y and settlements W_c of the rectangular punch centre on the external force eccentricity and, hence, on the external overturning moments, is observed. The structure-type nonlinearity, being revealed in such a way at the contact interaction, results in the inapplicability of the superposition principle. The calculations, performed for a square punch on a variable-thickness elastic layer ($x_c = 2a$), have shown (Fig. 4.20) that on the ranges $30° \leq \alpha \leq 60°$ and

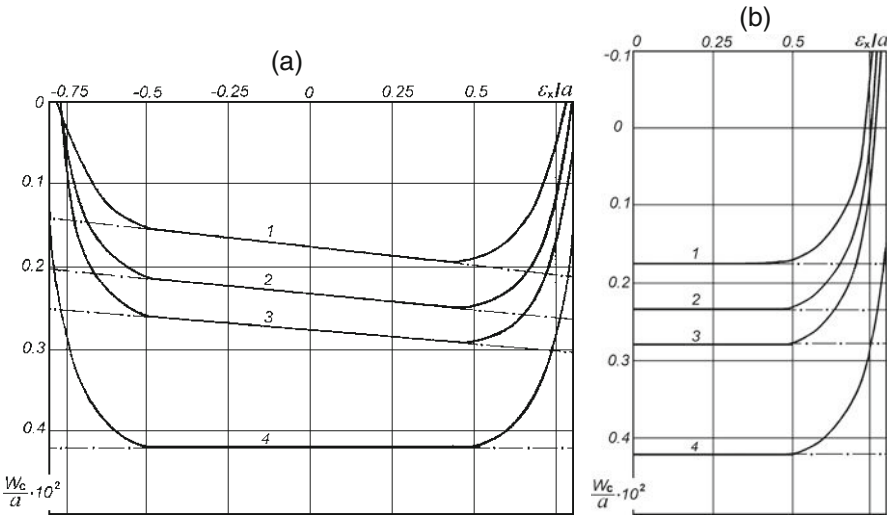

Fig. 4.20 Settlements of a centre of a square punch, resting on a variable-thickness elastic layer ($x_c = 2a$) depending on the force eccentricity: (**a**) $\varepsilon_x(\varepsilon_y = 0)$, (**b**) ε_y ($\varepsilon_x = 0$) at $\alpha = 30°$ (1), 45° (2), 60° (3); (4) elastic half-space. *Solid line* – with the account of uplifting of the punch from the base, *dashed line* – without the account of the punch uplifting

$-0.5\times a \leq \varepsilon_x \leq 0.4\times a$, $|\varepsilon_x| \leq 0.4\times a$ the contact interaction of the punch and the elastic base with the variable-thickness compressible soil mass goes without uplifting and, hence, the application of the superposition principle is correct.

Thus, it has been clearly shown with particular examples, that for rigid punches, using numerical calculations, one can determine the section kernel, i.e. the area of the vertical load application, for which the punch uplifting from the base does not arise. The problem of determination of the section kernel boundaries for rectangular punches at different values of *a/b*, α, x_c, ν, and β requires extensive special numerical calculations. The issues related to the calculation of the section kernel boundaries for foundation plates of non-canonical shape, often used for the design of new and renovated buildings, are considered systematically in Sect. 4.5. Here we only note that, contrary to the approximate estimation of the section kernel dimensions of rigid rectangular plates on an elastic half-space from the pressures or settlements [105], the numerical approach with the account of unilateral constraints proposed here enables reliable automatic determination of the section kernel boundaries for punches of a given shape resting on elastic bases of various type (constant- or variable-thickness layers, layered elastic bases, half-space with variable physical properties, etc.).

The analysis of the numerical calculations performed for the contact problems of off-centre loading of rectangular punches has shown that, similarly to the case of central loading, independently of the eccentricity of the impressing vertical force application, the settlements of the centre of the punch resting on an elastic half-space, also exceed the corresponding settlement values for the variable-thickness

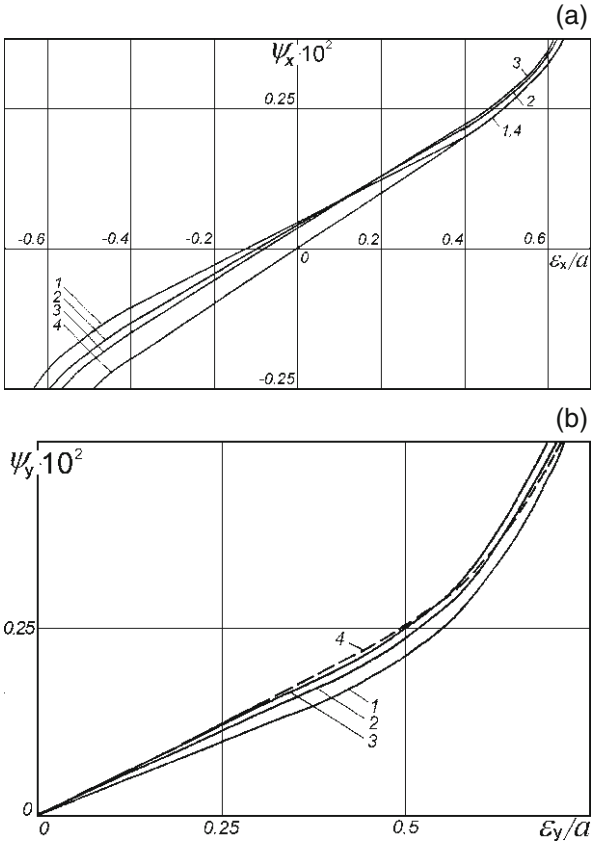

Fig. 4.21 Slopes of a square punch, resting on a variable-thickness elastic layer ($x_c = 2a$), versus the force eccentricity: (**a**) $\varepsilon_x(\varepsilon_y = 0)$, (**b**) ε_y $(\varepsilon_x = 0)$ at $\alpha = 30°$ (1), 45° (2), 60° (3); (4) half-space

bases with various α angle values. It follows from the calculated curves, plotted in Fig. 4.20a, that the dependences of the settlements of the centre of the square punch on the angle α at fixed values of eccentricity of the external force application point are monotonous and qualitatively similar. The square punch slope also monotonously depend on the eccentricity values (Fig. 4.21), but do not possess such a pronounced dependence on the angle α, as the settlements do. At full contact of the punch with the base (when the solutions with and without account of unilateral constraint coincide), the superposition principle holds and, as one should expect, the dependences of ψ_x and ψ_y on the eccentricity of the vertical resultant are practically linear. It is important to note that the dependences of slopes, corresponding to the off-centre loading of rectangular punches for $\varepsilon_y = 0$ (Fig. 4.21a), enable one to determine rather exactly (even graphically) the values of eccentricities ε_x, at which the punches do not undergo any slope ($\psi_x = 0$), i.e. have a uniform settlement.

The issues concerning providing uniform settlement of punches of various cross-section, resting on non-uniformly compressed bases, are considered in detail in Sect. 4.3.

With the beginning of formation of the zones of the square punch uplifting from the elastic base, the absolute values of the punch slopes vary nonlinearly, sharply increasing at $|\varepsilon_x|$, $|\varepsilon_y| \geq 0.6$, what finally results in the punch overturning. As follows from the calculations, performed for $\varepsilon_y = 0$ (Fig. 4.21a), the effect of the angle α at the vertex of the elastically compressible variable-thickness layer at $\varepsilon_x < 0$ is more essential than for $\varepsilon_x > 0$. In the case when $\varepsilon_x = 0$, the effect of the angle α on the dependence of the slopes ψ_y on ε_y is insignificant (Fig. 4.21b).

Thus, the numerical approach developed here enables the distribution of contact pressure over the foundation bottom to be studied in detail without any speculations or assumptions about the contact pressure character under external loading of spatial type. The numerical boundary-element algorithm being used is rather effective for solving spatial contact problems of essentially oblique punches when the area of the punch uplifting from the base is comparable or even larger than the contact area. Multivariant calculations have enabled us to find out that the account of spatial nonhomogeneity in the framework of the existing elastic base models or those proposed in Chap. 1, results in a considerably lower distributivity of the soil, essential reduction of the foundation settlements, redistribution of reactive pressures under their bottom in comparison with the most widely used homogeneous elastic half-space model. Since all real soils possess a rather pronounced nonhomogeneity of their elastic properties, it becomes possible to describe the contact interaction processes more accurately and substantiate the decrease of the calculated forces in shallow foundations and, hence, provide more economical use of materials at their construction.

4.3 Control of the Parameters of Loading and Shape to Provide a Uniform Settlement of Rigid Foundation Plates

The problem of providing a uniform settlement of punches (models of rigid foundations) under a vertical load is of great practical interest for foundation engineering.

Formation and development of foundation slopes results in the appearance of cracks and irreversible deformations of breakdown character in structures above the foundation. Special measures for the foundation reconstruction and reinforcement, required in such cases, are related to additional materials and labour expenses.

For homogeneous bases, the main reason for a slope in foundations with two or more symmetry axes is an off-centre load application. The presence of a single symmetry axis or a totally asymmetrical shape is another reason for the appearance of a foundation slope.

Non-uniform base compressibility on a relatively small area of a building or a structure, typical for a number of construction sites [86], results in slopes appearing for the foundations of symmetrical shape even at central loading. There are a lot of

references in the literature about breakdowns in the course of construction or functioning of objects of industrial and civil engineering, resulting from non-uniform deformations of soil bases (See, e.g. [90]).

The studies [122, 187] as well as the calculations we have performed for rectangular and round punches (Sect. 4.2, Appendix C) show that the variable thickness of the compressible layer in the base is the reason for an essentially non-uniform settlement and slopes of foundations, untolerable in most cases for engineering constructions.

In order to prevent dangerous foundation slopes, exceeding the limiting values (set by the regulations for the design of bases for building and structures), and to get rid of them, as a rule, the size of the foundation bottom is increased. In case of buildings being erected on non-uniformly compressible soils, an approach to eliminate slopes and level settlements by introduction of compensating systems into the base is also applied [211]. Note that both methods, depending on the soil conditions, result in an increase of the construction expenses.

Below a theoretical substantiation and numerical confirmation is given for two possible approaches to prevent punch slopes by controlling their shape and loading parameters.

The essence of the first approach is that, for a given punch shape and size, a location of the resultant vertical load is determined, for which the punch settlement occurs without a slope. The advantage of such approach consists in the fact that the problem solution always exists and its search does not require iterative processes for a complex shape of the punch. However, not always the solution found can have practical value since the resultant external load can appear too close to the punch edge or even beyond its boundary.

In the second approach, the punch bottom area and the load application point are fixed, and then a search for the punch bottom shape, providing its uniform settlement, is carried out. For the shape search, using a control parameter, a multiparametric family of contours of a certain type, bounding the punch, is given. For each punch shape a direct problem is solved, and then, by approximation of the solutions obtained, the control parameter value is determined, for which the punch slope is zero. This approach does not guarantee the uniqueness of the solution, requires time-consuming iterative procedures, but in most cases the results obtained are useful from the practical point of view.

For both approaches the area of the punch contact with the base remains unchanged and, hence, the corresponding practical implementation will not require any additional consumption of materials for the foundation.

4.3.1 Formulation of the Problem and Its Numerical Implementation

In both approaches the contact problem is solved by direct boundary-element method, using a piecewise constant approximation of the contact pressures

(Sect. 2.5.1). In the first approach the resolving equation system is given by

$$\begin{cases} \sum\limits_{j=1}^{n} p_j \cdot \delta_{ij} - W_c = 0, \quad \left(i = \overline{1,n}\right), \\ \sum\limits_{j=1}^{n} p_j \cdot \Delta s_j = P, \\ \sum\limits_{j=1}^{n} p_j \cdot \Delta s_j \cdot x_j + P \cdot \varepsilon_x = P \cdot x_c, \\ \sum\limits_{j=1}^{n} p_j \cdot \Delta s_j \cdot y_j + P \cdot \varepsilon_y = P \cdot y_c, \\ p_j \geq 0 \end{cases} \tag{4.1}$$

where the unknowns are contact pressures p_j within the boundary elements, the punch settlement W_c and eccentricities ε_x, ε_y of application of the resultant external load P with respect to a fixed punch point with the coordinates (x_c, y_c). The amount of the boundary elements in general is n, the j-th element area is Δs_j, and the coordinates of its centre of gravity are (x_j, y_j). The coefficients of the canonical equations are calculated from

$$\delta_{ij} = \int\limits_{F_j}\int \omega\,(x_i, y_i, \xi, \eta)\, d\xi d\eta$$

where $\omega(x_i, y_i, \xi, \eta)$ is the settlement of the point (ξ, η) within the domain of the j-th boundary element F_j due to a unit vertical force, applied to the base surface at the point (x_i, y_i), coinciding with the i-th element gravity centre. The function $\omega(x, y, \xi, \eta)$ is given in accordance with the elastic base model being used. Note that the δ_{ij} coefficients characterize the foundation shape.

While the system (4.1) is being solved, the eccentricities ε_x and ε_y play the role load control parameters. The fact that they are contained explicitly in the resolving linear equation system, essentially simplifies their calculation. For this purpose it is sufficient to solve the system (4.1) by any known method of linear algebra.

The second approach is based on the study of a somewhat different resolving equation system which can be written in the following way:

$$\begin{cases} \sum\limits_{j=1}^{n} p_j \cdot \delta_{ij} - \psi_x \cdot (x_i - x_c) - \psi_y \cdot (y_i - y_c) - W_c = 0 \left(i = \overline{1,n}\right), \\ \sum\limits_{j=1}^{n} p_j \cdot \Delta s_j = P, \\ \sum\limits_{j=1}^{n} p_j \cdot \Delta s_j \cdot x_j = -P \cdot x_c - M_y, \\ \sum\limits_{j=1}^{n} p_j \cdot \Delta s_j \cdot y_j = P \cdot y_c + M_x, \\ p_j \geq 0. \end{cases} \tag{4.2}$$

Here the same notations are used as those in Eq. (4.1). The unknowns are the contact pressures p_j, the punch slopes ψ_x and ψ_y and its settlement W_c due to the vertical force P and overturning moments M_x and M_y applied at the point (x_c, y_c).

The parameters, controlling the punch shape, are not contained explicitly in the equation system (4.2) what essentially encumbers the search for their optimal values corresponding to the condition $\psi_x = \psi_y = 0$. Therefore, for solving the problem in question the following algorithm is proposed. At the first stage the control parameters (u, v) are chosen, enabling the punch shape to be intentionally distorted along the main directions of variability of the base deformational properties. Then specified numerical values are assigned to the parameters with a step. These values correspond to the punches with different cross-section shape, but with the same area. For each punch shape the system (4.2) is solved with new coefficients. As a result, sets of tabulated functions $\psi_x(u, v)$, $\psi_y(u, v)$ are obtained.

From a combined consideration of equations

$$\begin{cases} \psi_x(u,v) = 0, \\ \psi_y(u,v) = 0, \end{cases} \tag{4.3}$$

the control parameter values can be found, resulting in such shape of the contact domain, at which the punch will have a zero slope.

The both approaches discussed were tested for solving problems for punches of various shape on a non-uniformly compressible base in the form of an elastic isotropic wedge with a pinched lower surface [89].

4.3.2 External Load Control

The solutions, proposed for consideration, were obtained for the punches of square, L-shaped and round shape. For each of the problems we determined the coordinates of the point, at which the resultant vertical external load should be applied in order to obtain a zero punch slope.

Square punch on an elastic wedge. The calculation scheme, used for this problem, is shown in Fig. 4.22. The numerical solutions were obtained at the wedge angles $\alpha = 30°$ and $60°$ and a relative distance of the punch centre from the wedge rib $2 \le x_c / a \le 20$ where a is a half of the punch side. The wedge-shaped base was characterized by the deformation modulus $E = 10$ MPa and the Poisson ratio $\nu = 0.25$. The calculations were preformed at a vertical load $P = 100$ kN, the punch side $2a = 2$ m. In order to describe the domain of the punch contact with the base, a uniform 12×8 boundary-element grid was used. The grid density along the OX axis is taken by factor of 1.5 higher than along the OY axis, following the direction of the greatest variation of the compressible soil mass thickness. The total amount of the unknowns in the problem was 99. The solution results in a dimensionless form are given in Table 4.5.

It follows from the table that in the whole range of variation of the geometrical parameters α and x_c / a under investigation, the calculated eccentricity ε_x of the

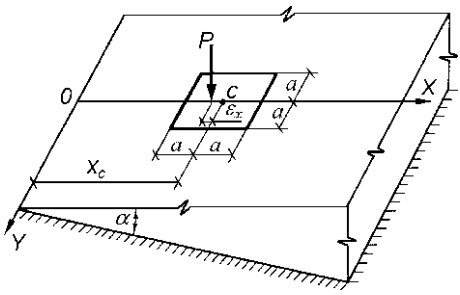

Fig. 4.22 Calculation scheme to determine the external load eccentricity, corresponding to the uniform settlement of a square punch

Table 4.5 Eccentricity ε_x of the resultant external vertical load, providing a uniform settlement W_c of a square punch on a wedge-shaped base

	ε_x/a		$(W_c/a) \times 10^2$	
x_c/a	α=30°	α=60°	α=30°	α=60°
2	0.11579	0.72108×10^{-1}	0.16996	0.27540
3	0.60385×10^{-1}	0.33134×10^{-1}	0.22605	0.32092
5	0.25334×10^{-1}	0.12219×10^{-1}	0.28937	0.35979
8	0.10534×10^{-1}	0.4694×10^{-2}	0.33444	0.38245
12	0.45538×10^{-2}	0.1791×10^{-2}	0.36219	0.39521
20	0.17548×10^{-2}	0.76294×10^{-3}	0.38536	0.40547

external load P, for which the punch slope will be zero, does not extend beyond the punch section kernel, i.e. a condition $|\varepsilon| < \rho$ holds, where ρ is the radius of the section kernel of a circle, inscribed into the square, $\rho = a/3$. Besides, for $x_c/a \geq 3$ an inequality $\varepsilon_x/a < \widetilde{\varepsilon}$ holds, where $\widetilde{\varepsilon} = a/15$ is the value of a random relative load eccentricity, usually taken at the foundation structure calculations.

The increase of x_c/a and α parameters results in a regular decrease of the required displacement value ε_x of the application point of the force P with respect to the punch centre. With a double increase of α (from 30° to 60°) the ε_x/a value decreases almost by the same factor. The increase of the distance x_c/a by factor of two results in a more pronounced decrease of the ε_x/a parameter – up to 5–6 times. Thus, the distance of the punch from the wedge rib affects the punch slope value much stronger than the wedge base angle α.

Regarding the punch settlement W_c/a, one should mention that at $x_c/a \geq 20$ and $\alpha = 30° \div 60°$ it is practically comparable with the settlement value for punch on an elastic half-space $W_c/a = 0.0042$. As follows from the calculations performed, the discrepancy does not exceed 10%.

L-shaped punch on an elastic compressible wedge and on an elastic half-space. The specific feature of the problem under consideration is the fact that even in the case of a homogeneous base and if the resultant of external vertical load is applied exactly in the gravity centre of the L-shaped punch, this will anyway result in its slope. This circumstance is due to the incomplete symmetry of the punch or its absence at all.

The contour of the punch, considered in the numerical experiments, is shown at the calculation scheme, given in Fig. 4.23. For building up the boundary-element grid the domain of the punch contact with the base was uniformly meshed into 72 rectangular boundary elements with sides of $0.167a$ along the OX axis and $0.25a$ along the OY axis, a being the characteristic size of the punch (Fig. 4.24). Two base models were used for the calculations: a linearly deformable homogeneous isotropic half-space and a linearly deformable homogeneous isotropic wedge with the vertex angle $\alpha = 45°$. The distance from the coordinate system origin OXY to the wedge rib, as shown in Fig. 4.23, was chosen as $L = 2a$. In both cases the Poisson ratio $\nu = 0.25$, the deformation modulus $E = 10$ MPa, the resultant vertical load $P = 100$ kN. The results obtained are shown in a dimensionless form in Table 4.6.

The analysis of the table data enables one to conclude on a noticeable difference of the calculated eccentricity values ε_x, ε_y from the corresponding distances to the

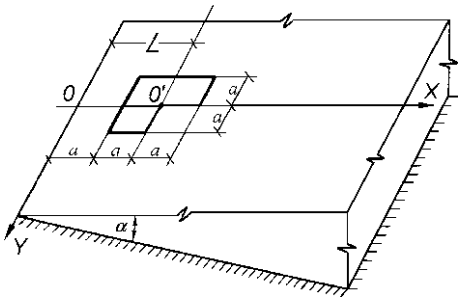

Fig. 4.23 Calculation scheme to determine the external load eccentricity, corresponding to the uniform settlement of an L-shaped punch

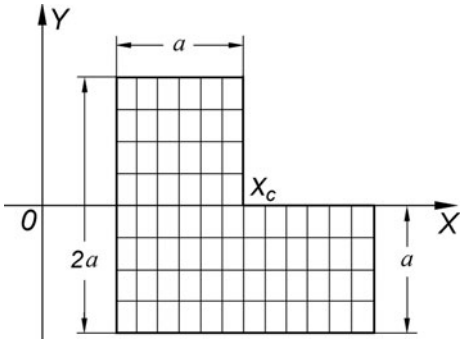

Fig. 4.24 Contact domain discretization for an L-shaped punch

Table 4.6 Contact interaction characteristics and eccentricities ε_x, ε_y of the resultant external vertical load, providing a uniform settlement W_c of an L-shaped punch on elastic bases

Base type	$\lvert\varepsilon_x\rvert/a$	$\lvert\varepsilon_y\rvert/a$	$\psi_x \times 10$	$\psi_y \times 10$	$(W_c/a) \times 10^2$
Elastic half-space	0.1472	0.1472	0	0	0.4608
	0	0	0.1281	0.1281	0.4986
Elastic wedge, α=45°, x_c=2a	0.2316	0.1265	0	0	0.2554
	0	0	0.1617	0.1165	0.3075

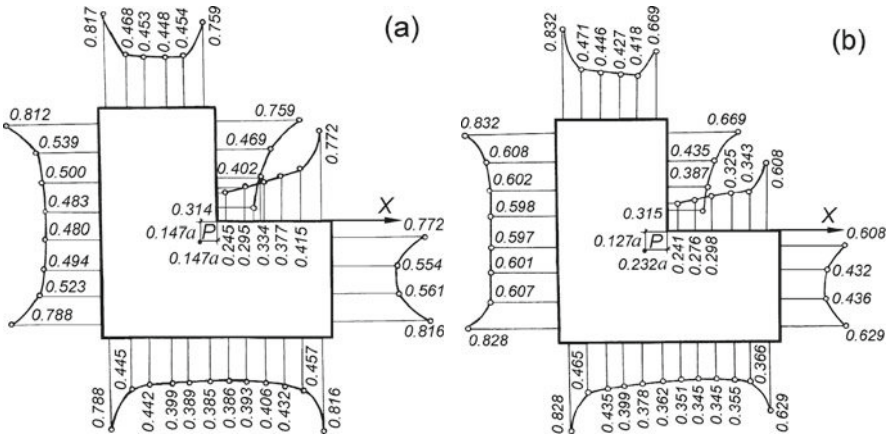

Fig. 4.25 Dimensionless contact pressures along the perimeter of an L-shaped punch with a uniform settlement at $x_c = 2a$, $\alpha = 45°$: (**a**) on an elastic half-space and (**b**) on an elastic wedge-shaped base

punch gravity centre $x_c = y_c = a/6 = 0.1667a$. Note that for the half-space the value $\sqrt{(\varepsilon_x)^2 + (\varepsilon_y)^2}$ does not exceed the random eccentricity value $\widetilde{\varepsilon} = a/15$.

Note that for the input data assumed the punch settlement on the half-space obtained from the calculation was almost twice the punch settlement on the wedge-shaped base.

Figure 4.25a,b illustrates the contact pressure profiles, plotted from the values in the boundary-element gravity centres for the elastic-half-space and the elastic wedge, respectively. The contact pressure values are given in the dimensionless form $\overline{p} = pa^2/P$. In both cases the punch slope is zero. It should be noted that since both models of the base are elastic, then in the angular points and near the punch edges the stress condensation occurs. The base model noticeably affects qualitatively on the character of the contact pressure distribution, and quantitative differences of stress values within similar boundary elements reach 30%.

Round punch on an elastic wedge. Consider some numerical results, obtained for a round punch. The calculation scheme, used for the problem, is shown in Fig. 4.26. The following parameter values, characterizing the elastic wedge, were assumed: the wedge angle $\alpha = 15°$, deformation modulus $E = 10$ MPa, Poisson ratio $\nu = 0.35$. The vertical load on the punch was $P = 10^3$ kN. The punch surface was meshed into 96 boundary elements by equidistant concentric circles and rays, centred in the punch centre. The distance of the punch centre from the wedge rib was assumed $L = 2r$ where r is the punch radius.

With the parameter values assumed, the contact problem solution was obtained, according to which the relative eccentricity value for the vertical load P, at which the punch slope is zero, should be $\varepsilon_x/r = 0.111$. In this case the contact pressure profile in the XOZ plane will have the shape shown in Fig. 4.27. In spite of the profile being essentially asymmetrical, the punch settlement is uniform.

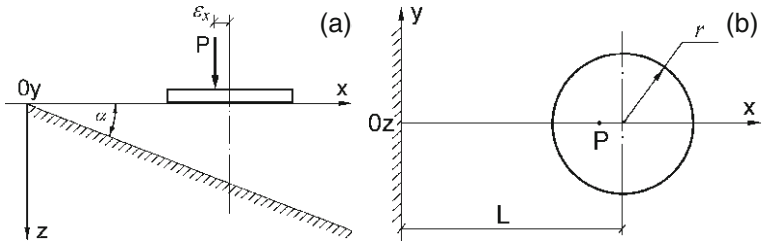

Fig. 4.26 Calculation scheme to determine the external load eccentricity, corresponding to a uniform settlement of a circular punch: (**a**) vertical section, (**b**) plan

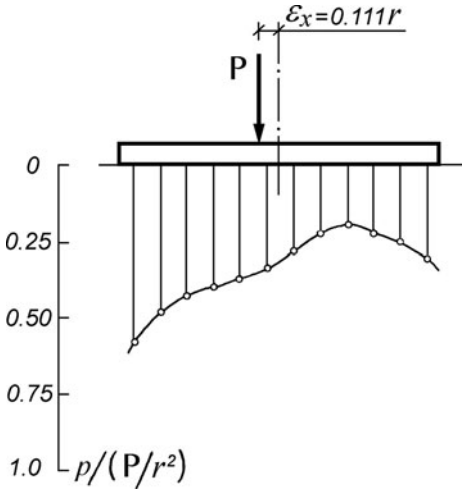

Fig. 4.27 Contact pressure under a round punch with a uniform settlement on an elastic wedge-shaped base ($\alpha = 15°$, $x_c = 2r$, $\nu = 0.35$)

4.3.3 Shape Parameter Control

Below we consider solutions, illustrating how a uniform settlement of a punch on a nonhomogeneous with depth base at a given external load can be achieved by the punch shape control.

Trapezoidal punch on an elastic wedge. The calculation scheme for this problem is shown in Fig. 4.28. A square punch with a side $2a$was taken as the initial configuration. In the course of the numerical studies its shape was intentionally distorted by a control parameter d/a. The control parameter was varied within $0 \le d/a \le 0.5$. Along with the shape, the boundary-element grid was also distorted, the total number of the boundary elements was taken 96 (Fig. 4.29).

The wedge angle was $\alpha = 45°$. The base parameter was the following: Poisson ratio $\nu = 0.25$, deformation modulus $E = 10$ MPa. The distance from the application point of the resultant vertical load $P = 100$ kN to the wedge rib was taken as $x_c = 2a$. The calculation results are presented in Table 4.7.

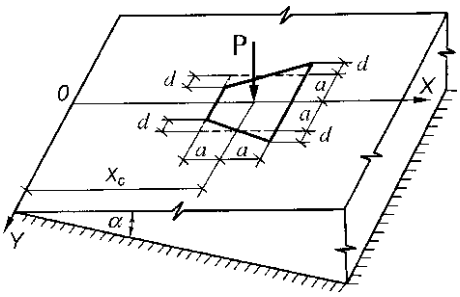

Fig. 4.28 Calculation scheme to determine the optimal size of a trapezoidal punch with a uniform settlement on a wedge-shaped elastic base

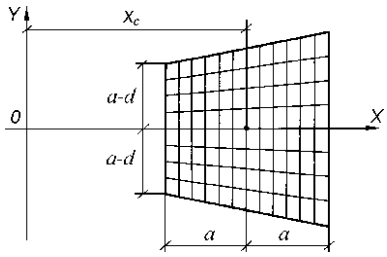

Fig. 4.29 Contact domain dicretization for a trapezoidal punch

Table 4.7 Slopes ψ_x and relative settlements W_c /*a* of a trapezoidal punch on a wedge-shaped base depending on the control parameter *d*/*a* values

d/*a*	0	0.1	0.237425	0.3	0.5
$\psi_x \times 10$	0.40033	0.23431	–0.04968	–0.10667	–0.47326
$(W_c/a) \times 10^2$	0.23395	0.23365	0.22737	0.23560	0.24190

Processing of the data of Table 4.7 by least-square method with subsequent numerical testing of the square approximation results enables us to conclude that the absence of the punch slope ($\psi_x = 0$) corresponds to the control parameter value $d/a = 0.2133$. In this case the relative settlement of the foundation is $W_c/a = 0.22692 \cdot \times 10^{-2}$.

It is known that at oblique position of the underlayer of a more dense soil the expected non-uniform settlements of a foundation can be reduced to the maximal tolerable value by broadening its bottom in the direction of the weak soil layer thickening [265, p. 93, Fig. III-26b]. The consideration of the contact problem for a trapezoidal punch performed here served as a calculation model enabling the foundation geometrical parameters, its settlement and contact stress over its bottom to be determined depending on the deformational and geometrical characteristics of the elastic layer [19].

Ring-shaped punch on a wedge base. The calculation scheme for this problem is shown in Fig. 4.30. The absence of the punch slope is achieved by shifting the inner circle of the ring by a value $\varepsilon = \varepsilon_0$ which serves as a control parameter.

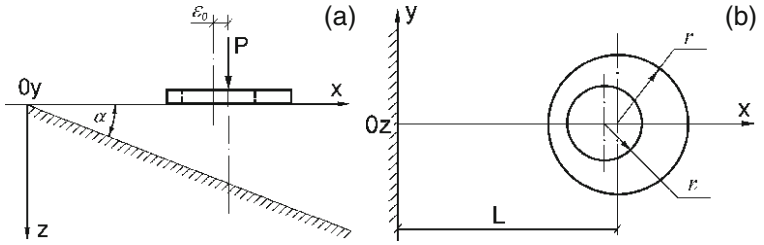

Fig. 4.30 Calculation scheme for an eccentric ring-shaped punch: (**a**) vertical section, (**b**) plan

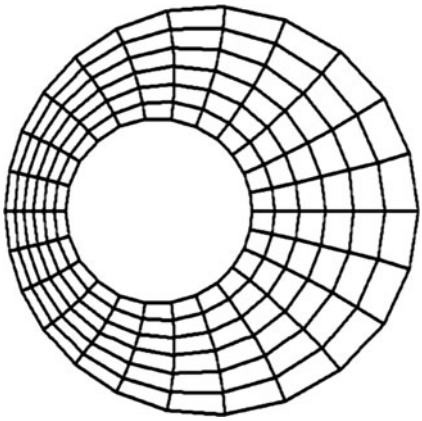

Fig. 4.31 Contact domain discretization for an eccentric ring-shaped punch

The resultant external load is applied at the symmetry centre of the outer circle of the punch, its value is $P = 10^3$ kN. The wedge-shaped base is characterized by the deformation modulus $E = 10$ MPa, Poisson ratio $\nu = 0.35$, wedge angle $\alpha = 30°$. The radii ratio of the inner and outer circles of the ring-shaped punch is taken $r_1/r = 0.6$, and the distance from the wedge rib to the ring-shaped punch centre is $L = 8r$. The boundary-element grid was built using a fractionally linear function of a complex variable $\zeta = (Az-1)/(A-z)$, conformally mapping a uniform grid, built in a circle, onto the ring interior, A is the transformation parameter, determined in terms of ε, r, and r_1. In order to obtain stable numerical results at various values of ε, the number of the boundary elements reaches 156 (Fig. 4.31). The calculation results are presented in Table 4.8.

It follows from the table that, contrary to the problems considered before where all unilateral constraints were involved into functioning, for the ring part of unilateral constraints appears to be open, i.e. a partial uplifting of the punch from the base is observed. The account of the uplifting essentially affects the calculation results.

Based on the approximation of the numerical values of the slope ψ_x, quoted in Table 4.8, the optimal value of the control parameter $\varepsilon_0 = 0.2088r$ is found, for which there will be no slope of the ring-shaped punch.

Table 4.8 Slopes ψ_x of a ring-shaped punch depending on the control parameter ε_0/r

ε_0/r	$\psi_x \times 10^3$	
	With the account of unilateral constraints	Without the account of unilateral constraints
0	5.3907	–
0.2	0.34688	–
0.208	0.072936	0.14653
0.20777	0.35083×10^3	0.85922×10^1
0.209	−0.049834	0.48411×10^1
0.21375	−0.24178	−0.10291
0.25	−2.1049	−7.4181

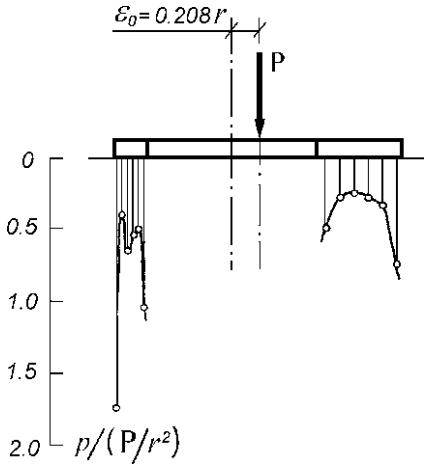

Fig. 4.32 Contact pressures for an eccentric ring-shaped punch with a translational motion on a variable-thickness elastic layer

Figure 4.32 shows the contact pressure profile under the ring-shaped punch in the *XOZ* plane at $\varepsilon_0/r = 0.2088$. Due to the contact pressure redistribution, the variation of the compressible base thickness will be compensated and the punch motion in this case will be translational.

Table 4.9 contains the optimal values of the control parameter ε_0/r for typical cases which can be practically important for construction of foundations under tower-type structures (funnels, water towers, TV towers, etc.) on a wedge-shaped base. The radii ratio here, similarly to the above case, is taken as $r_1/r = 0.6$.

By using the data of Table 4.9 for the foundation design, one can choose the required displacement ε_0 of the inner circle with respect to the outer one, for which the settlement of the ring-shaped foundation under consideration under a vertical load will be uniform. Application of the results of the solution of the contact problem for an eccentric ring-shaped punch for the design of foundations under tower-type structures in complicated engineering and geological conditions (on variable-thickness bases) is shown in Appendix C.

Table 4.9 Optimal values of the control parameter ε_0/r (for which the ring-shape punch slope is zero) depending on the wedge angle α and on the relative distance x_c/r of the punch centre from the wedge rib

x_C/r	$\alpha = 30°$	$\alpha = 45°$	$\alpha = 60°$
4	–	0.3398	0.3071
8	0.2088	0.1667	0.1413
12	0.1274	0.09828	0.08247

Thus, the numerical studies performed using the boundary-element method enable the following conclusions to be made:

- from the condition of providing the punch settlement uniformity, the use of control parameters while solving spatial contact problems enables the punch shape to be rationally assigned and the point of application of the resultant external vertical load to be shown;
- a considerable sensitivity of the punch slope to the control parameter variation as well as the comparability of the calculated and random values of eccentricity of the vertical load on the punch, revealed in the numerical experiments, prove the necessity of thorough monitoring of geotechnical survey results, as well as strict observance of the project prescriptions in the course of construction being performed on non-uniformly compressible bases;
- the computer software, worked out on the base of the proposed algorithms of the numerical solution of spatial contact problems, enables punches of a rather complex shape resting on elastic bases, for which fundamental solutions are known or can be obtained, to be studied under various combination of loads.

4.4 Spatial Stress-Strained State of the Base of a Rigid Strip Variable-Width Foundation

Variable-width foundations (VWFs) are rifid foundations of a progressive type [191]. Such foundations have a complex shape of the domain contacting with base, formed by a periodical system of cutouts of different configuration, depending on the foundation construction technology as well as on the specific feature of the above-foundation structures. Application of VWFs enables, in comparison with the solid plates, i.e. constant-width foundations (CWFs), concrete and steel consumption to be essentially reduced and rational design solutions in construction and reconstruction of foundations to be achieved in order to provide uniform settlement of structures (without slope).

At present no reliable methods of contact stress calculation of for VWFs have been elaborated, and the stress-strained state characteristics in the active zone of the base of such foundations are found rather approximately. In order to simplify the calculations, VWFs, as a rule, are treated as a regular repetition of similar fragments

along the foundation length, each of the fragments, in turn, consisting of a narrow block and a wide block. The pressure of each block on the soil is assumed constant. In spite of the limited foundation strip length, the edge effect revealed as the contact stress increase near the bottom boundaries, is not taken into account. At the design stage for the strip VWFs with different shape of cutouts the main task is the decrease of bending moments what reduces the consumption of materials (concrete and steel) in comparison with solid plates. The relevant instructions in the regulations result in cumbersome, very approximate and often not sufficiently substantiated calculations with a vast graphic and tabulated material being used. Reliable determination of the bending moments due to the reactive pressures in the VWFs sections requires a detailed account of the cutout shape.

The simplest example of a VWF is a foundation with a cross-shaped bottom which is used instead of square or rectangular foundations. Square and cross-shaped foundation tests with the load increase up to the limiting value have enabled the advantages of the foundations with angular cutouts to be estimated [257]: substitution of square foundations with cross-shaped ones with the same outer dimensions enables the metal consumption to be reduced by 26% and concrete consumption – by 15% for the same external load being transferred to the foundation.

The results of field tests of complex-shaped strip foundations with a flat surface of contact with a sand base are presented in [83, 257]. The studies have shown that the contact pressure distribution for a VWF essentially depends on its shape and the external load. It was proven experimentally that the ability of plates with cutouts to accept increased loads is caused by the specific features of the contact stress distribution. In the load range below the crack formation limit and at relatively small length VWFs on dense soils work as rigid punches.

Below we present some calculation data, obtained for strip CWFs and VWFs under central loading [18, 20]. Application of the elastic base model in the numerical algorithm elaborated is performed as a separate module and does not require the whole program resetting while different models of the elastic base with a known influence function being used.

4.4.1 Contact Problem for a Variable-Width Strip Foundation

As an example of a VWF consider a shallow foundation obtained by making ten symmetrical rectangular cutouts with the dimensions 1.2×0.4 m in a solid rectangular plate of 13.2×1.6 m. Since in design practice the base depth is to be set, from which the stress in the soil can be determined as for a CWF with the equal bottom area, the contact interaction parameters for the VWF were compared with the corresponding calculated characteristics for a rectangular foundation of the same length and a constant width of 1.237 m with equal area. The shapes of the VWF and CWF of equal areas with the corresponding contact surface discretization schemes are presented in Fig. 4.33. The calculation scheme for a rigid beam on an elastic base is accepted. Numerical modelling was performed for the case of the base being

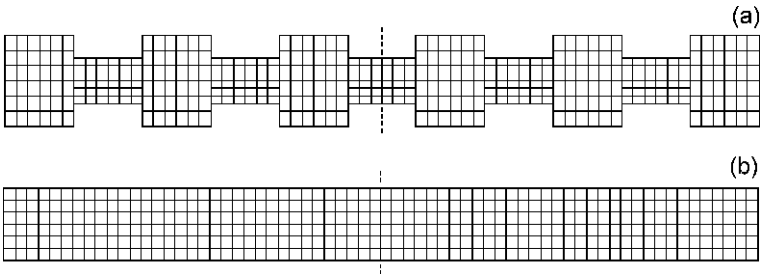

Fig. 4.33 Discretization of contact domains for rigid strip foundations of (**a**) variable and (**b**) constant width with equal areas and lengths, using 396 boundary elements

treated as an elastic half-space whose deformational properties are characterized by the elastic modulus $E = 10$ MPa and the Poisson ratio $\nu = 0.25$. The foundation was assumed to undergo a vertical load, reduced to a central force $P = 1000$ kN.

Multivariant calculations have shown that with the increase of the discretization degree the accuracy of the numerical results steadily grows. In order to estimate the convergence of the approximate solutions, the approximate values, obtained by Richardson method in the assumption of the second order of accuracy of the numerical method being applied, were used. On a uniform grid of 396 boundary elements (Fig. 4.33) the relative error of the boundary-element solutions did not exceed 1.5% for the settlements and 2% for the contact pressures, what is quite sufficient for practical calculations with a detailed graphic interpretation of the results. Thus, the approach used to calculate the VWFs with a given cutout shape, using the algorithms of numerical solution of spatial contact problems, is rather efficient: there are no difficulties with convergence, and the required accuracy does not demand high computation time and computer RAM resources.

Contact pressure isolines $p = p(x, y)$ on the foundation bottom are plotted in Fig. 4.34. The contact pressure distribution patterns for the CWF and the VWF are qualitatively different. In the first case for the rectangular strip foundation (of the constant width) an oval area of practically contact pressures exists, extended along the longitudinal axis of the bottom (Fig. 4.34b). With the increase of the distance from the centre the symmetrical ovals are transformed, and directly near the foundation edges the isobars have the shape of similar rectangles with rounded angles. On the foundation boundary contour the contact pressures increase unlimitedly.

As follows from the calculations, cutouts in the strip foundation bottom results in an essential transformation of the contact pressure field, which becomes nonuniform first of all due to the presence of additional angular points on the boundary contour (Fig. 4.34a). The shape of the isobars become complex and, at a given average pressure over the bottom, a distinct nonuniformity of the reactive pressures exists. In the areas of the bottom, corresponding to the larger foundation width, isolated discharge areas appear, being repeated along the whole foundation length. The numerical studies have shown that the perimeter increase due to the shape

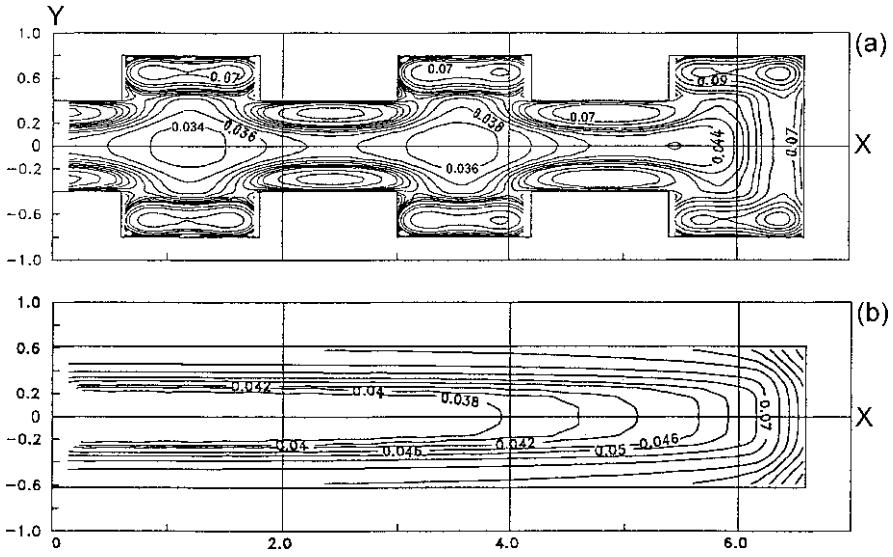

Fig. 4.34 Equal contact pressure lines (MPa) for foundations of (**a**) variable and (**b**) constant width

complication of the boundary contour plays the decisive role in the formation of the soil reactive pressures over the foundation bottom. At equal bottom area, its perimeter for the VWF (in the case of the cutout system under consideration, Fig. 4.33a) is by 30% longer than for the CWF.

Contact pressures in a vertical plane, including the longitudinal axis of the VWF and the CWF, are plotted in Fig. 4.35. As seen from the figure, almost along the whole VWF length, due to the repeated foundation widenings, the axial contact pressures oscillate with respect to the monotonously varying contact pressures for the CWF. In a narrow zone with the width of about the broadening step, adjacent to the edge part of thee foundations of both types, an unlimited growth of the contact pressures occurs. Due to this zone being broader for the VWF, the contact pressures there are essentially lower than the corresponding values for the CWF. The regularities of the contact pressure distribution in the area of the strip foundation width variation will be analyzed in detail in Sect. 4.4.3.

Note that, according to the calculations performed, the mentioned features in the contact pressure distribution are in a qualitative agreement for different models of elastic bases with distributive capability being used [205].

It is seen from the presented calculation data that the numerical method employed enables the contact pressures over the VWF bottom to be calculated from the given VWF shape. The detailed account of the contact pressures is quite important for the evaluation of internal forces in the foundation structures. When the considered regularity of the contact pressure field formation can be estimated at the design stage, a more strict substantiation of the choice of calculated forces in the VWF becomes

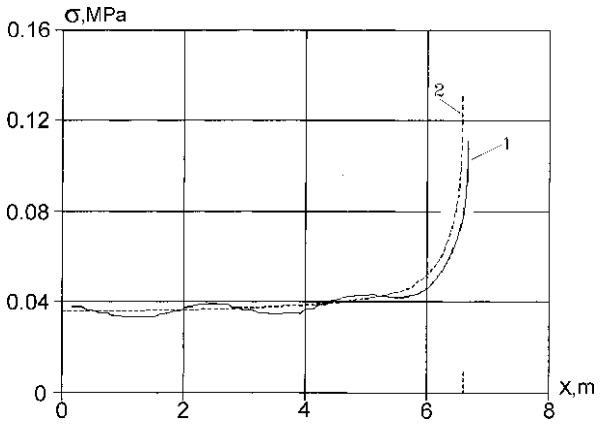

Fig. 4.35 Contact pressures σ (MPa) along the longitudinal axes of (1) variable-width and (2) constant-width foundations

possible; hence, the materials for its construction can be spent more rationally. Besides, the revealed features of the reactive stress distribution over the variable-width foundation bottom can serve as a basis to create an engineering method to calculate bending moments in the calculated foundation sections.

4.4.2 Stress-Strained State of a Strip Foundation Base

The increase of nonuniformity in the contact pressure distribution due to the presence of a cutout system in a VWF results in a decrease of its settlement. For the example under consideration the VWF settlement decrease was 2.8% in comparison with the CWF. In practice the settlement value will be even smaller than the calculated one since the soil in the cutout area participates in the VWF operation. The obtained result means that at a fixed load the bottom area decrease to a certain limit, related to the shape and number of cutouts in the bottom of a rectangular strip foundation, not only will not result in the settlement increase, but will also preserve it within the tolerance. The aforementioned fully agrees with the result of [83] where for a VWF on a medium-density sand the maximum size of curved cutouts was determined, for which the settlements do not increase. The mentioned trend should be taken into account at various stages of design when the VWF shape is chosen. Note that cross-shaped foundation tests also confirm the positive effect of angular cutouts on the decrease of the foundation settlements [257].

When foundations are designed with the account of their mutual influence, the compressive stress distribution in the thickness of the soil base should be taken into account. There is no special literature with instructions regarding the determination of additional pressure in the soil from the variable cross-section foundations. While calculating compressive stress in any base point both below the

foundation and outside it, the action of a uniformly distributed load on each rectangular boundary element is summated according to the known Love formula [92]. For the curved shape of the cutouts, we performed the most successful discretization of the contact surface, using triangular boundary elements (See Section 3.3.1 and [21]). Therefore, it is convenient to apply a more general approach [227], enabling vertical stress to be calculated at any depth in an elastic half-space, resulting from a load, uniformly distributed over triangular or quadrangular areas by algebraic summation of stresses under the vertices of acute angles of right-angle triangles formed by perpendiculars to the sides of the uniformly loaded domain.

The distribution of vertical compressive stresses σ_{CW} and σ_{VW} in the active zones of the CWF and VWF bases, obtained from the results of some of the calculations performed, is illustrated by Figs. 4.36–4.38. Figure 4.36 shows at various depths vertical compressive stresses in a vertical plane containing the CWF and VWF longitudinal axis. The comparison is performed for four different depths, starting from the near-contact area ($z = 0.1$ m) and moving away from the bottom surface ($z = 1.0$, 1.5, 2.0 m). As one should expect, the maximal difference in the calculated values was observed for $z \leq 0.1$ m. The compressive stresses along the VWF longitudinal axis are oscillating due to the periodical variation of the foundation width. At depths smaller than the average foundation halfwidth, due to the higher concentration of contact pressures under the narrow parts and the presence of the discharge zones under the broadenings, the stressed state in the soil qualitatively reproduces the stress distribution over the bottom. Compressive stresses for the CWF practically become averaged with respect to the corresponding oscillating values for the VWF. The maximal relative deviation of the discussed values at $z = 0.1$ m reaches 13% (Fig. 4.36). For the depths of the order of the foundation characteristic width, the vertical stresses for the VWF practically along the whole longitudinal axis are smaller than for the CWF and their oscillation amplitudes sharply decrease. Starting from the depth $z = 2$ m, the presence of the cutouts in the foundation bottom shows practically no effect on the characteristics of the stressed state of the soil. The compared compressive stress values become graphically indistinguishable and can be calculated as in the case of a rectangular foundation, i.e. using well known methods. The difference of the compressive stresses σ_{CW} and σ_{VW} at all depths of the soil base along the longitudinal axis outside the foundations is also quite insignificant (Fig. 4.36, x >6.6 m). Isolines of the vertical stress in horizontal planes at the depths 0.1, 0.5, 1.0, and 1.5 m for the CWF and VWF are plotted in Figs. 4.37 and 4.38. The zones of the foundation shape effect on the stressed state in the mass soil are clearly seen, enabling the “active” and “passive” zones of the base operation to be distinguished. Using similar plots for the investigated stages of the foundation loading, one can estimate at various depths the degree of the stressed state being close to the limiting one (in view of its strength) both under the centre and under the boundary contour of the foundation bottom. Now the combined effect of the VWF shape and the mechanical properties of the soil on the limiting load value for rigid strip foundations can be revealed.

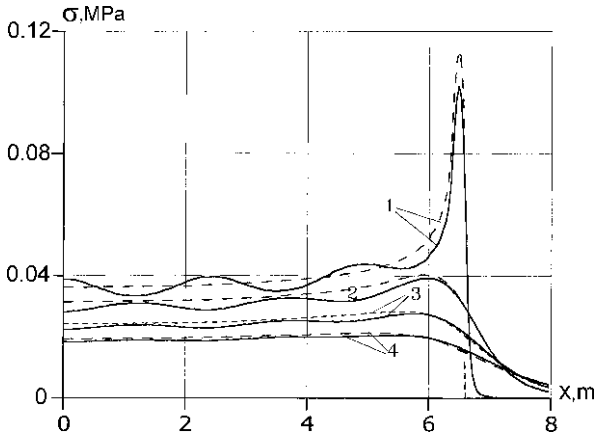

Fig. 4.36 Vertical compressive stress σ(MPa) in the soil base under the longitudinal axes of variable-width (*solid lines*) and constant-width (*broken lines*) foundations at the depth $z = 0.1$, 1.0, 1.5, 2.0 m (1–4)

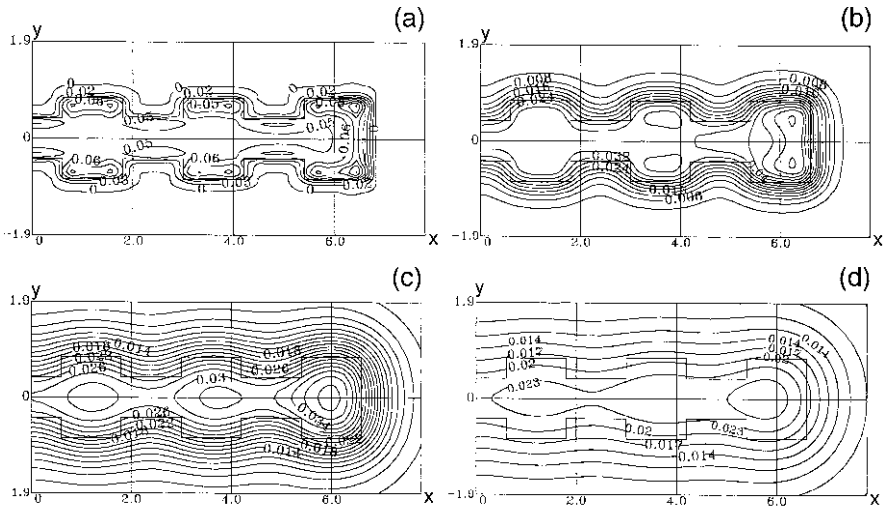

Fig. 4.37 Lines of equal vertical compressive stress σ (MPa) in the soil base for a variable-width foundation at the depths $z = 0.1$, 0.5, 1.0, 1.5 m (*a–d*)

4.4.3 Contact Pressure Distribution in the Area of the Strip Foundation Width Variation

From the results of [100], based on the data of [215], in the majority (69.5%) of the representative amount of the examined buildings in Moscow the ratio of minimal and maximal pressures over the foundation bottom was within 1.2–2.0.

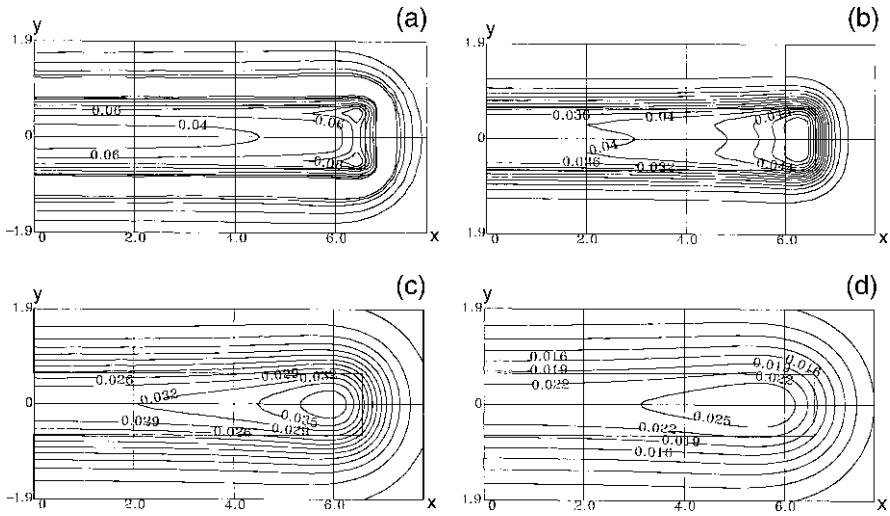

Fig. 4.38 Lines of equal vertical compressive stress σ (MPa) in the soil base for a constant-width foundation at the depths $z = 0.1, 0.5, 1.0, 1.5$ m (**a** – **d**)

Evidently, one of the reasons for this is the fact that when the load on the foundation strip is changed, its width is not always changed even in the case of absence of the expansion joints. Meanwhile, the pressures under a foundation could be to a considerable extent leveled by varying its width even by one nominal size grade according to the foundation plate production list. The load on the foundation can be treated as uniformly distributed. Such foundation is made as a strip consisting of the footing plates and several rows of wall blocks. Besides, such foundation supports an above-foundation structure – a carrying wall not less than 2.5 m high (the height of a storey). It is natural to consider such foundation structure as a rigid beam on an elastic base.

Here we study the contact pressure distribution in the area of the stepwise variation of the strip foundation width and quantitatively estimate additional pressures resulting in the decrease of the load due to the foundation on its narrow part and its increase on the broad part.

For the numerical solution of the problem we present the VWF as a strip consisting of the blocks A and B, located symmetrically (Fig. 4.39). The area, occupied by the strip foundation, is meshed in the longitudinal direction into regularly repeated fragments of variable cross-section, consisting of rectangular parts A and B. The latter are meshed into elementary rectangles (hereinafter elements), extended vertically. Within each element we consider the distribution of pressure on the base to be constant and equal to the pressure value in its gravity centre. This enables the variation of the non-uniform contact pressure field in the longitudinal direction to be studied, averaging it across the foundation strip.

The main difficulty for the compiling of the canonical equation system consists in the determination of influence coefficients which, in general, are found by numerical

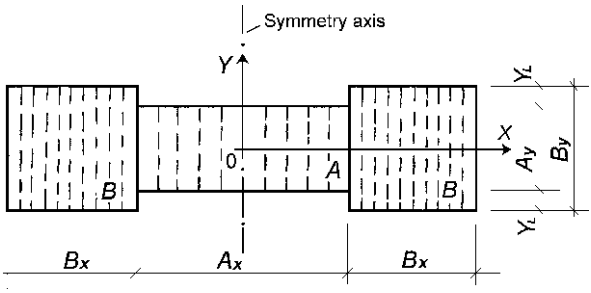

Fig. 4.39 Calculation scheme for a fragment of a strip foundation of variable cross-section for the case $A_y < B_y$

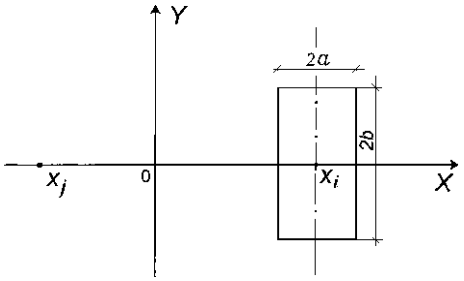

Fig. 4.40 To the calculation of the influence coefficients for rectangular boundary elements with centres, located on the longitudinal axis of a strip foundation

integration over the quadrature formuae of different orders. In the case under consideration all the boundary elements are rectangular with sides, parallel to the coordinate axes and centres lying on the same straight line. These circumstances enable the practical calculations to be facilitated by using an easily programmable formula. In the case of an elastic half-space the canonical equation system coefficients δ_{ij} are calculated in the finite form in terms of elementary functions

$$\delta_{ij} = x_1 \cdot \ln\left(\frac{R_1 + b}{R_1 - b}\right) + x_2 \cdot \ln\left(\frac{R_2 - b}{R_2 + b}\right) + 2b \cdot \ln\left(\frac{R_1 + x_1}{R_2 - x_2}\right)$$

where $x_1 = \bar{x} + a$, $x_2 = \bar{x} - a$, $\bar{x} = x_i - x_j$, $R_{1,2} = \sqrt{b^2 + x_{1,2}^2}$, a and b are the half-element dimensions in the direction of the X and Y axes, respectively, x_i is the element centre, x_j is the observation point (Fig. 4.40). This formula is a particular case of a more complicated Love formula [156] for the settlements of the elastic half-space points due to a uniform load, distributed over a rectangular domain.

The pressures, determined from the given calculation scheme, were used to construct the corresponding profiles according to the following method.

First the pressures were calculated due to a VWF and two CWFs, one of which had the width A_y and the other – B_y. The pressure due to the VWF was determined for two variants of mutual arrangement of the blocks A and B: variant 1: $A_y < B_y$ (Fig. 4.39) and variant 2: $A_y > B_y$.

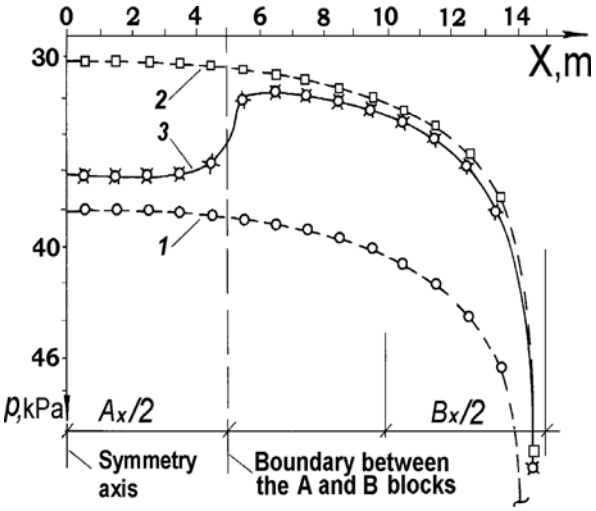

Fig. 4.41 Plots of contact pressures under the foundation at$P$= 100 kN: (1) foundation with a constant width $B_{\text{const}} = A_y = 0.8$ m; (2) the same, $B_{\text{const}} = B_y = 1.0$ m; (3) foundation with a variable width $A_y = 0.8$ m, $B_y = 1.0$ m

Then in each point a relative pressure deviation was determined as follows

$$p_{add} = \left[\left(\overline{p_1} - \overline{p_2} \right) / \overline{p_1} \right] \cdot 100\%,$$

where p_{add} is the relative deviation (in %) of the pressure under the VWF in comparison with the pressure under the CWF (hereinafter – the additional pressure), $\overline{p_1}$ and $\overline{p_2}$ are the higher and the lower (respectively) of the pressures under the VWF (hereinafter p_V) and under the CWF (hereinafter p_C) for each measurement point along the foundation length.

Then the profiles of relative additional pressures were built.

Figures 4.41 and 4.42 show the plots of the contact pressures in absolute (Fig. 4.41) and relative (Fig. 4.42) values for a foundation with widths $A_y = 0.8$ m and $B_y = 1.0$ m. The shape of these plots is typical for the VWFs with the size A_y and B_y considered. The plots, shown in Fig. 4.41, were obtained at a central force $P = 100$ kN and the soil deformation parameters $E = 10$ MPa, $\nu = 0.3$.

At further consideration the following restrictions are assumed.

The plates of width, specified by the GOST standard, were used [109]. With the account of this factor, the ledge values were assumed $Y_{\text{L}} = 0.1$ m and $Y_{\text{L}} = 0.2$ m. For each ledge only the minimal and maximal values of the block widths were taken. For example, for $Y_{\text{L}} = 0.2$ m only the blocks with $A_y^{\min} = 1.6$ m and $A_y^{\max} = 3.2$ m are accepted.

The block lengths $A_x = B_x = 10$ m were considered. A decrease of the length A_x increases the influence on the block A from the block B, opposite to the boundary considered. For example, while considering the right-side part of the

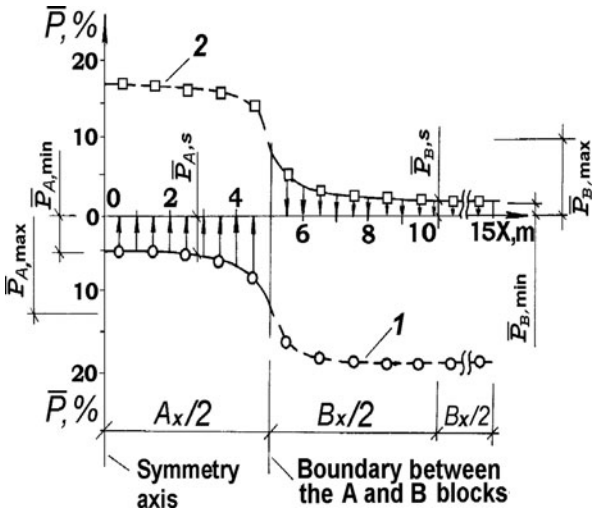

Fig. 4.42 Diagrams of additional pressures (in %) under the foundation with the size A_y= 0.8 m and B_y = 1.0 m: (1) foundation with a constant width $B_{const} = A_y = 0.8$ m, (2) the same, B_{const}= B_y= 1.0 m

foundation (Fig. 4.39), the decrease of A_x will result in the increase of influence of the left block B. Taking this circumstance into account, the pressures at A_x = B_x = 10 m and A_x =B_x = 20 m were compared. This study has shown that the lengths assumed (10 m) result in an excessive pressure. For the blocks A the excessive pressure is higher than for the blocks B. With the increase of the widths A_y and B_y the value of such error decreases within each ledge value. At $Y_L = 0.2$ m the error is higher than at $Y_L = 0.1$ m. However, in all cases this error does nor exceed 0.81%. Such value can be neglected and, therefore, the numerical studies were performed at $A_x = B_x = 10$ m.

Besides, the arrangement of the blocks A and B according to the variant 2 ($A_y > B_y$) enabled, at the data processing, p_{add} for the broad block to be taken from the calculation results according to the variant 1, and for the narrow block – according to the variant 2. This has also enabled the influence of the block B, opposite to the boundary under consideration, to be reduced. The profile in Fig. 4.42 was constructed using this approach.

The results of the studies are presented in Table 4.10. The signs "+" and "–" indicate the additional loading, downward with respect to the foundation bottom, and unloading, upward (respectively) action of the additional pressure. The additional pressure profile, characteristic for the cases under consideration, is shown in Fig. 4.42. In Table 4.10 the values of p_{min} for the block A were calculated according to the variant 2 at the distance A_x from the boundary between the blocks A and B.

The analysis of the results of the calculations performed has enabled the following conclusions:

Table 4.10 Additional pressures (p_{add}) under a variable-width foundation with respect to the pressure under a constant-width foundation

Y_L, m	Block width, m		p_{add} value at the segments, %					
				A			B	
	A_y	B_y	p_{min}	p_s	p_{max}	p_{max}	p_s	p_{min}
0.1	0.8	1.0	+1.64	+1.95	+9.54	−10.68	−1.86	−1.54
	1.4	1.6	+1.07	+1.33	+5.76	−6.10	−1.28	−1.04
0.2	1.6	2.0	+1.90	+2.36	+9.40	−10.28	−2.21	−1.76
	2.8	3.2	+1.28	+1.64	+5.60	−5.84	−1.56	−1.20

- p_{add}, arising in the area of a sharp variation of the foundation width, have different directions (under the block A they are unloading, and under the block B – additional loading);
- the maximal values of p_{add} are achieved at the boundary between the blocks A and B; its value depends on the Y_L value and on the block widths and lies within 5.6–9.54% under the block A and within 5.84–10.68% under the block B;
- the maximal values of p_{add} are achieved at $Y_L = 0.1$ m for the narrowest blocks ($A = 0.8$ m, $B = 1.0$ m);
- for each ledge size the value of p_{add} is inversely proportional to the block width;
- with the decrease of the relative ledge value ($\overline{Y}_L = Y_L/A_y$) the maximal p_{add} values decrease;
- the most considerable variations of p_{add} occur near the boundary; the length, at which the maximal pressure is reduced twice, is not more than 1.5 m for the block size combinations under investigation.

Using the relative values (%) has enabled the results, which can be extended to various loads and soils, to be obtained in a compact form.

The analysis performed has shown that the pressure redistribution in the area of the strip foundation width variation exists and should be taken into account. Additional pressures, arising in the area of the foundation width variation, are unloading for the narrow foundation parts and additional loading for the broad parts. In a short-length area (up to 1.5 m), adjacent to the boundary between the blocks, such pressures sharply increase, for the block widths under investigation the increase reaching 9.54% (for the narrow blocks) and 10.68% (for the broad blocks) of the pressure value arising under a constant-width foundation made of broad blocks loaded by above-foundation structures.

Thus, the account of regularities of stress distribution on the contact surface and in the soil at different geometrical shape of the foundation enables the methods for design of foundation structures to be improved. The calculations of the VWF bases of different type (periodical profile, symmetrical and asymmetrical with respect to the longitudinal axis, of sleeper type, etc.) can be carried out with higher reliability, the optimal size of such foundations can be chosen automatically, providing their minimal settlement without over-expenditure of expensive construction materials.

4.5 Calculation of the Section Kernel Boundary for Rigid Foundation Plates

As follows from the investigations performed (Sects. 4.2 and 4.3), in Sect. 2.5, based on the boundary-element method, an efficient and a rather general approach was developed to the numerical solution of spatial problems of contact interaction with the account of structural nonlinearity (unilateral constraints in the contact domain) for absolutely rigid punches of complex (practically any) shape on non-classical linearly deformable bases. Under a given spatial static load linear and angular punch displacements are determined, the pressure distribution in the contact domain is found. The account of unilateral constraints in the proposed numerical algorithm enables the rigid punch uplifting from the elastic base to be described as well as the pressure redistribution over the contact domain and slope increase with the external load application point approaching the punch boundary (or with the increase of an external overturning moment). Numerous calculations show that with the appearance of the zones of the punch uplifting from the elastic base surface and with the decrease of the contact area a nonlinear variation of the slopes and displacements of punches of various shapes with the external vertical force eccentricities (or external overturning moment values) is observed. Structural nonlinearity, revealed in such a way under the contact interaction, makes impossible the application of the superposition principle which is applied for almost all engineering calculation methods. Therefore, for a given punch geometry, the determination of the vertical load application area without the punch uplifting from the elastic base, is quite important.

A convenient geometrical characteristic of a shallow foundation bottom is section kernel [105], which denotes the part of the punch (a rigid foundation plate), within which a vertical load can be applied without causing a negative reactive pressure or, more exactly (since the soil does not work for tension), the punch uplifting from the base in any other point of the punch bottom.

Note once again that under an external vertical load within the section kernel the contact interaction of the punch with the elastic base occurs without uplifting and, hence, the superposition principle of linear theory of elasticity, being the basis for most engineering calculations, can be applied.

For a circular punch, as directly follows from [2, 74, 159], contact stress will be compressive in all points of the punch bottom only under a condition that the vertical force application point is located at a distance from the punch centre, not exceeding $a/3$ where a is the punch radius. Thus, the section kernel of a circular punch is also a circle whose radius is three times smaller than the punch radius. In [160] a contact problem is solved for an elliptical punch resting on an elastic half-space, loaded by a vertical eccentric force. From the solution obtained it follows that the section kernel of the elliptical punch is an ellipse with semiaxes three times smaller than the punch semiaxes.

When the vertical force goes beyond the section kernel, the punch uplifting from the base occurs, accompanied by the change of the contact stress distribution

character (the problem of an essentially oblique punch). Investigation of the problem of an essentially oblique circular punch, using the structural method, shows the possibility of the contact problem solution to be obtained for asymmetrical loading with the account of the punch uplifting from the base [225]. The contact area of the punch with the half-space, being a part of a circle, is determined depending on the force application point. The contact domain, bounded by the boundary condition separation line, will be unknown and is determined in the course of the problem being solved by iteration from the contact pressure sign change. However, the application of the structural method in the problem of an essentially oblique punch is encumbered by the necessity of the function, determining the family of the boundary condition separation lines for the contact stresses to be fully specified for the calculations. For a circular punch this function is assumed to be a biparametric parabola [225]. It is clear that for solving contact problems for essentially oblique complex-shaped punches the application of the structural method (*R*-function) is rather difficult from the practical point of view due to the impossibility of the contact domain on the punch bottom to be predicted.

At present, the complete data on the section kernel configurations neither for rectangular punches, nor (moreover) for the punches of more complex geometrical shapes, interacting with an elastic half-space, are available in the literature. A great practical interest is also attracted by the problems of design and estimation of stability of shallow foundations when the finite and variable depth of the compressible soil mass, layered superposition of rock strata, variation of the elastic properties with depth, etc. should be taken into account.

Here we describe the procedure of an approximate (with a given accuracy) determination of the section kernel boundary for punches of a complex geometrical shape, contacting with elastic bases, by invoking a numerical algorithm of solution of the spatial contact problem (Sect. 2.5.1).

In the punch bottom plane we introduce a polar coordinate system with a pole in an internal point (centre) of the punch (x_c, y_c) (Fig. 4.43). This point is the most convenient to be taken in the gravity centre or on the symmetry axis of the punch bottom. Then we fix a direction φ, $0 \le \varphi < 2\pi$, and carry out numerical calculations of the contact interaction of the punch with the elastic base for a vertical load, whose application point is varied along the segment $\rho_1(\varphi) < \rho(\varphi) < \rho_2(\varphi)$ (the choice of its ends will be specified below). The action of the vertical force in this case is equivalent to the action of a force P, applied in the punch centre (x_c, y_c), and moments $M_x = -P \times \rho \sin\varphi$, $M_y = P \times \rho\cos\varphi$. Then we apply a procedure similar to the bisection method of solving nonlinear equations.

At each value of φ, the polar radii of the zeroth approximation, bounding the section kernel boundary point, are chosen in such a way that for $\rho = \rho_1^{(0)}$ the contact interaction is without uplifting, and for $\rho = \rho_2^{(0)}$ at least for one boundary element $\rho_i < 0$. The interval $\rho_1^{(0)} < \rho < \rho_2^{(0)}$ is divided into the simples case in two and perform the calculations for $\overline{\rho} = (\rho_1^{(0)} + \rho_2^{(0)})/2$. If at $\rho = \overline{\rho}$ there will be a contact interaction without uplifting, then $\rho_1^{(1)} = \overline{\rho}$, $\rho_2^{(1)} = \rho_2^{(0)}$ is chosen as the first approximation. At the presence of areas of the punch uplifting from the elastic base

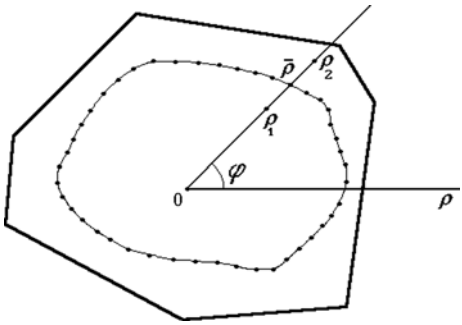

Fig. 4.43 Scheme for the algorithm to determine the section kernel of a rigid complex-shaped foundation plate, resting on an elastic base

for $\rho = \overline{\rho}$, one assumes $\rho_1^{(1)} = \rho_1^{(0)}$, $\rho_2^{(1)} = \overline{\rho}$. Then the calculations are performed according to the above scheme by iteration, until the condition

$$\left|\rho_1^{(k)} - \rho_2^{(k)}\right| \leq \varepsilon \cdot \left|\rho_1^{(k-1)} - \rho_2^{(k-1)}\right|$$

is fulfilled, where ε is the given relative accuracy of the calculations. Monotonous sequences $\left\{\rho_1^{(k)}\right\}$, $\left\{\rho_2^{(k)}\right\}$, obtained from the calculations, are limited and, within the given accuracy, after a finite number of iteration cycles each of them achieves its limiting value $\rho_*(\varphi)$ which determines the point $(\rho_*\cos\varphi, \times \rho_*\sin\varphi)$ of the punch section kernel for the chosen direction φ.

In the practical calculations of the section kernel boundary, depending on the complexity of the punch bottom shape, the angular interval $\{\varphi: 0 \leq \varphi < 2\pi\}$ was presented by discrete values

$$\varphi = \Delta\varphi \cdot (m-1), \quad \Delta\varphi = \frac{2\pi}{M}, \quad m = 1,2,...,M.$$

The calculation procedure is essentially shortened by the account of the external punch contour symmetry. It is also worth noticing that, in order to accelerate the iteration process convergence, we used the following technique: at each iteration step the values $\overline{\rho}(\varphi)$ were determined as

$$\overline{\rho}^{(k)} = \frac{\rho_1^{(k)} + \lambda_k \rho_2^{(k)}}{1 + \lambda_k}$$

where λ_k is a dimensionless parameter, characterizing at the k-th step the ratio of the total area F_1 of boundary elements, for which the contact stress is compressive ($\rho_i > 0$), to the total area F_2 of boundary elements, for which the contact stress is tensile ($\rho_i < 0$), $F_1 \cup F_2 = \Phi$, Φ being the whole punch bottom area.

As a test example to estimate the working efficiency of the algorithm proposed, we have chosen determination of the section kernel boundary for a round punch resting on a homogeneous elastic half-space. As noted above, this problem has an

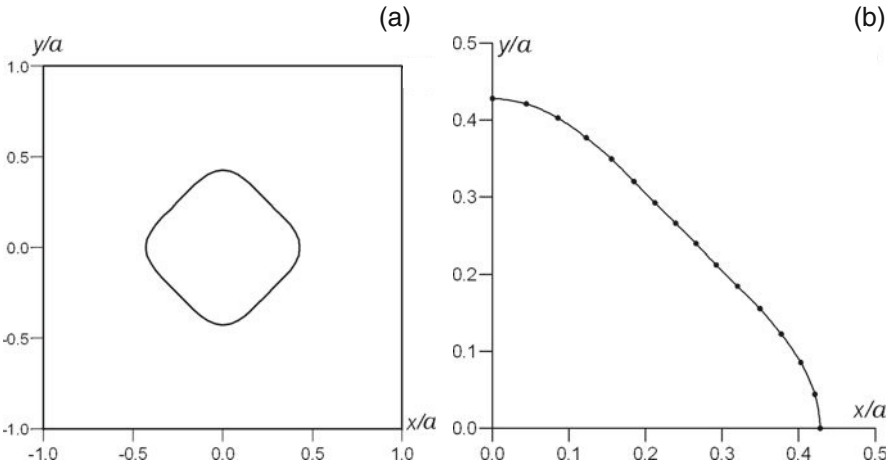

Fig. 4.44 Section kernel for a square punch on an elastic half-space: (**a**) location with respect to the punch contour, (**b**) calculated values of the polar radius of the boundary points

exact solution, $\rho_* = a/3$, a being the punch radius. Numerical calculations on the base of the method proposed with a uniform discretization of the circular contact domain into triangular and quadrangular boundary elements using 20 radii and 5 concentric circles, gives for $\varepsilon = 10^{-4}$ an approximate solution $\rho_* = 0.33486a$. The relative error is seen to be quite small, much less than 1%.

The results of calculations of the section kernel boundary for a square punch on an elastic half-space are presented in Fig. 4.44. Due to the symmetry of the problem, the calculations were performed for the angular interval $\{\varphi: 0 \leq \varphi \leq \pi/4\}$ with $\Delta\varphi = 3°$. As seen from the calculation data, the shape of the section kernel is a square-type figure with rounded angles, whose symmetry axes make an angle $\pi/4$ with the symmetry axes of the punch itself (Fig. 4.44a). For the example under consideration, the linear size of the section kernel is almost 2.8 times smaller than the punch itself.

The problem of pressure of a flat square punch, loaded by an eccentric force, was first solved approximately by Leonov, Posatskiy and Ivashchenko [154]. They applied the method of solving the problem of pressure under the punch bottom, resting on an elastic half-space, when the contact domain is close to circular. A circle is inscribed into the square contact domain. The pressure under the punch within the circle consists of the pressure, arising at the impression of a circular punch, and an additional pressure due to the application of a normal load, applied outside the circular punch, on the areas, complementing the circle to the square domain, required to provide the settlement under the punch on the whole square contact domain to coincide with the given settlement value. Solution of the problem at an eccentrically applied vertical force has shown that in order to obtain non-negative contact pressures under the punch, a condition for the eccentricity along the axis, normal to the square side with the length $2a$,

$$\rho \leq 0.45a$$

should hold. Note that the accuracy of the obtained value for the estimation of the section kernel size $\rho_*= 0.45a$ is low due to a rather approximate integration of the main equation of the problem with a large step $\Delta\alpha = 5^\circ$ along the angular coordinate as well as not quite efficient of subsequent approximation of the solution found. Besides, the method proposed in [154] does not possess high generality and, as noted earlier, is applicable only for contact domains, close to circular.

The results we have obtained are in a rather good agreement with the estimations for the section kernel boundaries for rigid rectangular plates on an elastic half-space, found in [105] by an approximate method, using the expansion of the contact pressure function into power series with a finite number of terms. It was also shown there that a point in the centre of the punch side is more dangerous in view of the punch uplifting than an angular point. The limit eccentricity value, above which the square punch uplifing from the soil occurs, obtained for this point in case the reactive pressure equation being taken as a sixth-order polynomial for a centred vertical load and a fifth-order polynomial for a momental load, equals $\rho_*/a = 0.425$ (a being half the side of the square). More exact calculations with eighth- and seventh-order polynomials being applied for the vertical and momental loads, respectively, give the value $\rho_*/a = 0.429$. According to our calculations for a square punch, discretized into 10×10 square boundary elements, at $\varepsilon = 10^{-4}$ the corresponding value will be $\rho_*/a = 0.4282$ (Fig. 4.44b).

The proposed numerical algorithm enables the problems of essentially oblique punches of a rather arbitrary shape to be solved and their section kernel boundaries to be found with a given accuracy, depending on the punch bottom domain discretization degree (number of the boundary elements) and the mesh grid quality. The calculation of the section kernel boundary for rigid punches with complex contours on elastic bases of various type is fully automated. From the geometrical point of view the problem is reduced to a rather detailed discretization of the flat domain, using triangular and quadrangular boundary elements, taking into account the contact stress concentration at the punch outer boundary. Application of any known software for building up high-quality grids for flat domains with a piecewise smooth boundary is possible, including those extensively used for finite-element calculations (See, e.g., [131, 228, 229]). We employed an intentionally elaborated software for solving spatial contact problems of theory of elasticity (FORTRAN-77 language) on the base of the algorithm described in Sect. 3.3.1. It enables discretization of flat domains, restricted by straight segments and arcs of smooth curves to be performed, what corresponds to the geometrical characteristics of foundation bottoms of various shape, used for construction and reconstruction of buildings and structures of known types.

In practical engineering, especially for construction of new foundations at constrained conditions of subterranean parts of buildings under reconstruction [226], complex-shaped foundations must often be used, as a rule, with a polygonal contour. Under considerable momental variable-sigh loads, or when there is a need to reduce the bottom length, foundations with I-shaped and T-shaped bottoms are applied. In

the cases of high momental loads, acting in perpendicular planes, L-shape bottom foundations are used. Cross-shaped foundations are used instead of rectangular ones in case lugs being provided for mounting closely located pillars or other structures of various design. Round foundations are often substituted by polygonal (hexa- or octagonal), since they are simpler for construction and their formwork production is less labour-consuming. These foundation types as well as other foundations with polygonal bottom are often used under various equipment and other technological structures [124, 257].

The abilities of the proposed method for estimation of stability of rigid foundation plates (interacting with the soil without their bottom uplifting) under an off-centre vertical load are illustrated (Figs. 4.45–4.48) by the calculations of the section kernel boundaries for polygonal punches (trapezoidal, cross-shaped, I-shaped, L-shaped), resting on an elastic half-space.

A common fact for all the examples under consideration is the presence of kinks at the section kernel boundaries, corresponding to the internal angular points on the contour of the punch itself. The presence of an external angle on the punch contour results in a smooth curving (rounding) between the practically linear segments at the section kernel boundaries. Besides, from the comparison of the section kernel configurations for a square and a trapezoidal punches with one common base (Figs. 4.44 and 4.45) it is seen that the punch contact domain broadening results in the stretching and displacement of the section kernel in the corresponding direction.

As follows from the calculations performed, the proposed numerical approach enables, from a given punch contour shape, the section kernel boundary (the domain of contact interaction without uplifting) to be effectively determined. This, in turn, provides important information at the stage of the complex-shaped foundation

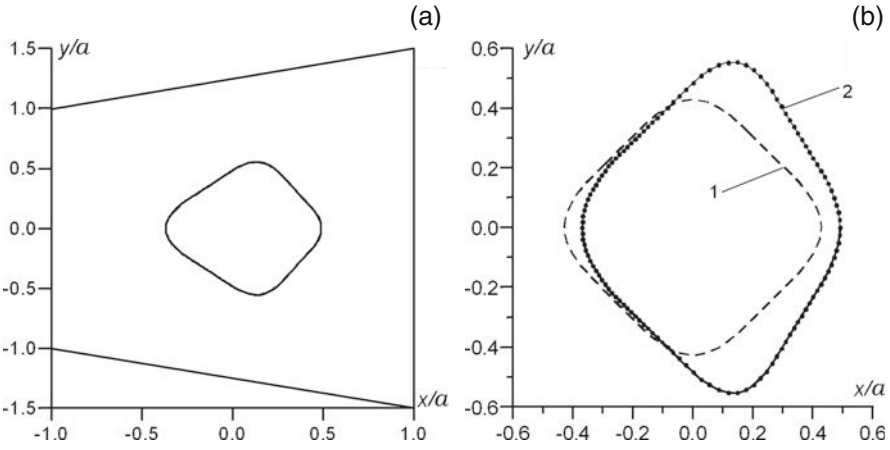

Fig. 4.45 Section kernel for a trapezoidal punch on an elastic half-space: (**a**) location with respect to the punch contour, (**b**) calculated values of the polar radius of the boundary points for a square (1) and a trapezoidal (2) punch

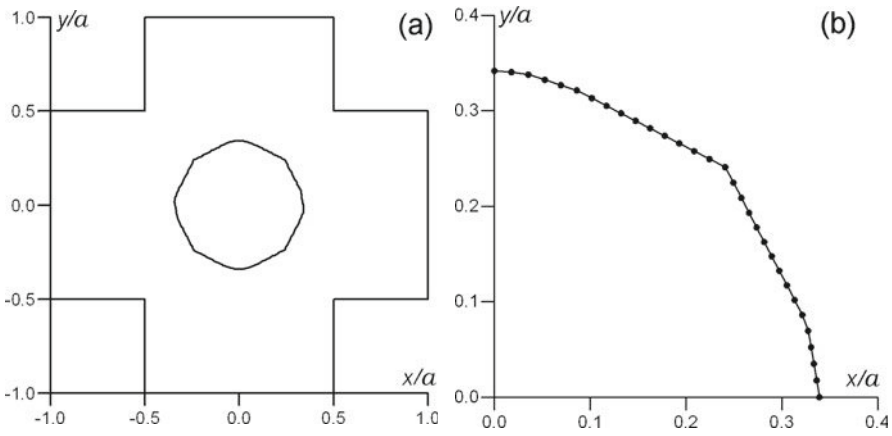

Fig. 4.46 Section kernel for a cross-shaped punch on an elastic half-space: (**a**) location with respect to the punch contour, (**b**) calculated values of the polar radius of the boundary points

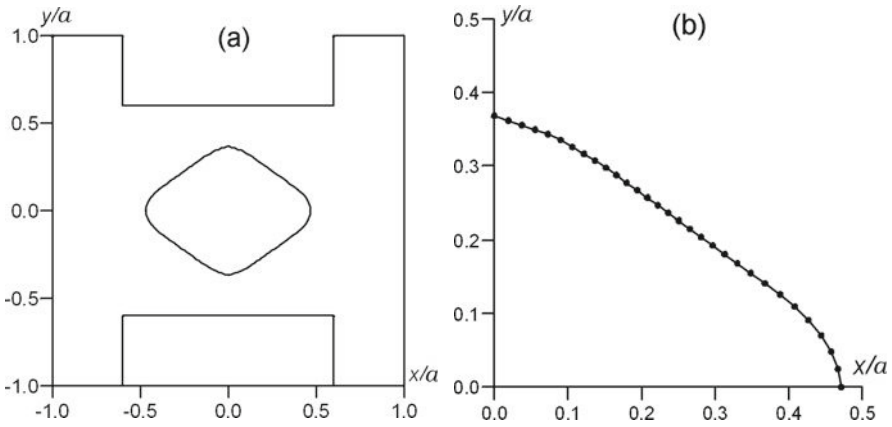

Fig. 4.47 Section kernel for an I-shaped punch on an elastic half-space: (**a**) location with respect to the punch contour, (**b**) calculated values of the polar radius of the boundary points

design when a strict account of the conditions of the punch bottom uplifting from the base is required. The relevant instructions available in the regulations [162, 249], result in cumbersome, very approximate and often not enough substantiated calculations with the use of vast graphic and table data. Therefore, the determination of the section kernel boundaries for foundations with bottom of a complex geometrical shape enables the methods of design and calculation of shallow foundations to be improved. In a number of practical cases, arising at the reconstruction of buildings, the maximal possible values of vertical load application eccentricities can be reliably determined. Thus, design of foundations with uplifting is avoided and high quality of the project solutions is provided.

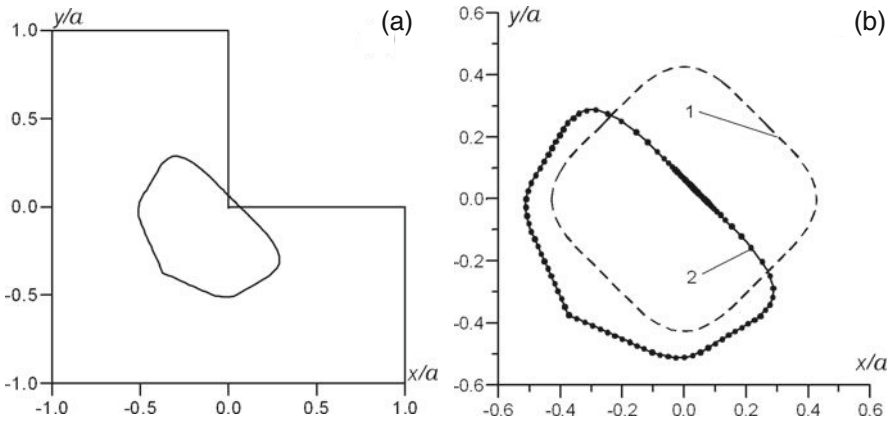

Fig. 4.48 Section kernel for an L-shaped punch on an elastic half-space: (**a**) location with respect to the punch contour, (**b**) calculated values of the polar radius of the boundary points for a square (1) and the L-shaped (2) punches

Application of the elastic base model in the elaborated numerical algorithm is performed as a separate module and does not require resetting of the whole program in case any other model of the elastic base being used, for which the influence functions have been obtained (See, e.g., [39, 73, 75, 89, 210, 225]). As a rather helpful illustration of the abilities of the proposed numerical method we consider a spatial contact model of an elastically compressible variable-thickness layer in the shape of a spatial wedge $0 \le x < \infty$, $-\infty < y < \infty$, $0 \le z \le x \times \tan\alpha$ with a central angle α at the rib, $0 < \alpha < 90°$ [89, 158]. The oblique plane, restricting the wedge from below, is completely restrained. The presence of an oblique underlayer makes the elastic base nonhomogeneous in depth and enables the account of variation of the compressed soil layer thickness under the bottom of large-scale foundations. Figures 4.49–4.54 present the calculated section kernel configurations for foundation plates of various, mostly polygonal shape, resting on an elastic compressible variable-thickness layer. It follows from the numerical calculations performed that for the foundations of the geometrical shapes under consideration their section kernels on an elastic compressible wedge always have smaller size than in the classical case (on an elastic homogeneous half-space). The corresponding reduction of the section kernel area, related to the non-uniform compressibility of the base, are rather essential and depend on the angle α of inclination of the rigid underlayer and on the punch distance from the elastic wedge rib, corresponding to the coordinate origin. With respect to the punch centre, one can observe a sort of the section kernel shift towards the wedge rib and its size decrease at the opposite side.

For the punches with a smooth contour (a circle, an ellipse) the section kernel boundaries are distorted and shift, remaining practically similar to the section kernel in the case of the half-space (Figures 4.49 and 4.50). However, for the polygonal punches, characterized by the presence of angular points on the contour, the section kernel boundaries acquire distinct straight segments and kinks, their location being

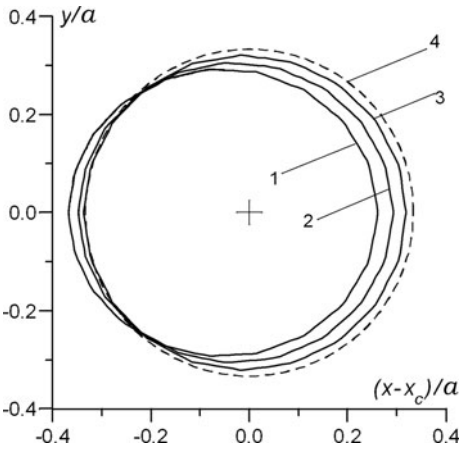

Fig. 4.49 Section kernel for a round punch with a radius a on a variable-thickness elastic layer. 1: $x_c = 1.5a, \alpha = 15°$; 2: $x_c = 1.5a$, $\alpha = 30°$; 3: $x_c = a$, $\alpha = 45°$; 4: elastic half-space

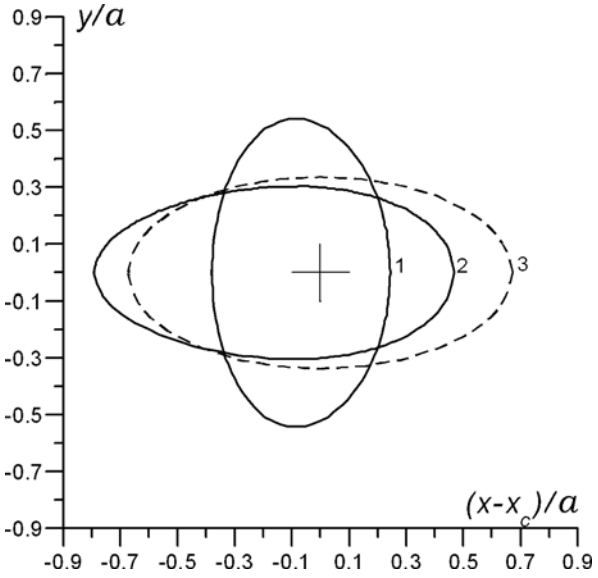

Fig. 4.50 Section kernel for an elliptical punch $(x–x_c)^2/a^2 + y^2/b^2 = 1$ on a variable-thickness elastic layer (α=30°). 1: $x_c = 2.5a$, $b = a/2$; 2: $x_c = 1.5a$, $b = 2a$; 3: elastic half-space

dependent of the nonhomogeneity degree of the compressed soil mass under the punch bottom (Figs. 4.51–4.54).

Note that the section kernel boundary configurations for the rigid foundation plates resting on elastic half-space-type bases with depth-dependent characteristics, calculated by the method proposed here, are similar to those obtained for the homogeneous half-space (Figs. 4.44–4.48), but their size depends on the nonhomogeneity parameters. Numerous calculations have shown that the method elaborated enables

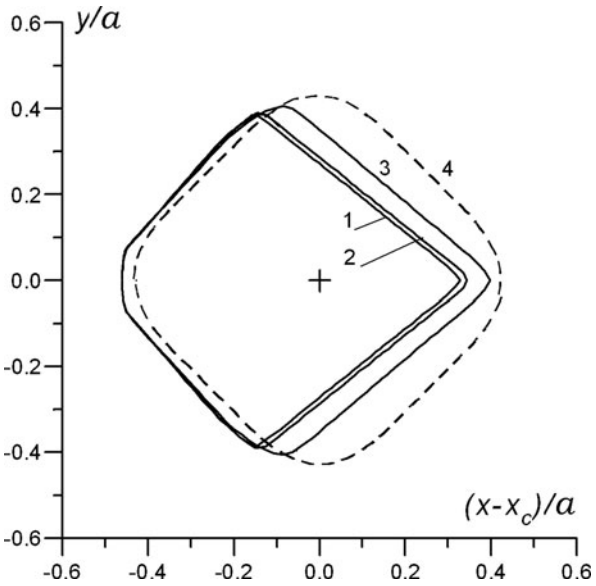

Fig. 4.51 Section kernel for a square punch on a variable-thickness elastic layer. 1: $x_c = 1.5a$, $\alpha = 15°$; 2: $x_c = 1.5a$,$\alpha = 30°$; 3: $x_c = a$,$\alpha = 45°$; 4: elastic half-space

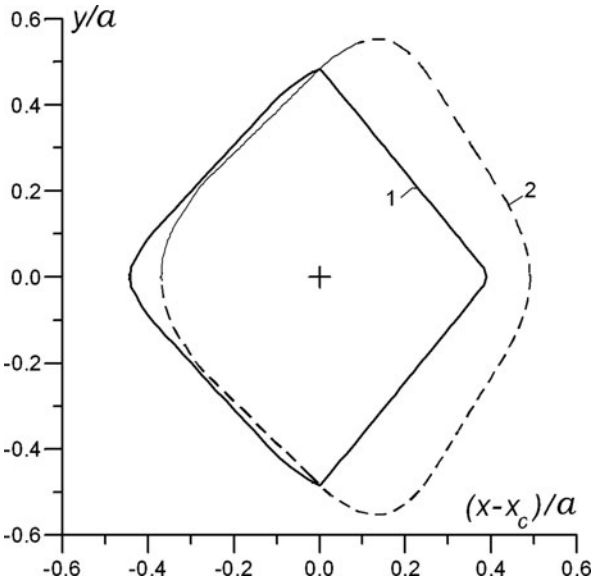

Fig. 4.52 Section kernel for a trapezoidal punch: (1) on a variable-thickness elastic layer, $x_c = 3a$, $\alpha = 15°$ and (2) on an elastic half-space

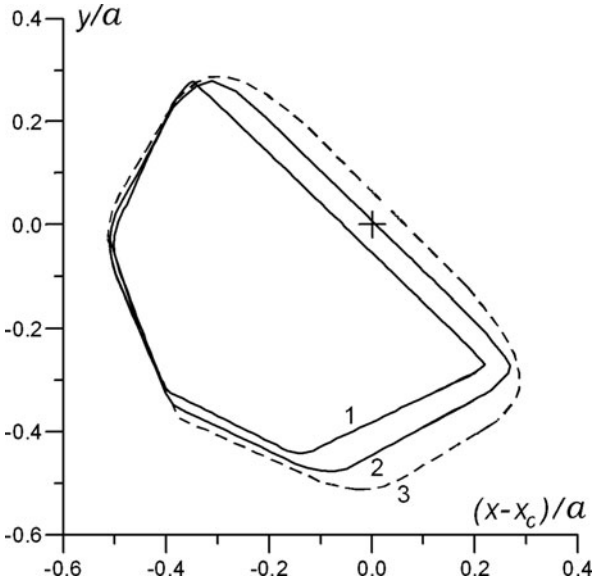

Fig. 4.53 Section kernel for an L-shaped punch on a variable-thickness elastic layer ($x_c = 2.5a$). 1:$\alpha = 15°$; 2: $\alpha = 30°$; 3: elastic half-space

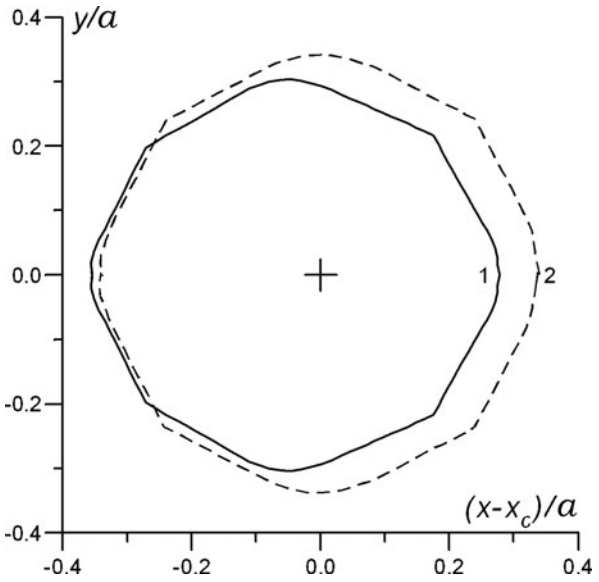

Fig. 4.54 Section kernel for a cross-shaped punch: (1) on a variable-thickness elastic layer, $x_c = 2a$, $\alpha = 30°$; and (2) on an elastic half-space

the effect of the elastic base nonhomogeneity degree (both in depth and over the area) on the size and shape of the rigid foundation plate section kernels to be estimated within the guaranteed accuracy.

Thus, the numerical algorithm elaborated enables the section kernel boundaries to be calculated from the given shape of the rigid foundation plate bottom and the mechanical characteristics of the elastic base and thereby the domains of application of a vertical resultant external load to be determined, for which the contact interaction of the rigid foundation plate occurs without the bottom uplifting from the soil base. The section kernel configurations have been obtained for the circular, elliptical, rectangular, trapezoidal, cross-shaped, I-shaped, L-shaped rigid foundation plates on spatially nonhomogeneous bases, for which obtaining analytical solutions has come across unsurmountable difficulties.

The obtained calculation data on the section kernel boundaries are important from the point of view of estimation of the complex-shaped rigid foundation plate stability for the spatial stress-strained state of the soil and can provide recommendations regarding the determination of optimal values of foundations operating without uplifting of the bottom from the base. The method requires short time for data preparation and numerical computations, provides stability and accuracy of the results obtained, sufficient for engineering applications.

4.6 Numerical Algorithms of Solving Boundary Integral Equations in Spatial Contact Problems for a Nonlinearly Deformable Base

The effective account of physical nonlinearity of soils is important for the rational design of bases and foundations [67, 94, 283]. At present, however, there is no unique and reliable approach to the solution of spatial problems of soil mechanics with the account of a wide variety of strength-related and deformational properties. As a rule, this is related to the lack of reliable data from stabilometric measurements of mechanical characteristic of soils for complex stress-strained states as well as with too high computer resources required for the calculations. Besides, one should note a rather narrow orientation of the existing software requiring large amount of information to prepare the input data for three-dimensional finite-element modelling. Therefore, it seems quite important to work out rather simple contact models with an ability to the account of nonlinear properties of various bases. Application of such models in combination with the efficient boundary-element method, enabling the problem dimensionality to be reduced, for a number of practical situations can lead to a considerable simplification of calculations, reduction of their scope, and a sufficiently accurate estimation of the qualitative and quantitative aspects of the contact interaction of the structures with the soil mass. Besides, as shown below, such an approach widely employs traditional numerical methods, popular for solving problems in the linear formulation with a wide range of contact models being applied, taking into account the base distributive properties.

4.6.1 Spatial Contact Model for a Nonlinearly Deformable Base

In practical calculations of soil bases for the linear deformation stage spatial contact models for a half-space [92, 128], a constant- or variable-thickness layer [75, 89], layered and nonhomogeneous with depth half-spaces, etc. have gained good reputation. The above noted contact models are the solutions of problems of the base surface settlement under a concentrated vertical load. The contact models, based on the strict solutions of a mixed spatial problem of theory of elasticity, are a relatively simple and convenient means to set a relationship between the pressure on the base and its settlement as given below:

$$W(x,y) = \frac{1-\nu^2}{\pi E} \int\int_S p(\xi,\eta)\, \omega(x,y,\xi,\eta)\, d\xi\, d\eta \tag{4.4}$$

where the function $\omega(x, y, \xi, \eta)$ is chosen, depending on the base model assumed. The contact models applied are linear and differ in the prediction of the base distributive properties. For the real conditions of soil deformation under the load increase, a nonlinear character of settlement-versus-load relation is revealed, and Eq. (4.4) requires a generalization.

Suppose the settlement in a given base surface point to be dependent of the loading level p/p_*. It can be given by

$$dW(x,y) = \varphi(p,p_*)\, \omega(x,y,\xi,\eta)\, d\xi\, d\eta$$

where $\varphi(p, p_*)$ is a function of the loading level, defining the law of nonlinear deformation of the surface under the load, p_* is the limiting contact pressure on the base surface, ξ and η are the coordinates of the centre of an elementary area, x and y are the coordinates of the point under consideration.

From mechanical speculations, qualitative conclusions on the form and properties of $\varphi(p, p_*)$ can be made. Thus,

$$\begin{aligned}
&\varphi(p,p_*) \sim p \text{ at } p << p_*,\\
&\varphi(p,p_*) \to \infty \text{ at } p \to p_*,\\
&\varphi'_p(p,p_*) > 0,\ \varphi''_{pp}(p,p_*) > 0,\ 0 < p < p_*.
\end{aligned}$$

The p_* value is considered as the contact model parameter, and we call it a limiting contact stress, since it has the dimensionality of stress and plays the role of a characteristic scale.

Specify the function $\varphi(p, p_*)$ using the following analytical approximation:

$$\varphi(p,p_*) = \frac{p}{\left[1-\left(p/p_*\right)^n\right]^m}$$

where $m, n > 0$ are dimensionless parameters which, along with p_*, are subject to identification based on the analysis of the experimental data. Hereinafter we

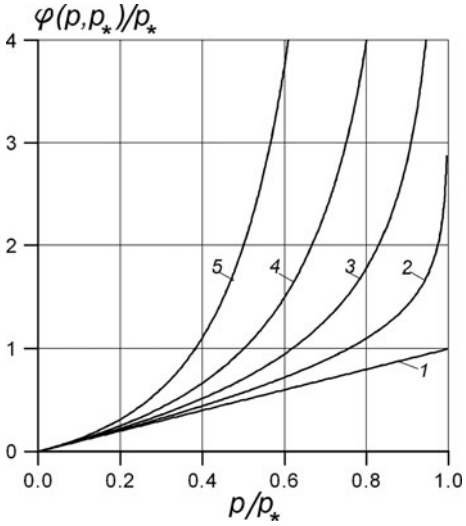

Fig. 4.55 Load function plots at the nonlinearity parameters $n = 1$; $m = 0$ (1), 0.2 (2), 0.5 (3), 2.0 (4), 5.0 (5)

consider $n = 1$. Parametric dependences, reflecting the character of the nonlinear behaviour of $\varphi(p, p_*)$ with the increase of the m parameter, are plotted in a dimensionless form in Fig. 4.55. Note that at small values of m one has the case of linear settlement-versus-load relationship practically in the whole range of the active stress variation.

Thus, the settlement of the nonlinearly deformable base surface under an external vertical load $p(x, y)$, distributed over the finite area S, will be presented in the following generalized form:

$$W(x,y) = \frac{1-\nu^2}{\pi E} \int\int_S p(\xi,\eta)\, \overline{\varphi}(\xi,\eta,p_*)\, \omega(x,y,\xi,\eta)\, d\xi\, d\eta \tag{4.6}$$

where $\overline{\varphi}(\xi,\eta,p_*) = \varphi(p,p_*)/p_*$. The form of Eq. (4.6) enables boundary contact problems to be built for given $\varphi(p,p_*)$ or $\overline{\varphi}(p,p_*)$ and for various fundamental solutions $\omega(x, y, \xi, \eta)$, known from the literature.

Note that in [282] a nonlinear dependence of the base settlement on the load is taken into account for the calculations of rigid beams on a nonhomogeneous Winkler base, obtained from an approximate formula

$$W = \frac{1-\nu^2}{E}\omega \cdot b \frac{p}{1-p/p_*} \tag{4.7}$$

where ω is a coefficient, depending on the rectangular foundation side ratio, p_* is the pressure corresponding to the loss of the carrying capacity by the base. Equation (4.7) was also used to set the coefficients of increase of the standard pressures on the soil in the mining underworking areas as well as to estimate the effect of nonlinear relationship between the foundation settlements and loads at the determination of

forces in buildings erected on the underworking territories. In [290], the shooting method was used for solving the problem of calculation of a rectangular plate on a nonlinearly deformable base, modelled by a solid half-space with the deformation modulus being a function of the load

$$E = E_0 \left[1 - \left(\frac{p}{p_*} \right)^{\gamma} \right]^{1/\gamma}$$

where E_0 is the initial deformation modulus, corresponding to the proportional dependence between the pressure on the soil and the displacements on its surface, p_* is the limiting pressure on the soil, determined from the punch tests, γ is the nonlinearity parameter.

4.6.2 System of Nonlinear Contact Equations of the Contact Problem for Absolutely Rigid Punches of a Complex Shape with a Flat Base

The spatial contact model of Eq. (4.6), using the dependences $\varphi(p,\ p_*)$ and $\omega(x,\ y,\ \xi,\ \eta)$, is applied to determine contact pressures $p(x,\ y)$, vertical displacements W_C and slopes ψ_x, ψ_y of rigid punches of arbitrary shape resting on the surface of a nonlinearly deformable base. Consider the punch to undergo a static load, reduced to a vertical resultant force P and moments M_x, M_y. Suppose also the vertical displacements of the punch and the base surface to be equal, and tangential stress in the contact plane to be zero.

For the spatial contact problem the equality of the vertical displacements of the punch with the area F and of the base surface results in the following nonlinear boundary integral equation to determine the unknown contact pressure and parameters of the punch displacement as a rigid solid:

$$\int\int_F p\,(\xi,\eta)\,\overline{\varphi}\,(p,\,p_*)\,\omega\,(x,y,\xi,\eta)\,d\xi\,d\eta\ = W_c + \psi_x \cdot (x - x_c) + \psi_y \cdot (y - y_c) \quad (4.8)$$

where F is the area of the contact between the punch and the base, $p(x,\ y)$ is the sought contact pressure function, W_C is the vertical displacement of the punch centre, x_c, y_c are the coordinates of the reduced external force application point. On the free surface of the base ($z = 0$) outside the contact domain $p(x,\ y) = 0$. Besides, the equilibrium equation system for the punch

$$\begin{gathered} \int\int_F p\,(\xi,\eta)\,d\xi\,d\eta = P, \\ \int\int_F p\,(\xi,\eta)\,\xi\,d\xi\,d\eta = P \cdot x_C - M_y, \quad \int\int_F p\,(\xi,\eta)\,\eta\,d\xi\,d\eta = P \cdot y_C - M_x \end{gathered} \quad (4.9)$$

should be satisfied.

Exact solutions of the formulated spatial contact problem exist only for a uniform isotropic linearly deformable half-space when the contact domain is of an elliptical or circular shape [74, 92, 98, 128, 203]. For punches of a more complex shape, as well as under interaction with the nonlinearly deformable base, the numerical boundary-element method will be used, which is successfully applied in the case of linearly deformable bases (See Sects. Section 4.2 – Section 4.5).

The nonlinear integral equation (4.8) is solved numerically in combination with the conditions of Eq. (4.9). For this purpose, the contact domain is meshed into N triangular or quadrangular elements. In the simplest case a piecewise constant approximation of the contact pressure function is assumed, hence within a separate element $p(x, y) = \text{const}$. In case of impossibility of the contact domain to be discretized into a rather large amount of elements and in order to increase the accuracy of the numerical solution, the calculations should be performed using the piecewise constant contact pressure function.

We successively substitute the coordinates of centres of gravity of all elements into Eq. (4.8) and replace the dual integrals over the area F by a sum of integrals over each element. The unknown contact pressures p_i on the elements (i=1,..,N) as well as the parameters W_C, ψ_x, and ψ_y of displacement of the punch as a rigid solid are determined from a system of (N+ 3) nonlinear (over p_i) algebraic equations

$$\begin{cases} p_1\overline{\varphi}\,(p_1,p_*)\,\delta_{i1} + p_2\overline{\varphi}\,(p_2,p_*)\,\delta_{i2} + \ldots + p_N\overline{\varphi}\,(p_N,p_*)\,\delta_{iN} - W_C - \\ -\psi_x\cdot(x_i - x_C) - \psi_y\cdot(y_i - y_C) = 0, \quad i = \overline{1,N}, \\ p_1\Delta S_1 + p_2\Delta S_2 + \ldots + p_N\Delta S_N = P, \\ p_1\Delta S_1 x_1 + p_2\Delta S_2 x_2 + \ldots + p_N\Delta S_N x_N = P\cdot x_C - M_y, \\ p_1\Delta S_1 y_1 + p_2\Delta S_2 y_2 + \ldots + p_N\Delta S_N y_N = P\cdot y_C + M_x. \end{cases} \tag{4.10}$$

Here, similarly to the above case, $\delta_{ij} = \int\limits_{F_j}\int \omega\,(x_i,y_i,\xi,\eta)\,d\xi\,d\eta$ is a vertical displacement of the surface of an elastic linearly deformable base in the point (x_i,y_i), coinciding with the centre of gravity of the i-th element, due to a unit load, uniformly distributed over the area F_j of the j-th element, ΔS_i is the i-th element area.

The numerical studies of the problem under consideration were carried out using a software, programmed by means of the FORTRAN language for punches of an arbitrary shape. According to the algorithm elaborated, the contact domain is successively discretized, the δ_{ij} coefficients are calculated from the given function $\omega(x, y, \xi, \eta)$, determining the distributive ability of the base, the equation system (4.10) is formed and solved for different values of the external forces and moments. The δ_{ij} coefficients are calculated semianalytically, as mentioned in Sect. 2.5.1.

4.6.3 Iterative Processes of Solving a Finite-Measure Analogue of the Spatial Contact Problem for a Nonlinearly Deformable Base

As a result of the discretization of the contact domain and the piecewise constant approximation of the contact pressure field, a finite-measure analogue of the spatial contact problem is obtained in the form of a system of N nonlinear equations (4.10), resulting from the nonlinear integral equation (4.8), as well as three linear equilibrium equations (4.9).

At $m = 0$, i.e. when the contact model is linear and the settlement of each point of the base surface is directly proportional to the contact pressures, Eqs. (4.10) become a system of linear algebraic equations and, due to the diagonal predominance, have good conditionality. This, in turn, enables standard methods of Gauss type to be used for the solution, without any special methods of regularization. For this case a rather general approach is developed for solving the spatial problems of contact interaction with the account of unilateral constraints for complex-shaped punches on no-classical linearly deformable bases (Sect. 2.5.1, Sects. 4.2–4.5).

At $m \neq 0$ the system (4.10) becomes nonlinear. Its solutions can be found by different methods, among which we used iterative ones [188, 230, 262]. Based on the experience of organization of different iterative algorithms, one can conclude about the efficiency of their application for the class of problems under consideration.

The simple iteration method can be the most easily realized for the system (4.10). First the system (4.10) is solved for the case of a linearly deformable base ($m = 0$). In this case all $\overline{\varphi}\,(p, p_*)=1$. The solution obtained $(p_1^{(0)}, p_2^{(0)}, \ldots, p_N^{(0)}; W_c^{(0)}, \psi_x^{(0)}, \psi_y^{(0)})$ is then used as an initial approximation in the following iterative process:

$$\begin{cases} p_1^{\alpha+1}\overline{\varphi}\,(p^{\alpha}, p_*)\,\delta_{i1} + p_2^{\alpha+1}\overline{\varphi}\,(p^{\alpha}, p_*)\,\delta_{i2} + \ldots + p_N^{\alpha+1}\overline{\varphi}\,(p^{\alpha}, p_*)\,\delta_{iN} - W_C^{\alpha+1} - \\ -\psi_x^{\alpha+1}\cdot(x_i - x_C) - \psi_y \cdot (y_i - y_C) = 0, \quad i = \overline{1,N}, \\ p_1^{\alpha+1}\Delta S_1 + p_2^{\alpha+1}\Delta S_2 + \ldots + p_N^{\alpha+1}\Delta S_N = P, \\ p_1^{\alpha+1}\Delta S_1 x_1 + p_2^{\alpha+1}\Delta S_2 x_2 + \ldots + p_N^{\alpha+1}\Delta S_N x_N = P \cdot x_C - M_y, \\ p_1^{\alpha+1}\Delta S_1 y_1 + p_2^{\alpha+1}\Delta S_2 y_2 + \ldots + p_N^{\alpha+1}\Delta S_N y_N = P \cdot y_C + M_x \end{cases} \tag{4.11}$$

where α is the iteration number. Numerous calculations have shown that the iterative process of Eq. (4.11), as a rule, converges for different values of the parameter m and punches of various configurations at a wide choice of the known influence functions $\omega(x, y, \xi, \eta)$ and external loading parameters. However, as follows from the practice of numerous calculations, direct application of the simple iteration method is hardly effective due to its slow convergence. With the increase of the m parameter values the convergence rate sharply decreases. Therefore, in order to speed up the convergence of the succession of approximation, the δ^2-Eitken transformation [115, 262] was used, convenient for the calculations and enabling the convergence of the iterative process of Eq. (4.11) for the class of problems under study to be speeded

up by dozens of times. The studies performed have shown that the use of such iterative processes as nonlinear relaxation methods, Jacobi or Seidel methods [230] have not revealed any advantages in comparison with the simple iteration methods and possess linear convergence. Meanwhile, the differential properties of nonlinear functions, contained in the equations of the system (4.10), enable the Newton method and its modifications to be used for its solution with any preset accuracy.

The Newton method for the system of nonlinear equations (4.10) is built in the following way. If p_i^{α}, $i = \overline{1,N}$,; $W_c^{(\alpha)}$,$\psi_x^{(\alpha)}$,$\psi_y^{(\alpha)}$ are already known, then

$$p_i^{\alpha+1} = p_i^{\alpha} + \Delta p_i^{\alpha}, \quad i = 1,...,N;$$

$$W_C^{\alpha+1} = W_C^{\alpha} + \Delta W_C^{\alpha}, \quad \psi_x^{\alpha+1} = \psi_x^{\alpha} + \Delta\psi_x^{\alpha}, \quad \psi_y^{\alpha+1} = \psi_y^{\alpha} + \Delta\psi_y^{\alpha},$$

where the values Δp_i^{α}, $i = \overline{1,N}$,; ΔW_C^{α}, $\Delta\psi_x^{\alpha}$, $\Delta\psi_y^{\alpha}$ are found from the following linear equation system:

$$\begin{cases} \delta_{i1}\varphi'\left(p_1^{\alpha}\right)\Delta p_1^{\alpha} + \delta_{i2}\varphi'\left(p_2^{\alpha}\right)\Delta p_2^{\alpha} + ... + \delta_{iN}\varphi'\left(p_N^{\alpha}\right)\Delta p_N^{\alpha} - \\ -\Delta W_C^{\alpha} - \Delta\psi_x^{\alpha}\cdot(x_i - x_C) - \psi_y^{\alpha}\cdot(y_i - y_C) = -\delta_{i1}\varphi\left(p_1^{\alpha}\right) - \\ -\delta_{i2}\varphi\left(p_2^{\alpha}\right) - ... - \delta_{iN}\varphi\left(p_N^{\alpha}\right) + W_C^{\alpha} + \psi_x^{\alpha}(x_i - x_C) + \\ +\psi_y^{\alpha}(y_i - y_C), \quad i = 1,2,...,N; \\ \Delta p_1^{\alpha}\Delta S_1 + \Delta p_2^{\alpha}\Delta S_2 + ... + \Delta p_N^{\alpha}\Delta S_N = P - p_1^{\alpha}\Delta S_1 - p_2^{\alpha}\Delta S_2 - ... - p_N^{\alpha}\Delta S_N, \\ \Delta p_1^{\alpha}\Delta S_1 x_1 + \Delta p_2^{\alpha}\Delta S_2 x_2 + ... + \Delta p_N^{\alpha}\Delta S_N x_N = P\cdot x_C - M_y - \Delta S_1 x_1 p_1^{\alpha} - \\ -\Delta S_2 x_2 p_2^{\alpha} - ... - \Delta S_N x_N p_N^{\alpha}, \\ \Delta p_1^{\alpha}\Delta S_1 y_1 + \Delta p_2^{\alpha}\Delta S_2 y_2 + ... + \Delta p_N^{\alpha}\Delta S_N y_N = P\cdot y_C + M_x - \Delta S_1 y_1 p_1^{\alpha} - \\ -\Delta S_2 y_2 p_2^{\alpha} - ... - \Delta S_N y_N p_N^{\alpha}. \end{cases} \tag{4.12}$$

As an initial approximation, here we also take the solution, corresponding to the case of a linearly deformable base. Due to the choice of such initial approximation and to the square convergence of the method, the succession of approximations converges rather quickly (3–5 iterations) in a broad range of variation of the nonlinearity parameter m. Note that in the case of large values of $m > 5$ the approximation processes considered give stable solutions together with the loading method with the parameter m [184].

Evidently, the boundary-element solutions p_i, $i = \overline{1,N}$, of the integral equation system (4.10) have the physical sense of contact stresses. Indeed, since the function $\overline{\varphi}(\xi,\eta,p_*)$ is dimensionless, the dimensionality of $p(\xi,\ \eta)$ does not change in case a nonlinear model being used. Besides, the nonlinear contact problem solutions, besides the integral representation of Eq. (4.8), with necessity satisfy the integral equilibrium conditions (4.9). Finally, in the limiting cases $p_* \to \infty$ or $m \to \infty$ the solutions obtained coincide with the contact stresses in the classical problem of theory of elasticity.

As follows from the theoretical study presented, the physical sense of the function $\omega(x, y, \xi, \eta)$ in the nonlinear contact model is not changed, i.e. it is supposed to be used from the consideration of linear deformation laws. It should be emphasized that the semiempirical model with the approximation of the loading function in the form of Eq. (4.6) should be treated as a complex representation of the dependence between the load and the settlement in the integral sense with invoking a dimensionless loading level function $\overline{\varphi}\,(p,p_*)$, and the functions $p(\xi, \eta)$ and $\omega(x, y, \xi, \eta)$ have their initial sense each (from the linear theory) – contact pressure and the influence function for a linearly deformable base without relation to any modifications.

According to the proposed numerical algorithm, the calculations are performed using a unique procedure, applicable for the cases of linear and nonlinear deformation. The influence functions are specified in a separate software module what does not require resetting of the whole algorithm.

4.6.4 Contact Problem for a Round Punch on a Nonlinearly Deformable Base

Consider, as an example, a spatial contact problem for a circular punch, interacting with a nonlinearly deformable base. We restrict our consideration by a punch loaded only by a vertical force P, as it is conventional at punch tests [110, 263]. To solve the problem numerically, the circular contact domain is discretized (Fig. 4.56) into triangular and quadrangular elements, using radii and concentric circles, condensing towards the boundary, what is related to a sharp change of the stressed state near the punch edge. The radii of the concentric circles are calculated using the following quasiuniform dependence:

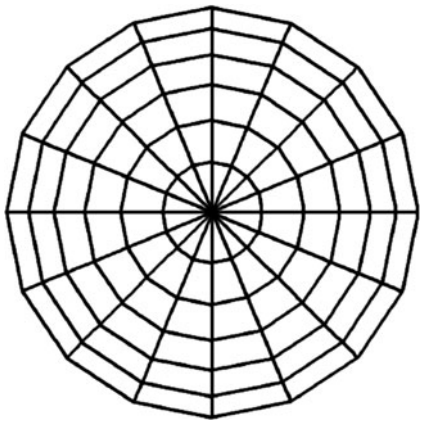

Fig. 4.56 Discretization of a circular contact domain

$$r_j = \alpha \frac{e^{\beta t_j} - 1}{e^{\beta} - 1}, \quad t_j = \frac{j-1}{L}, \quad j = 1,...,L.$$

The condensation degree is controlled by the choice of the parameter β.

In the case when the influence function is symmetrically differential, $\omega(x, y, \xi, \eta) = \omega(x–\xi, y–\eta)$, the system (4.10) for the round punch is essentially simplified

$$\begin{cases} \sum\limits_{j=1}^{L} A_{ij} p_j \overline{\varphi}\left(p_j, p_*\right) - W_c = 0, i = \overline{1,L}; \\ \sum\limits_{j=1}^{L} p_j \Delta S_j = \frac{P \cdot L}{N} \end{cases} \tag{4.13}$$

where the A_{ij} values are found using the influence coefficients δ_{ij} $(i, j = 1,...,N)$ from the formula

$$A_{ij} = \sum_{k=1}^{N/L} \delta_{i,j+L(k-1)}.$$

The dimensionality of the system (4.13) is $L+ 1$ where L is the number of the boundary elements in the radial direction.

Then consider the results of numerical modelling of the process of contact interaction of a round punch for the most popular models of elastic bases of a half-space type and of a finite-thickness layer type. The significance of such studies follows from the necessity of recovering nonlinear deformation diagrams from the punch test data.

Nonlinearly deformable half-space. Take the advantage of the known Boussinesq solution on the action of a unit concentrated force normally to the surface of the elastic linearly deformable half-space [128]. The influence function here is given by

$$\omega\,(x,y,\xi,\eta) = \frac{1-\nu^2}{\pi E} \frac{1}{\sqrt{(x-\xi)^2 + (y-\eta)^2}}. \tag{4.14}$$

In the case of interaction of a centrally loaded punch with a linearly deformable half-space, the problem has an analytical solution [98]

$$W_C = \frac{P\left(1-\nu^2\right)}{2Ea}, \psi_x = \psi_y = 0, p\,(r) = \frac{P}{2\pi a\sqrt{a^2 - r^2}}$$

where a is the punch radius, r is the distance from the centre to any point under the punch. This solution was a test for the algorithm constructed. Contact stress values of sufficient accuracy were obtained using $\beta = –1.0$ and the circle domain

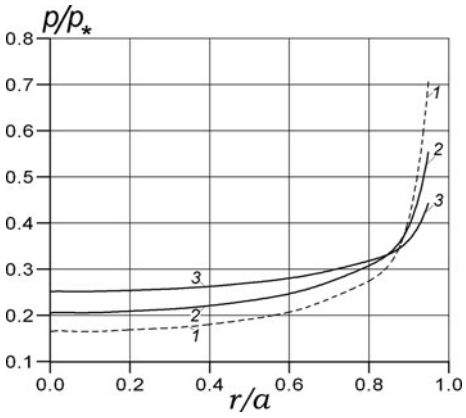

Fig. 4.57 Contact pressures under a round punch on a nonlinearly deformable half-space at $P = a^2 p^*$, m = 0 (1), 0.8 (2), 3.0 (3)

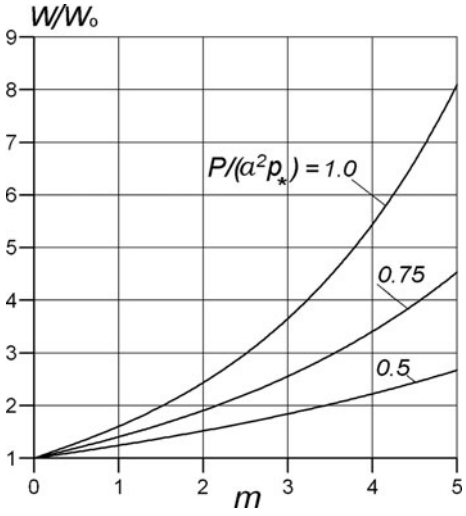

Fig. 4.58 Relative settlements of a round punch on a nonlinearly deformable half-space versus the nonlinearity parameter m at different loading values

discretization preformed using 96 elements, formed by six concentric circles and sixteen rays (Fig. 4.56).

The results of the calculations of contact pressures and displacements for a rigid punch on a nonlinearly deformable half-space are given in the dimensionless form in Figs. 4.57–4.59. It is seen from Fig. 4.57 that with the increase of the nonlinearity parameter m the contact pressure profiles are more flat, and the main change of the contact pressures occurs near the punch edge. The punch relative settlements at a given load increase nonlinearly with the m parameter increase, what is seen from Fig. 4.58. Nonlinear settlement-versus-load dependences are plotted in Fig. 4.59 at various values of the m parameter.

Nonlinearly deformable finite-thickness layer. The model of a linearly deformable half-space, in spite of wide application, still possesses certain

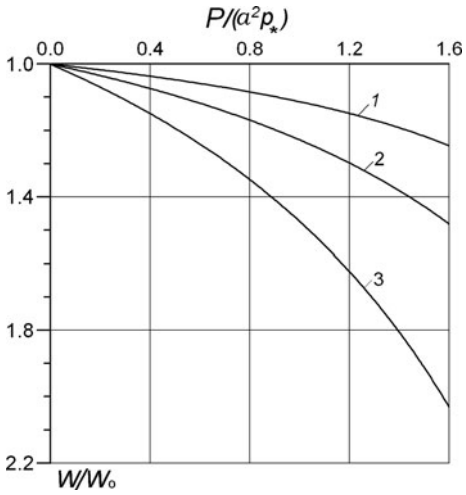

Fig. 4.59 Settlement versus load plots for a round punch on a nonlinearly deformable half-space at different values of the nonlinearity parameter m =0.2 (1), 0.4 (2), 0.8 (3)

shortcomings. In particular, the main of them is an assumption of the soil base being a spatially homogeneous semi-infinite medium. This essentially idealizes the situation and is not always confirmed at practical calculations. Application of a linearly deformable finite-thickness layer provides much better correlation with the foundation settlements on a soil base and enables the calculated values of forces and deformations in structures, resting on an elastic half-space, to be reduced.

In accordance with [203], the influence function $\omega(x, y, \xi, \eta)$, determining the vertical displacements of the surface points of a linearly deformable finite-thickness layer, caused by a unit normal concentrated force on its surface, is determined from the following integral dependence:

$$\omega\,(x,y,\xi,\eta) = \frac{1-\nu^2}{\pi E}\int\limits_0^\infty Q\,(H,t)\cdot J_0\,(R\cdot t)\,dt \tag{4.15}$$

where $R = \sqrt{(x-\xi)^2+(y-\eta)^2}$, J_0 is the first-order Bessel function of the 0th order.

The kernel $Q(t)$ of the integral representation (4.15) is given by

$$Q\,(H,t) = \frac{2\cdot\sinh^2(Ht)}{2Ht+\sinh(2Ht)} \tag{4.16}$$

where $0 < H < \infty$ is the thickness of an unlimited elastic layer, resting on an absolutely rigid base. Equation (4.16) was obtained using the Hankel transformation in the assumption of the absence of friction forces at the contact of the layer with the base. For a homogeneous elastic half-space $Q = 1$.

Table 4.11 Approximation parameters of the contact model for a constant-thickness elastic layer

k	1	2	3	4
A_k	0.8	1.4	2.0	2.6
B_k	0.426	−6.051	7.395	−2.770

The finite-thickness elastic layer model is in the mathematical sense more general than the elastic half-space model. At relatively high layer thickness $H >> a$, Eq. (4.15) is transformed into Eq. (4.14), i.e. calculations, based on Eq. (4.16), result in solutions of contact problems for the half-space as well.

It is known [150], that in the case of interaction of a centrally loaded punch with a linearly deformable finite-thickness layer, the contact problem solution is based on its reduction to even integral equations. This enables the punch displacements and contact stresses to be expressed in terms of an auxiliary function, satisfying the integral Fredholm equation with a continuous symmetrical kernel. Though this equation can be solved with a required degree of accuracy, this can be done only numerically.

While solving the contact interaction problem for punches of arbitrary shape with a finite-thickness elastic layer under a complex spatial loading, according to the numerical algorithm proposed here, the use of the integral representation of Eq. (4.15) is related to additional computational difficulties regarding the calculation of improper integrals containing oscillating Bessel functions. Therefore, when contact problems for a finite-thickness layer are to be solved, it is convenient to present the integrand of Eq. (4.16) in terms of a finite series of exponential functions. This enables the improper integrals to be calculated analytically, and thereby the computation accuracy to be increased and the computation time to be considerably shortened. In particular, a highly accurate approximation

$$\frac{2 \cdot \sinh^2(\alpha)}{2\alpha + \sinh(2\alpha)} = 1 + \sum_{k=1}^{4} B_k \exp(-A_k \cdot \alpha),$$

obtained by the least-square method in [33], enables the approximate solution for a concentrated normal force on the surface of a layer with a thickness H to be used in the form [75]

$$\omega(x,y,\xi,\eta) = \frac{1-\nu^2}{\pi E}\left(\frac{1}{R} + \sum_{k=1}^{4} \frac{B_k}{\sqrt{(A_k H)^2 + R^2}}\right) \tag{4.17}$$

where the coefficients A_k, B_k, $k=\overline{1,4}$ are listed in Table 4.11.

The first term in Eq. (4.17) corresponds to the Boussinesq solution and the rest of the terms, dependent of the layer depth H, can be treated as modifying terms. It is important to note that the function $Q(H, t)$ used is determined by one parameter of length dimensionality (the thickness of virtually compressible soil mass H), which

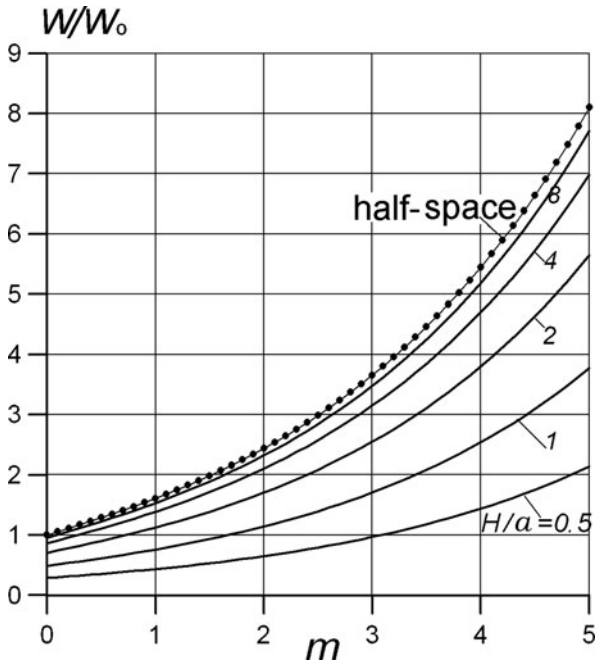

Fig. 4.60 Relative settlements of a round punch on a nonlinearly deformable finite-thickness layer versus the nonlinearity parameter m at different thicknesses of the elastic layer $P = a^2 p^*$

is the single geometrical parameter of the base. Due to this fact, the coefficients in Eq. (4.17) are fixed and, what is quite important, independent of the characteristics of mechanical properties of the base and its depth.

Numerical studies of the contact interaction of a round punch for the nonlinearly deformable finite-thickness layer, performed using the algorithm proposed, are in qualitative agreement with the calculation data for the half-space and are partly shown in Figs. 4.60–4.62. As one should expect, the contact pressure profiles become more flat both with the increase of the nonlinearity parameter m and with the decrease of the compressible layer thickness H (or a parameter $s = H/a$). The punch relative settlements under a given load nonlinearly increase with the increase of the m and s parameters, not exceeding the corresponding values for the half-space (Fig. 4.60).With the load increase this effect is revealed more noticeably (Fig. 4.61). The nonlinear character of the settlement-versus-load plots at different values of the m and H parameters is illustrated by Fig. 4.62.

As mentioned above, the calculations we have performed, are carried out in the assumption that there is no friction between the elastic layer and the rigid base. The presence of a contact surface between the elastic layer and the incompressible base in the soil at the depth H results in a nonuniformity of the stress-strained state. The studies, performed by a number of authors (See, e.g., [104]), have shown that the influence of the incompressible base on the stress concentration within the layer

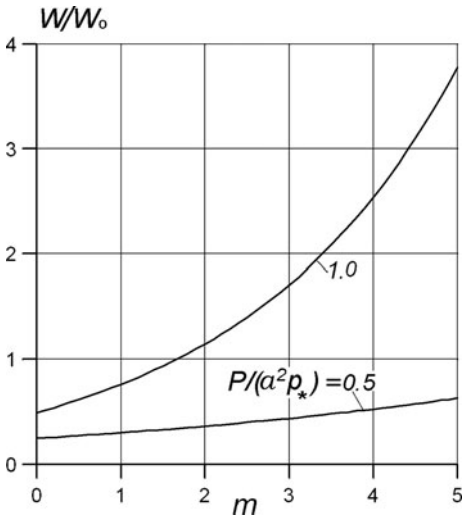

Fig. 4.61 Relative settlements of a round punch on a nonlinearly deformable finite-thickness layer (H/a= 1.0) versus the nonlinearity parameter$m$ at different load values

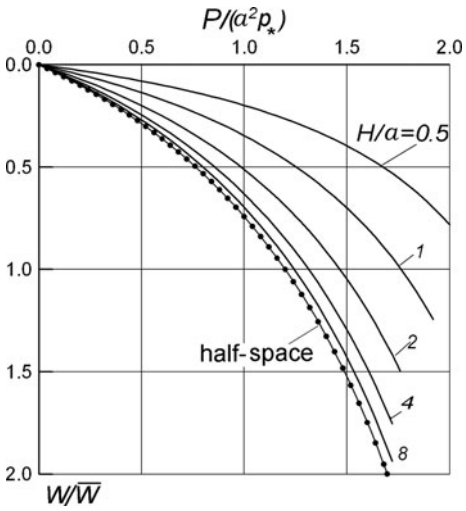

Fig. 4.62 Dimensionless settlement-versus-load plots for a round punch on a nonlinearly deformable finite-thickness layer W $=(1-\nu^{2})ap_{*}/2E$

becomes negligible only at $s = H/a > 5$. The concentration degree at $s < 5$ essentially depends on the conditions of the elastic layer sliding on the incompresible base. In particular, a detailed analysis shows that the condition of absence of tangential stress in comparison with the condition of the absence of displacements (restraint) on the lower boundary of the layer results in an increase of vertical displacements and compressive stresses. For real soil conditions, evidently, one should employ a boundary condition of the type of elastic constraints between an elastic body and an absolutely rigid body at their contact

$$u_j(x,y,H) = -\frac{1-\nu}{G}\mu \cdot \tau_{jz}(x,y,H), \quad j = x,y, \quad u_z(x,y,H) = 0,$$

proposed in [102], where μ is the coherence coefficient, resulting in an increase of the stress and displacement absolute values. The limiting cases of such conditions are coherence and smooth contact: at $\mu = 0$ the case of coherence of the layer and the base is obtained, at $\mu \to \infty$ the layer and the base can slide without friction along their whole common boundary.

A further approximation to the real deformation condition should be, evidently, considered modelling of a natural base as a scheme of an elastic finite-thickness layer on an elastic half-space. For example, when the elastic layer freely ($\mu = 0$) rests on the elastic half-space, the influence function is given by [11]

$$Q(\alpha,\chi) = \frac{\cosh 2\alpha - 1 + \chi\,(2\alpha + \sinh 2\alpha)}{2\alpha + \sinh 2\alpha + \chi\left(\cosh 2\alpha - 1 - \alpha^2\right)}. \tag{4.18}$$

This base model contains a ratio $\chi = \theta_1/\theta_2$ as a parameter, where $\theta_i = E_i/2(1-\nu_i^2)$, $i = 1,2$ are the mechanical characteristics of the layer and the half-space, respectively.

At $\chi \to 0$ one arrives at the scheme of an elastic layer on a rigid base, at $H/a \to \infty$ – at the elastic half-space scheme.

According to the module structure of the numerical algorithm developed, application of the influence function for the generalized model of a linearly deformable base of Eq. (4.18) does not result in any principal computational difficulties, leading only to the total increase of the computation time.

4.6.5 *Estimation of Nonlinear Deformation Effects from Punch Test Results*

From the calculation data presented in Sect. 4.6.4 it follows that, at the identification of the m, p_*, and H parameters, the contact model under consideration can be used to describe the deformational characteristics of bases as well as for the calculations of spatial contact interaction of foundation structures with soil at nonlinear deformation stage.

The qualitative character of the calculated dependences (Figs. 4.59–4.62) indicates the model applicability for the description of nonlinear deformation under foundations for both clay soils of soft and tough plastic consistency and sand soils of medium density with deformation diagrams without strengthening phenomena.

One of the possible algorithms of punch test data processing regarding the nonlinearly deformable base model under consideration can be the following.

First, the p_* parameter value can be estimated from the results of traditional punch tests [263], or the known formulae by Berezantsev [32] or Egorov [79] for initial critical load on the soil in the round punch case can be used for the first approximation.

Note that the calculation results, presented in Figs. 4.58, 4.60, and 4.61, are a sort of loading diagrams for a load series $P_t = K_t \times (a^2 p_*)$, i=1, 2, ...M (M is the number of the experimental points on a settlement versus load plot). If the experiments for the given loads P_i are carried out, then from the experimental data available $(W)_i$ one can, using the calculation diagrams, easily determine the corresponding $\{m_i\}$ values. Then a standard statistical processing of the obtained $\{m_i\}$ data array is performed [199] and the most probable (average) value for it $\overline{m}$ is evaluated. If the experimental data spread is small and the calculated data correspond to the experimental ones in accordance with the Fisher criterion at the given significance level, then the model based on the corresponding agreement criteria will be adequate to the experimental data and the $\overline{m}$ value is taken as a nonlinear model parameter.

As follows from the presented theoretical analysis of the spatial contact interaction at the nonlinear deformation stage, p_* and m are not independent parameters of the contact model, since the choice of the formula for the limiting contact pressure p_* (or its experimental determination) affects the $\overline{m}$ estimation.

The calculations performed (Fig. 4.62) are in agreement with the known results of practical observations indicating that one of the factors, essentially affecting the settlement value, is the depth H of the compressed soil base. It is determined rather accurately when the specific geotechnical conditions are known. The most typical are situations when, for example, under a compressible soil at a certain depth practically incompressible rock occurs; often under a structure season thawing out occurs to a finite depth, below which ever-frozen soils are located. Then it is natural to consider the whole deformable layer to be the compressible mass. Besides, there is a great number of calculation methods [104] to determine the compressible mass thickness: from the foundation width, from punch tests in combination with solutions for theory of elasticity, from the comparison of the natural and excessive pressures, etc.

The most popular approach to obtain the thickness H is its conditional calculation as the depth, at which the excessive pressure from the punch (the foundation model) is 10–20% of the natural value at the same depth. However, none of the known approaches to the compressible base thickness assignment is free from shortcomings. The values of the compressible soil mass depth, found for the same conditions by different methods, sometimes differ by factor of 2–5. Thus, the compressible base thickness is a conditional value being introduced into the calculation due to the difference of the real conditions from the half-space calculation model. This value should be assigned from the requirement of coincidence of the calculated and the actual settlements. Therefore, it is convenient to include the H value to the contact model nonlinear parameters and to determine it from the conditions of the calculated settlements approaching the real values. At such approach, the nonlinear character of the observed base thickness increase with load will be naturally taken into account as well as the influence of the punch area, soil condensation and a number of other factors.

The nonlinear parameters m, n, H of the model can be all together found by means of minimizing the mean square error at the mathematical processing of the punch test results by one of the nonlinear programming methods [60], e.g. by the

simplex method when a direct search is performed, using only the function values (without derivatives).

One should pay attention to the relation of p_* and m parameters to the form of the $\omega(x, y, \xi, \eta)$ function. According to the linearly deformable base theory [105], the influence function $\omega(x, y, \xi, \eta)$ determines the distributive properties of soil bases for the calculation model which in practice substitutes a real natural base. Many of these functions are at present widely used for the design and calculation of structures on an elastic base and are included into the regulations in action. A linearly deformable half-space, a linearly deformable finite-thickness layer, and the Fuss-Winkler model are most widely used in the calculation practice. Influence functions for many non-classical elastic bases have been obtained, with e.g. layered superposition of rock strata [210], variation of the elastic properties with depth [73], etc. being taken into account. Obviously, the choice of $\omega(x, y, \xi, \eta)$ at a given punch geometry determines, at different p_* and m parameter values, the characteristic settlement versus load diagram and thereby the evaluation of the nonlinearity parameters following from the experimental data processing. Calculations for the most widely used structures with the influence functions of Eqs. (4.14) and (4.17) are performed in Sect. 4.6.4. The choice of another $\omega(x, y, \xi, \eta)$ functions for the round punches will result in new calculated deformation diagrams, based on which, after the punch test experimental data processing, the model parameters p_*, m, and n will be identified. The presence of additional free parameters for the $\omega(x, y, \xi, \eta)$ function (e.g. the H parameter – the compressible soil base depth, or γ – the degree of nonuniformity of the mechanical properties with depth, etc.), enables the accuracy of approximating the experimental data to be increased. The example of a nonlinear contact problem for a finite-thickness elastic layer, considered above in Sect. 4.6.4, clearly and convincingly (in particular, the calculations presented in Figs. 4.60–4.62) shows a strong relationship of the p_* and m parameters with the influence function $\omega(x, y, \xi, \eta)$.

For the sake of completeness of the consideration one should make a note regarding the choice of the influence functions $\omega(x, y, \xi, \eta)$ themselves. It is well known [98, 128, 283] that until now the influence function $\omega(x, y, \xi, \eta)$, which would enable the behaviour of various soils to be described in a broad range of deformation conditions, has not been found. The results of comparison of different influence functions, referred to in the ample literature, do not enable one to determine, which of the influence functions available is the best for a satisfactory description of displacements and stresses for structures resting on elastic bases. Though each influence function $\omega(x, y, \xi, \eta)$ has its own physical background, at present it is impossible to make a preference for any of these functions. Therefore, the choice of the influence function $\omega(x, y, \xi, \eta)$ does not extend beyond the researcher's individual intuition based on a rational compromise between the complexity of the mathematical representations and the results of predictions regarding the functioning of bases for buildings and structures. Note once again that the use of an influence function $\omega(x, y, \xi, \eta)$ essentially affects the contact problem solution (Figs. 4.60–4.62), or, in other words, the nonuniformity degree of the reactive pressure distribution, which, in turn, affects the variation of the loading diagrams $W(m, H, p_*)$. The latter serve to estimate the nonlinearity parameters.

It is important to know that the nonlinearity parameters m, H, and p_* for a semi-empirical model are found from the condition of the best description of the experimental data at the non-linear stage of deformation. Such approach is generally accepted and widely used at the analysis of nonlinear mechanical models. The approach is most convincingly demonstrated in a number of publications (See, e.g., reviews [87, 181]), devoted to the issues of construction of nonlinear rheological calculation models of soil media. A lot of other references can be quoted, where the efficiency of the semi-empirical approach to describe various nonlinear mechanical phenomena is clearly demonstrated. Concerning the calculation of structures on an elastic base, two most important studies should be pointed out [282, 290]. In these publications, the ideology being used in this chapter, had been applied for the calculation of beam-type and plate-type structures, resting on an elastic nonlinearly deformable base.

Thus, a semiempirical contact model of a soil base is proposed, relating the nonlinearity parameters p_*, m, n with the distributive properties of the base. In the limiting cases ($p_* \to \infty$, or $m \to 0$) the contact model is linear, predicts a linear settlement-versus-load diagram and is fully characterized by the chosen influence function $\omega(x, y, \xi, \eta)$ for a linearly deformable base.

It is quite important that while formulating the calculation model proposed, contrary to the classical integral representations of theory of elasticity, the issue of the relationship between stress and deformation is not discussed. This is the specific feature and a certain advantage of the nonlinear integral representation of Eq. (4.6), relating the displacements and contact pressures only on the elastic base surface. The dimensionality of the foundation base calculation problems is reduced, and in a spatial (three-dimensional) formulation they become two-dimensional. One can treat the situation as a quite similar one to the application of the calculation models of one or two coefficients of subgrade reaction (Fuss-Winkler, Pasternak, or Filonenko-Borodich) which also do not imply the corresponding dependence between the stress and deformation tensor components. For practical engineering calculations, nonlinear contact models with coefficients of subgrade reaction depending on contact pressures or displacements, are successfully used [137, 139], and the variety of the soil properties and the complexity of their deformation processes quite justify the further development of the calculation methods invoking various modified calculation models of contact interaction.

4.7 Contact Problem for Orthotropic Foundation Plates with the Account of the Specific Features of Spatially Nonhomogeneous Base Deformation

Reinforced concrete plates are structural parts, widely used in practical engineering. When the plates serve as a foundation for a building or a structure, their functioning essentially affects the stress-strained state of the whole subterranean structure. The calculated values of separate structural parts in this case to a great extent depend on the soil base calculation model being employed.

4.7.1 Static Calculations of Foundation Plates on Elastic Bases

Reinforced concrete plate foundations of a rectangular, round, and ring-shaped cross-section are extensively applied for construction on natural bases (especially, on weak and nonhomogeneous soils) of multistorey buildings, elevators, funnels as well as dock bottoms, sluices, floors of industrial structures, airfield coverings, etc. [125].

Theoretical studies of plate foundation calculations are characterized by a quite great number of publications, based on some of which the computer software for the plate foundation calculations was worked out [105, 125]. Contrary to the traditional methods of calculations of proper plates of different shape and thickness, the calculations of the plate foundation structures are more complicated due to the necessity of account of the influence of a rigid above-foundation structure of the frame type, a system of constrained diaphragms, carrying walls of a very rigid above-foundation structure of funnel type, etc. The main specific features of the calculations result from the non-uniform base compressibility due to the natural soil nonhomogeneity within the plate foundation structures with large area.

The most popular scheme for the calculation of foundation plates on elastic bases is the one for the base with a variable rigidity coefficient which approximately takes into account the base nonhomogeneity with depth and over the area. Approaches, using this calculation scheme, as well as related ones based on the application of contact models with one or two coefficients of subgrade reaction (Winkler-type models), have been applied since the 1930s and are still used in the design practice. They are reflected in standards and regulations (See, e.g., [120, 121, 125]), and their theoretical substantiation with calculation examples is presented in detail in a vast number of books [5, 130, 134, 136, 143, 148, 189, 190, 257, 273, 274, 275, 280]. Note a publication [66] on an exact solution, directly related to the theory of design of rectangular foundation plates on Winkler-type elastic bases, which has not been included into books or handbooks, where a solution of the problem of bending of a plate with free edges, resting on a Winkler base, under a symmetrical load. This solution has not attracted the attention of design engineers due to the complexity of the expressions obtained for deflections, moments and transverse forces in the form of dual Fourier series whose coefficients should be found from the solution of infinite systems of linear algebraic equations. For practical purposes the foundation plate calculation by one of numerous methods (finite-difference, finite- or boundary-element) always appears more convenient due to its universality for the formulation of boundary conditions of various type, for the account of the complicate plate configuration and for a combined action of force and momental loads.

In spite of the disadvantages of the hypotheses concerning one and two coefficients of subgrade reaction, revealed in ambiguous dependences of the model parameters on the method of their determination, in the approximate account of the base distributive properties, in an additional concentrated lineal reaction along the plate contour, the base models with the use of the rigidity coefficients still remain applicable for practical calculations in view of their mathematical simplicity and convenience for software development.

Most of the above disadvantages of the Winkler-type elastic base contact models are overcome by using the base models, representing a spatial elastic continuum – an elastic half-space [105] or an elastic layer of constant and finite thickness [75]. Note that the model of an elastic layer, underlayered by an incompressible base, closer corresponds to the soil base properties and possesses the highest generality, since at considerable layer thicknesses it is reduced to the elastic half-space model, while at low thicknesses it is similar to the models of Winkler type (with an appropriate choice of the coefficients of subgrade reaction). Foundation plate calculations, using the contact models of spatial continuum type, enable the base distributive properties to be taken into account (formation of a sedimentary boot). While describing the base properties, these models take into account the deformation modulus and the Poisson ratio as parameters being, contrary to the coefficients of subgrade reaction, physical characteristics of the soil. It is especially important that the application of the elastic half-space and finite-thickness layer models enables the stress in the soil mass environment to be determined more reliably, the effect of foundations on each other to be taken into account, etc.

Theoretical studies devoted to the application of base models in the form of a half-space and a finite-thickness layer for the calculations of foundation plates, have been performed mostly by Russian researchers and are considered in detail in [105, 106, 291].

Gorbunov-Posadov [105] elaborated a method for approximate calculation of round and rectangular plates of various flexibility on an elastic half-space, based on the expansion of the plate deflections as a two-dimensional polynomial with unknown coefficients, determined by satisfying the plate bending differential equation, the boundary conditions on its contour, the equilibrium equations and the identity of the settlements of the plate and the base (half-space). A similar approach with some improvements in the technique of formation of the resolving system of linear equations was later implemented by Gorlov and Serebryanyi [106] for the calculations of rectangular foundation plates, resting on an elastic layer of a finite thickness.

In a method proposed by Zhemochkin [292], for the determination of the contact stress between the foundation plate and the base, vertical rod constraints are introduced, the forces in which are the resultants of the stresses in the soil near the surface of the foundation and the base contact. In such formulation the problem of calculation of the structures and the foundation is reduced to the determination of the forces in the constraints, i.e. to the construction and solution of a canonical system of equations of the mixed method of engineering mechanics.

The Zhemochkin approach is more labour-consuming than that of Gorbunov–Posadov, since it is related to much larger computation scope. However, it also possesses higher generality, enabling the variable rigidity of the plate to be taken into account as well as the base calculation model to be somewhat modified. The comparison of both methods for beams working at the conditions of the spatial problem, i.e. rectangular plates with the side ratio 7:1 and higher, has shown the difference in the application of these calculation methods to be small [106]. From the contemporary point of view, the method, proposed by Zhemochkin for a half-space, is in

fact the simplest form of the boundary-element method with a piecewise constant approximation of the contact pressure function.

Already in 1960 Solomin was one of the first to use the finite-difference method for the calculation of rectangular plates on an elastic half-space [250]. Later, finite-difference calculations for rectangular plates, resting on a finite-thickness elastic layer, were performed [251]. Further, the application of the variation-difference approach [271] has enabled Solomin et al. to extend the possibilities of the grid method to calculate complex-shaped foundation plates [253, 254]. The elaborated method of calculation appeared very efficient, and subsequently served as a basis for creation of a great number of professional software for foundation plate computations [105, 125].

The finite-difference method was of great importance at earlier stages of computer development, since the difference equation systems, having a simple and regular structure, can be efficiently solved using less powerful computer systems.

The book by Kączkowski [130], which is one of the most complete studies concerning static plate calculations, ranks the finite-difference method as the first among the approximate calculation methods. A special chapter there, devoted to the fundamentals of the finite-difference method application, proves that computations using the finite-difference method, do not encounter any serious programming difficulties, and the use of a sufficiently fine grid can provide results with an accuracy, quite sufficient for the practical purposes, to be obtained. The same chapter quotes the main studies concerning the finite-difference method application for plates of specific shapes (triangular, hexagonal, parallelogram-type, skew-angle).

The most significant among the recent papers, using the finite-difference method to calculate foundation plates on bases in the form of a rigid body, are [58, 126]. Reference [58] considers a plate (of beam type) on an elastic half-space, for its calculation a 40×10 finite-difference grid being employed. Variational principles are invoked to determine the contact domain of the plate and the base. An intentionally developed finite-difference software is used in [126] to perform extensive calculations, using a succession of condensing grids, of processes of interaction of a rectangular plate with an elastic half-space. A quite good convergence of the numerical results for the basic types of the external load (angular, edge, internal) is shown. The estimations of the finite-difference method efficiency have shown the computation time decrease by factor of 2–3 in comparison with the finite-element algorithms of a comparable accuracy. It is concluded that even now (in spite of the known popularity of the finite-element method) the finite-difference method is an effective tool for geotechnical calculations, especially for multiparametric studies.

Meleshenkov and Ozherelyev [168] present the results of a numerical experiment, performed for an example of plate bending problem solution by the finite-difference and finite-element methods. Depending on the density of a rectangular uniform grid, imposed on the plate, the accuracy of the solution and the number of arithmetic operation performed at the stage of solving the algebraic equation systems was compared. The finite-difference method is shown to be quite competitive with the finite-element method, and in some cases (a hinged plate under a uniformly distributed load) is has advantage over the finite-element method both in accuracy

and in the operation number. The finite-difference method is concluded to be rather efficient for solving some classes of problems of engineering mechanics and still remains a powerful tool for solving partial differential equations.

Application of the finite-element method for the calculation of foundation plates, resting on an elastic half-space, was first described in [65]. A quite detailed discussion of the calculation results obtained until 1979, including those obtained by the finite-element method, for foundation plates, resting on an elastic half-space, was performed by Selvadurai [234]. Due to the convenience of application of the finite-element method for the calculation of complex-shaped plates and simultaneous account of various nonlinear laws of their deformation, a lot of the developed software tools for foundation plate design use the finite-element method as the computation basis. However, the search performed has not revealed any professional software simultaneously including the use of the finite-element method and the elastic continuum models. Probably, this is explained by a sharp increase of the computer resources required and, consequently, by low efficiency of this type of algorithms in computer-aided design systems.

Among the publications, devoted to the finite-element calculation of of foundation plates, interacting with soil bases modelled by elastic spatial continua, some theoretical studies of the recent years should be mentioned [184, 206, 233, 237].

Contact interaction of two square plates, one of them being homogeneous, the other – three-layered, with an elastic half-space under a concentrated force, applied to the centre, is studied in [206]. Rectangular finite elements with a linear reactive pressure distribution were used.

In order to determine the deflection of a rectangular plate on an elastic half-space, Novotný and Hanuška [183] employed triangular finite elements, for which the plate deflection function is given by a full polynomial of the 5th order. Appearance of tensile contact stresses is excluded (the account of unilateral constraints), and the solution is found by iteration.

The Reisner square plate on an elastic half-space is calculated in [233] by using square isoparametric elements. The plate was supposed to bear on two opposite sides, the other two being gripped, and in the centre the plate bearing on a pole. The author claims this method, consisting in a choice of interpolation of the same order for the finite element geometry, displacement and reactive load fields, to result in a more exact and general solution than the known ones, since this solution is applicable not only for thin, but also for thick plates.

Contact pressure distribution under plates, resting on an elastic half-space, is investigated in [237]. The finite-element formulation of the problem is given with the application of eight-node isoparametric quadrangular elements. The numerical algorithm developed is capable of taking into account various shape of plates, whose material properties and thickness can vary from one element to another.

In the case of large areas the assumption of the soil working as a homogeneous isotropic elastic half-space is known to result in the overestimated values of deflections and bending moments in the foundation plates [105]. One of the reasons is a rather pronounced nonuniformity of the elastic properties of most soils over the depth. The most popular way of taking the base homogeneity into account is the use

of the deformation modulus, varying according to a power law. The layered superposition of soils is often taken into account as well as the Poisson ratio variation with depth. However, the rejection of the classical theory results in considerable complications of the calculation formulae, and only a small number of papers is devoted to the plate calculation with the account of the specific features of deformation of bases with variable physical and mechanical characteristics. In [73], the calculation for a rectangular plate, the soil deformation modulus under which varies with depth according to a power law, was performed by the finite-difference method. Mostly the studies are devoted to the calculations for round and ring-shaped plates, resting on bases with variable physical and mechanical characteristics under axisymmetric loading [4, 11, 38, 119, 164]. From the results of these studies it follows that the account of the increase with depth of the physical and mechanical parameters of the base can result in a reduction of the calculated values of the bending moments by up to 20%.

It follows from the analysis of the available literature that the issues of account of the base variable compressibility over the area, using the base continuum models for plate foundation design, have not been sufficiently developed. This results in a low reliability of the calculations for foundation plates, located on slope edges, near high-angle soil layers, on the bases with the compressible soil mass thickness increasing (decreasing) in a certain direction, as well as for a number of other complicated geotechnical conditions when the compressible soil mass thickness varies within the foundation plate area [125].

In the great majority of the calculation schemes at the studies of interaction of foundation plates with a soil base the plate material is assumed isotropic. However, even conventional ferroconcrete plates, reinforced in different directions, are characterized by different rigidity at bending, depending on its direction. This was noticed already by Huber [118] and Marcus [163], considering a ferroconcrete plate with orthogonal reinforcement as an orthotropic one. The anisotropic properties of plates should be taken into account in order to carry out more reliable calculations of mutual deformation of the above-foundation structure and the plate on a compressible base, to choose the reinforcement, to check the crack widths, to determine the calculated forces in the foundation.

Theory of calculations for anisotropic plates has been developed rather long ago and is in quite a detailed way described in a number of books, among which some are worth to be mentioned first of all [23, 152]. A particular case of anisotropy is orthotropy, which is characterized by three perpendicular directions of elastic symmetry in a plate. In practical engineering this type of anisotropy is the most common.

The orthotropic properties of plate foundations are in most cases induced by reinforcement, by smooth variation of thickness in a rather narrow range, by a one-side finning in one or two directions, by formation of cavities, by construction of box-like structures with ribs in two directions, etc. [105, 130]. The systems under consideration are, in general, plates of isotropic materials, but their bending rigidity varies over the area due to the variation of the plate cross-section. Many researchers come to a conclusion that the use of the mechanical model of a homogeneous orthotropic

plate with constant rigidities for the consideration of an elastic system, nonhomogeneous over the area, is evidently convenient for calculations (in case the averaged rigidities being determined correctly). The formulae to calculate the averaged elastic parameters of orthotropy for the above noted orthotropic systems, depending on the geometrical characteristics of the cross-section and the mechanical parameters of the plate material, are given, for instance, in [130].

In spite of the lack of principal difficulties for the calculation of anisotropic plates and the importance of the account of the foundation plate rigidity variation under bending in different directions, the programs, intended to be used for wide application in this field [105, 125], still do not take into account this orthotropy factor which is important for the foundation plate design.

Theoretical studies of calculation of orthotropic foundation plates are rather rare [129, 138, 247] and do not use, with a very rare exception [69], the soil base calculation models of spatial continuum type.

Klepikov and Malikova [138] formulated a problem of an orthotropic plate bending on an elastic Winkler base with a coefficient of subgrade reaction, variable in the plane of the contact between the plate and the base. The base displacements (subsidence) are taken into account, which essentially influence the stress-strained state of the whole structure, erected on underworked territories and collapsing soils. Unfortunately, the publication does not contain the calculation results.

The major part of a book by Kiselev [134] is devoted to the calculation of orthotropic rectangular plates, resting on an elastic base with two coefficients of subgrade reaction. It is considered that the plates can be supported differently at all four sides (hinge or fixation). The solutions are found, depending on the type of the boundary conditions in dual Fourier series or by an originally elaborated initial parameter method. In order to obtain the solution, a preliminary expansion of the external load in a Fourier series is required.

Smirnov [247] suggested to use an original numerical method employing differentiation matrices [246] to perform calculations for orthotropic rectangular plates, resting on an elastic base with a coefficient of subgrade reaction, variable over the area. The problems are solved for the case of the plate loading by a uniform load in case of a hinge-type support on a contour.

Kocatürk [141] performed calculations for a rectangular orthotropic plate with free edges, located on an elastic unilateral Winkler base and subject to a uniformly distributed load, a concentrated force and a moment at arbitrary points. The solution is obtained using the generalized Galerkin method, resulting in infinite systems of linear algebraic equations. The calculations have shown an essential influence of the orthotropic properties of the plate on the characteristics of the processes of its mutual contact deformation with the base.

The finite-element algorithm of calculation for a rectangular orthotropic piecewise homogeneous plate, resting on a Winkler base and undergoing an arbitrarily distributed normal load, is worked out in [129]. Software, developed on the basis of this algorithm, enables one to determine deflections, bending moments and stresses in the plates of road covering or floors of engineering structures, accepting the applied load and the base reaction.

The subsequent Sects. 4.7.2–4.7.4 are devoted to the account of the soil base compressible thickness variation and influence of conditions of different type on the stress-strained state of the orthotropic rectangular foundation plate structures. Such formulation of the contact problem is performed for further approaching of the calculation data to the real conditions of foundation plate interaction with nonhomogeneous and structurally unstable soils, when the account of the real nonuniform compressibility of the base under the large-size foundation plates bottom is required. The calculation method employed is applicable for any known contact models for elastic bases. As examples, numerical results for spatially nonhomogeneous bases of constant- and variable-thickness elastic layers are considered [75, 211]. No restrictions are assumed to be imposed on the characteristics of the plate flexibility, related to the relation of the deformation properties of the plate material and the base. An external transverse load on the plate can be given according to an arbitrary law.

4.7.2 System of Integro-Differential Equations of Bending of a Plate, Resting on an Elastic Base

Assuming the plate deflections small in comparison with its thickness, we consider the Kirchhof–Love hypotheses to be true. Then the differential equation for the curved surface of an orthotropic plate under a transverse load, resting on an elastic base (Fig. 4.63), is given by [152]:

$$D_1 \frac{\partial^4 W}{\partial x^4} + 2D_3 \frac{\partial^4 W}{\partial x^2 \partial y^2} + D_2 \frac{\partial^4 W}{\partial y^4} = q(x,y) - p(x,y) \tag{4.19}$$

where $W(x, y)$ is a vertical displacement of the median plane of the plate, $q(x,y)$ is the external load intensity, $p(x,y)$ is the contact pressure, D_1 and D_2 are cylindrical bending rigidities for the basic directions of elasticity, $D_i = E_i h^3/12(1 - \nu_1\nu_2)$, $i = 1, 2$, $D_3 = D_1\nu_2 + 2D_k = D_2\nu_1 + 2D_k$, $D_k = Gh^3/12$ is the torsion rigidity,

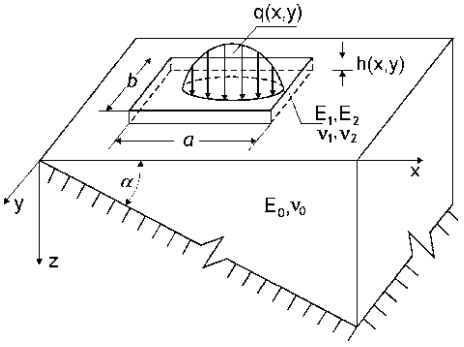

Fig. 4.63 Calculation scheme for an orthotropic plate, resting on an elastic base

E_1, E_2, ν_1, ν_2 are the elastic moduli and the Poisson ratios of the plate material, respectively, G is the shear modulus, h is the plate thickness.

For an orthotropic plate [152] the following relation holds:

$$E_1\nu_2 = E_2\nu_1.$$

In the isotropic plate case

$$E_1 = E_2 = E, \quad \nu_1 = \nu_2 = \nu, \quad G = E/2(1+\nu),$$

and all the rigidities are reduced to a single one

$$D_1 = D_2 = D_3 = D = Eh^3/12(1-\nu^2).$$

Similarly to the traditional approaches [105, 125, 252], friction at the contact domain is not taken into account; it is also assumed that the plate is completely adherent to the base, i.e. the vertical displacements of the plate and the base surface are equal. For the spatial contact problem the equality of the vertical displacements of the plate and the elastic base surface results [252] in an integral equation to determine the contact pressure

$$W(x,y) = \overline{W}(x,y) + A + B\cdot x + C\cdot y = \frac{1-\nu_0^2}{\pi E_0}\int\limits_S\int \omega(x,y,\xi,\eta)p(\xi,\eta)d\xi d\eta \quad (4.20)$$

where A, B, C are the parameters of the plate displacement as a rigid solid, E_0 and ν_0 are the elastic modulus and the Poisson ratio for the base, S is the domain of the plate contact with the base. The function $\omega(x, y, \xi, \eta)$ is given in accordance with the elastic base model being used.

The boundary conditions at the plate contour age given by

$$W|_{\Gamma_1} = 0, \left.\frac{\partial W}{\partial n}\right|_{\Gamma_1} = 0 \text{ (pinching)}, \quad (4.21)$$

$$W|_{\Gamma_2} = 0, M_n|_{\Gamma_2} = 0 \text{ (hinge)}, \quad (4.22)$$

$$M_n|_{\Gamma_3} = 0, \left.\left(Q_n + \frac{\partial M_{tn}}{\partial s}\right)\right|_{\Gamma_3} = 0 \text{ (free edge)} \quad (4.23)$$

where M_n and M_{tn} are the bending moments and torques, respectively, Q_n is the shearing force, $\partial/\partial n$ is a derivative over the normal, $\partial/\partial s$ is the derivative over the plate contour arc.

Note that the second equation in Eqs. (4.23) combines two necessary conditions $Q_n = 0$, $M_{tn} = 0$ on a free smooth contour of the plate when the distributed torque pairs are statically equivalent to the shearing force. If the free contour contains angular points, such kind of substitution results in concentrated forces, appearing in the

angular points [134, 157, 224, 261]. For example, in a detailed notation the formulation of the boundary conditions (4.23) for the most popular case of foundation plates of rectangular shape (a and b being the plate sides) with the account of the absence of concentrated forces in the angles, proportional to the torques

$$M_{xy} = M_{yx} = -2D_k \frac{\partial^2 W}{\partial x \partial y},$$

takes the following form with respect to the deflections: at $x = 0$, $x = a$

$$\frac{\partial^2 W}{\partial x^2} + \nu_2 \frac{\partial^2 W}{\partial y^2} = 0, \quad \frac{\partial^3 W}{\partial x^3} + \varepsilon_2 \frac{\partial^3 W}{\partial x \partial y^2} = 0; \tag{4.24}$$

at $y = 0$, $y = b$

$$\frac{\partial^2 W}{\partial y^2} + \nu_1 \frac{\partial^2 W}{\partial x^2} = 0, \quad \frac{\partial^3 W}{\partial y^3} + \varepsilon_1 \frac{\partial^3 W}{\partial x^2 \partial y} = 0; \tag{4.25}$$

at $x = 0$, $y = 0$; $x = 0$, $y = b$; $x = a$, $y = 0$; $x = a$, $y = b$

$$\frac{\partial^2 W}{\partial x \partial y} = 0. \tag{4.26}$$

Here the notations $\varepsilon_1 = (D_3 + 2D_k)/D_2$, $\varepsilon_2 = (D_3 + 2D_k)/D_1$ are introduced.

The problem is closed by a system of equilibrium equations for the plate, loaded by an external distributed load $q(x, y)$:

$$\begin{aligned}
\int\int_S p(\xi,\eta)\mathrm{d}\xi\,\mathrm{d}\eta &= \int\int_F q(\xi,\eta)\mathrm{d}\xi\,\mathrm{d}\eta, \\
\int\int_S p(\xi,\eta)\xi\,\mathrm{d}\xi\,\mathrm{d}\eta &= \int\int_F q(\xi,\eta)\xi\,\mathrm{d}\xi\,\mathrm{d}\eta, \\
\int\int_S p(\xi,\eta)\eta\mathrm{d}\xi\,\mathrm{d}\eta &= \int\int_F q(\xi,\eta)\eta\mathrm{d}\xi\,\mathrm{d}\eta
\end{aligned} \tag{4.27}$$

where S is the domain of the plate contact with the base, F is the domain of action of the external distributed load.

Thus, the mathematical formulation of the problem under consideration is reduced to the combined solution of a differential equation (4.19) and integral equations (4.20), (4.27) with the boundary conditions (4.21–4.23) on the plate contour.

The values of moments and transverse forces after the contact problem solution are determined by differentiating the deflection function and can be found from [152]

$$M_x = -D_1\left(\frac{\partial^2 W}{\partial x^2} + \nu_2\frac{\partial^2 W}{\partial y^2}\right), M_y = -D_2\left(\frac{\partial^2 W}{\partial y^2} + \nu_1\frac{\partial^2 W}{\partial x^2}\right), M_{xy} = -2D_k\frac{\partial^2 W}{\partial x \partial y},$$

$$Q_x = -D_1\left(\frac{\partial^3 W}{\partial x^3} + \frac{D_3}{D_1}\frac{\partial^3 W}{\partial x \partial y^2}\right), Q_y = -D_2\left(\frac{\partial^3 W}{\partial y^3} + \frac{D_3}{D_2}\frac{\partial^3 W}{\partial x^2 \partial y}\right). \quad (4.28)$$

4.7.3 *Calculation of Rectangular Orthotropic Plates Based on Combining Finite-Difference and Boundary-Element Methods*

Solving the spatial contact problem, formulated in Sect. 4.7.2 for any elastic base model requires considerable difficulties; for rectangular plates no exact solutions are known.

Our numerical calculations will be based on a combination of the grid method and the boundary-element method. A finite-difference grid of regular structure with the cell size of Δx and Δyin the direction of the coordinate axes, is imposed on the plate (Fig. 4.64). The finite-difference equation system will be given by

$$[H]\{W\} = \{q\} - \{p\}.$$

Here $[H]$ is the differential operator matrix with respect to the deflection vector $\{W\}$; $\{q\}$ and $\{p\}$ are the vectors of the external normal load and the reactive pressure, considered in the finite-difference grid nodes. The details of the finite-difference representation of the differential equation (4.19) and the boundary

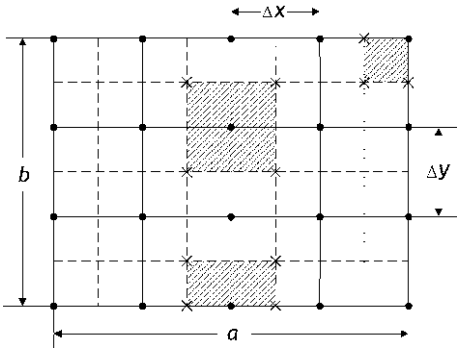

Fig. 4.64 Contact domain discretization

conditions (4.23) for orthotropic rectangular plates with free edges are given in Appendix E.

In order to obtain a matrix analogue of the integral equation (4.20), along with the regular finite-difference grid, consider an auxiliary grid (denoted by a dotted line in Fig. 4.64) whose cells are formed by straight lines, passing through the median points of the main grid cell sides. In assumption of the contact pressures being constant within each cell of the auxiliary grid, the integral equation (4.20) can be presented in the following discrete form of canonical equations:

$$\{W\} = [B]\{p\}$$

where $[B] = \|\delta_{ij}\|$ is the influence matrix, the elements of which are calculated as

$$\delta_{ij} = \int\int_{F_j} \omega(x_i, y_i, \xi, \eta) d\xi d\eta$$

and represent vertical displacements of the elastic half-space surface in the point (x_i, y_i), coinciding with the i-th element gravity centre, due to a unit load, equally distributed over the area F_j of the j-th element. The elements of the matrix $[B]$ are calculated by a procedure, described in detail in [15]. Solving the matrix equation (4.30) with respect to the contact pressures $\{p\}$, one obtains

$$\{p\} = [V]\{W\}$$

where $[V]=[B]^{-1}$ is the elastic base rigidity matrix. By substituting $\{p\}$ from Eq. (4.31) to Eq. (4.29), one obtains the solution of the problem under consideration

$$\{W\} = [\Sigma]^{-1}\{q\}, \; [\Sigma] = [H] + [B]^{-1}.$$

The contact pressures $\{p\}$ for the obtained solution $\{W\}$ are obtained using Eq. (4.31), and the distribution of the force factors in the plate is found based on a finite-difference approximation of the dependences (4.28).

After discretization the linear equation system for the deflection function in the node points of the plate is given by

$$[\Sigma]\{W\} = \{q\}$$

where $\{W\}$ is a vector of unknown deflections in the plate nodes, $\{q\}$ is a vector of generalized load parameters, $[\Sigma]$ is a matrix of the "plate + elastic base" contact system, being formed of the coefficients of the canonical equations of the force method for Eqs. (4.20), (4.27) and the coefficients of difference equations for Eq. (4.19). Thus, the elements of the matrix [S] depend on the stressed states of the base and

the plate. The system (4.32) is solved by the Gauss method with elimination of the main element in a row.

When the Gauss method is implemented for computations, arithmetic operations are performed by the processing unit with a fixed accuracy with, as a rule, 7 digits at single-precision and 16 digits with double-precision calculations. In the first case it results in rounding errors due to the truncation or rounding of the data and due to the accumulation of errors in the course of solving the problem. With the increase of the amount of unknowns, single-precision calculations may be not sufficient for the Gauss method. Then one should use the double-precision solution of the problem or apply a subsequent correction based on an iterative process.

At the single-precision calculations, due to the finite data length and an approximate calculation of derivatives, practically the computer is used to solve a system

$$(\Sigma + \Delta\Sigma)(W + \Delta W) = (q + \Delta q).$$

The error of its solution is given by

$$\frac{\|\Delta\Sigma\|}{\|\Sigma\|} \leq \sigma(\Sigma) \frac{\|\Delta q\|}{\|q\|}$$

where $\sigma(\Sigma) = \|\Sigma\| \cdot \left\|\Sigma^{-1}\right\|$ is the conditionality number [93]. If $\sigma(\Sigma)$ is great then the algebraic equation system is badly conditioned, and one should apply special methods of regularization in order to solve it.

In practical computations for the matrix of the linear equation system (4.32) we calculated its conditionality number s which shows how far are the results from the case of degeneracy. The estimations of conditionality, performed on the basis of numerous calculations, has shown that, though the matrix of the system (4.32) is nor sufficiently conditioned, still solving the equation system (due to the diagonal predominance of the influence matrix **B**) by the Gauss elimination method leads to quite quite acceptable results as the first approximation. In order to improve the solution obtained, it was further processed by iterative method. An extensive series of the calculations performed has shown that after 3–5 iterations the solution, as a rule, converges within the machine accuracy $\varepsilon = 10^{-5}$.

The numerical algorithm described above is implemented in a software module ORTOPLIT, written using the FORTRAN language, and includes formation of the system matrix and iterative refinement of the calculation results.

In the next subsection, using the calculation data obtained, the effect of spatial nonhomogeneity of the compressible soil mass, external transverse load distribution, different combinations of the plate fixation at its contour, and the degree of orthotropy of its material on the stress-strained states of the plate and the base is analyzed. An elastic linearly deformable half-space, a constant-thickness layer, and an elastic compressible wedge are considered as the soil base models.

4.7.4 Examples of Numerical Modelling of the Contact Interaction of Plates with Elastic Bases

Comparative calculations for an isotropic plate on an elastic half-space. In order to estimate the convergence of the numerical solutions and to illustrate the ability of the method proposed, consider a known example of calculation of a plate with free edges, resting on an elastic half-space [105, 183].

The input data for the calculation are the following: a reinforced concrete plate with the elastic module $E = 2.65 \cdot \times 10^4$ MPa, Poisson ratio $\nu = 0.1667$ and size 2 $\times$ 2 $\times$ 0.2 m, is located on a soil base which is treated as an elastic half-space with the characteristics $E_0 = 49$ MPa, $\nu = 0.4$.

$$\text{The plate flexibility index } r = \frac{3}{2} \cdot \pi E_0 a^3 \left(1 - \nu^2\right) / E h^3 \left(1 - \nu_0^2\right) \approx 10.$$

The plate is subject to a uniformly distributed load of the intensity $q = 1$ MPa.

The results of calculation of deflections, contact pressures, and bending moments in the plate centre along with the information on the conditionality number of the matrix of coefficients of the linear algebraic equation system (4.32) at various density of the finite-difference grid are shown in Table 4.12. For the sake of comparison, the table also contains the results, obtained by the finite-element method [183] and based on the Gorbunov-Posadov solution [105].

As follows from Table 4.12, with the increase of the discretization degree the accuracy of the obtained results increases; for the grids with the density of not less than 8 $\times$ 8 it is sufficient for carrying out engineering calculations. One can also easily estimate the limiting values from the data of Table 4.12. For the case of a linear dependence of the solution on n^{-1} where $n \times n$ is the grid size, at $n = 8$ and $n = 10$ one obtains

Table 4.12 Characteristics of convergence of numerical solutions for a square plate on an elastic half-space

$n \times n$	$\sigma(\Sigma)$	W_c, m	p_c/q	$4M_x/a^2 q$
Finite-difference method				
4 $\times$ 4	0.6487×10^3	0.02401	0.5204	0.07655
6 $\times$ 6	0.2206×10^4	0.02625	0.5286	0.08559
8 $\times$ 8	0.5826×10^4	0.02744	0.5448	0.08865
10 $\times$ 10	0.7442×10^4	0.02817	0.5539	0.08975
12 $\times$ 12	0.1435×10^5	0.02867	0.5598	0.09010
14 $\times$ 14	0.2449×10^5	0.02904	0.5647	0.09026
16 $\times$ 16	0.3847×10^5	0.02928	0.5671	0.09008
18 $\times$ 18	0.6694×10^5	0.02951	0.5697	0.08998
20 $\times$ 20	0.9135×10^5	0.02968	0.5719	0.09017
22 $\times$ 22	0.1217×10^6	0.03003	0.5780	0.09092
FEM [183], 10 $\times$ 10		0.03063	0.5747	0.1038
Gorbunov-Posadov [105]		0.0327	0.630	0.061

$$W_C = 0.03109 \text{ m}, \overline{p} = p_c/q = 0.5903, \overline{M}_x = 4M_x/a^2q = 0.09415.$$

The corresponding limiting values, obtained using the finite-element method [183], are the following:

$$W_C = 0.03115, \text{ m}, \overline{p} = 0.5815, \overline{M}_x = 0.0899.$$

The difference of the limiting calculated values, obtained by the two numerical methods, is seen not to exceed 1.5–4.5%. The result obtained enables a sort of the optimal density of the finite-difference grid to be chosen as 10×10, at which the accuracy of the deflection calculations is achieved, exceeding 92%.

Note that, contrary to the finite-difference method, application of the finite-element method to solving the equations of theory of thin plates is encumbered by a high degree of derivatives, contained in the initial equations and, consequently, in the expression for the potential energy functional. This results in the application of complex elements with a great number of degrees of freedom and is equivalent to the increase of the number of unknowns. The comparison of the finite-element and finite-difference methods that we have performed shows that both methods give practically the same accuracy of the solution. However, the finite-difference method applied here is expressed by a more compact linear equation system and requires essentially less computation time and computer RAM size. We should also, as noted in [183], point out an insufficient accuracy of the Gorbunov–Posadov solution, what is related to the use of partial sums of power series with insufficient number of terms for the sought functions.

Orthotropic plate with free edges on a variable-thickness elastic layer. Application of the proposed algorithm to estimate the effect of the thickness and nonhomogeneity of the compressible base on the plate bending will be illustrated by the results of calculations for a square plate of reinforced concrete ($E = 2\times10^4$ MPa, $\nu = 0.167$) with a side $a = 16$ m and thickness $h = 1$ m. For the account of the orthotropic properties of the plate we imply $E_1 = 2E$, $\nu_1 = 2\nu$, $E_2 = E$, $\nu_2 = \nu$, $G = 0.429{\cdot}E$. The following base characteristics are chosen: E_0 =29.1 MPa, ν_0= 0.25. The plate flexibility index in this case is estimated by a value

$$r = \frac{3}{2} \cdot \pi E_0 a^3 \left(1 - \nu^2\right) / Eh^3 \left(1 - \nu_0^2\right) \approx 29.$$

First consider the case of the plate being subject to a uniformly distributed load $q = 10^5$ N/m. The results of the calculated deflections of a plate with a non-fixed contour on an elastic half-space and on a variable-thickness layer are shown in Fig. 4.65. Figure 4.65a shows isolines of equal deflections for an isotropic plate on an elastic half-space, which are symmetrical with respect to the plate centre and practically do not differ from circles. With the increase of the distance from the centre, in the angles, the equal deflection lines become almost straight, parallel to the diagonals of the square. Figure 4.65b shows the deflection isolines for the same plate, but resting on an elastic compressible wedge ($\alpha = 30°$, the plate centre is located

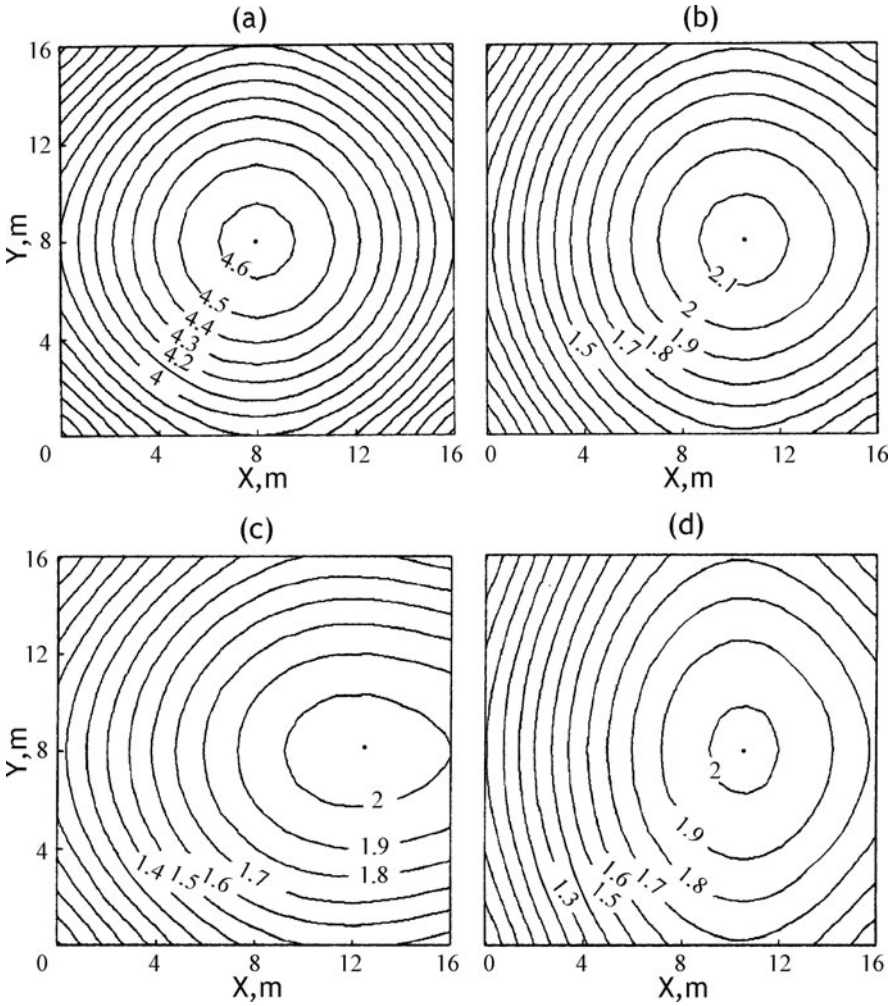

Fig. 4.65 Equal deflection W (cm) lines for a plate with free edges under a uniformly distributed load: (**a**): half-space, (**b**), (**c**), (**d**): elastic compressible wedge, $\alpha = 30°$ (**a**), (**b**): isotropic plate, (**c**), (**d**): orthotropic plate ($E_x = 2E$, $E_y = 2E$, respecively)

at a distance $x = 16$ m from the wedge rib). As one can see, the equal deflection line pattern is of an asymmetrical character with the contours being shifted with respect to the plate centre towards the increase of the non-uniformly compressed layer thickness. At the chosen values of the calculation parameters, the deflection values in the case of the elastic wedge appeared almost twice smaller than for the half-space. This is explained by the fact that soil under the plate on the half-space is deformed over an infinite depth. The calculation data for the deflections, obtained for an orthotropic plate on an elastic wedge, when $E_x = E_1$, are shown in Fig. 4.65c,

and Fig. 4.65d corresponds to a situation when the same plate is rotated with respect to its centre by a right angle (i.e. $E_y = E_1$). It is seen from the presented data that variable thickness of the elastic layer and variation of orientation of the orthotropy axes result in an essential asymmetry in the distribution of deflections. The maximal deflection area always shifts towards the base thickness increase and acquires the shape of an ellipse with the higher axis along the direction with the smallest deformation properties. As follows from the calculations, with the increase of the orthotropy degree and the elastic compressible layer thickness interval, at cylindrical bending this nonuniformity in the plate deformation character increases.

Thus, the calculations show that in order to reduce the deflection nonuniformity and, hence, to reduce the bending moments in the calculated sections of a plate, one should take into account the orientation of the orthotropy axes with respect to the rib of the elastic compressible wedge. As a recommendation for design, one should also keep in mind the requirement of the plate thickness to be increased or the load to be reduced in the direction of the increase of the compressed base thickness. The proposed calculation method enables one to obtain reasonable values of the corresponding parameters of the contact interaction in the "foundation plate + base" system.

Orthotropic plate with partly free, hinged, and pinched edges on elastic layers of variable and constant thickness. Consider the influence of the type of fixing at the plate contour in two cases: (i) a plate with two adjacent pinched sides (Fig. 4.66) and (ii) a plate with one hinge-born and one pinched side (Figs. 4.67 and 4.68). In both cases two sides are free.

Deflection isolines for a plate with the first type of the boundary conditions, loaded by a uniformly distributed load, are shown in Fig. 4.66. The equal deflection lines are plotted for an isotropic plate on a half-space (Fig. 4.66a) as well as on a variable-thickness layer at the rigid underlayer base tilt angle $\alpha = 45°$ (Fig. 4.66b). In order to take into account the orientation of the elasticity directions, similarly to Fig. 4.65, deflection isolines for an orthotropic plate are shown (Fig. 4.66c, d). It is seen from the calculations performed that the influence of the rigid underlayer tilt angle on the plate bending characteristics is also quite essential, similarly to the case of the plate with a totally free contour. This is the consequence of the nonuniform compressibility of the base within the foundation structure under consideration. Simultaneously, the comparison of the calculation data has shown that with the increase of the angle α the difference between the solutions for the half-space and the non-uniformly compressible base becomes smaller. The numerical results, obtained from the calculation of the plate, interacting with a variable-thickness elastic layer (Figs. 4.66 and 4.67), and their analysis show that substitution of pinching by hinge on a part of the plate contour makes a slight effect on the stress-strained state of the plate independently of the spatial nonhomogeneity of the compressed soil mass and the elastic base depth.

Consider the calculation results for a plate with the second type of the mixed boundary conditions. Deflection isolines for the plate with the account of the base thickness variation range, loading type, as well as the change of the orthotropy axes direction, are plotted in Figs. 4.67 and 4.68. Figure 4.67 shows the isolines for a

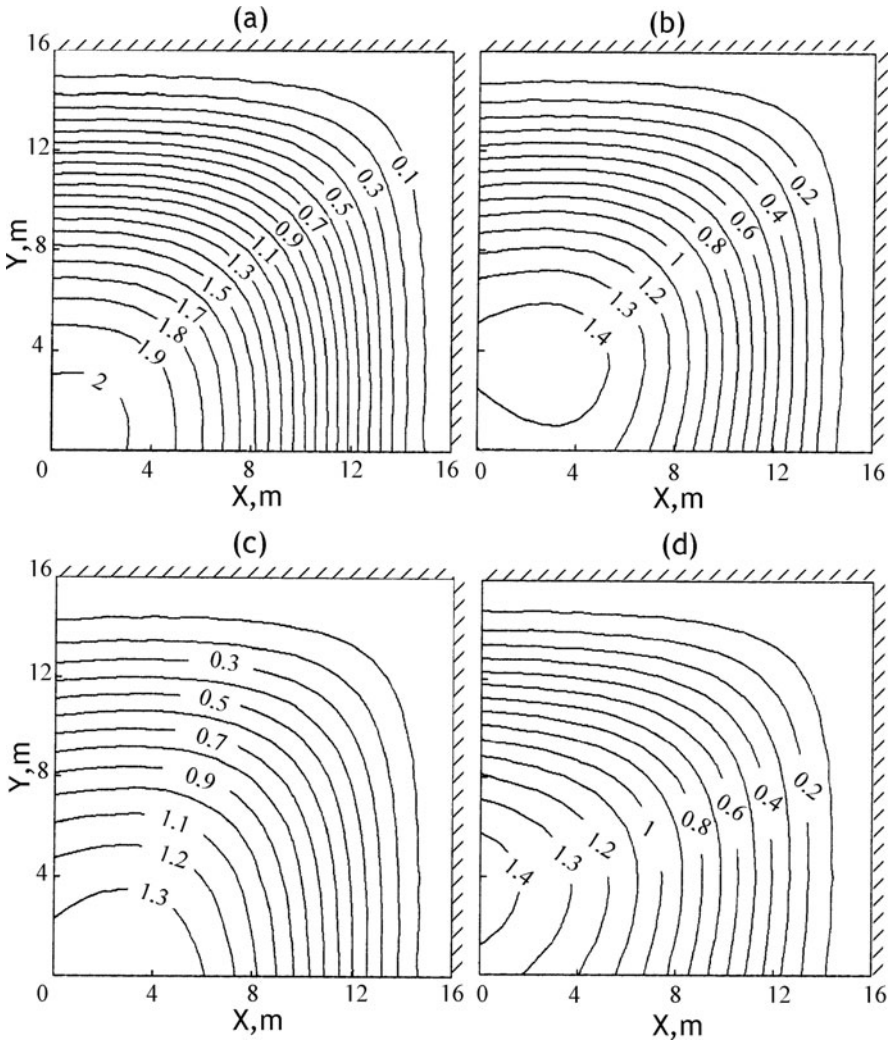

Fig. 4.66 Equal deflection W (cm) lines for a plate with the fixation conditions of type I under a uniformly distributed load: (**a**): half-space, (**b**),(**c**),(**d**): elastic compressible wedge, $\alpha = 45°$; (**a**), (**b**): isotropic plate, (**c**), (**d**): orthotropic plate ($E_x = 2E$, $E_y = 2E$, respecively)

plate under a uniformly distributed load, and Fig. 4.68 – for a plate, loaded in the centre by a force whose value is $Q = 0.256 \times 10^4$ N – the total force from the uniformly distributed load q. The force Q was distributed over the area 1.6×1.6 m^2, corresponding to one cell of the finite-difference grid. The calculated dependences, plotted in Figs. 4.67a and 4.68a, correspond to the isotropic plate interaction with a half-space, while Figs. 4.67b and 4.68b illustrate the effect of the non-uniform base compressibility (elastic wedge, $\alpha = 45°$) on the isotropic plate deflections

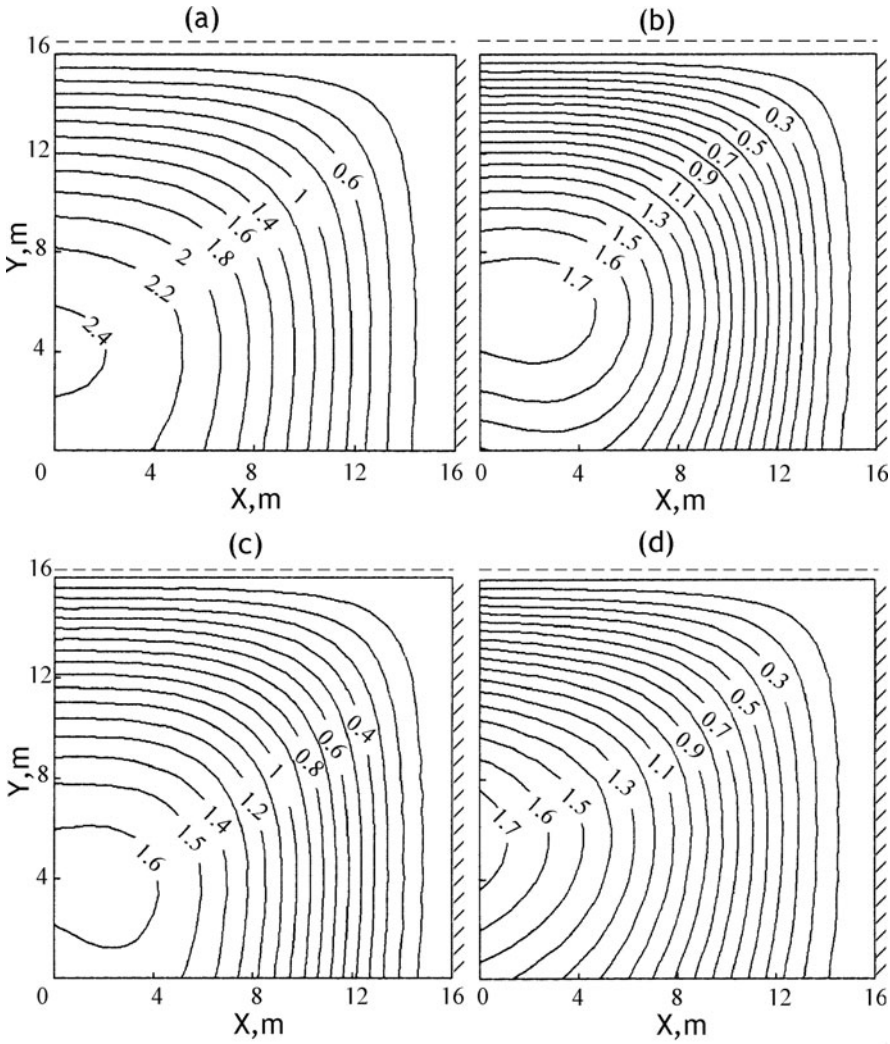

Fig. 4.67 Equal deflection W (cm) lines for a plate with the fixation conditions of type II under a uniformly distributed load: (**a**), (**b**), (**c**), (**d**): same as Fig. 4.66

under a uniformly distributed and a concentrated load, respectively. The effect of the orthotropic properties of the plate material on its bending is clearly seen from Figs. 4.67c and 4.68c ($E_x = 2E$), as well as from Figs. 4.67d and 4.68d ($E_y = 2E$). As one can see, the effect of the type of the plate loading (action of the concentrated and the uniformly distributed load) on its bending consists in a considerable difference in the distribution of deflections, bending moments, and reactive pressure intensity. As it should be expected, the stress-strained state of a plate of reinforced

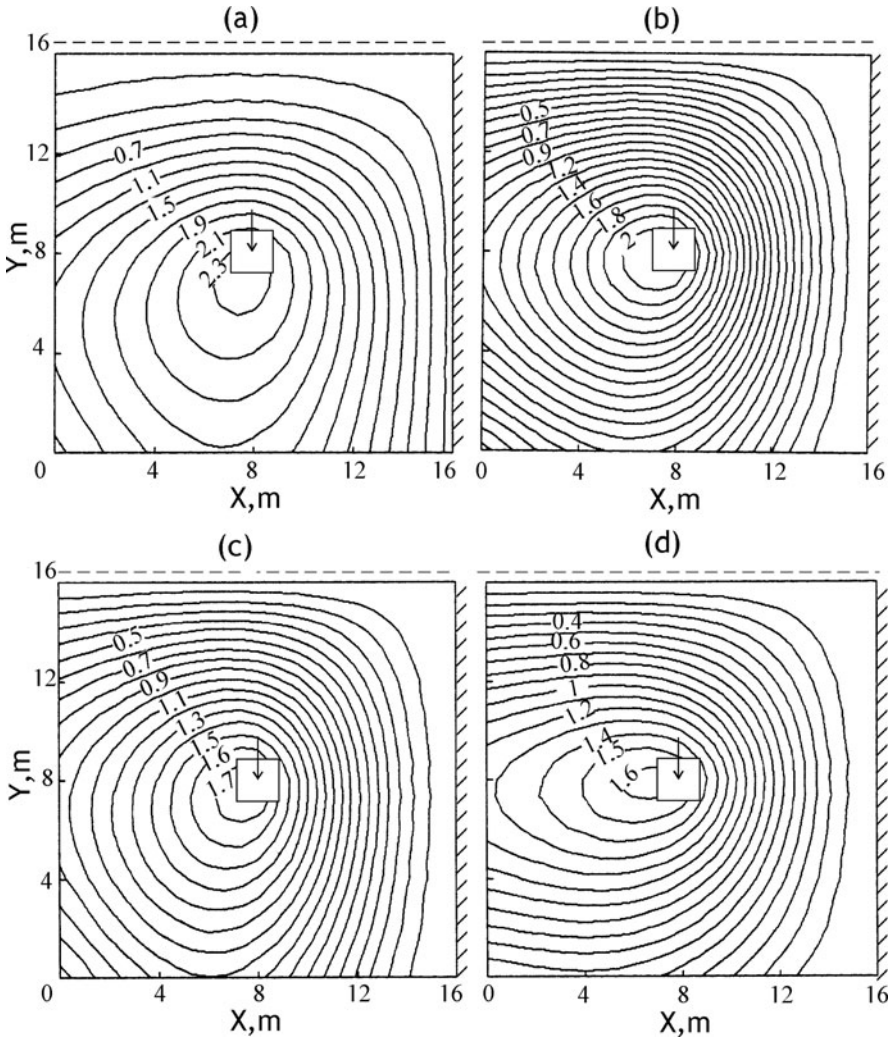

Fig. 4.68 Equal deflection W (cm) lines for a centrally loaded plate with the fixation conditions of type II. (**a**), (**b**), (**c**), (**d**): same as Fig. 4.66

concrete, loaded uniformly over its area, depends on the spatial nonhomogeneity of the base more essentially than under a concentrated force.

The numerical results, obtained for the variable-thickness layer, were compared with the results of calculations for a constant-thickness elastic layer. The depth H_c of the constant-thickness layer under the plate centre was determined from the condition $H_c = x_c \cdot \tan\alpha$. In Tables 4.13 and 4.14 two values for the maximal deflection are presented: the upper one corresponds to the variable-thickness layer with different angles α, and the lower one – to the constant-thickness layer. As follows from the

Table 4.13 Contact interaction characteristics for an orthotropic plate (boundary conditions of the first type)

Elastic base type	$W_{\max,}$cm	$4M_x/a^2q$	p_c/q	$W_{\max,}$cm	$4M_x/a^2q$	p_c/q
	$E_1 = 2 \times E$, $E_2 = E$			$E_1 = 2 \times E$, $E_2 = E$		
Variable-thickness layer:						
$\alpha=15°$, $H_c=0.27a$	0.658	0.791	0.438	0.720	0.504	0.456
	0.949	0.704	0.445	0.949	0.446	0.445
$\alpha=30°$, $H_c=0.58a$	1.087	0.851	0.315	1.182	0.576	0.320
	1.468	0.785	0.304	1.468	0.547	0.304
$\alpha=45°$, $H_c=a$	1.400	0.852	0.270	1.457	0.590	0.272
	1.716	0.807	0.252	1.716	0.572	0.252
$\alpha=60°$, $H_c=1.73a$	1.587	0.844	0.248	1.627	0.593	0.249
	1.853	0.813	0.231	1.853	0.581	0.231
Half-space	1.984	0.816	0.212	1.984	0.587	0.212

Table 4.14 Contact interaction characteristics for an orthotropic plate (boundary conditions of the second type)

Elastic base type	$W_{\max,}$cm	$4M_x/a^2q$	p_c/q	$W_{\max,}$cm	$4M_x/a^2q$	p_c/q
	$E_1 = 2 \times E$, $E_2 = E$			$E_1 = 2 \times E$, $E_2 = E$		
Variable-thickness layer:						
$\alpha=15°$, $H_c=0.27a$	0.812	0.952	0.587	0.883	0.505	0.545
	1.036	0.885	0.595	1.075	0.470	0.535
$\alpha=30°$, $H_c=0.58a$	1.311	1.156	0.441	1.437	0.622	0.395
	1.633	1.113	0.424	1.703	0.598	0.379
$\alpha=45°$, $H_c=a$	1.640	1.219	0.339	1.754	0.656	0.340
	1.990	1.197	0.375	2.022	0.642	0.320
$\alpha=60°$, $H_c=1.73a$	1.866	1.234	0.366	1.953	0.667	0.316
	2.200	1.232	0.350	2.190	0.659	0.296
Half-space	2.442	1.261	0.330	2.356	0.672	0.275

data quoted in Tables 4.13 and 4.14, the contact interaction characteristics (maximal settlements W_{max}, bending moments M_x and reactive pressures p_c in the plate centre) essentially depend on the base model being used. The analysis of the obtained results shows that variation of the base compressed soil mass thickness under the foundation structure affects first of all the character of distribution and the values of deflections. The deflection maximum W_{max} always shifts towards the increase of compressed base thickness. Variable compressibility of the base increases the nonuniformity of the stress-strained state of the plate. This trend should be taken into account at the design of foundation structures, since in the case of a momental stressed state an intense development of inelastic deformations in concrete is possible, leading to the formation of cracks [132].

The account of orthotropic properties of the plate material at a given type of it being fixed at its contour is also important for the estimation of the contact

interaction characteristics. In comparison with a freely resting plate, fixing of its sides has led to a decrease of the deflections and an increase of the bending moments. For the othotropic plate ($E_x = 2E$) at the boundary conditions of the first type (Table 4.13) the bending moments M_x in the plate centre are by factor of about 1.4 higher than the corresponding values for the plate, rotated with respect to its centre by a right angle. Note that for the boundary conditions of the second type (Table 4.14), at the same orthotropy parameters for the plate material, the bending moment values M_x increase almost twice. As follows from numerous calculations of bending of plates made of reinforced concrete, their orthotropic properties can essentially affect both the stress-strained state of the plate and the characteristics of the base reactive pressure.

Thus, the proposed numerical approach, based on a combination of the finite-difference and the boundary-element methods, enables effective solving of contact problems for rectangular plates, resting on non-classical elastic bases. The finite-difference method being used in the numerical algorithm is quite suitable to satisfy the boundary conditions which can be found in practice, and to perform the calculations on a computer far from the high-end level. The calculation examples presented confirm the applicability of the elaborated algorithm for the analysis of bending of rectangular plates on elastic spatially nonhomogeneous bases and illustrate its abilities regarding the design of foundation plates for complicated geotechnical conditions. The developed software module ORTOPLIT can be without any difficulties applied for the studies of complicated cases of loading and different combinations of boundary conditions at the plate contour. Besides, the application of a contact model of the elastic base is performed as a separate module and does not require the whole algorithm resetting.

References

1. Abramov V M (1937) Problems of contact of an elastic half-plane with an absolutely rigid foundation with the account of friction forces. Dokl AN SSSR 17 (issue 4):173–178 (in Russian)
2. Abramov V M (1939) Study of a case of asymmetric pressure of a punch of round cross-section on an elastic half-space. Dokl AN SSSR 23 (issue 8):759–763 (in Russian)
3. Abramowitz M, Stegun I A (1972) Handbook of mathematical functions with formulas, graphs, and mathematical tables, 10th edn. Dover, New York
4. Aizikovich S M, Trubchik I S, Shklyarova Ye V (1992) Calculation of a circular plate resting on a vertically inhomogeneous half-space. Mech Solids 27 (issue 4):163–171
5. Aleksandrov A V, Lashchenikov B Ya, Shaposhnikov N N et al. (1976) Computer-aided methods of calculation of rod systems, plates and shells. Stroyizdat, Moscow (in Russian)
6. Aleksandrov A Ya (1955) Some solutions of axially symmetrical contact problems of theory of elasticity. In: NIIZHT Works. Transzheldorizdat, Moscow, issue 11, pp. 29–61 (in Russian)
7. Aleksandrov A Ya (1955) Stresses and displacements in an elastic space and half-space under a load, uniformly distributed over a ring. In: NIIZHT Works. Transzheldorizdat, Moscow, issue 11, pp. 62–88 (in Russian)
8. Aleksandrov A Ya, Solovyov Yu I (1978) Spatial problems of theory of elasticity (application of methods of theory of complex-variable functions). Nauka, Moscow (in Russian)

9. Aleksandrov V M (1967) Axially symmetrical contact problem of the action of a ring-shaped punch on an elastic half-space. Inzh Zh Mekh Tverd Tela (issue 4):108–116 (in Russian)
10. Aleksandrov V M, Babeshko V A (1972) On the pressure on an elastic half-space by a wedge-shaped stamp. J Appl Math Mech 36:78–83
11. Aleksandrova G P (1973) Contact problems of bending of plates resting on an elastic base. Izv AN SSSR Mekh Tverd Tela (issue 1):97–106 (in Russian)
12. Aleksandrovich V F, Fedorovskii V G (1979) Round punch on an elastoplastic strengthening soil base. In: Experimental and theoretical studies of nonlinear problems in the field of bases and foundations. NPI, Novocherkassk, pp. 35–43 (in Russian)
13. Aleynikov S M (1991) Spatial contact problems for polygonal punches on elastic tapered basement. VISI, Voronezh, VINITI No. 1393-B91Dep (in Russian)
14. Aleynikov S M (1998) Method for the determination of modulus of deformation. Patent 2145655, MPK6 E02D 1/00; G01N 3/42. No. 98117270/28 (Russia)
15. Aleynikov S M, Ikonin S V (1990) Three-dimensional deformation of the surface of a tapered elastic layer. Soil Mech Found Eng 27:218–222
16. Aleynikov S M, Ikonin S V (1993) Numerical calculation of contact stresses in the base of a rectangular punch at off-centre loading. In: Issues of strength and plasticity. Dnipropetrovsk State University, Dnipropetrovsk, pp. 95–101 (in Russian)
17. Aleynikov S M, Kozlovtsev A M (1992) Numerical solution of spatial contact problems for rectangular punches on a variable-thickness elastic layer with the account of nuilateral constraints. Stroit Mekh Raschet Sooruzh (issue 3):18–23 (in Russian)
18. Aleynikov S M, Neiburg E V (1995) Contact pressure distribution in the area of strip foundation width variation. Izv Vuzov Stroit (issue 4):19–23 (in Russian)
19. Aleynikov S M, Neiburg E V (1997) Foundation. Patent 2080030 RU, MKI6 E 02 D 27/00. No. 94019239/33 (Russia)
20. Aleynikov S M, Nikolayev S N (1999) Spatial stress-strained state of the base of a variable-width rigid strip foundation. Izv Vuzov Stroit (issue 4):15–21 (in Russian)
21. Aleynikov S M, Sedaev A A (1995) Algorithm of grid generation in the boundary-element method for flat domains. Mat Modelirovanie 7 (issue 7):81–93 (in Russian)
22. Altenbach J, Sacharov A S (eds.) (1982) Die Methode der Finiten Elemente in der Festkörpermechanik. Fachbuchverlag, Leipzig
23. Ambartsumyan S A (1967) Theory of anisotropic plates. Nauka, Moscow (in Russian)
24. Amusin B Z, Fadeyev A B (1975) Finite-element method at the solution of problems of mining geomechanics. Nauka, Moscow (in Russian)
25. Antipov Yu A (1987) Exact solution of a problem of impression of a ring-shaped punch into a half-space. Doklady AN UkrSSR Ser A (issue 7):29–33 (in Russian)
26. Atopov V I, Serdobintsev Yu P, Slavin O K (1988) Contact stress modelling. Mashinostroyenie, Moscow (in Russian)
27. Babeshko V A, Glushkov Ye I, Glushkova N V (1981) On the singularities in the angular points of spatial punches in contact problems. Dokl AN SSSR 257 (issue 2): 289–294 (in Russian)
28. Babloyan A A, Tonoyan V S (1967) On the impression of a ring-shaped punch into an elastic half-space. Izv AN ArmSSR Mekh (issue 1):3–16 (in Russian)
29. Banerjee P K, Butterfield R (1981) Boundary element methods in engineering science. McGraw-Hill, New York
30. Barkan D D (1948) Dynamics of bases and foundations. Stroyvoyenmorizdat, Moscow (in Russian)
31. Basant Z P (1974) Three-dimensional harmonic functions near termination or intersection of gradient singularity lines: a general numerical method. Intern J Eng Sci 12:221–243.
32. Berezantsev V G (1970) Calculation of bases of buildings.Stroyizdat, Leningrad (in Russian)
33. Birman S Ye (1953) On the settlement of a rigid punch on an elastic layer resting on an incompressible base. Dokl AN SSSR 93 (issue 5):791–794 (in Russian)

34. Bokiy I B, Petrishin V I (1986) Algorithm of approximate solution of the problem of the pressure of a smooth square punch with a flat bottom on an elastic half-space. In: Stability and strength of structural elements. Dnipropetrovsk State University, Dnipropetrovsk, pp. 38–41 (in Russian)
35. Borodachev A N (1984) Pressure of an elliptical punch on a nonhomogeneous elastic half-space. Dokl AN UkrSSR Ser A (issue 7):30–33 (in Russian)
36. Borodachev A N (1985) Interaction of a rigid foundation with a nonhomogeneous elastic base. Izv Vuzov Stroit Arhit (issue 10):38–41 (in Russian)
37. Borodachev A N (1990) The influence tensor for an elastic medium with Poisson's ratio varying in one direction. J Appl Math Mech 54:242–249
38. Borodachev A N, Dudinskii V I (1986) Bending of a round plate on a nonhomogeneous elastic base. Izv Vuzov Stroit Arhit (issue 11):26–30 (in Russian)
39. Borodachev A N, Dudinskii V I (1986) Contact problem for an elastic half-space with a variable Poisson ratio. Mech Solids 21 (issue 1):86–91
40. Borodachev N M (1970) Impression of a punch with a footing in the shape of a narrow rectangle into an elastic half-space. Izv AN SSSR Mekh Tverd Tela (issue 4):135–141 (in Russian)
41. Borodachev N M (1976) Contact problem for a stamp with a rectangular base. J Appl Math Mech 40:505–512
42. Borodachev N M (1976) On the nature of the contact stress singularities under an annular stamp. J Appl Math Mech 40:347–352
43. Borodachev N M, Borodacheva F N (1966) Impression of a ring-shaped punch into an elastic half-space. Inzh Zh Mekh Tverd Tela (issue 4):158–161 (in Russian)
44. Borodachev N M, Galin L A (1974) Contact problem for a stamp with narrow rectangular base. J Appl Math Mech 38:108–113
45. Borodachev N M, Tarikov G P (1972) Determination of the reaction pressure under a foundation by the electrical modeling method. Soil Mech Found Eng 9:428–429
46. Borodachev N M, Tarikov G P (1974) Solution of three-dimensional contact problems in elasticity theory by the method of electrical simulation. Mech Solids 9 (issue 3):84–87
47. Borodacheva F N (1968) Action of a vertical eccentric force on an annular foundation situated on a compressible base. Soil Mech Found Eng 5:34–38
48. Borodacheva F N (1969) On indentation of a ring-shaped punch into an elastic half-space under an off-centre force. Izv Vuzov Stroit Arkhit (issue 8):15–20 (in Russian)
49. Borodacheva F N (1971) Determination of displacements of the boundary of an elastic half-space due to the action of a ring-shaped foundation. Izv Vuzov Stroit Arkhit (issue 5):80–86 (in Russian)
50. Borodacheva F N (1972) Displacements and stresses in the base of a rigid, symmetrically loaded ring foundation. Soil Mech Found Eng 9:217–221
51. Borodacheva F N (1973) Stresses in internal points of a half-space due to the action of a ring-shaped punch. Izv Vuzov Stroit i Arkhit (issue 3):58–65 (in Russian)
52. Borodacheva F N (1975) On the determination of main stresses in an elastic half-space under a ring-shaped punch. Izv Vuzov Stroit i Arkhit (issue 10):45–48 (in Russian)
53. Borowicka H (1943) Über ausmittig belaste starre Platten auf elastisch-isotropen Untergrund. Ing Arch 1:1–8
54. Botkin A I (1940) On the strength of friable and fragile materials. Izv VNIIG Vedeneeva 26:205–236 (in Russian)
55. Boussinesque J (1885) Applications des potintiels: l'etude de l'equilibre et du mouvement des solides e'lastiques. Gauthier-Villars, Paris
56. Brebbia C A, Walker S (1980) Boundary element techniques in engineering. Newnes-Butterworths, London
57. Brothers P W, Sinclair G B, Segedin C M (1977) Uniform indentation of the elastic half-space by a rigid rectangular punch. Intern J Solids Struct 13:1059–1072.
58. Bufler H, Lieb H, Meier G (1982) Frictionless contact between an elastic stamp and elastic foundation. Ing Arch 52:63–76.

59. Bugrov A K, Golubev A I (1993) Anisotropic soils and bases of buildings. Nedra, St. Petersburg (in Russian)
60. Bundy B D (1984) Basic optimization methods. Edward Arnold, Baltimore
61. Burmister D M (1956) Stress and displacement characteristics of a two-layer rigid base soil system: influence diagrams and practical applications. Proc Highw Res 35: 773–81
62. Burmistrov A N (1987) Contact problem of theory of elasticity for punches of oblong shape. In: Study of non-stationary motion of a solid medium. MFTI, Moscow, pp. 23–30 (in Russian)
63. Bycroft G N (1956) Forced vibrations of a rigid circular plate on a semi-infinite elastic space and on elastic stratum. Phil Trans Roy Soc London Ser A 248:327–368.
64. Chernousko F L, Banichuk N V (1973) Variational problems of mechanics and control. Numerical methods. Nauka, Moscow (in Russian)
65. Cheung Y K, Zienkiewicz O C (1965) Plates and tanks on elastic foundation: an application of finite element method. Intern J Solids Struct 1:451–461
66. Darevskii V M (1977) Bending of a rectangular plate with free edges. Izv AN SSSR Mekh Tverd Tela (issue 1):79–90 (in Russian)
67. Decisive laws of soil mechanics (1975) Mir, Moscow (in Russian)
68. Dempsey J P, Li H (1989) A rigid rectangular footing on an elastic layer. Geotechnique 9:147–152
69. Derkach V F (1971) Approximate calculation of thin constructive orthotropic ribbed plates on an elastic half-space. Izv Vuzov Stroit Arkhit (issue 4):50–54 (in Russian)
70. Desai C S, Christian J T (eds.) (1977) Numerical methods in geotechnical engineering. McGraw-Hill, New York
71. Dinnik A N (1952) Selected works. Vol 1. Impact and compression of elastic bodies. Ukr Acad Sci Publ, Kyiv (in Russian)
72. Dovnarovich S V, Pol'shin D E, Baranov D S, Sidorchuk V F (1981) Dependence of the stress state of the base on the form of the foundation in plan. Soil Mech Found Eng 150: 340–344
73. Durayev A Ye (1991) Calculation of structures on a soil base with a deformation modulus increasing with depth. Mordovian University, Saransk (in Russian)
74. Egorov K E (1948) Deformation of the base of a round rigid foundation under an eccentric load. In: Bases and foundations. Issues of soil mechanics. Tr NIIOSP 11:119–138 (in Russian)
75. Egorov K E (1958) On the deformation of a finite-thickness base. In: Bases and foundations. Soil mechanics. Tr NIIOSP 34:5–33 (in Russian)
76. Egorov K E (1963) Indentation of a punch with a flat ring-shaped bottom into a half-space. Izv AN SSSR Mekh i Mashinostr (issue 5):187–196 (in Russian)
77. Egorov K E (1965) Calculation of bed for foundation with ring footing. In: Proc 6th Intern Conf Soil Mech Found Eng, Vol. 2, pp. 41–45
78. Egorov K E, Barvashov V A, Fedorovskii V G (1973) On the application of theory of elasticity to the calculation of bases under structures. In: Proc 8th Intern Congr Soil Mech Found Eng. Stroyizdat, Moscow, pp. 72–83 (in Russian)
79. Egorov K E, Finaeva T I (1984) Initial critical load on the ground in the case of a circular foundation. Soil Mech Found Eng 21:269–272
80. Egorov K E, Kitaykina O V, Dokhnyanskii M P (1986) Calculation of bases for rong-shaped foundations. In: Efficient foundation design and methods of base preparation. Tr NIIOSP 85:104–116 (in Russian)
81. Egorov K E, Shelest L A (1985) Distribution of stresses and displacements in the base of a round foundation of tower structures. In: Numerical methods of solving the problems of soil mechanics and calculation of foundations at complex geotechnical conditions. Tr NIIOSP 84:46–64 (in Russian)
82. Egorov K E, Shelest L A, Sokolov N S (1988) Determination of the horizontal displacement of the base of a rigid round foundation on a finite-thickness layer. In: Theoretical and exper-

imental substantiation of new design and technology in foundation engineering. Tr NIIOSP 89:3–13 (in Russian)
83. Ermashov V P (1985) Effect of foundation shape on normal contact pressure distribution. Soil Mech Found Eng 22:61–64
84. Fabricant V I (1986) Inclined flat punch of arbitrary shape on an elastic half-space. Trans ASME J Appl Mech 53:798–806
85. Fadeev A B (1987) Finite-element method in geomechanics. Nedra, Moscow (in Russian)
86. Fedorov V I (1993) Design and construction of foundations for structures on a complex relief. Dalpress, Vladivostok (in Russian)
87. Fedorovskii V G (1985) Modern methods of description of mechanical properties of soils. VNIIS, Moscow (in Russian)
88. Fedorovskii V G, Dokhnyansky M P (1988) Settlements of round and ring-shaped foundations: prediction and comparison with field observation data. Baltic Conf on Soil Mechanics. Tallinn, Vol 2, pp. 99–106 (in Russian)
89. Fedorovskii V G, Onopa I A (1985) Surface settlements of a wedge-shape bed under a concentrated load. Soil Mech Found Eng 22:79–84
90. Filatov A V, Adigamov R Sh (1990) Emergencies and deformations of industrial buildings and structures. Soil Mech Found Eng 27:43–47
91. Florin V A (1936) On the calculation of structures on weak soils. In: Gidrostroyproekt Works: Gidrotekhnika, issue 1, pp. 21–34 (in Russian)
92. Florin V A (1959) Fundamentals of soil mechanics. Stroyizdat, Moscow/Leningrad (in Russian)
93. Forsythe G E, Malcolm M A, Moler C B (1977) Computer methods for mathematical computations. Prentice-Hall, Englewood Cliffs
94. Fourie A B, Beer G (1989) An illustration of the importance of soil non-linearity in soil-structure interaction problems. Comput Geotechnics 8:219–241
95. Fraser R A, Wardle L J (1976) Numerical analysis of rectangular rafts on layered foundations. Geotechnique 26:613–630
96. Galashev Yu V, Dyba V P, Murzenko A Yu (1979) Experimental studies of the depth od a compressible base loaded by a round punch. In: Experimental and theoretical studies of nonlinear problems in the field of bases and foundations. NPI, Novocherkassk, pp. 128–134 (in Russian)
97. Galin L A (1961) Contact problems in the theory of elasticity. North Carolina State College, Raleigh
98. Galin L A (1980) Contact problems of theory of elasticity and viscoelasticity. Nauka, Moscow (in Russian)
99. Galin L A (ed.) (1976) Development of theory of contact problems in the USSR, Nauka, Moscow (in Russian)
100. Gilman Ya D, Gilman Ye D (1989) Reinforcement and reconstruction of buildings on loess soils. Stroyizdat, Moscow (in Russian)
101. Glushkov V Ye (1990) Stress-strained state of elastoplastic bases of ring-shaped and circular foundations. In: Nonlinear methods of calculation of bases and foundations. Mariy Polytechnic Institute, Yoshkar-Ola, p 44–46 (in Russian)
102. Godes Yu Ya (1987) Functions of compliance of a multilayer base with elastic constraints between the layers. In: Nonlinear problems of hydroaeromechanics and theory of elasticity. Dnipropetrovsk State University, Dnipropetrovsk, pp. 92–97 (in Russian)
103. Godes Yu Ya, Privarnikov A K (1983) Quadrature formulae for Hankel integrals. Dnipropetrovsk State University, Dnipropetrovsk, VINITI No. 327-84Dep (in Russian)
104. Goldshtein M N, Kushner S G, Shevchenko M I (1977) Calculation of settlements and strength of bases of buildings and structures. Budivelnyk, Kyiv (in Russian)
105. Gorbunov-Posadov M I, Malikova T A, Solomin V I (1984) Calculation of structures on an elastic base. Stroyizdat, Moscow (in Russian)

106. Gorlov A M, Serebryaniy R V (1968) Automated calculation of rectangular plates on an elastic base. Stroyizdat, Moscow (in Russian)
107. Gorodetskiy A S, Zavoritskiy V I, Lantukh-Lyashchenko A I, Rasskazov A O (1989) Automation of calculations of transport buildings. Transport, Moscow (in Russian)
108. Goryacheva I G, Dobychin M N (1988) Contact problems in tribology. Mashinostroyeniye, Mosow (in Russian)
109. GOST 13580-85. Ferroconcrete plates of strip foundations. (1986) Standard Publishers, Moscow (in Russian)
110. GOST 20276-85. (1985) Soils. Methods of field determination of deformability characteristics Standard Publishers, Moscow (in Russian)
111. Gubenko V S (1960) Pressure of an axially symmetrical ring-shaped punch on an elastic layer and an elastic half-space. Izv AN SSSR Mekh Tverd Tela (issue 3):60–64 (in Russian)
112. Gubenko V S, Mossakovskii V I (1960) Pressure of an axially symmetric circular die on an elastic half-space. J Appl Math Mech 24:477–486
113. Gubenko V S, Nakashidze G M, Pyatovolenko V G (1986) Exact solution of the problem of a ring-shaped punch. Dokl AN UkrSSR Ser A (issue 3):40–44 (in Russian)
114. Gudehus G (ed.) (1977) Finite elements in geomechanics. Wiley, New York
115. Hamming R W (1962) Numerical methods for scientists and engineers. McGraw-Hill, New York
116. Hara T, Shibuya T, Koizumi T, Nakahara I (1978) An asymmetric mixed boundary value problem of the elastic half-space subjected to moment by an annular ring punch. Bull JSME 21:566–571.
117. Harr M E (1966) Foundations of theoretical soil mechanics. McGraw-Hill, New York
118. Huber M T (1914) Die Grundlagen einer rationellen Berechnung der Eisenbetonplatten. Z Österr Ing und Architektur Vereins:557
119. Il'inkova N I (1992) Bending of a plate of linearly variable thickness on an elastic half-space with modulus of elasticity varying along the depth. Intern Appl Mech 28:484–489
120. Instruction on design of blast-furnace foundations (1972) VSN 001-71, USSR Ministry of Ferrous Metallurgy, Stroyizdat, Moscow (in Russian)
121. Instruction on design of road coatings of non-rigid type (1985) VSN 46-83, USSR Ministry of Transport Engineering, Transport, Moscow (in Russian)
122. Instructions on design and erection of foundations for buildings and structures at hill slopes using the base settlement alignment method (1970) DVPromstroyniiproekt, Vladivostok (in Russian)
123. Instructions on design of foundations for machines subject to dynamic loads (1982) Gersevanov NIIOSP, Stroyizdat, Moscow (in Russian)
124. Instructions on design of foundations on a natural base of subcolumn for buildings and industrial structures (1978) Stroyizdat, Moscow (in Russian)
125. Instructions on design of plate foundations for tower-type skeleton buildings and structures (1984) Gersevanov NIIOSP, Stroyizdat, Moscow (in Russian)
126. Ioannides A M (1988) Finite difference solution for plate on elastic solid. J Transp Eng 114:57–75
127. Ivanov P L (1991) Soils and bases of hydrotechnical structures. Vysshaya shkola, Moscow (in Russian)
128. Johnson K L (1985) Contact mechanics. Cambridge University Press, Cambridge
129. Kachamkin A A, Tsukrov I I, Shvayko N Yu (1987) Application of the finite-element method to the calculation of variable-rigidity anisotropic plates on an elastic base. In: Issues of strength and plasticity. Dnipropetrovsk State University, Dnipropetrovsk, pp. 39–40 (in Russian)
130. Kączkowski Z (1968) Plyty – obliczenia statyczne. Arkady, Warszawa

131. Kalinnikov A Ye, Yefremov S M, Vakhrushev F V (1985) Algorithm for automatic mesh of a two-dimensional domain for solving contact problems by boundary-element method. Probl Prochnosti (issue 2):106–108 (in Russian)
132. Karpenko N I (1976) Theory of deformation of ferroconcrete with cracks. Stroyizdat, Moscow (in Russian)
133. Kim Yu A, Shebchuk L I (1978) Deformation of soil under a rigid punch. In: Theoretical and applied mechanics. Vysheyshaya Shkola, Minsk 5:109–112 (in Russian)
134. Kiselev V A (1973) Calculation of plates. Stroyizdat, Moscow (in Russian)
135. Kizyma Ya M (1973) Pressure of a circular punch on an elastic layer in the presences of tangential forces in the contact zone. Intern Appl Mech 9:901–904
136. Klepikov S N (1967) Calculation of structures on an elastic base. Budivelnyk, Kyiv (in Russian)
137. Klepikov S N (1972) Calculation of beams on a nonlinearly deformed Winkler base. Osnovaniya Fundamenty Mekh Gruntov (issue 1):8–10 (in Russian)
138. Klepikov S N, Malikova T A (1982) Bending of a variable-rigidity orthotropic plate on a nonlinearly deformable displaced base. In: Bases, foundations, and underground structures. Tr NIIOSP. 73:15–19 (in Russian)
139. Klepikov S N, Tregub A S, Matveyev I V (1987) Calculation of buildings and structures on subsiding soils. Budivelnyk, Kyiv (in Russian)
140. Knyazeva L P (1984) Solving mixed spatial problems of theory of elasticity of anisotropic media using the boundary integral equation method. Ph D thesis, Minsk (in Russian)
141. Kocatürk T (1995) Rectangular anisotropic (orthotropic) plates on a tensionless elastic foundation 31:378–386
142. Konik A Ya, Demin I I (1982) Calculation of temperature fields and stress-strained state of soil bases using the finite-element method. MISI, Moscow (in Russian)
143. Korenev B G, Chernigovskaya Ye I (1962) Calculation of plates on an elastic base. Gosstroyizdat, Moscow (in Russian)
144. Krivorotov A P (1963) Experimental studies of distribution of normal stress over the contact area for a punch with a sand base. Osnovaniya Fundamenty Mekh Gruntov (issue 2):8–12 (in Russian)
145. Krivorotov A P (1965) On the distribution of normal stress over the bottom of a rigid punch at the variation of the vertical load eccentricity. Izv Vuzov Stroit (issue 7):33–38 (in Russian)
146. Krivorotov A P (1969) State of stress of a sand mass under a plate lying at a shallow depth. Soil Mech Found Eng 6:22–24
147. Krivorotov A P, Babello V A (1981) Results of investigation of the stress state of a sandy bed for rigid plates. Soil Mech Found Eng 18:117–122
148. Kuznetsov V I (1952) Elastic base. Gosstroyizdat, Moscow (in Russian)
149. Lamzyuk V D, Privarnikov A K (1977) Mixed problems of theory of elasticity for multilayer bases with circular boundary condition separation lines. In: Mixed problems of mechanics of deformable bodies. Abstr 1st Sov Conf, Rostov-na-Donu, Pt 1, pp. 37–38 (in Russian)
150. Lebedev N N, Ufliand Ia S (1958) Axisymmetric contact problem for an elastic layer. J Appl Math Mech 22:442–450
151. Lee I K (1962) Bearing capacity of foundations with particular reference to the Melbourn area. J Instn Engrs Austr 34:283
152. Lekhnitskii S G (1947) Anisotropic plates. Gostekhizdat, Moscow/Leningrad (in Russian)
153. Leonov M Ya (1953) General problem of a pressure of a circular punch on an elastic half-space. Prikl Mat Mekh 17:87–98 (in Russian)
154. Leonov M Ya, Posatskii S L, Ivashchenko A N (1956) Calculation of a square-shaped foundation. Sci. Rep. Inst. Machinery and Automation, Ukr.Acad, Sci. 5 (issue 4):141–151 (in Russian)
155. Likhovtsev V M, Estrin I Yu (1985) Some aspects of numerical implementation of solving problems of interaction of a punch and a base by the finite-element method. In: Numerical methods of solving problems of soil mechanics and calculation of foundations in complicated geotechnical conditions. Tr NIIOSP 84:174–181 (in Russian)

156. Love A E H (1929) Stress produced in a semi-infinite solid by pressure on part of the boundary. Philos Trans Roy Soc London A 228:377–420.
157. Love A E H (1959) A treatise on the mathematical theory of elasticity, 4th edn. Cambridge University Press, Cambridge
158. Lubyagin I A, Pozharskii D A, Chebakov M I (1991) Generalization of Boussinesq and Cerruti problems for the case of an elastic spatial wedge. Dokl AN SSSR 321 (issue 1): 58–62 (in Russian)
159. Lur'e A I (1964) Three-dimensional problems in the theory of elasticity. Interscience, New York
160. Lur'e A I (1970) Theory of elasticity. Nauka, Moscow (in Russian)
161. Malyshev M V, Zaretskii Yu K, Shirokov V N, Cheremnykh V A (1973) On the combined functioning of rigid foundations and a nonlinearly deformable base. In: Proc 8th Intern Congr Soil Mech Found Eng. Stroyizdat, Moscow, pp. 97–104 (in Russian)
162. Manual for the design of bases for buildings and structures (for the Engineering Rules and Regulations 2.02.01.-83) (1986) Gersevanov NIIOSP, Stroyizdat, Moscow (in Russian)
163. Marcus H (1932) Die Theorie elastischer Gewebe und ihre Anwendungen auf die Berechnung biegsamer Platten, 2. Auflage, Springer-Verlag, Berlin
164. Martynenko M D, Dashkevich A A (1987) Bending of round plates on a nonhomogeneous base with a variable in depth Poisson ratio with the account of their thickness deformability. In: Non-axisymmetrical problems of hydromechanics and theory of elasticity. Dnipropetrovsk State University, Dnipropetrovsk, pp. 151–153 (in Russian)
165. Martynenko M D, Knyazeva L P, Romanchik V S (1979) Pressure of an absolutely rigid punch on an orthotropic half-space under cohesion. In: Current problems of mechanics of deformable media. Dnipropetrovsk State University, Dnipropetrovsk, pp. 156–161 (in Russian)
166. Martynenko M D, Knyazeva L P, Romanchik V S (1979) Pressure of an absolutely rigid punch on an orthotropic half-space in the absence of friction. Izv AN BSSR Ser Fiz Mat Nauk (issue 6):40–44 (in Russian)
167. Martynenko M D, Romanchik V S (1977) On one method of solving the main integral equation of the contact problem of theory of elasticity. Izv AN BSSR Ser Fiz Mat Nauk (issue 3):42–47 (in Russian)
168. Meleshenkov Ye I, Ozherelyev V A (1986) Some results of comparison of finite-element and finite-difference methods for the example of the problem of bending of a plate. In: Numerical methods in the studies of engineering structures. Kucherenko CNIISK Works, pp. 70–76 (in Russian)
169. Mindlin R D, Cheng D H (1950) Nuclei of strain in the semi-infinite solid. J Appl Phys 21:926–931
170. Mossakovskii V I (1953) General solution of a problem of determination of pressure under the bottom of a round punch without the account of friction. Scientific Records Inst Machinery and Automation Acad Sci UkrSSR 2 (issue 1):41–53 (in Russian)
171. Mossakovskii V I (1953) Pressure of a round punch on an elastic half-space. Scientific Records Inst Machinery and Automation Acad Sci UkrSSR 2 (issue 1):9–40 (in Russian)
172. Mossakovskii V I, Kachalovskaya N Ye, Golikova S S (1985) Contact problems of mathematical theory of elasticity. Naukova dumka, Kyiv (in Russian)
173. Mossakovskii V I, Kovura A B (1976) On one method of solving the problems of theory of potential and its application in theory of elasticity. Dokl AN UkrSSR Ser A (issue 1):44–47 (in Russian)
174. Mossakovskii V I, Kovura A B (1980) Contact problems for an elastic half-space with round and near-round boundary condition separation lines. In: Dnipropetrovsk State University, Dnipropetrovsk (issue 5):74–89 (in Russian)
175. Muki R (1960) Asymmetric problems of the theory of elasticity for a semi-infinite solid and a thick plate. In: Sneddon I N and Hill R (eds.) Progress in solid mechanics. North-Holland, Amsterdam, Vol. 1, pp. 399–439

176. Muravskii G B (1967) On the application of the Betti theorem for solving some problems for an elastic base. In: Works Mosc. Inst. Rail Transport Eng. 236:51–57 (in Russian)
177. Murzenko Yu N, Revenko V V (1976) Experimental studies of distribution of normal and tangential stresses in the base of a round punch using load-cell stress gauges. In: Bases and foundations. NPI, Novocherkassk, pp. 3–12 (in Russian)
178. Murzenko Yu N, Tarikuliyev Z A, Arinina E V, Revenko V V (1979) Results and prospects of experimental studies of the stress-strained state of bases of buildings. In: Experimental and theoretical studies of nonlinear problems in the field of bases and foundations. NPI, Novocherkassk, pp. 121–128 (in Russian)
179. Nikishin V S, Shapiro G S (1973) Problems of theory of elasticity for multilayer media. Naula, Moscow (in Russian)
180. Nikishin V S, Shapiro G S (1976) Problem of incomplete contact of annular or circular stamp with elastic laminated medium. Mech Solids 11 (issue 5):27–38
181. Nikolaevsky V N (1972) Mechanical properties of soil and theory of plasticity. VINITI AN SSSR, Moscow (in Russian)
182. Novotný B, Hanuška A (1985) Tuhy rasník obdĺžnikoveho podorysu na pruznom podlozí. Staveb. Cas. 33:521–540
183. Novotný B, Hanuška A (1987) Rectangular plate on an elastic half-space. Staveb Cas 35:359–376
184. Oden J T (1972) Finite elements of nonlinear continua. McGraw-Hill, New York
185. Olesiak Z (1965) Annular punch on elastic semi-space. Arch Mech Stosow 17:633–648
186. Onopa I A, Fedorovskii V G (1984) Calculation of contact stress under a rigid rectangular punch on a wedge-shaped base. In: Mechanics of soils and calculation of bases and foundations according to the limiting states. Tr NIIOSP 82:45–50 (in Russian)
187. Onopa I A, Fedorovskii V G (1984) Settlements and slopes of a rectangular punch on a wedge-shaped base. Izv Vuzov Stroit Arkhit (issue 5):47–50 (in Russian)
188. Ortega J M, Rheinboldt W C (1970) Iterative solution of nonlinear equations in several variables, Academic Press, New York
189. Palatnikov Ye A (1964) Rectangular plate on an elastic base. Stroyizdat, Moscow (in Russian)
190. Pasternak P L (1954) Fundamentals of a new method of calculation of foundations on an elastic base using two coefficients of subgrade reaction. Stroyizdat, Moscow (in Russian)
191. Perich A I (1994) Effective strip foundations. Zhilish Stroit (issue 4):11–13 (in Russian)
192. Petrukhin V P (1995) Calculation of suffosion deformations in saline soils. Soil Mech Found Eng 32:159–162
193. Pilyagin A V, Kazantsev S V (1986) Mixed elastoplastic problem of calculation of a soil base in a spatial formulation. In: Geotechnics of the Volga area, Kazan, pp. 44–47 (in Russian)
194. Pilyagin A V, Kazantsev S V (1990) Design of bases and foundations with the account of elastoplastic properties. Krasnoyarsk State University, Krasnoyarsk (in Russian)
195. Pilyagin A V, Kazantsev S V, Kazantseva N N (1985) Elastoplastic calculation of a soil base at the conditions of a spatial stress-strained state. Mariy Polytechnical Institute, Yoshkar-Ola, VNIIIS No. 5713 (in Russian)
196. PLAXIS – Finite Element Code for Soil and Rock Analyses. Ver. 7. General Information and Tutorial Manual (1998) Balkema, Rotterdam
197. Plevkov V S, Polishchuk A I (1990) Size determination of off-centre loaded foundations of various geometrical shape. TPI, Tomsk (in Russian)
198. Podgorniy A N, Gontarovskii P P, Kirkach B N et al. (1989) Problems of contact interaction of structural elements. Naukova Dumka, Kyiv (in Russian)
199. Pollard J H (1979) A handbook of numerical and statistical techniques. Cambridge University Press, Cambridge
200. Popov G Ya (1967) On an approximate method of solving a contact problem of a ring-shaped punch. Izv AN ArmSSR Mekh 20 (issue 2): 19–36 (in Russian)

201. Popov G Ya (1976) Mathematical problems of contact problems. Odesa State University, Odesa (in Russian)
202. Popov G Ya (1982) Concentration of elastic stress near punches, cuts, fine inclusions and supports. Nauka, Moscow (in Russian)
203. Popov G Ya (1982) Contact problems for a linearly deformable base. Vyshcha Shkola, Kyiv/Odesa (in Russian)
204. Poulos H G (1968) The behaviour of a rigid circular plate resting on a finite elastic layer. Civil Eng Inst Engrs Aust CE10:213–219
205. Poulos H G, Davis E H (1974) Elastic solutions for soil and rock mechanics. Wiley, New York
206. Prisyazhnyuk V K, Marchuk A V (1987) Boundary-element method in the problems of contact interaction of multilayer rectangular plates with an elastic half-space. Stroit Mekh Raschet Sooruzh (issue 4):9–12 (in Russian)
207. Proskuryakov S M, Malyshev M V (1979) Numerical solution of a spatial problem of a flexible load on a half-space. In: Experimental and theoretical studies of nonlinear problems in the field of bases and foundations. NPI, Novocherkassk, pp. 35–43 (in Russian)
208. Protsenko V S (1968) On the pressure under an annular punch. Intern Appl Mech 4 (issue 9):C51–53
209. Rabotnikov A I, Kovanev B M (1970) Experimental studies of deformations and stresses along the base depth under a rigid punch. In: Bases and foundations. Budivelnyk, Kyiv 3:59–64 (in Russian)
210. Rappoport L M (1948) Boussinesq problem for a layered elastic half-space. Works of Leningrad Polytechnical Institute (issue 5):3–18 (in Russian)
211. Recommendations on the calculation of settlements and slopes for rectangular foundations on a wedge-shaped base (1985) Gersevanov NIIOSP, Moscow (in Russian)
212. Reisner E, Sagoci H (1944) Forced torsional oscillation of an elastic half-space. J Appl Phys 15:652–662
213. Rekach V G (1984) Instructions for solving problems of applied theory of elasticity. Vysshaya Shkola, Moscow (in Russian)
214. Roitman A B, Shishkanova S F (1973) The solution of the annular punch problem with the aid of recursion relations. Intern Appl Mech 9:725–729
215. Roitman A G, Smolenskaya N G (1978) Renovation and reconstruction of residential and public buildings. Stroyizdat, Moscow (in Russian)
216. Rozin L A (1971) Computer-aided calculation of hydrotechnical structures. Finite-element method. Energia, Leningrad (in Russian)
217. Rozin L A (1990) Combination of the finite-element method and the Green-Somigliana formula. In: LPI Works 434:3–10 (in Russian)
218. Rozin L A (1998) Problems of theory of elasticity and numerical methods of their solution. SPBGTU, St. Petersburg (in Russian)
219. Rozin L A, Rukavishnikov V A (1995) Development of a combined method of calculation of structures and their bases of infinite length. Izv Vuzov Stroit Arkhit (issue 11):37–42 (in Russian)
220. Rozin L A, Rukavishnikov V A (1997) Problem of numerical calculation of structures, interacting with infinite bases. Izv Vuzov Stroit Arkhit (issue 4):47–52 (in Russian)
221. Rozin L A, Yevdokimov B M (1993) Method, based on a combination of the potential and finite-element methods. In: Issues od dynamics and strength, Zinatne, Riga, 43:49–55 (in Russian)
222. Rvachev V L (1959) The pressure on an elastic half-space of a stamp with a wedge-shaped planform. J Appl Math Mech 23:229–233
223. Rvachev V L (1982) Theory of R-functions and some of its applications. Naukova Dumka, Kyiv (in Russian)
224. Rvachev V L, Kurpa L V (1987) R-functions in the problems of theory of plates. Naukova Dumka, Kyiv (in Russian)

225. Rvachev V L, Protsenko V S (1977) Contact problems of theory of elasticity for nonclassical domains. Naukova Dumka, Kyiv (in Russian)
226. Rybin V S (1990) Design of foundations of buildings under reconstruction. Stroyizdat, Moscow (in Russian)
227. Rybin V S, Zakharchenko V E (1981) Vertical stresses in a bed stratum due to a load uniformly distributed over the area of a polygon. Soil Mech Found Eng 18:202–205
228. Sabonnadière J-C, Coulomb J-L (1986) La méthode des éléments finis. Du modèle. . . a la CAO. Hermes, Paris – Londres – Lausanne
229. Sakalo V I, Shkurin A A (1985) Universal program for triangulation of a two-dimensional domains of an arbitrary shape with grid condensations. Probl Prochn (issue 1):106–108 (in Russian)
230. Samarskiy A A, Gulin A V (1989) Numerical methods. Nauka, Moscow (in Russian)
231. Schiffman R L, Aggarwala D B (1961) Stresses and displacements produced in a semi-infinite elastic solid by a rigid elliptical footing, In: Proc 5th Intern Conf Soil Mech Found Eng, Vol. 1, pp. 795–801
232. Schofield A, Wroth P (1968) Critical state soil mechanics. McGraw-Hill, London
233. Sekulović M (1988) Metod konačnih elemenata. Gradevinska knjiga, Beoqrad
234. Selvadurai A P S (1979) Elastic analysis of soil-foundations interaction. Elsevier, Amsterdam
235. Seymov V M (1976) Dynamic contact problems. Naukova Dumka, Kyiv (in Russian)
236. Shapiro D M (1996) Finite-element calculation of structures and bases. VGASA, Voronezh (in Russian)
237. Sharma K G, Nagpal A K, Garg M K (1984) Finite element analysis of rafts resting on elastic half space. Indian Geotechn J 14:28–39
238. Shevchuk L I (1988) Method of calculation of frame systems on an anisotropic elastic layer. PhD thesis, Minsk (in Russian)
239. Shevlyakov Yu A (1977) Matrix algorithms in theory of elasticity of nonhomogeneous media. Vyshcha Shkola, Kyiv/Odesa (in Russian)
240. Shibuya T, Koizumi T, Nakahara I (1974) An elastic contact problem for a half-space indented by a flat annular rigid punch. Intern J Eng Sci 12:759–771
241. Shirinkulov T Sh (1969) Calculation of structures on a solid base. FAN, Tashkent (in Russian)
242. Shirinkulov T Sh (1972) Calculation of engineering structures on a nonhomogeneous elastic base. FAN, Tashkent (in Russian)
243. Shirokov V N, Solomin V I, Cheremnik V A, Malyshev M V, Zaretsky Yu K (1971) A circular rigid plate on a nonlinearly deforming base. In: Proc 4th Budapest Conf Soil Mech Found Eng. Akademiai Kiadó, Budapest, pp. 757–76
244. Shirokov V N, Solomin V I, Malyshev M V, Zaretski Yu K (1970) Stress state and displacements of a ponderable, nonlinearly deformable soil half-space under a circular rigid footing. Soil Mech Found Eng 7:2–8
245. Shtayerman I Ya (1949) Contact problem of theory of elasticity. Gostekhizdat, Moscow (in Russian)
246. Smirnov V A (1978) Calculation of plates of a complex contour. Stroyizdat, Moscow (in Russian)
247. Smirnov V A (1983) Calculation of orthotropic plates resting on an elastic base with a coefficient of subgrade reaction, variable over the area. In: Applied theory of elasticity. SPI, Saratov, pp. 12–21 (in Russian)
248. Sneddon I N (1946) Boussinesq's problem for a flat-ended cylinder. Proc Camb Phil Soc 42:29–39
249. SNIP (Construction Rules and Regulations) 2.02.01-83. Bases for buildings and structures (1985) Stroyizdat, Moscow (in Russian)
250. Solomin V I (1960) Calculation of rectangular plates on an elastic half-space by the grid method. Stroit Mekh Raschet Sooruzh (issue 6):12–17 (in Russian)

251. Solomin V I, Shirokov V N, Komarov E A (1968) Computation of rectangular plates on elastic layer of limited thickness. Soil Mech Found Eng 5:294–298
252. Solomin V I, Shmatkov S B (1986) Methods of calculation and optimal design of ferroconcrete foundation structures. Stroyizdat, Moscow (in Russian)
253. Solomin V I, Sytnik A S (1974) Design of foundation slabs of complex configuration and variable stiffness. Soil Mech Found Eng 11:300–305
254. Solomin V I, Sytnik A S, Vysokovskiy V L (1977) Calculation of foundation plates of complex configuration. Stroit Mekh Raschet Sooruzh (issue 2):39–41 (in Russian)
255. Solomon L, Zamirescu I (1963) Some approximate formulae and solutions in the contact problem for punches with a plane bounded non-elliptical basis. In: Applications of the theory of functions in continuum mechanics: Proc Intern Symp Tbilisi, pp. 400–409
256. Solovyov L Yu, Solovyov Yu I (1995) Distribution of stress at the action of a circular punch on an elastic half-space. Izv Vuzov Stroit (issue 9):22–26 (in Russian)
257. Sorochan E A (1986) Foundations of industrial buildings. Stroyizdat, Moscow (in Russian)
258. Sorochan E A, Trofimenkov Yu G (ed.) (1985) Bases, foundations and underground structures: designer's handbook. Stroyizdat, Moscow (in Russian)
259. Szegö G (1975) Orthogonal polynomials, 4th edn. Amer Math Soc, Colloquium Publ., Vol. 23__33 Providence, Rhode Island
260. Timoshenko S P, Goodier J N (1970) Theory of elasticity, 3rd edn, McGraw-Hill, New York
261. Timoshenko S, Wojnowski-Krieger S (1959) Theory of plates and shells. McGraw- Hill, New York
262. Traub J F (1982) Iterative methods for the solution of equations. Chelsea, New York
263. Trofimenkov Yu G, Vorobkov L N (1981) Field methods for the studies of constructive properties of soils. Stroyizdat, Moscow (in Russian)
264. Tsytovich N A, Abelev M Yu, Sidorchuk V F, Polishchuk A I (1979) Experimental investigation of the stress-strain state of loess soils in the base of rigid plates. Soil Mech Found Eng 16:140–145
265. Tsytovich N, Berezantsev V, Dalmatov B, Abelev M (1974) Foundation soils and substuctures. Mir, Mocow
266. Ufliand Ia S (1965) Survey of articles on the application of integral transforms in the theory of elasticity. North Carolina State University, Raleigh
267. Ufliand Ia S (1977) Method of coupled equations in mathematical physics problems. Nauka, Leningrad (in Russian)
268. Ukhov S B (1973) Calculation of structures and bases using the finite-element method. MISI, Moscow (in Russian)
269. Ukhov S B, Semenov V V, Znamenskii V V et al. (1994) Soil mechanics, bases and foundations. Association of Engineering Institutions, Moscow (in Russian)
270. Urisman V S (1976) Settlement and tilting of a rigid rectangular foundation on a compressible foundation bed of finite thickness. Soil Mech Found Eng 13:270–275
271. Vainberg D V, Gerashchenko V M, Roytfarb I Z et al. (1967) Grid equations of plate bending derived by variational method, In: Resistance of materials and theory of constructions. Budivelnyk, Kyiv, pp. 23–33 (in Russian)
272. Valov G M (1968) Infinite elastic layer and half-space under the action of a ring-shaped die. J Appl Math Mech 32:917–930
273. Varvak P M, Varvak L P (1977) Method of grids in problems of calculation of engineering structures. Stroyizdat, Moscow (in Russian)
274. Varvak P V, Ryabov A F (ed) (1971) Handbook on theory of elasticity (for engineers and builders). Budivelnyk, Kyiv (in Russian)
275. Vaynberg D V, Vaynberg Ye D (1970) Calculation of plates. Budivelnyk, Kyiv (in Russian)

276. Veryuzhskii Yu V, Ikonin S V, Savitskii V V (1982) Application of potential method in calculation of rigid foundations. In: Bases and foundations. Budivelnyk Kyiv 15:21–25 (in Russian)
277. Veryuzhskii Yu V (1978) Numerical methods of potential in some problems of applied mechanics. Vyshcha Shkola, Kyiv (in Russian)
278. Vinokurov L P (1956) Direct method of solving of spatial and contact problems for arrays and foundations. Kharkiv State University, Kharkiv (in Russian)
279. Vinokurov Ye F (1972) Iterative method of computation of bases and foundations. Nauka i tekhnika, Minsk (in Russian)
280. Vlasov V Z, Leontiev N N (1960) Beams, plates and shells on an elastic base. Phys. Math. Liter. Publ., Moscow (in Russian)
281. Vorovich I I, Aleksandrov V M, Babeshko V A (1972) Nonclassical mixed problems of theory of elasticity. Nauka, Moscow (in Russian)
282. Vronskii A V (1969) Considering the non-linear relationship between the settling of the foundation bed and load in the computation of rigid beams on non-uniform foundations. Soil Mech Found Eng 6:160–164
283. Vyalov S S (1978) Rheological principles of soil mechanics. Vysshaya shkola, Moscow (in Russian)
284. Way S (1940) Some observations on the theory of contact pressures. Trans ASME J Appl Mech 7:147–157
285. Whitman R V, Richart F E (1967) Design procedures for dynamically loaded foundations. J Soil Mech Founds Divn ASCE 93:169–193
286. Yegorov K E, Nitchiporovich A A (1961) Research on the deflection on foundations. In: Proc 5th Intern Conf Soil Mech Found Eng, Vol. 1, pp. 861–866
287. Yerzhanov Zh S, Karimbayev T D (1975) Finite-element method on problems of rock mechanics. Nauka, Almaty (in Russian)
288. Zaretskii Yu K (1989) Lectures on modern soil mechanics. Rostov State University, Rostov (in Russian)
289. Zaretskii Yu K, Lombardo V N (1983) Statics and dynamics of earth-fill dams. Energoatomizdat, Moscow (in Russian)
290. Zavarykin L G, Mazo B M (1989) Calculation of plates on a linearly deformable base by shooting method. In: Resistance of materials and theory of structures. Budivelnyk, Kyiv 54:43–46 (in Russian)
291. Zhemochkin B N, Sinitsyn A P (1962) Practical methods of calculation for beams and plates on an elastic base without Winkler hypothesis. Gosstroyizdat, Moscow (in Russian)
292. Zienkiewicz O C (1971) The finite element method in engineering science, McGraw-Hill, London
293. Zienkiewicz O C, Cheung Y K (1968) The finite element method in structural and continuum mechanics. McGraw-Hill, London
294. Zienkiewicz O C, Lewis R W, Stagg K G (eds.) (1979) Numerical methods in offshore engineering. Wiley, London

Chapter 6
Spatial Contact Problems for Porous Elastic Bases

Abstract The sixth chapter presents solutions of spatial problems of applied geomechanics related to variation of pore pressure in the soil. The influence of the pore pressure decline on the soil settlement and cracking as well as the induced seismicity and other environmental hazards due to pumping out gas and oil deposits or intense removal of underground water at industrial or civil engineering is discussed. The methods for numerical modelling of soil mass deformations due to the reduction of the pore pressure are described. The approach is based on the application of integral representations for displacements in a half-space saturated with liquid (or gas) according to the theory of linear pore-elasticity (filtration consolidation). Spatial deformation of the earth surface due to operating horizontal gas-and-oil wells or water drains is studied with the account of the run-off mode. Finally, the results for boundary-element solutions of the spatial contract interaction of structures with the soil at reduced pore pressure are presented.

Underground mining, intense employment of ground waters, oil and gas extraction result in violation of equilibrium in the geological environment and, first of all, in the changes in geostatic and geodynamic stress fields in the surrounding rock mass [22].

A pore pressure decline results in a volume decrease of the environment constituents due to the pore volume decrease. In the limiting case, if the ground skeleton is not rigid enough, pores can be completely occluded that causes volume reduction by the magnitude of the initial porosity, i.e. from 20 to 40% of the initial value. Pores and cracks can disappear due to their collapse, whose mechanism is related to the deformation process instability, as well as due to slow flowing processes in essentially viscous media. These changes can cause rock mass movement and land surface subsidence, resulting in complications of the conditions of functioning of surface and underground constructions as well as mining activities on vast areas. Land surface subsidence and trough formation are the most hazardous. They can lead to shear and tensile stresses in above-ground structures and finally to overstresses, inadmissible deformations, slopes and even breakdowns.

S.M. Aleynikov, *Spatial Contact Problems in Geotechnics*, Foundations of Engineering Mechanics, DOI 10.1007/b11479_6,

Cases of considerable decline of depressive sinkhole with underground water withdrawal by 100 m or more, and even up to 1000 m in coal fields have been reported (see [22]). Underground water level decline causes essential subsidence of the daylight surface over vast areas measuring sometimes hundreds of square kilometers. For example, according to the observation of scientists from Mexico Engineering Research Institute, during the period of 1900–1969 the territory of Mexico City gave subsidence to 7 m; moreover, in some places subsidence was non-uniform, which caused strong deformation of fundamental buildings such as the Theater Center, Shrine Museum and others. In Tokyo (Japan) where Artesian water is used, the subsidence has reached 3.3 m for 50 years, however at some places the subsidence rate was up to 18 cm per year. Only during 1971 in Tokyo and its suburbs the ground surface level had lowered by 10–20 cm (as a result of underground water withdrawal for the purposes of industrial and civil engineering), some sections of the city subway lines gave subsidence to 10 cm during a year and a half. Permanent land surface subsidence by tens of centimeters has been observed in Bangkok (Thailand) due to underground water withdrawal and rapid growth of skyscrapers, requiring deep foundations and deep water lowering. In Long Beach (the USA) land surface subsidence due to oil extraction has reached 7.6 m. In Niigata (Honshu Island, Japan) land surface subsidence due to gas extraction by up to 50 cm per year was observed and even after water having been pumped into the exhausted gas wells the settlement was just reduced to 25 cm per year. Land surface subsidence in Osaka (Japan) between 1935 and 1958 reached 175–190 cm, and in order to eliminate it, the land surface level was raised by putting in 26.5 million m^3 of soil and making a 124-km long levee.

At oil and gas field development sites the layer pressure decline is a serious environmental hazard. An increase of seismicity in oil and gas extraction areas has been observed in Russia (Northern Caucasus, the Urals and the Volga area, Sakhalin), in the Western part of Ukraine, and in Uzbekistan. It is related not only to the land surface subsidence and its cracking, but also to the induced seismicity due to the interaction of the changing effective stresses and tectonic anomalies. As a result, seismic activity bursts are possible, resulting in devastating earthquakes.

The most widely known are strong earthquakes in the Gazli gas field (Uzbekistan) on April 8, 1976 with a magnitude of $M = 7.0$ and on March 20, 1984 with $M = 7.2$ [13], as well as the earthquake with $M = 6.7$ at the depth of 9–10 km under Coalinga oil field in a non-seismic area of Southern California on May 2, 1983 [19]. In the latter case, all-round investigations have shown the seismicity to be related to a trigger action of the stressed state changes, generated by consolidation of the productive layer. At the earthquake, due to the man-triggered stress the limiting equilibrium was broken and relative motion of the break edges started.

The gas and oil fields in question were developed using vertical wells. Employment of horizontal wells for gas extraction [23], thereby intensifying the extraction process, resulting in the pore pressure changes in much greater layer volumes, can lead to a more significant effect on the rock mass stressed state. The length of the horizontal wells can reach 2 km. The pore pressure decline, arising in the vicinity

of wells, is spread unevenly over the layer, depending on the anisotropy of the layer permeability, over the whole thickness of the productive layer. It is important to perform mathematical modelling for horizontal gas wells functioning in relatively thick layers (3–20 m) with a width of 400 m or more.

Development of oil and gas fields leads to specific man-triggered geodynamic processes. References [18, 22] report on apparent consequences of processes related to land surface subsidence, pipe casing failures and crushing, pore liquid squeezing out of non reservoirs into the pore space of reservoirs, deformation of engineering and industrial constructions and, what is quite essential, the well sealing breakdown, changes of the reservoir characteristics of rocks due to the deformation of layers, containing mass, etc.

The experience of development of hydrocarbon fields using the horizontal wells has shown that man-triggered consequences sometimes result in a situation when the economic gain in development is less than the man-triggered damage [6, 26]. These consequences can be manifested as follows:

– man-triggered land surface subsidence (stable lowering) with a total amplitude up to several metres, as a rule non-uniformly distributed over the area;
– man-triggered "localized" earthquakes in seismic activity areas with a seismic focus, located much deeper than the object depth (Neftekamsk, Russia, 1995).

Such consequences lead to a whole series of complications in construction and functioning of civil and industrial structures:

– breaking the well airtightness, resulting in the gas eruptions into the upper layers and to the surface;
– deformation of industrial and engineering structures.

Displacements of the Earth surface points are caused by a complicated three-dimensional field of stress and deformation of both the reservoir bed itself and the surrounding rock mass. However, in the framework of the present-day approaches the reservoir bed deformation is studied separately from the deformation of its top and bottom as well as of the overlying and underlying rocks. Besides, the productive layer is usually considered to be of a very simple geometrical shape, and the loads are considered axisymmetric. In fact, the reservoir has a very complex shape, and the loads vary over the productive layer volume and surface. Calculations of the arising fields of rock displacements, deformations and stresses cannot be performed by the known methods. Elaboration of new mathematical models and new methods for solving the problem is required. In order to study and predict geodynamic processes occurring at oil, gas and water extraction, new mathematical models should be developed that would combine the reservoir bed and the surrounding rock mass into a single system.

In Russia, land surface subsidence, resulting from human activity, has been systematically observed at a number of fields since 1976, occasional observations having been carried out even before. The registered land surface subsidence over gas

fields has been ranging from 19 cm (North Stavropol oil field) to 27–37 cm per year (Gazli oil field, Uzbekistan). High-precision measurement data for spatial deformation of the land surface in the Shebelynka gas field area (the right bank of the Siverskiy Donets river, Kharkiv province, Ukraine) are analyzed in [5]. The comparison of the reference point coordinates, measured in different years, has shown the biggest displacements to have occurred before 1975, during the period of the most intense gas extraction. The observation point displacements are noted to occur at a variable rate even now, in the central area of the gas field they are larger – near 13 mm per year, at other points – 13 mm per year. Some coordination between vertical and horizontal displacements has been noticed, but not explained.

The predicted land surface subsidence values above the Astrakhan (Russia, seam thickness 100 m) and Qaragandy (Kazakhstan, seam thickness 1500 m) fields are equal to 0.3–0.4 and 1.0–2.0 m, respectively. One should note that the Earth's surface subsidence can be considerably (up to 5 times) larger than the productive layer thickness change due to the compression of overlying water-saturated sandy and clay soils. The subsidence of these soils is caused by squeezing out water into the pore space of the reservoir bed at the pressure decrease as well as by change of the level of near-surface and underground water, being pumped out for industrial and economic needs. Thus, the actual land surface subsidence can only be obtained by taking into consideration the deformation of the whole earth stratum thickness rather than solely the reservoir bed.

In the course of developing deformable reservoirs in the surrounding soil mass a field of normal and tangential stresses is formed. For large-thickness layers (of the order of 1000 m) tangential stress values can amount up to 50% of the seam pressure decline value, and if the seam thickness is about 200 m – not more than 20–30%. However, even in this case the stress can cause one-way flow of plastic soil along the stratification planes. In this case one has to do with transverse-and-longitudinal bending, the most hazardous kind of loading for the elements of industrial underground structures.

A rather detailed analysis of the most noticeable land surface subsidence cases due to decline of water table as well as gas and oil field development, having taken place in the world practice, is performed in reviews [7, 14, 18]. Note that the problem of land surface subsidence, caused by the pore pressure change due to development of oil and gas seams at shallow depth, has a rather complicated character. Traditional methods of estimation of the stress-strained state around the excavations at great depth are inapplicable in this case. The situation is aggravated by layered rock stratification and considerable nonhomogeneity. Hence, efficient investigations require invoking new numerical methods of structural and soil mechanics in spatial formulation. This will enable one to improve the existing prediction methods used to estimate the effect of large-scale hydrotechnical high-rise and underground construction on the environment and the existing buildings, in particular when erecting deepened structures and large-scale structures for oil and gas industry.

6.1 Soil Mass Deformation Due to the Pore Pressure Decline

6.1.1 Integral Representation of Displacements in a Porous Elastic Medium

Consider a porous elastic medium saturated with a fluid or a gas. The pore fluid rate is expressed, according to the Darcy's law, as follows [15]:

$$V_i = -k\frac{\partial H}{\partial x_i}$$

where k is isotropic permeability, $H = -\frac{P}{\rho g} + H_0$ is the total head, $H_0 = \text{const}$ is the excessive head, ρ is the liquid density, g is the acceleration of gravity, P is pressure.

Since the fluid flow rate from a unit volume of a porous body is given by $e_V = \frac{\partial V_i}{\partial x_i}$, then for an incompressible fluid the value e_V should be equal to the volume decrease rate which, in turn, is equal to the volume decrease rate with the opposite sign $\varepsilon_V = \varepsilon_{ii}$.

Thus,

$$\frac{\partial \varepsilon_V}{\partial t} = k\left(\frac{\partial^2 H}{\partial x^2} + \frac{\partial^2 H}{\partial y^2} + \frac{\partial^2 H}{\partial z^2}\right)$$

or

$$\frac{\partial \varepsilon_V}{\partial t} = -\frac{k}{\gamma_f}\Delta P\,, \tag{6.1}$$

where γ_f is the fluid specific gravity, Δ is the Laplace operator.

By introducing effective σ'_{ij} and total σ_{ij} stresses in a typical way for saturated porous media [4, 10], given by

$$\sigma_{ij} = \sigma'_{ij} + P\delta_{ij}\,, \tag{6.2}$$

one obtains

$$\frac{\partial \varepsilon_V}{\partial t} = \frac{1}{K}\frac{\partial \sigma'_0}{\partial t} = \frac{1}{K}\left(\frac{\partial \sigma_0}{\partial t} - \frac{\partial P}{\partial t}\right)\,, \tag{6.3}$$

where K is the bulk modulus of the soil skeleton deformation ($K = \frac{E}{3(1-2\nu)}$); $\sigma'_0 = \frac{\sigma'_{ii}}{3}$ and $\sigma_0 = \frac{\sigma_{ii}}{3}$ are the mean effective and total stresses, respectively; E is the modulus of elasticity, ν is the Poisson ratio.

Thus, from Eqs. (6.1) and (6.3) one arrives at the equation, which determines the pressure change in a porous medium:

$$C\Delta P = \frac{\partial P}{\partial t} - \frac{\partial \sigma_0}{\partial t},\ C = \frac{kK}{\gamma_f}. \tag{6.4}$$

The equations of equilibrium

$$\frac{\partial \sigma_{ij}}{\partial x_j} = 0, \quad i,j = 1, 2, 3,$$

with the account of Eq. (6.2), enable the pore pressure and the effective stresses to be related by

$$\frac{\partial \sigma'_{ij}}{\partial x_j} + \frac{\partial P}{\partial x_i} = 0 .$$

Assuming the soil skeleton material to obey the Hooke's law

$$\sigma'_{ij} = 2G\left(\varepsilon_{ij} + \frac{\nu}{1-2\nu}\sigma_{ij}\varepsilon_{kk}\right) ,$$

where $G = \frac{E}{2(1+\nu)}$ is shear modulus, $\varepsilon_{ij} = \frac{1}{2}(u_{i,j} + u_{j,i})$ is the deformation tensor, one arrives at three differential equations of elliptic type in displacements

$$\frac{2G(1-\nu)}{(1-2\nu)} \cdot \frac{\partial \varepsilon_V}{\partial x_i} + G\,\Delta u_i + \frac{\partial P}{\partial x_i} = 0 . \tag{6.5}$$

Equations (6.4) and (6.5) are interrelated and should be solved together. Note that the principal complications arise from the term $\frac{\partial \sigma_0}{\partial t} = q(x_i,t)$ in Eq. (6.4), whose value should be set from physical considerations [24]. When $\frac{\partial \sigma_0}{\partial t} = 0$ or $\sigma_0 = \text{const}$ (theory of simple consolidation), Eqs. (6.4) and (6.5) are separated from each other, and the situation is essentially simplified. In this case the system under consideration is similar to the thermoelasticity equation system [11], the equations of both systems coinciding at the substitution of P by $-\frac{E\alpha_t}{1-2\nu}T$, C by κ^2, where a_t is linear thermal expansion coefficient, κ is thermal conductivity coefficient, T is temperature.

Equations (6.4) and (6.5) should be complemented by boundary conditions for total surface forces

$$\sigma_{ij}n_j = \sigma'_{ij}n_j + Pn_i = t'_i + Pn_i = \sigma_i(N) , \quad N \in S_\sigma , \tag{6.6}$$

displacements

$$u_i(N) = f_i(N) , \quad N \in S_u , \quad S = S_u + S_\sigma , \tag{6.7}$$

as well as the initial and boundary conditions for the pore pressure

$$\begin{aligned} &P(N,O) = P_f(N) \quad \text{when } t = 0 , \quad N \in V , \\ &P(N,t) = P_g(N,t) , \quad N \in S_1 , \\ &-\frac{\partial P}{\partial x_i}n_i = P_h(N,t) , \quad N \in S_2 , \quad S = S_1 + S_2 , \quad t > 0 . \end{aligned} \tag{6.8}$$

In order to determine the field of displacements in a medium due to the pore pressure change only (uniform boundary conditions over S_u and S_σ), one can use

Maizel's method for thermoelasticity [9, 11], based on the application of the theorem of reciprocity in an auxiliary state chosen in a special way (with zero temperature). Then an integral representation for the field displacement component u_k is obtained:

$$u_k(\xi,\eta,\varsigma) = -\int_V P(N,t)U_{j,j}^{(k)}(N,K)dV(N)\,, \quad t > 0\,, \tag{6.9}$$

where $N = (x_1,x_2,x_3)$, and $U_{j,j}^{(k)}$ is the dilatation of the stressed state due to a concentrated unit force acting at the point in the direction parallel to the x_k axis. In Eq. (6.9) the pressure function $P(N, t)$ is assumed to be known (e.g., from the experimental data) or to be found according to Darcy's equation (6.4) with the initial and boundary conditions of Eq. (6.8).

The pore pressure can be obtained in an explicit form using a general integral representation [2]

$$\alpha P(N,t) = \int_S \left(F * P - G * \frac{\partial P}{\partial n}\right) dS + \int_V (G * \psi + f \cdot G)dV\,, \tag{6.10}$$

where $\alpha = 1$ for $N \in V$; $\alpha = 0$ for $N \notin V$; ψ is the volume source;
$F(N,t;\ K,\tau) = -\dfrac{\partial G}{\partial x_i} \cdot n_i$ is the directed flow due to G;
G is the Green's function (for an unlimited space)

$$G(N,t;\ K,\tau) = \exp\left(-\frac{r^2}{4(t-\tau)}\right) \cdot [4\pi(t-\tau)]^{3/2}\,;$$

n_i are the direction cosines of an external normal to the boundary S of the domain V; $r^2 = (x_i - \xi_i) \cdot (x_i - \xi_i)$. The asterisk in Eq. (6.10) means the Riemann convolution, determined according to the rule

$$(\varphi * \chi)(x,t) \equiv \int_0^t \varphi(x,t-\tau)\chi(x,\tau)d\tau\,.$$

In practice, the determination of the pressure field $P(N, t)$ for complex-shaped domains using the general integral representation (6.10), is encumbered, hence finite-difference-based [17] and finite-element-based [1] numerical methods as well as approaches, including Laplace transformations and step-by-step processes of time variation with spatial discretization according to the boundary-element method [2], are applied.

Thus, in the case the dilatation function being known, from the given or calculated pore pressure decline variation, displacements of any points of an elastic mass can be obtained using direct spatial integration with the representation of Eq. (6.9).

6.1.2 Dilatation Relations

The efficiency of application of the general integral representation (6.9) for the calculation of displacements of a porous elastic massif due to the pore pressure decline to a great extent depends on the availability of the explicit expression of the dilatation function $\varepsilon_V = U_{j,j}^{(k)}$ for the spatial stressed state. This, in turn, requires the availability of fundamental singular solutions of spatial problems of theory of elasticity $U_i^{(k)}$ (influence functions). In our case, accurate analytical solutions for concentrated forces for the case of infinite domains with boundary condition interfaces are of great interest. First of all, this category of domains includes an elastic homogenous half-space, two coupled half-spaces with different elastic properties and layered half-spaces. For these cases the Green's tensor $U_i^{(k)}(N, K)$ is given in Chap. 1 and in Appendix A. Application of such contact models is well suited for simulating elastic deformations of a layer and the surrounding rock mass in case of functioning of horizontal wells to be considered below.

Elastic half-space. The Green's tensor components in an expanded form

$$\left\| U_i^{(k)} \right\| = \left\{ U^{(k)}, V^{(k)}, W^{(k)} \right\}.$$

for a rectangular (Cartesian) coordinate system are given in Appendix A. Using these formulae and Hooke's law, the expressions $\sigma_{ij}^{(k)}$ for stresses arising in an elastic half-space due to a concentrated unit force, applied at a point $K(\xi,\eta,\zeta)$ in the direction of axis x_k, can be determined in a standard way. Then the dilatation relations are obtained in a standard way according to the known dependences

$$\varepsilon_V^{(k)} = \frac{1-2\nu}{E}\Theta^{(k)} = \frac{1-2\nu}{E}(\sigma_{xx}^{(k)} + \sigma_{yy}^{(k)} + \sigma_{zz}^{(k)})$$

or directly by the definition

$$\varepsilon_V^{(k)} = \frac{\partial U^{(k)}}{\partial x} + \frac{\partial V^{(k)}}{\partial y} + \frac{\partial W^{(k)}}{\partial z}.$$

Detailed computations in the general case lead to extremely bulky equations. The most simple form of the dependences under consideration is obtained in the case of the concentrated force being applied on the half-space surface, when $\varsigma = 0$, $R_1 = R_2 = R$ (i.e. when Boussinesq and Cerruti solutions are used) [8]

$$\varepsilon_V^{(1)} = \frac{1-2\nu}{E}\theta^{(1)} = -\frac{(1-2\nu)(1+\nu)}{\pi E} \cdot \frac{x_1}{R^3}, \tag{6.11}$$

$$\varepsilon_V^{(2)} = \frac{1-2\nu}{E}\theta^{(2)} = -\frac{(1-2\nu)(1+\nu)}{\pi E} \cdot \frac{y_1}{R^3}, \tag{6.12}$$

$$\varepsilon_V^{(3)} = \frac{1-2\nu}{E}\theta^{(3)} = -\frac{(1-2\nu)(1+\nu)}{\pi E} \cdot \frac{z}{R^3}. \tag{6.13}$$

Coupled elastic half-spaces. In order to calculate the deformation of surfaces, bounding the layer, one should know the dilatation functions of the stressed state caused by the concentrated unit forces on the interface of the elastic half-spaces. For this purpose, first of all, the Plevako fundamental solution is suitable [12]. Based on the equations of Sect. 1.3 for the Green's tensor components $U_i^{(k)} = \{U^{(k)},\ V^{(k)},\ W^{(k)}\}$ for the lower half-space, after conventional but cumbersome transformations, one arrives at the sought dilatation equations

$$\varepsilon_V^{(1)} = \frac{1}{16\pi(1-\nu_1)G_2}\left\{(\beta_1 - 2\lambda + \tau - \phi)\frac{x_1}{R^3} + 3(\beta_1+\tau)\frac{x_1 z^2}{R^5} + \right.$$
$$+ 4\chi\frac{x_1 z(2R+z)}{R^3(R+z)^2} - 4\delta\frac{x_1}{R(R+z)^2} + 2\chi\frac{x_1 z(R-z)}{R^4(R+z)} + \tag{6.14}$$
$$\left. + \delta\frac{x_1(R-z)(3R+z)}{R^3(R+z)^2} - \chi\frac{x_1 z(5R+3z)(R-z)(2R+z)}{R^5(R+z)^2}\right\},$$

$$\varepsilon_V^{(2)} = \frac{1}{16\pi(1-\nu_1)G_2}\left\{(\beta_1 - 2\lambda + \tau - \phi)\frac{y_1}{R^3} + 3(\beta_1+\tau)\frac{y_1 z^2}{R^5} + \right.$$
$$+ 4\chi\frac{H_1 Z\,(2R+z)}{R^3\,(R+z)^2} - 4\delta\frac{y_1}{R\,(R+z)^2} + 2\chi\frac{y_1 z\,(R-z)}{R^4\,(R+z)} + \tag{6.15}$$
$$\left. + \delta\frac{y_1(R-z)(3R+z)}{R^3(R+z)^2} - \chi\frac{y_1 z(5R+3z)(R-z)(2R+z)}{R^5(R+z)^2}\right\},$$

$$\varepsilon_V^{(3)} = (\tau - t)\frac{z}{R^3} - \frac{2\phi}{R(R+z)} + \phi\frac{(2R+z)(R-z)}{R^3(R+z)}\,. \tag{6.16}$$

In Eqs. (6.14), (6.15), and (6.16) the following notations are assumed:

$$\chi = 2(\alpha - \beta_1)\,,$$
$$\delta = (3-4\nu_2)\alpha + [1-2(\nu_1-\nu_2)]\beta_1 - 2\lambda\,,$$
$$\phi = (3-4\nu_2)\alpha - [3-2(\nu_1+\nu_2)]\beta_1\,,$$
$$\tau = (2\alpha - \beta_1)\,,$$
$$t = 2(\nu_2-\nu_1)\beta_1 + (3-4\nu_2)\alpha\,,$$
$$\beta_1 = \beta + 1\,,$$
$$\beta = \frac{\mu-1}{\mu(3-4\nu_1)+1},\ \mu = \frac{G_2}{G_1} = \frac{E_2(1+\nu_1)}{E_2(1+\nu_2)}\,,$$
$$\alpha = \frac{8\mu(1-\nu_1)[\mu(1-\nu_1)+(1-\nu_2)]}{(\mu+3-4\nu_2)[\mu(3-4\nu_1)+1]}\,,$$
$$\lambda = 4(1-\nu_1)\frac{\mu}{\mu+1}\,;\quad x_1 = x-\xi\,,\quad y_1 = y-\eta.$$

In case concentrated forces acting at a given depth in the lower (upper) half-space, dilatation relations are obtained in a quite similar way. They are not quoted here because of being too cumbersome. Note that for the case of a three-layer system with an internal productive layer, the dilatation relations are given in Chap. 1 in Fourier transforms (Sect. 1.4.3).

6.2 Distribution of Pressure in a Layer in Case of Functioning Horizontal Wells

6.2.1 Distributed Sources of Predetermined Intensity

Consider a well, whose axis presents a segment of a spatial straight line L between points M_1 and M_2, whose length is denoted as l (Fig. 6.1).

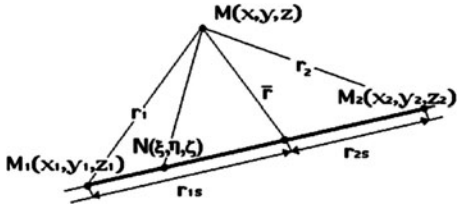

Fig. 6.1 To the determination of pressure near a well of finite length

Let sinks $q(s)$ of a specified intensity, calculated per unit length of the straight line L, be distributed along this segment. Then, the velocity potential $\varphi(x, y, z)$ due to the action of the sinks distributed along straight line L within an infinite space, is given by [15]

$$\varphi(x,y,z) = \frac{1}{4\pi} \int\limits_L \frac{q(s)ds}{\sqrt{(x-\xi)^2 + (y-\eta)^2 + (z-\varsigma)^2}}\,, \tag{6.17}$$

where s is the path length, measured from the starting point M_1 of the straight line L; ξ, η, ζ are Cartesian (rectangular) coordinates of points of this line, $M(x, y, z)$ is an arbitrary observation point.

Since the velocity potential can be written in the form [15]

$$\varphi(x,y,z) = -k\left(\frac{P}{\rho g} + z\right) + C\,,$$

then for the pore pressure one obtains

$$P = P_0 - \gamma_f \cdot z - \frac{\gamma_f}{4\pi} \int\limits_L \frac{q(s)ds}{\sqrt{(x-\xi)^2 + (y-\eta)^2 + (z-\varsigma)^2}} \tag{6.18}$$

where k is the coefficient of filtration, $\rho g = \gamma_f$ is the fluid or gas specific gravity, $P_0 = \text{const}$ is the reference pressure value, with respect to which the extra pressure is evaluated.

Let us reduce Eq. (6.18) to a form, suitable for practical calculations. We determine direction cosines of the segment M_1M_2, based on the relations

$$\cos\alpha = \frac{x_2 - x_1}{\ell}\,, \quad \cos\beta = \frac{y_2 - y_1}{\ell}\,, \quad \cos\gamma = \frac{z_2 - z_1}{\ell}\,,$$

then

$$\xi = x_1 + s \cdot \cos\alpha\ , \quad \eta = y_1 + s \cdot \cos\beta\ , \quad \varsigma = z_1 + s \cdot \cos\gamma$$

and Eq. (6.18) is finally written as

$$P(x,y,z) = P_0 - \gamma_f \cdot z - \frac{\gamma_f}{4\pi} \int_0^{\ell} \frac{q(s)ds}{\sqrt{r_1^2 - 2r_{1S}s + s^2}}\ . \tag{6.19}$$

Here the following notations are used:

$$r_1^2 = (x - x_1)^2 + (y - y_1)^2 + (z - z_1)^2\ ,$$

$$r_{1S} = (x - x_1)\cos\alpha + (y - y_1)\cos\beta + (z - z_1)\cos\gamma\ .$$

At a given function of the sink intensity $q(s)$, the regular integral, contained in Eq. (6.9), can be evaluated numerically with any accuracy, based on a suitable rule of integration. In practice, the $q(s)$ function is most often linear

$$q(s) = q_1 + \frac{q_2 - q_1}{\ell} s\ ,$$

where q_1 and q_2 are the sink intensity values at the beginning and at the end of the well. In this case, the integration is exact and Eq. (6.19) takes the following form:

$$\begin{aligned} P(x,y,z) =& P_0 - \gamma_f \cdot z - \frac{\gamma_f}{4\pi}\left[\frac{q_2 - q_1}{\ell}\left(\sqrt{\ell^2 - 2r_{1S}\ell + r_1^2} - r_1\right) + \right. \\ &\left. + \left(q_1 + \frac{q_2 - q_1}{\ell} r_{1S}\right) \ln \frac{\sqrt{\ell^2 - 2r_{1S}\ell + r_1^2} + \ell - r_{1S}}{r_1 - r_{1S}}\right]\ . \end{aligned} \tag{6.20}$$

Finally, in the simplest case, when $q_1 = q_2 = q = \text{const}$,

$$\begin{aligned} P(x,y,z) &= P_0 - \gamma_f \cdot z - \frac{\gamma_f}{4\pi} \ln \frac{\ell - r_{1S}\sqrt{(\ell - r_{1S})^2 + \bar{r}^2}}{r_1 - r_{1S}} = \\ &= P_0 - \gamma_f \cdot z - \frac{\gamma_f}{4\pi} \ln \frac{(r_1 + r_{1S})(r_2 + r_{2S})}{\bar{r}^2} \end{aligned} \tag{6.21}$$

where $\bar{r}$ is the distance from the point $M\,(x, y, z)$ to the segment M_1M_2, $\bar{r}^2 = r_1^2 - r_{1S}^2$, r_2 is the distance from the point $M\,(x, y, z)$ to the point $M_2(x_2, y_2, z_2)$, $r_2^2 = (x - x_2)^2 + (y - y_2)^2 + (z - z_2)^2$, r_{2S} is the projection of the segment MM_2 on the direction $M_1\,M_2$, $r_{2S} = (x_2 - x)\cos\alpha + (y_2 - y)\cos\beta + (z_2 - z)\cos\gamma = \ell - r_{1S}$.

6.2.2 Account of the Finite Radius of the Well

Potential representation of the pore pressure, Eq. (6.19), and its special cases, Eqs. (6.20) and (6.21), are convenient for engineering calculations, but do not contain some important characteristics of the inflow process to the wells, including the well radius and the size of the feed area. Hence, for the model calculations, along with Eqs. (6.19), (6.20), and (6.21) the following representations will be used. Let a cylindrical surface of radius R_2 (Fig. 6.2a) be treated as the feed area boundary for a well with radius R_1

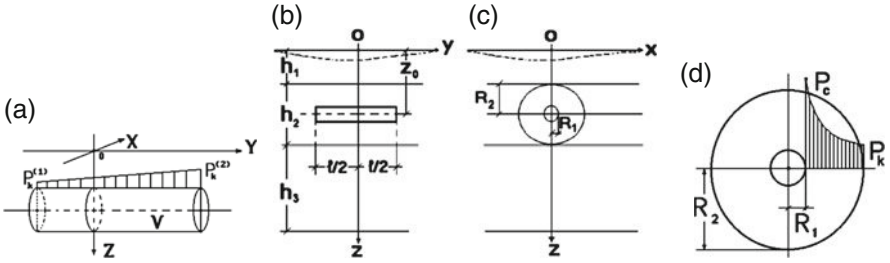

Fig. 6.2 Horizontal well feeding area (**a**, **b**, **c**) and pore pressure distribution in the near-face area (**d**)

In the simplest case, the well axis is considered horizontal, located at a depth z_0. The axes of the spatial rectangular co-ordinate system are chosen in a way, shown in Fig. 6.2a–c. The well length is considered to be equal to l. The pressure distribution is considered to be axisymmetric. In each section, perpendicular to the well axis (Fig. 6.2d), it varies according to a logarithmic law

$$\frac{P - P_k}{P_c - P_k} = \frac{\ln(r/R_2)}{\ln(R_1/R_2)}, \; r = \sqrt{y^2 + (z - z_0)^2} \; . \tag{6.22}$$

Furthermore, it is assumed that the pressure at the feed contour P_k and at the well P_c varies only along the well axis, this variation being linear:

$$P_k = P_k^{(1)} + \left(P_k^{(2)} - P_k^{(1)}\right) \frac{y - y_1}{y_2 - y_1} \; , \tag{6.23}$$

$$P_c = P_c^{(1)} + \left(P_c^{(2)} - P_c^{(1)}\right) \frac{y - y_1}{y_2 - y_1} \; . \tag{6.24}$$

Here $P_k^{(i)}$, $P_c^{(i)}$, $(i = 1, 2)$ are given constant pressure values at the left and the right well ends.

The model representations under consideration are easily generalized for the case of an inclined well with a given orientation within the layer as well as for more complicated laws of the pressure distribution in the feed area of the well. They can be used for quantitative and qualitative description of the processes of spatial fluid flow in a saturated porous medium.

6.3 Contact Problems for Foundation Structures at a Reduced Pore Pressure in the Soil

Sections 6.1 and 6.2 are devoted to the method of numerical modelling of soil mass deformation caused by the pore pressure decline due to oil and gas extraction or functioning of water supply drains. The approach is based on application of integral representations for spatial displacements, according to theory of linear pore elasticity. Mindlin solutions (for elastic half-spaces), Plevako solutions (for coupled half-spaces) as well as any other influence functions with known dilatation functions under spatial deformation can be used as fundamental solutions for the soil skeleton $U_i^{(j)} = \left\| U^{(k)}, V^{(k)}, W^{(k)} \right\|$. In this section, the formulations obtained are used for the description of the processes of spatial contact interaction of shallow and deep foundation structures with the soil mass. Formulations of the contact problems of such type are important due to the following reasons. If the area of the pore pressure reduction is comparable with the size of the foundation structure itself and is located close to it, then such a foundation undergoes inadmissible slopes and settlements which are sometimes very significant and lead to hazardous deformations of above-foundation structures. Besides, it is known that the pore fluid tends to flow to pile foundations what thereby results in the formation of a reduced pore pressure area in the foundation active area [3, 21]. In the course of a pile foundation loading, its additional indentation occurs with the formation of a contact layer on the surface of the stem. At a shear settlement, the grain structure of the contact layer tends to the state with a critical density. Thus, along the contact surface of the pile the conditions for water draining out of the soil are formed, i.e. a drain layer is formed around the pile. As a result, the existing load is increased by growing forces due to the pore pressure decline. All this leads to an additional settlement and sometimes even to the pile breakdown. The latter is especially dangerous in the case of compound pile structures. The analyzed features of behaviour of foundations are not manifested directly after the foundation having been constructed. The described contact filtration effect is revealed after some time, usually, a long period after the end of the foundation construction. As a result, the arising settlements are unexpected and it is difficult to find their reasons at once and to explain them correctly.

Therefore, it is quite clear that the studies of spatial contact interaction of deepened structures in case of a reduced pore pressure in the soil require further development.

6.3.1 Integral Equations of a Spatial Contact Problem

Consider a spatial contact problem for foundation structures located on the ground surface or deepened into the soil either in the vicinity of oil and gas deposits or close to watershed areas. A conventional consideration of the contact interaction here is complicated due to additional settlements caused by the pore pressure decline in the soil.

For further consideration the following assumptions will be made: (1) the foundation structure under study is an absolutely rigid body of a rather arbitrary shape; (2) the structure is subjected to the action of a static spatial system of forces, reduced to a basic force vector and a basic moment which are supposed to be known; (3) the soil base is treated as an isotropic, porous elastic, linearly deformable, homogeneous, weightless half-space; (4) the structure and the soil base are coupled over the contact surface.

The main integral equation of the contact problem is obtained, based on the similarity of consolidation and thermoelasticity problems, by introduction of a basic state and an auxiliary state, using Betti's theorem of reciprocity [11].

$$u_i(K) = \iint\limits_{\Gamma} \sigma_j(N)\, U_j^{(i)}(K,N)\, d\Gamma + \iiint\limits_{V} P(N)\, \Gamma_{k,k}^{(i)}(K,N)\, dV(N). \tag{6.25}$$

Here $K(\xi, \eta, \zeta)$ is the point of application of the concentrated unit force, σ_j are the components of the stress vector, distributed along the surface Γ of the soil base contact with the structure, $u_i(K)$ is the displacement of an arbitrary point K, situated on the contact surface. Equation (6.25) expresses the fact that the value of the displacement $u_i(K)$ is equal to the sum of the works of the arising contact stresses $\sigma_j(N)$ in the basic state on the displacements $U_j^{(i)}$ of the auxiliary state, plus the pore pressure work at the relative changes of the auxiliary state volume $U_{K,K}^{(i)}$, the values of the index $i = 1, 2, 3$ denoting the direction of the concentrated unit force parallel to the X, Y, Z axes, respectively. In Eq. (6.25), as usual, summation over repeated indices is assumed.

Then, similarly to the Sect. 2.1, we take into account the fact that the displacements of any point of the contact surface can be expressed in terms of displacements Δ_x, Δ_y, Δ_z of the whole rigid construction as well as angles of its rotation ψ_x, ψ_y, ψ_z with respect to the coordinate axes as follows:

$$\begin{aligned} U &= \Delta_x - z \cdot \psi_y + y \cdot \psi_z, \\ V &= \Delta_y - x \cdot \psi_z + z \cdot \psi_x, \\ W &= \Delta_z - y \cdot \psi_x + x \cdot \psi_y. \end{aligned} \tag{6.26}$$

The system of integral equations (6.25) in an expanded form is given by

$$\begin{aligned} &\iint\limits_{\Gamma} \left[\sigma_x(N)U^{(1)}(K,N) + \sigma_y(N)V^{(1)}(K,N) + \sigma_z(N)W^{(1)}(K,N)\right] d\Gamma - \\ &- \iiint\limits_{V} P(N)U_{k,k}^{(1)}(K,N)dV = \Delta_x - \zeta \cdot \psi_y + \eta \cdot \psi_z, \\ &\iint\limits_{\Gamma} \left[\sigma_x(N)U^{(2)}(K,N) + \sigma_y(N)V^{(2)}(K,N) + \sigma_z(N)W^{(2)}(K,N)\right] d\Gamma - \\ &- \iiint\limits_{V} P(N)U_{k,k}^{(2)}(K,N)dV = \Delta_y - \xi \cdot \psi_z + \zeta \cdot \psi_x, \\ &\iint\limits_{\Gamma} \left[\sigma_x(N)U^{(3)}(K,N) + \sigma_y(N)V^{(3)}(K,N) + \sigma_z(N)W^{(3)}(K,N)\right] d\Gamma - \\ &- \iiint\limits_{V} P(N)U_{k,k}^{(3)}(K,N)dV = \Delta_z - \eta \cdot \psi_x + \xi \cdot \psi_y. \end{aligned} \tag{6.27}$$

In order to make the system of Eqs. (6.25) and (6.27) we use, as usual, six static equations of equilibrium

$$\begin{aligned}
&\int\limits_{\Gamma}\int \sigma_x(N)d\Gamma = P_x, \quad \int\limits_{\Gamma}\int \sigma_y(N)d\Gamma = P_y, \quad \int\limits_{\Gamma}\int \sigma_z(N)d\Gamma = P_z,\\
&\int\limits_{\Gamma}\int \left[\sigma_z(N)y - \sigma_y(N)z\right]d\Gamma = M_x, \int\limits_{\Gamma}\int \left[\sigma_x(N)z - \sigma_z(N)x\right]d\Gamma = M_y,\\
&\int\limits_{\Gamma}\int \left[\sigma_y(N)x - \sigma_x(N)y\right]d\Gamma = M_z.
\end{aligned} \tag{6.28}$$

Note that the presence of the terms in Eqs. (6.27), obtained from the volume integration over the domain V of the pore pressure variation which do not contain unknown values, makes the pore pressure a loading parameter in the contact problem under consideration together with P_x, P_y, P_z, M_x, M_y, and M_z.

6.3.2 *Finite-Dimensional Algebraic Analogue of the Integral Equation System*

The spatial contact problem under consideration is represented in a rather general formulation by the system of integral equations (6.27) and (6.28), which can be solved numerically by the boundary-element method.

In order to obtain a finite-dimensional algebraic analogue of the system of Eqs. (6.27), we proceed similarly to Sect. 2.2. For this purpose, at first, the contact surface is discretized into triangular and quadrangular boundary elements is performed. Let m be a total number of the boundary contact elements. Then each surface integral in Eqs. (6.27) and (6.28) is substituted by the sum of integrals over individual boundary elements. The approximation of the contact stress functions is assumed to be piecewise constant, and the unknown contact forces are considered in the centres of the gravity of the boundary elements. The integral equations (6.27) with the account of the surface discretization only, are given by

$$\begin{aligned}
&\sum_{i=1}^{m}\left[\sigma_x(N_i)\int\limits_{\Delta\Gamma_i}\int U^{(j)}(K,N)d\Gamma + \sigma_y(N_i)\int\limits_{\Delta\Gamma_i}\int V^{(j)}(K,N)d\Gamma + \sigma_z(N_i)\int\limits_{\Delta\Gamma_i}\int W^{(j)}(K,N)d\Gamma\right] =\\
&= \int\limits_{v}\int\int P(N)U^{(j)}_{k,k}(K,N)dV + \begin{cases}\Delta_x - \zeta\cdot\psi_y + \eta\cdot\psi_z, j=1,\\ \Delta_x - \xi\cdot\psi_z + \zeta\cdot\psi_x, j=2,\\ \Delta_x - \eta\cdot\psi_x + \xi\cdot\psi_y, j=3.\end{cases}
\end{aligned} \tag{6.29}$$

The system of Eqs. (6.29) contains $3m$ unknown forces $\sigma_x(N_i)$, $\sigma_y(N_i)$, $\sigma_z(N_i)$ $(i = 1,...,m)$ and six unknown parameters Δ_x, Δ_y, Δ_z, ψ_x, ψ_y, ψ_z characterizing the displacement of the structure under consideration as an absolutely rigid body. The series of the first $3m$ equations is obtained by the collocation method by sequential substitution of coordinates of the gravity centre of the boundary elements into each equation of Eqs. (6.29) which is true for any point of the contact domain

$$\sum_{i=1}^{m}\left[\sigma_x(N_i)\int\limits_{\Delta\Gamma_i}\int U^{(j)}(K_f,N)d\Gamma+\sigma_y(N_i)\int\limits_{\Delta\Gamma_i}\int V^{(j)}(K_f,N)d\Gamma+\sigma_z(N_i)\int\limits_{\Delta\Gamma_i}\int W^{(j)}(K_f,N)d\Gamma\right]=$$
$$=\int\limits_{V}\int\int P(N)U^{(j)}_{k,k}(K_f,N)dV+\begin{cases}\Delta_x-\zeta_f\cdot\psi_y+\eta_f\cdot\psi_z, j=1,\\ \Delta_x-\xi_f\cdot\psi_z+\zeta_f\cdot\psi_x, j=2,\\ \Delta_x-\eta_f\cdot\psi_x+\xi_f\cdot\psi_y, j=3, f=1,...,m.\end{cases} \tag{6.30}$$

After the surface integral discretization, the equations of equilibrium (6.28) take the form

$$\sum_{i=1}^{m}\sigma_x(N_i)\Delta s_i=P_x, \tag{6.31}$$

$$\sum_{i=1}^{m}\sigma_y(N_i)\Delta s_i=P_y, \tag{6.32}$$

$$\sum_{i=1}^{m}\sigma_z(N_i)\Delta s_i=P_z, \tag{6.33}$$

$$\sum_{i=1}^{m}\left[\sigma_z(N_i)y_i-\sigma_y(N_i)z_i\right]\Delta s_i=M_x, \tag{6.34}$$

$$\sum_{i=1}^{m}\left[\sigma_x(N_i)z_i-\sigma_z(N_i)x_i\right]\Delta s_i=M_y, \tag{6.35}$$

$$\sum_{i=1}^{m}\left[\sigma_y(N_i)x_i-\sigma_x(N_i)y_i\right]\Delta s_i=M_z, \tag{6.36}$$

Thus, one obtains a finite-dimensional algebraic analogue of the system of integral equations (6.27) and (6.28) in the form of (3m+6) linear algebraic equations (6.30)–(6.36) with respect to 3m contact stresses $\sigma_x(N_j)$, $\sigma_y(N_j)$, $\sigma_z(N_j)$ ($j=1,...,m$), three displacements Δ_x, Δ_y, Δ_z, and three rotation anglesψ_x, ψ_y, ψ_z.

The obtained system of Eqs. (6.30)–(6.36) is similar to the system of Eqs. (2.13) and (2.14) for the contact problem without the account of the effect of the pore pressure reduction, the only difference being the fact that Eqs. (6.30)–(6.36) include the terms, caused by the volume integration. Finally they only result in a change of the load vector (the right-hand side vector).

6.3.3 Numerical Algorithm of Solution of the Contact Problem

The matrix notation of Eqs. (6.30)–(6.36) is given by

$$\mathbf{A}\cdot\mathbf{Z}=\mathbf{B} \tag{6.37}$$

where $\mathbf{A} = \begin{pmatrix} \mathbf{D}_{3m\times 3m} & \mathbf{C}_{3m\times 6} \\ \mathbf{T}_{6\times 3m} & 0 \end{pmatrix}$ is a square matrix of the (3*m*+6)-th order, $\mathbf{Z} = \begin{pmatrix} \mathbf{Q} \\ \mathbf{q} \end{pmatrix}$ is the column vector of (3*m*+6) unknowns, these factors exactly coincide with the corresponding ones in Eq. (2.15). The vector of the right-hand side $\mathbf{B} = \begin{pmatrix} H \\ h \end{pmatrix}$ of the same dimensionality as $\mathbf{Z}$ includes six components of the external load as well as a 3*m*- dimensional vector $\mathbf{H}$, responsible for the pore pressure reduction in the domain *V*. In a detailed notation these vectors are given by

$$\mathbf{Q} = \begin{pmatrix} \sigma_{x1} \\ \sigma_{y1} \\ \sigma_{z1} \\ \vdots \\ \sigma_{xm} \\ \sigma_{ym} \\ \sigma_{zm} \end{pmatrix}, \ \mathbf{q} = \begin{pmatrix} \Delta_x \\ \Delta_y \\ \Delta_z \\ \psi_x \\ \psi_y \\ \psi_z \end{pmatrix}, \ \mathbf{H} = \begin{pmatrix} H_{x1} \\ H_{y1} \\ H_{z1} \\ \vdots \\ H_{xm} \\ H_{ym} \\ H_{zm} \end{pmatrix}, \ \mathbf{h} = \begin{pmatrix} P_x \\ P_y \\ P_z \\ M_x \\ M_y \\ M_z \end{pmatrix},$$

where

$$H_{xi} = \int\int_V \int P(N)\varepsilon_v^{(1)}(K_i,N)dV, \ H_{yi} = \int\int_V \int P(N)\varepsilon_v^{(2)}(K_i,N)dV,$$
$$H_{zi} = \int\int_V \int P(N)\varepsilon_v^{(3)}(K_i,N)dV, \ i = 1,2,...,m.$$

Thus, the proposed numerical algorithm includes the following stages: (i) discretization of the contact surface of the foundation structure and the soil into boundary elements; (ii) discretization of the 3-dimensional domain of the pore pressure decline into finite 3-dimensional elements; (iii) calculation of the matrix coefficients at the unknowns and the load vector; (iv) formation and solving of the system of Eqs. (6.37) for various external force values and the given field of the pore pressure variation.

As mentioned above (see Sect. 3.2), the obtained algebraic systems have good conditionality, related to the diagonal predominance that enables one to use the standard solution methods of the Gauss type, without application of special regularization methods.

Here some explanations regarding the determination of the values H_{xi}, H_{yi}, H_{zi}, $i = 1,...,m$ should be made. The details of the numerical integration procedure over standard elements like pyramids, triangular and quadrangular prisms, are given in Appendix H. One should only discretize the given domain *V* of the pore pressure decline into 3-dimensional elements of the types mentioned. Here it seems possible to apply any algorithms for the discretization of complex-shaped spatial objects into 3-dimensional elements. First of all, this applies to the algorithms that are widely used at the finite-element simulation [1, 25]. However, taking into account the specific character of the problems under consideration, we propose the following approach. As a rule, the source of the pore pressure decline in the soil is a direct

sink (drainage, absorbing well with a central axis, etc.), and the form of the whole domain of the pore pressure decline is such that the sections, orthogonal to the sink axis, are of a similar shape. Hence, if a flat domain of a section, which is orthogonal to the preferred axis, is subjected to disretization, the whole domain V can be rather easily discretized into elementary pyramids, triangular and quadrangular prisms. The discretization of the flat domain itself into triangles and quadrangles can be performed using any of the known algorithms (see e.g. [16, 20]). The algorithm of automatic discretization of flat domains of a rather general type is described in detail in Chap. 3. It is sufficiently flexible and optimal and enables the procedure of generation of spatial grids for representation of the 3-dimensional domain of the pore pressure variation by a set of elementary pyramids as well as triangular and quadrangular prisms to be built up based on the geometrical characteristics of the cross-sections. This algorithm enables the mesh grid to be parametrically condensed in the vicinity of the source of the pore pressure decline (the corresponding examples of the discretization will be shown in Sect. 6.4). All this enables the volume integrals, contained in Eqs. (6.30)–(6.36), to be effectively computed using the numerical integration procedures for standard domains (see Appendix H).

6.3.4 Contact Problem for Shallow Foundations

For a visual illustration of the abilities of the approach considered in Sect. 6.3.3, we make some simplifying assumptions. As an object interacting with the porous elastic mass, we consider a shallow foundation structure (an absolutely rigid punch with a flat base of a rather arbitrary shape), resting on the surface of a half-space ($z = 0$). Similarly to the case, considered in Sect. 2.5.1, we do not take into account any friction in the contact domain and assume the punch to be loaded only under a static load reduced to a vertical force P_z and tilting moments M_x and M_y. Then, as usual, we assume that vertical displacements of the punch and the base surface are equal and there is no load outside the punch. Taking into consideration the pore pressure variation in the known domain of the soil mass (of the porous elastic half-space), one should determine the distribution of reaction pressures under the punch and the displacement parameters of the punch as a rigid body.

In this case, instead of three boundary integral equations (6.27), one has only one equation expressing the geometrical condition of the contact of the punch and half-space:

$$\frac{1-\nu^2}{\pi E}\int\limits_F\int \frac{p(\xi,\eta)d\xi\,d\eta}{\sqrt{(x-\xi)^2+(y-\eta)^2}} + \int\limits_F\int\int P(N)\varepsilon_v^{(3)}(K,N)dV(N) = \tag{6.38}$$

$$= W_c + \psi_x\cdot(x-x_c) + \psi_y\cdot(y-y_c)$$

where F is the area of the punch contact with the porous elastic base, $p(x, y) = \sigma_z(x, y, 0)$ is the sought contact pressures function, W_c is the vertical displacement of the punch centre (x_c, y_c), ψ_x, ψ_y are the punch slopes with regard to the OX and

OY axes, respectively, $\varepsilon_v^{(3)}(K,N) = \frac{(1-2\nu)(1+\nu)}{\pi E} \cdot \frac{z}{R^3}$ is the dilatation function for the elastic half-space due to a unit vertical concentrated force acting on the free surface. Taking into account that among the six equilibrium conditions of Eqs. (6.28) in the formulation of the contact problem under consideration. it is sufficient to analyze three integral equations which should be satisfied by the contact pressure field:

$$\begin{aligned} &\int\limits_F \int p(\xi,\eta)d\xi d\eta = P_z, \\ &\int\limits_F \int p(\xi,\eta)\xi d\xi d\eta = P_z \cdot x_c - M_y, \quad \int\limits_F \int p(\xi,\eta)\eta d\xi d\eta = P_z \cdot y_c - M_x. \end{aligned} \tag{6.39}$$

Thus, the spatial contact problem for a punch with a flat bottom, resting on the surface of a porous elastic half-space, is reduced to finding the parameters W_c, ψ_x, ψ_y, determining the punch location and the distribution of contact pressures $p(\xi, \zeta)$ over its bottom. After the punch being indented under the conditions of the pore pressure variation, they will be determined by solving the system of Eqs. (6.23) and (6.24).

For numerical solution of the system of integral equations (6.38) and (6.39) in the approximation of a piecewise constant function of contact pressures $p\ (\xi, \zeta) =$ const, one obtains the following finite-dimensional algebraic analogue in a more compact form than Eqs. (6.30)–(6.36):

$$\begin{cases} p_1\delta_{i1} + p_2\delta_{i2} + ... + p_m\delta_{im} - W_c - \psi_x \cdot (x_i - x_c) - \psi_y \cdot (y_i - y_c) + H_{iz} = 0,\ i = \overline{1,m}; \\ p_1\Delta s_1 + p_2\Delta s_2 + ... + p_m\Delta s_m = P_z, \\ p_1\Delta s_1 x_1 + p_2\Delta s_2 x_2 + ... + p_m\Delta s_m x_m = P_z \cdot x_c - M_y, \\ p_1\Delta s_1 y_1 + p_2\Delta s_2 x_2 + ... + p_m\Delta s_m x_m = P_z \cdot y_c - M_x, \end{cases} \tag{6.40}$$

being a linear equation system with (m+3) unknowns.

Here $p_i = p(\xi, \zeta)$ are contact pressures on the boundary elements, $\delta_{ij} = \int\limits_{F_j} \int \omega(x_i,y_i,\xi,\eta)d\xi d\eta$ are vertical displacements of the base surface at a point (x_i, y_i), coinciding with the centre of gravity of the i-th element, due to a unit load, uniformly distributed over the domain F_j of the j-th element, Δs_i is the area of the i-th element, $\omega\,(x_i,y_i,\xi,\eta) = \left(1-\nu^2\right) \Big/ \pi E\sqrt{(x-\xi)^2 + (y-\eta)^2}$ is the influence function (Boussinesq solution).

While solving the system of Eqs. (6.40), we use the matrix notation:

$$\mathbf{a} \cdot \mathbf{z} = \mathbf{b}, \tag{6.41}$$

where

$\mathbf{a} = \begin{pmatrix} d_{m\times m} & c_{3\times m} \\ t_{3\times m} & 0 \end{pmatrix}$ is a square matrix of the order (m+3), $d = \left\|\delta_{ij}\right\|$, $i,j = \overline{1,m}$;

$$c = -\begin{pmatrix} 1 & x_1 - x_c & y_1 - y_c \\ 1 & x_2 - x_c & y_1 - y_c \\ \cdots & \cdots\cdots & \cdots\cdots \\ 1 & x_m - x_c & y_1 - y_c \end{pmatrix}, \; t = \begin{pmatrix} \Delta s_1 & \Delta s_2 & \cdots & \Delta s_m \\ \Delta s_1 x_1 & \Delta s_2 x_2 & \cdots & \Delta s_m x_m \\ \Delta s_1 y_1 & \Delta s_2 y_2 & \cdots & \Delta s_m y_m \end{pmatrix},$$

Z and **B** are column matrices of the size (m +3),

$$\mathbf{Z} = \begin{pmatrix} \mathbf{Q} \\ \mathbf{q} \end{pmatrix}, \; \mathbf{B} = \begin{pmatrix} \mathbf{H} \\ \mathbf{h} \end{pmatrix},$$

$$[6pt]\mathbf{Q} = \begin{pmatrix} p_1 \\ p_2 \\ \vdots \\ p_m \end{pmatrix}, \; \mathbf{H} = \begin{pmatrix} H_{z1} \\ H_{z2} \\ \vdots \\ H_{zm} \end{pmatrix}, \; \mathbf{q} = -\begin{pmatrix} W_c \\ \psi_x \\ \psi_y \end{pmatrix}, \; \mathbf{h} = -\begin{pmatrix} P_z \\ P_z \cdot x_c - M_y \\ P_z \cdot y_c + M_x \end{pmatrix}.$$

Then the numerical-and-analytical method, described in Sect. 2.3, is used to calculate the surface integrals (both singular and regular) over an arbitrarily oriented boundary element with a polygonal contour. The components of the vector H are computed numerically, using the volume integration formulae in accordance with the discretization of the domain V into pyramids, triangular and quadrangular prisms (Appendix H). An example of the numerical calculation to estimate the pore pressure decline influence on the contact interaction process is given below in Sect. 6.4.3.

6.4 Examples of Numerical Calculations

The technique proposed in Sects. 6.1 and 6.2 for calculating the land surface deformation at oil and gas extraction and underground water withdrawal, is implemented in a PC software *Subsidence-01*, which does not require high-end PCs. According to the algorithm developed, all the above described stages are sequentially performed, the dilatation representations being applied are programmed as a separate routine that enables one to use a wide set of the known fundamental solutions for elastically deformable media, including nonclassical ones with a spatial non-uniformity of physical and mechanical parameters or anisotropy. According to the gas field extraction techniques, variation of the pore pressure in a layer is provided in the developed software product both based on the experimental database and using direct mathematical modelling of the filtration processes. The software outputs the values of the vertical and horizontal displacements of the land surface points and the soil mass for the specified set of observation points. The sought values are recommended to be obtained in the nodes of triangular or quadrangular grids for visual presentation of the results obtained on the basis of the numerical solution interpolation.

Numerical implementation of the method for the calculation of the land surface deformation and the contact deformation of the foundation structures with soil for the case of horizontal wells, developed in Sects. 6.1–6.4 on the basis of the concepts of spatial theory of elasticity, implies the stage of discretization of

the contact surfaces and spatial domains of the well feed into boundary and finite (3-dimensional) elements, respectively**.** For this purpose we use a program for discretization of single and multiply connected flat domains, bounded by linear segments or circular arcs, and a specially developed program for spatial discretization of complex-shaped 3-dimensional objects (mostly with geometrically similar configurations in sections, orthogonal to the specified directions, e.g. to a well axis, arbitrarily oriented within the layer under consideration). Figures 6.3, 6.4, and 6.5 show typical examples of discretization of flat doubly connected sections of spatial domains, bounding the well feed area for different engineering-and-geological conditions. As seen from the figures, the plotted grids enable one to characterize with sufficient accuracy the pore pressure field nonuniformity in the well feed area with the account of the filtration flow nonuniformity.

For visual representation of the possibilities of the approach developed for qualitative and quantitative estimation of the effect under investigation, model calculations have been carried out, part of which is presented below in Sects. 6.4.1–6.4.3.

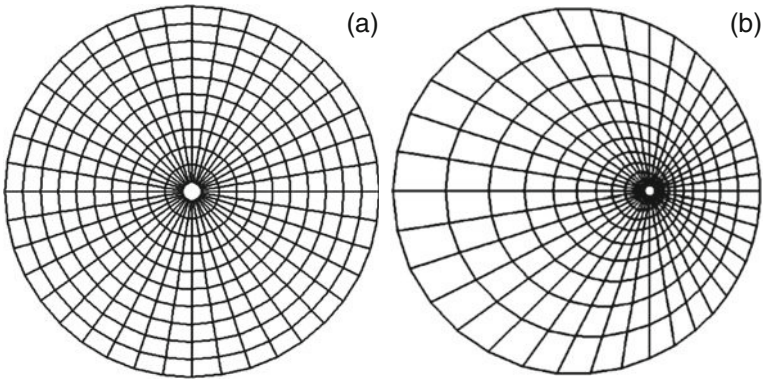

Fig. 6.3 Discretization of a ring-shaped centrosymmetric (**a**) and eccentric (**b**) feeding area with condensation near the horizontal well borehole

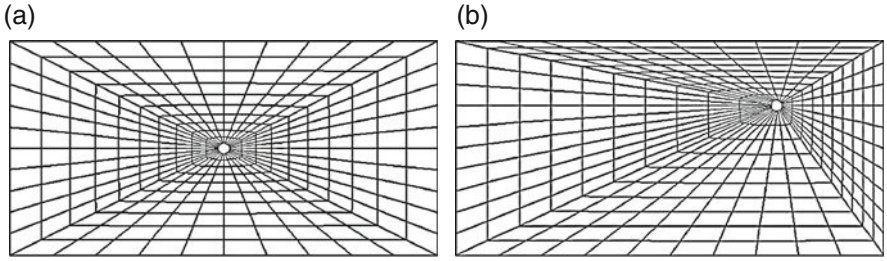

Fig. 6.4 Discretization of a centrosymmetric (**a**) and eccentric (**b**) feeding area with a rectangular contour near the horizontal well

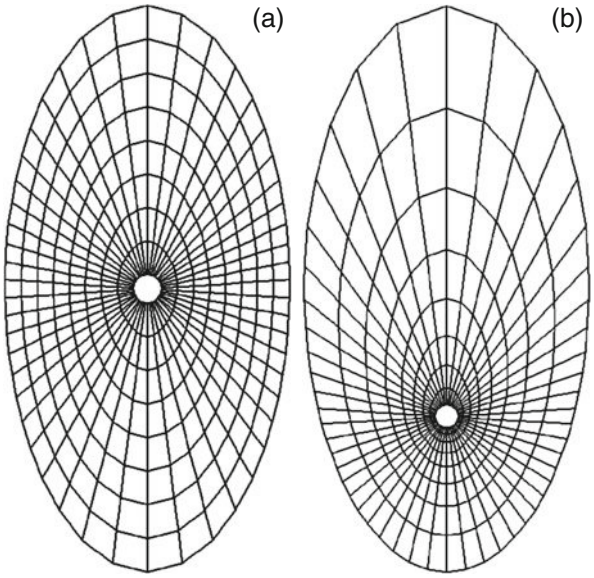

Fig. 6.5 Discretization of an elliptic centrosymmetric (**a**) and eccentric (**b**) feeding area near the horizontal well

6.4.1 Spatial Deformation of the Land Surface

Numerical calculations of spatial displacements of the land surface points are shown in Figs. 6.6–6.12. They were obtained for a horizontal gas well with a length l, whose axis is positioned at a depth z_0 in an elastic homogeneous half-space with the Poisson ratio $\nu = 0.3$. The feed contour of the well was bounded by the productive layer thickness $H_2 = 2\,h$, at the boundaries of which ($R_2 = h$) one assumes $P_k^{(1)} = P_k^{(2)} = 0$. At the well contour ($R_1 = 0.01\,h$) a constant $\left(P_c^{(1)}/P_c^{(2)} = Q = 1\right)$ or linearly variable along the well axis $\left(P_c^{(1)}/P_c^{(2)} = Q \neq 1\right)$ sink was given. In the calculations presented we use dimensionless spatial coordinates

$$\bar{x} = x/h,\ \bar{y} = y/h,\ \bar{z} = z/h$$

and displacements

$$\bar{U} = \frac{U \cdot E}{\Delta P \cdot h},\quad \bar{V} = \frac{V \cdot E}{\Delta P \cdot h},\quad \bar{W} = \frac{W \cdot E}{\Delta P \cdot h},$$

where $\Delta P = -P_c^{(1)}$; E is the soil deformation modulus.

From the calculation data presented one can clearly see the effect of the well depth on the deformation of the elastic half-space free surface (Figs. 6.6, 6.7).

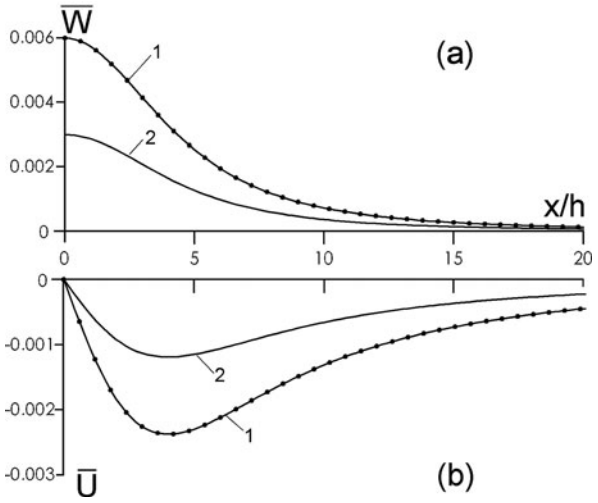

Fig. 6.6 Profiles of dimensionless vertical (**a**) and horizontal (**b**) displacements of the land surface in the cross-section orthogonal to the horizontal well axis ($l = 5\ h$) at different depths, 1: $z_0 = 2.5\ h$, 2: $z_0 = 5.5\ h$

Vertical displacements of the land surface are always of monotonous descending character, their absolute values decrease very fast as they move away from the well. Horizontal displacements, on the contrary, vary non-monotonously, with a specific extremum, located at a distance of the order of the longitudinal size of the well. It is important to note that the maximum absolute values of horizontal displacements appeared almost three times lower than the corresponding values for the vertical displacements, however, their decay rate was sufficiently lower. This feature should

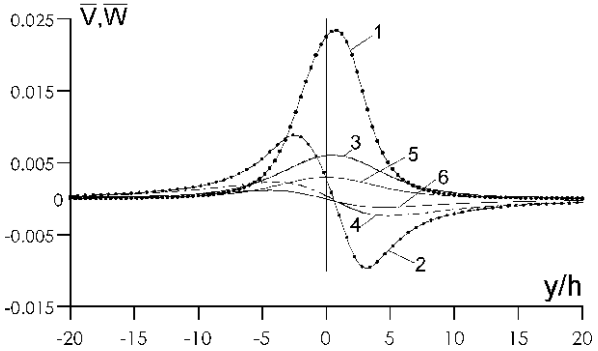

Fig. 6.7 Profiles of dimensionless vertical (1,3,5) and horizontal (2,4,6) displacements of the land surface in the vertical cross-section containing the axis of horizontal wells of different length, (1,2): $l = 10\ h$, (3–6): $l = 5\ h$, at different depths (1–4): $z_0 = 2.5\ h$, (5,6): $z_0 = 5.5\ h$; (1–4): sinks with linear variation of intensity ($Q = 3$), (5,6): sinks with constant intensity ($Q = 1$)

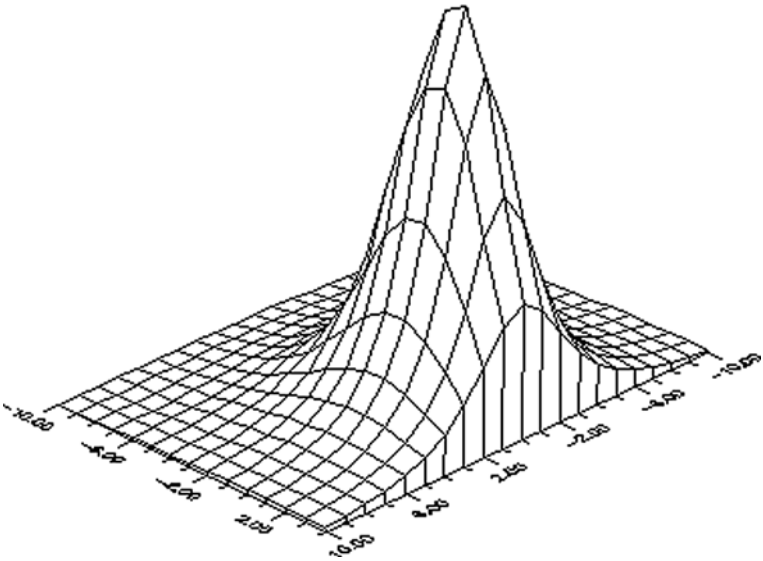

Fig. 6.8 Bowl of vertical deflections of the land surface formed due to a horizontal well functioning

be taken into account while estimating the consequences of functioning of horizontal wells. As one should expect, the irregularity of sink along the well axis makes the pattern of the land surface deformation essentially asymmetrical with respect to the transverse axis of the well (Figs. 6.7, 6.10, 6.11, and 6.12).

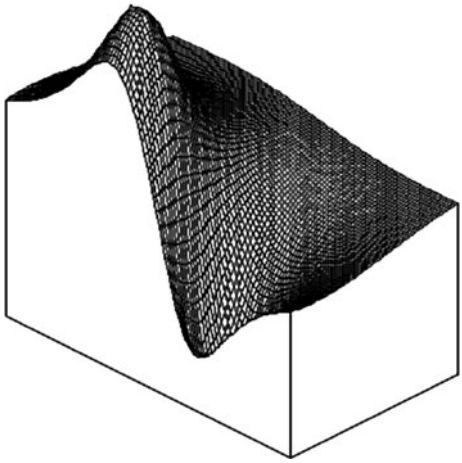

Fig. 6.9 Typical function of horizontal displacements of the land surface at a horizontal well functioning

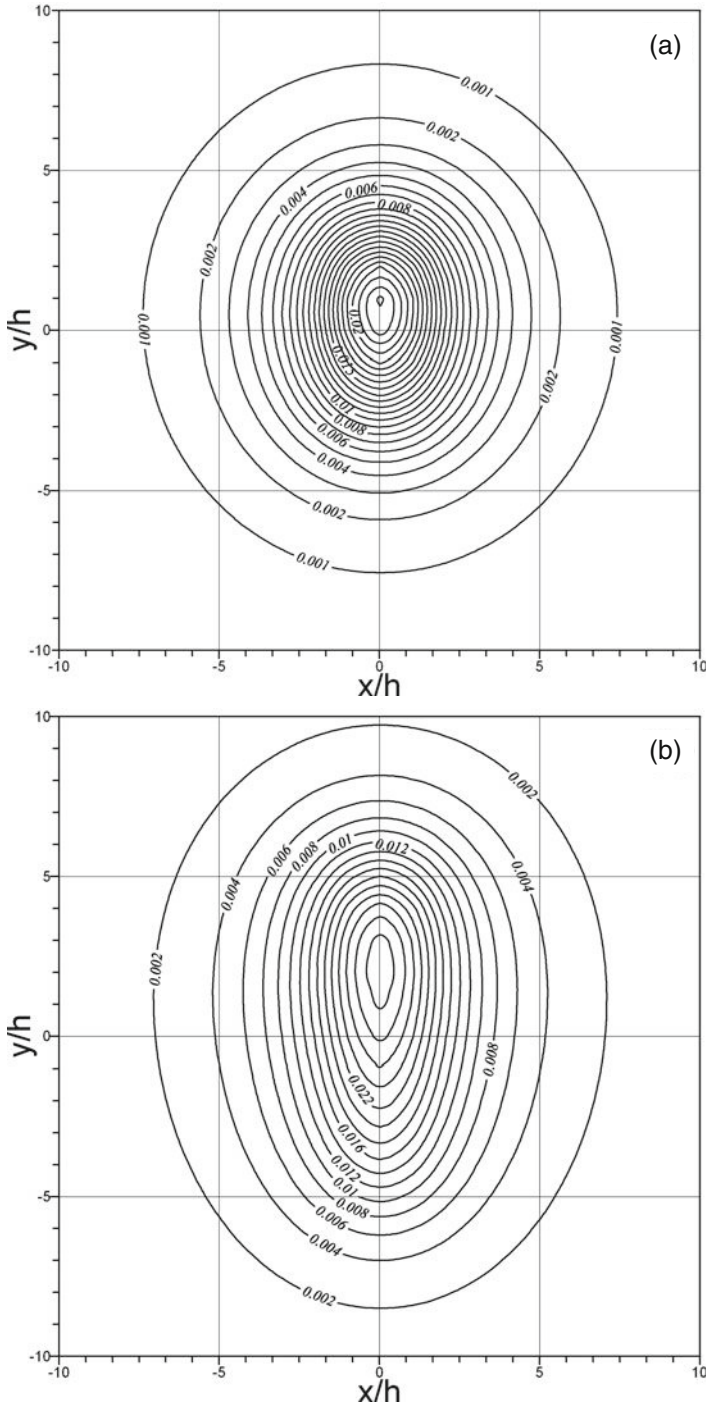

Fig. 6.10 Isolines of vertical displacements $W/(\Delta P \cdot h/E)$ of the land surface for horizontal wells of different length with a linear sink intensity variation ($Q = 3$), (**a**): $l = 5\ h$, (**b**): $l = 10\ h$

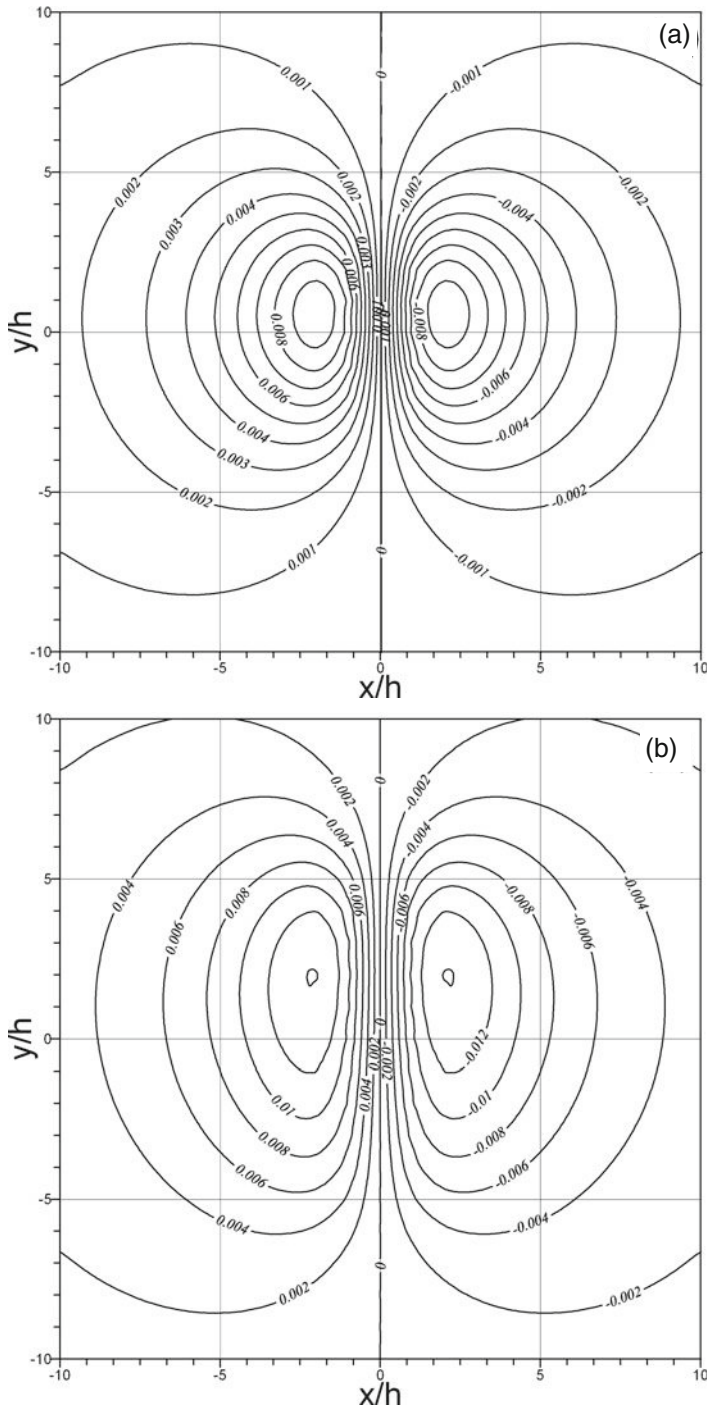

Fig. 6.11 Isolines of horizontal displacements $U/(\Delta P \cdot h/E)$ of the land surface for horizontal wells of different length with a linear sink intensity variation ($Q = 3$), (**a**): $l = 5\ h$, (**b**): $l = 10\ h$

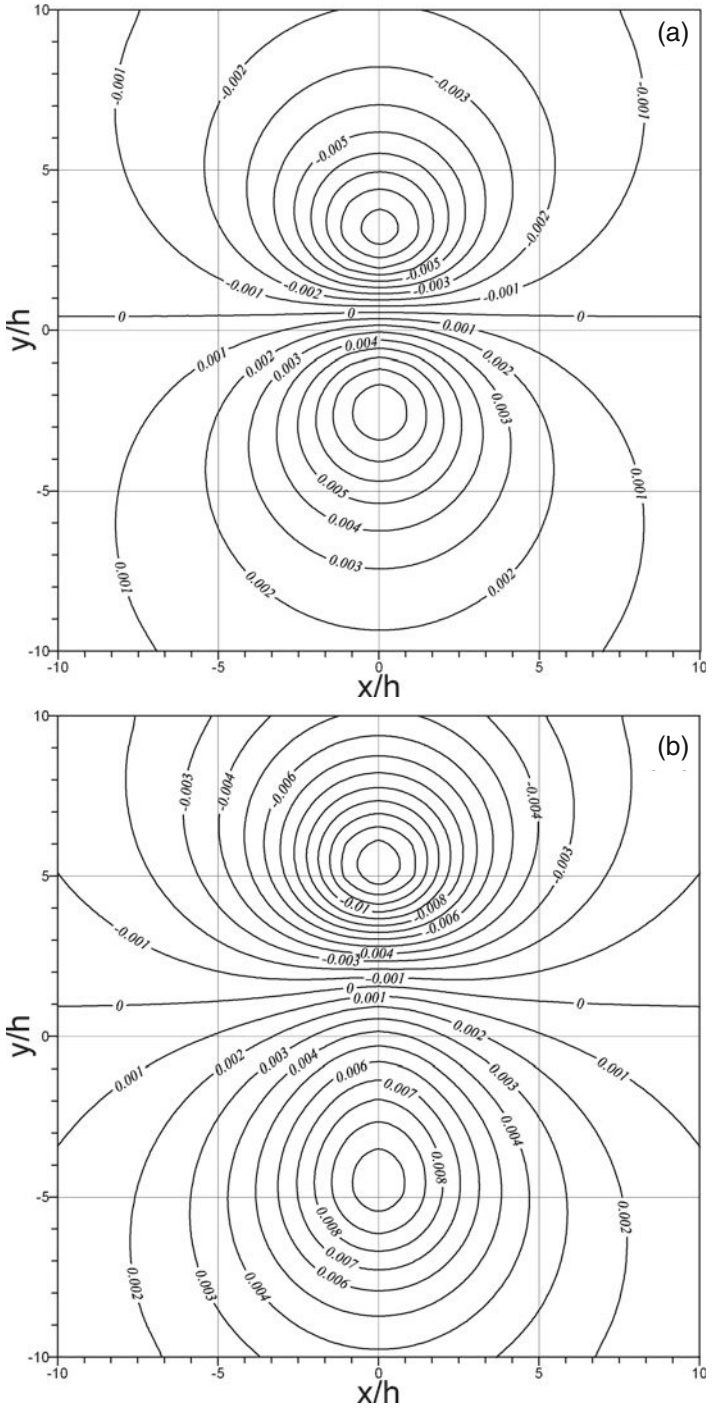

Fig. 6.12 Isolines of horizontal displacements $V/(\Delta P \cdot h/E)$ of the land surface for horizontal wells of different length with a linear sink intensity variation ($Q = 3$), (**a**): $l = 5\ h$, (**b**): $l = 10\ h$

The analysis of the calculations performed has shown the horizontal well depth and length, in comparison with its feed area radius, to be the factors providing the strongest effect on the land surface deformation.

6.4.2 Surface Deformations of the Layer

From the known dilatation relations (6.14–6.16) one can estimate the influence of the elastic properties of the layer and the surrounding rock mass on the deformation of their interface with the variation of the pore pressure in the productive layer. This is important in order to provide stability of the "layer + elastic mass" system and reliability of the horizontal well functioning.

We restrict our consideration to the vertical displacements of the contact surface of two coupled elastic half-spaces (Fig. 6.13). Figure 6.14 shows the calculation data (in the dimensionless form) for relative vertical displacements of two contacting half-infinite elastic masses for $\nu_1 = 0.3$ with the variation of the pore pressure in the oil- or gas-bearing (bottom layer No. 2 in Fig. 6.13). As follows from the calculations performed, the pore pressure decline results in a decrease of deforma-

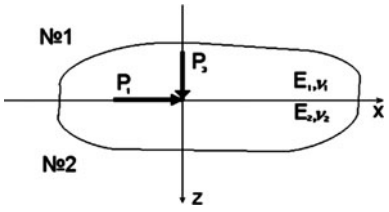

Fig. 6.13 Concentrated forces, acting on the boundary of two coupled elastic half-spaces

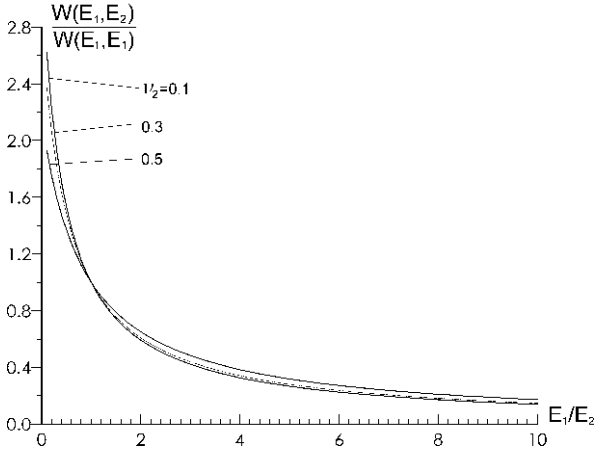

Fig. 6.14 Effect of elastic properties on the displacements of the boundary of the seam and the containing mass

tion the interface between the upper elastic layer and the oil- or gas-bearing layer in comparison with the system, possessing the same deformation parameters $E_1 = E_2$. The influence of the layer compressibilities (ν_1, ν_2) is negligible and can be revealed only if the upper layer deformation modulus is by an order of magnitude less than the deformation modulus of the oil- or gas-bearing layer, $E_1 \langle\langle E_2$.

6.4.3 Settlements and Slopes of Rigid Foundation Plates

Consider an example of numerical solution of a contact problem. Let a square punch with a side $2a$ rest on the surface of a porous elastic half-space and undergo a central loading by a vertical force P. A coordinate system is chosen with the origin in the punch centre, axes X and Y being directed perpendicularly to the sides of the square and axis Z is directed into the half-space.

A source of the pore pressure decrease (a horizontal well, a drain, etc.) with a length l is assumed to be located at a depth $z = z_0$ (Fig. 6.2a). While performing simulations, we consider a cylindrical surface with a radius R_2 (Fig. 6.2b, c) as the feed area boundary for the well with a radius R_1. Pressure distribution is considered to be axisymmetric, in each section perpendicular to the well axis (Fig. 6.2d) and varying according to the logarithmic law Eq. (6.22). The pressure at the feed contour P_k and at the well P_c linearly varies along the well axis according to Eqs. (6.23) and (6.24).

Numerical calculations of the contact interaction parameters for the spatial problem under consideration were performed for a porous elastic half-space with the Poisson ratio $\nu = 0.3$. At the feed contour of the well ($R_2 = a/2$), $P_k^{(1)} = P_k^{(2)} = 0$ was assumed. At the well contour ($R_1 = 0.01a$), a sink, linearly varying along the well axis, was specified ($P_c^{(1)}/P_c^{(2)} = Q = \text{const}$). $z_0 = 2.5a$; $l = 5a$, $Q = 3$, $P = Ea^2$ was taken, E being the soil deformation modulus.

The calculations performed have shown the contact deformation characteristics to be essentially affected by the well location depth and its length ratio to the feed contour radius as well as by the sink intensity parameters. For the example considered, a well located symmetrically with respect to the punch, leads to the punch slope $\psi_y = 4.1671 \cdot 10^{-3}$and settlement $W_c/a = 0.44675 \cdot 10^{-2}$ due to the non-uniform run-off along its axis. One should note for the sake of comparison that the corresponding classical solution of the contact problem for an elastic half-space gives the value of $W_c/a = 0.42032 \cdot 10^{-2}$ with zero slope. As one can see, besides the slope arising, the relative error in the determination of settlement with the account of the pore pressure decrease for the situation considered is 6.3%. The analysis of numerical computations has also shown the influence of the pore pressure variation on the redistribution of contact stresses $p(x, y)$ over the punch footing is negligible. This is explained by a specific character of the spatial contact problem, revealed in an unlimited growth of contact stresses while approaching the punch boundary. If the flexibility of the foundation structure is taken into account, the effect of the pore pressure decrease will be revealed to a greater extent.

Thus, an effective method for calculating the land surface deformation under functioning of horizontal wells in a complete spatial formulation has been developed. It takes into account the nonuniformity of the mechanical properties of the productive layer and the surrounding mass, a non-uniform sink mode along the well as well as its spatial orientation and location depth. The elaborated *Subsidence-01* software has a convenient module structure and enables the sought values of displacements to be obtained with high numerical stability. Discretization of spatial well feed areas of different complexity levels is provided, meeting the practical needs. It seems quite promising to develop an application software package based on the elaborated method that would enable, for a given trajectory of horizontal well systems on a vast territory of industrial extraction at complicated engineering-and-geological conditions, the processes of the well interference and the land surface lowering to be simulated, the optimal modes of oil and gas field operation, applicable from both environmental and technological point of view, to be interactively chosen. Such approach is helpful for the studies of large-scale effects in well drainage areas, providing more realistic predictions of gas extraction characteristics and application of various methods of intensification of intralayer cross flows on vast areas. In other words, the studies of geotechnical processes at oil, gas and water extraction enable, on the one hand, the material loss caused by these processes to be predicted and reduced and, on the other hand, these processes to be employed for controlling the filtration flows for industrial purposes.

Additionally, the model calculations performed have shown that based on the method proposed, one can carry out detailed studies of contact interaction of the soil mass with rigid foundation structures, located close to industrial mining areas and undergoing strong land surface deformation effects caused by the pore pressure decrease. Meanwhile, slopes and settlements of foundation structures with the development of oil and gas deposits or withdrawal of underground water are predicted with a sufficient accuracy. The corresponding algorithm of numerical calculation is based on the boundary-element method and enables one to estimate the deformation of bases of shallow and deep foundation structures under a system of spatial loads of general type. From the obtained solution of the contact problem one can calculate the stress-strained state of soil in the foundation active area and predict its slopes and displacements with the account of the processes of the pore pressure decline in the soil.

Among the important advantages of the approach proposed one should mention the absence of any iterative algorithmic processes, numerical stability of the results obtained that follows from the integral representation of the numerical solutions, as well as acceptable computation times required for practical purposes.

References

1. Altenbach J, Sacharov A S (eds.) (1982) Die Methode der Finiten Elemente in der Festkörpermechanik. Fachbuchverlag, Leipzig
2. Banerjee P K, Butterfield R (1981) Boundary element methods in engineering science. McGraw-Hill, New York

3. Bartolomei A A, Omelchak I M, Yushkov B S (1994) Principles of the prediction of pile foundation settlements. Stroyizdat, Moscow (in Russian)
4. Biot M A (1941) General theory of three-dimensional consolidation. J Appl Phys 12: 155–164
5. Bondar A L, Subbotin I E (1993) Study of land surface deformation in the area of Shebelynka gas field. Geod Kartogr (issue 4): 22–24 (in Russian)
6. Chernykh V A (1989) Geodynamics of processes of development of oil and gas fields. In: Problems of increase of efficiency of technology of natural gas field development. VNIIGAZ, Moscow, pp. 12–21 (in Russian)
7. Corapcioglu M Y (1984) Land subsidence – a state of the art review. In: J. Bear and M J. Corapcioglu (eds.) Fundamentals of transport phenomena in porous media. Noordhoff, Dordrecht, pp. 371–444
8. Johnson K L (1985) Contact mechanics. Cambridge University Press, Cambridge
9. Maizel V M (1951) Temperature problem of theory of elasticity. Ukr Acad Sci Publ., Kyiv (in Russian)
10. Nikolaevsky V N, Basniyev K S, Gorbunov A T et al. (1970) Mechanics of saturated porous media. Nedra, Moscow (in Russian)
11. Nowacki W (1970) Teoria sprezystosci. PWN, Warszawa
12. Plevako V P (1969) A point force inside a pair of cohering half-spaces. Soil Mech Found Eng 6: 165–169
13. Plotnikova L M, Flyonova M G, Machmudova V I (1990) Induced seismicity in the Gazly gas field region. Gerlands Beitr. Geophysik. Leipzig 99: 389–399
14. Poland J (ed.) (1984) Guidebook to studies of land subsidence due to groundwater withdrawal. UNESCO, Paris
15. Polubarinova-Kochina P Ya (1977) Theory of motion of ground waters. Nauka, Moscow (in Russian)
16. Sakalo V I, Shkurin A A (1985) Universal program for triangulation of a two-dimensional domains of an arbitrary shape with grid condensations. Probl Prochn (issue 1): 106–108 (in Russian)
17. Samarskiy A A, Gulin A V (1989) Numerical methods. Nauka, Moscow (in Russian)
18. Scott R F (1979) Subsidence: a review. In: Saxena S K (ed.) Evaluation and prediction of subsidence. ASCE, New York, pp. 1–25
19. Segall P, Yerkes R F (1990) Stress and fluid-pressure associated with oil-field operations: a critical assessment of effects in the focal region of the earthquake. In: Geological survey. Professional paper, pp. 259–272
20. Segerlind L J (1976) Applied finite element analysis. J Wiley & Sons, New York
21. Sobolevskiy D Yu (1994) Strength and bearing capacity of dilatating soil. Nauka i Tekhnika, Minsk (in Russian)
22. Tsytovich N A, Ter-Martirosyan Z G (1981) Fundamentals of applied geomechanics in engineering. Vysshaya Shkola, Moscow (in Russian)
23. Word Oil's Handbook of Horizontal Drilling and Completion Technology (1991). Gulf Publishing Company, Houston
24. Zaretskii Yu K (1967) Theory of soil consolidation. Nauka, Moscow (in Russian)
25. Zienkiewicz O C (1971) The finite element method in engineering science. McGraw-Hill, London
26. Zotov G A, Chernykh V A (1992) Geodynamic processes at development of hydrocarbon fields. In: Geotechnical problems of development of natural gas fields. VNIIGAZ, Moscow, pp. 24–30 (in Russian)

Chapter 5
Calculation of Bases for Rigid Complex-Shaped Deepened Foundations According to the Second Limiting State in a Three-Dimensional Formulation

Abstract In the fifth chapter boundary-element method is applied to calculate contact interaction of foundation structures with soil, taking into account the deepening factor. The need for spatially based calculation of bases of deepened foundations is explained. The principles for foundation structure calculations from the base deformations are briefly reviewed as well as the existing problem formulations and solution methods for spatial problems of contact interaction of deepened foundation structures with soil bases. Solutions of spatial contact problems for deepened monolithic-type foundation structures most widely used in the recent years are also considered, namely for (1) pyramidal piles; (2) foundations made of short vertical or inclined bored piles with caps; (3) bored pile foundations with support extensions; (4) slot foundations with the longitudinal cross-section of various shape. Heterogeneous stress-strained states of the base are taken into account as well as the formation of cavities between the soil and the foundation structures. The effect of the foundation shape on its displacement and slope at various spatial loading is estimated quantitatively. Numerous examples show the results of the boundary-element modeling to be in good agreement with the experimental measurements performed for spatial foundation structures, in most cases boundary-element method results being closer to the experiment than those obtained by other known calculation methods.

Large scale of engineering and related capital expenditures have set the problem of reduction of the engineering cost due to the decrease of consumption of materials and labour as well as the increase of the level of technology. Solution of these problems requires a rapid increase of development and implementation of efficient engineering structures, in particular, in foundation engineering.

There is a great variety of modern foundation structures related to the specific features of buildings and structures, methods of their construction, properties of soils in their bases, combinations of loads acting on them, etc. [19, 26, 31, 47, 50, 59, 65, 78, 90, 91, 94, 95, 97, 98, 100, 102, 136, 138, 149, 157, 160, 171, 172, 199, 202, 205, 206, 211, 218, 220, 224, 215, 227, 236, 244, 247]. Most of such foundations are traditional, the technology of their construction and methods of calculation having been well elaborated in practical engineering.

S.M. Aleynikov, *Spatial Contact Problems in Geotechnics*, Foundations of Engineering Mechanics, DOI 10.1007/b11479_5, © Springer-Verlag Berlin Heidelberg 2011

However, along with the advantages, many of the known foundation types, from the point of view of modern science and engineering, do not fully provide the required efficiency of foundation structures which should combine reliability, low labour consumption, speed of construction, reduced consumption of materials, etc. In order to reduce the labour consumption for the construction of foundation, new types of foundations are developed, more economical in comparison with the foundations of traditional type [224].

New solutions are related mostly to the improvement of the shape of the deepened parts of foundations and, consequently, to the development of special technologies of their construction. Among the new types of foundations elaborated in the recent years one should note some efficient modern structures with a complex-shaped deepened part, which have not yet been described in special literature.

At present, the most industrial foundation type are pile foundations, hence for them numerous attempts have been made to increase the pile bearing capacity by variation of their shape. Examples of successful application of some types of piles (triangular, pyramidal, trestle, with widenings, etc.) are quoted in the literature.

An effective trend to reduce the cost of foundations under buildings with strutted structures is the application of compaction piles of wegde-shaped and pyramidal type [79]. An improvement of the design of these piles consists in a cradle for a half-frame toe along the pile diagonal. The studies performed show the specific bearing capacity of such piles to be increased by 20–25% due to the increase of the soil back pressure area and application of a vertical load with high eccentricity.

A pyramidal displacement pile with a T-shaped cross-section in the medium part and a solid head was developed and found applications in Belarus [99]. The studies have shown that pyramidal displacement piles with a T-shaped cross-section, having the volume smaller than solid pyramidal piles (by a factor of about 1.9), are not worse than the latter in the soil base bearing capacity and meet all regulation standards in rigidity, crack-proofness, and strength.

Piles with *self-unfolding blades* with increased bearing capacity, were developed in Perm Technical University [11, 22, 23]. A pile consists of a shaft, in the lower part of which a widening in the shape of the self-unfolding blades is mounted. Due to afterdriving or under an applied load the pile settles together with the soil above the area of the blades, i.e. works as a small pile group. The experiments show that in the base of such piles a complex stress-strained state of the soil of the active area is formed, affecting the further functioning of the loaded pile.

A hollow *conical pile* is an example of a relatively new efficient foundation structure. The results of extensive experimental studies [14, 15, 144] have shown the hollow conical piles to possess high engineering and economical parameters. The efficiency of their application increases with their length.

A collaboration of technical universities of Perm and Mariy El [12] has resulted in the development and implementation of piles with a longitudinal sector-shaped cutout. Due to a broader involvement of soil into functioning, pile foundations *with a longitudinal cutout* provide high specific bearing capacity and low material consumption.

Among non-traditional efficient solutions of pile foundations for structures being erected on slopes, one should mention piles of reinforced concrete with a cross-section in a shape of an equilateral triangle [48]. *Piles with triangular cross-section* possess a developed lateral surface (with respect to the required direction) and, in comparison with traditional prismatic piles, higher bending rigidity. Piles with triangular cross-section are also efficient for construction of structures on a flat terrain when they are subject to horizontal loads, constantly acting in a fixed direction.

For construction of low-rise buildings a design and technology for strong foundations in the shape of *reverse arches*, deepened into soil, is proposed [191]. The internal contour of the arch elements is parabolic and the external one is a circular arc of a larger radius. The functioning of the arch-shaped foundations cannot be reduced to the conditions of a flat problem due to their length and width being approximately the same.

For a number of objects of rural engineering, being constructed in rock, sand, and clay soils in a stabilized state, *foundations with an inclined bottom* are used [160]. Construction of the foundations with an inclined bottom is most appropriate in the case of a considerable horizontal load to be transferred to the base, i.e. when the above-foundation structure is a strutted system of arc or frame type. A shortcoming of the foundations of such type is a low accuracy of their calculation method, involving numerous tables and nomographs.

Pile foundations and piles with a non-traditional shape of the below-grade part can be an efficient way to reduce vibrations for foundations under machines [199]. The studies of behaviour of piles with a variable shaft geometry (trapezoidal, pyramidal, with the shaft widening at the tip (alpha piles) and in the upper part) in a broad range of variation of the vibration direction and frequency, as well as dynamical load value at vertical and horizontal loading are reported in [81–83, 200, 237]. In particular, application of piles with one or several widenings of the shaft is shown to be appropriate. For the foundations under a horizontal load, application of piles with widenings in the upper part of the shaft is recommended. The main conclusion of the investigations performed is that construction of foundations with a complex shape of the below-grade part enables multiple reduction of the below-grade part volume with a corresponding saving of materials, the rigidity properties being preserved or even improved.

An example of short foundation structures of non-traditional shape can be *anchor structures*, applied for high metallic funnels, power transmission line supports, pipeline supports at irrigated territories. Among the anchor structures a special attention should be paid to the one with a shaft of a variable cross-section, proposed in [80] to reduce labour consumption and increase its reliability. In the longitudinal direction the structure has a wedge-like shape with anchor lugs on the inclined sides, their widened side facing the soil surface like a herringbone. Evidently, in order to provide efficient and reliable functioning of such anchor structures, especially under a pulling load, a calculation method for the base deformations in an essentially spatial formulation should be developed. Since in this case the contact

between the anchor and the soil will be violated, the method should undoubtedly take into account unilateral constraints.

Spatial foundations of structural type (with inclined panels) for ever-frozen soils are less investigated, but promising in view of the efficiency of their functioning and reduction of material consumption [145], as well as cross-shaped piles with diagonal reinforcement for bearing-wall residential buildings [32], pyramidal-prismatic foundations of short piles under strutted structures [113], prismatic, T-shaped, and pyramidal piles with a cantilever under strutted loads for construction sites on bases with an upper layer of humified or fill soil [170].

The quoted references to the literature regarding foundation structures with a complex-shaped deepened part do not exhaust the known sources and are just typical examples which can be further extended.

A considerable progress has been achieved in theory of foundation structure calculation what follows from a vast literature, including manuals, instructions, and handbooks. Nevertheless, many issues have still not been developed enough for practical solutions. For example, calculations of foundation structures, providing their reliable functioning, should, on one hand, be as reliable as possible, and, on the other hand, avoid excessive safety factors, implying unjustifiable expenditures of concrete and reinforcement. An optimal solution for these contradictory problems can be found only as a result of high-precision calculations for the foundation + base system.

For some foundation structure types there are either no recommendations for calculations, or they are not described sufficiently in special literature. Therefore, designers often encounter a number of difficulties and often use rather approximate and insufficiently substantiated calculation methods. As a result of such a situation, an additional safety factor is introduced into the approximately calculated foundation structures, this leading to the increase of material consumption. On the other hand, due to the low accuracy of the calculations, the foundation structures appear not reliable enough what results in a decrease of their lifetime or in emergency events.

Requirements for compliance with the Construction Rules and Regulations 2.02.01–83 [207], instructions for designers, and handbooks lead to cumbersome and labour-consuming calculations (especially for the foundations of a complex geometrical shape). In many cases the calculations are performed by iteration, with numerous tables and handbook data being invoked. As a consequence, in order to simplify the calculations, the dimensions of the foundation structures are taken a priori larger than the optimal required values. For the foundations with given dimensions, load values are reduced by using reliability coefficients that are not always substantiated.

For many foundation types, no special calculation methods, taking into account their structural features, friction resistance over the lateral surface and various combinations of acting forces and moments, have been created at all. For the calculation of new types of foundation structures a specially corrected scheme is created, based on assumptions and pre-conditions resulting, as a rule, in the application of an already known calculation method, in some cases being quite approximate. Often

the calculations are performed using an analogy with the known simplified methods, the simplest elastic soil model, based on the Winkler hypothesis, is used. Calculations according to the Construction Rules and Regulations 2.02.01–83 do not take into account the interaction of the foundation lateral surface with the soil and, therefore, the character of the unilateral constraint functioning in the areas of the structure uplifting from the base is not reflected.

Thus, due to the specific structural features of foundations, the insufficiency of the existing approaches to the foundation base calculation is evident. Broader and more universal approaches to the calculation of foundation structures are required, including non-traditional foundations, demanding more precise calculation methods. It should be also noted that the issue of the correct choice of the modified calculation scheme is of extreme importance as well in view of the spatial type of functioning of most of the foundation structures due to a combined action of vertical, horizontal, and momental loads.

Among the modern numerical methods that have found applications for calculation of structures in various fields of engineering, one should first of all mention the boundary-element method. Due to its sufficient universality, indifference to the shape of the structures, convenient data input, and possibility of consideration of infinite domains, this method is undoubtedly effective to calculate bases for foundations with a complex-shaped deepened part.

In the present chapter, the boundary-element method is used to analyze the results of mathematical modelling of the joint functioning of soil bases with complex-shaped rigid foundations under spatial loading of general type. The calculations are performed according to the method of solving a spatial contact problem of a rigid deepened punch, modelling the foundation. Numerical experiments are performed in two variants – with and without the account of unilateral constraints on the contact of the foundation with the soil. The calculation method is implemented in the *Rostwerk* software that does not require large computer resources.

Examples in Sect. 5.3–5.6 demonstrate the most typical calculations of base deformations for deepened foundation structures of monolithic type, having become most widely spread in the recent years:

(1) pyramidal piles,
(2) foundations of short vertical or inclined bored piles with pile rafts,
(3) bored pile foundations with support widenings,
(4) slotted foundations with different longitudinal cross-sections.

These sections are preceded by Sect. 5.1 where general information is given regarding the principles of calculation of foundation structures from the base deformation, and Sect. 5.2 with a brief review of the existing formulations and methods of solving spatial problems of contact interaction of deepened foundation structures with soil bases.

5.1 General Information on the Calculation of Bases for Foundation Structures from the Deformations

Design of foundation structures required an optimal solution to be found, providing fail-safe functioning of the structure. This is achieved by performing the calculations according to the principle of the limiting states [67, 101, 115, 215, 224]: forces, acting on the base, and stresses, displacements, and deformations, arising in the latter, should be restricted by corresponding limiting values.

Calculations according to the limiting states are divided into two groups [67, 115, 215, 224].

The first group includes carrying capacity-based calculations when the restrictions are introduced, enabling one to avoid excessive irreversible plastic deformation, deformations of creep, damage, resonance vibrations, etc. In case the limiting conditions of this group being violated, the base becomes completely unsuitable for the foundation structure functioning.

The second group is formed by deformation-based calculations, enabling such values of settlements, upheavals, horizontal displacements, deflections, slopes, vibration amplitudes, etc. to be set, for which no problems arise with normal functioning of the structures and their long-term reliability. Violation of the second-group calculation conditions, depending on the excess of the joint deformations of bases and structures over the limiting values, can result either in a state of the structure, unsuitable for normal functioning, or in its complete functional unsuitability.

Construction Rules and Regulations 2.02.01–83, taking into account a variety of features of interaction of foundation structures with bases, ordain the necessity of calculations for the bearing capacity in four most dangerous cases and for deformations – in all cases without exception [207]. Thus, for industrial and civil engineering, calculation according to the second group of limiting states (base deformations) is decisive.

Base deformations are caused by various reasons and can be of the following type [224]:

- *settlements* – deformations due to the soil compression (without changes of their structure) under an external load as well as the influence of neighbouring structures, the intrinsic weight of the soil,
- *collapsing* – deformations due to the soil compression (with a change of their structure) under an external load and the intrinsic weight of the soil as well as due to such processes as soaking of collapsing soils, thawing of frost soils, etc.,
- *upheaval*or *shrinkage* of the base surface – deformations, related to the change of volume of some soils due to physical or chemical processes (frost heave, swelling, chemical ground stabilization, etc.),
- *subsidence* – deformations of the land surface due to mining, soil excavation at underground construction work, intense water intake, etc.,
- *horizontal displacements* – common deformations of bases and structures at high values of horizontal components of the total load (at the erection of sheet

pile constructions, retaining walls, foundations of spacer structures, etc.) as well as at large vertical displacements of the ground surface at settlements and collapsing,

non-uniform deformations of the base – due to the soil nonhomogeneity within the construction site and misadjustment of loads on separate foundations.

The following basic types of the common deformations of a structure and its base are considered.

An important quantitative characteristics of settlement or horizontal displacement of a separate foundation is its *absolute displacement W*, determined as vertical and horizontal displacements of a selected point of the foundation (on its bottom, edge, on the base surface level, etc.) or as their average displacement, respectively [70, 115, 215, 224].

From the W values, known for different foundations, the non-uniformity of the base deformations is evaluated. For example, the *average settlement*of the base $\overline{W}$ can be estimated from the equation

$$\overline{W} = \frac{\sum_{i=1}^{n} W_i A_i}{\sum_{i=1}^{n} A_i}$$

where W_i is the absolute settlement of the i-th foundation, A_i is its base area. Knowing the values W_i (i=1,. . .n) along with $\overline{W}$, one can choose the design solutions to reduce the settlement non-uniformity.

In order to evaluate additional forces, arising in structures under a non-uniform deformation of bases, a *relative settlement non-uniformity* for two foundations is introduced into consideration:

$$\hat{W} = \frac{|W_2 - W_1|}{L}$$

where L is the distance between the foundations.

The foundation *slope* ψ in the simplest case can be defined as a ratio of the difference of settlements of the extreme points of its bottom to the distance between them

$$\psi = \frac{W_\alpha - W_\beta}{L}.$$

The foundation slope value enables one to estimate additional forces in the foundations as well as in the above-foundation structures.

In case forces acting on the foundation ends in different directions, a torsionof the structure arises. In order to characterize the spatial functioning, a *relative torsion angle* θ is introduced into consideration, its value enabling the additional forces in bearing structures and ceilings to be evaluated.

Non-uniform settlements of foundation structures arise additional stress in the latter, what can result in the formation of cracks and even to the structure breakdown, while slopes and deflections can violate the normal functioning of the equipment installed. Therefore, the design of foundation structures implies a condition of all kinds of deformation not to exceed the limiting values set by the project (the second group of limiting states) [115, 215]:

$$W \leq W_{LIM} \tag{5.1}$$

where W is the generalized displacement of the foundation (the foundation edge, the pile head, etc.), determined by calculation according to one of the recommended methods, W_{LIM} is the admissible generalized displacement of the foundation, given as a reference value, depending on the building strength and deformability as well as on the requirement to the building functioning and installation of equipment. The W_{LIM} value can be modified according to the design assignment or to the combined calculation of the base + foundation + building system.

In some cases, according to the tables of the Construction Rules and Regulations, deformations due to the soil shrinkage and swelling as well as to the suffusion-related base settlement, are determined.

The values of W and W_{LIM} can mean all the above mentioned deformation types: (1) absolute vertical settlement of the base of a separate foundation, (2) horizontal displacement of the foundation, (3) average settlement of the base of the structure, (4) relative non-uniformity of settlements of two foundations, etc.

Thus, the deformation-based calculation of the foundation bases is performed with the account of the common functioning of the building and the base. The limiting values of the common deformation of the base and the structure in the course of the building functioning (soil compression, swelling, collapsing, suffusion-related settlement) are set from the technological or architectural requirements as well as from the conditions of strength, stability and crack-proofness of the structure. Only in the case the structures being not intended to bear the forces arising at the common functioning with the base, and the W_{LIM} values being not set in the design assignment, the limiting values of the base deformations (relative settlement difference, slopes, average or maximal settlements, etc.) for different structures are set in accordance with the tables of the Construction Rules and Regulations [207].

The condition of Eq. (5.1) is reduced to a condition

$$P \leq P_{LIM} \tag{5.2}$$

where P is the load on the foundation; P_{LIM} is the load corresponding to the admissible displacement. The conditions of Eqs. (5.1) and (5.2) are written for the simplest cases of loading in a selected direction. At complex spatial loading, in the general case vertical, longitudinal, and transverse displacements arise; consequently, the displacement and load become vectors and the W and P values mean the absolute values of the corresponding displacement and load vectors, respectively

$$W = \sqrt{W_x^2 + W_y^2 + W_z^2},\ P = \sqrt{P_x^2 + P_y^2 + P_z^2}.$$

Besides, for some cases of spatial loading a restriction of the type of Eq. (5.2) should be also introduced for momental loads.

Consider some examples of typical conditions of calculations of foundations from the base deformations.

Instructions [67] give recommendations regarding calculation and design of foundations for machines with operation-related dynamical loads due to the action of unbalanced forces and moments, motion of masses, impacts of moving or falling parts of the machines, including foundations for machines with rotating parts, machines with crank mechanisms, forging hammers, precast reinforced concrete forming machines, pile drivers, crushers, rolling equipment, metal-cutting machines, and rotating furnaces.

According to [67], the foundation vibration amplitudes should satisfy a condition

$$A \leq A_{adm} \tag{5.3}$$

where A is maximal amplitude of the foundation vibrations determined from the calculations, A_{adm} is the maximal admissible amplitude of the foundation vibrations. The A_{adm} value can be modified according to the design assignment.

If due to the machine operation vertical A_V, horizontal longitudinal A_{HL} and transverse A_{HT} vibrations arise, then the condition of Eq. (5.3) is recommended to be used in the form

$$\sqrt{A_V^2 + A_{HL}^2 + A_{HT}^2} \leq A_{adm}.$$

The vibration amplitudes A_V, A_{HL}, and A_{HT} should be determined from a system of differential equations of vertical and horizontal-rotational vibrations of the foundation [67].

Calculation of pile foundations according to the second-group limiting conditions (based on deformations) under vertical loading is carried out, based on a condition [224]

$$S \leq S_U$$

where S is the deformation of the pile foundation base (settlement and relative settlement difference), determined by the calculations, S_U is the limiting admissible value of the pile foundation base deformation, determined from the Construction Rules and Regulations 2.02.01–83 or set by the design assignment.

The pile foundation settlement is determined as for a nominal foundation, transferring to the soil a uniformly distributed pressure in the horizontal plane passing through the lower ends of the piles. Due to the functioning of the lateral surface of

the piles, the nominal foundation bottom size is taken bigger than the pile group lateral size.

Foundations of piles, working as end-bearing piles, do not require calculations based on the deformations due to the vertical load.

Calculation for pile foundation displacements due to horizontal loads and moments consists in the fulfillment of conditions

$$U_p \leq U_u; \psi_p \leq \psi_u$$

where U_p and ψ_p are the calculated values of the pile head horizontal displacement and its rotation angle, respectively, U_u and ψ_u are their limiting values, set in the design assignment.

Prediction of additional settlements of bases under reconstructed buildings is recommended [225] to be performed by a special calculation in two stages: (1) calculation of the initial (before the reconstruction) stress-strained state of the base, (2) determination of the additional settlement of the foundation after the reconstruction. The first stage enables one to estimate the base settlement value over the period before the reconstruction and to build up a scheme of local non-uniformity in the base of the existing foundation with pointing out the soil compression (decompression) zones, determining their size and configuration. This enables the variants and schemes of the foundation reinforcement to be assigned in a more substantiated way. Further, the deformation-based calculation of the base under reconstruction can be carried out from the condition

$$S \leq S_U, J \leq J_U$$

where S is the additional settlement of the foundation as per the calculation, due to the load increase under the reconstruction, S_U is the limiting additional settlement, J is the calculated skew of two neighbouring foundations after the reconstruction, J_U is the limiting skew value.

The limiting value of the additional settlement of a building after the reconstruction S_U can be within the first approximation determined from the condition

$$S_U = K_C \cdot S_{\max,U}$$

where $S_{\max,U}$ is the maximal limiting settlement, recommended by Appendix D of the Construction Rules and Regulations 2.02.01–83 for a new construction, K_C is the coefficient of reduction of the limiting settlement value due to the structure ageing (at the wear of 20% K_C=0.4, at the wear above 30% K_C=0.3). In order to determine the additional settlements, various numerical methods are used as well as the methods of layer summation, equivalent layer, limited compressible thickness, etc.

Base deformations due to the soil compression are determined by calculation from analytical and approximate solutions, obtained by simplifying assumptions [70, 101, 115, 215, 224] (the method of a linearly deformable half-space or a

limited-thickness soil layer; the layer summation method, the equivalent layer method), as well as by approximate numerical methods of calculation (the finite-difference method, the finite-element method, the boundary-element method), using the apparatus of mechanics of condensed media, applied mathematics and computational engineering [66, 116].

In order to calculate foundation bases according to the second-group of limiting states we apply the BEM, being the most efficient among the known numerical methods for solving engineering problems of essentially spatial type for linearly deformable soil masses. Appraisal and improvement of the developed method will further enable this method to be spread to the cases of elastoplastic deformation of soil bases, processes of consolidation, creep, etc. when numerous specific features of the soil media are taken into account and the linear solutions remain the basic ones.

As noted above, most of the practical methods of calculation of settlements of structures are based on using a linear dependence between the settlement and the load at any intensity of the latter. In fact, the development of domains of plastic deformation with the load increase results in a nonlinearity of the settlement-vs-load plot. Therefore, in case the foundation structures being designed using linear calculation methods, the following condition is introduced:

$$\sigma \leq R$$

where σ is the average stress over the foundation bottom and R is the calculated soil resistance, admitting the development of areas of plastic deformations to the depth of a quarter of the foundation width and being determined from the Construction Rules and Regulations [207]. In other words, at $\sigma > R$ the Construction Rules and Regulations do not guarantee the correct value of the settlement of the structure, determined from the linear calculations. It should be also noted that the value of the linearity limit of the quarter of the foundation width is rather arbitrary and not substantiated for different types of soils. For example, the calculations [70] have shown that at high internal friction angles of soils $\varphi > 20°$ the linearity of the settlement-vs-load plot is preserved far beyond R. Practically, for such soils the solutions of theory of elasticity can be used for settlement determination within a small error up to the loads of $2 \cong 3\ R$ and even more.

To a considerable extent the introduction of the value R is caused by insufficient development and practical implementation of solutions of nonlinear problems of soil mechanics [70, 224]. With the development of techniques for mathematical modelling of elastoplastic (nonlinear) deformation of soils, more possibilities are open to determine settlements at any stage of loading, up to the limiting value.

The only possibility to estimate the reliability of the existing methods for the calculation of foundation bases is the comparison of the base settlement values, determined from the calculation (W_c) and from the field observations (W_f). Sotnikov [216] generalized and analyzed long-term field observation data regarding the settlements of a great number of buildings and structures in comparison with the calculation data for the same values. In order to perform such a comparison, over

200 research papers have been analyzed with the observation data regarding the settlements of several hundreds buildings and structures in different countries of the world after 1938. Average settlement values were compared as well as characteristics of the settlement non-uniformity (maximal difference, deflections, skews, slopes). Objects under investigation were residential and industrial buildings of various type (brick, bearing-wall, skeleton-type), round-type structures (funnels, towers, tanks), rectangular-shape structures, extended structures (concrete dams, sluices), etc. A both-side spread of the calculated values was revealed, the errors reaching hundreds per cent both sides. Based on the results of observations and calculations from many publications, it was concluded that coincidence of the calculation results with the measurement data can be treated as a mere accident. In most cases calculations resulted in considerable errors. It is also noted that for loose soils (oozes, varved clays, peaty sand-clays, etc.) the settlement calculation results in lowered data (in 72% cases). For dense soils (bedrock of various composition – clays, marls, limestones, till of semihard and hard consistency, sand, etc.) W_c in most cases (78%) appeared higher than W_f (the calculations result in overstated data). In the first case the understatement of W_c is dangerous, since the error does not increase the safety factor. However, the increase of W_c by factor of 1.5–2, proposed by some authors, found no reflection in the Construction Rules and Regulations. The main result of an extensive and detailed study of Sotnikov [216] is the conclusion: reliability of determination of the calculated values of W_c at present stage of development of foundation construction and soil mechanics is absolutely insufficient for efficient design.

Section 5.2 contains a review of the existing approaches to the calculation of foundation bases (with the account of the deepening factor), their specific features being noted and a short comparative characteristics being given. It also contains information on the practical possibilities of the calculation methods proposed in the literature. Restrictions for their application for the design of foundation structures of an essentially spatial type are also given.

5.2 Spatial Problems for Calculation of Foundation Bases with the Account of the Depth Factor

An extensive literature is devoted to the problem of foundation base calculation based on their deformation. Studies [51, 71, 99, 243, 244] give a review of formation of modern calculation schemes, taking into account the spatial character of the base and foundation functioning under a load. The variety of the calculation methods is related to the existence of a great number of models, being various modifications of the Winkler model, the elastic half-space model as well as numerous nonlinear (elastoplastic) models.

Winkler model. Due to its simplicity and convenience, the most widely spread in practice ate methods based on the hypothesis of a coefficient of subgrade reaction (Winkler model). The simplest solutions in this case are obtained when the foundation calculation scheme is taken as an absolutely rigid body [51, 87, 88, 98, 217, 244]. Note that most of the shallow foundations correspond to such calculation

scheme. In this case, depending on the longitudinal-to-transverse dimension ratio, the foundations are considered as three-dimensional bodies or as rods. In the latter case the load from the rod to the base is supposed to be transferred via fictitious areas whose dimensions are chosen in a specific way. The proposed methods differ in a number of components of the soil reactive forces being taken into account. In [51, 87, 98] two coefficients of subgrade reaction (in vertical and horizontal directions, respectively), determining the soil back pressure normally to the foundation surfaces, are introduced into the calculation. For a more adequate modelling of contact interaction over the foundation bottom, Zavriyev and Shpiro [244] introduce an additional coefficient characterizing the foundation shift in the horizontal direction (exactly equal to half of the coefficient of subgrade reaction in the vertical direction). Kiselev [88] and Ten [217] in their solutions fully take into account the base reaction, using all components of the soil reactive back pressure. For a better fit of the proposed calculation models to the real functioning of a foundation in the soil, the coefficients of subgrade reaction are supposed to be linearly [51, 87, 88, 98] or arbitrarily [244] variable with depth. The sought foundation settlements, displacements, and slopes are found by invoking equilibrium equations, displacement method, and the principle of superposition.

A scheme of a foundation in the form of an elastic bar has been widely spread for the calculation of long piles. In this case, when the soil base is described using the Winkler model, the calculation methods [84, 111, 209, 242] are well elaborated, experimentally substantiated, and form a basis for the instructions on pile foundation design [68]. A theoretical basis for the calculation methods used in the quoted papers, is a fourth-order differential equation of simple bending of beams [203]. By invoking a system of equations of the initial parameter method [226] solutions have been obtained at various boundary conditions at the pile ends [111, 242]. For the coefficients of subgrade reaction triangular [242] or trapezoidal [111, 209] profiles were used. Reference [84] gives numerical solutions for a triangular and a trapezoidal coefficient of subgrade reaction profiles, practically coinciding with the results of [209], however, being obtained on the base of a specially developed numerical approach using the possible displacement method and integral equilibrium equations.

Elastic half-space model. Method of calculation of deepened foundations based on base deformations using the elastic half-space model have not been widely developed due to essential mathematical difficulties. This concerns calculation schemes of foundations not only as three-dimensional bodies, but also as an elastic or a rigid rod.

The problem of a horizontally loaded absolutely rigid rod, interacting with an elastic half-space, was first considered by Zhemochkin [245]. The essence of the proposed approach is reduced to a substitution of the contact between the rod and the elastic isotropic linearly deformable half-space by a point contact using arbitrary rod constraints. The resolving system of canonical equations is obtained based on the mixed method of engineering mechanics after cutting the above constraints and introduction of a rigid fixation on the rod axis. Friction forces on the contact of the fixation and the soil are not taken into account. The canonical equation system

coefficients are sought using the fundamental solution for a unit horizontal force acting near the half-space boundary. Later, in [117] the fundamental Zhemochkin solution was generalized for a soil medium with a variable deformation modulus. A further development of the Zhemochkin method for the calculation scheme of a foundation as a nondeformable rod was performed by Levenstam [108]. He considered a granular medium of Kandaurov type [73] as the soil base model and elaborated a corresponding fundamental solution for a unit horizontal force. One should note that the results, obtained for the granular medium and for the elastic half-space, are qualitatively similar.

The simplest implementation of the Zhemochkin method is proposed in [19, 100] where a simplified approach is developed by means of restriction of the number of constraints by two pairs only. It also takes into account the anisotropy of the soil base properties in the horizontal and vertical directions. For this purpose, the soil deformation modulus, determined using a vertical punch, is multiplied by a reduction coefficient 0.8. Such assumption enables the higher deformability of the base in the horizontal direction to be taken into account in the simplest way. Note that solutions, using the Zhemochkin method for a linearly deformable half-space [19, 117, 245], later were used as a basis for the recommendations for calculation of pile foundations for vertical and horizontal loads [93].

A pile deformation in the approximation of simple bending is considered by Simvulidi [203], using the nonhomogeneous half-space model with a smoothly variable deformation modulus. After the pile length having been partitioned, simplifying assumptions are made. First, the friction forces at the contact between the pile and the soil base are neglected. Second, no mutual influence of the pile partitions is supposed. Then the soil deformation modulus within each of the partitions is averaged and the function, approximating the base reaction, is taken as a third-order polynomial of the reduced coordinate for each partition. After the force method being applied, the proposed approach enables a closed system of linear equations to be formed for the unknown coefficients of each polynomial.

For the design and evaluation of functioning of deepened foundations like bored piles, anchor foundations, etc., a solution of the problem of a deepened punch settlement in a spatial formulation is required. For example, bored and pyramidal piles transfer a considerable part of load to the soil by means of a footing whose base is a rigid deepened punch. Besides, the foundations of various structures, as a rule, are located not on the surface, but inside the soil. Rather approximate solutions for the settlement of rigid foundations incorporated into a linearly deformable half-space, have been obtained based on the Mindlin's solution. They are determined as average vertical displacements of a uniformly loaded circle [198] or rectangle [106], treated as nominal rigid foundations. In order to obtain more exact settlement values, one should apply solutions of spatial contact problems of deepened punches. Direct solving of such problems is known to be rather difficult and not always justified for engineering calculation purposes.

The labour-consuming solution of contact problems can be avoided if, due to some speculations, one can predict the contact pressure distribution over the foundation bottom. In [109, 110] approximate values for the rigid deepened punch

settlements are obtained using the semi-inverse method, when for setting the contact pressures a known exact solution of the problem of a circular rigid punch on a half-space surface is invoked. In order to take into account the displacement pile tip functioning, in [204] the Boussinesq solution for the settlement of a round punch on a half-space surface is used, with an additional coefficient 0.5 being introduced. This assumption is rather rough, it can be used only for the displacement piles, for which the cross-section radius is small in comparison with their length.

Settlements of rigid foundations with small relative depth values (h/a=0.5, 1.0) were determined in [197] using the solution for a rigid punch on a half-space. The contact pressure distribution under the deepened punch is given similarly to the punch on a half-space, with a 6th order polynomial being added to take into account the foundation deepening. The contact pressure profile under a deepened rigid punch appeared to be practically the same as for a punch on the surface of an elastic half-space. This enabled the author of [163] to find the settlement of a round rigid deepened punch as well as vertical compressive stress under, based on the Mindlin's solution with the contact pressure distribution over the bottom according to the Boussinesq law. A good agreement of the obtained solution with the results of [198] (the difference does not exceed 4%) has shown the assumptions, performed in [163] for the determination of a circular rigid deepened punch settlement, to be correct. For practical convenience, [163] also gives tabulated values of the dimensionless punch settlements for different Poisson ratio values ν and relative depths h/a.

The elastic base settlements are shown to be noticeably reduced with depth [106, 198], what, in turn, affects the displacements of rigid foundation structures and the internal force distribution in flexible structures. Therefore, for rational design of foundation beams and plates, as exact as possible solutions are required, based on the analysis of spatial contact problems for deepened rigid punches.

Ogranovich [133, 134] has solved numerically spatial problems of determination of the settlement of centrally loaded round and rectangular foundations located at a given depth form the surface of a linearly deformable elastic isotropic half-space. In both cases the solution is reduced to the canonical equations of the mixed method of engineering mechanics. The author uses the improved Zhemochkin method of piecewise uniform elements [246], being, in fact, the simplest form of the boundary-element method. The canonical equation system matrix is determined using the Mindlin vertical displacement function. For the rigid punch the contact domain is meshed into separate elements with a shape of a circle (the central element) and rings with their thickness decreasing near the contour. For the rectangular punch the contact domain is meshed into a grid or rectangular elements, condensing towards the angular points. Within each element the soil back pressure was assumed constant. The optimal number and size of the elements are determined by test calculations for punches located on the half-space surface, when there is an exact solution for a circle (according to Boussinesq [219]) or an approximate solution for a rectangle [54]. The calculations have convincingly shown that the account of the foundation deepening results in an essential decrease of the settlement in comparison with the same foundation resting on the half-space surface (for the circular foundation at the relative depth h/b=5 and ν=0.35 the settlement decrease

was 66%). Simultaneously an important for practical purposes conclusion is made on a quite small error, introduced by non-accounting of the pit, on the bottom of which the foundation structure is located. Note that the same author considered in the spatial formulation the problem of a beam, deepened into an elastic half-space, loaded by a concentrated force or a uniformly distributed load [132]. The deepening effect was also revealed in an essential decrease of bending moments both under the concentrated force (of the order of 30% at relative depth $h/b=10$ and flexibility index $t=10$) and under a uniformly distributed load (of the order of 100%).

Solutions of contact problems of plate-type objects deepened into an elastic medium are of considerable interest for the estimation of functioning loads on anchor-type structures. The calculation scheme in the form of a low anchor plate, fully bonded with the soil, presents a rather adequate model for the case of a flat anchor domain, formed in a saturated soil mass. In this case the contact is provided by the cohesive forces and the intrinsic weight of the soil weakly affects the axial rigidity at low depth.

The solution of the problem of a rigid anchor disk, fixed into an isotropic elastic infinite medium, was first given in [24]. This solution was developed by Selvadurai [176–178] for a transversely isotropic elastic medium with the account of the plate flexibility as well as under an eccentric load. The problem of the anchor plate can be considered as a limiting case of a spherical anchor subject to an axial load. Such solutions were developed in [74, 175] based on the application of the singularity method and using the expansions over spherical harmonic functions. In [251] these studies were extended to the case of transversely isotropic media. Non-classical effects related to partial uplifting of the anchor plate from the soil, were considered by Keer [77] and Selvadurai [183]. Similar phenomena, related to anchor plates, deepened into crumbling domains, localized in an elastic space, were studied in [181, 188]. The generalized rigidity-related properties of anchor plates, deepened into a transversely isotropic medium or resting on a surface of separation of two contacting half-spaces, were studied in [179, 184]. Due to essential mathematical simplifications, many solutions for anchor plates in an infinite elastic space can be obtained in an analytical form. However, one should keep in mind that the assumption of the elastic medium infinity is justified only for the cases when the anchor plate is deepened into the elastic base by a sufficiently large distance from the surface.

In the case when the anchor plate is located near the elastic-half-space boundary, the load-free plane makes an essential influence on the rigidity-related characteristics of the deepened anchor plate. The mathematical formulation of the contact problem for a rigid disc-shaped anchor, deepened into an elastic half-space, was first considered in [62]. Besides the main attention in this paper being paid to the consideration of the effect of the compressed elastic medium, the authors also consider an uplifting effect on the contact surface of the plate and the soil. Besides, for shallow soil anchors the solution of the contact problem of a disc, deepened into an elastic half-space, was used for in situ tests on loading conventional and helical plates [185, 186], and Rower and Booker [165] numerically studied contact problems for anchors, horizontally deepened into an elastic half-space.

Contact problems for anchors, deepened into a homogeneous and a nonhomogeneous half-space, were studied by means of variation schemes and discretization procedures in [152, 155]. An axisymmetric problem for a rigid disc, deepened into a half-space, when the conditions for common displacements on the boundary surface being fulfilled only partially, is considered in [135]. Some specific aspects for a disc anchor in an elastic half-space were considered in the review papers [121, 122]. Later Selvadurai [189] solved an interesting from the practical point of view problem of the influence of the surface load on a disc anchor, deepened into an elastic half-space. An elastostatic problem for an absolutely rigid anchor disc (a round plate of neglectably small thickness), deepened into a half-space, welded with the elastic medium and subject to an axial loading, is considered in [182]. The problem was solved using the Hankel transformation and reduced to a system of the second-order Fredholm equations with subsequent numerical implementation. The calculation results were presented by the plots of the plate settlements versus its distance from the half-space surface and, in fact, represent the anchor axial rigidity depending on its depth.

Less known are solutions for the calculation scheme of a foundation as a spatial block, when for the soil base an elastic half-space model is applied and, consequently, Mindlin equations are to be used for the displacements under concentrated forces in the directions of the coordinate axes. The possibility of the Mindlin's solutions to be used was first substantiated by Gersevanov already in 1948, with the limits of applicability being indicated [49]. However, due to considerable mathematical difficulties at the integration of the fundamental Mindlin's solutions, no general approaches to the calculation of deepened foundations of spatial type according to the second group of limiting states have been developed yet. In scarce studies some Mindlin's solutions were used for geotechnical calculations (under the action of a vertical or a horizontal force). Lapshin, using the Mindlin's solutions, considered an issue of determination of additional horizontal and vertical stresses on the boundary of a bored pile under loading due to the resistance of a clay soil over the lateral surface above the considered cross-section [102]. Separate Mindlin's solutions were applied by Vasilenko, Petrenko, Orobchenko, Tsymbal for the calculation of piles in sands [139, 140].

In relatively recent papers by Ogranovich [129, 130] the Mindlin's solutions were successfully used for the calculation of rigid piles of variable cross-section (pyramidal and conical) subject to horizontal, vertical, and momental loads. Besides, the same author, for the calculation of rigid pyramidal piles under horizontal and momental loads, took into account formation of a gap between the foundation and the soil [131]. The engineering method of calculation of pile foundations with the account of the depth factor, developed in detail by Ogranovich, is discussed in Sect. 5.3.1, specially devoted to the calculation of rigid pyramidal piles under spatial loading.

A combined deformation of cylindrical piles and the surrounding homogeneous mass under a central load was considered in [125, 127]. The soil was considered as a linearly deformable half-space with the average deformation modulus E_o and lateral expansion coefficient ν_0. The pile deformability was taken into account according

to the Hooke's law as compression of a straight short beam with a deformation modulus E. The contact is supposed to be a full cohesion of the pile and the soil. The mutual influence of the pile and the soil is approximated by a system of fictitious forces, acting along the pile axis and related by boundary conditions at the contact surface. The pile length is divided into n equal partitions. The authors assume the fictitious forces to act in the centre of each partition and at the tip level. Tangentail stress within the lateral surface of each partition is assumed constant. It is calculated using the Mindlin's solution for a horizontal unit force applied inside an elastic half-space. The problem is solved by the finite-difference method, based on the relationship between the variation of the fictitious forces and the tangential stresses at chosen neighbouring partitions of the pile. The proposed approach enables the pile settlements to be determined with the account of its geometry (length and cross-section diameter) without any preliminary assumptions on the tangential stress distribution character. The numerical investigations performed have shown that at a considerable relative depth the pile material compressibility essentially affects the stress distribution character and the pile settlements. In particular, at the diameter d=0.3 m, length L=6 m, n=10, E_o =30 MPa, E=15·10^4 MPa, and axial load N=200 kN the pile material compression was 0.6 mm, or 22% of the pile head settlement (2.7 mm). Later the method, having been proposed in [125, 127], was applied for the problem of studying stress and displacements in the soil in case a vertical static load being transferred by a conical pile [126]. In order to simplify the calculation scheme, the conical pile was proposed to be considered as a telescopic one with the account of the load transfer by ledge rings and cylindrical lateral surface of each telescopic part of the pile.

A method, applicable for rigid off-centre loaded pier foundations [104], appeared to be rather general and simultaneously experimentally substantiated. The method is based on the application of partial solutions for a separate partition of the contact surface, obtained on the base of the Mindlin's solutions for an isotropic and homogeneous elastic half-space. In order to find the general solution, the finite-difference method is applied. The calculation results appeared to be in a good agreement with the experimental data.

The elastic half-space model was used for the calculation of short cylindrical bored piles subject to a spatial load system of a general type [63, 64]. The pile body was assumed to be non-deformable, no slippage of the soil particle with respect to the pile surface was assumed. The calculation was based on the potential method [228]. The contact interaction model took into account unilateral constraints, not working in tension, and under compression having an unlimited resistance to friction (structural nonlinearity). The Mindlin's solution is taken as the fundamental one. The analysis of numerous calculations has shown the profiles of normal and tangential contact stress to be in a good qualitative agreement with the known experimental data. The only exceptions are the boundary parts of the profiles where a concentration of stress is observed, typical for the contact deformation of ideally elastic media. No such concentration was observed experimentally. A satisfactory description of kinematics of the pile interaction with the surrounding soil base. Comparison of the calculations with the experimental plots and the calculation data

based on the Construction Rules and Regulations 2.02.03–85 (using the Winkler model) for horizontal displacements, settlements, and slopes of the pile under a horizontal load has shown that a much better agreement with the experimental data is observed for the elastic half-space model calculations than for those based on the Construction Rules and Regulations 2.02.03–85. An important conclusion is made that the development of deformation-based calculation methods for short bored pile bases under a spatial load system with the application of the soil model in the form of an elastic half-space is advisable and promising. This model enables the soil mass behaviour under a load to be described in a more adequate way than the hypothesis of the coefficient of subgrade reaction. Unfortunately, the approach of [63, 64], based on the numerical-and-analytical potential method, has appeared not to be sufficiently universal. Its application for solving the problems of deepened punches (foundation models) with an arbitrary configuration of the contacting surfaces could not be realized. This is related to the method of analytical calculation of the influence matrix coefficients being developed only for the case of flat boundary elements, parallel to the coordinate axes, approximating the contact surface between the foundation and the soil. Therefore, the performed calculations were restricted by the consideration of cylindrical bored piles (with a special boundary-element grid) as well as prismatic and benched block foundations.

It is known that deepened piled foundations can be subject to loading by a torque due to different off-centre lateral forces. In particular, foundations undergo due to storm winds and earthquakes. In the case of foundations under machines, unbalanced masses at the operation of engines also result in torque loads. Another typical example are bored foundations of power transmission line supporting structures, subject to considerable torsional loads due to non-uniform stress in the electric cables and due to wind or snow. Consequently, the evaluation of torsional rigidity of deepened foundation structures is important for the static and dynamical analysis of the foundation+structure system. However, this important geotechnical problem has not found its proper development yet. In this connection one should mention [28, 60, 76, 112, 148, 153, 154, 156, 164, 180, 187], devoted to the analysis of contact interaction of deepened structures under torsion.

The stress-strained state of a circular cylinder and a half-space welded to it, subject to a torque, applied to the free end of the cylinder, is investigated in [60]. The cylinder and the half-space are elastic isotropic materials with different deformational characteristics. The torque is considered to rotate the cylinder's free end as a rigid body, i.e. radial displacement in the cylinder varies in each section linearly along the radius. Besides, the lateral surface of the cylinder and the half-space surface beyond the cylinder are assumed to be free from the external load. The Fourier method is used for finding the solution for the cylinder, and in the case of the half-space the integral Hankel transformation is applied. Explicit formulae for all the values, characterizing the stress-strained state, are obtained. If the half-space is an absolutely rigid body, the obtained formulae give the known solution of the problem of strength of materials regarding a round rod torsion. In another limiting case, corresponding to the geotechnical problem formulation, when the cylinder is an absolutely rigid body, results in the Reisner and Sagoci formulae [164] to determine the

contact stresses and displacements in a half-space subject to torsion by a rigid cylindrical punch. Finally, the problem solution is reduced to the solution of an infinite algebraic equation system, having a symmetrical matrix with a determinant without singularities. Numerical calculations, performed in [60] for a 16th order system, enabled the stress-strained state characteristics in the cylinder and in the half-space to be obtained, areas of influence of fixation (with respect to the cylinder depth) to be determined for various ratios of the elastic properties of the cylinder and the half-space. Subsequently the solutions of the problem under consideration were used to describe the torsional behaviour of rigid piled foundations, using the function of torsion rigidity in a homogeneous half-space [148, 180] as well as in a layered base when a layer and a half-space beneath it are assumed to be homogeneous [76, 112, 153, 187]. Torsion of rigid foundations, deepened into a nonhomogeneous elastic soil with a residuum, is studied in [154]. The residuum shear modulus is assumed to decrease linearly with depth and the shear modulus of the underlying nonhomogeneous soil – to increase with depth. Problems for rigid foundations of flat circular and cylindrical shape are considered. The boundary integral equation method, based on the Green's functions for displacements and forces in a nonhomogeneous elastic medium, is applied. Numerical solutions with respect to the torsion rigidity function are presented for various depths, shear modulus gradients, and residuum thickness. A detailed analysis of the obtained results has shown the torsional rigidities to vary linearly at the variation of the shear modulus gradient and the residuum thickness and parabolically at the variation of the cylindrical foundation length.

Based on the approaches, considered in [60, 76, 112, 148, 153, 154, 164, 180, 187] to the setting of the stress field in the near-pile space, different approximate solutions were obtained in a closed form [28, 156]. Randolph [156] presented an approximate analytical solution, based on a simplification of the stress field in the soil, and obtained torsional rigidities of an elastic pile, deepened into a homogeneous soil as well as into a linearly nonhomogeneous soil with zero shear modulus on the daylight surface. The main result of this study was a strict consideration of the influence of the underlying soil nonhomogeneity on the rotation of the deepened rigid foundation. Based on the simplest assumptions on the stress field in the soil, a closed form of the solution for a torsion rigidity of an absolutely rigid or flexible single cylindrical pile in a homogeneous isotropic soil was obtained [28]. Using the same finite-difference method, a numerical solution was found for the rotation angle of the pile in the soil whose shear modulus varies arbitrarily with depth. The calculations were performed in the assumption of soil to be deformed as a linear elastic medium. The calculation results were compared with the Poulos experimental data [148]. A good correlation of the calculated and the measured data was observed. In the authors' opinion, in order to describe a more realistic picture of the pile behaviour under torsion (up to its breakdown), a more adequate concept should be introduced into the numerical algorithm, based on the dependence of the shear stress versus the rotation angle along the pile length, similar to the known hypothesis of the coefficient of subgrade reaction for horizontally loaded piles.

Nonlinear soil base models. To calculate the foundation settlements for a linear settlement-vs-load plot, an elastic solution is applied, taking into account only

the deformational characteristics of the soil (E – deformation modulus, ν – Poisson ratio). At the pressure over the foundation bottom, exceeding the calculated pressure, the settlement-vs-load plot becomes nonlinear, and the account of strength-related and elastoplastic properties of the soil is required to calculate the settlements (recommendations of the Construction Rules and Regulations 2.02.01–83, Sect. 24).

Fedorovskii [43, 107] has proposed a method for the calculation of nonlinear settlements (at the soil deformation in the shear phase) of deep supports of bored pile type. The calculation method according to the second limiting state is based on the application of theory of elasticity to the interaction of a cylindrical rod (pile) with a soil base. The soil is considered as an elastic half-space with an incorporated cylindrical non-deformable pile. The soil daylight surface is free from loads. The bored pile is loaded by a vertical force, it can be with or without an broadened footing. In the shear phase, i.e. at loads, exceeding the proportionality limit, the soil slippage occurs at the pile lateral surface, due to its insufficient cohesion with the pile, or to an extremely stressed state arising in a thin layer, surrounding the pile. Since at the pile sliding practically all the soil mass remains in the elastic state, the calculation of the pile settlement can be performed using the methods of theory of elasticity. Gorbunov-Posadov was the first to pay attention to this fact [55].

In the approach, proposed by Fedorovskiy, the stress-strained state of the soil mass is presented as a superposition of Mindlin's solutions for a concentrated force in a half-space. The half-space with a cutout, corresponding to the pile volume, is substituted by a full half-space, and a fictitious load in the form of vertical and double horizontal forces is distributed along the pile axis. Such approach is based on the studies performed by Poulos [150] who has shown the difference between the solutions obtained based on the fictitious load distribution along the pile axis and over its lateral and end surfaces to be quite small and noticeable only in small areas near the pile ends. In order to increase the calculation accuracy, Fedorovskiy applied concentrated forces at the pile head and tip: vertical forces as well as double vertical and horizontal forces. A principal difference from the known boundary integral equation method (BIEM) is in the fact that fictitious forces are applied not on the contact boundary of the pile and the soil, but at a certain distance from it (along the pile axis), what is quite justified only for long piles. The integral equations are not written in an explicit form, but substituted by conditions at separate points (collocation points), lying on frontal and rear generatrices of the pile in the centre of the constant load areas. Due to such simplifications, all the calculations, preceding the solution of the resolving equation system, are performed analytically, and no numerical integration is required, as in the boundary-element method.

The fictitious load distribution along the pile axis in the fedorovskiy method is assumed piecewise linear. The sought unknowns are the fictitious force values at the points on the pile's axis as well as concentrated load values at the pile ends. The influence matrix (displacements and stresses due to unit fictitious loads) of the resolving equation system is obtained, using the Mindlin formulae and integrals of them. At the initial stage of calculation, the conditions of full cohesion between the

soil and the pile both over the lateral surface and over the tip, i.e. the conditions of equal displacements of the pile and the soil at their contact, are set as the contact conditions. Then, with the load increase, in the upper part of the pile the soil slippage areas arise, gradually widening and involving the whole lateral surface and the tip. The plot of the pile settlement versus load $s=s(p)$ becomes curved and the settlements increase in comparison with a purely elastic calculation. In order to take this increase into account, the method implies a search for the boundary of separation of the areas of slippage and full cohesion. In the slippage area, the condition of equality of tangential (with respect to the pile surface) displacements is substituted by the slippage condition, which is taken in the form of the Coulomb's friction law

$$\tau = \sigma_n \cdot \tan\varphi + C$$

where φ and C are the parameters of the contact friction between the soil and the pile, τ and σ_n are the friction and normal pressure on the pile at the contact points, calculated with the account of the initial stressed state and additional stresses due to the pile loading. In the case of the presence of a broadened footing at the pile end, which is assumed spherical, the calculation tales into account the experimentally observed [9] uplifting of the soil from the upper part of the widening. At the numerical implementation of the proposed approach, the author recommends the dependence $s=s(p)$ to be found by a semiinverse method, i.e. the load on the pile is determined from the given settlement.

The method for calculation of deep pile settlements, proposed by Fedorovskii, was subsequently implemented as a computer code. Additional features are introduced into the calculation algorithm, taking into account the pile shaft compressibility, what is essential for the piles with a high ratio of the length to the diameter. Besides, in order to make a transition from homogeneous to multilayer bases, the Mindlin formulae for the calculation of the stress-strained state of the medium under concentrated forces are substituted by the corresponding formulae for a layered medium according to the method, described in [44]. Based on the elaborated software and on the results of the performed numerical studies, recommendations for the design of bored piles with and without a broadened footing, as well as shell piles in sand and clay soils were elaborated [161], helpful (along with static tests) for the optimal choice of piles at the assignment of load on the piles of a given size. It should be noted that, though, in the authors' opinion, the method elaborated produces quite acceptable results. it is not applicable for short piles and piles with considerable widenings. Besides, the loading is assumed to be strictly axial, and small widenings of spherical shape should be located under the pile footing. Finally, the development of zones of extremely stressed state, resulting in additional pile settlement increase, is not taken into account.

Using a method, identical to the one, proposed by Fedorovskii for the problem of calculation of a vertically loaded pile with the account of contact slippage [43, 107], later the problems of functioning of a single pile or a pile group in an elastic homogeneous half-space under a horizontal load were solved [46]. Comparison of the calculation results with the known solutions and data of model experiments [146,

147] have shown the account of the pile uplifting from the soil in the course of loading considerably approaches the calculated mutual influence of the piles in the group by means of the soil to the experimental values.

The results of theoretical studies of nonlinear (elastoplastic) displacements of a pile, subject to an axial load, are given in [86]. The pile absolute rigidity is assumed, as well as the equality of displacements of the pile shaft and the contacting soil layer. The mathematical model of the soil in the framework of theory of plastic flow with strengthening is applied [85]. The author characterizes the stressed state of the base by the Lode parameter, equal to zero. Different strength hypotheses can be applied (Mises–Schleicher–Botkin, More–Coulomb, Hill–Tresk). It is noted by the author that practical application of his formula for a pile settlement has essential difficulties, related to the experimental determination of mechanical characteristics of the soil: in order to obtain the deformation-related and strength-related parameters, a special non-standard equipment should be applied or even constructed, what leads to complicated and expensive studies. This made the author of the proposed calculation method to apply approximate equations of state as well as to neglect elastic deformations. The results of the calculations performed and the field studies give a satisfactory qualitative agreement. Quantitatively, a satisfactory agreement of the calculation and the experiment is observed up to the load value, not exceeding about 60% of its carrying capacity. Note also that the proposed method of the deformation-based pile calculation contains an assumption of zero influence of the pile tip, i.e. is restricted to the consideration of a pile of infinite length. Therefore, recommendations, setting the limits of applicability of the proposed method regarding the pile relative depth, are required. This limit can be set only based on comparison of numerous test data and model calculations. Hence, the proposed method of estimation of nonlinear settlements of piles is far from being complete and its practical application is encumbered.

One of the main tasks of soil mechanics and foundation construction is development of such a method of calculation of bases and foundations, which would enable the deformation processes to be described simultaneously in the whole range of loads, including the limiting values, with the account of both deformation-related and strength-related characteristics of soils (C – cohesion, φ – internal friction angle) [123], and in case the behaviour of a structure with time being considered, viscosity-related (fluidity-related) properties should be also taken into account [36].

The class of problems under consideration is characterized by a strong nonlinearity. Their complex solution is possible only in case efficient numerical methods being used on modern computers. However, in spite of overall intense application of powerful computers for solving nonlinear problems in the recent years, this complex problem of soil mechanics and foundation construction is still far from its admissible solution. Noticeable success has been achieved, using the finite-element method for deepened foundations in the form of rotation bodies (piles, anchors, round foundations) under axisymmetric loading [36]. For such foundations their geometry and loading conditions are independent of the azimuthal coordinate. Therefore, they are considered in a two-dimensional space of cylindrical coordinates (z-coordinate and

polar radius), what is to a great extent similar to the case of well studied flat problems [6, 35, 42, 56, 174, 223].

In a series of papers by Fadeev and collaborators [7, 36, 37, 41], a method of boundary-element solution of elastoplastic and elastoviscoplastic problems of determination of the stress-strained state of the base + foundation system is developed with the account of rheological properties of soils at axisymmetric deformation. This method is implemented in the *Geomechanics Creep-3* computer code, using the initial stress procedure [37]. The program enables one to model axisymmetric problems, arising in the practice of industrial, civil, hydrotechnical, and transport engineering, and provides a series of elastoplastic solutions for a given sequence of loading by gravitational forces, stepwise application of construction loads, stagewise excavation of ditches or below-grade workings by introduction of structural elements and given displacements in the nodes at any stage. A bilinear elastoplastic model of soil with the Coulomb fluidity criterion serves as a rheological model in the proposed calculation scheme. It is characterized by parameters, determined at conventional engineering-and-geological studies: deformation modulus, Poisson ratio, cohesion, internal friction angle, density. In the numerical finite-element procedure linear ring-shaped elements of triangular cross-section are used. They are most convenient for the solution of elastoplastic problems. Their rotation results in a triangular torus. The domain of calculation can contain up to 20 element types with different set of properties. Obtaining the elastoplastic solution is based on a multiple repetition of elastic solutions with modified values of the node forces, the system rigidity matrix remaining constant (i.e. the rigidity matrix inversion being performed only once). The natural stressed state is modelled by an all-round hydrostatic stress tensor which is summed up with the actual principal stress value. At first the problem is solved for the given node force values and boundary conditions. Then, in order to find the elastoplastic solution in each of the elements, a sequential procedure is performed, stated in detail in [6, 35, 36, 41, 42, 56, 174, 223]. For the stress-strained state analysis with the account of the soil creep the Shvedov–Bingham model is applied [229]. In this case, for each finite element the characteristics of long-term strength and viscosity coefficients are added, and then the elastoviscoplastic solution is found similarly to the elastoplastic one, using a temporal stepwise procedure.

Using the *Geomechanics Creep-3* software, calculations for some typical schemes of foundation design were performed and analyzed.

A central loading of a low-deepened (H/d=0.125) rigid punch was considered in [41]. Plastic areas in the base were found and their development with the external load increase was traced. The obtained settlement-vs-load curves enabled the levels of the average pressure over the foundation bottom, for which the settlements on an elastic and on an elastoplastic base practically coincide, to be separated from those, for which the presence of plastic deformations results in an enhanced increase of settlements in comparison with the purely elastic solution.

The analysis of settlements and carrying capacity of a single conical pile is given in [7]. A full cohesion is assumed both over the lateral surface of the foundation and over the bottom of the foundation and the base. The pile rigidity is given by the

description of its geometrical shape and the concrete characteristics. An axisymmetric elastoplastic solution has shown a satisfactory coincidence (the discrepancy did not exceed 15%) with the experimental settlement-vs-load plots, built based on the data of static tests of equivalent 4.4–70–20 pyramidal piles, equal in volume and in length to the conical one, assumed for the calculation.

The analysis of calculations of the stress-strained state in the active area of a foundation, performed in [7, 36, 37, 41], has shown quite convincingly that the proposed finite-element method for the calculation of settlements and carrying capacity of axisymmetric foundations enables a combined calculation to be performed according to the first and the second limiting conditions and settlements at the limiting loads to be predicted. It is quite important that the calculation enables the nonhomogeneity of the base soil layers to be taken into account, a combined calculation of the base + pile foundation system to be performed with the account of formation of the pile compression area at the pile driving and loading, plastic deformation development areas to be detected with the account of the load on the foundation.

Aleksandrovich and Fedorovskii [2] also used the finite-element method for solving the problem of interaction of a rigid deepened foundation and a base represented by a model of an elastoplastic strengthening medium (of Cam-Clay type [45, 173]) for the case of axial symmetry under vertical central loading. The base model, chosen for the investigation is based on the associated plastic flow law. The plasticity potential includes a strengthening parameter, depending on the stress-strained state. Finally, the problem becomes nonlinear and is solved by the incremental method with iterations at each loading step. Over the foundation – base contact special contact elements were located, simulating the Coulomb friction and the foundation detachment from the soil. The elaborated approach enabled foundations of various depth in the range from surface punches to piles to be calculated in the same way. A series of calculations performed with input data, differing only in the foundation depth, has enabled the character of the foundation interaction with the base to be traced with deepening. The nonlinear character of the settlement-vs-load curve is revealed in a more pronounced way with depth, ending with the foundation fall-in. The authors explain this deepening effect by an increase of the lateral surface contribution into the total area of the contact between the base and the foundation and by the increasing role of the lateral surface in this interaction.

Boyko and co-workers [1] applied finite-element modelling for automated calculations of interaction of deepened foundation structures with the soil medium at elastoplastic deformation of the base. This method was implemented into a *Rosinka* software [168], based on the Mises–Schleicher–Botkin criterion of limiting equilibrium and theory of plastic flow in the form of the non-associated law. The usage of the latter is due to the fact that the associated flow law, widely used for calculations, is not confirmed for non-rock soils, as follows from most experiments. The main advantage of this approach is the account of formation of limiting state areas in the soil, what enables the stress-strained state of the soil mass to be traced of the foundation + base system operation: from the beginning of loading to the loss of the bearing capacity. As an example of application of the proposed method for calculation of foundations, the problems of interaction of deepened punches with various tip

configurations with the soil medium were solved. Numerical solutions, confirmed by field experiments, have shown a slight (below 5%) discrepancy in the characteristics of the stress-strained state for all punch shapes. The authors explain this fact by the decisive role of formation of an elastic kernel under the punch footing.

A method for calculation of bored piles in the case of nonlinear behaviour of the soil base is proposed in [238, 239, 241]. The mathematical model, used for the description of the mechanical properties of the soil [240], is formulated in the framework of theory of plastic flow. The parameters of three strengthening functions, being contained in the corresponding loading functions, are specified from the data of shear and compression soil tests. The model is implemented by means of a finite-element solution of axisymmetric boundary problems. The results of interaction of the bored piles with the soil base are considered. The calculation domain is approximated by second-order triangular elements with a condensation at the contact of the pile with the soil. The pile was modelled by a set of "rigid" elements with the elastic moduli, by 3–4 orders of magnitude higher than the soil moduli. Full cohesion was assumed as a boundary condition at the contact between the foundation and the soil. Thus, a possible pile slippage with respect to the soil can occur only with a "capture" of part of the soil. As reasonably noted in [239], the latter circumstance is quite realistic for bored piles and is determined by the technology of their production. At the calculations for displacement piles and other types of foundations, boundary conditions should be introduced with the account of slippage. Based on the calculation, the pile settlement is plotted vs the vertical load. With the pile length increase a linear part of the calculated settlement-vs-load curve becomes more pronounced. The areas of the limiting state of the soil are formed along the pile lateral surface, starting from its lower end, and develop with the load increase. The proposed method enables one to trace the transformation of the tangential stress profile as well as horizontal pressures along the pile contact with the soil, which have appeared to be linear practically in the whole load range. The bored pile settlements are essentially different for different assumptions of the initial loading surface in the mathematical soil model even for the same soil conditions. The most important advantages of the proposed method are the possibilities of the bored piles calculation for the base collapsing, as well as for two limiting states (both the admissible deformations and the bearing capacity) in the framework of one theory.

The axisymmetric calculation scheme was also employed by Shapiro for solving the soil elastoplastic problem in his studies, devoted to the modelling of a pile loading by an axial impressive force [193, 196]. The calculation procedure is based on the initial stress method in a combination with the finite-element method. The theoretical basis of the method is the soil description as a solid isotropic medium, modelled according to theory of plastic flow. The axisymmetric version of the numerical calculation method is employed, which had been approved earlier at the design of structures with a calculation scheme corresponding to the flat deformation conditions [192, 194, 195]. Continual ring-shaped finite elements of a triangular cross-section are used. The calculation simulates the pile loading by a stepwise increasing force. The natural stressed state is assumed to be hydrostatically distributed. The following hypotheses are applied for the formulation of the elastoplastic problem:

(1) the nonlinearities, being taken into account, include plastic deformation of the shape change type for the complex stressed state, unobstructed deformation under tension, shear along the pile lateral surface,
(2) for the complex stressed state the total deformation includes an elastic (linear) a plastic component, the latter arising after the stressed state having reached the strength limit in according with the Mises–Schleicher–Botkin condition [30],
(3) the vectors of principal plastic deformations and principal stresses are assumed coaxial,
(4) at the plastic deformation stage, the non-associated flow law is applied with a dilatancy rate being introduced.

Based on the calculations performed for cylindrical piles, the boundaries of the prelimit and limiting stressed state areas of the soil are determined and a settlement-vs-load plot is built. The results of the mathematical modelling are compared with the static test data for bored piles and pile foundations in boreholes. The calculation data on the settlement-vs-load plots are noted to be close to those obtained from the static tests of the piles in the boreholes. This is, to a considerable extent, due to the mechanical characteristics of the soil, determined from the all-round studies of the foundation active areas being taken as the input data. The results of calculations for bored piles of 1.7-m diameter for bridges show a possibility of increase (in comparison with the Construction Rules and Regulations 2.02.03–85) of the predicted bearing capacity of both single foundations and components of pile rafts. For both types of pile foundations many settlement-vs-load dependences appeared practically linear and the number of iterations, required for the achievement of a given accuracy level, is quite significant (30–50). In the author's opinion, in spite of well checked and extensively used assumptions, the proposed method of pile foundation calculations still requires further studies and modifications.

Among rare studies, devoted to essentially spatial interaction of foundations with nonlinearly deformed bases, one should first of all note a series of studies by Fadeyev and Matveyenko [38–40] regarding a method of solving the spatial contact problem by means of a semianalytical finite-element method, first proposed by Wilson [232] and developed by Zienkiewicz et al. [233, 248]. The approach, elaborated in [38–40], is applicable for axisymmetric rigid foundations, loaded by vertical and horizontal forces, and can be implemented in both elastic and elastoplastic formulations. The base stress-strained state characteristics (node loads and displacements) are determined as a product of two functions, one of which being found by the finite-element method, and the other one being given in the form of a trigonometric series. In case the trigonometric function orthogonality and the axial symmetry of the domain under consideration being taken into account, the three-dimensional problem is separated into a series of independent two-dimensional problems. The axisymmetric domain of the soil base calculation is discretized by a set of ring-shaped triangular finite element, interconnected by node circles. A procedure of obtaining an elastoplastic solution by the initial stress method for a medium with internal friction is proposed in [6, 35]. The soil is considered as an ideal elastoplastic medium with a fluidity surface, described by the Botkin criterion in octahedral

stresses. The elastoplastic solution is reached by multiple repetition of elastic solutions with variable node force values and a variable rigidity matrix of the system. The numerical algorithm of spatial problem solution for axisymmetric foundations is implemented in a *Geomechanics ADA* code. This software was tested for the elastic stage of the base functioning by a comparison with the known theoretical solution by Egorov [33] for the problem of an off-centre loading of a round foundation plate. A rather good agreement was obtained for the solution of an axisymmetric problem of a rigid shallow foundation in an elastoplastic base [41]. The studies of efficiency of the semianalytical finite-element method have shown that, in comparison with the full three-dimensional analysis, the developed method enables the calculation time for the stress-strained state of bases under axisymmetric foundation structures subject to a horizontal load to be reduced by an order of magnitude.

Today the elaborated approach using the semianalytical finite-element method should be considered one of the most efficient for the finite-element prediction of spatial stress-strained states of axisymmetric foundation bases. However, no other studies have been performed for deepened foundations, except for solving one problem of pile behaviour under a horizontal load [39].

Among other studies regarding nonlinear calculation of bases for foundations of spatial type with the account of the depth factor, one should note the most perfect, in our opinion, finite-element approaches [143, 231] as well as the calculation of pile foundation settlements using transformational functions [61].

A professional software *PLAXIS*, worked out in the Delft University (the Netherlands) [143], is at present one of the most successful software tools, intended for numerical studies of interaction of foundation structures with the soil. The *PLAXIS* software employs the finite-element method, using two type of elements fifteen (their amount can be up to 200) and six (up to 800) node triangular elements. It is designed for solving a class of axisymmetric problems at elastoplastic deformation. On the surface of interaction of the foundation and the soil, special contact elements are introduced, for with the strength-related parameter values (internal friction angle and cohesion) are used, different from the corresponding values for the soil. In such a way a thin near-surface layer of the soil is modelled, in which the shear deformation processes are the most intense. The *PLAXIS* software allows several soil models to be employed in order to describe the mechanical behaviour of the soil:

– a linearly deformable medium (a zeroth order model – for strong bedrock bases),
– the Mohr-Coulomb model (a first-order model – for the most of engineering-and-geological conditions),
– the Cam-Clay model (a second-order model – for soft soils).

Note that the second-order model is practically very seldom used because of its high sensitivity to the soil nonlinearity parameters: overconsolidation and transverse stress coefficients, which are determined in the geotechnical practice with great difficulties. *PLAXIS* has no new conceptual achievements, in comparison with the Russian software. Only due to quite convenient service and graphical functions

this software is widely apply the professional version of *PLAXIS*, whose first release was produced in 1988. Numerous examples of practical application of *PLAXIS* for the analysis of geotechnical problems are quoted in [143]. The *PLAXIS*-based results of numerical modelling of interaction of a group of four C4–30 prismatic piles with the surrounding soil are presented in [128]. The problem is solved in an axisymmetric formulation. The ideal elastoplastic Mohr-Coulomb model is taken as the soil base model. The numerical modelling results show two important features of the *PLAXIS* software. First, an additional study should be performed regarding the correct assignment of the dimensions of the pile foundation active area. Second, when the characteristics of the soil, compressed due to the pile submergence, were introduced into the calculation, doubtful results were obtained. In the author's opinion [128], after the load being applied, the plastic deformation areas begin to develop very rapidly and a considerable soil squeeze out towards the half-space boundary occurs. As a result, the obtained pattern appears very far from being realistic.

Essentially three-dimensional finite-element calculations were performed [231] for a rigid deepened prismatic foundation under an eccentric inclined force due to the organization of comparative test calculations in 1990 in order to study the possibilities of modelling of an intentionally planned experiment at the Institute of Soil Mechanics and Rock Mechanics at the University of Karlsruhe (Germany). The results, presented in [231], appeared to be the closest to those obtained from field measurements among the 17 calculation predictions from different countries (Great Britain, Germany, France, Slovakia, Italy). A MONOT model of elastoplastic type with double strengthening [120] was taken as the model to describe the rheological properties of the soil medium (sand). The three-dimensional version of the model was calibrated using the results of standard punch tests of the base. Three-dimensional calculations (with the account of a symmetry plane in the calculation scheme), in spite of being labour-consuming, resulted in exaggerated settlements, and no satisfactory prediction of the base rigidity was obtained. The finite-element calculation results are shown to be essentially determined by the friction at the contact of the foundation and the soil.

In the Technical University of Gdańsk, since the 1970s the studies have been performed to find the analytical dependences of nonlinear settlements of vertical cylindrical piles on vertical loads in order to describe the whole settlement-vs-load plot based on the geotechnical parameters, corresponding to the properties of the soil base before the pile installation. A method of so-called transformational functions [61], describing the dependences between the lateral resistance and the settlement (t–z curves) as well as between the pressure under the pile and its settlement (q–z curves) is developed. Using the approximate theoretical solutions and the experimental data, an extensive analysis of the transformational functions is performed. In order to identify the empirical parameters being contained in the transformational functions, a colossal amount of the experimental data was required to be processed (260 piles with the account of several variants of choice of transformational functions for each of them). The calculations were carried out, using an intentionally elaborated *PALOS* software, automatically performing iterative process of approximation from the experimental pile settlements and the given nonlinear elasticity

law. In each separate case a good agreement of the calculated values with the field test data was obtained. However, the method is hardly applicable for practical purposes in view of the requirement of a group of empirical parameters, obtained from a great number of penetration tests, to be given for each transformational function. The method is mostly oriented at cylindrical piles of a large diameter under vertical central loading. Another restriction for its application is related to the fact it being essentially based on Polish engineering regulations.

It follows from the presented analysis that a certain success has been achieved in the methods of foundation calculations with the account of the depth factor. A sufficient amount of calculation schemes has been proposed, reflecting a variety of properties of soils, loading type, relative depth, and other factors. However, each of the methods has its own specific features, and all of them are different in accuracy and convenience of application.

The simplest and most convenient for engineering calculations are methods, using the Winkler base model and its modifications. Meanwhile, they do not enable the desired accuracy of the project solutions, require the superposition principle to be fulfilled, what is known not to be confirmed experimentally in most cases. Tangential contact stresses, comprising up to 50% of total reactive resistance of the soil, depending on the shape of the foundation deepened part and on the loading type, are either not taken into account by these methods, or taken into account by assignment of the corresponding coefficients of subgrade reaction without proper substantiation of their numerical values.

Calculations, using the elastic half-space model, are more preferable. They take into account the distributive and deformational properties of the soil base in a rather adequate way. However, in view of essential mathematical difficulties, there are no closed solutions for deepened foundation structures at all, and obtaining numerical solutions is quite labour-consuming even for the simplest-shape foundations. For practical calculations, solutions for centrally loaded circular and rectangular areas are used, simulating the functioning of separate parts of the foundations (s a rule, only its footing). None of the desired solutions of contact problems for foundations with a given shape of the deepened part under spatial force and momental loading of general type have been found yet.

As follows from the reference data, application of the soil base nonlinear models enables the calculation conditions to be essentially shifted towards higher loads, up to the limiting values. In most cases the nonlinear calculation methods are based on the finite-element modelling of axisymmetric modelling of axisymmetric foundation structures (of cylindrical or conical shape), subject to a central loading. The authors pay the greatest attention to the studies of influence of the strength-related soil properties on the character of the settlement-vs-load dependence. All methods of evaluation of deformability of nonlinear (elastoplastic) bases are characterized by high labour consumption in input data preparation, a great number of iteration cycles at each loading step as well as insufficient substantiation of the choice of an elastoplastic deformation law. A disadvantage of the existing nonlinear methods of foundation base calculation consists in the spatial functioning of the nonlinearly deformed base being taken into account only for the simplest case of centrally

loaded foundations in the form of rotation bodies, what is actually equivalent to a consideration of the problem of a flat stress-strained state. In such a formulation it is not possible to perform deformation-based foundation calculations for off-central loading, the most widely used in design practice. The above speculations are even more applicable to foundations with a complex geometrical shape of the deepened part, which for any loading conditions determine the spatially non-uniform stress-strained state in the foundation active area, i.e. in all cases determine the complex functioning of a base.

The subsequent sections of the chapter contain the results of boundary-element modelling for the most popular foundations with a complex (non-traditional) shape of the deepened part, applied in the modern practice of enabling works. The design of such foundations requires the account of real depth, specific features of the geometrical shape of the contact surface with the soil above the footing, load application eccentricity, etc. Calculation of bases for such foundation structures leads with necessity to the solution of spatial contact problems, since reliability in the determination of the foundation settlements, horizontal displacements and slopes depends to a great extent on the accuracy of determination of tangential and normal stress on the contact surface of the foundation with the soil.

5.3 Calculation of Bases for Pyramidal Piles Under Vertical, Horizontal, and Momental Loads

It is well known from the literature on foundation engineering that traditional foundations of long prismatic piles have low economic efficiency [13, 102, 149]. One of the alternative solutions for loose soils, covered by a layer of a stronger soil (3–6 m thick), is the application of short pyramidal piles.

Short pyramidal piles began to be introduced into engineering in the mid-1970s and soon became very popular due to their high efficiency in comparison with the prismatic piles [78]. The experiments [4, 13, 31, 94, 172] show the pyramidal piles to have carrying capacity by factor of 1.5–3 higher than prismatic piles of the same volume. Such increase of the pyramidal pile bearing capacity is explained by a considerable compression of soil around them and a specific character of their interaction with the surrounding soil. In particular, pyramidal piles have large lateral surface and, due to their faces being inclined, the soil resistance to normal stress increases. Due to these circumstances, rather large loads can be transferred to the piles, even for loose soils in their bases.

Pyramidal piles are successfully used for objects of industrial, civil, rural engineering [13, 53, 57, 58, 433]. Construction on such piles is economically justified for the most of engineering-and-geological conditions, including the bases consisting of nonhomogeneous, collapsing, swelling, heaving soils [8, 213, 249, 250]. As shown by recent all-round studies [172], application of pyramidal piles in freezing heaving soils can provide reliable functioning of light buildings and structures with an essential reduction of the foundation cost. Note that introduction of pyramidal piles instead of strip foundations enables the foundation cost to be reduced by half,

labour consumption for their construction – by up to 60%, concrete consumption – by up to 70%, the foundation material consumption – by a factor of 3 [69].

5.3.1 Existing Approaches to the Calculation of Piles with a Variable Cross-Section

The experimental proof of the efficiency of pyramidal pile application in engineering became an impetus to the development of a theory of their calculation. The problem of creation a method for pyramidal pile calculation has been studied extensively since the 1970s. The relevant papers [7, 13, 52, 57, 58, 69, 102, 103, 129–131, 249, 250] should be mentioned as giving the most complete characteristics of the existing approaches to the pyramidal pile calculations.

A calculation of pyramidal piles under a combined action of vertical, horizontal, and momental loads is proposed in [57, 249, 250]. A pile is considered as a rigid volumetric punch and the base – according to the Fuss-Winkler model. Components of the soil reactive back pressure over all four inclined sides of the pile are taken into account in [57, 249]. In [250] the soil back pressure only at the front and rear sides of the pile lateral surface is taken into account. In these papers the method of determination of coefficients of subgrade reaction are also different, the later being introduced in the calculation as constant values. The authors of [58] propose the coefficients of subgrade reaction, nonlinearly dependent of the contact stress values and the calculated soil resistance, to be applied for the pyramidal pile calculations. A simplified solution of the elastoplastic problem for a vertically loaded pyramidal pile is obtained by the finite-element method in a flat formulation in [13]. A similar approach is applied in [52] to the studies of obliquely and off-centre loaded pyramidal piles. The authors of [8, 69, 151] recommend the principle of independent action of forces to be applied for the pyramidal pile calculation. At such approach the pile calculation is performed separately for the vertical load, on one hand, and on the horizontal and momental loads, on the other hand. In the case of calculation for the horizontal and momental loads, a pyramidal pile is modelled as a rigid trapezoidal plate, restrained in the base. In [69] the soil properties are described by the Fuss-Winkler model, while in [131] an elastic linearly deformable half-space is used. When the calculation for vertical and horizontal loads is performed, the pile is treated as a rigid volumetric punch, fixed in a linearly deformable elastic half-space [129, 130]. A paper [7] and a book [102] are devoted to the pyramidal pile calculation for a vertical load in an axisymmetric formulation when the pile is modelled by a truncated cone, equal in height and in volume. An advantage of these studies is that the calculation scheme takes into account the soil nonhomogeneity due to its compression at the pile driving. In [7] the finite-element method is employed for the studies of the pyramidal pile interaction with soil, and in [102] an approximate analytical solution of the mixed problem of theory of elasticity and plasticity is obtained.

Thus, at present several methods for base deformation-based calculation of pyramidal piles have become popular. The main shortcomings of these methods should be mentioned as follows:

– lack of account of combined action of vertical, horizontal, and momental loads,
– introduction of coefficients of subgrade reaction for determination of horizontal and vertical reactive pressures of the soil and their rather approximate assignment for different soil types and states,
– application of a rectangular profile for the coefficients of subgrade reaction which does not take into account their variation with depth,
– presence of extensive auxiliary tables, applicable only for separate nominal sizes of pyramidal piles and physical and mechanical parameters of soils,
– substitution of a pyramidal pile by a deepened conical punch with a surface equal to those of the pile, and application of solutions of the axisymmetric problem of limit equilibrium theory.

A required increase of the pyramidal foundation efficiency can be achieved by application of solutions of mixed problems of theory of elasticity and plasticity in a spatial formulation [142]. However, in this case essential mathematical difficulties arise. Even the attempts to apply well elaborated numerical methods (FEM) for the studies of soil bases in a flat or axisymmetric stress-strained state due to static loads result in a great increase of the required memory size and computation time [141]. Besides, consideration of the soil as an ideal elastoplastic medium in the framework of the associated and non-associated plastic fluidity laws does not enable the solutions of essentially three-dimensional problems to be applied for the development of engineering methods for the calculation of foundations of various type since they are mostly of theoretical character.

To our knowledge, among the papers, devoted to pyramidal pile calculations, only [129, 130] contain calculations according to the second group of limiting states, based on the application of solutions of spatial problems of theory of elasticity. The boundary-element method in its simplest form is applied. A pyramidal pile of square cross-section is substituted by a telescopic absolutely rigid body. At vertical or horizontal loading, only the Mindlin's solution components, corresponding to the load direction, are used, with the soil Poisson ratio ν=0.35. Integration of displacement functions over each vertical lateral side of the telescopic body is substituted by summation of displacements from our concentrated forces as well as sixteen concentrated forces at the lower horizontal end. This calculation method was applied for comparison with the test results [53] for a pyramidal pile with a square cross-section of 70×70 cm^2 near the surface and 10×10 cm^2 at the depth of 5 m. The soil deformation modulus was determined by punch tests and at the construction site it was within 2.5 to 3 MPa. Under the load on the pile of 500 kN the settlement was 5 cm. Even for a rather small number of telescopic part (n= 5) and the deformation modulus, taken as the average value over the site 2.75 MPa, the settlement value of 0.0467 m was obtained, the discrepancy with the experiment being only 6.6% [130]. This enabled a conclusion to be made that the application of rectangular and "telescopic" elements in the calculations of pyramidal pile settlements considerably simplifies the solution in comparison with the finite-element method and even for a small mesh (5–7 elements) is quite applicable for obtaining results, sufficiently accurate for practical purposes.

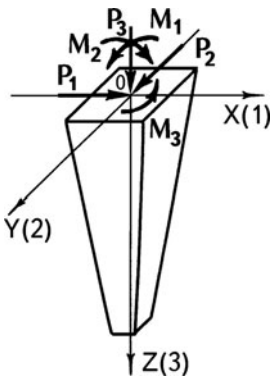

Fig. 5.1 Calculation scheme for the spatial loading of a pyramidal pile

Developing the above approach for the pyramidal pile calculation under simultaneous action of vertical, horizontal, and momental loads (Fig. 5.1), we apply an original modern numerical method of solving the spatial contact problem, based on the direct boundary-element method.

While formulating the contact problem, we present the pile calculation scheme as a rigid volumetric deepened punch in the shape of the pyramidal pile to be calculated. We assume a linearly deformable half-space with a cavity, whose boundaries coincide with the pile contact surface, as a model for the base. For modelling the contact interaction of the pile with the soil, we apply unilateral constraints, which do not work in tension and possess an unlimited resistance to friction under compression. The system of equations (2.9) and (2.10), corresponding to the spatial contact problem of theory of elasticity for a deepened punch whose surface is bonded with the base, is complemented by a restriction

$$p^{(n)}(N) \geq 0 \tag{5.4}$$

where $p^{(n)}(N)$is the contact surface vector projection in the point N onto a normal, external to the pile structure surface, contacting with the soil.

The system of Eqs. (2.9) and (2.10) with a restriction of Eq. (5.4), due to the presence of an inequality, results in a class of contact problems with a construction type nonlinearity; hence, the principle of independence of forces is not applicable for solving it. For each separate case of spatial loading of the pile, a separate calculation should be performed.

The system of Eqs. (2.9), (2.10), and (5.4) is solved, using the direct boundary-element method (Sect. 2.2) in accordance with the following modification, taking into account the presence of unilateral constraints. If there is no preliminary information on the contact domain, then after the coefficient matrix having been formed, an iterative program mode is entered, at each step of which the solution of the system of Eqs. (2.13) and (2.14) is determined. At the full contact of the pile foundation with the base the system of Eqs. (2.13) and (2.14) is a closed system of (3M+6)

linear algebraic equations where M is the total number of the boundary elements. At each step of iteration the values $p^{(n)}(N_t) \geq 0$ ($t=1, 2, \ldots M$) are analyzed in order to determine the boundary elements, at which tensile normal stress arises. The rows and columns of the matrix of the equation system (2.13) and (2.14), corresponding to such elements, are made zero at subsequent steps. The iteration process is finished when there is no tensile stress along the normal to the foundation contact surface. The experience of the program operation shows that the iteration number is within 4–7, no program cycling being observed.

The routine for the pyramidal pile calculation under a combined action of vertical, horizontal, and momental loads from the elaborated *Rostwerk* software kit is simple in operation and requires the following input data: total number of the boundary elements, into which the pile contact surface is meshed (Fig. 5.2), the size of the upper and lower pile ends and the pile height, projections of force and moment vectors, applied to the pile head, the deformation modulus and the Poisson ratio of the soil.

Note that in the numerical method applied here for pyramidal piles, the geometrical shape of the foundation is exactly described and the tangential conditions at the contact surface of the pile and the soil are taken into account. Therefore, the boundary-element approach in the full spatial formulation with the application of the pyramidal pile discretization into several hundreds of boundary elements will undoubtedly provide higher level of accuracy of characteristics of the contact interaction of the pyramidal piles with the soil than the "telescopic element" method.

The efficiency and reliability of the proposed method for pyramidal pile calculation are estimated in the subsequent sections by comparison of the numerical results with the experimental data.

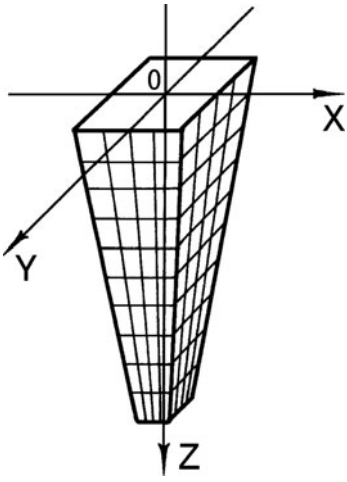

Fig. 5.2 Discretized surface of the pyramidal pile contact with the soil

5.3.2 Calculation for the Vertical Load

The results of static tests of a pyramidal pile under a vertical load are given in [53]. The pile was 5 m long, the side of the upper square end of the pile was 0.7 m, the lower end side 0.1 m. The pile base was a high-plasticity clayey, the average deformation modulus value E=2.75 MPa was found from the punch test data. The density and strength-related parameters of the clayey were the following: γ=16.3 kN/m^3, φ=10°, C=15 kPa. The Poisson ratio of the clayey is assumed ν=0.35.

Figure 5.3 shows the settlement-vs-load plots for the pyramidal pile under consideration, obtained experimentally (line 1) and from the calculation (line 2). In the same figure the pile settlement curve is shown (line 3), obtained in Appendix F according to the method, quoted in the instruction [69]. Comparison of the experimental and calculated data (lines 1 and 2) leads to a conclusion that the settlement-vs-load plots, obtained experimentally and from the solution of the spatial contact problem, are practically parallel, with the exception of the initial part (in particular, this is the evidence for the correct evaluation of the high-plasticity clayey deformation modulus from the punch test data). Note that the contact problem solution can be made even closer to the experimental results, if one takes into account the fact that when the stress in the soil is lower than its structural strength, the soil deformations are extremely small. According to the experimental data (limit 1), the soil structural strength limit is overcome at the vertical load $P_3 \approx 50$ kN. Then the contact problem solution with the account of the soil structural strength can be presented by a plot (line 4) which is essentially closer to the experimental curve. Note also that the results of the pile settlement calculation (line 3) according to the instruction [69] are in a good agreement with the experiment only at the very initial stage of the pile loading, and at other stages they are quite far from the reality.

5.3.3 Calculation for the Action of a Horizontal Load

The results of the numerical studies were also compared with some of the experimental data published in [57]. Horizontally loaded pyramidal piles of two nominal sizes were considered: one pile with the length of 5.5 m with the head size 0.6 × 0.6 m and the footing size 0.2 × 0.2 m, and a second pile with the length of 4.4 m and the head and the footing size 0.75 × 0.8 m and 0.3 × 0.3 m, respectively. The piles were tested at four experiment sites, three of which were on water-saturated clayeys and one – on water-saturated clays. Table 5.1 presents the results of our calculations of piles along with the average values of physical and chemical parameters of soils of the experiment sites which were kindly provided by the author of [57].

The analysis of the data, quoted in Table 5.1, has shown that the boundary-element results give a satisfactory agreement with the experimentally measured pile displacements. Note that for the piles Nos. 4 and 6 the boundary-element method gives the results close to the field measurements than the finite-element method [57].

Table 5.1 Parameters of the test site soil physical and mechanical properties and results of pyramidal pile calculations

Pile no. according to the table in [57]	Parameters of the test site soil physical and mechanical properties					Pile dimensions		Load on pile		Horizontal displacement of the pile head Δ_1, mm		
	Density in natural state γ, g/cm^3	Unit cohesion C, MPa	Internal friction angle φ, deg	Deformation modulus (punch)E, MPa	Poisson ratio ν	Head / Tip,cm	Length, m	Horizontal P_1,kN	Momental M_2, kN·m	Test	Calculation according to [57]	Calculation according to the BEM
2	1.95	0.043	12.3	11	0.47	$\frac{60 \times 60}{20 \times 20}$	5.5	160	30	10	9.0	$\frac{7.7}{8.1}$
3	2.02	0.027	5	8.5	0.49	$\frac{60 \times 60}{20 \times 20}$	5.5	144	30	10	10.0	$\frac{9.0}{9.5}$
4	1.83	0.041	19.7	11	0.42	$\frac{60 \times 60}{20 \times 20}$	5.5	200	40	10	13.9	$\frac{9.8}{10.3}$
6	1.90	0.047	16.6	6.0	0.44	$\frac{75 \times 80}{30 \times 30}$	4.4	115	20	10	11.3	$\frac{10.2}{10.8}$

Note. The last column of the table contains the displacement values with (denominator) and without (numerator) unilateral constraints on the pile–soil contact.

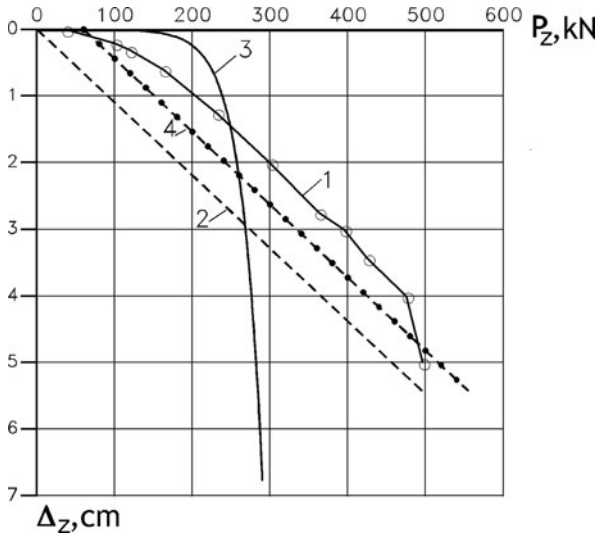

Fig. 5.3 Dependences of the pyramidal pile settlements on the vertical load: 1– experiment, 2–4 – calculation

5.3.4 Calculation for the Action of an Inclined Load

Figure 5.4 shows the calculation scheme and the discretized surface of a prismatic-pyramidal pile loaded by a vertical and a horizontal force. The pile length is 3 m, the head size 0.6 × 0.6 m, the footing size 0.1 × 0.1 m, in the upper part the pile is prismatic, this partition length being 0.8 m. The given pile was tested under an inclined load at two test sites [5]. The first site was located on a stift clay with the following physical and mechanical parameters: γ=19.7 kN/m, φ=19°, C=0.033 MPa, E=18 MPa, ν=0.426. The angle of inclination of the external load, applied to the pile head, with respect to the horizon, was α=55°. The second site was located on a stift clayey: γ=17.7 kN/m, φ=20°, C=0.015 MPa, E=14 MPa, ν=0.417. At this site the pile was tested by the load at an inclination angle α=68°.

The horizontal displacement of the pile head is plotted across the inclined load in Fig. 5.5. Lines (1) and (2) in the figure correspond to the experimental dependences [5], and lines (3) and (4) are plotted according to the calculation, performed by the boundary-element method. Comparison of the results, shown in Fig. 5.5, leads to a conclusion that in the major part of the whole load range the experimental and theoretical dependences are close to each other. This range is restricted by a load of 65–70% of the pile bearing capacity what, in turn, corresponds to the admissible calculation load on a pile at the reliability coefficient near 1.4, what is specified by the Construction Rules and Regulations for the pile foundation design.

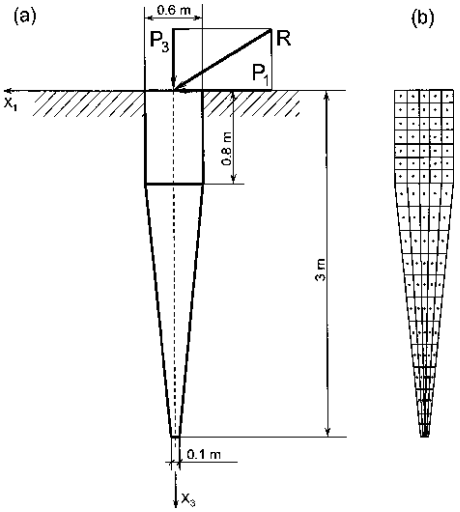

Fig. 5.4 Calculation scheme (**a**) and discretized surface of contact with the soil (**b**) for a pyramidal-prismatic pile loaded by an inclined force

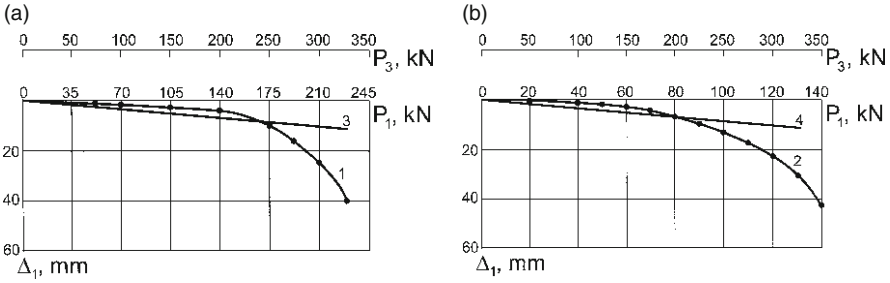

Fig. 5.5 Dependence of the pile head horizontal displacement on the joint action of vertical and horizontal loads: 1,2 – experiment [76], 3,4 – calculation; (**a**) site No. 1 (semihard clay); (**b**) site No. 2 (semihard clayey)

5.3.5 Calculation for the Combined Action of an Inclined Force and a Moment

We have analyzed an example of calculation of a pyramidal pile with the upper end size 0.68 × 0.68 m, the lower end size 0.1 × 0.1 m, length 2.9 m, loaded by a vertical load of 155 kN, a horizontal load of 83 kN, and a momental load of 22 kN·m, taken from the instruction book [69]. The soil is represented by a fine damp sand with the following physical and mechanical characteristics: γ=17.4 kN/m^3, φ=28°, C=3 kPa, E=18 MPa. The soil Poisson ratio is taken as ν=0.25. The calculation results for this pile from the instruction book [69] and obtained by the method proposed here, are listed in Table 5.2.

Table 5.2 Parameters of contact interaction of the pyramidal pile with the soil, loaded by an inclined force and a moment

Calculation method	Settlement Δ_z, mm	Horizontal displacement Δ_x, mm	Slope $\psi \cdot 10^2$, rad
Instruction book [69]	6.2	5.0	0.32
Boundary-element method	3.7	3.6	0.16

It follows from the table that, similarly to the earlier comparison, for a centrally loaded pyramidal pile the numerical boundary-element solution of the spatial contact problem for the case of loading by an inclined force and a moment, results in essentially smaller deformations of the pile base than for the predictions of the instruction book [69].

Thus, the studies performed show the evidence for the proposed approach being promising for the pyramidal pile base calculations in the most general spatial formulation. Its further improvement is related to a detailed experimental testing at different engineering-and-geological conditions that will enable reliable range of the method applicability to be established and the method itself to be suggested for application in the development of regulations.

5.4 Interaction of Bases and Rigid Bored Foundations with Vertical and Inclined Piles

In many countries the fraction of pile foundations is above 25% of the gross foundation volume, and in some regions up to 40–70% buildings and structures are erected on pile foundations [10]. Development and implementation of new pile structures with high technological parameters is considered to be one of the major trends to solve the problem of pile foundation efficiency. This can provide an essential economic effect and qualitatively improve the figures.

Extensive application of rational structures of rigid pile foundations in engineering [20, 75, 114, 210] is hampered by a low reliability level of the practical calculation methods, based on separate empirical data and extremely simplified theoretical models of soil. For example, according to the design regulations, accepted in Russia, pile foundation base deformations are studied for a vertical load using a linearly deformed half-space model, and separately for a horizontal and a momental load using the coefficient of subgrade reaction (Winkler) model [208]. Dependence of the foundation calculation scheme and the base model on the external load direction is the reason for the low reliability of the results of calculations to determine the pile foundation displacements in the soil at the stage of its functioning.

A considerable economy due to a reduction of materials consumption can be obtained due to the account of functioning of a low pile raft in pile foundations [190]. As follows from the estimations, a pile raft can accept from 20 to 70% of

the total load on the foundation. The method, used in the Construction Rules and Regulations 2.02.03–85 [208] for the design of pile foundations, does not take into account the soil distributive properties in case the load being transferred by the pile lateral surface and tip, as well as the low pile raft functioning.

5.4.1 Structure, Design, and Specific Features of Calculation of Rigid Pile Foundations with Short Piles and a Pile Raft

Pile foundations with short rigid piles have found applications in various fields of engineering [151, 169, 235, 247]. In particular, for rural engineering (cattle farms, warehouses, hangars, etc.), with bearing structures in the form of three-hinge frames or arches as well as vaulted folded plates, one of the most rational foundation types are short vertical and inclined bored piles with a raft in the form of a washer or a cantilever [105, 222].

When inclined piles are used, their longitudinal axis is put along the direction of the resultant of the main external load combination. This results in an essential improvement of conditions of functioning of the soil, surrounding the pile. As follows from the field experiments data [118, 119], the foundation slope is reduced, horizontal displacements of the mounting groups of bearing structures are reduced to a minimum. The stress in the pile cross-sections is purely compressive, what essentially favours the decrease of the bending moments and transverse forces in the pile body and enables one to use the only reinforcement to conjugate the pile shaft with the pile raft. In case the horizontal loads exceed the vertical ones, the pile rafts are made in the form of an unloading cantilever what is also helpful to reduce the foundation slope and its horizontal displacements. Such pile foundation structure is one of the most rational foundation structures, applied under legs of aerial power transmission line supports [100].

In Russia, no special regulations for the design of pile raft foundations with vertical and inclined piles have been developed so far. Therefore, for substantiating the engineering calculations, in the first approximation the regulations for the design of conventional pile foundations are used. However, the calculation schemes, provided by the Construction Rules and Regulations [208], do not reflect some essential features of interaction of bases and pile raft foundations. In particular, the calculations according to the Construction Rules and Regulations do not take into account the soil reaction over the pile raft bottom as well as mutual influence of the pile raft and the pile. This is the reason for the behaviour of inclined foundations under an operating load being hardly predictable with sufficient reliability.

Another rational field of application for short piles are foundations under pipeline trestles, power line supports, contact-wire line supports [96, 166, 167]. In this case the lower part of the support, sunk into a preliminarily drilled well, is often used as a pile. In order to increase the bearing capacity for a horizontal load at the base surface level, the piles are reinforced with washers or soleplates [17, 72].

Technology of construction of short pile foundation with rafts is highly mechanized. After the site planning, wells are drilled. Compression of the residual slime at the hole bottom is performed by impression of the working part of the drill without rotation into the well bottom. After drilling, reinforcing cages are installed and fixed in the wells. Then pile construction process is begun. A concrete-delivery truck arrives directly at the construction site and supplies concrete directly from the agitator to the well through a filling funnel. The concrete mixture compaction is performed using vibration tools. The concrete should have pourable consistency. After the piles having been produced, reinforcing fabrics and raft formwork are set. Concrete is supplied into the formwork directly from the agitator with its subsequent compaction by a platform vibrator. The productivity is even more increased in case a gap between the concrete placement into the pile and the raft can be avoided.

In order to achieve higher adequacy between the calculation and experimental data, we use the spatial contact problem formulation for a complex-shaped rigid punch, deepened into a soil base, performed in Chap. 2. The calculations are performed according to the second limiting state for rigid pile foundations of a constant cross-section, both with and without a raft.

We accept initially that the external load (from the power line support or other above-foundation structures) is transferred to the base not only by the pile contact surface, as it is set in [208], but also by the pile raft bottom. Interaction of the raft lateral surface with the soil is not taken into account due to a high friability of the back fill soil as well as due to the fact that for power line supports and many other engineering structures, as a rule, higher pile rafts are used, located on the base surface.

Since the flexibility of a short pile foundation is low (with respect to the soil base), it can be treated as an absolutely rigid volumetric deepened punch. Small pile length (2–4 m) provides, as a rule, their location within the same engineering-and-geological layer. Therefore, in the first approximation for the simulation of the soil distributive property and the possibility of account of mutual influence of the pile raft and the pile on the stressed state of the soil, the base model is taken in the form of a homogeneous isotropic linearly deformable half-space with a vertical or inclined cavity. The pile raft bottom is resting on the half-space surface, and the cavity is fully filled with the pile.

Since the soil practically does not work in tension, the numerical modelling should take into account the unilateral character of the foundation contact with the base: in the areas of the foundation uplifting from the soil, all contact stress components are zero.

Some examples of automatic boundary-element discretization of contact surfaces of pile foundations with inclined and vertical piles and pile rafts of various shapes, used for practical calculations, are shown in Figs. 5.6 and 5.7.

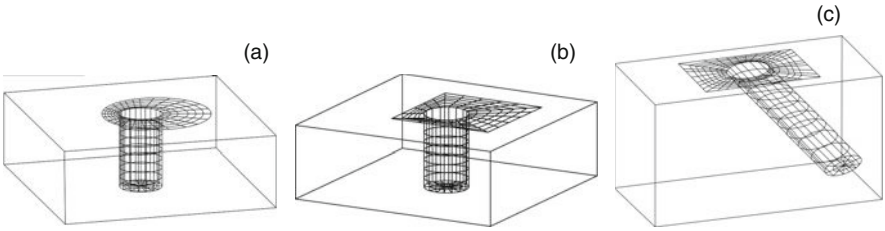

Fig. 5.6 Discretized surfaces of contact of soil and a vertical pile with (**a**) a circular and (**b**) a rectangular eccentric pile raft, as well as (**c**) of soil and an inclined pile with a rectangular pile raft

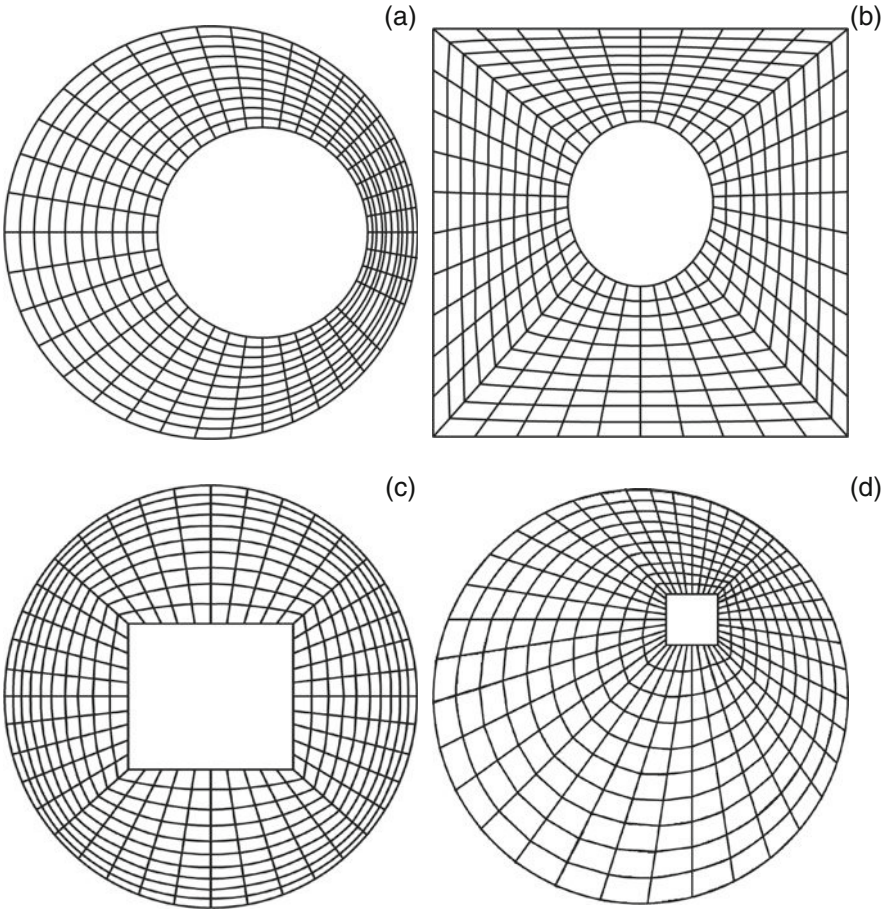

Fig. 5.7 Discretized surfaces of contact of soil with (**a**) a circular eccentric pile raft for a vertical cylindrical pile, (**b**) a rectangular pile raft for an inclined cylindrical pile, (**c**) and (**d**) a circular pile raft for piles with square cross-section

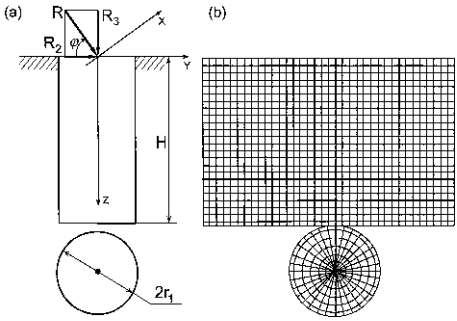

Fig. 5.8 Cylindrical punch, deepened into an elastic half-space: (**a**) calculation scheme, (**b**) deconvolution of the lateral surface and discretization of the contact domain

5.4.2 Vertical Cylindrical Piles Under an Inclined Load

Piles without a pile raft. A series of numerical experiments was devoted to the studies of the influence of a cylindrical pile length and the direction of an inclined load on the character of the pile displacement in the soil. The calculation scheme, corresponding to the case in question, is presented in Fig. 5.8. The same figure shows the discretization of the contact surface of the pile and the soil into boundary elements. The external load values, contained in the equation system (2.13) and (2.14), are taken as follows:

$$P_1 = 0,\ P_2 = R\cos\varphi,\ P_3 = R\sin\varphi,\ M_1 = M_2 = M_3 = 0.$$

Calculations of characteristics of contact interaction of separate cylindrical piles depending on the inclined load direction are presented in Figs. 5.9 and 5.10. Due to the calculation scheme symmetry with respect to the vertical pile axis, the calculations are performed for the external force inclination angles within the range of $90° \le \varphi \le 180°$. In order to plot the results graphically (most of the plots appeared to be quite monotonous), the calculations were performed with a step of 6°. In some cases the step was reduced to 3°, 1°, and even 0.5°. The relative pile length H/r_1 was 3, 10, and 20, r_1 being the pile cross-section radius. The calculations were carried out in two variants – with and without the account of unilateral constraints at the pile–soil contact and the values of $R/Er_1{}^2 = 1$, ν=0.3.

Figures 5.9 and 5.10a show the calculation data for a short pile ($H/r_1 = 3$). Numerical results, obtained under a vertical load without the account of unilateral constraints, were the test data and are in part described in Sect. 3.5.2. With the increase of the angle of inclination of the force R the horizontal component of the inclined load $R\sin\varphi$ increases while its vertical component $R\cos\varphi$ simultaneously decreases. This results in the absolute values of the vertical and horizontal displacements decrease and increase, respectively. Simultaneously the slope ψ_x increases, its maximal value being achieved under a purely horizontal load.

The account of the unilateral constraints in the contact domain results in considerable quantitative changes. This is related to the contact area decrease due to the formation of contact zones where tensile normal stresses act. As follows from the numerical experiments, the zones with negative stress arise at the lower end of the pile shaft (Fig. 5.9) and increase towards the foundation bottom, encompassing larger areas both with the increase of the load absolute value R and with the relative deepening parameter H/r_1. Here a "wedging" effect is revealed: on the lower part of the pile lateral surface a tension zone is formed as well as a gap between the pile and the soil, while on the upper part a compression zone arises.

The strongest effect of the "wedging" on the pile behaviour is for the φ angles, close to 90°, for the solutions, obtained with the account of the gap formation between the pile and the soil. In our opinion, this effect is to a considerable degree related to the specific features of the contact pressure formulation. They consist in the fact that on the boundary elements where compressive normal stress acts, no possibility of the pile slippage with respect to the base is provided and, as a consequence, no restrictions are imposed on the tangential stress values. In the course of the numerical solution of the contact problem, at each iteration step, boundary elements on the pile lateral surface are consecutively (from the bottom up) excluded, since the stresses on these elements are tensile (See the test example from Sect. 3.5.2 as well as Fig. 5.9). In the course of the iterations part of the lateral surface of the vertically loaded pile is excluded from the contact domain between the pile and the soil. As a result, the load is transferred from the pile to the soil only by its bottom and a ring-shaped area of the lateral surface, represented by the upper rows of the boundary elements. With the account of the possibility of the pile slippage

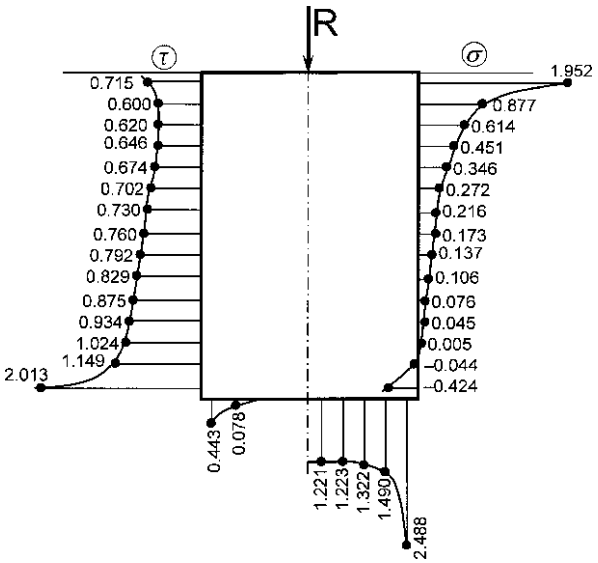

Fig. 5.9 Profiles of tangential (τ) and normal (σ) contact stresses at central loading of a short pile ($H/r_1=3$) without a pile raft

with respect to the base surface, the influence of the "wedging" effect on the pile behaviour can be smoothed.

For all external load inclination angles, the "wedging" effect results in an increase of the absolute values of horizontal displacements Δ_y and slopes ψ_x. The maximum relative difference for these values, due to the account of the unilateral constraints, for a short pile (with a relative depth of $H/r_1 = 3$) reaches 25% and 37%, respectively. With the increase of the resultant force inclination angle, the Δ_z values, with the account of the unilateral constraints, almost up to $\varphi \approx 125°$ exceed the corresponding values, obtained without the unilateral constraint account. At $\varphi \approx 125°$ the two plots intercept (Fig. 5.10a) what is the evidence for the fact that the contact interaction with the formation of a gap between the pile and the soil at such φ does not lead to any changes of vertical displacement. At further increase of the resultant force angle φ, the account of the unilateral constraints results in an increase

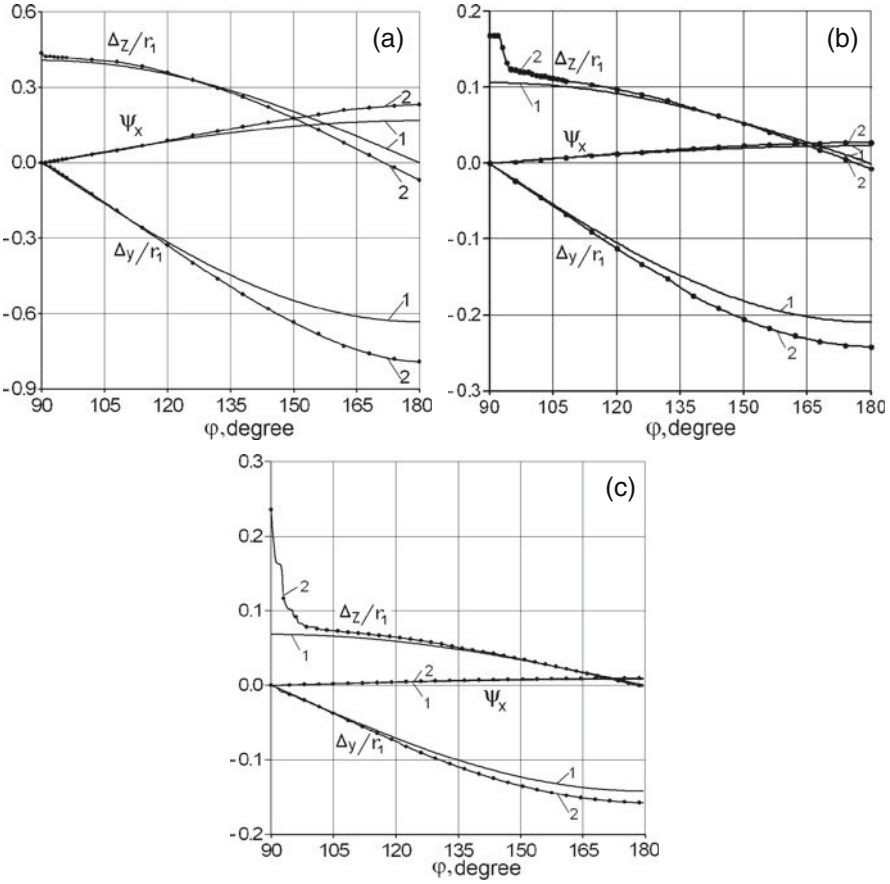

Fig. 5.10 Displacements and loads of a cylindrical pile depending on the inclined load direction without (1) and with (2) the account of unilateral constraints; $H/r_1 = 3$ (**a**); 10 (**b**); 20 (**c**)

of the absolute values of horizontal displacements Δ_y and slopes ψ_x. However, the increase of the external load horizontal component, increasing with φ, results in a sharp decrease of vertical displacements Δ_z. At the load, practically close to horizontal ($\varphi \geq 170°$), there are practically no vertical displacements near the pile head, and with the further increase of the load inclination angle the pile can even go up ($\Delta_z<0$). In other words, at horizontal (or close to horizontal) pile loading it can be squeezed out of the soil towards the base surface. With the increase of the relative pile length this effect becomes less noticeable (Fig. 5.10b, c). Note that in case unilateral constraints being not taken into account, no such effect is observed, i.e. always $\Delta_z \geq 0$ and the pile does not move upward.

Consider the effect of the relative depth H/r_1 on the linear and angular displacements of the pile. It can be analyzed from the comparison of the calculated dependences, plotted in Fig. 5.10. The numerical analysis performed has shown all the calculated dependences to be qualitatively similar. As one could expect, the pile displacement under the same external load essentially decreases with the increase of the relative pile length. With the relative length decrease, the discrepancies between the solutions, obtained with and without the account of unilateral constraints, become more and more noticeable. The pile settlement behaviour depending on the conditions, accepted for the contact surface, is ambiguous. At the angles φ, close to 90°, the account of unilateral constraints results in the pile settlement increase. In the range of φ variation from 90 to 180°, starting from a certain value of φ, depending on the pile length, a reverse dependence is observed, namely the settlement decrease with the account of the unilateral constraints. Variation of the H/r_1 parameter provides the strongest effect on the vertical pile displacements. The relative depth increase plays an important role only under almost vertical loading ($\varphi \approx 90° \pm 6°$), when the effect of horizontal forces is small yet, and the decisive role is played by the "wedging" effect. At such loading conditions, the account of unilateral constraints results in considerable additional settlements, whose values can be compared with the settlement values calculated without the gap formation, using Table 5.3.

The obtained calculation data for the settlements and slopes of separate short, medium, and long cylindrical piles enable, with the account of the pile uplifting from the soil base, the displacements and slopes under an arbitrary inclined load, the settlements and slopes under an arbitrary inclined load to be evaluated without the hypothesis of the coefficient of subgrade reaction. Besides, the data quoted here, will be used in subsequent chapters for comparative estimations of the obtained

Table 5.3 Effect of relative depth on the settlement of piles without a raft under vertical loading without (numerator) and with (denominator) the account of unilateral constraints

H/r_1	3	10	20
	0.406	0.106	0.0685
Δ_z/r_1	0.436	0.165	0.2355
Settlement increment, %	7.4	54	244

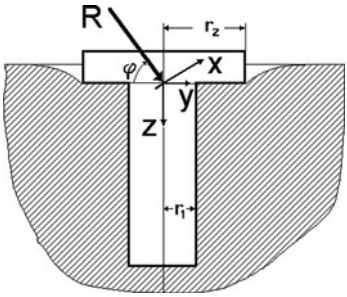

Fig. 5.11 Calculation scheme for a vertical pile with a circular pile raft

calculation results for pile raft foundation structures with both vertical and inclined piles.

Vertical short piles with a low circular pile raft. The presence of a low pile raft is known [20, 167] to produce an essential effect on the load transfer to the base and, in particular, to enable the load increase on a pile foundation.

We studied the effect of the pile raft size on the interaction of the pile foundation with the soil for the example of vertical cylindrical piles with a circular cylindrical pile raft. The calculation scheme for this case is presented in Fig. 5.11. The general outlook and the discretization of the contact surface of the pile foundation with the soil into boundary elements are shown in Fig. 5.6a. The discretization of the pile raft contact surface is illustrated by Fig. 5.7a.

For the calculations the following parameters were fixed: the pile diameter r_1 and its length $H = 10r_1$. The pile raft radius ($r_2/r_1 = 0$, 2, and 4) and the external load vector value were varied. The latter value was chosen from the condition of the average contact pressure being constant for the piles with different pile rafts. The load direction was varied within $0° \leq \varphi \leq 180°$. In a separate study the influence of the pile raft location eccentricity with respect to the pile axis on the characteristics of the pile foundation displacement in the soil. The solutions were obtained both with and without the account of unilateral constraints on the contact of the pile with the soil.

The results of the performed numerical studies of processes of interaction of separate piles with a low circular raft with soil are shown in Figs. 5.12, 5.13, and 5.14.

Comparison of the plots, presented in Figs. 5.12 and 5.13, shows that the presence of a circular pile raft with a radius of $r_2 = 2\ r_1$ (the pile frat of such size increases the surface of the foundation contact with the soil by 14.3%) does not result in any essential qualitative changes of the contact interaction characteristics, in comparison with the case of a pile without a raft. At a fixed external load value, the decrease of horizontal displacements both with and without the account of unilateral constraints in the example under consideration achieves 20.1% with the slope decrease up to 25.8%. The most essential effect of the pile raft presence is for the case of vertical displacements Δ_z at a vertical or near-vertical load. This is revealed, first of all, in a decrease of settlements for the pile with a raft. With the general pattern of the

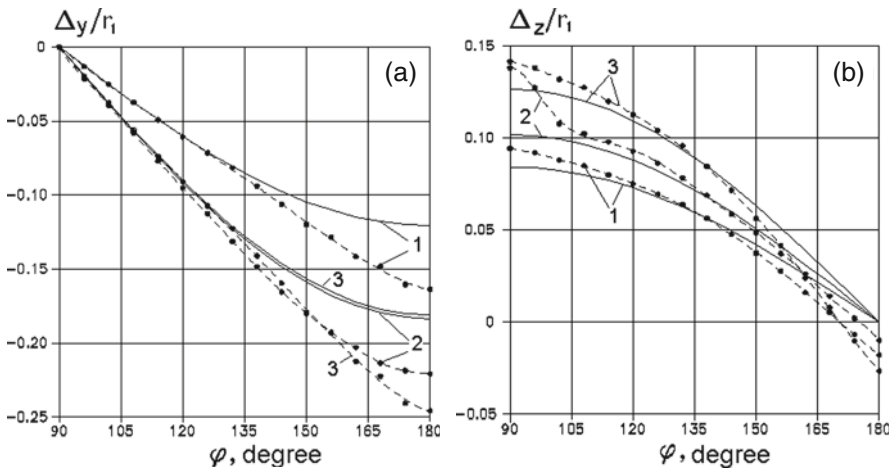

Fig. 5.12 Horizontal (**a**) and vertical (**b**) displacements of pile foundations (H/r_1=10) with a circular pile raft depending on the inclined load direction without (*solid lines*) and with (*dashed lines*) the account of unilateral constraints: (1) r_2=4r_1 , $R = r_1^2 \cdot E$; (2) r_2=2r_1, $R = r_1^2 \cdot E$; (3) r_2=4r_1 , R =1,5$r_1^2 \cdot E$

"wedging" effect being preserved, at the increase of the load inclination angle the presence of the pile raft results in a smoother decrease of settlements at the account of unilateral constraints and, on the contrary, to their sharper decrease in case the gap formation not being taken into account. With the further increase of the pile raft size (r_2= 4 r_1) at vertical or near-vertical loading the "wedging" effect is still preserved (Figs. 5.12 and 5.13); however, it is less pronounced. It follows from the calculations performed that the pile raft size increase essentially affects the displacements and slopes at a load close to horizontal, when a considerable part of the pile raft is excluded from the interaction with the soil. The data for the comparative analysis of the displacement and slope numerical values under vertical and horizontal loading are presented in Table 5.4.

Table 5.4 Effect of pile raft size on the characteristics of contact interaction of the soil and the pile foundation (H/r_1 =10) under vertical (Δ_z) and horizontal (Δ_y, ψ_x) loading without (numerator) and with (denominator) the account of unilateral constraints

r_2/r_1	Δ_y/r_1	Horizontal loading ψ_x (rad)	Vertical loading Δ_z/r_1
2	0.184 / 0.221	0.0193 / 0.0244	0.102 / 0.138
4	0.121 / 0.164	0.0107 / 0.0166	0.0842 / 0.0943
4 ($R\prime$=1.5·R)	0.181 / 0.246	0.0160 / 0.0249	0.126 / 0.141

$R\prime$ is the increased load (by factor of 1.5).

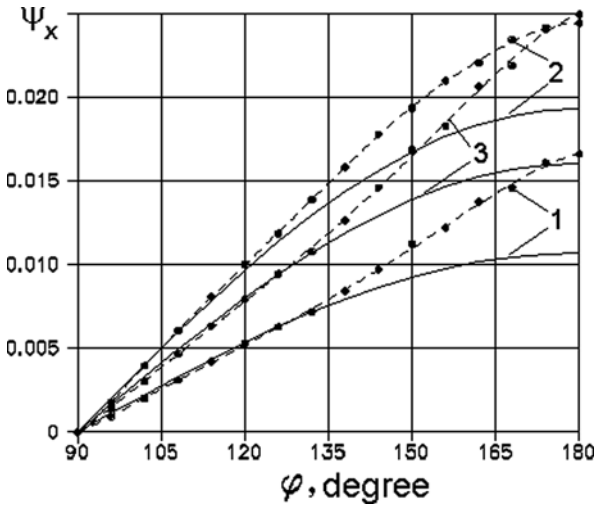

Fig. 5.13 Slopes of vertical cylindrical piles ($H/r_1=10$) with a circular pile raft depending on the inclined load direction without (*solid lines*) and with (*dashed lines*) the account of unilateral constraints. (1) $r_2=4r_1$, $R = r_1^2 \cdot E$; (2) $r_2=2r_1$, $R = r_1^2 \cdot E$; (3) $r_2=4r_1$, $R =1{,}5\ r_1^2 \cdot E$

As one should expect, the slopes of a pile foundation structure decrease with the pile raft size (Fig. 5.13). An increase of the load absolute value results in a practically similar increase of slopes and displacements. The comparison of calculations, performed under a fixed average contact pressure for pile structures with rafts of different size and piles of the same length, shows the pile raft size increase to result in an essential slope decrease.

Independently of the pile raft size and the external load absolute value, there is a direction of the load action, for which the account of unilateral constraints does not result in any change of the pile structure settlements. In this case the decisive parameter is the relative pile depth H/r_1. As shown by the calculations, at $H/r_1 = 10$ such situation is observed at $\varphi \approx 135°–140°$ (Fig. 5.12b). Horizontal displacements (without the account of unilateral constraints) decrease, though slightly, with the pile raft size increase. This is the evidence for the main effect on the horizontal displacements in the case of a full contact of the pile foundation with the soil is produced by the pile length. On the other hand, with the increase of the pile raft size, as seen from Fig. 5.12a, the account of unilateral constraints results in the Δ_y displacement increase with the increase of the horizontal load component.

At $45° \leq \varphi \leq 135°$ the settlements of a pile structure with a larger raft are higher than for the one with a smaller raft, while at a horizontal or near-horizontal loading the situation is opposite (Fig. 5.12b). This is related to the fact that, when the vertical component of the external load exceeds the horizontal one, the major part of force is taken up by the pile tip and its lateral surface. The redistribution of forces over the pile raft surface makes less effect on the contact interaction characteristics. At a horizontal load, a considerable part of the structure with a pile raft does not participate

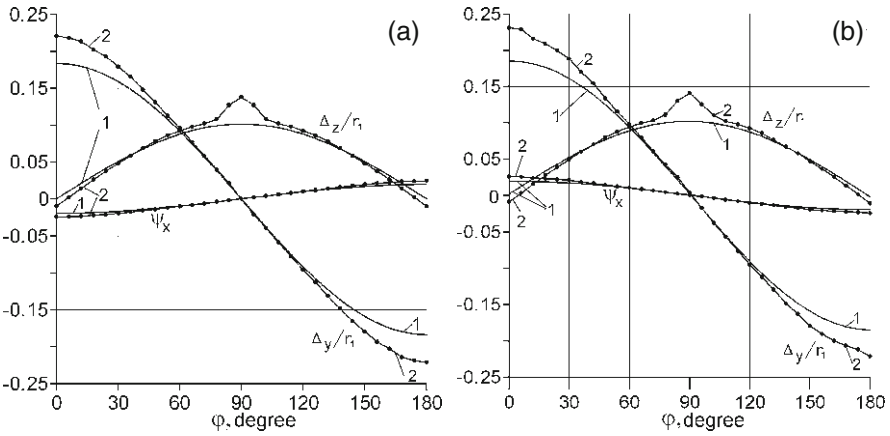

Fig. 5.14 Displacements and slopes of a vertical cylindrical pile (H/r_1=10) with (**a**) a concentric and (**b**) an eccentric (ϵ_x/r_1=0.3) round pile raft (r_2=2r_1) depending on the inclined load direction (1) without and (2) with the account of unilateral constraints

in the contact interaction with the soil and, to a considerable extent, the increase of the specific contact pressure results in the increase of vertical displacements for the foundation with a larger pile raft.

By comparing the plots, presented in Fig. 5.14, one can estimate the effect of an eccentrically located pile raft on the slopes and settlements of a pile structure in the soil. First of all, as follows from the comparative analysis, even a relatively slow eccentricity in the pile raft location with respect to the pile symmetry axis (ϵ_x/r_1= 0.3) results in rather noticeable slopes in the opposite direction. This is an additional theoretical confirmation for the applicability of asymmetrical foundation structures of console type, accepting simultaneous horizontal and vertical loads from structures with a spacer-type scheme [105, 113, 170]. For the horizontal and vertical displacements the effect of an asymmetrical pile raft is less noticeable: the highest asymmetry is observed in the difference of horizontal displacements at φ=0° and φ=180°. For the example under consideration this difference is negligibly small without the account of unilateral constraints in the contact domain and reaches 4.5% in case them being taken into account.

5.4.3 Foundations with Inclined Piles and a Rectangular Pile Raft

A separate series of numerical experiments was carried out for the estimation of the effect of the pile inclination angle on the pile raft foundation displacements. Piles with a given angle α of deviation from the vertical direction were considered, conjugated with a rectangular pile raft. The calculation scheme is shown in Fig. 5.15. The shape of the surface of the foundation and the soil contact, subject to discretization,

is shown in Fig. 5.6c. The total number of the boundary elements on the pile and the pile raft did not exceed 500.

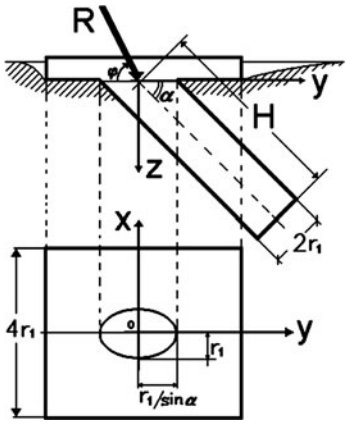

Fig. 5.15 Calculation scheme for an inclined pile with a square pile raft

Figures 5.16 and 5.17 show the calculated dependences of slopes and displacements for a foundation with piles of a fixed length $H/10r_1$, inclined to the base surface at angles $\alpha=30°$ and $\alpha=60°$, for the different angles of the resultant inclination. The pile raft was assumed to be a square with a side $4r_1$ and the inclined axis of the pile to pass through its centre. The inclined load acts in the symmetry plane of the pile foundation (Fig. 5.15).

As follows from the data obtained (Figs. 5.16 and 5.17), all the calculated curves are considerably asymmetrical. It is seen from Fig. 5.17 that there are no horizontal displacements at the load inclination at an angle $\varphi = \varphi_0 \approx 75°$. The value of φ_0 is practically not related to the angle α of the inclination of the pile itself and

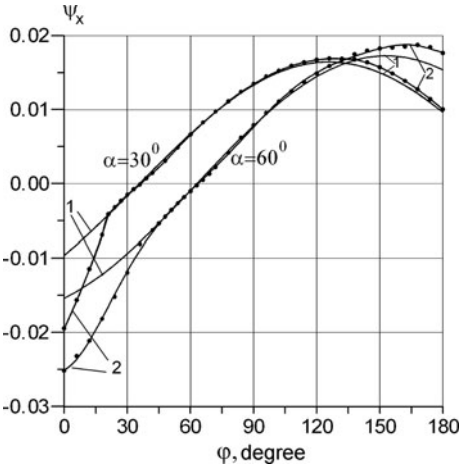

Fig. 5.16 Slopes of foundations with an inclined pile ($H/r_1=10$) and a square pile raft depending on the inclined load direction (1) without and (2) with the account of unilateral constraints

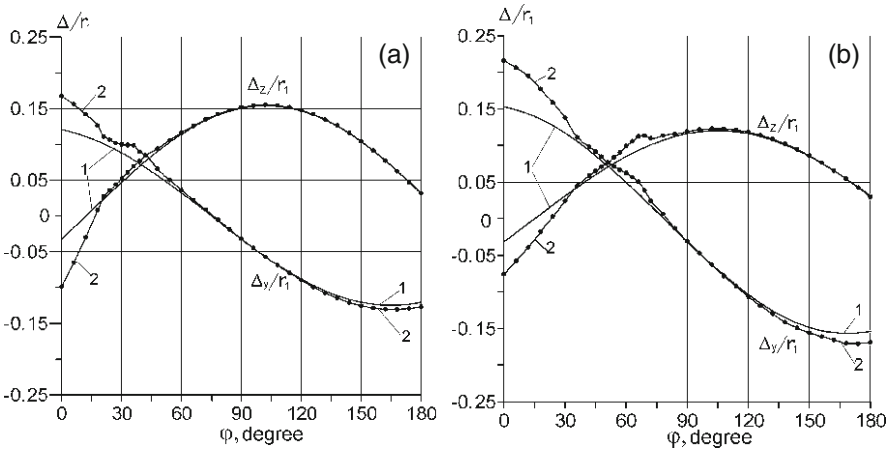

Fig. 5.17 Relative displacements of foundations with an inclined pile ($H/r_1=10$) and a square pile raft depending on the inclined load direction (1) without and (2) with the account of unilateral constraints; $\alpha=30°$ (**a**), 60° (**b**)

is determined mostly by the foundation structure size. Up to the value of φ_0 the account of unilateral constraints plays an important role for the determination of the displacement values. The largest difference is observed at a horizontal load ($\varphi = 0°$), when the foundation structure is most uplifted from the soil. The same holds for slopes (Fig. 5.16). With the increase of the angle φ of the resultant force inclination, its horizontal component decreases and the conditions are achieved, at which the structure and the soil are in contact over the entire surface of the pile and the pile raft. At $\alpha=30°$ the mentioned angle of the load inclination is $\varphi\approx15°$, while for $\alpha=60°$ $\varphi\approx45°$. However, when the load direction slightly deviates from the pile axis ($\varphi\approx\alpha\pm15°$), the "wedging" effect is noticeably revealed, leading to additional displacements both in the horizontal and the vertical direction. In this case the pile structure slope due to the account of unilateral constraints, is small what is important for the foundation design. A subsequent (up to $\varphi\approx120°$–$135°$) increase of the resultant inclination angle practically does not result in any noticeable uplifting of the structure from the soil. With the further increase of the φ angle the role of the horizontal component of the external load vector becomes increasingly important. Due to the increasing uplifting of the structure from the soil, an additional slope arises and the horizontal displacement absolute values increase. Simultaneously, the uplifting of the structure from the soil does not make any noticeable influence on the development of vertical displacements.

Thus, from the calculations using the proposed boundary-element method, one can obtain the main features of contact interaction of pile structures with low pile rafts of various geometry. This will enable the pile foundation displacements and slopes depending on the external force direction and value to be reliably determined at the stage of design by variation of the pile raft shape and location as well as the pile size and inclination angle.

5.5 Spatial Contact Problem for a Bored Pile Foundation with a Widening

Bored pile foundations are successfully used for construction of buildings and structures of various type (industrial, social, residential, rural, etc.) on cohesive (clay) soils, especially under high concentrated vertical and horizontal loads as well as on construction sites with complicated geotechnical conditions [97, 162, 166, 247]. High bearing capacity and lower settlements of bored pile foundations in comparison with those, performed in open trenches, are explained by the preserved soil base structure, rational bottom shape and good contact of the foundation with soil.

Application of efficient structures of bored pile foundations enables the degree of work mechanization to be increased, material consumption for the foundation to be decreased, the work to be performed in any season, the construction duration to be reduced. The expenses for the foundation construction are reduced on the average by 60%. Application of bored pile foundations enables one to decrease the consumption of metal, fuel, and power resources, to reduce essentially transportation expenditures, as well as to exclude the pile cut-off.

Bored pile foundations are also effective from the point of view of technical solutions:

- in case of necessity of the piles to be bored through embankments with hard inclusions (in the form of fragments of destroyed stone, concrete, ferroconcrete buildings and structures) or through natural layers of hard clay soil, soils with frequent boulders, etc., when pile driving or immersion cannot be performed;
- on constrained sites where it is difficult to transport and install displacement piles;
- near the existing buildings and structures where inadmissible deformation of elements of bearing structures or equipment can arise due to the pile driving or vibroimmersion.

The practical experience of foundation engineering has shown bored pile foundations to be suitable for bearing-wall buildings with bearing basement and ground floor outer walls as well as for bearing-wall or brick buildings with pile rafts or edge beams. Besides, bored pile foundations are applicable for skeleton-type buildings without basements. In this case the excavation bulk-up is minimal and equal to the volume of excavation work under the foundations. The most advisable (from the technical and economical point of view) is application of bored piles in case of the possibility of their placement without strengthening the walls of the well.

The bearing capacity of bored pile foundations can be increased both by the pile length increase (this is, however, related to the considerable work complexity and labour consumption) and due to the bored piles with widenings resulting in the increase of the bearing capacity due to the development of a part of the shaft (footing, head, or the intermediate part).

5.5.1 Production and Structures of Bored Pile Foundations with a Support Widening

Technology of production of bored pile foundations consists of the following operations: well sinking using a rock drill, construction of the widening, installation of the reinforcement, and placement of concrete.

Widenings are mostly constructed by soil drilling out and compression by an impact or a static load.

Bored piles with radial widenings, produced by the soil compression by an impact load, are used for construction of rural objects on collapse soils of I type [234]. The experience of construction work testifies for a high speed of the whole cycle of construction of each well with a broadened footing. Short bored piles with a radially broadened footing are effectively applied in clay soils (including collapse soils of type I and swelling soils) of hard, semihard, and low-plasticity consistency.

For construction of foundations under supports of aerial power lines in ever-frozen soil, for which labour consumption reaches 40%, an efficient technological solution is anchoring of metallic piles of steel pipes [92]. This enables the bearing capacity with respect to pulling loads in summer as well as with respect to the frost heave to be increased. The most simple and natural is application of the pile body widening as anchor elements. An effective energy source, providing the pile shape change and impression of the pile body widening into the soil, is a concentrated explosive charge, exploded in the pile cavity, since the produced pressures are sufficient for the deformation of soil of any strength. In the course of the pile shaft deformation, the widening shape is a part of a toroidal surface, described by a semicircle, rotating around the pile axis. Due to the widening formed, the force provided by conventional lifting means is insufficient and the bearing capacity considerably exceeds the operational requirements.

Bored pile foundation structures with spheroconical widenings have appeared to be quite reliable [211, 212, 227]. Wide possibilities for the variation of the widening diameter and depth enable one to adjust the bored pile foundation settlements at drastically different loads on separate foundations, at the variation of the deformational characteristics of the soil base under the building as well as in the case of oblique soil base layers. The advantages of the foundations of this type are relative simplicity of the fully mechanized construction technology, absence of the soil collapse from the walls of the conical part of the widening during the whole work cycle. Corresponding typical solutions of bored pile foundations have been worked out, used for residential houses of 5–14 storeys. The high efficiency of the bored pile foundations has been shown by the construction of 14-storeyed brick buildings; the settlements of a building on a bored pile foundation appeared close to those of a building, constructed on displacement piles. Technical and economic parameters of conventional pier foundations and bored pile foundations with spheroconical widenings were determined on the base of estimate calculations (for bored pile foundation being used instead of conventional pier ones, the excavation work is shortened by 94%, concrete consumption – by 19%, metal consumption – by 63%, general expenses – by 41%, and labour consumption – by 55%) [211].

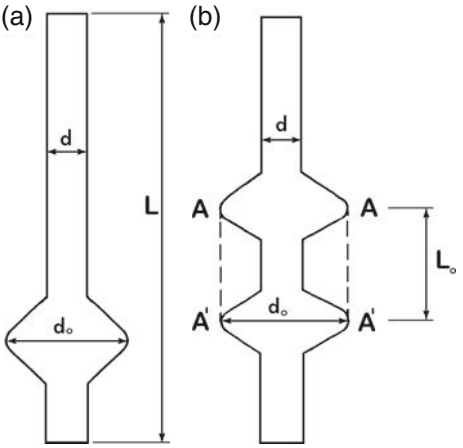

Fig. 5.18 Bored pile foundations with widenings: (**a**) with a single widening, (**b**) with a double widening

Bored pile foundations with widenings were extensively applied in India for construction on swelling soils as anchor type piles as well as load-carrying piles [149]. For anchor piles, as a rule, one widening is used (Fig. 5.18a); for load-carrying piles several widenings can be used (Fig. 5.18b). Bored pile foundations with a single widening are used in the same way as piles with a broadened footing, the widening can be located above the footing.

For bored pile foundations with two or more widenings, separated by a certain distance, the soil between the widenings functions as a part of the pile in such a way that the total soil resistance can be taken on the A–A' surface of a cylinder with a diameter, equal to the widening, and height, equal to the L_o step (Fig. 5.18b). These features of the contact interaction were confirmed by model experiments [149]. Besides, it was shown by the Indian researchers that in order to achieve the maximal efficiency, the optimal step between the widenings in a multiple-widening foundation should be within 1.25–1.5 of the widening diameter. As an example for economy of materials, the application of bored pile foundations with multiple widenings, working in London clays, is mentioned: for the same bearing capacity the concrete volume in a homogeneous pile should be increased by more than four times.

Finally note that a cylindrical footing, present for all bored pile foundation structures under consideration, is required not only from the point of view of their production technology, but also from the point of view of the structure stability; in this case the possibility of a unilateral hear of the widening base is excluded and the vertical character of displacements is provided.

In case developed and perfect methods of calculation and design as well as appropriate technical and economic substantiation being used, bored pile foundations with widenings can be applied for various types of industrial and civil buildings. As shown by the experience of engineering [227], the method for construction of bored

pile foundations with support widenings is a promising one, and, hence, requires further development of the corresponding methods for calculation and design.

5.5.2 *Engineering Methods for Calculation of Bored Pile Foundation Bases from the Base Deformation*

For the further development of the existing engineering methods for calculation of bored pile foundations according to the limiting states and for working out new methods one should have a clear and full concept of the character of functioning of each separate part of the foundation. First of all, it is important to elucidate the role of the widening and the cylindrical footing of the foundation in the load transfer from the building to the soil, i.e. to determine the quantitative distribution of load between the main structural parts of the foundation.

Field tests have enabled the qualitative pattern of interaction of the main parts of foundation with the base to be studied, the soil deformation character and the conditions of formation of condensed zones (kernels) in it under the widening bottom and the cylindrical footing bottom to be elucidated, the stress distribution character on the contact of the bottom and the soil to be determined, quantitative relationship between the loads on the widening and the footing to be found. However, the experiments on the elucidation of the specific features of the condensed kernel formation and the displacement distribution in the foundation model base give only the qualitative description of the effect.

Quantitative estimations of the experimentally observed facts of the effect of the widening bottom shape on the base deformation character are required. In particular, it has been found that at equal displacements in the widening bottom boundary areas, the shear areas are less developed for a more convex bottom. Besides, with the increase of the convexity degree the development of the vertical deformation area decreases. Therefore, data regarding the limiting diameter value for the foundations with a convex bottom, are required. In case this limiting value being exceeded, the relative bearing capacity (i.e. the ratio of the bearing capacity to the foundation concrete volume) of the foundation decreases.

Finally, quantitative estimations of the available test data for the bored pile foundations (of various diameter, with various widening depth, with footing excluded) at various soil conditions are required, that will enable the distribution of the overall load among the foundation elements to be specified.

The currently available calculation methods and schemes do not fully comply with the specific features of bored pile foundation structures and do not take into account the functioning of the footing together with the widening as well as the geometrical characteristics of the widening and a number of other factors. Therefore, a further development of the calculation method is required with the account of a spatial formulation, suitable for different bored pile foundation types and sizes with different geometry of the widening and its different location with respect to the cylindrical footing.

A simplified method for the bored pile foundation calculation (only for the vertical load), proposed in [227], is based on an assumption of the whole structure functioning being divided into the functioning of two independent elements – a widening and a footing, interaction between them being formally excluded. A vertical load N, applied to the foundation, is divided into the parts λN and $(1–\lambda)N$, accepted by the widening (λN), considered as a ring, and by the footing, $(1–\lambda)N$. A coefficient of participation of the ring-shape widening λ is introduced, being taken into account in the calculations in accordance with the values of the widening diameter and the footing height, according to the Table 6 of [227]. The calculation method is based on the choice of such value of the λ parameter, for which the settlements of the ring-shaped widening S_1 and the cylindrical footing S_2, rigidly assembled into a unique solid structure, are equal. The settlement values S_1 and S_2 are found in a rather approximate way using a known layer summation method. It is a rather labour-consuming task to provide the main condition $S_1 = S_2$ to be fulfilled with an accuracy of 5%. It is performed in several stages using a plenty of tabulated data. For the determination of stress in the base of a bored pile foundation, a theoretical solution by Egorov [34] under a flat punch with a ring-shaped bottom is used. The roles of the conical and spherical parts of the widening are not being taken into account. Besides, for the sake of simplification of the calculations, the contact stress profile over the ring-shaped widening bottom and the nominal shaft toe footing is taken rectangular.

Experimental studies of functioning of an off-centre loaded bored pile foundation with a widening were performed in [211, 212], where the recommendation regarding their calculation were also worked out. The effect of eccentricity on the average settlement, slope, horizontal displacements, rotation centre position, etc. was found. The proposed method for the calculation of bored pile foundations with the account of the resistance of the soil above the bottom, is based on the method for the calculation of deep massive foundations [244]. The Fuss-Winkler base model is taken as the calculation model. Note that usage of the coefficient of subgrade reaction for the calculation of piles only for the horizontal load was earlier proposed by Tsymbal [222].

Spatial functioning of the foundation was considered by Sorochan and Gruodis [211, 212] only in the vertical plane of its symmetry under a horizontal force and a moment. The effect of the vertical force is taken into account only for the determination of pressures under the footing of the foundation widening.

The crucial point of the calculation method, proposed in [211, 212], to a great extent determining the reliability of the calculations, is the choice of the coefficient of subgrade reaction C variation with depth. Horizontal coefficients of subgrade reaction are calculated on the base of the experimental data and essentially depend on the geometrical shape of the support widening. For comparison of the calculation and the experimental data, two laws of the C variation with depth were used:

linear $C_z = C \cdot \frac{z}{h_f}$,

nonlinear $C_z = C \cdot \sqrt{\frac{z}{h_f}}$

where h_f is the footing bottom depth, $C=k\cdot C_0$ is the non-uniform compression coefficient (a characteristic of the base rigidity), $k$is a coefficient, taking into account the relationship between the uniform and non-uniform compression coefficients (for round foundations $k=2.68$), p_0 is the average additional pressure under the widening bottom, $\overline{W}$ is the foundation settlement, determined from the Construction Rules and Regulations as for a nominal foundation on a natural base.

The application of both hypotheses gives a rather high discrepancy with the experimental results of the slope determination (for the linear law – by factor of up to 2.5, for the nonlinear law – by factor of 1.5). One can just make the calculations according to the Construction Rules and Regulations more specified as well as trace a general trend of the increase of slopes, settlements, and horizontal displacements at a fixed average pressure under the bored pile foundation widening bottom.

The method for the calculation of bored pile foundations with widenings, elaborated in [211, 212], due to its simplicity and visuality, was included into a designer's handbook [215]. However, one should take into account that it enables the calculations to be preformed according to the second group of limiting states with insufficient accuracy and only with a great amount of field test data being available.

Thus, the complicated character of functioning of bored pile foundations with widenings at the interaction with the soil base requires additional detailed studies of the soil reactive pressure over the lateral surface based on the formulation and solution of the spatial contact problem (as a rule, bored pile foundations transfer a spatial force system to the base, this force system being in the general case a combination of a vertical, a horizontal, and a momental load).

Since bored pile foundations with support widenings, having rather small relative depth, are characterized by high rigidity, for them a calculation scheme in the form of a volumetric deepened punch seems natural to be applied. The base model will be treated as a linearly deformable half-space, weakened by a cavity, whose boundaries are in full correspondence with the contact surface of the foundation structure to be calculated.

Below the examples of numerical boundary-element calculation of bored pile foundations with spheroconical widenings under a vertical and an inclined load are considered.

5.5.3 Calculation of Deformations of the Base of a Bored Pile Foundation with a Spheroconical Widening Under a Central Loading (Axisymmetric Contact Problem)

Consider a bored pile foundation in the form of a deepened punch with a spheroconical widening, fixed in an elastic half-space. In the simplest case it is assumed to be loaded only by a vertical force along the symmetry axis. Due to the axial symmetry, the deepened absolutely rigid punch in the shape of a rotation body with a spherical and a conical widening will be displaced only vertically. The stressed state of the elastic half-space (the soil base) is characterized by a radial and a tangential component of the contact stress vector (tangential stress is zero due to the

axial symmetry) and depends only on the vertical coordinate. The system of integral equations, written on the base of the reciprocality theorem, including the punch equilibrium equations, is considered above in Sect. 2.4.1.

For the numerical solution of the system of Eqs. (2.30) and (2.34), the contact surface of the foundation and the soil is partitioned into meridional zones, each of them being divided by horizontal planes into triangular and quadrangular boundary elements. On each boundary element the contact stress functions are averaged. The dimensionality of the boundary-element problem is reduced and equals $(2M+1)$ with respect to the values $p_r^{(i)}$, $p_z^{(i)}$ $(i=1, 2,...M)$ and Δ_z where M is the total number of the boundary elements along the generatrix of the bored pile foundation. The averaged contact force values are expressed only in terms of the punch rigid axial displacement. As noted above in Sect. 2.4.1, in the cylindrical coordinate system the problem is essentially simplified and becomes in fact a one-dimensional one.

In the practical calculations, the generatrix of the bored pile foundation was partitioned by horizontal planes into 25, and along the angular coordinate – into 16 equal partitions. As above, regular integrals were computed using the cubature formulae of the highest accuracy degree, singular integrals were calculated semi-analytically with selection of the singularity. The calculation scheme for the general case and the boundary-element grid, used for the numerical solution, are shown in Figs. 5.19 and 5.20.

Figure 5.21 presents the results of the contact problem solution in the form of normal and tangential contact stress profiles for a meridional cross-section of a short bored pile foundation ($h/2a=3$) in the fractions of the contact pressure average value $\sigma_{av} = N/F$where F is the contact surface area, N is the vertical load on the foundation. The Poisson ratio value was taken $\nu=0.3$. The widening dimensions are determined by the ratios $b/a=2.5$, $r_f/a=3$, its depth $h_f/a=2.5$, 4.0. A specific feature of the normal stress σ profile should be noted, consisting, as one should expect,

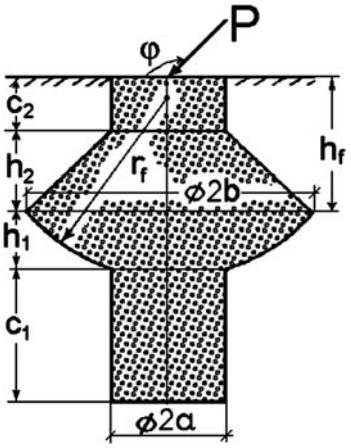

Fig. 5.19 Calculation scheme for a bored pile foundation with a support widening under an inclined load

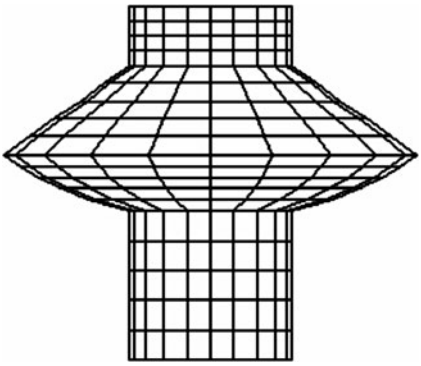

Fig. 5.20 Discretization of the contact surface of the foundation and the soil using boundary elements

in the presence of tensile stresses in the conical part of the deepened punch lateral surface what is related to the lack of account of unilateral constraints in the contact domain.

The calculation results for the bored pile settlements, using the boundary-element method (requiring only the deformational characteristics of the soil E and ν to be used), are listed in Table 5.5. The calculations were performed both with and without the account of unilateral constraints.

The geometrical dimensions of the bored pile foundation with a support widening and its loading conditions are presented in Fig. 5.22. The following physical and mechanical characteristics of the soil were taken (sand-clays and clayeys of low-plasticity and semihard consistency):

deformation modulus E=1270 t/m^2,
Poisson ratio ν=0.3,
density =1.7 t/m^3,
internal friction angle δ=16°,
cohesion C=2.9 t/m^2.

As follows from Table 5.5, an increase of the contact surface discretization degree above 400 elements by each 100 elements results in the increase of the numerical solution accuracy by less than 1%. Assuming the calculation results to be linearly dependent of the value n^{-1} (n being the number of the boundary elements), one can easily find the limiting values of the foundation settlement: S=3.829 cm without

Table 5.5 Settlement (cm) of a bored pile foundation with a support widening, calculated by the boundary-element method

Number of boundary elements	$n = 400$	$n = 500$	$n = 600$
Without the account of unilateral constraints	3.881	3.870	3.864
With the account of unilateral constraints	4.127	4.113	4.105

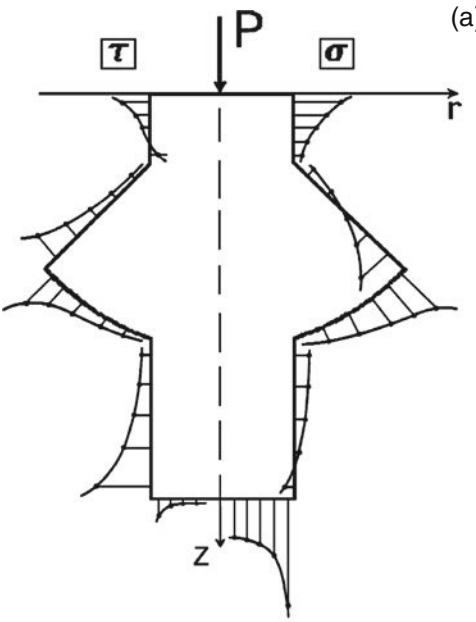

n	z/a	r/a	τ	σ
1	0.1	0.981	0.257	0.927
2	0.3	0.981	0.121	0.563
3	0.5	0.981	0.078	0.449
4	0.7	0.981	0.042	0.351
5	0.9	0.981	-0.008	0.233
6	1.157	1.134	0.087	0.132
7	1.455	1.427	0.151	0.034
8	1.754	1.721	0.204	-0.081
9	2.054	2.014	0.268	-0.211
10	2.353	2.308	0.579	-0.584
11	2.599	2.363	0.895	1.088
12	2.798	2.165	0.393	0.646
13	2.998	1.927	0.279	0.587
14	3.197	1.631	0.158	0.515
15	3.394	1.235	0.004	0.326
16	3.75	0.981	0.089	0.140
17	4.25	0.981	0.268	0.086
18	4.75	0.981	0.395	0.043
19	5.25	0.981	0.519	0.009
20	5.75	0.981	0.874	-0.112
21	6.0	0.886	0.476	2.004
22	6.0	0.691	0.076	1.051
23	6.0	0.497	0.046	0.948
24	6.0	0.305	0.023	0.884
25	6.0	0.131	0.008	0.857

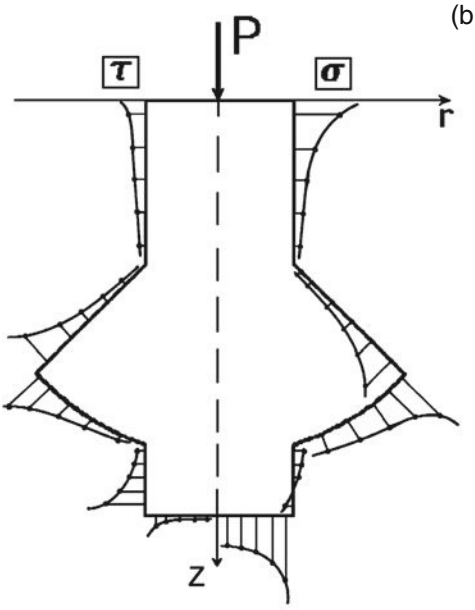

n	z/a	r/a	τ	σ
1	0.25	0.981	0.277	0.757
2	0.75	0.981	0.209	0.338
3	1.25	0.981	0.191	0.233
4	1.75	0.981	0.159	0.153
5	2.25	0.981	0.078	0.071
6	2.657	1.134	0.065	-0.076
7	2.955	1.427	0.144	-0.156
8	3.254	1.721	0.199	-0.232
9	3.554	2.014	0.261	-0.328
10	3.853	2.308	0.564	-0.691
11	4.099	2.363	0.976	1.047
12	4.298	2.165	0.456	0.630
13	4.498	1.927	0.349	0.597
14	4.697	1.631	0.229	0.559
15	4.894	1.235	0.039	0.391
16	5.1	0.981	0.008	0.153
17	5.3	0.981	0.180	0.117
18	5.5	0.981	0.293	0.069
19	5.7	0.981	0.413	0.021
20	5.9	0.981	0.915	-0.192
21	6.0	0.886	0.291	1.383
22	6.0	0.691	0.621	0.865
23	6.0	0.497	0.041	0.785
24	6.0	0.305	0.021	0.739
25	6.0	0.131	0.008	0.718

Fig. 5.21 Profiles of dimensionless contact normal (σ) and tangential (τ) stresses in a meridional cross-section of bored pile foundations with widenings. (**a**) $h_f/a = 2.5$, (**b**) $h_f/a = 4.0$

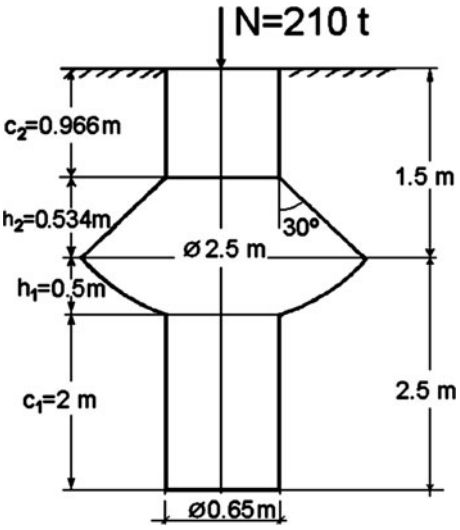

Fig. 5.22 Scheme for the example of calculation of a bored pile foundation with a support widening for a vertical load

the account of unilateral constraints and S=4.060 cm with the account of unilateral constraints. Thus, if unilateral constraints are not taken into account, under vertical loading, an error of up to 6% in the determination of the settlement value can arise.

According to the method of calculation for the same foundation, quoted in [237], in assumption of the building being without a basement, at first the condition of applicability of the deformation-based calculation is checked: $P_{\text{av}} = N/F \leq R$. Since the average pressure over the foundation surface (in the widening plane) $P_{\text{av}} =$ 43 t/m^2, and the calculated pressure on the base without the account of the cylindrical footing (included into the safety factor), obtained on the base of the Puzyrevsky solution (Construction Rules and Regulations 11–15–74) R=43.5 t/m^2, then the check is performed. Then, using the method and the tables, quoted in [227], one can show the required equality of the nominal settlements $S = S_1 = S_2$ to be provided if the coefficient of participation of the widening in the foundation functioning λ=0.65. The distribution of load $N = N_{\text{B}} + N_{\text{F}}$ between the ring-shaped widening and the footing is the following:

ring-shaped widening $N_K = \lambda N = 137\text{t}$,
footing $N_F = (1 - \lambda)\, N = 73\,\text{t}$.

Finally, the calculation of the foundation settlement [227] gives a final result

$$S = S_1 \approx S_2 = 2.94\,\text{cm}.$$

Thus, an approximate calculation, performed according to the recommendations for the design of bored pile foundations [227], has a discrepancy with our data, obtained by the boundary-element method, by 23–27%. Such discrepancy, evidently, is a consequence of a rather rough account of the widening geometry in [227], of unilateral constraints being not taken into account as well as of using a

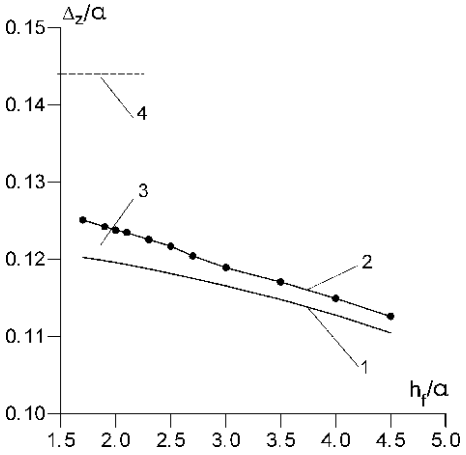

Fig. 5.23 Relative settlements of bored pile foundations of equal volume at a fixed vertical load: (1) foundation with a support widening, without the account of unilateral constraints; (2) foundation with a support widening, without the account of unilateral constraints; (3) foundation without a support widening, with a given height; (4) foundation without a widening, with a given diameter

rather approximate tabulated data for references. Note that in the case of an inclined load, the calculation according to [227] cannot be performed at all.

Figure 5.23 shows the results of boundary-element calculations, characterizing the effect of the widening and its depth on the bored pile foundation settlements under a vertical load. Relative settlements of the foundation with a widening are compared to the settlements of cylindrical bored piles of the same volume as the initial foundation with a widening, but of the same length (then, of a larger diameter) or of the same diameter (then, of a larger length). The calculations are performed in two variants – with and without the account of unilateral constraints on the contact between the foundation and the soil and the values $P/Ea^2 = 1$, $\nu = 0.3$. The geometrical dimensions of the bored pile foundation are the following: $b/a = 2.5$, $h_1/a = 1$, $h_2/a = 1.5$, $r_f/a = 3$. The vertical load on the foundation was fixed. As one could expect, the settlements of the bored pile foundation with a widening are practically always smaller than for cylindrical piles. Besides, with the increase of the relative depth of the support widening h_f/a the settlements decrease, varying practically linearly. Meanwhile, the account of unilateral constraints results in a considerable increase of settlements what is related to the decrease of the contact domain between the foundation and the soil.

5.5.4 Calculation of Displacements and Slopes of a Bored Pile Foundation Under an Inclined Load

In our calculations, performed using the direct boundary-element method in a full formulation, the boundary-element grid on the punch surface was generated according to the same principle as for the problem in an axisymmetric formulation. The total number of the boundary elements did not exceed 400. Surface integrals were computed using a proposed numerical-and-analytical method. If the dimensionality

of the linear algebraic equation system in the axisymmetric formulation was n=51, in the full formulation it was n=1206. Note that the dimensionality of the finite-measure analog of the problem can be reduced in the presence of symmetry planes in the foundation structure loading scheme.

Model experiments have shown that for the practical purposes of determination of such integrated characteristics as displacements and slopes, the number of boundary elements can be reduced almost twice without a loss of accuracy. On the contrary, for the studies of the stress-strained state of the soil in the foundation active zone one should apply a dense grid of boundary elements, corresponding to the contact stress condensation degree. A developed *Rostwerk* software enables the contact surface to be automatically partitioned into boundary elements, using the given shape of the bored pile foundation axial cross-section. Axial cross-sections of bored pile foundations with widenings of the most frequently used types are shown in Fig. 5.24. The same figure shows the schemes of discretization of the near-pile space, required for the postprocessor processing of the contact problem solution results (construction of stress isolines, deformations and their invariants, displacements, etc.).

The calculated dependences of settlements, horizontal displacements, and slopes of a bored pile foundation with a support widening of a spheroconical shape under an inclined load are presented in Figs. 5.25, 5.26, and 5.27.

An inclined force of a constant value was supposed to be applied in the centre of the top edge of the foundation, its direction being determined by the angle φ of its deviation from the horizontal plane. Due to the calculation scheme symmetry with respect to the vertical axis of the foundation, the calculations were performed

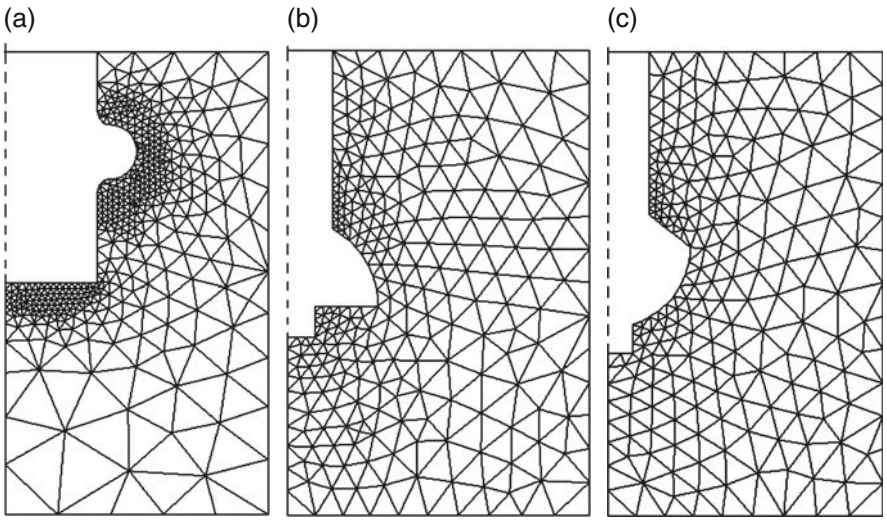

Fig. 5.24 Discretization of the active area of bored pile foundations with support widenings of various type: (**a**) toroidal, (**b**) hemispherical, (**c**) spheroconical

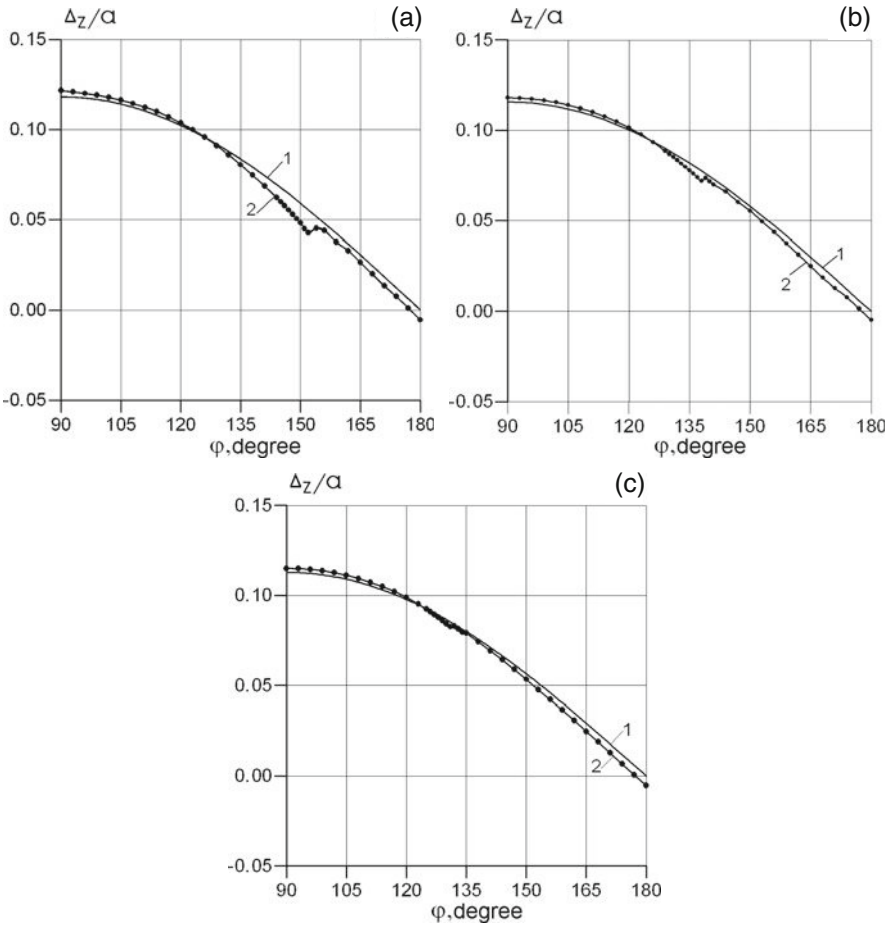

Fig. 5.25 Relative settlements of a bored pile foundation with a support widening versus the inclined load direction (1) without and (2) with the account of unilateral constraints; h_f/a=2.5 (**a**); 3.25 (**b**); 4.0 (**c**)

for the external force inclination angles in the range $90° \leq \varphi \leq 180°$. For plotting the calculations were carried out mostly with a step of 6°. Within the ranges of non-monotonous variation of displacements and slopes the step value was decreased down to 3°, 1°, or even 0.5°.

The obtained dependences of the contact interaction characteristics without the account of unilateral constraints are rather monotonous (Figs. 5.25, 5.26, and 5.27, lines 1). With the increase of the angle of inclination of the force P the horizontal component of the inclined load vector $P \cdot \sin\varphi$ increases and simultaneously its vertical component $P \cdot \cos\varphi$ decreases. This results in the decrease and increase of the vertical and horizontal displacements, respectively. Simultaneously, the slope ψ_x increases, reaching its maximal value under horizontal loading.

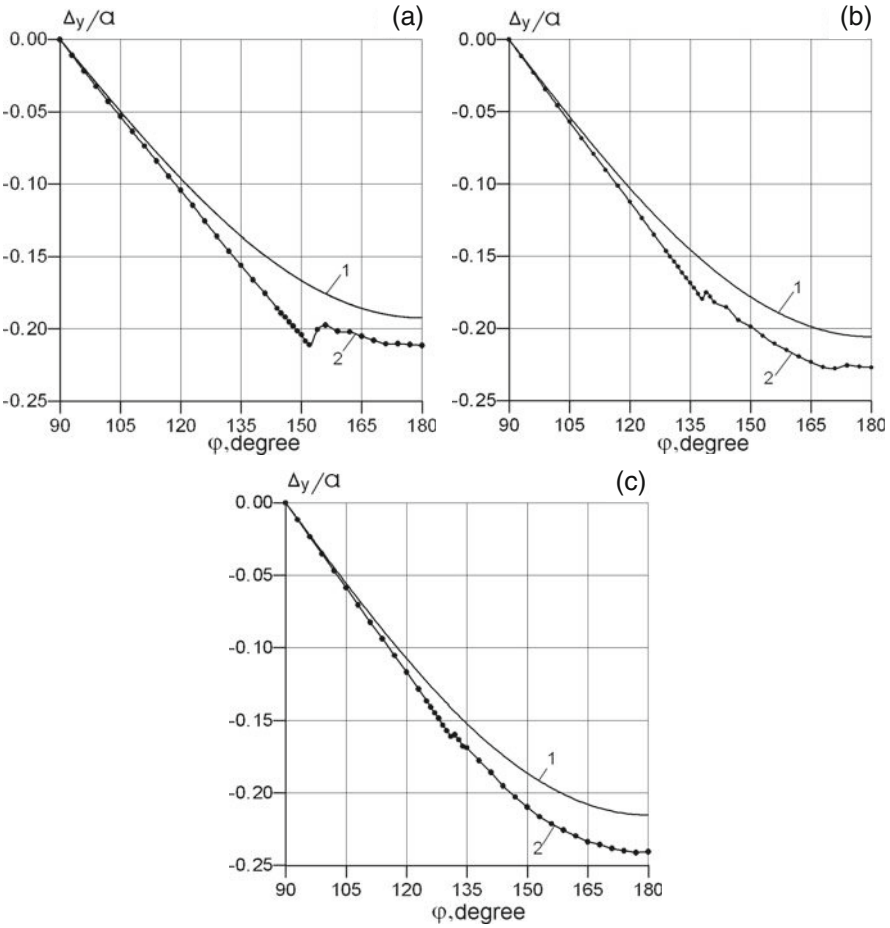

Fig. 5.26 Horizontal displacements of a bored pile foundation with a support widening versus the inclined load direction (1) without and (2) with the account of unilateral constraints; h_f/a=2.5 (**a**); 3.25 (**b**); 4.0 (**c**)

The account of unilateral constraints in the contact domain results in quantitative and qualitative changes (Figs. 5.25, 5.26, and 5.27, lines 2). This is related to the decrease of the contact area due to the formation of areas with tensile stress on the foundation surface. Since the soil does not work in tension, in the corresponding areas gaps are formed between the foundation and the soil. As shown by numerical experiments, at vertical loading, the areas with negative stress emerge on the conical part of the widening, expanding with the absolute load value *P*as well as with the parameter of the relative depth of the widening location h_f/a. A similar situation is also observed in the lower part of the cylindrical footing, in some sense resembling the "wedging" effect, at which a tension area is formed in the lower part of a cylindrical surface as well as a gap between the foundation and the soil.

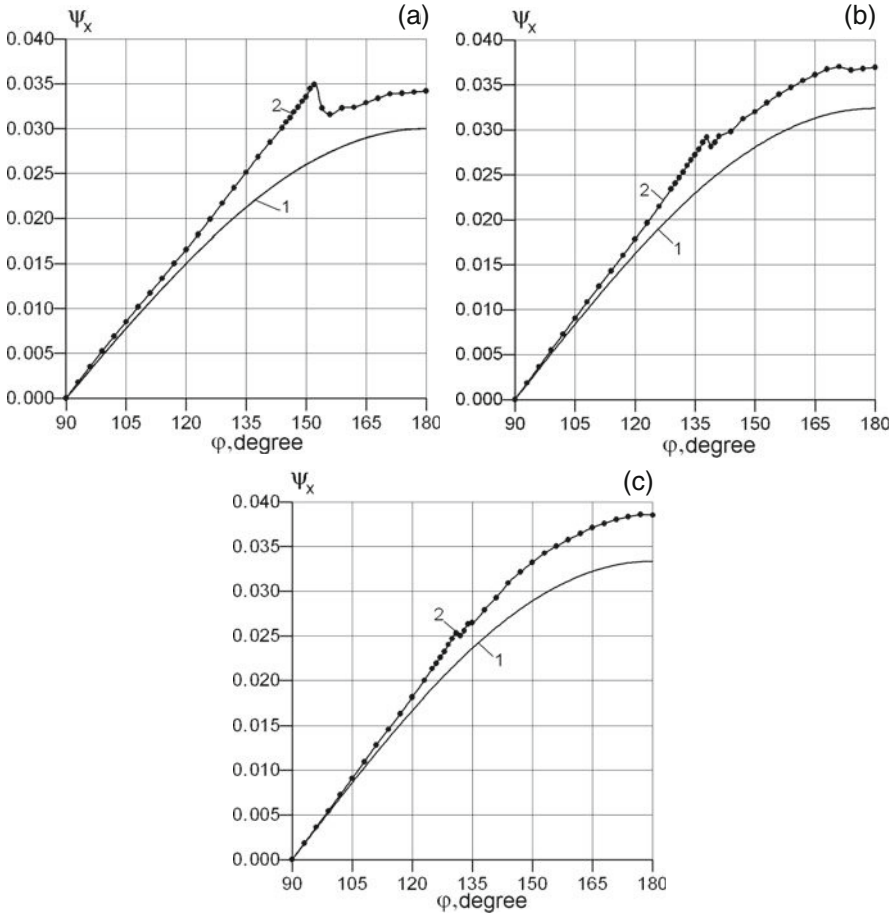

Fig. 5.27 Slopes of a bored pile foundation with a support widening versus the inclined load direction (1) without and (2) with the account of unilateral constraints; h_f/a=2.5 (**a**); 3.25 (**b**); 4.0 (**c**)

Note that the "wedging" effect is also observed in the case of a cylindrical pile without a widening; however, it is revealed even more strongly. Under an inclined load, the formation and development of tension areas is irregular and can rather hardly be traced due to an essentially non-uniform stress-strained state in the foundation active area. Finally this process is reflected in the values of the integrated characteristics: displacements and rotation of the bored pile foundation as a rigid solid. We proceed with a more detailed description of dependence of these values on the inclined force direction.

For all external load inclination angles, the account of the foundation uplifting from the soil always results in an increase of absolute values of horizontal displacements Δ_z and slopes ψ_x.

The influence of the "wedging" effect and underpressure in the conical part of the widening affects the increase of the bored pile foundation settlements at $90° \leq \varphi \leq 120°$, i.e. in this range of variation of the resultant force inclination angle, the Δ_z values with the account of unilateral constraints exceed the corresponding values without the account of unilateral constraints. Depending on the ratio of the widening size and its depth, at a certain value of φ from the range $125° \leq \varphi \leq 135°$ both settlement curves intercept (Figs. 5.25a, 5.26, and 5.27a). Hence, there exists such resultant direction, for which the account of unilateral constraints results in the settlement values equal to those for the contact problem solution in a linear formulation (without the account of unilateral constraints).

At the further increase of the φ angle, the effect of the increase of the horizontal component of the external load vector goes on. Due to the uplifting of the structure from the soil, the slope further increases and the absolute values of the foundation horizontal displacements increase (Figs. 5.25b, c, 5.26, and 5.27b, c). Simultaneously, the vertical displacements Δ_z decrease (Figs. 5.25a, 5.26, and 5.27a).

As follows from the calculation data (Figs. 5.25, 5.26, and 5.27), there is a threshold value of the angle φ^*, at which a qualitative change of the contact deformation pattern occurs. The account of unilateral constraints results in the foundation slope and the absolute values of the foundation horizontal displacements increase up to the φ^* value increasing strictly linearly along the tangents, built at $\varphi = 90°$ (vertical loading) to the corresponding plots, obtained without the account of unilateral constraints. When the threshold value of the inclined force φ^* is reached, the calculated curves become non-monotonous. After a certain decrease of the slope and horizontal displacement values and a settlement increase, these characteristics continue to vary nonlinearly. The threshold value φ^* is most essentially affected by the depth h_f of the support widening location. In particular, for the series of calculation we have performed, the influence of the depth on the φ^* value can be seen from Table 5.6.

Table 5.6 Values of ϕ^* at different depth h_f of the location of the support widening

h_f/a	2.5	3.25	4.0
ϕ^*	152°	138°	132°

Hence a practically important result is obtained: in order to predict slope and horizontal displacements of a foundation within the range of the inclined force angle $90° \leq \varphi \leq \varphi^*$, it is sufficient to have the results of only one calculation of these characteristics.

At a near-horizontal load ($\varphi \geq 175°$), at the foundation head vertical displacements are practically zero, and the further increase of the load inclination value even leads to the foundation uplifting ($\Delta_z < 0$). In other words, at a horizontal (or a near-horizontal) loading of the bored pile foundation its uplifting towards the base surface occurs. Note that in case unilateral constraints not being taken into account, this phenomenon is not observed, i.e. always $\Delta_z \geq 0$ and the bored pile foundation is not uplifted.

Thus, from the performed analysis of deformations of bases of bored pile foundations with support widenings under a complex spatial loading one can conclude that the proposed numerical boundary-element approach enables one to take into account the non-uniform stress-strained state of the base and formation of cavities between the soil and the widening in the course of the foundation displacement. This approach is effective for the practical calculation of bored pile foundations with various shapes of support widenings, without appealing to various regulating documents, where the specific features of bored pile foundation functioning are taken into account rather roughly.

5.6 Calculation of Contact Interaction of Bases with Slotted Foundations of Industrial and Civil Buildings

The experience of design and construction of objects of industrial and civil engineering in Russia has shown [214] that in cohesive and low-watered soils of natural (as a rule, eluvial) origin, application of shallow monolithic foundations with working lateral surface is justified. The most important feature of such foundations is an effective technology of their construction, where the back fill is excluded. This enables lateral friction over the walls to be actualized, that cannot be achieved at the construction of traditional foundations in open pits. It is also advisable to apply shallow (up to 6–8 m) foundations not only due to the possibility to use common excavating machines, but also because in non-watered soils one can refuse from making trenches under the protection of clay mixture. The most efficient, in comparison with different traditional (pile, strip, pier) structures of shallow monolithic foundations with lateral working surface, are slotted foundations applied for both industrial and civil engineering [136]. The role of slotted foundations increases for low-rise engineering of residential buildings (cottages) and light skeleton-type industrial buildings [21, 137, 211] in view of modern environmental requirements to the foundation engineering, construction cost reduction, high bearing capacity, simplification of the construction procedure.

5.6.1 Slotted Foundations of Various Structural Shapes

Slotted foundations are a sort of an engineering solution of foundations, built by the diaphragm wall technique [47, 206]. They are made as a narrow wall of concrete or reinforced concrete in a soil base. Structures with a raftless joint of a window-sill type or with a pile raft for the load transfer from the above-ground structures to the walls are possible (Fig. 5.28). The load is transferred to the base by lateral planes, wall ends, and the pile raft plate bottom. Therefore, the geometrical shape of the slot, the pile raft, and the lateral surface is determined depending on the above-foundation structure size, load direction and value, geological conditions, depth of the soil freezing or weathering. In the recent years, based on the

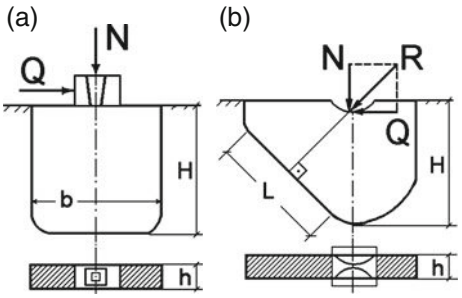

Fig. 5.28 Calculation schemes for slotted foundations: (**a**) under a column of reinforced concrete, (**b**) under a three-hinge frame

experience of construction of foundations using the diaphragm wall technique [206], Russian researchers and engineers have proposed and worked out new structures and technologies of construction of slotted foundations, being successfully applied for industrial and civil buildings [136, 214]: foundations with cavities, two-slot foundations with a low pile cap, wedge-slotted foundations with monolithic plates, slotted foundations with a widened footing, etc. (Fig. 5.29).

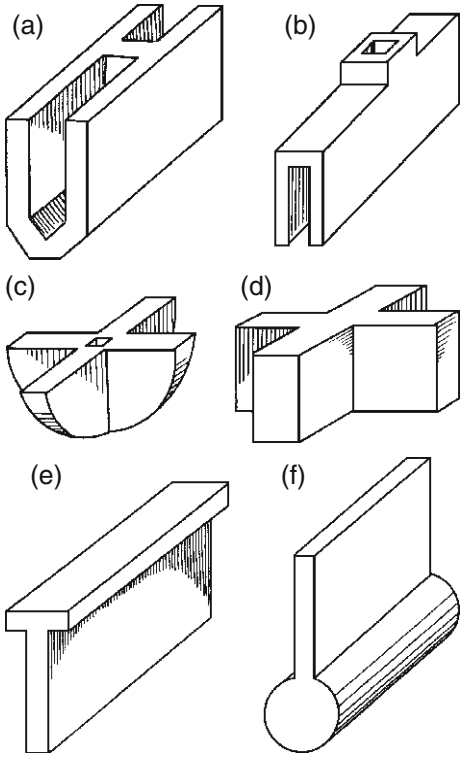

Fig. 5.29 General view of slotted foundation of various structure: (**a**) with cavities; (**b**) double-slotted; (**c**, **d**) cross-shaped; (**e**) with a pile raft; (**f**) with a bottom widening

The technology of slotted foundation construction is highly mechanized. After the site grading, slots are made in the soil using earth-moving excavator-based machines with a special working equipment of backhoe, narrow grab bucket, or rotor type. Narrow slots are often produced using a bar or a slot-profiling machine. The residual sludge in the face is removed or compressed by impression or tamping. Then reinforcing cages are installed and fixed in the slotted pit. While producing the foundation, concrete is supplied directly into the foundation body. Vibrating tampers are used for the concrete compaction. The concrete should have sufficiently semifluid or pourable consistency. A subsequent concrete compaction by a platform vibrator is useful. After the concreting being finished, maintenance of the placed concrete is performed during the whole period of its strengthening.

Slotted foundations have the advantages of both shallow and pile foundations. It is shown in [136, 214] that structural solutions of the slotted foundations as well as their construction technology enable a number of shortcomings of traditional foundation types to be avoided. In particular, they do not require deep pits under the whole building to be made, the amount of formwork is strongly reduced, they can be constructed at different depth without a surcharge of materials. The slotted foundation structures having been proposed, enable technical and economic characteristics of these foundations as well as their competitiveness to be considerably increased in comparison with the known solutions. The experience of application of slotted foundations for the construction of a number of industrial and civil objects at various soil conditions has shown [137, 214] that, in comparison with the foundations, produced in a pit or using the displacement piles, they enable the excavation work volume to be reduced by 40–50% (in the case of specific structural solutions – up to 70–80%), concrete consumption – by 5–6%, reinforcement consumption – by 15–20%, and formwork – by 70–100%.

In spite of the efficiency of the foundation structures under consideration, they have not found proper wide application in engineering. One of the essential restrictive reasons is a low level of reliability of practically applied calculation methods, based on separate empirical data and simplest calculation schemes [158, 159]. Until now, no special methods for calculation of slotted foundations have been created, which would take into account their structural features, friction resistance over the developed lateral surface, and various combination of active forces and moments. The calculations are performed similarly to the known methods for nominal and pile foundations. A simplified elastic model of the soil medium based on the Winkler hypothesis is used. Calculation of slotted foundations for off-centre loads is performed with the account of their fixation in the soil according to the scheme of a fixed absolutely rigid rod [159].

It should be noted that for the calculation of the settlement of the base of a rigid slotted foundation, application of the calculation scheme of a nominal foundation, developed for pile foundations, is not quite correct. For shallow slotted foundations one should take into account the effect of the lateral surface geometry on the foundation displacements. As a rule, slotted foundations transfer to the base a system of forces, represented, in the general case, by a vertical, a horizontal, and a momental load. According to the design rules, adopted in Russia [115, 215], the stress-strained

state of the base of a slotted foundation should be studied separately: for the vertical load, using the model of a linearly deformable half-space, and for the horizontal and momental loads, invoking the Winkler model. Dependence of the foundation calculation scheme and the base model on the external load direction is also a reason for the low level of reliability of determination of displacements and slopes of slotted foundation structures at the stage of their operation.

Thus, at efficient and rather well elaborated construction technology at various soil conditions, the methods for calculation of settlements and slopes of slotted foundations require further improvement on the base of theoretical studies with the account of spatial formulations and detailed analysis of the processes of contact interaction of the foundation with the soil.

5.6.2 Calculation of Slotted Foundations Based on the Base Deformation

Slotted foundations are characterized by high rigidity, hence we assume a calculation scheme in the form of a volumetric punch, deepened in a soil base, treated as a linearly deformable half-space, weakened by a cavity whose boundaries are identical to the contact surface of the foundation structure to be calculated.

The developed *Rostwerk* software is a rather universal one, enabling numerical experiments to be performed in order to evaluate the effect of various factors on the slotted foundation displacements and the contact stress distribution over the lateral and end surface and bottom. The input data preparation is simple, totally automated, and suitable for discretization of the contact surface and active area of slotted foundations of the known types. Typical examples are shown in Figs. 5.30 and 5.31.

Subsequent sections of the chapter are devoted to the systematic studies of the processes of contact interaction of slotted foundations with soil bases. At the calculations, the load, acting on the slotted foundation, is considered known and given. The effect of the geometrical shape of the foundation on its displacements and on the stress-strained state of the base is evaluated. The influence of the inclination angle and eccentricity of the resultant external load on the slotted foundation displacement is investigated. The results of the settlement and slope calculation are compared with the data of the field experiments as well as with the existing approximate calculation methods. The analysis of this comparison has enabled the accuracy of the approximate engineering methods to be estimated and the admissible range of their application to be specified.

Effect of the degree of discretization of the contact surface of the foundation with the soil. For numerical experiments a separate (or, using the terms of [136], pier) slotted foundation with a bottom of a rectangular shape was considered (this is the simplest solution for a foundation under ferroconcrete and steel columns). The foundation dimensions as well as the chosen coordinate system are shown in Fig. 5.32a, b. The soil base had the following deformational characteristics: deformation modulus E=20 MPa, Poisson ratio ν=0.4 what corresponds to firm-structure

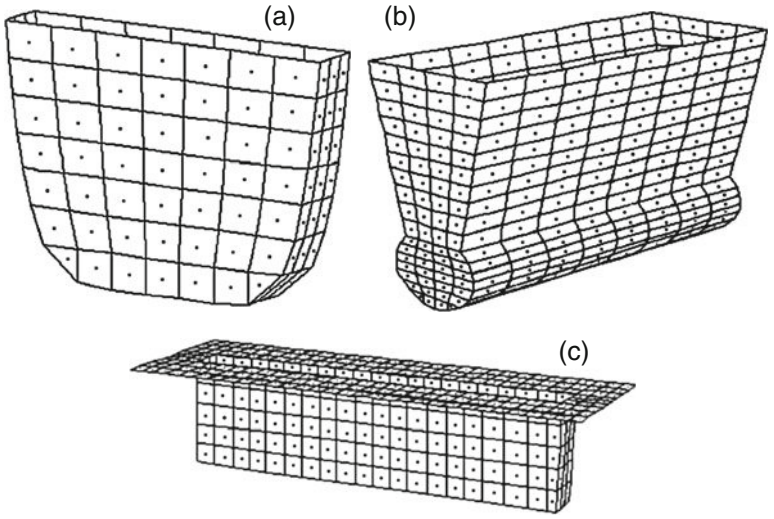

Fig. 5.30 Discretization of the contact surface of interaction with the soil for slotted foundations of various types by a boundary-element grid: (**a**) pier foundation, (**b**) wedge-slotted foundation with a widening, (**c**) pile raft foundation

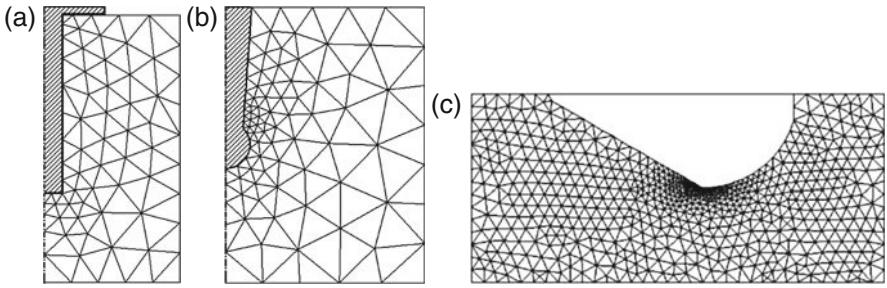

Fig. 5.31 Discretization of the active area of the base for slotted foundations: (**a**) with a pile raft, (**b**) with a widening, (**c**) with an inclined bottom

low-moisture eluvial clayeys in a hard state. The foundation was subject to an essentially spatial load by an inclined force $P=10^3$ kN which had an angle of 45° with the vertical axis, acting in a plane, passing through the foundation centre and perpendicular to the slot plane (Fig. 5.32b). The results of calculations with sequential condensation of the calculation grid at different discretization degree on the width (n_1), length (n_2), and depth (n_3) of the foundation block are given in Table 5.7.

Settlements Δ_z, displacements Δ_x, and slopes ψ_x were calculated (Table 5.7). For comparative evaluation and search for optimal (from the point of view of economy and accuracy) results, this table also contains the total number of boundary elements K. Using the data of Table 5.7 and assuming the dependence of the numerical solutions on K^{-1} to be linear, one can readily obtain the extrapolated values $\bar{\Delta}_z$,

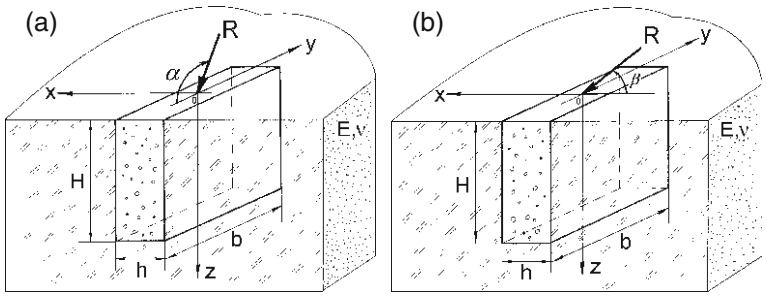

Fig. 5.32 Calculation schemes for a slotted foundation with a rectangular longitudinal cross-section under an inclined force: (**a**) within the slot plane, (**b**) orthogonally to the slot plane

Table 5.7 Convergence of numerical solutions for a slotted foundation with a rectangular bottom under an inclined load

n_1	n_2	n_3	K	$-\Delta_x \cdot 10^2$,m	$\Delta_z \cdot 10^3$,m	$-\psi_y \cdot 10^3$,rad
3	7	7	161	1.12439	7.35481	3.64699
3	8	8	200	1.12233	7.34523	3.63504
3	9	9	243	1.12079	7.33774	3.62609
3	10	10	290	1.11959	7.33171	3.61910
3	10	11	316	1.11892	7.32869	3.61489
3	10	12	342	1.11839	7.32616	3.61148
3	10	13	368	1.11795	7.32406	3.60863
3	10	14	394	1.11759	7.32227	3.60626
3	11	14	425	1.11726	7.32026	3.60467
3	12	14	456	1.11698	7.31859	3.60337
2	14	14	476	1.11828	7.32487	3.61159
3	13	14	487	1.11674	7.31719	3.60226
1	15	15	495	1.12108	7.34259	3.62836
2	15	14	506	1.11802	7.32352	3.61044
2	14	15	508	1.11793	7.32308	3.60911
Extrapolated values				1.11461	7.30782	3.58971

$\overline{\Delta}_x$, $\overline{\psi}_y$ at $K \to \infty$. These values are also given in Table 5.7, they enable the accuracy of the approximate solution to be estimated.

As follows from the calculations performed, the approximate numerical solutions, obtained by the boundary-element method, rather soon stabilize with the increase of the degree of discretization of the contact surface of the foundation and the soil. The obtained data can serve to optimize the discretization degree for further series of calculations. As one can see, the boundary-element grid $(n_1) \times (n_2) \times (n_3) = 3 \times 10 \times 14$ with the total number of elements K=394 is suitable both in view of the computation time and for obtaining the approximate values of the contact deformation parameters with a high accuracy (0.3% regarding the displacements and 0.5% regarding the slopes).

The calculations have also shown that a decrease of the discretization degree over the end surface of the slotted foundation ($n_1 < 3$) results in a decrease of the accuracy

of the numerical results in spite of the increase of the number of boundary element on the lateral surface. Therefore, we have taken $n_1 = 3$ as the minimal discretization degree over the foundation end surface. Note that while calculating such integrated characteristics of the contact interaction as displacements and slopes, one can practically without any loss in accuracy restrict oneself by the discretization degree over the foundation lateral surface of the order of $(n_2) \times (n_3) = 7 \times 7$. However, this is obviously insufficient for the studies of the two-dimensional contact stress field and three-dimensional stress-strained state in the foundation active area.

Settlements and slopes under a complicated spatial loading. Calculation of slotted foundations based on the base deformations is performed for the main load combinations. Settlements and slopes of a separate slotted foundation, as of any other foundation structure, depend on its shape and size, mechanical properties of the soil base, conditions at the surface of the contact of the foundation and the base, loading type, influence of the neighbouring foundations and loads on adjacent areas, and a number of other factors [101, 201] (the rigidity of the foundation itself, its depth, size of plastic areas beneath it, depth of the compressed base, character and rate of loading, conditions of work). Account of all these factors makes the problem of calculation of a slotted foundation practically horizonless.

For deepened foundations of a block type, to which the slotted foundations belong, the most important characteristics of the base deformations under a spatial load system of the most general type will be the dependences of displacements versus size, shape and conditions on the contact of the foundation with the soil. Since the slotted foundations are spatial structures with finite and different size in three coordinate directions, and the above-foundation structures transfer to them vertical, horizontal and momental loads, numerical studies of contact interaction of slotted foundations for the following typical cases of spatial loading were performed:

- action of an inclined force in the plane of the foundation longitudinal cross-section, applied in the centre of its top edge (Fig. 5.32a),
- action of an inclined force, applied in the centre of the foundation top edge in the plane, orthogonal to the longitudinal cross-section of the foundation (Fig. 5.32b),
- vertical force, applied with an eccentricity ϵ_y in the longitudinal cross-section of the foundation.

The geometrical shape of the slotted foundation and the surrounding soil characteristics were the same as considered above.

The dependences of the slotted foundation displacements and slopes for the loading types under consideration are presented in Figs. 5.33, 5.34, and 5.35.

The calculation data, shown in Fig. 5.33, enable one to estimate the soil resistance due to the development of tangential and normal forces developing mostly on the lateral surface and partially on the bottom and end faces of the slotted foundation, located parallelly or orthogonally to the acting force planes, respectively (at different inclination angles). For the slotted foundation under consideration with a relative depth H/b= 3.5 m/2.6 m = 0.74, the action of inclined forces in orthogonal planes results at each inclination angle of the resultant $\alpha(\beta)$ to different horizontal displacements and slopes of the slotted foundation. As one should expect, the

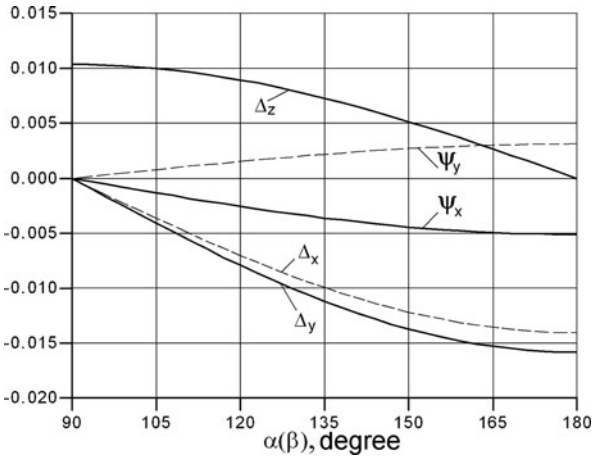

Fig. 5.33 Displacements Δ (m) and slopes ψ (rad) of a slotted foundation under a longitudinal (*solid line*) and transverse (*dashed line*) loading by an inclined force

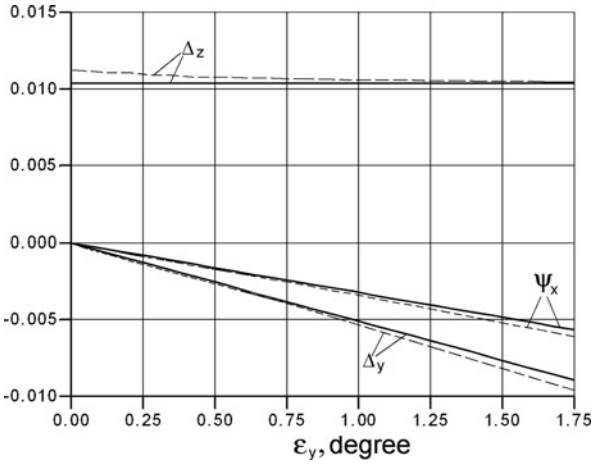

Fig. 5.34 Displacements Δ (m) and slopes ψ (rad) of a slotted foundation versus the longitudinal eccentricity of a vertical load with (*dashed lines*) and without (*solid lines*) the account of unilateral constraints

biggest difference in these values is observed in the absence of the vertical component of the inclined force (i.e. at horizontal loading, $\alpha(\beta)$ 180°) and reaches 20% for the displacements and 40% for the slopes. As follows from the calculations, with the relative depth increase the noted discrepancies in the displacements and slopes are also revealed, but to a lower extent. Since at each value of the angle $\alpha(\beta)$ of the external load inclination the vertical component does not change under longitudinal and transverse loading, this does not lead to any changes of the settlements Δ_z, which decrease with $\alpha(\beta)$ according to the sine law (Fig. 5.33).

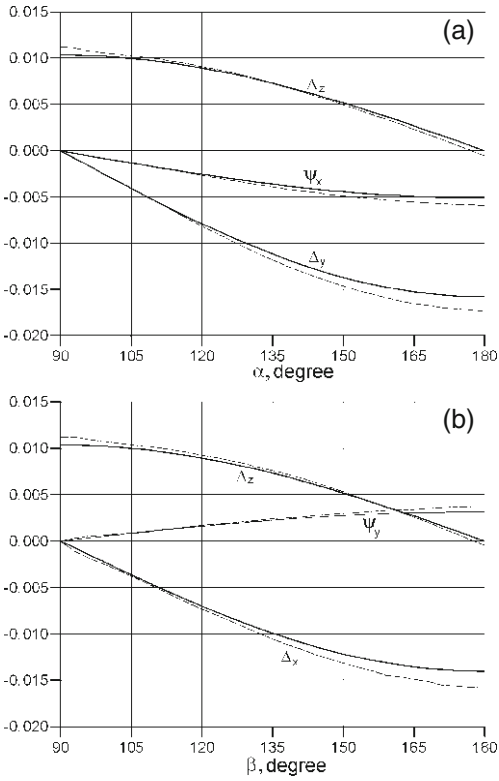

Fig. 5.35 Displacements Δ (m) and slopes ψ (rad) of a slotted foundation under (**a**) longitudinal and (**b**) transverse loading by an inclined force with (*dashed lines*) and without (*solid lines*) the account of unilateral constraints

Figure 5.34 shows the results of calculation of displacements and slopes under a vertical force with the eccentricity $0 \leq \epsilon_y \leq b/2 = 1.75$ m acting on the top edge of the slotted foundation along the longitudinal axis. Since this loading is equivalent to a central vertical force P and a moment $M = -P \cdot \epsilon_y$, with the increase of ϵ_y the values ψ_x and Δ_y should increase proportionally, and the settlement Δ_z should remain unchanged what is confirmed with high accuracy by the calculation results.

Figures 5.34 and 5.35 enable one to judge upon the account of unilateral constraints in the contact domain of the slotted foundation with the soil. As seen from the calculations, due to the contact area decrease the horizontal displacements have an additional development. The account of the unilateral constraints provides maximal effect at horizontal loading when the vertical load component is zero. Quantitatively the account of unilateral constraints at the longitudinal (Fig. 5.35a) and transverse (Fig. 5.35b) loading is similar, not exceeding 10%. This is evidently explained by the fact that the detachment area on one lateral side under the transverse loading is comparable with the total area of symmetrical detachment zones on two lateral sides under the longitudinal loading.

A somewhat different situation is observed in the settlement character with the account of unilateral constraints under the longitudinal and transverse loading

(Fig. 5.35). At such loading types the account of unilateral constraints can result both in an additional settlement increase and in their decrease. For the calculation example under consideration the change of the increment sign is observed for $\bar{\alpha} \approx 135°$ under the longitudinal loading and for $\bar{\beta} \approx 160°$ at the transverse loading. Below the quoted values of the inclined force action $\bar{\alpha}(\bar{\beta})$ its vertical component results in a "wedging" effect being noticeably revealed (See Sect. 5.4) and, hence, the settlement increment is positive. The maximal relative value of this increment is observed for purely vertical loading (90°) and for both loading types does not exceed 7.5%. For $\alpha\ (\beta) > \bar{\alpha}(\bar{\beta})$ the increment of the settlement for the centre of the slotted foundation top edge with the account of unilateral constraints is negative, i.e. with the approach of the force direction to the horizontal one, the settlements decrease in comparison with the case of total cohesion of the slotted foundation with the soil. At almost horizontal loading, the account of unilateral constraints results in the absolute values of the settlement increments even exceeding the settlements for the calculation in the linear formulation. As a consequence, at $\alpha(\beta) \approx 180°$ the slotted foundation has negative settlements what, for the chosen coordinate system, corresponds to the slotted foundation uplifting. In other words, the slotted foundation is squeezed out of the soil. Note that the maximal value of such vertical displacement is quite small – near 0.5 mm for both longitudinal and transverse loading.

The account of unilateral constraints at loading by a vertical force and a moment (Fig. 5.34) increases both the slopes and the displacements in the whole range of the ϵ_y variation. The maximal relative increase of ψ_x and Δ_y (by 8.2%) is achieved at the maximal value of the moment. The maximal relative increase of the settlement Δ_z, similarly to the above examples with an inclined force, is obtained at central vertical loading, i.e. at $\epsilon_y = 0$.

The results for convergence of iteration processes for the cases of spatial loading under consideration are shown in Fig. 5.36. The highest computation resources were required by the calculation of the transverse loading of a slotted foundation (the average iteration number for each load direction angle was $N_{\text{av}}=10$, $N_{\max}=12$ at $\beta=135°$, $N_{\min}=7$, at $\beta=180°$). Under the longitudinal loading, the iteration process characteristics were the following: $N_{\text{av}}= 6$ at $N_{\max}= 9$, $N_{\min}= 3$, for the greater part of the inclined force angle variation interval ($\alpha \geq 120°$) $N= 4$. Under an eccentric load with the increase of ϵ_y the number of iterations monotonously decreased from $N_{\max}=10$ to $N_{\min}= 4$, and $N_{\text{av}}= 7$.

Thus, it follows from the analysis of the iteration process convergence data that though the account of the structure nonlinearity in the calculation of slotted foundations with a rectangular shape of longitudinal cross-section in this specific case results in a correction of the contact interaction parameters, it still requires the computation time increase by factor of 6–10. For the practical purposes such amount of computational work for the calculation result correction within not more than 10% is not always justified. Therefore, for the calculation of slotted foundations according to the second limiting state at a complex spatial loading with a relative error not more than 10%, the calculation can be performed without the account of unilateral constraint and, what is important for practical purposes, the superposition principle can be applied. With the increase of the absolute values of

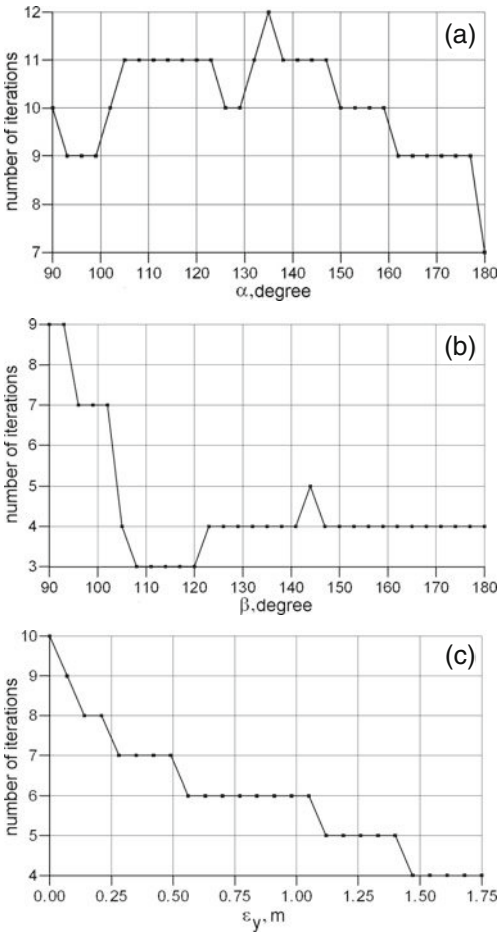

Fig. 5.36 Scheme of the iteration process at the account of unilateral constraints for a slotted foundation under: (**a**) an inclined force within the transverse cross-section plane; (**b**) an inclined force within the longitudinal cross-section plane; (**c**) a vertical force with a longitudinal eccentricity

forces and moments applied to the slotted foundation from the above-foundation buildings and structures, the structure nonlinearity will be revealed to a higher extent and a reliable prediction of the slotted foundation displacements and slopes will require mandatory account of unilateral constraints in the contact domain.

Effect of the shape of the slotted foundation longitudinal cross-section. Depending on the trench excavation procedure due to the application of various types of earth-moving machines [136], the longitudinal cross-section of the slotted foundations can be rectangular, rectangular with a curved bottom, or curved. Since the slotted foundations are subjected to high vertical and horizontal loads from the above-foundation structures, the quality of the trench excavation and its geometrical shape in the longitudinal cross-section essentially affect the technical and economic parameters of the design solutions. As follows from the construction experience [136], high requirements to the narrow trench excavation under slotted foundations

are in general satisfied by using common dipper mechanisms with a rather high productivity. Meanwhile, it is noted by the specialists that at short trench excavation a constant check and correction of the geometrical size of the trench is required. Therefore, the most promising is application of rod grab buckets with high productivity, capable of digging trenches of large depth (20–25 m), providing the trench verticality and the required geometrical size in the longitudinal direction.

Hence, the spatial shape of the trench and, accordingly, of the slotted foundation, is rather effectively checked in the course of excavation and production of the foundation. However, at the design stage the calculation methods are used, operating, for example, with the foundation depth parameters, its size, slot width. At the calculations of slotted foundations according to the scheme of an absolutely rigid rod, fixed in the soil [136, 159] only the foundation bottom resistance moment and its size in the plane, perpendicular to the load, are taken into account. Due to this inconsistency, we have performed numerical studies in order to reveal the influence of the shape of the slotted foundation longitudinal cross-section on its displacements and slopes along each coordinate axis direction under all components of both force and momental loads. In the calculations the following dimensions of the slotted foundation were fixed: the foundation size ($h\times\ b$= 0.6 × 3.5 m) and depth (H= 2.6 m). The deformation parameters of the soil are taken the same as above (E= 20 MPa, ν= 0.4).

The shape of the lateral surface for the case of curved longitudinal cross-section was given using a power law (Fig. 5.37a)

$$z = H\left[1 - \left(\frac{2|y|}{b}\right)^m\right]. \tag{5.5}$$

At such dependence, the increase of the m parameter results in the longitudinal cross-section shape approaching the rectangular one (Fig. 5.37b).

The lateral surface of the slotted foundations of a rectangular shape with a curved bottom was considered by a conjugation of a rectangle with the sides $(2b) \times (h–R)$ and a semicircle with a radius R=b (Fig. 5.37c). The z-coordinate of the bottom points was calculated as follows:

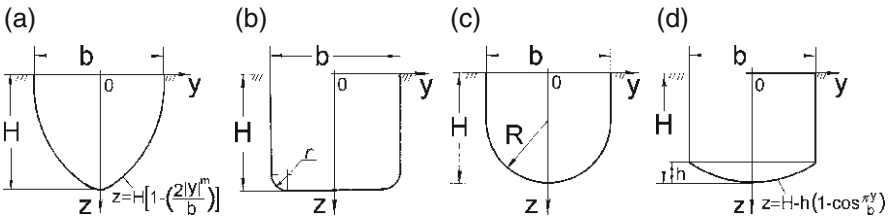

Fig. 5.37 Longitudinal cross-sections of slotted foundations: (**a**) curved; (**b**) rectangular; (**c**, **d**) rectangular with a curved bottom

$$z = H - b + \sqrt{b^2 - y^2}. \tag{5.6}$$

Here one should note that the choice of formulae of the type of Eqs. (5.5) and (5.6) is not crucial and they can be easily replaced for a specific practically applied bottom contour according to the trench excavation procedure applied. It is also convenient to use the bottom contour in the form of, for example:

a circular arc with a diameter larger than the slotted foundation length,
a cosinusoid $z = H - h\left(1 - \cos\frac{\pi y}{b}\right)$ (Fig. 5.37d),
a lower part of an ellipse $z = H - h + \frac{h}{b}\sqrt{b^2 - y^2}$, etc.

Here b, H, h are the slotted foundation shape parameters in its longitudinal cross-section.

In the cross-section of the slotted foundation of a rectangular shape the lower corners were supposed to be rounded by arcs of a radius r (Fig. 5.37b). At $r \to 0$ the slotted foundation has the shape of a rectangular paralellepiped. The examples of dicretization of the lateral surface of the slotted foundations of the forms under consideration using a program for automated construction of boundary-element grids are shown in Fig. 5.38.

The results of calculation of the contact interaction parameters for slotted foundations with the longitudinal cross-section of various shape under force and momental loads with respect to three coordinate directions are presented in Tables 5.8 and 5.9. For each of the slotted foundation structure types the upper row gives the absolute values of slopes and displacements at Q_x (Q_y, Q_z) = 10 kN (Table 5.8) and M_x (M_y,

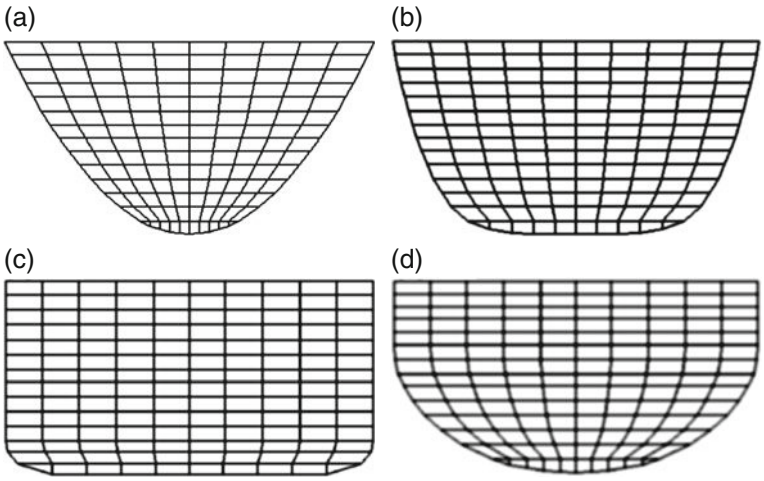

Fig. 5.38 Discretization of the lateral surface of slotted foundations with longitudinal cross-section of various type: (**a**) curved, $m = 2$; (**b**) curved, $m = 5$; (**c**) rectangular, (**d**) rectangular with a curved bottom

Table 5.8 Displacements and slopes of slotted foundations under force loads at different longitudinal cross-section shape *

Load	Q_x=10^3 kN			Q_y=10^3 kN			Q_z=10^3 kN
Displacements Δ, m and slopes ψ, rad	$\Delta_x.10^2$	$\Delta_z.10^4$	$\psi_y.10^3$	$\Delta_y.10^2$	$-\Delta_z.10^4$	$-\psi_x.10^3$	$\Delta_z.10^2$
Curved cross-section, $m = 2$;	1.71929	–	6.14466	1.59813	–	4.25920	1.25841
$S_{lat} = 16.05$ m^2, $V = 9.63$ m^3	1.91831	8.36191	7.25658	1.76358	6.30197	5.07059	1.30388
$m = 4$;	1.65872	–	5.67023	1.52879	–	3.88333	1.17008
$S_{lat} = 18.8$ m^2, $V = 11.28$ m^3	1.83744	7.18912	6.61700	1.72982	6.42275	4.75172	1.20826
$m = 6$;	1.63529	–	5.49618	1.49733	–	3.70465	1.13395
$S_{lat} = 20$ m^2, $V = 12$ m^3	1.81236	6.75855	6.40984	1.69372	5.81801	4.49710	1.19123
$m = 8$;	1.62291	–	5.40697	1.47907	–	3.59981	1.11406
$S_{lat} = 20.7$ m^2, $V = 12.42$ m^3	1.79198	6.34471	6.26931	1.67015	5.49375	4.34559	1.18714
$m = 12$;	1.61015	–	5.31764	1.45861	–	3.48191	1.09271
$S_{lat} = 21.4$ m^2, $V = 12.84$ m^3	1.77479	6.03288	6.14541	1.64559	5.18912	4.18594	1.18252
Rectangular with curved bottom shape,							
$r = 1.75$ m,	1.62335	–	5.62670	1.47109	–	3.59539	1.13768
$S_{lat} = 19.9$ m^2, $V = 11.94$ m^3	1.79531	7.23652	6.54792	1.68722	6.42676	4.47109	1.15162
$r = 0.45$ m,	1.58567	–	5.16954	1.41265	–	3.22471	1.04995
$S_{lat} = 23$ m^2, $V = 13.8$ m^3	1.74983	5.66163	5.97709	1.58541	4.38824	3.84372	1.08510
Rectangular,							
$r = 0$ m,	1.58051	–	5.10002	1.40291	–	3.14488	1.03552
$S_{lat} = 23.4$ m^2, $V = 14.04$ m^3	1.73554	5.32605	5.86361	1.56926	4.32280	3.73618	1.12331

∗ The upper row presents the data without the account of unilateral constraints, the lower one – those with the account of unilateral constraints.

Table 5.9 Displacements and slopes of slotted foundations under momental loads at different longitudinal cross-section shape *

Load	M_x=10^3 kN·m			M_y=10^3 kN·m			M_z=10^3 kN·m
Displacements Δ, m and slopes ψ, rad	$-\Delta_y \cdot 10^3$	$-\Delta_z \cdot 10^3$	$\psi_x \cdot 10^3$	$\Delta_x \cdot 10^3$	$-\Delta_z \cdot 10^4$	$\psi_y \cdot 10^3$	$\psi_z \cdot 10^3$
Curved cross-section, $m = 2$;	4.26069	–	3.48175	6.14423	–	4.87393	3.98424
$S_{lat} = 16.05$ m^2, $V = 9.63$ m^3	4.26069	–	3.48175	6.14423	–	4.87393	3.98424
$m = 4$;	3.88402	–	2.88659	5.66971	–	4.09107	3.12596
$S_{lat} = 18.8$ m^2, $V = 11.28$ m^3	7.62012	1.87499	6.86811	6.61246	3.21264	4.69717	3.41242
$m = 6$;	3.70510	–	2.64377	5.49563	–	3.82166	2.80387
$S_{lat} = 20$ m^2, $V = 12$ m^3	12.2946	11.3150	13.5728	6.36248	2.87255	4.36469	3.05412
$m = 8$;	3.60014	–	2.51124	5.40642	–	3.68641	2.63404
$S_{lat} = 20.7$ m^2, $V = 12.42$ m^3	12.1117	11.2701	13.2226	6.25191	2.69309	4.21045	2.86849
$m = 12$;	3.48212	–	2.37049	5.31707	–	3.55237	2.45789
$S_{lat} = 21.4$ m^2, $V = 12.84$ m^3	11.8629	11.3008	12.9047	6.13102	2.53637	4.04332	2.67473
Rectangular with curved bottom shape,							
$r = 1.75$ m,	3.59569	–	2.70129	5.62619	–	4.10169	2.69669
S_{lat}= 19.9 m^2, $V = 11.94$ m^3	10.9798	7.06645	12.1986	6.51721	2.88868	4.69139	2.93986
$r = 0.45$ m,	3.22484	–	2.10258	5.16913	–	3.33392	2.11851
S_{lat}= 23 m^2, $V = 13.8$ m^3	4.90505	0.83356	3.05339	5.90579	1.90846	3.78202	2.29878
Rectangular,							
$r = 0$ m,	3.14461	–	1.98897	5.09949	–	3.22714	2.03725
$S_{lat} = 23.4$ m^2, $V = 14.04$ m^3	4.61144	0.75369	2.73880	5.81562	2.02085	3.65644	2.21143

∗ The upper row presents the data without the account of unilateral constraints, the lower one – those with the account of unilateral constraints.

M_z) = 10 kN·m (Table 5.9). In the lower rows the values of Δ_z (m) and ψ (rad), respectively, with the account of unilateral constraints are given.

As one should expect, the absolute values of the displacements and slopes decrease with the increase of the contact surface area (the foundation volume). The calculation data for the case of a moment M_x, rotating the slotted foundation in the longitudinal cross-section plane, make an exception. A non-monotonous behaviour of the contact interaction parameters observed here for the calculations with the account of unilateral constraints is explained by an insufficiently uniform discretization of the end surface.

For the foundations with almost equal contact surface area (equal volume) and a close geometrical shape of the longitudinal cross-section (Tables 5.8 and 5.9) the difference in the contact interaction parameters does not increase 5–7%. The results for the foundations with a longitudinal cross-section of a rectangular shape are also rather close. At it could be expected, the best parameters (in the sense of the smallest slopes and displacements) are obtained for the foundations with a linear bottom shape.

On the other hand, unit values of the displacements and slopes (for the foundations with equal average values of forces and moments) have essential differences (up to 30%) depending on the longitudinal cross-section shape. It especially concerns the foundations with a curved bottom shape. With the increase of the dimensionless shape parameter m these differences decrease.

Thus, the account of the longitudinal cross-section shape for the calculation of slotted foundations based on the base deformations is quite important and can result in the lower materials consumption and excavation volume for slotted foundations. The noted trend to the decrease of slopes and displacements can be used to improve the technical and economic parameters of design solutions. Namely, application of slotted foundation with a curved bottom instead of those with a rectangular longitudinal section is possible; according to our calculations, it will result in the decrease of concrete consumption at the foundation production, the restrictions on the displacements and slope, specified by the design assignments, being obeyed.

Besides, the obtained data provide the evidence for both the area and the shape of the lateral surface essentially affecting the slopes and settlements of the slotted foundations. In order to optimize the foundation parameters, while comparing the calculation results one can also specify as characteristics [16] unit settlements Δ_z (1/m^2) and slopes ψ_x (rad/m^3), given by

$$\overline{\Delta} = \Delta / V, \overline{\psi} = \psi / V$$

where V is the foundation volume.

As follows from Tables 5.8 and 5.9, with the increase of S_{lat} the unit slopes and unit settlements will also decrease, even faster than the absolute values. The highest values of the slopes and the settlements correspond to the foundations with a curved bottom shape. Based on the calculation data obtained, it can be noted that the geometrical parameters of slotted foundations with a curved bottom shape should be assigned with high m index value. On the other hand, application of slotted

foundations with a rectangular bottom shape can result in an excessive (≈ 30%) consumption of concrete for producing foundations without the corresponding (≈ 10%) decrease of their base deformation parameters.

Thus, based on the analysis of the calculation data obtained, one can conclude on the necessity of a substantiated assignment of the geometrical size of slotted foundations with different longitudinal cross-section shape.

Comparison of calculated and experimental data under a vertical compressive load acting on a slotted foundation. The numerical results, obtained using the proposed boundary-element method, will be compared with the field test data. In order to estimate the possibilities of the proposed calculation method we compare the plotted dependences of the slotted foundation settlements on the loads with the static test plots. As follows from the references [3, 29, 136], due to a rather labour-consuming and expensive performance of field experiments, the experimental studies of interaction of slotted foundations with soil bases were mostly carried out in laboratory with models of various scale. In order to use the results of testing of the slotted foundation models of various scale by a static load, for the determination of the characteristics of their interaction with the soil bases of industrial foundations, empirical formulae are required [221]. At present they are missing for the slotted foundations of various shape and at various soil conditions. Taking into account these complications at the transfer form the laboratory studies to the field experiments, in order to provide the most complete and reliable study of the calculation and experimental data for the construction sites, we will give a certain priority to the field experiments.

Among the rare field experiments available we will use the data [136] of static tests by a vertical compressive load of a slotted foundation with the size of 1×0.6 m and the depth of 4 m by a vertical compressive load. The field slotted foundation was performed in a trench, worked out dry at a test site in Yekaterinburg.

Soil conditions. The base of the slotted foundation was formed by a loose saturated alluvial clayey with liquidity index from low-plasticity to high-plasticity. The physical and mechanical characteristics of the soil, determined from the drilling of a 15 m deep well, were the following:

natural humidity $w = 0.27$,
compressive deformation modulus $E_c = 4.8$ MPa,
soil density $\gamma = 19.8$ kN/m^3,
internal friction angle $\varphi = 16°$,
unit cohesion $C = 0.013$ MPa,
liquidity index $I_L = 0.55$.

Figure 5.39 shows an experimentally obtained [136] dependence of settlement versus vertical compressive load for a field slotted foundation under consideration. In the same figure the calculation of settlements of a slotted foundation using the boundary-element method is shown both with and without the account of unilateral constraints. A uniform discretization of the contact surface of the soil and the slotted foundation with a rectangular bottom shape consisted of 394 quadrangular boundary elements. The Poisson ratio value ν=0.445 and the total deformation modulus,

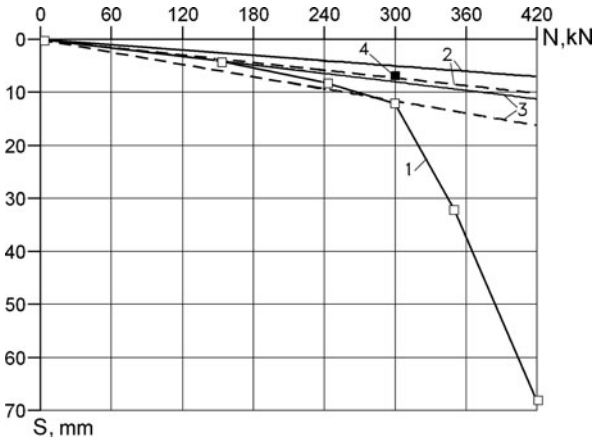

Fig. 5.39 Dependence of the settlement of a test slotted foundation on load: (1) experiment, (2) boundary-element method (m_k= 4); (3) boundary-element method (m_k= 2.5); (4) layered summation method (m_k= 2.5); calculation with (*dashed line*) and without (*solid line*) the account of unilateral constraints

corrected in accordance with [215], $E = 4 \cdot E_K = 19.2$ MPa, were used for the calculations. The foundation weight was $G_F = V_F \cdot \gamma_b = 2.4$ m $\times$ 25 kN/m = 60 kN. The analysis of the data, presented in Fig. 5.39, has shown the results of the boundary-element calculation of the base deformations of the slotted foundation are in a rather good agreement with the field experiment at load values of 75–80% of the limiting load. The settlement discrepancy did not exceed 3–5 mm.

Note that the agreement of the experimental and calculated data essentially depends on the accuracy of assignment of the deformational characteristics of soils (first of all, the calculated deformation modulus) which can become sufficient only in the case of field methods of their determination. The lack of data for the punch deformation modulus resulted in the necessity of a correction factor m_c to be introduced. Though this correction factor correctly reflects the necessity of the compressive deformation modulus to be increased (the deformation modulus values obtained from the compression tests practically always appear to be lowered), however, the choice of its value is rather arbitrary. Note that the values of m_c, quoted for clayeys in [215, Table 1.16] with the intervals of 0.5 and 1.0, are rather essentially dependent of the soil porosity coefficient for all liquidity indices $I_L \leq 0.75$. Application of tabulated values of the deformation modulus E according to [215, Table 1.13] with a more detailed account of the liquidity index in the interval $0.5 < I_L \leq 0.75$ enables in the specific case under our consideration ($I_L = 0.55$) the value of $E = 12$ MPa to be used for the calculations. Computations, performed for this value of the calculated deformation modulus (i.e. for $m_c = 2.5$) enabled the calculation and experimental data to be obtained practically identical (lines 3 in Fig. 5.39). In this case, the experimentally obtained plot of settlement versus load in the load range, not exceeding the calculation load $N \leq 300$ kN, appeared exactly between the theoretical dependences with and without the account of unilateral constraints.

For the calculation load, equal to N=300 kN, using the layer summation method, we have determined the settlement of the slotted foundation under consideration as for a nominal foundation according to Appendix B of the Construction Rules and Regulations 2.02.01–83. The settlement value was 6.875 mm (Fig. 5.39). For the same load value the linear boundary-element method calculation (i.e. without the account of unilateral constraints) gives the settlement value of 8.035 mm. As one can see, in the load range where the linear calculation can be performed, both methods – layered summation and boundary-element – produce not only comparable, but also practically hardly distinguishable results (the difference of settlements is 1.16 mm, being within the measurement accuracy). It is important to note that the account of the structure nonlinearity (unilateral constraints) in the developed boundary-element approach results in the calculated settlement value of 11.572 mm what is by factor of 1.7 larger than according to the Construction Rules and Regulations, and practically coincides with the experimental value of 12 mm (Fig. 5.39).

Thus, the proposed numerical calculation method according to the second limiting state enables the slotted foundation settlements in the phase of compression and local shears to be reliably predicted and, hence, the boundary-element solutions to be recommended for implementation in the calculation practice for mass engineering when the application of the linearly deformable half-space model is most justified.

Prediction of deformations of the slotted foundation base under an off-centre loading. From the point of view of the method of production, slotted foundations belong to the structures, made in cavities, formed inside the soil itself and, contrary to the foundations, produced in open pits, for them, as for deep structures, the known simplified methods of calculation of pile foundations and deep bored supports [51], as fixation in the soil, can be applied. In spite of the greater preference of the elastic half-space method, for practical calculations still a more simple calculation model of an elastic medium, based on the Winkler hypothesis, is applied. A proportional increase of the coefficient of subgrade reaction with depth is assumed.

The book by Pavlov [136] contains general considerations regarding the calculation of foundations with the account of their fixation in the soil as well as an example of calculation of a slotted pier foundation for the action of an off-centre load. The slotted foundation calculation method applied there (with the account of the fixation in the soil) does not take into account the soil resistance to friction at the lateral faces, parallel to the action of the forces and moments. Since the slotted foundations have a rather developed lateral surface, the actual stability of the slotted foundation will always be higher than the calculated one what is noted in [136] at the analysis of the experimental data. A lack of specific methods of calculation for slotted foundations, in opinion of [136], essentially affects their economic efficiency. Therefore, it is advisable to carry out an extended (with the account of contact tangential and normal stresses) calculation of deformation of the slotted foundation base for the elastic half-space model and, based on its results, to evaluate the reliability overestimation, obtained using the traditional calculation method [136, 159].

The example of calculation for an off-centre load, quoted in [136], concerns the design of the foundation of a one-storeyed industrial building with a ferroconcrete frame and travelling cranes with rated load capacity of 50 tons. The bay width 24 m, the step of columns of the main frame 12 m. The column cross-section 600 × 600 mm.

Input data. For the calculation the most loaded foundation of the external row is taken, for which the calculated forces at the top edge level are

$N = 1720.8$ kN,
$M_x = M_y = 458.3$ kN·m,
$H_x = H_y = 37.5$ kN.

Soil conditions. From the soil surface to the depth of 5 m tough clay (E=15 MPa, γ=18.3 kN/m, φ=14°, C=0.043 MPa, I_L =0.37), below – to the depth of 10 m – eluvial clayey (E=27 MPa, γ=21.2 kN/m, φ=25°, C=0.04 MPa, I_L = 0).

The foundation dimensions are 3.5×0.6 m. The slot depth is 5 m. The slotted foundation has a rectangular longitudinal cross-section with a curved bottom shape, r=1.75 m (Fig. 5.40). The slotted foundation calculation is performed in [136]

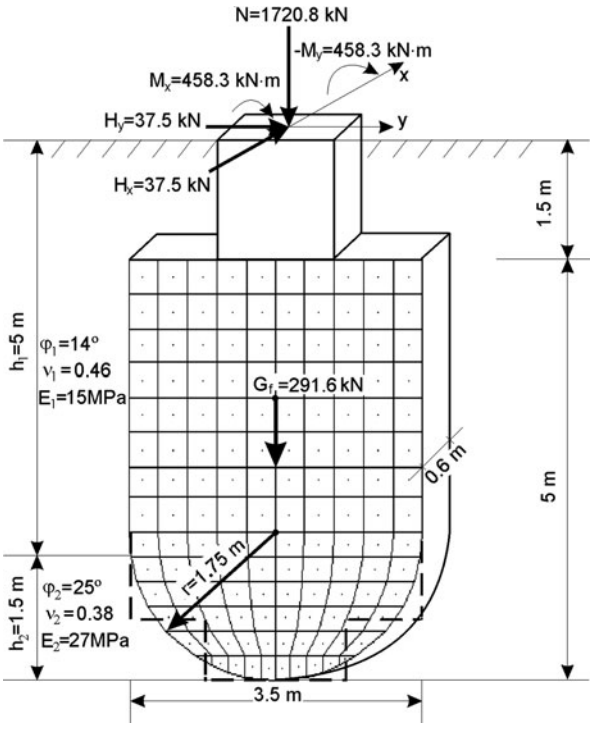

Fig. 5.40 Scheme for the calculation of a slotted foundation with a rectangular longitudinal cross-section with a curved bottom for an off-centre load

according to the scheme of an absolutely rigid rod. In order to simplify the calculations the curved contour of the foundation bottom is substituted by a rectangular one with a ledge. The ledge value is determined from the condition of the equality of volumes of the real and the equivalent foundations. The tests for the foundation bearing capacity, based on the soil base resistance, as well as for the foundation bearing capacity and stability in the plane perpendicular to the slot plane, were performed with a considerable reserve. The calculated foundation weight is $G_F = V_F \cdot \gamma_b = 291.6$ kN ($\gamma_b = 25$ kN/m is the density of the concrete, class B15).

Based on the test for the foundation stability in the plane, perpendicular to the slot plane, the angle of the foundation rotation around the rotation centre, located at the depth of $z = 3.42$ m, was calculated:

$$\psi = 2.14 \cdot 10^{-2} \text{rad}$$

The calculation using the layered summation method was performed as for a nominal foundation according to the Appendix B to the Construction Rules and Regulations 2.02.01–83. As a result, the settlement value was obtained:

$$S = 2.06\,\text{cm}$$

For the calculation of the slotted foundation according to the proposed approach using the boundary-element method, the point of application of external forces and moments is considered to be the centre of the top edge of the foundation on the level of the calculated soil surface (Fig. 5.40). The absolute values of momental loads, applied to the slotted foundation, should be increased by a value $H_x(H_y) \cdot h = 37.5$ kN $\times$ 1.5 m $= 56.25$ kN·m where $h = 1.5$ m is the height of the base of the column. The calculation scheme for the slotted foundation under the specified off-centre load and discretization of its lateral surface into the boundary elements are shown in Fig. 5.40. The total number of the boundary elements on the contact surface of the slotted foundation and the soil was 388.

Since two layers of soil are located above the foundation bottom, the calculations are performed for three variants of given base parameters:

(1) $E = E_1 = 15\,\text{MPa}, \ \nu = \nu_1 = 0.46,$
(2) $E = E_2 = 27\,\text{MPa}, \ \nu = \nu_2 = 0.38,$
(3) $E = \frac{E_1 \cdot h_1 + E_2 \cdot h_2}{h_1 + h_2} = 17.8\,\text{MPa}, \ \nu = \frac{\nu_1 \cdot h_1 + \nu_2 \cdot h_2}{h_1 + h_2} = 0.44$

being the weighted deformation parameter values, $h_1 = 5$ m, $h_2 = 1.5$ m being the soil layer thicknesses.

The Poisson ratio values ν_1 and ν_2 were determined using the Wet [240] from the tabulated internal friction values φ_1 and φ_2 of the upper and the lower soil layers, respectively.

The results of calculation using all the three mentioned variants of the base deformational parameters are listed in Table 5.10 where the contact interaction parame-

Table 5.10 Parameters of a slotted foundation base deformation under off-centre loading

Displacements (cm)			Slopes (rad)		
$\Delta_x \cdot 10$	$\Delta_y \cdot 10$	Δ_z	$-\psi_x \cdot 10^4$	$\psi_y \cdot 10^4$	$-\psi_z \cdot 10^4$
		$E = 15$ MPa, $\nu = 0.46$			
2.3327	2.4824	2.1809	8.0619	7.5369	0
2.7854	2.8139	2.3489	8.2212	9.1031	1.0898
		$E = 27$ MPa, $\nu = 0.38$			
1.2771	1.3973	1.2124	4.5279	4.0663	0
1.4362	1.6503	1.3211	4.9139	4.4970	0.0772
		$E = 17.8$ MPa, $\nu = 0.44$			
1.9606	2.1011	1.8401	6.8229	6.3134	0
2.5239	2.3691	1.9884	7.0115	8.2887	1.1693

ters are presented both with (the upper row) and without (the lower row) the account of unilateral constraints.

As one should expect, the account of unilateral constraints for all calculation variants leads to an increase of absolute values of the slotted foundation displacements and slopes. For settlements this increase was 7–8%, for horizontal displacements – 10–21%, for slopes – 2–28%. Thus, for slotted foundations with a developed lateral surface, the account of unilateral constraints in the calculations is necessary. Besides, due to the action of forces and moments in orthogonal directions, a slight rotation of the slotted foundation around the central symmetry axis appears. This rotation is due to the account of the structure nonlinearity and in principle cannot be obtained by any of the methods in linear formulation.

Calculations of the foundation settlements Δ_z according to the first and the third calculation variants are in a rather good agreement with the calculation data according to the absolutely rigid rod scheme [136]. A minimal discrepancy was obtained for the third variant with the account of unilateral constraints, its value being only 4%. The calculation according to the second variant, when the whole base parameters are associated with the deformational parameters of the soil layer in the bottom, results in the discrepancies of the results both for the settlements and the slopes more than by 40%. This, in particular, confirms that for a slotted foundation the lateral surface bearing capacity value is much more important than that for the bottom.

If the calculation is based on the third variant, i.e. with the averaged soil deformational parameters, then application of the numerical approach based on the boundary-element method results in a decrease of the slotted foundation settlements. This is even more applicable for slopes which for all the three variants appeared almost three times smaller than for the calculation using the coefficient of subgrade reaction. Since according to the calculation of the foundation as a fixation in the soil $\Delta_x = z_0 \cdot \tan\psi = 3.42 \text{ m} \cdot 2.14 \cdot 10^{-3} \approx 0.0073$ m, for the boundary-element modelling a decrease of horizontal displacements is also noted (Table 5.10).

Thus, the boundary-element approach enables a designer to obtain a full pattern of the spatial strained state of the soil base of a slotted foundation subject to

an off-centre load of a general kind. The performed comparison of our numerical calculations with the data of [136], obtained using the deformation-based method of calculation of a slotted foundation as a nominal foundation on a natural base in accordance with the requirements of the Construction Rules and Regulations, is the evidence for the importance of the account of the soil back pressure forces for the reliable determination of the slotted foundation displacements and slopes. In comparison with the design regulations being used [215], the approach proposed here is sufficiently universal and results in a more economical design solutions since it enables the pressure transferred to the soil to be increased and the foundation size to be reduced. Besides, the results of the comparison performed have shown a possibility of effective application of the boundary-element method in practical design of slotted foundations at various shape of the deepened part.

5.6.3 Contact Stress on the Lateral Surface of a Slotted Foundation

Slotted foundations are bearing structures which accept all types of loads from the above-earth parts of buildings and structures. The loads are transferred to the base by the bottom and lateral surfaces of the slotted foundations. The slotted foundation thickness, corresponding to its width, is by an order of magnitude lower than its other dimensions. Therefore, the studies of distribution of tangential and normal stress over the slotted foundation lateral surface, developed in depth and in the longitudinal direction, are of the main interest. Here one should note that the experimental studies of formation and transformation of the contact stress field, required for better understanding of the processes of the slotted foundation interaction with the soil medium at different loading conditions, is rather difficult due to technical reasons, the most essential of which are errors induced in the pressure cell readings in the course of their installation and concrete placement, structural features of the equipment, high measurement errors (of the order of 20%), etc. [136]. Therefore, technical results for the determination of forces of contact interaction of slotted foundations with soil by means of mathematical modelling are of great importance for soil mechanics and foundation engineering.

The known mathematical difficulties and total lack of analytical solutions of spatial contact problems for slotted foundations with all features of contact surfaces lead to a necessity of the contact forces to be studied only approximately, using numerical methods and computations.

Application of numerical solutions of spatial contact problems for deepened punches, obtained using the boundary-element method, enables all components of the contact stress vector for the slotted foundations to be estimated without invoking expensive and labour-consuming field measurements. The proposed approach to the contact stress studies enables the experiments to be much simplified and a sufficiently complete information to be obtained on the contact stress field distribution with an accuracy, a priori not worse than the experimental one.

The most evident is consideration of the contact stress fields for a prismatic slotted foundation whose all sides are perpendicular to the coordinate axes, since for the corresponding faces one of the following relations will be fulfilled:

$$\sigma_n = \pm p_x,\ \sigma_n = \pm p_y,\ \sigma_n = \pm p_z.$$

On a slotted foundation lateral surface ($x=\pm h/2$), in a pre-chosen coordinate system (Fig. 5.32), the normal stresses $\sigma_n=\pm p_x$, and the tangential stress vector will always belong to the flat contact surface. Therefore, in order to indicate the tangential stress vector, a direction field is convenient, determined in each contact point by the following angle:

$$\Theta = \begin{cases} \arctan\left(\frac{p_z}{p_y}\right), p_y > 0; \\ \pi + \arctan\left(\frac{p_z}{p_y}\right), p_y < 0, p_z \geq 0; \\ -\pi + \arctan\left(\frac{p_z}{p_y}\right), p_y < 0, p_z < 0. \end{cases} \tag{5.7}$$

For the numerical modelling of the contact stress consider a typical pier slotted foundation with a rectangular longitudinal cross-section and the dimensions of 3.5 $\times$ 2.6 $\times$ 0.6 m, subject to spatial loads of the following type:

(1) central vertical compressive load,
(2) eccentric vertical load,
(3) inclined force load in the plane of the longitudinal cross-section,
(4) momental load in the plane of the longitudinal cross-section,
(5) inclined force load, acting orthogonally to the plane of the longitudinal cross-section,
(6) momental load, acting orthogonally to the plane of the longitudinal cross-section,
(7) torque along the vertical axis.

The contact stress field analysis was carried out for the following fixed values of the base deformational parameters: E=20 MPa, ν=0.4, corresponding to the conditions of construction of slotted foundations in firm-structure soils of low-moisture clayey type.

Knowing the direction cosines and stress vector components p_x, p_y, p_z for each boundary element, one can calculate tangential $\tau = \pm\sqrt{p_y^2 + p_z^2}$ and normal σ_n contact stresses for all faces of the slotted foundation.

A rather full pattern of contact stress distribution for slotted foundations with a rectangular lateral surface is obtained from a numerical boundary-element solution of the spatial contact problem and plotted in Figs. G.2–G.15 of Appendix G, using the isolines of dimensionless stresses $\bar{\sigma}_n = \pm\bar{p}_x$, $\bar{p}_y$, $\bar{p}_z$, $\bar{\tau}$. As a scale for the contact stress we used the average pressure $p_{av}=10^2$kN/S_F=42.69 kN/m^2 where S_F=23.42 m^{2}is the surface of the contact of the foundation and the soil.

The vector contact stress fields, shown in Figs. 5.41–5.48, enable the soil resistance to the friction on the slotted foundation lateral surfaces under spatial static loads to be studied quite effectively and with an accuracy, sufficient for practical purposes, avoiding complex and expensive field measurements. The information about the tangential stress vector value and direction enables the tangential contact stress field over the whole slotted foundation lateral surface to be visualized on a boundary-element grid of even a moderate density. Thereby the mechanism of the slotted foundation lateral surface resistance to the shear deformation can be studied with the account of the three-dimensionality of the stress-strained state of the base. Figures 5.49–5.53 contain isolines of the reduced direction angle $\bar{\theta} = 2\theta/\pi$ for the tangential stress vector as an additional geometrical characteristics of the contact stress field.

As seen from Figs. 5.41–5.53 and Appendix G, the calculation using the boundary-element method has enabled rather distinct patterns of the tangential stress field characteristics on the lateral surface of the slotted foundations to be obtained, what does not seem to be possible in the framework of traditional calculation schemes.

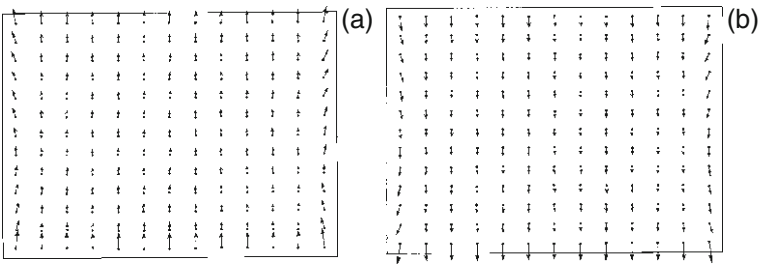

Fig. 5.41 Tangential contact stress vector fields on the lateral surface of a slotted foundation under an overturning moment M_y=1.4·10^3 kN·m, (**a**):x=0.3 m, (**b**): x= –0.3 m

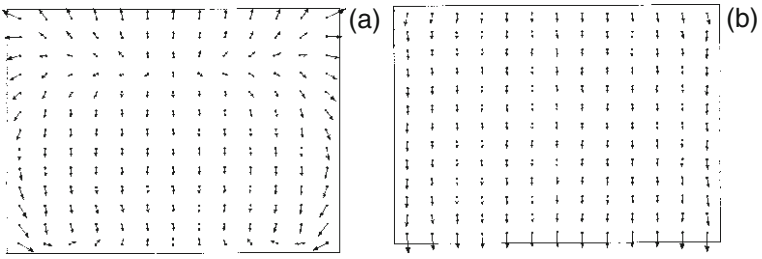

Fig. 5.42 Tangential contact stress vector fields on the lateral surface of a slotted foundation under a combined action of a force and a momental load P_z=10^3 kN, M_y=1.4·10^3 kN·m, (**a**):x=0.3 m, (**b**): x= –0.3 m

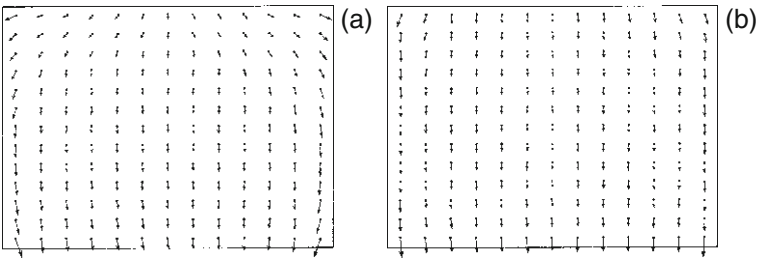

Fig. 5.43 Tangential contact stress vector fields on the lateral surface of a slotted foundation under a combined action of a force and a momental load $P_z=10^3$ kN, $M_y=0.7\cdot10^3$ kN·m, (**a**)x=0.3 m, (**b**) x= –0.3 m

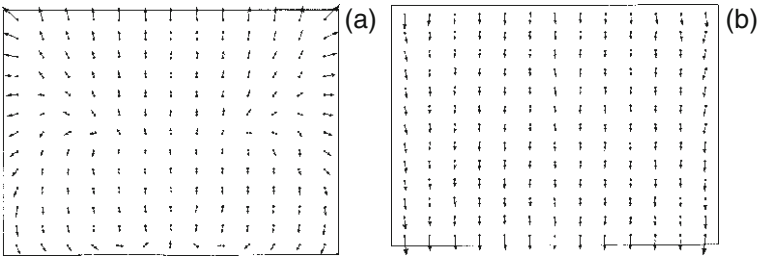

Fig. 5.44 Tangential contact stress vector fields on the lateral surface of a slotted foundation under an inclined force $R=10^3$ kN, $\beta=135°$ perpendicularly to the longitudinal cross-section plane, (**a**)x=0.3 m, (**b**) x= –0.3 m

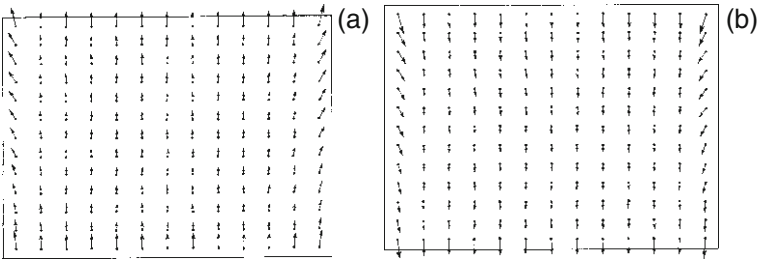

Fig. 5.45 Tangential contact stress vector fields on the lateral surface of a slotted foundation under a horizontal force $R=10^3$ kN, $\beta=180°$ perpendicularly to the longitudinal cross-section plane, (**a**)x=0.3 m, (**b**) x= –0.3 m

Consider how the contact stress field components, obtained from the calculations, help one to estimate the main features of the slotted foundation lateral surface functioning at different spatial loading conditions.

First of all, from the value and the distribution character of normal and tangential stresses one can study the resistance of the soil to the friction over the contact surface under vertical, horizontal, and momental loads as well as their combinations, acting on a slotted foundation.

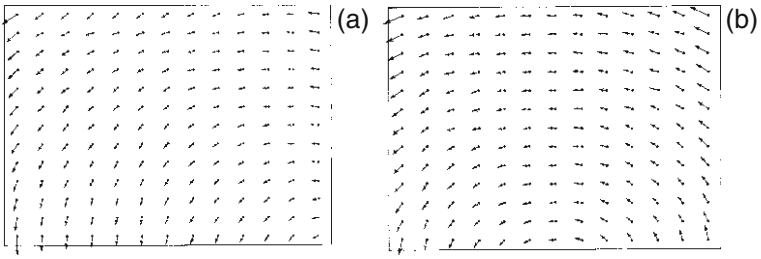

Fig. 5.46 Tangential contact stress vector fields on the lateral surface of a slotted foundation (x= ±0.3 m) under an inclined force R=10^3 kN within the longitudinal cross-section plane, (**a**)α=135°, (**b**) α=180°

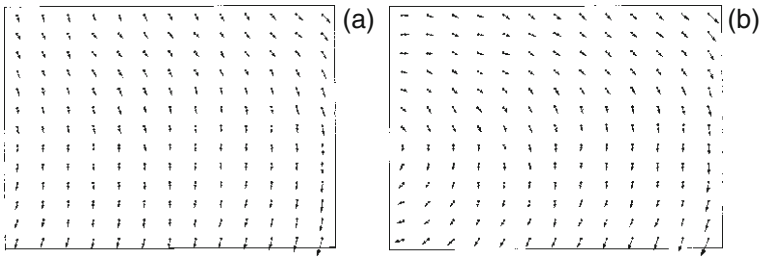

Fig. 5.47 Tangential contact stress vector fields on the lateral surface of a slotted foundation (x= ±0.3 m) under an eccentric vertical force P_z=10^3 kN, (**a**)ϵ_y= –0.7 m, (**b**) ϵ_y= –1.4 m

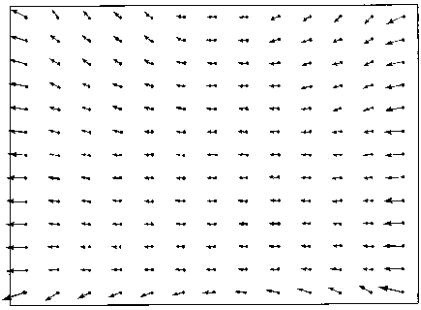

Fig. 5.48 Tangential contact stress vector field on the lateral surface of a slotted foundation (x= 0.3 m) under a torque M_z= 0.5·10^3 kN·m

The data on the contact stresses are important for the analysis of the stress-strained state in the foundation active area. With an assumption, common for the soil mechanics, that the stress components in case of a small development of plastic deformation areas, can be determined from the solutions of theory of elasticity, one can easily determine the calculated pressures on the soil base for slotted foundations of different size and depth under a complex spatial loading.

The solution of the problem of increase of reliability and improvement of calculation methods for slotted foundations is impossible without the account of strength-related characteristics of the soil base. As noted above, application of the contact

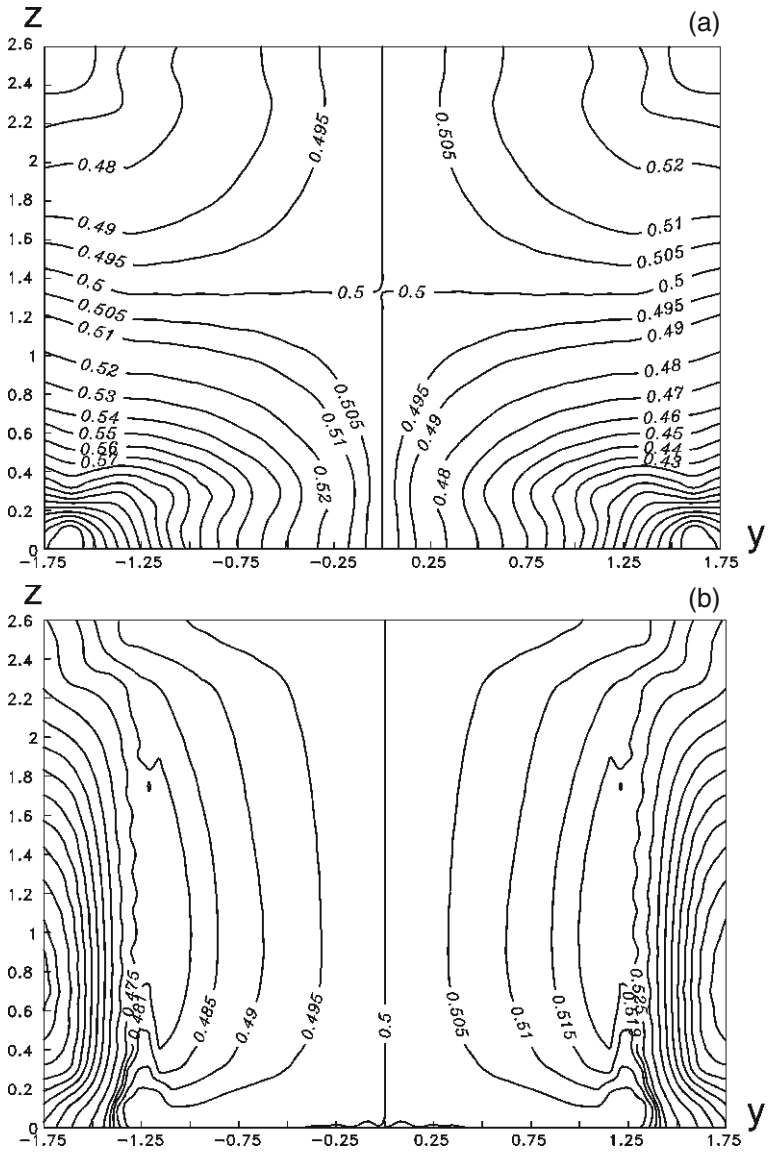

Fig. 5.49 Isolines of reduced direction angles $\bar{\theta} = 2\theta/\pi$ of the tangential contact stress vector on the lateral surface of a slotted foundation (x= 0.3 m) under a central force R=10^3 kN: (**a**) vertical force, (**b**) horizontal force

stress data enables the resistance to shear on the contact surface of the slotted foundation and the soil to be estimated. Here we show, how the knowledge of the contact stress field on the lateral surface of a slotted foundation and the knowledge of the

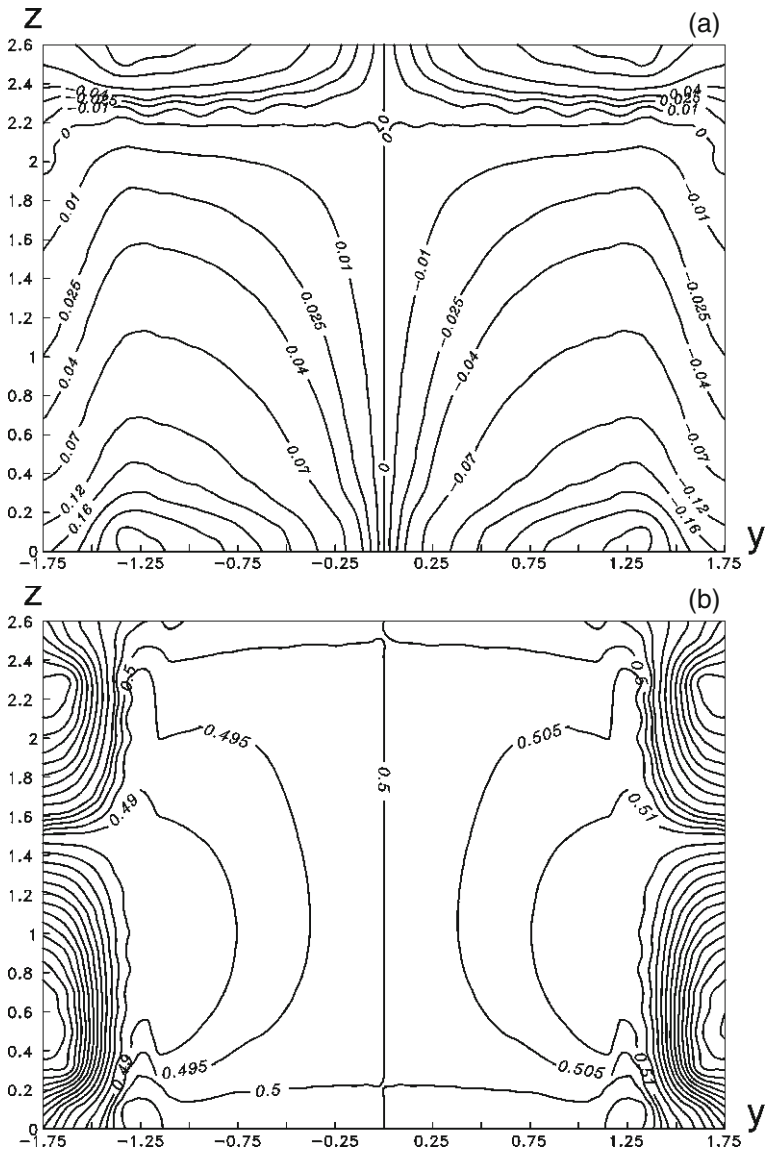

Fig. 5.50 Isolines of reduced direction angles $\bar{\theta} = 2\theta/\pi$ of the tangential contact stress vector on the lateral surface of a slotted foundation (x= 0.3 m) under: (**a**) a torque M_z=0.5·10^3 kN·m and (**b**) an overturning moment M_y=1.4·10^3 kN·m

limiting state condition for the soil enables the contact strength of the foundation structure binding to the base can be checked.

For the mechanical behaviour of soil, at each site the Coulomb friction law should hold

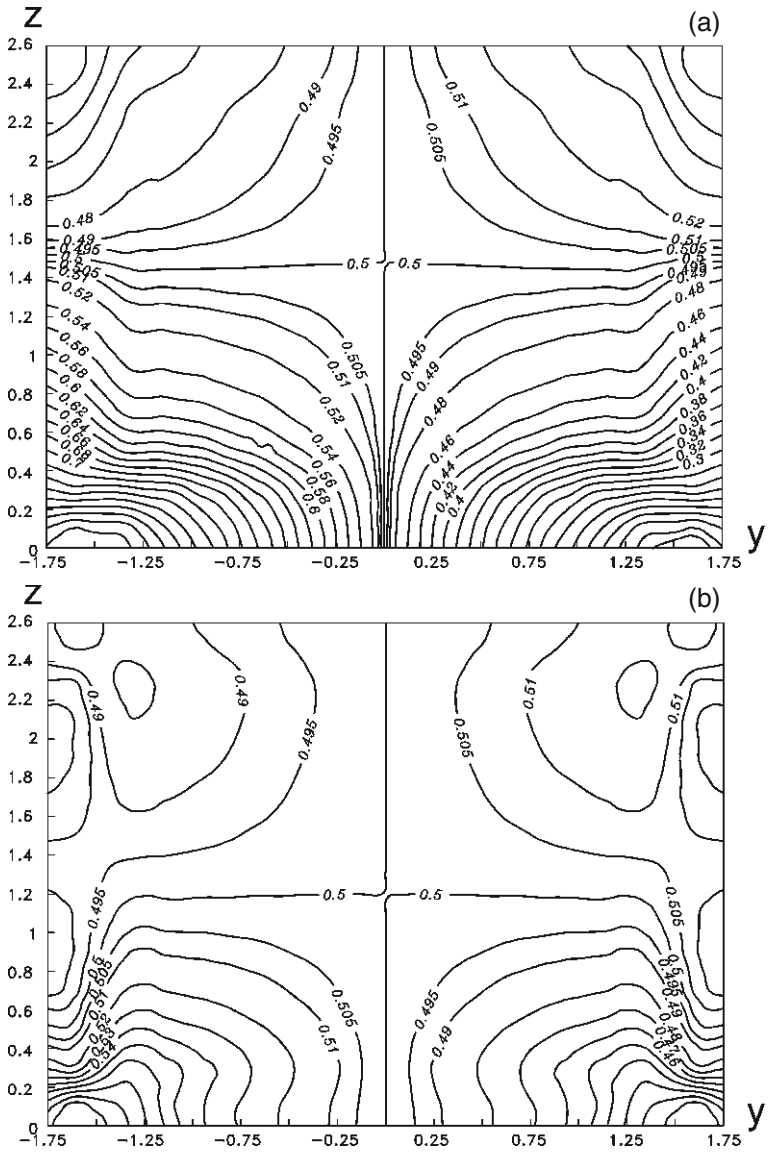

Fig. 5.51 Isolines of reduced direction angles $\bar{\theta} = 2\theta/\pi$ of the tangential contact stress vector on the lateral surface of a slotted foundation (x= 0.3 m) under a combined action of a force and a momental load P_z=10^3 kN, M_y=0.7·10^3 kN·m: (**a**) x= 0.3 m, (**b**) x= –0.3 m

$$|\tau| \leq C + \sigma_n \cdot \tan\varphi \tag{5.8}$$

where C is cohesion, φ is the internal friction angle. As known from [25], in the points where the tangential component τ of the reactive soil pressure exceeds the

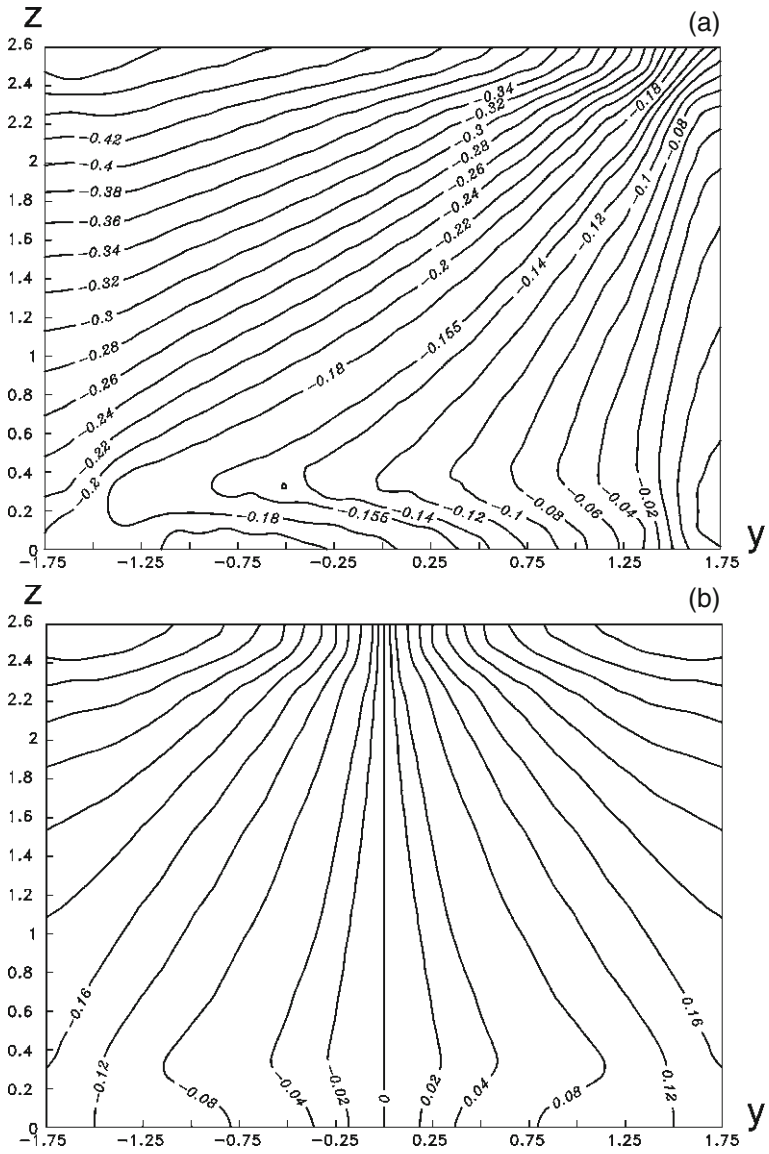

Fig. 5.52 Isolines of reduced direction angles $\bar{\theta} = 2\theta/\pi$ of the tangential contact stress vector on the lateral surface of a slotted foundation ($x = \pm 0.3$ m) under an inclined force $R = 10^3$ kN within the longitudinal cross-section plane: (**a**) $\alpha = 135°$, (**b**) $\alpha = 180°$

value, determined by the strength condition of Eq. (5.8), slippage occurs. The condition of Eq. (5.8) is applicable for the points inside a soil medium. On the contact surface of the base and the foundation the following condition is fulfilled:

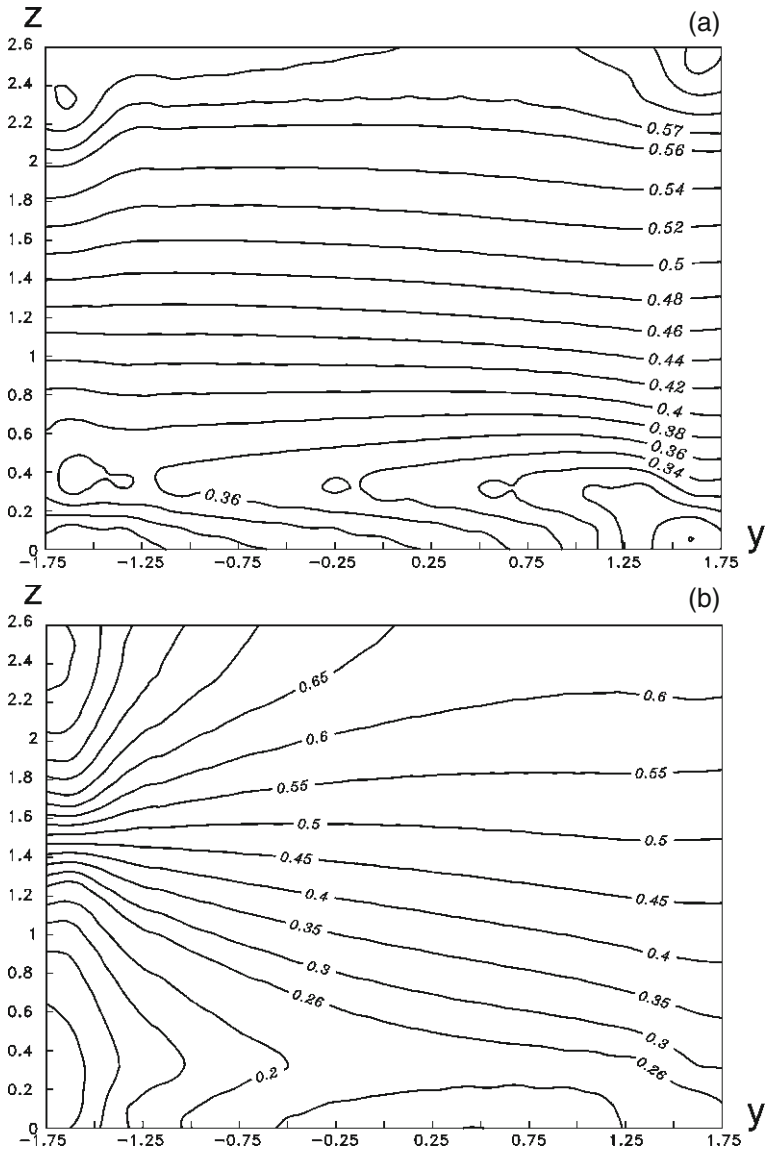

Fig. 5.53 Isolines of reduced direction angles $\bar{\theta} = 2\theta/\pi$ of the tangential contact stress vector on the lateral surface of a slotted foundation ($x = \pm 0.3$ m) under an eccentric vertical force $P_z = 10^3$ kN: (**a**) $\epsilon_y = -0.7$ m, (**b**) $\epsilon_y = -1.4$ m

$$|\tau| \leq a + \sigma_n \cdot \tan\delta \tag{5.9}$$

where $|a| \leq C$, τ and σ_n are the components of the stress vector in the point of the soil contact with the foundation, δ ($\leq \varphi$) is the angle of the soil friction across the

foundation (measure of roughness). It is known from the experiments [25] that $m = a/C = \tan\delta$, $0 \le m \le 1$. At $\tau = 0$, i.e. when $\delta = a = 0$, an absolutely smooth surface is obtained, and at $|\tau| \le C + \sigma_n \cdot \tan\varphi$, i.e. when $\delta = \varphi$ and $a = C$ one obtains an absolutely rough surface. For the calculations of concrete gravity retaining walls with a flat boundary, for the sake of simplicity $\delta = 2\varphi/3$ is usually accepted [25]. For drift sand, obeying the Coulomb strength law and interacting with concrete foundation structures, the value of $m = a/C = 0.8$ is suggested to be chosen [27]. The relation of the internal friction angle φ and the angle δ of friction on the contact surface will be hereinafter estimated using a theoretically substantiated formula

$$\tan\delta = \sin\varphi \tag{5.10}$$

which was obtained in [124] for a soil with plastic incompressibility.

Since for the soil masses the most dangerous is violation of cohesion due to shear, then, knowing the parameters of resistance to shear for different parts of the contact surface, one can, according to Eq. (5.9), from the tangential stresses on the boundary elements, determine the contact slippage areas where the tangential component of the reactive soil pressure exceeds the value, determined from the strength condition. In the first approximation, in order to estimate the strength of the contact between the foundation and the soil, one should built, based on the calculation results, the lines of equal level of a function

$$f\left(\sigma_{ij}\right) = |\tau| - a - \sigma_n \cdot \tan\delta.$$

The areas with $f < 0$ give the evidence for the lack of slippage, on a contact surface with $f = 0$ a limiting state is achieved, at $f > 0$ no cohesion of the foundation with the soil is provided. Building up areas with different cohesion level enables the areas of most probable slippage to be identified what, in turn, enables the necessary recommendation to be worked out for the rational design of slotted foundations.

One should note that while performing calculations for slotted foundations, whose lateral surface can be oriented depending on the slot location and the external force direction, in firm-structure soils, it is important to take onto account the soil base anisotropy. The slippage areas in this case are revealed in a similar way, using the method considered, invoking anisotropic strength conditions [18] as well as experimental data on the studies of strength-related characteristics of soils and rock masses. The effect of anisotropy on the resistance to shear is especially pronounced for varved clays with a layered structure. For such clay the vertical cohesion value can be several times higher than cohesion in the horizontal direction [102]. The account of anisotropy as one of the essential and common features of rocks and soils will enable the efficiency of design of slotted foundations to be increased; in particular, it will enable the slot plane orientation on the construction site to be purposefully chosen as well as the length-to-depth ratio of the slotted foundations to be improve in order to reduce the possibility of formation of slippage areas at their developed lateral surface.

Consider the effect of the strength-related soil properties on the features of the shape and size of the contact strength fault areas over the slotted foundation lateral surface, in case the "elastic" field of the contact stress being known. The studies of the contact strength fault areas is important from the practical point of view for reliable assignment of the slotted foundation shape and loading parameters as well as for the formulation of criteria for the safety factor assignment in the design regulations.

Studies of the spread of the contact strength fault areas over the slotted foundation lateral surface was carried out for five variants of the strength-related parameters of the soil, presented in Table 5.11. The same table contains the strength parameters δ and a, characterizing the friction and cohesion on the contact surface of the foundation and the soil and related to the soil strength parameters φ and C by Eq. (5.10) and a ratio $m = a/C = 0.8$.

Using the calculated contact stress values (Appendix G), in Fig. 5.54 lines, for which $f(\sigma_{ij}) = |\tau| - a - \sigma_n \cdot \tan\delta = 0$, are built. Consequently, the configuration of areas, for which Eq. (5.9) is violated and slippage is possible, are indicated.

Table 5.11 Parameters of internal and contact friction and cohesion

Strength parameters	Variants				
	1	2	3	4	5
ϕ, deg	17	27	37	37	37
δ, deg	16.3	24.4	31	31	31
C, kPa	6.25	6.25	6.25	11.25	18.75
a, kPa	5	5	5	9	15

Analyzing the presented calculation data, one can note the following qualitative and quantitative features of the contact interaction of slotted foundations with soil.

First, the presence of slippage areas on the slotted foundation lateral surface is revealed for all five characteristic types of spatial loading (Fig. 5.54, Table 5.12). Numerical modelling of the contact interaction has shown that, depending on the loading type and the soil strength-related properties, the slippage can occur over rather extensive areas on the foundation lateral surface, comparable with the full cohesion areas.

It is seen from the calculation data, presented in Fig. 5.54 that the slippage area configurations are essentially dependent of the contact strength characteristics as well as the load value and direction on the top edge of the foundation. The slippage areas can be simply or multiply connected, usually, originating from the ribs, in the vicinity of which the contact stress field is characterized by the highest nonhomogeneity degree. Under a force or a momental load across the plane of the slotted foundation longitudinal cross-section, the slippage areas arise in the range of its bottom on the lateral side where tensile normal stress is observed. On the opposite side of the lateral surface, where the foundation is pressed to the soil (i.e. compressive normal stress is developed), the tangential stress field is rather uniform, no areas of shear contact strength faults are observed.

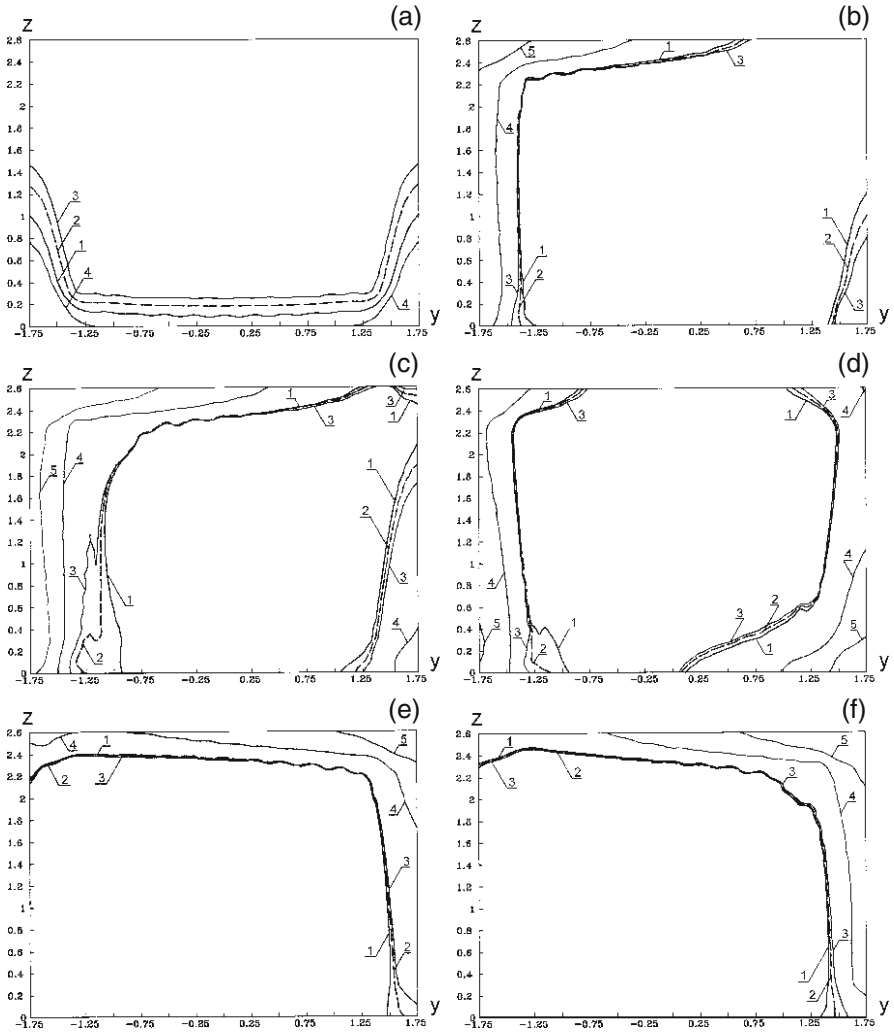

Fig. 5.54 Boundaries of contact strength fault areas on the lateral surface of a slotted foundation under different loading conditions (**a–f**) at the friction and soil cohesion parameters (1–5), determined according to Table 5.6

The effect of the cohesion parameters (C, a) on the development of the slippage areas is more noticeable than that of the internal and contact friction angles (φ,δ). A double increase of δ under different type of loading in the plane of the slotted foundation longitudinal cross-section results in an increase of the slippage areas only by 3–5% (See the areas restricted by curves 1, 2, and 3 in Figs. 5.54b–f). This is the evidence for the resistance to shear on the slotted foundation lateral surface being determined mostly by cohesive forces. A somewhat different situation occurs

Table 5.12 Maximal values of the function $f(\sigma_{ij}) = |\tau| - a - \sigma_n \cdot \tan\delta \geq 0$ (kPa) on the lateral surface of a slotted foundation with different parameters of contact friction and cohesion under spatial loading

Loading type	Strength parameters				
	1 $a = 5$ kPa, $\delta = 16.3^\circ$	2 $a = 5$ kPa, $\delta = 24.4^\circ$	3 $a = 5$ kPa, $\delta = 31^\circ$	4 $a = 9$ kPa, $\delta = 31^\circ$	5 $a = 15$ kPa, $\delta = 31^\circ$
Transverse load (a) $R = 1000$ kN, $\alpha = 135°$	4.869	7.100	9.141	5.141	–
Longitudinal load					
(b) R=1000 kN, $\alpha = 135^\circ$	13.918	14.789	15.587	11.587	05.587
(c) $R = 1500$ kN, $\alpha = 135^\circ$	23.376	24.683	25.879	21.879	15.879
(d) R=1000 kN, $\alpha = 90^\circ$	13.945	14.838	15.653	11.653	05.653
Eccentric vertical load R=1000 kN,					
(e) $\epsilon_y = 0.7$ m	16.259	16.904	17.495	13.495	7.495
(f) $\epsilon_y = 1.4$ m	23.292	24.032	24.709	20.709	14.709

at the foundation being loaded across the slot plane. For such loading type, the presence of a component, orthogonal to the foundation lateral surface, increases the role of the internal friction forces in the soil, whose growth results in a practically proportional expansion of the slippage areas (Fig. 5.54a).

As follows from the calculations, at a fixed value of the contact friction δ, the increase of the soil contact cohesion parameter a rather essentially affects the decrease of the fault areas for the strength of the contact between the foundation and the soil (Fig. 5.54, curves 3, 4, and 5). In particular, at "transverse" loading of the slotted foundation by an inclined force the increase of the a parameter from 5 kPa to 15 kPa (i.e. by factor of 3) at δ=31° has led not only to a sharp decrease of the slippage areas, but even to their total absence (Fig. 5.54a).

The increase of the load on the foundation, as one could expect, results in an increase of areas where the contact cohesion of the foundation with soil is violated. It is seen, for instance, from the comparison of Figs. 5.54b and 5.54c where the shear areas are shown on the lateral surface of the slotted foundation loaded by an inclined force acting in the plane of its longitudinal cross-section. The load increase by factor of 1.5 has led to a clearly revealed expansion of the slippage areas. The discussed expansion (or appearance) of the slippage areas is revealed for all variants of the strength-related parameters under consideration (Table 5.11). A general trend to the expansion of the contact strength fault areas from the boundaries towards the central part of the lateral surface along the inclined external force direction is observed.

The effect of the resultant inclination angle on the configuration of the contact strength fault areas can be revealed from the analysis of Figs. 5.54b and 5.54d. As noted above, the inclined force (α=135°), acting in the longitudinal cross-section of the foundation (Fig. 5.32a), forms slippage areas on its lateral surface, adjacent to the opposite angles in accordance with the inclined force direction. Such

configuration of the slippage areas is naturally determined by the presence of a vertical (impressing) and a horizontal (shearing) components of the inclined force. Contrary to the above case, at $\alpha=180°$, i.e. under a horizontal force, the mechanism of formation of the slippage areas on the slotted foundation lateral surface is qualitatively different. In this case the highest increase of tangential stress occurs on the zones, adjacent to the vertical faces of the slotted foundation. A rather essential irregularity of the slippage area boundaries is noted, due to the slotted foundation size, loading level, and contact strength parameters.

Numerous calculations have shown that under a vertical load on a slotted foundation, applied to its centre, the areas with highest tangential stress are localized near its bottom. As follows from the data illustrated by Figs. 5.54e and 5.54f, the contact strength fault areas under an eccentric loading are transformed and, besides the areas, adjacent to the bottom, include also a more loaded vertical face. As a result, the slippage area if formed at the loaded rib and the face which form it. An increase of the vertical load eccentricity (double, for the case under consideration) results in hardly noticeable deformations of the slippage area boundary contours. The slippage area boundaries are more sensitive to the variation of the contact cohesion parameter a than to the variation of the contact friction angle δ.

The presented method of delineation of slippage areas on the lateral surfaces of slotted foundations enables one, in case of a considerable growth of their fraction, exceeding a certain threshold value (which for better reliability should be set, invoking the empirical data), to conclude on the inapplicability of the linear elastic state model and on a need for application of more complex calculation schemes of nonlinear deformation. On the other hand, a considerable complexity and high labour consumption of solving nonlinear (elastoplastic) problems for a spatial stress-strained state of the base essentially encumbers implementation of such solutions into the practice of foundation engineering even at the modern level of mathematical modelling. Therefore, in view of the slippage areas of different size, arising under loading on the developed lateral surface of slotted foundations, for calculations it is convenient to introduce a safety factor whose value for soils with known strength-related characteristics can be assigned depending on the slotted foundation size, required calculation accuracy, and the category of the building to be constructed, based on multivariant boundary-element solutions, similar to those discussed above.

The calculations presented also enable one to make a conclusion, important for practical purposes, that for soils with higher values of the C parameter the slippage areas on the slotted foundation lateral surface will shrink and, consequently, the possibility of application of the elastic half-space model for base deformation-based calculation of slotted foundations will be more justified. this will enable the calculation loads to be noticeably increased and the slotted foundation economical parameters to be improved.

In order to elucidate the contact deformation pattern in more detail one should take into account that the stress-strained state of the slotted foundation + base system, determined in the first cycle, will correspond to the real one only to a certain extent: due to the soil slippage over the foundation the contact stress field will be transformed what will result in the slippage area variation. Further improvement of

the contact interaction results will require a series of calculations to be performed and a special stepwise computation procedure to be organized. however, the trend to the slippage development or stabilization will enable one to conclude on the change of the calculation scheme, assignment of the foundation size and load values on its top edge. The most important for practical purposes is to set the optimal size of the slotted foundation. On one hand, the desire to decrease the foundation volume is quite reasonable; however, it is related to an inadmissible increase of its settlements and slopes. On the other hand, formation of contact strength fault areas on the lateral surface of slotted foundations, even designed in an optimal way, but without a check for sufficient cohesion over the contact surface, can reduce the quality of the design solution, leading to an additional unpredicted increase of displacements and slopes.

Thus, theoretical studies of variation of contact stress fields enables the results of base deformation-based calculations and field studies of slotted foundations to be treated more exactly. Determination of contact stress fields on the slotted foundation lateral surfaces by mathematical modelling and obtaining their qualitative and quantitative dependences on the force, geometrical, physical and mechanical, strength-related and other characteristics of the foundation+soil system will enable purposeful control of the slotted foundation displacement parameters and check of their stability to external spatial loads. As a result, the efficiency of application of slotted foundations in the industrial and civil engineering will increase due to the practical recommendations regarding the choice of the calculation schemes, optimization of the shape parameters and loading as well as formation of substantiated methods of calculation applicable for their design and functioning.

5.6.4 Slotted Foundations with Lateral Widenings

Based on the calculation experience, we propose new structures of slotted foundations with lateral widenings in the form of longitudinal ribs of different cross-section configuration (Fig. 5.55a). The horizontal support ribs result in additional support area, increase the area of the contact surface with the soil. The geometrical characteristics of a support widening are determined depending on the value and direction of the external load, applied to the foundation, as well as on the physical and mechanical properties of the soil. The presence of the support widenings in the structure of the slotted foundations enables the settlements under vertical load to be essentially ($\approx$12%) reduced in comparison with the foundations without widenings. The support widenings are the stress concentrators in the foundation active area. Under inclined or momental loads the widening ribs prevent the foundation slopes in both longitudinal and transverse directions, i.e. prevent the foundation overturning effect under eccentric loading. At a given slotted foundation depth this is achieved by a slight increase of the concrete volume in comparison with traditional slotted foundations.

The analysis of the calculations performed has shown that the settlements and slopes of the slotted foundations with lateral widening ribs are essentially affected

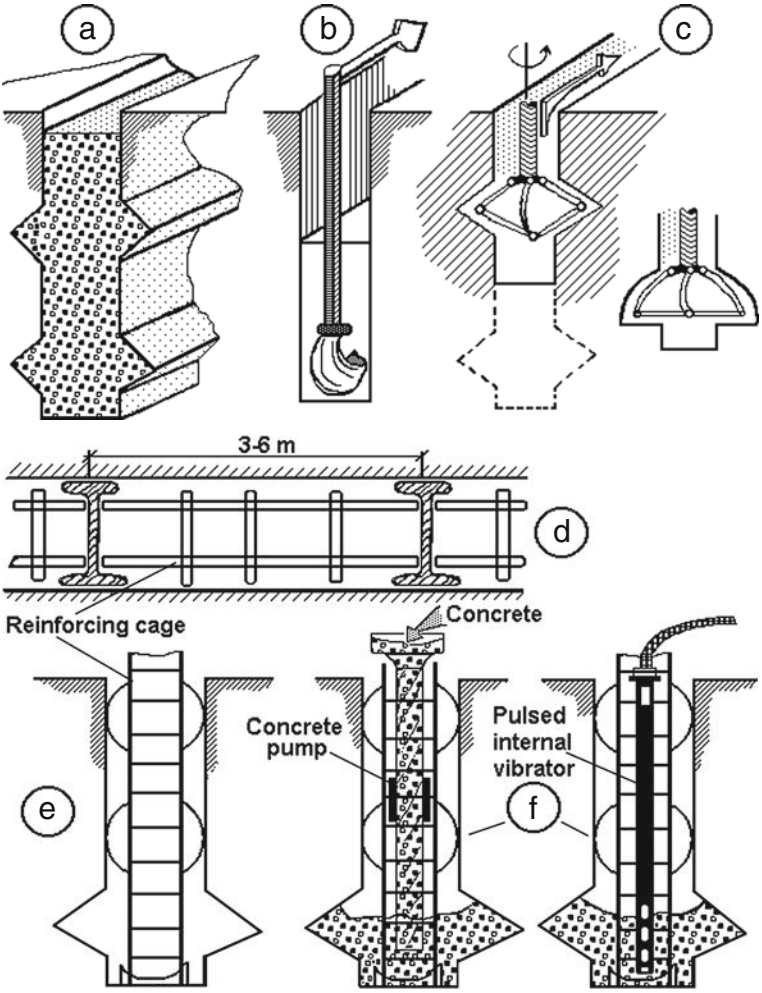

Fig. 5.55 Technological scheme of production of a slotted foundation with support widenings: (**a**) ready slotted foundation with support widenings; (**b**) trench digging; (**c**) making a support widening; (**d**) reinforcement with reinforcement cages; (**e**) concreting

by such factors as the widening rib relative depth, cross-section shape and size. By variation of these factors the settlement-vs-load characteristic (the main calculated characteristic of a foundation) can be effectively controlled.

From the point of view of technology of production the slotted foundations with support widenings can be attributed to the fast type. When a working is made for a lateral widening of a foundation in a slot, a longitudinal cutting (Figs. 5.55b, c) is performed by a basic machine, equipped with a special widener of a pantograph or a tab type [47, 206]. As a result, a working with the required configuration of the support rib is formed in the trench for the foundation. The

construction of a rotor widener presumes the presence of hard cutting elements providing the efficient functioning of the widener in the soil mass with the account of the speed of its forward motion. At the slotted foundation depth above 3.5 m a second pass of the machine is possible in order to form the second widening rib (Fig. 5.55c). Additional operations for the slot grading practically do not increase the total labour consumption, do not make the cycle more complicated, do not slow down the general pace of work. After the excavation work for the trench digging and formation of a working for the support widening is finished, the foundation reinforcement is performed by means of volume block reinforcement cages (Fig. 5.55d). The reinforcement cages are joined into a single structure by vertical groove elements with an additional function of restriction of the slotted foundation length. Then the concreting stage follows (Fig. 5.55e) when the concrete mixture is conveyed and placed by a force concrete pump, providing the required concreting pace. The mixture distribution and compression is recommended to be performed using a deep vibrator with a pulse effect on the concrete mixture. This provides full air removal and formation of the concrete structure with high reliability and guaranteed absence of structural defects of the foundation structure.

References

1. Aleksandrov A V, Lashchenikov B Ya, Shaposhnikov N N et al. (1976) Computer-aided methods of calculation of rod systems, plates and shells. Stroyizdat, Moscow (in Russian)
2. Aleksandrovich V F, Fedorovskii V G (1982) Finite-element calculation of interaction of a deepened foundation with an elastoplastic base. In: Engineering properties of soil and calculation of the bearing capacity and settlements of foundations. Tr NIIOSP 78: 106–113 (in Russian)
3. Alekseyev A I, Nikiforov Yu N, Derevyanko V M (1985) Experimental studies of functioning of slotted foundations. In: Bases and foundations in the geological conditions of the Urals. PPI, Perm, pp. 31–35 (in Russian)
4. Alekseyev V M, Lipson G A, Mitrenko Yu A (1980) Study of the bearing capacity of pyramidal piles on a vertical load. In: Soil mechanics, bases and foundations. Voronezh State University, Voronezh, pp. 72–81 (in Russian)
5. Alekseyev V M, Lipson G A, Mitrenko Yu A (1984) Studies of bearing capacity of pyramidal piles under an inclined force. In: Studies of rational structures of foundations. Voronezh State University, Voronezh, pp. 17–24 (in Russian)
6. Amusin B Z, Fadeyev A B (1975) Finite-element method at the solution of problems of mining geomechanics. Nauka, Moscow (in Russian)
7. Bakenov Kh Z, Bizhanov K S, Repina P I (1984) On the calculation of settlements and bearing capacity of pyramidal piles using the finite-element method. In: Bases and foundations in weak and heaving soils. LISI, Leningrad, pp. 32–42 (in Russian)
8. Bakholdin B V, Kolesnikov L I, Shikalovich N S (1989) Effect of frost-heave forces of soils on the bearing capacity of pyramidal piles. Soil Mech Found Eng 26: 243–248
9. Baranov V S, Romanov D A, Romanov K D, Sidorchuk V F (1973) Investigation of the pressure distribution in the soil around piles with spherical enlarged bases. Soil Mech Found Eng 10: 96–99
10. Bartolomei A A (1994). Modern state and problems of pile foundation engineering. In: Proc 4th Int Conf Pile Foundation Engineering Problems. Pt 1. Improvement of methods of calculation and technology of pile foundations. PGTU, Perm, pp. 38–43 (in Russian)

11. Bartolomei A A, Chikishev V M, Yushkov B S, Malyugin V P (1994) Experimental and theoretical studies of interaction of foundations of piles with blades with the soil base. In: Bases and foundations at the geological conditions of the Urals. PPI, Perm, pp. 3–13 (in Russian)
12. Bartolomei A A, Lavrentyev V A (1988) Pile foundations of increased bearing capacity. In: Bases and foundations in geological conditions of the Urals. PPI, Perm, pp. 8–13 (in Russian)
13. Bartolomei A A, Pilyagin A V (1988) Stress-strain state of the beds of pyramidal pile foundations. Soil Mech Found Eng 25: 136–140
14. Bartolomei A A, Ponomaryov A B, Yushkov B S (1994) Foundations of hollow conical piles. In: Bases and foundations in geological conditions of the Urals. PPI, Perm, pp. 13–17 (in Russian)
15. Bartolomei A A, Yushkov B S, Ponomaryov A B (1990) Experimental studies of the stress-atrained state of the active zone of a hollow conical pile. In: Bases and foundations in geological conditions of the Urals. PPI, Perm, pp. 60–66 (in Russian)
16. Bekbasarov I I, Shilibekov S K, Kushekbayev B Z (1989) On the effect of some geometrical parameters of foundations in tamped pits on their resistivity to static vertical load. In: Bases and foundations in geological conditions of the Urals. PPI, Perm, pp. 88–93 (in Russian)
17. Budanov V G (1975) Functioning of a base at cross-beam fixation of horizontally loaded power line support pillars. Energet Stroit (issue 7): 52–54 (in Russian)
18. Bugrov A K, Golubev A I (1993) Anisotropic soils and bases of buildings. Nedra, St. Petersburg (in Russian)
19. Bukharin Ye M, Gabliya Yu A, Levin L E (1971) Design of foundations for power line supports. Energiya, Moscow (in Russian)
20. Bykov V I (1975) Experimental investigations of performance of horizontally loaded pile foundations. Soil Mech Found Eng 12: 102–104
21. Bykov V I (1995) Foundations for individual residential buildings. Soil Mech Found Eng 32: 66–68
22. Chikishev V M, Bay V F, Dolgov V N, Shmidt V G (1994) Studies of functioning of foundations of piles with enhanced bearing capacity in clay soils. In: Bases and foundations at the geological conditions of the Urals. PPI, Perm, pp. 18–26 (in Russian)
23. Chikishev V M, Bay V F, Malyshkin A P (1990) Experimental studies of the stress-strained state of soils in the base of group of piles with self-unfolding blades. In: Bases and foundations at the geological conditions of the Urals. PPI, Perm, pp. 53–60 (in Russian)
24. Collins W D (1962) Some axially symmetric stress distributions in elastic solids containing penny-shaped cracks. I. Cracks in an infinite solid and a thick plate. Proc Roy Soc Ser A 203: 359–386
25. Costet J, Sanglerat D (1975) Cours practique de mechanique des sols. Bordas, Paris
26. Dalmatov B I (1981) Mechanics of soils, foundations and bases. Stroyizdat, Moscow (in Russian)
27. De Buhan P, Siad L (1989) Influence of a soil-strip interface failure condition on the yield-strength of reinforced earth. Computers Geotech 7: 3–18
28. Dembicki E, Sieradzki M (1988) Analysis of the behaviour of piles in high compressible soil subjected to torsion. In: Baltic Conf Soil Mech Found Eng. vol. 2: Construction on heats and deformation of structures on highly compressible soils. Tallinn, pp. 160–163
29. Derevyanko V M (1990) Experimental studies of the slotted foundation + soil system. In: Bases and foundations in the geological conditions of the Urals. PPI, Perm, pp. 100–104 (in Russian)
30. Drucker D C, Prager W (1952) Soil mechanics and plastic analysis or limit design. Quart Appl Math 10:157–165
31. Druzhinin G A, Komzina A A (1988) Rational construction of shallow foundations for rural buildings on a natural base. Kuibyshev State University, Kuibyshev (in Russian)

32. Dubov K A (1992) Calculation of piles with cross-shaped cross-section with diagonal reinforcement for raftless pile foundations of large-panel residential buildings. In: Increase of efficiency of application of equipment and improvement of technology of engineering. VPI, Vladimir, pp. 54–58 (in Russian)
33. Egorov K E (1948) Deformation of the base of a round rigid foundation under an eccentric load. In: Bases and foundations. Issues of soil mechanics. Tr NIIOSP 11:119–138 (in Russian)
34. Egorov K E (1958) On the issue of the base calculation under a foundation with a ring-shaped footing. In: Bases and foundations. Soil mechanics. Tr NIIOSP 34:34–57 (in Russian)
35. Fadeev A B (1987) Finite-element method in geomechanics. Nedra, Moscow (in Russian)
36. Fadeev A B, Bakenov Kh Z, Repina P I (1988) Finite-element calculation of settlements for round punches and single piles with the account of strength-related and rheological properties of soils. LISI, Leningrad (in Russian)
37. Fadeev A B, Bakenov Kh Z, Repina P I et al. (1987) Geomekhanika CREEP-3 software for finite-element calculation of stress-strained state of round foundations with the account of deformational, strength-related and rheological properties of medium. Gos FAP SSSR No. 50870000956, Moscow (in Russian)
38. Fadeev A B, Matveyenko G A (1983) Semianalytical finite-element method for prediction of stress-strained state of bases for axisymmetrical foundations. In: Nonlinear soil mechanics: Proc 6th Rus Conf St Petersburg, vol. 1, pp. 146–149 (in Russian)
39. Fadeev A B, Matveyenko G A (1988) Semianalytical finite-element method for solving spatial problems of foundation engineering in elastic and elastoplastic formulation. Izv Vuzov Stroit (issue 12): 113–116 (in Russian)
40. Fadeev A B, Matveyenko G A (1990) Semianalytical finite-element method for solving spatial problems of geomechanics. In: Studies and developments on computer-aided design of foundations and bases. NPI, Novocherkassk, pp. 28–35 (in Russian)
41. Fadeev A B, Preger A L (1984) Solution of the combined axisymmetric problem of the theory of elasticity and plasticity by the finite-element method. Soil Mech Found Eng 21: 181–184
42. Fadeev A B, Repina P I, Abdyldayev E K (1982) Finite-element method for solving geotechnical problems and Geomekhanika software. LISI, Leningrad (in Russian)
43. Fedorovskii V G (1973) Algorithm of calculation of settlements of deep supports with the account of gliding. In: Engineering constructions and theory of structures: Bases, foundations and soil mechanics. Vysheyshaya Shkola, Minsk (issue 2): 123–128 (in Russian)
44. Fedorovskii V G (1975) Settlements of piles in homogeneous and multilayer bases. In: Proc 1st Baltic Conf Mech Soil Found Eng, Gdansk, pp. 50–59 (in Russian)
45. Fedorovskii V G (1985) Modern methods of description of mechanical properties of soils. VNIIS, Moscow (in Russian)
46. Fedorovskii V G, Kurillo S V, Kulakov N A (1988) Computing the lateral load on piles and pile groups from the model of a linearly deformable half space. Soil Mech Found Eng 25: 166–172
47. Filakhtov A L, Lubenets G K, Pisanko N V et al. (1981) Experience of construction using the "wall in ground" method. Budivelnyk, Kyiv (in Russian)
48. Gabibov F G (1995) Technology of production of a bored pile with a cross-section in the shape of an equilateral triangle, In: Proc 2nd Ukr Sci Eng Conf Soil Mech Found Eng. Pt 2. Efficient foundations produced with soil excavation, Poltava, pp. 114–117 (in Russian)
49. Gersevanov N M (1948) Experience of application of theory of elasticity to the determination of admissible loads on the soil based on experimental data. In: Selected works, vol. 1. Pile bases and calculation of foundations. Stroyvoyenmorizdat, Leningrad, pp. 236–260 (in Russian)
50. Glotov N M, Luga A A, Silin K S et al. (1975) Pile foundation. Transport, Moscow (in Russian)

51. Glushkov G I (1977) Calculation of structures, deepened into soil. Stroyizdat, Moscow (in Russian)
52. Glushkov V Ye, Mamayev N G, Kislitsyn S A (1994) Elastoplastic calculation of piramidal pile bases under inclined and off-centre loads, In: Proc Int Conf Pile Found Eng Problems. Pt 1. Improvement of methods of calculation and technology of pile foundation production. PGTU, Perm, pp. 86–88 (in Russian)
53. Golubkov V N, Morgulis N L, Nikitin V F (1977) Tapered-pile foundations with intermediate cushion. Soil Mech Found Eng 14: 331–334
54. Gorbunov-Posadov M I, Malikova T A, Solomin V I (1984) Calculation of structures on an elastic base. Stroyizdat, Moscow (in Russian)
55. Gorbunov-Posadov M I, Sivtsova Ye P (1966) Check of a pile for sliding. In: Bases and foundations. Tr NIIOSP 56: 36–41 (in Russian)
56. Gorodetskiy A S, Zavoritskiy V I., Lantukh-Lyashchenko A I, Rasskazov A O (1989) Automation of calculations of transport buildings. Transport, Moscow (in Russian)
57. Gotman A L (1987) Analysis of tapered piles under combined action of vertical, horizontal, and flexural loads. Soil Mech Found Eng 24: 7–12
58. Gotman A L (1996) On the calculation of variable cross-section piles on the horizontal load with the account of nonlinearity of deformation of soil and the pile material. In: Proc 5th Intern Conf Pile Found Eng Problems. RNKMGF, Moscow, vol. 1, pp. 41–46 (in Russian)
59. Grigoryan A A (1984) Pile foundations of buildings and structures on subsiding soils. Stroyizdat, Moscow (in Russian)
60. Grilitskii D V, Kizyma Ya M (1967) Concomitant torsion of a rod and half-space. Intern Appl Mech 3(issue 2): 54–59
61. Gwizdala K (1996) Analiza osiodan pali przy wykorzystaniu funkcji transformacyjnych. Zeszyty Naukowe Politechniki Gdanskiej. Nr. 532. Budownictwo Wodne, vol. XLI.
62. Hunter S C, Gamblen D (1975) The theory of a rigid circular disc ground anchor buried in an elastic soil either with adhesion or without adhesion. J Mech Phys Solids 22: 371–399
63. Ikonin S V (1988) Application of an elastic half-space model for the calculation of short bored piles under a horizontal loading. In: Voronezh State University, Voronezh, pp. 103–107 (in Russian)
64. Ikonin S V (1992) Contact interaction of a deepened punch with a base at arbitrary static loading. In: Calculation and design of bases and foundations at complicated geotechnical conditions, VISI, Voronezh, pp. 82–86 (in Russian)
65. Ilyichev V A, Mongolov Yu V, Shayevich V M (1983) Pile foundations in seismic areas. Stroyizdat, Moscow (in Russian)
66. Ilyin V P, Karpov V V, Maslennikov A M (1990) Numerical methods of solving problems of engineering mechanics. Handbook. Vysheyshya shkola, Minsk (in Russian)
67. Instructions on design of foundations for machines subject to dynamic loads (1982) Gersevanov NIIOSP, Stroyizdat, Moscow (in Russian)
68. Instructions on design of pile foundations (1980) Stroyizdat, Moscow (in Russian)
69. Instructions on design of pyramidal pile foundations (1983) Glavn Upr Project Organiz, Moscow (in Russian)
70. Ivanov P L (1991) Soils and bases of hydrotechnical structures. Vysshaya shkola, Moscow (in Russian)
71. Kananyan A S, Kurnosov A I, Gorelov A V (1977) Designing the foundation bed of free-standing reinforced-concrete standards from deformations. Soil Mech Found Eng 14: 23–27
72. Kananyan A S, Nikitenko M I (1973) Experimental studies of functioning of bases of horizontally loaded rigid pillars. In: Engineering structures and theory of buildings: Bases, foundations, and soil mechanics. Vysheyshaya shkola, Minsk 2: 185–194 (in Russian)
73. Kandaurov I I (1988) Mechanics of grain media and its application in engineering. Stroyizdat, Leningrad (in Russian)
74. Kanwal R P, Sharma D L (1976) Singularity methods for elasto-statics. J Elasticity 6: 405–418

75. Karasev O V, Talanov G P, Benda S F (1977) Investigation of the work of single situ-cast piles under different load combinations. Soil Mech Found Eng 14: 173–177
76. Karasudhi P, Rajapakse R K N D, Hwang B Y (1984) Torsion of a long cylindrical elastic bar partially embedded in a layered elastic half space. Intern J Solids Struct 20: 1–11
77. Keer L M (1975) Mixed boundary value problems for a penny-shaped cut. J Elasticity 5: 89–98.
78. Khazin V I (1984) Foundation structures for rural buildings on short pyramidal piles. Budivelnyk, Kyiv (in Russian)
79. Khazin V I (1990) Study of functioning of new compaction piles for rural buildings. In: Bases and foundations at geological conditions of the Urals. PPI, Perm, pp. 23–24 (in Russian)
80. Khazin V I, Khazin S V (1995) Study of functioning of anchor piles for pulling load. In: Proc 2nd Ukr Sci Conf Soil Mech Effect Eng. Pt 1. Effective foundations erected without soil excavation. PTU, Poltava, pp. 56–59 (in Russian)
81. Kholmyanskii M L (1991) Consideration of the effect of embedment depth and lateral backfilling of machine foundations on the dynamic properties of their beds. Soil Mech Found Eng 28: 223–228
82. Kholmyanskii M L (1993) Effect of the complex shape of the underground part on the dynamical properties of deepened foundations for machines. Izv Vuzov Stroit (issue 2): 101–104 (in Russian)
83. Khozhmetov G Kh, Shakasymov Sh (1986) Interaction of complex foundations with bases. Izv AN UzSSR Ser Tekhn (issue 2): 44–46 (in Russian)
84. Kirilin V M (1975) Calculation of piles for horizontal and momental loads using the possible displacement method. Izv AN KazSSR Ser Fiz-Mat (issue 3): 53–58 (in Russian)
85. Kirillov V M (1983) Plastic flow of soils. Izv Vuzov Stroit Arkhit (issue 5): 20–25 (in Russian)
86. Kirillov V M (1986) Nonlinear pile settlement. Izv Vuzov Stroit Arkhit (issue 6): 26–31 (in Russian)
87. Kirillov V S (1980) Bases and foundations. Transport, Moscow (in Russian)
88. Kiselev V A (1976) Engineering mechanics. Stroyizdat, Moscow (in Russian)
89. Klein G K (1977) Engineering mechanics of granular bodies. Stroyizdat, Moscow (in Russian)
90. Klein G K, Cherkasov I I (1985) Foundations of urban transport structures. Stroyizdat, Moscow (in Russian)
91. Klimanov V I, Litvinenko A G, Kavayeva V P (1988) Conical shell foundations. Stroyizdat, Moscow (in Russian)
92. Kofman M M, Gumerov A G, Bikbayev A Z, Molodtsov G I (1993) Erection of tubular piles in frozen soils using explosion energy. In: Functioning of oil industry equipment and pipelines. Institute of Problems of Power Resources for Transport, Ufa, pp. 100–108 (in Russian)
93. Kogan B M, Zinchenko V D (1960) Stressed state of a nonhomogeneous layer, resting on an elastic half-space. Izv Vuzov Stroit Arkhit (issue 3): 8–18 (in Russian)
94. Komzina A A (1984) Foundations of agricultural buildings. Kuibyshev State University, Kuibyshev (in Russian)
95. Konovalov P A (1988) Soil bases and foundations of buildings under reconstruction. Stroyizdat, Moscow (in Russian)
96. Korzh I V, Buslov A S (1972) Experience of application of short bored piles. Transport Stroit (issue 9): 49 (in Russian)
97. Kosorukov I I (ed) (1974) Pile works. Vysshaya Shkola, Moscow (in Russian)
98. Kosterin E V (1978) Bases and foundations. Vysshaya Shkola, Moscow (in Russian)
99. Kravtsov V N (1990) Experimental studies of driven pyramidal piles with T-shaped section. In: Bases and foundations in the geological conditions of the Urals. PPI, Perm, pp. 14–16 (in Russian)

100. Kryukov K P, Kurnosov A I, Novgorodtsev B P (1975) Construction and design of metal and ferroconcrete power line supports. Energiya, Leningrad (in Russian)
101. Kushner S G (1990) Calculation of settlements of bases under buildings and structures. Budivelnyk, Kyiv (in Russian)
102. Lapshin F K (1979) Calculation of piles according to limiting conditions. Saratov State University, Saratov (in Russian)
103. Lazarev G B (1977) Use of pyramidal piles for greenhouse foundations. Soil Mech Found Eng 14: 20–22
104. Ledenev V V (1973) Study of interaction of a pier foundation, fixed in the soil, with the base under an off-centre load. Ph D thesis, Novocherkassk (in Russian)
105. Ledenev V V (1978) Experience of implementation of bored pile foundations at the construction of buildings with a spacer-type scheme. In: Mechanics of soils, bases and foundations. Voronezh State University, Voronezh, pp. 103–109 (in Russian)
106. Ledenev V V, Shelyapin R S (1973) Approximate determination of the settlement of a rigid rectangular deep foundation by their corner point method. Soil Mech Found Eng 10: 22–24
107. Levachev S N, Fedorovskiy V G, Kurillo S V, Kolesnikov Yu M (2002) Piles in hydrotechnical engineering. Balkema, Rotterdam
108. Levenstam V V (1973) Study of interaction of short pile foundations with soil under a horizontal load. Ph D thesis, Rostov-na-Donu (in Russian)
109. Likhovtsev V M (1976) Displacement and contact pressures for a rigid sunken plate. Soil Mech Found Eng 13: 414–419
110. Likhovtsev V M (1978) Deformation of an elastic half-space with a cylindrical cutout. In: Bases, foundations and underground structures. Tr NIIOSP 69: 73–78 (in Russian)
111. Luchkovskii I Ya, Lekumovich G S (1971) Analysis of laterally loaded piles in cohesive soils. Soil Mech Found Eng 8: 184–187
112. Luco J E (1976) Torsion of a rigid cylinder embedded in an elastic half space. Trans ASME J Appl Mech 43: 419–423
113. Malatsidze E G, Slyusarenko S A (1977) Design of foundations of short piles operating at horizontal loads. Bases and foundations. Budivelnyk, Kyiv 10: 69–72 (in Russian)
114. Mal'tsev A T, Sazhin V S (1980) Behavior of short piles in collapsible soils under the action of inclined forces. Soil Mech Found Eng 17: 235–239
115. Manual for the design of bases for buildings and structures (for the Construction Rules and Regulations 2.02.01-83) (1986) Gersevanov NIIOSP, Stroyizdat, Moscow (in Russian)
116. Milligan G W E, Houlsby G T, Onisi Yu et al. (1991) Software for soil mechanics and foundation engineering. Likhovtsev V M (ed). Stroyizdat, Moscow (in Russian)
117. Mironov V S (1955) Practical method for calculation of piles for the action of horizontal loads. Izv Vuzov Stroit Arkhit (issue 5): 24–32 (in Russian)
118. Mironov V S, Krovyakov V N (1978) Testing of batter piles under the combined effect of vertical and horizontal loads. Soil Mech Found Eng 15: 299–303
119. Mironov V S, Krovyakov V N (1980) Experimental studies of resistance of vertical and inclined piles to the action of inclined loads. Izv Vuzov Stroit Arkhit (issue 8): 123–126 (in Russian)
120. Molenkamp F (1981) Elasto-plastic double hardening model MONOT. LGM ReportCO-218595. Geotechnics, Delft
121. Mura T (1982) Micromechanics of defects in solids. Nijhoff, the Hague/Boston
122. Mura T (1988) Inclusion problems. Appl Mech Rev 41: 15–20
123. Murzenko Yu N (1989) Computer-aided calculation of bases fir buildings and structures at the elastoplastic stage of functioning. Stroyizdat, Leningrad (in Russian)
124. Nikolaevsky V N, Kuznetsov A S, Bellendir E N (1991) Mathematical dilatancy theory and conditions at strong discontinuities. Intern J Eng Sci 29: 1375–1389.
125. Oding B S (1968) Investigation of the stressed state and deformations of soil at the transfer of load by means of a pile. Izv Vuzov Stroit Arkhit (issue 10): 38–42 (in Russian)

126. Oding B S (1984) On the interaction of a conical pile with soil. In: Investigation of rational foundation structures. Voronezh State University, Voronezh, pp. 67–74 (in Russian)
127. Oding B S, Shelyapin R S (1964) Application of Mindlin's solution for the determination of stress around piles. In: Theory of buildings and structures, No. 10(issue 1): 134–153 (in Russian)
128. Ofrikhter V G (1996) Numerical modelling of interaction of pile foundations with the surrounding soil. In: Proc 5th Inter Conf Problems Pile Found Eng, RNKMGF, Moscow, vol. 1, pp. 124–126 (in Russian)
129. Ogranovich A B (1989) Calculation of a rigid pyramidal pile for a horizontal load in an elastic half-space. Stroit Mekh Raschet Sooruzh (issue 4): 7–9 (in Russian)
130. Ogranovich A B (1990) Calculation of settlement for a variable cross-section pile. Izv Vuzov Stroit Arkhit (issue 12): 97–100 (in Russian)
131. Ogranovich A B (1991) Consideration of soil discontinuities in the analysis of tapered piles under horizontal loading. Soil Mech Found Eng 28: 40–43
132. Ogranovich A B (1992) Calculation of a deepened beam on an elastic base (spatial problem). Izv Vuzov Stroit (issue 9–10): 25–28 (in Russian)
133. Ogranovich A B (1992) Numerical method of calculation of settlement and slope of a rigid foundation with a rectangular bottom, deepened into an elastic half-space. Izv Vuzov Stroit (issue 1): 114–117 (in Russian)
134. Ogranovich A B (1992) Settlement of a round rigid foundation, deepened into an elastic half-space. Izv Vuzov Stroit (issue 11–12): 29–33 (in Russian)
135. Pak R Y S, Gobert A T (1989) Computational aspects in a mathematical analysis of an inclusion problem. Proc Can Congr Appl Mech 2: 542–543
136. Pavlov V V (1992) Slotted foundation of buildings. Stroyizdat, Krasnoyarsk (in Russian)
137. Pavlov V V, Katsov K P, Smorodinov M I (1992) Slit foundations of industrial and civic buildings in the middle Urals. Soil Mech Found Eng 29: 140–143
138. Perley Ye M (1969) Tubular ferroconcrete piles for industrial and civil engineering. Stroyizdat, Leningrad (in Russian)
139. Petrenko G M, Orobchenko P A, Tsymbal S I (1972) Data for the calculation of piles from the base deformations. In: Osnovaniya i fundamenty. Budivelnyk, Kyiv (issue 5): 78–85 (in Russian)
140. Petrenko G M, Vasilenko A Yu (1972) On the methods of determination of stress in the base of a hanging pile. In: Bases and foundations. Budivelnyk, Kyiv (issue 5): pp. 20–26 (in Russian)
141. Pilyagin A V (1992) Nonlinear methods deformation-based of calculation of bases of foundations of various type. In: Efficiency of foundation design solutions, Mariy Polytechnical Institute, Yoshkar-Ola, pp. 94–99 (in Russian)
142. Pilyagin A V, Kazantsev S V, Kazantseva N N (1985) Elastoplastic calculation of a soil base at the conditions of a spatial stress-strained state. Mariy Polytechnical Institute, Yoshkar-Ola, VNIIIS No. 5713 (in Russian)
143. PLAXIS – Finite Element Code for Soil and Rock Analyses. Ver. 7. General Information and Tutorial Manual (1998) Balkema, Rotterdam
144. Ponomarev A B (1988) Study of bearing capacity of hollow conical piles. In: Bases and foundations in the geological conditions of the Urals. PPI, Perm, pp. 29–33 (in Russian)
145. Popovich A P, Koldyrev V I (1991) Spatial foundations of structural type. In: Spatial constructions in Krasnoyarsk region. KISI, Krasnoyarsk, pp. 107–116 (in Russian)
146. Poulos H G (1971) The behaviour of laterally loaded piles: I. Single piles. J Soil Mech Founds Divn ASCE 97: 711–731
147. Poulos H G (1971) The behaviour of laterally loaded piles: II. Pile groups. J Soil Mech Founds Divn ASCE 97: 733–751
148. Poulos H G (1975) Torsional response of piles. J Geotech Eng ASCE 101: 1014–1035
149. Poulos H G, Davis E H (1980) Pile foundation analysis and design. Wiley, New York

150. Poulos H G, Davis E N (1968) The settlement behaviour of single axially-loaded incompressible piles and piers. Geotechnique 18: 351–371.
151. Rabotnikov A, Zats S (1970) Experience of application of short bored piles. Promysh Stroit Inzh Sooruzh (issue 6): 6–7 (in Russian)
152. Rajapakse R K N D (1988) The interaction between a circular elastic plate and a transversely isotropic elastic halfspace. Intern J Num Anal Method Geomech 12: 419–436.
153. Rajapakse R K N D, Selvadurai A P S (1985) Torsional stiffness of non-uniform and hollow rigid piers embedded in isotropic elastic media. Intern J Num Anal Method Geomech 9: 1213–1229.
154. Rajapakse R K N D, Selvadurai A P S (1989) Torsion of foundations embedded in a non-homogeneous soil with a weathered crust. Geotechnique 39: 485–496
155. Rajapakse R K N D, Selvadurai A P S (1991) Response of circular footings and anchor plates in non-homogeneous elastic soils. Intern J Num Anal Method Geomech 15: 457–470
156. Randolph M F (1981) Piles subjected to torsion. J Geotech Eng ASCE 107: 1095–1111.
157. Rausch E (1959) Maschinenfundamente und Andere Dynamisch Beanspruchte Baukonstruktionen. VDI-Verlag, Düsseldorf
158. Recommendations on design and construction of slotted foundations (1982) Gersevanov NIIOSP, Moscow (in Russian)
159. Recommendations on design and construction of slotted foundations in the conditions of the Central Urals (1990) UPI, Sverdlovsk (in Russian)
160. Recommendations on the calculation of bases under foundations with an inclined bottom (1983) Gersevanov NIIOSP, Moscow (in Russian)
161. Recommendations on the calculation of nonlinear settlements of deep supports using a computer (1974) Gersevanov NIIOSP, Moscow (in Russian)
162. Recommendations on the rational usage of piles of various type in engineering (1982) Gersevanov NIIOSP, Moscow (in Russian)
163. Redkov V I (1982) Calculation of the settlement of a round rigid punch, deepende into an elastic half-space. In: Bases and foundations. PPI, Perm, pp. 44–51 (in Russian)
164. Reisner E, Sagoci H (1944) Forced torsional oscillation of an elastic half-space. J Appl Phys 15: 652–662.
165. Rower R K, Booker J R (1979) A method of analysis of horizontally embedded anchors in an elastic soil. Intern J Num Anal Method Geomech 3: 187–203.
166. Rybalko Yu Ya (1968) Foundations of short bored post piles. Promysh Stroit (issue 6): 46 (in Russian)
167. Ryzhenko A P (1973) Work of a pile raft of bored piles for the action of horizontal forces. Transport Stroit (issue 4): 43–44 (in Russian)
168. Sakharov A S, Boyko I P, Kozak A L (1983) Summary of the Rosinka software. Osnovaniya, Fundamenty Mekh Gruntov (issue 5): 7 (in Russian)
169. Saprykina N M (1977) Application of short bored piles in rural engineering. Promysh Stroit (issue 9): 25 (in Russian)
170. Savchenko F M, Oding B S (1988) Economically efficient foundations under strutted structures of agricultural buildings. In: Pile foundation studies. Voronezh State University, Voronezh, pp. 162–167 (in Russian)
171. Savinov O A (1979) Modern design of foundations under machines and their calculation. Stroyizdat, Leningrad (in Russian)
172. Sazhin V S, Shishkin V A, Zhanalinov B N (1991) Design and technology of erection of foundations on heaving soils. Gylym, Almaty (in Russian)
173. Schofield A, Wroth P (1968) Critical state soil mechanics. McGraw-Hill, London.
174. Segerlind L J (1976) Applied finite element analysis. John Wiley & Sons, New York
175. Selvadurai A P S (1976) The load-deflexion characteristics of a deep rigid anchor in an elastic medium. Geotechnique 26: 603–612
176. Selvadurai A P S (1979) An energy estimate of the flexural behaviour of a deep rigid anchor embedded in an isotropic elastic medium. Intern J Num Anal Method Geomech 3: 285–292.

177. Selvadurai A P S (1979) On the displacement of a penny-shaped rigid inclusion embedded in a transversely isotropic elastic medium. Solid Mech Arch 4: 163–172.
178. Selvadurai A P S (1980) The eccentric loading of a rigid circular foundation embedded in an isotropic elastic medium. Intern J Num Anal Method Geomech 4: 121–129
179. Selvadurai A P S (1984) Elastostatic bounds for the stiffness of an elliptical disk inclusion embedded at a transversely isotropic bi-material elastic interface. J Appl Math Phys (ZAMP) 35: 64–77.
180. Selvadurai A P S (1984) Torsional stiffness of rigid piers embedded in isotropic elastic soils. Laterally loaded deep foundations: analysis and performance. ASTM STP 835: 49–55
181. Selvadurai A P S (1989) The influence of a boundary fracture on the elastic stiffness of a deeply embedded anchor plate. Intern J Num Anal Method Geomech 13: 159–170.
182. Selvadurai A P S (1993) The axial loading of a rigid circular anchor plate embedded in an elastic half-space. Intern J Num Anal Method Geomech 17: 343–353.
183. Selvadurai A P S (1994) A unilateral contact problem for a rigid disk inclusion embedded between two dissimilar elastic half-spaces. Q J Mech Appl Math 47: 493–510.
184. Selvadurai A P S, Au M C (1986) Generalized displacements of a rigid elliptical anchor embedded at a bi-material geological interface. Intern J Num Anal Method Geomech 10: 633–652
185. Selvadurai A P S, Bauer G E, Nicholas T J (1980) Screw plate testing of a soft clay. Can Geotechn J 17: 465–472
186. Selvadurai A P S, Nicholas T J (1979) A theoretical assessment of the screw plate test. In: Wittke W (ed) Proc 3rd Intern Conf Numerical Methods Geomech 3: 1245–1252
187. Selvadurai A P S, Rajapakse R K N D (1987) Variational scheme for analysis of torsion of embedded nonuniform elastic bars. J Eng Mech ASCE 113: 1534–1550.
188. Selvadurai A P S, Singh B M (1986) The axial displacement of a disc inclusion embedded in a penny-shaped crack. J Appl Math Phys (ZAMP) 37: 64–77
189. Selvadurai A P S, Singh B M, Au M C (1990) The in-plane loading of a rigid disk inclusion embedded in an elastic halfspace. Trans ASME J Appl Mech 58: 362–369
190. Shadunts E G (1973) Calculation of one-row pile foundations with a pile raft, resting on the soil. Izv Vuzov Stroit Arkhit (issue 9): 22–27 (in Russian)
191. Shadunts K Sh, Podetlkov V V (1990) Arch foundations and their calculation with the account of sliding on the base. In: Studies and developments on computer-aided design of foundation and bases. NPI, Novocherkassk, pp. 87–95 (in Russian)
192. Shapiro D M (1985) Practical method of analysis of bases and earth structures in nonlinear formulation. Soil Mech Found Eng 22: 182–187
193. Shapiro D M (1993) Mathematical modelling of limiting states of bored piles. In: Nonlinear soil mechanics. Proc 4th Russ Conf St Petersburg 1: 140–145 (in Russian)
194. Shapiro D M, Poltorak G V (1989) Program for elastoplastic numerical calculation of soil structures and structures, interacting with soil. Osnovaniya Fundamenty Mekh Gruntov (issue 5): 20 (in Russian)
195. Shapiro D M, Poltorak G V (1990) Implementation of nonlinear calculation method at the design of bases and soil structures. In: Nonlinear methods of calculation of bases and foundation. Mariy Polytechnical Institute, Yoshkar-Ola, pp. 24–27 (in Russian)
196. Shapiro D M, Zotsenko N L, Beda S V (1996) Elastoplastic calculation of bearing capacity of piles. Izv Vuzov Stroit Arkhit (issue 6): 34–39 (in Russian)
197. Shekhter O Ya (1956) On the calculation of a deepened rigid foundation. In: Mechanics of soils. Tr NIIOSP 30: 45–60 (in Russian)
198. Shelyapin R S (1965) Approximate determination of settlement of a rigid round deepened foundation. Izv Vuzov Stroit Arkhit (issue 6): 11–18 (in Russian)
199. Shvets N S, Sedin V L, Kirichek Yu A (1987) Structural methods of reduction of vibrations of foundations for machines with dynamical loads. Stroyizdat, Mocsow (in Russian)

200. Shvets N S, Zakhvatkin M P (1995) Study of functioning of piles of non-traditional shape at horizontal dynamic load. In: Proc 2nd Ukr Sci Conf Soil Mech Found Eng. Pt 1: Efficient foundations, erected without soil excavation. PTU, Poltava, pp. 69–71 (in Russian)
201. Shvets V B, Ginzburg L L, Goldshtein V M et al. (1987) Handbook on mechanics and dynamics of soils. Budivelnyk, Kyiv (in Russian)
202. Silin K S, Glotov N M, Zavriev K S (1981) Design of deep foundations. Transport, Moscow (in Russian)
203. Simvulidi I A (1978) Calculation of engineering structures on an elastic base. Vysshaya Shkola, Moscow (in Russian)
204. Sivtsova Ye P (1963) Calculation of settlement of a single pile with the account of the tip functioning. Tr NIIOSP 53: 47–66 (in Russian)
205. Smorodinov M I (1983) Anchors in engineering. Stroyizdat, Moscow (in Russian)
206. Smorodinov M I, Fedorov B S (1986) Construction of structures and foundations using a "wall in the soil" method. Stroyizdat, Moscow (in Russian)
207. SNIP (Construction Rules and Regulations) 2.02.01-83. Bases for buildings and structures (1985) Stroyizdat, Moscow (in Russian)
208. SNIP (Construction Rules and Regulations) 2.02.03-85. Pile foundations (1986) Stroyizdat, Moscow (in Russian)
209. Snitko N K, Snitko A N (1967) Calculation of rigid and flexible supports embedded in the ground under the simultaneous action of horizontal and vertical forces. Soil Mech Found Eng 4: 153–156
210. Solovyov Yu I, Vlasov Yu V (1974) Investigations and engineering calculation method of short piles in subsidence soil on the action of horizontal loads. In: Engineering and geological conditions and specific features of foundation engineering in Siberia. Proc NIIZHTA, Novosibirsk 152: 108–119 (in Russian)
211. Sorochan E A (1986) Foundations of industrial buildings. Stroyizdat, Moscow (in Russian)
212. Sorochan E A, Gruodis R Yu (1983) Performance of cast-in-place concrete foundations in interaction with the soil. Soil Mech Found Eng 20: 204–208
213. Sorochan E A, Li E A (1993) Investigation of the operation of pyramidal piles in swelling soils. Soil Mech Found Eng 30: 42–46
214. Sorochan E A, Piven V G, Rybnikov A M (1991) Monolithic foundations with an effective lateral surface. Soil Mech Found Eng 28: 99–102
215. Sorochan E A, Trofimenkov Yu G (ed) (1985) Bases, foundations and underground structures: Designer's handbook. Stroyizdat, Moscow (in Russian)
216. Sotnikov S N (1992) On the evaluation of reliability of results of calculation of final settlement of bases under buildings and structures. In: Erection and reconstruction of foundations on weak soils. SPBISI, St. Peterburg, pp. 5–13 (in Russian)
217. Ten I A (1964) Effect of friction forces at the calculation of foundations with the account of fixation. Transport Stroit (issue 10): 39–41 (in Russian)
218. Tetior A N, Felkin V I, Surguchev V G (1981) Design of foundations. Budivelnyk, Kyiv (in Russian)
219. Timoshenko S P, Goodier J N (1970) Theory of elasticity, 3rd edn. McGraw-Hill, New York
220. Tishin V G (1985) Bases and foundations of objects of oil and gas industry. Stroyizdat, Moscow (in Russian)
221. Trofimenkov Yu G, Vorobkov L N (1981) Field methods for the studies of constructive properties of soils. Stroyizdat, Moscow (in Russian)
222. Tsiprianovich I V (1971) On the calculation of piles with widenings for horizontal load from the base deformations. In: Bases and foundations. Budivelnyk. Kyiv 4: 122–127 (in Russian)
223. Ukhov S B (1973) Calculation of structures and bases using the finite-element method. MISI, Moscow (in Russian)
224. Ukhov S B, Semenov V V, Znamenskii V V et al. (1994) Soil mechanics, bases and foundations. Association of Engineering Institutions, Moscow (in Russian)

225. Ulitskiy V M, Shashkin A G (1999) Supervision of urban reconstruction (investigation, calculations, works implementation, monitoring). ASV, Moscow (in Russian)
226. Urban I V (1939) Calculation of thin walls with the account of elastic properties of the soil and the wall. In: Issues of Engineering Mechanics. MIIT Works 55: 43–69 (in Russian)
227. Vershinin V P, Kovalev I P, Chelnokov Ye L (1978) Bored pile foundations with support widenings. Stroyizdat, Leningrad (in Russian)
228. Veryuzhskiy Yu V (1978) Numerical methods of potential in some problems of applied mechanics. Vyshcha Shkola, Kyiv (in Russian)
229. Vyalov S S (1978) Rheological principles of soil mechanics. Vysshaya shkola, Moscow (in Russian)
230. Wet J (1966) Application of energy hypothesis in soil mechanics. In: Soil mechanics and foundation engineering. Proc 5th Intern Conf Stroyizdat, Moscow, pp. 105–114 (in Russian)
231. Williams I, Hiecks M A (1992) Finite-Elemente-Prognose für ein schrag belastetes Fundament. Geotechnik 15: 66–72.
232. Wilson E L (1965) Calculation of strength of axially symmetrical bodies. Raket Tekh Kosmonavt (issue 12): 124–131 (in Russian)
233. Winnicki L A, Zienkiewicz O C (1979) Plastic (or visco-plastic) behaviour of axisymmetric bodies subjected to nonsymmetric loading – semi-analytical finite element solution. Intern J Num Method Eng 14: 1399–1412
234. Yagudin A M, Druzhinin G A (1968) Foundations for buildings of driven piles with a radial widened footing. Promyshlennoye Stroitelstvo (issue 11): 19–22 (in Russian)
235. Yarutin V M (1974) Flow-line construction of cast-in-place pile foundations of farm buildings. Soil Mech Found Eng 11: 375–380
236. Zabylin M I, Linovskii S V, Nuzhdin L V (1991) Design of pile foundations under machines. NISI, Novosibirsk (in Russian)
237. Zakhvatkin M P, Shvets N S (1989) Studies of functioning of piles of various shape under dynamic loads. In: Foundations under machines with dynamic loads. Proc Intern Symp Stroyizdat, Leningrad, pp. 195–198 (in Russian)
238. Zaretskii Yu K, Karabaev M I (1985) Limit-state design of cast-in-place piles. Soil Mech Found Eng 22: 169–175
239. Zaretskii Yu K, Karabaev M I (1987) Analysis of settlements of bored-cast-in-place piles in collapsible soils. Soil Mech Found Eng 24: 13–19
240. Zaretskii Yu K, Lombardo V N (1983) Statics and dynamics of earth-fill dams. Energoatomizdat, Moscow (in Russian)
241. Zaretskii Yu K, Orekhov V V, Karabayev M I (1984) Application of the finite-element method to the calculation of bored pile foundations. In: Modern computer-based methods of calculation of hydropower and nuclear power plants. Tr Gidroproekta im S Zhuka 100: 3–10 (in Russian)
242. Zavriev K S (1976) Approximate method of designing piles for horizontal loading and determining their flexibility. Soil Mech Found Eng 13: 152–156
243. Zavriev K S, Kryukov Ye P, Shpiro G S (1960) Study of the bearing capacity of foundations under contact line suports. Tr VNIITS. Transzheldorizdat, Moscow, 39: 1–216 (in Russian)
244. Zavriev K S, Shpiro G S (1970) Calculation of foundations under deep bridge piers. Transport, Moscow (in Russian)
245. Zhemochkin B N (1948) Calculation of the elastic fixation of a rod (rod bending in an elastic half-space). Stroyizdat, Moscow (in Russian)
246. Zhemochkin B N, Sinitsyn A P (1962) Practical methods of calculation for beams and plates on an elastic base without Winkler hypothesis. Gosstroyizdat, Moscow (in Russian)
247. Zhukov N V, Dondysh A M, Pogosyan Z G et al. (1972) Short piles in rural engineering. ONTI CNIIEPSelstroy, Moscow (in Russian)
248. Zienkiewicz O C (1971) The finite element method in engineering science. McGraw-Hill, London

249. Ziyazov Ya Sh (1977) On the calculation of pyramidal piles in a nonhomogeneous base under a vertical and a horizontal load. In: Foundation engineering issues. Niipromstroy, Ufa 21: 40–45 (in Russian)
250. Zotsenko N L (1988) On the calculation of pyramidal piles under a combined action of vertical and horizontal loads. In: Pile foundation studies, Voronezh State University, Voronezh, pp. 94–102 (in Russian)
251. Zureick A H (1988) Transversely isotropic elastic medium with a rigid spheroidal inclusion under an axial pull. Trans ASME J Appl Mech 55: 495–497

Conclusions

In modern geotechnical engineering, field and laboratory experiments have become complicated, durable and expensive, and the simplified formulae of soil mechanics, based on analytical solutions of separate problems, no longer correspond to the increased requirements of design. In various fields of science and engineering computational experiments have been widely introduced, being a powerful tool for studies of engineering problems. Computational experiment plays an important role in soil mechanics and foundation engineering, hence once can claim a new field of knowledge, computational geotechnics, to have been formed. The aim of computational geotechnics is modelling of stress-strained states of soil bases and foundations by numerical solutions of equations of mathematical physics. For the design of engineering constructions, the computational experiment enables real situations to be predicted and practical economical effect to be achieved.

Boundary-element method, being developed in this study, due to its visual character and indifference to the object geometry, is undoubtedly an efficient numerical method for solving many spatial problems in geotechnical engineering.

Evident advantages of the boundary-element method are revealed first of all at the studies of stress-strained states in unlimited domains (half-space, constant- and variable-thickness layers, etc.) which serve as models for soil bases in geotechnical problems.

Using flat boundary elements of triangular or quadrangular shape, one can rather accurately reproduce the surface of contact with soil practically for all existing foundation structures. Besides, in comparison with other popular numerical methods (e.g., finite-difference or finite-element methods, requiring discretization of not only the boundaries, but also of the interior of the calculation domains), the base free surface does not need discretization into boundary elements and, consequently, the input data amount is considerably reduced and their preparation is much simplified.

The studies performed have shown that the universality of the boundary-element method can be compared with that of the finite-element method, which is generally considered to be the main method of structural analysis in various fields of science and engineering. Meanwhile, in spatial problems of a foundation structure contact with a linearly deformable soil base, application of the boundary-element method is more reasonable and more efficient for practical purposes since the boundary-element algorithms do not require large computation time and memory size.

S.M. Aleynikov, *Spatial Contact Problems in Geotechnics*, Foundations of Engineering Mechanics, DOI 10.1007/b11479_BM2,

Test and model calculations, performed using the *Rostwerk* software described here, have been compared for the problems having an analytical solution or for those which had been also solved by other approximate methods.

Extensive methodological calculations show a good convergence of the numerical results and high accuracy of the boundary-element method, sufficient for the practical purposes, even at piecewise constant approximation of the contact stress field. On the other hand, the obtained estimation of the boundary-element method calculation accuracy is of great importance for practical engineering, especially due to the necessity of setting the applicability limits for various empirical formulae, recommended in handbooks.

One should note that an important feature of the developed boundary-element algorithms is their applicability for a wide range of spatial contact models (influence functions) – both the existing ones and those to be developed. The results of calculations, using the available methods, enable the suitability of the influence functions to be estimated, their features to be revealed at the modelling of spatial contact interaction processes.

Due to their sufficient universality, the developed boundary-element method without any essential additional processing can be applied for the calculation of base deformations for practically all existing foundation structures, used in industrial, civil, and transport engineering, including non-traditional complex-shaped rigid foundation structures. This enables the foundation base calculations to be unified and development of special calculation methods for each foundation structure type and loading conditions to be avoided. From the boundary-element calculations the designer can see the whole pattern of the spatial stress-strained state of the soil base for foundations of various depth, subject to a spatial load of a general type. In comparison with the engineer-oriented methods and regulations being currently in use, the boundary-element calculation methods enable a discrepancy between the theoretical and experimental data to be considerably reduced; they lead to more economical design solutions enabling the pressure, transmitted to the soil, to be increased and the foundation size to be decreased. All this enables the methods developed to be recommended for application at the calculations of base deformations for both high-priority foundation structures and large-scale housing construction. A considerable increase of computer speed and memory parameters and application of an efficient numerical method are the reasons for an optimistic view in case a large amount of calculation work is to be carried out in order to determine stress-strained states in three-dimensional active areas of bases for complex-shaped foundation structures.

The presented analysis of numerous calculation examples shows rather convincingly wide opportunities being open while solving spatial contact problems by boundary-element method in engineering mechanics, soil mechanics, mathematical physics, etc. Simultaneously, the ideas and methods of numerical solution of integral equations of mechanics of deformable solids, presented in the book, set a number of problems which have not been fully solved yet and still require further studies. Note some of the promising trends that, in our opinion, need further theoretical development and implementation into practical engineering.

1. Further *development and analysis of contact models* of soil bases of anisotropic and nonhomogeneous half-space and layer type are required, what will enable, using the BEM, the effect of the soil base mechanical properties on the processes of spatial contact interaction to be studied.

2. Undoubtedly important is the *improvement of calculation schemes* for spatial contact deformation (account of the contact friction, effect of the soil intrinsic weight, presence of initial stresses, finite rigidity of foundation structures at their interaction with soils, etc.) in order to have a distinct idea about the limits of rational application of boundary-element methods in geotechnical engineering. It is especially helpful to determine the conditions, for which more complicated calculation schemes are required in order to take into account the essential features of contact deformation processes.

3. The progress in computer industry along with the application of the boundary-element method opens the possibility for a transition from simple calculation of deformation of bases of complex foundation structures to the search of *optimal solutions*, i.e. to the application of optimization methods in design process. Mathematical optimization methods are rather effectively used in various fields of science and engineering; however, their implementation for optimization of foundation structures has just begun. The reason for this is the fact that solution of the optimization problem for foundations of various depth is very cumbersome: even a single calculation of contact interaction characteristics is related to considerable computational expenses which are multiplied by any iterative process. In the present study, the search for optimal solutions was performed only for shallow foundation structures, resting on non-uniformly compressible bases. The calculation models and efficient boundary-element algorithms proposed here, will further become a reliable basis for the development of mathematical means for *computer-aided design* of foundation structures.

4. Application of the developed boundary-element methods seems promising for the solution of essentially spatial contact problems *of inelastic deformation* (with the account of elastoplastic properties, viscoplasticity, creep, etc.) which have been studied quite insufficiently yet. Elastoplastic solutions in the problems of engineering mechanics and mechanics of deformable solids can be at small increments implemented by iterative processes on the basis of a well-known method of "elastic solutions". Solutions of spatial dynamic problems, problems of viscoplasticity and creep can be obtained according to a stepwise procedure of integration over time. Some approaches to the solution of inelastic deformation problems by boundary-element method (as a rule, in a two-dimensional formulation or for finite-size bodies) have been already carried out in a number of publications. In future, while solving spatial contact problems, using the boundary-element method for rheologically complicated bases, one can expect application of a formalism with a fictitious matrix of "elastic equivalent", reducing the decisive equations in increments to the relations of linear theory of elasticity (in the general case, anisotropic and non-uniform).

5. In the future studies of the base+foundation+structure system, based on the proposed boundary-element methods, it is natural to perform the three-dimensional

analysis of *rigidity coefficients* for complex-shaped punches, deepened into the elastic base.

Elastic properties of soil bases are known to be quite effectively described by a rigidity coefficient matrix. This is a symmetrical, positively determined square matrix of the sixth order. Its elements are reactions due to unit progressive displacements or rotations of a rigid punch. Application of the rigidity coefficient matrix enables the number of degrees of freedom due to the elastic base reaction to be reduced to six and, consequently, essentially simplifies calculation of foundation structures from the base deformations. In the cases when undular processes in the soil can be neglected, application of the rigidity coefficients is possible not only for static, but also for dynamical problems. Application of rigidity coefficients of soil bases is efficient for static calculations as well as the calculations of vibration of machine foundations when the complex shape of their below-grade part should be taken into account. The problems of determination of the rigidity coefficients are rather important at the account of soil-mediated interaction of parts of foundations made by different techniques and at different depths (piles and a pile raft; foundations on natural bases, reinforced by piles; deepened foundations, reinforced by plates; slotted foundations, combined by a plate resting on the soil, etc.). Often the deepened part of foundations is intentionally made more complicated in order to reduce vibrations and to improve the contact with the soil.

In practical calculations, due to the absence of exact solutions for spatial contact problems of theory of elasticity for complex-shaped punches with different depth, rigidity coefficients are used only for foundations of simple shape resting on the elastic base surface or, with the account of depth, at the flat problem conditions.

In the framework of the developed boundary-element method the rigidity coefficients for complex-shaped punches, deepened into an elastic base, can be conveniently calculated, by setting unit loads and moments in the coordinate axes directions and subsequent inversion of the obtained matrix of displacements and rotations.

6. For specific types of foundations, the results of boundary-element calculations for the determination of settlement-vs-load dependences and characteristics of the stress-strained states in the active areas of the foundation structure bases should be accumulated and generalized. After a detailed experimental testing at various engineering-and-geological conditions, the reliable limits of applicability of the method can be determined, and the method can be recommended for *correction and improvement of design regulations*.

7. The developed methods of numerical modelling of spatial contact interaction are sufficiently *general*, applicable not only for calculation and design of foundation structures, but also in other areas where methods of engineering mechanics and mechanics of deformable solids are applied (strength calculations in machine-building, calculation and design of road coverage, studies of mechanical properties of materials by impression of indentors, mining, etc.). Therefore, it is important to continue further improvement of the known three-dimensional calculation schemes of the boundary-element method as well as development of new ones in order to extend their application area, based on (i) use of boundary elements of higher order,

(ii) efficient discretization of the boundary (contact) domains, (iii) elaboration of special methods of numerical and analytical integration of fundamental solutions, (iv) application of the boundary-element method in combination with other numerical methods of solution of problems of mathematical physics.

Appendix A
Fundamental Solutions of Spatial Theory of Elasticity for a Homogeneous Isotropic Half-Space

Equations (A.1–A.9) give an extended form of the Green's displacement tensor components $\left\| \Gamma_i^{(k)} \right\| = \{\mathrm{U}^{(k)}, \mathrm{V}^{(k)}, \mathrm{W}^{(k)}\}$ for a rectangular Cartesian coordinate system (Fig. A.1)

$$U^{(1)}(K,N) = \frac{1}{8\pi G(1-\nu)} \left\{ \frac{3-4\nu}{2} \left(\frac{1}{R_1} + \frac{1}{R_2} \right) + \frac{x_1^2}{2} \left(\frac{1}{R_1^3} + \frac{1}{R_2^3} \right) + z\zeta \frac{R_2^2 - 3x_1^2}{R_2^5} \right.$$
$$\left. -(1-2\nu) \left[2(1-\nu) z_2 \frac{R_2(R_2+z_2) - x_1^2 \left(2 + \frac{z_2}{R_2} \right)}{R_2^2 (R_2+z_2)^2} - (1-2\nu) \frac{R_2^2 - x_1^2}{R_2^3} \right] \right\}, \tag{A.1}$$

$$V^{(1)}(K,N) = -\frac{x_1 y_1}{8\pi G(1-\nu)} \left\{ -\frac{1}{2} \left(\frac{1}{R_1^3} + \frac{1}{R_2^3} \right) \right.$$
$$\left. +(1-2\nu) \left[\frac{1-2\nu}{R_2^3} - 2(1-\nu) z_2 \frac{2 + \frac{z_2}{R_2}}{R_2^2 (R_2+z_2)^2} \right] + 3z\zeta \frac{z_2}{R_2^5} \right\}, \tag{A.2}$$

$$W^{(1)}(K,N) = \frac{x_1}{8\pi G(1-\nu)} \left[\frac{1}{2} \left(\frac{z_1}{R_1^3} + \frac{z_2}{R_2^3} \right) + \frac{2(1-\nu)(1-2\nu)}{R_2(R_2+z_2)} \right.$$
$$\left. - \frac{2(1-\nu)\zeta - (1-2\nu)z}{R_2^3} - 3z\zeta \frac{z_2}{R_2^5} \right], \tag{A.3}$$

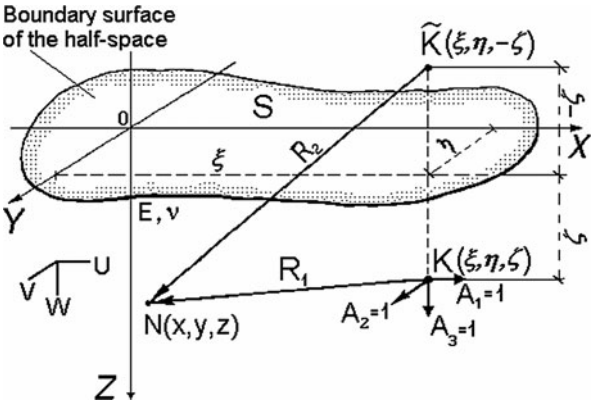

Fig. A.1 Geometric representations at the formulation of fundamental solutions of the spatial theory of elasticity for a homogeneous isotropic half-space

$$U^{(2)}(K,N) = -\frac{x_1 y_1}{8\pi G(1-\nu)}\left\{-\frac{1}{2}\left(\frac{1}{R_1^3}+\frac{1}{R_2^3}\right)\right.$$
$$\left.+(1-2\nu)\left[\frac{1-2\nu}{R_2^3}-2(1-\nu)z_2\frac{2+\frac{z_2}{R_2}}{R_2^2(R_2+z_2)^2}\right]+\frac{3z\zeta}{R_2^5}\right\}, \tag{A.4}$$

$$V^{(2)}(K,N) = \frac{1}{8\pi G(1-\nu)}\left\{\frac{3-4\nu}{2}\left(\frac{1}{R_1}+\frac{1}{R_2}\right)+\frac{y_1^2}{2}\left(\frac{1}{R_1^3}+\frac{1}{R_2^3}\right)+z\zeta\frac{R_2^2-3y_1^2}{R}-\right.$$
$$\left.-(1-2\nu)\left[2(1-\nu)z_2\frac{R_2(R_2+z_2)-y_1^2(2+\frac{z_2}{R_2})}{R_2^2(R_2+z_2)^2}-(1-2\nu)\frac{R_2^2-y_1^2}{R_2^3}\right]\right\} \tag{A.5}$$

$$W^{(2)}(K,N) = \frac{y_1}{8\pi G(1-\nu)}\left[\frac{1}{2}\left(\frac{z_1}{R_1^3}+\frac{z_2}{R_2^3}\right)+\frac{2(1-\nu)(1-2\nu)}{R_2(R_2+z_2)}\right.$$
$$\left.-\frac{2(1-\nu)\zeta-(1-2\nu)z}{R_2^3}-3z\zeta\frac{z_2}{R_2^5}\right], \tag{A.6}$$

$$U^{(3)}(K,N) = \frac{x_1}{8\pi G(1-\nu)}\left[\frac{z_1}{2R_1^3}+(3-4\nu)\frac{z_1}{2R_2^3}+3z\zeta\frac{z_2}{R_2^5}-\frac{2(1-\nu)(1-2\nu)}{R_2(R_2+z_2)}\right], \tag{A.7}$$

$$V^{(3)}(K,N) = \frac{y_1}{8\pi G(1-\nu)}\left[\frac{z_1}{2R_1^3} + (3-4\nu)\frac{z_1}{2R_2^3} + 3z\zeta\frac{z_2}{R_2^5} - \frac{2(1-\nu)(1-2\nu)}{R_2(R_2+z_2)}\right], \tag{A.8}$$

$$\begin{aligned} W^{(3)}(K,N) = \frac{1}{8\pi G(1-\nu)}\Bigg[&\frac{3-4\nu}{2R_1} + \frac{z_1^2}{2R_1^3} + \frac{1-\nu^2+(2-3\nu)^2}{2R_2} \\ &+(3-4\nu)\frac{z_2^2}{2R_2^3} - z\zeta\frac{R_2^2-3z_2^2}{R_2^5}\Bigg], \end{aligned} \tag{A.9}$$

where

$$x_1 = x-\xi, y_1 = y-\eta, z_1 = z-\zeta, z_2 = z\zeta,$$

$$R_1 = \sqrt{x_1^2+y_1^2+z_1^2}, \qquad R_2 = \sqrt{x_1^2+y_1^2+z_2^2},$$

ξ, η, ζ are the coordinates of the point K where a unit concentrated force is applied; x, y, z are the coordinates of the observation point N.

Using Eqs. (A.1–A.9) and Hooke's law relations one can obtain expressions for the stress $\sigma_{ij}^{(k)}$ (A.10–A.17), arising in an elastic half-space from the action of a unit concentrated force at the point $K(\xi, \eta, \zeta)$ in the direction of the X_k axis:

$$\begin{aligned} \tau_{xy}^{(1)} = \frac{1}{8\pi(1-\nu)}\Bigg\{&-(1-2\nu)\frac{y_1}{R_1^3} - 3\frac{y_1x_1^2}{R_1^5} - (8\nu^2-10\nu+3)\frac{y_1}{R_2^3} + \\ &+(8\nu^2-8\nu+1)\frac{3y_1x_1^2}{R_2^5} - \frac{6z\zeta y_1}{R_2^5} + \frac{30y_1z\zeta x_1^2}{R_2^7} + \\ &+4(1-2\nu)(1-\nu)\left[\frac{y_1z_2\left(2+\frac{z_2}{R_2}\right)\left(1-3\frac{x_1^2}{R_2^2}\right)}{R_2^2(R_2+z_2)^2} - \frac{2y_1z_2x_1^2}{R_2^3(R_2+z_2)^3}\right]\Bigg\}, \end{aligned} \tag{A.10}$$

$$\tau_{xy}^{(2)} = \frac{1}{8\pi(1-\nu)} \left\{ -(1-2\nu)\frac{x_1}{R_1^3} - 3\frac{y_1^2 x_1}{R_1^5} - (8\nu^2 - 10\nu + 3)\frac{x_1}{R_2^3} + \right.$$

$$+ (8\nu^2 - 8\nu + 1)\frac{3y_1^2 x_1}{R_2^5} - \frac{6z\zeta x_1}{R_2^5} + \frac{30x_1 z\zeta y_1^2}{R_2^7} +$$

$$\left. + 4(1-2\nu)(1-\nu)\left[\frac{x_1 z_2 \left(2 + \frac{z_2}{R_2}\right)\left(1 - 3\frac{y_1^2}{R_2^2}\right)}{R_2^2(R_2 + z_2)^2} - \frac{2x_1 z_2 y_1^2}{R_2^3(R_2 + z_2)^3} \right] \right\}, \tag{A.11}$$

$$\tau_{xy}^{(3)} = \frac{1}{8\pi(1-\nu)} \left[-\frac{3x_1 y_1 z_1}{R_1^5} - 3(3-4\nu)\frac{x_1 y_1 z_1}{R_2^5} - \frac{30x_1 y_1 z z_2 \zeta}{R_2^7} + \right.$$

$$\left. + 4(1-2\nu)(1-\nu)\frac{x_1 y_1 \left(2 + \frac{z_2}{R_2}\right)}{R_2^2(R_2 + z_2)^2} \right], \tag{A.12}$$

$$\tau_{yz}^{(1)} = \frac{1}{8\pi(1-\nu)} \left\{ -\frac{3x_1 y_1 z_1}{R_1^5} - [2(1-\nu)z_2 + (1-2\nu)z_1]\frac{3y_1 x_1}{R_2^5} + \frac{30x_1 y_1 z z_2 \zeta}{R_2^7} \right\}, \tag{A.13}$$

$$\tau_{yz}^{(2)} = \frac{1}{8\pi(1-\nu)} \left\{ -(1-2\nu)\frac{z_1}{R_1^3} - \frac{3z_1 y_1^2}{R_1^5} + (1-2\nu)\frac{z_1}{R_2^3} - \frac{6z z_2 \zeta}{R_2^5} + \frac{30z z_2 \zeta y_1^2}{R_2^7} - \right.$$

$$\left. - [(1-2\nu)z_1 + 2(1-\nu)z_2]\frac{3y_1^2}{R_2^5} \right\}, \tag{A.14}$$

$$\tau_{yz}^{(3)} = \frac{1}{8\pi(1-\nu)} \left\{ -(1-2\nu)\frac{y_1}{R_1^3} - \frac{3z_1^2 y_1}{R_1^5} + (1-2\nu)\frac{y_1}{R_2^3} - \frac{30y_1 z z_2^2 \zeta}{R_2^7} - \right.$$

$$\left. - \left[2(1-2\nu)z_2 z - z_2^2 + 2z^2\right]\frac{3y_1}{R_2^5} \right\}, \tag{A.15}$$

$$\tau_{zx}^{(1)} = \frac{1}{8\pi(1-\nu)} \left\{ -(1-2\nu)\frac{z_1}{R_1^3} - \frac{3z_1 x_1^2}{R_1^5} + (1-2\nu)\frac{z_1}{R_2^3} - \frac{6z z_2 \zeta}{R_2^5} + \frac{30z z_2 \zeta x_1^2}{R_2^7} - \right.$$

$$\left. - [(1-2\nu)z_1 + 2(1-\nu)z_2]\frac{3x_1^2}{R_2^5} \right\}, \tag{A.16}$$

$$\tau_{zx}^{(2)} = \frac{1}{8\pi(1-\nu)}\left\{-\frac{3x_1y_1z_1}{R_1^5} - [(1-2\nu)z_1 + 2(1-\nu)z_2]\frac{3x_1y_1}{R_2^5} + \frac{30x_1y_1zz_2\zeta}{R_2^7}\right\}, \tag{A.17}$$

$$\tau_{zx}^{(3)} = \frac{1}{8\pi(1-\nu)}\left\{-(1-2\nu)\frac{x_1}{R_1^3} - \frac{3x_1z_1^2}{R_1^5} + (1-2\nu)\frac{x_1}{R_2^3} - \frac{30x_1\zeta zz_2^2}{R_2^7} - \right.$$
$$\left. - \left[2(1-2\nu)z_2z - z_2^2 + 2z^2\right]\frac{3x_1}{R_2^5}\right\}, \tag{A.18}$$

$$\sigma_x^{(1)} = \frac{1}{4\pi(1-\nu)}\left\{-\frac{1}{2}(1-2\nu)\frac{x_1}{R_1^3} - \frac{3}{2}\frac{x_1^3}{R_1^5} - (8\nu^2 - 11\nu + 3.5)\frac{x_1}{R_2^3} + (4\nu^2 - \right.$$
$$- 4\nu + 0{,}5)\frac{3x_1^3}{R_2^5} - \frac{9z\zeta x_1}{R_2^5} + \nu\frac{6x_1\zeta z_2}{R_2^5} + \frac{15z\zeta x_1^3}{R_2^7} +$$
$$\left. + 2(1-2\nu)(1-\nu)\left[\frac{3z_2x_1\left(2+\frac{z_2}{R_2}\right)\left(1-\frac{x_1^2}{R_2^2}\right)}{R_2^2(R_2+z_2)^2} - \frac{2x_1^3z_2}{R_2^3(R_2+z_2)^3}\right]\right\}, \tag{A.19}$$

$$\sigma_x^{(2)} = \frac{1}{4\pi(1-\nu)}\left\{\frac{1}{2}(1-2\nu)\frac{y_1}{R_1^3} - \frac{3}{2}\frac{x_1^2y_1}{R_1^5} - \frac{1}{2}(1-2\nu)\frac{y_1}{R_2^3} + \right.$$
$$+ (12\nu^2 - 12\nu + 1.5)\frac{y_1x_1^2}{R_2^5} - \frac{3y_1z\zeta}{R_2^5} + \nu\frac{6y_1\zeta z_2}{R_2^5} + \frac{15y_1z\zeta x_1^2}{R_2^7} + \quad ,$$
$$\left. + 2(1-2\nu)(1-\nu)\left[\frac{y_1z_2\left(2+\frac{z_2}{R_2}\right)\left(1-3\frac{x_1^2}{R_2^2}\right)}{R_2^2(R_2+z_2)^2} - \frac{2y_1z_2x_1^2}{R_2^3(R_2+z_2)^3}\right]\right\} \tag{A.20}$$

$$\sigma_x^{(3)} = \frac{1}{4\pi(1-\nu)} \left\{ \frac{1}{2}(1-2\nu)\frac{z_1}{R_1^3} - \frac{3}{2}\frac{x_1^2 z_1}{R_1^5} - (1-2\nu)(1.5-2\nu)\frac{z_2}{R_2^3} - \right.$$
$$- 3(1-2\nu)\frac{\zeta}{R_2^3} - \frac{3}{2}(3-4\nu)\frac{z_1 x_1^2}{R_2^5} - \nu\frac{6\zeta z_2^2}{R_2^5} - \frac{15 z z_2 \zeta x_1^2}{R_2^7} + \frac{3 z z_2 \zeta}{R_2^5} -,$$
$$\left. -2(1-2\nu)(1-\nu)\left[\frac{1}{R_2(R_2+z_2)} - \frac{x_1^2\left(2+\frac{z_2}{R_2}\right)}{R_2^2(R_2+z_2)^2} \right] \right\} \tag{A.21}$$

$$\sigma_y^{(1)} = \frac{1}{4\pi(1-\nu)} \left\{ \frac{1}{2}(1-2\nu)\frac{x_1}{R_1^3} - \frac{3}{2}\frac{y_1^2 x_1}{R_1^5} - \frac{1}{2}(1-2\nu)\frac{x_1}{R_2^3} + \right.$$
$$+ (12\nu^2 - 12\nu + 1.5)\frac{x_1 y_1^2}{R_2^5} - \frac{3 x_1 z\zeta}{R_2^5} + \nu\frac{6 x_1 \zeta z_2}{R_2^5} + \frac{15 x_1 z \zeta y_1^2}{R_2^7} +$$
$$\left. +2(1-2\nu)(1-\nu)\left[\frac{x_1 z_2\left(2+\frac{z_2}{R_2}\right)\left(1-3\frac{y_1^2}{R_2^2}\right)}{R_2^2(R_2+z_2)^2} - \frac{2 x_1 z_2 y_1^2}{R_2^3(R_2+z_2)^3} \right] \right\}, \tag{A.22}$$

$$\sigma_y^{(2)} = \frac{1}{4\pi(1-\nu)} \left\{ -\frac{1}{2}(1-2\nu)\frac{y_1}{R_1^3} - \frac{3}{2}\frac{y_1^3}{R_1^5} - (8\nu^2 - 11\nu + 3{,}5)\frac{y_1}{R_2^3} + \right.$$
$$+ (12\nu^2 - 12\nu + 1.5)\frac{y_1^3}{R_2^5} - \frac{9 z\zeta y_1}{R_2^5} + \nu\frac{6 y_1 \zeta z_2}{R_2^5} + \frac{15 z\zeta y_1^3}{R_2^7} +$$
$$\left. + 2(1-2\nu)(1-\nu)\left[\frac{3 z_2 y_1\left(2+\frac{z_2}{R_2}\right)\left(1-\frac{y_1^2}{R_2^2}\right)}{R_2^2(R_2+z_2)^2} - \frac{2 y_1^3 z_2}{R_2^3(R_2+z_2)^3} \right] \right\}, \tag{A.23}$$

$$\sigma_y^{(3)} = \frac{1}{4\pi(1-\nu)}\left\{\frac{1}{2}(1-2\nu)\frac{z_1}{R_1^3} - \frac{3}{2}\frac{y_1^2 z_1}{R_1^5} - (1-2\nu)(1.5-2\nu)\frac{z_2}{R_2^3} - \right.$$
$$-3(1-2\nu)\frac{\zeta}{R_2^3} - \frac{3}{2}(3-4\nu)\frac{z_1 y_1^2}{R_2^5} - \nu\frac{6\zeta z_2^2}{R_2^5} - \frac{15 z_2 z \zeta y_1^2}{R_2^7} + \frac{3 z z_2 \zeta}{R_2^5} -$$
$$\left. -2(1-2\nu)(1-\nu)\left[\frac{1}{R_2(R_2+z_2)} - \frac{y_1^2\left(2+\frac{z_2}{R_2}\right)}{R_2^2(R_2+z_2)^2}\right]\right\}, \tag{A.24}$$

$$\sigma_z^{(1)} = \frac{1}{4\pi(1-\nu)}\left\{\frac{1}{2}(1-2\nu)\frac{x_1}{R_1^3} - \frac{3}{2}\frac{z_1^2 x_1}{R_1^5} - \frac{1}{2}(1-2\nu)\frac{x_1}{R_2^3} + \right.$$
$$\left. +[(\nu-0.5)z_1 z_2 - (1-\nu)z_2^2 + \zeta^2]\frac{3x_1}{R_2^5} + \frac{15 z_2^2 z \zeta x_1}{R_2^7}\right\}, \tag{A.25}$$

$$\sigma_z^{(2)} = \frac{1}{4\pi(1-\nu)}\left\{\frac{1}{2}(1-2\nu)\frac{y_1}{R_1^3} - \frac{3}{2}\frac{z_1^2 y_1}{R_1^5} - \frac{1}{2}(1-2\nu)\frac{y_1}{R_2^3} + \right.$$
$$\left. +[(\nu-0.5)z_1 z_2 - (1-\nu)z_2^2 + \zeta^2]\frac{3y_1}{R_2^5} + \frac{15 z_2^2 z \zeta y_1}{R_2^7}\right\}, \tag{A.26}$$

$$\sigma_z^{(3)} = \frac{1}{4\pi(1-\nu)}\left\{-\frac{1}{2}(1-2\nu)\frac{z_1}{R_1^3} - \frac{3}{2}\frac{z_1^3}{R_1^5} + \frac{1}{2}(1-2\nu)\frac{z_1}{R_2^3} + \right.$$
$$\left. +[(\nu-0.5)z_1 z_2 + (\nu-0.25)z_2^2 - \frac{3}{4}z_1^2]\frac{3z_2}{R_2^5} - \frac{15\zeta z z_2^3}{R_2^7}\right\}. \tag{A.27}$$

At the action of the concentrated force at the half-space surface, i.e. when $\zeta = 0$, $R_1 = R_2 = R$, Eqs. (A.10)–(A.27) lead to the Boussinesq and Cerruti solutions presented in the following combined form:

$$U^{(1)} = \frac{1}{4\pi G}\left\{\frac{1}{R} + \frac{x_1^2}{R^3} + (1-2\nu)\left[\frac{1}{R+z} - \frac{x_1^2}{R(R+z)^2}\right]\right\}, \tag{A.28}$$

$$V^{(1)} = \frac{1}{4\pi G}\left[\frac{x_1 y_1}{R^3} - (1-2\nu)\frac{x_1 y_1}{R(R+z)^2}\right], \tag{A.29}$$

$$W^{(1)} = \frac{1}{4\pi G}\left[\frac{x_1 z}{R^3} + (1-2\nu)\frac{x_1}{R(R+z)}\right], \tag{A.30}$$

$$U^{(2)} = \frac{1}{4\pi G}\left[\frac{x_1 y_1}{R^3} - (1-2\nu)\frac{x_1 y_1}{R(R+z)^2}\right], \tag{A.31}$$

$$V^{(2)} = \frac{1}{4\pi G}\left\{\frac{1}{R} + \frac{y_1^2}{R^3} + (1-2\nu)\left[\frac{1}{R+z} - \frac{y_1^2}{R(R+z)^2}\right]\right\}, \tag{A.32}$$

$$W^{(2)} = \frac{1}{4\pi G}\left[\frac{y_1 z}{R^3} + (1-2\nu)\frac{y_1}{R(R+z)}\right], \tag{A.33}$$

$$U^{(3)} = \frac{1}{4\pi G}\left[\frac{x_1 z}{R^3} - (1-2\nu)\frac{x_1}{R(R+z)}\right], \tag{A.34}$$

$$V^{(3)} = \frac{1}{4\pi G}\left[\frac{y_1 z}{R^3} - (1-2\nu)\frac{y_1}{R(R+z)}\right], \tag{A.35}$$

$$W^{(3)} = \frac{1}{4\pi G}\left[\frac{z^2}{R^3} + \frac{2(1-\nu)}{R}\right], \tag{A.36}$$

$$\tau_{xy}^{(1)} = \frac{y_1}{2\pi R^3}\left[-\frac{3x_1^2}{R^2} - \frac{(1-2\nu)}{(R+z)^2}\left(R^2 - \frac{2Rx_1^2}{R+z} - x_1^2\right)\right], \tag{A.37}$$

$$\tau_{xy}^{(2)} = \frac{x_1}{2\pi R^3}\left[-\frac{3y_1^2}{R^2} - \frac{(1-2\nu)}{(R+z)^2}\left(R^2 - \frac{2Ry_1^2}{R+z} - y_1^2\right)\right], \tag{A.38}$$

$$\tau_{xy}^{(3)} = -\frac{x_1 y_1}{2\pi R^3}\left[\frac{3z}{R^2} - (1-2\nu)\frac{2R+z}{(R+z)^2}\right], \tag{A.39}$$

$$\tau_{yz}^{(1)} = -\frac{3x_1 y_1 z}{2\pi R^5}, \tag{A.40}$$

$$\tau_{yz}^{(2)} = -\frac{3x_1 y_1 z}{2\pi R^5}, \tag{A.41}$$

$$\tau_{yz}^{(3)} = \frac{3y_1 z^2}{2\pi R^5}, \tag{A.42}$$

$$\tau_{zx}^{(1)} = -\frac{3x_1^2 z}{2\pi R^5}, \tag{A.43}$$

$$\tau_{zx}^{(2)} = -\frac{3y_1^2 z}{2\pi R^5}, \tag{A.44}$$

$$\tau_{zx}^{(3)} = \frac{3x_1 z^2}{2\pi R^5}, \tag{A.45}$$

$$\sigma_x^{(1)} = \frac{x_1}{2\pi R^3}\left[-\frac{3x_1^2}{R^2} + \frac{1-2\nu}{(R+z)^2}\left(R^2 - \frac{2Ry_1^2}{R+z} - y_1^2\right)\right], \tag{A.46}$$

$$\sigma_x^{(2)} = \frac{y_1}{2\pi R^3}\left[-\frac{3y_1^2}{R^2} - \frac{1-2\nu}{(R+z)^2}\left(R^2 - \frac{2Rx_1^2}{R+z} - x_1^2\right)\right], \tag{A.47}$$

$$\sigma_x^{(3)} = \frac{1}{2\pi R^3}\left\{-3\frac{x_1^2 z}{R^2} + (1-2\nu)\left[\frac{x_1^2(2R+z)}{(R+z)^2} - \frac{R^2 - Rz - z^2}{R+z}\right]\right\}, \tag{A.48}$$

$$\sigma_y^{(1)} = \frac{x_1}{2\pi R^3}\left[-\frac{3y_1^2}{R^2} + \frac{1-2\nu}{(R+z)^2}\left(3R^2 - \frac{2Rx_1^2}{R+z} - x_1^2\right)\right], \tag{A.49}$$

$$\sigma_y^{(2)} = \frac{y_1}{2\pi R^3}\left[-\frac{3x_1^2}{R^2} + \frac{1-2\nu}{(R+z)^2}\left(3R^2 - \frac{2Ry_1^2}{R+z} - y_1^2\right)\right], \tag{A.50}$$

$$\sigma_y^{(3)} = \frac{1}{2\pi R^3}\left\{-3\frac{y_1^2 z}{R^2} + (1-2\nu)\left[\frac{y_1^2(2R+z)}{(R+z)^2} - \frac{R^2 - Rz - z^2}{R+z}\right]\right\}, \tag{A.51}$$

$$\sigma_z^{(1)} = -\frac{3x_1 z^2}{2\pi R^5}, \tag{A.52}$$

$$\sigma_z^{(2)} = -\frac{3y_1 z^2}{2\pi R^5}, \tag{A.53}$$

$$\sigma_z^{(3)} = -\frac{3z^3}{2\pi R^5}, \tag{A.54}$$

$$\varepsilon_V^{(1)} = \frac{1-2\nu}{E}\theta^{(1)} = -\frac{(1-2\nu)(1+\nu)}{\pi E}\frac{x_1}{R^3}, \tag{A.55}$$

$$\varepsilon_V^{(2)} = \frac{1-2\nu}{E}\theta^{(2)} = -\frac{(1-2\nu)(1+\nu)}{\pi E}\frac{y_1}{R^3}, \tag{A.56}$$

$$\varepsilon_V^{(3)} = \frac{1-2\nu}{E}\theta^{(3)} = -\frac{(1-2\nu)(1+\nu)}{\pi E}\frac{z}{R^3}, \tag{A.57}$$

Equations (A.55)–(A.57) give the dilatation functions of the stressed state $\varepsilon_v^{(i)}$, $i = 1,2,3$.

Further simplification of Eqs. (A.28)–(A.54) corresponds to the case when the components of the displacement and stress tensors are determined only at the boundary plane of the half-space.

Taking into account that at $z = 0$

$$R = r = \sqrt{(x_1 - \xi)^2 + (x_2 - \eta)^2},$$

the combined fundamental Boussinesq–Cerruti solution is given in the simplest form

$$U^{(1)} = \frac{1}{2\pi G}\left[(1-\nu)\frac{1}{r} + \nu\frac{x_1^2}{r^3}\right], \tag{A.58}$$

$$V^{(1)} = \frac{\nu}{2\pi G}\frac{x_1 y_1}{r^3}, \tag{A.59}$$

$$W^{(1)} = \frac{1-2\nu}{4\pi G}\frac{x_1}{r^2}, \tag{A.60}$$

$$U^{(2)} = \frac{\nu}{2\pi G}\frac{x_1 y_1}{r^3}, \tag{A.61}$$

$$V^{(2)} = \frac{1}{2\pi G}\left[(1-\nu)\frac{1}{r} + \nu\frac{y_1^2}{r^3}\right], \tag{A.62}$$

$$W^{(2)} = \frac{1-2\nu}{4\pi G}\frac{y_1}{r^2}, \tag{A.63}$$

$$U^{(3)} = -\frac{1-2\nu}{4\pi G}\frac{x_1}{r^2}, \tag{A.64}$$

$$V^{(3)} = -\frac{1-2\nu}{4\pi G}\frac{y_1}{r^2}, \tag{A.65}$$

$$W^{(3)} = \frac{1-\nu}{2\pi G}\frac{1}{r}, \tag{A.66}$$

$$\tau_{xy}^{(1)} = \frac{-y_1}{2\pi r^3}\left[\frac{6\nu x_1^2}{r^2} + (1-2\nu)\right], \tag{A.67}$$

$$\tau_{xy}^{(2)} = \frac{-x_1}{2\pi r^3}\left[\frac{6\nu y_1^2}{r^2} + (1-2\nu)\right], \tag{A.68}$$

$$\tau_{xy}^{(3)} = (1-2\nu)\frac{x_1 y_1}{\pi r^5}, \tag{A.69}$$

$$\tau_{yz}^{(1)} = \tau_{yz}^{(2)} = \tau_{yz}^{(3)} = \tau_{zx}^{(1)} = \tau_{zx}^{(2)} = \tau_{zx}^{(3)} = 0, \tag{A.70}$$

$$\sigma_x^{(1)} = \frac{x_1}{\pi r^3}\left[-(1+\nu) + \frac{3\nu y_1^2}{r^2}\right], \tag{A.71}$$

$$\sigma_x^{(2)} = \frac{y_1}{\pi r^3}\left[-(1+\nu) + \frac{3\nu x_1^2}{r^2}\right], \tag{A.72}$$

$$\sigma_x^{(3)} = \frac{(1-2\nu)}{2\pi r^3}\left[\frac{x_1^2 - y_1^2}{r}\right], \tag{A.73}$$

$$\sigma_y^{(1)} = -\frac{3\nu x_1 y_1^2}{\pi r^5}, \tag{A.74}$$

$$\sigma_y^{(2)} = -\frac{3\nu x_1^2 y_1}{\pi r^5}, \tag{A.75}$$

$$\sigma_y^{(3)} = \frac{(1-2\nu)}{2\pi r^3}\left[\frac{y_1^2 - x_1^2}{r}\right], \tag{A.76}$$

$$\sigma_z^{(1)} = \sigma_z^{(2)} = \sigma_z^{(3)} = 0. \tag{A.77}$$

Appendix B
Numerical Schemes for Surface Integral Calculations

B.1 Parametric Representation of Surface Integrals

While calculating surface integrals of the form

$$\iint_{\Gamma} f(x,y,z)d\Gamma \tag{B.1}$$

we assume the surface Γ, restricted by a contour $\mathcal{L}$, to be given parametrically by equations

$$x = x(u,v)\ , \quad y = y(u,v)\ , \quad z = z(u,v) \tag{B.2}$$

where the parameters u and v vary within a domain ω, restricted by a piecewise-smooth contour l on the (u,v) plane (Fig. B.1). Let one-to-one correspondence be set between the points of the surface Γ and the domain ω, and the contour $\mathcal{L}$ be transformed into l. Consider a matrix

$$\mathbf{D} = \begin{Vmatrix} x'_u & y'_u & z'_u \\ x'_v & y'_v & z'_v \end{Vmatrix}$$

and denote its determinants as A, B, and C:

$$A = \begin{vmatrix} y'_u & z'_u \\ y'_v & z'_v \end{vmatrix}\ , \quad B = \begin{vmatrix} z'_u & x'_u \\ z'_v & x'_v \end{vmatrix}\ , \quad C = \begin{vmatrix} x'_u & y'_u \\ x'_v & y'_v \end{vmatrix}\ .$$

The surface area element in the parametric coordinates (B.2) is given by [20]

$$d\Gamma = \sqrt{A^2 + B^2 + C^2}du\ dv\ . \tag{B.3}$$

Then for any function $f(x,y,z)$ limited at the surface Γ the following formula is valid:

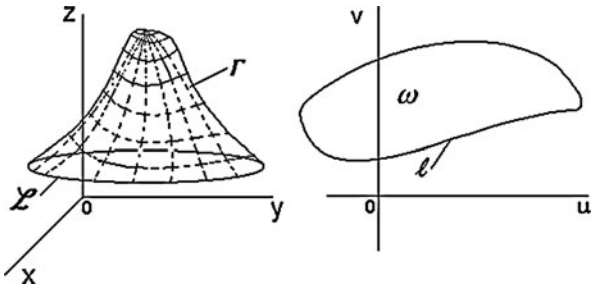

Fig. B.1 Surface parametrization

$$\iint_{\Gamma} f(x,y,z)d\Gamma = \iint_{\omega} f(x(u,v),y(u,v),z(u,v))\sqrt{A^2+B^2+C^2}dudv$$

Thus, in order to reduce the surface integral under consideration (B.1) to a double integral one should substitute coordinates x, y, z by the expressions using the u and v parameters while the surface area element $d\Gamma$ should be substituted by the expression in accordance with Eq. (B.3).

The contact surface of the 3-dimensional volumetric deepened punches can practically always be approximated with sufficient accuracy by a set of plane boundary elements (see B.4). Usually only elements of the two types – triangular and quadrangular – are used. For each element a local coordinate system is introduced, linked to the global system (surface parametrization). In the local coordinate system (within the parameter plane) the surface integrals under consideration are reduced to double integrals over the areas of simplex and standard square type.

Triangular boundary elements. A separate triangular element and its local coordinate system ξ_1, ξ_2 are shown in Fig. B.2. Global Cartesian coordinates of the triangular element points can be given by [11]

$$\begin{bmatrix} x \\ y \\ z \end{bmatrix} = \begin{bmatrix} x_1 & x_2 & x_3 \\ y_1 & y_2 & y_3 \\ z_1 & z_2 & z_3 \end{bmatrix} \begin{bmatrix} \xi_1 \\ \xi_2 \\ \xi_3 \end{bmatrix} \tag{B.4}$$

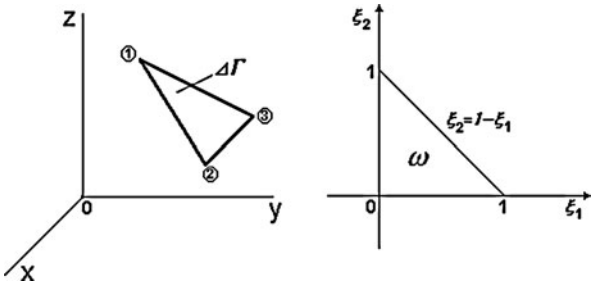

Fig. B.2 A flat triangular boundary element and its parametrization

where ξ_1, ξ_2, ξ_3 are*triangular coordinates*, related by a formula

$$\xi_1 + \xi_2 + \xi_3 = 1 \ .$$

Applied to a triangular integration area, the calculations result in

$$A = \begin{vmatrix} y'_{\xi_1} & z'_{\xi_1} \\ y'_{\xi_2} & z'_{\xi_2} \end{vmatrix} = \begin{vmatrix} (y_1 - y_3) & (z_1 - z_3) \\ (y_2 - y_3) & (z_2 - z_3) \end{vmatrix} ,$$

$$B = \begin{vmatrix} z'_{\xi_1} & x'_{\xi_1} \\ z'_{\xi_2} & x'_{\xi_2} \end{vmatrix} = \begin{vmatrix} (z_1 - z_3) & (x_1 - x_3) \\ (z_2 - z_3) & (x_2 - x_3) \end{vmatrix} ,$$

$$C = \begin{vmatrix} x'_{\xi_1} & y'_{\xi_1} \\ x'_{\xi_2} & y'_{\xi_2} \end{vmatrix} = \begin{vmatrix} (x_1 - x_3) & (y_1 - y_3) \\ (x_2 - x_3) & (y_2 - y_3) \end{vmatrix} ,$$

$$\sqrt{A^2 + B^2 + C^2} = 2S_\Delta$$

where S_Δ is the area of the triangular element.

For the calculation of a surface integral over a triangular boundary element the following calculation formula is obtained:

$$\begin{aligned} \iint\limits_\Gamma f(x,y,z)d\Gamma \ &= 2S_\Delta \iint\limits_\Delta f(x(\xi_1,\xi_2), y(\xi_1,\xi_2), z(\xi_1,\xi_2))d\xi_1,\xi_2 = \\ &= 2S_\Delta \int\limits_0^1 \int\limits_0^{1-\xi_1} \tilde{f}(\xi_1,\xi_2)d\xi_1 \ d\xi_2 \ . \end{aligned} \tag{B.5}$$

Quadrangular boundary elements. A separate quadrangular element and its local coordinate system ξ_1, ξ_2 are shown in Fig. B.3. Global Cartesian coordinates of the quadrangular element can be found from the following equations [11]:

$$\begin{cases} x = \varphi_1 x_1 + \varphi_2 x_2 + \varphi_3 x_3 + \varphi_4 x_4 \ , \\ y = \varphi_1 y_1 + \varphi_2 y_2 + \varphi_3 y_3 + \varphi_4 y_4 \ , \\ z = \varphi_1 z_1 + \varphi_2 z_2 + \varphi_3 z_3 + \varphi_4 z_4 \end{cases} \tag{B.6}$$

where $x_i, y_i, z_i, i = \overline{1,4}$ are the coordinates of the quadrangular cell vertices,

$$\begin{cases} \varphi_1 = \dfrac{1}{4}(1-\xi_1)\cdot(1-\xi_2) \ , & \varphi_2 = \dfrac{1}{4}(1+\xi_1)\cdot(1-\xi_2) \\ \varphi_3 = \dfrac{1}{4}(1+\xi_1)\cdot(1-\xi_2) \ , & \varphi_4 = \dfrac{1}{4}(1-\xi_1)\cdot(1+\xi_2) \ , \end{cases} \tag{B.7}$$

are interpolating functions; ξ_1, ξ_2 are point coordinates of a standard square $|\xi_1| \le 1 \ , \quad |\xi_2| \le 1 \ .$

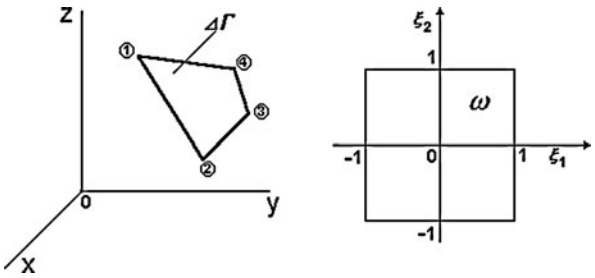

Fig. B.3 A flat quadrangular boundary element and its parametrization

Using Eqs. (B.7), we find $\partial\varphi_i/\partial\xi_j$, $i = \overline{1,4}$, $j = 1,2$, and then A, B, and Cvalues. For the calculation of surface integrals over a flat quadrangular boundary element the following calculation formula is obtained:

$$\iint_{\Gamma} f(x,y,z)d\Gamma = \int_{-1}^{1}\int_{-1}^{1} f(x(\xi_1,\xi_2), y(\xi_1,\xi_2), z(\xi_1,\xi_2))\sqrt{A^2+B^2+C^2}d\xi_1 d\xi_2 \tag{B.8}$$

where

$$A = \frac{1}{4}(a_1\varphi_1 + a_2\varphi_2 + a_3\varphi_3 + a_4\varphi_4$$

$$B = \frac{1}{4}(b_1\varphi_1 + b_2\varphi_2 + b_3\varphi_3 + b_4\varphi_4)\,,$$

$$C = \frac{1}{4}(c_1\varphi_1 + c_2\varphi_2 + c_3\varphi_3 + c_4\varphi_4)\,,$$

$$a_1 = \begin{vmatrix} y_{21} & z_{21} \\ y_{41} & z_{41} \end{vmatrix}, a_2 = \begin{vmatrix} y_{21} & z_{21} \\ y_{32} & z_{32} \end{vmatrix}, a_3 = \begin{vmatrix} y_{34} & z_{34} \\ y_{32} & z_{32} \end{vmatrix}, a_4 = \begin{vmatrix} y_{34} & z_{34} \\ y_{41} & z_{41} \end{vmatrix},$$

$$b_1 = \begin{vmatrix} x_{41} & z_{41} \\ x_{21} & z_{21} \end{vmatrix}, b_2 = \begin{vmatrix} x_{32} & z_{32} \\ x_{21} & z_{21} \end{vmatrix}, b_3 = \begin{vmatrix} x_{32} & z_{32} \\ x_{34} & z_{34} \end{vmatrix}, b_4 = \begin{vmatrix} x_{41} & z_{41} \\ x_{34} & z_{34} \end{vmatrix},$$

$$c_1 = \begin{vmatrix} x_{21} & y_{21} \\ x_{41} & z_{41} \end{vmatrix}, c_2 = \begin{vmatrix} x_{21} & y_{21} \\ x_{32} & z_{32} \end{vmatrix}, c_3 = \begin{vmatrix} x_{34} & y_{34} \\ x_{32} & z_{32} \end{vmatrix}, c_4 = \begin{vmatrix} x_{34} & y_{34} \\ x_{41} & z_{41} \end{vmatrix},$$

$$\begin{aligned} &x_{21} = x_2 - x_1, \quad y_{21} = y_2 - y_1, \quad z_{21} = z_2 - z_1, \\ &x_{32} = x_3 - x_2, \quad y_{32} = y_3 - y_2, \quad z_{32} = z_3 - z_2, \\ &x_{41} = x_4 - x_1, \quad y_{41} = y_4 - y_1, \quad z_{41} = z_4 - z_1, \\ &x_{34} = x_3 - x_4, \quad y_{34} = y_3 - y_4, \quad z_{34} = z_3 - z_4\,. \end{aligned}$$

B.2 Gauss Cubature Formulae for a Standard Simplex and a Standard Square

Surface integrals, contained in discretized integral equations, require different schemes of numerical integration, depending on where the application point of the concentrated force is located. When the point $K(\xi, \eta, \zeta)$ is outside the cell of the boundary element under consideration, the integrand function remains bounded (a regular integral) and, hence, can be integrated numerically by some cubature formulae of different orders. Since the calculation of such integrals requires the major part of the processing time, this procedure should be optimized. Such optimizing is achieved by setting a given maximal upper limit of uncertainty. This means that the order of the cubature formulae should flexibly vary depending on the distance between the boundary element and the $K(\xi, \eta, \zeta)$ point. Below the cubature formulae for a simplex and a standard square are given, constructed using the Gauss quadrature formula. Using the Gauss quadratures has an advantage over conventional methods (trapezoid rule, Simpson etc.): the given accuracy of the result can be achieved by using a twice smaller number of summands. This is related to the optimal choice of both weights and nodes at the approximation of an integral by a sum (see also B.4).

Numerical integration over *triangular* boundary elements is performed using the cubature formulae for a simplex $0 \le \xi_1 \le 1,\ \ 0 \le \xi_2 \le 1 - \xi_1$ (Fig. B.4a). Node coordinates and weights of the corresponding cubature formulae of the Gaussian type [13]

$$\int_0^1 \int_0^{1-\xi_1} \hat{f}(\xi_1,\xi_2,\xi_3)\, d\xi_1\, d\xi_2 = \sum_{i=1}^{n} w_i \cdot \hat{f}(\varsigma_1^i,\varsigma_2^i,\varsigma_3^i) \tag{B.9}$$

are listed in Table B.1. Contrary to the formulae given in the known books on numerical methods [8, 10, 12, 14, 16, 26, 31], this formula at high accuracy is completely symmetrical with respect to the triangle vertices. The symmetry means that if a

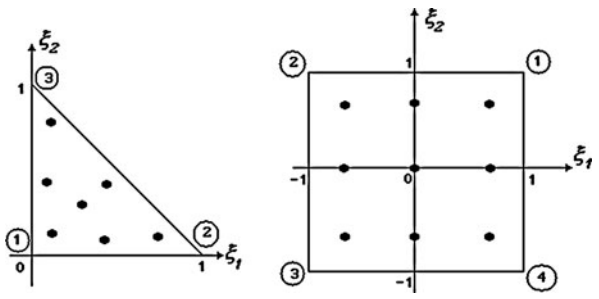

Fig. B.4 Location of the nodes of cubature formulae for a standard simplex (**a**) and a standard square (**b**)

Table B.1 Weights w_i and nodes ζ_i of cubature formulae for a simplex [13]

$2w_i$	ζ_1	ζ_2	ζ_2	Multiplicity
3-point formula (degree of accuracy 2)				
0.333333	0.666667	0.166667	0.166667	3
4-point formula (degree of accuracy 3)				
−0.562500	0.333333	0.333333	0.333333	1
0.520833	0.600000	0.200000	0.200000	3
6-point formula (degree of accuracy 4)				
0.109952	0.816847	0.091576	0.091576	3
0.223381	0.108103	0.445948	0.445948	3
7-point formula (degree of accuracy 5)				
0.225000	0.333333	0.333333	0.333333	1
0.125939	0.797426	0.101286	0.101286	3
0.132394	0.470142	0.470142	0.059716	3
12-point formula (degree of accuracy 6)				
0.050845	0.873821	0.063089	0.063089	3
0.116786	0.501427	0.249286	0.249286	3
0.082851	0.636502	0.310352	0.053145	6
13-point formula (degree of accuracy 7)				
−0.149570	0.333333	0.333333	0.333333	1
0.175615	0.479308	0.260346	0.260346	3
0.053347	0.869739	0.065130	0.065130	3
0.077114	0.638444	0.312865	0.486903	6

cubature node $(\zeta_1, \zeta_2, \zeta_3)$ occurs, all its permutations will also necessarily occur. If all ζ_i are different, then there are six such nodes in the cubature; if two values of ζ_i coincide, then there are three such nodes. In case of one term (linear interpolation) the central point (1/3, 1/3, 1/3) is used with the weight of 1/2. The nodes and weights of Eq. (B.9) are determined from the systems of strongly nonlinear equations. The requirement of symmetry of nodes with respect to the triangle vertices enables the number of the unknown values (and, hence, the number of equations) to be reduced to a minimum.

Numerical integration over quadrangular boundary elements is performed using the cubature formulae for a standard square (Fig. B.4b)

$$\int_{-1}^{1}\int_{-1}^{1} \hat{f}(\xi_1,\xi_2)\, d\xi_1\, d\xi_2 \approx \sum_{i=1}^{n}\sum_{j=1}^{m} w_i w_j \cdot \hat{f}(\varsigma_1^i,\varsigma_2^j)\,. \tag{B.10}$$

Such formulae are obtained by generalization (direct product) of one-dimensional Gaussian quadrature formulae over each variable

$$\int_{-1}^{1} \hat{f}(\xi)\, d\xi = \sum_{i=1}^{n} w_i \cdot \hat{f}(\varsigma_i) + \varepsilon_n\,, \quad \varepsilon_n = O\left(\frac{\partial^{2n} f}{\partial \varsigma^{2n}}\right)\,. \tag{B.11}$$

Table B.2 Nodes and weights of the Gauss cubature formula [10]

n	$\pm\zeta_i$	w_i
1	0.000000	2.000000
2	0.577350	1.000000
3	0.000000	0.555556
	0.774596	0.888889
4	0.339981	0.652145
	0.861136	0.347855
5	0.000000	0.568889
	0.538469	0.478629
	0.906179	0.236927
6	0.238619	0.467914
	0.661209	0.360762
	0.932469	0.171324
7	0.000000	0.417959
	0.405845	0.381830
	0.741531	0.279705
	0.949108	0.129485
8	0.183435	0.362684
	0.525532	0.313707
	0.796666	0.222381
	0.960289	0.101229

Here ε_n is the uncertainty of the quadrature formula of the n-th order. The weights w_i and nodes ζ_i of the Gaussian quadrature formulae for $n \leq 8$ are listed in Table B.2. For $n > 8$ the corresponding values can be found in a special literature (see, e.g. [1, 8, 10, 12, 14, 21, 22, 26, 31]).

B.3 Transformation of Coordinates, Reducing the Order of the Integrand Function Singularities

Integration over a triangular element, arbitrarily oriented in space, according to the cubature formula (B.9), is performed by transformation to a simplex using a local triangular coordinate system. In this case the presence of a singularity in one of the element nodes will by no means be taken into account. Evidently, direct usage of such cubature formulae is not applicable for the calculation of surface improper and singular integrals. In this case an additional subdivision of the boundary element (adaptive algorithm of integration [29]) or usage of cubature formulae of a special type [12] is required. The latter can be applied only for the integrals with weak singularities, their accuracy being not high enough.

Consider a coordinate transformation at which the order of the integral function singularity is reduced by a unit. Without narrowing the generality, one can assume that the point of application of the unit force $K(\xi, \eta, \zeta)$ is located in one of the triangle vertices. Such triangles represent the subdivision of the boundary element

into subelements for which the mass center of the boundary element is the common vertex $K(\xi, \eta, \zeta)$ (see Sect. B.3, Fig. 2.4).

According to [23, 29], the coordinates of the triangular element points are given by

$$\begin{bmatrix} x \\ y \\ z \end{bmatrix} = \begin{bmatrix} x_1 & x_2 & x_3 \\ y_1 & y_2 & y_3 \\ z_1 & z_2 & z_3 \end{bmatrix} \begin{bmatrix} 1-\sigma_1 \\ \sigma_1 \cdot (1-\sigma_2) \\ \sigma_1 \sigma_2 \end{bmatrix} . \tag{B.12}$$

Under such a transformation a unit square [0,1] x [0,1] in the (σ_1, σ_2) plane is transformed into a spatial triangular element (Fig. B.5a, b, c). Comparing Eqs. (B.4) and (B.12) one can see that the new local coordinates σ_1 and σ_2 are related to conventional *triangular* coordinates ξ_1, ξ_2, ξ_3 by equations

$$\xi_1 = 1 - \sigma_2 , \quad \xi_2 = \sigma_1 \cdot (1 - \sigma_2) , \xi_3 = \sigma_1 \cdot \sigma_2 . \tag{B.13}$$

It is easily seen that the condition $\xi_1 + \xi_2 + \xi_3 = 1$ holds identically. In order to find the differential surface area $d\Gamma = \sqrt{A^2 + B^2 + C^2} d\sigma_1 \, d\sigma_2$ in the new local coordinates (σ_1, σ_2) define

$$A = \begin{vmatrix} y'_{\sigma_1} & z'_{\sigma_1} \\ y'_{\sigma_2} & z'_{\sigma_2} \end{vmatrix} = \sigma_1 \begin{vmatrix} (y_1 - y_3) & (z_1 - z_3) \\ (y_2 - y_3) & (z_2 - z_3) \end{vmatrix} ,$$

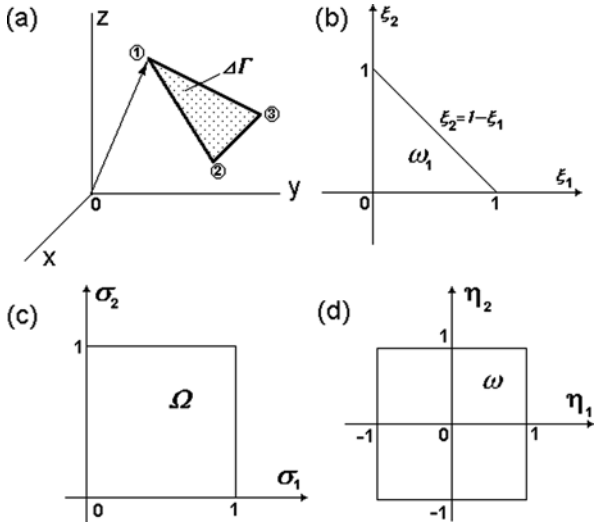

Fig. B.5 A flat triangular boundary element with an integrand function singularity in the first node (**a**) and consecutive transformations of the local coordinates to a standard square (**b–d**)

$$B = \begin{vmatrix} z'_{\sigma_1} & x'_{\sigma_1} \\ z'_{\sigma_2} & x'_{\sigma_2} \end{vmatrix} = \sigma_1 \begin{vmatrix} (z_1 - z_3) & (x_1 - x_3) \\ (z_2 - z_3) & (x_2 - x_3) \end{vmatrix},$$

$$C = \begin{vmatrix} x'_{\sigma_1} & y'_{\sigma_1} \\ x'_{\sigma_2} & y'_{\sigma_2} \end{vmatrix} = \sigma_1 \begin{vmatrix} (x_1 - x_3) & (y_1 - y_3) \\ (x_2 - x_3) & (y_2 - y_3) \end{vmatrix}$$

Now an equation for the calculation of a surface integral over a triangular element with a singularity of the integrand function in the first node is obtained:

$$\int_{-1}^{1}\int_{-1}^{1} f(x(\sigma_1,\sigma_2), y(\sigma_1,\sigma_2), z(\sigma_1,\sigma_2))\sqrt{A^2 + B^2 + C^2}d\sigma_1 d\sigma_2 = \\ = 2S_\Delta \int_0^1\int_0^1 \tilde{f}(\sigma_1,\sigma_2)\ \sigma_1\ d\sigma_1\ d\sigma_2\ . \tag{B.14}$$

Here, as above, S_Δ is the triangular boundary element area; $\tilde{f}(\sigma_1,\sigma_2) = f(x(\sigma_1,\sigma_2), y(\sigma_1,\sigma_2), z(\sigma_1,\sigma_2))$. Note that the fact conditions (B.13) being fulfilled and the form of Eq. (B.14) enabled the authors of [23] to call the variables (σ_1, σ_2) *triangular polar coordinates*.

All the quadrature and cubature formulae quoted in handbooks use nodes defined at the standard interval $[a, b] = [-1,1]$. Therefore, for the convenience of handbook data application we perform one more linear substitution of variables

$$\sigma_1 = \frac{1}{2}(1 + \eta_1)\ ,\sigma_2 = \frac{1}{2}(1 + \eta_2)\ .$$

Now in the new local variables (η_1,η_2), $\{\ |\eta_1| \le 1\ ,\quad |\eta_2| \le 1\ \}$ the integration will be performed for a standard square ω (Fig. B.5d) according to a formula

$$\iint_\Gamma f(x,y,z)d\Gamma = \frac{1}{4}S_\Delta \int_{-1}^{1}\int_{-1}^{1} \tilde{f}(\eta_1,\eta_2)(1 + \eta_1 d\eta_1 d\eta_2 \tag{B.15}$$

It follows from Eq. (B.15) that along the side $\eta_1 = -1$ of the square ω the integrand function equals to zero. According to the considered train of transformations, this side corresponds to the first node of the triangular element. Therefore, the either present singularity of the integrand function in one of the triangular element vertices can be eliminated, or its degree can be reduced by unit.

Thus, after the transformation

$$\begin{bmatrix} x \\ y \\ z \end{bmatrix} = \begin{bmatrix} x_1 & x_2 & x_3 \\ y_1 & y_2 & y_3 \\ z_1 & z_2 & z_3 \end{bmatrix} \begin{bmatrix} \frac{1}{2}\cdot(1 - \eta_1) \\ \frac{1}{4}(1 + \eta_1)\cdot(1 - \eta_2) \\ \frac{1}{4}(1 - \eta_2)^2 \end{bmatrix} \tag{B.16}$$

having been applied, numerical integration over triangular boundary elements with an integrand function singularity in one of the nodes can be carried out uniformly and efficiently on the base of cubature formulae for a standard square (B.10).

B.4 Highest Algebraic Order of Accuracy Cubature Formulae of Interpolation-Orthogonal Type Based on Chebyshev Polynomials

A formula is at present considered the best from the point of view of accuracy at a given number of points [12]. However, in case the Gaussian quadrature being used, a certain practical inconvenience is related to the need of the nodes and weights corresponding to a great number of integration point to be input in the computer memory by typing. Using of additional software capable of relatively fast calculations of quadrature nodes and weights for a given order of accuracy, seems a more rational way. We have elaborated such software based on the first-order Chebyshev polynomials, following [19, 24, 25, 30]. The developed algorithms and software on their base can be readily introduced into the existing boundary-element or finite-element software.

In the theory of quadrature formulae for a given n a problem is set for such a choice of nodes x_k and weights A_k $(k = 1, 2,...,n)$, at which Eq. (B.11) will be exact for all polynomials of the highest degree. Since each polynomial of the degree $N = 2n-1$ has also $2n$ parameters to be determined, once can choose the parameters x_k and A_k in such a way that the quadrature formulae will be exact. The quadratures possessing this property belong to the quadratures of the highest algebraic degree of accuracy [24, 27]. Besides, it is proven in [27] that there is no choice of nodes and weights at which a n-th order quadrature formula can possess the algebraic degree of accuracy higher than $N = 2n-1$. Therefore, in order to calculate surface (two-dimensional) improper and singular integrals it is natural to use the quadrature formulae with the highest algebraic degree of accuracy. If zeros of classical orthogonal polynomials [27] are used as nodes of the quadrature formulae given by Eq. (B.11), then the quadrature formulae of interpolation-orthogonal type with the highest degree of accuracy are obtained.

If the zeros of $x = x_k^{(n)}$, $(k = 1, 2,...,n)$ of Legendre polynomials $P_n(x)$ are chosen as nodes, one obtains the above mentioned widely known Gaussian quadrature formulae. The weights of these formulae are determined from the relation [27]

$$A_k^{(n)} = \frac{1}{1-(x_k^{(n)})^2} \cdot \frac{2}{\left[P_n'(x_k^{(n)})\right]^2} . \tag{B.17}$$

For instance, in the handbook [1] one of the most complete tables of nodes and weights of the Gaussian quadratures is given, but it contains the data only for some values of $n = 2...12,16(4)24(8)48(16)96$. Direct use of this table as well as other tables in regular computations of surface integrals over triangular and quadrangular boundary elements with check for accuracy is not convenient enough. The weights

can be calculated using Eq. (B.17) after the zeros of the Legendre polynomials having been determined with the required accuracy. However, this is an iterative process requiring initial approximations to be given and, besides, recurrent formulae to be used both for the Legendre polynomials and for their derivatives. Evidently, such a way will result in a considerable growth of the machine time.

A great convenience is application of zeros of first-order Chebyshev polynomials T_n [1]

$$x_k^{(n)} = \cos\theta_k\ , \quad \theta_k = \frac{2\,k-1}{2n}\pi \tag{B.18}$$

as integration nodes $x = x_k^{(n)}$, ($k = 1, 2,...,n$). Then calculations with the application of the weight function $1\Big/\sqrt{1-x^2}$ result in a quadrature with coefficients [24]

$$B_k^{(n)} = \pi/n\ , \quad k = 1,2,...,n\ . \tag{B.19}$$

As a result, the following convenient and practical quadrature formula of the highest algebraic degree (Hermit formula) is obtained:

$$\int_{-1}^{1} \hat{f}(\xi)\,d\xi \approx \frac{\pi}{n}\sum_{k=1}^{n}\sqrt{1-(x_k^{(n)})^2}\cdot\hat{f}(x_k^{(n)})\ . \tag{B.20}$$

The node coordinates and weight factors of the quadrature formula (B.20) are easily calculated at arbitrary n and input in a computer's random-access memory or a disk prior to the operation of the boundary-element software main routines. As an illustration, the corresponding quadrature parameters, computed for $n \le 8$, are listed in Table B.3.

In [19] a problem of calculation of definite integrals by approximation of the integrand by an interpolation Chebyshev polynomial [25] is considered. It can be shown [9] that interpolation of functions over nodes being the roots of first-order Chebyshev polynomials (B.18) possesses the property of optimality. After using the integration formula for Chebyshev polynomials [19] a quadrature formula of the type of Eq. (B.11) with the nodes of Eq. (B.18) and the weights of

$$A_k^{(n)} = \frac{2}{k}(-1)^{k-1}\sin\theta_k \sum_{j=1}^{n}{}''' \frac{1-(-1)^j}{j}\cos(n-j)\theta_k\ , \quad k = \overline{1,n} \tag{B.21}$$

is finally obtained [30].

Explicit formulae for the approximation of a function of two variables $F(x, y)$ in a standard square $(x, y) \in [-1,1] \times [-1,1]$ by a two-dimensional interpolation Chebyshev polynomial built in [25], appeared very helpful for practical calculation of surface integrals in the boundary-element method. If the zeros of the first-order Chebyshev polynomials

Table B.3 Nodes and weights of the Hermit cubature formula (B.20)

n	$\pm\zeta_i$	w_i
1	0.000000	2.000000
2	0.707107	1.000000
3	0.000000	1.111111
	0.866025	0.444444
4	0.382683	0.735702
	0.923880	0.264298
5	0.000000	0.613333
	0.587785	0.525552
	0.951056	0.167781
6	0.258819	0.503561
	0.707107	0.377778
	0.965926	0.118661
7	0.000000	0.454422
	0.433884	0.398242
	0.781832	0.287831
	0.974928	0.086716
8	0.195090	0.385877
	0.555570	0.324152
	0.831477	0.222988
	0.980785	0.066983

$$x_i^{(n)} = \cos\frac{2i-1}{2n}\pi, \quad y_k^{(m)} = \cos\frac{2k-1}{2m}\pi, \quad i = \overline{1,n}\,; \quad k = \overline{1,m} \tag{B.22}$$

are again taken as the interpolation nodes, then termwise integration if a two-dimensional interpolation polynomial results in a cubature formula [19]

$$\int_{-1}^{1}\int_{-1}^{1} F(\xi_1,\xi_2)\,d\xi_1\,d\xi_2 \approx \sum_{i=1}^{n}\sum_{k=1}^{m} A_{ik}\cdot F(\xi_i,\xi_k) \tag{B.23}$$

with the coefficients

$$A_{ik} = \frac{16(-1)^{i+k}}{m\cdot n}\sum_{r=0(2)}^{n-1\prime}\frac{1}{1-r^2}\sin\frac{(n-r)(2i-1)\pi}{2n}\times \\ \times\sum_{s=0(2)}^{m-1\prime}\frac{1}{1-s^2}\sin\frac{(m-s)(2k-1)\pi}{2m} \tag{B.24}$$

If a case when the nodes being the extremal points of the first-order Chebyshev polynomials

$$x_i^{(n)} = \cos\frac{i\pi}{n-1}, \quad y_k^{(m)} = \cos\frac{k\pi}{m-1}, \quad i = \overline{0,n-1}\,; \quad k = \overline{0,m-1} \tag{B.25}$$

is considered, then a quadrature formula

$$\int_{-1}^{1}\int_{-1}^{1} F(\xi_1,\xi_2)\, d\xi_1\, d\xi_2 \approx \sum_{i=0}^{n-1}\sum_{k=0}^{m-1} B_{ik}\cdot F(\xi_i,\xi_k) \tag{B.26}$$

holds [19] where

$$B_{ik} = \frac{16}{(n-1)\cdot(m-1)} \sum_{r=0(2)}^{n-1\,\prime\prime} \frac{1}{1-r^2}\cos\frac{ir\pi}{n-1} \times \sum_{s=0(2)}^{m-1\,\prime\prime} \frac{1}{1-s^2}\cos\frac{is\pi}{m-1}\,. \tag{B.27}$$

In Eqs. (B.21), (B.24), and (B.27) a prime near the summation symbol means that the first term of the sum should be taken with a factor of 1/2, two primes mean that the first and the last terms of the sum are taken with the coefficient 1/2. Three primes indicate that only the last term has the factor of 1/2.

Numerical calculations have shown that the cubatures (B.20), (B.21), (B.24), and (B.27), obtained on the base of the Chebyshev polynomials, are easily realized on a computer by explicit formulae, being convenient from the point of view of programming (the use of tabulated data is not required), provide high accuracy of calculations (very close to the accuracy of the Gaussian formula) and enable, contrary to the Gaussian formulae, the order to be easily changed without additional partitioning of boundary elements into subelements, what is especially convenient at the calculation of both regular and improper surface integrals.

Appendix C
Round Punch on an Elastic Layer of Variable Thickness at Central and Off-Centre Load

This appendix contains the results of numerical boundary-element solution of a spatial contact problem for a rigid round punch with a flat bottom, located on a $z = 0$ surface of an elastic layer $x \geq 0$, $|y| < \infty$, $0 \leq z \leq h$ whose thickness varies as h $= x \cdot \tan\alpha$, $\alpha < \pi/2$. The lower boundary of the layer is rigidly fixed. The influence function for such a base is described in detail in Sect. 1.4.2. The punch is suppose to undergo a spatial static load reduced to a vertical resulting force P, eccentric in general case. There are neither friction forces between the punch and the base, nor any load outside the punch. The calculation scheme for the problem is shown in Fig. C.1.

The calculation data are obtained using STAMP-C software, composed for a EC-1060 computer (FORTRAN-IV programming language), implementing the boundary-element algorithm, described in в Sect. 2.5.1. The lack of tensile stress in the soil is achieved by imposing unilateral constraints in the contact area.

For the numerical solution of the contact problem the contact area is discretized into triangular and quadrangular elements by means of radii and concentric circles, getting more condensed towards the boundary near which contact pressures have higher gradients. The radii of the concentric circles are calculated using the following quasiuniform relation:

$$r_j = \alpha \frac{e^{\beta t_j} - 1}{e^{\beta} - 1}, t_j = \frac{j}{L} j = 1, \ldots, L.$$

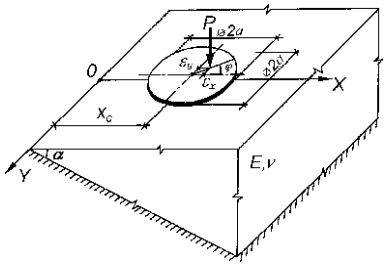

Fig. C.1 Calculation scheme for a round punch on an elastic layer of variable thickness at off-centre loading

The condensation degree is controlled by the choice of the parameter β. The contact pressure values of required accuracy were achieved at $\beta = -1$ and discretization of the circular area using up to 400 boundary elements. In order to calculate integrated characteristics of the contact interaction in most cases it is sufficient to perform the discretization of a circle using 96 boundary elements, formed by six concentric circles and sixteen rays (see the discretization diagram in Fig. C.2).

The results for the calculated parameters of the contact interaction of the punch on an elastic half-space and an elastic layer of variable thickness are shown in Figs. C.3–C.17 and in Table C.1. In the calculations we used $E = 10$ MPa, $P = (10a)$ kN, a being the punch radius. A constant vertical load was applied at the point with coordinates $\bar{x} = x_c + \varepsilon_x$, $\bar{y} = y_c + \varepsilon_y$ where ε_x , ε_y is the eccentricity of the force P along the OX, OY axes with respect to the punch centre $(x_c\ ,\ y_c\ )$, $y_c\ = 0$.

Figures C.3, C.4, and C.5 show the plots of the contact pressures under a centrally loaded rigid punch at certain values of the tilt angle α of the seat layer and the fixed values of $\nu = 0.25$ and $x_c = 2a$. For comparison the same figures show the contact pressures corresponding to the exact solution of the axially symmetrical contact problem for the round punch on a half-space

$$W_c = \frac{P(1-\nu^2)}{2Ea}, p(r) = \frac{P}{2\pi a\sqrt{a^2 - r^2}}.$$

The pressure values p_j in the centres of gravity of the elements located along the radius, calculated from the solution of the contact problem, were interpolated by cubic splines. As follows from the comparison of the calculated dependences,

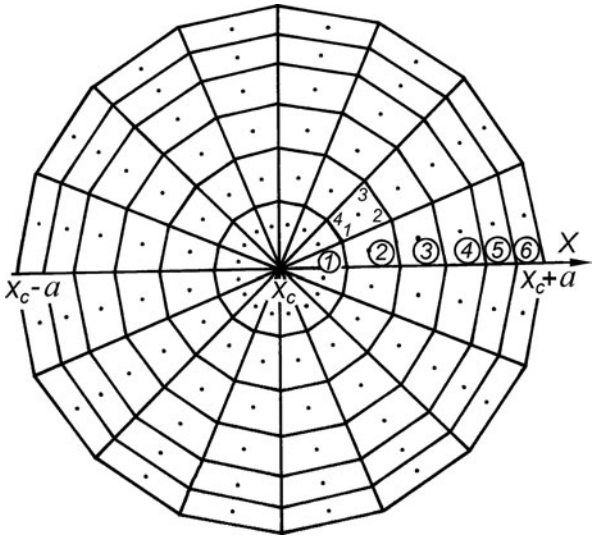

Fig. C.2 Discretization of the contact domain into boundary elements

Table C.1 Characteristics of linear and angular displacements of a round punch at $\nu = 0.25$, $x_c = 2a$, $\varepsilon_y = 0$

Foundation type	Central load, $\varepsilon_x = 0$		Off-centre load, $\varepsilon_x = 0.5a$		Off-centre load, $\psi_y = 0$
	$\varepsilon_x = 0$	$\varepsilon_x = 0$	$\varepsilon_x = 0$	$\varepsilon_x = 0$	$\varepsilon_x = 0$
Elastic layer					
$\alpha = 15°$	0.124	0.454	0.147 / 0.106	0.262 / 0.379	1.048
$\alpha = 30°$	0.221	0.513	0.247 / 0.213	0.368 / 0.458	0.809
$\alpha = 45°$	0.290	0.441	0.312 / 0.285	0.400 / 0.470	0.619
$\alpha = 60°$	0.346	0.355	0.361 / 0.334	0.421 / 0.489	0.460
$\alpha = 75°$	0.373	0.281	0.387 / 0.363	0.408 / 0.466	0.370
Elastic half-space	0.485	0.0	0.485 / 0.461	0.390 / 0.449	0.0

the pressure under the punch on a layer of variable thickness is essentially non-monotonous. With the increase of α values the difference between the exact solution for a half-space and the calculation results for a compressed wedge decreases what is explained by the increase of the compressed layer thickness under the punch. For the values $\alpha<15°$ the pressure profiles at the interval $0 < r < 3a/4$ are practically constant what corresponds to a rather uniform distribution of forces in the central part of the punch bottom. In order to visualize the asymmetric character of the pressure field in the contact area, the dependences, corresponding to the diameter sections of the punch at the angles of $\varphi = 0, \pm\pi/2, \pi$ with the X axis, are plotted (Figs. C.3, C.4, and C.5). The comparison of the obtained results shows an asymmetry,

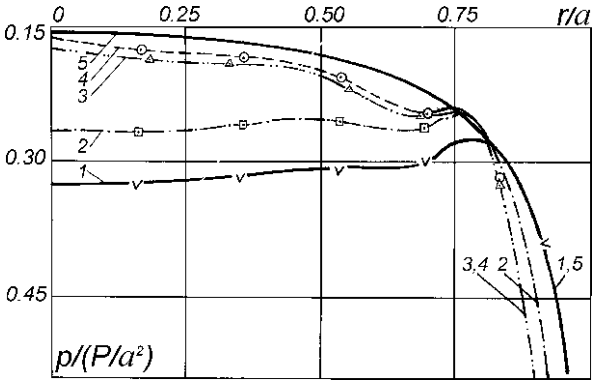

Fig. C.3 Contact pressures ($\varphi = 0°$, $\nu = 0.25$; $x_c = 2a$, $\varepsilon_x = \varepsilon_y = 0$) at $\alpha = 5°, 15°, 45°, 75°$ (1–4), 5 – half-space

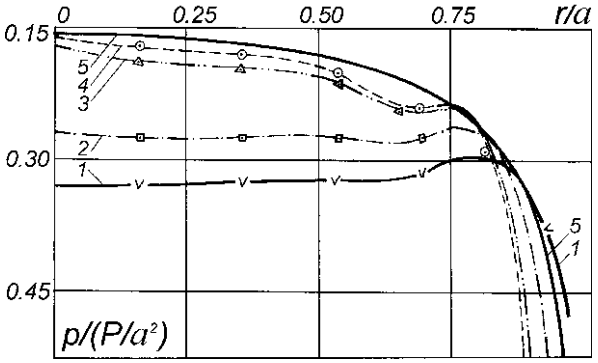

Fig. C.4 Contact pressures ($\varphi = 90°$, $\nu = 0.25$; $x_c = 2a$, $\varepsilon_x = \varepsilon_y = 0$) at $\alpha = 5°$, 15°, 45°, 75° (1–4), 5 – half-space

the most pronounced in the $0 - \pi$ direction. A more detailed view of the asymmetric character of the contact phenomena can be seen from the angular dependences shown in Fig. C.6. The tilt angle of the lower face of the elastic seat layer imposes the most essential effect on the distribution of the contact pressures for the values $\alpha \leq 30°$. For example, variation of α from 5 to 15° results in a decrease of the contact pressure in the punch centre almost by 20%. As one should expect, the contact pressures unlimitedly increase with the approach to the domain boundary. The non-axially symmetrical character of the contact pressure distribution is seen also from the fact that near the circular punch boundary for the variable-thickness elastic layer they can be both larger and smaller than for the half-space, depending on the chosen direction φ. Note that with the decrease of α the contact pressures are concentrated in the central part of the punch.

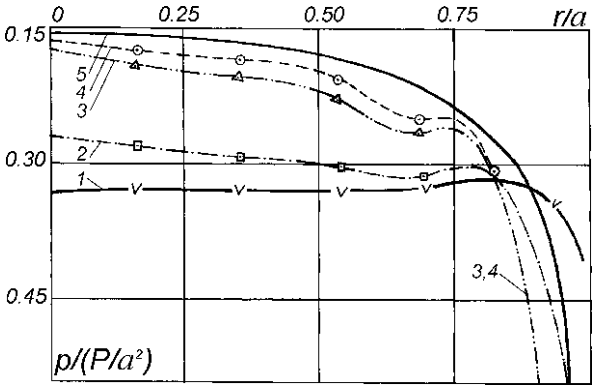

Fig. C.5 Contact pressures ($\varphi = 180°$, $\nu = 0.25$; $x_c = 2a$, $\varepsilon_x = \varepsilon_y = 0$) at $\alpha = 5°$, 15°, 45°, 75° (1–4), 5 – half-space

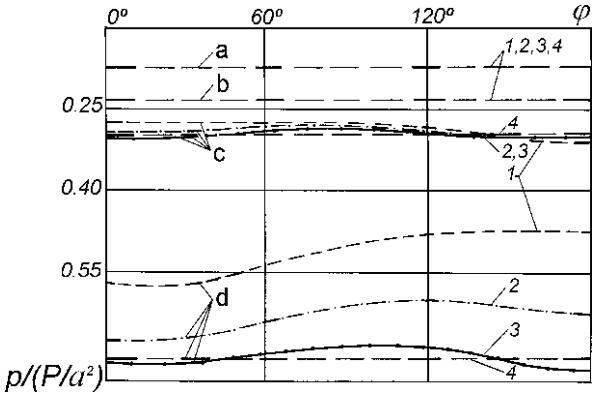

Fig. C.6 Contact pressures for $r/a = 0.16$ (**a**), 0.69 (**b**), 0.82 (**c**), 0.93 (**d**), $\nu = 0.25$; $x_c = 2a$, $\varepsilon_x = \varepsilon_y = 0$ at $\alpha = 15°, 45°, 75°$ (1–3), 4 – half-space

Figures C.7, C.8, and C.9 show the variation of the contact pressures in the punch centre p_c, displacements W_c, and punch slopes ψ_x with the distance from the elastic wedge rib $x = 0$. As seen from Fig. C.7, with the increase of α the pressures in the punch centre grow rapidly. With the increase of $p_c\,/a$ the values of p_c equalize independently of the tilt angle α. In this case the difference from the corresponding value of the contact pressure for the half-space $p_c = P/2\pi a^2$ does not exceed 10%. Settlements of the punch centre increase both with its distance from the rib of the elastic layer of variable thickness and with the angle α of tilt of the bottom plane of the distorted foundation (Fig. C.8, Table C.1). With the increase of x_c/a the settlement values asymptotically approach the corresponding values of the punch settlements on the half-space.

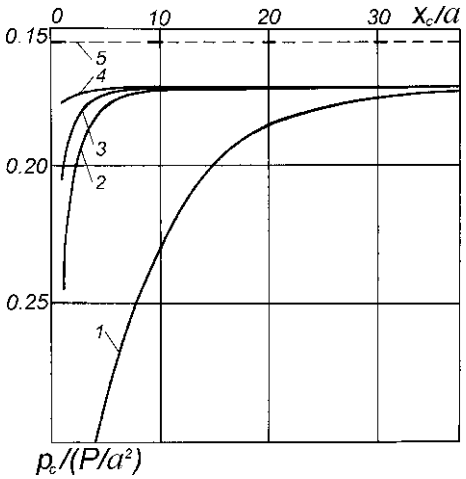

Fig. C.7 Pressures in the punch centre versus the distance from the wedge rib for $\nu = 0.25$; $\varepsilon_x = \varepsilon_y = 0$ at $\alpha = 5°, 30°, 45°, 60°$ (1–4), 5 – half-space

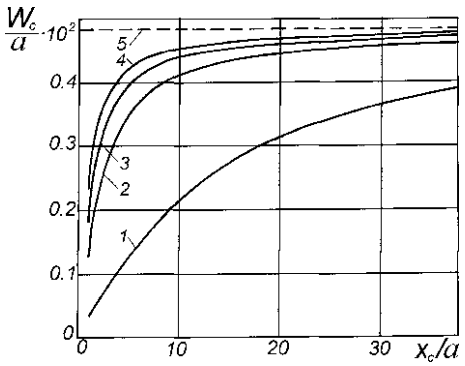

Fig. C.8 Settlements of the punch centre versus the distance from the wedge rib for $\nu = 0.25; \varepsilon_x = \varepsilon_y = 0$ at $\alpha = 5°, 30°, 45°, 60°$ (1–4), 5 – half-space

Figure C.9 illustrates the effect of relative distance x_c/a and angle α on the punch slopes at central load. The calculations show that for $\alpha = 5°$ a characteristic maximum of the slope ψ_x occurs, observed at $x_c \approx 2a$, what possibly results from the approximate character of the fundamental solution being used or the specific stress-strained state features of the thin layer. With the increase of the relative distance x_c/a the punch slopes rapidly decrease to zero, the greater α value the higher the slope variation rate.

Plots in Figs. C.10, C.11, and C.12 show the effect of the base Poisson's ratio on the contact pressures, punch centre displacements and punch slopes with distance from the $x = 0$ rib. As seen from extraneous dependences (Fig. C.10), the increase of ν results in the increase of p_c values. Already for $x_c > 10a$ the contact pressure values in the punch centre are practically the same for the Poisson's ratio ν values in the whole range of its possible variation. Variation of the Poisson's ratio most essentially affects the punch centre settlement value. With the punch distance from

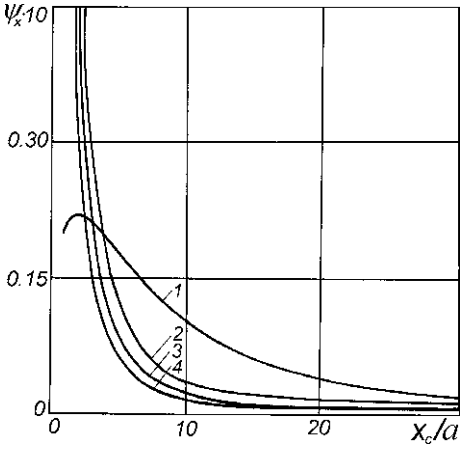

Fig. C.9 Punch slopes versus the distance from the wedge rib for $\alpha = 5°, 30°, 45°, 60°$ (1–4), $\nu = 0.25$; $\varepsilon_x = \varepsilon_y = 0$

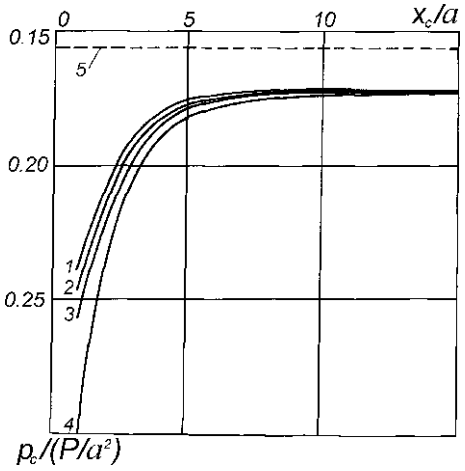

Fig. C.10 Pressures in the punch centre versus the distance from the wedge rib for $\alpha = 30°$, $\varepsilon_x = \varepsilon_y = 0$ at $\nu = 0, 0.25; 0.35, 0.5$ (1–4), 5 – half-space ($\nu = 0.25$)

the wedge rib the relative settlements achieve the values corresponding to the punch settlements on the half-space (Fig. C.11). Dependence of the punch rotation angles on the Poisson's ratio is illustrated by Fig. C.12. As follows from the quoted calculations, at $x_c > 4a$ the punch slopes cannot be noticed, and already at $x_c > 5a$ there is practically no punch slope ($\psi_x < 10^{-2}$) independently of ν y values.

Numerical studies show that at off-centre punch load negative-pressure zones arise in the contact area. Therefore, for a correct description of the contact interaction of the punch with the base when the soil cannot bear the tensile stress, unilateral character of constraints in the contact area should be introduced. Thus adjusted problem qualitatively changes the contact interaction pattern. Figures C.13, C.14, C.15, and C.16 and Table C.1 show the calculation results for the centre displacements and the punch slopes for various cases of the off-centre load with the account of the unilateral constraints. The punch distance from the $x = 0$ wedge rib and the

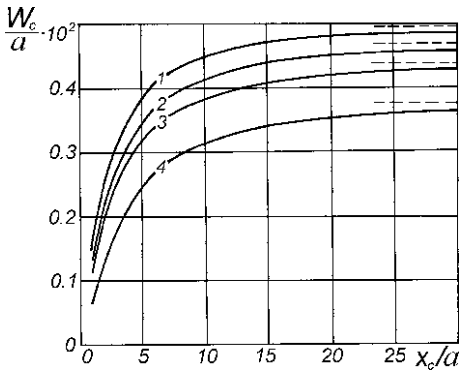

Fig. C.11 Settlements of the punch centre versus the distance from the wedge rib for$\alpha = 30°$, $\varepsilon_x = \varepsilon_y = 0$ at $\nu = 0, 0.25, 0.35, 0.5$ (1–4)

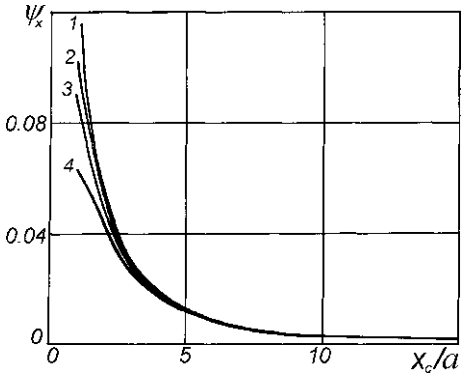

Fig. C.12 Punch slopes versus the distance from the wedge rib for$\alpha = 30°$, $\varepsilon_x = \varepsilon_y = 0$ at $\nu = 0$; 0.25, 0.35, 0.5 (1–4)

Poisson's ratio for the distorted base were fixed: $x_c = 2a$, $\nu = 0.25$. The plots in Figs. C.13 and C.16a show that the dependences of the punch centre settlements on eccentricities ε_x and ε_y without the account of unilateral constraints are strictly linear. In the case of $\varepsilon_y = 0$ (Fig. C.13) the angular coefficients of the corresponding straight lines are evidently nonzero and practically independent of the angle α. At $\varepsilon_x = 0$ (Fig. C.16a) the punch centre settlement does not depend on ε_y.

Evidently, the approach without the account of unilateral constraints cannot show the separation of parts of the punch from the base and the essential punch slope at high eccentricities of the applied load. This shortcoming is overcome for the solution with the account of the unilateral character of constraints in the contact

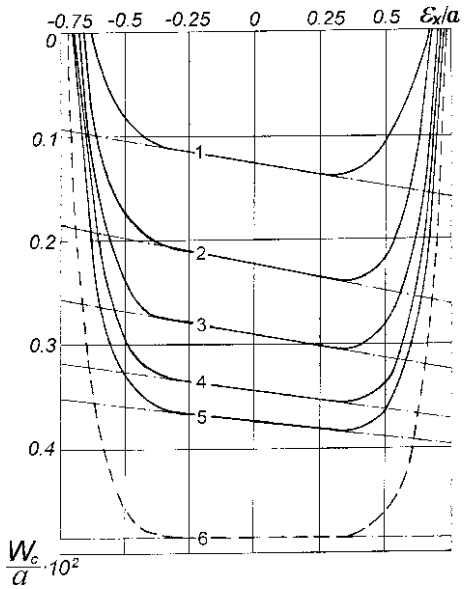

Fig. C.13 Punch centre settlements for $\nu = 0.25$; $\varepsilon_x = 0$, $x_c = 2a$at $\alpha = 15°$, 30°, 45°, 60°, 75° (1–5), 6 – half-space with the account of the punch separation (*solid curve*) and without account of separation (*chain curve*)

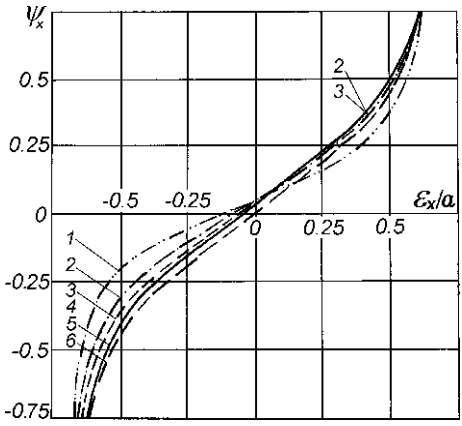

Fig. C.14 Punch slopes versus ε_x for $\nu = = 0.25$; $\varepsilon_y = 0$; $x_c = 2a$ at $\alpha = 15°$, 30°, 45°, 60°, 75° (1–5), 6– half-space

area. At partial separation of the punch from the layer surface the plots (Figs. C.13, C.16a) begin to show the nonlinear law of settlement variation. For ε_x (ε_y) > $0.75a$ a sharp increase of displacements W_c is observed what corresponds to even stronger shrinkage of the contact area and the punch turnover. The analysis of numerous calculations enables one to conclude that in the intervals $-0.4a < \varepsilon_x < 0.3a$ ($\varepsilon_y = 0$, Fig. C.13) and $|\varepsilon_y| < 0.35a$ ($\varepsilon_x = 0$, Fig. C.16a) the contact interaction of the punch and the distorted layer goes without separation. Besides, independently of the eccentricity of the resultant force application, the increment of the settlements of the punch centre applied to a half-space over the corresponding values for the wedge bases is preserved. The plots in Fig. C.15 clearly show that the dependences of the punch centre settlement on the angle α for the fixed eccentricity values are similar and their character is monotonous. The punch slopes (Figs. C.14, C.16b) do

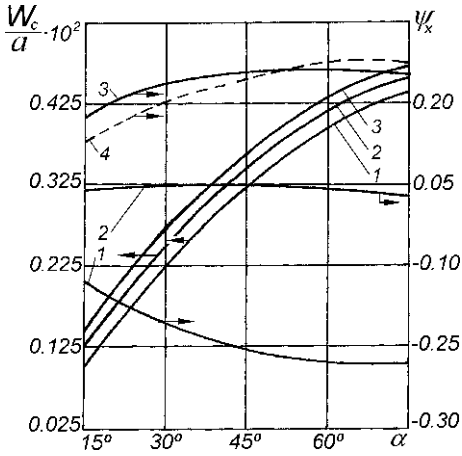

Fig. C.15 Punch centre settlements and punch slopes versus the angle α for $\nu = 0.25$, $\varepsilon_y = 0$, $x_c = 2a$ at$\varepsilon_x/a = –0.4$ (1); 0 (2); 0.3 (3); 4 – $|\psi_x|$ at $\varepsilon_x/a = –0.4$

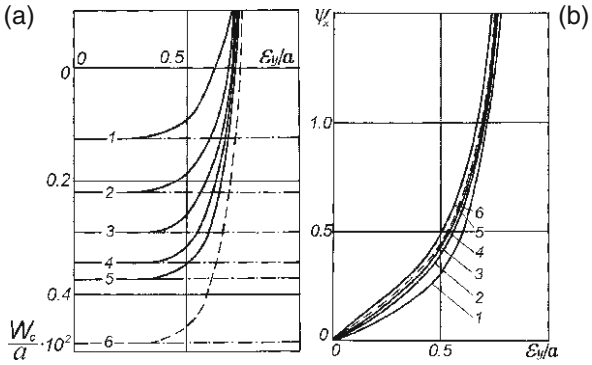

Fig. C.16 Punch centre settlements (**a**) and punch slopes (**b**) versus$\varepsilon_y$for $\nu = 0.25$, $\varepsilon_x = 0$, $x_c = 2a$ at $\alpha = 15°, 30°, 45°, 60°, 75°$ (1–5), 6 – half-space with the account of the punch separation (*solid curve*) and without account of separation (*chain curve*)

not possess such a pronounced dependence on the angle α, as the settlements. At the intervals of coincidence of the solutions, obtained with and without account of the unilateral character of constraints, the dependences of the slopes and the settlements on ε_x (ε_y) are rather close to linear. At high eccentricities the slope absolute values infinitely grow what corresponds to the punch turnover. The solution for the half-space, as seen from Figs. C.14, C.15, and C.16b, is intermediate, i.e. for different tilt angles α the punch slopes can be both higher or lower than the corresponding values for the half-space.

Figures C.14 and C.15 indicate some specific features of the off-centre punch loading when $\varepsilon_y = 0$. At such loading the slope $\psi_y = 0$. Depending on the values of ε_x, the punch slopes ψ_x can acquire values of different signs (Fig. C.14). Table C.1 gives the calculated values for the eccentricities ε_x for the case, the most important in practice when the punch has no slope ($\psi_x = 0$). In the same table for $\varepsilon_x = 0.5a$ the punch displacement parameters without the account of unilateral constraints are shown in the numerator, and those obtained with the account of unilateral constraints – in the denominator. The dependences of the punch slopes ψ_x on the tilt angle of the rigid seat base do not have such pronounced monotonous character as settlement curves (Fig. C.15, Table C.1), their character being essentially dependent of the sign and value of the eccentricity ε_x. At $\varepsilon_x = 0$ the slope ψ_x is practically constant, rather close to zero.

Figure C.17 enables one to compare the calculation results for the contact pressures under a round punch interacting with the layers of constant and variable thickness. In the last case the known Egorov influence function for an elastic layer of finite thickness with a smooth contact with the rigid base was used. The depth of both layers H_c under the punch centre was fixed, the tilt angles of the bottom plane of the elastically compressible layer were varied. The contact pressure distributions at $H_c/a = 2$ for $\alpha = 60°, 45°$ are shown in Fig. C.17.

The calculation data, given in Appendix C, give the evidence for the efficiency of the proposed method to be applied for design of foundations under tower-type struc-

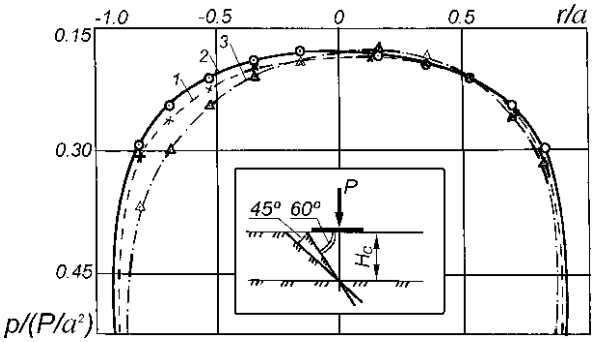

Fig. C.17 Contact pressures along the punch diameter (0–π) at $\nu = 0.25$; $H_c = 2a$; 1, 3 – wedge base, $\alpha = 45°$ (1), 60° (3), 2 – layer of constant thickness

tures to be constructed at complicated geotechnical conditions (with the account of the actual character of occurrence of weakly compressible soils). This enables the method to be recommended for practical application for search of rational project solutions, calculation of base deformations and determination of preliminary size of foundations, round in plane.

Appendix D
Foundation Under a Tower-Type Structure on a Wedge Base

Under tower-type structures (compact in plan high public and dwelling buildings, chimneys, water towers, TV towers, masts, etc.), constructed on a wedge foundation, as a rule, rigid foundation plates are used with flat bottom of simple geometric shape: a square, a rectangle, a circle, or a ring. The wedge base is understood as a layer of compressible soil of non-uniform thickness restricted by a horizontal flat surface from above and by an oblique plane resting on an uncompressible massive rock. The most important aspect of design of the foundations in question is restriction of non-uniformity of the wedge base settlements and, hence, the slope of the structure in general.

It follows from the experience of practical applications of traditional calculation methods that foundation plates with a symmetrical bottom have high consumption of material since, due to the non-uniform compressibility of the wedge base, in order the condition $(i_v+i_m) \leq i_u$ to be fulfilled, the plate part of the foundation should be essentially extended in plan against the calculated values obtained from the conditions $p_{\min} \geq 0$, $p_{\max} \leq 1.2R$, $p \leq R$. Here i_v, i_m are the components of the total slope of the foundation i, resulting from vertical V and moment M loads, respectively, transmitted by the foundation to the base, i_u is the maximal admissible slope for the given class of structures, $p_{\min}$ and $p_{\max}$ are the minimal and maximal pressures on the soil under the fundament plate bottom edges, respectively, p is the average pressure on the soil over the plate bottom, R is the calculated soil resistance.

Thus, the non-uniform compressibility of the wedge base is the reason for the underutilization of the soil strength capacity and, hence, excessive consumption of reinforced concrete for foundation plates.

We propose a foundation for tower-type structures in the shape of a round plate with a hole in the bottom whose longitudinal axis is displaced with respect to the plate centre towards the wedge base rib by the value of eccentricity determined by the wedge angle, the distance to the rib, the geometrical size of the foundation and the deformational characteristics of the base. Due to the eccentric location of the hole the pressure is essentially concentrated under the plate edge where the wedge thickness is minimal what, in turn, contributes to the foundation slope removal.

Figure D.1 shows the in-plan view and section of a foundation intended for the construction of tower-type structures on a wedge base. The considered foundation is a round in plan plate 1 with a hole 2 whose longitudinal axis is displaced by the

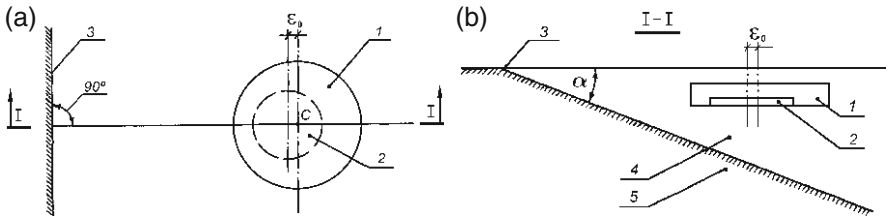

Fig. D.1 Plan (**a**) and vertical section (**b**) of the foundation under a tower-type structure on a wedge base

value ε_0 with respect to the plate centre (point *C*) towards the rib 3 of the wedge base 4 resting on a massive rock 5. The hole in the foundation bottom can be either blind, or through. The hole depth should exceed the expected base settlement under the plate. The eccentricity value ε_0, by which the hole axis is displaced with respect to the plate centre, is determined depending on the wedge angle, distance from the foundation to the wedge rib, geometrical size of the foundation and the deformational characteristics of the base. The proposed construction of the foundation plate enables the pressure over the bottom on the wedge base to be redistributed in such a way that the foundation slope component due to the vertical load resultant be excluded, and under the variable-sign moment loads the wedge base becomes equally compliant (the foundation slope depends only on the moment value, but not on its direction).

The calculation scheme explaining the character of interaction of the proposed foundation construction with the wedge shape at vertical loading is shown in Fig. D.2a, while Fig. D.2b shows a similar situation with the account of the moment loading. The vertical load resultant on the base *V* causes translational (without slope) downward vertical shift of the proposed foundation. It happens so due to the presence of an eccentrically displaced hole in the bottom that enables the adjustment of the distribution of the contact pressures on the wedge base, and thus affects the foundation slope. The increase of the eccentricity ε_0 results in a considerable

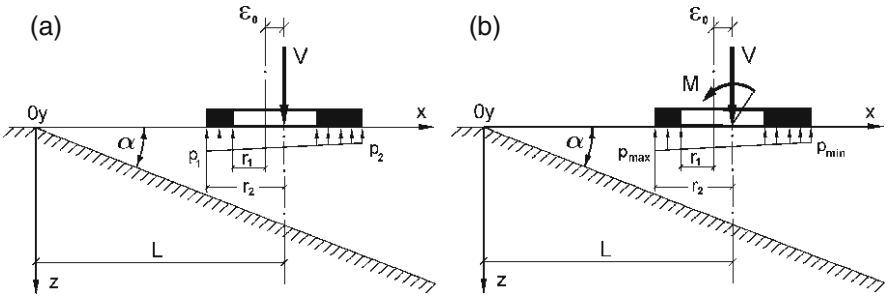

Fig. D.2 Calculation scheme of interaction of the foundation with the wedge base under central (**a**) and off-centre (**b**) vertical load

concentration of pressures p_1 under the plate edge where the wedge thickness is the smallest and, on the contrary, at the opposite side of the plate the pressures p on the soil become minimal, as shown in Fig. D.2a. As a result, with the increase of ε_0 the foundation slope in the direction of the wedge base thickness increase, induced by the vertical load resultant V, will decrease and at certain values of ε_0 can even change its sign to the opposite. The eccentricity value ε_0 required in order to provide the foundation settlement uniformity is found from the solution of the known integral equation of the soil mechanics contact problem

$$W(x,y) = \iint_F p(\xi,\eta) \cdot \omega(x,y,\xi,\eta) d\xi d\eta \tag{D.1}$$

where $W(x, y)$ is the base settlement in the point (x, y), $p(\xi, \eta)$ is the contact pressure value in the point (ξ, η), $\omega(x,y, \xi, \eta)$ is the base surface settlement in the point (ξ, η) due to the vertical unit concentrated force applied to the base in the point (x,y), F is the area of the foundation contact with the base. The contact pressures $p(\xi, \eta)$ in Eq. (D.1) should obey the equilibrium conditions

$$\iint_F p(\xi,\eta) d\xi d\eta = V, \iint_F p(\xi,\eta) d\xi d\eta = V \cdot L + M_y, \iint_F p(\xi,\eta) d\xi d\eta = M_x \tag{D.2}$$

where L is the distance from the point of application of the vertical load resultant V to the wedge rib, M_x and M_y are the moment load components with respect to OX and OY axes, respectively.

In the case under consideration the contact area F has the shape of an eccentric ring shown in Fig. D.3. By substitution in an explicit form of the integration limits in the polar coordinate system (the pole being in the centre of the outer circle) and taking into account the main condition of the problem $W(x,y) = \overline{W} = \text{const}$ (corresponding to a vertical translational shift of the foundation without any slope),

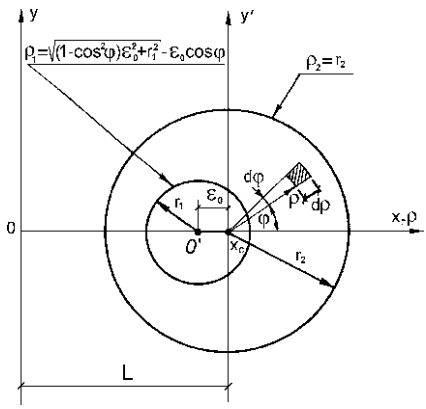

Fig. D.3 Geometrical scheme of the contact area of the foundation and the base

Eq. (D.1) is given by

$$2\int_0^{\pi} d\varphi \int_{\sqrt{(1-\cos^2\varphi)\varepsilon_0^2+r_1^2}-\varepsilon_0\cos\varphi}^{r_2} p(\rho,\varphi)\cdot\omega(x,y,\rho,\varphi)\rho d\rho - \overline{w} = 0. \tag{D.3}$$

The search parameter ε_0, settlement $\overline{W}$ and contact stresses $p(\rho,\varphi)$ can be found from the joint solution of Eq. (D.3) and the conditions of Eq. (D.2) from numerical computations. We assume $M_x = 0$ and $M_y = 0$ in Eq. (D.2). The chosen bottom shape in the form of an eccentric ring and its size its afterwards used to determine the foundation plate slopes induced by variable-sign moment loads M_x and M_y. For this purpose we jointly solve numerically Eq. (D.1) with the conditions of Eq. (D.2). The base settlement function in the left-hand side of Eq. (D.1) is given by

$$W(x,y) = \overline{W} + \psi_x \cdot (x - x_c) + \psi_y \cdot (y - y_c)$$

where ψ_x and ψ_y are the foundation plate slopes around the OX and OY axes due to the moments M_x and M_y, respectively.

As an example we use the relative eccentricity values ε_0/r_2 from Table D.1, calculated at the radii ratio $r_1/r_2 = 0.6$ and Poisson's ratio of the soil $\nu = 0.35$ (see also Sect. 4.3.3). The function $\omega(x,y,\xi,\eta)$ is determined according to the formulae of Sect. 1.4.2. The soil deformation modulus E and the vertical force value V were assumed dimensionless $E = 1$, $V = 1$, since they do not affect the ε_0 values what follows from the structure of Eq. (D.1). Numerical computer experiments were carried out using boundary-element method (Sect. 2.5.1).

The data quoted in Table D.1 give the evidence for the necessity of the eccentricity ε_0 increase with the decrease of the wedge angle α and distance L.

As noted above, the specific feature of the proposed foundation plate is the dependence of its slope only on the absolute value of the moment load $|M|$ and does not depend on its direction. This was shown by the numerical computations, some of the results being given in Table D.2. The parameter values in this case were the following: $L/r = 8$, $r_1/r_2 = 0.6$, $\alpha = 30°$, $E = 1$, $\nu = 0.35$, $\varepsilon_0/r_2 = 0.2088$, $|M| = \sqrt{M_x^2 + M_y^2} = 1$.

The quoted results of the numerical experiments confirm that a hole made in the bottom of a round foundation plate with a longitudinal axis shifted with respect

Table D.1 Relative eccentricity values ε_0/r_2 at which the centrally loaded foundation with the bottom in the shape of an asymmetric ring possesses uniform settlement on a wedge base

ε_0/r_2	$\alpha = 30°$	$\alpha = 45°$	$\alpha = 60°$
4	–	0.3398	0.3071
8	0.2088	0.1667	0.1413
12	0.1274	0.09828	0.08247

Table D.2 Slope values ψ_x, ψ_y at moment loads of various direction on a foundation in the shape of an asymmetric ring

M_y	M_x	ψ_x	ψ_y
1	0	0.73464	0
−1	0	−0.73573	0
0	±1	0	±0.74105

to the foundation centre towards the wedge base rib by the calculated value of ε_0, provides equal compliance of the wedge base both to the vertical load $V$and the variable-sign moment load M. That is, the character of the plate displacements under external loading is the same as if it rested on the surface of a homogeneous half-space or a constant-thickness layer.

The most unfavourable case of the combined action of the vertical and moment loads is shown in Fig. D.2b. In this case the edge stresses under the foundation bottom achieve extreme values $p_{\min}$ and $p_{\max}$. The dotted line shows the contact pressure profile without the moment load. The scheme shown in Fig. D.2b should be taken as the calculation one and serve as the basis for the choice of the foundation size. The calculation procedure can be illustrated by an example.

The foundation plate bottom size should be chosen for the following initial data: load at the foundation edge $N = 100000$ kN, $M = 60000$ kNm, $Q = 700$ kN, foundation depth $d = 2.5$ m, the soil specific weight above the foundation bottom $\gamma'_{II} = 15$ kN/m^3, the base is formed by plastic sand loam $I_L = 0.4$ with the following characteristics: $\varphi_{II} = 24°$, $C_{II} = 15$ kPa, $\gamma_{I\,I} = 19$ kN/m^3, $E = 16000$ kPa, $\nu = 0.35$, the inclination angle of the massive rock seat to the horizon $\alpha = 30°$, the distance from the load application point to the wedge rib $L = 120$ m, averaged specific weight of the reinforced concrete and the soil $\gamma_{mt} = 20$ kN/m^3, the maximal admissible slope $i_u = 0.0025$.

Assume the radii ratio $\beta = r_1/r_2 = 0.6$. In the first approximation consider the bottom to be in the shape of an axially symmetrical ring.

Put $r_2 = 12$ m. Then $r_1 = \beta r_2 = 0.6{\cdot}12 = 7.2$ m.

The ring width $b = r_2(1-\beta) = 12 \cdot (1-0.6) = 4.8$ m .
The ring area $F = \pi \cdot r_2^2(1-\beta^2) = \pi \cdot 12^2 \cdot (1-0.6^2) = 289.5$ m^2 .
The ring moment of inertia

$$I_c = \pi \cdot r_2^4(1-\beta^4)/4 = \pi \cdot 12^4(1-0.6^4)/4 = 14175.4 \text{ m}^4.$$

The average pressure over the bottom

$$p = N/F + \gamma_{m\,t} d = 100000/289.5 + 20 \cdot 2.5 = 395 \text{ kPa}.$$

The maximal pressure over the bottom

$$p_{\max} = p + \frac{(M + Q \cdot d)r_2}{I_c} = 395 + (60000 + 700 \cdot 2.5) \cdot 12/14175.4 = 448 \text{ kPa}.$$

The minimal pressure over the bottom

$$p_{\min} = p - \frac{(M + Q \cdot d)r_2}{I_c} = 395 - (60000 + 700 \cdot 2.5) \cdot 12/14175.4 = 343 \text{ kPa}.$$

The calculated soil resistance of the soil under the foundation bottom

$$R = \frac{\gamma_{c\,1} \cdot \gamma_{c\,2}}{K}(M_\gamma \cdot k_z \cdot b \cdot \gamma_{I\,I} + M_q \cdot d \cdot \gamma'_{I\,I} + M_c \cdot C_{I\,I}) =$$
$$= 1.2 \cdot 1.1 \cdot (0.72 \cdot 0.53 \cdot 4.8 \cdot 19 + 3.87 \cdot 2.5 \cdot 18 + 6.45 \cdot 15) = 404 \text{ kPa}$$

where K is a coefficient depending on the way of determination of physical and mechanical characteristics of the soil, k_z is a coefficient depending on the foundation width: $k_z = z/(2r_2) + 0.2 = 8/24 + 0.2 = 0.53$, $1.2R = 485$ kPa. Check: $p \le R$ (395 kPa < 404 kPa), $p_{\max} \le 1.2R$ (448 kPa < 485 kPa), $p_{\min} \ge 0$ (343 kPa > 0).

The check holds.

The ratio $L/r_2 = 120/12 = 10$. At this ratio and the wedge angle $\alpha = 30°$ Eq. (D.3) should be solved jointly with the conditions (D.2), having set $M_x = 0$ and $M_y = 0$. In our case one can use the results available from Table D.1. According to the tabulated data, the relative displacement of the hole axis in the foundation bottom towards the wedge rib should be $\varepsilon_0/r_2 = (0.2088 + 0.1274)/2 = 0.1681$. The absolute value $\varepsilon_0 = 0.1681 \cdot 12 = 2.02$ m.

The coordinate x_0 of the gravity centre of the foundation bottom in the shape of an asymmetric ring is calculated as

$$x_0 = \frac{S_y}{F} = \frac{\pi \cdot r_1^2 \varepsilon_0}{\pi \cdot r_2^2(1 - \beta^2)} = \frac{\beta^2 \varepsilon_0}{1 - \beta^2} = \frac{0.6^2 \cdot 2.02}{1 - 0.6^2} = 1.136 \text{ m}$$

where S_y is the static moment of inertia with respect to OY axis.

The moment of inertia of the foundation bottom in the shape of an asymmetric ring with respect to the main axis of symmetry is as follows:

$$I = I_c + \pi \cdot r_2^2 x_0^2 - \pi r_1^2 (x_0 + \varepsilon_0)^2 = \frac{\pi}{4} r_2^4 (1 - \beta^4) + \pi r_2^2 \left[x_0^2 - \beta^2 \cdot (x_0 + \varepsilon_0)^2\right] =$$
$$= \frac{\pi}{4} 12^4 (1 - 0.6^4) + \pi \cdot 12^2 \left[1.136^2 - 0.6^2 (1.136 + 2.02)^2\right] = 13137 \text{ m}^4.$$

The ring width in the narrowest part

$$b = r_2 - r_1 - \varepsilon_0 = 12 - 7.2 - 2.02 = 2.78 \text{ m}.$$

The maximal pressure under the foundation bottom edge

$$p_{\max} = p + \frac{(M + Qd + Nx_0)(r_2 + x_0)}{I} = 395$$
$$+ \frac{(6000 + 700 \cdot 2.5 + 100000 \cdot 1.136) \cdot (12 + 1.136)}{13137} = 570 \text{ kPa}.$$

Check: $p_{\max} \le 1.2R$ (570 kPa > 485 kPa).
The check does not hold. We increase the foundation bottom size.
Assume $r_2 = 15$ m. Then $r_1 = 0.6 \cdot 15 = 9$ m, $L/r_2 = 120/15 = 8$.

According to Table D.1 $\varepsilon_0/r_2 = 0.2088$, $\varepsilon_0 = 0.2088 \cdot 15 = 3.132$ m, $x_0 = 0.6^2 \cdot 3.132/(1-0.6^2) = 1.762$ m, $F = \pi \cdot 15^2 \cdot (1-0.6^2) = 452.4$ m^2, $I_c = \pi \cdot 15^4 \cdot (1-0.6^4)/4 = 34607.8$ m^4, $I = 34607.8 + \pi \cdot 15 \cdot \left[1.762^2 - 0.6^2 \cdot (1.762 + 3.132)^2\right] = 30707.5$ m^4 .

The pressures over the foundation bottom

$$p = \frac{100000}{452.4} + 20 \cdot 2.5 = 271 \text{ kPa}$$

$$p_{\max} = 271 + \frac{(60000 + 700 \cdot 2.5 + 100000 \cdot 1.762) \cdot (15 + 1.762)}{30707.5} = 401 \text{ kPa}$$

$$p_{\min} = 271 - \frac{(60000 + 700 \cdot 2.5 + 100000 \cdot 1.762) \cdot (15 - 1.762)}{30707.5} = 168 \text{ kPa}$$

The soil resistance is calculated as

$$R = \frac{1.2 \cdot 1.1}{1.0} \cdot (0.72 \cdot 0.467 \cdot 2.78 \cdot 19 + 3.78 \cdot 2.5 \cdot 18 + 6.45 \cdot 15) = 381 \text{ kPa}$$

where $k_z = 8/30 + 0.2 = 0.467$. $1.2R = 1.2 \cdot 381 = 457$ kPa.

Check: $p \le R$ (271 kPa < 381 kPa), $p_{\max} \le 1.2R$ (401 kPa < 457 kPa), $p_{\min} \ge 0$ (168 kPa > 0). The check holds.

Thus, the size is determined, for which the foundation plate under vertical load will uniformly settle on a wedge base ($i_v = 0$).

Now the foundation slope from the moment load should be determined; for this purpose Eq. (D.1) should be solved jointly with the conditions of Eq. (D.2) at the value $\varepsilon_0/r_2 = 0{,}2088$. In this example the data from Table D.2 can be used as well as a formula for the transition from the tabulated data to the foundations of real dimensions:

$$i_m = \frac{(M + Q \cdot d)\psi_x^{\text{tab}}}{E\, r_2^3} = \frac{(60000 + 700 \cdot 2.5)}{16000 \cdot 15^3} \cdot 0.73573 = 0.00084.$$

The total foundation slope $i = i_v + i_m = 0.00084$.
Check: $i \le i_u$ (0.00084 < 0.0025). The check holds.
The foundation plate settlement in this case is $\overline{W} = 0.105$ m .

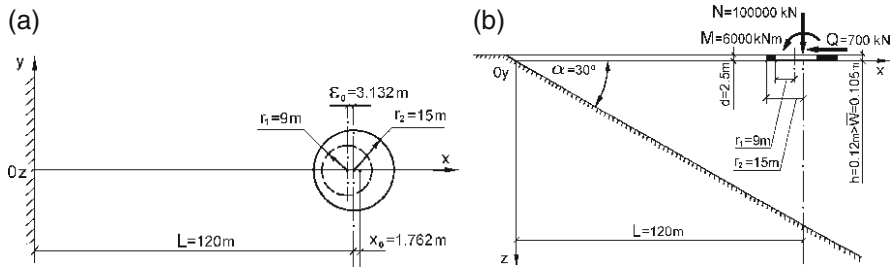

Fig. D.4 Plan (**a**) and sectional view (**b**) of the designed foundation

The plan of the designed foundation is shown in Fig. D.4a and its sectional view together with the wedge base is shown in Fig. D.4b. The hole in the foundation is set through. If the foundation plate had been designed as a symmetric ring, then, in order the condition $i \leq i_u$ to be satisfied, its size should be essentially increased, since in this case the vertical load component V results in a considerable foundation slope.

Thus, due to a hole made in a round foundation plate from the bottom side with the depth $h > \overline{W}$ and the longitudinal axis, shifted from the foundation centre towards the wedge rib by the calculated value ε_0, the following results are achieved:

1. Uniformity of the settlement of a tower-type structure on a wedge base due to the vertical load V.
2. Essential (by factor of up to 1.5) saving of reinforced concrete for the foundation, in comparison with traditional structures.

The considered foundation design is covered by Russian Federation patent No. 043462 of September 10, 1995.

A solution, close to the above foundation design, is a ring-shaped foundation whose central hole is performed in the shape of a truncated circle [2, 3]. The chord in this case is displaced from the circumference of the part of the circle, cut off as a segment, at a distance D, corresponding to the segment height, directed towards the increase of the base thickness (Fig. D.5). The value D is determined, depending

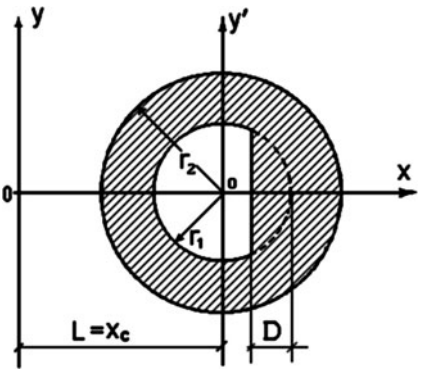

Fig. D.5 Contact area for a ring-shaped foundation with a truncated internal circle

on the angle of the elastically compressible wedge, the distance from the foundation centre to the wedge rib, the geometrical size of the foundation bottom and the deformational characteristics of the base, from the results of the spatial contact problem for a ring-shaped punch located on an elastic wedge shape.

Similarly to the case of the eccentric inner circle, this foundation design enables a uniform settlement of the structure under vertical load and a uniform compliance of the base with respect to a variable-sign moment load to be provided. Simultaneously, construction of such foundation is technologically convenient since traditional symmetric ring-shaped foundations can be used with a minor constructional finishing. Similar minor constructional changes of standard ring-shaped foundations (with *D*value correction) can be recommended for avoiding overcritical slope values at reconstruction and reinforcement of tower-type structures subject to moment loads constantly applied in a given direction.

Appendix E
Finite-Difference Equations of Cylindrical Bend of Orthotropic Slabs Located on an Elastic Foundation

The differential equation (4.19) of bend of an orthotropic slab at given boundary conditions of Eqs. (4.21)–(4.23) for deflections and forces on the rectangular slab contour (fixing, hinged-supporting, or free edges) is solved by the finite difference method, partial derivatives of the deflection function $W(x,y)$ being substituted by the corresponding finite-difference expressions. As a result, the boundary-value problem is reduced to a system of linear algebraic equations with a matrix whose order equals to the number of unknown deflections of the slab in the chosen discrete population of points.

At first a discrete model of the rectangular elastic slab is built. The origin is put into the lower left corner of the slab. On a domain $0 \le x \le a$, $0 \le y \le b$, occupied by the slab, a mesh is put along the X an Y axes with the array pitch Δx along the OX axis and Δy along the OY axis (Fig. E.1). The coordinates of the mesh nodes are determined as $\{\Delta x\cdot(i-1),\Delta y\cdot(j-1)\}$, $i = 1, 2,...,M+1$; $j = 1, 2,...,N+1$; $\Delta x = a/M$, $\Delta y = b/N$; M and N denote the number of intervals of the slab sides being partitioned by the mesh along the X and Y axes, respectively. The mesh density is characterized by the number $M\cdot N$, the total number of nodes on the slab is $(M+1)\times(N+1)$.

Consider Eq. (4.19) in an internal node of the finite-difference mesh (i, j)

$$D_1\left(\frac{\partial^4 W}{\partial x^4}\right)_{i,j} + 2D_3\left(\frac{\partial^4 W}{\partial x^2 \partial y^2}\right)_{i,j} + D_2\left(\frac{\partial^4 W}{\partial y^4}\right)_{i,j} = q_{i,j} - p_{i,j} \qquad \text{(E.1)}$$

$i = 3, 4,...,M-1$; $j = 3, 4,...,N-1$.

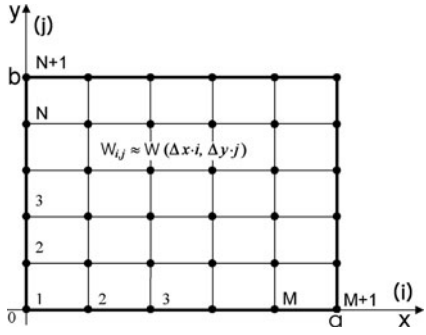

Fig. E.1 Finite-difference mesh plotted on the slab

Partial derivatives in each summand of the left-hand side of Eq. (E.1) are approximately represented in the extended form, using the known finite-difference relations for derivatives

$$\left.\frac{\partial^2 W}{\partial x^2}\right|_{i,j} = \frac{W_{i+1,j} - 2W_{i,j} + W_{i-1,j}}{\left(\Delta x^2\right)}, \tag{E.2}$$

$$\left.\frac{\partial^2 W}{\partial y^2}\right|_{i,j} = \frac{W_{i,j+1} - 2W_{i,j} + W_{i,j-1}}{\left(\Delta y^2\right)}, \tag{E.3}$$

$$\left.\frac{\partial^2 W}{\partial x \partial y}\right|_{i,j} = \frac{W_{i+1,j+1} - W_{i-1,j+1} - W_{i+1,j-1} - W_{i-1,j-1}}{4\Delta x \Delta y}, \tag{E.4}$$

$$\left.\frac{\partial^3 W}{\partial x^3}\right|_{i,j} = \frac{W_{i+2,j} - 2W_{i+1,j} + 2W_{i-1,j} - W_{i-2,j}}{2\left(\Delta x\right)^3}, \tag{E.5}$$

$$\left.\frac{\partial^3 W}{\partial y^3}\right|_{i,j} = \frac{W_{i,j+2} - 2W_{i,j+1} + 2W_{i,j-1} - W_{i,j-2}}{2\left(\Delta y\right)^3}, \tag{E.6}$$

$$\left.\frac{\partial^3 W}{\partial x \partial y^2}\right|_{i,j} = \frac{W_{i+1,j+1} - 2W_{i+1,j} + 2W_{i-1,j} - W_{i-1,j+1} + W_{i+1,j-1} - W_{i-1,j-1}}{2\left(\Delta x\right)\left(\Delta y\right)^2}, \tag{E.7}$$

$$\left.\frac{\partial^3 W}{\partial x^2 \partial y}\right|_{i,j} = \frac{W_{i+1,j+1} - 2W_{i,j+1} + 2W_{i,j-1} - W_{i+1,j-1} + W_{i-1,j+1} - W_{i-1,j-1}}{2\left(\Delta x\right)^2\left(\Delta y\right)}, \tag{E.8}$$

$$\left.\frac{\partial^4 W}{\partial x^4}\right|_{i,j} = \frac{W_{i+2,j} - 4W_{i+1,j} + 6W_{i,j} - 4W_{i-1,j} + W_{i-2,j}}{\left(\Delta x\right)^4}, \tag{E.9}$$

$$\left.\frac{\partial^4 W}{\partial y^4}\right|_{i,j} = \frac{W_{i,j+2} - 4W_{i,j+1} + 6W_{i,j} - 4W_{i,j-1} + W_{i,j-2}}{\left(\Delta y\right)^4}, \tag{E.10}$$

$$\left.\frac{\partial^4 W}{\partial x^2 \partial y^2}\right|_{i,j} = \frac{W_{i+1,j+1} + W_{i+1,j-1} + W_{i-1,j+1} - W_{i-1,j-1} - 2W_{i,j+1} -}{\left(\Delta x\right)^2\left(\Delta y\right)^2} \\ \frac{-2W_{i,j-1} - 2W_{i+1,j} - 2W_{i-1,j} + 4W_{i,j}}{\left(\Delta x\right)^2\left(\Delta y\right)^2}. \tag{E.11}$$

Equation (E.1) in the finite-difference form for the internal node (i, j) are given by

$$\begin{aligned}&\left[6D_1\lambda^2 + 8D_3\lambda + 6D_2\right] W_{i,j} - \left[4D_1\lambda^2 + 4\lambda D_3\right]\left(W_{i+1,j} + W_{i-1,j}\right) + \\ &+D_1\lambda^2\left(W_{i-2,j} + W_{i+2,j}\right) - \left[4\lambda D_3 + 4D_2\right]\left(W_{i,j+1} + W_{i,j-1}\right) + \\ &+2D_3\lambda\left(W_{i+1,j+1} + W_{i-1,j-1} + W_{i+1,j-1} + W_{i-1,j+1}\right) + D_2\left(W_{i,j+2} + W_{i,j-2}\right) = \\ &= q_{i,j}\left(\Delta y^4\right) - p_{i,j}\left(\Delta y^4\right),\end{aligned} \tag{E.12}$$

$i = 3, 4,...,M-1; j = 3, 4,...,N-1.$

Hereinafter a dimensionless geometrical parameter of the finite-difference mesh $\lambda = (\Delta y/\Delta x)^2$ is used, being the ratio of the squared array pitches of the finite-difference mesh along the *OY* and *OX* axes, respectively. Equations (E.12) relate the deflections of the slab middle plane in thirteen nodes (Fig. E.2a). The finite-difference equations can be conveniently composed using a 13-point pattern (Fig. E.2b), by making its centre to coincide with the mesh nodes and noting the coefficients C_k $(k = 1, 2,...,13)$ at each variable.

While setting up the difference equations for (E.1) in the precontour and the contour nodes using the 13-point pattern one should know not only the deflections in the nodes of the mesh plotted on the slab, i.e. inside the contour and on it, but also the deflections of two series of points outside the slab contour (Fig. E.3). It is convenient to give such deflections at these outside-contour mesh nodes that at the nearest node edge the boundary conditions would be satisfied. For this purpose Eqs. (4.21−4.23) are subjected to difference discretization. Below, as an example, consider the main and the most complicated type of boundary conditions for a free contour of Eqs. (4.24–4.26) which are most often used at the calculation of slabs on an elastic foundation and which for the contour mesh nodes are given by
at $i = 1, j = 1, 2,...,N+1$; $i = M+1, j = 1, 2,...,N+1$,

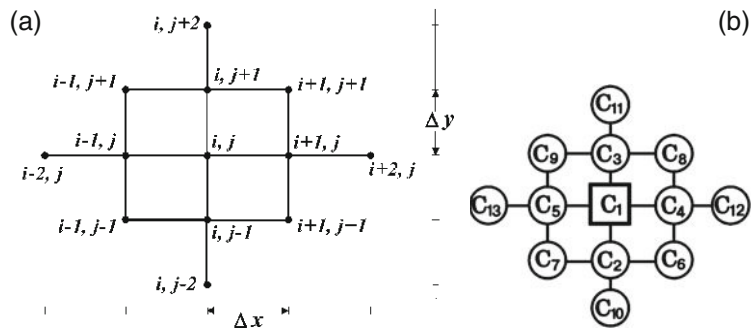

Fig. E.2 Part of the finite-difference mesh for the internal node (i, j) with the accepted numbering notations (**a**) and schematic representation of the finite-difference equation structure using a 13-point pattern (b)

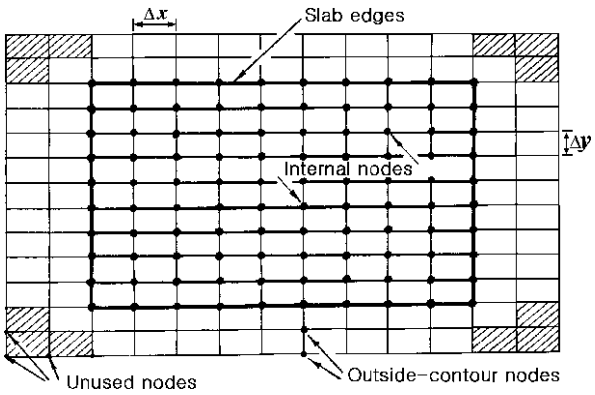

Fig. E.3 Extension of the finite-difference mesh beyond the slab contour

$$\left(\frac{\partial^2 W}{\partial x^2}\right)_{i,j} + \nu_2 \left(\frac{\partial^2 W}{\partial y^2}\right)_{i,j} = 0, \quad \left(\frac{\partial^3 W}{\partial x^3}\right)_{i,j} + \varepsilon_2 \left(\frac{\partial^3 W}{\partial x \partial y^2}\right)_{i,j} = 0;, \tag{E.13}$$

at $j = 1$, $i = 1, 2,...,M+1$; $j = N+1$, $i = 1, 2,...,M+1$,

$$\left(\frac{\partial^2 W}{\partial y^2}\right)_{i,j} + \nu_1 \left(\frac{\partial^2 W}{\partial x^2}\right)_{i,j} = 0, \quad \left(\frac{\partial^3 W}{\partial y^3}\right)_{i,j} + \varepsilon_1 \left(\frac{\partial^3 W}{\partial x^2 \partial y}\right)_{i,j} = 0; \tag{E.14}$$

at $i = 1, j = 1$; $i = M+1, j = 1$; $i = 1, j = N+1$; $i = M+1, j = N+1$,

$$\left(\frac{\partial^2 W}{\partial x \partial y}\right)_{i,j} = 0. \tag{E.15}$$

For the finite-difference approximation of the boundary conditions, as before, we use the formulae for approximate calculation of derivatives of different order from the function of two variables (E.2–E.11). After substitution of all partial derivatives by expressions in finite differences the boundary conditions of Eqs. (E.13)–(E.15) are given by

$$\begin{aligned} &2(\lambda + \nu_2) W_{i,j} - \nu_2 \left(W_{i,j+1} + W_{i,j-1}\right) - \lambda \left(W_{i+1,j} + W_{i-1,j}\right) = 0, \\ &2\sqrt{\lambda}(\lambda + \varepsilon_2)\left(W_{i+1,j} - W_{i-1,j}\right) - \varepsilon_2 \sqrt{\lambda}\left(W_{i+1,j+1} + W_{i-1,j+1} - W_{i+1,j-1} - W_{i-1,j-1}\right) \\ &-\lambda\sqrt{\lambda}\left(W_{i+2,j} - W_{i-2,j}\right) = 0 \end{aligned} \tag{E.16}$$

at $i = 1, j = 1,...,N+1$, $i = M+1$; $j = 1,...,N+1$;

$$\begin{aligned} &2(1 + \lambda\nu_1) W_{i,j} - W_{i,j+1} - W_{i,j-1} - \lambda\nu_1 \left(W_{i+1,j} + W_{i-1,j}\right) = 0, \\ &2(1 + \lambda\varepsilon_1)\left(W_{i,j+1} - W_{i,j-1}\right) - \lambda\varepsilon_1 \left(W_{i+1,j+1} + W_{i+1,j-1} - W_{i-1,j+1} - W_{i-1,j-1}\right) \\ &-W_{i,j-2} + W_{i,j+2} = 0 \end{aligned} \tag{E.17}$$

at $i = 1,...,M+1, j = 1$; $i = 1,...,M+1$, $j = N+1$;

$$W_{i-1,j-1} + W_{i+1,j+1} - W_{i+1,j-1} - W_{i-1,j+1} = 0 \tag{E.18}$$

at $i = 1, j = 1$; $i = 1, j = N+1$; $i = M+1, j = 1$; $i = M+1, j = N+1$.

The finite-difference approximation of the boundary conditions (E.16)–(E.18) enables the unknown outside-contour deflections to be included into the overall equation system and to be expressed in terms of deflections of the nearest inside-contour points and finally to be excluded from the overall equation system. Then the difference equations will contain the number of unknowns equal to the number of the mesh nodes plotted on the slab.

Thus, after the outside-contour deflections having been excluded, in any node of the slab (i, j) the difference equations are written in the following general form:

$$\begin{aligned} &C_1(i,j)\,W_{i,j} + C_2(i,j)\,W_{i,j-1} + C_3(i,j)\,W_{i,j+1} + C_4(i,j)\,W_{i+1,j} + \\ &+C_5(i,j)\,W_{i-1,j} + C_6(i,j)\,W_{i+1,j-1} + C_7(i,j)\,W_{i-1,j-1} + \\ &+C_8(i,j)\,W_{i+1,j+1} + C_9(i,j)\,W_{i-1,j+1} + C_{10}(i,j)\,W_{i,j-2} + \\ &+C_{11}(i,j)\,W_{i,j+2} + C_{12}(i,j)\,W_{i+2,j} + C_{13}(i,j)\,W_{i-2,j} = \\ &=(\Delta y)^4\,\alpha q_{i,j} - p_{i,j}\,, \end{aligned} \tag{E.19}$$

$i = 1, 2,...,M+1; j = 1, 2,...,N+1$

where $C_k(i,j)$, $k = 1,...,13$ are the difference coefficients; the values of $p_{i,j}$ are set according to the model of the elastic foundation being used, $q_{i,j}$ are external load intensity values in the finite-difference mesh nodes;

$$\alpha = \begin{cases} 1 \ - \ \text{for an internal node,} \\ 0.5 \ - \ \text{for a node located on the side,} \\ 0.25 \ - \ \text{for a node in an corner point of the slab.} \end{cases}$$

Difference equations (E.19), corresponding to each node depending on its location at the difference mesh (Fig. E.1), can be built using the patterns given for each type of the boundary conditions, respectively. There are totally 25 such patterns, corresponding to the number of subdomains shown in Fig. E.4. For a partial (and the most complicated) case of the slab with free edges, the corresponding patterns are given in the end of this appendix.

Patterns No. 1, 5, 21, 25 correspond to the corner points of the difference mesh. Using patterns No. 2, 3, 4 and No. 22, 23, 24 one can build difference equations for horizontal boundary points. In order to build difference equations for vertical boundary points one should use patterns No. 6, 11, 16 and No. 15, 10, 20.

Patterns No. 7, 8, 9 and No. 17, 18, 19 correspond to precontour horizontal points, while those No. 7, 12, 17 and No. 14, 9, 19 correspond to precontour vertical points. The most often used is pattern No. 13 intended for building up difference equations in the internal nodes of the finite-difference mesh being more than two node rows distant from the slab edges.

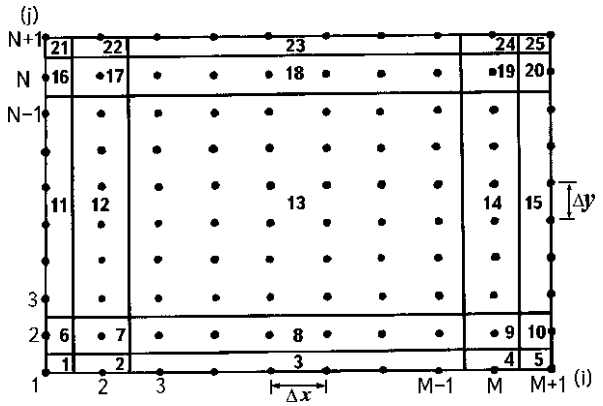

Fig. E.4 Subdomains of the slab (1–25) in which the finite-difference equations are built up according to the same patterns

The values A_i ($i = 1, 2,...,36$), quoted in patterns No. 1–25, are determined as follows:

$$
\begin{aligned}
A_1 &= D_2,\\
A_2 &= 2\lambda D_3,\\
A_3 &= -4\left(\lambda D_3 + D_2\right),\\
A_4 &= \lambda^2 D_1,\\
A_5 &= -4\lambda\left(\lambda D_1 + D_3\right),\\
A_6 &= 6\lambda^2 D_1 + 8\lambda D_3 + 6D_2,\\
A_7 &= A_6 + 2\left(A_3 + A_5\right) + 2A_2\left(a_2 + a_4\right) + 2D_1\left(a_4 a_5 + a_6\right) + 2A_1\left(a_2 a_7 + a_8\right),\\
A_8 &= A_6 + A_3 a_1 + A_2 a_2 - A_4 + A_1 a_2 a_7 + A_1 a_1 a_8,\\
A_9 &= A_6 + a_1\left(A_3 + a_8 A_1\right) + 2a_2\left(A_2 + a_7 A_1\right),\\
A_{10} &= A_6 + a_3\left(A_5 + a_6 D_1\right) + a_4\left(A_2 + a_5 D_1\right) - A_1,\\
A_{11} &= A_6 - A_1 - A_4,\\
A_{12} &= A_6 - A_1,\\
A_{13} &= A_6 + a_3\left(A_5 + a_8 D_1\right) + 2a_4\left(A_2 + a_5 D_1\right),\\
A_{14} &= A_6 - A_4,\\
A_{15} &= A_5 + a_2\left(A_3 + a_8 A_1\right) + 2A_2 + 2A_4 + 2a_7 A_1,\\
A_{16} &= A_5 + a_2\left(A_3 + a_8 A_1\right) + A_1\left(A_2 + a_7 A_1\right),\\
A_{17} &= 2\left[a_1\left(A_2 + a_7 A_1\right) - a_6 D_1\right],\\
A_{18} &= A_5 + a_3 A_4,\\
A_{19} &= -2a_6 D_1,\\
A_{20} &= A_4 + a_2\left(A_2 + a_7 A_1\right),\\
A_{21} &= 2\left(a_2 A_2 + a_2 a_7 A_1\right) + D_1,\\
A_{22} &= 2A_4,\\
A_{23} &= -2a_5 D_1,
\end{aligned}
$$

$$
\begin{aligned}
&A_{24} = A_2 + a_4A_4, A_{25} = A_2 + a_4A_4 + a_2A_1, A_{26} = -4\left(a_5D_1 + a_7A_1 + A_2\right),\\
&A_{27} = A_3 + 2\left(A_1 + A_2\right) + a_4\left(A_5 + a_6D_1\right) + 2a_5D_1,\\
&A_{28} = A_3 + a_1A_1,\\
&A_{29} = A_3 + a_4\left(A_5 + a_6D_1\right) + a_3\left(A_2 + a_5D_1\right),\\
&A_{30} = -2a_8A_1,\\
&A_{31} = 2\left[a_3\left(A_2 + a_5D_1\right) - a_8A_1\right],\\
&A_{32} = A_1 + a_4\left(A_2 + a_5D_1\right),\\
&A_{33} = 2\left[a\quad_4\left(A_2 + a_5D_1\right) + A_1\right],\\
&A_{34} = 2A_1,\\
&A_{35} = -2a_7A_1,\\
&A_{36} = A_2 + a_2A_1
\end{aligned}
$$

where a_i ($i = 1, 2,...8$) are introduced to make the notation shorter and are given by

$$
\begin{aligned}
&a_1 = 2\left(1 + \lambda\nu_1\right),\ a_2 = -\lambda\nu_1,\ a_3 = 2\left(1 + \nu_2/\lambda\right),\ a_4 = -\nu_2/\lambda\ ,\\
&a_5 = -\lambda\varepsilon_2,\ a_6 = 2\lambda\left(\lambda + \varepsilon_2\right),\ a_7 = -\lambda\varepsilon_1,\ a_8 = 2\left(1 + \lambda\varepsilon_1\right)\ .
\end{aligned}
$$

Comparison of the common 13-point pattern (Fig. E.2b) with patterns No. 1–25 for the known values of A_i ($i = 1, 2,...36$) enables one to identify the difference coefficients $C_k(i,j)$ ($k = 1, 2,...,13$), i.e. to develop from the known formulae a global rigidity matrix solving the linear algebraic equation system

$$
[\Sigma]\{W\} + \{p\} = \{q\}\,.
$$

After solving the algebraic equation system (E.19) and finding the node deflections $W_{i,j}$ ($i = 1,...,M{+}1$; $j = 1,...,N{+}1$) bending moments M_x, M_y and torques M_{xy} as well as lateral forces Q_x, Q_y are calculated using the known formulae [15, 18, 28]

$$
M_x = -D_1\left(\frac{\partial^2 W}{\partial x^2} + \nu_2\frac{\partial^2 W}{\partial y^2}\right),\ M_y = -D_2\left(\frac{\partial^2 W}{\partial y^2} + \nu_1\frac{\partial^2 W}{\partial x^2}\right), \tag{E.20}
$$

$$
M_{xy} = M_{yx} = -2D_{KP}\frac{\partial^2 W}{\partial x\partial y}, \tag{E.21}
$$

$$
Q_x = -D_1\left(\frac{\partial^3 W}{\partial x^3} + \frac{D_3}{D_1}\frac{\partial^3 W}{\partial x\partial y^2}\right),\ Q_y = -D_2\left(\frac{\partial^3 W}{\partial y^3} + \frac{D_3}{D_2}\frac{\partial^3 W}{\partial x^2\partial y}\right). \tag{E.22}
$$

Having presented Eqs. (E.20)–(E.22) in the finite-difference form, one obtains

$$
\begin{aligned}
(M_x)_{i,j} &= -\frac{D_1}{(\Delta y)^2}\left[\lambda\left(W_{i+1,j} + W_{i-1,j}\right) + \nu_2\left(W_{i,j+1} + W_{i,j-1}\right) - 2\left(\lambda + \nu_2\right)W_{i,j}\right]\ ,\\
(Q_x)_{i,j} &= -\frac{D_1}{2\Delta x\,(\Delta y)^2}\left[\lambda\left(W_{i+2,j} - W_{i-2,j}\right) - 2\left(\lambda + \frac{D_3}{D_1}\right)\left(W_{i+1,j} - W_{i-1,j}\right) + \right.\\
&\left. + \frac{D_3}{D_1}\left(W_{i+1,j+1} + W_{i-1,j+1} - W_{i+1,j-1} - W_{i-1,j-1}\right)\right]
\end{aligned}
$$

for

$$j = 1;\ i = 2,...,M;$$
$$j = 2;\ i = M{+}3,...,2(M{+}1){-}1;$$
$$j = N{+}1;\ i = N(M{+}1){+}2,...,(N{+}1)(M{+}1){-}1;$$

$$\left(M_y\right)_{i,j} = -\frac{D_2}{(\Delta y)^2}\left[\lambda\nu_1\left(W_{i+1,j} + W_{i-1,j}\right) + W_{i,j-1} + W_{i,j+1} - 2\left(1 + \lambda\nu_1\right)W_{i,j}\right], \tag{E.25}$$

$$\left(Q_y\right)_{i,j} = -\frac{D_2}{2\left(\Delta y\right)^3}\left[W_{i,j-2} - W_{i,j+2} - 2\left(1 + \frac{\lambda D_3}{D_2}\right)\left(W_{i,j+1} - W_{i,j-1}\right) + \right.$$
$$\left. + \frac{\lambda D_3}{D_2}\left(W_{i+1,j+1} + W_{i+1,j-1} - W_{i-1,j+1} - W_{i-1,j-1}\right)\right] \tag{E.26}$$

for

$$j = 2;\ i = M{+}2,...,2(M{+}1);$$
$$j = 3;\ i = 2(M{+}1){+}1,...,3(M{+}1);$$
$$j = N;\ i = (N{-}1)(M{+}1){+}1,...,N(M{+}1);$$

$$\left(M_{xy}\right)_{i,j} = -\frac{D_{KP}}{\Delta x \Delta y}\left[W_{i+1,j+1} + W_{i-1,j-1} - W_{i+1,j-1} - W_{i-1,j+1}\right] \tag{E.27}$$

for

$$j = 1;\ i = 2,...,M;\ j = 2;$$
$$i = (M{+}1){+}1,...,2(M{+}1);$$
$$j = N{+}1;\ i = N(M{+}1){+}2,...,(N{+}1)(M{+}1){-}1.$$

Based on the algorithm described in this appendix, an "ORTOPLIT" software was elaborated for studies of contact bending of rectangular slabs located on elastic nonclassical foundations. The results obtained have shown the efficiency of application of the finite-difference method for solving contact problems of statical bending of orthotropic slabs when a half-space and layers of constant and variable thickness are used as models for the elastic foundations (see Sects. Section 4.7.3, Section 4.7.4, [5–7]). Using an elastic foundation model with rigidity coefficient variable over the foundation area, a project of a potable water basin reinforcement by piles foundations was performed [4]. From the values of the foundation rigidity function, variable over the foundation area, at the finite-difference mesh nodes, found from the solution of the contact problem, the rigidities of the supplied pile foundations were calculated what enabled the basin bottom deflections to be adjusted. From the rigidity values found, the loads on each piles foundation were determined and the size of the piles was chosen.

Patterns for Building up Finite-Difference Equation of Cylindrical Bend of an Orthotropic Slab

Pattern No. 1: $i = 1, j = 1$.
Pattern No. 2: $i = 2, j = 1$.
Pattern No. 3: $i = 3, 4, \ldots, M-1, j = 1$.
Pattern No. 4: $i = 1, j = M-1$.
Pattern No. 5: $i = 1, j = M$.
Pattern No. 6: $i = 2, j = 1$.
Pattern No. 7: $i = 2, j = 2$.
Pattern No. 8: $i = 2, j = 3, 4, \ldots, M-2$.
Pattern No. 9: $i = 2, j = M-1$.
Pattern No. 10: $i = 2, j = M$.
Pattern No. 11: $i = 3, 4, \ldots, N-1, j = 1$.
Pattern No. 12: $i = 3, 4, \ldots, N-2, j = 2$.
Pattern No. 13: $i = 3, 4, \ldots, N-2, j = 3, 4 \ldots, M-2$.
Pattern No. 14: $i = 3, 4, \ldots, N-2, j = M-1$.
Pattern No. 15: $i = 3, 4, \ldots, N-2, j = M$.
Pattern No. 16: $i = N, j = 1$.
Pattern No. 17: $i = N-1, j = 2$.
Pattern No. 18: $i = N-1, j = 3, 4, \ldots, M-2$.
Pattern No. 19: $i = N-1, J = M-1$.
Pattern No. 20: $i = N-1, j = M$.
Pattern No. 21: $i = N, j = 1$.
Pattern No. 22: $i = N, j = 2$.
Pattern No. 23: $i = N, j = 3, 4, \ldots, M-2$.
Pattern No. 24: $i = N, j = M-1$.
Pattern No. 25: $i = N, j = M$.

Pattern No. 1 :
i=1, j=1

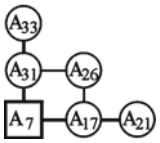

Pattern No. 2 :
i=2, j=1

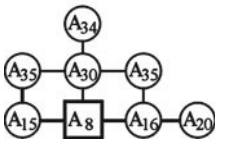

Pattern No. 3 :
i=3,4,...,M–1, j=1

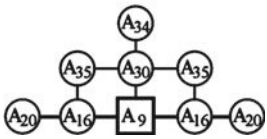

Pattern No. 4 :
i=1, j=M–1

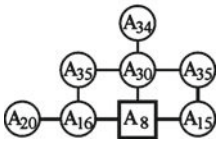

Pattern No. 5 :
i=1, j=M

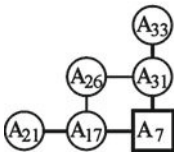

Pattern No. 6 :
i=2, j=1

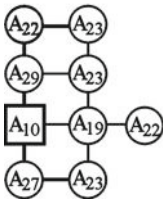

Pattern No. 7 :
i=2, j=2

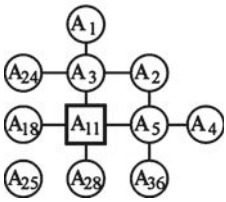

Pattern No. 8 :
i=2, j=3,4,...,M–2

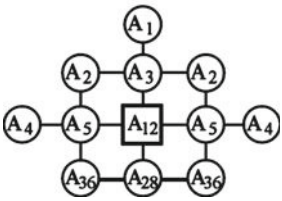

Pattern No. 9 :
i=2, j=M–1

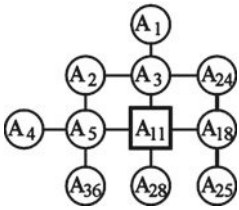

Pattern No. 10 :
i=2, j=M

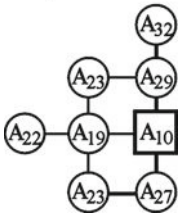

Pattern No. 11 :
i=3,4,...,N–1, j=1

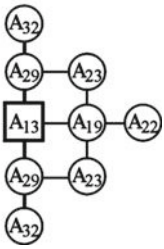

Pattern No. 12 :
i=3,4,...,N–2, j=2

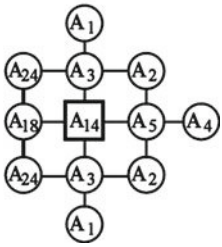

Pattern No. 13 :
i=3,4,...,N–2, j=3,4...M–2

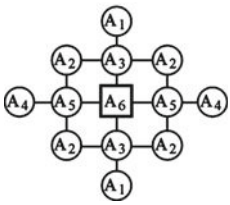

Pattern No. 14 :
i=3,4,...,N–2, j=M–1

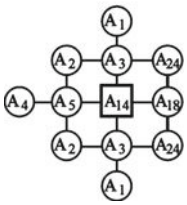

Pattern No. 15 :
i=3,4,...,N–2, j=M

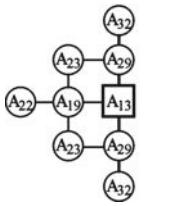

Pattern No. 16 :
i=N, j=1

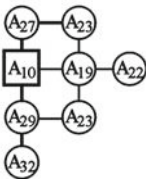

Pattern No. 17 :
i=N–1, j=2

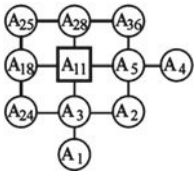

Pattern No. 18 :
i=N–1, j=3,4,...,M–2

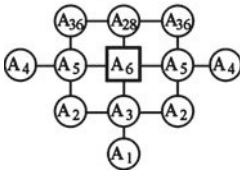

Pattern No. 19 :
i=N–1, J=M–1

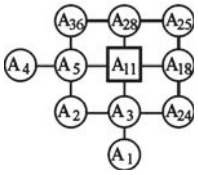

Pattern No. 20 :
i=N–1, j=M

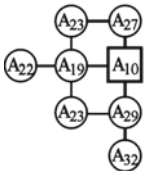

Pattern No. 21 :
i=N, j=1

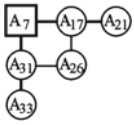

Pattern No. 22 :
i=N, j=2

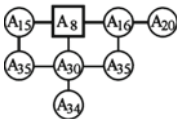

Pattern No. 23 :
i=N, j=3,4,...,M–2

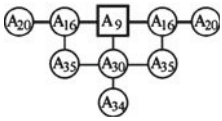

Pattern No. 24 :
i=N, j=M–1

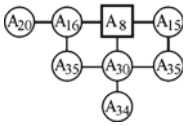

Pattern No. 24 :
i=N, j=M–1

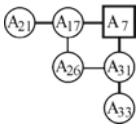

Appendix F
Calculation of the Base for a Pyramidal Pile Under Vertical Load According to the "Instructions Manual for Design of Foundations Made of Pyramidal Piles"

The aim is to build a graph of settlements of the base of a 5-m long $\frac{0.7 \times 0.7}{0.1 \times 0.1}$ m pyramidal pile, submerged in a high-plasticity clayey soil with the following physico-mechanical properties: internal friction angle $\varphi = 10°$, specific resistance $C = 15$ kPa, specific weight of the soil $\gamma = 16.3$ kN/m^3, modulus of deformation of the soil, determined from the punch test data $E_p = 2750$ kPa.

F.1 General

Settlement of the base of a single pile S (Fig. F.1) due to the transfer of pressure on the soil by the pile lateral surface according to [17] is given by

$$S = \frac{2\,(1+\mu)\cdot(1-2\mu)}{E}\cdot\rho\cdot\left[P_H\left(\frac{P_{F,6n}+C\cdot\cot\varphi}{P_H+C\cdot\cot\varphi}\right)\frac{1+\sin\varphi}{\sin\varphi}-P_{F,6n}\right] \quad \text{(F.1)}$$

where μ is the soil transverse expansion coefficient, determined for clayeys and clays from the formula [17]

$$\mu = 0.1\cdot(1+3J_L\text{`}) \quad \text{(F.2)}$$

J_L is the soil consistency index, ρ is a geometric characteristic of the pile (m), given by

$$\rho = \frac{l}{d_B^2}\left[d_H^2 + 2\,l\cdot\tan\alpha\left(d_H+\frac{2}{3}l\cdot\tan\alpha\right)\right] \quad \text{(F.3)}$$

where d_H, d_B, l, α are the notations shown in Fig. F.1: $d_H$is the diameter (cross-section side) of the bottom end of the pile, d_B is the diameter (cross-section side) of the upper part of the pile in the level of the calculated soil surface, l is the pile submergence depth, α is the pile convergence angle, E is the calculated modulus of

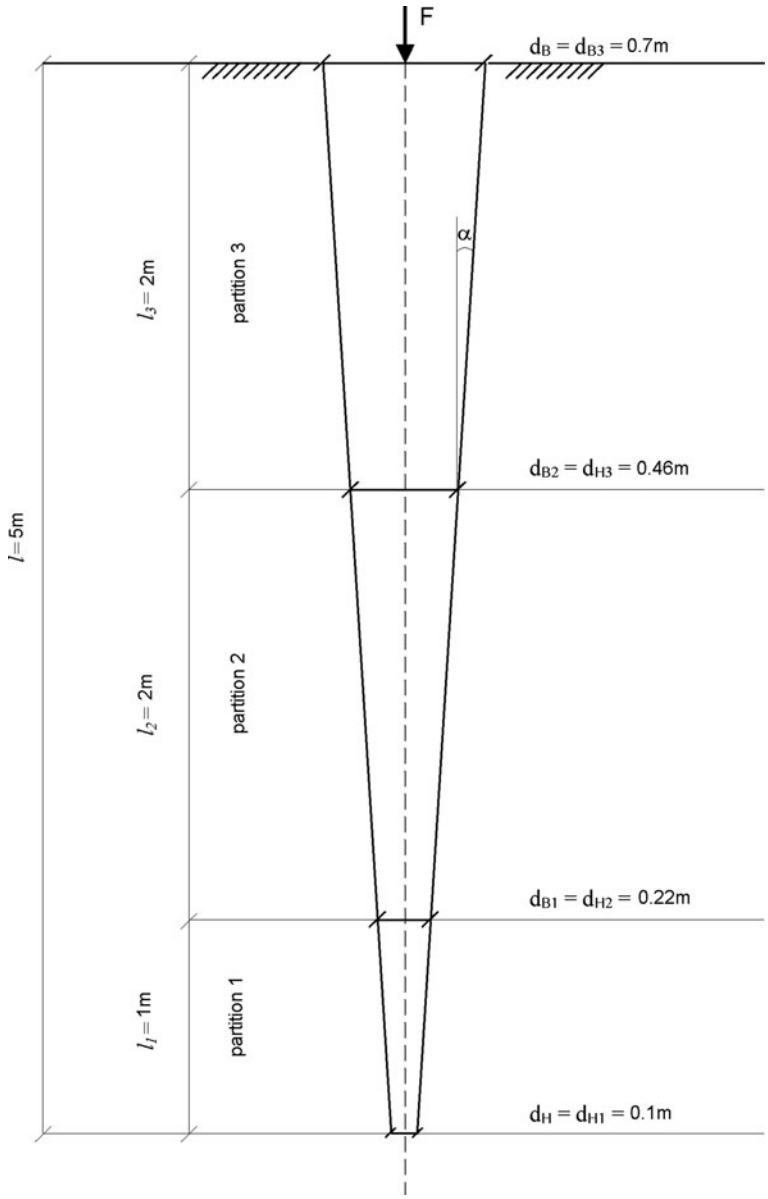

Fig. F.1 Scheme for calculation of the pyramidal pile settlements under a vertical load

deformation of the soil (kPa), determined from durable pressiometric or punch tests, using a relationship

$$E = \eta \cdot E_p, \tag{F.4}$$

η is an adjustment factor, taking into account the type of the soil, P_H is the initial squeezing pressure (kPa), given by

$$P_H = P_0(1 + \sin\varphi) + C \cdot \cos\varphi \tag{F.5}$$

P_0 is the natural lateral soil pressure (kPa), given by

$$P_0 = \frac{\mu}{1-\mu} \cdot \gamma \cdot h, \tag{F.6}$$

γ is the natural weighted average specific weight of the soil within the pile submergence depth (kN/m), h is the distance from the grading level to the middle of the pile part under consideration (m), $P_{F,\text{lat}}$ is the squeezing pressure (kPa), on the pile from the load F, determined as

$$P_{F,\text{lat}} = \frac{F_{\text{lat}} - \Phi \cdot \cos\alpha \cdot C}{\Phi \cdot \cos\alpha \cdot (\tan\alpha + \tan\varphi)} \tag{F.7}$$

where F_{lat} is the calculated load on the soil, transferred by the pile lateral surface (kN), Φ is the pile lateral surface area (m^2).

The settlement of the base under the pile's bottom end S_0 is given by

$$S_0 = \frac{0.3(1+\mu)\cdot(1-2\mu)}{E} d_H \cdot D \cdot \left[P_H \left(\frac{P_{F,0} + C \cdot \cot\varphi}{P_H + C \cdot \cot\varphi} \right)^{\frac{1+\sin\varphi}{\sin\varphi}} - P_{F,0} \right] \tag{F.8}$$

where $P_{F,0}$ is the soil resistance (kPa) under the bottom end of the pile, given by

$$P_{F,0} = A \cdot \frac{F_0}{d_H^2} - B \cdot C, \tag{F.9}$$

where F_0 is the calculated load on the soil, transferred by the bottom end of the pile (kN), d_{H} is the diameter (side) of the bottom section of the pile (m), *A, B,* and *D* are the coefficients, taken from Table 2.1 in the instructions manual [17] depending on the calculated value of the internal friction angle φ.

While calculating pyramidal piles from the base deformations, one should, in accordance with the instructions manual [17], partition soil seams (along the pile length) with respect to the base deformations into homogeneous layers (parts) not more than 2-m thick (long). Then the calculated load on the soil, transferred by the whole pile surface, is determined as the sum of loads transferred by the bottom end F and the lateral surfaces of the pile partitions F_i ($i = 1,...n$) at a given settlement S

$$F = F_0 + \sum_{i=1}^{n} F_i. \tag{F.10}$$

At the final stage the calculated loads F, corresponding to the given pile settlements S, are determined from the $S = f(F)$ plots and, vice versa, the settlements S, corresponding to the given loads F are determined from the $F = g(S)$ plots.

F.2 Calculation Procedure

For clayeys $J_L = \eta = 1$, hence

$$E = \eta E_p = 2750\,\text{kPa},$$

$$\mu = 0.1(1 + 3J_L) = 0.1(1 + 3.1) = 0.4$$

In the calculation example under consideration for $\varphi = 10^\circ$

$\sin 10^\circ = 0.1736$, $\cos 10^\circ = 0.9848$, $\tan 10^\circ = 0.1763$, $\cot 10^\circ = 5.6714$,

$$\frac{1 + \sin 10^\circ}{\sin 10^\circ} = 6.759.$$

According to Table 2.1 of the instructions manual [17], we imply

$$A = 0.445,\ B = 0.851,\ D = 2.428.$$

Now we calculate the geometrical characteristics of the pile and its three marked partitions 1 m, 2 m, and 2 m long, respectively (Fig. F.1):

side of the pile lower section $d_\text{H} = d_{\text{H}1} = 0.1$ m,
side of the 1st section of the pile $d_{\text{B}1} = d_{\text{H}2} = 0.22$ m,
side of the 2nd section of the pile $d_{\text{B}2} = d_{\text{H}3} = 0.46$ m,
side of the pile head $d_\text{B} = d_{\text{B}3} = 0.7$ m,
length of the lower partition of the pile $l_1 = 1$ m,
length of the medium partition of the pile $l_2 = 2$ m,
length of the upper partition of the pile $l_3 = 2$ m,
overall pile length $l = l_1 + l_2 + l_3 = 5$ m,
depth of the centre of the 1st partition $h_1 = l_1/2 + l_2 + l_3 = 4.5$ m,
depth of the centre of the 2nd partition $h_2 = l_2/2 + l_3 = 3$ m,
depth of the centre of the 3rd partition $h_3 = l_3/2 = 1$ m,
tangent of the pile convergence angle $\tan\alpha = (d_\text{B} - d_\text{H})/2/l = 0{,}06$,
cosine of the pile convergence angle $\cos\alpha = 0{,}9982$,
lateral surface area of the 1st partition of the pile

$$\Phi_1 = 4 \cdot \frac{(d_{H1} + d_{B1})}{2} \cdot \frac{l_1}{\cos\alpha} = 0.6412\,\text{m}^2,$$

lateral surface area of the 2nd partition of the pile

$$\Phi_2 = 4 \cdot \frac{(d_{H2} + d_{B2})}{2} \cdot \frac{l_2}{\cos\alpha} = 2.7249\,\mathrm{m}^2,$$

lateral surface area of the 3rd partition of the pile

$$\Phi_3 = 4 \cdot \frac{(d_{H3} + d_{B3})}{2} \cdot \frac{l_3}{\cos\alpha} = 4.6484\,\mathrm{m}^2,$$

geometrical characteristics of the 1st partition of the pile

$$\rho_1 = \frac{l_1}{d_{B1}^2}\left[d_{H1}^2 + 2l_1 \cdot \tan\alpha\left(d_{H1} + \frac{2}{3}l_1 \cdot \tan\alpha\right)\right] = 0.5537\,\mathrm{m},$$

geometrical characteristics of the 2nd partition of the pile

$$\rho_2 = \frac{l_2}{d_{B2}^2}\left[d_{H2}^2 + 2l_2 \cdot \tan\alpha\left(d_{H2} + \frac{2}{3}l_2 \cdot \tan\alpha\right)\right] = 1.138\,\mathrm{m},$$

geometrical characteristics of the 3rd partition of the pile

$$\rho_3 = \frac{l_3}{d_{B3}^2}\left[d_{H3}^2 + 2l_3 \cdot \tan\alpha\left(d_{H3} + \frac{2}{3}l_3 \cdot \tan\alpha\right)\right] = 1.3927\,\mathrm{m}.$$

F.3 Determination of the Base Settlements S_0 Under the Bottom End of the Pile

At $d_\mathrm{H} = d_{\mathrm{H1}} = 0.1$ m and $l = 5$ m using Eq. (F.9) we calculate the soil resistance at the given value of $F = 3.3$ kN:

$$P_{F,0} = A \cdot \frac{F_0}{d_H^2} - B \cdot C = 0.445 \cdot \frac{3.3}{0.01} - 0.851 \cdot 15 = 134.085\,\mathrm{kPa}$$

and, having calculated

$$P_0 = \frac{\mu}{1-\mu} \cdot \gamma \cdot h = \frac{0.4}{0.6} \cdot 16.3 \cdot 5 = 54.33\,\mathrm{kPa},$$

$$P_H = P_0 \cdot \left(1 + \sin 10^\circ\right) + 15 \cdot \cos 10^\circ = 54.33 \cdot 1.1736 + 15 \cdot 0.9848 = 78.54\,\mathrm{Kpa},$$

according to Eq. (F.8), we determine the base settlements under the bottom end of the pile

Table F.1 The load under the bottom end of the pile versus the loads on the soil

F_0 (kN)	$P_{F,0}$ (kPa)	S_0 (cm)
3.3	134.085	0.3206
3.6	147.435	0.5170
3.9	160.785	0.7943
4.2	174.135	1.1768
4.5	187.485	1.6947
4.8	200.835	2.3845
5.1	214.185	3.2899
5.4	227.535	4.4634
5.7	240.885	5.9665
6.0	254.235	7.8719

$$S_0 = \frac{0.3 \cdot 1.4 \cdot 0.2}{2750} \cdot 0.1 \cdot 2.428 \cdot \left[78.54 \left(\frac{134.085 + 15 \cdot 5.67}{78.54 + 15 \cdot 5.67} \right)^{6.759} - 134.085 \right]$$
$$= 0.3206\,\text{cm}.$$

Then we perform calculations, varying the load within the range, corresponding to the settlement variation within the operating interval 0.3−8.0 cm under the bottom end of the pile versus the loads on the soil are given in Table F.1. The data obtained are approximated using the least-square method by a logarithmic dependence

$$F_0 = 0.84743 \ln (10^{-2} \cdot S_0) + 8.0383, \tag{F.11}$$

its plot being shown in Fig. F.2.

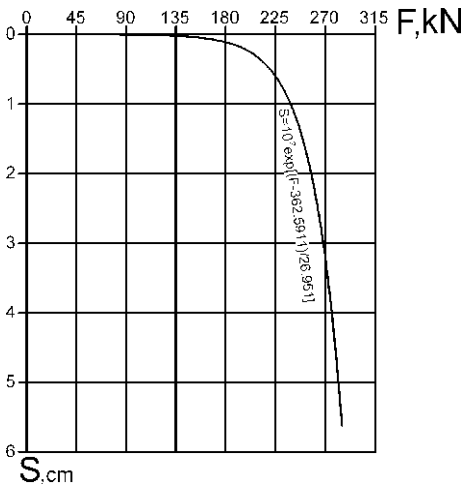

Fig. F.2 Plots of calculated loads on the soil for separate partitions of the pile, resulting in the same given base settlements: F_0 is the load on the pile's lower end, F_1,F_2,F_3 are the loads on the lateral surfaces of the pile partitions, F is the sum of the loads transferred by the lower end and the lateral surface of the pyramidal pile at a given settlement

F.4 Determination of the Base Settlements S_1 of the Lower Part of the Pile (Partition 1)

At $d_{H1} = 0.1$ m, $d_{B1} = 0.22$ m, $h_1 = 4.5$ m, $l_1 = 1$ m, $\Phi_1 \cdot \cos 10^\circ = 0.64$ m^2, $\rho_1 = 0.5537$ m, using Eq. (F.7), at the given value of $F_1 = 22$ kN we determine the squeezing pressure, acting on the 1st partition of the pile:

$$P_{F,1} = \frac{F_1 - \Phi_1 \cdot \cos\alpha \cdot C}{\Phi_1 \cdot \cos\alpha \cdot (\tan\alpha + \tan\varphi)} = \frac{22 - 0.64 \cdot 15}{0.64 \cdot (0.06 + 0.1763)} = 81.985\,\text{kPa}.$$

Then, having calculated

$$P_0 = \frac{\mu}{1-\mu} \cdot \gamma \cdot h_1 = \frac{0.4}{0.6} \cdot 16.3 \cdot 4.5 = 48.9\,\text{kPa},$$

$$P_H = P_0 \cdot \left(1 + \sin 10^\circ\right) + 15 \cdot \cos 10^\circ = 32.6 \cdot 1.1736 + 15 \cdot 0.9848 = 53.03\,\text{kpa},$$

using Eq. (F.1), we determine the settlements of the base of the pile's lower partition S_1:

$$S_1 = \frac{2 \cdot 1.4 \cdot 0.2}{2750} \cdot 0.5537 \cdot \left[72.16 \left(\frac{81.985 + 15 \cdot 5.67}{72.16 + 15 \cdot 5.67}\right)^{6.759} - 81.985\right] = 0.3011\,\text{cm}.$$

Then we perform calculations, varying the load within the range, corresponding to the settlement variation within the interval 0.3/8.0 cm. The values of the base settlements S_1 of the lower partition of the pile versus the loads on the soil are given in Table F.2.The data obtained are approximated using the least-square method by a logarithmic dependence

$$F_1 = 2.79232 \ln\left(10^{-2} \cdot S_1\right) + 37.3238, \tag{F.12}$$

its plot being shown in Fig. F.2.

Table F.2 The values of the base settlements of the lower partition of the pile versus the loads on the soil

F_1 (kN)	$P_{F,1}$ (kPa)	S_1 (cm)
22.0	81.985	0.3011
23.0	88.597	0.5942
24.0	95.209	0.9773
25.0	101.820	1.4681
26.0	108.432	2.0864
27.0	115.044	2.8555
28.0	121.655	3.8013
29.0	128.267	4.9533
30.0	134.879	6.3459
31.0	141.491	8.0137

F.5 Determination of the Base Settlements S_2 of the Medium Part of the Pile (Partition 2)

At $d_{H2} = 0.22$ m, $d_{B2} = 0.46$ m, $h_2 = 3$ m, $l_2 = 2$ m, $\Phi_2 \cdot \cos 10^\circ = 2.72$ m^2, $\rho_2 = 1.138$ m, using Eq. (F.7) at the given value of $F_2 = 79.5$ kN we determine the squeezing pressure, acting on the 2nd partition of the pile:

$$P_{F,2} = \frac{F_2 - \Phi_2 \cdot \cos\alpha \cdot C}{\Phi_2 \cdot \cos\alpha \cdot (\tan\alpha + \tan\varphi)} = \frac{79.5 - 2.72 \cdot 15}{2.72 \cdot (0.06 + 0.1763)} = 60.205\,\text{kPa}.$$

Then, having calculated

$$P_0 = \frac{\mu}{1-\mu} \cdot \gamma \cdot h_2 = \frac{0.4}{0.6} \cdot 16.3 \cdot 3.0 = 32.6\,\text{kPa},$$

$$P_H = P_0 \cdot \left(1 + \sin 10^\circ\right) + 15 \cdot \cos 10^\circ = 32.6 \cdot 1.1736 + 15 \cdot 0.9848 = 53.03,\text{kPa}$$

using Eq. (F.1), we determine the settlements of the base of the pile's medium partition S_2:

$$S_2 = \frac{2 \cdot 1.4 \cdot 0.2}{2750} \cdot 1.138 \cdot \left[53.03 \left(\frac{60.285 + 15 \cdot 5.67}{53.03 + 15 \cdot 5.67}\right)^{6.759} - 60.205\right] = 0.3528\,\text{cm}.$$

Then we perform calculations, varying the load within the range, corresponding to the settlement variation within the interval $0.3 \div 8.0$ cm. The values of the base settlements S_2 of the medium partition of the pile versus the loads on the soil are given in Table F.3. The data obtained are approximated using the least-square method by a logarithmic dependence

$$F_2 = 8.9314 \ln(10^{-2} \cdot S_2) + 127.66, \tag{F.13}$$

its plot being shown in Fig. F.2.

F.6 Determination of the Base Settlements S_3 of the Upper Part of the Pile (Partition 3)

At $d_{H3} = 0.46$ m, $d_{B3} = 0.7$ m, $h_3 = 3$ m, $l_3 = 2$ m, $\Phi_3 \cdot \cos 10^\circ = 4.64$ m^2, $\rho_3 = 1.393$ m, using Eq. (F.7), at the given value of $F_3 = 110.5$ kN we determine the squeezing pressure, acting on the 3rd partition of the pile:

$$P_{F,3} = \frac{F_3 - \Phi_3 \cdot \cos\alpha \cdot C}{\Phi_3 \cdot \cos\alpha \cdot (\tan\alpha + \tan\varphi)} = \frac{110.5 - 4.64 \cdot 15}{4.64 \cdot (0.06 + 0.1763)} = 37.3\,\text{kPa},$$

Then, having calculated

$$P_0 = \frac{\mu}{1-\mu} \cdot \gamma \cdot h_3 = \frac{0.4}{0.6} \cdot 16.3 \cdot 1.0 = 10.87\,\text{kPa},$$

$$P_H = P_0(1 + \sin 10^\circ) + 15\cos 10^\circ = 10.87 \cdot 1.1736 + 15 \cdot 0.9848 = 27.53.\,\text{kPa},$$

using Eq. (F.1), we determine the settlements of the base of the pile's upper part S_3:

$$S_3 = \frac{2 \cdot 1.4 \cdot 0.2}{2750} \cdot 1.393 \cdot \left[27.53\left(\frac{37.3 + 15 \cdot 5.67}{27.53 + 15 \cdot 5.67}\right)^{6.759} - 37.3\right] = 0.3124\,\text{cm}.$$

Then we perform calculations, varying the load within the range, corresponding to the settlement variation within the interval 0.3/8.0 cm. The values of the base settlements S_3 of the upper part of the pile versus the loads on the soil are given in Table F.4. The data obtained are approximated using the least-square method by a logarithmic dependence

$$F_3 = 14.3802 \ln(10^{-2} \cdot S_3) + 189.57, \tag{F.14}$$

its plot being shown in Fig. F.2.

Table F.3 The values of the base settlements of the medium partition of the pile versus the loads on the soil

F_2 (kN)	$P_{F,2}$ (kPa)	S_2 (cm)
79.5	60.205	0.3353
82.5	64.873	0.6395
85.5	69.540	1.0245
88.5	74.207	1.5033
91.5	78.874	2.0898
94.5	83.541	2.8001
97.5	88.208	3.6518
100.5	92.875	4.6644
103.5	97.542	5.8598
106.5	102.209	7.2619
109.5	106.876	8.8969

Table F.4 The values of the base settlements of the upper partition of the pile versus the loads on the soil

F_3 (kN)	$P_{F,3}$ (kPa)	S_3 (cm)
110.5	37.299	0.3124
115.0	41.403	0.5383
119.5	45.507	0.8343
124.0	49.611	1.2122
128.5	53.714	1.6849
133.0	57.818	2.2669
137.5	61.922	2.9746
142.0	66.026	3.8259
146.5	70.129	4.8409
151.0	74.234	6.0421
155.5	78.337	7.4539

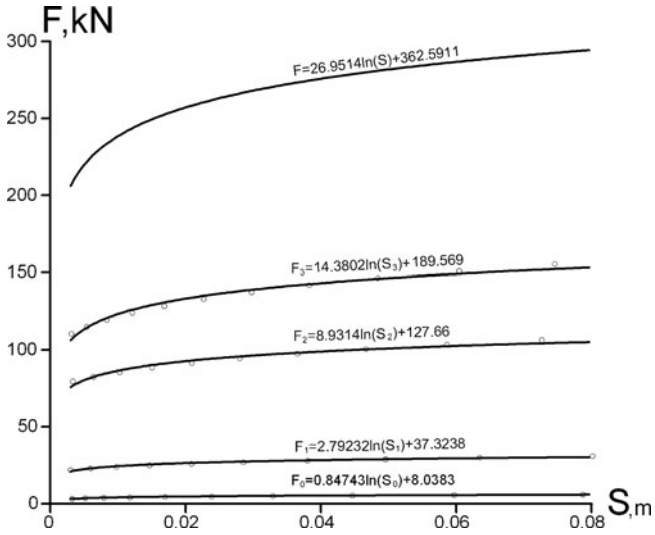

Fig. F.3 Generalized plot of load versus settlement for the pyramidal pile under vertical loading

The calculated load on the pile F at the given settlement S is obtained as the sum of loads, transferred by the bottom end and the whole lateral surface of the pile

$$F = F_0 + F_1 + F_2 + F_3. \tag{F.15}$$

The corresponding functional dependence after the summation of Eqs. (F.11)–(F.14) is given by

$$F = 26.951 \ln (10^{-2} \cdot S) + 362.591, \tag{F.16}$$

its plot also being shown in Fig. F.2. Figure F.3 shows the sought plot of the pyramidal pile's base settlements at vertical load built in a convenient practical form using Eq. (F.16).

Appendix G
Isolines of Contact Stress on a Lateral Surface of a Slotted Foundation

The appendix contains the results of boundary-element calculations of contact stress at the lateral faces of a slotted foundation with a rectangular shape of the longitudinal cross-section (the simplest construction of a foundation under columns of reinforced concrete and steel). The calculation scheme for the corresponding spatial problem is shown in Fig. G.1.

The deformation parameters of the soil base are taken as follows: deformation modulus $E = 20$ MPa, Poisson coefficient $\nu = 0.4$ (cohesive slightly wet eluvial clayey in a solid state).

The following spatial actions on the slotted foundation are considered:

(1) a central vertical compressive load;
(2) a combined action of a central vertical force and a tilting moment, acting within the longitudinal cross-section plane (a vertical load with an eccentricity in the longitudinal direction);
(3) a tilted force load within the longitudinal cross-section plane;
(4) a torque around the vertical axis;
(5) a tilted force load acting orthogonally to the longitudinal cross-section plane;
(6) a torque load acting orthogonally to the longitudinal cross-section plane;

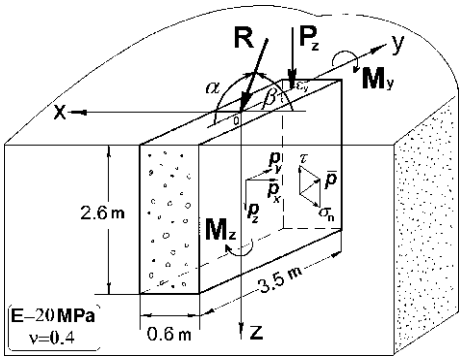

Fig. G.1 Calculation scheme at spatial loads of a slotted foundation with a rectangular longitudinal cross-section

(7) a combined action of a central vertical force and a tilting moment, acting orthogonally to the longitudinal cross-section plane (a vertical load with an eccentricity in the lateral direction)

which are typical for calculations of bases for deformations under the main combinations of loads when the above-foundation constructions transmit, in general case, tilted forces and torques onto the slotted foundations.

At the chosen coordinate system on the lateral surface of the slotted foundation the normal stress are $\sigma_n = \pm p_x$, and the tangential stress vector lies within the contact surface (Fig. G.1).

Figures G.2–G.15 represent isolines of dimensionless contact stress:

(a) normal $\overline{\sigma}_n = \sigma_n / p_{av}$,
(b) tangential $\overline{\tau} = \tau / p_{av}$,
(c) horizontal $\overline{p}_y = p_y / p_{av}$,
(d) vertical $\overline{p}_z = p_z / p_{av}$.

As a scale factor for the contact stress the average pressure $p_{av} = 10$ kN/$S_f = 42.69$ kN/m was used where $S_f = 23.42$ m^2 is the area of the foundation and soil contact surface.

Taking into account the fact that in the case of the above listed (1)–(4) type loads the medial longitudinal cross-section is a symmetry plane in the calculation scheme, the isolines of the contact stress on the lateral faces will be symmetric or skew symmetric, and, hence, for these cases only the calculation results for the slotted foundation face $x = 0.3$ m are given (Figs. G.2, G.3, G.10–G.15).

For the case of (5)–(7) type loads the medial longitudinal cross-section is not a symmetry plane in the calculation scheme, and the spatial stressed states of the base are symmetric only with respect to the medial lateral cross-section; hence, the isolines of the contact stress are given for both lateral faces of the slotted foundation at $x = \pm 0.3$ m (Figs. G.4–G.9).

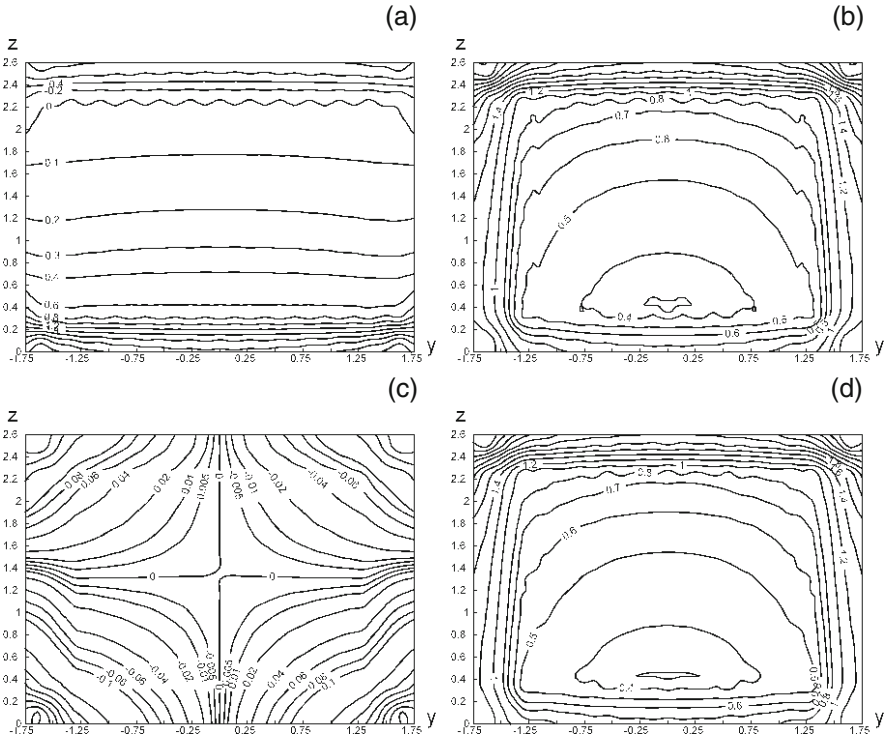

Fig. G.2 Contact normal σ_n/p_{pv} (**a**), tangential τ/p_{av} (**b**), horizontal p_y/p_{av} (**c**), and vertical p_z/p_{av} (**d**) stresses at the lateral surface of a slotted foundation ($x = 0.3$ m) under a central vertical force $P_z = 10^3$ kN

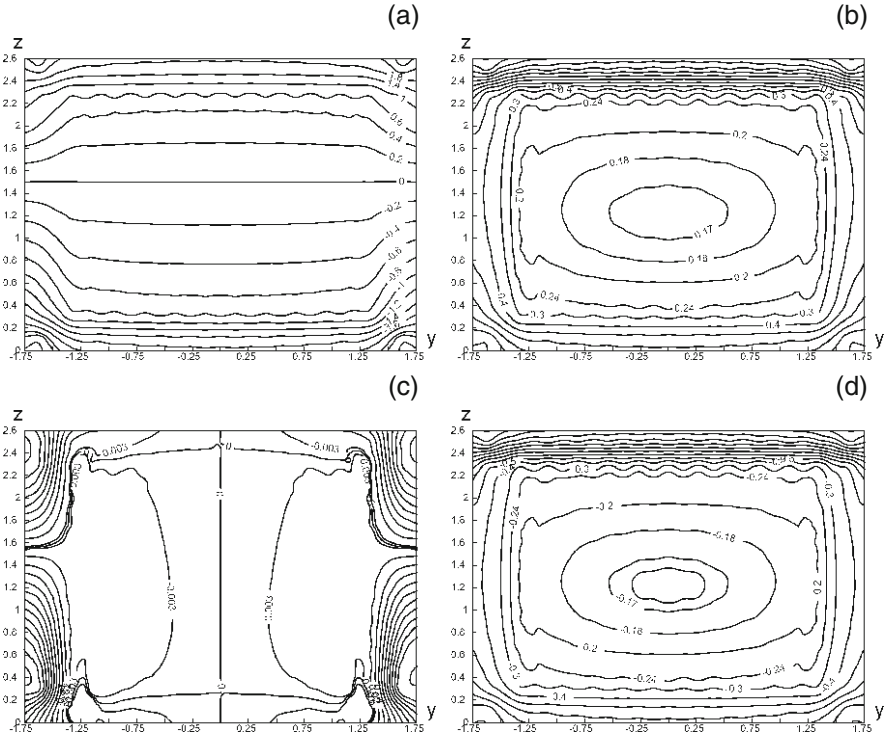

Fig. G.3 Contact normal σ_n/p_{pv} (**a**), tangential τ/p_{av} (**b**), horizontal p_y/p_{av} (**c**), and vertical p_z/p_{av} (**d**) stresses at the lateral surface of a slotted foundation ($x = 0.3$ m) under the action of a tilting moment $M_y = 1.4{\cdot}10^3$ kN·m

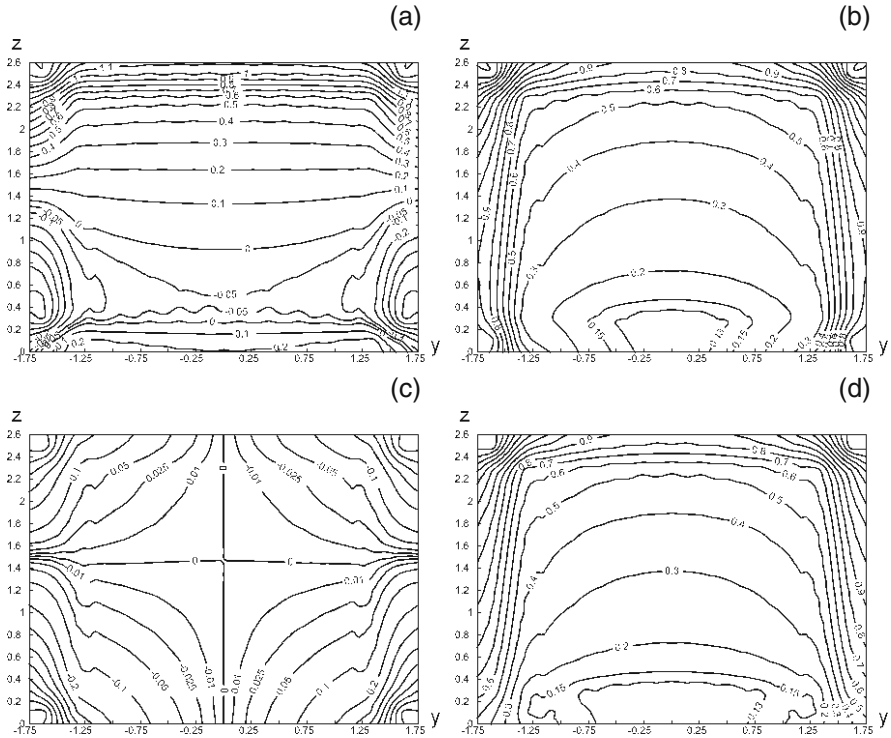

Fig. G.4 Contact normal σ_n/p_{pv} (**a**), tangential τ/p_{av} (**b**), horizontal p_y/p_{av} (**c**), and vertical p_z/p_{av} (**d**) stresses at the lateral surface of a slotted foundation ($x = 0.3$ m) under the combined action of a force and a torque load, $P_z = 10^3$ kN, $M_y = 0.7{\cdot}10^3$ kN·m

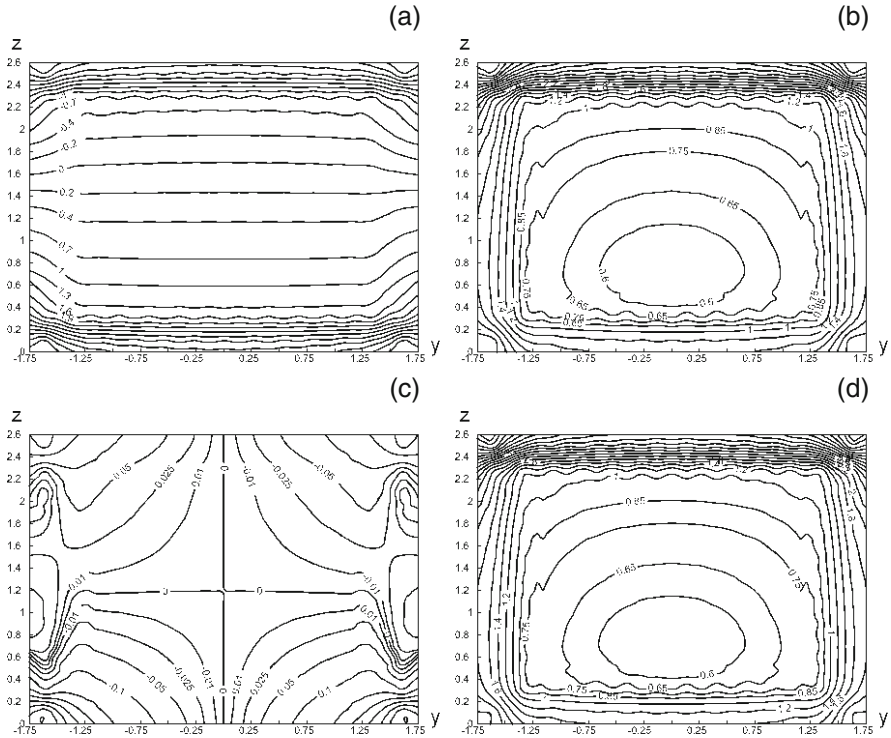

Fig. G.5 Contact normal σ_n/p_{pv} (**a**), tangential τ/p_{av} (**b**), horizontal p_y/p_{av} (**c**), and vertical p_z/p_{av} (**d**) stresses at the lateral surface of a slotted foundation ($x = –0.3$ m) under the combined action of a force and a torque load, $P_z = 10^3$ kN, $M_y = 0.7 \cdot 10^3$ kN·m

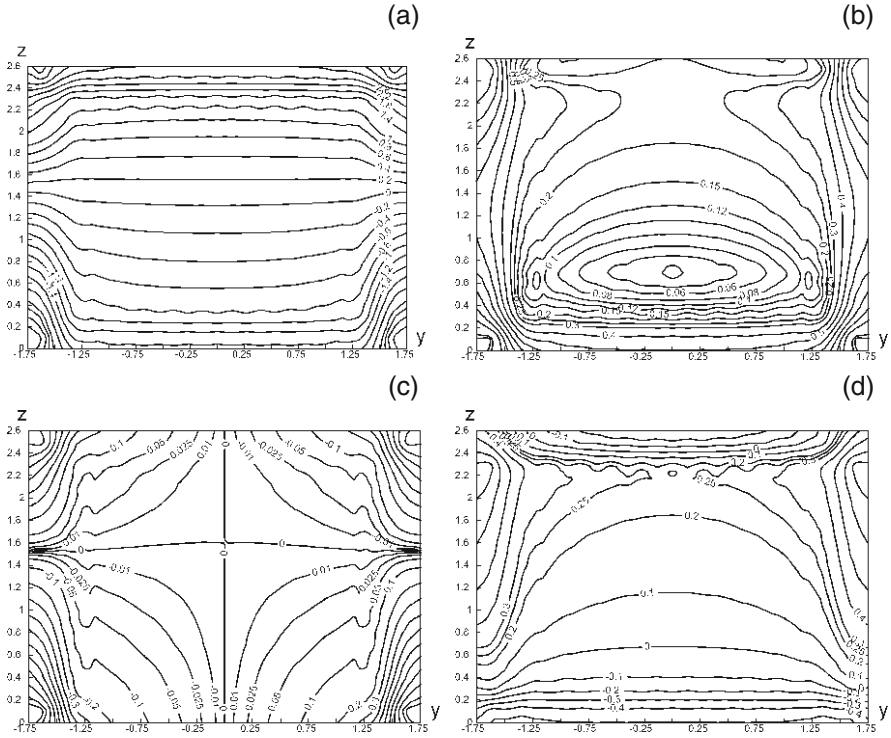

Fig. G.6 Contact normal σ_n/p_{pv} (**a**), tangential τ/p_{av} (**b**), horizontal p_y/p_{av} (**c**), and vertical p_z/p_{av} (**d**) stresses at the lateral surface of a slotted foundation ($x = 0.3$ m) under the combined action of a force and a torque load, $P_z = 10^3$ kN, $M_y = 1.4{\cdot}10^3$ kN·m

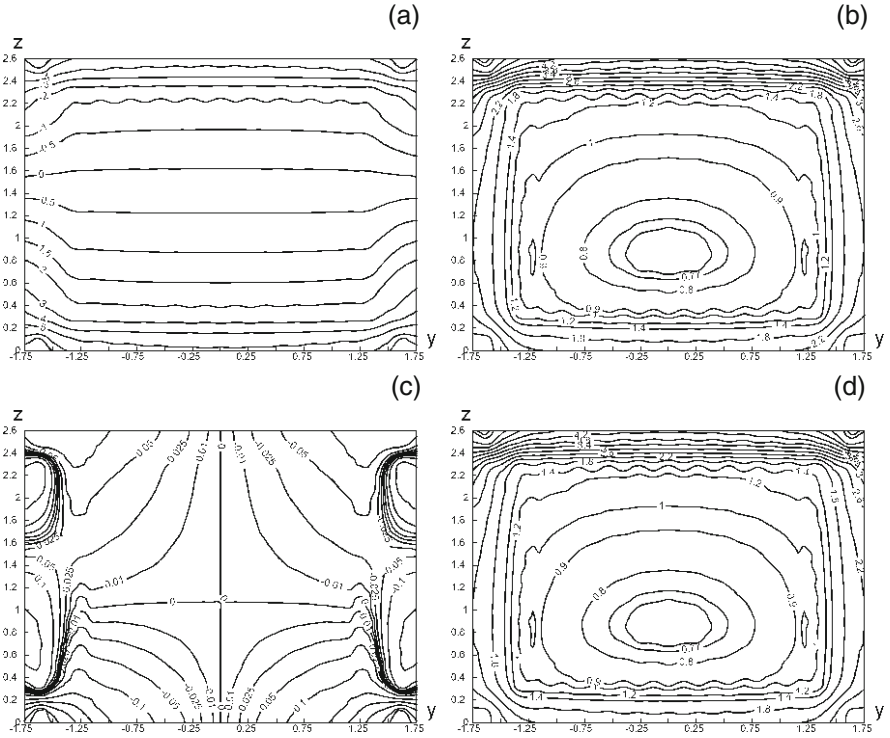

Fig. G.7 Contact normal σ_n/p_{pv} (**a**), tangential τ/p_{av} (**b**), horizontal p_y/p_{av} (**c**), and vertical p_z/p_{av} (**d**) stresses at the lateral surface of a slotted foundation ($x = –0.3$ m) under the combined action of a force and a torque load, $P_z = 10^3$ kN, $M_y = 1.4{\cdot}10^3$ kN·m

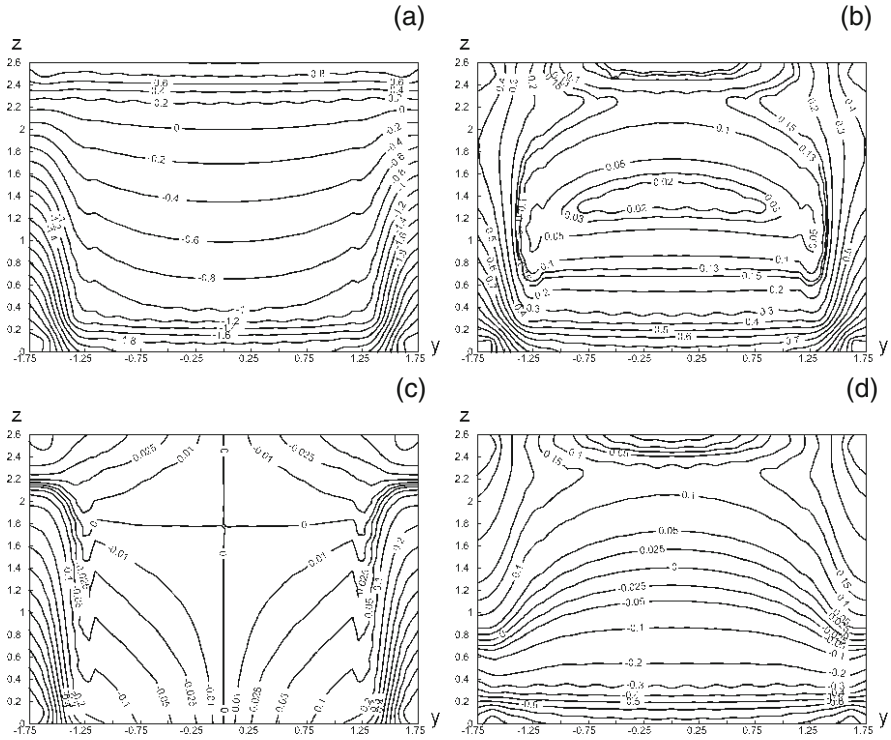

Fig. G.8 Contact normal σ_n/p_{pv} (**a**), tangential τ/p_{av} (**b**), horizontal p_y/p_{av} (**c**), and vertical p_z/p_{av} (**d**) stresses at the lateral surface of a slotted foundation ($x = 0.3$ m) under a tilting force $R = 10^3$kN, $\beta = 135°$ normally to the longitudinal cross-section plane

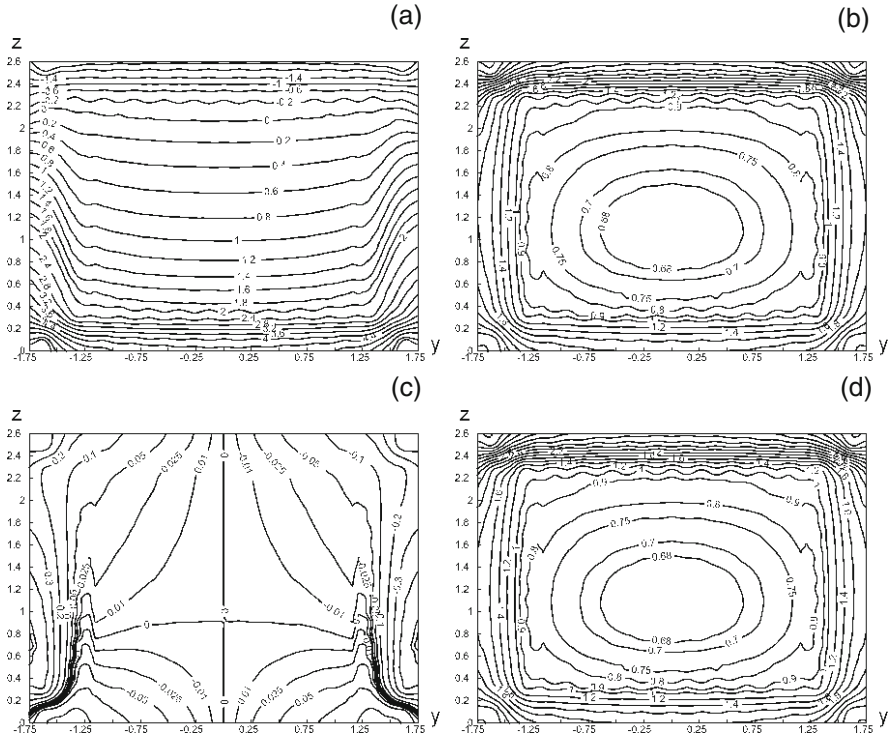

Fig. G.9 Contact normal σ_n/p_{pv} (**a**), tangential τ/p_{av} (**b**), horizontal p_y/p_{av} (**c**), and vertical p_z/p_{av} (**d**) stresses at the lateral surface of a slotted foundation ($x = -0.3$ m) under a tilting force $R = 10^3$kN, $\beta = 135°$ normally to the longitudinal cross-section plane

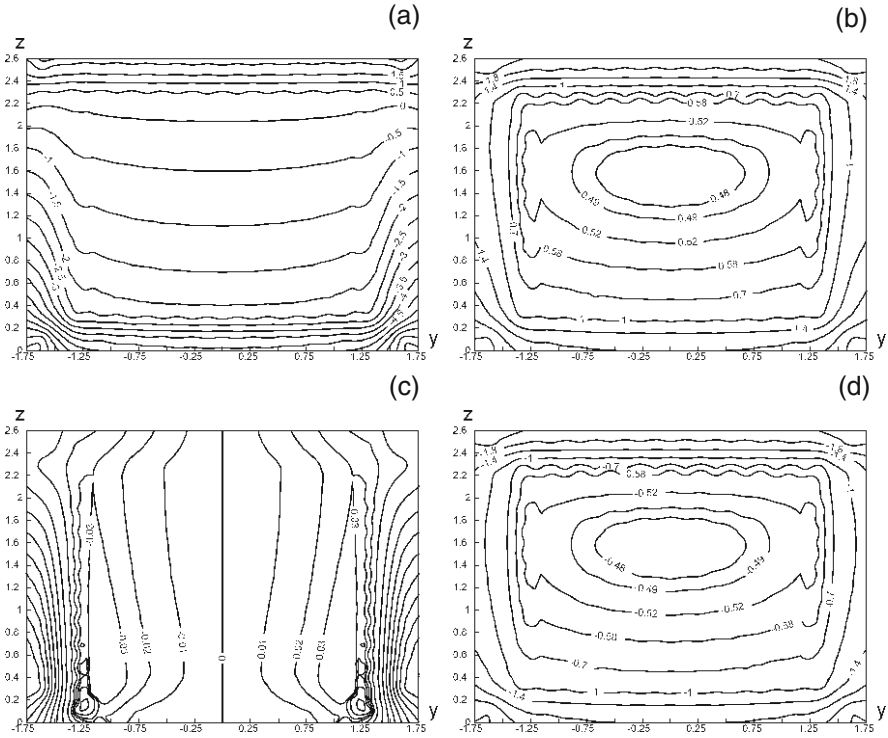

Fig. G.10 Contact normal σ_n/p_{pv} (**a**), tangential τ/p_{av} (**b**), horizontal p_y/p_{av} (**c**), and vertical p_z/p_{av} (**d**) stresses at the lateral surface of a slotted foundation ($x = 0.3$ m) under a horizontal force $R = 10^3$kN, $\beta = 180°$ normally to the longitudinal cross-section plane

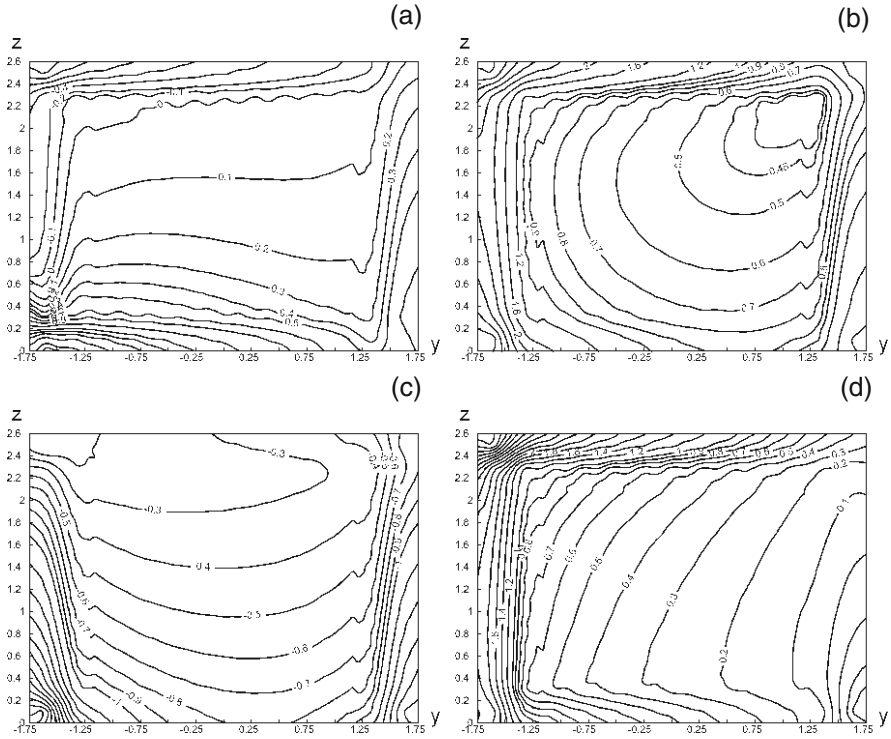

Fig. G.11 Contact normal σ_n/p_{pv} (**a**), tangential τ/p_{av} (**b**), horizontal p_y/p_{av} (**c**), and vertical p_z/p_{av} (**d**) stresses at the lateral surface of a slotted foundation ($x = 0.3$ m) under a tilting force $R = 10^3$kN within the longitudinal cross-section plane; $\alpha = 135°$

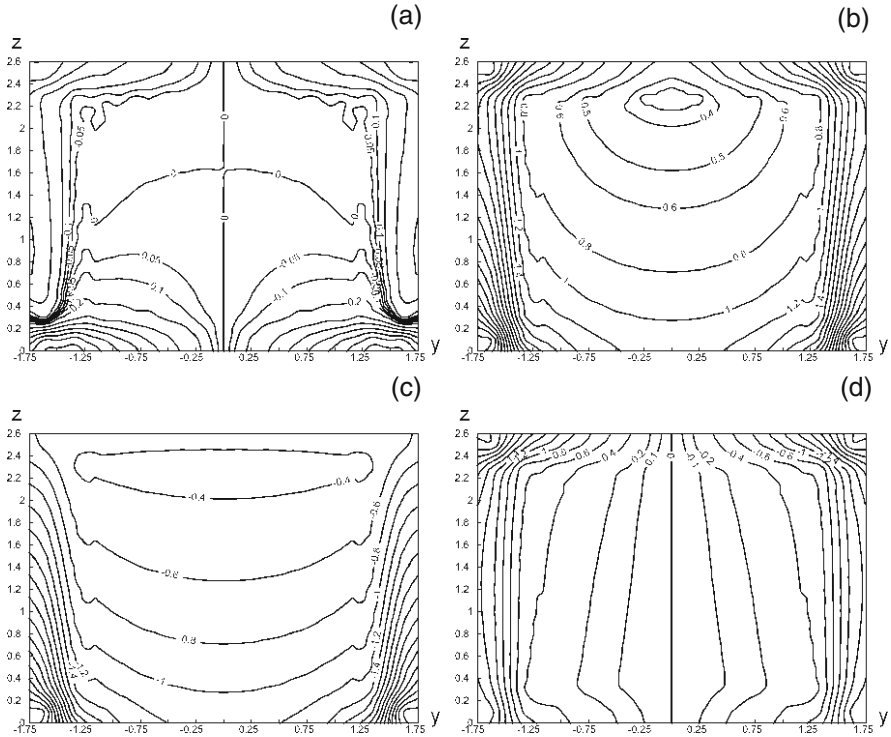

Fig. G.12 Contact normal σ_n/p_{pv} (**a**), tangential τ/p_{av} (**b**), horizontal p_y/p_{av} (**c**), and vertical p_z/p_{av} (**d**) stresses at the lateral surface of a slotted foundation ($x = 0.3$ m) under a tilting force $R = 10^3$kN within the longitudinal cross-section plane; $\alpha = 180°$

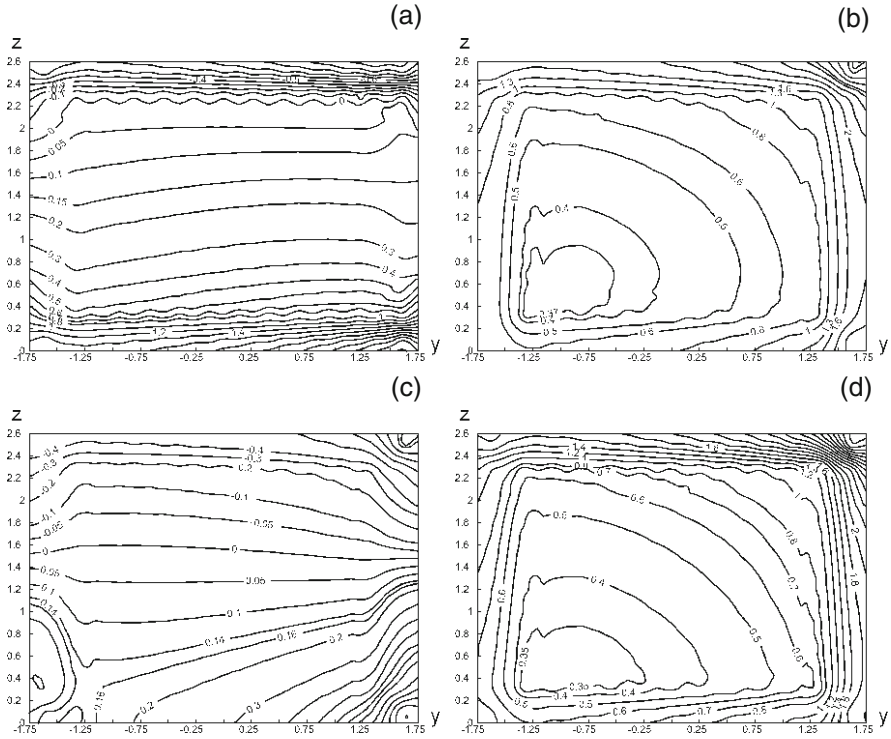

Fig. G.13 Contact normal σ_n/p_{pv} (**a**), tangential τ/p_{av} (**b**), horizontal p_y/p_{av} (**c**), and vertical p_z/p_{av} (**d**) stresses at the lateral surface of a slotted foundation ($x = 0.3$ m) under an eccentric vertical force $P_z = 10^3$ kN; $\varepsilon_y = -0.7$ m

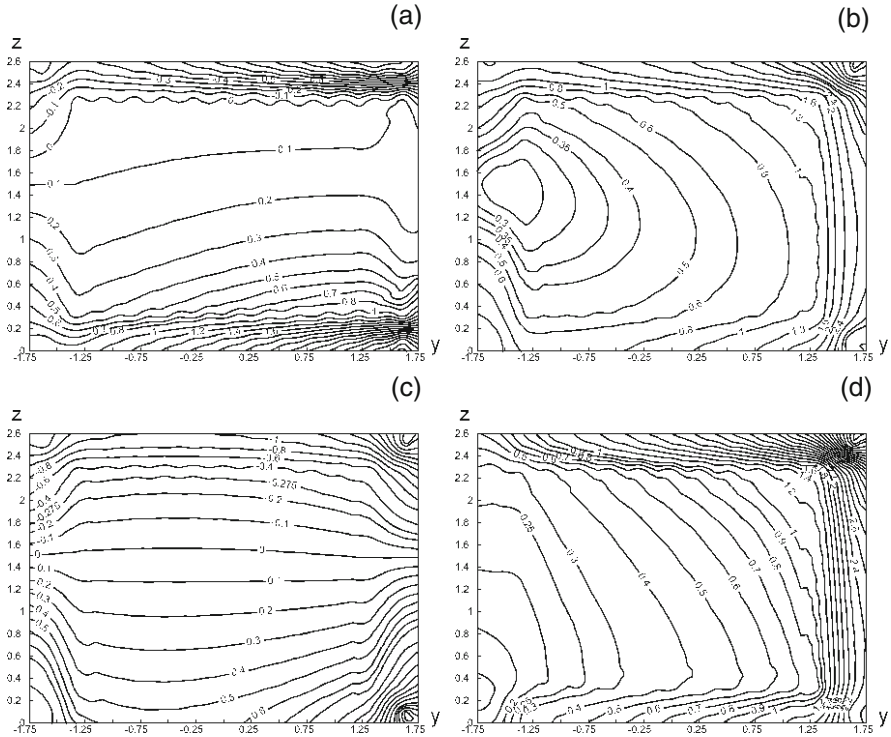

Fig. G.14 Contact normal σ_n/p_{pv} (**a**), tangential τ/p_{av} (**b**), horizontal p_y/p_{av} (**c**), and vertical p_z/p_{av} (**d**) stresses at the lateral surface of a slotted foundation ($x = 0.3$ m) under an eccentric vertical force $P_z = 10^3$ kN; $\varepsilon_y = -1.4$ m

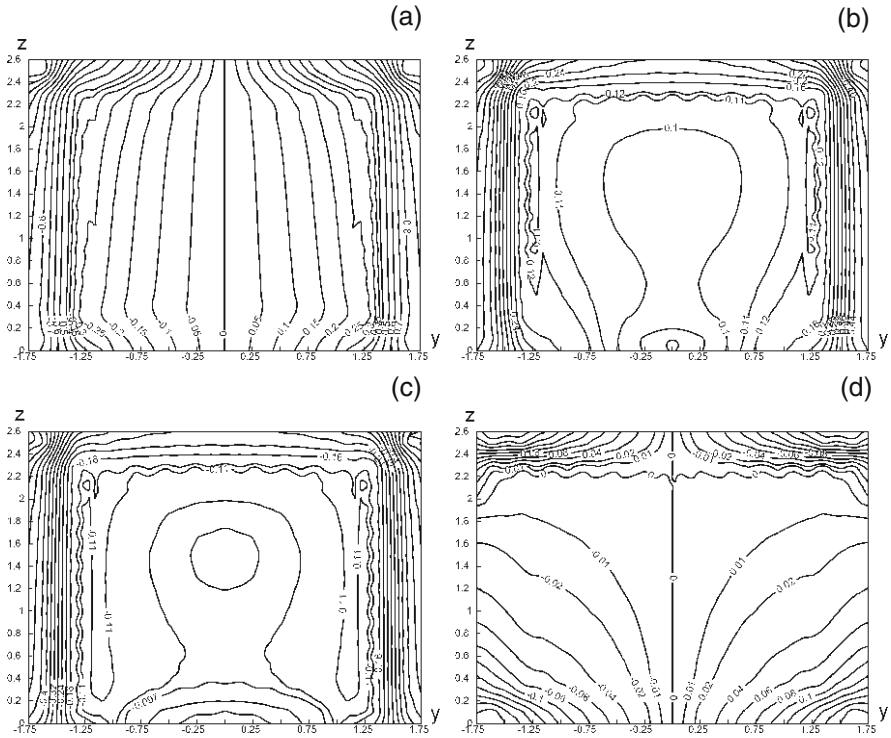

Fig. G.15 Contact normal σ_n/p_{pv} (**a**), tangential τ/p_{av} (**b**), horizontal p_y/p_{av} (**c**), and vertical p_z/p_{av} (**d**) stresses at the lateral surface of a slotted foundation ($x = 0.3$ m) under the action of a torque $M_z = 0.5{\cdot}10^3$ kN·m

Appendix H
Numeric Schemes of Volume Integration

The volume integrals contained in the integral representations of Chap. 6 are finally reduced to the integrals of the form

$$\iiint\limits_V P(x,y,z)\epsilon_V(x,y,z)dV = \iiint\limits_V f(x_1,x_2,x_3)dV \tag{H.1}$$

which, as a rule, cannot be calculated analytically due to a complicated form of the integrands and the intervals of integration. Since in this case the integrand functions remain limited in the corresponding ranges, i.e. all the volume integrals under consideration do not contain singular parts, one does not need to use any special regularization techniques, and the integration can be performed numerically.

In order to calculate the integrals of the form of Eq. (H.1) in the point $K(\xi, \eta, \zeta) \notin V$ we perform a discretization of the interval V to elementary volumes $\Delta V_i, i = \overline{1,n}$. Further we assume the global interval V of a sufficiently arbitrary shape to be presented with any degree of accuracy as a combination of a finite number of pyramids, triangular and quadrangular prisms. Some details of such representation were considered in Sect. 6.4. Besides, we consider that in the vertices of the elementary volumes (the nodes of the spatial network) the integrand function values are known or can be rather easily calculated. Each of the elementary volumes under consideration admits transformation into canonical elements with standard integration limits. Figure H.1 presents three types of spatial basic elements with the introduced system of local coordinates ℓ_1,ℓ_2,ℓ_3, used at the numerical integration. Equation (H.1) is transformed in the local coordinates to the form [8, 10]

$$\iiint\limits_V f(x_1,x_2,x_3)dV = \sum_j \iiint\limits_{\Delta V_j} \tilde{f}\ell_1,\ell_2,\ell_3)fracD(x_1,x_2,x_3)D(\ell_1,\ell_2,\ell_3)d\ell_1\ d\ell_2\ d\ell \tag{H.2}$$

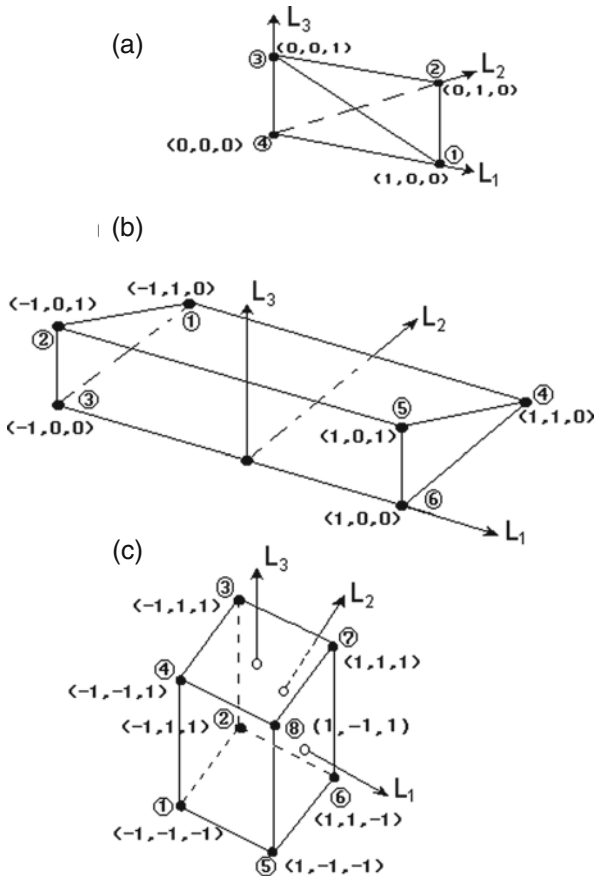

Fig. H.1 Three types of canonical volume elements

$$J(x,\ell) = \frac{D(x_1,x_2,x_3)}{D(\ell_1,\ell_2,\ell_3)} = \begin{vmatrix} \frac{\partial x}{\partial \ell_1} & \frac{\partial x}{\partial \ell_2} & \frac{\partial x}{\partial \ell_3} \\ \frac{\partial y}{\partial \ell_1} & \frac{\partial y}{\partial \ell_2} & \frac{\partial y}{\partial \ell_3} \\ \frac{\partial z}{\partial \ell_1} & \frac{\partial z}{\partial \ell_2} & \frac{\partial z}{\partial \ell_3} \end{vmatrix} = \begin{vmatrix} G_1 & G_2 & G_3 \\ G_4 & G_5 & G_6 \\ G_7 & G_8 & G_9 \end{vmatrix} =$$

$$= G_1(G_5G_9 - G_8G_6) - G_2(G_4G_9 - G_7G_6) + G_3(G_4G_8 - G_7G_5)$$

where ΔV_i is the standard volume, $J(x,\ell)$ is the transformation Jacobian.

Since the procedure of the volume integral calculation should be optimized, we assume the integrand function to vary linearly at each element. The use of a quadratic or cubic approximation results in a considerable increase of the number of nodes at each element. This, in turn, due to the complicated form of the integrand

function and a great number of calls to them, leads to a considerable increase of the computation time. Then the accuracy, required for the practical purposes, will be achieved for the expense of the increase of the integration interval discretization degree, as a rule, by an adaptive increase of the calculation network density at the sections with higher gradients.

Thus, we restrict ourselves to the linear isoparametric volume elements for which the geometrical and functional nodes coincide. Global Cartesian coordinates of any internal points of the element and integrand functions are presented by an expansion over the same basis functions $N^\alpha(\ell_i)$

$$x_i(\ell_i) = \sum_{\alpha=1}^{\rho} N^\alpha(\ell_i) \cdot X_i^\alpha \ ,$$
$$f(\ell_i) = \sum_{\alpha=1}^{\rho} N^\alpha(\ell_i) \cdot f_\alpha \ , \quad i = 1,2,3$$

where X_i^α are the geometric node coordinates, f_α are the functional values in the nodes, ρ is the number of nodes of the isoparametric element.

Here we give the detailed expressions for the basic functions and Jacobians for the three types of volume elements most often used in practice (Fig. H.1) as well as present the formulae for the transition from the corresponding triple integrals to the iterated integrals included into the software elaborated.

Tetrahedral element, $\rho = 4$ (Fig. H.1a)

$$N_\alpha = \ell_\alpha \qquad (\alpha = 1,2,3,4)$$

where $0 \le \ell_\alpha \le 1$ are the space coordinates,

$$\ell_1 + \ell_2 + \ell_3 + \ell_4 = 1 \quad (\text{or } \ell_4 = 1 - \ell_1 - \ell_2 - \ell_3) \ ,$$
$$x = \ell_1 X^1 + \ell_2 X^2 + \ell_3 X^3 + (1 - \ell_1 - \ell_2 - \ell_3) X^4 \ ,$$
$$y = \ell_1 Y^1 + \ell_2 Y^2 + \ell_3 Y^3 + (1 - \ell_1 - \ell_2 - \ell_3) Y^4 \ ,$$
$$z = \ell_1 Z^1 + \ell_2 Z^2 + \ell_3 Z^3 + (1 - \ell_1 - \ell_2 - \ell_3) Z^4 \ ,$$
$$\frac{\partial N_\alpha}{\partial \ell_i} = \delta_{\alpha i} \ ; \qquad \frac{\partial N_4}{\partial \ell_i} = -1 \ ,$$
$$G_1 = X^1 - X^4 \ , \quad G_2 = X^2 - X^4 \ , \quad G_3 = X^3 - X^4 \ ,$$
$$G_4 = Y^1 - Y^4 \ , \quad G_5 = Y^2 - Y^4 \ , \quad G_6 = Y^3 - Y^4 \ ,$$
$$G_7 = Z^1 - Z^4 \ , \quad G_8 = Z^2 - Z^4 \ , \quad G_9 = Z^3 - Z^4 \ ,$$
$$\frac{D(x_1,x_2,x_3)}{D(\ell_1,\ell_2,\ell_3)} = \begin{vmatrix} X^1 - X^4 & X^2 - X^4 & X^3 - X^4 \\ Y^1 - Y^4 & Y^2 - Y^4 & Y^3 - Y^4 \\ Z^1 - Z^4 & Z^2 - Z^4 & Z^3 - Z^4 \end{vmatrix} = \text{mes } \Delta V_j \ ,$$

$$
\begin{aligned}
&= \iiint_{\Delta V_j} g(\ell_1,\ell_2,\ell_3)d\ell_1 d\ell_2 d\ell_3 = \int_0^1 d\ell_1 \int_0^{1-\ell_1} d\ell_2 \int_0^{1-\ell_1-\ell_2} g(\ell_1,\ell_2,\ell_3)d\ell_3 = \\
&\int_0^1 (1-\ell_1)^2 d\ell_1 \int_0^1 (1-\ell_2')d\ell_2' \int_0^1 g(\ell_1,\ell_2,\ell_3)d\ell_3' = \\
&= \left(\frac{1}{2}\right)^6 \int_{-1}^1 (1-\ell_1')^2 d\ell_1' \int_{-1}^1 (1-\ell_2'')d\ell_2'' \int_{-1}^1 g(\ell_1,\ell_2,\ell_3)d\ell_3'' = \\
&= \left(\frac{1}{2}\right)^6 \iiint_{\Omega} (1-\ell_1')^2(1-\ell_2'')g(\ell_1,\ell_2,\ell_3)d\ell_1' d\ell_2'' d\ell_3''
\end{aligned}
\tag{H.3}
$$

where Ω is a standard (unit) cube,

$$
g(\ell_1,\ell_2,\ell_3) = V_j \cdot \bar{f}(\ell_1,\ell_2,\ell_3)\ , \ell_1 = \frac{1}{2}(1+\ell_1')\ , \quad \ell_2 = \frac{1}{4}(1-\ell_1')(1+\ell_2'')\ ,
$$
$$
\ell_3 = \frac{1}{8}(1-\ell_1')(1-\ell_2''^2)\ .
$$

Triangular-prismatic element, $\rho = 6$ (Fig. H.1b),

$$
\begin{aligned}
N_1 &= \frac{1}{2}(1-\ell_1)\ell_2\ , \\
N_2 &= \frac{1}{2}(1-\ell_1)\ell_3\ , \\
N_3 &= \frac{1}{2}(1-\ell_1)(1-\ell_2-\ell_3)\ , \\
N_4 &= \frac{1}{2}(1+\ell_1)\ell_2\ , \\
N_5 &= \frac{1}{2}(1+\ell_1)\ell_3\ , \\
N_6 &= \frac{1}{2}(1+\ell_1)(1-\ell_2-\ell_3)\ , \\
&-1 \le \ell_1 \le 1\ , \quad 0 \le \ell_2\ , \quad \ell_3 \le 1\ . \\
x &= N_1X^1 + N_2X^2 + N_3X^3 + N_4X^4 + N_5X^5 + N_6X^6\ , \\
y &= N_1Y^1 + N_2Y^2 + N_3Y^3 + N_4Y^4 + N_5Y^5 + N_6Y^6\ , \\
z &= N_1Z^1 + N_2Z^2 + N_3Z^3 + N_4Z^4 + N_5Z^5 + N_6Z^6\ , \\
\frac{\partial N_1}{\partial \ell_1} &= \frac{\partial N_4}{\partial \ell_1} = \frac{1}{2}\ell_2\ , \\
\frac{\partial N_1}{\partial \ell_2} &= \frac{\partial N_4}{\partial \ell_3} = -\frac{\partial N_3}{\partial \ell_2} = -\frac{\partial N_3}{\partial \ell_3} = \frac{1}{2}(1-\ell_1)\ , \\
\frac{\partial N_1}{\partial \ell_3} &= \frac{\partial N_2}{\partial \ell_2} = -\frac{\partial N_4}{\partial \ell_3} = -\frac{\partial N_5}{\partial \ell_2} = 0\ ,
\end{aligned}
\tag{H.4}
$$

$$\frac{\partial N_2}{\partial \ell_1} = -\frac{\partial N_5}{\partial \ell_1} = -\frac{1}{2}\ell_3 \,,$$
$$\frac{\partial N_3}{\partial \ell_1} = -\frac{\partial N_6}{\partial \ell_1} = -\frac{1}{2}(1-\ell_2-\ell_3) \,,$$
$$\frac{\partial N_4}{\partial \ell_2} = \frac{\partial N_5}{\partial \ell_3} = -\frac{\partial N_6}{\partial \ell_2} = -\frac{\partial N_6}{\partial \ell_3} = \frac{1}{2}(1+\ell_1) \,,$$
$$\iiint\limits_{\Delta V_j} \tilde{f}(\ell_1,\ell_2,\ell_3)\frac{D(x_1,x_2,x_3)}{D(\ell_1,\ell_2,\ell_3)}d\ell_1 d\ell_2 d\ell_3 = \iiint\limits_{\Delta V_j} g(\ell_1,\ell_2,\ell_3)d\ell_1 d\ell_2 d\ell_3 =$$
$$= \int\limits_{-1}^{1} d\ell_1 \int\limits_{-1}^{1} d\ell_2 \int\limits_{-1}^{1-\ell_2} g(\ell_1,\ell_2,\ell_3)d\ell_3 = \frac{1}{8}\int\limits_{-1}^{1} d\ell_1 \int\limits_{-1}^{1}(1-\ell_2')d\ell_2' \int\limits_{-1}^{1} g(\ell_1,\ell_2,\ell_3)d\ell_3' =$$
$$\frac{1}{8}\iiint\limits_{\Omega}(1-\ell_2')g(\ell_1,\ell_2,\ell_3)d\ell_1 d\ell_2' d\ell_3' \tag{H.4}$$

where $\ell_2 = \frac{1}{2}(1+\ell_2')$; $\quad \ell_3 = \frac{1}{4}(1+\ell_3')(1-\ell_2')$.

Hexahedral element, $\rho = 8$ (Fig. H.1c)

$$N_\alpha = \frac{1}{8}(1+S_{\alpha 1}\ell_1)(1+S_{\alpha 2}\ell_2)(1+S_{\alpha 3}\ell_3) \,, \quad \alpha = 1,2,...,8.$$

$$\|S_{\alpha i}\| = \begin{bmatrix} -1\,, & -1\,, & -1 \\ -1\,, & 1\,, & -1 \\ -1\,, & 1\,, & 1 \\ -1\,, & -1\,, & 1 \\ 1\,, & -1\,, & -1 \\ 1\,, & 1\,, & -1 \\ 1\,, & 1\,, & 1 \\ 1\,, & -1\,, & 1 \end{bmatrix} \text{ arethei} - \text{th uniform coordinates of the node} \alpha,$$

$$-1 \le \ell_1,\ell_2,\ell_3 \le 1 \,,$$
$$x = N_1X^1 + N_2X^2 + \quad \ldots \quad + N_8X^8 \,,$$
$$y = N_1Y^1 + N_2Y^2 + \quad \ldots \quad + N_8Y^8 \,,$$
$$z = N_1Z^1 + N_2Z^2 + \quad \ldots \quad + N_8Z^8 \,,$$
$$\frac{\partial N_\alpha}{\partial \ell_1} = \frac{S_{\alpha 1}}{8}(1+S_{\alpha 2}\ell_2)(1+S_{\alpha 3}\ell_3) \,,$$
$$\frac{\partial N_\alpha}{\partial \ell_2} = \frac{S_{\alpha 2}}{8}(1+S_{\alpha 1}\ell_1)(1+S_{\alpha 3}\ell_3) \,,$$

$$\frac{\partial N_\alpha}{\partial \ell_3} = \frac{S_{\alpha 3}}{8}(1 + S_{\alpha 1}\ell_1)(1 + S_{\alpha 2}\ell_2)\,,$$

$$\iiint\limits_{\Delta V_j} \bar{f}(\ell_1,\ell_2,\ell_3)\frac{D(x_1,x_2,x_3)}{D(\ell_1,\ell_2,\ell_3)}d\ell_1\, d\ell_2\, d\ell_3 = \iiint\limits_{\Delta V_j} g(\ell_1,\ell_2,\ell_3)d\ell_1\, d\ell_2\, d\ell_3 =$$

$$= \int\limits_{-1}^{1} d\ell_1 \int\limits_{-1}^{1} d\ell_2 \int\limits_{-1}^{1} g(\ell_1,\ell_2,\ell_3)d\ell_3 = \iiint\limits_{\omega} g(\ell_1,\ell_2,\ell_3)d\ell_1\, d\ell_2\, d\ell_3$$

The integrals of Eq. (H.3)–(H.5) are reduced to the same canonical form with the unit integration limits admitting multiplicative approximation [8, 10]

$$\int\limits_{-1}^{1}\int\limits_{-1}^{1}\int\limits_{-1}^{1} F(q_1,q_2,q_3)dq_1\, dq_2\, dq_3 = \sum_{i=1}^{n}\sum_{j=1}^{m}\sum_{k=1}^{p} w_i^{(n)} w_j^{(m)} w_k^{(p)} F(q_{1i}^{(n)},q_{2j}^{(m)},q_{3k}^{(p)})$$

where (q_{1i}, q_{2j}, q_{3k}) are coordinates of the nodes whose location is determined by the type of the integration formula applied, and w_i, w_j, w_k are the corresponding weight factors. As known from [10], the greatest effect is achieved by the application of the Gauss formulae, enabling the number of integration points to be essentially reduced. This gives the required achievement of the given calculation accuracy with a simultaneous reduction of the machine time. Due to the regularity of the integrals under consideration we used in our calculations the nodes and weights of the two-point Gaussian quadrature formula $q^{(1)} = -q^{(2)} = 0.5773503$, $w^{(1)} = w^{(2)} = 1.0$, providing exact integration of the third-order polynomials. The number of the integration points over each coordinate is assumed to be the same ($n = m = p = 2$) and the integrand should be calculated in eight points. Besides, note that at large-scale calculations of the volume integrals the presence of the unit weight factors in the quadrature used enables the number of arithmetic actions to be to a certain extent reduced and the total calculation uncertainty to be lowered.

References

1. Abramowitz M, Stegun I A (1972) Handbook of mathematical functions with formulas, graphs, and mathematical tables, 10th edn. Dover, New York
2. Aleynikov S M (1996) Ring-shaped foundation with an internal cut-off circle. In: Calculation and design of bases and foundations at complex geotechnical conditions. VGASA, Voronezh, pp. 9−16 (in Russian)
3. Aleynikov S M, Belozerov V A (1999) Ring-shaped foundation under tower-type constructions on a wedge-shaped base. Patent 2135694 RU, MPK^6 E 02 D 27/42.No. 98102534/03 (Russia)
4. Aleynikov S M, Ikonin S V (1998) Reinforcement of a potable water reservoir by means of piles. In: Proc. 6th Intern Conf Pile Found Eng, vol. 4. Reinforcement of bases and foundations under the reconstruction of buildings. RNKMGIF, Moscow, pp. 5−10 (in Russian)
5. Aleynikov S M, Nekrasova N N (1992) Numerical calculations of orthotropic plates on a variable-thickness elastic base. In: Calculation and design of bases and foundations at complex geotechnical conditions. VISI, Voronezh, pp. 22–31 (in Russian)

6. Aleynikov S M, Nekrasova N N (1996) Bending of otrhotropic foundation plates resting on elastic nonclassical bases. Izv Vuzov Stroit (issue 9): 65–71 (in Russian)
7. Aleynikov S M, Nekrasova N N (1996) Contact problem for orthotropic foundation slabs with consideration of deformation peculiarities of spatial and nonhomogeneous bases. Studia Geotechnica et Mechanica 20: 63–104
8. Altenbach J, Sacharov A S (eds) (1982) Die Methode der Finiten Elemente in der Festkörpermechanik. Fachbuchverlag, Leipzig
9. Bakhvalov N S (1973) Numerical methods, vol. 1. Nauka, Moscow (in Russian)
10. Banerjee P K, Butterfield R (1981) Boundary element methods in engineering science. McGraw-Hill, New York
11. Brebbia C A, Walker S (1980) Boundary element techniques in engineering. Newnes-Butterworths, London
12. Brebbia C, Telles J, Wrobel L (1984) Boundary element techniques. Springer-Verlag, Berlin
13. Cowper G R (1973) Gaussian quadrature formulas for triangles. Intern J Num Method Eng 7: 405–408
14. Engels H (1980) Numerical quadrature and cubature. Academic Press, London/New York
15. Gorbunov-Posadov M I, Malikova T A, Solomin V I (1984) Calculation of structures on an elastic base. Stroyizdat, Moscow (in Russian)
16. Hammer P C, Marlowe O P, Stroud A H (1956) Numerical integration over simplexes and cones. Math Tables Aids Comp 10: 130–137
17. Instructions on design of pyramidal pile foundations (1983) Glavn Upr Project Organiz, Moscow (in Russian)
18. Kiselev V A (1973) Calculation of plates. Stroyizdat, Moscow (in Russian)
19. Klokov Yu A, Shkerstena A Ya (1986) Numerical integration of functions using interpolational polynomials of Chebyshev type. Latvian Math Annual 30: 207–217 (in Russian)
20. Korn G A, Korn T M (1961) Mathematical handbook for scientists and engineers. McGraw-Hill, New York
21. Kronrod A S (1965) Nodes and weights of quadrature formulas. Consultants Bureau, New York
22. Krylov V I, Shulgina L T (1966) Handbook on numerical analysis. Nauka, Moscow (in Russian)
23. Li H B, Han G M, Mang H A (1986) Quadrature of singular integral in the direct BEM applied to tree-dimensional elasto-plasticity. Z Angew Math Mech 66: 314–316
24. Paszkowski S (1975) Zastosowania numerycne wielomianów i szeregów Czebyszewa. PWN, Warszawa
25. Shkerstena A Ya (1984) Interpolated Lagrange formulae, constructed from Chebyshev polynomial node. Latv Mathem Ann 28: 130–142 (in Russian)
26. Stroud A H, Secrest D (1966) Gaussian quadrature formulas. Prentice-Hall, Englewood Cliffs
27. Suyetin P K (1976) Classical orthogonal polynomials. Nauka, Moscow (in Russian)
28. Timoshenko S, Wojnowski-Krieger S (1959) Theory of plates and shells. McGraw-Hill, New York
29. Ugodchikov A G, Khutoryanskiy N M (1986) Boundary-element method in mechanics of deformable solids. Kazan State University, Kazan (in Russian)
30. Vasilyev N I, Klokov Yu A, Shkerstena A Ya (1984) Application of Chebyshev polynomials in numerical analysis. Zinatne, Riga (in Russian)
31. Zienkiewicz O C (1971) The finite element method in engineering science. McGraw-Hill, London

Index

A
Abramov effect, 257
Accuracy cubature formula, 562
Adaptive integration schemes, special, 75
Alpha piles, 387
Analytical-and-numerical integration method, 106
Analytical solutions, 109, 138, 197, 216, 242, 255, 257–259, 268, 334, 476, 512
Analytic language, 107
Anchor axial rigidity, 401
Anchor foundation plates, 224
Anchor structures, 387
Anisotropic properties of the soil, 238
Anisotropic strength conditions, 486
Anisotropy, 4, 263, 266, 277, 356, 398, 486, 507, 524
Approximate analytical solutions, 258
Artesian water, Japan, 506
Asymmetrical foundation structure, 435
Asymptotic methods of 'large and small λ', 261
Automatic boundary-element grid formation, 143
Axial rigidity, 400
Axisymmetric
  calculation scheme, 410
  contact problem, 125

B
Back fill, 426, 454
Backhoe, 456
Back pressure forces, 476
Bangkok, 506
Base deformations, 390, 394
Bases and rigid bored foundations, 424–437
  inclined piles and rectangular pile raft, 435–437
  structure, design, and specific features, 425–428
  vertical cylindrical piles, 428–435
Base settlements, determination of, 601, 603–604
BEM-based numerical modeling, 91
Bending moments, 216, 252–253, 271, 312, 315, 355–357, 359, 364, 367, 369, 371–372, 400, 425, 592
Berezantsev's formulae, 348
Bessel function, 14, 32–33, 52, 71, 204, 345
  first-order, 344
Betti's theorem, 92–93, 273, 518
Biharmonic Love function, 26
Block diagonalization, 146
Bored pile foundation, 187, 385, 389, 438–445, 447–454
Bored pile foundation with widening, 438–454
  deformations calculation, 443–448
  displacements calculation of and slopes, 448–454
  engineering methods for calculation, 441–443
  production and structures, 439–441
Botkin criterion, 411
Botkin dependence, 265
Botkin model, 271
Boundary-element
  algorithm, 109, 131, 136, 139, 197, 216, 229, 233, 242, 253, 300, 538–539, 566
  approach, 205, 223–224, 228, 243, 252, 276, 419, 454, 472, 475
  discretization, 98, 186, 192, 426
  grid, 171, 174, 176–177, 179–180, 183–184, 190, 195, 198, 203, 208, 222–223, 229, 232, 273, 279, 303, 305, 307, 444, 448, 458–459, 478

method (BEM), 1, 27, 52, 54, 82–93, 96, 98–101, 113, 118–119, 121, 123, 128, 131, 135–137, 151, 162–163, 167–168, 171, 174, 176, 192, 195–196, 202, 204–206, 216–217, 219, 225, 228–229, 233, 242–243, 251, 264, 272–277, 279, 311, 323, 334, 338, 354, 361, 372, 385, 389, 395, 399, 405, 417, 420, 422, 437, 445, 447, 459, 470–472, 474–476, 478, 511, 519, 534, 538–541
node, 106, 138, 190
plane, 106
polyhedron surface, 228
solution, characteristics of the, 194, 202
Boundary integral equations, 64, 91–96, 99, 106, 111, 116, 119–120, 146, 151, 162, 217, 272, 405, 522
numerical algorithms, 334–351
finite-measure analogue, 339–341
nonlinear contact equations, 337–338
nonlinear deformation effects, 348–351
nonlinearly deformable base, 335–337
round punch contact problem, 341–348
Boundary macroelement, 176–180, 184–186, 188–190, 192
Boundary node, 155, 163–164, 168
Boundary-superelement method, 146
Boussinesq-Cerruti solution, 12, 120, 131, 551
Boussinesq equation, 60, 274
Boussinesq fundamental solutions, 8
Boussinesq law, 399
Boussinesq solution, 7, 14, 16, 59, 65–66, 68, 76, 272–273, 342, 345, 399, 512, 523, 548
Bubnov-Galerkin type method, 262
Bulk deformation modulus, 265
Burmister solution, 17, 275

C

Cam-Clay model, 412
Canonical equations, 302, 362, 397, 399
Capacity-based calculations, 390
Carrying capacity, analysis of, 408
Cartesian coordinate system, 12, 28, 62, 92, 102, 105, 107, 110, 137, 176, 218, 542, 625
Cauchy principal value, 94
Cauchy relations, 94
Cerruti displacement functions, 127
Cerruti solution, 7–8, 127, 129
Chebyshev polynomials, 204, 562–565
Cinematic loading scheme, 271
Circular foundation bases, 269
Circular (or ring-shaped) punch, indentation of, 125
Circular punches, 128, 255, 259, 272
slopes, 286
smooth punches, 276
Clayey sands, 236
Coalinga oil field, 506
Coefficient matrix, 139, 144, 265, 418, 540
Cohesion parameters, 488
Collapsing, 357, 390–392, 410, 415
Collocation method, 97
Complex-shaped foundation, 188, 252, 294, 327, 538
rigid, 389
Complex-shaped punches, 91, 123, 163, 216, 251, 255, 295, 324, 339, 540
Compliance functions, 37
Compressed soil mass thickness, 286, 371
Compressibility effect, 50
Compression tests, 471
Computer-aided design, 146, 355, 539
Concrete mixture, 426, 493
Condensation subdomain, 155
Condensed zones (kernels) formation of, 441
Conditionality estimations, 363
Cone generatrix, 229–230, 232
Conical punches, 233, 235
Constant-width foundations (CWFs), 311, 312–315, 320
Construction Rules and Regulations
2.02.01–83, 388–390, 393–394, 405, 472, 474
2.02.03–85, 403, 411, 425
Contact deformation, semi-empirical models, 253
Contact friction, 277, 487–490, 539
parameters of, 406
Contact interaction characteristics, 279, 289, 371, 432, 450, 539
Contact models, development and analysis of, 539
Contact pressure
curve, 282
function, 121–122, 195, 257, 260, 262, 327, 337–338, 354
isolines, 203, 313
Contact problems for anchors, 401
Contact stress, determination of, 92, 258
Contact stress functions, 120, 274, 444, 519
Contact tangential stress functions, 127
Contact zones formation, 429

Correction and improvement of design regulations, 540
Coulomb fluidity, 408
Coulomb friction law, 406, 482
Coulomb strength law, 486
Coupled elastic half-spaces, 513
Coupled half-spaces, 8–12
Crack-proofness, 386, 392
Crank mechanisms, 393
Cross-shaped foundation, 328
  tests, 312, 315
Crushers, 180, 393
Cyclic discretization, 113, 118, 125, 130
Cylindrical coordinate system, 59, 61–62, 108, 110–111, 115, 184, 444
Cylindrical foundations, 186–187
Cylindrical punch, 224, 428
  axisymmetrical contact problem, 225

D

2-D and 3-D images, visualization of, 141
Darcy's equation, 509, 511
Deepening effect, 400, 409
Deep pile settlements, 406
Deflection isolines, 367
Deflection nonuniformity, 367
Deformable reservoirs, 508
Deformation-based calculation, 390, 392, 394, 403, 415–416, 447, 490–491
Deformation characteristics, 8, 56, 234, 242, 271–272, 278, 403, 405, 439, 445, 457, 471, 577–578, 585
Deformation components, 270
Deformation modulus, 1, 55–58, 60, 64–70, 72–75, 78–82, 135, 201, 203, 228, 234, 238–239, 242, 253, 261, 265, 275, 292–294, 305, 309, 337, 353, 356, 398, 401–402, 405, 408, 419–420, 445, 457, 471, 607
  parabolic law of, 65
  square law of, 67
Deformation of soil, spatial processes of, 255
Deformation parameters, 12, 43, 238, 243, 459, 465, 474–475, 477, 533, 607
Deformation properties, 1, 4, 55, 234, 242, 251, 265, 269–270, 276, 292, 313, 334, 358, 367, 414
  variation of, 14, 74
Deformations due to soil compression, 390
Deformation stage spatial contact models, 335
Deformation tensor, 351, 510
Delaunay triangulation, 165
Desalination degree, 275
Detachment zones, 251, 462
3-D finite-element, 166, 174
Diaphragm wall technique, 454–455
Differential equation, 29–30, 264, 270, 277, 353, 358, 360–361, 393, 510, 586
Dilatation, 30, 32, 36, 39, 62, 270, 511–513, 517, 523–524, 532, 550
  equations, 513
  function, 30, 32, 36, 39, 511–513, 517, 523, 550
Dinite-difference equation, 264, 361, 586, 588, 591
Dipper mechanisms, 465
Dirac delta function, 2
Dirac δ-function, 66
Direct boundary-element
  formulation, 118
  method, 96, 106, 112, 116–117, 218, 301, 418, 448
Dirichlet cell, 167
Dirichlet problem, 5
Dirichlet-Voronoy cells, 171, 193
  polygons, 173, 195, 197–198
Discretization
  circular domain, 161
  complex-shaped surface, 175
  contact domain, 121, 124, 128, 204, 216, 339, 428
  contact surface, 97, 177, 229, 445, 458
  2-D domains, 150–174
    algorithm of triangulation, 151–162
    dual grids applications, 162–174
  degree, 102, 142, 175, 195, 265, 292, 313, 327, 364, 457, 459–460, 625
  domain, 162
  foundations with pile rafts, 190
  numerical modeling, 151
  procedure, 154, 159, 401
  rigid inclusion contact surface, 218
  rotation surface, 185
  scheme of, 179, 191
  spherical surface, 220
  triangular boundary, 180
Disc-shaped anchor, 400
Displacement
  components, 256
  decay, 67
  matrix, 3
  piles, 181, 386, 399, 410, 438–439, 456
  tensor, 3, 8–9, 542
  vector components, 3, 9, 26, 93, 121
Double-precision calculations, 363
Drop caissons, calculation of, 55

Dual boundary-element grids, efficiency characteristics, 217
Dual grid, 151, 162–166, 168–173, 194, 201, 212, 216
application, 216
cell, 169
examples, 165
polygonal, 197, 205–216
rectangular, 166

E
Earth-moving excavator-based machines, 456
Earthquakes, 403, 506–507
Eccentric ring-shaped punch, 210, 213, 309–310
Egorov influence function, 275, 575
Egorov solution, 15, 17, 290
δ^2-Eitken transformation, 339
Elastic base rigidity matrix, 362
Elastic bases with deformation modulus, 55–82
nonhomogeneous half-space surface, 63–82
normal concentrated force, 58–63
variation with depth, 55–58
Elastic compressible wedge, 285, 290, 304, 363, 365–368
Elastic foundation model, 593
Elastic half-space, 93, 292, 397, 512
boundary, 400
homogeneous, 91, 130, 192, 200, 203–205, 212, 219, 228, 273, 292, 406, 526
model, 397
torsion, 116, 130
Elastic homogeneous isotropic half-space, 5–8
Boussinesq and Cerruti solutions, 6–8
Mindlin's solution, 5–6
Elastic layered bases, 12–55
constant-width layer, 12–17
multilayer half-space, 25–55
variable-thickness layer, 17–25
Elastic modulus, 77, 91, 258, 313
Elastic non-classical models, 253
Elastic spatial wedge, 17
Elastic wedge, 17, 22, 281, 284–287, 290, 296, 306–307, 366, 368, 585
rib, 281, 284–287, 296
Elastoplastic deformation law, 414
Elastoplastic deformation of soil bases, 395
Elastoplastic problem, 410
Elastoplastic solution, 408–409, 411–412, 539
Elastostatic problem, 401
Elastoviscoplastic problems, 408
Electric modelling, 255
Elliptical contact domains, 123
Elliptical punches, 128, 259
Elliptical-shaped contact domains, 123
Elliptic centrosymmetric, 526
Eluvial clayeys, 458
Engineering-and-geological conditions, 25, 56, 79, 242, 252, 412, 415, 424, 525, 534, 540
Engineering theory of beam bending, 263

F
Fatigue crack nucleation, 279
FEM, *see* Finite-element method
Ferroconcrete, 356, 438, 457, 473
Fictitious force method, 22
Field experiments, 56, 410, 425, 457, 470
Filtration
coefficient, 514
consolidation, 505
Finite-difference approximation, 264, 362, 589–590
Finite-difference grid, 174, 265, 354, 361–362, 364–365, 368
nodes, 361
Finite-difference method (FDM), 136, 138, 145, 253, 264–266, 270, 354–356, 365, 372, 395, 402, 404, 593
Finite-difference relations, 587
Finite-difference software, 354
Finite-element algorithm, 354, 357
Finite-element formulation, 355
Finite-element method, 146, 175–176, 218, 242, 264, 266–272, 277–278, 354–355, 364–365, 395, 407, 409–412, 416–417, 420
computer implementation, 176
matrix, 146
Finite-measure analogue, 96–101
Finite-thickness elastic layer, 27, 43, 50, 275, 345, 354
First-order model, *see* Mohr-Coulomb model
Fisher criterion, 349
Flat-base punch settlement, 232
Flat boundary macroelements, 177
Flat graph theory, 165
Flat ring-shaped punch, 131, 261
Flexible punch, calculation scheme for, 252
Forging hammers, 180, 393
FORTRAN, 137, 145, 159, 173, 178, 241, 327, 338, 363, 566
FORTRAN-77, 137, 159, 173, 327
FORTRAN-IV programming language, 566
Foundation bases with account of depth factor, 396–415

Foundation engineering, 252, 276, 300, 385, 415, 438, 454, 490
Foundation models, 254, 272, 403, 470
Foundation slope, 300–301, 391, 425, 577–579, 583–584
Foundation structure, calculation of, 17, 64, 389, 540
  methods, 136
  principles for, 385
  theory, 388
Foundation structures at reduced pore pressure, 517–524
  finite-dimensional algebraic analogue, 519–520
  integral equations, 517–519
  numerical algorithm, 520–522
  shallow foundations, 522–524
Foundation structures from deformations, calculation of bases, 390–396
Fourier method, 257, 403
Fourier series, 27, 352, 357
Fourier transformation, 5, 26, 30–31, 33, 52, 513
  two-dimensional, 1, 27, 29, 54
Fourth-order differential equation, 397
Fredholm equation, 263, 345, 401
Fredholm integral equations, 259
Friction resistance, 388, 456
Functional coefficient, Dependence of, 46–48
Functioning horizontal wells, 514–516
  finite radius of well, 516
  predetermined intensity sources, 514–516
Fuss-Winkler model, 350, 416, 442

G

Galerkin method, 261, 357
Galerkin vector, 9, 26
Gauss Cubature formulae, 557
  nodes and weights of, 559
Gauss elimination, 101, 119, 139, 147–148, 363
Gauss formulae, 628
Gaussian function, 262
Gaussian surface equations, 174
Gauss-Legendre quadrature formula, 52, 77, 79
Gauss method, 52, 147–148, 150, 363
GAUSS program, 139
Gauss type methods, 521
Gazli gas field, Uzbekistan, 506, 508
Geogrids, 54
Geomechanics ADA code, 412
Geomechanics Creep–3, 408
Geometrical scheme, 6, 124, 579
Geotechnics, 1, 25–26, 97, 224, 234
Geotextiles, 54
Gilbert boundary problem, 18
Gorbunov-Posadov solution, 364–365
GOST standard, 320
Green's displacement functions, 3
Green's displacement tensor, 8, 542
Green's formulae, 18
Green's function, 3, 5, 404
Green's tensor, 512–513
Grid
  approximations, 192
  condensation, 152, 194–195
  nodes, 174, 198, 211, 268

H

Half-round abutting ends, 212
Half-space
  model, 255, 257, 300, 345, 353, 396–398, 401–403, 414, 424, 472, 490
  surface settlements, 64, 71–72, 78
  theory, 91
Hankel integrals, 27, 39, 52, 54
Hankel operator, 258
Hankel transformation, 26–27, 259, 276, 401, 403
Hard cutting elements, 493
Heaviside function, 241
Hermit cubature formula, 563
  nodes and weights of, 564
Heterogeneous stress-strained states, 385
High λ method, 22
Hill-Tresk hypotheses, 407
Hollow conical pile, 386
Homogeneous half-space model, 64
Homogeneous isotropic half-space, 542
Homogeneous layer, 15, 599
Hooke equations, 94
Hooke's law, 4, 30, 60, 270, 402, 510, 512, 544
Horizontal displacements, 15, 183, 256, 258–259, 263, 390–391, 403, 415, 425, 430–432, 435–436, 442–443, 449, 452–453, 462, 475, 508, 524, 527–528, 530–531
Hydrocarbon fields, 507
Hydrotechnical engineering, 54
Hypergeometrical function, 52

I

Ilyushin elastic solution, 270
Inadmissible deformations, 505
Inclination angle, 428, 430, 433, 435, 437, 450, 452, 457, 460, 489
Inclined bottom foundations, 183, 387

Industrial engineering, 181
Inelastic deformation, 539
  development of, 371
Infinite-measure matrix, 257
Infinite stripe punch, 257
Influence matrix, 106–107, 115, 119, 121, 129–131, 141, 265, 273–274, 276, 362–363, 403, 405
  coefficients, 119, 130, 273–274, 403
Integral-differential operators, 13, 256
Integral equation, two-dimensional, 128, 263
Integral transformations, 26, 257–258
Integrand function singularities, 559
Integration procedure, 102, 121, 521–522
Internal graphic software tool, 162
Inverse Fourier transformation, 32, 38
Inverse trigonometric law, 80
Irregular grids of boundary elements, 197
Isobars, 198, 209, 212, 293, 313
Isolines of contact stress, 607
Isomorphism, 163
Isotropic media, 400
Iteration processes, 463

J
Jacobian transformation, 624
Jacobi or Seidel methods, 340

K
Kantorovich-Lebedev transformation, 21
Kelvin displacements, 4
Kelvin influence matrix, 107
Kelvin's kernels, 138
Kelvin's solution, 3–6, 12, 26, 102, 106–107, 119
Kelvin transformation, 257
Kernel boundary point, 324
Kirchhof–Love hypotheses, 358
Koltso software, 276
Kronecker symbol, 2

L
Labour-consuming
  calculations, 388
  solution, 398
Lamé equations, 2, 29
Landau order symbol, 67
Land surface
  deformation, 524, 528, 532, 534
  subsidence, 505–506
Laplace operator, 509
  three-dimensional, 3
Lateral expansion coefficient, 401
Lateral friction, 454
Layer permeability, 507
Layer summation method, 395, 472
Least-square method, 27, 171, 255, 275, 308, 345, 602–605
Legendre polynomials, 562–563
Limiting transition, 12, 47, 81, 94, 203, 232
Linear algebraic equation system, 101, 139, 146–151, 218, 274, 364, 449, 592
Linear algebra method, 302
Linear and angular displacements, characteristics of, 568
Linear law of deformation modulus, 64
Linearly deformable base theory, 350
Liquidity index, 470–471
Load-carrying capacity, 183, 187–188
Logarithmic law, 516, 533
Lommel function, 52
Long Beach, USA, 506
Longitudinal-to-transverse dimension ratio, 397
Love formula, 316, 319
L-shaped punch, 304–306, 330, 333

M
Macdonald function, 19
Macrofragmental soils, 236
Maizel's method for thermoelasticity, 511
Man-triggered damage, 506–507
Maple, 107
Masts, 186, 577
Matcad, 107
Material nonhomogeneity, 277
Mathematica, 107
Mathieu functions, 257
Mechanical behaviour of soil, 482
Mechanical properties of soils, determination of, 234–235
Meridional zone, 113–114, 444
Mesh condensation, 154
Metal-cutting machines, 393
Mexico Engineering Research Institute, 506
Mindlin displacement, 5–6, 102
Mindlin equation, 93, 102, 401
Mindlin's solution, 5–6, 8, 12, 27, 47, 91, 96–97, 101, 106–107, 110, 119, 121, 218–219, 273, 398–399, 401–402, 405, 417, 517
Mises plasticity, 270
Mises–Schleicher–Botkin hypotheses, 407, 409, 411
Mises–Schleicher–Botkin strength condition, 267
Mohr-Coulomb model, 412

Mohr-Coulomb strength condition, 267
Moment of inertia, 216, 582
Monolithic
  blocks, 180
  foundation structures, 385
  plates, 455
MONOT model of elastoplastic type, 413
Multiparametric method, 149
Multivariant calculations, 300, 313

N
Narrow grab bucket, 456
Navier's equations, 27
NBE array, 167
NBK array, 167, 173
Negative (tensile) contact stress, 202
Neumann series, 18, 20
  convergence of, 22
Newton method of nonlinear equations, 340
Niigata, Honshu Island, Japan, 506
NNBK arrays, 173
Non-classical model, 258
Nondeformable rod, 398
Nonhomogeneous half-space settlements, 82
Nonlinear (elastoplastic) displacements, 407
Nonlinear law of settlement variation, 574
Nonlinearly deformable
  finite-thickness layer, 343
  half-space, 342
Nonlinear programming methods, 349
Nonlinear settlement-versus-load dependences, 343
Nonlinear soil base models, 404
Non-linear stage of deformation, 351
Non-uniform base compressibility, 300, 577
Non-uniform compression coefficient, 443
Non-uniform deformations, 301, 391
Nonuniformity function, dimensionless, 79
Nonuniformity parameter, 73, 78, 80
Non-uniform settlements, 392
North Stavropol oil field, 508
Numerical algorithm testing, tool for, 131
Numerical-and-analytical method, 52, 54, 75, 82, 91, 101–107, 115, 131, 148, 218, 238, 239, 273, 403, 448, 524
Numerical calculations examples, 524–534
  settlement and slopes of rigid foundation plates, 533–534
  spatial deformation of land surface, 526–532
  surface deformations of layer, 532–533
Numerical modeling test examples, 192–243
  axisymmetric punches, factor for, 218–243
  flat punches with a smooth base, 192–217
Numeric schemes of volume integration, 623

O
Obtuse-angle conical punches, 231–233
Obtuse-angled cones, dimensionless settlements, 233
Oozes, 396
Optimal solutions, 539
Orthogonal polynomials, 262
Orthotropic foundation plates, contact problem, 351–372
  integro-differential equations, 358–361
  numerical modelling, 364–372
  rectangular orthotropic plates, 361–363
  static calculations, 352–358
Orthotropic plate with free edges, 365
ORTOPLIT software, 363, 372, 593
Osaka, Japan, 506

P
Paired integral equations method, 258
PALOS software, 413
P-analytic functions, 109
Papkovic-Neuber representation, 21
Parabola, 204, 324
Partial differential equations, 14, 255, 355
Peaty sand-clays, 396
Physical nonlinearities, 277
Pile calculations, 224, 416–417
Pile drivers, 393
Pile foundation, 181, 183, 187, 190, 276, 386–387, 393–394, 397, 409, 411–413, 418, 422, 424–426, 432–434, 437–441, 443, 454, 456, 517, 593
  calculation of, 398, 401, 411, 472
  construction, 181
  deformation of, 393
  displacement, 394, 424, 432, 437
  settlement, 393, 412
Pile raft foundations, 189–190, 425, 432
Pile rigidity, 408
Pile settlement
  behaviour, 431
  curve, 420
Pile shaft compressibility, 406
Pile sliding, 405
Piles with self-unfolding blades, 386
Piles with triangular crosssection, 387
Pipe casing failures and crushing, 507
Planar graph theory, duality in, 151
Plastic deformation, 234, 278, 390, 395, 408–409, 411, 413, 480

Plastic flow theory, 270, 407, 409–410
Plastic fluidity laws, 417
Plate flexibility index, 364–365
Plate foundations, orthotropic properties of, 356
PLAXIS software, 412–413
Plevako solution, 9, 12, 513, 517
Poisson coefficient, 607
Poisson ratio, 5, 8, 14–15, 17–18, 22–23, 50, 54–55, 57–58, 70–71, 91, 143, 192, 195, 222–223, 228–232, 234, 236, 256, 258–259, 263, 265, 274, 281, 290, 296, 303, 307, 309, 313, 353, 356, 359, 364, 399, 408, 417, 419, 445, 457, 470, 474, 526, 533, 571–573, 580
Polar coordinate systems, 104
Polish engineering regulations, 414
Polygonal cross-section punches, 208–209
Polygon-type boundary elements, 129
Polynomial
  approximation, 263
  coefficients, 275
Pore liquid squeezing, 507
Pore pressure, 505–506, 508, 510–512, 514, 516–517, 519–522, 524–525, 532–534
Pores and cracks, 505
Porous elastic massif, 512
Postprocessor algorithm, 171
Power law, 56, 69–70, 73, 356, 465
Prandtl-Reiss equation, 270
Pre-conditions resulting, 388
Preprocessor algorithm, 151, 167, 169, 173
Prismatic foundations, 181
Pulse effect, 493
Punch boundary, 97, 194–195, 297, 323
Punch centre settlement, 285, 571, 574
Punch contour, 204, 279, 325–326, 328–330
Punch displacement, 91, 100, 115, 122, 147, 149, 202, 204, 275, 323, 337, 345
Punch equilibrium equations, 225, 259, 444
Punch foundation, 255, 272
Punch generatrix, 113, 115, 118
Punch indentation, 121, 125–126
Punch settlement values, 273, 286
Punch in the shape of a rotation body, 108–119
  axisymmetric contact problem, 110–115
  axisymmetric punch torsion, 115–119
Punch test, 68, 234, 238, 251, 341–342, 348–349, 413, 420, 598
Punch uplifting zone, 296
Punch vertical displacement, 260
Puzyrevsky solution, 447
Pyramidal displacement pile, 386
Pyramidal piles, 415–424
  application, 416
  horizontal load action, 420–422
  inclined force and moment, 423–424
  inclined load action, 422–423
  piles with variable cross-section, 416–420
  settlements, 422
  vertical load, 420
Pyramidal-prismatic foundations, 388

Q

Quadrangular boundary elements, 555
Quadratic approximation, 240
Quasiuniform dependence, 193, 341
Quasiuniform discretization of a square domain, 281
Quasi-uniform grids, 180
Q–Z curves, 413

R

Radial deformations, 58
Reciprocality theorem, 260, 444
Rectangular punch, 212
Reference vertices, 154, 156, 160
Reinforced concrete forming machines, precast, 393
Reisner square plate, 355
Relative punch displacement, 230
Relative settlement difference, 391–393
Relative torsion angle, 391
Reverse arches, 387
R-function, 212, 216, 262, 324
Rheological calculation models, 351
Rheological properties, 267, 277, 408, 413
Richardson method, 292, 313
Riemann convolution, 511
Rigid disc, axisymmetric problem for a, 401
Rigid displacements, 95
Rigid flat-bottom punches, spatial contact problems, 253–278
Rigid foundation plates, 300–311
  external load control, 303–307
  kernel boundary for, 323–334
  problem formulation and numerical implementation, 301–303
  shape parameter control, 307–311
  structural analysis, 243
Rigidity coefficients, 352, 540
Rigidity matrix, 267, 271, 408, 412, 592
Rigidity-related characteristics, 400
Rigid plates, 180
Rigid punch displacement, 274

Rigid punches contact problems, 119–131
elastic half-space torsion, 126–131
punch indentation, 121–126
Rigid rectangular punches, contact problems, 278–300
contact interaction at central loading, 282–294
contact interaction at off-centre loading, 295–300
Rigid ring-shaped punches, 276
Rigid rod scheme, 475
Rigid sphere, displacements of, 223
Rigid spherical inclusion, 135, 219
Rigid strip variable-width foundation, 311–322
contact pressure distribution, 317–322
strip foundation base, 315–317
variable-width strip foundation, 312–315
Ring-shape
belts, 224–225
centrally loaded punch, 268
centrosymmetric, 525
conductor, 260
foundation, 269, 276, 310, 584–585
punch, 128, 130–131, 211, 213–215, 255, 257, 260–261, 272, 276, 308, 310, 585
problem, 131
rotation, 130
Roben elastostatic problem, 223
Roben equation, 239
Rock stratification, 508
Rolling equipment, 393
Romberg integration scheme, 53
Rosinka software, 409
Rostwerk software, 135–137, 139–140, 143–146, 150, 242, 389, 419, 449, 457, 538
block structural scheme of, 139
deep foundations in, 142
shallow foundations in the, 141
Rotating furnaces, 393
Roughness measure, 486
Round punch, 130–131, 194, 197, 200, 202–204, 256, 258–259, 266, 270, 273, 287, 301, 306–307, 325, 331, 342–344, 346–347, 399, 566, 568, 575
Round punch on an elastic wedge, 306
Russia, 424–425, 454, 456, 506–508
Russian Federation patent No. 043462, 584
Russian handbooks and regulations, 258

S

Schleicher formula, 273, 276
Second-order Bessel function, *see* Macdonald function
Second-order model, *see* Cam-Clay model
Section kernel boundary configurations, 331
Seidel method, 265
Semihard and hard consistency, 396
Semi-inverse method, 261–262, 399
Settlements and slopes, 281, 289, 460
Settlement-vs-load curve, 408–410
Shallow foundations, 82, 91, 138, 141, 190, 251–253, 255, 300, 324, 329, 396
design of, 252
Shallow monolithic foundations, 454
Shallow slotted foundations, 456
Shandru problem, 12
Shearing force, 252–253, 359
Shear modulus, 5, 14, 55, 265, 270, 404
Shebelynka gas field area, 508
Shekhter method, 26
Shrine Museum, 506
Shvedov–Bingham model, 408
Similarity function, approximation of, 241–242
Simpson rule, 16
Single-precision calculations, 272, 363
Singularities and irregularities, 155
Slippage, 16, 268, 274, 277–278, 402, 405–406, 410, 429, 484, 486–491
delineation of, 490
Slotted foundations, 181, 189, 454, 456–457, 476
calculation of, 456, 460, 474
construction technology, 456
contact interaction calculation of industrial and civil buildings, 454–493
base deformation calculation, 457–476
contact stress on the lateral surface, 476–491
lateral widenings, 491–493
structural shapes, 454–457
geometrical shape, 460
Soatial contact problems for, 241
Sobolev δ-shaped averaging functions, 274
Soil back pressure, 386, 397, 399, 416, 476
Soil compression, 392, 394, 439
Soil conditions, 470, 473
Soil consistency index, 597
Soil deformability, 56
Soil deformation modulus, 1, 64, 143, 147, 238, 242, 356, 398, 526
Soil deformation parameters, 320
Soil deformation properties, 76, 141

Soil drilling technology, 187
Soil grain composition, 238
Soil linear displacement phase, 238
Soil mass deformation, 509–513
  dilatation relations, 512–513
  porous elastic medium, 509–511
Soil mechanics, 64, 82, 252, 254, 267–268, 272, 277, 334, 395–396, 407, 476, 480, 508, 538, 579
Soil nonhomogeneity, 82, 352, 391, 404, 416
Soil properties, characterization of, 234
Soil resistance, 224, 268, 415–416, 440, 460, 472, 478, 582–583, 599, 601
Soil skeleton deformation, bulk modulus of, 509
Soil tests, 56, 234, 410
Soil transverse expansion coefficient, 597
Somigliana formula, 93, 273, 278
Somigliana identity, 93
Southern California, 506
Spacer-type scheme, 435
Spatial contact interaction processes, 254, 263, 517, 539
Spatial contact models, 1, 131, 207, 538
Spatial contact problem, 21, 82, 91, 95–97, 113, 118–123, 128, 130, 135–136, 147–148, 163, 173, 175, 192, 204–205, 207–208, 211–213, 215, 218–219, 228, 234, 242, 251, 253–259, 263–264, 271–273, 277–278, 292, 300, 311, 313, 324, 327, 337–339, 341, 359, 361, 389, 398–399, 411, 415, 418, 420, 424, 426, 443, 476–477, 517, 519, 523, 538–540, 566, 585
  equations of, 91, 99, 110–111
  numerical solution of, 192
  rigid punches, 175, 277
  solutions of, 385
  theory of elasticity, 21, 118, 258, 327, 540
Spatial deformation, 505, 508
Spatial discretization, 135, 186, 511, 525
Spatial elastic layer, 12
Spatial elastoplastic problem, 266
Spatial formulations, 264, 457
Spatial foundations of structural type, 388
Spatial functioning, 442
Spatial grids of boundary elements, 174–192
Spatial loading, 121, 162, 196–197, 202, 228, 278, 345, 385, 389, 392–393, 401, 418, 454, 460, 463, 479–480, 487
Spatial nonhomogeneity, 137, 300, 363, 370
Spatial problems solving software, 136–146
Spatial theory of elasticity, fundamental solutions, 1–4
  Concentrated forces, 1–2
  Green's displacement tensor, 2–3
  Kelvin's tensor, 3–4
Spatial triangular element, 560
Spatial wedge, 21–22, 330
Spherical harmonic functions, 400
Square punch, 173, 195–196, 208–210, 213, 216, 264, 273, 282–283, 285–286, 288–290, 292, 294, 296–300, 304, 307, 326–327, 332, 533
  orientation scheme, 290
Squeezing pressure, 603
STAMP-C software, 566
Strength-related characteristics, 407, 480, 486, 490
Strength-related soil properties, 238, 414, 487
Stress components, 256, 351
Stress distribution, 109, 136, 143, 188, 219, 231, 252, 262, 273, 312, 315, 322–323, 402, 441, 457, 477
Stress extrapolation, 229
STRESS program, 139
Stress-strained state, 7–8, 12, 25–26, 31, 36, 39–40, 55, 58, 60–61, 70–71, 92, 97, 109, 135–136, 218–219, 251, 253–254, 256, 264–268, 270–271, 276, 311, 334, 346, 351, 357–358, 363, 369, 371–372, 386, 394, 403–406, 408–409, 411–412, 415, 417, 449, 452, 454, 457, 460, 478, 480, 490, 508, 534, 538
  characteristics of, 30, 39, 50, 118, 311, 404, 410–411, 540
Stress tensors, 6, 550
  components, 30, 94
Stress vector, 108–111, 116, 139, 141, 150, 219, 443, 476–480
  components of the, 518
Strip discretization, algorithm of, 152
Stripe-shaped punches, 257
Strip foundation, 251, 260, 263, 312–315, 318–319, 322, 415
Strip punch, 209
Structural nonlinearity, 323
Structure-type nonlinearity, 297
Subsidence-01 software, 524, 534
Suffusion-related
  compression, 275
  settlement, 392
Superposition principle, 7, 277, 296, 298–299, 323, 397, 463

Surface approximation, 175
Surface discretization, 175, 190, 224, 228, 312, 445, 519
Surface integrals, parametric representation of, 553
Surface parametrization, 554
Surface subsidence, 505–508
Swelling, 390, 392, 415, 439–440

T
Tangential stress, 9, 13, 15, 61, 110, 121, 126–128, 130, 137, 144–145, 231, 256, 264, 279, 347, 402, 410, 443, 478–479, 486–487, 490, 508
  determination of, 272
Taylor polynomial, first-order, 171
Tectonic anomalies, 506
Telescope-shaped cylindrical foundations, 187
Telescopic element method, 419
Tensile forces, 54
Tensile functioning of soil, 136
Tensile stress, 141, 202, 216, 419, 445, 451, 505, 566, 572
Tetrahedral element, 625
Theater Center, 506
Theoretical substantiation, 301, 352
Theory of elasticity, 1–4, 25–26, 52, 55–56, 64, 72, 98, 108–109, 118–120, 123, 128, 147, 224–225, 258, 272, 277, 335, 349, 351, 405, 416–418, 480
  axisymmetric problem of, 112
  classical, 63
  edge effects in, 143
  equations of, 73
  inverse symmetrical problem of, 116
  linear, 2, 234, 257, 268, 539
  spatial problems of, 4, 12, 27, 54, 71, 106–107, 109, 171, 257, 417, 512
  three-dimensional, 138, 175, 261
Thermoelasticity equation system, 510
6th order polynomial, 399
9th order polynomial approximation, 240
Torque load, 136, 259, 403, 607
Torsional rigidities, 404
Total (mean square) error, 195
Tower-type structures, 213, 256, 258, 276, 310, 577, 585
Transformational functions, 412–413
Translational displacements, 95
Transverse loading, 462–463
Transverse-and-longitudinal bending, 508
Trapezoidal punches, 307, 328
Trapezoid rule, 557
Travelling cranes, 473
Trench, 238, 464–466, 470, 492–493
Triangular boundary
  elements, 554
  macroelement, 179–180
Triangular discretization, 195
  algorithm of, 152
Triangular grid, 216
Triangular polar coordinates, 561
Triangular-prismatic element, 626
Triangulation of a 2-D domain, algorithm of, 151
Triangulation algorithm, 162
Tridiagonalization, 146
Trough formation, 505
T-shaped cross-section, 386
Two-dimensional integral Fourier transformation theory, 14
Two-layer deformable system, 42
Two-slot foundations, 455
T–Z curves, 413

U
Ukraine, 506, 508
Underground mining, 505
Underground water level decline, 506
Unilateral constraints, 202–204, 218, 281, 296, 309, 323, 339, 355, 388–389, 402, 418, 428–437, 445, 447–448, 450–452, 462–464, 469–472, 475, 566, 572–573
Uplifting zone, 202, 296

V
Variable-sign moment load, 578, 581, 585
Variable-thickness elastic layer, 17–18, 25, 253, 279, 282, 287–289, 291, 296–299, 310, 331–333, 358, 365
Variable-thickness elastic layer, 291
Variable-thickness elastic wedge, 23
Variable-width foundations (VWFs), 311–315, 318–320, 322
Variation-difference problem, 270
Varved clays, 396, 486
Vasilyev solution, 12
Vertical displacements, 61, 279, 337, 522
Vertical resultant force, 279
Vertical rod constraints, 353
Vibroimmersion, 438
Viscosity-related (fluidity-related) properties, 407
Volumetric punch, 92, 416, 457
Voronoy polygons, 151, 164–165, 195

W
Wedge rib, 23, 287, 366, 570–573, 578–579, 584–585
Wedge-slotted foundation, 183, 190, 455, 458
Wedging, 429–431, 433, 437, 451–452, 463
Wet formula, 234
Winkler base, 336, 352, 357, 414
Winkler constraints, 55
Winkler hypothesis, 389, 456, 472
Winkler model, 55, 257, 352, 396–397, 403, 416, 424, 457
Winkler-type elastic bases, 352–353

Y
Yekaterinburg test site, 470

Z
Zero deformation modulus, 261
Zeros of classical orthogonal polynomials, 562
Zeroth order model, 412
Zhemochkin method, 353, 398–399